

James J. (Jong Hyuk) Park
Leonard Barolli
Fatos Xhafa
Hwa Young Jeong *Editors*

Information Technology Convergence

Security, Robotics, Automations and
Communication

Lecture Notes in Electrical Engineering

Volume 253

For further volumes:
<http://www.springer.com/series/7818>

James J. (Jong Hyuk) Park
Leonard Barolli · Fatos Xhafa
Hwa Young Jeong
Editors

Information Technology Convergence

Security, Robotics, Automations
and Communication

 Springer

Editors

James J. (Jong Hyuk) Park
Department of Computer Science
and Engineering
Seoul National University of Science
and Technology (SeoulTech)
Seoul
Republic of South Korea

Leonard Barolli
Faculty of Information Engineering
Department of Information
and Communication Engineering
Fukuoka Institute of Technology
Fukuoka
Japan

Fatos Xhafa
Departament de Llenguatges i Sistemes
Informàtics
Universitat Politècnica De Catalunya
Barcelona
Spain

Hwa Young Jeong
Humanitas College
Kyung Hee University
Seoul
Republic of South Korea

ISSN 1876-1100

ISBN 978-94-007-6995-3

DOI 10.1007/978-94-007-6996-0

Springer Dordrecht Heidelberg New York London

ISSN 1876-1119 (electronic)

ISBN 978-94-007-6996-0 (eBook)

Library of Congress Control Number: 2013940289

© Springer Science+Business Media Dordrecht 2013, corrected publication 2024

This work is subject to copyright. All rights are reserved by the Publisher, whether the whole or part of the material is concerned, specifically the rights of translation, reprinting, reuse of illustrations, recitation, broadcasting, reproduction on microfilms or in any other physical way, and transmission or information storage and retrieval, electronic adaptation, computer software, or by similar or dissimilar methodology now known or hereafter developed. Exempted from this legal reservation are brief excerpts in connection with reviews or scholarly analysis or material supplied specifically for the purpose of being entered and executed on a computer system, for exclusive use by the purchaser of the work. Duplication of this publication or parts thereof is permitted only under the provisions of the Copyright Law of the Publisher's location, in its current version, and permission for use must always be obtained from Springer. Permissions for use may be obtained through RightsLink at the Copyright Clearance Center. Violations are liable to prosecution under the respective Copyright Law. The use of general descriptive names, registered names, trademarks, service marks, etc. in this publication does not imply, even in the absence of a specific statement, that such names are exempt from the relevant protective laws and regulations and therefore free for general use.

While the advice and information in this book are believed to be true and accurate at the date of publication, neither the authors nor the editors nor the publisher can accept any legal responsibility for any errors or omissions that may be made. The publisher makes no warranty, express or implied, with respect to the material contained herein.

Printed on acid-free paper

Springer is part of Springer Science+Business Media (www.springer.com)

Message from ITCS 2013 General Chairs

The International Conference on Information Technology Convergence and Services (ITCS 2013) is the FTRA 5th event of the series of International Scientific Conference. This conference takes place on July 8–10, 2013 at Fukuoka Institute of Technology, Fukuoka, Japan.

The aim of the ITCS 2013 was to provide an international forum for scientific research in the technologies and application of Information Technology Convergence and its Services. The ITCS previous editions were held successful Gwangju, Korea, September 2012 (ITCS 2012), Gwangju, Korea, October 2011 (ITCS 2011), Cebu, Philippines, August 2010 (ITCS 2010), and Bangalore, India, January 2009 (ITCS 2009).

The papers included in the proceedings cover different topics such as: Advanced Computational Science and Applications, Advanced Electrical and Electronics Engineering and Technology, Intelligent Manufacturing Technology and Services, Advanced Management Information Systems and Services, Electronic Commerce, Business and Management, Intelligent Vehicular Systems and Communications, Bio-inspired Computing and Applications, Advanced IT Medical Engineering, Modeling and Services for Intelligent Building, Town, and City.

The accepted and presented papers highlight new trends and challenges of Information Technology Convergence and its Services. They present new research ideas which could lead to novel and innovative applications. We hope you will find these results useful and inspiring for your future research.

We would like to express our sincere thanks to Steering Chairs: James J. (Jong Hyuk) Park (Seoul National University of Science and Technology, Korea). Our special thanks go to the Program Chairs: Minoru Uehara (Toyo University, Japan), Markus Aleksy (ABB AG, Germany), Hwa-Young Jeong (Kyung Hee University, Korea), and Jinjun Chen (Swinburne University of Technology, Australia). We also thank all Program Committee members and all additional reviewers for their valuable efforts in the review process, which helped us to guarantee the highest quality of the selected papers for the conference.

We cordially thank all authors for their valuable contributions and other participants of this conference. The conference would not have been possible without their support. Many thanks also for many experts who contributed to making the event a success.

We would like to give special thanks to FIT and especially Mr. Yoji Unoki, Chairman of Board of Trustees of FIT and Prof. Teruo Shimomura, President of FIT for hosting ITCS 2013, providing the university facilities and their continuous support.

We would like to thank Fukuoka Convention Bureau and Fukuoka City for their great support, help, advices, and local arrangement.

Finally, we would like to thank the Local Arrangement Team at FIT and the Administration Staff of FIT for their support and for making excellent local arrangement for the conference.

We do hope that you will enjoy the conference and beautiful city of Fukuoka.

Leonard Barolli
Fukuoka Institute of Technology
Japan

Young-Sik Jeong
Dongguk University
Korea

David Taniar
Monash University
Australia

Message from ITCS 2013 Program Chairs

Welcome to the 5th FTRA International Conference on Information Technology Convergence and Services (ITCS 2013) which will be held at Fukuoka Institute of Technology (FIT), Fukuoka, Japan on July, 8–10, 2013. The ITCS 2013 will be the most comprehensive conference focused on the various aspects of advances in information technology convergence, applications, and services. The ITCS 2013 will provide an opportunity for academic and industry professionals to discuss the latest issues and progress in the area of ITCS. In addition, the conference will publish high quality papers which are closely related to the various theories, modeling, and practical applications in ITCS. Furthermore, we expect that the conference and its publications will be a trigger for further related research and technology improvements in this important subject.

For ITCS 2013, we received many paper submissions. After a rigorous peer review process, we accepted 40 high quality papers for ITCS 2013 proceedings, which will be published by the Springer. All submitted papers have undergone blind reviews by at least two reviewers from the technical program committee, which consists of leading researchers around the world. Without their hard work, achieving such a high quality proceeding would not have been possible.

We take this opportunity to thank them for their great support and cooperation. We would like to sincerely thank the Keynote Speakers who kindly accepted our invitations and helped to meet the objectives of the conference. Finally, we would like to thank all of you for your participation in our conference, and also thank all the authors, reviewers, and organizing committee members. Thank you and enjoy the conference!

Minoru Uehara
Toyo University
Japan

Markus Aleksy
ABB AG
Germany

Michael H. (Hwa-Young) Jeong
Kyung Hee University
Korea

Jinjun Chen
Swinburne University of Technology
Australia

Organization

Honorary Chair

Teruo Shimomura, FIT President, Japan
Makoto Takizawa, Seikei University, Japan

Steering Chairs

James J. Park, SeoulTech, Korea

General Chairs

Leonard Barolli, Fukuoka Institute of Technology, Japan
Young-Sik Jeong, Dongguk University, Korea
David Taniar, Monash University, Australia

Program Chairs

Minoru Uehara, Toyo University, Japan
Markus Aleksy, ABB AG, Germany
Hwa-Young Jeong, Kyung Hee University, Korea
Jinjun Chen, Swinburne University of Technology, Australia

Workshop Chairs

Tomoya Enokido, Risho University, Japan
Hui-Huang Hsu, Tamkang University, Taiwan
Eric Pardede, La Trobe University, Australia
Seung-Ho Lim, Hankuk University of Foreign Studies, Korea

Publication Chair

Akio Koyama, Yamagata University, Japan
Jaehwa Chung, Korea National Open University, Korea

International Advisory Committee

Doo-soon Park, SoonChunHyang University, Korea
Siao-Hwa Chen, National Cheng Kung University, Taiwan
Habib F. Rashvand, University of Warwick, UK
Andrew Kusiak, The University of Iowa, USA
Yang Xiao, The University of Alabama, USA
Jianhua Ma, Hosei University, Japan
Qun Jin, Waseda University, Japan
Wenny Rahayu, La Trobe University, Australia
Fatos Xhafa, Technical University of Catalonia, Spain
Yoshitaka Shibata, Iwate Prefectural University, Japan

Publicity Chairs

Takahiro Hara, Osaka University, Japan
Farookh Hussain, University of Technology, Sydney, Australia
Hangbae Chang, Sangmyung University, Korea

Invited Speakers

Fatos Xhafa, Technical University of Catalonia (BarcelonaTech), Spain

Message from STA 2013 General Chairs

Welcome to the 10th FTRA International Conference on Secure and Trust Computing, Data Management, and Applications (STA 2013), which will be held at Fukuoka Institute of Technology (FIT), Fukuoka, Japan from July 8–10, 2013.

The aim of the conference is to deliver a platform of scientific interaction between challenging areas of research and development of future IT-enabled applications. The STA 2013 is an open forum for researchers to discuss theories and practical applications of secure and trust computing and data management. These problems are very important for the Internet and IT applications. Therefore, during the conference, it will be presented important results to solve the application services and various problems within the scope of STA 2013. In addition, we expect it will trigger further related research and technology developments which will improve our lives in the future.

The organization of an International Conference requires the support and help of many people. A lot of people have helped and worked hard to produce a successful STA 2013 technical program and conference proceedings. First, we would like to thank all authors for submitting their papers, the Program Committee Members, and the reviewers who carried out the most difficult work by carefully evaluating the submitted papers.

We are grateful to Honorary Co-Chairs: Prof. Teruo Shimomura, FIT President, and Prof. Makoto Takizawa, Hosei University, Japan. We would like to thank the Steering Committee Chair of STA Prof. James J. (Jong Hyuk) Park for his strong encouragement and guidance. We give special thanks to STA 2013 PC Chairs: Dr. Alfredo Cuzzocrea, ICAR-CNR and University of Calabria, Italy, Prof. Tomoya Enokido, Risho University, Japan, Prof. Hiroaki Kikuchi, Meiji University, Japan, and Dr. Young-Gab Kim, Catholic University of Daegu, Korea for their great efforts to make the conference successful. This year together with STA 2013, we have four International Workshops. We would like to thank Workshops Chairs: Dr. Neil Y. Yen, Dr. Jin-Mook Kim, Dr. Muhamed Younas, and Dr. Makoto Ikeda for organizing STA 2013 workshops.

We would like to give special thanks to FIT and especially Mr. Yoji Unoki, Chairman of Board of Trustees of FIT for hosting STA 2013, providing the university facilities and his continuous support. We would like to thank Fukuoka Convention Bureau and Fukuoka City for their great support, help, advices, and

local arrangement. Finally, we would like to thank the Local Arrangement Team at FIT and the Administration Staff of FIT for their support and for making excellent local arrangement for the conference. We hope you will have a good experience and enjoy the beautiful city of Fukuoka.

Leonard Barolli
Fukuoka Institute of Technology
Japan

Mohammad S. Obaidat
Monmouth University
USA

Martin Sang-Soo Yeo
Mokwon University
Korea

Fatos Xhafa
Technical University of Catalonia
Spain

Message from STA 2013 Program Chairs

Welcome to the 10th FTRA International Conference on Secure and Trust Computing, Data Management, and Applications (STA 2013). The STA 2013 is held in conjunction with the 5th FTRA International Conference on Information Technology Convergence and Services (ITCS-13) and the 3rd International Conference on Intelligent Robotics, Automations, Telecommunication Facilities, and Applications (IRoA 2013) from July 8–10, 2013 at Fukuoka Institute of Technology (FIT), Fukuoka, Japan.

Information technology issue is emerging rapidly as an exciting new paradigm with user-centric environment to provide computing and communication services. In order to realize IT advantages, it requires integrating security and data management to be suitable for future computing environments. However, there are still many problems and major challenges waiting for us to solve such as the security risks in resource sharing, which could occur when data resources are connected and accessed by anyone. Therefore, it is needed to explore more secure and trust and intelligent data management mechanism.

STA 2013 contains high quality research papers submitted by researchers from all over the world. Each submitted paper was peer-reviewed by reviewers who are experts in the subject area of the paper. Based on the review results, the Program Committee accepted 16 papers. For organizing an International Symposium, the support and help of many people is needed. First, we would like to thank all authors for submitting their papers. We also appreciate the support from program committee members and reviewers who carried out the most difficult work of carefully evaluating the submitted papers.

We would like to give special thanks to Prof. James J. (Jong Hyuk) Park, the Steering Committee Chair of STA for his strong encouragement and guidance to organize the conference. We would like to thank STA 2013 General Co-Chairs, Prof. Leonard Barolli, Prof. Mohammad S. Obaidat, Prof. Martin Sang-Soo Yeo, and Prof. Fatos Xhafa for their advices to make possible organization of STA 2013. We also thank the Workshops Chairs, Dr. Neil Y. Yen, Dr. Jin-Mook Kim, Dr. Muhamed Younas, and Dr. Makoto Ikeda for organizing STA 2013 workshops. We would like to express special thanks to FTRA members and the Local Organization Team at FIT for their timely unlimited support.

We hope you will enjoy the conference and readings and have a great time in Fukuoka.

Hiroak Kikuchi
Meiji University
Japan

Young-Gab Kim
Catholic University of Daegu
Korea

Tomoya Enokido
Risho University
Japan

Alfredo Cuzzocrea
ICAR-CNR and University of Calabria
Italy

Organization

Honorary Chair

Teruo Shimomura, FIT President, Japan
Makoto Takizawa, Seikei University, Japan

Steering Chairs

James J. Park, Seoul National University of Science and Technology, Korea

General Chairs

Leonard Barolli, Fukuoka Institute of Technology, Japan
Mohammad S. Obaidat, Monmouth University, USA
Martin Sang-Soo Yeo, Mokwon University, Korea
Fatos Xhafa, Technical University of Catalonia, Spain

Program Chairs

Hiroaki Kikuchi, Tokai University, Japan
Young-Gab Kim, Korea University, Korea
Tomoya Enokido, Risho University, Japan
Alfredo Cuzzocrea, ICAR-CNR and University of Calabria, Italy

Workshop Chairs

Neil Y. Yen, the University of Aizu, Japan
Jin-Mook Kim, Sunmoon University, Korea
Muhamed Younas, Oxford Brookes University, UK
Makoto Ikeda, Fukuoka Institute of Technology, Japan

Publication Chair

Hwa Young Jeong, Kyung Hee University, Korea

International Advisory Committee

Doo-Soon Park, SoonChunHyang University, Korea
 Hai Jin, Huazhong University of Science and Technology, China
 Yanchun Zhang, Victoria University, Australia
 Gail-Joon Ahn, Arizona State University, USA
 Wanlei Zhou, Deakin University, Australia
 Steganos Gritzalis, University of the Aegean, Greece
 Hsiao-Hwa Chen, National Sun Yat-Sen University, Taiwan
 M. Atiquzzaman, University of Oklahoma, USA
 Young-Sik Jeong, Dongguk University, Korea
 Feng Bao, Institute of Infocomm Research (I2R), Singapore
 Xiaobo Zhou, University of Colorado at Colorado Springs, USA
 Tok Wang Ling, National University of Singapore, Singapore
 Philip S. Yu, University of Illinois at Chicago, USA
 Timothy K. Shih, National Central University, Taiwan
 Minoru Uehara, Toyo University, Japan
 Irfan Awan, University of Bradford, UK

Publicity Chairs

Deqing Zou, Huazhong University of Science and Technology, China
 Jun Hong, Queen's University Belfast, UK
 Hung-Min Sun, National Tsing Hua University, Taiwan
 Takuo Nakashima, Tokai University, Japan

Local Arrangement Chairs

Makoto Ikeda, Fukuoka Institute of Technology, Japan
 Tao Yang, Fukuoka Institute of Technology, Japan

Program Committee

Akimitsu Kanzaki, Osaka University, Japan
 Akio Koyama, Yamagata University, Japan
 Apostolos N. Papadopoulos, Aristotle University of Thessaloniki, Greece
 Bo-Yeon Song, National Institute for Mathematical Sciences, Korea
 Carson K. Leung, University of Manitoba, Canada
 Chan Yeun Yeob, Khalifa University of Science, UAE

Cliff Zou, University of Central Florida, USA
Dimitrios Skoutas, IMIS Athena RC, Greece
Dimitris, Sacharidis, IMIS Athena RC, Greece
Edward Hua, QED Systems, USA
Emmanuelle Anceaume, IRISA/CNRS, France
Eric Pardede, La Trobe University, Australia
Fabrizio Angiulli, University of Calabria, Italy
Hamidah Ibrahim, Universiti Putra Malaysia, Malaysia
Harald Kosch, University of Passau, Germany
Hasan Jamil, University of Idaho, USA
Hongmei Chi, Florida A&M University, USA
Jemal Abawajy, Deakin University, Australia
Jin Li, Guangzhou University, China
Jongsub Moon, Korea University, Korea
Jose A. Onieva, University of Malaga, Spain
Katerina Doka, National Technical University of Athens, Greece
Le Gruenwald, University of Oklahoma, USA
Ligang He, University of Warwick, UK
Manolis Terrovitis, Institute for the Management of Information Systems, Greece
Markus Aleksy, ABB AG, Germany
Maytham Safar, Kuwait University, Kuwait
Minoru Uehara, Toyo University, Japan
Mohamed Gaber, University of Portsmouth, UK
Motoi Yamagiwa, Toyo University, Japan.
Roberto Caldelli, University of Florence, Italy
Ruben Rios delPozo, University of Malaga, Spain
Ruth Breu, University of Innsbruck, Austria
Ruzana Ishak, Universiti Teknologi Malaysia, Malaysia
Sherif Sakr, National ICT Australia, Australia
Soon M. Chung, Department of Computer Science and Engineering, Wright State University, USA
Stefanos Gritzalis, University of the Aegean, Greece
Tomoki Yoshihisa, Osaka University, Japan
Vincent Rijmen, TU Graz KULeuven, Belgium
Walter Colin, University of London, UK
Wei Feng Chen, California University of Pennsylvania, USA
Wei Wang, Wang, University of New South Wales, Australia
Wei-Chuen Yau, Multimedia University, Malaysia
Wenny Rahayu, La Trobe University, Australia
Xiaofeng Chen, Xidian University, China
Yuxin Peng, Peking University, China

Message from the IRoA 2013 General Chairs

On behalf of the organizing committees, it is our pleasure to welcome you to the 3rd International Conference on Intelligent Robotics, Automations and Applications (IRoA 2013), which will be held at Fukuoka Institute of Technology (FIT), Fukuoka, Japan on 8–10 July, 2013. IRoA 2013 is hosted by FIT and it is technically sponsored by Future Technology Research Association International (FTRA) and Korea Information Technology Convergence Society (KITCS). We believe the IRoA is a major forum for professors, scientists, professional engineers, and practitioners throughout the world to present the latest research, results, ideas, developments, and applications in all areas of intelligent robotics and automations. Furthermore, we expect that the IRoA 2013 and its publications will be a trigger for further related research and technology improvements in this important subject.

First we would like to thank our Honorary Chairs, Prof. Teruo Shimomura (President of FIT, Japan) and Prof. Makoto Takizawa (Hosei University, Japan) for their kind support for the conference. We also give special thanks to our Steering Committee Chairs: Prof. Leonard Barolli (FIT, Japan) and Prof. James J. Park (Seoul National University of Science and Technology, Korea) for their hard work and their continuous supports. We are very grateful to Prof. Fatos Xhafa (Technical University of Catalonia, Spain) for his full and wholehearted support and for his prestigious invited talk. We would like to thank all our chairs and committees for their great efforts to make IRoA 2013 very successful.

We would like to give special thanks to FIT and especially Mr. Yoji Unoki, Chairman of Board of Trustees of FIT for hosting STA 2013 and for providing the university facilities and his continuous support. We would like to thank Fukuoka Convention Bureau and Fukuoka City for their great support, help, advices, and local arrangement. Finally, we would like to thank the Local Arrangement Team at FIT and the Administration Staff of FIT for their support and for making excellent local arrangement for the conference.

We hope you find IRoA 2013 enjoyable and please let us know any suggestions for improvement in this event and also in next events.

Sang-Soo Yeo
Mokwon University
Korea

Kok-Meng Lee
Georgia Institute of Technology
USA

Hitoshi Kino
Fukuoka Institute of Technology
Japan

Message from IROA 2013 Program Chairs

We would like to welcome you to the 3rd International Conference on Intelligent Robotics, Automations, Telecommunication Facilities, and Applications (IROA 2013), which will be held at Fukuoka Institute of Technology (FIT), Fukuoka, Japan on 8–10 July, 2013.

IROA 2013 is focused on the various aspects of advances in intelligent robotics and automations including the latest research, results, ideas, developments, and its applications and provides an opportunity for academic and industry professionals to discuss the latest issues and progress in all areas of intelligent robotics and automations. We expect that the conference and its publications will be a trigger for further related research and technology improvements in this important subject.

We received a lot of paper submissions from many countries. Due to many high quality paper submissions and the lack of space in proceedings, we accepted 30 papers out of 72 submissions after a rigorous peer review process. Each paper was reviewed by at least three reviewers.

Finally, we would like to sincerely thank all authors of submitted papers and all attendees for their contributions and participation. And we would like to give a special thanks to all Track Chairs and Program Committee members for their hard work. We would like to thank the reviewers and organizers who supported this event as a whole and, in particular, helped in the success of IROA 2013.

Hiroyuki Fujioka
Fukuoka Institute of Technology
Japan

Yong-Ho Seo
Mokwon University
Korea

Organization

Honorary Chair

Teruo Shimomura, FIT President, Japan
Makoto Takizawa, Seikei University, Japan

Steering Chairs

James J. Park, Seoul National University of Science and Technology, Korea
Leonard Barolli, Fukuoka Institute of Technology, Japan

General Chairs

Sang-Soo Yeo, Mokwon University, Korea
Kok-Meng Lee, Georgia Institute of Technology, USA
Hitoshi Kino, Fukuoka Institute of Technology, Japan

Program Chairs

Hiroyuki Fujioka, Fukuoka Institute of Technology, Japan
Yong-Ho Seo, Mokwon University, Korea

Track Chairs

Track 1. Intelligent Robotics
Wada Takahiro, Ritsumeikan University, Japan
Keun-Chang Kwak, Chosun University, Korea

Track 2. Intelligent Perception Systems
Kenji Tahara, Kyushu University, Japan
Ji-Hwan Kim, Sogang University, Korea

Track 3. Automations and Simulation

Fumiaki Takemura, Okinawa National College of Technology, Japan
Giljin Jang, UNIST, Korea

Track 4. Control Systems

Tomonori Kato, Fukuoka Institute of Technology, Japan
Cheong Ghil Kim, Namseoul University, Korea

Track 5. Telecommunication Facilities

Tatsushi Tokuyasu, Fukuoka Institute of Technology, Japan
Kang-Hee Lee, Soongsil University, Korea

Track 6. Smart Space and Context-Awareness

Ken Shimoto, Fukuoka Institute of Technology, Japan
Dong-Han Kim, Kyunghee University, Korea

Track 7. Artificial Intelligence

Tetsuya Morizono, Fukuoka Institute of Technology, Japan
Tae-Woo Han, Woosong University, Korea

Track 8. Manufacturing Techniques and Systems

Takuya Tajima, Fukuoka Institute of Technology, Japan
Se-Jun Park, Mokwon University, Korea

Workshop Chairs

Akio Koyama, Yamagata University, Japan
Yunhui Liu, Chinese University of Hong Kong, China
Honghai Liu, University of Portsmouth, UK

Publication Chair

Hwa Young Jeong, Kyung Hee University, Korea

Publicity Chairs

Lianqing Liu, Chinese Academy of Sciences, China
Makoto Ikeda, Fukuoka Institute of Technology, Japan
Ho-Sub Yoon, ETRI, Korea
Jeong-Sik Park, Mokwon University, Korea

International Advisory Committee

Marco Ceccarelli, University of Cassino, Italy
Panos J. Antsaklis, University of Notre Dame, USA
Tzyh-Jong Tarn, Washington University, USA

Kazuhiro Saitu, University of Michigan, USA
David Atkinson, Air Force Office of Scientific Research, USA
Shigeki Sugano, Waseda University, Japan
Hyun S. Yang, KAIST, Korea
Sung-Kee Park, KIST, Korea
Tae-Kyu Yang, Mokwon University, Korea

Local Arrangement Chairs

Makoto Ikeda, Fukuoka Institute of Technology, Japan
Tao Yang, Fukuoka Institute of Technology, Japan

Invited Speakers

Fatos Xhafa, Technical University of Catalonia (Barcelona Tech), Spain

Program Committee

Abdel Aitouche, Hautes Etudes d'Ingenieur, France
Abdel-Badeeh Salem, Ain Shams University, Egypt
Adil Baykasoglu, University of Gaziantep, Turkey
Ahmed Zobaa, Brunel University, UK
Ajay Gopinathan, University of California, Merced, USA
Alessandra Lumini, University of Bologna, Italy
Alessandro Giua, Universita'di Cagliari, Italy
Alexandre Dolgui, Ecole Nationale Suprieure des Mines de Saint Etienne, France
Andrea Garulli, Universita'di Siena, Italy
Andreas C. Nearchou, University of Patras, Greece
Angel P. del Pobil, Universitat Jaume I, Spain
Angelos Amanatiadis, Democritus University of Thrace, Ksanthi, Greece
Anthony A. Maciejewski, Colorado State University, USA
Anthony Tzes, University of Patras, Greece
Anton Nijholt, University of Twente, The Netherlands
Antonios Tsourdos, Cranfield University, UK
Arijit Bhattacharya, Dublin City University, Ireland
Arvin Agah, The University of Kansas, USA
Asokan Thondiyath, Indian Institute of Technology Madras
Barry Lennox, The University of Manchester, UK
Ben-Jye Chang, Chaoyang University of Technology, Taiwan
Bernard Brogliato, INRIA, France
Bernardo Wagner, University of Hannover, Germany
Carla Seatzu, University of Cagliari, Italy
Carlo Alberto Avizzano, Scuola Superiore S. Anna, Italy

Carlo Menon, Simon Fraser University, Canada
 Cecilia Sik Lanyi, University of Pannonia, Hungary
 Ching-Cheng Lee, Olivet University and California State University at East Bay,
 USA
 Choon Yik Tang, University of Oklahoma, USA
 Chunling Du, Division of Control and Instrumentation, School of Electrical and
 Electronic Engineering, Singapore
 Clarence de Silva, UBC, Canada
 Claudio Melchiorri, University of Bologna, Italy
 Daizhan Cheng, Academy of Mathematics and Systems Science, China
 Dan Zhu, Iowa State University, USA
 Daniel Thalmann, EPFL Vrlab, Switzerland
 Denis Dochain, Universite catholique de Louvain, Belgium
 Dianhui Wang, La Trobe University, Australia
 Djamila Ouelhadj, University of Portsmouth, UK
 Dongbing Gu, University of Essex, UK
 Eloisa Vargiu, University of Cagliari, Italy
 Erfu Yang, University of Strathclyde, UK
 Evangelos Papadopoulos, NTUA, Greece
 Fang Tang, California State Polytechnic University, USA
 Federica Pascucci, University Roma Tre, Italy
 Frank Allgower, University of Stuttgart, Germany
 Frans Groen, University of Amsterdam, The Netherlands
 Frantisek Capkovic, Slovak Academy of Sciences, Slovak Republic
 Fumiya Iida, Institute of Robotics and Intelligent Systems ETH Zurich,
 Switzerland
 Georg Frey, Saarland University, Germany
 George L. Kovacs, Hungarian Academy of Sciences, Hungary
 Gerard Mckee, The University of Reading, UK
 Gheorghe Lazea, Technical University of Cluj-Napoca, Romania
 Giovanni Indiveri, University of Salento, Italy
 Graziano Chesi, University of Hong Kong, Hong Kong
 Guilherme N. De Souza, University of Missouri-Columbia, USA
 Gurvinder S. Virk, Massey University, New Zealand
 Hairong Qi, University of Tennessee, USA
 Helder Araujo, University of Coimbra, Portugal
 Helen Ryaciotaki-Boussalis, California State University, Los Angeles, USA
 Hemant A. Patil, Gandhinagar, Gujarat, India
 Hideyuki Sotobayashi, Aoyama Gakuin University, Japan
 Hiroyasu Iwata, Waseda University, Japan
 Hongbin Zha, Peking University, China
 Huei-Yung Lin, National Chung Cheng University, Taiwan
 Hung-Yu Wang, National Kaohsiung University of Applied Sciences, Taiwan
 Ichiro Sakuma, The University of Tokyo, Japan
 Irene Yu-Hua Gu, Chalmers University of Technology, Sweden

Jean-Daniel Dessimoz, Western University of Applied Sciences, Switzerland
Jing-Sin Liu, Institute of Information Science, Academia Sinica, Taiwan
Jingang Yi, The State University of New Jersey, USA
Jiunn-Lin Wu, National Chung Hsing University, Taiwan
Jonghwa Kim, University of Augsburg, Germany
Joris De Schutter, Katholieke Universiteit Leuven, Belgium
Jose Tenreiro Machado, Institute of Engineering of Porto
Jose Valente de Oliveira, Universidade do Algarve, Portugal
Juan J. Flores, University of Michoacan, Mexico
Jun Ota, The University of Tokyo, Japan
Jun Takamatsu, Nara Institute of Science and Technology, Japan
Kambiz Vafai, University of California, Riverside, USA
Karsten Berns, University of Kaiserslautern, Germany
Kauko Leiviska, University of Oulu, Finland
Lan Weiyao, Department of Automation, Xiamen University, China
Leonardo Garrido, Monterrey Tech., Mexico
Libor Preucil, Czech Technical University in Prague, Czech Republic
Loulin Huang, Massey University, New Zealand
Luigi Villani, University di Napoli Federico II, Italy
Mahasweta Sarkar, San Diego State University, USA
Maki K. Habib, Saga University, Japan
Manuel Ortigueira, Universidade Nova de Lisboa, Portugal
Marek Zaremba, UQO, Canada
Maria Gini, University of Minnesota, USA
Mario Ricardo Arbulu Saavedra, University Carlos III of Madrid, Spain
Masao Ikeda, Osaka University, Japan
Matthias Harders, Computer Vision Laboratory ETH Zurich, Switzerland
Mehmet Sahinkaya, University of Bath, UK
Michael Jenkin, York University, Canada
Mitsuji Sampei, Tokyo Institute of Technology, Japan
Nitin Afzulpurkar, Asian Institute of Technology, Thailand
Olaf Stursberg, Technische Universitaet Muenchen, Germany
Panagiotis Petratos, California State University, Stanislaus, USA
Pani Chakrapani, University of Redlands, USA
Paul Oh, Drexel University, USA
Peng-Yeng, National Chi Nan University, Taiwan
Peter Xu, Massey University, New Zealand
Pieter Mosterman, The Math works, Inc.
Plamen Angelov, Lancaster University, UK
Prabhat K. Mahanti, University of New Brunswick, Canada
Qinggang Meng, Research School of Informatics, UK
Qurban A. Memon, United Arab Emirates University, UAE
Radu Bogdan Rusu, Technical University of Munich, Germany
Ragne Emardson, SP Technical Research Institute of Sweden
Ren C. Luo, National Taiwan University, Taiwan

Rezia Molfino, Universitadegli Studi di Genova, Italy
Riad I. Hammoud, DynaVox and Mayer-Johnson Innovation Group, USA
Richard J. Duro, Universidade da Corunña, Spain
Robert Babuska, Delft University of Technology, The Netherlands
Rolf Johansson, Lund University, Sweden
Romeo Ortega, LSS Supelec, France
Ruediger Dillmann, University of Karlsruhe, Germany
Ryszard Tadeusiewicz, AGH University of Science and Technology, Poland
Saeid Nahavandi, CISR, New Zealand
Sarith Kodagoda, University of Technology, Sydney, Australia
Sean Mc Loone, National University of Ireland (NUI) Maynooth, Ireland
Selahattin Ozcelik, University-Kingsville, USA
Sergej Fatikow, University of Oldenburg, Germany
Seth Hutchinson, University of Illinois, USA
Shu-Ching Chen, Florida International University, USA
Shugen Ma, Ritsumeikan University, Japan
Shuro Nakajima, Chiba Institute of Technology, Japan
Shuzhi Sam Ge, National University of Singapore, Singapore
Simon G. Fabri, University of Malta, Malta
Stjepan Bogdan, University of Zagreb, Faculty of EE&C, Croatia
Tariq Shehab, California State University, Long Beach, USA
Taskin Padir, Worcester Polytechnic Institute, USA
Thira Jearsiripongkul, Thammasat University, Thailand
Thomas C. Henderson, University of Utah, USA
Tomonari Furukawa, Virginia Polytechnic Institute and State University, USA
Tong Heng Lee, NUS, Singapore
Tongwen Chen, University of Alberta, Canada
Tsai-Yen Li, National Chengchi University, Taiwan
Uwe R. Zimmer, The Australian National University, Australia
Venketesh N. Dubey, Bournemouth University, UK
Venzeslav (Venny) Valev, Bulgarian Academy of Sciences, Bulgaria
Wail Gueaieb, University of Ottawa, Canada
Wang Qing-Guo, National University of Singapore, Singapore
Waree Kongprawechnon, Thammasat University, Thailand
Weihua Sheng, Oklahoma State University, USA
Weizhong Dai, Louisiana Tech University, USA
Wen-Hua Chen, Loughborough University, UK
Wladyslaw Homenda, Warsaw University of Technology, Poland
Wolfgang Halang, Fernuniversitaet, Germany
Won-jong Kim, Texas A&M University, USA
Xun W. Xu, University of Auckland, New Zealand
Yang Dai, University of Illinois at Chicago, USA
Yangmin Li, University of Macau, Macao
Yantao Shen, University of Nevada, USA
Yugeng Xi, Shanghai Jiaotong University, China

Yun Wang, University of California, Irvine, USA
Zhijun Yang, University of Edinburgh, UK
Zidong Wang, Brunel University, UK
Zongli Lin, University of Virginia, USA
Vasily Sachnev, The Catholic University of Korea, Korea
Elena Tsomko, Namseoul University, Korea
Jin Young Kim, Kwangwoon University, Korea
Ki-Hyung Kim, Ajou University, Korea
Nammee Moon, Hoseo University, Korea
Taesam Kang, Konkuk University, Korea
Hwa-Jong Kim, Kangwon National University, Korea
Yeonseok Lee, Kunsan National University, Korea
Cheong Ghil Kim, Namseoul University, Korea
SanghyunJoo, ETRI, Korea
Wei Wei, Xi'an Jiaotong University, China

Message from DMFIT-2013 Workshop Chair

Welcome to the International Workshop on Data Management for Future Information Technology (DMFIT-2013), which will be held from July 8–10, 2013 in FIT, Fukouka, Japan. The main objective of this workshop is to share information on new and innovative research related to advanced technologies and applications in the areas of data management on cloud computing, mobile computing, ubiquitous computing, data mining, and databases. Many advanced techniques and applications in these areas have been developed in the past few years. DMFIT-2013 will bring together researchers and practitioners who are interested in both the technical and applied aspects of advanced techniques and applications on data management for future information technology. Furthermore, we expect that the DMFIT-2013 and its publications will be a trigger for further related research and technology improvements in this important subject.

DMFIT-2013 contains high quality research papers submitted by researchers from all over the world. Each submitted paper was peer-reviewed by reviewers who are experts in the subject area of the paper. Based on the review results, the Program Committee accepted seven papers.

We hope that you will enjoy the technical programs as well as the social activities during DMFIT-2013. We would like to send our sincere appreciation to all of the Organizing and Program Committees who contributed directly to DMFIT-2013. Finally, we specially thank all the authors and participants for their contributions to make this workshop a grand success.

Jun-Hong Shen
Asia University
Taiwan

Ming-Shen Jian
National Formosa University
Taiwan

Tien-Chi Huang
National Taichung University of Science and Technology
Taiwan

Message from PSSI-2013 Workshop Chairs

The organizing committee of the FTRA International Workshop on Pervasive Services, Systems and Intelligence (PSSI 2013) will like to welcome all of you to join the workshop as well as the FTRA MUE 2013. Advances in Information and Communications Technology (ICT) have presented a dramatic growth in merging the boundaries between physical space and cyberspace, and go further to improve human being's daily life. One typical instance is the use of smartphone. Modern smartphone is equipped with a variety of sensors that are used to collect activities, locations, and situations of its user continuously and provide immediate helps accordingly. Some commercial products (e.g., smart house, etc.) also demonstrate the feasibility of comprehensive supports by deploying a rapidly growing number of sensors (or intelligent objects) into our living environments. These developments are collectively best characterized as ubiquitous service that promises to enhance awareness of the cyber, physical, and social contexts. As such, researchers (and companies as well) tend to provide tailored and precise solutions (e.g., services, supports, etc.) wherever and whenever human beings are active according to individuals' contexts. Making technology usable by and useful to, via the ubiquitous services and correlated techniques, human beings in ways that were previously unimaginable has become a challenging issue to explore the picture of technology in the next era. This workshop aims at providing a forum to discuss problems, studies, practices, and issues regarding the emerging trend of pervasive computing. Researchers are encouraged to share achievements, experiments, and ideas with international participants, and furthermore, look forward to map out the research directions and collaboration in the future.

With an amount of submissions (13 in exact), the organizing chairs decided to accept six of them based on the paper quality and the relevancy (acceptance rate at 46 %). These papers are from Canada, China, and Taiwan. Each paper was reviewed by at least three program committee members and discussed by the organizing chairs before acceptance. We would like to thank three FTRA Workshop Chair, Young-Gab Kim from Korea University, Korea for the support and coordination. We thank all authors for submitting their works to the workshop.

We also appreciate the program committee members for their efforts in reviewing the papers. Finally, we sincerely welcome all participants to join the discussion during the workshop.

James J. Park
Neil Y. Yen

Message from ASNT 2013 Workshop Chairs

We are very proud and honored to organize the 2013 International Workshop on Advanced Social Network Technologies (ANST 2013), in conjunction with the 10th FTRA International Conference on Secure and Trust Computing, Data Management, and Applications (STA 2013), in FIT, Fukouka, Japan, July 8–10, 2013.

Social Networks have been applied in various domains. A social network is a social structure made up of a set of actors (such as individuals or organizations) and the dyadic ties between these actors. The social network perspective provides a clear way of analyzing the structure of whole social entities. The overall goal of the data mining process is to extract information from a data set and transform it into an understandable structure for further use. The major issue of this workshop is to present novel technologies and ideas for social network analysis, intelligent technologies, data mining, and social network-related researches.

This year, we have received 16 submissions. All manuscripts underwent a rigorous peer-review process with three reviewers per paper. Only seven papers were accepted for presentation and inclusion in the proceedings, comprising a 44 % acceptance rate. Thanks to all authors who contributed to the success of this workshop.

Finally, we especially like to thank the organization team of the STA 2013 conference, for their organization of the proceedings, the invitation of valuable speakers, and the social events. The conference and STA 2013 were not been successful without their great contributions.

Yung-Hui Chen
Lung Hwa University of Science and Technology
Taiwan

Lawrence Y. Deng
St. John's University
Taiwan

Contents

Part I Information Technology Convergence and Services

Novel Handoff Frequency Algorithms for Vehicular Area Networks . . .	3
Shih-Chang Huang and Yu-Shenq Tzeng	
RC4-2S: RC4 Stream Cipher with Two State Tables	13
Maytham M. Hammood, Kenji Yoshigoe and Ali M. Sagheer	
Genetic Algorithm-Based Relocation Scheme in Electric Vehicle Sharing Systems	21
Junghoon Lee and Gyung-Leen Park	
Improvement of Wireless LAN Connectivity by Optimizing Placement of Wireless Access Points	29
Taiki Honda and Makoto Ikeda	
Performance Comparison of OLSR and AODV Protocols in a VANET Crossroad Scenario	37
Evjola Spaho, Makoto Ikeda, Leonard Barolli and Fatos Xhafa	
WMN-GA System for Node Placement in WMNs: Effect of Grid Shape	47
Tetsuya Oda, Evjola Spaho, Admir Barolli, Leonard Barolli, Fatos Xhafa and Makoto Takizawa	
DCT-Based Watermarking for Color Images via Two-Dimensional Linear Discriminant Analysis	57
I-Hui Pan, Ping Sheng Huang and Te-Jen Chang	
Human Action Recognition Using Depth Images.	67
Chaur-Heh Hsieh, Chin-Pan Huang and Jian Ming Hung	

Performance Analysis of OLSR with ETX_ff for Different HELLO Packet Interval in a MANET Testbed. 77
 Masahiro Hiyama, Elis Kulla, Makoto Ikeda, Leonard Barolli and Makoto Takizawa

Multi-Flow Traffic Investigation of AODV Considering Routing Control Packets. 89
 Elis Kulla, Masahiro Hiyama, Makoto Ikeda, Leonard Barolli, Fatos Xhafa and Makoto Takizawa

An Estimation Method for Amplitude Modification Factor Using Floor Area Ratio in Urban Areas. 101
 Kazunori Uchida, Keisuke Shigetomi, Masafumi Takematsu and Junich Honda

A SURF Feature Based Building Recognition System for Distinctive Architectures 111
 Shio-Wen Chen, Yi-Hao Chung, Hsin-Fu Chien and Chueh-Wei Chang

A Kinect-Based System for Golf Beginners’ Training 121
 Yi-Hsuan Lin, Shih-Yu Huang, Kuei-Fang Hsiao, Kuei-Ping Kuo and Li-Tieng Wan

A Hill Climbing Algorithm for Ground Station Scheduling. 131
 Fatos Xhafa, Xavier Herrero, Admir Barolli and Makoto Takizawa

A Ferry Dispatching Optimization for Mobile Ad-Hoc Networks Using the Virtual Multiple Message Ferry Backbone Routing Scheme 141
 Chu-Fu Wang and Ya-Chi Yang

A Location-Estimation Experimental Platform Based on Error Propagation for Wireless Sensor Networks 151
 Yih-Shyh Chiou, Sheng-Cheng Yeh and Shang-Hung Wu

Performance Evaluation of WMNs Using Hill Climbing Algorithm Considering Giant Component and Different Distributions 161
 Xinyue Chang, Tetsuya Oda, Evjola Spaho, Makoto Ikeda, Leonard Barolli and Fatos Xhafa

Performance Evaluation of WMNs Using Simulated Annealing Algorithm Considering Different Number Iterations per Phase and Normal Distribution 169
 Shinji Sakamoto, Tetsuya Oda, Elis Kulla, Makoto Ikeda, Leonard Barolli and Fatos Xhafa

UBMLRSS–Cognitive Financial Information Systems 177
 Lidia Ogiela and Marek R. Ogiela

A Framework of Static Analyzer for Taint Analysis of Binary Executable File 185
 Young-Hyun Choi, Jae-Won Min, Min-Woo Park, Jung-Ho Eom and Tai-Myoung Chung

An IoT-Based Framework for Supporting Children with Autism Spectrum Disorder 193
 Ardiana Sula, Evjola Spaho, Keita Matsuo, Leonard Barolli, Fatos Xhafa and Rozeta Miho

Improvement of Fingerprint Verification by Using the Similarity Distribution. 203
 Seung-Hoon Chae and Sung Bum Pan

Improvement of Lung Segmentation Using Volume Data and Linear Equation. 213
 Seung-Hoon Chae, Daesung Moon, Deok Gyu Lee and Sung Bum Pan

WMN-GA System for Node Placement in WMNs: Performance Evaluation for Weibull Distribution of Mesh Clients 223
 Admir Barolli, Tetsuya Oda, Fatos Xhafa, Leonard Barolli, Petraq Papajorgji and Makoto Takizawa

Indoor Navigation System for Wheelchair Using Smartphones 233
 Nattapob Wattanavarangkul and Toshihiko Wakahara

Performance Comparison of Wireless Sensor Networks for Different Sink Speeds. 243
 Tao Yang, Elis Kulla, Leonard Barolli, Gjergji Mino and Makoto Takizawa

Induction Motor Drive Based Neural Network Direct Torque Control. 255
 Sy Yi Sim, Wahyu Mulyo Utomo, Zainal Alam Haron, Azuwien Aida Bohari, Nooradzianie Muhd. Zin and Roslina Mat Ariff

Adaptive Keyword Extraction System for the Hierarchical Category Search 263
 Toshitaka Maki and Toshihiko Wakahara

Fuzzy Logic Control Design for Induction Motor Speed Control Improvement Through Field Oriented Control 273
 Roslina Mat Ariff, Dirman Hanafi, Wahyu Mulyo Utomo, Kok Boon Ching, Nooradzianie Muhd Zin, Sy Yi Sim and Azuwien Aida Bhohari

Considering Lifetime of Sensors for Clusterhead Selection in WSN Using Fuzzy Logic 281
 Qi Wang, Leonard Barolli, Elis Kulla, Gjergji Mino, Makoto Ikeda and Jiro Iwashige

Speed Control of Permanent Magnet Synchronous Motor Using FOC Neural Network 295
 Nooradzianie Muhd. Zin, Wahyu Mulyo Utomo, Zainal Alam Haron, Azuwien Aida Bohari, Sy Yi Sim and Roslina Mat Ariff

An Interactive Learning System Using Smartphone for Improving Students Learning Motivation 305
 Noriyasu Yamamoto and Toshihiko Wakahara

Design and Implementation of H.264/AVC Reverse Biorthogonal Wavelet-Based Flexible Macroblock Ordering 311
 Jing-Siang Wei, Zeng-Yao Lin and Chian C. Ho

Design and Characteristics of Two-Dimensional Color Code Editor with Dotted Images 323
 Toshihiko Wakahara, Damri Samretwit, Toshitaka Maki and Noriyasu Yamamoto

Studies on Loss Evaluation of Bending in Post Wall Waveguide for Microwave Transmission 333
 Hiroshi Maeda, Kazuya Tomiura, Huili Chen and Kiyotoshi Yasumoto

Resource Management for Hybrid 3.75G UMTS and 4G LTE Cellular Communications 341
 Ben-Jye Chang, Ying-Hsin Liang and Kai-Xiang Cao

Automatic Travel Blog Generator Based on Intelligent Web Platform and Mobile Applications 355
 Yi-Jiu Chen, Wei-Sheng Zeng and Shian-Hua Lin

Thai Wikipedia Link Suggestion Framework 365
 Arnon Rungsawang, Sompop Siangkho, Athasit Surarerk
 and Bundit Manaskasemsak

**Computing Personalized PageRank Based on Temporal-Biased
 Proximity** 375
 Bundit Manaskasemsak, Pramote Teerasetmanakul, Kankamol Tongtip,
 Athasit Surarerks and Arnon Rungsawang

**KSVTs: Towards Knowledge-Based Self-Adaptive Vehicle
 Trajectory Service.** 387
 Jin-Hong Kim and Eun-Seok Lee

**Part II Secure and Trust Computing, Data Management,
 and Applications**

**Secure and Reliable Transmission with Cooperative Relays
 in Two-Hop Wireless Networks** 397
 Yulong Shen, Xiaohong Jiang, Jianfeng Ma and Weisong Shi

RC4 Stream Cipher with a Random Initial State 407
 Maytham M. Hammood, Kenji Yoshigoe and Ali M. Sagheer

**Improved Redundant Power Consumption Laxity-Based
 (IRPCLB) Algorithm
 for Server Clusters** 417
 Tomoya Enokido, Ailixier Aikebaier and Makoto Takizawa

Security of Cognitive Information Systems 427
 Marek R. Ogiela and Lidia Ogiela

**The Design of a Policy-Based Attack-Resilient Intrusion Tolerant
 System** 435
 Jungmin Lim, Yongjoo Shin, Seokjoo Doo and Hyunsoo Yoon

**Algorithms for Batch Scheduling to Maximize the Learning
 Profit with Learning Effect and Two Competing Agents** 445
 Jen-Ya Wang, Yu-Han Shih and Jr-Shian Chen

**A Fuzzy-Based System for Evaluation of Trustworthiness
 for P2P Communication in JXTA-Overlay** 451
 Kouhei Umezaki, Evjola Spaho, Keita Matsuo, Leonard Barolli,
 Fatos Xhafa and Jiro Iwashige

**Applying Cluster Techniques of Data Mining to Analysis
the Game-Based Digital Learning Work.** 461
Shu-Ling Shieh, Shu-Fen Chiou, Gwo-Haur Hwang and Ying-Chi Yeh

**Design and Implementation of Social Networking System for Small
Grouped Campus Networks.** 469
Jung Young Kim and Seung-Ho Lim

**Effective Searchable Symmetric Encryption System Using
Conjunctive Keyword** 477
Sun-Ho Lee and Im-Yeong Lee

**Secure Method for Data Storage and Sharing During
Data Outsourcing** 485
Sun-Ho Lee, Sung jong Go and Im-Yeong Lee

Study on Wireless Intrusion Prevention System for Mobile Office. . . . 495
Jae Dong Lee, Ji Soo Park and Jong Hyuk Park

**A Component Model for Manufacturing System
in Cloud Computing** 501
HwaYoung Jeong and JongHyuk Park

**Traditional Culture Learning System for Korean Folk Literature,
Pansori** 509
Dong-Keon Kim and Woon-Ho Choi

**Auction Based Ticket Selling Schemes with Multiple Demand
from the Agents in Static Environment** 519
Sajal Mukhopadhyay, D. Ghosh, Narayan C. Debnath and N. RamTeja

A Decision Tree-Based Classification Model for Crime Prediction. . . . 531
Aziz Nasridinov, Sun-Young Ihm and Young-Ho Park

Part III Artificial Intelligence Applications for E-Services

**Innovation Performance on Digital Versatile Disc (DVD) 3C Patent
Pool Formation** 541
Yu-Hui Wang

**Top-k Monitoring Queries for Wireless Sensor Database Systems:
Design and Implementation** 547
Chi-Chung Lee and Yang Xia

Protection Management of Enterprise Endpoint Based on the ITIL Management Framework 557
 Mei-Yu Wu, Shih-Fang Chang and Wei-Chiang Li

Adaptive Content Recommendation by Mobile Apps Mash-Up in the Ubiquitous Environment 567
 Chih-Kun Ke, Yi-Jen Yeh, Chang-Yu Jen and Ssu-Wei Tang

A Real-Time Indoor Positioning System Based on RFID and Kinect 575
 Ching-Sheng Wang, Chien-Liang Chen and You-Ming Guo

Intuitional 3D Museum Navigation System Using Kinect 587
 Ching-Sheng Wang, Ding-Jung Chiang and Yu-Chia Wei

Application of QR-Code Steganography Using Data Embedding Technique 597
 Wen-Chuan Wu, Zi-Wei Lin and Wei-Teng Wong

Combining FAHP with MDS to Analyze the Key Factors of Different Consumer Groups for Tablet PC Purchasing 607
 Chen-Shu Wang, Shiang-Lin Lin and Heng-Li Yang

Game-Based History Ubiquitous Learning Environment Through Cognitive Apprenticeship 617
 Wen-Chih Chang, Chiung-sui Chang, Hsuan-Che Yang and Ming-Ren Jheng

The Behavioral Patterns of an Online Discussion Activity in Business Data Communication Class 627
 Chiu Jui-Yu and Chang Wen-Chih

Integration of a Prototype Strategical Tool on LMS for Concept Learning 635
 David Tawei Ku and Chi-Jie Lin

Part IV Advanced Social Network Technologies

Application-Driven Approach for Web Site Development 649
 Chun-Hsiung Tseng

The Analysis of the Participants' Personality for the Contestants of the National Skills Competition 659
Kung-Huang Lin, You-Syun Jheng, Lawrence Y. Deng and Jiung-Yao Huang

Ontology-Based Multimedia Adaptive Learning System for U-Learning 669
Lawrence Y. Deng, Yi-Jen Liu, Dong-Liang Lee and Yung-Hui Chen

The Taguchi System-Neural Network for Dynamic Sensor Product Design. 677
Ching-Lien Huang, Tian-Long John Wan, Lung-Cheng Wang and Chih-Jen Hung

Using Decision Tree Analysis for Personality to Decisions of the National Skills Competition Participants. 683
Dong-Liang Lee, Lawrence Y. Deng, Kung-Huang Lin, You-Syun Jheng, Yung-Hui Chen, Chih-Yang Chao and Jiung-Yao Huang

Intelligent Reminder System of Having Medicine for Chronic Patients 693
Dong-Liang Lee and Chun-Liang Hsu

Part V Data Management for Future Information Technology

A Skewed Spatial Index for Continuous Window Queries in the Wireless Broadcast Environments 707
Jun-Hong Shen, Ching-Ta Lu, Ming-Shen Jian and Tien-Chi Huang

Advancing Collaborative Learning with Cloud Service 717
Yong-Ming Huang, Chia-Sui Wang, Jia-Ze Guo, Huan-Yu Shih and Yong-Sheng Chen

Using MapReduce Framework for Mining Association Rules 723
Shih-Ying Chen, Jia-Hong Li, Ke-Chung Lin, Hung-Ming Chen and Tung-Shou Chen

Cloud Feedback Assistance Based Hybrid Evolution Algorithm for Optimal Data Solution 733
Ming-Shen Jian, Fu-Jie Jhan, Kuan-Wei Lee and Jun-Hong Shen

Molecular Simulation Methods for Selecting Thrombin-Binding Aptamers 743
 Jangam Vikram Kumar, Wen-Yih Chen, Jeffrey J. P. Tsai and Wen-Pin Hu

An Efficient Group Key Management Scheme for Web-Based Collaborative Systems 751
 Yung-Feng Lu, Rong-Sheng Wang and Shih-Chun Chou

The Diagnosis of Mental Stress by Using Data Mining Technologies 761
 Hsiu-Sen Chiang, Liang-Chi Liu and Chien-Yuan Lai

Part VI Intelligent Agent System and Its Applications

Intelligent Rainfall Monitoring System for Efficient Electric Power Transmission 773
 Rong-Chi Chang, Teng-Shih Tsai and Leehter Yao

A Computational Data Model of Intelligent Agents with Time-Varying Resources 783
 Anthony Y. Chang

An Intelligent Energy-Saving Information Interface Agent with Web Service Techniques 793
 Sheng-Yuan Yang, Dong-Liang Lee, Kune-Yao Chen and Chun-Liang Hsu

Part VII Intelligent Robotics, Automations, Telecommunication Facilities, and Applications

3D Trajectory Planning for a 6R Manipulator Robot Using BA and ADAMS 807
 P. Masajedi, Kourosh Heidari Shirazi and Afshin Ghanbarzadeh

Performance Improvement of Human Detection Using Thermal Imaging Cameras Based on Mahalanobis Distance and Edge Orientation Histogram 817
 Ahra Jo, Gil-Jin Jang, Yongho Seo and Jeong-Sik Park

Sensibility to Muscular Arrangement of Feedforward Position Control for Non-Pulley-Musculoskeletal System 827
 Hitoshi Kino, Shiro Kikuchi, Yuki Matsutani and Kenji Tahara

Mobile Sensing-Based Localization Method for Illegal Electricity Usage by Using Inspection Robot 835
 Bat-Erdene Byambasuren, Mandakh Oyun-Erdene and Dong-Han Kim

Development Age Groups Estimation Method Using Pressure Sensors Array 847
 Junjirou Hasegawa, Takuya Tajima, Takehiko Abe and Haruhiko Kimura

Bio Rapid Prototyping Project: Development of Spheroid Formation System for Regenerative Medicine. 855
 Takeshi Shimoto, Nozomi Hidaka, Hiromichi Sasaki, Koichi Nakayama, Shizuka Akieda, Shuichi Matsuda, Hiromasa Miura and Yukihide Iwamoto

Robot Control Architectures: A Survey 863
 Evjola Spaho, Keita Matsuo, Leonard Barolli and Fatos Xhafa

Experiment Verification of Position Measurement for Underwater Mobile Robot Using Monocular Camera 873
 Natsuki Uechi, Fumiaki Takemura, Kuniaki Kawabata and Shinichi Sagara

Emergency Detection Based on Motion History Image and AdaBoost for an Intelligent Surveillance System 881
 Jun Lee, Jeong-Sik Park and Yong-Ho Seo

Marker Tracking for Indirect Positioning During Fabric Manipulation 889
 Mizuho Shibata

Vision-Based Human Following Method for a Mobile Robot Using Human and Face Detection 897
 Se-Jun Park, Tae-Kyu Yang and Yong-Ho Seo

Precise Location Estimation Method Using a Localization Sensor for Goal Point Tracking of an Indoor Mobile Robot. 905
 Se-Jun Park and Tae-Kyu Yang

Motion Capture Based Dual Arm Control of a Humanoid Robot Using Kinect 913
 Kyo-Min Koo, Young Joon Kim and Yong-Ho Seo

Scalable Building Facade Recognition and Tracking for Outdoor Augmented Reality 923
 Suwon Lee, Yong-Ho Seo and Hyun S. Yang

Head Pose Estimation Based on Image Abstraction for Multiclass Classification. 933
 ByungOk Han, Yeong Nam Chae, Yong-Ho Seo and Hyun S. Yang

Recovering Human-Like Drawing Order from Static Handwritten Images with Double-Traced Lines 941
 Takayuki Nagoya and Hiroyuki Fujioka

Noise Reduction Scheme for Speech Recognition in Mobile Devices. . . 949
 Jeong-Sik Park, Gil-Jin Jang and Ji-Hwan Kim

Implementation of a Large-Scale Language Model in a Cloud Environment for Human-Robot Interaction. 957
 Dae-Young Jung, Hyuk-Jun Lee, Sung-Yong Park, Myoung-Wan Koo, Ji-Hwan Kim, Jeong-sik Park, Hyung-Bae Jeon and Yun-Keun Lee

Speed Control Using a PID Algorithm for an Educational Mobile Robot 967
 Se-Young Jung, Se-Jun Park, Yong-Ho Seo and Tae-Kyu Yang

Performance Analysis of Noise Robust Audio Hashing in Music Identification for Entertainment Robot. 977
 Namhyun Cho, Donghoon Shin, Donghyun Lee, Kwang-Ho Kim, Jeong-Sik Park, Myoung-Wan Koo and Ji-Hwan Kim

Preliminary Experiments of Dynamic Buoyancy Adjusting Device with an Assist Spring. 985
 Norimitsu Sakagami, Amira Shazanna Binti Abdul Rahim and Satoshi Ishikawa

Optimization of a Cart Capacity Using the Three-Dimensional Single Bin Packing Problem for a Serving Robot 995
 Ara Khil and Kang-Hee Lee

A Study on Splitting LPC Synthesis Filter 1003
 Kwang-Bock You and Kang-Hee Lee

Teleoperation of a Master–Slave Pneumatic Robot Arm System Over the Internet: Consideration of Delay Between Oregon and Fukuoka. 1011
 Shunta Honda, Tomonori Kato, Hiromi Masuda and Ittirattana Jullakarn

Fundamental Study of a Virtual Training System for Maxillofacial Palpation 1019
 Tatsushi Tokuyasu, Erina Maeda, Takuya Okamoto, Hiromu Akita, Kazuhiko Toshimitsu, Kazutoshi Okamura and Kazunori Yoshiura

Design of a 2-DOF Wearable Mechanism for Support of Human Elbow and Forearm 1027
 Tetsuya Morizono and Motoki Suzuki

Variable Quantile Level Based Noise Suppression for Robust Speech Recognition 1037
 Kangyeoul Lee, Gil-Jin Jang, Jeong-Sik Park and Ji-Hwan Kim

An Efficient Resource Management Scheme Based on Locality for P2P Overlay Network 1047
 Chung-Pyo Hong, Jin-Chun Piao, Cheong-Ghil Kim, Sang-Yeob Na and Tae-Woo Han

Parallel SAD for Fast Dense Disparity Map Using a Shared Memory Programming 1055
 Cheong Ghil Kim

A Study on Object Contour Tracking with Large Motion Using Optical Flow and Active Contour Model. 1061
 Jin-Woo Choi, Taek-Keun Whangbo and Nak-Bin Kim

Correction to: 3D Trajectory Planning for a 6R Manipulator Robot Using BA and ADAMS C1
 P. Masajedi, Kourosh Heidari Shirazi and Afshin Ghanbarzadeh

Author Index 1071

Part I
Information Technology Convergence
and Services

Novel Handoff Frequency Algorithms for Vehicular Area Networks

Shih-Chang Huang and Yu-Shenq Tzeng

Abstract In the vehicular area networks (VANETs), mobile station will frequently switch the associated base station. Reducing the number of handoff times is an import issue on retaining the quality of connection. In this paper, we propose two algorithms to solve this issue. The first one is named the Longest Distance Algorithm (LDA). We transform the handoff problem as finding the cross points of multiple circles and a line in a graph. The base station whose cross point is closest to the destination will be the candidate. The second one is called as Least Handoff Frequency Algorithm (LHFA). In the LHFA, the base stations are treated as the vertices. The link between two base stations implies mobile station can perform the handoff operation. The LHFA uses the Dijkstra's shortest path algorithm to optimize the number of handoff times. The simulation results show that both the proposed LDA and LHFA algorithms can greatly reduce the numbers of handoff operations than the signal-strength algorithm.

Keywords Vehicular area networks · Handoff · Shortest path algorithm · Destination greedy algorithm

1 Introduction

The wireless communication techniques have been rapidly developed in the recent years. Users can freely move here and there while they access the network. When the Mobile Station (MS) moves out of the radio coverage of its associated Base

S.-C. Huang (✉) · Y.-S. Tzeng
Department of Computer Science and Information Engineering, National Formosa University, Yunlin, Taiwan, ROC
e-mail: schuang@nfu.edu.tw

Y.-S. Tzeng
e-mail: p7689love@gmail.com

Station (BS), the network connection may break. The MS needs to associate a new BS to continue the network service. We named this process as handoff. In the handoff process, MS needs to exchange information with the next potential BS. Delivering data packets at this time is temporarily unavailable. So, shortening the time spent on the handoff process can explicitly improve the delay time.

The handoff process has three phases. They are the probe, authentication and re-association. In the probe phase, the MS monitors the channels to collect the information of neighbor BSs. MS can probe the channels actively or passively. In the active mode, the MS will send out a probe frame to inform the neighbor BSs that it is probing. In the passive mode, the MS will stay in each channel for a while to collect the beacon frames broadcasted by the BSs. The time spent on scanning the channels is called as *probe delay*. In the authentication phase, MS sends an authentication request to the new BS. The time spends on this phase is called as *authentication delay*. After the MS passes the authentication phase, MS will negotiate the communication parameters with the new BS. This is called as *re-association delay*. The handoff process is complete when re-association phase terminates.

In these three phases, the probe phase spends most of the time in the handoff process. Many studies have been done to improve the delay. For example, the SyncScan [1] lets the MS scan the nearby BSs in advance to reduce the delay time wasted in the handoff process. When the MS enters the handoff process, it can simply select the candidate BS from the previous scanning results. The SyncScan method needs to scan channels continuously for maintaining the newest information of all nearby BSs. The DeuceScan [2] collects and sorts the BSs in advance based on their quality of Received Signal Strength (RSS) to solve the problem of SyncScan. Only the top three best BSs are traced. When the MS enters the handoff process, one of these three BS is selected. DeuceScan can reduce the time to maintain all neighbor BSs. A similar method calls SelectiveScan [3], which only scans the channels that are non-overlapping. These methods will scan full channels when the MS fails to find the BS in the designated channels.

The neighbor nodes around the MS are used for assisting the channel scanning [4]. The MS will designate each neighbor a set of channels to scan. After collecting the results of all neighbors, MS will choose a desired BS. These assistant scanners can effectively reduce the handoff delay. However, their scanning results are not always trustable because their positions to scan the channels are different.

The location information of MS [5] can also be applied to reduce the probing delay. The distance between MS to BS is used as the criterion to select the target BS. The BS with the closest distance will be associated by the MS. The overhead on computing distance between MS and BS must be reduced when nodes are densely deployed. The artificial neural network (ANN) is used to find the better handoff locations [6]. The data of radio coverage of BSs will be stored for the ANN algorithm to train the suitable handoff locations. MS changes BSs at the specific locations scheduled by the algorithm. The cost of ANN technique is the long training time.

The Lookahead [7] method divides the moving track of MS into multiple slots. The available BSs in each slot will be stored in the database. When the MS stays in a slot and prepares to switch to the new BS, it does not need to scan the channel for searching a BS but just looks up the database to find the BS that covers the longest continuous slots as the candidate. Additional memory space is necessary for the database in this method. In addition to probe delay, some methods [8] use the pre-authenticate mechanism to reduce the authentication delay.

All above methods focus on shortening the time spent on a handoff process. The handoff frequency is not considered. Reducing the handoff frequency may efficiently shorten the total handoff delay time. So, we propose two methods in this paper. The first one is the Longest Distance Algorithm, which use simple geometry to calculate the distance between the MS and BS. The second is Least Handoff Frequency Algorithm, which is a pre-scan method.

This rests of this paper is organized as following. We illustrate the main idea of our proposed methods in Sect. 2. In Sect. 3, we show the simulation results to compare with the existing handoff methods. The results prove that our proposed methods are well enough on reducing the handoff frequency. At last, the conclusions and the future works are given in Sect. 4.

2 Proposed Methods

The detail operations of our proposed methods will be given in this section. Firstly, we introduce the Longest Distance Algorithm which determines the next potential BS when the signal of associated BS becomes weak. Then, we introduce the LHFA which can schedule the handoff BSs in advance to optimize the number of handoff times. We assumed the radio coverage of every BS is a perfect circle. The radio range of each BS is irregular. The MS equips with the Global Position System (GPS) to get its current position. We use the forthright to elaborate the main idea. In the latter, we will show how to extend our methods to grid roads in the urban district.

2.1 The Longest Distance Algorithm (LDA)

Let the current associated BS of MS be BS_c . When the RSS of BS_c is less than the predefined threshold, MS starts to collect the data of each nearby BS_i . The data includes the coordinate (x_i, y_i) and the radio radius R_i . Let Ω is the set contain all these BSs. The next potential BS will be the BS which can provide the longest service time.

Figure 1a is a handoff scenario in the VANETs. Seven BSs are installed aside the road. Their radio range is r_i , $i = 1 \dots 7$. Their edge of the radio coverage is represented as the dash line circle C_i , $i = 1 \dots 7$. Initially, MS associates with BS_1 .

It straightly moves from location S to the destination Z . The maximal service distance (MSD) that a BS_i can provide to MS on this moving path is also shown in Fig. 1a. We can represent this scenario as the geometric graph in Fig. 1b. The radio coverage of each BS_i is a circle. The moving path of MS is a line. The MSD of each BS_i is the length of the chord that L cuts on C_i .

At the location A, MS detects the signal down and triggers the handoff process. MS collects the neighbor BSs, the BS_2 and BS_5 , into set Ω and computes the remaining service distance (RSD) of every BS in Ω . The RSD of a BS_i is part of its MSD. It computes from MS's current location to the end point of the chord that is near the destination. The BS with longest RSD is selected. Computing the RSD of BS_i needs the coordinates of the endpoints of the chord. We use the geometric graph in Fig. 1b to compute the RSD.

The history position of MS helps us to get the line equation L . Let (x_Z, y_Z) be the coordinate of destination and (x_c, y_c) be the coordinate of current position P_c . The line equation L can be obtained from (1).

$$y = m(x - x_c) + y_c. \quad (1)$$

In (1), $m = \frac{y_c - y_Z}{x_c - x_Z}$. It is the slope of L . For circle C_i , MS has the coordinate of BS_i which is the center point of C_i and the radio range r_i . Therefore, each C_i can be represented as (2).

$$r_i^2 = (x - x_i)^2 + (y - y_i)^2. \quad (2)$$

By solving the simultaneous equations of (1) and (2), we can get the two cross points P_i^a and P_i^b that L crosses on C_i . Let $P_i^* = \min(|ZP_i^k|)$, where $k = a, b$, The RSD of BS_i will be $|P_c P_i^*|$. The BS with which MS will associate will be the one as (3).

$$\max(|P_c P_i^*|), \quad \forall BS_i \in \Omega. \quad (3)$$

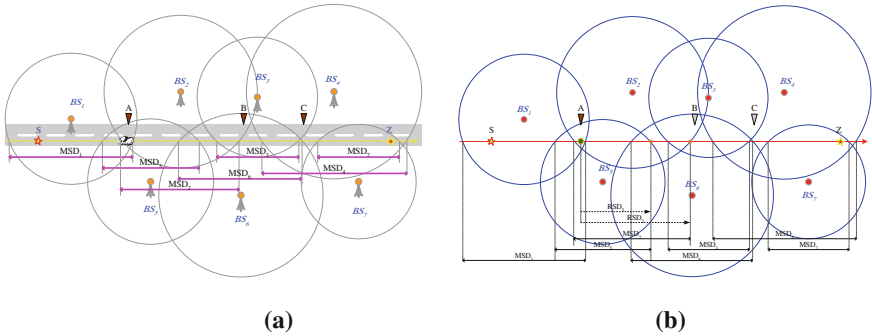


Fig. 1 The MSDs and RSDs, **a** The handoff scenario. **b** The geometric graph of (a)

2.2 The Minimal Handoff Frequency Algorithm

In the LDA method, MS still needs to go through the three phases during the handoff process. It only reduces the number of times that MS switches the BSs. The handoff delay in every handoff process is not explicitly saved. To improve the delay time in a handoff process, we propose a pre-scheduled method named the Minimal Handoff Frequency Algorithm.

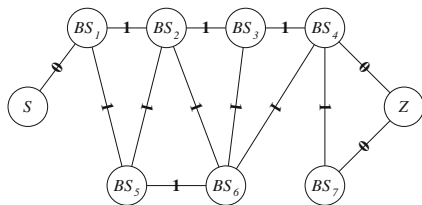
Generally, a BS is stationary after it is installed. If the BSs' position information can be obtained in advance, we can schedule the most suitable BSs for the MS at the beginning that MS enters the road. Consequently, MS can also authenticate to these BSs beforehand. So, the delay time spent on both probing and authentication phases can be reduced.

The LHFA needs to build the handoff-graph which exhibits the possible handoff relation between BSs. The corresponding handoff-graph for Fig. 1a will be shown as Fig. 2. A vertex in the handoff-graph represents a BS. The link between two vertices implies that MS can switch service between these two BSs. To have a link between two vertices in the handoff-graph, the corresponding two BSs must satisfy two conditions. Firstly, their radio coverage must overlap with each other. Secondly, their overlapping coverage must cover the moving path of the MS. For example, there is no link between the BS₆ and BS₇ in Fig. 1a. Although these two BSs overlap their radio coverage with each other, the area does not cover the path of the MS.

When the MS switches from one BS to another, it is similar to move from one vertex to another in the handoff-graph. Thus, we weight each link in the handoff-graph to 1. In addition, the S and Z are also added into this graph. The BSs that cover Z will add a link to it, but the weight is set to 0. The S adds a link the BS with which MS initially associates. The weight is also set to 0.

Finding the minimal number of handoff times from S to Z is similar to find the shortest path from S to Z in the handoff-graph. So, we can use the Dijkstra's algorithm to solve the problem. In the Fig. 2, $S \rightarrow BS_1 \rightarrow BS_2 \rightarrow BS_6 \rightarrow BS_4 \rightarrow Z$ is one of the shortest paths. The sequence $BS_1 \rightarrow BS_2 \rightarrow BS_6 \rightarrow BS_4$ will be the scheduled handoff BS sequence which has the minimal number of handoff times. Note that the MS may not discover a scheduled BS in the sequence due to the signal interference. In this situation, MS will switch to the LDA method to collect the information of BSs. And then, a new handoff sequence will be rescheduled for MS via the LHFA algorithm.

Fig. 2 The handoff-graph for Fig. 1a



2.3 Extend to Grid Roads in Urban District

In the practical case, the MS will not always move over a forthright. The road in city is similar to the grid on the checkerboard. To extend the LDA and LHFA to the urban scenario, we transform the grid roads to a forthright in this section. In the example of Fig. 3a, we have three forthright segments $\{\overline{SX}, \overline{XY}, \overline{YZ}\}$ between S and Z. They are separated and reassembled as Fig. 3b. For the LDA, we can treat each forthright between S and Z as a sub-handoff problem. The street corners will be an intermediate start and the destination locations.

To extend the LHFA to the scenario of grid roads, we compute the MSD of every BS in every segment. If the MSD of a BS is out of the road segment, the MSD is set to the end point of the road segment. At last, all road segments are reassembled as a forthright. The MSDs of the same BSs will be concatenated. For example, the final MSDs of BSs will be constructed as Fig. 3b.

3 Simulation

The simulation results are given in this section. We implemented the LDA, Lookahead (LOOK_1), strongest RSS(S-RSS), LHFA and the hard-handoff (HARD) methods with the C# program. BSs are randomly installed aside the road. We assume that the installed BSs will fully cover the road. Each BS randomly chooses an operation channel. The active channel scanning is used in probing phase.

In the practical active channel scanning operation, the MS will listen to a channel for a time period. If the channel is idle during this time, the scanning is finished and the channel is declared empty. This time period is named as *MinChannelTime*. If there is any traffic during this time, the station must wait for a longer time period. This time period is named as *MaxChannelTime*. To obtain

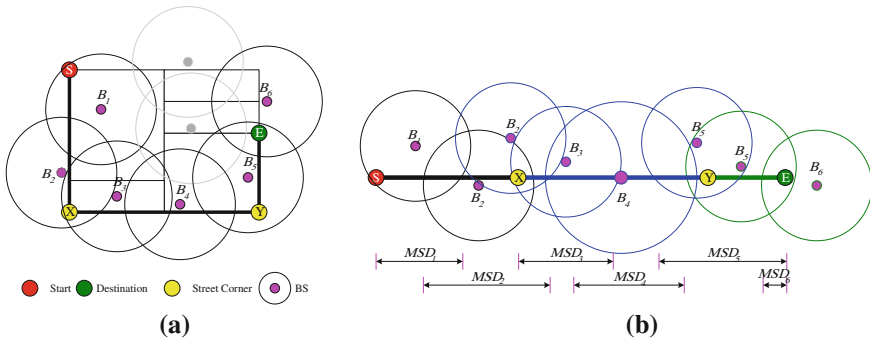


Fig. 3 Transform grid road to a forthright. **a** Original road. **b** Reassembled forthright

more realistic delay time, we use the following formula to estimate the channel scanning time.

$$(11 - C_u) \times \beta + C_u \times \alpha \quad (4)$$

The C_u is the total number of channels. The α is the MaxChannelTime and the β is the MinChannelTime. Both the authentication delay and re-association delay are 1 ms. The packet loss rate is also involved. The other related simulation parameters are listed in Table 1. All results are averaged from 1000 random topologies.

3.1 Simulation Results

Figure 4 shows the results of the number of handoff times. The RSS is always eager to find the BS with the best signal. So, it has the worst results in this index. Its number of handoff times is more than twice of the other methods. Because RSS method always associates with the BS with the best signal, its number of handoff times is not influenced when we increase the maximum radio range of BS. For the other methods, the service time period of a BS will be extended when the maximum range of BS increases. Therefore, the number of handoff times in other methods will decrease. The HARD handoff method is worse than other methods except the RSS because it does not choose the BS which has the longest service time. Instead, when the signal of previous associated BS completely loses, it selects the BS with the best signal. A special note is the LDA. Its number of handoff times is close to the pre-scan methods. It proves that LDA is an excellent online method.

Figure 5 is the accumulated handoff delay time over all simulation period. High frequently switching the BSs cause the S-RSS method has the worst results. The increasing of radio range will raise the probability for MS to find the BS with better signal. So, the accumulated handoff delay increase with the growing of radio range. For the LDA and HRAD methods, their delay time is heavy depended on the number of handoff times. LDA exhibits better results than HRAD.

Without the time spent on channel probing, the pre-scan methods LDA and LOOK have their accumulated handoff delay time approximate to zero. In Fig. 6, three LOOK_x methods with different size of time slot are implemented. The x represents

Table 1 Simulation parameters

Simulation parameters	Values	Simulation parameters	Values
Simulation duration	450 s	MaxchannelTime(α)	11 ms
Max radio range of a BS	200, 300, 400, 500, 600	MinchannelTime(β)	5 ms
Min radio range	150	Used channel (C_u)	1-11
Distance from BS to road	-125 m ~ 125 m	Authentication delay	1 ms
Total available channels	11 channels	Association delay	1 ms
Probe delay (ms)	$(11 - C_u) \times \beta + C_u \times \alpha$	Moving speed of MS	10 m/s
Lookahead time slot (*50)	1 ms, 5 ms, 10 ms	Inter BS distance gap	50 m ~ 200 m

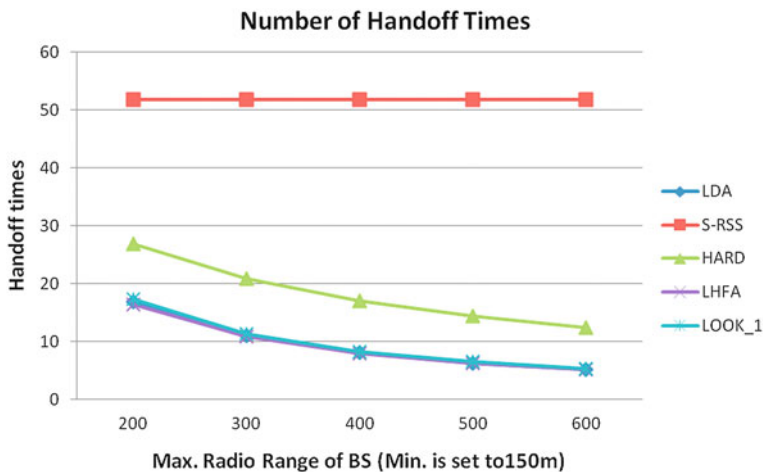


Fig. 4 The number of handoff times

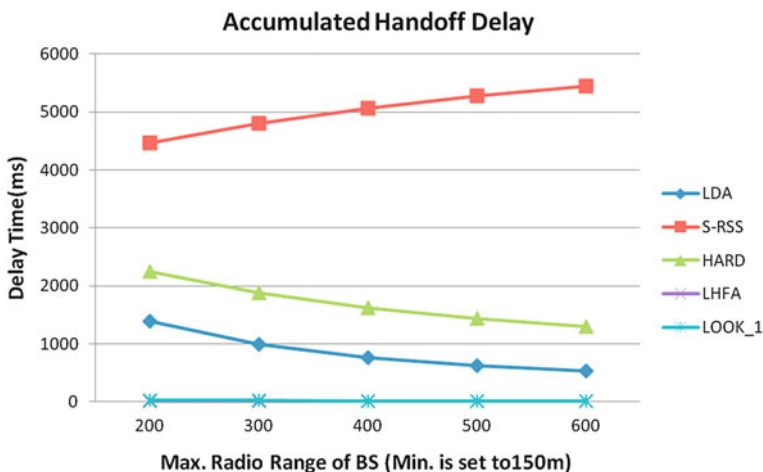


Fig. 5 Accumulated of the BSs handoff delay

the size of slot time. For example, LOOK_1 represents the slot time is 1×50 ms and so on. Shortening the size of slot time can slightly reduce the number of handoff times. The explicitly influence can be observed from the case of 400 m radio range. The difference of LOOK_1 and LOOK_10 is about two times. However, shortening the size of slot time implying more memory space is required for storing the slot information. As we find that the LHFA is still the best one. Without slotting the time, the number of handoff time in LDA will be better than that of LOOK.

At last, we show the impacts caused by the number of deployed BSs in Fig. 7. The handoff times of S-RSS increases when the total deployed BSs increases.

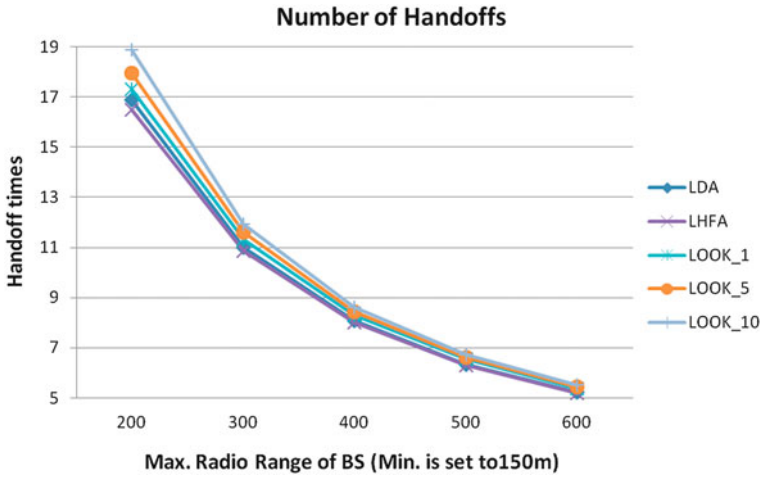


Fig. 6 Compare the pre-scan methods

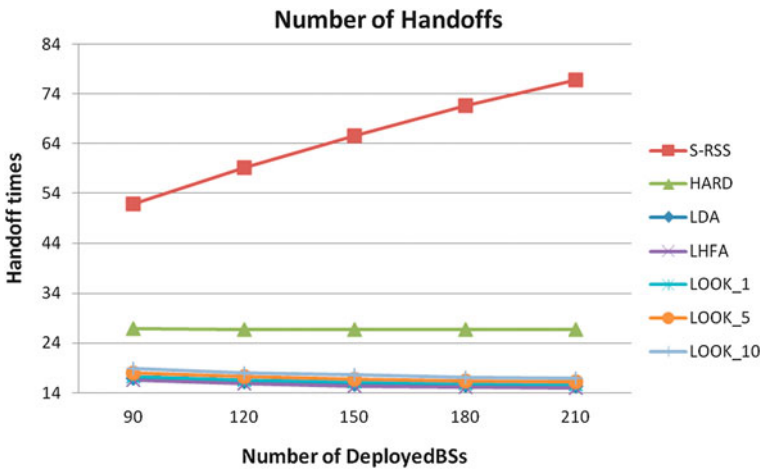


Fig. 7 The impacts of the deployed BSs

For the HARD method, the densely deployed BSs will increase the probability for the MS to find the new BS near the position that the previous BS loses the signal. So, it does not respond to the number of BSs. LDA, LHFA, and LOOK will slightly reduce the number of handoff times.

4 Conclusions

This paper proposed two handoff methods to reduce the handoff frequency in the vehicular area network. The LDA is an online method which needs to probe the channels during the handoff process. The LHFA is a pre-schedule method. It transforms the handoff problem to the shortest path problem in the graph. The probing and authentication phases in LHFA can be done beforehand to shorten the handoff delay in a handoff process. The simulation results prove that both LDA and LHFA are better than the Lookahead method. In our further works, we will extend the model of LHFA to the scenario that the radio coverage of every BS is not a perfect circle and to improve signal quality and loading balance during the handoff process.

Acknowledgments This work was supported in part by the National Science Council, Taiwan, ROC, under grant NSC100-2221-E-150-087.

References

1. Ramani I, Savage S (2005) SyncScan: practical fast handoff for 802.11 infrastructure networks. In: Proceedings of the 24th IEEE INFOCOM, vol 1, pp 675–684
2. Chen YS, Chuang MC, Chen CK (2008) DeuceScan: deuce-based fast handoff scheme in IEEE 802.11 wireless networks. In: IEEE transactions on vehicular technology, vol 57, pp 1126–1141
3. Shin S, Forte AG, Rawat AS, Schulzrinne H (2004) Reducing MAC layer handoff latency in IEEE 802.11 wireless LANs. In: Proceedings of the 2nd international workshop on mobility management and wireless access protocols (MobiWac04), pp 70–83
4. Zhang ZX, Pazzi RW, Boukerche A (2011) A fast MAC layer handoff protocol for WiFi-based wireless networks. In: Proceedings of the 35th IEEE conference on local computer networks (LCN), pp 684–690
5. Sarddar D, Banerjee J, Chakraborti T, Sengupta A, Naskar MK, Jana T, Biswas U (2011) Fast handoff implementation using distance measurements between mobile station and APs. In: Proceedings of IEEE students' technology symposium (TechSym), pp 81–86
6. Wu TY, Weng WF (2011) Reducing handoff de-lay of wireless access in vehicular environments by artificial neural network-based geographical fingerprint. In: IET communications, vol 5, pp 542–553
7. Kim M, Liu Z, Parthasarathy S, Pendarakis D, Yang H (2008) Association control in mobile wireless networks. In: Proceedings of the 27th conference on computer communications, pp 1256–1264
8. Pack S (2005) SNC: A selective neighbor caching scheme for fast handoff in IEEE 802.11 wireless networks. ACM Mobile comput Commun 9(4):39–49

RC4-2S: RC4 Stream Cipher with Two State Tables

Maytham M. Hammood, Kenji Yoshigoe and Ali M. Sagheer

Abstract One of the most important symmetric cryptographic algorithms is Rivest Cipher 4 (RC4) stream cipher which can be applied to many security applications in real time security. However, RC4 cipher shows some weaknesses including a correlation problem between the public known outputs of the internal state. We propose RC4 stream cipher with two state tables (RC4-2S) as an enhancement to RC4. RC4-2S stream cipher system solves the correlation problem between the public known outputs of the internal state using permutation between state 1 (S_1) and state 2 (S_2). Furthermore, key generation time of the RC4-2S is faster than that of the original RC4 due to less number of operations per a key generation required by the former. The experimental results confirm that the output streams generated by the RC4-2S are more random than that generated by RC4 while requiring less time than RC4. Moreover, RC4-2S's high resistivity protects against many attacks vulnerable to RC4 and solves several weaknesses of RC4 such as distinguishing attack.

Keywords Stream cipher · RC4 · Pseudo-random number generator

This work is based in part, upon research supported by the National Science Foundation (under Grant Nos. CNS-0855248 and EPS-0918970). Any opinions, findings and conclusions or recommendations expressed in this material are those of the author (s) and do not necessarily reflect the views of the funding agencies or those of the employers.

M. M. Hammood

Applied Science, University of Arkansas at Little Rock, Little Rock, USA

e-mail: mmhammood@ualr.edu

K. Yoshigoe (✉)

Computer Science, University of Arkansas at Little Rock, Little Rock, AR, USA

e-mail: kxyoshigoe@ualr.edu

A. M. Sagheer

College of Computer, University of Anbar, Anbar, Iraq

e-mail: ali_makki@ieee.org

1 Introduction

Cryptographic algorithms that can provide fast implementation, small size, low complexity, and high security for resource-constrained devices such as wireless sensor devices are imperative. Conventional cryptographic algorithms are very complex and consume significant amount of energy when used by resource-constrained devices for the provision of secure communication, and public key algorithms are still not feasible in sensor networks for several reasons including limited storage and excessive energy usage [1]. Therefore, security schemes should rely on a symmetric key cryptography especially when systems have limited hardware resources.

There are a number of stream cipher algorithms presented to implement high performance software including IDEA, ORYX, LEVIATHAN, MUGI, RC4, Helix, SEAL, SOBER, and SNOW. One-time pad, which is stronger than all these aforementioned algorithms, is unbreakable since it never uses the same key more than once. Consequently, it is impossible to deduce any information about the key from ciphertext by an attacker. The robustness of stream ciphers depends on Pseudo-Random Number Generator (PRNG) which has proved to be resistant to the attacks if it passes the statistical tests.

RC4 is a proprietary stream cipher which was designed in 1987 by Ron Rivest. RC4 is widely used in security software based on stream cipher including one in the encryption of traffic to and from secure web sites such as Transport Layer Security (TLS), Secure Socket Layer (SSL), and Wired Equivalent Privacy (WEP) implementations. RC4 is fast in comparison to other algorithms and it has a simple design hardware implementation [2]. For instance, RC4 is five times faster than Data Encryption Standard (DES) and fifteen times faster than Triple-DES [3].

Many stream ciphers use de-facto RC4 standard for meeting specific requirements such as limited storage size and power of devices; however, there are many weaknesses found in stream ciphers caused by mathematical relations between the key, ciphertext, and plaintext with which attackers can assess the security of the cryptographic algorithms via cryptanalysis. Thus the goal is to create a sequence of keys that approaches to true randomness [4]. The rest of the paper is organized as follows: [Section 2](#) reviews related works. [Section 3](#) presents the description of RC4, and [Sect. 4](#) shows some weaknesses of RC4. We then present our proposed algorithm to enhance RC4 technique in [Sect. 5](#), followed by description of randomness testing and NIST in [Sect. 6](#). [Section 7](#) presents analysis and implementation followed by the conclusion in [Sect. 8](#).

2 Related Work

Numerous researchers attempt to enhance the RC4 and create variant algorithms. Paul and Preneel [5] explored a new statistical weakness in the first two output bytes of the RC4 key stream generator. They showed that the number of outputs

required distinguishing the output of the RC4 of the random sequence with the presence of which bias is 128, and they recommended using 256 to overcome this bias. The authors were also creating a new pseudo-random number generator, RC4A, which is characterized by being more resistant against most attacks that apply to RC4 especially the weakness of distribution in the first two output bytes. However, the RC4A did not completely remove the autocorrelations, and it was broken with a distinguishing attack by Maximov [6]. Zoltak [4] proposed Variably Modified Permutation Composition (VMPC) which was designed to be efficient in software implementations and solving a weakness found in the RC4 Key Scheduling Algorithm (KSA) that was described by Fluhrer et al. in [7]. The structure of Pseudo-Random Generation Algorithm (PRGA) in VMPC was more complex in comparison with the RC4 that makes it more resistant against attacks. However, it was again broken by distinguishing attack [6].

Yu and Zhang [8] presented RC4 state combined with the hash function without affecting the simplicity and efficiency. The RC4 state based on hash function can generate Message Authentication Code (MAC). The enhancement includes the offset, forward, and backward properties of RC4 states where the authors use offset to ignore the first few bytes of the key and started encrypt the data in determine position which has led to increase the time of execution. Pardeep and Pateriya [9] proposed Pardeep Cipher (PC-RC4) which is adding a new improvements and extension to RC4 algorithm. In the PC-RC4, randomness in KSA and PRGA are improved to make it stronger but it again increased the time of execution [9]. Kadry and Smaili [10] presented Vigenère RC4 (VRC4) which is a combination of the RC4 and the poly alphabetic cipher Vigenère. The plain text encrypted by using the classic RC4 cipher followed by re-encrypting by Vigenère which results in increased time of execution. Mousa and Hamad examined the analysis of the effect of different parameters of the RC4 algorithm such as the execution time and the file size where they conclude that the speed of encryption and decryption time is affected by length of encryption key and the size of data file [11]. Yao, et al. presented analysis and enhancement of the security of RC4 algorithm by using public key encryption with RC4 which has led to increase the size of the system and the time of execution [12]. Hammood et al. proposed an RRC4 random initial state algorithm in which a new enhancement of RC4, and its improved randomness compared against the traditional RC4. However, the issue of the speed was not addressed [13].

3 Description of RC4

RC4 design avoids the use of Linear Feedback Shift Registers (LFSRs) where many stream cipher algorithms depend on it, especially in hardware. It attempts to achieve highest randomness via swapping of elements in arrays. The RC4 algorithm has variable key length which ranges between 0 to 255 bytes for initializing 256-byte array in initial state by elements from $S[0]$ to $S[255]$. As recommended in [7, 14], RC4 must use a key longer than 128 bytes. The algorithm consists of

KSA and PRGA which are executed sequentially. RC4 Key is initialized by KSA while the pseudo-random number is produced by PRGA.

The pseudo codes for the two parts of RC4 algorithm are shown in Algorithm 1 and Algorithm 2 where m is the message length of a plain text, L is the length of the initial key in bytes, N is the size of the array or state S , and i and j are index pointers. Such a self-modifying lookup table is simple and has been applied efficiently in software [15]. The output of the PRGA algorithm is a key sequence that will be XOR-ed with plaintext (or ciphertext) to get ciphertext (or plaintext).

Sharif and Mansoor provided comparison between different encryption algorithms using different data sizes and key sizes. The simulation results clarified preponderance of RC4 algorithm over other algorithms in terms of speed and throughput [16].

Algorithm 1. KSA for RC4

INPUT: $K [k_1, k_2, \dots, k_L], m$
OUTPUT: S
 1. $S[i] = i$, for $i=0, 1, 2, \dots, 255$
 2. $j \leftarrow 0$;
 3. For $i \leftarrow 0$ to 255 Do
 3.1. $j \leftarrow (j + S[i] + K[i \bmod L]) \bmod 256$
 4. Swap $S[i]$ with $S[j]$
 5. Return (S)

Algorithm 2. PRGA for RC4

INPUT: State S
OUTPUT: Key sequence $Kseq$
 1. $j \leftarrow 0$
 2. $i \leftarrow 0$
 3. While not end of sequence Do
 3.1. $i \leftarrow (i+1) \bmod 256$
 3.2. $j \leftarrow (j + S[i]) \bmod 256$
 3.3. Swap $S[i]$ with $S[j]$
 3.4. $Kseq \leftarrow S [(S[i] + S[j]) \bmod 256]$
 4. Return ($Kseq$)

4 The Weaknesses of RC4

Several weaknesses in RC4 were identified. Some of these weaknesses are simple and can be solved easily, but others are critical because they can be exploited by the attackers. Two of the problems of RC4 are 1) the weakness of the KSA and 2) the weakness of relations between the S-box in different time. Initial state of the PRGA achieves a pretty good efficiency against a number of attempted attacks. In [17] Mantin and Shamir, distinguished statistical weakness inside RC4 algorithm that the probability of the second round output byte generated is zero output byte is twice than other values, which can be exploited this weakness by practical ciphertext only attack. This ciphertext only attack is limited to broadcast applications where different keys are used to encrypt the same plaintext for multiple recipients. There are many other attacks described in [7] such as subkey guessing attack, linear consistency attack, inversion attack, etc. In addition, an algebraic attack is a new type of higher order correlation attack. Since a fairly straight forward approach such as brute force attack infers the internal state of the PRGA, increased internal state size is recommended, yet it results in increased encryption and decryption time.

5 RC4 Stream Cipher With Two State Tables

As discussed in the previous section, RC4 has significant number of weaknesses in the phases of KSA and PRGA. In this section, we propose RC4 stream cipher with two state tables (RC4-2S) algorithm as an improvement to RC4. It is one of the RC4 stream cipher algorithm family proposed to reduce the correlation problem between the public known outputs of the internal state while improving the speed of the encryption and decryption. The new algorithm consists of initialization phase (KSA) and output phase (PRGA) as shown in Algorithm 3 and 4, respectively. All addition operations are carried out modulo N . KSA takes a key, k , consisting of 16 n -bit words. After the setup, the round algorithm is executed once for each word output. In reality, all practical applications of the developed RC4 is implemented with $n = 8$ in which case all entries of S along with i and j are bytes.

In the first phase of KSA, S_1 is filled from 0 to $(N/2)-1$ and S_2 gets the remaining $N/2$ numbers from $N/2$ to $N-1$. The input secret key, k , is used as a seed for the two states S_1 and S_2 . k is used to make permutation and swapping of the elements of S_1 and S_2 . Therefore S_1 and S_2 become two secret random inputs for second phase.

In the second phase, S_1 and S_2 produce two keys in each loop cycle instead of one as with the standard RC4. In this algorithm, there are more elements to be swapped between S_1 and S_2 by three pointers: i , $j_1 = j_1 + S_1[i]$, and $j_2 = j_2 + S_2[i]$ in the S -box. S_1 and S_2 in PRGA are used to produce the sequence of output stream which is XOR-ed with plaintext (or ciphertext) to generate ciphertext (or plaintext).

Algorithm3. KSA for RC4-2S

```

INPUT:  $k, m$ 
OUTPUT:  $S_1, S_2$ 
1. For  $i \leftarrow 0$  to  $N/2 - 1$  Do
     $S_1[i] \leftarrow i$ 
2. For  $i \leftarrow N/2$  to  $N - 1$  Do
     $S_2[i-N/2] \leftarrow i$ 
3.  $j \leftarrow 0$ .
4. For  $i \leftarrow 0$  to  $N/2 - 1$  Do {
    4.1.  $j \leftarrow (j + S_1[(i + k[i \bmod L]) \bmod N/2] + k[i \bmod L]) \bmod N/2$ 
    4.2. Swap  $S_1[i]$  with  $S_1[j]$  }
5.  $j \leftarrow 0$ .
6. For  $i \leftarrow 0$  to  $N/2 - 1$  Do {
    6.1.  $j \leftarrow (j + S_2[i] + k[i \bmod L]) \bmod N/2$ 
    6.2. Swap  $S_2[i]$  with  $S_2[j]$  }
Return ( $S_1$  and  $S_2$ )

```

Algorithm4. PRGA for RC4-2S

```

INPUT:  $S_1, S_2$ 
OUTPUT: Key sequence  $Kseq$ 
1.  $i, j_1, j_2 \leftarrow 0$ 
2. While not end of half sequence Do
    2.1  $i \leftarrow (i+1) \bmod N/2$ 
    2.2  $j_1 \leftarrow (j_1 + S_1[i]) \bmod N/2$ 
    2.3 Swap  $S_1[i]$  with  $S_2[j_1]$ 
    2.4  $t_1 \leftarrow S_1[(S_1[i] + S_1[j_1]) \bmod N/2]$ 
    2.5  $j_2 = j_2 + S_2[i] \bmod N/2$ 
    2.6 Swap ( $S_2[i]$  with  $S_1[j_2]$ )
    2.7  $t_2 = S_2[(S_2[i] + S_2[j_2]) \bmod N/2]$ 
    2.8  $Kseq = [t_1, t_2]$ 
Return ( $Kseq$ )

```

RC4-2S is faster than RC4 because RC4-2S requires two swaps and five modulo functions to generate two bytes of key per iteration in the PRGA algorithm

while RC4 requires one swap and three modulo functions to generate only one byte of key.

This technique combines increasing randomness of the initial internal states with permutation of the two state tables during key generation to solve the correlation problem between the public known outputs of the internal.

6 Randomness Test

The binary generated sequences are tested by National Institute of Standards and Technology (NIST) Test Suite which is a statistical package for random number generation test which consists of 16 statistical tests to measure the randomness of the output sequences of true random number generators or pseudo-random number generators.

7 Result Analysis

The design of the RC4-2S was done using MATLAB and the tests of this PRNG were done using NIST STS-1.6 [18]. Key generation time of RC4-2S was faster than that of the original RC4 by approximately 20 % for various amount of keys generated as shown in Table 1. This is expected because RC4-2S, which can generate two bytes of key per iteration in the PRGA algorithm, requires two swaps and five modulo functions while RC4, which generates only one byte of key, requires one swap and three modulo functions.

We check the produced binary sequence from RC4-2S by NIST statistical tests. The probability of a good or bad random number generator is represented by the p value. Testing process compared p -value to 0.01. If the p -value is more than 0.01, then the process accepts the sequence, else rejects the sequence because the sequence is non-randomness. Conversely, some tests accept large sizes of sequence and fail in the small size as well as other tests accept both sizes. In our program, we use a large size 134,000 bytes (1,072,000 bits); generated by each keys and these sequences were tested, and subsequently calculated the average of the p -values result from these tests. As shown in Table 2, the p -values are acceptable when greater than 0.01, and the produced sequence can be deemed random, uniformly distributed, and suitable for cryptography.

Table 1 Key generation time for RC4 and RC4 -2S

Amount of keys in KB	RC4 (ms)	RC4-2S (ms)
100	232.726	189.4
500	1372.36	970.195
1000	2407.425	1932.196

Table 2 Result of running the NIST suite over the set data produced by the proposed RC4-2S and standard RC4

Test no.	Statistical test name	RC4		RC4-2S	
		p-value	Conclusion	p-value	Conclusion
1	Approximate entropy	0.444380	SUCCESS	0.273897	SUCCESS
2	Block frequency	0.453253	SUCCESS	0.529301	SUCCESS
3	Cumulative sums (Forward)	0.406619	SUCCESS	0.544359	SUCCESS
4	Cumulative sum (Reverse)	0.394456	SUCCESS	0.448504	SUCCESS
5	FFT	0.492610	SUCCESS	0.451043	SUCCESS
6	Frequency	0.426195	SUCCESS	0.502214	SUCCESS
7	Lempel–Ziv compression	1.000000	SUCCESS	1.000000	SUCCESS
8	Linear complexity	0.425838	SUCCESS	0.631859	SUCCESS
9	Longest runs	0.462975	SUCCESS	0.460664	SUCCESS
10	Non periodic templates	0.501925	SUCCESS	0.485355	SUCCESS
11	Overlapping template	0.395097	SUCCESS	0.418021	SUCCESS
12	Random excursions	0.500386	SUCCESS	0.527889	SUCCESS
13	Random excursions variant	0.530319	SUCCESS	0.439212	SUCCESS
14	Rank	0.451984	SUCCESS	0.382616	SUCCESS
15	Runs	0.575766	SUCCESS	0.604976	SUCCESS
16	Serial	0.496741	SUCCESS	0.386188	SUCCESS
17	Universal statistical	0.356271	SUCCESS	0.542075	SUCCESS

If the tests give p-value asymptotically to 1, then the sequence appears to have perfect randomness. A p-value of zero indicates that the sequence appears to be completely nonrandom. The SUCCESS indicates the sequence is acceptable and has good randomness, where the FAILURE mean the sequence is not acceptable due to non-randomness. There are some statistical tests of PRBG that are very common and must be included in test suite such as *Runs* test, *Frequency* test, and *Universal* test [19]. In these tests, the p-values of the proposed RC4-2S algorithm are greater than the p-values of the standard RC4 as shown in the Table 2. Moreover, RC4-2S is better than RC4 in most of the other tests.

8 Conclusion

The RC4 cipher system is an important encryption algorithm that can be used to protect the information on the common channel as its implementation is simpler and its cryptographic function is faster than that of DES. The proposed RC4 stream cipher with two state tables (RC4-2S) offers an enhanced randomness in the generated key sequences while the key generation time of RC4-2S is faster than that of RC4. The generated output sequences of RC4-2S have passed the NIST suite of statistical tests. The suggested RC4-2S algorithm is not a complicated one. Thus, it can be implemented in either software or hardware.

References

1. Sharma K, Ghose MK, Kumar D, Singh RPK, Pandey VK (2010) A comparative study of various security approaches used in wireless sensor networks. *Int J Adv Sci Technol* 177(77)
2. Gupta SS, Chattopadhyay A, Sinha K, Maitra S, Sinha B (2013) High-performance hardware implementation for RC4 stream cipher. *IEEE Trans Comput* 62(4):730–743
3. Ahmad S, Beg MR, Abbas Q, Ahmad J, Atif S (2010) Comparative study between stream cipher and block cipher using RC4 and Hill Cipher. *Int J Comput Appl* (0975–8887), 1(25)
4. Zoltak B (2004) VMPC one-way function and stream cipher. *Fast software encrypt FSE 2004, LNCS 3017*. Springer-Verlag, New York, pp 210–225
5. Paul S, Preneel B (2004) A new weakness in the RC4 keystream generator and an approach to improve the security of the cipher in fast software encrypt. *FSE 2004, LNCS 3017*. Springer-Verlag, New York, pp 245–259
6. Maximov A (2005) Two linear distinguishing attacks on VMPC and RC4A and weakness of the RC4 family of stream ciphers. *Fast software encryption, FSE*
7. Fluhrer S, Mantin I, Shamir A (2001) Weaknesses in the key scheduling algorithm of RC4. In: *Proceedings of annual workshop on selected areas in cryptography*, vol 2259, Springer, Toronto, pp 1–24
8. Yu Q, Zhang C (2011) RC4 state and its applications. In: *Ninth annual international conference on privacy, security and trust*, pp 264–269
9. Pardeep Pateriya P (2012) PC-RC4 algorithm: an enhancement over standard RC4 algorithm. *Int J Comput Sci Netw* 1(3)
10. Kadry S, Smaili M (2010) An improvement of RC4 cipher using vigenère cipher. *Int J Comput Intell Inform Secur* 1(3)
11. Mousa A, Hamad A (2006) Evaluation of the RC4 algorithm for data encryption. *Int J Comput Sci Appl* 3(2)
12. Yao Y, Chong J, Xingwei W (2010) Enhancing RC4 algorithm for WLAN WEP protocol. In: *control and decision conference (CCDC)*, IEEE, pp 3623–3627
13. Hammood MM, Yoshigoe K, Sagheer AM (2013) RC4 stream cipher with a random initial state. In: *Proceedings of 10th FTRA international conference on secure and trust computing, data management, and applications (STA'13)*. Lecture notes in electrical engineering, Springer, Heidelberg
14. Grosul A, Wallach D (2000) A related-key cryptanalysis of RC4. Department of computer science, Rice University, Technical report TR-00-358, June 2000
15. Stamp M (2006) *Information security principles and practice*. Wiley, New York
16. Sharif SO, Mansoor SP (2010) Performance analysis of stream and block cipher algorithms. In: *3rd international conference on advanced computer theory and engineering (ICACTE)*, IEEE vol 1, pp 522–525
17. Mantin I, Shamir A (2001) A practical attack on broadcast RC4. In: *8th international workshop, FSE*, PP 152–164
18. Rukhin A, Soto J, Nechvatal J, Smid M, Barker E, Leigh S, Levenson M, Vangel M, Banks D, Heckert A, Dray J, Vo S (2001) A statistical test suite for random and pseudorandom number generators for cryptographic applications. NIST special publication 800-22, National institute of standards and technology (NIST), Gaithersburg. <http://csrc.nist.gov/rng/>
19. Stallings W (2011) *Cryptography and network security principles and practices*, 5th edn. Prentice Hall Pearson, New Jersey

Genetic Algorithm-Based Relocation Scheme in Electric Vehicle Sharing Systems

Junghoon Lee and Gyung-Leen Park

Abstract This paper designs a genetic algorithm-based relocation scheme for electric vehicle sharing systems, which suffer from the stock imbalance problem due to different rent-out and return patterns in different stations. To improve the service ratio, the relocation scheme explicitly moves vehicles from overflow stations to underflow stations. Each relocation plan is encoded to an integer-valued vector, based on two indexes, one for the overflow list, and the other for the underflow list. In each list, stations are bound to specific locations according to the number of surplus or needed vehicles. For a vector element, its location is the overflow station index, while the value is the underflow index. Iterative genetic operations improve the population quality, computed by the relocation distance, generation by generation. The simulation result shows that the proposed relocation scheme finds an efficient relocation plan in the early stage of iterations for the given parameter set.

Keywords Smart transportation · Electric vehicle sharing system · Vehicle relocation · Genetic algorithms · Relocation distance

This research was financially supported by the Ministry of Knowledge Economy (MKE), Korea Institute for Advancement of Technology (KIAT) through the Inter-ER Cooperation Projects.

J. Lee (✉) · G.-L. Park
Department of Computer Sciences and Statistics, Jeju National University, Jeju,
Republic of Korea
e-mail: jhlee@jejunu.ac.kr

G.-L. Park
e-mail: glpark@jejunu.ac.kr

1 Introduction

In spite of many benefits in environmental aspects such as high energy efficiency and low carbon emissions, electric vehicles, or EVs in short, cannot easily penetrate into our daily lives [1]. To say nothing of long charging time, they are still expensive for personal ownership. In the mean time, there is quite a lot of demand to buy a second car from many households while the second cars are not so intensively used as the first cars. Hence, carsharing is a very economic service for such households, and will be a prospective business model for EVs for the time being [2]. As a short time rental, which lasts just for a few hours, a group of users share EV pool, and each EV is parked, charged, and maintained in charging stations [3]. They rent out an EV on necessary basis and returns at a station. On the one-way rental, drivers are allowed to return an EV to a different station they have taken the EV.

Even though the one-way rental is most convenient to users, a stock imbalance problem cannot be avoided. That is, due to different demand density, the number of EVs will be different in each station [4]. EVs can get stuck in stations having low demand density, while some hot-spot stations runs out of EVs to meet the user requests. Vehicle relocation can solve this problem to balance between demand and supply for EV sharing. EV relocation can be performed either by human staffs or by vehicle transporters. As such methods are all costly, an efficient strategy is necessary. As an example, [5] presents a two-step relocation algorithm for optimal positioning and strategy selection. In their scheme, Step 1 conducts demand clustering to identify spatio-temporal hot spots and cold spots. Step 2 continuously measures the current state of spatial vehicle distribution to decide whether to trigger relocation procedures.

Anyway, a relocation procedure moves EVs in overflow stations to underflow stations. In overflow station, the current number of EVs is larger than the target distribution. Hence, the relocation is the process of matching two items in each of both parties so as to meet a given system goal such as relocation distance minimization. Even though a set of computer algorithms can be exploited for this problem, its execution time can grow too much when the number of EVs to be relocated gets larger. Accordingly, this paper designs an EV relocation scheme based on genetic algorithms, which are known to be a very efficient suboptimal search technique capable of finding reasonable quality solutions within a limited time bound [6]. In the core of this work, we encode a relocation plan to an integer-valued vector to run genetic operations such as selection, reproduction, and mutation. Then, its performance is assessed using the traffic pattern in Jeju city area.

2 Relocation Scheduler

2.1 Preliminaries

Before designing a relocation algorithm, it is necessary to introduce our previous work for background. First, a performance analysis framework has been built to assess a service in EV sharing systems, such as relocation schemes and renting policies [7]. For relocation, this framework allows a designer to virtually place sharing stations on the city map, set the number of EVs, and finally analyze the service ratio for a given relocation strategy using the real-life traffic pattern in the Jeju city. Actually, this pattern is obtained from pick-up and drop-off records in a taxi telematics system. However, it will be very similar to the EV sharing request pattern, as most forms of transport have many common features. Here, for the given parameters including the number of EVs and the access distance to the stations, the framework can measure service ratio, moving distance, and per-station EV distribution at relocation time.

Next, as for relocation strategies, which decide the target EV distribution [8], has considered 3 intuitive strategies including even, utilization-based, and morning-focused schemes, upon a practical assumption that the relocation procedure is carried out during non-operation hours. The relocation procedure reassigns EVs to make the current distribution equal to the target distribution. The even relocation scheme makes all station have the same number of EVs. It doesn't consider demand patterns, but may have reasonable service ratio in the long term. The utilization-based scheme relocates EVs according to the demand ratio of each station. It assigns more EVs to the station having more pick-ups. The morning-focused scheme redistributes EVs according to just the pick-up requests during the first few hours after the operation starts. It has also proposed a relocation procedure based on the stable marriage problem solver, but the execution time can get extended when the number of moves increases.

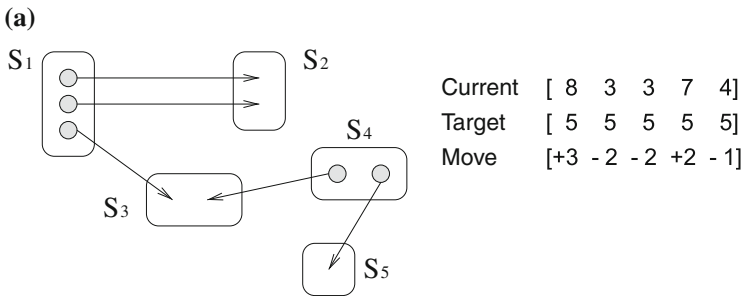
2.2 Genetic Algorithm Design

For a station set, $S = \{S_1, S_2, \dots, S_n\}$, let $C = \{C_1, C_2, \dots, C_n\}$ be the current distribution and $T = \{T_1, T_2, \dots, T_n\}$ be the target distribution, where n is the number of stations. Then, the relocation vector, $\{V_i\}$, can be calculated by $C_i - T_i$ for all S_i . If V_i is positive, S_i is an overflow station having surplus EVs which should be moved to other stations. As contrast, if V_i is negative, S_i is an underflow station and wants to receive EVs. If an EV, say E_k , currently belonging to a station, say S_i , will be relocated to another station, S_j , it is denoted by (S_i, S_j) , and it is equivalent to (E_k, S_j) . If there are m EVs to be relocated, its relocation plan consists of m (EV, Station) pairs, namely, $\{(S_i, S_j)\}$. Here, each EV is all different, but a station can appear e times, if it wants to replenish e EVs. The relocation distance is

the sum of distances for all (EV, station) pairs in the relocation plan. To calculate the relocation distance, it is necessary to be aware of distances between all individual station pairs.

To find an efficient relocation plan taking advantage of genetic algorithms, it is necessary to encode a relocation plan to the corresponding integer-valued vector called chromosome as well as to evaluate the quality of each plan. Our work selects the relocation distance as quality criteria for better energy saving and service staff efficiency. The shorter the distance, the better the relocation plan. Next, for encoding two indexes are defined, one for overflow stations and the other for underflow stations. Each index points to the location of overflow station and underflow station lists, respectively. Each station appears in the list as many times as the number of overflow (underflow) EVs. In the encoded vector, each number is ordered sequentially. Then, the location of the number is the pointer to the overflow index while a number, or a vector element, is the pointer to the underflow index.

This encoding scheme can be explained by an example shown in Fig. 1. There are 5 stations from S_1 to S_5 and 25 EVs in a sharing system. Current and target EV distributions are shown in Fig. 1a, and the corresponding relocation vector is



(b)

Index	0	1	2	3	4
Overflow stations	S_1	S_1	S_1	S_4	S_4
Underflow stations	S_2	S_2	S_3	S_3	S_5

- (c)
- [0 1 2 3 4]: (S_1, S_2) + (S_1, S_2) + (S_1, S_3) + (S_4, S_3) + (S_4, S_5)
 - [0 4 2 1 3]: (S_1, S_2) + (S_1, S_5) + (S_1, S_3) + (S_4, S_2) + (S_4, S_3)
 - [3 4 0 2 1]: (S_1, S_3) + (S_1, S_5) + (S_1, S_2) + (S_4, S_3) + (S_4, S_2)

Fig. 1 Encoding of relocation plans. **a** Current and target distribution. **b** Overflow and underflow indexes. **c** Example of encoded relocation plans

(3, -2, -2, 2, 1). S_1 and S_4 are overflow stations having 3 and 2 surplus EVs, respectively. Figure 1a also shows a sample relocation plan of $\{(S_1, S_2), (S_1, S_2), (S_1, S_3), (S_4, S_3), (S_4, S_5)\}$. In each pair, the first element is an overflow station from which an EV departs, while the second is an underflow station to which EV is relocated. The total number of EVs to be relocated is the same as the number of total surplus EVs and it is 5, so the relocation plan has 5 entries.

Figure 1b describes how to build overflow and underflow indexes. Each station is put to one of the two lists according to whether it is an overflow or underflow station. Hence, S_1 , an overflow station, appears 3 times from location 0 to 2 in the overflow list, while S_5 , an underflow station, appears once at location 4 in the underflow list. Now, consider the vector (0, 4, 2, 1, 3). Value 0 is located at the first place having index 0. Index 0 is the pointer to the first element in the overflow list, namely, S_1 . Value 4 is the pointer to the first element in the underflow list, namely, S_2 . Hence, value 0 in the first place is the relocation pair of (S_1, S_2) . In addition, value 4 comes next place having index 1. Index 1 points the second element in the overflow list, S_1 again. Value 4 points the fifth element in the underflow list, namely, S_5 , resulting in the relocation pair of (S_1, S_5) . As such, an integer vector can be mapped to a relocation plan and 3 examples are shown in Fig. 1c.

This encoding scheme makes the EV relocation procedure equivalent to a well-known Traveling Salesman Problem (TSP). Its genetic algorithm solver begins with initial population consisting of specific number of feasible solutions, each of which is a permutation of numbers from 0 to $m - 1$, where m is the number of relocation pairs [6]. Figure 1c shows 3 examples of them and each one has its own cost value determined by the total relocation distance. Then, genetic loops iterates with selection, reproduction, and mutation operations until a given time bound comes or a reasonable quality relocation plan is obtained. Here, by a simple reproduction, some genes are highly likely to appear more than once in a chromosome. To overcome this problem, we implement a modified reproduction. After generating a new chromosome from two parents, the controller invalidates duplicated elements from the vector, replacing it with disappearing ones.

3 Experiment Result

We have implemented a prototype of the proposed relocation scheme using the C programming language for the assessment purpose. Five stations are placed as described as in our previous work [8]. According to the number of EVs, which ranges from 25 to 200, the end-of-day distribution is generated for each simulation day from the analysis framework [7]. This distribution corresponds to $C:\{C_1, C_2, \dots, C_n\}$. The distributions of about 1.5 months are fed to our relocation scheme one by one. Target distribution is selected by even, utilization-based, and morning-focused scheme, respectively. Then, our solver creates the relocation plan for each day by means of the genetic algorithm-based relocation scheme. For a relocation plan, this section measures the relocation distance.

The first experiment measures the effect of population size for 3 strategies. Here, the number of EVs is set to 200 and the number of iteration to 500. Three curves rarely change for the given range of population size, as the proposed scheme finds an efficient solution in the early stage of iterations, as shown in Fig. 2. In the even strategy, gradual reduction of relocation distance is detected, even the amount is not so much, less than 1 km. In the utilization-based strategy, the relocation distance remains unchanged after the population size of 30. The next experiment measures the effect of number of iterations in the genetic algorithm. Here, the population size is set to 50, while the number of iterations ranges from 100 to 1,000. The performance graph of Fig. 3 is quite similar to that of Fig. 2. These results indicate that the effect of genetic parameters is not so significant, as the number of stations is not large.

Figure 4 plots the effect of number of EVs to the relocation distance. Here, the population size is set to 50 and the number of iterations to 500. The experiment changes the number of EVs from 50 to 200. For the even strategy, the relocation distance almost linearly increases according to the increase in the number of EVs, and thus the number of moves. On the contrary, the utilization-based and morning-focuses strategies prevent the relocation distance from sharply increasing as in the even strategy. For more than 125 EVs, the morning-focused strategy better benefits from the genetic algorithm implementation.

Finally, Fig. 5 plots the probability distribution of the number of moves for each scheme to catch the insight of the vector length. As shown in the figure, the even strategy has much more moves around 50 and reaches almost 125. The utilization-based strategy has a peak around 20 and reaches 87 at maximum. The morning-focused strategy has many relocation plans having less than 5 moves due to the symmetric traffic patterns in urban area. After all, the utilization-based strategy seems to have more EVs to relocate, but shows the almost same relocation distance as the morning-focused strategy. Any other relocation strategies can be easily combined with our relocation procedure.

Fig. 2 Population size effect

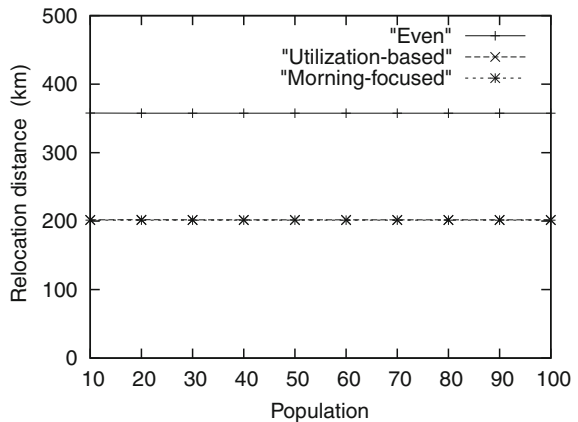


Fig. 3 Iteration effect

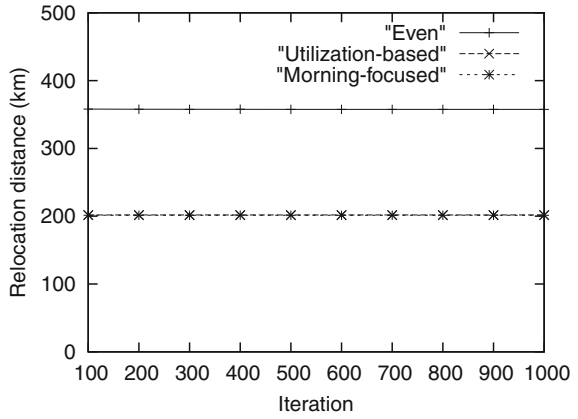


Fig. 4 Effect of number of EVs

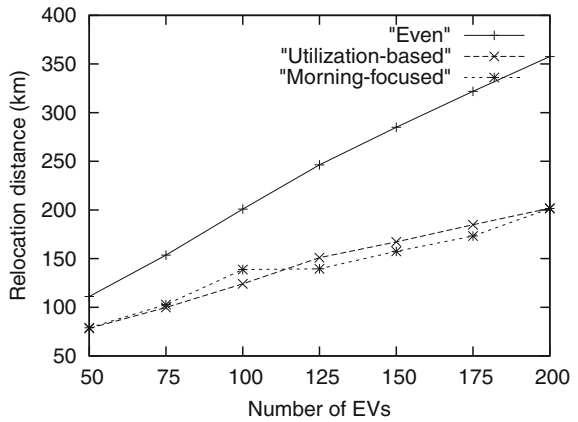
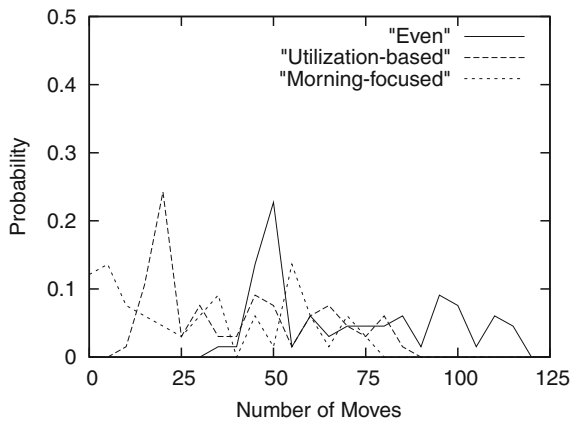


Fig. 5 Policy effect



4 Conclusions

EVs are the key element of future transportation systems pursuing energy efficiency, while the EV sharing system is a prospective business model capable of coping with their high cost. To build a relocation plan using genetic algorithms, each relocation plan is encoded to an integer-valued vector, based on two indexes, one for the overflow list, and the other for the underflow list. In each list, stations are bound to specific locations according to the number of surplus or needed vehicles. For a vector element, its location is the overflow station index, while the value is the underflow index. According to the performance measurement results obtained from a prototype implementation and actual traffic pattern in Jeju city, our relocation scheme can find an efficient relocation plan in the early stage of genetic iterations even with small population size. After all, this scheme can alleviate the stock imbalance problem and improve the serviceability of EV sharing systems.

References

1. Ipakchi A, Albuyeh F (2009) Grid of the future. *IEEE Power Energy Mag* 7(2):52–62
2. Cepolina E, Farina A (2012) A new shared vehicle system for urban areas. *Transp Res Part C* 230–243
3. Correia G, Antunes A (2012) Optimization approach to depot location and trip selection in one-way carsharing systems. *Transp Res Part E* 48(1):233–247
4. Kek A, Cheu R, Meng Q, Fung C (2009) A decision support system for vehicle relocation operations in carsharing systems. *Transp Res Part E* 45:149–158
5. Weikl S, Bogenberger K (2012) Relocation strategies and algorithms for free-floating car sharing systems. In: *IEEE conference on intelligent transportation systems*, 355–360
6. Giardini G, Kalmar-Nagy T (2011) Genetic algorithm for combinational path planning: the subtour problem. *Mathematical Problems in Engineering*
7. Lee J, Kim H, Park G, Kwak H, Lee M (2012) Analysis framework for electric vehicle sharing systems using vehicle movement data stream. In: Wang H et al (eds) *APWeb 2012, LNCS*, vol 7234. Springer, Heidelberg, pp 89–94
8. Lee J, Kim H, Park G (2012) Relocation action planning in electric vehicle sharing systems. In: Sombattheera C et al (eds) *MIWAI 2012, LNCS*, vol 7694. Springer, Heidelberg, pp 47–56

Improvement of Wireless LAN Connectivity by Optimizing Placement of Wireless Access Points

Taiki Honda and Makoto Ikeda

Abstract By rapid evolution of information terminals, such as tablets and smart phones, people having multiple wireless communication terminals are expected to increase the information access and traffic amount. In public facilities, hot spots, and university campuses, the coverage area of the wireless Access Points (APs) is limited because of high cost. Therefore, it is difficult to provide stable network connectivity. In this paper, we focus on measurement of the coverage in our university campus. Using network simulation, we measured field strength and throughput for wireless APs. We optimized AP placement and improved the connectivity in our campus.

1 Introduction

In recent years, with the spread of mobile terminals such as smart phone and tablet PCs, connecting to wireless networks quickly and easily has significantly increased. Free wireless Access Points (AP) available have appeared in various facilities such as airports, shopping mall, university campuses. Location of the wireless APs will affect the quality of the communication, which is determined by measuring the field strength and throughput using different instruments. In general, it is difficult to provide stable network service and find dead spots in Wi-Fi networks [1]. Also, it is difficult to cover the university campus by wireless AP for

T. Honda

Graduate School of Engineering, Fukuoka Institute of Technology (FIT),
3-30-1 Wajiro-Higashi, Higashi-Ku, Fukuoka 811-0295, Japan
e-mail: taiki.hnd@gmail.com

M. Ikeda (✉)

Department of Information and Communication Engineering, Fukuoka Institute of
Technology (FIT), 3-30-1 Wajiro-Higashi, Higashi-Ku, Higashi-Ku 811-0295, Japan
e-mail: makoto.ikd@acm.org

wide range communication and complicated applications [2]. Until now, many researchers performed valuable research in the area of wireless networks by computer simulations, as in general, a simulator can give a quick and inexpensive understanding of protocols and algorithms. Most of them are focused on connectively improvement and optimal replacement considering two-dimensional space.

In [3], the authors proposed a method of optimize the AP placement with Genetic Algorithm (GA). They consider the location of antenna, as well as the transmission power and frequency channels. In addition, the authors of [4] have conducted a study by placing additional wireless AP using a heuristic algorithm in Wireless Distribution System (WDS), to reduce the number of hops between wireless APs.

In this paper, we focus on measurement of the wireless coverage in our university campus. Using QualNet network simulator [5], we measured field strength and throughput for wireless APs. We optimized AP placement and improved the connectivity in our campus. The rest of the paper is organized as follows. The overview of wireless LAN technologies are described in Sect. 2. The simulation settings are explained in Sect. 3. The simulation results are presented in Sect. 4, followed by the conclusion in Sect. 5.

2 Wireless LAN

Wireless Local Area Network (WLAN) has been developed as one of the solutions to avoid the inconvenience of cable rewire due to the changes in the layout of facilities. In the period of the mainstream desktop PC, users were almost static when accessing the Internet. However, by the appearance of tablet PCs and laptops, the number of users which are not able to choose the time and place to access the Internet has increased. In this way, WLAN has made significant progress toward the development of the hardware technologies. Nowadays, WLAN has become popular for home users, due to ease of installation and use.

Most modern WLANs are based on IEEE 802.11 standards, marketed under the Wi-Fi brand name [6]. WLANs have a great deal of applications. Modern implementations of WLANs range from small in-home networks to large campus-sized ones or large mobile networks on aircraft and trains. Users can also access the Internet from WLAN hotspots in restaurants and hotels, with portable devices that connect to 3G or 4G networks.

The Wi-Fi Passpoint [7] is now the focus of public attention. Wi-Fi certified Passpoint assures simple and secure connection to public Wi-Fi hotspots for off-loading cellular data, ensuring lower overall total cost of ownership (TCO). There are three technology pillars to Passpoint: IEEE 802.11u [8], WPA2-Enterprise and EAP-based authentication [9].

The next generation standard of IEEE 802.11vht (ac/ad) have been de-veloped [10]. It is an extension to the 802.11 family of protocols also known as Wi-Fi.

It allows for multi-user MIMO and 256-QAM (Quadrature Amplitude Modulation), at 5 GHz and can go up to 1.3 Gbps (physical rate) with 3 streams and a theoretical maximum throughput of 7 Gbps (8×8 MIMO with 160 MHz channel width) [11].

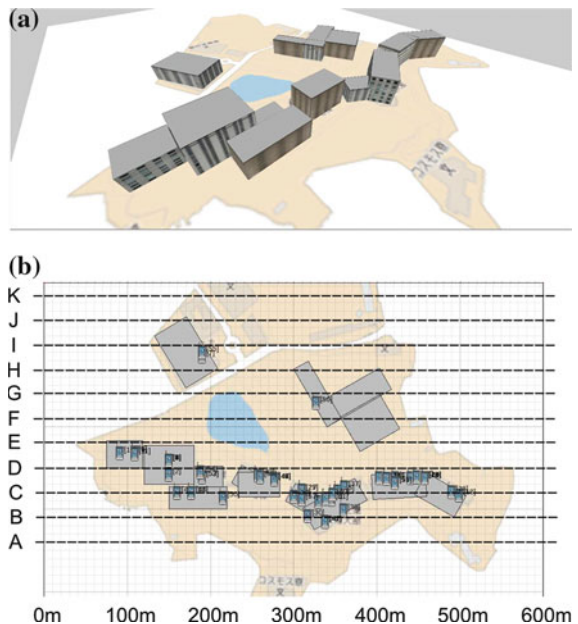
In this way, WLAN technology has become an important technology offering large capacity contents. However, the performance of WLAN communication changes regarding the position of wireless APs. For this reason, AP placement is a very important factor, which has also become one of the issues to improve the wireless connectivity.

3 Simulation Setting

In Fig. 1, is shown the placement of the Aps actually being used by our university. Our simulations are conducted in the area shown in Fig. 1b. In our simulation scenario the client moves horizontally through lines A to K. The client communicates with the destination via wireless APs. We in investigate whether the mobile client on each line can connect to Aps. we evaluated the performance considering connection rate (Conn rate). throughput (Thr), packet loss (Pkt loss), received power (Rx power) and number of dead spots (DSs).

We defines a DS a point where the number of sent packets and the number of lost packets is the same, meaning that no packet reached the destination. Otherwise, the connection to AP is possible. After analyzing the simulation data, we

Fig. 1 Simulation scenarios.
a Three-dimensional model of our campus.
b Measurement environment



focus on the improvement of the coverage for campus area, by repositioning wireless Aps.

The simulation input, constraint condition and the output are as follows.

1. Goal
 - (a) Minimizing the number of dead spots.
2. Input parameters
 - (a) Field information.
 - (b) Location information of each wireless AP.
 - (c) Upper limit value of client radio transmission range (RH_{\max}).
3. Constraint condition
 - (a) Prohibited area for wireless AP placement.
 - (b) Clients can connect to any wireless AP in one session.
 - (c) Wireless AP can be placed indoor only.
4. Output
 - (a) Connection rate, throughput, packet loss, received power and number of dead spots.

4 Simulation

4.1 Simulation Description

We evaluated by simulation the network performance of WLAN environment that our university is currently providing. Simulations are carried out moving in linear lines from 0 to 600 m, as shown in Fig. 1b. We do not consider the space outside of the university campus (white space in Fig. 1) to analyze the network performance. Other simulation parameters are shown in Table 1. Wireless AP has Layer 3 (L3) roaming capabilities. In this case, mobile clients move from one AP to another within university network. They decide to re-associate with an AP, which have a stronger wireless signal. However, they may loose connection with the actual AP before associating with another AP. In this paper, a mobile client is considered to be a laptop PC or a smart phone that communicates via wireless AP.

4.2 Simulation Results

In Table 2, we show the simulation results for each evaluation metric for the actual APs placement. We considered lines from A to E, which cover the area of the main buildings where students and staff often use. The connection rate can be calculated

Table 1 Simulation parameters

Parameter	Value
Simulation time	600 [S]
Scenario dimensions (X, Y)	600 [m] × 800 [m]
Number of APs	59
Roaming	Enable
Beacon interval	200 [TUs]
Application	CBR (8000 [bytes], 125 [pps])
Propagation limit	−111.0 [dBm]
Radio type	IEEE802.11 g
Transmission power	20 [dBm]
Receive sensitivity	−85 [dB]
Antenna model	Ommidirectional
Antenna gain	−11.5 [dBm]

as $n(1)/N \times 100$, where $n(1)$ is the number of points where the client is not able to connect to at least one AP. While, $n(0)$ is the number of points where the client can not connect to any AP. A DS is a measuring point inside each line where no packet can be delivered to destination. Therefore, the total number of measuring data N on each line can be calculated by $n(0) + n(1)$. Each line has 600 measuring points (every 1 m), but we did not consider some points, which are located outside of university campus. From the results, we can see that there are many DSs in lines B, D and E.

In Fig. 2, we show the Rx power and throughput results for actual placement of APs, in order to understand the locations where there is no connectivity in points inside campus. We found that the actual APs placement can not cover the D line which is around buildings, especially cannot cover hot-spot areas where students often stay or move during break times. Most of packets have been dropped in outdoor areas. Also, we see that there are many DSs in outdoor areas, as shown in Fig. 2a–e. After, analyzing the results from the actual placement of APs, we tried to improve the wireless coverage by repositioning the APs.

In fact, the actual placement of APs is intended to mostly cover the indoor environment. However, the AP transmission radius is at least 40 m, so it is able to cover the area inside the classrooms. In order to increase the coverage of the outdoor areas, we relocated the APs in places by the windows inside classrooms and the antenna directivity moved outside of the buildings.

Table 2 Mean results of actual placement

Line id	Conn. rate [%]	Thr [Mbps]	Pkt loss [pkt]	Rx power [dBm]	No. of DSs
A	95.62	7.48	8.13	−70.21	12
B	44.60	3.55	69.56	−71.19	236
C	96.98	7.70	4.67	−66.87	13
D	16.59	1.92	95.04	−73.87	372
E	23.91	1.31	104.51	−74.11	385

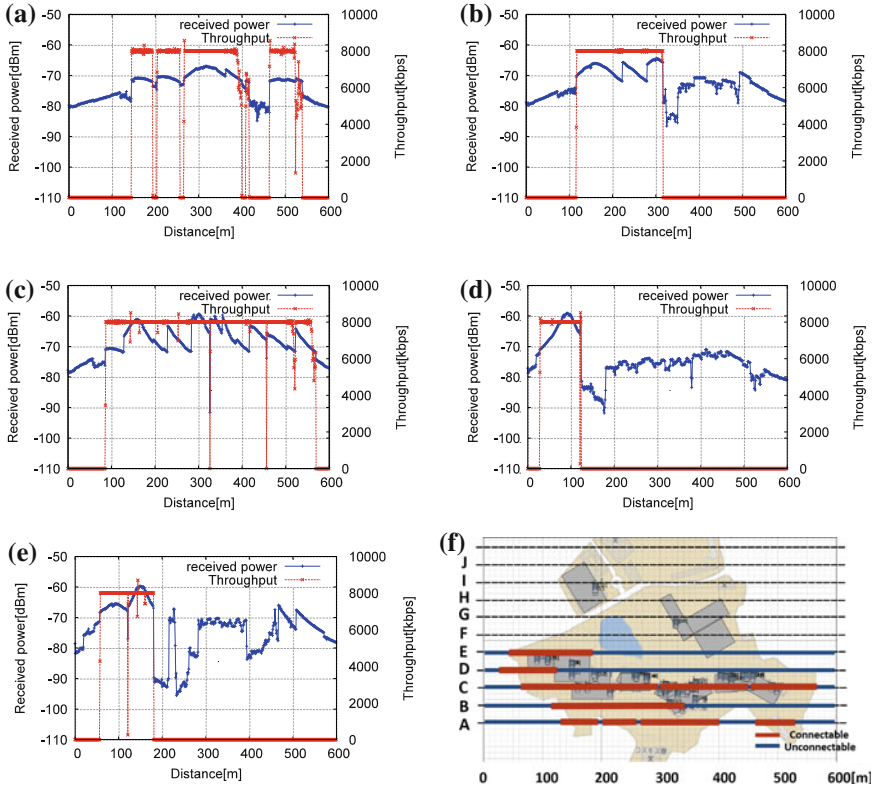


Fig. 2 Results of actual placement. **a** Line A. **b** Line B. **c** Line C. **d** Line D. **e** Line E. **f** Coverage area

Table 3 Mean results of optimized replacement

Line id	Conn.rate [%]	Thr [Mbps]	Pkt loss [pkt]	Rx power [dBm]	No. of DSs
A	95.62	7.45	9.05	-78.23	12
B	98.82	7.94	1.35	-67.74	5
C	97.72	7.95	0.94	-66.67	2
D	99.97	7.94	1.04	-67.21	1
E	33.79	2.67	83.29	-71.68	335

After the repositioning we measured the same area again. We show the results in Table 3 and Fig. 3. The number of DSs has decreased noticeably, as shown in Table 3. In Fig. 3, we can also notice an improvement in the Rx power and throughput results for optimized replacement.

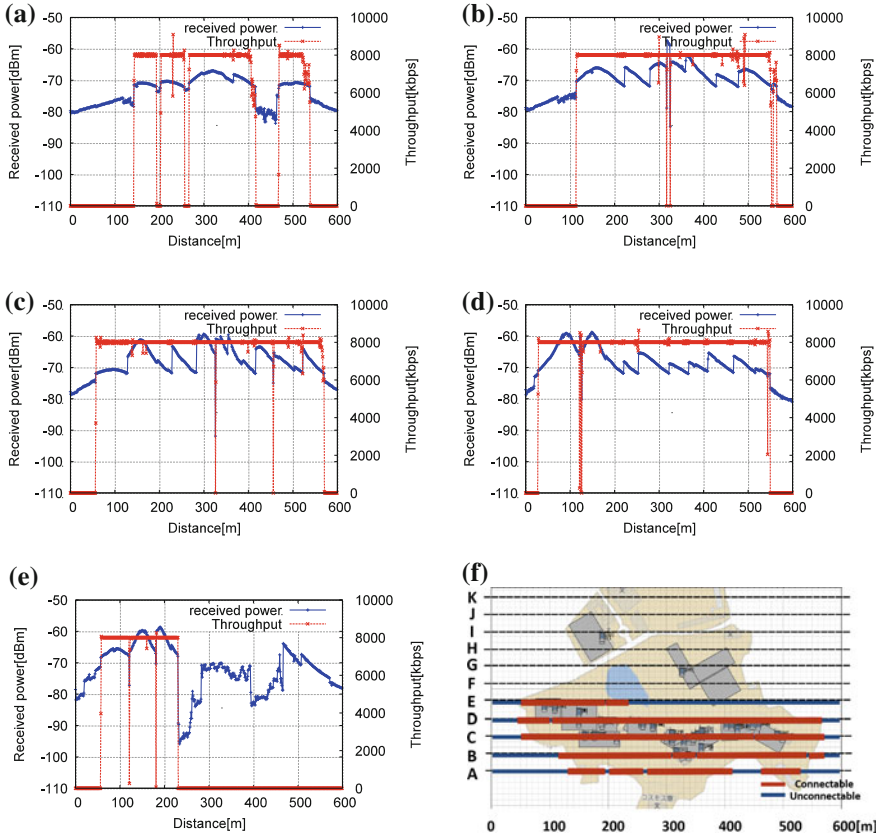


Fig. 3 Results of optimized replacement. **a** Line A. **b** Line B. **c** Line C. **d** Line D. **e** Line E. **f** Coverage area

5 Conclusions

In this paper, we focused on measurement of the wireless coverage in our university campus. Using QualNet network simulator, we measured different metrics considering three-dimensional space for replacement of wireless APs. Based on simulation results, we proposed the rules for optimization of AP placement, in order to improve the connectivity in our university campus.

For actual AP placement, we found out that most of packets have been dropped in outdoor areas and the number of DSs was high. After AP replacement, the network performance improved in terms of wireless coverage. We also noticed an improvement of Rx power and throughput in all areas of our university campus.

In our future work, we would like to extend our simulation system and propose a standard method for optimizing AP placement, to adapt to various public facilities. In addition, we will investigate the campus site survey and improve its accuracy.

Acknowledgments This work is supported by a Grant-in-Aid for scientific research of Japan Society for the Promotion of Science (JSPS). The authors would like to thanks for the financial support.

References

1. Motomura S, Kimoto M, Ohno K (2011) Improved utilization of wireless LAN by planning the placement of wireless access points [in Japanese]. *J Acad Comput Networking* 15:40–45
2. Kamenetskyt M, Unbehau M (2007) Coverage planning for outdoor wireless LAN systems. In: Proceedings of international Zurich seminar on broadband communications, Access-transmission-networking, 49:1–49:6
3. Vanhatupa T, Hannikainen M, Hamalainen TD (2007) Genetic algorithm to optimize node placement and configuration for WLAN planning. In: Proceedings of 4th international symposium on wireless communication systems, 612–616
4. Nomura Y, Funabiki N, Nakanishi T (2005) An improvement of an access-point location algorithm for wireless LAN, IEICE technical report, NS2005-73, 49–52
5. QualNet, <http://www4.kke.co.jp/network/qualnet/>
6. Wi-Fi Alliane’s web page, <http://www.wi-fi.org/discover-and-learn>
7. Wi-Fi Alliance, Wi-Fi CERTIFIED Passpoint (2012) A new program from the Wi-Fi alliance to enable seamless Wi-Fi access in hotspots. <http://www.wi-fi.org/discover-and-learn/wi-fi-certified-passpoint%E2%84%A2>
8. The IEEE Standard 802.11u (2011) IEEE, 1–190
9. Aboba B, Blunk L, Vollbrecht J, Carlson J, Levkowitz H (2004) Extensible authentication protocol (EAP), RFC 3748 (Proposed standard), updated by 5247
10. Vaughan-Nichols SJ (2010) Gigabit Wi-Fi Is on its way. *IEEE J Mag* 43(11):11–14
11. Cordeiro C, Akhmetov D, Park M (2010) IEEE 802.11ad: introduction and performance evaluation of the first multi-Gbps wifi technology: In Proceedings of ACM international workshop on mmWave communications, 3–7

Performance Comparison of OLSR and AODV Protocols in a VANET Crossroad Scenario

Evjola Spaho, Makoto Ikeda, Leonard Barolli and Fatos Xhafa

Abstract In this work, we evaluate the performance of OLSR and AODV protocols in a VANET crossroad scenario. As evaluation metrics, we use Packet Delivery Ratio (PDR), Throughput and Delay. We analyse the performance of the network by sending Constant Bit Rate (CBR) traffic and considering different number of connections. The simulation results show that when the number of connections is high, OLSR performs better than AODV protocol in this VANET scenario.

Keywords VANETs · Routing protocols · OLSR · AODV

1 Introduction

Vehicular Ad-hoc networks (VANETs) are a special type of Ad-hoc networks that can be utilized for road safety, comfort, entertainment and make new forms of inter-vehicle communications. Due to the high cost of deploying and implementing

E. Spaho (✉)

Graduate School of Engineering, Fukuoka Institute of Technology (FIT), 3-30-1 Wajiro-Higashi, Higashi-Ku, Fukuoka 811-0295, Japan
e-mail: evjolaspaho@hotmail.com

M. Ikeda · L. Barolli

Department of Information and Communication Engineering, Fukuoka Institute of Technology (FIT), 3-30-1 Wajiro-Higashi, Higashi-Ku, Fukuoka 811-0295, Japan
e-mail: makoto.ikd@acm.org

L. Barolli

e-mail: barolli@fit.ac.jp

F. Xhafa

Technical University of Catalonia, Department of Languages and Informatics Systems, C/Jordi Girona 1-3 08034 Barcelona, Spain
e-mail: fatos@lsi.upc.edu

VANET systems in a real environment, most of research is concentrated on simulations.

In the recent years, a lot of simulators for VANETs have been emerging [1]. For example, the IMPORTANT framework has been one of the first attempt to understand the dependence between vehicular traffic and communication performance [2, 3]. The authors analyzed the impact of the node mobility on the duration of communication paths.

In [4], the authors present a simulator written in Java, which can generate mobility traces in several formats. There are also other powerful traffic simulators, like TranSim [5], which makes use of a cellular automaton for simulating the interaction of vehicles. Also, SUMO is another powerful traffic simulator, intended for traffic planning and road design optimization. There is an attempt to interface SUMO with NS2 [6].

In this regard, we used a lightweight simulator called Cellular Automaton based Vehicular NETWORK (CAVENET) [7] which can be used to understand the properties of the mobility models of vehicular traffic and their impact on the performance of VANETs and interface it with NS3 to evaluate the performance of routing.

CAVENET vehicular mobility model is a microscopic model. The core of the simulator is 1-dimensional CA (Cellular Automaton) model, which has been first studied by Nagel and Schreckenberg (NaS) [8] in a stochastic setting. The CA is a discrete time model of the vehicle traffic.

Since VANETs are a specific class of ad-hoc networks, the commonly used ad-hoc routing protocols initially implemented for MANETs have been tested and evaluated for VANET environments. VANETs share some common characteristics with MANETs. They are both characterized by the movement and self-organization of the nodes. We consider the possibility of using ad-hoc and MANET protocols for VANET scenarios.

In our previous work [9], we evaluated the performance of three routing protocols: Ad-hoc On-demand Distance Vector (AODV) [10], Optimized Link State Routing (OLSR) [11] and Dynamic MANET On Demand (DYMO), using NS2 simulator.

In this work, we use NS3 to evaluate and compare the performance of two routing protocols (OLSR and AODV) in a VANET crossroad scenario.

The rest of the paper is structured as follows. In Sect.2, we briefly describe OLSR and AODV protocols. The simulation system design and description is presented in Sect.3. In Sect.4, we show the simulation results. Finally, the conclusions and future work are presented in Sect.5.

2 Routing Protocols

For our performance comparison study, we choose two ad hoc routing protocols OLSR and AODV. We will shortly describe these protocols in following.

2.1 OLSR Protocol

The OLSR protocol [11] is a pro-active routing protocol, which builds up a route for data transmission by maintaining a routing table inside every node of the network. The routing table is computed upon the knowledge of topology information, which is exchanged by means of Topology Control (TC) packets. OLSR makes use of HELLO messages to find its one hop neighbours and its two hop neighbours through their responses. The sender can then select its Multi Point Relays (MPR) based on the one hop node which offer the best routes to the two hop nodes. By this way, the amount of control traffic can be reduced. Each node has also an MPR selector set which enumerates nodes that have selected it as an MPR node. OLSR uses TC messages along with MPR forwarding to disseminate neighbour information throughout the network. Host Network Address (HNA) messages are used by OLSR to disseminate network route advertisements in the same way TC messages advertise host routes.

2.2 AODV Protocol

The AODV is an improvement of DSDV [13] to on-demand scheme. It minimizes the broadcast packet by creating route only when needed. Every node in network maintains the route information table and participate in routing table exchange. When source node wants to send data to the destination node, it first initiates route discovery process. In this process, source node broadcasts Route Request (RREQ) packet to its neighbours. Neighbour nodes which receive RREQ forward the packets to its neighbour nodes. This process continues until RREQ reach to the destination or the node who know the path to destination.

When the intermediate nodes receive RREQ, they record in their tables the address of neighbours, thereby establishing a reverse path. When the node which knows the path to destination or destination node itself receives RREQ, it sends back Route Reply (RREP) packet to source node. This RREP packet is transmitted by using reverse path. When the source node receives RREP packet, it can know the path to destination node and it stores the discovered path information in its route table. This is the end of route discovery process. Then, AODV performs route maintenance process. In route maintenance process, each node periodically transmits a Hello message to detect link breakage.

3 Simulation System Design and Description

3.1 Simulation System Structure

The simulation system structure is shown in Fig. 1. The behavioural analyzer block (CAVENET), generates the movement pattern of the vehicles that is used then by the communication protocol analyzer (NS3 simulator).

The detailed simulation model is based on NS-3 (ver-3.14.1) [15]. The NS3 simulator is developed and distributed completely in the C++ programming language, because it better facilitated the inclusion of C-based implementation code. The NS3 architecture is similar to Linux computers, with internal interface and application interfaces such as network interfaces, device drivers and sockets.

The goals of NS3 are set very high: to create a new network simulator aligned with modern research needs and develop it in an open source community. Users of NS3 are free to write their simulation scripts as either C++ main() programs or Python programs. The NS3 s low-level API is oriented towards the power-user but more accessible “helper” APIs are overlaid on top of the low-level API.

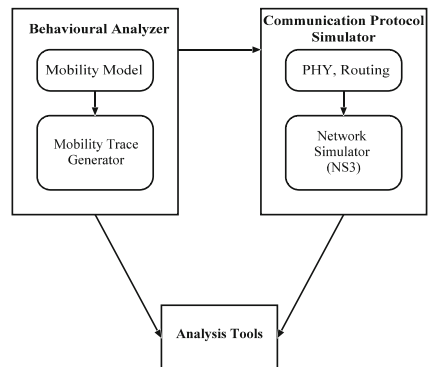
In order to achieve scalability of a very large number of simulated network elements, the NS3 simulation tools also support distributed simulation. The NS3 support standardized output formats for trace data, such as the pcap format used by network packet analyzing tools such as tcpdump, and a standardized input format such as importing mobility trace files from NS2 [14].

The NS3 simulator has models for all network elements that comprise a computer network. For example, network devices represent the physical device that connects a node to the communication channel. This might be a simple Ethernet network interface card or a more complex wireless IEEE 802.11 device.

In our simulations we used IEEE 802.11p standard and TwoRayGround PropagationLossModel.

IEEE 802.11p: Is an approved amendment to the IEEE 802.11 standard to add Wireless Access in Vehicular Environments (WAVE). It defines enhancements to

Fig. 1 Simulation system structure



802.11 required to support Intelligent Transportation Systems (ITS) applications. The 802.11p standard is based on the 802.11 architecture, but version “p” is aimed at communications between vehicles and between them and fixed infrastructure. This new technology uses the 5.9 GHz band in various propagation environments: vehicle, open, urban, and so on. This standard defines the WAVE as the signalling technique and interface functions that are controlled by the physical layer (MAC) devices where the physical layer properties change rapidly and where the exchanges of information have a short duration. The purpose of this standard is to provide a set of specifications to ensure interoperability between wireless devices trying to communicate in rapidly changing environments and in particular time periods.

TwoRayGroundPropagationLossModel: It considers the direct path and a ground reflection path. The received power at distance t is calculated with the following equation:

$$Pr(d) = PtGtGrht^2hr^2/d^4L.$$

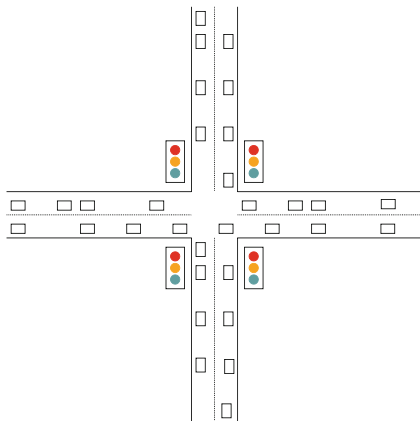
where ht and hr are the heights of the transmit and receive antennas.

Simulation Environment: The simulations are carried out in Ubuntu 11.10.

Traffic Model: Constant bit rate (CBR) traffic sources and 512-byte data packets are used. Other simulation parameters are shown in Table 1.

Table 1 Simulation parameters

Network simulator	NS3
Routing protocols	OLSR, AODV
Simulation time	50 s
Simulation area	200 m x 200 m
Simulation scenario	Crossroad
Number of nodes	32
Max speed (km/h)	135
Incidence of decelerating	30 %
Traffic source/destination	Deterministic
DATA TYPE	CBR
Packet size	512 bytes
MAC protocol	IEEE802.11 p
MAC rate	2 Mbps
RTS/CTS	None
Transmission range	250 m
Radio propagation model	TwoRayGround
Network simulation time	5–45 s

Fig. 2 Simulation scenario

3.2 Implementation of a Crossroad Scenario with CAVENET and Simulation Description

In this work, we consider a two lane crossroad scenario (see Fig. 2). During the simulations, 32 vehicles move in roads according to CA model and respecting the traffic light. Vehicles are randomly positioned at the beginning of the intersection.

The maximum speed of the vehicles is 135 km/h. The vehicles accelerate and decelerate according to CA model. The incidence of decelerating is considered 30 %. The vehicles follow each other and when a vehicle reaches at the end of the road it is shifted at the beginning of the same road. When a vehicle goes near the intersection, it checks for the state of the traffic light. The traffic lights change the state in a constant time period. If the traffic light is red, it decelerates and stop. If the traffic light is green it reduce the speed and enter to the intersection.

The cars in front of the crossroad and in the junction will have a speed of 27 km/h (minimal).

For simulations, we used OLSR and AODV protocols and sent multiple CBR flows over UDP. Different number of connections are created and the same pairs source–destination are used for both protocols. The simulation time is 50 s.

4 Simulation Results

We present here some simulation results for OLSR and AODV protocols done by means of CAVENET and NS3. For performance evaluation, we use three metrics: the average PDR, throughput and delay. We carried out simulations for 2, 4, 6, 8, 10, 12 and 14 connections in the network. The CBR data sent in one connection during all simulation time is 256 kbps. Based on the number of connections, the total rate transmitted in the network changes.

Fig. 3 Simulation results for PDR

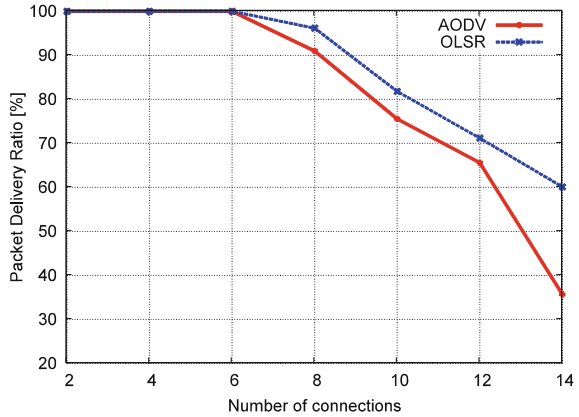
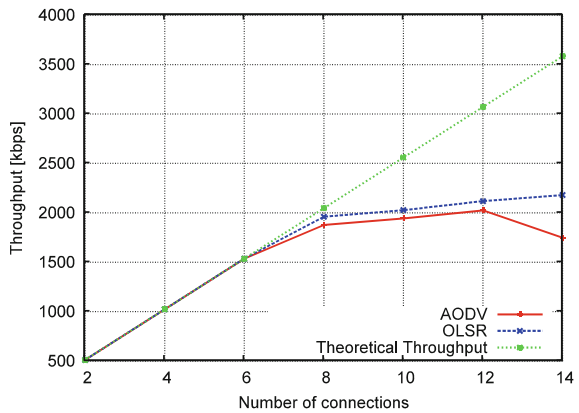


Fig. 4 Simulation results for throughput

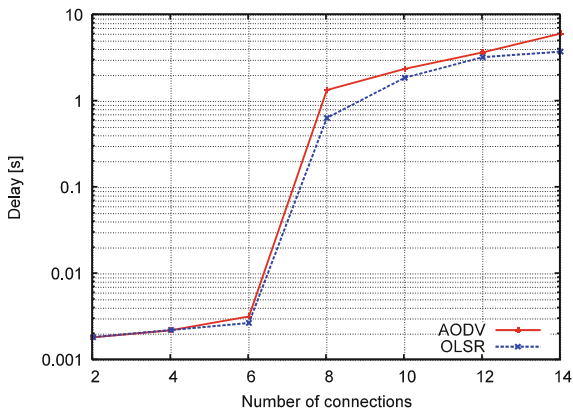


In Fig. 3 are shown the simulation results of number of connections vs. PDR for OLSR and AODV protocols. For less than 6 connections in the network, both protocols have a maximal PDR and a very good performance. For number of connection from 6 to 12 connections, because of the amount of data sent in the network is increased, the PDR for both protocols is decreased (however it is higher than 65 % for both protocols). In this case, OLSR protocol has better PDR. For 14 connections in the network, the information sent between the pairs source–destination is very high and a lot of packets are dropped. The PDR of AODV is highly decreased compared with OLSR.

In Fig. 4 are shown the simulation results of number of connection vs. throughput. When the number of connections in the network is less than 6, PDR is maximal and the throughput is theoretical. For number of connections between 6 and 12, the throughput is slowly increased for both protocols.

For number of connections 14, the throughput of OLSR continues to increase slowly but the throughput of AODV is decreased.

Fig. 5 Simulation results for delay



The simulation results for number of connection vs. delay are shown in Fig. 5. For number of connections less than 8, the delay for both protocols is less than 1 s and they can be both used for real time applications, but after 8 connections, delay is high.

5 Conclusions

In this work, we evaluated the performance of OLSR and AODV routing protocols in a VANET crossroad scenario considering PDR, throughput and delay as evaluation metrics. We used CAVENET to generate the movement of the vehicles and NS3 to test the performance of routing protocols. For simulations, we considered different number of connections in the network, sent multiple CBR flows over UDP and use IEEE 802.11p standard and TwoRayGroundPropagationLossModel.

From the simulation results, we conclude as follows.

- For small number of connections in the network, both protocols have a very good performance with maximal PDR, theoretical throughput and a very small delay.
- For average number of connection in the network, the performance of both protocols is decreased, but PDR is higher than 65 %. In this case, OLSR performs better than AODV.
- For big number of connections in the network, the amount of data sent in the network is very high, the network is congested, many packets are dropped and the delay is increased. In this case, the PDR and throughput of OLSR are higher than AODV.

In the future, we plan to extend our work for different radio propagation models and environments [16]. We also would like to consider other parameters for evaluation such as routing overhead, traffic quantity and topology change.

Acknowledgments This work was supported by Japanese Society for the Promotion of Science (JSPS). The authors would like to thank JSPS for the financial support.

References

1. Harri J, Filali F, Bonnet C (2009) Mobility models for vehicular ad hoc networks: a survey and taxonomy. *IEEE Commun Surv Tuto* 11(4):19–41
2. Bai F, Sadagopan N, Helmy A (2003) MPORTANT: a framework to systematically analyze the impact of mobility on performance of routing protocols for ad-hoc networks. In: *Proceedings of the IEEE INFOCOM-2003*, Mar–Apr 2003, pp 825–835
3. Sadagopan N, Bai F, Krishnamachari B, Helmy A (2003) PATHS: analysis of path duration statistics and their impact on reactive manet routing protocols. In: *Proceedings of the 4-th ACM international symposium on mobile ad hoc networking and computing (mobihoc 2003)*, pp 245–256
4. Fiore M, Harri J, Filali F, Bonnet C (2007) Vehicular mobility simulation for VANETs. In: *Proceedings of the 40-th annual simulation symposium (ANSS-2007)*, pp 301–309
5. Smith L, Beckan R, Anson R, Nagel K, Williams M (1995) TRANSIMS: transportation analysis and simulation system. In: *Proceedings of the 5-th national transportation planning methods applications conference*, LA-UR 95–1664 Apr 1995
6. Piorkowski M, Raya M, Lugo AL, Grossglauser M, Hubaux JP (2006) Joint traffic and network simulator for VANETs. In: *Proceedings of the mobile and information communication systems conference (MICS-2006)* Oct 2006, Available online at: <http://www.mics.ch/>
7. De Marco G, Tadauchi M, Barolli L (2007) Description and analysis of a toolbox for vehicular networks simulation. In: *Proceedings of the IEEE ICPADS/PMAC-2WVN*, vol 2, pp 1–6
8. Nagel K, Schreckenberg M (1992) A cellular automaton model for freeway traffic. *J Physics I Fr* 2:2221–2229
9. Spaho E, Mino Gj, Barolli L, Xhafa F (2011) Goodput and PDR analysis of AODV, OLSR and DYMO protocols for vehicular networks using CAVENET. *Int J Grid Util Comput (IJGUC)* 2(2): 130–138
10. Perkins C, Belding-Royer E, Das S (2003) Ad hoc on-demand distance vector (aodv) routing. In: *IETF RFC 3561 (Experimental)*
11. Clausen T, Jacquet P (2003) Optimized link state routing protocol (OLSR). In: *IETF RFC 3626*, Oct 2003
12. Sommer C, Dressler F (2007) The DYMO routing protocol in VANET scenarios. In: *Proceedings of the 66-th IEEE vehicular technology conference (VTC2007-Fall)*, pp 16–20
13. Perkins CE, Bhagwat P (1994) Highly dynamic destination-sequenced distance vector routing (dsv) for mobile computers. *ACM* 234–244
14. Information science institute (ISI), Network simulator version 2 (NS-2) <http://www.isi.edu/nsnam>
15. The ns-3 network simulator. <http://www.nsnam.org>
16. Dhoutaut D, R'egis A, Spies F (2006) Impact of radio propagation models in vehicular ad hoc networks simulations. In: *Proceedings of the VANET-2006*, pp 40–49

WMN-GA System for Node Placement in WMNs: Effect of Grid Shape

Tetsuya Oda, Evjola Spaho, Admir Barolli, Leonard Barolli, Fatos Xhafa and Makoto Takizawa

Abstract In WMNs mesh routers provide network connectivity services to mesh client nodes. The good performance and operability of WMNs largely depends on placement of mesh routers nodes in the geographical deployment area to achieve network connectivity, stability and user coverage. In this paper, we evaluate the performance of WMN-GA system for node placement problem in WMNs. For evaluation, we consider Normal, Exponential and Weibull Distribution of mesh clients and different grid size. The simulation results show that the grid size effects in the performance of WMN-GA. The system performs better for Normal distribution.

T. Oda (✉) · E. Spaho

Graduate School of Engineering, Fukuoka Institute of Technology (FIT),
3-30-1 Wajiro-Higashi, Higashi-Ku, Fukuoka 811-0295, Japan
e-mail: oda.tetsuya.fit@gmail.com

E. Spaho

e-mail: evjolaspaho@hotmail.com

A. Barolli

Canadian Institute of Technology, Zayed Center, Rr. Sulejman Delvina,
Tirana, Albania

e-mail: admir.barolli@gmail.com

L. Barolli

Department of Information and Communication Engineering, Fukuoka Institute of
Technology (FIT), 3-30-1, Wajiro-Higashi, Higashi-Ku, Fukuoka 811-0295, Japan
e-mail: barolli@fit.ac.jp

F. Xhafa

Department of Languages and Informatics Systems, Technical University
of Catalonia, C/Jordi Girona 1-3, 08034 Barcelona, Spain

e-mail: fatos@lsi.upc.edu

M. Takizawa

Department of Computers and Information Science, Seikei University,
3-3-1, Kichijoji-Kitamachi, Musashino-Shi, Tokyo 180-8633, Japan

e-mail: makoto.takizawa@computer.org

Keywords Genetic algorithms · Mutation operators · Crossover operators · Size of giant component

1 Introduction

WMNs distinguish for their low cost nature that makes them attractive for providing wireless Internet connectivity. Moreover, such infrastructure can be used to deploy community networks, metropolitan area networks, municipal and, corporate networks.

The main issue of WMNs [1] is to achieve network connectivity and stability as well as QoS in terms of user coverage. This problem is very closely related to the family of node placement problems in WMNs [2–5], among them, the mesh router mesh nodes placement. Here, we consider the version of the mesh router nodes placement problem in which we are given a grid area where to deploy a number of mesh router nodes and a number of mesh client nodes of fixed positions (of an arbitrary distribution) in the grid area. As node placement problems are known to be computationally hard to solve for most of the formulations [6, 7], Genetic Algorithms (GAs) have been recently investigated as effective resolution methods. However, GAs require the user to provide values for a number of parameters and a set of genetic operators to achieve the best GA performance for the problem [8–10].

In this paper, we deal with connectivity in WMN. Because this problem is known to be NP-Hard, we propose and implement a system based on GAs, called WMN-GA. We evaluate the performance of the proposed system considering different grid size scenarios and using giant component and number of covered mesh client metrics. We compare the performance of the system for Normal, Exponential and Weibull Distribution of mesh clients.

The rest of the paper is organized as follows. The mesh router nodes placement problem is defined in Sect. 2. The WMN-GA system and a brief introduction of GAs is presented in Sect. 3. The simulation results are given in Sect. 4. In Sect. 5, we give some conclusions and future work.

2 Mesh Router Node Placement Problem

In this problem, we are given a grid area arranged in cells where to distribute a number of mesh router nodes and a number of mesh client nodes of fixed positions (of an arbitrary distribution) in the grid area. The objective is to find a location assignment for the mesh routers to the cells of the grid area that maximizes the network connectivity and client coverage. Network connectivity is measured by the size of the giant component of the resulting WMN graph, while the user coverage is simply the number of mesh client nodes that fall within the radio coverage of at least one mesh router node. An instance of the problem consists as follows.

- N mesh router nodes, each having its own radio coverage, defining thus a vector of routers.
- An area $W \times H$ where to distribute N mesh routers. Positions of mesh routers are not pre-determined, and are to be computed.
- M client mesh nodes located in arbitrary points of the considered area, defining a matrix of clients.

It should be noted that network connectivity and user coverage are among most important metrics in WMNs and directly affect the network performance.

3 Proposed and Implemented WMN-GA System

GAs have shown their usefulness for the resolution of many computationally hard combinatorial optimization problems. They are, of course, a strong candidate for efficiently solving mesh router nodes placement problem in WMNs. For this reason we implemented a simulation system based on GA to solve the node placement problem in WMNs.

3.1 Genetic Algorithms

For the purpose of this work we have used the template given in Algorithm 1.

Algorithm 1 Genetic Algorithm Template

```

Generate the initial population  $P^0$  of size  $\mu$ ;  $t = 0$ .
Evaluate  $P^0$ ;
while not termination-condition do
  Select the parental pool  $T^t$  of size of size  $A$ ;
   $T^t := \text{Select}(P^t)$ ;
  Perform crossover procedure on pairs of individuals in  $T^t$  with probability  $pc$ ;  $P_c^t := \text{Cross}(T^t)$ ;
  Perform mutation procedure on individuals in  $P_c^t$  with probability  $pm$ ;  $P_m^t := \text{Mutate}(P_c^t)$ ;
  Evaluate  $P_m^t$ ;
  Create a new population  $P^{t+1}$  of size  $\mu$  from individuals in  $P^t$  and/or  $P_m^t$ ;
   $P^{t+1} := \text{Replace}(P^t; P_m^t)$ 
   $t := t + 1$ ;
end while
return Best found individual as solution;

```

As can be seen from the template, several parameters intervene in the GAs: population size, intermediate population size, number of evolution steps, crossover probability, mutation probability and parameters for replacement strategies. On the other hand, there are the (families of) genetic operators: crossover operators, mutation operators, selection operators and replacement operators.

Selection Operators: In the evolutionary computing literature we can find a variety of selection operators, which are in charge of selecting individuals for the

pool mate. Some of these operators are: Random Selection, Best Selection, Linear Ranking Selection, Exponential Ranking Selection, Tournament Selection etc. The operator considered in this work, Exponential Ranking Selection is based on Implicit Fitness Re-mapping technique. It should be noted that selection operators are generic ones and do not depend on the encoding of individuals.

Mutation Operators: In the case of mesh routers node placement, the matrix representation is chosen for the individuals of the population, in order to keep the information on mesh router nodes positions, mesh client positions, links among routers and links among routers and clients. The definition of the mutation operators is therefore specific to matrix-based encoding of the individuals of the population. Some move-based and swap-based operators are SingleMutate, RectangleMutate, SmallMutate, SmallRectangleMutate etc.

Crossover Operators: The crossover operator selects individuals from the parental generation and interchanging their genes, thus new individuals (descendants) are obtained. The aim is to obtain descendants of better quality that will feed the next generation and enable the search to explore new regions of solution space not explored yet.

There exist many types of crossover operators explored in the evolutionary computing literature. It is very important to stress that crossover operators depend on the chromosome representation. This observation is especially important for the mesh router nodes problem, since in our case, instead of having strings we have a grid of nodes located in a certain positions.

3.2 WMN-GA System

In this section, we present WMN-GA system. Our system can generate instances of the problem using different distributions of client and mesh routers.

The GUI interface of WMN-GA is shown in Fig. 1. The left side of the interface shows the GA parameters configuration and on the right side are shown the network configuration parameters.

For the network configuration, we use: distribution, number of clients, number of mesh routers, grid size, radius of transmission distance and the size of subgrid. For the GA parameter configuration, we use: number of independent runs, GA evolution steps, population size, population intermediate size, crossover probability, mutation probability, initial methods, select method.

4 Simulation Results

In this work, we took in consideration different grid size. The number of mesh routers for all the scenario is considered 16 and the number of mesh clients 48. Normal, Exponential and Weibull distribution methods of mesh clients are used.

Fig. 1 GUI tool for WMN-GA system



As selection operator we use Linear Ranking and single mutate as mutation operator. We carried out many simulations to evaluate the performance of WMNs using WMN-GA system.

In Figs. 2, 5 and 8 are shown the simulation results for grid size (8 × Y) for Normal, Exponential and Weibull distribution, respectively. In every simulation, Y is considered 8, 16, 32, 64 and 128. In Fig. 2a are shown the simulation results of the average size of giant component vs. number of generations. As can be seen, the average size of giant component is maximized (all mesh routers are connected with each other) for all grid dimensions. In Fig. 2b, is shown the average number of mesh clients versus the number of generation. For grid size (8 × 8), (8 × 16) and (8 × 32) all mesh routers are covered, but for other dimension of grid size, not all mesh clients are covered. For grid size (8 x 128) because the grid area is big, only 50 % of mesh clients are covered. The simulation results for grid size (32 × Y) are shown in Fig. 3. When the grid size is big (128 × Y), the size of giant component only for the grid size (128 × 128) is not maximal (see Fig. 4). In this scenario, the average number of covered mesh clients is small.

In Fig. 5, are shown the simulation results for Exponential distribution and grid size (8 x Y). As can be seen from Fig. 5a, the average size of giant component is

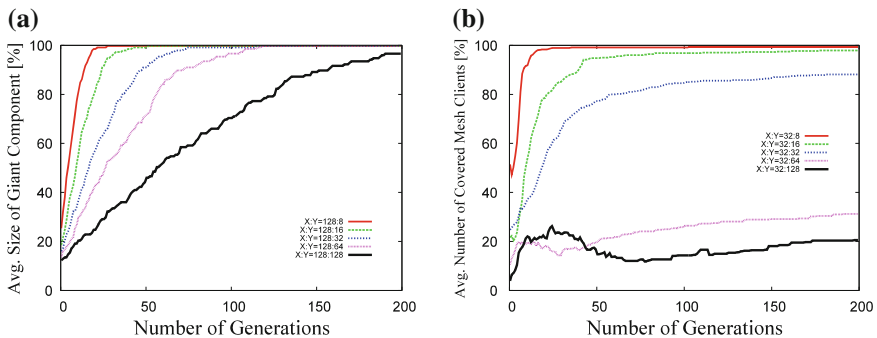


Fig. 2 Simulation results for Normal distribution and grid size (8 × Y). **a** Average size of giant component versus number of generations. **b** Average number of covered mesh clients versus number of generations

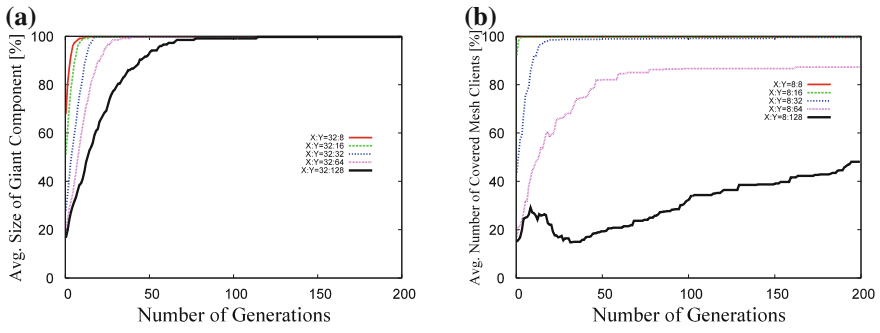


Fig. 3 Simulation results for Normal distribution and grid size (32 × Y). **a** Average size of giant component versus number of generations. **b** Average number of covered mesh clients versus number of generations

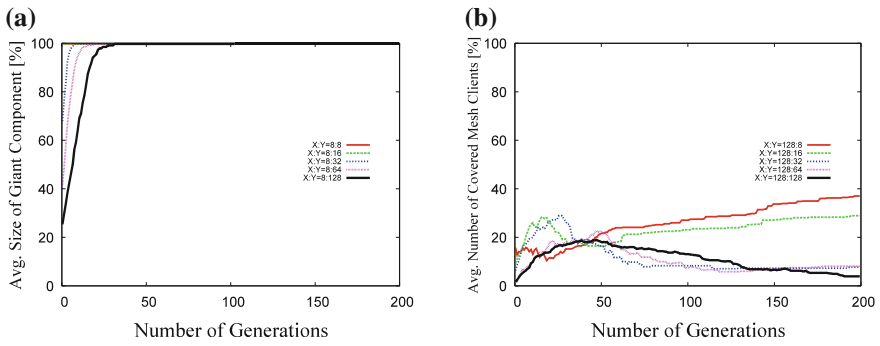


Fig. 4 Simulation results for Normal distribution and grid size (128 × Y). **a** Average size of giant component versus number of generations. **b** Average number of covered mesh clients versus number of generations

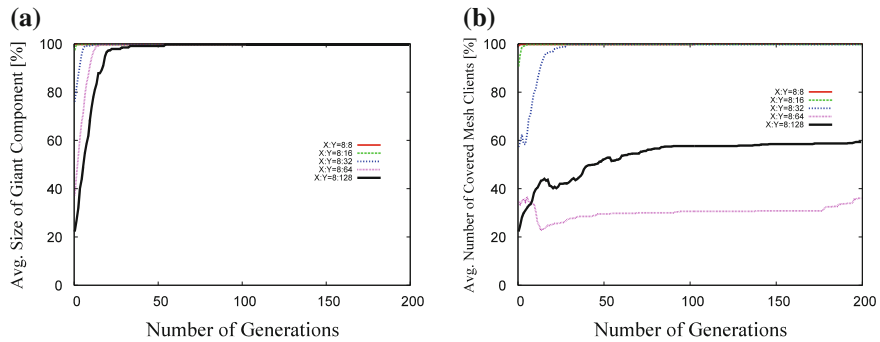


Fig. 5 Simulation results for Exponential distribution and grid size (8 × Y). **a** Average size of giant component versus number of generations. **b** Average number of covered mesh clients versus number of generations

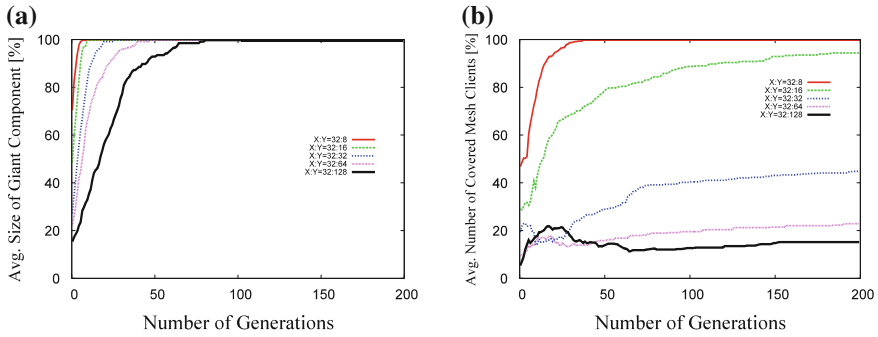


Fig. 6 Simulation results for Exponential distribution and grid size ($32 \times Y$). **a** Average size of giant component versus number of generations. **b** Average number of covered mesh clients versus number of generations

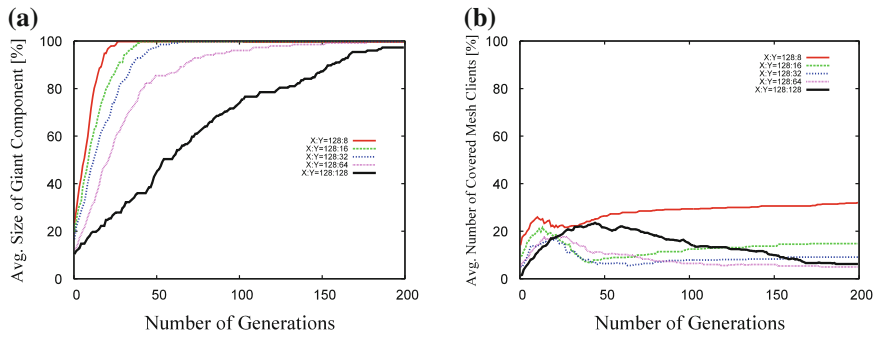


Fig. 7 Simulation results for Exponential distribution and grid size ($128 \times Y$). **a** Average size of giant component versus number of generations. **b** Average number of covered mesh clients versus number of generations

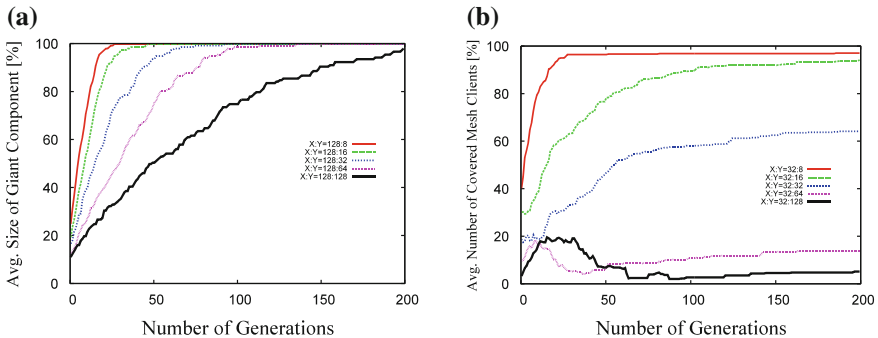


Fig. 8 Simulation results for Weibull distribution and grid size ($8 \times Y$). **a** Average size of giant component versus number of generations. **b** Average number of covered mesh clients versus number of generations

maximized for all grid dimensions. In Fig. 5b, is shown the average number of mesh clients versus the number of generation. From the results, we can see that for grid size (8×8) , (8×16) and (8×32) all mesh routers are covered, but for other dimension of grid size, the average number of covered mesh clients is not maximal. In Fig. 6, are shown the simulation results for Exponential distribution and grid size $(32 \times Y)$. Also in this scenario, the giant component is maximal for all grid dimensions (see Fig. 6a). In Fig. 6b the performance of the system is decreased with the increasing of grid size. When the grid size is big $(128 \times Y)$, the size of giant component is almost 100 %, but the average number of covered mesh clients is less than 35 % (Fig. 7).

In Figs. 8, 9 and 10 are shown the simulation results for Weibull distribution of mesh clients and grid size $(8 \times Y)$, $(32 \times Y)$ and $(128 \times Y)$, respectively. The performance of Weibull distribution is almost the same with Exponential distribution.

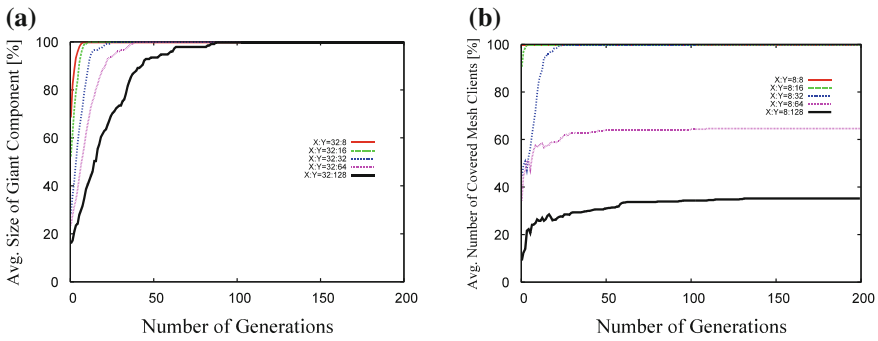


Fig. 9 Simulation results for Weibull distribution and grid size $(32 \times Y)$. **a** Average size of giant component versus number of generations. **b** Average number of covered mesh clients versus number of generations

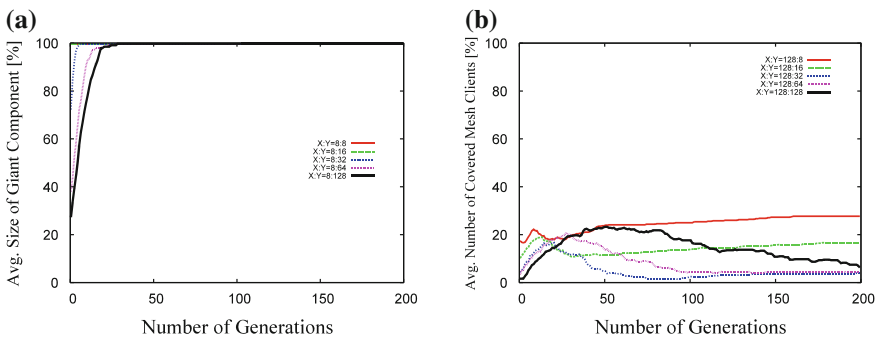


Fig. 10 Simulation results for Weibull distribution and grid size $(128 \times Y)$. **a** Average size of giant component versus number of generations. **b** Average number of covered mesh clients versus number of generations

If we compare the results for all distributions, we can notice that for Normal distribution the system performs better. Also, for the same surface of the grid area with size $(X \times Y)$, the system has better performance when X is smaller than Y .

5 Conclusions

In this work, we used our proposed and implemented WMN-GA for node placement problem in WMNs. We evaluate and compare the performance of WMN-GA system for Exponential and Weibull distribution of mesh clients considering different grid sizes and using giant component and number of covered mesh client metrics.

The simulation results show that the system performs better for Normal distribution of mesh clients. For a given number of mesh routers and mesh clients, with the increasing of the grid size, because the surface is increased, mesh routers cannot cover all mesh clients in the grid size and the performance of the system is decreased. The shape of grid size effects in the performance of the system. For the same surface of the grid area with size $(X \times Y)$, the system has better performance when X is smaller than Y .

In the future work, we would like to carry out extensive simulations for different scenarios.

Acknowledgments This work is supported by a Grant-in-Aid for Scientific Research from Japanese Society for the Promotion of Science (JSPS). The authors would like to thank JSPS for the financial support.

References

1. Akyildiz FI, Wang X, Wang W (2005) Wireless mesh networks: a survey. *Comput Netw* 47(4):445–487
2. Franklin A, Murthy C (2007) Node placement algorithm for deployment of two-tier wireless mesh networks. In: *IEEE GLOBECOM-2007*, pp 4823–4827
3. Muthaiah NS, Rosenberg C (2008) Single gateway placement in wireless mesh networks. In: *8th international IEEE symposium on computer networks*, pp 4754–4759
4. Tang M (2009) Gateways placement in backbone wireless mesh networks. *Int J Commun Netw Syst Sci* 2(1):45–50
5. Vanhatupa T, Hännikäinen M, Hämäläinen DT (2007) Genetic algorithm to optimize node placement and configuration for WLAN planning. In: *4th international symposium on wireless communication systems*, pp 612–616
6. Lim A, Rodrigues B, Wang F, Xua Zh (2005) k-center problems with minimum coverage. *Theor Comput Sci* 332(1–3):1–17
7. Wang J, Xie B, Cai K, Agrawal PD (2007) Efficient mesh router placement in wireless mesh networks. In: *MASS-2007, Pisa, Italy*, pp 9–11
8. Khafa F, Barolli L, Durresi A (2007) An experimental study on genetic algorithms for resource allocation on grid systems. *J Interconnect Netw* 8(4):427–443

9. Xhafa F, Sanchez C, Barolli L (2009) Ad Hoc and neighborhood search methods for placement of mesh routers in wireless mesh networks. In: ICDCS workshops of the IEEE 29th international conference on distributed computing systems (ICDCS-2009), pp 400–405
10. Yao X (1993) An empirical study of genetic operators in genetic algorithms. In: 19th EUROMICRO symposium on microprocessing and microprogramming on open system design: hardware, software and applications, Elsevier Science Publishers, pp 707–714

DCT-Based Watermarking for Color Images via Two-Dimensional Linear Discriminant Analysis

I-Hui Pan, Ping Sheng Huang and Te-Jen Chang

Abstract In this paper, we propose a watermarking algorithm based on Discrete Cosine Transform (DCT) using Two-dimensional Linear Discriminant Analysis (2DLDA) for color images. At first, the color image is converted into the YIQ color space and then transformed into the frequency domain by DCT. During the embedding stage, two watermarks of reference and logo are embedded into the Q component. Then, watermark extraction is done by 2DLDA from the Q component based on the frequency domain of DCT. By considering the Human Visual System (HVS), experimental results have shown that the watermark can be correctly extracted and better robustness is provided after various image attacks.

Keywords Two-dimensional linear discriminant analysis (2DLDA) • Watermarking • Discrete cosine transform (DCT) • YIQ color space

1 Introduction

The invisible or visible digital watermarking is an important technology to protect the copyright of digital contents such as video, audio and images from the illegal users. In addition, the watermarking should be robust to versatile attacks such as image compressions, geometric distortions and typical image transformations. For

I.-H. Pan
School of Defense Science, Chung Cheng Institute of Technology, National Defense University, No. 75, Shiyuan Road, Daxi, Taoyuan 333, Taiwan

P. S. Huang (✉)
Department of Electronic Engineering, Ming Chuan University, No. 5 De Ming Road, Gui Shan, Taoyuan 333, Taiwan
e-mail: pshuang@mail.mcu.edu.tw

T.-J. Chang
Department of Electrical and Electronic Engineering, Chung Cheng Institute of Technology, National Defense University, No. 75, Shiyuan Road, Daxi, Taoyuan 333, Taiwan

those methods in spatial domain [1–8], watermark embedding is achieved by modifying the pixel values of the host image with computational efficiency. For schemes in the transform domain [9–11], the pixel values of the host image in the spatial domain are firstly converted into their corresponding coefficients in the frequency domain by a transformation method such as the discrete cosine transform (DCT), discrete Fourier transform (DFT) or discrete wavelet transform (DWT), etc. Then, the coefficients are further utilized or modified to embed the watermark. An overview of image watermarking techniques can be found in Trémeau and Muselet [12].

By exploiting the fact that human eyes are less sensitive to changes in the blue component, Kutter et al. [1] proposed embedding the watermark in the blue component by changing a selected set of pixel values. Recently, Support Vector Machines (SVMs) [2, 3] and Linear Discriminant Analysis (LDAs) [4–6, 13] have been successfully applied in various applications including pattern recognition, classification, function estimation, and medicine, and so on. Much of literature seems to indicate that the performance of SVMs and LDAs are superior to those of traditional training models. However, for applications related to image processing, although LDA has adopted the class separation ability to extract watermark pixels, the region relationship of pixel neighboring is not considered and this is essential for classification of image regions. Therefore, Two-dimensional Linear Discriminant Analysis (2DLDA) [5] is used for tackling watermarking problems in this paper.

2 Related Works

YIQ Color Space

The YIQ color model is formed by a linear transformation of the RGB cube. The Y component represents the luminance and this is the only component used by black-and-white television receivers. Then, I and Q represent the chrominance information in which I represents in-phase, while Q stands for quadrature information referring to the component used in quadrature amplitude modulation. The transform matrix of RGB to YIQ is given by

$$\begin{bmatrix} Y \\ I \\ Q \end{bmatrix} = \begin{bmatrix} 0.299 & 0.587 & 0.114 \\ 0.596 & -0.274 & -0.322 \\ 0.212 & -0.523 & 0.311 \end{bmatrix} \begin{bmatrix} R \\ G \\ B \end{bmatrix} \quad (1)$$

In Eq. (1), the first line $Y = (0.299, 0.587, 0.144)(R, G, B)$ also gives pure black-and-white translation for RGB. The inverse transformation matrix that converts YIQ to RGB is given by

$$\begin{bmatrix} R \\ G \\ B \end{bmatrix} = \begin{bmatrix} 1.0 & 0.956 & 0.621 \\ 1.0 & -0.272 & -0.647 \\ 1.0 & -1.105 & 1.702 \end{bmatrix} \begin{bmatrix} Y \\ I \\ Q \end{bmatrix} \quad (2)$$

Discrete Cosine Transform

According to the discrete cosine transform (DCT) definition, an image can be converted from the spatial domain into the DCT domain by a two-dimensional forward transform. In the DCT domain, this image is represented by the combination of DC and AC components with different frequencies. Then, the image can be recovered from the DCT domain by a two-dimensional inverse transform. Either the forward transform or the inverse transform requires complicated computation. The forward DCT and inverse DCT to an image $f(x, y)$ are given by

$$C(u, v) = \alpha_u \alpha_v \sum_{x=0}^{M-1} \sum_{y=0}^{N-1} f(x, y) \cos \frac{\pi(2x+1)u}{2M} \cos \frac{\pi(2y+1)v}{2N} \quad (3)$$

and

$$f(x, y) = \sum_{u=0}^{M-1} \sum_{v=0}^{N-1} \alpha_u \alpha_v C(u, v) \cos \frac{\pi(2x+1)u}{2M} \cos \frac{\pi(2y+1)v}{2N} \quad (4)$$

where $u = 0, 1, 2, \dots, M-1$, $v = 0, 1, 2, \dots, N-1$, $x = 0, 1, 2, \dots, M-1$, and $y = 0, 1, 2, \dots, N-1$. M and N are row and column sizes of image $f(x, y)$. The coefficients of α_u and α_v are given by

$$\alpha_u = \begin{cases} \sqrt{1/M}, & u = 0 \\ \sqrt{2/M}, & 1 \leq u \leq M-1 \end{cases} \quad \text{and} \quad \alpha_v = \begin{cases} \sqrt{1/N}, & u = 0 \\ \sqrt{2/N}, & 1 \leq u \leq N-1 \end{cases}$$

Two-dimensional Linear Discriminant Analysis (2DLDA)

2DLDA is an extension of LDA and the difference between 2DLDA and LDA is that 2DLDA works on the matrix representation of images directly, while LDA uses a vector representation. By considering the meaning of statistical analysis, the matching or classification of image regions should take 2DLDA into consideration, rather than LDA. Furthermore, 2DLDA has asymptotically minimum memory requirements, and lower time complexity than LDA. Therefore, 2DLDA is adopted in this paper.

Let m_i be the mean of the i -th class ($i = 1, 2, \dots, L$) and m_x be the global mean. They can be obtained by

$$m_i = \frac{1}{N_i} \sum_{j=1}^{N_i} x_j \quad (5)$$

$$m_x = \frac{1}{L \times N_i} \sum_{i=1}^L \sum_{j=1}^{N_i} x_j \quad (6)$$

In 2DLDA, under this metric, the within-class and between-class distances of S_{wz} and S_{bz} can be computed by

$$S_{wz} = \sum_{i=1}^k \sum_{j=1}^{N_i} [(x_j^{(i)} - m_x)X] [(x_j^{(i)} - m_x)X]^T \quad (7)$$

$$S_{bz} = \sum_{i=1}^k [(m_i - m_x)X][(m_i - m_x)X]^T \quad (8)$$

The optimal projection matrix X is decided when the criterion is maximized, i.e.,

$$\text{Max}_X \text{ trace} \left((X^T S_{wz} X)^{-1} (X^T S_{bz} X) \right) \quad (9)$$

The optimal transformation X can maximize S_{bz} and minimize S_{wz} simultaneously. If S_{wz} is nonsingular, the solution of above optimization problem is to solve the generalized eigenvalue problem. Traditional LDA always suffers from the singularity problem. However, 2DLDA can overcome this problem successfully. Note that the size of matrices S_{wz} and S_{bz} is $n \times n$. This is much smaller than the size of $n^2 \times n^2$ for S_{wz} and S_{bz} in classical LDA.

3 Proposed Watermarking Scheme

In this paper, we propose a novel watermarking scheme based on 2DLDA for color images. Before the watermark bits embedded are extracted, the reference watermark bits are firstly trained by 2DLDA and the optimal transformation matrices are created for further watermark extraction. During the extraction stage, every watermark bit is determined by calculating the similarity to two class centers of 0 and 1. The details of the proposed watermark embedding and extraction schemes are described in [Sects. 3.1](#) and [3.2](#), respectively.

3.1 Watermark Embedding

The block diagram of the proposed watermark embedding procedure is shown in [Fig. 1](#). The steps of watermark embedding are described as follows.

- Step 1: Converting the original image from the RGB color space to the YIQ color space. Then, DCT is used to transform the Q component into the frequency domain. Selecting the AC frequency coefficients from the DCT for watermark embedding
- Step 2: The embedded watermark is composed of the reference watermark and the true watermark data. The reference watermark $R = r_1 r_2 \dots r_x$ is a binary sequence randomly generated according the given key $K1$ and this is used

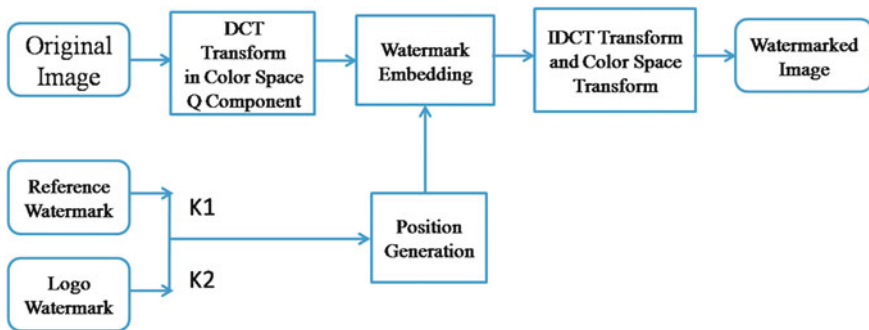


Fig. 1 Block diagram of watermark embedding

for 2DLDA training. The logo watermark $G = g_1g_2 \dots g_{m \times n}$ is permuted according to the copyright owner's private key K_2

Step 3: For each embedding position selected, the average pixel intensity A_{pt} on the cross-shaped region with the size of 7×7 is computed by

$$A_{pt}(i, j) = \left(\sum_{x=-3}^3 P(i+x, j) + \sum_{x=-3}^3 P(i, j+x) - P(i, j) \right) / .13 \quad (10)$$

To embed the watermark data, the pixel intensity of each selected embedding position is modified by

$$P_{pt} \leftarrow A_{pt} + \alpha w_t, \quad t = 1, 2, \dots, T \quad (11)$$

where α is the scaling factor in the Q channel.

Step 5: Using the updated AC components to compose the Q component by IDCT. Then, replacing the Q component by the new ones, and transforming the image back to the RGB watermarked image

3.2 Watermark Extraction

The block diagram of the proposed watermark extraction procedure is shown in Fig. 2. The watermark extraction procedure can be summarized as follows.

Step 1: Transforming the original image from the RGB color space to the YIQ color space. Then, Using DCT to transform the Q component into the frequency domain. Selecting the AC components from the DCT for watermark extraction

Step 2: Hiding position generation of watermark bits: Generating the hiding position sequence $\{p_t = (i_t, j_t)\}_{t=1,2,\dots,T}$ according to the secret key K provided by the copyright owner

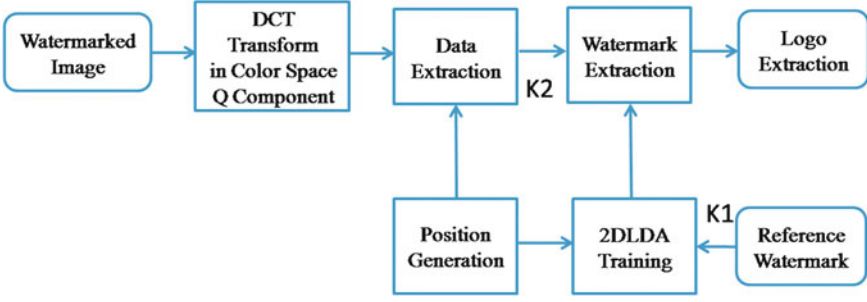


Fig. 2 Block diagram of watermark extraction

Step 3: For each embedding position selected, compute the difference $\delta_{i,j} = \tilde{P}(i,j) - \tilde{A}(i,j)$ between the intensity of the central pixel and the average in a sliding cross-shaped window with the size of 7×7 . The average in a sliding cross-shaped window is computed by

$$\tilde{A}_{P_t}(i,j) = \left(\sum_{x=-3}^3 \tilde{P}(i,j+k) + \sum_{x=-3}^3 \tilde{P}(i+k,j) - 2\tilde{P}(i,j) \right) / 12 \quad (12)$$

where $\tilde{P}(i,j)$ is the pixel value at position (i,j) . Before performing the 2DLDA training, the training dataset can be constructed by the reference positions from the embedding position sequence $D_i = \{\vec{D}_t\}_{t=1,2,\dots,T}$. Then the selected data extracted from the reference positions form the training dataset $T_{si} = \{\vec{D}_t, r_t\}_{t=1,2,\dots,x}$. After 2DLDA training, the watermarking bits belonging to the logo can be obtained from the projection and form the extraction dataset $E_{si} = \{\vec{D}_t\}_{t=x+1,\dots,x+m \times n}$.

Step 4: After 2DLDA training and the optimal projection matrices of X is obtained. Then we can compute optimal discriminant matrices B_i and F_i for T_{si} and E_{si} by

$$B_i = X_y^T T_{si}^{(j)} X_y, \quad j = 1, \dots, x \quad (13)$$

$$F_i = X^T E_{si}^{(j)} X, \quad j = R+1, \dots, m \times n \quad (14)$$

Step 5: Computing every arithmetic mean for C_{1i} and C_{0i} between 1 and 0 on the training dataset T_{si} by

$$\begin{aligned} C_{1i} &= C_{1i} + B_i, \text{ if reference watermark} = 1 \\ C_{0i} &= C_{0i} + B_i, \text{ else} \end{aligned} \quad (15)$$

The total means of C_{1i} and C_{0i} can be assigned as the centers of class 0 and 1.

Step 6: Extracting the embedded watermark bits by the trained 2DLDA on the extraction dataset E_{si} . So the similarity on E_{si} is defined as $Diff_1 = F_i - C_{1i}$ and $Diff_0 = F_i - C_{0i}$. The distance between 0 and 1 is calculated by

$$w'_i = \begin{cases} 1, & \text{if } Diff_0^2 > Diff_1^2 \\ 0, & \text{else} \end{cases} \quad (16)$$

where $i = 1, 2, \dots, m \times n$. The measure of BER (Bit Error Rate) is used and given by

$$BER = \frac{\sum_{i=1}^m w_i \oplus w'_i}{m} \quad (7.17)$$

4 Simulation Results

In this section, the proposed watermarking scheme is applied to a host color image of size 512×512 in which each pixel is represented by 24 bits in RGB color space. The watermark of a recognizable pattern of size 35×28 is embedded into the host color image. To demonstrate the effectiveness of the proposed scheme, we have tested the proposed watermarking scheme on different images including “Lena”, “Baboon” and “Peppers”, that represent different texture complexity.

The original 512×512 images of Lena, Baboon and Peppers are shown in Fig. 3a–c, and the corresponding watermarked images with PSNR 44.49, 44.78, 44.38 dB are demonstrated, respectively in Fig. 3d–f. The extracted watermarks with 0 error bits are shown in Fig. 3g–i.

In the experiments, we found that the length of 50 bits for the reference watermark can make a good compromise between two necessities of transparency and robustness. We have tested the watermarked image under several attacks such as cropping, distortion, blurring, noisy and so on. $\alpha = 40$ is selected for watermark embedding and the proposed algorithm is applied for watermark extraction. Experimental results have demonstrated that the watermark can be extracted without the need of any original image by only the aid of the reference data.

The watermark embedding strength in Kutter’s method and Fu’s method are decided experimentally to get watermarked images with similar PSNR values. Due to the limitation of space, only part of the comparison results on Baboon against Kutter et al.’s [1] and Fu et al.’s [4] methods are shown. Kutter et al. [1] proposed to embed the watermark into the blue channel of the color images, in which the watermark detection threshold is only decided by two special data embedded in the host image. Fu et al. [4] proposed to embed the watermark into the RGB channel of color images and the watermark was extracted by the aids of a well trained LDA. For the purpose of comparison, we have added different image attacks from

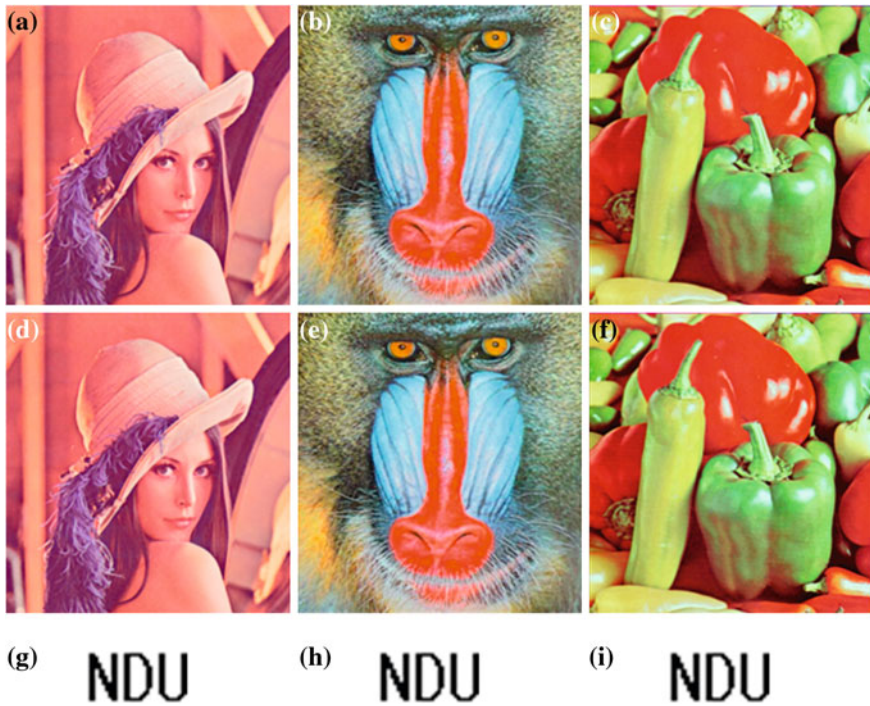


Fig. 3 Original images of **a** Lena, **b** Baboon, and **c** Peppers. Watermarked images for **d** Lena, **e** Baboon, and **f** Peppers. Extracted watermarks: **g** from **d**; **h** from **e**; **i** from **f**

Table 1 Experimental results compared with Kutter's and Fu's methods on Baboon image [4]

Attacks	PSNR (dB)	BER (Bit error rate)		
		Kutter's method	Fu's method	2DLDA method
Attack free	41.46	0.009	0.001	0.000
Blurring	28.65	0.031	0.003	0.003
Noisy (density = 0.02)	23.24	0.035	0.015	0.009
Cropping (25 % removed)	12.15	0.154	0.050	0.015
Distortion (degree of 2)	26.02	0.326	0.131	0.018
Luminance and contrast adjustment (enhance 50 %)	11.12	0.164	0.011	0.011

blurring, noise, cropping, distortion, luminance and contrast attacks to the watermarked image. The measured quantitative results are shown in Table 1. As we can see from Table 1, the extracted watermark by the proposed method has demonstrated much better performance than Kutter's and Fu's methods.

5 Conclusions

This paper presents a new watermarking algorithm using the classification approach from machine learning. Based on DCT, the watermark is embedded in the Q component and watermark extraction is performed by adopting the training and classification performance from 2DLDA. The proposed watermark embedding and extraction procedures are imposed on the host image by DCT and the watermark is embedded into the AC components. Experimental results show that the proposed scheme can indeed provide a strong robustness for watermarked images with 2DLDA. Although promising performance has shown in this paper, a larger color image database is needed in the future for testing the efficacy of the proposed approach.

Acknowledgments This research is supported in part by the National Science Council, Taiwan under the grant of NSC 101-2221-E-130-026.

References

1. Kutter M, Jordan F, Bossen F (1998) Digital watermarking of color images using amplitude modulation. *J Electron Imaging* 7:326–332
2. Tsai H-H, Sun D-W (2007) Color image watermark extraction based on support vector machines. *Inf Sci* 177(2):550–569
3. Wang X-Y, Yang H-Y, Cui C-Y (2008) An SVM-based robust digital image watermarking against desynchronization attacks. *Signal Process* 88:2193–2205
4. Fu Y-G, Shen R-M (2008) Color image watermarking scheme based on linear discriminant analysis. *Comput Stand Interfaces* 30:115–120
5. Ye J, Janardan R, Li Q (2004) Two-dimensional linear discriminant analysis. *Adv Neural Inf Process Syst* 17:1569–1576
6. Li M, Yuan B (2005) 2D-LDA: A statistical linear discriminant analysis for image matrix. *Pattern Recogn Lett* 26:527–532
7. Pizzolante R, Carpentieri B, Castiglione A, Giancarlo D-M (2011) The AVQ algorithm: watermarking and compression performances. In: *Third international conference on intelligent networking and collaborative systems*, Fukuoka, Japan, pp 698–702
8. Pizzolante R, Carpentieri B (2012) Copyright protection for images on mobile devices. In: *Sixth international conference on innovative mobile and internet services in ubiquitous computing*, Palermo, Italy, pp 585–590
9. Wang Y-P, Chen M-J, Cheng P-Y (2000) Robust image watermark with wavelet transform and spread spectrum techniques. In: *Conference record of the thirty-fourth Asilomar conference on signals, systems and computers*, vol 2, pp 1846–1850
10. Ali A-H (2007) Combined DWT-DCT digital image watermarking. *J Comput Sci* 3(9):740–746
11. Phadikar A, Maity SP, Verma B (2011) Region based QIM digital watermarking scheme for image database in DCT domain. *Comput Electr Eng* 37:339–355
12. Trémeau A, Muselet D (2009) Recent trends in color image watermarking. *J Imaging Sci Technol* 53:010201-1–010201-15
13. Zhang D, Jing X, Yang J (2006) *Biometric image discrimination technologies*. Idea Group Publishing, Hershey

Human Action Recognition Using Depth Images

Chaur-Heh Hsieh, Chin-Pan Huang and Jian Ming Hung

Abstract This paper presents a human action recognition algorithm using a depth image. First, 3D coordinates of the body's joints of each frame are generated from the depth image. Then, the proposed method applies normalization and quantization processes to the body joints of all frames of the action video to obtain a 3D histogram. The histogram is projected onto xy, xz, and yz plans sequentially and combined into a one-dimensional feature vector. For dimension reduction, the principal component analysis (PCA) technique is applied to the feature vector to generate an action descriptor. To further improve the recognition performance, a decision tree method is developed to divide input actions into four main categories. The action description vectors of each category are used to design its respective support vector machine (SVM) classifier. Each SVM classifies the actions of a category into one type of actions. Experimental results verify that our approach effectively rules out the interference of background and improves the recognition rate.

Keywords Decision tree · Human action recognition · Principal component analysis · Support vector machine

1 Introduction

Human action recognition has recently been an important subject in computer vision. Several schemes for this topic utilize low level features from the RGB cameras such as colors, shapes, motion, and local information. However, these methods suffer from reducing the discrimination rate in case of the complex

C.-H. Hsieh (✉) · C.-P. Huang · J. M. Hung
Department of Computer and Communication Engineering, Ming Chuan University, 5 Der
Ming Road, Gwei Shan, Taoyuan 333, Taiwan
e-mail: harrishsieh@gmail.com

background in the image or different wearing of action performers. In this paper, we propose to use a depth map to conquer the deficiencies of the traditional methods. A depth map is a three-dimension feature retrieved from the body joints. Using the features of a depth map has advantage of not only its sufficient spatial information but also its avoidance of interference of background and wearing effects of the user. Furthermore, our method employs the decision tree technique to divide the actions into four main categories and designs its respective SVM classifier to improve recognition rate and expedite the system processing speed.

Among recently introduced action recognition techniques, Fujjyoshi et al. [1] first presented to use color and shape information as features for action recognition. The scheme uses distance between outline of the figure and its centroid to recognize actions. The features of this method are generated by two phases. First, extracting silhouette of the figure is via the binarization image with dilation and erosion processes. Then the boundary extraction is obtained by extracting the outline of the generated silhouette. The distances of the longest few lines between the centroid and the boundary are used to represent the features of the movement of the user. The drawbacks of the method are that the distances will be different from the different users with the same action, and the segment distribution will also change. The other scheme based on outline of the user is to calculate the direction of the gradient histogram (Histograms of Oriented Gradient; HOG). Bobick and Davis [2] proposed two temporal template representations for action recognition. The first representation is motion energy image (MEI). The method employs continuous image binarization to obtain pixel changes, the action occurrences, marking in white to form a binary cumulative motion image, called the motion-energy image. The method gives each of the continuous images with the same weight, so that it cannot distinguish each image in the sequence. The second representation is motion history image (MHI). It gives each image with different weights; the old frame is given lower weights, while the new one with higher weights. The disadvantage of this method is that it is only suitable for simple actions, such as stand up, sit down, waving. In case of too complex actions, it overwrites the old motion information, so that it becomes less reliable. For usage of mobile features, Li [3] proposed to calculate the optical flow field between two frames to obtain the horizontal and vertical components of optical flow field and the strength and direction information for every pixel. The method takes the obtained optical flow information to draw gradient in the direction of histogram (HOG). Due to high feature dimensions, principal component analysis (PCA) technique is used to reduce the dimension and a Hidden Markov Model (HMM) model is adopted. Regarding local features, Jianhao et al. [4] use the silhouette image to find the local maxima of the gradient, apply a series of quantization to find the relatively bright portion of the picture, and adopt the tangent circle and silhouette Edge to filter the produced picture. The brightest point of the local area is thus obtained and the human skeleton features can be found by linking its neighbor points in four directions.

Recently, the depth map from 3D camera has been used to capture information in some researches for action recognitions. Cherla et al. [5] use the Kinect camera

to capture 20 joint points of x, y coordinates and a depth value of z to form a three-dimensional coordinate position, obtain features through quantization processes, and apply linear discriminant analysis (LDA) technique to recognize the actions. Yang et al. [6] use motion information of the depth map with the HOG for action recognition. Zainordin et al. [7] employ the depth map with a body skeleton for pose recognition.

In this paper, we propose a human action recognition algorithm using a depth map made by the Kinect 3D camera. Through normalization and quantization processes, our method obtains a 3D histogram which is then projected onto the xy, xz, and yz planes to form three one-dimensional feature vectors. After that, the generated vectors are fused to obtain an action description vector which will be used for action recognition through the SVM classifier. Because the feature dimension is extremely high, the PCA technique is utilized to reduce its dimension. Moreover, to further speed up the processing and improve the recognition rate, a decision tree method is developed to divide input actions into four main categories. The action description vectors of each category are used to design its respective support vector machine (SVM) classifier. Each SVM classifies the actions of a category into one type of actions. The rest of this paper is organized as follows. Section 2 introduces the proposed method. Section 3 describes the experimental results. Finally, Sect. 4 gives conclusions.

2 Proposed Method

The system block diagram of our proposed method is shown in Fig. 1. The detailed techniques are described as follows.

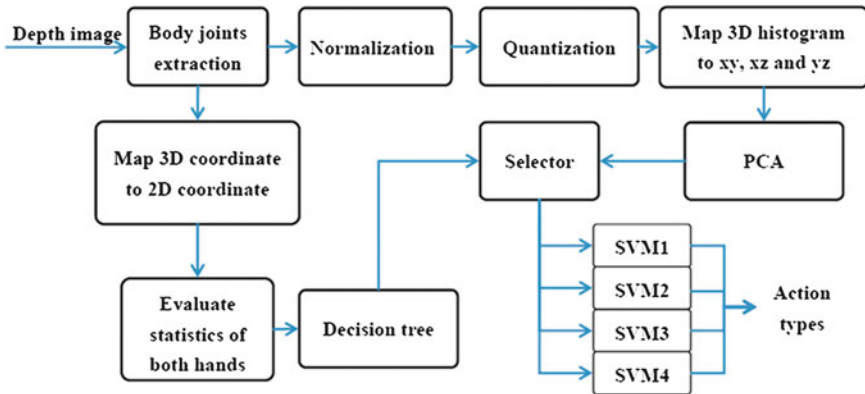


Fig. 1 System block diagram of our proposed method

2.1 Feature Extraction

We utilize Microsoft Kinect 3D camera with the OpenNI drivers to capture a depth map with 15 human body joints as shown in Fig. 2.

The position of a joint point is a 3-D vector (x,y,z) , where (x,y) represents spatial location and z denotes depth value. Thus an action can be described as several sequences of 3-D joints, each corresponding to the trajectory over time of each joint. The recognition of actions from the sequences of 3-D joints faces two major challenges: (a) RST (rotation, scaling and translation) problem: for same action, the trajectory of each joint will vary with the geometric changes of the actor including rotation, scaling and translation. (b) Temporal variations: different actors produce different lengths of trajectories even they perform same action. Furthermore, the same actor performing the same action at different time often generates different lengths of trajectories. To solve this problem, a coordinate transform in (1) is performed to normalize the 3D position of a joint.

$$C_t(x, y, z) = (P_t(x, y, z) - \text{Torso}(x, y, z)) / D_{HT} \quad (1)$$

where $P_t(x,y,z)$ denotes the 3D position of a joint at time t ; $\text{Torso}(x,y,z)$ is the position of Torso at the initial time; and D_{HT} is the Euclidean distance between Head position and Torso position. After the coordinate transform, the 3D positions of joints of different persons will have the same scale space. Consequently, same actions performed by different persons produce similar patterns.

First of all, we collect the joint positions of an action over a period of time T . Secondly, the joint position sequence is normalized by the coordinate transformation, and the result is denoted as $C_T(x,y,z)$. Next, the $C_T(x,y,z)$ is projected into x - y plane, x - z plane, and y - z plane, and the corresponding projections are denoted as $C_T(x,y)$, $C_T(x,z)$ and $C_T(y,z)$, respectively. For each plane, we divide it into

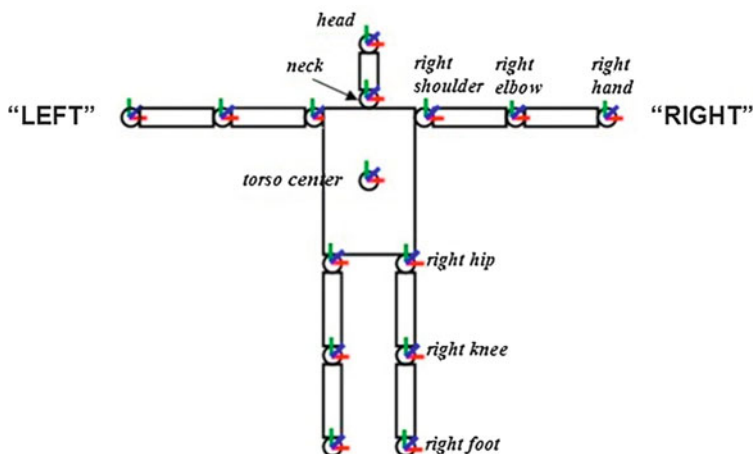


Fig. 2 A depth map with 15 body joints

several blocks and calculate the histogram for each block. Finally, the histograms of the three planes are fused together to form a descriptor of the action.

For x-y plane, we divide x axis into m partitions, and y axis into n partitions. As a consequence, it produces $m \times n$ blocks in x-y plane. Then we compute the occurrence frequency of each block $H_{xy}(i)$, which is defined as the number of data points lying in each block of x-y plane as shown in (2). The occurrence frequency of all blocks is regarded as the histogram feature of x-y plane.

$$H_{xy}(i) = \#\{C_T(x, y, z) | C_T(x, y) \in block_i, i = 1, 2, \dots, m \times n\} \quad (2)$$

The above procedure is also applied to x-z plane and y-z plane. Then we obtain histogram $H_{xz}(i)$ and $H_{yz}(i)$ defined in the following

$$H_{xz}(i) = \#\{C_T(x, y, z) | C_T(x, z) \in block_i, i = 1, 2, \dots, m \times k\} \quad (3)$$

$$H_{yz}(i) = \#\{C_T(x, y, z) | C_T(y, z) \in block_i, i = 1, 2, \dots, n \times k\} \quad (4)$$

The H_{xy} , H_{xz} , and H_{yz} are further normalized to the range of [0,1] using L2-norm, and concatenated to form a final feature vector $H = [H_{xy} \ H_{xz} \ H_{yz}]$.

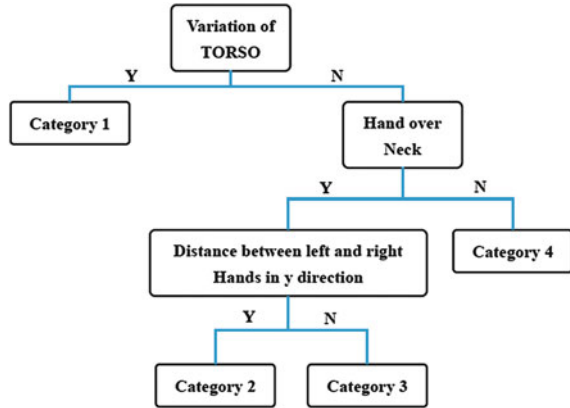
2.2 Principal Component Analysis

Principal component analysis (PCA) uses an orthogonal transformation to convert high dimensional data into principal components (eigenvectors) associated with their weights (eigenvalues). The results can be used to explain the variance in the original data to show the direction of greatest impact on the variance. In other words, PCA provides an effective way to reduce the data dimension. Components may be ruled out in the original data corresponding to smaller eigenvalues and then it results in low-dimensional data. Because the length of the feature vector mentioned above is very large (3360) and the majority of its bin is 0, the PCA technique is employed to reduce its dimension to expedite the processing speed.

2.3 Decision Tree

In this study, the feature vector is generated based on torso joint over a time interval of the action frames as described in feature extraction subsection. The drawbacks of using that method are two folds. The first one is lacking translation information and second one is missing body movement sequence data. Those defects may affect the action recognition accuracy. In order to solve these problems, decision tree technique with three classification criteria is adopted. Those criteria are as follows: the relative 2D coordinate position between joints of two hands and those of neck of the extracted features, large displacement of the torso, and distance between two hands in y direction. They are applied to categorize the actions into four main categories as shown in Fig. 3.

Fig. 3 Decision tree with four categories



2.4 Training and Recognition

In training phase, the actions are trained according to the categorized classes of the decision tree. It results in four trained SVM classifiers (i.e. SVM1 ~ SVM4) which will be used in recognition phase. In recognition phase, test actions will be classified by the criteria of decision tree to obtain their classified category number which then be used to select the appropriate SVM classifier for further discriminate the action types. Through the chosen SVM classifier, the test actions can be correctly recognized.

3 Experimental Results

To best of our knowledge, no datasets of actions collected with Kinect sensor containing depth map are available. We collect one dataset consisting of twelve action types selected from the National Health gymnastics and performed by thirty students wearing different color clothes in complex background environment for the experiment. The action types are classified into four main categories in accordance with those of decision tree as shown in Table 1. There are 360 action video samples in the database. Several action examples are shown in Fig. 4.

3.1 Experiments on Decision Tree

In this experiment, the actions were classified in two cases: Case I classifying directly; Case II classifying with decision tree. Experimental results are shown in Table 2. It is clear that the case of classifying with decision tree has higher

Table 1 Categories of action types

Category 1	Category 2	Category 3	Category 4
Knee bending	Single-hand held Up punches	Up punches Hands on the move Enlarge bosom Hand pushing	Turn pose Lift the knee Mark time Zhan yi Elbow folding

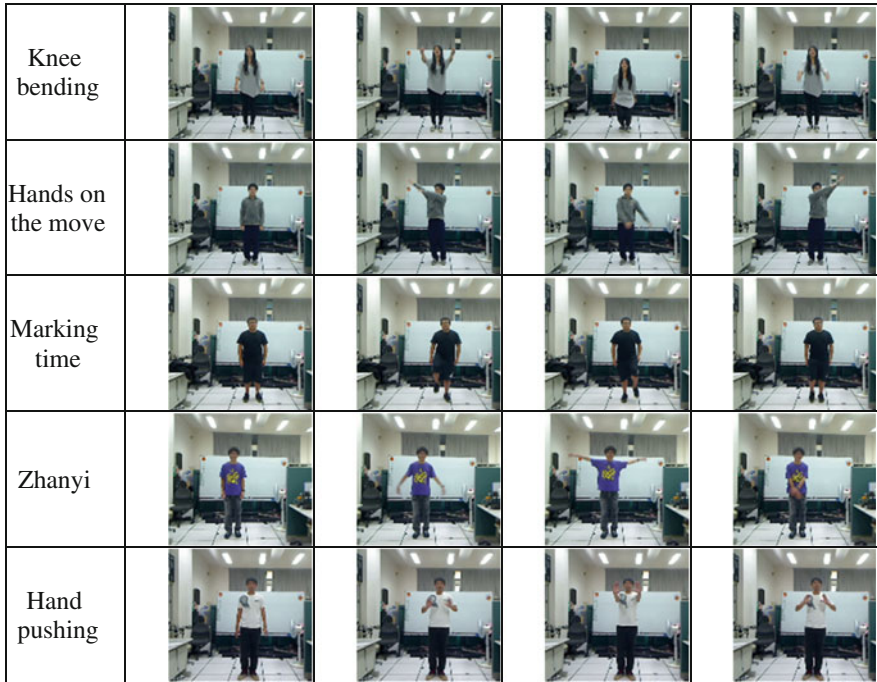


Fig. 4 Action examples

recognition rate than that of case of classifying directly. These results verify that the proposed method improves the recognition accuracy by using decision tree.

3.2 Experiments on Dimension Reduction

In this experiment, the PCA technique is employed to reduce the dimensions. In order to realize the impact of the dimensions on the recognition rate, comprehensive experiments were conducted with dimensions ranging from 130 to 2.

Table 2 Experimental results on decision tree

	Without decision tree (%)	With decision tree (%)
Knee bending	85	100
Single-hand held	100	100
Up punches	70	100
Hands pushed	55	90
Hands on the move	100	100
Enlarge bosom	90	90
Turn pose	90	100
Lift the knee	95	95
Mark time	95	95
Zhan yi	70	75
Elbow folding	95	95
Hand pushing	90	95
Total	86.25	94.58

Table 3 PCA dimension versus recognition rate

Reduced dimension	Recognition rate (%)
130	94.14
110	94.17
90	94.17
70	94.58
50	94.58
30	95.42
25	95.83
20	95.83
15	96.25
10	96.25
8	95.42
6	95
4	92.08
2	84.16

Results are shown in Table 3. The results indicate that the recognition rate will be optimal at dimension of 15. This gives an insight of dimension reduction that it may not achieve better recognition rate when using higher dimension.

3.3 Comparisons

In this experiment, the proposed method is compared with the 3DHOG (three-dimensional histogram orientation gradient) method [9, 10]. Both methods are performed to all actions to measure their recognition rates. The results are shown in Table 4. It is clear that the proposed method has higher recognition rate than that of 3DHOG method.

Table 4 Recognition rate comparison with other method

	Proposal method (%)	3DHOG (%)
Knee bending	100	92.86
Single-hand held	100	85.71
Up punches	100	85.71
Hands pushed	90	85.71
Hands on the move	100	92.86
Enlarge bosom	95	78.57
Turn pose	100	100
Lift the knee	100	100
Mark time	100	92.86
Zhan yi	85	78.57
Elbow folding	95	100
Hand pushing	95	92.86
Total	96.25	90

4 Conclusions

This paper has presented an effective and efficient algorithm for human action recognition based on a depth map extracted from joints of human skeleton. To improve recognition rate and expedite the processing speed, the decision tree technology has been adopted. Experimental results have verified that our approach effectively prevent from the interference of background and demonstrated the promising recognition accuracy, extremely low computational load, and highly suitable for real-time applications.

Acknowledgements This research is supported in part by the National Science Council, Taiwan under the grants of NSC 99-2632-E130-001-MY3 and NSC 99-2221-E130-011-MY3.

References

1. Fujiyoshi H, Lipton AJ (1998) Real-time human motion analysis by image skeletonization. In: Fourth IEEE workshop on applications of computer vision, WACV 1998, pp 15–21
2. Bobick F, Davis JW (2001) The recognition of human movement using temporal templates. *IEEE Trans Pattern Anal Mach Intell* 23:257–267
3. Li X (2007) HMM based action recognition using oriented histograms of optical flow field. *Electron Lett* 43:560–561
4. Jianhao D et al (2010) Extraction of human body skeleton based on silhouette images. In: 2010 second international workshop on education technology and computer science (ETCS), pp 71–74
5. Cherla S et al (2008) Towards fast, view-invariant human action recognition. In: IEEE computer society conference on computer vision and pattern recognition workshops, 2008, CVPRW '08. pp 1–8

6. Yang X et al (2012) Recognizing actions using depth motion maps-based histograms of oriented gradients. In: The 20th ACM international conference on multimedia, pp 1057–1060, Nara, Japan
7. Zainordin FD et al (2012) Human pose recognition using Kinect and rule-based system. In: World automation congress (WAC), 2012, pp 1–6
8. Chang CC, Lin CJ (2001) LIBSVM: a library for support vector machines. Software available at <http://www.csie.ntu.edu.tw/~cjlin/libsvm>
9. Hwang WY, Hsieh CH (2010) Human action recognition using 3-D HOG and key-point distribution. In: Proceedings of 23th IPPR conference on computer vision, graphics and image processing (CVGIP2010), Taiwan
10. Kläser A et al (2008) A spatio-temporal descriptor based on 3d-gradients. In: BMVC, pp 99.1–99.10

Performance Analysis of OLSR with ETX_ff for Different HELLO Packet Interval in a MANET Testbed

Masahiro Hiyama, Elis Kulla, Makoto Ikeda, Leonard Barolli and Makoto Takizawa

Abstract Recently, Mobile Ad-hoc Networks (MANETs) have an increased interest in applications for covering rural areas due to the possibility of usage of low-cost and high-performance mobile terminals, without having to depend on the network infrastructure. Because the terminals are mobile, the routes change dynamically, so routing algorithms are very important for operation of MANETs. In this paper, we investigate the performance of Optimized Link State Routing (OLSR) protocol with ETX_ff, for different scenarios in indoor and outdoor environment considering throughput and packetloss metrics. We design and implement two experimental scenarios in our academic environment and compare their performance behaviour for different HELLO packets interval of OLSR protocol.

M. Hiyama (✉) · E. Kulla
Graduate School of Engineering, Fukuoka Institute of Technology (FIT),
3-30-1 Wajiro-Higashi, Higashi-Ku, Fukuoka 811-0295, Japan
e-mail: masahiro.hiyama@gmail.com

E. Kulla
e-mail: eliskulla@yahoo.com

M. Ikeda · L. Barolli
Department of Information and Communication Engineering, Fukuoka Institute of
Technology (FIT), 3-30-1 Wajiro-Higashi, Higashi-Ku, Fukuoka 811-0295, Japan
e-mail: makoto.ikd@acm.org

L. Barolli
e-mail: barolli@fit.ac.jp

M. Takizawa
Department of Advanced Sciences, Hosei University, 3-7-2, Kajino-machi, Koganei-shi,
Tokyo 184-8584, Japan
e-mail: makoto.takizawa@computer.org

1 Introduction

A Mobile Ad hoc Network (MANET) is a collection of wireless mobile terminals that are able to dynamically form a temporary network without any aid from fixed infrastructure or centralized administration.

Most of the work for MANETs has been done in simulation, as in general, a simulator can give a quick and inexpensive understanding of protocols and algorithms. However, experimentation in the real world are very important to verify the simulation results and to revise the models implemented in the simulator. A typical example of this approach has revealed many aspects of IEEE 802.11, like the gray-zones effect [1], which usually are not taken into account in standard simulators, as the well-known ns-2 simulator.

So far, we can count a lot of simulation results the performance of MANET, e.g. in terms of end-to-end throughput, delay and packetloss. However, in order to assess the simulation results, real-world experiments are needed and a lot of testbeds have been built to date [2]. In [3], the authors analyze the performance of an outdoor ad-hoc network, but their study is limited to reactive protocols such as Ad hoc On Demand Distance Vector (AODV) and Dynamic Source Routing (DSR). The authors of [4] perform outdoor experiments of non standard pro-active protocols. Other ad-hoc experiments are limited to identify MAC problems, by providing insights on the one-hop MAC dynamics as shown in [5].

In [6], the authors present an experimental comparison of OLSR using the standard hysteresis routing metric and the Expected Transmission Count (ETX) metric in a 7 by 7 grid of closely spaced Wi-Fi nodes to obtain more realistic results. The throughput results are similar to our previous work and are effected by hop distance [7]. The closest work to ours is that in [8]. However, the authors did not care about the routing protocol. In [9], the disadvantage of using hysteresis routing metric is presented through simulation and indoor measurements. Our experiments are concerned with the interaction of transport protocols and routing protocol, for instance OLSR. In our previous work [10–12], we carried out many experiments with our MANET testbed. We proved that while some of the OLSR's problems can be solved, for instance the routing loop, this protocol still have the self interference problem. There is an intricate inter-dependence between MAC layer and routing layer, which can lead the experimenter to misunderstand the results of the experiments. For example, the horizon is not caused only by IEEE 802.11 Distributed Coordination Function (DCF), but also by the routing protocol.

In this work, we investigate the performance of OLSR in a MANET testbed in indoor-outdoor environment, considering different values of HELLO packets interval and ETX_ff algorithm. We implemented two MANET scenarios and evaluated the performance considering throughput and packetloss metrics.

The structure of the paper is as follows. In [Sect. 2](#), we show an overview of OLSR routing protocol. In [Sect. 3](#), we introduce the implementation of our testbed. In [Sect. 4](#), we give experimental results. Finally, conclusions are given in [Sect. 5](#).

2 OLSR Overview

The link state routing protocol that is most popular today in the open source world is OLSR from olsr.org. OLSR with Link Quality (LQ) extension and fisheye-algorithm works quite well. The OLSR protocol is a proactive routing protocol, which builds up a route for data transmission by maintaining a routing table inside every node of the network. The routing table is computed upon the knowledge of topology information, which is exchanged by means of Topology Control (TC) packets. The TC packets in turn are built after every node has filled its neighbors list. This list contains the identity of neighbor nodes. A node is considered a neighbor if and only if it can be reached via a bidirectional link.

OLSR makes use of HELLO messages to find its one hop neighbors and its two hop neighbors through their responses. The sender can then select its Multi Point Relays (MPR) based on the one hop node which offer the best routes to the two hop nodes. By this way, the amount of control traffic can be reduced. Each node has also an MPR selector set which enumerates nodes that have selected it as an MPR node. OLSR uses TC messages along with MPR forwarding to disseminate neighbor information throughout the network. OLSR checks the symmetry of neighbor nodes by means of a 4-way handshake based on HELLO messages. This handshake is inherently used to compute the packetloss probability over a certain link. This can sound odd, because packetloss is generally computed at higher layer than routing one. However, an estimate of the packetloss is needed by OLSR in order to assign a weight or a state to every link. Host Network Address (HNA) messages are used by OLSR to disseminate network route advertisements in the same way that TC messages advertise host routes.

In our previous OLSR code, a simple RFC-compliant heuristic was used to compute the MPR nodes [13]. Every node computes the path towards a destination by means of a simple shortest-path algorithm, with hop-count as target metric. In this way, a shortest path can result to be also of good, from the point of view of the packet error rate. Accordingly, recently `olsrd` has been equipped with the LQ extension, which is a shortest-path algorithm with the average of the packet error rate as metric. This metric is commonly called as ETX, which is defined as $ETX(i) = 1/(NI(i) \times LQI(i))$. Given a sampling window W , $NI(i)$ is the packet arrival rate seen by a node on the i -th link during W . Similarly, $LQI(i)$ is the estimation of the packet arrival rate seen by the neighbor node which uses the i -th link. When the link has a low packet error rate, the ETX metric is higher. The LQ extension greatly enhances the packet delivery ratio with respect to the hysteresis-based technique [14]. In our experiments we used `ETX_ff`, which calculates ETX value based only on HELLO packets received.

`ETX_ff` (ETX Funkfeuer/Freifunk) is the current default LQ algorithm for `OLSRd`. It uses the sequence number of the OLSR packets (which are link specific) to determine the current packet loss rate. `ETX_ff` includes a hysteresis mechanism to suppress small fluctuations of the LQ and NLQ values. If no packets are received from a certain neighbor at all, a timer begins to lower the calculated LQ

value until the next packet is received or the link is dropped. ETX_ff uses only integer arithmetic, so it performs well on embedded hardware having no FPU.

3 Testbed Description

Our testbed is composed of five laptops machines. The operating system mounted on these machines is Fedora 14 Linux with kernel 2.6.35, suitably modified in order to support the wireless communications. In our testbed, we have two systematic background or interference traffic we could not eliminate: the control traffic and the other wireless Access Points (APs) interspersed within the campus. The control traffic is due to the ssh program, which is used to remotely start and control the measurement software on the source node. The other traffic is a kind of interference, which is typical in an academic scenario.

3.1 Scenario Description

We constructed two experimental scenarios in our testbed. Node states for each scenario are shown in Table 1. In Fig. 1a, all nodes are in a static state. Two nodes (node 1 and 2) are in the fifth floor of building D of our campus and two other nodes (node 3 and 4) are inside building C. We call this Static (STA) scenario. In Moving (MOV) scenario, node 5 moves from position of node 1 to the position of node 4 and back, for 80 s, as shown in Fig. 1b.

Table 1 Number of nodes for each experimental scenario

Scenario	Number of nodes			
	Building D	Bridge	Building C	Moving
STA	2	0	2	0
MOV	2	0	2	1

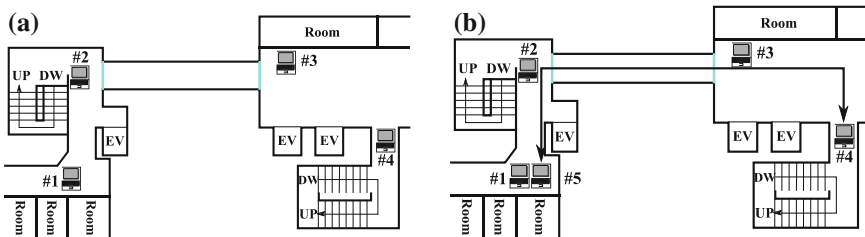


Fig. 1 Experimental scenarios. **a** Static scenario (STA). **b** Moving scenario (MOV)

4 Experimental Results

4.1 Experimental Settings

The experimental parameters are shown in Table 2. We study the impact of best-effort traffic for Mesh Topology (MT). In the MT scheme, the MAC filtering routines are not enabled. We collected data for throughput metric. These data are collected using the Distributed Internet Traffic Generator (DITG) [15], which is an open-source Internet traffic generator.

The transmission rate of the data flow is $122 \text{ pps} = 499.712 \text{ Kbps}$, i.e. the packet size of the payload is 512 bytes. All experiments have been performed in the fifth floor of our department buildings. All laptops are in radio range of each other. The experimental time for one experiment was about 80 s.

We measured the throughput, which is computed at the receiver. For OLSR, $w\text{HELLO} < T_{\text{Exp}}$, where T_{Exp} is the total duration of the experiment, i.e., in our case, $T_{\text{Exp}} = 80 \text{ s}$, and HELLO is the rate of the HELLO messages. However, the testbed was turned on even in the absence of measurement traffic. Therefore, the effective T_{Exp} was much greater.

As MAC protocol, we used IEEE 802.11b. The transmission power was set in order to guarantee a coverage radius big enough to cover all one-hop physical neighbors of each node in the network. Since we were interested mainly in the performance of the routing protocol, we kept unchanged all MAC parameters, such as the carrier sense, the retransmission counter, the contention window and the RTS/CTS threshold. Moreover, the channel central frequency was set to 2.412 GHz (channel 1). In regard to the interference, it is worth noting that, during our tests, almost all the IEEE 802.11 spectrum had been used by other APs disseminated within the campus. In general, the interference from other APs is a non-controllable parameter.

Table 2 Experimental parameters

Function	Value
Number of nodes	4 or 5
Logical link	Mesh
MAC	IEEE 802.11b
Traffic generator	D-ITG-2.8.0-rc1
Flow type	CBR
Packet rate	122 pps
Packet size	512 bytes
Number of trials	10
Duration	80 s
Routing protocol	OLSRd 0.6.4
LQWS of OLSR	10

4.2 Results Discussion

Here, we show the measured data by time-domain graphs, in Figs. 2, 3, 4 and 5. In this way we can have a better observation of the oscillations occurring during

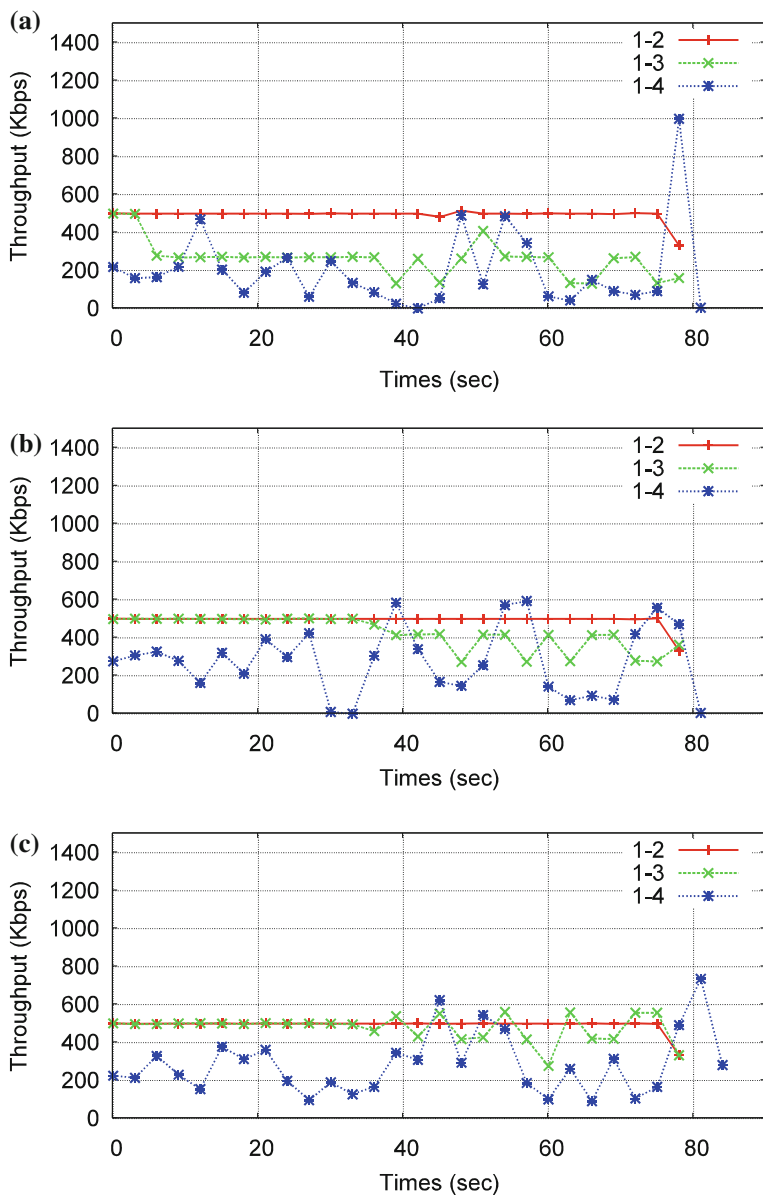


Fig. 2 Throughput results for static scenario. Interval: = 0.5 s (a), 1.0 s (b), 2.0 s (c)

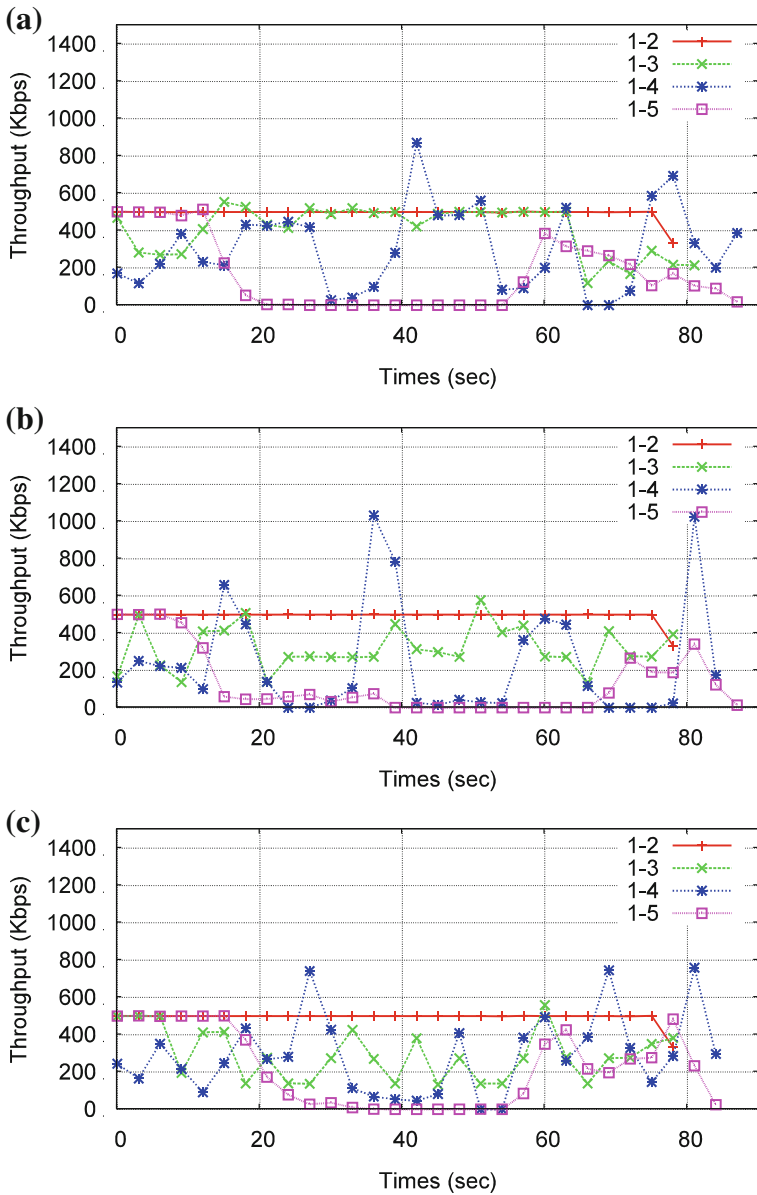


Fig. 3 Throughput results for moving scenario. Interval = 0.5 s (a), 1.0 s (b), 2.0 s (c)

transmission as well as the effects of mobility. Moreover, we show the average throughput and packetloss data for each experiment in Tables 3 and 4, respectively.

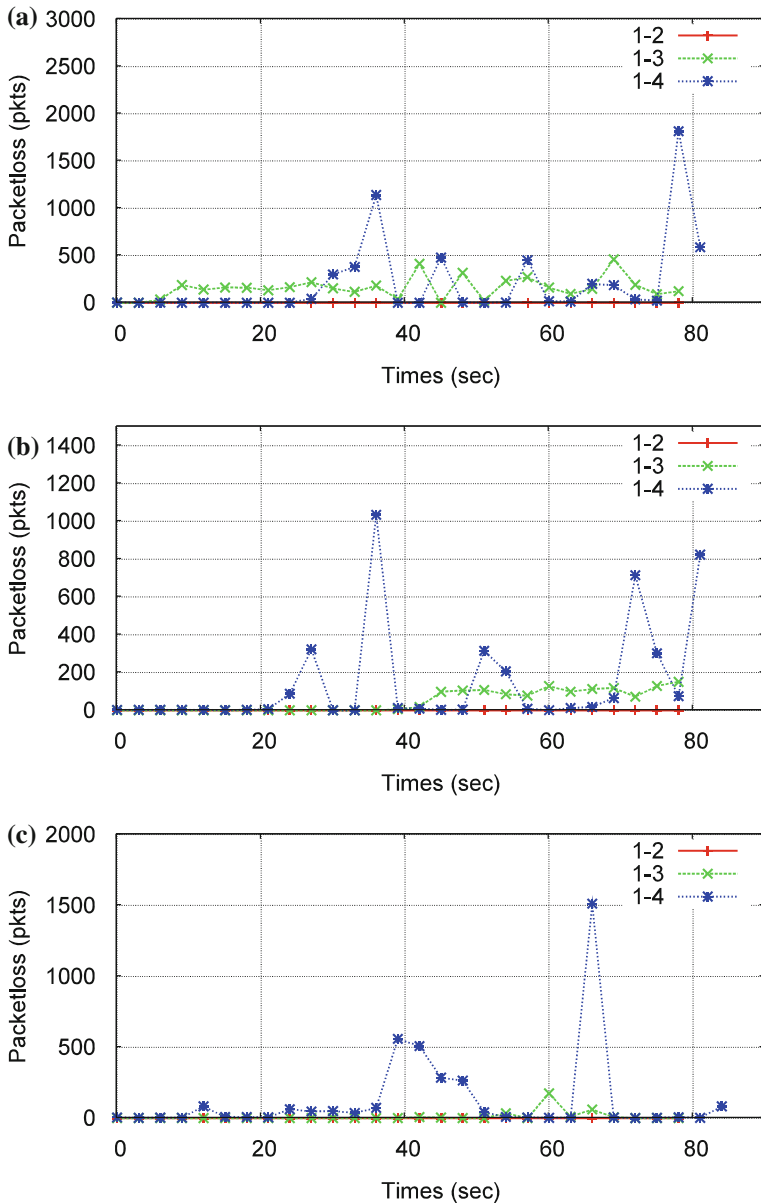


Fig. 4 Packetloss results for static scenario. Interval: = 0.5 s (a), 1.0 s (b), 2.0 s (c)

In Fig. 2, we show the throughput results for STA scenario. We can see that, when the destination is on the other building (node 3 or node 4), there are more oscillations than when destination is node 2, which is in the same building with the source node. From Table 3, we can also notice that the average throughput

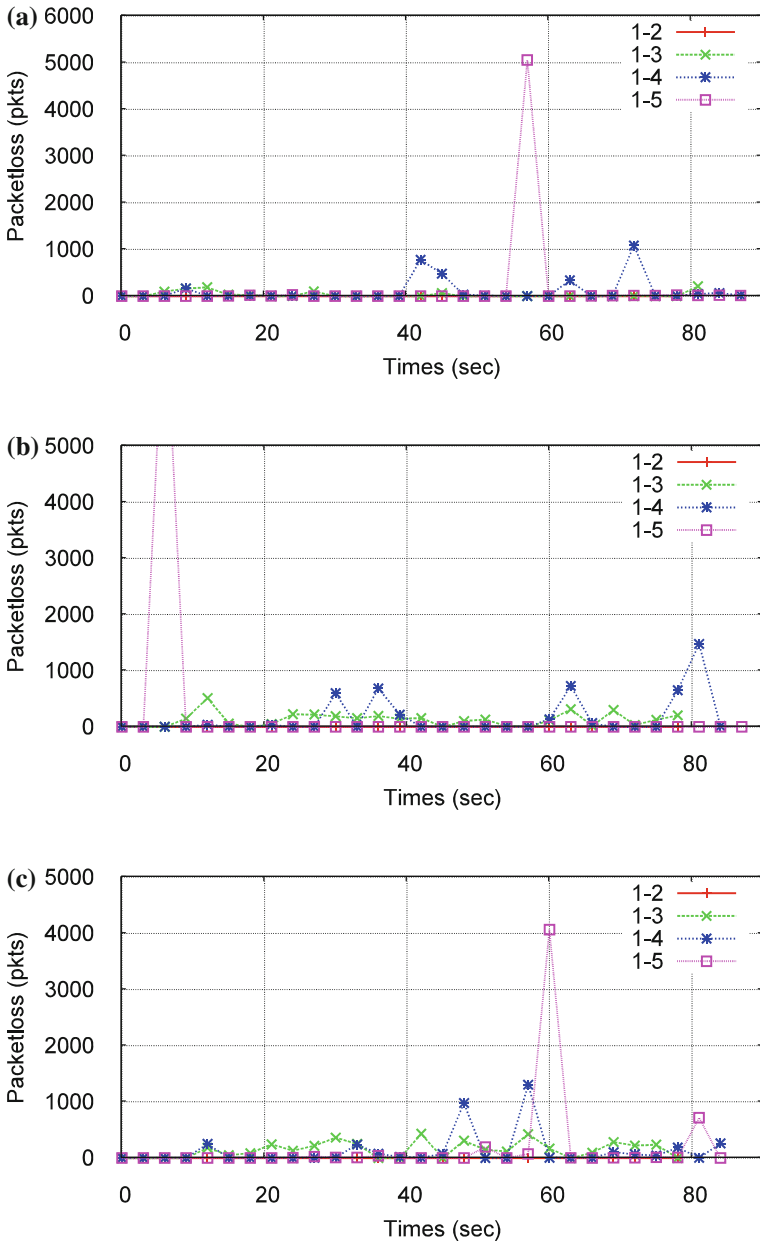


Fig. 5 Packetloss results for moving scenario. Interval: = 0.5 s (a), 1.0 s (b), 2.0 s (c)

decreases further for 1- > 3 and 1- > 4 flows. When the number of hops increases, throughput decreases. On the same case, we see from Table 3, that packetloss also increases from 0 to 94.80 pps. When the interval of HELLO packets increases,

Table 3 Throughput results (kbps)

Scenario	Hello interval (s)	Source node - > Destination node			
		1 - > 2	1 - > 3	1 - > 4	1 - > 5
STA	0.5	499.77	264.81	205.67	-
	1.0	499.79	431.68	280.03	-
	2.0	499.75	483.48	288.51	-
MOV	0.5	499.77	404.83	309.74	164.40
	1.0	499.77	324.31	245.02	133.95
	2.0	499.77	296.61	291.66	223.12

Table 4 Packet loss results (pps)

Scenario	Hello interval (sec)	Source node - > Destination node			
		1 - > 2	1 - > 3	1 - > 4	1 - > 5
STA	0.5	0	70.25	94.80	-
	1.0	0	21.82	75.62	-
	2.0	0	4.93	61.20	-
MOV	0.5	0	14.93	51.72	87.20
	1.0	0	56.88	78.00	114.73
	2.0	0	65.98	60.98	86.25

throughput also increases, because the overhead of HELLO packets decreases. Thus, packetloss decreases and have more oscillations (see Fig. 4).

In Fig. 3, the throughput results for MOV scenario. The mobility of node 5, brings more oscillations than in STA scenario. Because of the mobility, the routes in the network become more dynamic. Thus, the best performance is achieved when the interval of HELLO packets is 0.5.

5 Conclusions

In this paper, we conducted experiments by our MANET testbed for two scenarios. We used OLSR protocol, with ETX_ff for experimental evaluation. We changed the HELLO interval from the default value and compared the effect of different HELLO interval values and mobility. We assessed the performance of our testbed in terms of throughput and packetloss and from our experiments, we found the following results.

- When the destination is on the other building, there are more oscillations than when destination is node 2, which is in the same building with the source node, because the communication happens in a heterogeneous environment (indoor and outdoor).

- When the number of hops increases, throughput decreases. On the same case, packetloss also increases from 0 to 94.80 pps.
- When the interval of HELLO packets increases, throughput also increases, because the overhead of HELLO packets decreases. Packetloss decreases and have more oscillations.
- Because of the mobility of node 5, the routes in the network become more dynamic. Thus, the best performance is achieved when the interval of HELLO packets is lower (0.5 s).

In this work, we carried out the experiments with OLSR. We would like to compare the results with different settings and algorithms of OLSR. We would also like to compare experimental and simulation results. We believe that MAC layer has an effect on the performance, so we would like to use IEEE 802.11g/n for future evaluations.

Acknowledgments This work is supported by a Grant-in-Aid for scientific research of Japan Society for the Promotion of Science (JSPS). The authors would like to thank JSPS for the financial support.

References

1. Lundgren H, Nordstrom E, Tschudin C (2002) Coping with communication gray zones in IEEE 802.11b based ad hoc networks. In: Proceedings of the 5-th ACM international workshop on wireless mobile multimedia (WOWMOM-2002), pp 49–55
2. Kiess W, Mauve M (2007) A survey on real-world implementations of mobile ad-hoc networks. *Ad Hoc Netw* 5(3):324–339
3. Maltz DA, Broch J, Johnson DB (2001) Lessons from a fullscale multihop wireless ad hoc network testbed. *IEEE Pers Commun* 8(1):8–15
4. Gray RS, Kotz D, Newport C, Dubrovsky N, Fiske A, Liu J, Masone C, McGrath S, Yuan Y (2004) Outdoor experimental comparison of four ad hoc routing algorithms. In: Proceedings MSWiM-2004, pp 220–229
5. Anastasi G, Borgia E, Conti M, Gregori E (2005) IEEE 802.11b ad hoc networks: performance measurements. *Cluster Comput* 8(2–3):135–145
6. Johnson D, Hancke G (2009) Comparison of two routing metrics in OLSR on a grid based mesh network. *Ad Hoc Netw* 7(2):374–387
7. De Marco G, Ikeda M, Yang T, Barolli L (2007) Experimental performance evaluation of a pro-active ad-hoc routing protocol in outdoor and indoor scenarios. In: Proceedings of IEEE AINA-2007, pp 7–14, May 2007
8. Kawadia V, Kumar PR (2005) Experimental investigations into TCP performance over wireless multihop networks. In: Proceedings of E-WIND-2005, pp 29–34
9. Clausen T, Hansen G, Christensen L, Behrmann G (2001) The optimized link state routing protocol, evaluation through experiments and simulation. In: Proceedings of IEEE symposium on wireless personal mobile communications. <http://hipercom.inria.fr/olsr/wpmc01.ps>, Sept 2001
10. Kulla E, Ikeda M, Barolli L, Miho R (2010) Impact of source and destination movement on MANET performance considering BATMAN and AODV protocols. In: Proceedings of BWCCA-2010, pp 94–101

11. Hiyama M, Ikeda M, Barolli L, De Marco G, Xhafa F, Durresi A (2009) Mobility effects in mobile ad hoc networks. In: Proceedings of international workshop on network traffic control, analysis and applications (NTCAA-2009), Vol 2, pp 679–684, Dec 2009
12. Tonnesen A () OLSRd: implementation code of the OLSR. <http://www.olsr.org/>
13. ClausenT, Jacquet P (2009) Optimized link state routing protocol (OLSR), RFC 3626 (Experimental)
14. Couto DSJD, Aguayo D, Bicket J, Morris R (2003) A high throughput path metric for multi-hop wireless routing. In: Proceedings of MobiCom-2003, pp 134–146
15. Botta A, Dainotti A, Pescapè A (2007) Multi-protocol and multiplatform traffic generation and measurement. In: Proceedings of INFOCOM-2007, Demo session, pp 1–2, May 2007

Multi-Flow Traffic Investigation of AODV Considering Routing Control Packets

Elis Kulla, Masahiro Hiyama, Makoto Ikeda, Leonard Barolli,
Fatos Xhafa and Makoto Takizawa

Abstract Recently, wireless communication systems are oriented to mobile communications, because of the increasing number of smart phones and tablets in today's market. The interest on Mobile Ad hoc Networks (MANETs) is also increasing due to their potential use in several fields such as collaborative computing and multimedia communications. Thus, there is an increasing need to minimize the overhead introduced by routing protocols in the network. In this paper, we analyze the performance of a MANET by simulations, investigating the effects of RREQ, RREP and RERR, considering Random Waypoint Mobility (RWM) model. We consider the case when source and destination nodes are static.

E. Kulla (✉) · M. Hiyama
Graduate School of Engineering, Fukuoka Institute of Technology (FIT),
3-30-1 Wajiro-Higashi, Higashi-Ku, Fukuoka 811-0295, Japan
e-mail: bd10002@bene.fit.ac.jp

M. Hiyama
e-mail: masahiro.hiyama@gmail.com

M. Ikeda · L. Barolli
Department of Information and Communication Engineering, Fukuoka
Institute of Technology (FIT), 3-30-1 Wajiro-Higashi, Higashi-Ku,
Fukuoka 811-0295, Japan
e-mail: makoto.ikd@gmail.com

L. Barolli
e-mail: barolli@fit.ac.jp

F. Xhafa
Technical University of Catalonia, Department of Languages and Informatics Systems,
C/Jordi Girona 1-3 08034 Barcelona, Spain
e-mail: fatos@lsi.upc.edu

M. Takizawa
Department of Advanced Sciences, Hosei University, 3-7-2 Kajino-machi,
Koganei-shi, Tokyo 184-8584, Japan
e-mail: makoto.takizawa@computer.org

We evaluate the performance by measuring the throughput and AODV control packets, for single-flow and multiple-flow communication.

Keywords NS2 · MANET · Random way-point mobility model · AODV · Static nodes · RERR · RREQ · RREP · Throughput · Single flow · Multiple flows

1 Introduction

Recently, Mobile Ad hoc Networks (MANETs) are continuing to attract the attention for their applications in several fields, where the communication infrastructure is expensive and/or time consuming. In MANET, mobile hosts act as routers and end nodes. Mobility and the absence of any fixed infrastructure make MANET very attractive for rescue operations and time-critical applications. However, they are prone to isolated nodes, limited transmission ability and so on. This brings the need to design routing protocols with increased control capability, by increasing the control packets in the network.

In a research environment, research tools are required to test, verify and identify problems of an algorithm or protocol. These tools are classified in three major techniques: simulators, emulators and real-world experiments. Simulators are a very powerful tool to test the new methods, algorithms and protocols. Experiments in the real world are very important to verify the simulation results and to revise the models implemented in the simulator. Emulators use a hybrid environment, using simulations in an experimental fashion.

We conducted many experiments with our MANET testbed, which are shown in our previous works [1, 2]. We proved that while some of the Optimized Link State Routing (OLSR) problems can be solved, for instance the routing loop, this protocol still has the self-interference problem. There is an intricate inter-dependence between MAC layer and routing layer, which can lead the experimenter to misunderstand the results of the experiments. For example, the horizon is not caused only by IEEE 802.11 Distributed Coordination Function (DCF), but also by the routing protocol.

We carried out the experiments with different routing protocols such as OLSR and Better Approach to Mobile Ad-hoc Networks (BATMAN) and found that throughput of TCP was improved by reducing Link Quality Window Size (LQWS), but there were packet loss because of experimental environment and traffic interference. For TCP data flow, we got better results when the LQWS value was 10. Moreover, we found that the node join and leave operations affect more the TCP throughput and Round Trip Time (RTT) than UDP [3]. In [4], we showed that BATMAN buffering feature showed a better performance than Ad-hoc On-demand Distance Vector (AODV), by handling the communication better when routes changed dynamically.

In [5], we considered the case when source and destination nodes are static and the other nodes are mobile. We evaluated the performance by measuring the number of hops and throughput of one-flow traffic. From results, we found that density and moving speed makes routes more unstable, thus presenting oscillations in number of hops and throughput. In [6], we created different scenarios with different number of static nodes. For all scenarios, the average throughput was around 5 times lower than sent data rate. The number of hops was higher and had more oscillations for denser networks. In this paper, we analyze the performance of AODV routing protocol [7] by NS2. Different from other works, we investigate the performance regarding the route control packets of AODV. We evaluate the performance by measuring the RREQ, RREP and RERR packets as well as throughput of one-flow and multi-flow traffic. The structure of the paper is as follows. In Sect. 2, we show the related work. In Sect. 3, we give an overview of AODV routing protocol. In Sect. 4, we describe our MANET simulation system. In Sect. 5, we discuss the simulation results. Finally, we draw conclusions in Sect. 6.

2 Related Work

Many researchers performed valuable research in the area of wireless multi-hop networks by computer simulations and experiments [8, 9]. Most of them are focused on throughput improvement, but they do not consider mobility [10]. In [11], the authors implemented multi-hop mesh network called Massachusetts Institute of Technology (MIT) Roofnet, which consists of about 50 nodes. They consider the impact of node density and connectivity in the network performance. The authors show that the multi-hop link is better than single-hop link in terms of throughput and connectivity. In [12], the authors analyze the performance of an outdoor ad-hoc network, of AODV and Dynamic Source Routing (DSR) [13] reactive routing protocols.

In [14], the authors perform outdoor experiments of non standard proactive protocols. Other ad-hoc experiments are limited to identify MAC problems, by providing insights on the one-hop MAC dynamics as shown in [15]. In [16], the disadvantage of using hysteresis routing metric is presented through simulation and indoor measurements.

In [17], the authors presents performance of OLSR using the standard hysteresis routing metric and the Expected Transmission Count (ETX) metric in a 7 by 7 grid of closely spaced Wi-Fi nodes to obtain more realistic results. The throughput results are affected by hop distance, similar to our previous work [1].

In [18, 19], the authors propose a dynamic probabilistic broadcasting scheme for mobile ad-hoc networks where nodes move according to different mobility models. Simulation results show that their approach outperforms the Fixed Probability Ad hoc On-demand Distance Vector (FP-AODV) and simple AODV in terms of saved rebroadcast under different mobility models. It also achieves higher

saved rebroadcast and low collision as well as low number of relays than the fixed probabilistic scheme and simple AODV.

The authors of [20], evaluate the robustness of simplified mobility and radio propagation models for indoor MANET simulations. They show that common simplified mobility and radio propagation models are not robust. By analyzing their results, they cast doubt on the soundness of evaluations of MANET routing protocols based on simplified mobility and radio propagation models, and expose the urgent need for more research on realistic MANET simulation.

In [21], three metrics are recommended to construct a credible MANET simulation scenario: average shortest path hop count, average network partitioning, and average neighbour count. The main contribution of this work is to provide researchers with models that allow them to easily construct rigorous MANET simulation scenarios.

3 Overview of AODV Routing Protocol

AODV is one of the most popular reactive routing protocols for MANET. In the following, we will explain its functionalities in a general view. For more detailed description, see [7].

As a reactive (on demand) protocol, when a node wants to transmit data, it first starts a route discovery process, by flooding a RREQ (Route Request) packet. The RREQ packets are forwarded by all nodes by which it is received, until the destination is found. On the way to destination, the RREQ informs all intermediate nodes about a route to the source.

When the RREQ reaches the destination, destination sends a Route Reply (RREP) packet which follows the reverse path discovered by RREQ. This informs all intermediate nodes about a route to the destination node. After RREQ and RREP are delivered to their destination, each intermediate node on the route knows what node to forward data packets in order to reach source or destination. Thus, the data packets do not need to carry addresses of all intermediate nodes in the route. It just carries the address of the destination node, decreasing noticeably routing overheads.

A third kind of routing message, called route error (RERR), allows nodes to notify errors, for example, because a previous neighbour has moved and is no longer reachable. If the route is not active (i.e., there is no data traffic flowing through it), all routing information expires after a timeout and is removed from the routing table. When a link break in an active route occurs, the node upstream of that break may choose to repair the link locally if the destination was no farther than a number of hops away.

AODV is based on DSDV and DSR algorithms. The best advantage to DSR and DSDV is that in AODV, packets being sent (the RREP packet also) carry only the address of the destination and not the addresses of all intermediate nodes to make the delivery. This lowers routing overheads. In AODV, the route discovery process

may last for a long time, or it can be repeated several times, due to potential failures during the process. This introduces extra delays, and consumes more bandwidth as the size of the network increases.

4 Simulation System

Simulation is the process of designing a model of a real system and conducting experiments with this model for the purpose of understanding the behaviour of the system and/or evaluating various strategies for the operation of the system [22]. In MANET, simulations are very important to understand the behaviour of routing protocols, addressing mechanisms, security algorithms, mobility models, and so on. There are a number of network simulators such as NetSim [23], OPNET [24], NS2/NS3 [25, 26], which are usually used in the network simulations. In this work we used NS2, which is equipped with enough modules and analyzing tools.

4.1 NS2

Network Simulator version 2 (NS2) is a discrete event simulator. It is primarily unix-based simulator build on different modules and uses TCL scripting language for varying parameters and C++ structured code. The modules included in NS2 are nodes, links, SimpleLink objects, packets, agents, and applications. There are also three helper modules: timers, random number generators, and error models. NS2 also consists of radio propagation models, traffic generators, topology generators for different mobility models and so on.

4.2 Random Way-Point Mobility Model

Random Way point Mobility (RWM) model was proposed in [27] and it is used widely in simulating MANETs. In NS2, this mobility model can be modelled by using the *setdest* tool. In RWM model, the moving directions of nodes are uncorrelated to each-other.

1. Selects a random starting position in the simulation area ($L \times W$).
2. Selects a random location in the area as the next way-point (W).
3. Starts moving towards the destination W , with a randomly chosen speed between V_{\min} and V_{\max} .
4. After reaching destination W , the node pauses for T_p s.
5. Then it repeats steps 2–4, until the simulation time T_{\max} finishes.

The movement speed is a key parameter to decide the dynamism of the topology and therefore changes in routes. For low speeds the topology is almost static and for high speeds the topology becomes dynamic and the routes change frequently.

4.3 Simulation Topologies

We prepared the simulation environment, considering the parameters during simulation time, as shown in Table 1. The size of the simulation area is 1000×1000 and we use 5 cases with 20, 40, 60, 80 and 100 nodes distributed and moving randomly in this area. For each case, the nodes move with different uniformly distributed speeds, based on RWM model. The pause time is considered 2 s. We investigate the effect of node density and speed in AODV performance, by sending single- and multiple-flow data.

In our previous works, we investigated the performance of the network, in the case when all nodes were mobile, including source and destination. But, when source and destination nodes are moving, the number of hops that a packet needs to reach the destination is strongly related to the distance between the two nodes (there are also other factors). On the other hand, the distance between source and destination is a function, which is related to the randomness of way-point selection. Thus, the communication will be mostly affected by the randomness of the RWM model, than by any properties of routing protocols. Thus, we chose a static source and static destination in our scenario.

In Fig. 1, we describe the static position of nodes for our scenario. We send single-flow data from source and destination nodes, which are positioned in S(200, 200) and D(800, 800), respectively (as shown in Fig. 1a). All other nodes are moving according to RWM model. We should note that the distance between static nodes is around 850 m and the packets need at least 4 hops to reach the destination. In Fig. 1b, we show the scenario, when we send 4 flows in the network, using two source nodes and two destination nodes. The distance between sources and destinations is 600 or 850 m.

Table 1 Simulation settings

Functions	Values	Functions	Values
Area size	1000×1000 m	Pause time	2 s
Number of nodes	20, 40, 60, 80 and 100	Packet rate	200 pps
Transmission range	250 m	Packet size	230 bytes
Simulation time	300 s	Routing protocol	AODV
Speed distributions	1–5, 5–10, 10–20, 20–30		

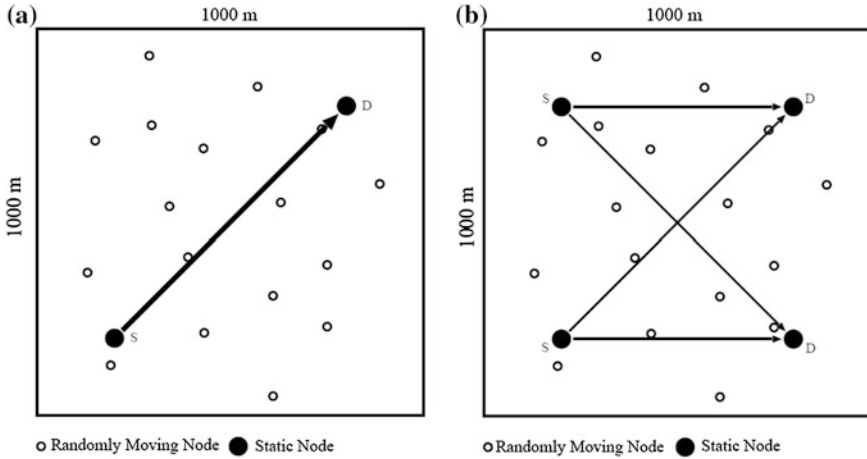


Fig. 1 Simulation Scenarios. **a** One-flow data. **b** Multi-flow data

5 Simulation Results

In this section, we will present the simulation results. We show the total number of RREQ and RERR as well as the rate of RREP packets over RREQ, in Figs. 2, 3, in order to understand how is affected the throughput, which is shown in Fig. 4 in average values during 300-second simulation.

The number of RREQ packets increases when the number of nodes in the network increases (see Fig. 2a), because RREQ packets are broadcast in a larger network. We notice also that as the speed of nodes increases, there are more RREQ packets in the network. We have similar results for RERR also, as shown in Fig. 2c. In fact, RREP packets are responsible for transmitting route information, so we show the rate of RREP packets over RREQ packets in Fig. 2b. We show the rate because RREP packets are sent in response to RREQ packets. In this case when number of nodes is smaller, the rate is bigger, because the number of RREQ packets is small.

We also sent multiple flows in the network and show results in Fig. 3. The dependence from the movement speed is similar as in the single-flow case. We notice that, the number of RREQ packets is smaller than in single-flow case. This is an interesting result, as we expected to have more RREQ packets in the case where there are more data sent in the network. On the other hand, the number of RERR packets is increased, because the nodes are busier and they may serve to different routes at the same time. The rate of RREP over RREQ packets has similar values. We will investigate further in this rate, which seems to be dependent only on physical conditions of the network and not on the amount of data sent.

Fig. 2 AODV control packets (Single-flow data).
a RREQ. **b** RREP/RREQ. **c** RERR

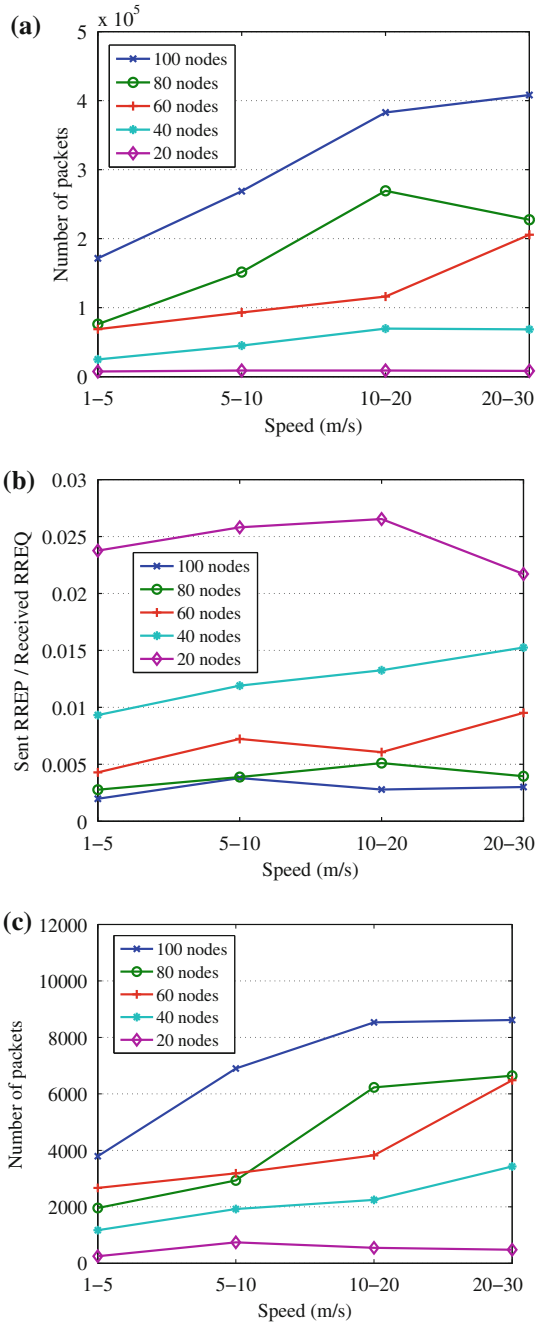
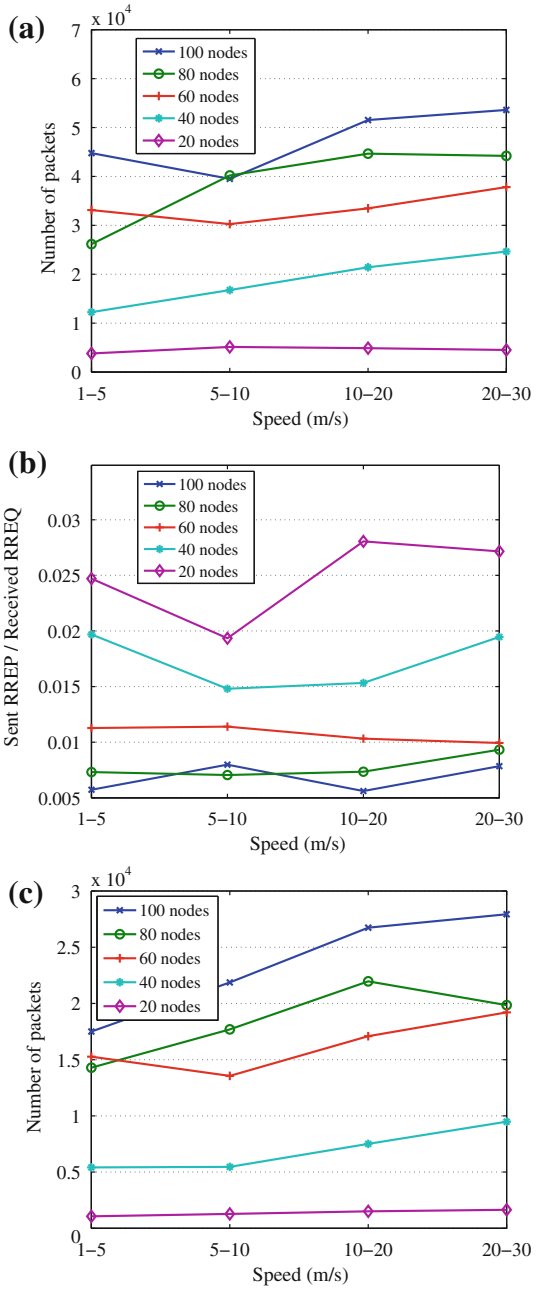


Fig. 3 AODV control packets (Multiple-flow data).
a RREQ. **b** RREP/RREQ. **c** RERR



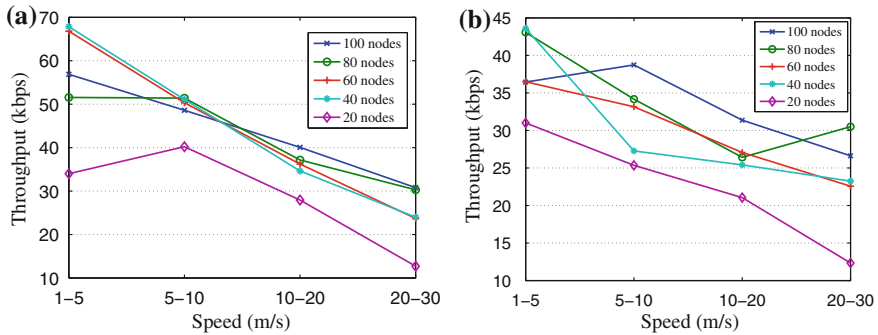


Fig. 4 Average throughput. **a** Single-flow. **b** Multi-flow

In Fig. 4, we show the throughput results for both single-flow and multi-flow traffic. Throughput for multiple-flow communication is shown as the average value for all four flows. In general, throughput decreases as the moving speed increases, because the routes become unstable from dynamic topology changes. When there are 20 nodes in the network, the performance is lower, because the area is too big to get covered by 20 nodes. When the number of nodes increases, throughput becomes a little better. The area is covered for 40 or more nodes. In the case of multi-flow communication the average throughput is lower than the single-flow case. But if we consider that there are four flows, the quality is still good.

6 Conclusions and Future Work

In this paper, we analysed the performance of a AODV by NS2 simulations. We sent one flow and four flows of data in the network and measured the number of control packets and throughput, in order to analyze the performance of the network with different number of nodes and different movement speed of nodes. All nodes were moving, while source and destination nodes were static. From the simulation results, we conclude as follows.

- The number of RREQ packets increases when the number of nodes in the network increases. The number of RREQ packets is smaller in multi-flow case.
- As the speed of nodes increases, there are more RREQ packets in the network for single-flow and multi-flow cases.
- The rates of RREP over RREQ have similar values for both cases. This rate seems to be independent on the amount of data sent.
- In general, throughput decreases as the moving speed increases.
- When there are 20 nodes in the network, the performance is lower, because the area is too big to get covered by 20 nodes. When the number of nodes increases, throughput improves.

- In the case of multi-flow communication the average throughput is lower than the single-flow case.

As future work, we would like to continue the investigation of AODV routing control packets. For multi-flow communication, we will make a detailed investigation of each flow. We will also consider a more realistic mobility model, which can test the properties of MANET routing protocols and applications.

Acknowledgments This work is supported by a Grant-in-Aid for Scientific Research from Japanese Society for the Promotion of Science (JSPS). The authors would like to thank JSPS or the financial support.

References

1. De Marco G, Ikeda M, Yang T, Barolli L (2007) Experimental performance evaluation of pro-active adhoc routing protocol in outdoor and indoor scenarios. In: Proceedings of AINA-2007, pp 7–14, May 2007
2. Barolli L, Ikeda M, De Marco G, Durresi A, Xhafa F (2009) Performance analysis of OLSR and BATMAN protocols considering link quality parameter. In: Proceedings of AINA-2009, pp 307–314, May 2009
3. Ikeda M, Barolli L, Hiyama M, Yang T, De Marco G, Durresi A (2009) Performance evaluation of a MANET testbed for different topologies. In: Proceedings of NBiS-2009, Indianapolis, pp 327–334, Aug 2009
4. Kulla E, Ikeda M, Barolli L, Miho R (2010) Impact of source and destination movement on MANET performance considering BATMAN and AODV protocols. In: Proceedings of BWCCA-2010, pp 94–101
5. Kulla E, Ikeda M, Barolli L, Younas M, Uchida K, Takizawa M (2012) Simulation performance of a MANET using static source and destination considering AODV routing protocol. In: Proceedings of NBiS-2012, pp 141–147
6. Kulla E, Hiyama M, Ikeda M, Barolli L, Uchida K, Takizawa M (2012) Setting up static components for investigating MANET performance: a simulation case. In: Proceedings of BWCCA-2012, pp 53–59, 2012
7. Perkins C, Belding-Royer E, Das S (2003) Ad hoc on-demand distance vector (AODV) routing, RFC3561. Nokia Research Center, University of California, University of Cincinnati. <http://www.ietf.org/rfc/rfc3561.txt>. Accessed May 2012
8. Nordström E (2002) APE—a large scale ad-hoc network testbed for reproducible performance tests, Master's thesis, Uppsala University
9. Owada Y, Takahashi Y, Suda T, Terui H, Taki F, Yagi T, Mase K (2005) A large scale wireless mobile adhoc network testbed. In: Proceedings of IEEE vehicular technology conference, pp 324–328, Sept 2005
10. Draves R, Padhye J, Zill B (2004) Comparison of routing metrics for static multi-hop wireless networks. In: Proceedings of SIGCOMM-2004, pp 133–144
11. Bicket J, Aguayo D, Biswas S, Morris R (2005) Architecture and evaluation of an unplanned 802.11b mesh network. In: Proceedings of MOBICOM-2005, pp 31–42
12. Maltz DA, Broch J, Johnson DB (2001) Lessons from a full-scale multihop wireless ad-hoc network testbed. *J Pers Commun* 8(1):8–15
13. Johnson DB, Maltz DA, Broch J (2001) DSR: the dynamic source routing protocol for multi-hop wireless ad-hoc networks. *J Ad-Hoc Netw* 5:139–172

14. Gray RS, Kotz D, Newport C, Dubrovsky N, Fiske A, Liu J, Masone C, McGrath S, Yuan Y (2004) Outdoor experimental comparison of four ad-hoc routing algorithms. In: Proceedings of MSWiM-2004, pp 220–229
15. Borgia E, Conti M, Gregori E (2005) IEEE 802.11b ad-hoc networks: performance measurements. *J Cluster Comput* 8(2–3):135–145
16. Clausen T, Hansen G, Christensen L, Behrmann G (2001) The optimized link state routing protocol, evaluation through experiments and simulation. In: Proceedings of IEEE symposium on wireless personal mobile communications. <http://hipercom.inria.fr/olsr/wpmc01.ps>, Sept 2001
17. Johnson D, Hancke G (2009) Comparison of two routing metrics in OLSR on a grid based mesh network. *J Ad-Hoc Netw* 7(2):374–387
18. Hanashi AM, Siddique A, Awan I, Woodward M (2007) Performance evaluation of dynamic probabilistic flooding under different mobility models in MANETs. In: Proceedings of ICPADS-2007, Vol 2, pp 1–6, Dec 2007
19. Hanashi AM, Awan I, Woodward M (2009) Performance evaluation with different mobility models for dynamic probabilistic flooding in MANETs. *J Mobile Inf Sys* 5(1):65–80
20. Cavilla AL, Baron G, Hart TE, Litty L, de Lara E (2004) Simplified simulation models for indoor MANET evaluation are not robust. Proceedings of annual IEEE communications society SECON-2004 conference, pp 610–620, Oct 2004
21. Munjal A, Camp T, Navidi WC (2010) Constructing rigorous MANET simulation scenarios with realistic mobility. Proceedings of European wireless (EW-2010) conference, pp 817–824, Apr 2010
22. Shannon RE (1998) Introduction to the art and science of simulation. In: Proceedings of WSC-98
23. NETSIM—the cisco network simulator & router simulator. <http://www.boson.com/netsimcisco-network-simulator>. Accessed Mar 2012
24. OPNET—optimized network engineering tools. <http://www.opnet.com/>. Accessed Mar 2012
25. NS2—network simulator version 2. <http://www.isi.edu/nsnam/ns/>. Accessed Mar 2012
26. NS3—network simulator version 3. <http://www.nsnam.org/>. Accessed Mar 2012
27. Broch J, Maltz DA, Johnson DB, Hu Y-C, Jetcheva J (1998) A performance comparison of multi-hop wireless ad hoc network routing protocols. In: Proceedings of the fourth annual ACM/IEEE Mobicom-98, ACM, Oct 1998

An Estimation Method for Amplitude Modification Factor Using Floor Area Ratio in Urban Areas

Kazunori Uchida, Keisuke Shigetomi, Masafumi Takematsu
and Junich Honda

Abstract This paper is concerned with a numerical simulation of electric field distributions in urban areas by using the 1-ray model combined with 2-ray model. Introducing amplitude modification factor α and propagation order β of distance, this model is arranged so that we can deal with propagation in complicated electromagnetic environments. We show that the two parameters α and β can be obtained from Hata's empirical equations. In this paper, we propose an estimation method for the electric field distributions in complicated propagation environments in addition to those areas defined by the Hata's equations by employing statistical data such as building coverage and floor area ratios. Numerical analyses are carried out to show an example of distribution of amplitude modification factor α in Fukuoka city.

Keywords Radio propagation · 1-ray model · Amplitude modification factor · Propagation order

1 Introduction

Recently, demands for wireless communications, such as cellular phones, wireless LANs, ad hoc networks, sensor networks etc., have rapidly been increasing. In many wireless systems, base stations (BSs) and/or mobile stations (MSs) are sometimes located in complicated natural or artificial propagation environments;

K. Uchida (✉) · K. Shigetomi · M. Takematsu
Fukuoka Institute of Technology, Fukuoka 811-0295, Japan
e-mail: k-uchida@fit.ac.jp

J. Honda
Electronic Navigation Research Institute, Cyofu 182-0012, Japan
e-mail: jhonda.fit@gmail.com

for examples, random rough surfaces (RRSs) such as desert, hilly mountain, sea surface and so on, or urban, suburban and rural areas. Thus it is important for wireless communication engineers to estimate propagation characteristics in these complicated electromagnetic environments in order to achieve the objectives to construct reliable and low-cost wireless networks [1].

For the simulation of electromagnetic (EM) wave propagation in complicated propagation environments described above, we have so far proposed field expressions based on 1-ray and 2-ray models by introducing the modification factor α and the propagation order β of distance [2]. The latter parameter was originally introduced by Hata to empirically estimate the path losses in urban, suburban and open areas for the introduction of vehicular phone systems in Japan [3].

The two parameters α and β have also been successfully applied to the problem of EM wave propagation along RRSs [1, 4, 5]. The most interesting feature of the parameters is that we can evaluate EM field distributions in a simple way based on the 1-ray or 2-ray model by choosing the parameters appropriately [6, 7]. Moreover, we can easily evaluate communication distance along RRSs when the input power of a transmitter and the detectable minimum power of a receiver are given [1, 5].

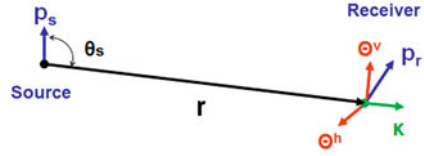
It is interesting that the propagation order β of distance depends only on the height of BS antenna according to the Hata's empirical equations from which we can obtain an explicit form of path loss L_p in urban, suburban and open areas, respectively [3]. The 1-ray model, on the other hand, enables us to analytically compute α in terms of β and L_p , and consequently we can estimate α as long as the propagation environments are restricted only to urban, suburban or open area. In case of propagation along RRSs, the above mentioned parameters should be closely related to the statistical quantities related to RRSs such as deviation of height and correlation length as well as antenna height of BSs [9, 10]. In urban areas, on the other hand, the amplitude modification factor α might be closely associated with the complexity of propagation environments, for example, high density of high-rise buildings in urban areas.

The main purpose of this paper is to propose an estimation method for the amplitude modification factor α in terms of building coverage ratio and floor area ratio in urban or suburban areas. The basis of the present view point is that the complexity of a city is well explained in terms of these two statistical ratios. We also show some numerical examples for distributions of the building coverage and floor area ratios as well as an estimated amplitude modification factor in Fukuoka.

2 Field Expression Based on 1-Ray Model

Now we review the 1-ray model introduced by the authors based on the incident wave in the free space weighted by amplitude modification factor α , propagation order β of distance and field matching factor γ [6, 7]. It should be noted that the model is simple but it can be applied effectively to the estimation of EM field

Fig. 1 Incident ray related vectors



distributions in many complicated propagation environments, such as urban, suburban and open areas as well as RRSs. In other words, we can always approximate EM field distributions in any complicated propagation environments, only if the parameters α and β are employed appropriately for numerical computations. The electric field expression in far zone ($r \gg \lambda$) is summarized as follows [6, 7]:

$$\mathbf{E}(r) = 10^{\alpha/20} 10^{(\beta-1)\gamma/20} r^{(1-\beta)} \mathbf{E}_i(r) \tag{1}$$

where $r = |\mathbf{r}|$ is the distance from the source antenna to a receiving antenna as shown in Fig. 1. The field matching factor γ is defined by

$$\gamma = 20 \log_{10}[\Gamma(r)] \tag{2}$$

where the field matching distance is defined by

$$\Gamma(r) = r|\mathbf{E}_t(r)|/|\mathbf{E}_i(r)| \tag{3}$$

It is sufficient for the distance r to be chosen as a maximum communication distance.

The incident field in the free space is expressed as follows [11, 12]:

$$\mathbf{E}_t(r) = \mathbf{E}_i(r) + \sqrt{30G_s P_s} \cdot \frac{|\mathbf{p}_s \times \mathbf{r}_s|}{r_s} \cdot \frac{e^{-jk_0 r_0}}{r_0} \mathbf{e}_r(r). \tag{4}$$

where the time dependence $e^{j\omega t}$ is assumed and $\kappa_0 = \omega\sqrt{\epsilon_0\mu_0}$ is the wave number in free space with permittivity ϵ_0 and permeability μ_0 . In Eq. (4) we have assumed that the source is a small dipole antenna with input power P_s and gain $G_s = 1.5$.

On the other hand, the total field above a ground plane is given by the sum of the incident and reflected fields as follows:

$$\mathbf{E}_t(r) = \mathbf{E}_i(r) + \sqrt{30G_s P_s} \cdot \frac{|\mathbf{p}_s \times \mathbf{r}_s|}{r_s} \cdot \frac{e^{-jk_0 r_0}}{r_0} \mathbf{e}_r(r). \tag{5}$$

The electric field vector for the reflected wave is given by

$$\begin{aligned} \mathbf{e}_r(r) = & R^v(\theta_i)[\Theta^v(\mathbf{r}_s, \mathbf{p}_s) \cdot \Theta^v(\mathbf{r}_s, \mathbf{n})]\Theta^v(\mathbf{r}_r, \mathbf{n}) \\ & + R^h(\theta_i)[\Theta^h(\mathbf{r}_s, \mathbf{p}_s) \cdot \Theta^h(\mathbf{r}_s, \mathbf{n})]\Theta^h(\mathbf{r}_r, \mathbf{n}) \end{aligned} \tag{6}$$

where \mathbf{r}_s is the position vector from the source to the reflection point, and \mathbf{r}_r is the position vector from the reflection point to the receiving antenna as shown in

Fig. 2 Reflection ray and related vectors

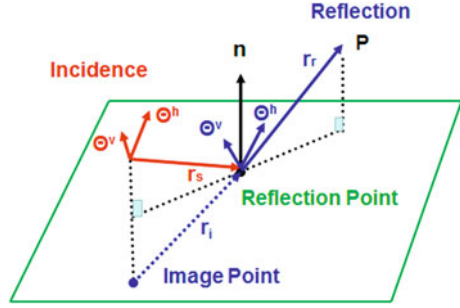


Fig. 2 together with $r_0 = |\mathbf{r}_s| + |\mathbf{r}_r|$. The vertical and horizontal unit vectors used in Eqs. 4 and 6 are defined by

$$\Theta^v(\mathbf{r}, \mathbf{p}) = \frac{(\mathbf{r} \times \mathbf{p}) \times \mathbf{r}}{|(\mathbf{r} \times \mathbf{p}) \times \mathbf{r}|}, \quad \Theta^h(\mathbf{r}, \mathbf{p}) = \frac{\mathbf{r} \times \mathbf{p}}{|\mathbf{r} \times \mathbf{p}|} \quad (7)$$

where \mathbf{p} is an arbitrary unit vector. Moreover, the Fresnel reflection coefficients for the vertical and horizontal electric field components are given by [11, 12]

$$R^h(\theta_i) = \frac{\cos \theta_i - \sqrt{\epsilon_c - \sin^2 \theta_i}}{\cos \theta_i + \sqrt{\epsilon_c - \sin^2 \theta_i}}, \quad R^v(\theta_i) = \frac{\epsilon_c \cos \theta_i - \sqrt{\epsilon_c - \sin^2 \theta_i}}{\epsilon_c \cos \theta_i + \sqrt{\epsilon_c - \sin^2 \theta_i}} \quad (8)$$

where $\epsilon_c = \epsilon_r - j\sigma/\omega\epsilon_0$ is the complex permittivity of the ground plane with dielectric constant ϵ_r and conductivity σ . In the subsequent numerical examples we select the parameters such that $\epsilon_r = 5.0$ and $\sigma = 0.0023$ [S/m] corresponding to a dry soil constituting the ground plane. The angle θ_i in Eq. (8) is the incident angle of the incident ray at the reflection point.

In the far zone ($r \gg \lambda$), the field matching distance $\Gamma(r)$ can be approximated as follows:

$$\Gamma(r) \simeq \Gamma_0 \simeq 2\kappa_0 h_b h_m. \quad (9)$$

It should be noted that Eq. (9) holds within 91.5 % numerical error for $r = \Gamma_0$ and within 99.3 % for $r = 5\Gamma_0$. As a result, it can be concluded that the electric field intensity above a plane ground plane is enhanced as the source and receiving antenna heights are increased.

3 Communication Distance and Path Loss

Since the direction vectors of the source and receiving antennas are \mathbf{p}_s and \mathbf{p}_r as shown in Fig. 1, the received power of the small dipole antenna can be expressed as follows [11, 12]:

$$P_r = \lambda^2 G_r |\mathbf{E} \cdot \mathbf{p}_r|^2 / (4\pi Z_0) \quad (10)$$

where $G_r = 1.5$ is the gain of the small dipole receiving antenna and $Z_0 \simeq 120\pi \text{ } [\Omega]$ is the intrinsic impedance of the free space. Combining Eqs. (1) and (4), the electric field intensity according to the 1-ray model is given by

$$|E_1| = 10^{\frac{\alpha}{20}} \cdot 10^{\frac{(\beta-1)r}{20}} \cdot \sqrt{30G_s P_s} \cdot r^{-\beta} \quad (11)$$

where the antenna orientation is assumed to be arranged so that the maximum received power may be obtained. Let E_{\min} be the minimum detectable electric field intensity. Then, Eq. (11) yields the maximum communication distance D_c as follows:

$$D_c = 10^{\frac{\alpha}{20\beta}} \times 10^{\frac{(\beta-1)D_c}{20\beta}} \times (30G_s P_s)^{\frac{1}{2\beta}} \times (E_{\min})^{-\frac{1}{\beta}}. \quad (12)$$

Assuming the ideal isotropic source and receiving antennas with unit gain $G_s = G_r = 1$ in accordance with the Hata's empirical equations, the received power in Eq. (10) can be rewritten in [dB] as follows:

$$P_r[\text{dBW}] = |\mathbf{E}|[\text{dBV/m}] - 10 \log_{10} Z_0 + 10 \log_{10} (\lambda^2 / 4\pi) \quad (13)$$

where $\lambda = c/f = 2\pi c/\omega$ is the wave length in the free space with frequency f [Hz] and light velocity $c = 3 \times 10^8$ [m/s].

Since the path loss L_p is given by the difference between the transmitted and received powers in [dB], it is described as follows [3]:

$$\begin{aligned} L_p[\text{dB}] &= P_s[\text{dBW}] - P_r[\text{dBW}] \\ &= P_s[\text{dBW}] - |\mathbf{E}|[\text{dBV/m}] + 10 \log_{10} Z_0 - 10 \log_{10} (\lambda^2 / 4\pi). \end{aligned} \quad (14)$$

Equation (14) indicates that the received electric field can be derived from the path loss L_p as long as the input power P_s is specified. According to the 1-ray model in Eq. (1), the path loss defined in Eq. (14) is rewritten for the 1-ray model as follows:

$$\begin{aligned} L_p[\text{dB}] &= -\alpha - (\beta - 1)\Gamma + 20\beta \log_{10} r - 10 \log_{10} 30 \\ &\quad + 10 \log_{10} Z_0 - 10 \log_{10} (\lambda^2 / 4\pi). \end{aligned} \quad (15)$$

As a result, the relation between α and β can be explicitly described by Eq. (15), as far as the path loss L_p is known experimentally or theoretically.

Path losses in the urban, suburban and open areas can be estimated from the Hata's empirical equations [3]. One of the important features is that β depends only on the BS antenna height h_b [m] as follows:

$$\beta = (44.9 - 6.55 \log_{10} h_b) / 20 \simeq 2.25 - 0.33 \log_{10} h_b. \quad (16)$$

It is interesting that β is independent on other parameters which would be affected by natural or artificial environments where experimentations were performed.

Thus Eq. (15) leads to an explicit expression for α based on the 1-ray model as follows:

$$\begin{aligned} \alpha = & -L_p[\text{dB}] - (\beta - 1)\Gamma + 20\beta \log_{10} R \\ & + 20 \log_{10} f_c + 60\beta + 20 \log_{10}(4\pi/300) \end{aligned} \quad (17)$$

where some unit conversions have been made in accordance with the Hata's results; that is, $f[\text{Hz}] \rightarrow f_c[\text{MHz}]$ and $r[\text{m}] \rightarrow R[\text{Km}]$. It should be noted that the above formulation is restricted only to the urban, suburban and open areas, and thus we must interpolate the amplitude modification factor α in other regions approximately [13].

For example, if we select as $h_b = 30$ [m], Eq. (16) yields $\beta = 1.76$. And if we choose as $f_c = 800$ [MHz], $h_m = 1.5$ [m], $\varepsilon_r = 5.0$ and $\sigma = 0.0023$ [S/m], Eq. (17) together with L_p from Hata's empirical equations provides amplitude modification factors $\alpha_u = -37.3$ [dB], $\alpha_s = -27.7$ [dB] and $\alpha_o = -9.3$ [dB] in urban, suburban and open areas, respectively.

4 Building Coverage Ratio and Floor Area Ratio

In Japan the statistics of buildings and houses in a city are described in terms of the two parameters; one is the building coverage ratio KD indicating the total covered area on all floors of all buildings on a certain site area, and the other is the floor area ratio YD denoting the ratio of the total floor area of buildings to the site area. They are classified into gross and net data, that is, (GKD, GYD) and (NKD, NYD) depending on whether they include road and park areas or not. We have obtained these data from the local government in Fukuoka. Figure 3 shows the net building

Fig. 3 Net building coverage ratio

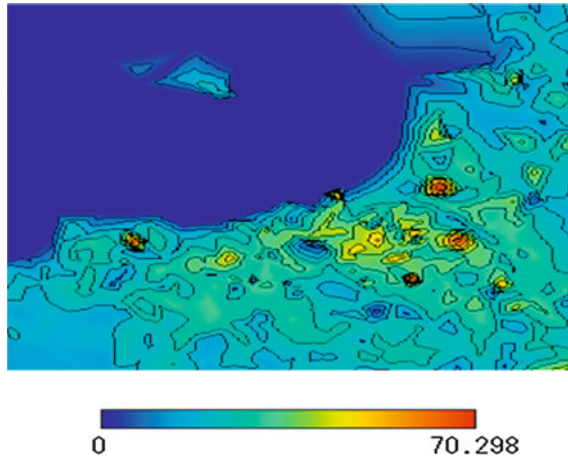
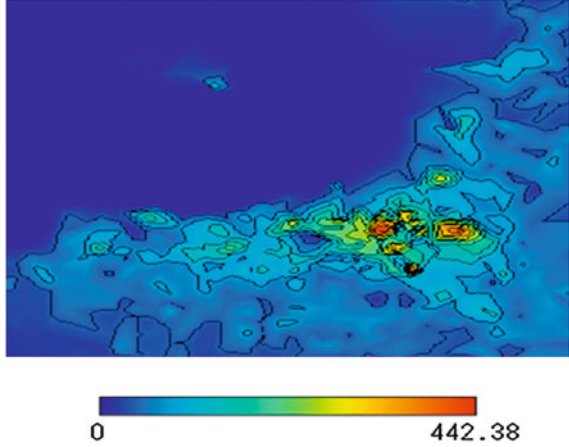


Fig. 4 Gross floor area ratio



coverage ratio GKD in Fukuoka, and Fig. 4 depicts the gross floor area ratio GYD in Fukuoka.

Now we assume that α can be approximated by the Lagrange interpolation in terms of the gross floor area ratio GYD as follows [14]:

$$\alpha = \frac{(y - y_s)(y - y_o)}{(y_u - y_s)(y_u - y_o)}\alpha_u + \frac{(y - y_u)(y - y_o)}{(y_s - y_u)(y_s - y_o)}\alpha_s + \frac{(y - y_u)(y - y_s)}{(y_o - y_u)(y_o - y_s)}\alpha_o \quad (18)$$

where α_u , α_s and α_o are the amplitude modification factors α in urban, suburban and open areas, respectively. The parameter y is given in the form of a parametric representation with respect to GDY as follows:

$$y_p = f(x_p) \quad (p = u, s, o) \quad (19)$$

where x_u , x_s and x_o are the gross floor area ratios GYD in urban, suburban and open areas, respectively.

Figures 5 and 6 shows an example of interpolated α in Fukuoka where we have selected “Tenjin” as an urban area with $x_u = 435.8$, “Hakozaki” as a suburban area with $x_s = 87.2$ and “Heiwa” as an open area with $x_o = 5.2$, respectively. It is worth noting that “Tenjin” area is the center of commercial district and “Heiwa” area is one of the graveyards in Fukuoka. Moreover, we have assumed that the parametric function is denoted by $y = x^\eta$, and we have selected as $\eta = 0.4$ in this numerical example.

Fig. 5 Interpolated α by GVD

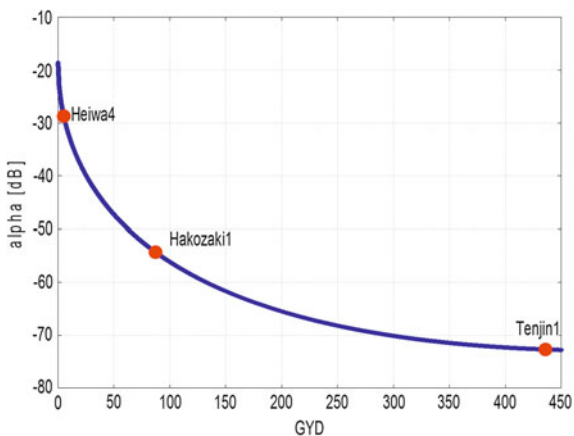
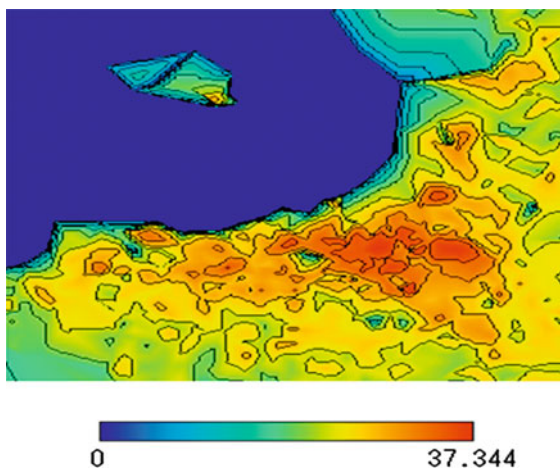


Fig. 6 Amplitude modification factor ($-\alpha$)



5 Conclusion

In this paper, first we have reviewed the 1-ray model combined with the 2-ray model to estimate propagation characteristics in complicated electromagnetic environments such as urban, suburban and open areas. Second, we have shown the building coverage ratio GKD and the floor area ratio GVD of Fukuoka city in terms of the method of vector interpolation. Finally, we have proposed an approximate estimation algorithm for the relationship between amplitude modification factor α and gross floor area ratio GVD . Some numerical results have also been shown to demonstrate the effectiveness of the proposed estimation method.

Estimation for path loss and communication distance in cities deserves as a future problem.

Acknowledgments The work was supported in part by a Grand-in Aid for Scientific Research (C) (24560487) from Japan Society for the Promotion of Science.

References

1. Uchida K, Honda J (2010) Estimation of propagation characteristics along random rough surface for sensor networks. In: Merret GV, Tan YK (eds.) *Wireless sensor networks: application-centric design*, Chapter 13. InTech, pp 231–248
2. Uchida K, Honda J (2011) An algorithm for allocation of base stations in inhomogeneous cellular environment. In: *Proceedings of 2011 international conference on network-based information systems (NBIS-2011)*, pp 507–512, Sept 2011
3. Hata M (1980) Empirical formula for propagation loss in land mobile radio services. *IEEE Trans Veh Technol* VT-29(3):317–325
4. Uchida K, Honda J, Yoon KY (2011) An algorithm for rough surface generation with inhomogeneous parameters. *J Algorithm Comput Technol* 5(2):259–271
5. Honda J, Uchida K, Yoon KY (2010) Estimation of radio communication distance along random rough surface. *IEICE Trans Electron* E93-C(1):39–45
6. Uchida K, Honda J, Tamaki T, Takematsu M (2011) Two-rays model and propagation characteristics in view of hata's empirical equations. *IEICE technical report AP2011-14:49–54*
7. Uchida K, Honda J, Lee JH (2011) A study of propagation characteristics and allocation of mobile stations. *IEICE technical report IN2011-98:31–36, MoMuC2011-32:31–36*
8. Uchida K, Honda J, Yoon KY (2009) Distance characteristics of propagation in relation to inhomogeneity of random rough surface. In: *Proceedings of 12th international symposium on microwave and optical technology*, pp 1133–1136, Dec 2009
9. Uchida K, Takematsu M, Honda J (2012) An algorithm to estimate propagation parameters based on 2-ray model. In: *Proceedings of NBIS-2012, Melbourne*, pp 556–561, Sept 2012
10. Uchida K, Takematsu M, Lee JH, Honda J (2012) Field distributions of 1-ray model using estimated propagation parameters in comparison with DRTM. In: *Proceedings of BWCCA-2012, Victoria*, pp 488–493, Nov 2012
11. Mushiake Y (1985) *Antennas and radio propagation*. Corona Publishing Co. Ltd, Tokyo
12. Collin RE (1985) *Antennas and radiowave propagation*. McGraw-Hill, New York
13. Shigetomi K, Honda J, Uchida K (2012) On estimation of amplitude modification factor and propagation order of 1-ray and 2-ray models in comparison with Hata's equations. In: *Proceedings of KJJC-2012, Seoul, Korea*, pp 145–148, May 2012
14. Press WH, Flannery BP, Teukolsky SA, Vetterling WT (1992) *Numerical recipes in FORTRAN: the art of scientific computing*, 2nd edn. Cambridge University Press, Cambridge, pp 99–122

A SURF Feature Based Building Recognition System for Distinctive Architectures

Shio-Wen Chen, Yi-Hao Chung, Hsin-Fu Chien
and Chueh-Wei Chang

Abstract Buildings plays a very important role in the development of culture, art, history, and in our daily life. If we can retrieve unique features for describing a building, it might have some helps for architecture history, digital resources of architecture, even for determining the position of a person in the urban area. As the popularity of smart mobile devices, if we could have some interesting application for getting information of buildings around user, by captured building images in any direction and view, it will be a great help for the promotion of culture and tourism industry. In this paper, we propose a preliminary building recognition system using the SURF and color features for distinctive buildings in a city. This system using Google Street View's images as a feature learning database. Based on the research of buildings' characteristics in a modern city, the recognition system can identify buildings efficiently in different scales, rotation, and partial occlusion of the building's image in this system.

Keywords Building recognition · SURF · Object recognition · Google street view

S.-W. Chen · Y.-H. Chung · H.-F. Chien · C.-W. Chang (✉)
Department of Computer Science and Information Engineering, National
Taipei University of Technology, Taipei, Taiwan
e-mail: cwchang@ntut.edu.tw

S.-W. Chen
e-mail: t9598003@ntut.edu.tw

Y.-H. Chung
e-mail: t96599008@ntut.edu.tw

H.-F. Chien
e-mail: t9599004@ntut.edu.tw

1 Introduction

Buildings plays a very important role in the development of culture, art, history, and in our daily life. Buildings is a visible object every where in the modern city around the world. For object recognition, a building's appearance can extract many classification features. If we can extract these features, it can help the digital archive of architecture resources. Due to the popularity of smart mobile devices, if there has some application for tourists [1] or foreigners to get some interesting information, it will improve the promotion of the city and tourism Industry. Also the density of buildings is very high in urban city, we could use this recognition technology to improve GPS localization [2].

Object Recognition usually faced the following problems: lighting condition, rotation, displacement, and scale changes. Building recognition also includes these problems because of the difference between construction materials, weather, and shooting time. One of the characteristics of cities in Taiwan is the high density of every kinds of buildings, and the color of building is usually in the same tone. Since the variation of residential buildings is not many and usually with familiar design and color, the combination of residential and commercial buildings give a great chance for distinctive building recognition.

Base on the specific design attribute in Taiwan, we want to focus on those special architectures, because these attributes should become many great landmarks, as well as for the building object recognition. The color feature of these buildings will also become one of the important features. In this paper, we will propose a method for recognizing distinctive buildings based on Taipei city. By this color and feature point matching method, we can recognize those buildings in different position, scale, and in different parts.

2 Related Works

Since the 1980's, the building recognition is an important issue for sense remote [3]. In 2000's, there are some researches of building recognition based on high-resolution aerial images [4]. Due to the advances of object recognition methods and the population of mobile device, there have been some building recognition researches that attempted to recognize architectures with special meanings in our life.

Lim and Kim [2] proposed a building recognition system of mobile device. They used GPS to limit the range of retrieval. Chung et al. [5] proposed the building recognition with huge change in scales and perspectives. Besides, Zhang and Kosecka [6] present the building recognition use localization based features. From those researches, we can find out that the suggested method of feature extraction for building recognition is the SIFT feature. We will use SIFT's scale-invariant based descriptor for providing a robust building recognition.

Those researches of building recognition used the ZuBuD database [7] for building feature learning. The ZuBuD database contains many building images that captured in Zurich city. In order to construct a similar database for building recognition in Taiwan, we want to use the Street View function provided by the Google Map to extract the building images for this building database.

The Scale-Invariant Feature Transform (SIFT) that we will use is proposed by D. Lowe in 1999. This algorithm is widely used in object recognition, because it can work robustly in many common problems of recognition, such as scale changing, light changing, rotation, and displacement of matching objects.

Because the SIFT algorithm spends lots of time on computing Difference of Gaussian (DoG) and constructing image pyramid, Bay [8] proposed another SIFT improved method called SURF (Speed up Robust Feature). By using integral image and the Hessian Matrix, the SURF can speed up the computation of DoG and image pyramid.

Juan et al. [9] have made a comparison of time consumption for scale, rotation, blur, illumination, and affine transform between SIFT, PCA-SIFT and SURF methods. From the results shown in their paper, SURF is much more robust and fast than SIFT. We also did the same experiments to compare the SIFT and SURF features. The results support that the SURF feature extraction and matching takes less time than SIFT, also matches between feature points quite well. So we will use the SURF feature for one of our features in this building recognition system.

In general, there are several problems such as camera angle, distance between building and user, lighting, the image quality and color tone will severely affect the matching efficiency. To find the limitation of our system, we test some matching condition of SURF and color:

(1) Too many buildings in one picture.

When the distance between building and user who shot the picture is too far, the image could include too many buildings and hence makes the recognition fail.

(2) Camera angle.

If user is too close to the building, the camera angle is not appropriate for shooting. Because the sun light and the image would contain the eaves, the recognition will fail.

(3) Lighting effect.

At night, there might be some different light source with colors, or the image is too vague because of dark.

(4) Image quality.

The quality of image resolution and camera lens is important for the color matching. In mobile devices, there also have many application software for adding special effect on images that will cause a bad matching result.

By these tests, we can realize that this building recognition system still has many limitations. It won't be easy to solve all these problems at any places and any time.

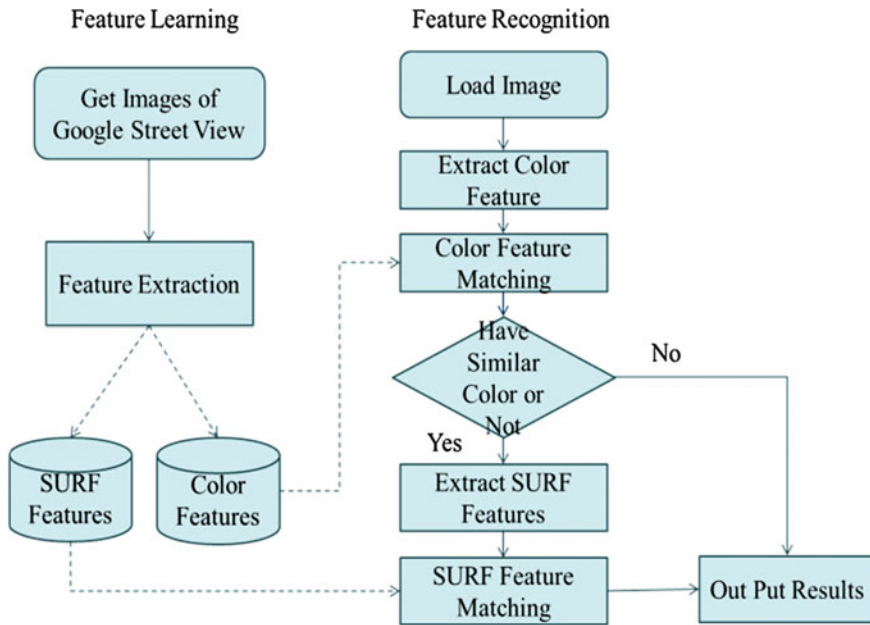


Fig. 1 System architecture diagram

3 Systeem Architecture

According to the above related works and characteristics of building in Taiwan, this system is divided in two parts: (1) Building Feature Learning Phase and (2) Building Feature Recognition Phase (searching and matching), as shown in Fig. 1.

In Feature Learning, our system will attempt to extract features from the Google Street View images. For getting more features for recognition, this system will use three images of the same building of different angles. These three images are grabbed from different positions from the Google Street View. For recognition accurately, our system will use color feature to find the same building in different images. Then we can specify the region of building (ROB), and extract those common SURF features from the ROB.

In Feature Recognition, our system will use color feature first, to examine the color of building between query image and learning database is similar or not to speed up the recognition process speed. After matching color, our system will next extract the SURF features of image and output the searching and matching results.

Several major processing modules in our system are listed and described as followings:

- (1) Get Images from Google Street View:

Download street view images from the Google Map by specific API function calls.

(2) Building Feature Extraction:

First, we can combine several designate parts of street view images according to the specific order and place provided by the Google to put the building together. Then extract the color feature of this building. Use color histogram to extract color of this building and store the color feature information. According to the color feature, get the ROB for extracting SURF feature. Finally we store both color and SURF features into learning database for recognition.

(3) Load Contents of a Query Image.

(4) Extract Color Feature from Query Image.

(5) Color Feature Matching:

Matching color feature from query image and database that try to find if there has similar color in both. If matched, extract SURF features for feature matching next. Otherwise, output the result.

(6) Extract SURF Features.

(7) SURF Feature Matching:

First, our system will match sign of the Laplacian. Next, use NNDR method to compute the Euclidean distance between SURF feature descriptors. It will be introduce in the next Section.

(8) Output Results:

Report the name and image of the building or similar buildings.

4 Feature Learning

In feature learning phase, we need to get the image of the Google Street View and extract color and SURF features from the buildings.

For the first step, we have to get the Google Street View for feature learning. Google street view image has its pano_id. So we have to find the pano_id for download the images. From Google Street Static API [10], we know that we can access the Google Street View image database by using the URL command, such as, [http://cbk0.google.com/cbk?output=xml&ll=\[x,y\]](http://cbk0.google.com/cbk?output=xml&ll=[x,y]).

Then, we can download each part of image as shown in Fig. 2. By the regular arrangement, we could only download and cut the parts of we need. We use three images of different viewpoints of each building for corresponding feature learning.

Because the regular arrangement and the building's characters, we can also get the color histogram from parts of the buildings, and store the histogram of this image. In most of the cases, we can see there are still many other objects in this image. So we use try to remove those irrelevant objects by using the image processing method from the back projection, the dilation and erosion, to find the ROB shown in Fig. 3.



Fig. 2 The Google street view images

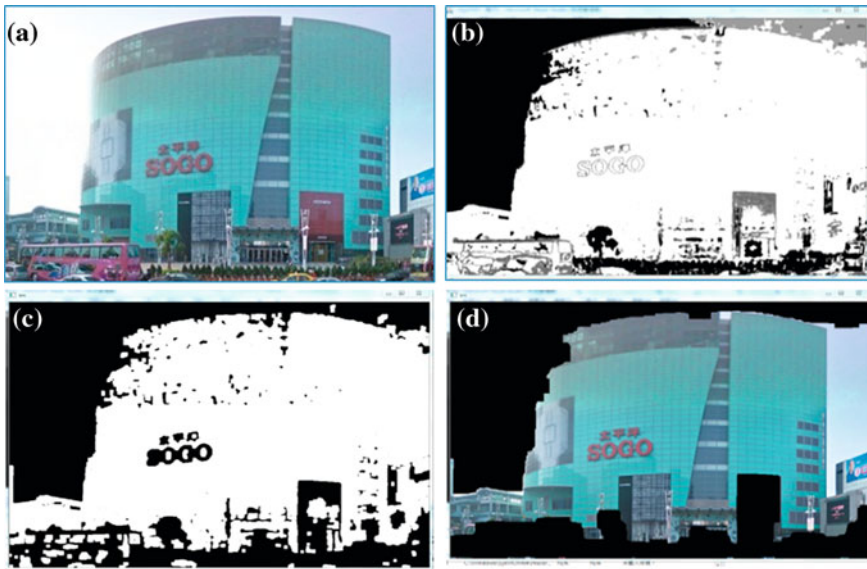


Fig. 3 The region of building (ROB) operations. **a** Original image. **b** After the back projection. **c** After the erosion and dilation operation. **d** The region of building

Next, we will extract the SURF feature from the ROB. The major operation of SURF [11] extraction is as follows:

- (1) Create an Integral Image.
- (2) Use Hessian Matrix and filter box to replace DoG (Difference of Gaussian) and Image pyramid for finding extreme value and construct scale space.
- (3) Use Haar-Like features to define the orientation of keypoints.
- (4) Compute the descriptors of keypoints.

We use the open SURF library for SURF extraction. Our system will store the SURF features of this building in a surf learning database.

5 Feature Matching

After feature extraction, we can load image for building recognition. As shown in Fig. 4, we have to extract and matching the color feature first for speed up efficiency.

We use correlation coefficient to decide the color is match or not. In Eq. (1), H_1 is the histogram of query image, and H_2 is the histogram of learning images. The correlation coefficient $r(H_1, H_2)$ is defined as:

$$r(H_1, H_2) = \frac{\sum_i^n (H_1(i) - \bar{H}_1)(H_2(i) - \bar{H}_2)}{\sqrt{\sum_i^n (H_1(i) - \bar{H}_1)^2 (H_2(i) - \bar{H}_2)^2}} \tag{1}$$

where

$$\bar{H}_1 = \frac{1}{n} \sum_i^n H_1(i), \tag{2}$$

$$\bar{H}_2 = \frac{1}{n} \sum_i^n H_2(i). \tag{3}$$

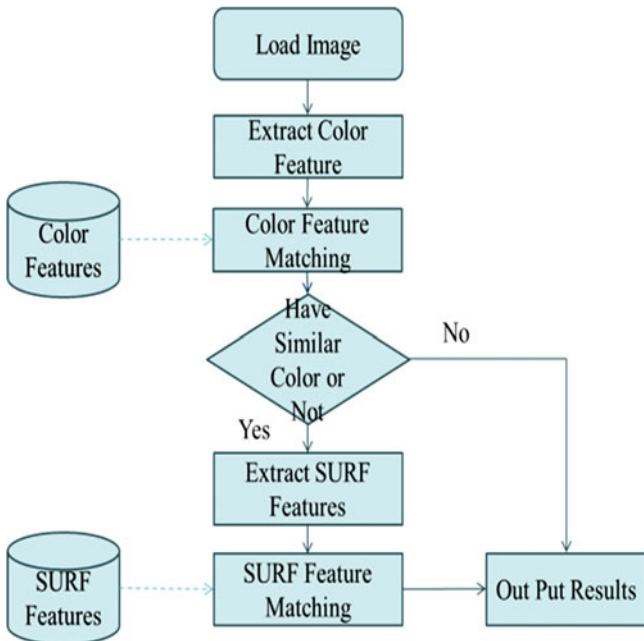


Fig. 4 Feature matching diagram

If the query image has a similar color of buildings, system will extract SURF features for next step building recognition. For accelerating, system will compare sign of Laplacian first. To match the sign of the Laplacian means to decide the Hessian matrix is the local extreme value or not. This is a very simple and effective way for the first step of SURF feature filtering and matching.

Then we use Nearest Neighbor Distance Ratio (NNDR) [11] for feature matching. Assuming X and Y are the features points of query image and feature data. We can get $\Pi(X, Y)$ which is a set of Euclidean distances between X, Y . And $\pi_1(X, Y), \pi_2(X, Y)$ are the first and second nearest distance. As the Eq. (4), we could get a ρ presents a threshold of descriptor matching.

$$\frac{\pi_1(X, Y)}{\pi_2(X, Y)} < \rho, \quad \rho \in [0, 1] \quad (4)$$

Because query images would only have part of buildings, we chose $\rho = 0.5$ and $r(H_1, H_2) \in [0.3, 1]$ for the boundary of recognition.

6 Experimental Result

We choose the characteristic buildings along the Nangang Line of MRT in Taipei. And the test query images are grabbed in different viewpoints, weather, and lighting conditions.

For increasing the accuracy, user can select a specific region in the query image with a building that want to query. Then system will output the result(s) on the right side of the system interface. The result in the Rank 1 should be the correct answer.

Table 1 is the experimental results of this system. For each building, we choose 10 to 20 images in different position, scale, weather and lighting. There also has 30 wrong images included in learning database for recognition.

The false case of the Guang Hua mall2 indicates a big Ad on the wall. Once the Ad is changed, the building recognition will cause a wrong matching result.

Table 1 Experimental results

Building name	Total images	TP	FP	FN	Precision rate (%)	Recall rate (%)
Belavita	46	16	0	0	100	100
Shin Kong A8	50	20	0	0	100	100
BR4	48	18	0	0	100	100
Eslite	45	15	0	0	100	100
Guang Hua mall	45	0	0	15	0	0
Sunyung building	45	15	1	0	90.9	100

TP True positive, *FP* False positive, *FN* False negative

7 Conclusion and Future Work

In this paper, we proposed a preliminary system using appearance of the building for recognizing distinctive architectures in Taipei. This system used color for filtering the buildings and speed up processing time. Then, this system matches buildings by SURF features. There are some limitations such as too many buildings in one picture, lighting condition and the Ads on the buildings.

Some of the special functions will be improved for this system in the future, such as clustering and indexing algorithm for the database construction. We will also attempt to design a fully automatic robot to download the Google Street View, and can create the whole city image for feature learning.

References

1. Hu J, Sawyer J, Herve JY (2006) Building detection and recognition for an automated tour guide. In: IEEE international conference on systems, man and cybernetics, pp 283–289
2. Lim B, Kim J (2009) Efficient database reduction method of building recognition using global positioning system on mobile device. In: IEEE international symposium on wireless pervasive computing, pp 1–5
3. Levitt S, Aghdasi F (1997) Texture measures for building recognition in aerial photographs. In: Proceedings of south African symposium on communications and signal processing, pp 75–80
4. Michaelsen E, FGAN-FOM, Ettlingen, Doktorski L, Soergel U, Stilla U (2007) Perceptual grouping for building recognition in high-resolution SAR images using the GESTALT-system. In: IEEE urban remote sensing joint event, pp 1–6
5. Chung YC, Han TX, He Z (2009) Building recognition using sketch-based representations and spectral graph matching. In: International conference on computer vision, pp 2014–2020
6. Zhang W, Kosecka J (2005) Localization based on building recognition. In: Computer society conference on computer vision and pattern recognition, p 21
7. Shao TSH, Gool LV (2003) Zurich buildings database for image based recognition. In: Technical report no. 260. Swiss Federal Institute of Technology, May 2003
8. Bay H, Tuytelaars T, Van Gool L (2006) SURF: speeded up robust features. In: Proceedings of European conference on computer vision, pp 404–417
9. Juan L, Gwon O (2009) A comparison of SIFT, PCA-SIFT and SURF. *Int J Image Process* 3:143–152
10. Google Streetview Static API. <http://jamiethompson.co.uk/web/2010/05/15/google-streetview-static-api/>
11. Open SURF. <http://www.chrisevansdev.com/computer-vision-opensurf.html>

A Kinect-Based System for Golf Beginners' Training

Yi-Hsuan Lin, Shih-Yu Huang, Kuei-Fang Hsiao, Kuei-Ping Kuo
and Li-Tieng Wan

Abstract Golf is well known worldwide as a prestigious and enjoyable sport. However, access to golf has been limited by high training costs, such as coaching fees, equipment, and course/driving range fees. This paper proposed a cost-effective golf assistive system, which is designed for golf beginners. This system uses Kinect sensor to detect beginners common swing mistakes. The experimental results indicate that the accuracy ratio in detection of errors is over 80 %. This paper provides a useful alternative assistive system for improving golf swings.

Keywords Golf swing · Posture movement · Kinect

1 Introduction

Golf is a sport pursuing both accuracy and distance. Unlike other sports, lower number of strokes has a better performance in the Golf. Nevertheless, an effective swing plays an important issue in this sport, and swing accuracy carries more weight than hitting distance for all golf players. A swing is composed by many copulative movements including the motion of knees and wrist, and spins of shoulder, hip and spine. Constantly practicing and practicing in a proper way are critical matters in picking up accuracy.

Y.-H. Lin (✉) · S.-Y. Huang · L.-T. Wan
Department of Computer Science and Information Engineering,
Ming Chuan University, Taoyuan, Taiwan
e-mail: 0136640@me.mcu.edu.tw

K.-F. Hsiao
Department of Information Management, Ming Chuan University,
Taoyuan, Taiwan

K.-P. Kuo
National Pingtung University of Science and Technology,
Office of Physical Education, Pingtung, Taiwan

General speaking, an upswing is triggered by the foot and followed by the torso. Firstly, the body's center-of-gravity position moves to the right foot, then waist, shoulder and arms are spin one after the other near simultaneously. When comes to down swing, body's center-of-gravity position shifts from the right foot to the left. Following the body movement, arms fall naturally as drawing a circle and the impact of the club and the ball takes place thereafter. Many crucial factors involved in the swing which demands excessive practice specially the coordination of foot, lower body, upper body, arms, hand and even head. It is so challenging that frustrated many beginners.

In order to improve the swing skills for beginners, a common practice is to hire instructor to provide hands-on lessons at the golf range. Other than the considerably expense of hiring instructor, experienced and capable instructors are not available everywhere all the time. In order not to discourage beginners, many golf swing assist systems that use modern technology have been proposed. In the related studies, sensor [1–7], motion capture [8, 9], and video processing [10–17] are the three most popular approaches. For example, Ghasemzede et al. (2009) [1, 2] and K-Vest [3] install sensors on player, and Ghasemzede [4, 5] also designed clubs with built-in sensors. King [6] and Burchfield [7] designed the swing assist system by using accelerometer and gyroscope. Blake et al. [8] (2008) adopted Motion Capture to analyze the swing. Urtasun et al. [16] (2006) use human body 3D motion detector to track 3D motion. I. Karliga et al. [17]. (2006) collected 2D objects from video, and then use this objects to build 3D motion.

This research proposed a swing assistive system aiming to help beginning players. Based on previous studies of swing theory and established model, this research first introduces 6 common mistakes on swing motion. A swing assistive system utilized the Microsoft Kinect to capture the swing motion, and automatically detect the swing mistakes. The remainder of this paper is organized as follows. The common mistakes on swing motion of golf beginners are shown in [Sect. 2](#). [Section 3](#) describes schemes utilized in the proposed Kinect-based assistive system. The experimental results are given in [Sect. 4](#). Conclusions are provided in [Sect. 5](#).

2 Common Mistakes on Swing Motion

Common mistakes comprised improper motions of knee, shoulder, head, hand, and the most important center-of-gravity. [Figure 1](#) summarizes those common mistakes on swing motion obtained by 67 students from a 2011 Physical Education class. Though there are right-handed player and left-handed players in golf, this research focused on right-handed players, since it can be quickly reversed for Left-handed player. Common mistakes of golf beginners can be classified into 6 types. [Table 1](#) gives incidences of these 6 types of mistakes. The details of them are described in the following.

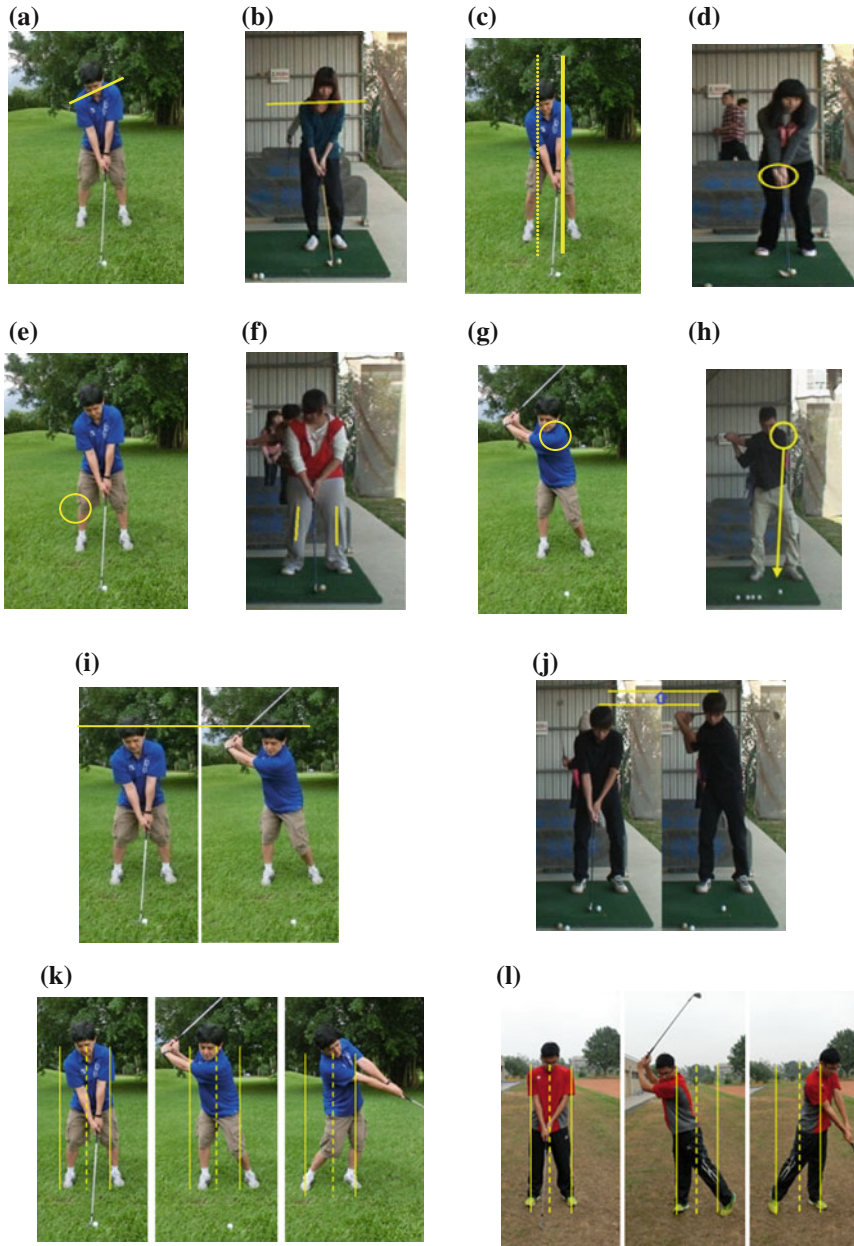


Fig. 1 Common mistakes on swing motion. **a** Correct SE1. **b** Incorrect SE1. **c** Correct SE2. **d** Incorrect SE2. **e** Correct SE3. **f** Incorrect SE3. **g** Correct SE4. **h** Incorrect SE4. **i** Correct SE5. **j** Incorrect SE5. **k** Correct SE6. **l** Incorrect SE6

Table 1 Incidences of common mistakes

Types of mistakes	SE1	SE2	SE3	SE4	SE5	SE6
Incidence	0.82	0.81	0.40	0.78	0.54	0.54

- **SE1: In ready position, the position of left shoulder is lower or equal to that of right shoulder**

SE1 type mistake is one of common mistake in swing. The incidence of SE1 is about 0.82. This mistake will decrease the spin power, and the impact of the sweet point will be missed. As a consequence, the flying distance and accuracy of the golf ball will be ineffectively.

- **SE2: In ready position, the hand grip position isn't close to left leg**

Golf beginners usually put their hand grip in the middle of two legs. The correct hand grip position should be closed to left leg. SE2 type mistake is also one of common mistake in swing. The incidence of SE2 is about 0.81. If SE2 occurs, it will cause the golf ball fly to the left of the course.

- **SE3: In ready position, knees are not bent**

SE3 type mistake would lead to the insufficient swing scale. The flying ball may shoot high but not far. Keep knees bend could stabilize body and increase swing stability.

- **SE4: In upswing, left shoulder fails to rotate to the center**

During swing, the upper body should be the axis of the spin. To have the correct swing, shoulders should rotate thereafter against the axis, so does the club. Therefore the tip of club will draw a cycle in the air, and the center is the torso. Fail to rotate the shoulder indicates the upper body is not spin, and the club is not drawing the cycle.

- **SE5: In upswing, the height level of the body is not maintained**

The SE4 type mistake will make the player shift his/her aiming point. By missing the sweet point, the flying direction and distance of the golf ball is not possible to foresee.

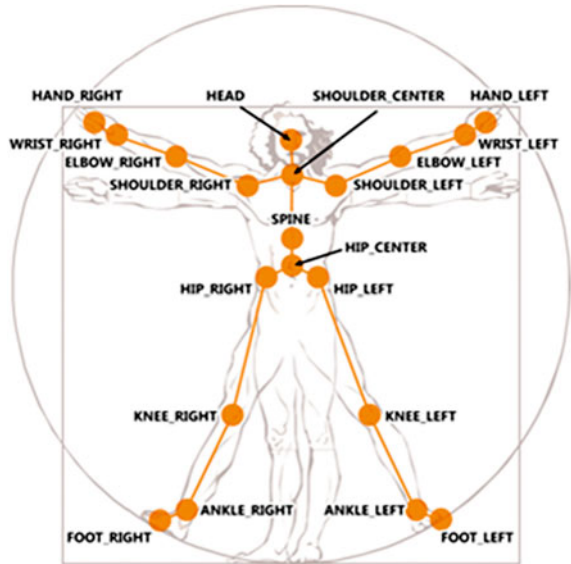
- **SE6: In backswing, center-of-gravity shifts too much in the final stage**

The shift of body's center-of-gravity from right to left renders extra power in the ball hitting during the backswing. This move can reinforce the strength of spin that increases flying distance. However gravity shifting is a very touchy and fine act, and easily over do. The movement starts moment before the impact of the club and the ball. Major action mainly takes place in the lower body particularly between two legs.

3 The Proposed Detection System

This System collects human body's information from Kinect sensor to detect mistakes of a golf swing. Kinect provides 20 different joints of human skeleton shown in Fig. 2. All of the joints are displayed as a set of coordinates (x, y, z),

Fig. 2 Human skeleton information from Kinect

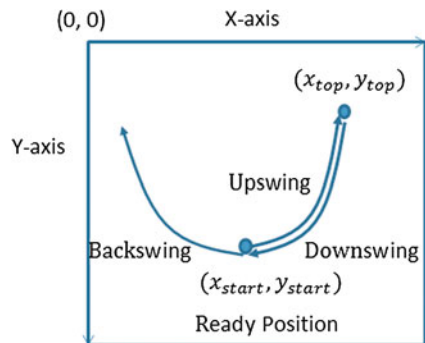


where CCD capture offer x and y value and infrared capture offer z value. The following discussed mathematical techniques used in the system for detection.

• **Golf swing phase detecting technique**

This technique uses HAND_LEFT joint's x value and y value to apart each phase of golf swing. Figure 3 displays the trajectory of HAND_LEFT joint's on x-y plane. Figure 3 has two important points. One is swing start point (x_{start}, y_{start}) another is the highest point of upswing (x_{top}, y_{top}) . Swing start point is the first point of swing, and usually stays the same position in little time. Let (x_i, y_i) be HAND_LEFT joint's x value and y value at frame i. If (x_i, y_i) are similar in continuous frame's, then record as swing start point (x_{start}, y_{start}) . This system will determine the phase to address whether (x_i, y_i) differs from (x_{start}, y_{start}) due to some people test the swing but not impact the ball.

Fig. 3 The trajectory of HAND_LEFT joint's on x-y plane



When $x_i > x_{\text{strt}}$ and $y_i < y_{\text{start}}$, the swing phase is upswing. In this phase, the system will check current y_i , which is continuous decreasing. In other words, HAND_LEFT joint continued rise up. If y_i becomes to the minimum value, HAND_LEFT joint's x and y value will be $(x_{\text{top}}, y_{\text{top}})$, that is the end of upswing. Number N will count how many frames in upswing, and use in backswing.

When HAND_LEFT joint leave the point $(x_{\text{top}}, y_{\text{top}})$, the system will determine the phase is downswing. In this phase the system will check current x_i , which is continuous decreasing. If x_i equals to x_{start} , then it ends downswing and turns to backswing. This system use Heuristic to determine the end of backswing. This system considers the frame count of upswing and backswing are similar, so when it comes to backswing, N will decrease as the frame count of backswing increase. If $N = 0$, then it ends back swing.

- **SE1 detecting technique**

The system use SHOULDER_LEFT and SHOULDER_RIGHT joints to detect this mistake. If SHOULDER_RIGHT joint's y value greater than SHOULDER_LEFT joint's y value, the player right shoulder higher than left shoulder. In other words, $y_{\text{SHOULDER_RIGHT}}$ minus $y_{\text{SHOULDER_LEFT}}$ greater than a threshold number, this means the action correctly. Equation 1 gives the detecting details of SE1.

$$\begin{cases} \text{if}(y_{\text{SHOULDER_RIGHT}} - y_{\text{SHOULDER_LEFT}}) \geq \text{TH}_1, & \text{SE1} = 0 \\ \text{Otherwise,} & \text{SE1} = 1 \end{cases} \quad (1)$$

where TH_1 is a threshold, which is set by system.

- **SE2 detecting technique**

The system use HAND_RIGHT, HIP_CENTER and KNEE_RIGHT joint's x value to detect SE2 mistake. Equation 2 gives the detecting details of SE2.

$$\begin{cases} \text{if}(x_{\text{KNEE_RIGHT}} < x_{\text{HAND_RIGHT}}) \text{ and } (x_{\text{HAND_RIGHT}} < x_{\text{HIP_CENTER}}), & \text{SE2} = 0 \\ \text{Otherwise,} & \text{SE2} = 1 \end{cases} \quad (2)$$

- **SE3 detecting technique**

SE3 could be detecting by HIP, KNEE and FOOT joint, which form a triangle. If HIP to KNEE joint's distance plus KNEE to FOOT joint's distance longer than HIP to FOOT joint's distance, knees should bend. Equation 3 gives the detecting details of SE3.

$$\begin{cases} \text{if}(D_{\text{HK}}^{\text{R}} + D_{\text{KF}}^{\text{R}}) - D_{\text{HF}}^{\text{R}} > \text{TH}_2, & \text{SE3} = 0 \\ \text{if}(D_{\text{HK}}^{\text{L}} + D_{\text{KF}}^{\text{L}}) - D_{\text{HF}}^{\text{L}} > \text{TH}_2, & \text{SE3} = 0 \\ \text{Otherwise,} & \text{SE3} = 1 \end{cases} \quad (3)$$

where

$$\begin{aligned}
 D_{HK}^R &= \sqrt{(x_{HIP_RIGHT} - x_{KNEE_RIGHT})^2 + (y_{HIP_RIGHT} - y_{KNEE_RIGHT})^2}, \\
 D_{KF}^R &= \sqrt{(x_{KNEE_RIGHT} - x_{FOOT_RIGHT})^2 + (y_{KNEE_RIGHT} - y_{FOOT_RIGHT})^2}, \\
 D_{HF}^R &= \sqrt{(x_{HIP_RIGHT} - x_{FOOT_RIGHT})^2 + (y_{HIP_RIGHT} - y_{FOOT_RIGHT})^2}, \\
 D_{HK}^L &= \sqrt{(x_{HIP_LEFT} - x_{KNEE_LEFT})^2 + (y_{HIP_LEFT} - y_{KNEE_LEFT})^2}, \\
 D_{KF}^L &= \sqrt{(x_{KNEE_LEFT} - x_{FOOT_LEFT})^2 + (y_{KNEE_LEFT} - y_{FOOT_LEFT})^2}, \\
 D_{HF}^L &= \sqrt{(x_{HIP_LEFT} - x_{FOOT_LEFT})^2 + (y_{HIP_LEFT} - y_{FOOT_LEFT})^2},
 \end{aligned}$$

where TH_2 is a threshold, which is set by system.

- **SE4 detecting technique**

SE4 could be detecting by use SHOULDER_LEFT and SHOULDER_CENTER joint's x value and z value, which form the plane. But when shoulder rotates around SHOULDER_CENTER could be cover joint's position. This situation could get error skeleton information. This paper propose a method, which use HIP_CENTER joint's x value and z value to approach SHOULDER_CENTER joint's x value and z value. Equation 4 gives the detecting details of SE4.

$$\begin{cases} A_{SHip}^{LC} > TH_3, SE4 = 0 \\ \text{Otherwise, } SE4 = 1 \end{cases} \quad (4)$$

where $A_{SHip}^{LC} = \tan^{-1}(z_{SHOULDER_LEFT} - z_{HIP_CENTER}) / (x_{SHOULDER_LEFT} - x_{HIP_CENTER})$, and TH_3 is a threshold, which is set by system, and $0^\circ < TH_3$.

- **SE5 detecting technique**

SE5 could be detecting by HEAD joint's y value. Suppose a swing have n HEAD points, which $\{y_{Head1}, y_{Head2}, \dots, y_{Headn}\}$ are HEAD joint's y value. Assumed $V_{Head} = \text{Var}\{y_{Head1}, y_{Head2}, \dots, y_{Headn}\}$, which is y value variance. Equation 5 gives the detecting details of SE5.

$$\begin{cases} V_{Head} < TH_4, SE5 = 0 \\ \text{Otherwise, } SE5 = 1 \end{cases} \quad (5)$$

where TH_4 is a threshold which is set by system and $0 < TH_4$.

- **SE6 detecting technique**

SE6 could be detecting by HIP_CENTER joint and x_{start} . Equation 6 gives the detecting details of SE6.

$$\begin{cases} \text{if } (x_{start} - x_{HIP_CENTER}) < TH_8, SE6 = 0 \\ \text{Otherwise, } SE6 = 1 \end{cases} \quad (6)$$

where TH_5 is a threshold which is set by system and $0 < TH_5$.

Fig. 4 The proposed stem architecture



4 Experimental Results

This system is implemented on the PC Platform utilizing Kinect to detect beginner's common mistakes in golf swing. Microsoft Kinect device has two CCDs, one for color image, and the other for image depth by using infrared. Figure 4 shows the system architecture. Table 2 displays detection's results obtained by 26 golf beginners. This paper uses R to explain the performance of the proposed system. R is denoted as the percentage that golf coach and this system have the same judgment for each swing. For SE1, $R_{SE1}=0.88$. The number means 4 beginners were determined correct by the coach whereas this system determine 1 player is correct and 22 beginners were determined error by the coach whereas this system also determines 22 players are error. So, $R_{SE1}=(1 + 22)/26$.

Overall, the detection rates of the proposed system are more than 80 %. Only SE4 correct rate is lower than 80 %. This is the results of occlusions among skeleton joints in a shoulder's rotations. SHOULDER_LEFT and SHOULDER_RIGHT joints would be covered when shoulder rotation since this system's Kinect sensor was be located in the front of players. In this situation, Kinect sensor cannot provide enough skeleton information as a result of lower values of R .

Table 2 The performance of the proposed system

Common swing mistake	R	Number of correct swings judged by coach		Number of error swings judged by coach	
		Number of correct swings judged by the proposed system	Number of error swings judged by the proposed system	Number of correct swings judged by the proposed system	Number of error swings judged by the proposed system
SE1	0.88	1	3	0	22
SE2	1.00	13	0	0	13
SE3	1.00	11	0	0	15
SE4	0.69	15	7	1	3
SE5	0.84	7	3	1	15
SE6	1.00	13	0	0	13

5 Conclusions and Future Works

This paper proposed a Kinect-based assistive system to detect beginner's swing common mistakes. The experimental results shows that the proposed system could effective detect these mistakes. However, it is still needed to be further investigated to provide helpful guidance to improve swing motion after mistakes are detected.

Acknowledgments This research is supported in part by the National Science Council, Taiwan under the grant of NSC 101-2221-E130-024-MY2 and NSC 100-2511-S-130-003-MY2.

References

1. Ghasemzadeh H, Loseu V, Guenterberg E, Jafari R (2009) Sport training using body sensor networks: a statistical approach to measure wrist rotation for golf swing. In: BodyNets'09: proceedings of the fourth international conference on body area networks, pp 1–8
2. Ghasemzadeh H, Loseu V, Jafari R (2009) Wearable coach for sport training: A quantitative model to evaluate wrist-rotation in golf. *J Ambient Intell Smart Environ* 1:173–184
3. K-vest website (2009) <http://www.k-vest.com/>
4. Sonic golf website (2009). <http://www.sonicgolf.com/>
5. Smartswing golf website (2009). <http://www.smartswinggolf.com/site/>
6. King K, Yoon SW, Perkins NC (2008) Wireless mems inertial sensor system for golf swing dynamics. *Sens Actuators A* 141(2):619–630
7. Burchfield R, Venkatesan S (2010) A framework for golf training using low-cost inertial sensors. In: Body sensor networks (BSN'10), pp 267–272
8. Blake, Grundy C (2008) Evaluation of motion capture systems for golf swings: optical versus gyroscopic. In: Information technology interfaces (ITI'08), pp 409–414
9. Blair D (2007) Unique golf teaching System. <http://www.ugt.co.uk/>
10. Howe N, Leventon M, Freeman W (1999) Bayesian reconstruction of 3-D human motion from single-camera video. In: NIPS'99
11. DiFranco DE, Tat-Jen C, Rehg JM (2001) Reconstruction of 3D figure motion from 2D. In: CVPR, pp 307–314
12. Goncalves L, Perona P (1995) Monocular tracking of human arm in 3D. In: ICCV'95, Boston, USA, Jul 1995
13. Sappa A, Aifanti N, Malassiotis S, Strintzis MG (2003) Monocular 3D human body reconstruction towards depth augmentation of television sequences. In: IEEE ICIP 2003
14. Luo Y, Hwang J-N (2005) A comprehensive coarse-to-fine sports video analysis framework to infer 3D parameters of video objects with application to tennis video sequences. In: IEEEICASSP 2005
15. Hwang J-N, Karliga I, Cheng H-Y (2006) an automatic 3-D human behavior analysis system for video surveillance applications. In: IEEE ISCAS
16. Urtasun R, Fleet DJ, Fua P (2005) Monocular 3-D tracking of the golf swing. In: IEEE CVPR, pp 932–939
17. Karliga, Hwang J-N (2006) Analyzing human body 3-D motion of golf swing from Single-camera video sequences. In: IEEE ICASSP

A Hill Climbing Algorithm for Ground Station Scheduling

Fatos Xhafa, Xavier Herrero, Admir Barolli and Makoto Takizawa

Abstract Ground Station Scheduling arises in satellite mission planning and belongs to scheduling family with time windows. It is known for its high computational complexity and hardness to solve to optimality. In fact, in some cases it is even hard to find a feasible solution that satisfies all user requirements and resource constraints. In this paper we present a Hill Climbing (HC) algorithm for the problem, which is a fast local search algorithm. Despite of being a simple search method, HC showed a good performance for small size instance while could not cope with medium and large size instances. The Satellite Toolkit is used for its experimental study and performance evaluation.

Keywords Hill climbing · Ground station scheduling · Spacecrafts · Multi-objective optimization · Satellite toolkit

1 Introduction

Scheduling with window times is a large family of problems that arise in logistics, in airport aircraft maintenance process, schedules for bus-drivers, project planning, logistics, etc. (see e.g. [1–4]). These problems are usually classified as either fixed time task scheduling, when the window start time and length are *a priori* fixed, or

F. Xhafa (✉) · X. Herrero
Universitat Politècnica de Catalunya, Barcelona, Spain
e-mail: fatos@lsi.upc.edu

A. Barolli
Canadian Institute of Technology, Tirana, Albania
e-mail: admir.barolli@gmail.com

M. Takizawa
Hosei University, Tokyo, Japan
e-mail: makoto.takizawa@computer.org

variable task scheduling when the window start time and length are variable. Such scheduling problems have been also studied in the satellite mission-planning domain, where teams of ground stations are to communicate with spacecrafts. For instance, in scheduling earth observation activities [6] or satellite imagery tasks [7].

Most formulations of both fixed time scheduling and variable time scheduling have been shown NP-hard and thus their resolution is addressed through heuristic and meta-heuristic methods [8–10]. In this paper we present a local search algorithm, namely, a Hill Climbing algorithm, for solving the Ground Station Scheduling.

The rest of the paper is organized as follows. We introduce the problem definition in Sect. 2. The Hill Climbing algorithm and its instantiation for the problem is presented in Sect. 3. The experimental evaluation of the algorithm using STK-Satellite Toolkit is given in Sect. 4. We conclude the paper in Sect. 5 with some remarks.

2 Ground Station Scheduling

Ground Station Scheduling aims at finding an optimal planning of communications between spacecraft (SC) and operations teams of Ground Station (GS). In its general formulation one assumes that there are multi-ground stations to satisfy mission-planning allocations. In fact, even in its version of one ground station, this scheduling problem is a complex combinatorial optimization problem. We assume that there is one antennae associated with every ground station. The need for automatic planning software to assist the operations staff comes from the increasing complexity of space systems. The number of satellite missions keeps increasing and thus automated planning has a direct impact in reducing the operational costs of ground station teams.

The Ground Station Scheduling receives in *input* the information on spacecrafts, the information on ground stations, spacecraft usage requests (missions), and other constraints such as ground station visibility. It then should compute a schedule of the operations of the spacecrafts within the requested constraints. The output of the scheduling is a detailed planning of task allocations with start time and duration rime for the spacecraft and the ground stations. We resume in Tables 1 and 2 the input and output parameters of the scheduling problem.

Several objectives (fitness functions) can be defined for the problem, which is multi-objective in its general formulation. The most usual ones are: (a) time

Table 1 Input instance

Parameter	Description
$SC\{i\}$	List of spacecrafts in the planning
$GS\{g\}$	List of ground station in the planning
N_days	Number of days for the schedule
$TAOS_VIS(i)(g)$	Visibility time of GS to SC
$TLOS_VIS(i)(g)$	Time GS loses signal from SC
$TReq(i)$	Communication time required for spacecrafts

Table 2 Output

Parameter	Description
$T_{Start}(i)(g)$	Starting time of the communication $SC(i)-GS(g)$
$T_{Dur}(i)(g)$	Duration time of the communication $SC(i)-GS(g)$
$SC_GS(i)$	The GS assigned to every $SC(i)$
$Fit_{LessClash}$	The fitness of minimizing the collision of two or more SC to the same GS for a given time period (measured from 0 to 100)
$Fit_{TimeWin}$	The fitness value corresponding to time access window for every pair $GS-SC$ (measured from 0 to 100)
Fit_{Reg}	Fitness value corresponding to satisfying the requirement on the mission communication time (measured from 0 to 100)
Fit_{GSU}	Fitness value corresponding to maximizing the usage of all GS during the planning (measured from 0 to 100)

windows fitness; (b) clash fitness; (c) requirement time fitness and (d) ground station usage fitness. The formulae for these fitness functions are given through Eqs. (1)–(7):

- *Time windows fitness.*

$$f(n) = \begin{cases} 1, & \text{if } [T_{Start}(n), T_{Start}(n) + T_{Dur}(n)] \subseteq \\ & \subseteq AW(n_g, n_i), \\ 0, & \text{otherwise.} \end{cases} \quad (1)$$

$$Fit_{AW} = \frac{\sum_{n=1}^N f(n)}{N} * 100, \quad (2)$$

- *Communication clashes fitness.*

$$f(n) = \begin{cases} -1, & \text{if } T_{Start}(n+1) < T_{Start}(n) + T_{Dur}(n), \\ 0 & \text{otherwise.} \end{cases} \quad (3)$$

$$Fit_{CS} = \frac{N + \sum_{n=1}^N f(n)}{N} \quad (4)$$

- *Communication time requirement fitness.*

$$\begin{aligned} T_{Start}(m) &> T_{From}(k) \\ T_{Start}(n) + T_{Dur}(n) &< T_{TO}(k) \\ T_{Comm}(k) &= T_{Dur}(j) \end{aligned} \quad (5)$$

$$f(k) = \begin{cases} 1, & \text{if } T_{Comm}(k) \geq T_{REQ}(k), \\ 0 & \text{otherwise.} \end{cases}$$

$$FIT_{TR} = \frac{\sum_{k=1}^K f(k)}{N} \cdot 100. \quad (6)$$

- *Resource usage fitness.*

$$Fit_{GU} = \frac{\sum_{n=1}^N T_{Dur}(n)}{\sum_{g=1}^G T_{Total}(g)} \cdot 100. \quad (7)$$

These fitness functions can then be sought into one single fitness function by assigning weights (or priorities) to the particular fitness.

3 Hill Climbing Algorithm

We present first a template of Hill Climbing algorithm and then its instantiation for the Ground Station Scheduling.

3.1 Instantiation of HC for Ground Station Scheduling

Hill Climbing (HC) algorithm is a basic local search algorithm (see Algorithm 1). Starting from an initial solution, the algorithm constructs a path of solutions through the search space aiming to reach the optimal solutions. The move from one solution to another one is done through the definition of neighborhood, which defines the condition under which two solutions are considered neighbors. The algorithm then jumps from one solution to a neighboring solution that improve—in terms of fitness—the best so far solution, until no further improvements. The acceptability criteria thus define the convergence of the algorithm and in most cases HC ends up to a local optimal solution.

Algorithm 1 Hill Climbing algorithm for maximization. f is the fitness function.

- 1: **Start:** Generate an initial solution s_0 ;
 - 2: $s = s_0$; $s^* = s_0$; $f^* = f(s_0)$;
 - 3: **repeat**
 - 4: **Movement Selection:** Choose a movement $m = \text{select_movement}(s)$;
 - 5: **Evaluate & Apply Movement:**
 - 6: **if** $\delta(s, m) \geq 0$ **then**
 - 7: $s' = \text{apply}(m, s)$;
 - 8: $s = s'$;
 - 9: **end if**
 - 10: **Update Best Solution:**
 - 11: **if** $f(s') > f(s^*)$ **then**
 - 12: $f^* = f(s')$;
 - 13: $s^* = s'$;
 - 14: **end if**
 - 15: **Return** s^*, f^* ;
 - 16: **until** (stopping condition is met)
-

3.2 Instantiation of HC for Ground Station Scheduling

Solution representation. We first note that a solution to the problem has been defined as follows:

$$\begin{array}{cc}
 \text{Planning :} & \text{Resources :} \\
 \left[\begin{array}{ccc}
 SC[1] & T_{start} & T_{dur} \\
 SC[2] & T_{start} & T_{dur} \\
 \vdots & \vdots & \vdots \\
 SC[i] & T_{start} & T_{dur}
 \end{array} \right] & \left[\begin{array}{cc}
 SC[1] & GS[g1] \\
 SC[2] & GS[g2] \\
 \vdots & \vdots \\
 SC[i] & GS[gi]
 \end{array} \right]
 \end{array}$$

where SC[i] indicate the spacecrafts and GS[k] represent the Ground Stations.

Initial Solution. The initial solution (starting point of the exploration process) is computed by some *ad hoc* method (see [10] for details).

Neighborhood definition. The neighborhood of a solution is defined by a local perturbation of a given solution, that is, a small change to its combinatorial structure, leading to another similar yet different solution to the problem. The premise is that small changes could lead to improvements of best so far solution. The definition of a local movement defines the neighborhood as follows:

$$\text{Movement } m : \{s' : s' = s \rightarrow m, s, s' \in S\}$$

where *s* is the current solution and *s'* the new solution obtained by applying a local change to *s*. For the coding of movement, use two structures *scheduleRow* and *resourceRow*, containing the local modification, which corresponds to the position and the modified values in the solution.

Acceptability. In moving from one solution to another one, the acceptability criteria is that of *steepest ascent policy*, that is, a solution that yields improvement in fitness function.

4 Experimental Evaluation of the Hill Climbing Algorithm

In this section we present the evaluation of the Hill Climbing algorithm for the Ground Station Scheduling. We present first the set of instances used and then the computational results.

4.1 Problem Instances

We have used the STK—Satellite Toolkit for simulating various scenarios for evaluating the performance of HC algorithm for the problem (Tables 3, 4 and 5).

Table 3 Small size instances

Parameter	Value
Ground stations (GS)	5
Spacecrafts	10
Number of days for planning	10

Table 4 Medium size instances

Parameter	Value
Ground stations (GS)	10
Spacecrafts	15
Number of days for planning	10

Table 5 Large size instances

Parameter	Value
Ground stations (GS)	15
Spacecrafts	20
Number of days for planning	10

A total of 48 instances,¹ classified into small, medium and large size, have been generated. Their characteristics are as follows:

4.2 Computational Results

Results below are averaged over 10 independent runs; standard deviation is also given.

Small size instances. The HC algorithm performed a total of 10000 evolution steps (Table 6).

Medium size instances. The HC algorithm performed a total of 15000 evolution steps (Table 7).

Large size instances. The HC algorithm performed a total of 25000 evolution steps (Table 8).

¹ Instances can be downloaded from <http://www.lsi.upc.edu/~fatos/GSSchedulingInputs.zip>.

Table 6 Fitness values for small size instances

Instance	Fit _{win}	Fit _{LessClash}	Fit _{TimeReq}	Fit _{GSU}	Fit _{TOT}	Ex. Time(s)
I_S_01	100.00	77.00	100.00	77.71	258.48	7.05
I_S_02	100.00	72.00	100.00	86.48	258.07	7.10
I_S_03	100.00	78.00	100.00	77.57	258.58	7.28
I_S_04	100.00	70.00	100.00	83.14	257.83	7.12
I_S_05	100.00	81.00	100.00	74.41	258.84	7.25
I_S_06	100.00	77.00	100.00	78.93	258.49	7.26
I_S_07	100.00	74.00	100.00	82.26	258.22	7.22
I_S_08	100.00	70.00	100.00	82.94	257.83	7.20
I_S_09	100.00	67.00	100.00	77.73	257.48	7.13
I_S_10	100.00	77.00	100.00	80.71	258.51	7.30
I_S_11	100.00	79.00	100.00	76.81	258.67	7.22
I_S_12	99.00	76.00	100.00	78.71	256.89	7.31
I_S_13	100.00	77.00	100.00	78.23	258.48	7.30
I_S_14	100.00	76.00	100.00	79.76	258.40	7.29
I_S_15	100.00	79.00	98.89	76.42	257.55	7.28
I_S_16	79	83	100	96.69	227.77	6.93
		Fit _{win}	Fit _{LessClash}	Fit _{TimeReq}	Fit _{GSU}	Fit _{TOT}
Average		99.93	75.33	99.93	79.45	258.15
Standard deviation (σ)		0.26	3.94	0.29	3.14	0.54

Table 7 Fitness values for small size instances

Instance	Fit _{win}	Fit _{LessClash}	Fit _{TimeReq}	Fit _{GSU}	Fit _{TOT}	Ex. Time(s)
I_M_01	100.00	78.67	100.00	63.23	258.50	15.88
I_M_02	99.33	73.33	100.00	62.76	256.96	15.81
I_M_03	100.00	79.33	100.00	56.50	258.50	15.77
I_M_04	98.67	82.67	100.00	61.40	256.88	15.80
I_M_05	99.33	75.33	100.00	63.28	257.17	15.84
I_M_06	100.00	76.00	100.00	65.52	258.26	15.81
I_M_07	99.33	78.00	100.00	64.04	257.44	15.93
I_M_08	100.00	84.67	100.00	62.68	259.09	15.81
I_M_09	100.00	79.33	100.00	66.52	258.60	15.85
I_M_10	99.33	82.00	100.00	63.95	257.84	15.88
I_M_11	99.33	80.00	100.00	65.87	257.66	15.82
I_M_12	99.33	84.00	100.00	64.95	258.05	16.09
I_M_13	100.00	80.00	100.00	58.95	258.59	15.96
I_M_14	99.33	86.67	100.00	64.70	258.31	15.92
I_M_15	100.00	83.33	100.00	61.44	258.95	16.01
I_M_16	62	94	100	89.1	203.29	15.9
		Fit _{win}	Fit _{LessClash}	Fit _{TimeReq}	Fit _{GSU}	Fit _{TOT}
Average		99.60	80.22	100.00	63.05	258.05
Standard deviation (σ)		0.42	3.71	0.00	2.67	0.70

Table 8 Fitness values for small size instances

Instance	Fit _{win}	Fit _{LessClash}	Fit _{TimeReq}	Fit _{GSU}	Fit _{TOT}	Ex. Time(s)
I_L_01	100.00	78.00	100.00	56.36	258.36	34.42
I_L_02	99.00	83.00	100.00	55.28	257.35	34.67
I_L_03	99.50	84.00	100.00	58.77	258.24	34.64
I_L_04	99.50	79.00	100.00	58.89	257.74	34.31
I_L_05	99.00	85.00	100.00	55.96	257.56	34.19
I_L_06	100.00	77.00	100.00	56.41	258.26	34.32
I_L_07	99.50	82.50	100.00	55.98	258.06	34.43
I_L_08	100.00	82.00	100.00	55.19	258.75	34.49
I_L_09	99.00	86.00	100.00	58.19	257.68	34.61
I_L_10	99.50	78.50	100.00	59.20	257.69	34.43
I_L_11	99.00	74.50	100.00	55.78	256.51	34.45
I_L_12	99.00	83.00	100.00	59.63	257.40	34.44
I_L_13	99.50	79.50	100.00	57.99	257.78	34.4
I_L_14	99.50	85.00	100.00	60.08	258.35	34.4
I_L_15	99.50	84.00	100.00	56.26	258.21	34.32
I_L_16	61.50	96.00	100.00	80.10	202.65	34.25
		Fit _{win}	Fit _{LessClash}	Fit _{TimeReq}	Fit _{GSU}	Fit _{TOT}
Average		99.43	81.40	100.00	57.33	257.86
Standard deviation (σ)		0.37	3.42	0.00	1.69	0.55

5 Conclusions

In this paper we have presented a Hill Climbing algorithm for the Ground Station Scheduling problem. The problem arises in mission planning of communications of teams of ground stations with spacecrafts and is know for its high complexity. The Hill Climbing algorithm showed a good performance for small size instances but shows its limitations to solving mediums and especially large size instances, for which the algorithms most potently got stuck into local maximum solutions. Its advantage however is the fast execution times, which makes the algorithm an interesting resolution method when a large number of mission planning have to be computed in short times.

References

1. Fischetti M, Martello S, Toth P (1992) Approximation algorithms for fixed schedule problems, *Oper Res* 40/1:96-S108
2. Jansen K (1994) An approximation algorithm for the license and shift class design problem. *Eur J Oper Res* 73:127-131
3. Kolen A, Lenstra JK, Papadimitriou C, Orlin J Interval scheduling problems, Manuscript, Center of Mathematics and Computer Science, C.W.I., Amsterdam

4. Kolen AWJ, Kroon LG (1993) On the computational complexity of (maximum) shift class scheduling. *Eur J Oper Res* 64:138–151
5. Pemberton JC, Greenwald L (2004) On the need for dynamic scheduling of imaging satellites. *Proceedings of AAAI'04*, pp 723–728
6. Vaghei BG, Moghadam RA, Bagheri A, Sarkheyli A (2010) Scheduling earth observation activities in LEO satellites using graph coloring problem. In 2010 5th international symposium on telecommunications (IST), 4–6 Dec 2010, pp 928–931
7. Harrison SA, Price ME, Philpott MS (1999) Task scheduling for satellite based imagery. In: The eighteenth workshop of the UK planning and scheduling, special interest group, University of Salford, UK
8. Barbulescu L, Howe A, Watson J, Whitley L (2002) Satellite range scheduling: a comparison of genetic, heuristic and local search. *Parallel problem solving from Nature –PPSN, VII*: 611–620
9. Sarkheyli A, Vaghei BG, Bagheri A (2010) New tabu search heuristic in scheduling earth observation satellites. In: *Proceedings of 2nd international conference on software technology and engineering (ICSTE)*, pp V2-199–V2-203
10. Xhafa F, Barolli A, Takizawa M (2013) Steady state genetic algorithm for ground station scheduling problem. In: *IEEE 27th international conference on advanced information networking and applications, AINA-2013, Spain, 25–28 Mar 2013*, pp 153–160

A Ferry Dispatching Optimization for Mobile Ad-Hoc Networks Using the Virtual Multiple Message Ferry Backbone Routing Scheme

Chu-Fu Wang and Ya-Chi Yang

Abstract A virtual multiple message ferry backbone routing scheme dynamically adopts roaming mobile nodes as Virtual Message Ferries (VMFs) to be responsible for the message carrying and relaying tasks, but it does not alter the moving direction or speed of the chosen mobile nodes. In this routing scheme, the intermittent connected routing problem of a Mobile Ad-hoc Network (MANET) can be much relieved by properly planned multiple VMF trajectories and the respective VMF dispatch time scheduling. In our previous research works [1], we discussed a VMF dispatch time scheduling optimization problem called the Virtual Multiple Message Ferry Dispatch Scheduling (VMMFDS) problem to minimize the total transfer waiting time of all-pair source–destination paths. In this paper, we provide a further theoretical property of the VMMFDS solution. Besides, a ring-based VMF backbone routing scheme, which includes the ring pattern VMF trajectory planning and the respective VMF dispatch time scheduling is also addressed.

Keywords Virtual multiple message ferry backbone routing · Mobile ad-hoc network · Intermittent connected routing problem · Backbone routing

1 Introduction

As network technology has advanced, diverse applications have been proposed for enhancing our daily life. Wireless communication systems are one of the most promising recent network technologies, due to the communication devices no longer being limited by wire, but communicating with each other via radio signals.

C.-F. Wang (✉) · Y.-C. Yang
Department of Computer Science, National Pingtung University
of Education, Pingtung, Taiwan
e-mail: cfwang@mail.npue.edu.tw

Y.-C. Yang
e-mail: cdcdd5203@gmail.com

This development quickly received much attention and research efforts from researchers and enterprises alike. Many practical technologies (such as RFID, Bluetooth, HomeRF, WLAN, etc.) were quickly applied to real world usage; for example, a user can answer a phone call by using a smart phone with a bluetooth earphone via a Piconet that is formed by bluetooth devices, or he/she can use the same smart phone to acquire the local weather forecast or nearby restaurant information from the Internet via WiFi or 4G technologies.

Wireless networks can be classified into two categories, namely infrastructure-based wireless networks and infrastructure-less wireless networks (also known as ad-hoc networks). The ad-hoc networks, each node in the network plays both roles of a terminal and a router. The message transmission can be accomplished via the help of nodes around the network in a multihop communication fashion. Due to there being no need for centrally deployed equipment and the fact that the network operates with a self-organized and self-management mechanism, the range of applications is much more extensive than for infrastructure-based wireless networks. A Mobile Ad-hoc Network (MANET) is a special type of ad-hoc network, which enables the mobility of wireless nodes. Recently, the applications of MANETs for vehicles have received much attention from both researchers and car manufacturers. This special type of MANET is known as a Vehicular Ad-hoc Network (VANET). Drivers can gain help from the VANET to increase both the safety and the quality of their driving.

However, the network designs of MANETs are much more difficult than those of traditional wireless networks, due to node mobility causing the communication links to be frequently broken, and consequently the routing protocols will be busy repairing or reestablishing the communication paths. The situation may be even worse when the nodes are sparse; then the network topology may be disconnected and connected interchangeably as time evolves, which is known as the Intermittent connected routing problem. There are many studies that have proposed solutions for relieving the Intermittent connected routing problem [2, 3]. The promising approaches include Realistic Message Ferrying (RMF) [4–6] and Virtual Message Ferrying (VMF) [1] to assist message forwarding in such a network environment.

In the former approach, MF is performed by a realistic ferry (for example, a bus moving along a fixed planning trail); as the ferry approaches a source node with a message relaying demand (see the left part of Fig. 1), it will make the decision as to whether or not to forward the carrying messages to the ferry. In the case of an increase in the chance of messages eventually arriving at the destination via the MF relaying, then it will relay the message to the MF. As the MF passes through the position of the destination node, the transmitted message can then be relayed to the destination. The right part of Fig. 1 gives an example of two MFs with two different trajectories (shown by the dashed line) in the network environment, which will expand the covering range of the MF routing. The main drawback of the traditional realistic MF routing mechanism is that the arrival time at each stop of the bus is not accurate enough for mobile nodes to make the relaying decision. For the VMF mechanism, a VMF is performed by a temporarily chosen mobile node. That is, any mobile node has the chance of being temporarily chosen as the

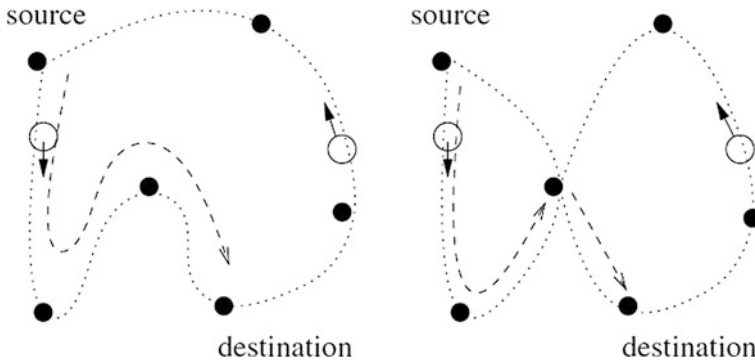


Fig. 1 An example of the realistic message ferry routing scheme

VMF when needed, but later it may be dismissed from its duty of being an VMF and turn back to being a normal mobile node (the details of this mechanism are described in the next section). Our previous research work [1] proposed a hierarchy multiple VMF backbone routing mechanism to relieve the above drawback of the realistic MF mechanism, and to provide a precise VMF arrival time at each position of the VMF trajectories.

The remainder of this paper is organized as follows. In Sect. 2, the VMF backbone routing scheme and the VMMFDS problem are described briefly. In Sect. 3, a proposed complete planning of the ring-based VMF backbone routing scheme and a theoretical property for the optimum solutions of the VMMFDS problem are discussed in detail. The concluding remarks are given in Sect. 4.

2 The Multiple VMF Backbone Routing Scheme and the VMMFDS Problem Formulation

In order to relieve the drawbacks of the realistic MF routing scheme described previously, we proposed a two-tiered multiple VMF backbone routing scheme in [1]. In the following, we will use Fig. 2 as an example to illustrate the basic ideas of the routing scheme. The multiple VMF backbone routing scheme consists of two layers. The lower layer of the routing scheme focuses on how a VMF is implemented. The upper layer focuses on the backbone routing planning, which includes how to arrange the multiple VMF trajectories and the design of the respective VMF dispatch time scheduling. Note that the trajectory of a VMF may consist of several line segments and is separated by checkpoints. For example, the trajectory of the VMF_7 in Fig. 2 consists of 4 line segments. The VMF travels along line segment $i(1 \leq i \leq 4)$ with constant velocity v_i . Notice that, due to the trajectory and the moving speed of a VMF being determined, the position of the VMF at any given time can be easily predicted.

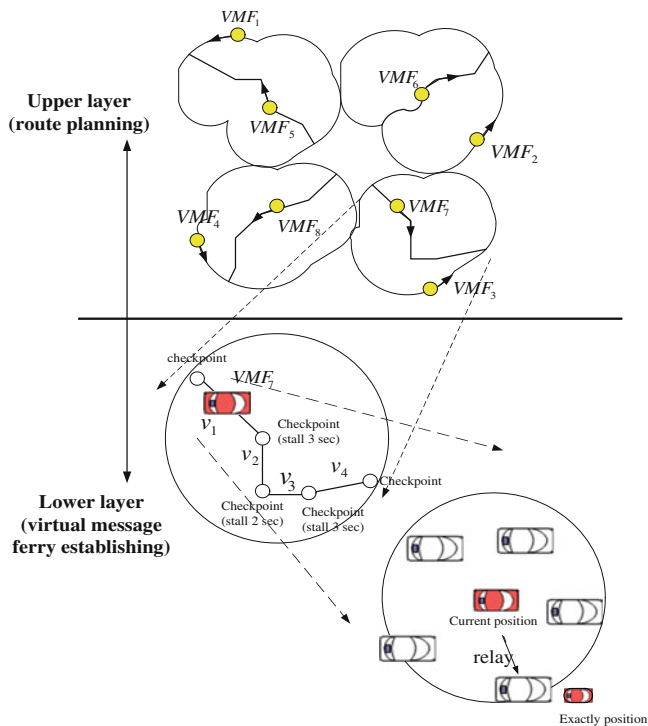


Fig. 2 An example of the two-tiered multiple VMF backbone routing scheme [1]

The implementations of the VMF in the lower layer are as follows. As shown in Fig. 2, let the red car denote a realistic mobile node that is currently playing the role of VMF_7 . Whenever the distance between the position of the red car and the position that the VMF_7 should be in is far beyond a given threshold, then the red car has to perform a handover procedure. The handover procedure will dismiss the red car's VMF role playing and select another car in the red car's neighborhood which is the closest to the position that the VMF should be in, to be the new VMF. It will then transmit every message that is carried in the current VMF node to the newly chosen node. In this way, at any time, on each VMF trajectory, there will be a mobile node playing the role of the VMF that shows up at the preplanned position to perform the task of message carrying.

In this routing scheme, the crucial problem is how to arrange multiple VMF trajectories to cover the network environment to form a backbone network for message relaying. In addition, the VMF dispatch time scheduling with respect to the VMF trajectories will affect the routing performance significantly. Figure. 3 shows four ring-shaped trajectories, each of which has a VMF traveling along the trajectory in a clockwise direction. There are 12 checkpoints in each trajectory. The distances between any two adjacent checkpoints are all equal to d .

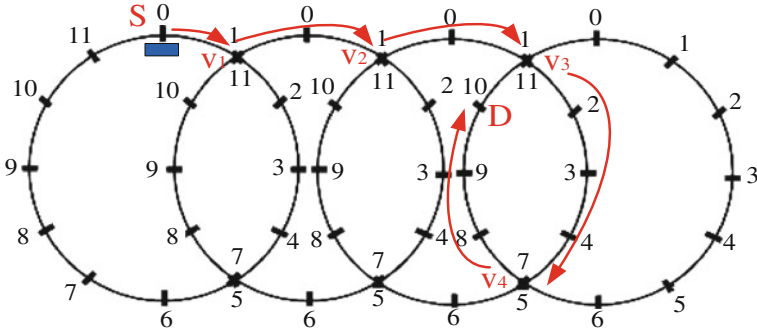


Fig. 3 An example of the VMF dispatch time scheduling

The collection of these checkpoints and the link between any two adjacent checkpoints will form a graph $G = (V, E)$, which is called the **VMF backbone graph**. Assume the moving speed of each VMF is constant and is d . Then the traveling time between any two adjacent nodes is equal to 1 ($d/d = 1$) unit of time. The labeling value (range from 0–11) associated with each node stands for the VMF show-up time at the checkpoint (i.e., the VMF dispatching time scheduling). For example, the value associated with node v_1 is 1 in the first trajectory (and 11 in the second trajectory), which means at time $t \bmod 12 = 1$ ($t \bmod 12 = 11$) there will be a VMF showing up at this intersection.

Assume that the all-pair of the source and destination paths in the VMF backbone graph are given in advance. For example, the routing path between the source node S and the destination node D in Fig. 3 is shown by the red arrow lines. Firstly, the messages are transmitted to the first VMF at time $t = 0$; and then at time $t = 1$, the message will arrive at the intersection point v_1 and wait for the second VMF to pass at time $t = 11$. Thus the transfer waiting time at the intersection point v_1 will be equal to $10 (= 11 - 1)$. Continuing in the same way, the message will eventually arrive at the destination node D with a total transfer waiting time of $(11 - 1) + (11 - 1) + (11 - 1) + (7 - 5) = 32$. We use $T_R^A(v_s, v_d)$ to denote the total transfer waiting time between the source v_s and the destination v_d , where R denotes the given all-pair routing paths and A denotes the VMF dispatch time scheduling. Our considered network optimization problem, the *Virtual Multiple Message Ferries Dispatch Scheduling problem* (VMMFDS), is defined as: given a VMF backbone graph (G) and the all-pair source–destination routing paths (R), the VMMFDS tries to find the optimum VMF dispatch time scheduling (A^*) such that the all-pair total transfer waiting time $\sum_{v_s, v_d \in V, v_s \neq v_d} T_R^{A^*}(v_s, v_d)$ is as small as possible.

3 The Proposed Ring-Based VMF Backbone Routing Scheme and a Property of the VMMFDS Problem Solutions

In the following, we firstly describe the proposed VMF backbone graph (G) that consist of multiple ring pattern trajectories and its optimum VMF dispatch time scheduling (A^*) for the VMMFDS problem. A theoretical property of the VMMFDS problem solutions for any given VMF backbone graph (G) (not limited to the ring-pattern VMF backbone graph) and its optimum VMF dispatch time scheduling (A^*) are then described in the next section.

3.1 The Ring-Based VMF Backbone Routing Scheme

Figure 4 gives an example of the proposed ring-pattern VMF backbone graph. The numbers associated with each checkpoint in the graph form an optimum VMF dispatch time scheduling (A^*) for the VMMFDS problem. Since the transfer waiting time at each intersection is 0, the total transfer waiting time for any given source–destination path will be equal to the trivial lower bound (0). Due to the article length limit, we omit the labeling method of the optimum scheduling (A^*) here and only briefly describe it using the example in Fig. 4.

In the upper-left corner of Fig. 4, there are two VMFs located at the checkpoint with label 4. The value 4 in the two checkpoints mean that there will be two VMFs passing through the checkpoints and moving toward the next checkpoints in a clockwise direction at time $t \pmod{6} = 4$ and $t + 6 \pmod{6} = 4$, respectively. Then the message routing by the aid of the VMFs is very similar to a passenger relocating his/her position to the destination via the mass rapid transit system in a city. In our proposed VMF dispatch time scheduling, the message relaying from one VMF to another in different trajectories at the intersection will not cause any delay, since the two VMFs will arrive at the intersection at the same time. Therefore it not only gains the advantage of a total transfer waiting time of 0, but the proposed scheduling also has the benefit of no extra facilities being required to be installed at each intersection to buffer the transferring messages, which is more practical than other scheduling systems. In the following, we call the optimum solution for the VMMFDS problem with a transfer waiting time at each intersection point of 0, the *seamless VMF dispatch time scheduling*.

3.2 The Property of the VMMFDS Problem Solutions

Due to different VMF backbone graphs, the respective optimum VMF dispatch time scheduling, the frequency of VMF dispatching, and the VMF speed will all affect the performance of the message transmission significantly. For instance,

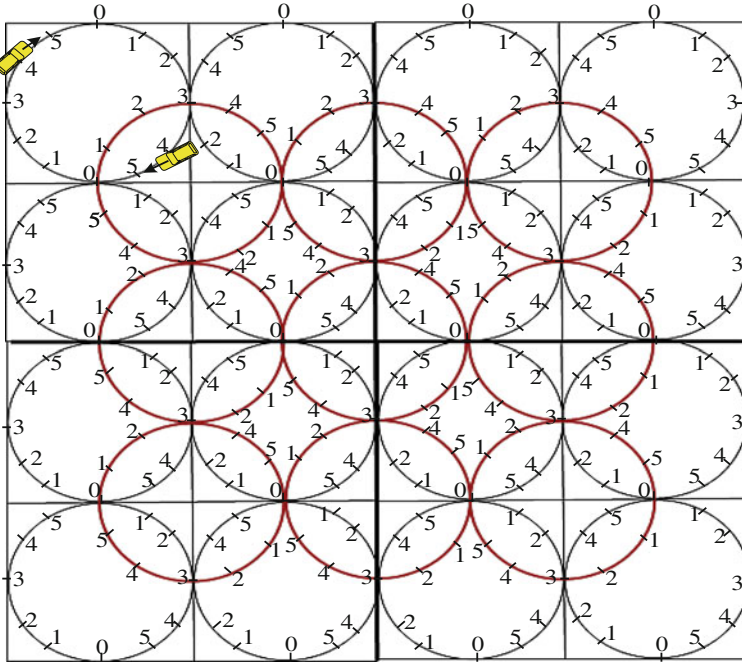


Fig. 4 An example of a ring-pattern VMF backbone graph and the optimum solution of the VMMFDS problem

shortening the frequency of VMF dispatching in a VMF trajectory (such as the frequency of VMF dispatching in the ring trajectory of Fig. 4 being a half of the frequency of Fig. 3) will increase the total number of VMFs required in the network environment. However, it will gain the benefit of shortening the message transmission delay. Therefore, how to adjust the VMF dispatch frequency of an optimum VMF dispatch time scheduling to gain another optimum solution by only minor computations is contributable. The following theorem gives a property for the seamless optimum solution of the VMMFDS problem.

Theorem 1 *Given a VMF backbone graph (G) and a respective optimum seamless VMF dispatch time scheduling (A*), let the VMF dispatching frequency of A* be k. For any factor m of value k (i.e., $m|k$), if we replace each value a of A* that is associated with a checkpoint by $[a \bmod m]$, then the resulting VMF dispatch time scheduling A** will also be an optimum seamless solution for the VMMFDS problem.*

Proof For any three adjacent nodes u, v, w in the VMF backbone graph (G), let the labeling values that are associated with these nodes be $[a \bmod k]$, $[(a + 1) \bmod k]$, and $[(a + 2) \bmod k]$, respectively. Now, we want to show that $[[a \bmod k] \bmod m]$, $[[a + 1] \bmod k] \bmod m]$, and $[[a + 2] \bmod k] \bmod m]$ are adjacent values in a

cyclic number series of modular m (i.e., $0, 1, 2, \dots, m-2, m-1, 0, 1, 2, \dots$). Conditioning on the possible outcomes for the three initial numbers, we have that,

Case 1 if $a + 2 \leq k - 1$

The value $[[a \bmod k] \bmod m] = [a \bmod m]$, value $[[a + 1] \bmod k] \bmod m = [(a + 1) \bmod m]$, and value $[[a + 2] \bmod k] \bmod m = [(a + 2) \bmod m]$. Obviously, the resulting three values are adjacent values in a cyclic number series of modular m .

Case 2 if $a \bmod k = k-2, (a + 1) \bmod k = k-1, (a + 2) \bmod k = 0$

The value $[[a \bmod k] \bmod m] = [(k-2) \bmod m] = [(-2) \bmod m] = [(m-2) \bmod m]$ (since mk). The value $[[a + 1] \bmod k] \bmod m = [(d-1) \bmod m] = [(-1) \bmod m] = [(m-1) \bmod m]$. And the value $[[a + 2] \bmod k] \bmod m = [0 \bmod m]$. Thus the resulting three values $[(m-2) \bmod m], [(m-1) \bmod m]$, and $[0 \bmod m]$ are also adjacent values in a cyclic series of numbers of modular m .

Case 3 if $a \bmod k = k-1, (a + 1) \bmod k = 0, (a + 2) \bmod k = 1$

Similar arguments can be applied for deducting the results, but we omit them here.

To conclude the above three cases, we have that the resulting values are also a feasible optimum seamless VMF dispatch time scheduling for the VMMFDS problem. \square

Figure 5 gives an example to demonstrate the property for the optimal seamless solution of the VMMFDS problem in Theorem 1. Obviously, the scheduling A^* in

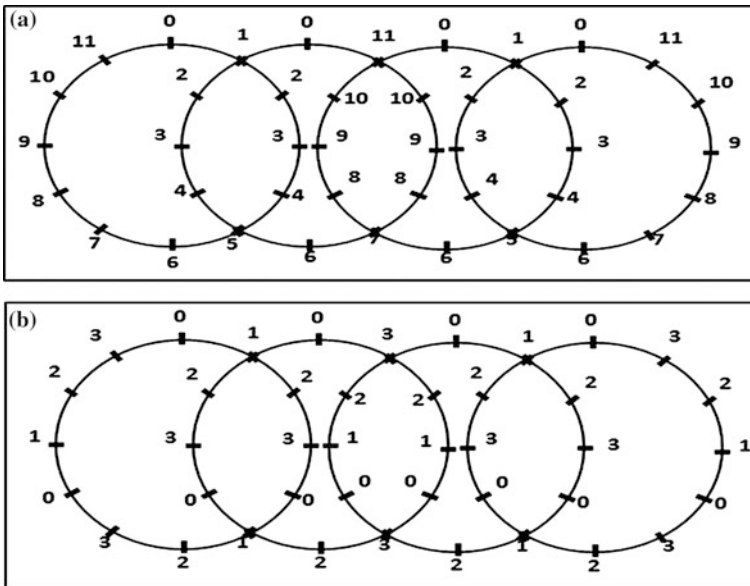


Fig. 5 An example to demonstrate the property for the seamless optimal solution of the VMMFDS problem

Fig. 5a is optimum with a transfer waiting time at any trajectory intersection of 0. Note that the VMF dispatching frequency (k) in Fig. 5a is equal to 12. Since 4 is a factor of 12 (i.e., $4|12$), we thus replace each value (a) shown in Fig. 5a by $(a \bmod 4)$. The resulting scheduling A^{**} is shown in Fig. 5b. Obviously, the scheduling A^{**} is also an optimum seamless solution of the VMMFDS problem with shorter frequency.

4 Concluding Remarks

In this paper, an optimization problem (VMMFDS) for the VMF Backbone Routing Scheme to minimize the total transfer waiting time of all-pair source–destination paths is considered. We propose a ring-pattern VMF backbone graph and the respective optimum seamless VMF issuing time scheduling. Besides, we also give a theoretical property related to the seamless VMMFDS solution to ease the network design.

Acknowledgments This work was supported in part by the National Science Council, Taiwan, Republic of China, under grant NSC 101-2221-E-153 -004.

References

1. Wang CF (2012) A virtual multiple message ferry backbone routing scheme for mobile ad-hoc networks. *Ad-Hoc Netw* 10:1399–1418
2. Liu C, Wu J (2007) Scalable routing in delay tolerant networks. In: 8th ACM international symposium on mobile ad hoc networking and computing, pp 51–60
3. Ali S, Qadir J, Baig (2010) A routing protocols in delay tolerant networks—a survey. In: 6th international conference on emerging technologies (ICET'10), pp 70–75
4. Zhang Z, Fei Z (2007) Route design for multiple ferries in delay tolerant networks. In: The IEEE wireless communications and networking conference (WCNC'07), pp 3462–3467
5. Zhao W, Ammar M, Zegura E (2004) A message ferrying approach for data delivery in sparse mobile ad hoc networks. In: 5th ACM international symposium on mobile ad hoc networking and computing (MobiHoc'04), pp 187–198s
6. Wu J, Member S, Yang S, Member S, Dai F (2007) Logarithmic store-carry-forward routing in mobile ad hoc networks. *IEEE Trans Parallel Distrib Syst* 18:735–748

A Location-Estimation Experimental Platform Based on Error Propagation for Wireless Sensor Networks

Yih-Shyh Chiou, Sheng-Cheng Yeh and Shang-Hung Wu

Abstract This paper presents a location-estimation experimental platform based on the error propagation approach to reduce the computational load of traditional algorithms. For the experimental platform with the scalar information, the proposed technique based on the Bayesian approach is handled by a state space model; a weighted technique with the reliability of the information passing is based on the error propagation law. As compared with a traditional Kalman filtering (KF) algorithm, the proposed algorithm has much lower computational complexity with the decoupling approach. Numerical simulations and experimental results show that the proposed location-estimation algorithm can achieve the location accuracy close to that of the KF algorithm.

Keywords Bayesian filtering · Error propagation · Location estimation · Wireless sensor networks · ZigBee positioning system

1 Introduction

Location-based services (LBS) have received great attention for commercial, public-safety, and military applications [1]. In the literatures, a number of positioning schemes have been reported [2]. Most of location-estimation approaches are based on the received signal strengths (RSSs) in wireless network

Y.-S. Chiou

Department of Electronic Engineering, Chung Yuan Christian University,
Jhongli, Taoyuan 32023, Taiwan
e-mail: choice@alumni.ncu.edu.tw

S.-C. Yeh (✉) · S.-H. Wu

Department of Computer and Communication Engineering, Ming Chuan University,
Guishan, Taoyuan 33324, Taiwan
e-mail: peteryeh@mail.mcu.edu.tw

environments. For positioning systems based on RSSs in small areas, there are two major approaches for location estimation of a mobile terminal (MT) in wireless networks: one using wireless local area networks (WLANs) and the other using wireless sensor networks (WSNs). However, providing customers with tailored location-based services is a fundamental problem. In terms of previous study, the location accuracy and the computational complexity are two major technical challenges in location-estimation systems. In other words, not only are accurate positioning algorithms essential to useful positioning systems, but also to reduce energy consumption with low-complexity schemes is worth developing for wireless networks [3–5].

Traditionally, an accurate location can be improved with tracking algorithms, which is to perform recursive state estimation by the state equation and the observation equation [3–5]. Furthermore, because Kalman filtering (KF) algorithm is considered an optimal recursive computation of the least-squares algorithm, it has been introduced to enhance the accurate estimation of the location-estimation system [4–8]. Nevertheless, the high location accuracy in terms of the conventional KF coupling algorithm requires high computational complexity, and direct implementation of the KF equations may be too complex to be applied to practical systems [4, 5]. In addition, for a linear dynamic system, a location tracking scheme based on a state space model can be derived from the Bayesian dynamic model [9–11]. Therefore, the scheme can be viewed as the reliability information passing on a state space model. In short, to improve localization efficiency, it would be useful to develop algorithms with reduced-complexity approaches in practical systems.

In this paper, a localization technique with low computational complexity is proposed to obtain a location of the MT in the experimental platform for WSNs, where the network scenario combining WSNs with WLANs is used for the proposed experimental platform. To improve the location accuracy, the proposed technique is to perform recursive state estimation given by the state equation and the observation equation. And then, a procedure based on the forward error propagation (FEP) approach [12] is used to simplify the implementation of Bayesian filtering and based on adaptive weighting approach for localization. Furthermore, in terms of a classical decoupling approach for different tracking groups, its computational complexity is much lower than that of the traditional KF coupling tracking scheme.

2 Background

2.1 Error Propagation Law

The error propagation is the problem of finding the distribution of a function of random variables in terms of the output as a function of the input and the system components. For a multi-input multi-output system, if the mathematical model of

the system and the distribution of the input are well known, the error propagation law is to desire the distribution of the output [5, 12]. Suppose that the vector $\mathbf{x} = [x_1, x_2, \dots, x_n]^T$ is distributed with known mean and variance. Let \mathbf{x} is an $n \times 1$ random vector with the mean matrix $\boldsymbol{\mu}_x$ and the covariance matrix \mathbf{P}_x . The known function $\mathbf{z} = f(\mathbf{x}) = \mathbf{A}\mathbf{x} + \mathbf{b}$ is a linear transformation function, where $\mathbf{z} = [z_1, z_2, \dots, z_m]^T$, \mathbf{A} , and $\mathbf{b} = [b_1, b_2, \dots, b_m]^T$ are $m \times 1$ vector, $m \times n$ matrix, and $m \times 1$ vector, respectively. Consequently, the mean matrix of the \mathbf{z} , $\boldsymbol{\mu}_z$, and the covariance matrix of the \mathbf{z} , \mathbf{P}_z , resulting from the linear function are given by

$$\boldsymbol{\mu}_z = \mathbf{A}\boldsymbol{\mu}_x + \mathbf{b} \quad (1)$$

$$\mathbf{P}_z = \mathbf{A}\mathbf{P}_x\mathbf{A}^T. \quad (2)$$

2.2 Bayesian Filtering Approach

For the Bayesian filtering at time k , assume that $p(\mathbf{x}_k|\mathbf{z}_{0:k})$ is well known, and we want to find $p(\mathbf{x}_{k+1}|\mathbf{z}_{0:k+1})$. According to the Markov structure and Bayes's theorem, the prediction-correction recursion can be written as follows [5, 9–11].

Prediction step (time update)

$$p(\mathbf{x}_{k+1}|\mathbf{z}_{0:k}) = \int p(\mathbf{x}_k, \mathbf{x}_{k+1}|\mathbf{z}_{0:k})d\mathbf{x}_k = \int p(\mathbf{x}_k|\mathbf{z}_{0:k})p(\mathbf{x}_{k+1}|\mathbf{x}_k, \mathbf{z}_{0:k})d\mathbf{x}_k \quad (3)$$

Correction step (measurement update)

$$p(\mathbf{x}_{k+1}|\mathbf{z}_{0:k+1}) = \frac{p(\mathbf{z}_{k+1}|\mathbf{x}_{k+1}, \mathbf{z}_{0:k})p(\mathbf{x}_{k+1}|\mathbf{z}_{0:k})}{p(\mathbf{z}_{k+1}|\mathbf{z}_{0:k})} \quad (4)$$

where $p(\mathbf{x}_{0:K}, \mathbf{z}_{0:K}) \square p(\mathbf{x}_0, \dots, \mathbf{x}_K, \mathbf{z}_0, \dots, \mathbf{z}_K)$, $p(\mathbf{z}_{k+1}|\mathbf{z}_{0:k})$ is the predictive distribution of \mathbf{z}_{k+1} given the past observations $\mathbf{z}_{0:k}$. The recursion relations in (3) and (4) form the basis for the Bayesian approach.

2.3 ZigBee Positioning System (ZPS)

The ZigBee network is based on IEEE 802.15.4, which can exchange information during the route maintenance process with the features of low transfer rate, low power, and low cost. A positioning system based on ZigBee network for location estimation is illustrated in [13], where the RSS is a measurement of the power of the received radio signal. This kind of ZigBee positioning system (ZPS) includes three type nodes: coordinator, reference node (RN), and blind node (BN), as shown

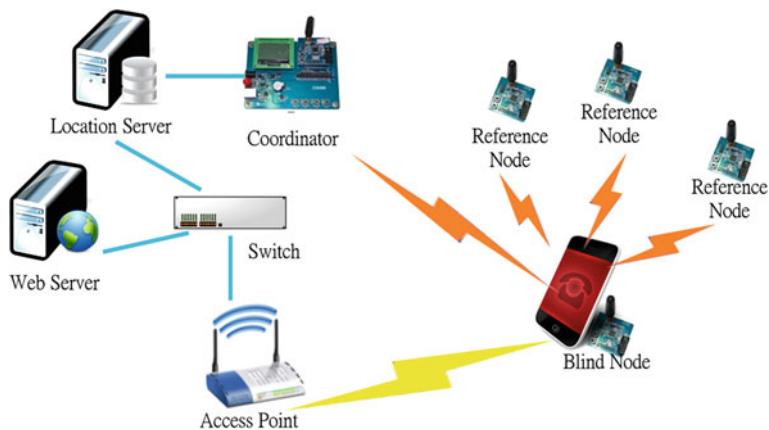


Fig. 1 The network scenario for estimating the BN's location in terms of ZPS

in Fig. 1. The coordinator is directly connected to a computer; RNs placed at a known position would send device identifications and coordinates to BNs. The BN is a node collects signals from all RNs responding to the respective RSS values of RNs for location estimation. When a BN receives signal information from neighboring RNs, the distance between the BN and RNs can be calculated by the collecting RSSI samples and the path-loss model [14], and then the location of the BN can be obtained with well known coordinates of RNs. Afterward, the estimated location of the BN (MT) is sent to the coordinator through the WSN system.

3 The Proposed Algorithm

For the approaches of incorporated measurement uncertainties in WSNs, one of the popular commercial ZPS systems is based on the CC2431 location engine developed by Texas Instruments (TI) [14]. The BN (TI CC2431) is a hardware location engine targeting low-power ZigBee applications in WSNs; it is used to estimate the position of nodes in an ad-hoc wireless network with RSS values from known RNs (TI CC2430) based on a centralized computation approach. In terms of the RSSI values, the TI CC2431 location engine outputs X and Y locations individually. Consequently, this paper focuses on a location-estimation approach in terms of X and Y groups individually in two-dimensional (2-D) coordinate system. That is, in terms of the idea of a classical decoupling approach for different tracking groups, the proposed filtering procedure is used to simplify the implementation of location estimation [15].

3.1 Experiment Setup

In this paper, the experimental platform was located on the sixth floor of a building (Department of Computer and Communication Engineering, Ming Chuan University, Taiwan). The floor layout and the setup of the experimental environment are shown in Fig. 2; the sampled locations are denoted by red hollow circles with 1 meter separation between adjacent points. RNs (RN: 1–8) are widely distributed over the hallway. Furthermore, to achieve the best possible accuracy of estimated locations, antennas having near-isotropic radiation characteristics are used for the positioning system; to measure the RSSI information more accurately, the simple antenna pattern-measurement method described in [13] was adopted. Using these techniques, the RSS information in terms of different distances in the four directions was measured, the four measurements were averaged, and then the information was entered into the TI CC2431 for localization.

3.2 Problem Formulation

The TI CC2431 is based on the RSSI information, where the distances between an MT (BN) and base nodes (RN) are calculated by the collecting RSSI information and the path-loss model. Afterward, the MT location is addressed by combining all the available distance measurements using a least-squares solution [14], and then it provides 2-D estimated-location information about the MT. As a result, the idea of decoupling X and Y dimensions for different groups is used to reduce the computational complexity [15]. For a 2-D model in this paper, the vector $[x_k \ y_k \ s_{x,k} \ s_{y,k}]^T$ denotes the state of the MT at time k , where x_k and y_k are the

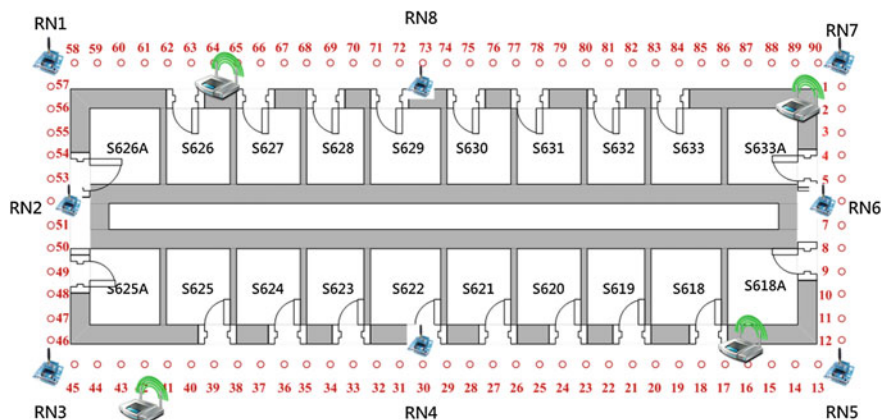


Fig. 2 The floor layout and the setup of the experimental environment

locations in the X and Y directions; $s_{x,k}$ and $s_{y,k}$ are the speeds in the X and Y directions. For the motion model of the MT based on acceleration noise, by adding a normal random component to the MT, the 2-D model describing the motion and observing the location of the MT is taken as

$$\begin{bmatrix} x_{k+1} \\ y_{k+1} \\ s_{x,k+1} \\ s_{y,k+1} \end{bmatrix} = \begin{bmatrix} 1 & 0 & \Delta_k & 0 \\ 0 & 1 & 0 & \Delta_k \\ 0 & 0 & 1 & 0 \\ 0 & 0 & 0 & 1 \end{bmatrix} \begin{bmatrix} x_k \\ y_k \\ s_{x,k} \\ s_{y,k} \end{bmatrix} + \begin{bmatrix} \Delta_k^2/2 & 0 \\ 0 & \Delta_k^2/2 \\ \Delta_k & 0 \\ 0 & \Delta_k \end{bmatrix} \begin{bmatrix} \eta_{x,k} \\ \eta_{y,k} \end{bmatrix} \quad (5)$$

$$\begin{bmatrix} z_{x,k} \\ z_{y,k} \end{bmatrix} = \begin{bmatrix} 1 & 0 & 0 & 0 \\ 0 & 1 & 0 & 0 \end{bmatrix} \begin{bmatrix} x_k \\ y_k \\ s_{x,k} \\ s_{y,k} \end{bmatrix} + \begin{bmatrix} v_{x,k} \\ v_{y,k} \end{bmatrix}, \quad (6)$$

where Δ_k is the measurement interval between k and $k + 1$; $[\eta_{x,k} \ \eta_{y,k}]^T$ is the process noise; $[z_{1,k} \ z_{2,k}]^T$ and $[v_{x,k} \ v_{y,k}]^T$ are the observed information and measurement noise, corresponding to the MT at time k , respectively. However, according to (5, 6), many elements in the matrices are zeros for the KF tracking algorithm [4, 5]. In other words, the computational load of the traditional KF techniques must be considered and should be reduced for practical real-time applications. Therefore, the results of X and Y estimated locations are decoupled as individual observed information for location estimation, and then the idea of scalar for different groups is used to replace the vector and to reduce the computational complexity [15]. That is, the 2-D problem in (5) and (6) is reduced to two one-dimensional (1-D) problems, and the example of the 1-D model describing the motion and observing the location for X-coordinate group is taken as

$$\begin{bmatrix} x_{k+1} \\ s_{k+1} \end{bmatrix} = \begin{bmatrix} 1 & \Delta_k \\ 0 & 1 \end{bmatrix} \begin{bmatrix} x_k \\ s_k \end{bmatrix} + \begin{bmatrix} \Delta_k^2/2 \\ \Delta_k \end{bmatrix} \cdot \eta_{x,k} \quad (7)$$

$$z_k = [1 \ 0] \begin{bmatrix} x_k \\ s_k \end{bmatrix} + v_{x,k}, \quad (8)$$

where the Y-coordinate group also can be described similarly. In terms of (1–8), it is to perform recursive state estimation with the error propagation law, which is given by the state equation for the time update phase and given by observation equation for the measurement update phase [5]. As a result, time update and measurement update are the fundamental phases of a recursive tracking approach. In addition, for the linear Gaussian model, the sum of two independent Gaussian probability density function (PDF) is Gaussian; the product of any two Gaussian PDF is Gaussian [5]. Consequently, the idea of decoupling X and Y dimensions for different groups can be used to reduce the complexity of the location-estimation approach in WSNs.

However, in terms of the Gaussian random components, according to (8), the observed information is based only on the location information. If the speed tracking scheme is performed without a speed observation, it may cause error propagation in speed and thus reduce location accuracy. In terms of the error propagation law and the relation in (9), two estimated locations and the known measurement interval can be used to refine the speed observation for location estimation [16].

$$s_{k-1} = \frac{x_k}{\Delta_{k-1}} - \frac{x_{k-1}}{\Delta_{k-1}} - \frac{\Delta_{k-1}}{2} \eta_{x,k-1} \leftrightarrow N\left(s_{k-1}; \frac{x_k - x_{k-1}}{\Delta_{k-1}}, \frac{\Delta_{k-1}^2}{4} Q_{x,k-1}\right), \quad (9)$$

where $N(ar; me, va)$ is defined as a Gaussian density function; ar , me , and va are the argument, mean, and variance, respectively; Q is the model noise variance. As a result, in terms of the Gaussian random components, the error propagation calculation and the scalar information passing of (7) and (8) are given as (10–12).

$$x_{k+1} = x_k + \Delta_k s_k + \frac{\Delta_k^2}{2} \eta_{x,k} \leftrightarrow N\left(x_{k+1}; x_k + \Delta_k s_k, \frac{\Delta_k^4}{4} Q_{x,k}\right) \quad (10)$$

$$s_{k+1} = s_k + \Delta_k \eta_{x,k} \leftrightarrow N(s_{k+1}; s_k, \Delta_k^2 Q_{x,k}) \quad (11)$$

$$z_k = x_k + v_{x,k} \leftrightarrow N(z_k; x_k, R_{x,k}), \quad (12)$$

where R is the measurement noise variance. The experimental results of a 1-D location-estimation technique based on the proposed FEP approach (FEP-based) are illustrated in the following sections.

4 Experimental Results

The experimental investigation combines TI CC2430/CC2431 ZPS platform with FEP approach for location estimation. As an MT moved along the test path in Fig. 2, the experimental results of location estimation using the TI ZPS platform with resolution 0.25 m are illustrated in Fig. 3. To verify the performances of estimation results introduced by the proposed schemes, the location parameters are based on the estimated result from TI ZPS platform. Without loss of generality, it is assumed that the MT has a steady state in (5); Δ_k , the measurement interval (sampling time) between k and $k + 1$, is set to one second. In addition, the model describing the observation location of the MT taken in (6) is based on the results in Fig. 3, and the estimated results are conducted to demonstrate the accuracy of the proposed approach.

In terms of the cumulative distribution function (CDF) of the error distance, the simulation results of the location-estimation schemes are given in Fig. 4a. The results demonstrate that more than 90 (60) percent of the non-tracking scheme, the KF-based scheme, and the proposed FEP-based scheme had error distances of

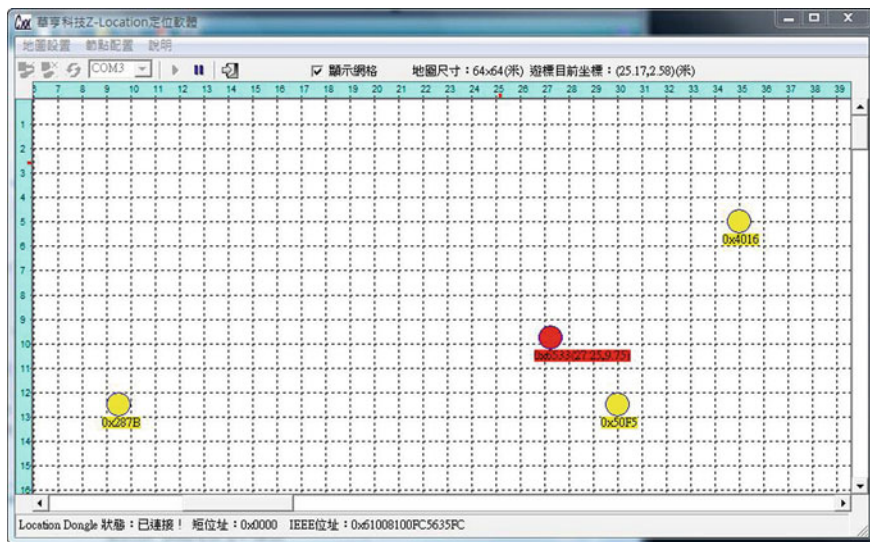


Fig. 3 An illustration for the localization using ZPS as a BN moves along the test path in Fig. 2

less than 4.6 (2.9) m, less than 3.2 (2.0) m, and less than 3.4 (2.1) m, respectively. According to the results, the location accuracy of the proposed schemes is better than that of the non-tracking scheme. In fact, the KF algorithm is an optimal tracking scheme for the linear Gaussian model, and it gives the best linear estimator in a mean-square error sense. Additionally, as an MT moved along the same path in terms of accumulative laps of 10 in Fig. 2, the estimated results in terms of the CDF of the error distance are given in Fig. 4b. As a nearly constant-speed motion model is under the environment in Fig. 2, the results demonstrate that more than 90 (60) % of the estimated locations with the TI ZPS have error distances less than 6.32 (4.14) m. More than 90 (60) % of the estimated locations with the KF-based scheme and the FEP-based scheme have error distances less than 5.21 (3.50) m and 5.29 (3.56) m, respectively. In a real environment with the ZPS platform, the distribution of RSSs in a fixed location is close to a Gaussian distribution [7], and the motion path of the BN (MT) close to a linear trajectory. However, the KF-based and FEP-based approaches are derived from the linear Gaussian model; the multipath effect is much more complex than the simulation in indoor environments. That is, in terms of the experimental results, the output of the estimated locations (X and Y) with the ZPS is only Gaussian-like distributions. Therefore, Fig. 4b illustrated that the ZPS cannot estimate the location of the BN (MT) very well in the complexity environment. Nevertheless, the proposed algorithm using adaptive weighting scheme based on FEP approach can improve the location accuracy.

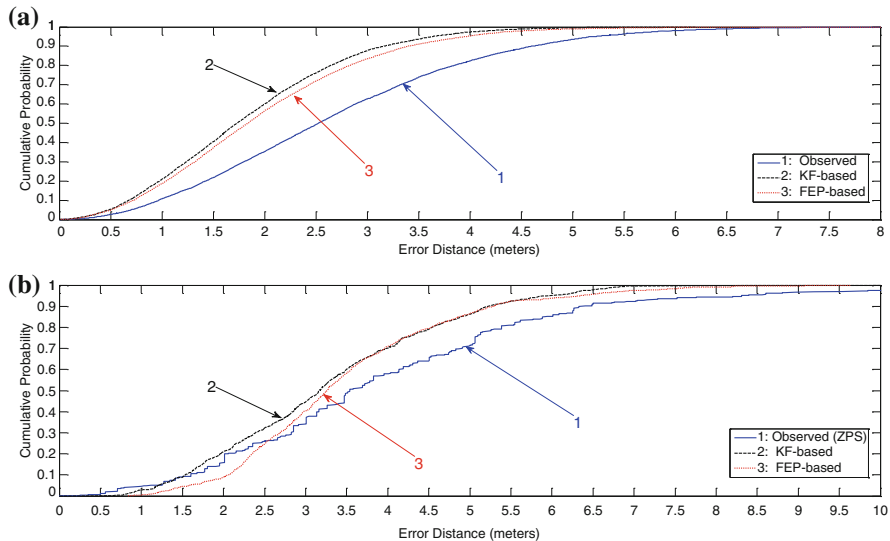


Fig. 4 Comparison of the non-tracking (observed), KF-based tracking, and FEP-based tracking schemes in terms of the CDF of the error distances. **a** Simulation, **b** ZPS: a BN moving along the same path with accumulative laps of 10 in Fig. 2

5 Conclusion

In this paper, we have proposed the FEP algorithm to implement the Bayesian filtering approach for location-estimation platform in WSNs. The FEP algorithm is based on passing the scalar reliability information between the prediction phase and the observation phase. Therefore, the location accuracy of the proposed FEP-based scheme is weighted and dominated by the information that has higher reliability information between the prediction and observation, and then the error propagation of the estimate results can be avoided in either high-reliability incoming information. As compared the conventional KF tracking scheme with proposed FEP tracking scheme, the differences between them are the decoupling and scalar-distributive designs. For the purpose of increasing the execution speed, the high computational complexity algorithms are not practical to implement for location- estimation systems. Nevertheless, because of the proposed approach with the feature of the lower computational complexity, the FEP-based approach is worth presenting for estimating the location of an MT. By taking error-propagation procedure based on weighting the scalar-information reliability and with the idea of decoupling X and Y dimensions to simplify the implementation of location estimation, the numerical simulations and experimental results show that the proposed FEP approach based on the error propagation law, in comparison with the conventional KF coupling scheme, achieves acceptable location accuracy and makes it suitable for practical implementation. To sum up, the proposed FEP

location-estimation approach, with features of both acceptable location accuracy and low computational complexity, is attractive for use in LBS applications.

Acknowledgments This work was supported in part by the National Science Council of the Republic of China (R.O.C.) under Grants NSC 101-2218-E-033-007 and NSC 101-2221-E-130 - 017.

References

1. Rantakokko J, Rydell J, Stromback P, Handel P, Callmer J, Tornqvist D, Gustafsson F, Jobs M, Gruđen M, Gezici M (2011) Accurate and reliable soldier and first responder indoor positioning: multisensor systems and cooperative localization. *IEEE Wirel Commun* 18(2):10–18
2. Barton RJ, Zheng R, Gezici S, Veeravalli VV (2008) Signal processing for location estimation and tracking in wireless environments. *EURASIP J Adv Signal Process* 2008:1–3
3. Pahlavan K, Li X, Makela JP (2002) Indoor geolocation science and technology. *IEEE Commun Mag* 40:112–118
4. Chiou Y-S, Wang C-L, Yeh S-C (2011) Reduced-complexity scheme using alpha-beta filtering for location tracking. *IET Commun* 5(13):1806–1813
5. Chiou Y-S, Tsai F, Wang C-L, Huang C-T (2012) A reduced-complexity scheme using message passing for location tracking. *EURASIP J Adv Signal Process* 2012(1):18
6. Chiou Y-S, Wang C-L, Yeh S-C, Su M-Y (2009) Design of an adaptive positioning system based on WiFi radio signals. *Elsevier Comput Commun* 32:1245–1254
7. Chiou Y-S, Wang C-L, Yeh S-C (2010) An adaptive location estimator using tracking algorithms for indoor WLANs. *ACM/Springer Wirel Netw* 16(7):1987–2012
8. Chen B-S, Yang C-Y, Liao F-K, Liao J-F (2009) Mobile location estimator in a rough wireless environment using extended Kalman-based IMM and data fusion. *IEEE Trans Veh Tech* 58(3):1157–1169
9. Arulampalam MS, Maskell S, Gordon N, Clapp T (2002) A tutorial on particle filters for nonlinear/non-Gaussian Bayesian tracking. *IEEE Trans Signal Process* 50:174–188
10. Fox D, Hightower J, Liao L, Schulz D, Borriello G (2003) Bayesian filtering for location estimation. *IEEE Pervasive Comput* 2(3):24–33
11. Cappé O, Godsill SJ, Moulines E (2007) An overview of existing methods and recent advances in sequential Monte Carlo. *Proc IEEE* 95(5):899–924
12. Koch K-R (1999) Parameter estimation and hypothesis testing in linear models. Springer, Berlin
13. Tsai F, Chiou Y-S, Chang H (2013) A positioning scheme combining location tracking with vision assisting for wireless sensor networks. *J Appl Res Technol* (in press)
14. CC2431 Location engine. <http://www.tij.co.jp/jp/lit/an/jaja175/jaja175.pdf>
15. Farina A, Studer FA (1985) Radar data processing, vol 1: introduction and tracking. Research Studies Press, Letchworth
16. Wang C-L, Chiou Y-S, Tsai F (2013) Reduced-complexity tracking scheme based on adaptive weighting for location estimation. *IET Commun* (in press)

Performance Evaluation of WMNs Using Hill Climbing Algorithm Considering Giant Component and Different Distributions

Xinyue Chang, Tetsuya Oda, Evjola Spaho, Makoto Ikeda,
Leonard Barolli and Fatos Xhafa

Abstract In this paper, we propose and implement a system based on Hill Climbing algorithm, called WMN-HC. We evaluate the performance of the proposed system by different scenarios using giant component and different distribution of mesh clients. We present some evaluation scenarios and show that the proposed approach has a good performance.

Keywords Wireless mesh networks · Hill climbing · Node placement · Giant component

X. Chang (✉) · T. Oda · E. Spaho
Graduate School of Engineering, Fukuoka Institute of Technology (FIT),
3-30-1 Wajiro-Higashi, Higashi-Ku, Fukuoka 811-0295, Japan
e-mail: keigetjyou@gmail.com

T. Oda
e-mail: oda.tetsuya.fit@gmail.com

E. Spaho
e-mail: evjolaspaho@hotmail.com

M. Ikeda · L. Barolli
Department of Information and Communication Engineering, Fukuoka Institute of
Technology (FIT), 3-30-1 Wajiro-Higashi, Higashi-Ku, Fukuoka 811-0295, Japan
e-mail: makoto.ikd@acm.org

L. Barolli
e-mail: barolli@fit.ac.jp

F. Xhafa
Department of Languages and Informatics Systems, Technical University of Catalonia,
C/Jordi Girona 1-3 08034 Barcelona, Spain
e-mail: fatos@lsi.upc.edu

1 Introduction

Wireless Mesh Networks (WMNs) are gaining a lot of attention because of their low cost nature that makes them attractive for providing wireless Internet connectivity. A WMN is dynamically self-organized and self-configured, with the nodes in the network automatically establishing and maintaining mesh connectivity among them-selves (creating, in effect, an ad hoc network). This feature brings many advantages to WMNs such as low up-front cost, easy network maintenance, robustness, and reliable service coverage [1]. Moreover, such infrastructure can be used to deploy community networks, metropolitan area networks, municipal and corporative networks, and to support applications for urban areas, medical, transport and surveillance systems.

The main issue of WMNs is to achieve network connectivity and stability as well as QoS in terms of user coverage. This problem is very closely related to the family of node placement problems in WMNs [2, 4–6], among them, the mesh router mesh nodes placement. Here, we consider the version of the mesh router nodes placement problem in which we are given a grid area where to deploy a number of mesh router nodes and a number of mesh client nodes of fixed positions (of an arbitrary distribution) in the grid area. Node placement problems are known to be computationally hard to solve [3, 7], in some previous works, Genetic Algorithms (GAs) have been recently investigated [8–10].

In this paper, we deal with connectivity and coverage in WMNs. Because this problem is known to be NP-Hard, we propose and implement a system based on Hill Climbing algorithm, called WMN-HC. We evaluate the performance of the proposed system by different scenarios using giant component and different distribution of mesh clients.

The rest of the paper is organized as follows. The mesh router nodes placement problem is defined in Sect. 2. We give an introduction of our proposed and implemented simulation system WMN-HC for mesh router placement of and Hill Climbing algorithm in Sect. 3. The simulation results are given in Sect. 4. In Sect. 5, we give some conclusions and future work.

2 Node Placement Problem in WMNs

In this problem, we are given a grid area arranged in cells where to distribute a number of mesh router nodes and a number of mesh client nodes of fixed positions (of an arbitrary distribution) in the grid area. The objective is to find a location assignment for the mesh routers to the cells of the grid area that maximizes the network connectivity and client coverage. Network connectivity is measured by the size of the giant component of the resulting WMN graph, while the user coverage is simply the number of mesh client nodes that fall within the radio coverage of at least one mesh router node.

An instance of the problem consists as follows.

- N mesh router nodes, each having its own radio coverage, defining thus a vector of routers.
- An area $W \times H$ where to distribute N mesh routers. Positions of mesh routers are not pre-determined, and are to be computed.
- M client mesh nodes located in arbitrary points of the considered area, defining a matrix of clients.

It should be noted that network connectivity and user coverage are among most important metrics in WMNs and directly affect the network performance. In this work, we have considered a bi-objective optimization in which we first maximize the network connectivity of the WMN (through the maximization of the size of the giant component) and then, the maximization of the number of the user coverage.

3 Proposed and Implemented WMN-HC System

We proposed and implemented a new simulator that uses Hill Climbing algorithm to solve the problem of node placement in WMNs. We called this simulator WMN-HC. Our system can generate instances of the problem using different distributions of client and mesh routers. The GUI interface of WMN-HC is shown in Fig. 1.

3.1 Hill Climbing Algorithm for Mesh Router Node Placement

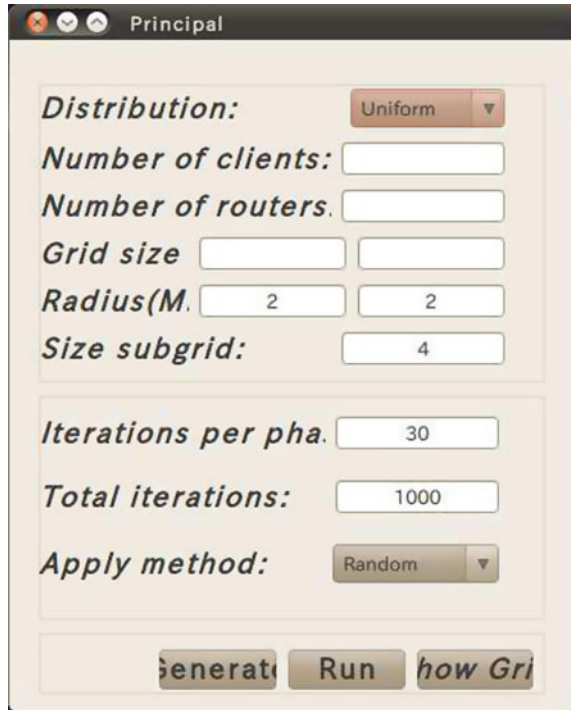
We present here the particularization of the Hill Climbing algorithm (see Algorithm. 1) for the mesh router node placement problem in WMNs.

Initial solution: The algorithm starts by generating an initial solution either random or by ad hoc methods [9].

Evaluation of fitness function: An important aspect is the determination of an appropriate objective function and its encoding. In our case, the fitness function follows a hierarchical approach in which the main objective is to maximize the size of giant component in WMN.

Neighbor selection and movement types: The neighborhood $N(s)$ of a solution s consists of all solutions that are accessible by a local move from s . We have considered three different types of movements. The first, called Random, consists in choosing a router at random in the grid area and placing it in a new position at random. The second move, called Radius, chooses the router of the largest radio and places it at the center of the most densely populated area of client mesh nodes (see Algorithm. 2). Finally, the third move, called Swap, consists in swapping two routers: the one of the smallest radio situated in the most densely populated area of

Fig. 1 GUI tool for WMN-
HC system



client mesh nodes with that of largest radio situated in the least densely populated area of client mesh nodes. The aim is that largest radio routers should serve to more clients by placing them in more dense areas.

Algorithm 1 Hill Climbing algorithm for maximization of f (fitness function).

- 1: Start: Generate an initial solution s_0 ;
 - 2: $s = s_0$; $s^* = s_0$; $f_- = f(s_0)$;
 - 3: repeat
 - 4: Movement Selection: Choose a movement $m = \text{select movement}(s)$;
 - 5: Evaluate & Apply Movement:
 - 6: if $\delta(s, m) \geq 0$ then
 - 7: $s' = \text{apply}(m, s)$;
 - 8: $s = s'$;
 - 9: end if
 - 10: Update Best Solution:
 - 11: if $f(s') > f(s^*)$ then
 - 12: $f^* = f(s')$;
 - 13: $s^* = s'$;
 - 14: end if
 - 15: Return s^*, f^* ;
 - 16: until (stopping condition is met)
-

We also considered the possibility to combine the above movements in sequences of movements. The idea is to see if the combination of these movements offers some improvement over the best of them alone. We called this type of movement Combination:

$\langle \text{Rand}_1, \dots, \text{Rand}_k; \text{Radius}_1, \dots, \text{Radius}_k; \text{Swap}_1, \dots, \text{Swap}_k \rangle$, where k is a user specified parameter.

Acceptability criteria: The acceptability criteria for newly generated solution can be done in different ways (simple ascent, steepest ascent, or stochastic). In our case, we have adopted the simple ascent, that is, if s is current solution and m is a movement, the resulting solution s' obtained by applying m to s will be accepted, and hence become current solution, iff the fitness of s' is at least as good as fitness of solution s . In terms of δ function, s' is accepted and becomes current solution if $\delta(s,m) \geq 0$. It should be noted that in this definition we are also accepting solutions that have the same fitness as previous solution. The aim is to give chances to the search to move towards better solutions in solution space. A more strict version would be to accept only solutions that strictly improve the fitness function ($\delta(s,m) > 0$).

Algorithm 2 Radius movement.

1: Input: Values H_g and W_g for height and width of a small grid area.

2: Output: New configuration of mesh nodes network.

3: Compute the most dense $H_g \times W_g$ area and $(x_{\text{dense}}, y_{\text{dense}})$ its central cell point.

4: Compute the position of the router of largest radio coverage $(x_{\text{largest_cov}}, y_{\text{largest_cov}})$.

5: Move router at $(x_{\text{largest_cov}}, y_{\text{largest_cov}})$ to new position $(x_{\text{dense}}, y_{\text{dense}})$.

6: Re-establish mesh nodes network connections.

4 Simulation Results

In this work, the number of Mesh Routers is considered 16 and the number of mesh clients 48. We took in consideration two distribution methods: Exponential and Weibull. For the simulations we used the combination method. The total number of iterations is considered 102400, the iterations per phase is considered 512. We carried out many simulations to evaluate the performance of WMNs using WMN-HC system.

In Figs. 2 and 3 are shown the simulation results for Exponential and Weibull, respectively. In Fig. 2a are shown the simulation results for size of giant component versus number of generations for Exponential distribution. After 200 generations, all the 16 routers are connected with each-other. The number of covered mesh routers versus the number of generations is shown in Fig. 2b. After 200 generations, all the mesh clients are covered by mesh routers.

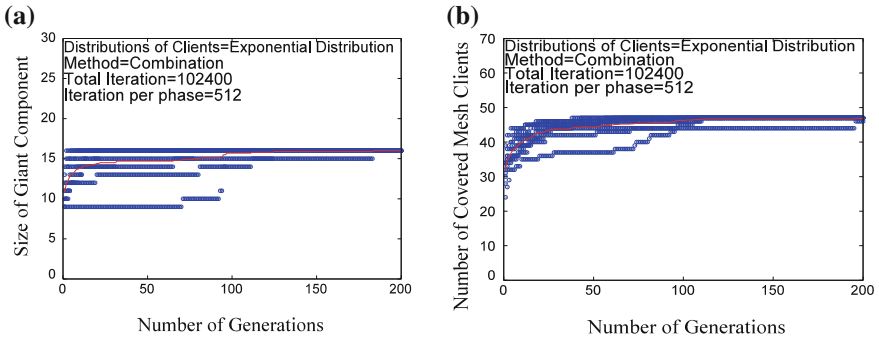


Fig. 2 Simulation results for exponential distribution **a** Size of Giant Component, **b** Number of covered mesh clients

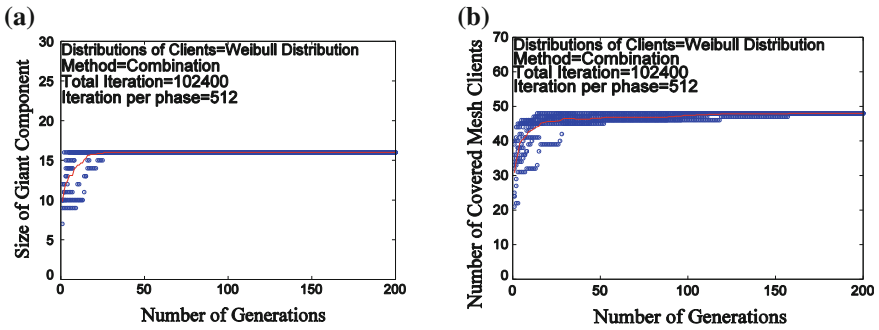


Fig. 3 Simulation results for Weibull distribution. **a** Size of Giant Component, **b** Number of covered mesh clients

In Fig. 2a are shown the simulation results for size of giant component versus number of generations for Weibull distribution. Also for Weibull distribution, all 16 mesh routers are connected with each other and they cover all mesh clients in the grid size (see Fig. 3b).

The system has a very good performance for both distribution methods.

5 Conclusions

In this work, we evaluated the performance of Hill Climbing for the problem of mesh router placement problem in WMNs. For evaluation, we have proposed and implement a simulation system based on Hill Climbing algorithm called WMN-HC and used Exponential and Weibull distributions of mesh node clients.

From the simulation results we observed that the system has a very good performance for Exponential and Weibull distributions.

In the future work, we would like to carried out extensive simulations and evaluate the performance of the proposed system for different scenarios.

Acknowledgments This work is supported by a Grant-in-Aid for Scientific Research from Japanese Society for the Promotion of Science (JSPS). The authors would like to thank JSPS for the financial support.

References

1. Akyildiz FI, Wang X, Wang W (2005) Wireless mesh networks: a survey. *Comput Netw* 47(4):445–487
2. Franklin A, Murthy C (2007) Node placement algorithm for deployment of two-tier wireless mesh networks. In: *IEEE GLOBECOM-2007*, pp 4823–4827
3. Lim A, Rodrigues B, Wang F, Xua Zh (2005) k-Center problems with minimum coverage. *Theor Comput Sci* 332(1-3):1–17
4. Muthaiah NS, Rosenberg C (2008) Single gateway placement in wireless mesh networks. In: *8th international IEEE symposium on computer networks*, pp 4754–4759
5. Tang M (2009) Gateways placement in backbone wireless mesh networks. *Int J Commun Netw Syst Sci* 2(1):45–50
6. Vanhatupa T, Hännikäinen M, Hämmäläinen DT (2007) Genetic algorithm to optimize node placement and configuration for WLAN planning. In: *4th international symposium on wireless communication systems*, pp 612–616
7. Wang J, Xie B, Cai K, Agrawal PD (2007) Efficient mesh router placement in wireless mesh networks. In: *MASS-2007, Pisa, Italy*, pp 9–11
8. Xhafa F, Barolli L, Durresi A (2007) An experimental study on genetic algorithms for resource allocation on grid systems. *J Interconnect Netw* 8(4):427–443
9. Xhafa F, Sanchez C, Barolli L (2009) Ad Hoc and neighborhood search methods for placement of mesh routers in wireless mesh networks. In: *ICDCS workshops of the IEEE 29th international conference on distributed computing systems (ICDCS-2009)*, pp 400–405
10. Yao X (1993) An empirical study of genetic operators in genetic algorithms. In: *19th EUROMICRO symposium on microprocessing and microprogramming on open system design: hardware, software and applications, Elsevier Science Publishers*, pp 707–714

Performance Evaluation of WMNs Using Simulated Annealing Algorithm Considering Different Number Iterations per Phase and Normal Distribution

Shinji Sakamoto, Tetsuya Oda, Elis Kulla, Makoto Ikeda,
Leonard Barolli and Fatos Xhafa

Abstract Wireless Mesh Networks (WMNs) currently have a lot of attention in wireless research and technology community due to their importance for providing cost-efficient broadband connectivity. Issues for achieving the network connectivity and user coverage are related with the node placement problem. In this work, we consider the router node placement problem in WMNs. We want to find the most optimal distribution of router nodes in order to provide the best network connectivity and provide the best client coverage in a set of uniformly distributed clients. We use our WMN-SA simulation system to calculate the size of Giant Component (GC) and number of covered users with different number of iterations per phase of Simulated Annealing (SA) algorithm calculations. From results, SA is good algorithm for optimizing the size of GC. While in terms of number of covered users, it does not cover all users. The performance of WMN-SA system increases when we use more iterations per phase.

S. Sakamoto (✉) · T. Oda · E. Kulla
Graduate School of Engineering, Fukuoka Institute of Technology (FIT), 3-30-1
Wajiro-Higashi, Higashi-Ku, Fukuoka 811-0295, Japan
e-mail: shinji.t.sakamoto@gmail.com

T. Oda
e-mail: oda.tetsuya.fit@gmail.com

E. Kulla
e-mail: eliskulla@yahoo.com

M. Ikeda · L. Barolli
Department of Information and Communication Engineering, Fukuoka Institute
of Technology (FIT), 3-30-1 Wajiro-Higashi, Higashi-Ku, Fukuoka 811-0295, Japan
e-mail: makoto.ikd@acm.org

L. Barolli
e-mail: barolli@fit.ac.jp

F. Xhafa
Department of Languages and Informatics Systems, Technical University of Catalonia,
C/Jordi Girona 1-3 08034 Barcelona, Spain
e-mail: fatos@lsi.upc.edu

Keywords WMNs · Simulated annealing · Number of generations · Number of iterations · Connectivity · Coverage

1 Introduction

Wireless Mesh Networks (WMNs) [1–3] are important network infrastructure for providing cost-efficient broadband wireless connectivity. They are showing their applicability in deployment of medical, transport and surveillance applications in urban areas, metropolitan, neighboring communities and municipal area networks. At the heart of WMNs are the issues of achieving network connectivity and stability as well as QoS in terms of user coverage. These issues are very closely related to the family of node placement problems in WMNs, such as mesh router nodes placement.

Node placement problems have been long investigated in the optimization field due to numerous applications in location science (facility location, logistics, services, etc.) and classification (clustering).

Facility location problems are thus showing their usefulness to communication networks, and more especially from WMNs field. WMNs are currently attracting a lot of attention from wireless research and technology community for providing cost-efficient broadband wireless connectivity.

WMNs are based on mesh topology, in which every node (representing a server) is connected to one or more nodes, enabling thus the information transmission in more than one path. The path redundancy is a robust feature of this kind of topology. Compared to other topologies, mesh topology needs not a central node, allowing networks based on such topology to be self-healing. These characteristics of networks with mesh topology make them very reliable and robust networks to potential server node failures. In WMNs mesh routers provide network connectivity services to mesh client nodes. The good performance and operability of WMNs largely depends on placement of mesh routers nodes in the geographical deployment area to achieve network connectivity, stability and user coverage. The objective is to find an optimal and robust topology of the mesh router nodes to support connectivity services to clients.

For most formulations, node placement problems are shown to be computationally hard to solve to optimality [4–7], and therefore heuristic and metaheuristic approaches are useful approaches to solve the problem for practical purposes. Several heuristic approaches are found in the literature for node placement problems in WMNs [8–12].

In this work, we use our proposed and implemented WMN-SA system that is based on SA to deal with the node placement problem in WMNs. For simulations, we consider normal distribution of 48 mesh clients in a 32×32 sized grid. Then we deploy 16 mesh routers and apply SA, to calculate the optimum solution for the maximum size of GC, and then maximize the number of covered users.

The rest of the paper is organized as follows. The definition of node placement problem is shown in Sect. 2. The proposed and implemented WMN-SA system is presented in Sect. 3. The simulation results are given in Sect. 4. We give some concluding remarks and future work in Sect. 5.

Algorithm 1 :Pseudo-code of SA.

```

t:= 0
Initialize T
s0 := Initial Solution()
v0 := Evaluate(s0)
while(stopping condition not met) do
  whilet mod MarkovChainLen = 0 do
    t:= t+1
    s1 := Generate(s0,T) //Move
    v1 := Evaluate(s1)
    ifAccept(v0,v1,T) then
      s0 := s1
      v0 := v1
    end if
  end while
  T := Update(T)
end while
returns0

```

2 Node Placement Problem in WMNs

In this problem, we are given a grid area arranged in cells where to distribute a number of mesh router nodes and a number of mesh client nodes of fixed positions (of an arbitrary distribution) in the grid area. The objective is to find a location assignment for the mesh routers to the cells of the grid area that maximizes the network connectivity and client coverage. Network connectivity is measured by the size of the GC of the resulting WMN graph, while the user coverage is simply the number of mesh client nodes that fall within the radio coverage of at least one mesh router node.

An instance of the problem consists as follows.

- N mesh router nodes, each having its own radio coverage, defining thus a vector of routers.
- An area $W \times H$ where to distribute N mesh routers. Positions of mesh routers are not pre-determined, and are to be computed.
- M client mesh nodes located in arbitrary points of the considered area, defining a matrix of clients.

It should be noted that network connectivity and user coverage are among most important metrics in WMNs and directly affect the network performance.

In this work, we have considered a bi-objective optimization in which we first maximize the network connectivity of the WMN (through the maximization of the size of the GC) and then, the maximization of the number of covered users.

3 Proposed and Implemented WMN-SA System

In this section, we present WMN-SA system. Our system can generate instances of the problem using different distributions of client and mesh routers.

The GUI interface of WMN-SA is shown in Fig. 1. We set the network configuration parameters as distribution, number of clients, number of mesh routers, grid size, radius of transmission distance and the size of subgrid.

Fig. 1 GUI tool for WMN-SA system

The screenshot shows a GUI window titled "Principal" with the following parameters and controls:

- Distribution:** A dropdown menu set to "Uniform".
- Number of client:** An empty text input field.
- Number of route:** An empty text input field.
- Grid size:** Two empty text input fields.
- Radius(M):** Two text input fields, both containing the value "2".
- Size subgrid:** A text input field containing the value "4".
- Iterations per phase:** A text input field containing the value "30".
- Temperature:** A text input field containing the value "3".
- Total iterations:** A text input field containing the value "1000".
- Apply method:** A dropdown menu set to "Random".
- Buttons:** At the bottom, there are three buttons: "Generat", "Run", and "how Gri".

3.1 Simulated Annealing

3.1.1 Description of Simulated Annealing

SA algorithm [13] is a generalization of the metropolis heuristic. Indeed, SA consists of a sequence of executions of metropolis with a progressive decrement of the temperature starting from a rather high temperature, where almost any move is accepted, to a low temperature, where the search resembles Hill Climbing. In fact, it can be seen as a hill-climber with an internal mechanism to escape local optima (see pseudo-code in Algorithm 1). In SA, the solution s' is accepted as the new current solution if $\delta \leq 0$ holds, where $\delta = f(s') - f(s)$. To allow escaping from a local optimum, the movements that increase the energy function are accepted with a decreasing probability $\exp(-\delta/T)$ if $\delta > 0$, where T is a parameter called the "temperature". The decreasing values of T are controlled by a *cooling schedule*, which specifies the temperature values at each stage of the algorithm, what represents an important decision for its application (a typical option is to use a proportional method, like $T_k = \alpha T_{k-1}$). SA usually gives better results in practice, but uses to be very slow. The most striking difficulty in applying SA is to choose and tune its parameters such as initial and final temperature, decrement of the temperature (cooling schedule), equilibrium detection, etc.

For further details on initial solution, fitness evaluation and movement types, refer to [14].¹ However, the acceptability criteria of neighboring solutions is now different, as explained next.

3.1.2 Acceptability Criteria

The acceptability criteria for newly generated solution is based on the definition of a threshold value (accepting threshold) as follows. We consider a succession tk such that $tk > tk + 1$, $tk > 0$ and tk tends to 0 as k tends to infinity. Then, for any two solutions si and sj , if $fitness(sj) - fitness(si) < tk$, then accept solution sj .

For the SA, tk values are taken as accepting threshold but the criterion for acceptance is probabilistic:

- If $fitness(sj) - fitness(si) \leq 0$ then sj is accepted.
- If $fitness(sj) - fitness(si) > 0$ then sj is accepted with probability $\exp[(fitness(sj) - fitness(si))/tk]$ (at iteration k the algorithm generates a random number $R \in (0,1)$ and sj is accepted if $R < \exp[(fitness(sj) - fitness(si))/tk]$).

¹ Initial solution, fitness evaluation and movement types are the same for Hill Climbing and Simulated Annealing

In this case, each neighbor of a solution has a positive probability of replacing the current solution. The tk values are chosen in way that solutions with large increase in the cost of the solutions are less likely to be accepted (but there is still a positive probability of accepting them).

4 Simulation Results

We carried out many simulations to evaluate the performance of WMNs using WMN-SA simulation system. In these simulation scenarios, we consider a grid with 32×32 size. The number of mesh routers is considered 16 and the number of mesh clients 48. For evaluation, we considered normal distribution of mesh clients. We set the value of SA temperature to 1 and conduct simulations for different number of iterations for each phase.

In Figs. 2 and 3, we show results of size of GC and number of covered users, respectively. For each phase of calculations, SA runs a number of 64, 128, 256 and 512 iterations. Because of the presence of random processes in our simulation system, we conduct the simulations 10 times, in order to create a general view of results. The maximum size of GC is 16, as we have 16 routers in our scenario. In Fig. 2a, b, the performance of the system for optimizing the size of GC, is almost the same. After 25 iterations the router backbone is completed with all 16 routers. While in the cases of 256 and 512 iterations (Fig. 2c, d), the performance increases, as the max size of GC is reached for less generations (10 and 8, respectively). We show the results for 50 generations as the size of GC is always maximum for more generations.

In Fig. 3 is shown the covered users for each iterations. First, we conducted simulations with 50 generations. In that case, not all users were covered. Then, we increased the number of generations per simulation to 200. The algorithm runs in similar ways for all cases when number of iterations is different. The maximum number of covered users goes up to 46. The performance becomes a little better

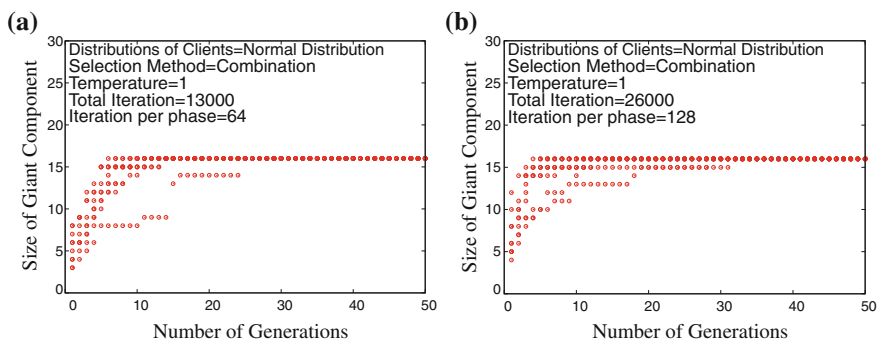


Fig. 2 Size of GC for different numbers of iterations

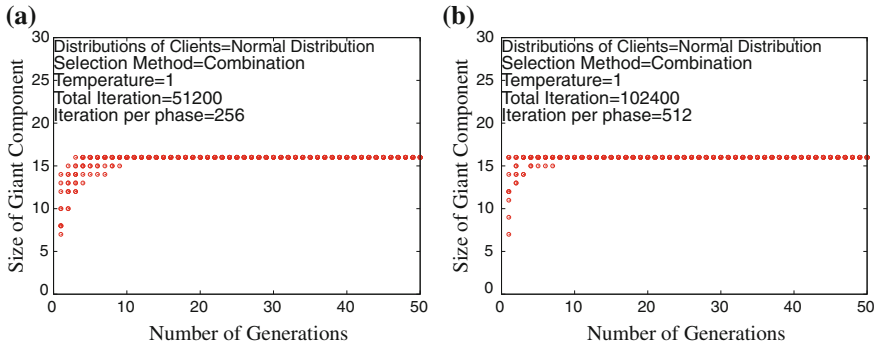


Fig. 3 Number of covered users for different numbers of iterations

when we move from 64 iterations up to 512 (see Fig. 3a–d), in terms of faster optimization. In the cases of 256 and 512 iterations per phase, in Fig. 3c, d, in around 10 phases there are more than 40 users covered. For less iterations per phase the performance is worse.

5 Conclusions

We conducted simulations with our WMN-SA system, in a grid with size 32×32 , where we deployed 48 mesh clients and 16 mesh routers. Using SA, we optimized the size of GC and then the number of covered users for different number of iterations per phase.

From the simulation results, we conclude that, SA is a good algorithm for optimizing the size of GC, while in terms of number of covered users, it does not cover all the users. The performance of WMN-SA system increases when we use more iterations per phase. In the case of the size of GC, all the routers were connected for less than 10 phases, when the number of iterations were 512.

In our future work, we would like to make a quantitative evaluation of the calculation time for all cases and compare the performance with other approaches. Moreover, we would like to implement other search optimization algorithms in our simulation system.

References

1. Akyildiz F, Wang X, Wang W (2005) Wireless mesh networks: a survey. *Comput Netw* 47(4):445–487
2. Nandiraju N, Nandiraju D, Santhanama L, He B, Wang J and Agrawal D (2007) Wireless mesh networks: current challenges and future direction of web-in-the-sky. *IEEE Wireless Commun*, pp 79–89

3. Chen Ch, Chekuri Ch (2007) Urban wireless mesh network planning: the case of directional antennas. Tech report no. UIUCDCS-R-2007-2874, Department of computer science, University of Illinois at urbana-champaign
4. Garey MR, Johnson DS (1979) Computers and intractability : a guide to the theory of np-completeness. Freeman, San Francisco
5. Lim B, Rodrigues F, Wang, Xua Zh (2005) k- center problems with minimum coverage. *Theoret Comput Sci* 332(1-3):1–17
6. Amaldi E, Capone A, Cesana M, Filippini I, Malucelli F (2008) Optimization models and methods for planning wireless mesh networks. *Comput Netw* 52:2159–2171
7. Wang J, Xie B, Cai K, Agrawal DP (2007) Efficient mesh router placement in wireless mesh networks. In: *Proceedings of MASS-2007, Pisa, Italy*, pp 9–11
8. Muthaiah SN, Rosenberg C (2008) Single gateway placement in wireless mesh networks. In: *Proceedings of 8th international IEEE symposium on computer networks, Turkey*, pp 4754–4759
9. Zhou P, Manoj BS, Rao RA (2007) Gateway placement algorithm in wireless mesh networks. In: *Proceedings of the 3rd annual international wireless internet conference (WICON-2007)*, pp 1–9
10. Tang M (2009) Gateways placement in backbone wireless mesh networks. *Int J Commun Net Syst Sci* 2(1):45–50
11. Franklin A and Siva Ram Murthy C (2007) Node placement algorithm for deployment of two-tier wireless mesh networks. In: *Proceedings of IEEE GLOBECOM-2007, Washington, USA*, pp 4823–4827
12. Vanhatupa T, Hannikainen M and Hamalainen TD (2007) Genetic algorithm to optimize node placement and configuration for WLAN planning. In: *Proceedings of 4th international symposium on wireless communication systems*, pp 612–616
13. Kirkpatrick S, Gelatt CD, Vecchi MP (1983) Optimization by simulated annealing. *J Sci* 220:671–680
14. Xhafa F, Sanchez Ch, Barolli L, Miho R (2010) An annealing approach to router nodes placement problem in wireless mesh networks In: *Proceedings of CISIS-2010*, pp 245–252
15. Holland J (1975) *Adaptation in natural and artificial systems*. University of Michigan Press, Ann Arbor
16. Xhafa F, Sanchez C, Barolli L, (2010) Genetic algorithms for efficient placement of router nodes in wireless mesh networks. In: *Proceedings of AINA 2010*, pp 465–472

UBMLRSS–Cognitive Financial Information Systems

Lidia Ogiela and Marek R. Ogiela

Abstract Intelligent information management systems that analyse management processes and support strategic decision taking will be discussed based on the example of cognitive data management systems. This group of information management systems is about taking strategic decisions at enterprises by semantically analysing selected groups of economic and financial ratios. This publication will discuss systems classed as UBMLRSS (*Understanding Based Management Liquidity Ratios Support Systems*)–cognitive systems for analysing enterprise liquidity ratios which will reason about the resources and the solvency of the working capital of the company as well as about its current operations based on a semantic analysis of a set of selected ratios. UBMLRSS systems represent one of four classes of Cognitive Financial Analysis Information Systems.

Keywords UBMLRSS systems · Semantic analysis · Cognitive systems · CFAIS systems

1 Introduction

The purpose of management information systems is to support decision-making processes [7]. A new direction in the development of these management information systems is their ability to semantically reason based on analysed data sets about possible future developments and the overall condition of the enterprise in

L. Ogiela (✉) · M. R. Ogiela
AGH University of Science and Technology, Al. Mickiewicza 30 PL-30-059 Krakow,
Poland
e-mail: logiela@agh.edu.pl

M. R. Ogiela
e-mail: mogiela@agh.edu.pl

the future. Hence work was undertaken to develop new classes of information systems [1, 5] for analysing and interpreting economic and financial data, which will support intelligent enterprise management. The development of cognitive financial data analysis systems [6, 7] is made possible by the elaboration of IT semantic reasoning formalisms [2–4] necessary for this purpose, which are used to design systems supporting the perceptive interpretation of patterns presented in the form of numerical sets. More precisely, these sets take the form of numerical sequences and the purpose of the analysis is to support taking decisions of strategic importance for enterprises [7].

The proposed approach is primarily based on the correct description, and secondly on the correct building of new classes of systems for analysing and interpreting numerical data, namely financial ratios selected for this analysis. The ratio analysis systems currently developed operate using semantic analysis [5–7]. Thus the design of information systems is based on mathematical techniques of linguistic reasoning used to describe the analysed data [7]. This description is especially geared towards a perceptive analysis and the interpretation of the analysed data sets.

2 CFAIS Systems as an Example of Systems for Semantically Analysing Financial Ratios

Systems used for the semantic analysis of financial ratios represent one of three types of systems for cognitive data analysis [7] (Fig. 1), which include:

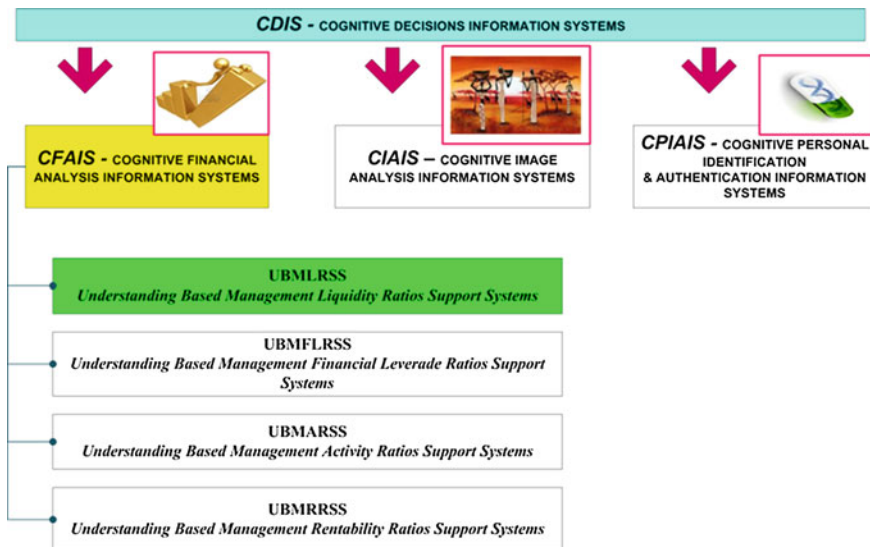


Fig. 1 The classification of cognitive decision information systems

- CFAIS systems–Cognitive Financial Analysis Information Systems,
- CIAIS systems–Cognitive Image Analysis Information Systems,
- CPIAIS systems–Cognitive Personal Identification and Authentication Information Systems.

The CFAIS class of systems is divided into four sub-classes which include the following new classes of systems cognitively analysing economic and financial data (Fig. 2):

- UBMLRSS—Understanding Based Management Liquidity Ratios Support Systems,
- UBMFLRSS—Understanding Based Management Financial Leverage Ratios Support Systems,
- UBMARSS—Understanding Based Management Activity Ratios Support Systems,
- UBMPRSS—Understanding Based Management Profitability Ratios Support Systems.

The UBMLRSS are the cognitive systems for analysing enterprise liquidity ratios which will reason about the resources and the solvency of the working capital of the company as well as about its current operations based on a semantic analysis of a set of ratios.

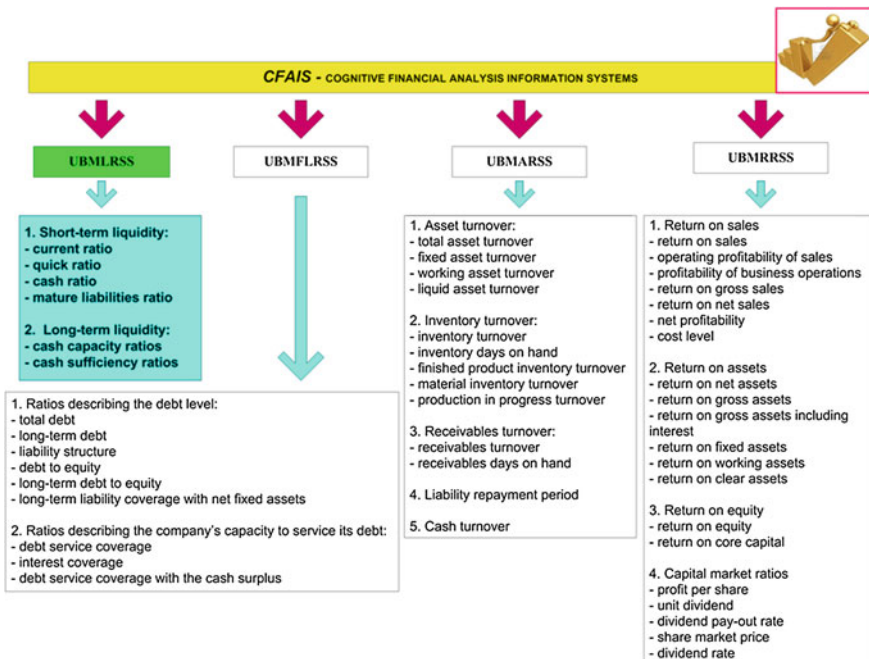


Fig. 2 The CFIAS information systems

The UBMFLRSS are the cognitive systems for analysing financial leverage ratios (financial debt ratios) which will reason about the sources financing the company's assets and the proportion of external capital by analysing short-term and long-term liabilities, as well as the effectiveness of outlays and the interest paid.

The UBMARSS are the cognitive systems for analysing turnover ratios which will reason about how fast assets rotate and how productive they are.

The UBMPRSS are the cognitive systems for analysing profitability ratios which will reason about the financial efficiency of business operations of a given unit based on the relationship between financial results and the sales of goods and services as well as the cost of sales.

Systems for the automatic interpretation of the analysed economic and financial ratios use computational intelligence and mathematical linguistic algorithms. This view of information systems for describing and interpreting the analysed data distinguishes cognitive systems from traditional information systems operating based on traditional informatics formalisms, e.g. neural networks or database reasoning systems based on predicate calculus.

The methodology of designing information systems which improves processes of automatic analysis and semantic interpretation of data forms the foundation of the research work carried out.

The semantic analysis of financial ratios carried out using techniques of the automatic interpretation and analysis of data, which work on the basis of the semantic analysis of the analysed data, makes it possible to conduct a gradual and comprehensive automatic semantic analysis of selected information.

3 Liquidity Analysis

Liquidity analysis is aimed at assessing the liquidity of an enterprise in the context of servicing its debts. The main ratios used to assess this type of standing are as follows:

1. In static methods:

- current ratio—the ratio of current assets (i.e. working assets made up of the inventory, receivables and cash) to current liabilities (i.e. current liabilities consisting of liabilities maturing within a short period of time and long-term liabilities maturing in the specific period),
- quick ratio—shows the level to which current liabilities are covered by highly liquid assets (i.e. receivables, short-term securities and cash),
- cash ratio—the ratio of cash and short-term securities available for sale to current liabilities,
- mature liabilities ratio—describing the relationship of cash to mature liabilities.

Fig. 3 The set of terminal symbols



2. In dynamic methods:

- cash capacity ratios—describe the level of cash receipts generated by the enterprise at a given time from sales or invested assets,
- cash sufficiency ratios—tell about the relationship of cash (generated by the primary business lines) to expenses and total liabilities of the enterprise.

Liquidity ratios are used to assess both short- and long-term liquidity. The first type of assessment focuses on short-term forecasting of enterprise receipts and expenditure using static methods. The second type of assessment is used to analyse expenditure over a long period of time and has a dynamic character.

4 UBMLRSS Systems

The UBMLRSS system class serves to assess current liquidity by using static methods of analysing liquidity ratios. The following formal grammar is proposed for analysing current liquidity:

$$G_L = (V_{NL}, V_{TL}, P_L, S_L)$$

where:

V_{NL} —the set of non-terminal symbols:

$V_{NL}\{\text{LIQUIDITY, EXCESS_LIQUIDITY, OPTIMAL_LIQUIDITY, SOLVENCY_PROBLEMS}\}$,

V_{TL} —the set of terminal symbols:

$V_{TL}\{a, b, c, d, e\}$ —Fig. 3.

where:

$a \in [0; 1)$, $b \in [1, 1, 2)$, $c \in (1, 2; 1, 5)$, $d \in [1, 2, 5]$, $e \in (2; +\infty)$.

$S_L \in V_{NL}$, $S_L \text{LIQUIDITY}$.

P_L — set of productions:

1. $\text{LIQUIDITY} \rightarrow \text{EXCESS_LIQUIDITY} \mid \text{OPTIMAL_LIQUIDITY} \mid \text{SOLVENCY_PROBLEMS}$
2. $\text{EXCESS_LIQUIDITY} \rightarrow \text{EEE} \mid \text{EDE} \mid \text{EED}$
3. $\text{OPTIMAL_LIQUIDITY} \rightarrow \text{DCA} \mid \text{DCB} \mid \text{DBB} \mid \text{DBC} \mid \text{DBA} \mid \text{CBA} \mid \text{CCA} \mid \text{CBD}$
4. $\text{SOLVENCY_PROBLEMS} \rightarrow \text{DEE} \mid \text{AAA} \mid \text{ABA} \mid \text{AAB} \mid \text{ABB} \mid \text{BAB} \mid \text{BBA} \mid \text{ABC} \mid \text{BAC} \mid \text{ACB} \mid \text{BCA} \mid \text{AAC} \mid \text{ACA} \mid \text{CAA} \mid \text{AAD} \mid \text{ADA} \mid \text{DAA} \mid \text{AAE} \mid \text{AEA} \mid \text{EAA} \mid \text{ACD} \mid \text{ADC} \mid \text{ABD} \mid \text{ADB} \mid \text{DAB} \mid \text{ABE} \mid \text{AEB} \mid \text{BAA} \mid \text{BAD} \mid \text{BAE} \mid \text{BEA} \mid \text{EAB} \mid \text{EBA} \mid \text{CAB} \mid \text{ACC} \mid \text{CAC} \mid \text{BCC} \mid \text{CAD} \mid \text{CDA} \mid \text{CAE} \mid \text{CEA} \mid \text{ACE} \mid \text{ADE} \mid \text{AED} \mid \text{DAE} \mid \text{DEA} \mid \text{EAD} \mid \text{EDA} \mid \text{BBB} \mid \text{CCC} \mid \text{DDD} \mid \text{BBC}$

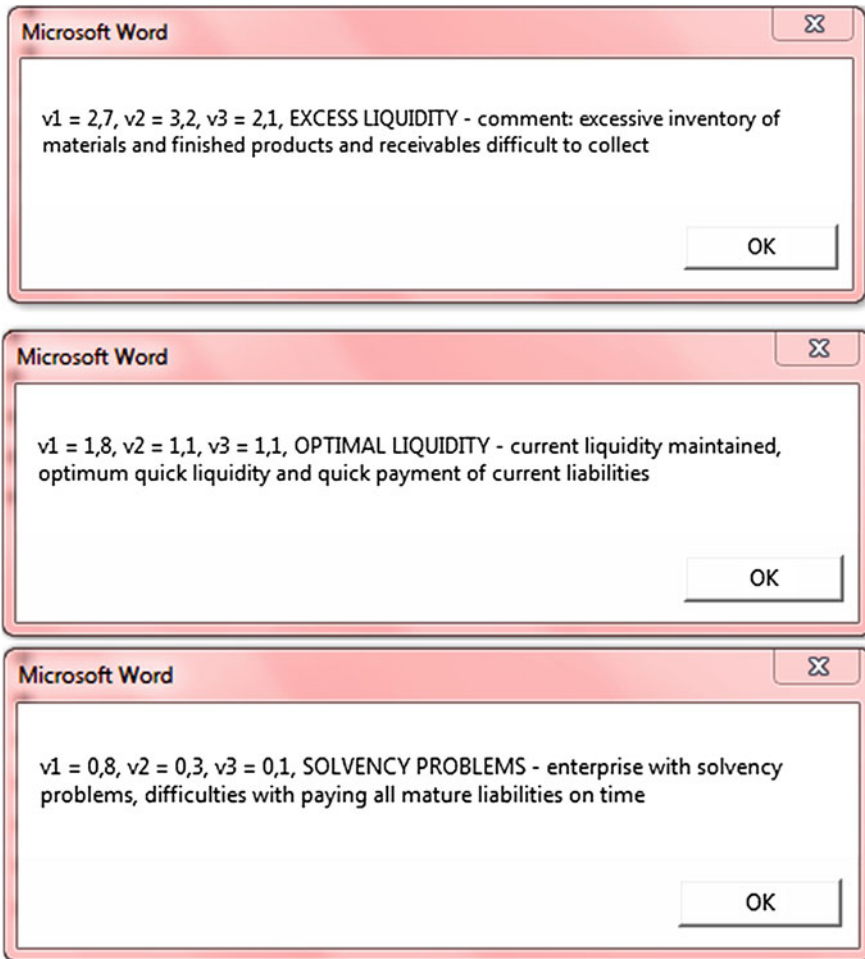


Fig. 4 The examples of UBMLRSS system

CBB | BDA | BCB | BBD | BDB | BBE | BEB | EBB | CCD | CDC | DCC | CCE |
 CEC | ECC | DDE | DED | EDD | BCD | BDC | CDB | BCE | BEC | ECB | EBC |
 CBE | CEB | CDE | CED | EDC | ECD | DEC | DCE | EEA | EAE | AEE | EEB |
 EBE | BEE | CEE | ECE | EEC | DDA | DAD | ADD | BDD | DBD | DDB | DDC
 | CDD | DCD | BDE | BED | CBC | CCB | DAC | DBE | EAC | EBD | ECA |
 EDB | AEC | DEB

5. A → a
6. B → b
7. C → c
8. D → d
9. E → e

The semantic analysis of the liquidity of an enterprise is determined by the assessment of the current and quick ratios of liquidity as well as of cash and mature liabilities. Examples of cognitive analysis conducted by an UBMLRSS system, which comprises not only the assessment of the current company standing but primarily reasoning based on the analysed data, are shown in Fig. 4.

5 Conclusion

The UBMLRSS systems for analysing enterprise liquidity presented here have been developed for analysing the short-term or current liquidity. The data collected in the knowledge base of the system makes it possible to carry out an analysis of groups of financial ratios and to reason about the future of the enterprise. The purpose of the analysis carried out is to identify the directions of changes within the enterprise aimed at ensuring its current liquidity, and if the system identifies optimum values of liquidity ratios of the enterprise, to maintain this situation for as long as possible.

UMBLRSS systems, as a sub-class of cognitive data analysis systems, are designed based on linguistic algorithms and formal grammars [8, 9].

Acknowledgments This work has been supported by the National Science Centre, Republic of Poland, under project number DEC-2012/05/B/HS4/03625.

References

1. Cohen H, Lefebvre C (eds) (2005) Handbook of categorization in cognitive science. Elsevier, The Netherlands
2. Ogiela L (2008) Cognitive systems for medical pattern understanding and diagnosis. LNAI 5177:394–400
3. Ogiela L (2009) UBIAS systems for cognitive interpretation and analysis of medical images. Opto-Electron Rev 17(2):166–179
4. Ogiela L (2010) Cognitive informatics in automatic pattern understanding and cognitive information systems. In: Wang Y, Zhang D, Kinsner W (eds) Advances in cognitive informatics and cognitive computing, Studies in computational intelligence (SCI), vol 323. Springer, Berlin, pp 209–226
5. Ogiela L, Ogiela MR (2009) Cognitive techniques in visual data interpretation, Studies in computational intelligence, vol 228. Springer, Berlin
6. Ogiela L, Ogiela MR (2011) Semantic analysis processes in UBIAS systems for cognitive data analysis. In: You I, Barolli L, Tang F, Xhafa F (eds), IMIS 2011 - 2011 5th International conference on innovative mobile and internet services in ubiquitous computing, Seoul, Korea, 30 June–2 July, pp 182–185
7. Ogiela L, Ogiela MR (2012) Advances in cognitive information systems, cognitive systems monographs, vol 17. Springer, Berlin

8. Ogiela MR, Ogiela U (2012) DNA-like linguistic secret sharing for strategic information systems. *Int J Inf Manage* 32(2):175–181
9. Ogiela MR, Ogiela U (2012) Linguistic protocols for secure information management and sharing. *Comput Math Appl* 63(2):564–572
10. Zhong N, Raś ZW, Tsumoto S, Suzuki E (eds) (2003) *Foundations of intelligent systems*. 14th International symposium, ISMIS, Maebashi City, Japan

A Framework of Static Analyzer for Taint Analysis of Binary Executable File

Young-Hyun Choi, Jae-Won Min, Min-Woo Park, Jung-Ho Eom and Tai-Myoung Chung

Abstract In this paper, we proposed a tool framework of static analyzer for taint analysis of binary executable file. Dynamic taint analysis is becoming principal technique in security analysis. In particular, proposed system focuses on tracing a dynamic taint analysis. Moreover, most existing approaches are focused on data-flow based tainting. The modules of this paper use two kinds of input file type which are taint_trace file and binary executable file. Proposed system analyzes the result of dynamic taint analysis and makes control flow graph. Our proposed system is divided by three modules; taint reader, crash analyzer and code tracker. Trace reader converts trace file into readable/traceable information for a manual analyzer. Crash analyzer find out a vulnerability that is a causative factor in accrued crash. Code tracker supports a variety of binary executable file analysis. In this paper, we suggest a tool framework for dynamic taint analysis.

Keywords Binary analysis · Vulnerability analysis · Static analysis · Taint analysis

Y.-H. Choi · J.-W. Min · M.-W. Park · J.-H. Eom (✉) · T.-M. Chung
Internet Management Technology Laboratory, Electrical and Computer Engineering,
Sungkyunkwan University, Seoul, Republic of Korea
e-mail: eomhun@gmail.com

Y.-H. Choi
e-mail: yhchoi@imtl.skku.ac.kr

J.-W. Min
e-mail: jwmin@imtl.skku.ac.kr

M.-W. Park
e-mail: mwpark@imtl.skku.ac.kr

T.-M. Chung
e-mail: tmchung@imtl.skku.ac.kr

Y.-H. Choi · J.-W. Min · M.-W. Park · J.-H. Eom · T.-M. Chung
Daejeon University, Daejeon, Republic of Korea

1 Introduction

Dynamic taint analysis is a principal technique for tracking information flow. And dynamic taint analysis is available approach to binary executable file without source code. Dynamic taint analysis works by tagging inputs to a program as tainted. And tainted data taints to other values that are influenced tainted inputs. We can check for information well-known vulnerability in a application by marking inputs as tainted, and then checking whether they propagate to inappropriate outputs.

Our proposed system is divided by three modules; taint reader, crash analyzer and code tracker. Trace reader converts trace file into readable/traceable information for a manual analyzer. Crash analyzer find out a vulnerability that is a causative factor in accrued crash. Code tracker supports a variety of binary executable file analysis. Code tracker draws a control flow graph for static analysis with binary executable file. The control flow graph node represents a basic block in the graph.

In this paper we present our approach, a tool framework of static analyzer for taint analysis of binary executable file, as an advantage to an existing similar tools. We also show demonstration of taint trace reader.

The rest of the paper is organized as follows. We provide related work and motivation for the work in [Sect. 2](#). [Section 3](#) presents our approach, and [Sect. 4](#) provides result demonstration. Finally, we conclude and discuss future-work directions in [Sect. 5](#).

2 Related Work and Motivation

There is plenty of related work for a tool framework for the static analyzer for taint analysis of binary executable file. We discuss the most closely-related approaches.

2.1 *Dynamic Taint Analysis*

Taint analysis is a kind of data flow analysis. Other data are influenced by the data flows. Dynamic taint analysis is a mechanism which tracks incoming data from the user input throughout whole process. The reason why marking ‘tainted’ is that data originating from the user input is untrusted. Operations on this data are kept tagging, and taint tagging propagates to the result of operations.

The purpose of dynamic taint analysis is to trace information flow between sources and sinks in accordance with the taint policies.

A taint policy determines exactly the way of tainted data flows as a program executes and the consequences from influence of tainted value [1, 2] [DTA++][ddd].

2.2 Motivation

Taint analysis provides various approach and powerful techniques to detect attacks on vulnerabilities. For example, analyzer protects zero-day attacks using that trace of the control flow and detection of an exploit. Analyzer do not need to well-known vulnerabilities. Many intrusions are untrusted input data principal to a process executing unexpected code. In fact, more than one third of all vulnerabilities notes reported by US-CERT in 2012 consisted of buffer overflows. An attacker try to buffer overrun attack using inject code.

3 Our Approach

In this section, we describe our generic approach for static taint analysis. We provide a general description of our framework, details of the inner module of the framework. The inner module analyses a `taint_trace` file and a binary executable file.

The taint information is the result of taint analysis of binary executable file. Taint information pack into a trace file.

Proposed system can draw to analyze information of processor from disassembled code. Proposed system is divided into a crash analyzer, a taint reader and a code tracker.

A taint reader can determine the overall information of the results of the taint analysis. A crash analyzer estimates a variety of vulnerability of activated processor through the `taint_trace` file. A code tracker generates the assembly code of binary executable file.

The `taint_trace` files generated by the taint analysis are used experimentally to create brand new pieces of analysis policy.

3.1 Proposed Framework

Proposed framework statically analyzes the information of process. Proposed framework consists of taint reader, crash analyzer and code tracker. Trace reader converts trace file into readable/traceable information for a manual analyzer. Crash analyzer finds out a vulnerability that is a causative factor in accrued crash. Code tracker supports a variety of binary executable file analysis.

Figure 1 depicts the overall structure of proposed framework.

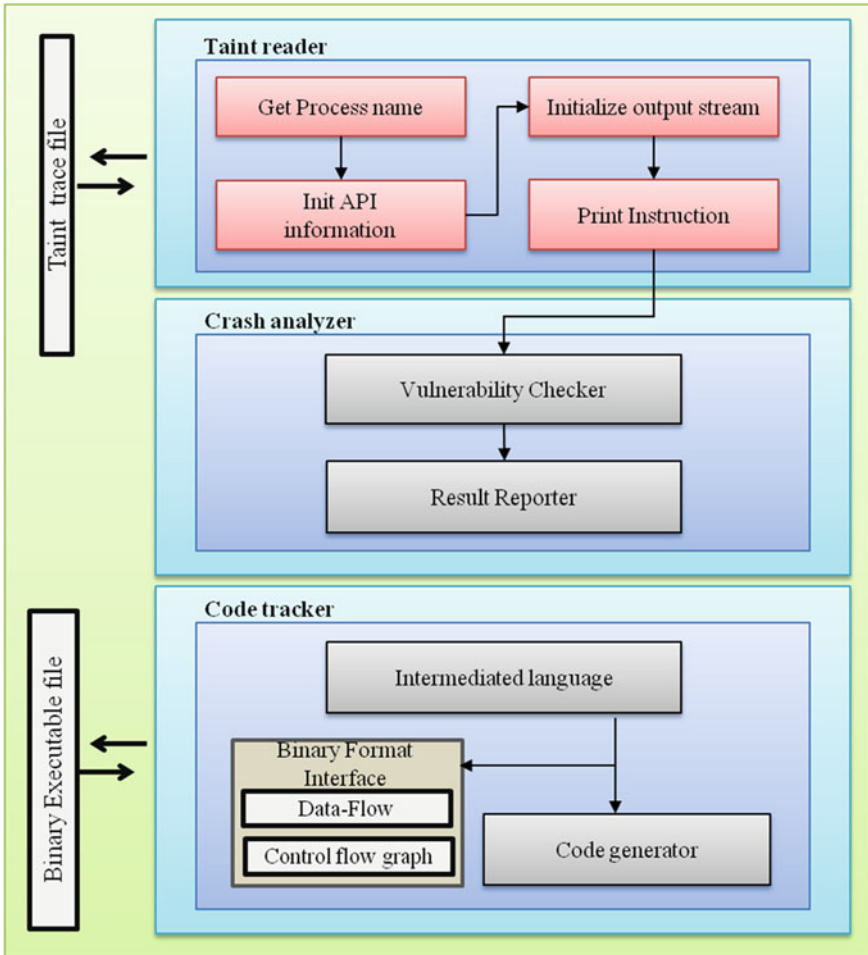


Fig. 1 Framework of proposed static analyzer

3.2 Trace Reader

Trace Reader is comprised of Get Process Name, Init Module Information, Initialize Output Stream, and Print Instruction.

Get Process Name is proposed system gets the subject’s process name of taint analysis of program. Init Module Information initializes the information of loaded modules on taint analysis of program. Initialize Output Stream is allowed to designate an output stream to print the trace information of taint_trace file. Print Instruction prints instructions in the trace information of taint_trace file through the output stream.

3.3 Crash Analyzer

Crash analyzer analyzes trace information of abnormal termination program. Because of crash analyzer finds the software vulnerability on the inner program and reports to user of proposed system. Crash analyzer is comprised of Parser, Vulnerability Checker, Result Reporter.

First of all, Parser, the trace information converts to the token through the tokenization. The tokenization is the process of demarcating and possibly classifying sections of a string of input characters. The resulting tokens are then passed on to the vulnerability checker. The meaningful token has been saved the information at field in the structure. The Vulnerability checker compares with vulnerability information and taint_trace information, and then the vulnerability checker detects concerned vulnerability for a program crash. The result reporter sends the crash analysis information to user.

3.4 Code Tracker

Code Tracker supports a variety of binary executable file analysis. Code Tracker is comprised of Intermediated Language, Binary Format Interface, Code Generator.

An intermediate language is the language of an abstract machine designed to aid in the analysis of computer programs, as well as the analysis language for binary format and code generator. The semantics of the intermediate language are designed to be faithful to assembly languages [11]. Binary format interface supports to analysis program flow, instruction list, address of instruction, etc. Binary format interface has two engines which a control flow graph engine and a data-flow engine. Control flow graph engine generates to facilitate the graph for analysis of data flow of binary code. Data-flow engine traces the extracted data flow through intermediate language information. Data-flow engine verifies that there is accurate operand available of binary codes. Code generator generates the code from intermediate language to machine-level language.

4 Demonstration and Comparison

In this section, an explanation for the demo of trace reader in the proposed system and making a comparison between the proposed system and other similar static analysis programs will be followed.

Trace reader indicates the data of instruction address, instruction information, operand information of source and operand information of destination condition.

Instruction address represents physical address for instruction. Instruction information shows the entire process of instruction and operands.

Table 1 Comparison with other static analysis tools

Name	Control flow graph	Static analysis technique	Input	Note
Airac	No	Abstract interpretation	Source code	Implemented in nML
Sparrow	Yes	Semantic and syntactic, etc.	Source code	Server-client system Early detection
Vine	Yes	Program verification analyses	Binary file	Hybrid with TEMU in BitBlaze project
Proposed system	Yes	Taint analysis	Binary file and taint_trace file	Practical use taint_trace file

Operand information of source and operand information of destination gives specific information of operands such as all kinds of the storage, value and taint information. Users can confirm all of the information mentioned as above so that they can find out what they want like vulnerability and carry out crash analysis Table 1.

The demonstration of trace reader is shown by Fig. 2.

One of static analysis tools called ‘Airac’, which doesn’t have control flow graph differ from the other tools, has abstract interpretation as a static analysis technique. Also ‘Airac’ uses source code for input and ‘Airac’ is implemented in nML. Other three tools named ‘Sparrow’, ‘Vine’ and ‘Proposed system’ provide control flow graph, especially ‘Sparrow’ uses source code for input same as ‘Airac’ and using semantic and syntactic, etc. for static analysis, server-client system and early detection. ‘Vine’ uses binary file for input and has program

```

=====
Instruction addr::77cf9194
Instruction:    mov    $0x7ffe0300,%edx
Operand info::I@0x00000000[0x7ffe0300][4](R)          Untainted
Operand info::R@edx[0x00000000][4](W)                Untainted

=====
Instruction addr::77cf9199
Instruction:    call  *(%edx)
Operand info::M@0x7ffe0300[0x7c93eb8b][4](R)          Untainted
Operand info::M@0x0007febc[0x0007fe9c][4](W)          Untainted

=====
Instruction addr::7c93eb8b
Instruction:    mov    %esp,%edx
Operand info::R@esp[0x0007febc][4](R)                Untainted
Operand info::R@edx[0x7ffe0300][4](W)                Untainted

```

Fig. 2 Trace reader: taint_trace demonstration file

verification analysis as a static analysis technique. Also hybrid with TEMU Bit-Blaze project is on 'Vine'. Lastly, in terms of 'Proposed system', it has taint analysis as a static analysis technique and uses binary file and taint_trace file for input. Practical use taint_trace file is one of its specific characters.

5 Conclusion and Future Work

We presented our framework for static analysis, which provides several approaches. First, it is flexible input files that are taint_trace file and executable binary file. Second, it is practicable taint analysis on static analysis. Finally, it works at the application level and doesn't need the source code.

Proposed system analyzes the result of dynamic taint analysis and makes control flow graph. Our proposed system is divided by three modules; taint reader, crash analyzer and code tracker. Trace reader converts trace file into readable/traceable information for a manual analyzer. Crash analyzer finds out vulnerability that is a causative factor in accrued crash. Code tracker supports a variety of binary executable file analysis.

Proposed a Framework for Static Analyzer for Taint Analysis of Binary Executable File is different detecting whole crash situation on the runtime. However, analysis based on executable file can be efficiently the program without source code supporting. Proposed system has wide range and finds out relatively much vulnerability.

Acknowledgments This work (Grants No. 00044301) was supported by Business for Cooperative R&D between Industry, Academy, and Research Institute funded Korea Small and Medium Business Administration in 2012.

References

1. Scholten M (2007) Taint analysis in practice. Vrije Universiteit Amsterdam, Amsterdam, pp 1–29
2. Newsome J, Song D (2004) Dynamic taint analysis for automatic detection, analysis, and signature generation of exploits on commodity software. Technical report. School of computer science, Carnegie Mellon University
3. Christopher DM, Prabhakar R, Hinrich S (2008) Introduction to information retrieval. Technical report, Cambridge University Press, United Kingdom
4. Denning DE, Denning PJ (1977) Certification of programs for secure information flow. *Commun ACM* 20:504–513
5. Kang MG, McCamant S, Poesankam P, Song D (2011) DTA ++: dynamic taint analysis with targeted control-flow propagation. In: 18th annual network and distributed system security symposium
6. Chow J, Pfaff B, Garnkel T, Christopher K, Rosenblum M (2004) Understanding data lifetime via whole system simulation. In: 13th USENIX security symposium, San Diego, pp 321–336

7. Song D, Brumley D, Yin H, Caballero J, Jager I, Kang MG, Liang Z, Newsome J, Poosankam P, Saxena P (2008) BitBlaze: a new approach to computer security via binary analysis. In: 4th international conference on information systems security (ICISS), information systems security. Lecture notes in computer science, pp 1–25
8. Yin H, Song D, Egele M, Kruegel C, Kirda E (2007) Panorama: capturing system-wide information flow for malware detection and analysis. In: Computer and communication security (CCS), Alexandria
9. US-CERT. Vulnerability notes database. <http://www.us-cert.gov>
10. Rahbar A Stack overow on windows vista. White paper, Sysdream

An IoT-Based Framework for Supporting Children with Autism Spectrum Disorder

Ardiana Sula, Evjola Spaho, Keita Matsuo, Leonard Barolli, Fatos Xhafa and Rozeta Miho

Abstract In this paper, we propose a framework based on Internet of Things (IoT) and P2P technology for supporting learning and improving the quality of life for children with Autism Spectrum Disorder (ASD). Many children with autism are highly interested and motivated by smart devices such as computers and touch screen tablets. These types of assistive technology devices get children with autism to interact, make choices, respond, and tell parents what they want, need, think, and maybe even feel. Our framework uses JXTA-Overlay platform and smartbox device to monitor the children and create P2P communication between children,

A. Sula
Ministry of Education and Science of
Albania, Rr. Durrës, Nr 23 1001 Tirana, Albania
e-mail: asula@mash.gov.al

E. Spaho
Graduate School of Engineering, Fukuoka Institute of Technology (FIT),
3-30-1 Wajiro-Higashi, Higashi-Ku, Fukuoka 811-0295, Japan
e-mail: evjolaspaho@hotmail.com

K. Matsuo
Fukuoka Prefectural Kaho-Sogo High School, 1117-1 Haji, Keisen-machi,
Kaho-gun, Fukuoka 820-0607, Japan
e-mail: matuo-k7@fku.ed.jp

L. Barolli (✉)
Department of Information and Communication Engineering,
Fukuoka Institute of Technology (FIT), 3-30-1 Wajiro-Higashi, Higashi-Ku,
Fukuoka 811-0295, Japan
e-mail: barolli@fit.ac.jp

F. Xhafa
Technical University of Catalonia, Department of Languages and Informatics
Systems, C/Jordi Girona 1-3 08034 Barcelona, Spain
e-mail: fatos@lsi.upc.edu

R. Miho
Polytechnic University of Tirana, Mother Teresa Square, Nr. 4, Tirana, Albania
e-mail: rmiho@fti.edu.al

parents and therapists. Various visual systems, such as objects, photographs, realistic drawings, line drawings, and written words, can be used with assorted modes of technology, as long as the child can readily comprehend the visual representation. Vocabulary skills such as names of common everyday objects, fruits, animals, toys, names of familiar people can be taught through our proposed framework.

Keywords Assistive technologies · Smart environment · Assistive learning · IoT · P2P

1 Introduction

Most of the socially assistive research to date is focused on Autism Spectrum Disorder (ASD). Autism is a neurological disorder that affects the ability to communicate and interact socially.

One of the issues to cope with this problem is how to benefit from the technology to help these children. Individuals with cognitive disabilities and developmental and social disorders constitute another growing population that may benefit from assistive applications in the contexts of special education, therapy, and training.

The cause of the increasing number of children with autism is not yet known. However, early intervention is critical to enabling a positive long-term outcome, and even with early intervention, many individuals will need high levels of support and care throughout their lives.

An assistive smart environment has the potential to enhance the quality of life for broad populations of users: the elderly, individuals with physical impairments and those in rehabilitation therapy, and individuals with cognitive disabilities and developmental and social disorders [1].

The advance of the technology is leading to smart objects being capable of identifying, locating, sensing and connecting and thus leading to new forms of communication between people and things and things themselves. Now in the process of development is an increasing number of smart devices that allow users to control and monitor events in consumer-based appliances, home electronics, and home-security systems. As these devices become more common, the need will increase for a home networking strategy that will allow all data, voice, and smart devices to be accessed at anytime from anywhere.

IoT will be a key part of the future Internet. Radio Frequency Identification (RFID) tags, allow objects to be uniquely identified, to determine the location, to sense changes in physical data and to connect and communicate with a corresponding transponder.

Children with autism are the subjects of the research presented here. As there is no current cure for autism and the primary care goal is in creating a supportive

environment. We propose a framework based on an assistive smart environment for supporting learning and improving the quality of life.

The rest of the paper is organized as follows. In Sect. 2, we give an overview of the various current networking technologies. An introduction of IoT and RFID is given in Sect. 3. In Sect. 4, we discuss the proposed framework for children with ASD. We present conclusions and future work in Sect. 5.

2 Networking Technologies

Advances in data collection technology, such as embedded devices and RFID technology have lead to an increasing number of smart devices (see Fig. 1) that allow users to control and monitor events in consumer-based appliances, home electronics, and home-security systems. As these devices become more common, the need will increase for a home networking strategy that will allow all data, voice, and smart devices to be accessed at anytime from anywhere [2].

Home networking is the collection of elements that process, manage, transport, and store information, enabling the connection and integration of multiple computing, control, monitoring, and communication devices in the home.

Robots are being steadily introduced into modern everyday life and are expected to play a key role in the near future. Typically, the robots are deployed in situations where it is too dangerous, expensive, tedious, and complex for humans to operate. Robots offer many advantages to accomplish a wide variety of tasks given their strength, speed, precision, repeatability, and ability even in extreme environments. Socially intelligent robotics is the pursuit of creating robots capable of exhibiting natural-appearing social qualities. Beyond the basic capabilities of moving and acting autonomously, research is focused on the use of the robot's physical embodiment to communicate and interact with users in a social

Fig. 1 Smart devices in children environment



and engaging manner. Assistive robotics in general and socially assistive robotics in particular have the potential to enhance the quality of life for broad populations of users: the elderly, individuals with physical impairments and those in rehabilitation therapy, and individuals with cognitive disabilities and developmental and social disorders [3].

A number of research groups have examined the response of children with autism to robots [4–8]. Each of these studies has demonstrated that robots generate a high degree of motivation and engagement in subjects, including subjects who are unlikely or unwilling to interact socially with human therapists. This presents the hope that a robot might be used to teach them social skills incrementally, and assists in the transfer of this knowledge to interactions with humans.

Peer to Peer (P2P) systems appeared as a new paradigm after client–server and became quite popular for file-sharing among internet users. Such systems benefit from high scalability and fault tolerance. Today research is focused on the design, implementation and deployment of full featured P2P networks that integrate end-devices. P2P is a very good approach to an efficient platform for e-learning and robot control.

A Wireless Personal Area Network (WPAN) is a low-range wireless network which covers an area of only a few dozen meters. This sort of network is generally used for linking peripheral devices (like printers, cellphones, tablets and home appliances) or a Personal Digital Assistant (PDA) to a computer, or just two nearby computers, without using a hard-wired connection. There are several kinds of technology used for WPANs, but the main WPAN technology is Bluetooth.

Emerging WPAN standards (IEEE 802.15 standards) are focused in general to provide cost effective and innovative smart wireless applications such as: Wireless Sensor Networking and RFID Applications. Most popular WPAN Standards are: Bluetooth IEEE 802.15.1, Zigbee IEEE 802.15.4, UWB (Ultra Wide Band) IEEE 802.15.3a and Proprietary standards based on Embedded Wireless Chips.

Wireless Sensor Networks (WSNs) are increasingly gaining impact in our daily lives. They are finding a wide range of applications in various domains, including health-care, assisted and enhanced-living scenarios, industrial and production monitoring, control networks, and many other fields.

3 Internet of Things (IoT)

The term Internet of Things has recently become popular to emphasize the vision of a global infrastructure of networked physical objects. IoT enables the things/objects in our environment to be active participants with other members of the network, often using the same Internet Protocol (IP) that connects the Internet.

In this way the things/objects are capable of recognizing events and changes in their surroundings and are acting and reacting autonomously largely without human intervention in an appropriate way.

The major objectives for IoT are the creation of smart environments/spaces and self-aware things for smart transport, products, cities, buildings, energy, health and living applications (see Fig. 2).

The Internet of Things will accelerate and expand, since the IPv6 (Internet Protocol version 6) implementation is to result in a tremendous growth of IP addresses, giving broader ability for every physical thing to connect to the Internet and communicate with any other object.

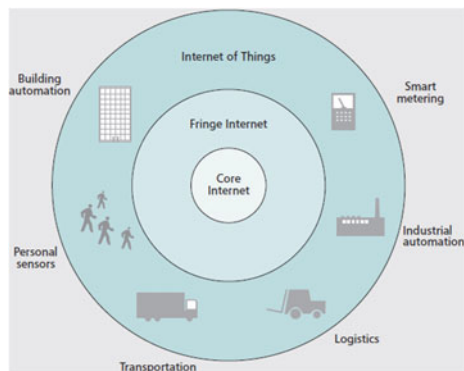
The IoT is partly inspired by the success of RFID technology, which is now widely used for tracking objects, people, and animals.

RFID and sensor network technologies will rise to meet this new challenge, in which information and communication systems are embedded in the environment. RFID is primarily used to identify objects from a distance of a few meters, with a stationary reader typically communicating wirelessly with small battery-free functions for an IoT identification and communication RFID can also be used to determine the approximate location of objects provided the position of the reader is known.

RFID systems consist of three main components. They are RFID tags, the RFID readers, and RFID software. An RFID tag or transponder carries the ID data which is a unique string or code. In addition, a tag can also store information contents depending on the size of its memory. A tag is tagged or attached physically to the object to be identified. The tag is an electrical device designed to receive a specific signal and automatically transmit a specific reply.

It consists of a coupling element (such as a coil, or a microwave antenna) and an electronic microchip. Tags can be passive, semi-passive or active, based on their power source and the way they are used, and can be read-only, read/write or read/write/re-write, depending on how their data is encoded. Passive RFID tags take the energy from the electro-magnetic field emitted by readers. An RFID reader or interrogator is a hardware device that is used to read the transmitted data from the tag. RFID software is a middleware that runs on the RFID reader.

Fig. 2 IoT applications



4 Proposed System for Supporting Children with ASD

Technological advancements lead to smart objects being capable of identifying, locating, sensing and connecting and thus leading to new forms of communication between people and things and things themselves. Assistive Technologies (ATs) such as Ambient Assisted Living (AAL) encompasses technical systems to support children with autism in their daily routine to allow an independent and safe life-style and an assistive learning environment. The combination of smart technologies results in an applied IoT infrastructure for AAL scenarios. A central AAL paradigm can be realized through the IoT, where the children with autism live in their homes with smart objects, thus smart homes, communicating to the outside world in an intelligent and goal-orientated manner.

We propose the combination of IoT, P2P, Web and sensor technologies for monitor, check, control the health situation and assist children with ASD. Our proposed IoT based framework is shown in Fig. 3. Our system sends information about the children state in real time to therapists using P2P technology and also allows children to interact with other children and parents.

P2P communication can be build using JXTA-Overlay Platform. JXTA-Overlay project is an effort to use JXTA technology for building an overlay on top of JXTA offering a set of basic primitives (functionalities) that are most commonly needed in JXTA-based applications. The proposed overlay comprises the following primitives: peer discovery, peer's resources discovery, resource allocation, task submission and execution, file/data sharing, discovery and transmission, instant communication, peer group functionalities (groups, rooms etc.), monitoring of peers, groups and tasks.

Fig. 3 Proposed IoT based framework for supporting children with ASD

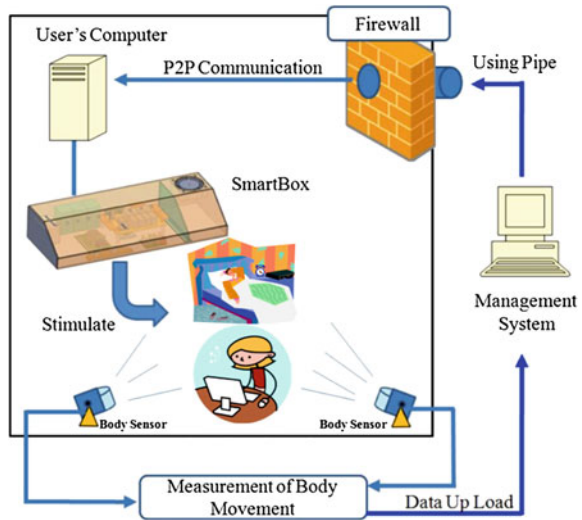
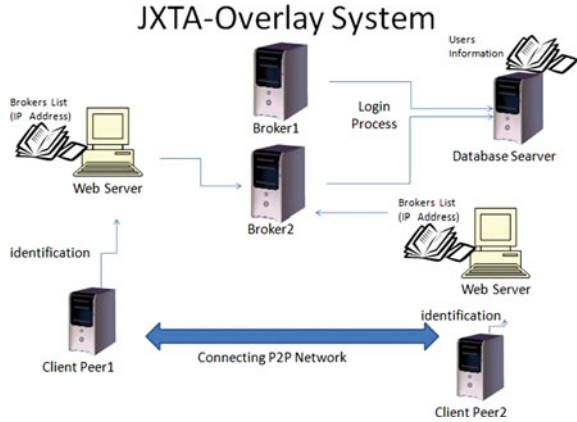


Fig. 4 Structure of JXTA-overlay system

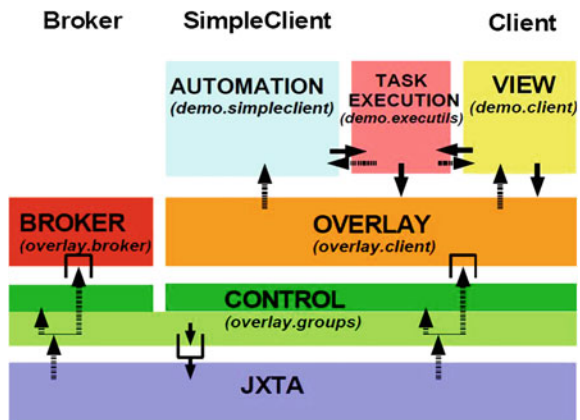


The overlay is built on top of JXTA layer and provides a set of primitives that can be used by other applications, which on their hand, will be built on top of the overlay, with complete independence. The JXTA-Overlay project has been developed using the ver-2.3 JXTA libraries. In fact, the project offers several improvements of the original JXTA protocols/services in order to increase the reliability of JXTA-based distributed applications [9] and to support group management and file sharing.

The architecture of P2P distributed platform which can be developed using JXTA technology has two main peers: Broker and Client. Altogether these two peers form a new overlay on top of JXTA. The structure of JXTA-Overlay is shown in Fig. 4.

Except Broker and Client peers, the JXTA-Overlay has also Simple Client peers as shown in Fig. 5. The control layer interacts with the JXTA layer, and is divided into two parts: a lower part with functionality common to any kind of peer, and a higher part with functionality specific to Brokers and Clients.

Fig. 5 JXTA-overlay architecture



- The common part provides functionality for doing JXTA messaging, discovery and advertisement.
- The Broker specific part provides functionality for managing groups of Brokers and keeping broker statistics.
- The Client specific part provides functionality for managing groups of Clients, keeping client statistics, managing its shareable files, managing the user configuration and creating the connection with a Broker.

The lower part queues the JXTA messages to be sent. Whenever a message arrives, the JXTA layer fires an event to the lower layer, which in turn fires a notifications to the upper layers.

The most important part in a P2P system is the communication between peers. By using JXTA-Overlay, it is possible to overcome, firewalls, routers, NATs, and bridges in the private networks.

We explain in following the message transmission by the JXTA-Overlay.

JXTA-Overlay uses Universally Unique Identifier (UUID) in order to identify the peers in the private network from the Internet. The UUID is a general unique identifier. It is generated by the NIC address of the computer, date and time.

By knowing the UUID and TCP address, it is possible to make address translation.

A control system that is able to control a peer in a private network from a peer in the Internet as showing in Fig. 6. The control targets are considered the network devices such as RS232C port, LPT port and USB port. By implementing this kind of control system, we are able to collect data and control the peers in a Wide Area Network (WAN). Thus, we will be able to control all devices that are connected to the peers. We can control the USB devices and RS232C equipment. This is because USB devices are very popular and are used almost in every computer. Also, by using USB it is possible to control motors and LEDs. The RS232C is a legal interface and many devices have implemented it.

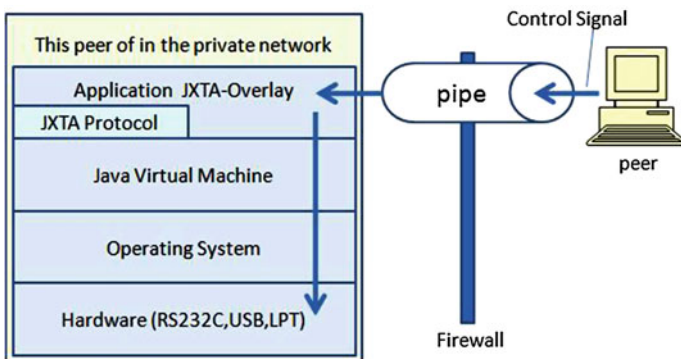


Fig. 6 Remote control in JXTA-overlay

The SmartBox device is integrated with our system as a useful tool for monitoring and controlling children activities. The size of the SmartBox is $35 \times 7 \times 12$ cm. The SmartBox has the following sensors and functions:

- **Body Sensor** for detecting body movement
- **Chair or Bed Vibrator Control** for vibrating the chair or bed
- **Light Control** for adjusting the room light
- **Smell Control** for controlling the room smell
- **Sound Control** to emit relaxing sounds, and
- **Remote Control Socket** for controlling AC 100 V socket (on–off control).

These functions can calm and relax children with ASD that are anxious or on a panic attack and increase concentration on tasks.

Assistive Technologies (ATs) are often presumed to improve health and social care services for children with autism spectrum disorders.

Tagging physical objects to find and analyze data about the object is one way the IoT can be used in education. In Fig. 7 is shown a part of the proposed framework for assistive learning. A child can learn new words through touching the physical objects that are in their vocabulary list.

Each physical object would have a RFID tag placed on the item. When this tag is read by a RFID reader or scanned by an application running on a computer or mobile device it would prompt the device to open up a page of information or send a command for an action to happen.

RFID tags can be created and attached by the parents for each of the physical items in the vocabulary list. When the child places the RFID card on the RFID reader, it will say the word for the item in their native language. Touching the item will give to the child another sense to be engaged and may help them learn new words faster.

Fig. 7 Part of the proposed framework for assistive learning



5 Conclusions and Future Work

Assistive applications are a new research area with large horizons of fascinating and much needed research. Even IoT technology for assistive applications is still in its early stages of development, the next decade promises systems that will be used in schools and homes in therapeutic programs that monitor, encourage, and assist children with autism.

In this work, we proposed a framework based on IoT and P2P for monitoring, supporting learning and improving the quality of life for children with ASD. We believe that smart environment help children with autism to learn language, social skills, appropriate behavior and academic skills.

In the future, we would like to implement the proposed framework and make experiments to evaluate its effectiveness.

References

1. American Psychiatric Association (2000) Diagnostic and statistical manual of mental disorders, 4th edn. Washington
2. Home Networking. <http://www.iec.org>
3. Tapus A, Matarich M, Scassellati B (2007) The grand challenges in socially assistive robotics. *Robotics Autom Mag IEEE* 14(1):35–42
4. Werry P, Dautenhahn K (1999) applying mobile robot technology to the rehabilitation of autistic children. In: Proceedings of the 7th international symposium on intelligent robotics systems (SIRS99), Coimbra, Portugal
5. Michaud F, Clavet A (2001) Robotoy contest—designing mobile robotic toys for autistic children. In: Proceedings of the American society for engineering education (ASEE01), Albuquerque, NM, USA
6. Robins B, Dautenhahn K, te Boekhorst R, Billard A (2005) Robotic assistants in therapy and education of children with autism: can a small humanoid robot help encourage social interaction skills? *Universal Access in the Information Society (UAIS)*
7. Kozima H, Nakagawa C, Yasuda Y (2005) Interactive robots for communication-care: a case-study in autism therapy. In: Proceedings of the IEEE international workshop on robot and human interactive communication (RO-MAN05), pp 341–346
8. Scassellatti B (2005) How Social Robots will help us to diagnose, treat and understand autism. In: Proceedings of the 12th international symposium of robotics research (ISSR05), San Francisco, CA, USA
9. Xhafa F, Fernandez R, Daradoumis T, Barolli L, Caballe S (2007) Improvement of JXTA protocols for supporting reliable distributed applications in P2P systems. In: Proceedings of NBIIS-2007, Germany, pp 345–354

Improvement of Fingerprint Verification by Using the Similarity Distribution

Seung-Hoon Chae and Sung Bum Pan

Abstract Mobile devices, with their excellent portability and increasing computational power, are increasingly being used for communication and financial transactions. As they are used in close relation to people, their security is becoming more important. Faceless verification systems with improved security performance, including face or fingerprint verification, are recently being required. Fingerprint verification is a suitable method in a faceless environment. However, the commonly used Minutiae-based fingerprint verification shows a drop in the performance of fingerprint verification, due to the decreased number of minutiae, when the number of acquired images is small. Especially since the values around the threshold of similarity are similar in the genuine and imposter, many errors could occur here. The minutiae-based fingerprint verification has a limitation in addressing these problems. A hybrid-based verification method that uses two or more fingerprint matching methods can address these problems better. Therefore, this paper has conducted the binary-image-based fingerprint verification in the partial band around the threshold. From the results of the experiment, it can be seen that the Equal Error Rate (EER) was improved by a total of 42 %, from 3.01 % to 1.73 %, by reducing the False Match Rate (FMR) in the partial band area around the threshold. In addition, it was improved by reducing the FMR by a total of 89 % from 2.77 % to 0.28 %.

Keywords Biometrics • Fingerprint verification • Hybrid fingerprint verification

S.-H. Chae

The Research Institute of IT, Chosun University, 309, Pilmun-daero, Dong-gu, Gwangju 501-759, Korea
e-mail: ssuguly@gmail.com

S. B. Pan (✉)

Department of Control, Instrumentation, and Robot Engineering, Chosun University, 309, Pilmun-daero, Dong-gu, Gwangju 501-759, Korea
e-mail: sbpan@chosun.ac.kr

1 Introduction

Mobile devices such as computer, smart phones, PDAs, and mobile phones are providing a wide range of applications and conveniences to users. With their portability, miniaturization, price fall, diverse applications, and performance improvements, their penetration rate is rapidly increasing. Community websites such as Social Networking Services (SNSs) that are based on mobile devices are recently being developed, and communication activities via mobile devices are increasing. Accordingly, individual activities and financial information can be known by analyzing the mobile device information of an individual. With the increase in the number of activities for which mobile devices are used, the loss or hacking of such devices is resulting in much more mental and financial damage than before. Leaked information often leads to crimes. Thus, mobile device security and privacy protection are the most important issues for mobile devices, which have become very closely related to human life. Also, in the modern society, the importance of faceless verification system has been increased from the development of communication technology. The traditional authentication system of using password and Personal Identification Number (PIN) holds the problem of forgetting and misuse. Especially when the false-matching was successful in the verification with the information illegally acquired, this may raise a security problem. The biometrics draws a lot of attention as a method appropriate to solve these problems. The biometrics can be owned only by oneself and has no risk of forgetting or loss [1, 2].

As shown in Fig. 1, Android of Google, which is the representative operating system for mobile devices, has released an OS that has a face unlock feature that uses face verification, and has developed a smart-phone with a fingerprint sensor for fingerprint verification. The biometric system is increasingly being introduced to mobile devices. With the improvement of mobile device performance, the performance of the camera installed in the device is also improving. Contactless fingerprint verification methods are being studied to enable the use of high-performance cameras in mobile devices to obtain fingerprint images, which eliminates the need for an additional accessory [3, 4].

The fingerprint verification is the most widely used method of various biometrics. The Minutiae-based Fingerprint Verification (MFV) is generally used as the fingerprint verification method. Recently as the fingerprint verification system is miniaturized, the size of fingerprint scan sensor has become small and hence, the acquired size of fingerprint got smaller as well. Accordingly, this can raise the problem that the number of extracted minutiae and region with two fingerprints overlapped may not be sufficient from the fingerprint image acquired, hence reducing the verification performance. The problem with the lack of minutiae cannot be addressed using the conventional MFV that extracts minutiae only from one fingerprint image. The methods that have been proposed to solve these problems, include that of generating a super template by accepting several fingerprints [5], and that of improving the template quality [6]. There is also the



Fig. 1 The smart phones using biometrics

Hybrid-based Fingerprint Verification (HFV) that uses minutiae and phase information [7], which is different from the method of using merely minutiae.

In this paper, HFV, which is based on MFV and uses, to a limited degree, the Binary-image-based Fingerprint Verification (BFV), was proposed to improve the fingerprint verification performance. Simultaneously using MFV and BFV for each verification process will improve security, but the resulting increase in the calculation volume will reduce the convenience of the user's fingerprint verification. Therefore, BFV was used to a limited extent to ensure security while addressing the problem of the user's long verification time. Since the value around the threshold of similarity are similar to those of genuine and imposter, the overall fingerprint verification performance could be reduced. In order to improve the verification result of holding the similarity around the threshold of MFV, this paper proposes the HFV that uses the BFV in the band around the threshold of minutiae similarity. Generally although the binary fingerprint image is the information generated and discarded for the extraction of minutiae, the binary fingerprint image holds more information than minutiae. Accordingly when performing the fingerprint verification around the threshold of MFV by using the binary fingerprint image of holding more comparison information than minutiae with the same image size, the false matching error around the threshold could be reduced. According to the result of experiment, we could see that the False Match Rate (FMR) was reduced by 89 % from 2.77 % of the MFV to 0.28 % of the proposed method. Also, we could check that the Equal Error Rate (EER) of fingerprint verification was improved as well from 3.01 % to 1.73 %. The remainder of this paper is organized as follows. In Sect. 2, we describe the HVF used by the proposed method. The experimental results are presented in Sect. 3, and we conclude in Sect. 4.

2 Proposed Hybrid Fingerprint Verification Using Partial Band

In this paper, the conventional MFV and the BFV were combined to improve the fingerprint verification performance. The HFV is described, and then the combined method that uses minutiae and binary images is described.

2.1 Hybrid Fingerprint Verification System

The HFV combines two or more supplemental verification methods. In this paper, the conventional MFV and BFV were used. The hybrid-based verification method that uses both the MFV and BFV methods are described as follows. Let $\omega_1, \omega_2, \dots, \omega_n$ represent the n users enrolled in the database. Minutiae (M), which is extracted from the input fingerprint image using the minutiae extraction module, is inputted into the matching module of the first system. The result of the first system is $S(\omega_i | M)$, wherein $S(\omega_i | M)$ is the similarity of the minutiae of the input fingerprint (M) to ω_i . In the second system, matching is conducted using the additional information on the fingerprints. In this paper, the binary image of fingerprint (B) was used as the additional fingerprint information. The user is verified using the result of the first and second systems, $S(\omega_i | M, B)$. Figure 2 shows the integration of the two systems. Unlike the conventional verification method that involves only one piece of information and one verification process, the hybrid-based verification method has two or more verification processes that use different pieces of information. Accordingly, it can reduce the security errors that may occur in the conventional verification process.

In order to solve the problem held by the MFV, this paper has used the image-based fingerprint verification method of using fingerprint image. Since the fingerprint image holds more comparable information than minutiae, it can perform

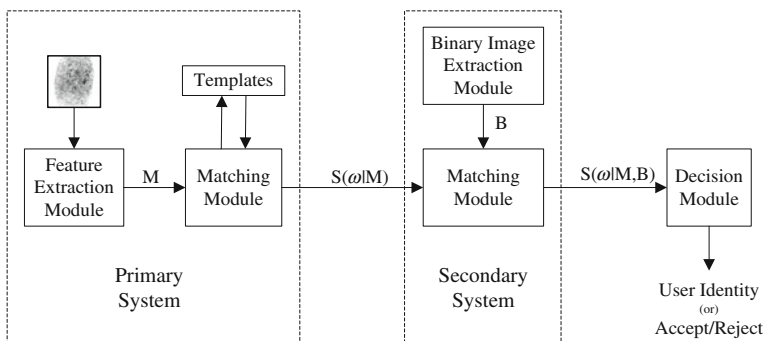


Fig. 2 Integration of BFV with MFV

more accurate verification than minutiae when the overlapped area of two fingerprints is small or the acquired fingerprint image is small.

The Fig. 3 shows the HFV that uses the minutiae and binary image proposed in this paper. Since the fingerprint information is not aligned properly, this requires a process of aligning two fingerprints. As for the alignment methods that use only the finger image, there are the method [8] of using ridges and the method [9] of using the singular points such as core and delta. However, the method of using only the image has some limitations since this requires a lot of calculations and there may be the cases that the singular points do not exist. Therefore, the fingerprint correction of using only the image is less efficient than the method of using minutiae. And, the BFV used in this paper has required more processing time than the method of using minutiae. Accordingly, the BFV should be conducted only to a limited extent. Also while the performance of MFV was excellent in the place of high minutiae similarity, the fingerprint verification error has occurred around the threshold low in the similarity. In this case, this paper refers the area around the threshold as partial band. Accordingly as for the area excluding the partial band high in the reliability, this paper intends to propose the HFV that uses the BFV for the fingerprints holding the minutiae similarity of partial band without performing the BFV. As for the fingerprint image, this paper has used the binary fingerprint image that has gone through the fingerprint quality improvement and binarization occurring in the process of MFV. The binary fingerprint image is small in the data size as compared to that of gray-scale image. And, the contrast of fingerprint image is more obvious than that of gray-scale. Also while going through the image quality improvement and binarization process, it becomes more appropriate for the fingerprint verification as the small noises such as skin wrinkles and pores are removed. For these reasons, in this paper image verification stage is done after the binarization of images.

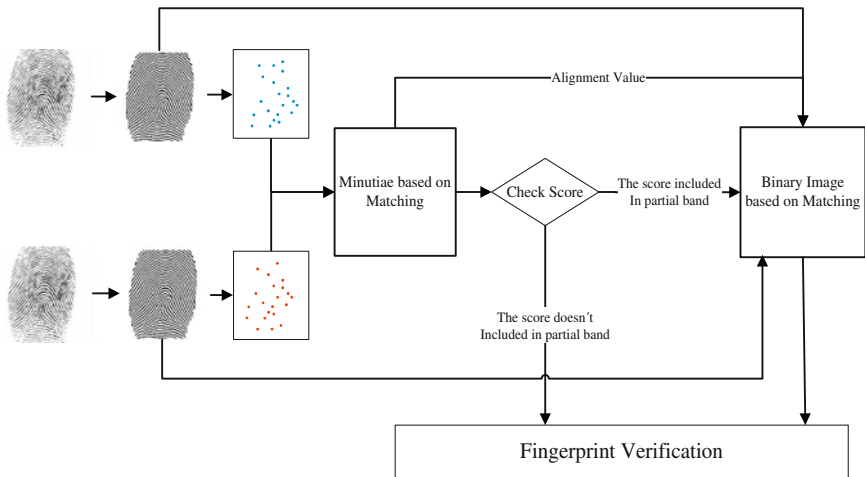


Fig. 3 Proposed HFV system

2.2 Partial Band of Similarity Distribution

The proposed method in this paper has first performed the MFV. And then, this paper determines whether or not to perform the BFV. If the minutiae similarity is held in the partial band necessary to have the BFV, the verification is performed by using the result of BFV after executing the BFV. However when the result of MFV holds the minutiae similarity of the area excluding the reliable partial band, the matching is performed only with the MFV. As for the correction phase of BFV, this paper has used the correction result of MFV. The partial band, which determines execution of the BFV, uses the similarity distribution of MFV. The Fig. 4a shows the similarity distribution of MFV.

The errors in the MFV are distributed around the threshold value th as shown in the Fig. 4a. The cases, which errors have occurred in the MFV, were the case that

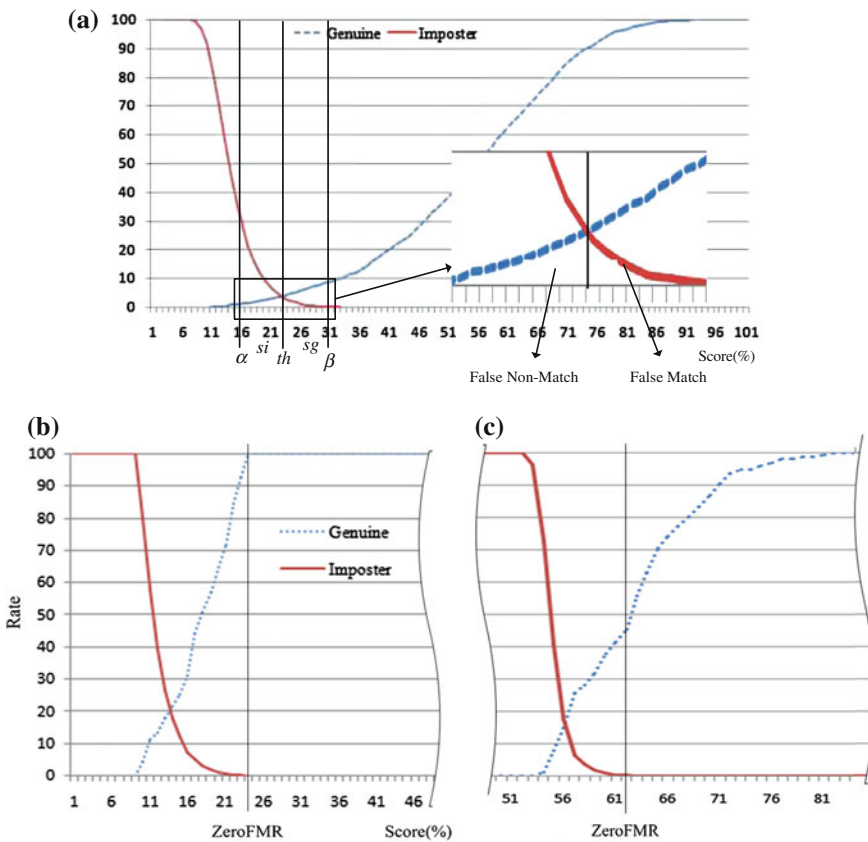


Fig. 4 Similarity distribution of fingerprint verification. **a** Similarity distribution of MFV, **b** Similarity distribution of MFV within the partial band, **c** Similarity distribution of BFV within the partial band

the similarity of genuine becomes below the threshold value as well as the case that the similarity of imposter exceeds the threshold value. These errors are respectively referred to as ‘False Non-Match’ and ‘False Match’. As shown in the Fig. 4a, this paper has used the partial band between the similarity α (where the ‘False Non-Match’ becomes ‘0’) and similarity β (where the ‘False Match’ becomes ‘0’) as the maximum band. The S_i and S_g hold the similarity value between th and α and the value between th and β , which are in the similarity range of partial band. Since the similarity values of genuine and imposter around the threshold within the partial band are similar from each other, this is the range that errors occur most frequently. When performing the BFV excellent in the performance of rejecting false matching within this partial band, the verification performance could be improved.

Since the BFV has a lot of comparison information, the FMR could be reduced. However as the False Non-Match Rate (FNMR) is raised, the EER performance could be reduced as compared to the MFV. However as for the minutiae similarity distribution, the gain obtained by the reduction of FMR is larger than the loss by the mismatching error when performing the BFV within the partial band around the threshold. Accordingly from the result of the BFV performed within the partial band, the MFV holds the Zero False Match Rate (ZeroFMR) of 100 % as shown in the similarity distribution of Figs. 4b and c. However since the ZeroFMR of BFV holds the performance of 60 %, it is better than the BFV. Accordingly, this paper has improved the security performance of fingerprint verification by reducing FMR within the partial band area around the threshold. Also, the EER performance was improved by the FMR reduction effect.

3 Experimental Results

This paper has performed the experiment by using the Set A of FVC [10]-DB1 fingerprint database [10]. In case of genuine and imposter, the test was performed respectively for 2,800 times and 4,950 times. As for the similarity partial band of the minutiae to execute the binary image fingerprint verification, this paper has used the similarity distribution. The minutiae similarity partial band that holds the P distribution is selected by using the Eq. (1).

$$P = \frac{I(th, S_i) + G(th, S_i)}{I(th, \alpha) + G(th, \alpha)} \times 100 = \frac{I(th, S_g) + G(th, S_g)}{I(th, \beta) + G(th, \beta)} \times 100 \quad (1)$$

$I_{(i,j)}$: Number of imposter between the similarity i and j

$G_{(i,j)}$: Number of imposter between the similarity i and j

In other words, the fingerprint verification performance was tested on the basis of threshold value after finding the similarity below the threshold and above the threshold that hold as many fingerprints for the P ratio. The Fig. 4 shows the

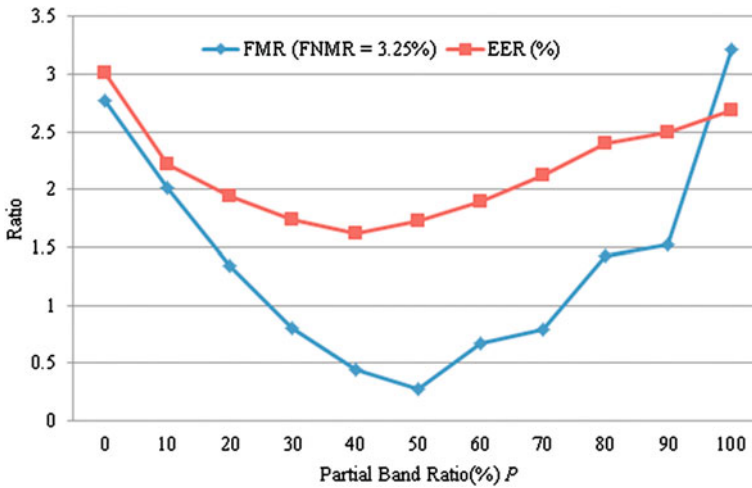


Fig. 5 Fingerprint verification performance by the value of P

fingerprint verification performance in accordance with the P ratio. As for the partial band ratio, this experiment has checked the performance after measuring the matching result within the partial band for the P value of 0 % up to 100 %. Binary fingerprint matching used Dice overlap, define as $2(R \cap B)/(R + B)$ where R is registration binary fingerprint image and B is input binary fingerprint image [11].

From the Fig. 5, the case with the partial band ratio P of 0 shows the experimental result that has used only the MFV without using the BFV. In order to check the improvement effect of FMR, this experiment has tested the changes in FMR by fixing FNMR and has measured EER to evaluate the verification performance.

According when having fixed FNMR to 3.25 %, the FMR performance was improved more than having used the MFV. Especially when having used only the partial band ratio of 50 %, we could see that the performance was improved from 2.77 % to 0.28 %. Also, the EER of proposed method was improved to 1.62 % from 3.01 %. Through these experimental results, we have verified that the proposed fingerprint verification method not only improves the FMR but also the verification performance.

4 Conclusions

The MFV is the fingerprint verification method most widely used due to its excellent performance and quick processing speed. However, the verification performance is reduced in the case when the acquired image is small. Likewise in order to solve the problem of MFV and to improve the FMR in security, this paper has proposed the HFV that uses both the MFV and BFV methods. In order to

combine two verification methods effectively, we have performed the BFV only within the partial band with similar minutiae. After using the proposed method by using the band ratio of 50 %, we could see that the FMR of proposed method was improved by 89 % from 2.77 % to 0.28 % as compared to the MFV and the EER performance was improved by 42 % when having fixed FNMR to 3.25 %. In the future, we plan to study on the image comparison method to improve the processing speed of image based fingerprint verification method.

Acknowledgments This research was supported by Basic Science Research Program through the National Research Foundation of Korea (NRF) funded by the Ministry of Education, Science and Technology (2011-0023147).

This research was supported by Basic Science Research Program through the National Research Foundation of Korea (NRF) funded by the Ministry of Education, Science and Technology (No. 2010-0005091).

References

1. Jin C, Kim H (2009) High-resolution orientation field estimation based on multi-scale gaussian filter. *IEICE Electron Express* 6(24):1781–1787
2. Lee S, Choi WY, Moon D, Chung Y (2009) Secure fuzzy fingerprint vault against correlation attack. *IEICE Electron Express* 6(18):1368–1373
3. Palma J, Liessner C, Mil'Shtein S (2007) Contactless optical scanning of fingerprints with 180° view. *Scanning* 28(6):204–301
4. Labati, RD (2011) A neural-based minutiae pair identification method for touch-less fingerprint images. In: *Computational intelligence in biometrics and identity management*, pp 96–102
5. Ryu C, Han Y, Kim H (2005) Super-template generation using successive bayesian estimation for fingerprint enrollment. In: Kanade T, Jain AK, Ratha NK (eds) *AVBPA 2005, LNCS*, vol 3546. Springer, Heidelberg, pp 261–277
6. Lee K, Park KR, Jang J, Lee S, Kim J (2005) A study on multi-unit fingerprint verification. In: Kanade T, Jain AK, Ratha NK (eds) *AVBPA 2005, LNCS*, vol 3546. Springer, Heidelberg, pp 141–150
7. Ito K, Morita A, Aoki T, Nakajima H, Kobayashi K, Higuchi T (2005) A fingerprint recognition algorithm combining phase-based image matching and feature-based matching. In: Zhang D, Jain AK (eds) *ICB 2006, LNCS*, vol 3832. Springer, Heidelberg, pp 316–325
8. Uludag U, Jain AK (2006) Securing fingerprint template: fuzzy vault with helper data. In: *CVPRW 2006*, pp 163–163
9. Jain AK, Prabhakar S, Hong L, Pankanti S (2000) Filterbank-based fingerprint matching. *Image Process* 9:846–859
10. FVC2002 database. <http://bia.csr.unibo.it/fvc2002/databases.asp>
11. Dice L (1945) Measures of the amount of ecologic association between species. *Ecology* 26(3):297–302

Improvement of Lung Segmentation Using Volume Data and Linear Equation

Seung-Hoon Chae, Daesung Moon, Deok Gyu Lee and Sung Bum Pan

Abstract Medical image segmentation is an image processing technology prior to performing a variety of medical image processing. Therefore, a variety of methods have been researched for fast and accurate medical image segmentation. Performing segmentation in various organs, you need the accurate judgment of the interest region in medical image. However, the removal of interest region occurs by the lack of information to determine the interest region in a small region. In this paper, we improved segmentation results in a small region in order to improve the segmentation results using volume data with a linear equation. In order to verify the performance of the proposed method, lung region by chest CT images was segment. As a result of experiments, volume data segmentation accuracy rose from 0.978 to 0.981 and from 0.281 to 0.187 with a standard deviation improvement was confirmed.

Keywords Medical image · Image segmentation · CT

S.-H. Chae

The Research Institute of IT, Chosun University, 309,
Pilmun-daero, Dong-gu, Gwangju 501-759, Korea
e-mail: ssuguly@gmail.com

D. Moon · D. G. Lee

Electronics and Telecommunications Research Institute,
161, Gajeong-dong, Yuseong-gu, Daejeon 305-350, Korea
e-mail: daesung@etri.re.kr

D. G. Lee

e-mail: deokgyulee@etri.re.kr

S. B. Pan (✉)

Department of Control, Instrumentation, and Robot Engineering,
Chosun University, 309, Pilmun-daero, Dong-gu, Gwangju 501-759, Korea
e-mail: sbpan@chosun.ac.kr

1 Introduction

By the improvement of the performance of medical imaging equipment, in accordance with the acquisition of high-resolution digital images, computer image analysis is being actively applied in the field of medical diagnosis and treatment. Especially, the field of medical imaging are growing rapidly by new ways to extract or visualize the organ tissue information from diagnostic medical images obtained by a variety of medical imaging equipment such as X-Ray, Computerized Tomography (CT), Magnetic Resonance Imaging (MRI), Ultrasound, Positron Emission Tomography (PET), etc. [1]. Ritter et al. divided the major issues in the field of medical image processing into Image Enhancement, Image Segmentation, Image Registration, Quantification, Visualization, Computer-aided Detection [2]. Image Segmentation of these are important image processing that need to be ahead of a variety of medical image processing such as Image Registration, Quantification, Visualization, Computer-aided Detection. It is difficult for a radiologist to manually segment the large size of data, and because of the similarity of the biological characteristics of human organs, accurate medical image segmentation is not easy. So, in the field of medical image segmentation, many researchers are studying a variety of ways to obtain fast and accurate automatic segmentation methods for medical images.

Many methods such as Threshold method, Watershed, Region Growing, Active Shape Models (ASM), Clustering, Level-set, etc. have been researched for medical image segmentation [3–8]. In performing segmentation, accurate judgment is necessary in order to exactly extract the region of interest from medical images in the presence of other organs. For example, if you want to segment the lung region in chest CT images, the bronchi can be segment that exists within a chest CT images. In case sufficient information is obtained from the region of the lungs and bronchial region, the segmentation can be performed accurately distinguishing the two regions. On the other hand, in case the size of the region, as shown in Fig. 1, is small, the region could not be determined as lung region by the lack of information for selecting the lung region.

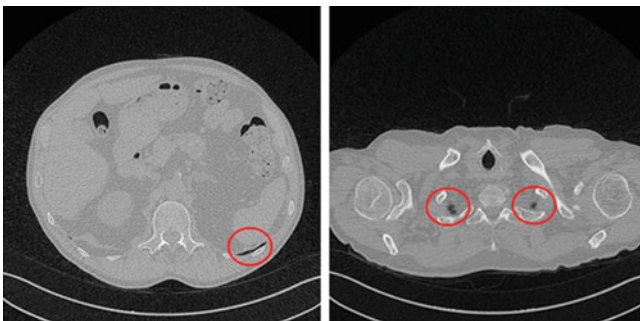


Fig. 1 The small lung region

In this paper, we researched how to improve the performance of exact segmentation of small region with volume data which is a bunch of medical images. Using chest CT images among the medical images, we improved the segmentation result and evaluated the performance through the proposed method.

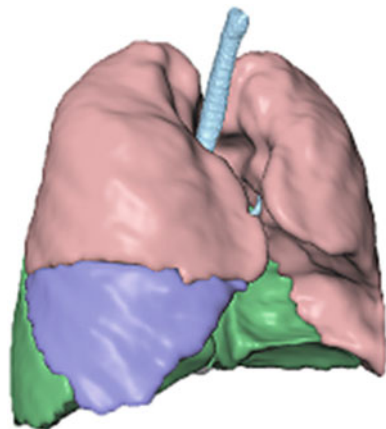
2 Proposed Improvement Method Using Volume Data and Linear Equation

2.1 Chest CT Image

Chest CT images of human body uses the 12 bit images instead of general 8 bit images. Generally 300 ~ 500 chest CT images region obtained from a patient, and it varies depending on the performance of the CT scan equipment. Figure 2 shows the representation of three-Dimensional modeling of lungs. Because the top and bottom parts of the lungs have diminishing structure becoming smaller and smaller, the lung region of the top and bottom is small. It is difficult to determine and segment lung region because small region of the top and bottom of the lungs don't have many features of the lung.

Chest CT images of the dataset consist of axial chest image slices as shown in Fig. 3a. The bundle of axial chest CT images consisting dataset of chest image is able to generate a volume data. Also, it is able to generate the coronal chest image through the volume data as shown in Fig. 3b. Through coronal chest CT image, we can find that shape of lung image doesn't consist of drastic changes but naturally connected slices. It means the previous form of lung slices and the next slices are similar to each other and there are natural connections. Using such chest CT images of volume data, predictions of small lung area can improve segmentation results.

Fig. 2 Representation of three-dimensional modeling of lungs



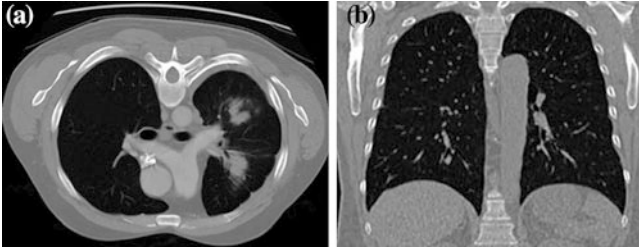


Fig. 3 The configuration of chest CT images. **a** Axial chest CT image, **b** coronal chest CT image

2.2 Linear Equation

The connection form of the coronal plane of the lungs does not have a complex shape. In addition, because the information of the next slice is predicted using standard slices, lung region was predicted without using higher-order linear equations, but by the first linear equation which has less computation. The first equation or linear equation is equation with the highest order term of the order of 1. The first equation may have more than one variable. Linear equations with two variables are actually linear functions. In addition, this is called ‘equation of the straight line’ because it is a straight line in the coordinate plane and associated with the geometric properties of the straight lines. If given two different points (x_1, f_1) and (x_2, f_2) , the equation of a straight line is defined as follows.

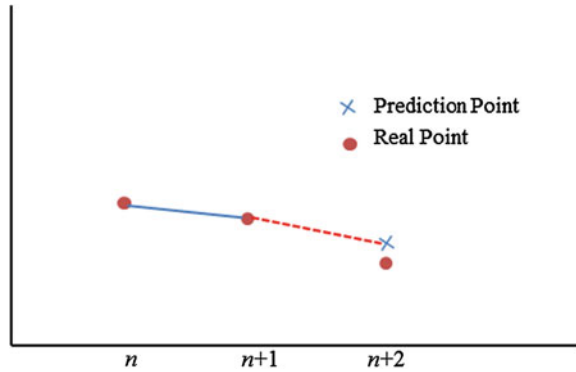
$$\begin{aligned} f_1 &= ax_1 + b \\ f_2 &= ax_2 + b \end{aligned} \quad (1)$$

Using Eq. (1), a random coordinate (x, f) on the line can be obtained as the following equation.

$$\begin{aligned} a &= \frac{f_2 - f_1}{x_2 - x_1} \\ b &= f_2 - \left(\frac{f_2 - f_1}{x_2 - x_1} \right) x_2 \\ f &= \frac{f_2 - f_1}{x_2 - x_1} (x - x_1) + f_1 \end{aligned} \quad (2)$$

That is, given (x_1, f_1) and (x_2, f_2) , (x_n, f_n) is able to be predicted through the linear equations. As shown in Fig. 4, after contour information of lung is extracted in the n -th and $n + 1$ th slices of chest CT images, the coordinates similar to the actual contours coordinates can be obtained if the outline of the results of the $n + 2$ th second installment is predicted through the linear equation.

Fig. 4 Principles of prediction using linear equations



2.3 Improvement of Segmentation

Figure 5 is a flow chart of the whole, improving the segmentation results. First, perform segmentation of lung region of each slice of chest CT image dataset. In order to set the standard slices, measure the dispersion of each slice and select two consecutive slices with low the dispersion. After selecting anchor points on the contours of the reference slices, adjust results for the segmentation

In order to apply linear equations to segment region, the coordinate information of contour should be extracted. Using the coordinates of all contour information is not efficient. So, after setting the anchor point at regular intervals, linear equations between the anchor points should be obtained. As shown in Fig. 6a, set the anchor points on contour point of the segmentation results of n and $n + 1$ th slice at regular intervals. Then, select a fixed pair of points of the shortest distance from n and $n + 1$ th slice. Figure 6b shows the difference between the actual results (dotted line

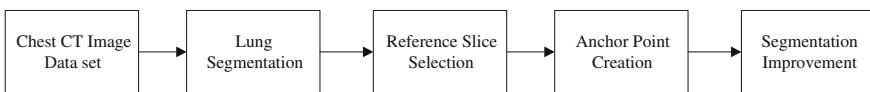


Fig. 5 The flow chart of proposed segmentation method

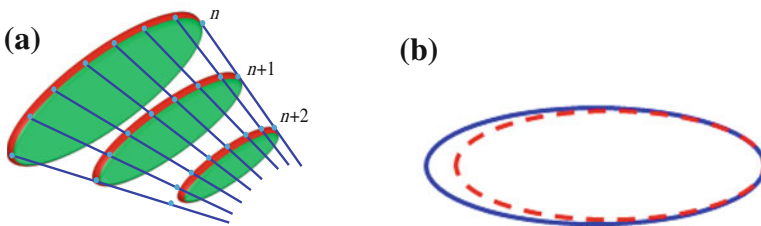


Fig. 6 Prediction process using a linear equation. **a** Building a linear equation, **b** measured results and the predicted results

of red) and predicted (line of blue). After searching a pair of fixed points of the shortest distance between the two results, use the actual results if they exist within a certain distance. On the other hand, if the actual results do not exist within a certain distance, adjust segmentation results using the predicted results as the final result.

Lung region can be generated on lung slices that the region does not exist using a linear equation to predict the contour of the segmentation results. Lung candidate region information was generated by the threshold in order to solve this problem, and the predictions were applied. Using reference image m_n and m_{n+1} , generate P_{n+2} , segmentation prediction. Then, combining P_{n+2} and m_{n+2} , the actual segmentation the result, with correction makes the results M_L . M_L predicted by the linear equation creates the prediction region in a region that does not exist when you choose a wrong pair of anchor points. In order to reduce such errors segmentation information I_{n+2} using threshold was used. I_{n+2} is initial segmentation information which contains all the regions of lung and bronchial. Therefore, given that threshold segmentation region T_{n+2} combined with M_L which predicted only lung region, not the region that cannot be lung region but only the lung region is detected. This can be expressed as the following equation.

$$\begin{aligned} P_{n+2} &= F(m_n, m_{n+1}) \\ M_L &= P_{n+2} + m_{n+2} \\ I_{n+2} &= M_L \cap T_{n+2} \end{aligned} \quad (3)$$

In order to obtain such linear equations at least two reference chest CT imaging slice is needed. Objects having simpler shapes, the lower the probability of occurrence of segmentation fault. Therefore, we used the dispersion which can express the simplicity of the form in a numerical value to automatically select the reference slice. By the perimeter of the image (p), and the region of the image (a), the dispersion can be summarized as Eq. (4) [9]. Here, the lower the dispersion, the object with the simpler form.

$$D = \frac{p^2}{a} \quad (4)$$

The results of performing segmentation improvement generate rough segmentation results because interval occurs between anchor points set for the linear equation. Therefore, an extension of the segmentation results fit to the object is necessary. In this paper, the segmentation results using the Level-set segmentation method was extended to fit the object.

3 Experimental Results

In this paper, to improve the performance of segmentation Vessel Segmentation in the Lung 2012 (VESSEL12) DB using experiments were carried out. The VESSEL12 was held as a workshop of International Symposium on Biomedical Imaging 2012

(ISBI2012) introduced through the Grand Challenges in Medical Image Analysis [10]. VESSEL12 DB is consists of a total of 20 chest CT image dataset and segmentation mask dataset which is lung region segmentation information. Chest CT images in VESSEL12 dataset are composed of $512 \times 512 \times 12$ bit images. The segmentation mask file consists of a $512 \times 512 \times 8$ bit and, lung region were classified as 0, 1. One dataset consists of average 430 slices and a total of 8,593 chest CT image slices. Dice's Overlap methods were used to measure lung region segmentation performance. Result of lung segmentation A and segmentation mask image B in VESSEL12 DB was calculated using the following equation [11].

$$Score = \frac{2(A \cap B)}{(A + B)} \quad (5)$$

Figure 7 shows the appearance that did not segment small lung region and the result of the proposed method improves the segmentation results. Before using the proposed method, small lung region was removed in the segmentation results as shown in the Fig. 7b, in the lung segmentation process and lung region determination process. However, the segmentation improvement method using volume data and linear equations shows segmentation result restoring the small lung region as shown in Fig. 7c.

Level-set was used as the method to medical image segmentation, DRLS was used for the speed function of the Level-set [12]. Table 1 shows the performance of the existing segmentation methods and the proposed method. Score for chest CT imaging of a volume data (S) was measured using Dice's Overlap, and standard deviation of score (Std) for each slice was measured. Compared to the conventional method, score of the proposed method was improved from 0.978 to 0.981 and the standard deviation was improved from 0.281 to 0.187. Because the size of

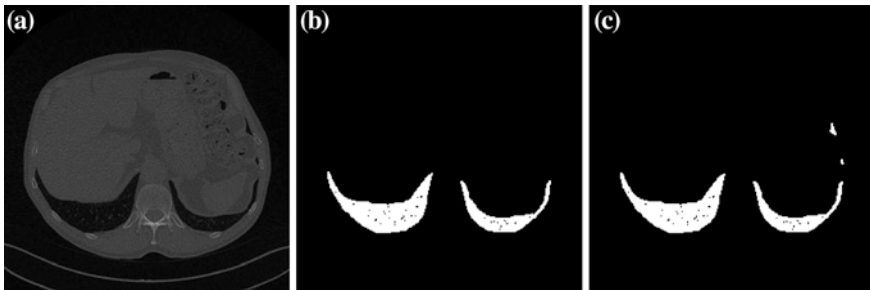


Fig. 7 Result of lung segmentation improvement. **a** Original CT image, **b** segmentation result, **c** proposed method

Table 1 Experiment result

	Existing segmentation result	Proposed method
S	0.978	0.981
Std	0.281	0.187

the improved segmentation area was small, the overall accuracy of the impact was small. But, as shown in the Fig. 7, even in the slice of which lung region is too small to perform lung region segmentation, lung region segmentation was performed.

4 Conclusions

As the performance of medical imaging equipment improving, medical diagnostic using a computer-assisted image analysis is becoming more important. In order to effectively use the medical images, many researchers have been researching a variety of methods for fast and accurate segmentation of medical images. In performing segmentation, accurate judgment is necessary in order to exactly extract the region of interest from medical images in the presence of other organs. But the removal of interest region occurs by the lack of information to determine the interest region in a small region. Because the top and bottom parts of the lungs have diminishing structure becoming smaller and smaller, the lung region of the top and bottom is small. It is difficult to determine and segment lung region because small region of the top and bottom of the lungs don't have many features of the lung.

In this paper, we studied how to improve the performance of exact segmentation of small region with volume data and linear equation. Through coronal lung image, we can find that shape of lung image doesn't consist of abrupt changes but naturally connected slices. Therefore, linear equations using two standard slices can predict the segmentation region of the next slice. Using dispersion information of segmentation image, two standard slices were set, and then anchor points were set on the contour of segmentation region in the slices. After obtaining a linear equation using a pair of anchor points set in the two slices, segmentation region of the next slice of the standard slice was predicted. By the combination of the predicted results and the actual segmentation result, performance of segmentation was improved. As a result of experiment, performance of segmentation was improved from 0.978 to 0.981. In particular, the standard deviation of the slices of the volume data is improved from 0.281 to 0.187, and even improvement of segmentation performance in each slice was confirmed.

In the future, I plan to perform image segmentation using a variety of medical imaging DB and conduct researches to detect lesions which exist within the segmented region.

Acknowledgments This research was supported by Basic Science Research Program through the National Research Foundation of Korea (NRF) funded by the Ministry of Education, Science and Technology (2011-0023147).

References

1. Costaridou L (2005) *Medical Image analysis methods*. Taylor&Francis, Florida
2. Ritter F, Boskamp T, Homeyer A, Laue H, Schwier M, Link F, Peitgen H (2011) Medical image analysis. *IEEE Pulse* 2(6):60–70
3. Zhu Y, Parademetris X, Sinusas AJ, Duncan JS (2010) Segmentation of the left ventricle from cardiac mr images using a subject-specific dynamical model. *IEEE Trans Med Imaging* 29(3):669–687
4. Badakhshannory H, Saeedi P (2011) A model-based validation scheme for organ segmentation in CT scan volumes. *IEEE Trans Biomed Eng* 58(9):2681–2693
5. Zhang J, Yan CH, Chui CK, Ong SH (2010) Fast segmentation of bone in CT images using 3D adaptive thresholding. *Comput Biol Med* 40(2):231–236
6. Christ MCJ, Parvathi RMS (2012) Segmentation of medical image using k-means clustering and marker controlled watershed algorithm. *Eur J Sci Res* 71(2):190–194
7. Kaur P, Soni AK, Gosain A (2013) A robust kernelized intuitionistic fuzzy c-means clustering algorithm in segmentation of noisy medical images. *Patten Recognit Lett* 34(2):163–175
8. Chen S, Kohlberger T, Kirchberg KJ (2011) Advanced level set segmentation of the right atrium in MR. In: *Proceedings SPIE 2011*, vol 7964
9. Lipton AJ (1998) Moving target classification and tracking from real-time video. In *Proceedings applications of computer vision*, pp 8–14
10. VESsel segmentation the lung 2012 (VESSEL12). <http://vessel12.grand-challenge.org>
11. Dice L (1945) Measures of the amount of ecologic association between species. *Ecology* 26(3):297–302
12. Li C, Xu C, Gui C, Fox MD (2010) Distance regularized level set evolution and its application to image segmentation. *IEEE Trans Image Process* 19(12):3224–3254

WMN-GA System for Node Placement in WMNs: Performance Evaluation for Weibull Distribution of Mesh Clients

Admir Barolli, Tetsuya Oda, Fatos Xhafa, Leonard Barolli, Petraq Papajorgji and Makoto Takizawa

Abstract In this paper, we evaluate the performance of WMN-GA system for node placement problem in WMNs. For evaluation, we consider Weibull Distribution of mesh clients and different selection and mutation operators. The population size is considered 64 and the number of generation 200. For evaluation, we consider the giant component and the number of covered users metrics. The simulation results show that the WMN-GA system performs better for Single Mutation and Linear Ranking.

Keywords Genetic algorithms · Mutation operators · Selection operators · Size of giant component

A. Barolli (✉) · P. Papajorgji
Canadian Institute of Technology, Zayed Center, Rr. Sulejman Delvina, Tirana, Albania
e-mail: admir.barolli@gmail.com

P. Papajorgji
e-mail: petraq@gmail.com

T. Oda
Graduate School of Engineering, Fukuoka Institute of Technology (FIT), 3-30-1
Wajiro-Higashi, Higashi-Ku, Fukuoka 811-0295, Japan
e-mail: oda.tetsuya.fit@gmail.com

F. Xhafa
Department of Languages and Informatics Systems, Technical University of Catalonia,
C/JordiGirona 1-3 08034 Barcelona, Spain
e-mail: fatos@lsi.upc.edu

L. Barolli
Department of Information and Communication Engineering, Fukuoka Institute of
Technology (FIT), 3-30-1 Wajiro-Higashi, Higashi-Ku, Fukuoka 811-0295, Japan
e-mail: barolli@fit.ac.jp

M. Takizawa
Department of Advanced Sciences, Hosei University, 3-7-2, Kajino-machi, Koganei-shi,
Tokyo 184-8584, Japan
e-mail: makoto.takizawa@computer.org

1 Introduction

Wireless Mesh Networks (WMNs) are based on mesh topology, in which every node (representing a server) is connected to one or more nodes, enabling thus the information transmission in more than one path. The path redundancy is a robust feature of this kind of topology. Compared to other topologies, mesh topology needs not a central node, allowing networks based on such topology to be self-healing. These characteristics of networks with mesh topology make them very reliable and robust networks to potential server node failures. In WMNs mesh routers provide network connectivity services to mesh client nodes. The good performance and operability of WMNs largely depends on placement of mesh routers nodes in the geographical deployment area to achieve network connectivity, stability and user coverage. The objective is to find an optimal and robust topology of the mesh router nodes to support connectivity services to clients. WMNs [1–3] are important networking infrastructure for providing cost-efficient broadband wireless connectivity. They are showing their applicability in deployment of medical, transport and surveillance applications in urban areas, metropolitan, neighboring communities and municipal area networks.

Node placement problems have been long investigated in the optimization field due to numerous applications in location science (facility location, logistics, services, etc.) and classification (clustering). In such problems, we are given a number of potential facilities to serve to costumers connected to facilities aiming to find locations such that the cost of serving to all customers is minimized. In traditional versions of the problem, facilities could be hospitals, polling centers, fire stations serving to a number of clients and aiming to minimize some distance function in a metric space between clients and such facilities.

For most formulations, node placement problems are shown to be computationally hard to solve to optimality [4–7], and therefore heuristic and meta-heuristic approaches are useful approaches to solve the problem for practical purposes. Several heuristic approaches are found in the literature for node placement problems in WMNs [8–12].

Genetic Algorithms (GAs) have been recently investigated as effective resolution methods. In this work, we use our proposed and implemented WMN-GA system that is based on GA to deal with the node placement problem in WMNs. For evaluation, we consider Weibull Distribution of mesh clients and different selection and mutation operators. The population size is considered 64 and the number of generation 200. For evaluation, we consider the giant component and the number of covered users metrics.

The rest of the paper is organized as follows. In [Sect. 2](#) is presented Genetic Algorithm template and its application to mesh router nodes placement. The proposed and implemented WMN-GA system is presented in [Sect. 3](#). The simulation results are given in [Sect. 4](#). We give some concluding remarks and future work in [Sect. 5](#).

2 Genetic Algorithms

Genetic Algorithms (GAs) [13] have shown their usefulness for the resolution of many computationally combinatorial optimization problems. For the purpose of this work we have used the template given in Algorithm 1.

We present next the particularization of GAs for the mesh router nodes placement in WMNs (see [14] for more details).

2.1 Encoding

The encoding of individuals (also known as chromosome encoding) is fundamental to the implementation of GAs in order to efficiently transmit the genetic information from parents to offsprings.

In the case of the mesh router nodes placement problem, a solution (individual of the population) contains the information on the current location of routers in the grid area as well as information on links to other mesh router nodes and mesh client nodes. This information is kept in data structures, namely, pos routers for positions of mesh router nodes, routers links for link information among routers and client router link for link information among routers and clients (matrices of the same size as the grid area are used). Based on these data structures, the size of the giant component and the number of users covered are computed for the solution.

It should be also noted that routers are assumed to have different radio coverage, therefore to any router could be linked to a number of clients and other routers. Obviously, whenever a router is moved to another cell of the grid area, the information on links to both other routers and clients must be computed again and links are re-established.

Algorithm 1 Genetic algorithm template

Generate the initial population P^0 of size μ ; $t = 0$.

Evaluate P^0 ;

while not termination-condition do

Select the parental pool T^t of size of size λ ;

$T^t := \text{Select}(P^t)$;

Perform crossover procedure on pairs of individuals in T^t with probability pc ;

$P_c^t := \text{Cross}(T^t)$;

Perform mutation procedure on individuals in P_c^t with probability pm ; $P_m^t := \text{Mutate}(P_c^t)$;

Evaluate P_m^t ;

Create a new population P^{t+1} of size μ from individuals in P^t and/or P_m^t ;

$P^{t+1} := \text{Replace}(P^t, P_m^t)$

$t := t + 1$;

end while

return Best found individual as solution;

2.2 Selection Operators

In the evolutionary computing literature we can find a variety of selection operators, which are in charge of selecting individuals for the pool mate. The operators considered in this work are those based on Implicit Fitness Re-mapping technique. It should be noted that selection operators are generic ones and do not depend on the encoding of individuals.

- **Random Selection:** This operator chooses the individuals uniformly at random. The problem is that a simple strategy does not consider even the fitness value of individuals and this may lead to a slow convergence of the algorithm.
- **Best Selection:** This operator selects the individuals in the population having higher fitness value. The main drawback of this operator is that by always choosing the best fitted individuals of the population, the GA converges prematurely.
- **Linear Ranking Selection:** This operator follows the strategy of selecting the individuals in the population with a probability directly proportional to its fitness value. This operator clearly benefits the selection of best endowed individuals, which have larger chances of being selected.
- **Exponential Ranking Selection:** This operator is similar to Linear Ranking but the probabilities of ranked individuals are weighted according to an exponential distribution.
- **Tournament Selection:** This operator selects the individuals based on the result of a tournament among individuals. Usually winning solutions are the ones of better fitness value but individuals of worse fitness value could be chosen as well, contributing thus to avoiding premature convergence. Particular cases of this operator are the Binary Tournament and N-Tournament Selection, for different values of N.

2.3 Mutation Operators

Mutation operator is one of the GA ingredients. Unlike crossover operators, which achieve to transmit genetic information from parents to offsprings, mutation operators usually make some small local perturbation of the individuals, having thus less impact on newly generated individuals.

Crossover is “a must” operator in GA and is usually applied with high probability, while mutation operators when implemented are applied with small probability. The rationale is that a large mutation rate would make the GA search to resemble a random search. Due to this, mutation operator is usually considered as a secondary operator.

In the case of mesh routers node placement, the matrix representation is chosen for the individuals of the population, in order to keep the information on mesh router nodes positions, mesh client positions, links among routers and links among

routers and clients. The definition of the mutation operators is therefore specific to matrix-based encoding of the individuals of the population. Several specific mutation operators were considered in this study, which are move-based and swap-based operators.

Single Mutate

This is a move-based operator. It selects a mesh router node in the grid area and moves it to another cell of the grid area.

Rectangle Mutate

This is a swap-based operator. In this version, the operator selects two “small” rectangles at random in the grid area, and swaps the mesh routers nodes in them.

Small Mutate

This is a move-based operator. In this case, the operator chooses randomly a router and moves it a small (a priori fixed) number of cells in one of the four directions: up, down, left or right in the grid. This operator could be used a number of times to achieve the effect of Single Mutate operator.

Small Rectangle Mutate

This is a move-based operator. The operator selects first at random a Small Mutate. This is a move-based operator. In this case, the operator chooses randomly a router and moves it a small (a priori fixed) number of cells in one of the four directions: up, down, left or right in the grid. This operator could be used a number of times to achieve the effect of Single Mutate operator.

Small Rectangle Mutate

This is a move-based operator. The operator selects first at random a rectangle and then all routers inside the rectangle are moved with a small (a priori fixed) numbers of cells in one of the four directions: up, down, left or right in the grid.

3 Proposed and Implemented WMN-GA System

In this section, we present WMN-GA system. Our system can generate instances of the problem using different distributions of client and mesh routers.

The GUI interface of WMN-GA is shown in Fig. 1. The left side of the interface shows the GA parameters configuration and on the right side are shown the network configuration parameters.

For the network configuration, we use: distribution, number of clients, number of mesh routers, grid size, radius of transmission distance and the size of subgrid.

For the GA parameter configuration, we use: number of independent runs, GA evolution steps, population size, population intermediate size, crossover probability, mutation probability, initial methods, select method.



Fig. 1 GUI tool for WMN-GA system

4 Simulation Results

We carried out many simulations to evaluate the performance of WMNs using WMN-GA system. The grid size is considered 32×32 . The number of mesh routers is considered 16 and the number of mesh clients 48. For evaluation, we considered Normal Distribution of mesh clients and six different selection operators (Best, Binary Tournament, N Tournament, Exponential Ranking, Linear Ranking and Random) and four mutation operators (Rectangle Mutate, Single Mutate, Small Mutate, Small Rectangle Mutate). The population size is considered 64 and the number of generation 200. As evaluation metrics, we consider the giant component and the number of covered users. The WMN-GA system, first maximizes the connectivity among mesh routers and, then optimizes the mesh clients coverage.

In Figs. 2, 3, 4 and 5 are shown the simulation results for Rectangle Mutate, Single Mutate, Small Mutate and Small Rectangle Mutate operators, respectively. In Fig. 2a, are shown the simulation results for Average size of giant component versus number of generations for six different selection operators (Best, Binary Tournament, N Tournament, Exponential Ranking, Linear Ranking and Random). For all selection methods, the size of giant component is not maximized. In Fig. 2b, are shown the results for average number of covered mesh clients versus number of generations for different selection operators. The performance for all selection operators is low and less than 40 % of the mesh clients are covered. For Binary Tournament, all mesh routers are connected with each other but the number of mesh clients that they cover is very small.

In Fig. 3a, for N Tournament only 80 % of mesh routers are connected with each other but for other selection operators after 50 generations all mesh routers

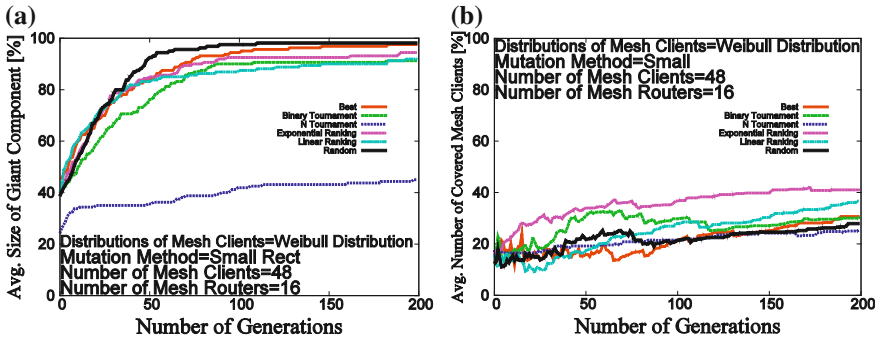


Fig. 2 Simulation results for rectangle mutate. **a** Average size of giant component versus number of generations, **b** Average number of covered mesh clients versus number of generations

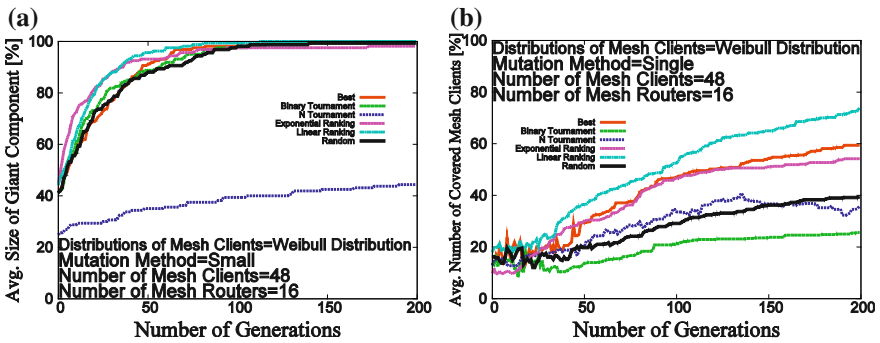


Fig. 3 Simulation results for single mutate. **a** Average size of giant component versus number of generations, **b** Average number of covered mesh clients versus number of generations

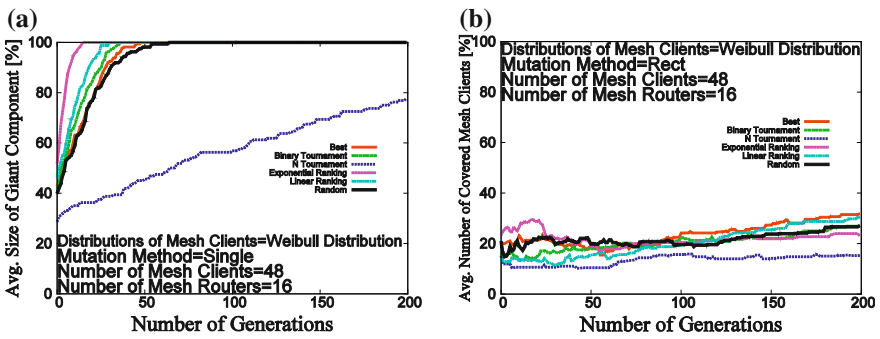


Fig. 4 Simulation results for small mutate. **a** Average size of giant component versus number of generations, **b** Average number of covered mesh clients versus number of generations

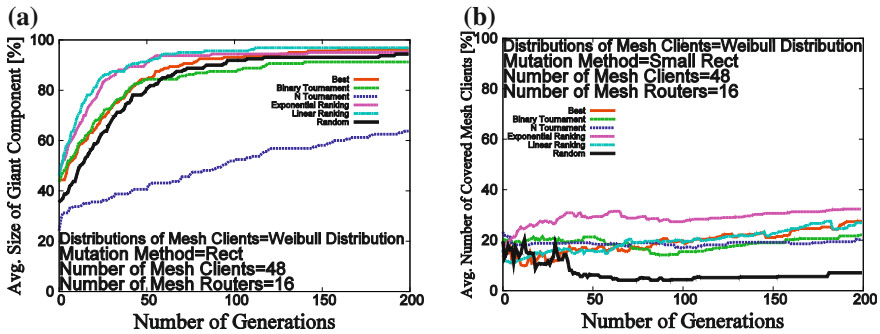


Fig. 5 Simulation results for small rectangle mutate. **a** Average size of giant component versus number of generations, **b** Average number of covered mesh clients versus number of generations

are connected (see Fig. 3a). In this case, the best performance is achieved for Linear Ranking operator where 75 % of mesh clients are covered.

In Fig. 4b, Exponential Ranking performs better than other selection operators but it has still a low performance (only 40 % of mesh clients are covered).

Rectangle Mutate and Small Rectangle mutate have almost the same performance (see Figs. 2 and 5).

5 Conclusions

In this work, we used WMN-GA system to deal with the node placement problem in WMNs. For evaluation, we considered Weibull Distribution of mesh clients and different selection and mutation operators.

From the simulations, we found out the following results.

- For all mutation methods and selection operators, the routers have a good connectivity except the N Tournament.
- The best results for Weibull distribution are achieved for Single Mutate. In this scenario, for Linear Ranking operator, number of covered mesh clients is higher than all other operators.

In the future work, we would like to make extensive simulations for different scenarios and compare the performance of WMN-GA system with other optimization algorithms.

References

1. Akyildiz IF, Wang X, Wang W (2005) Wireless mesh networks: a survey. *Comput Netw* 47(4):445–487
2. Nandiraju N, Nandiraju D, Santhanama L, He B, Wang J, Agrawal D (2007) Wireless mesh networks: current challenges and future direction of web-in-the-sky. *IEEE Wirel Commun* 14(4):79–89
3. Chen Ch, Chekuri ch (2007) Urban wireless mesh network planning: the case of directional antennas, Tech Report No.UIUCDCS-R-2007-2874, Department of Computer Science, University of Illinois at Urbana-Champaign
4. Garey MR, Johnson DS (1979) *Computers and intractability -a guide to the theory of NP-completeness*. Freeman, San Francisco
5. Lim A, Rodrigues B, Wang F, Xua Zh (2005) k-Center problems with minimum coverage. *Theor Comput Sci* 332(1–3):1–17
6. Amaldi E, Capone A, Cesana M, Filippini I, Malucelli F (2008) Optimization models and methods for planning wireless mesh networks. *Comput Netw* 52:2159–2171
7. Wang J, Xie B, Cai K, Agrawal DP (2007) Efficient mesh router placement in wireless mesh networks, MASS-2007. Pisa, Italy, pp 9–11
8. Muthaiah SN, Rosenberg C (2008) Single gateway placement in wireless mesh networks. In *Proceedings of 8th international IEEE symposium on computer networks*, Turkey, pp 4754–4759
9. Zhou P, Manoj BS, Rao R (2007) A gateway placement algorithm in wireless mesh networks. In: *Proceedings of the third annual international wireless internet conference (WICON-2007)*, pp 1–9
10. Tang M (2009) Gateways placement in backbone wireless mesh networks. *Int J Commun Netw Syst Sci* 2(1):45–50
11. Antony Franklin A, Siva Ram Murthy C (2007) Node placement algorithm for deployment of two-tier wireless mesh networks. In: *Proceedings of IEEE GLOBECOM- 2007*, Washington, USA, pp 4823–4827
12. Vanhatupa T, Hännikainen M, Hämmäläinen TD (2007) Genetic algorithm to optimize node placement and configuration for WLAN planning. In: *Proceedings of 4th international symposium on wireless communication systems*, pp 612–616
13. Holland J (1975) *Adaptation in natural and artificial systems*. University of Michigan Press, Ann Arbor
14. Khafa F, Sanchez C, Barolli L (2010) Genetic algorithms for efficient placement of router nodes in wireless mesh networks. *Proc AINA 2010*:465–472

Indoor Navigation System for Wheelchair Using Smartphones

Nattapob Wattanavarangkul and Toshihiko Wakahara

Abstract Recently, in order to assist the disabled people moving around, many support systems and tools have been developed. However, a moving person supported by wheelchairs in the building has a significant problem of lacking GPS signal. This paper presents a new indoor navigation system for wheelchairs, using smartphones as a sensor and navigation medium. In this navigation system, the wheel sensor in the wheelchair and the digital compass of the smartphone are used to calculate the current location accurately. Moreover, the navigation system provides a map function that displays possible and optimum routes of passage in a wheelchair from the current location to a destination in the building. The experimental results and evaluation are also presented.

Keywords Smartphone · Indoor · Navigation · Wheelchair · Disabled

1 Introduction

In this study, we build a navigation system for disabled people who are using wheelchairs, in order that the wheelchair can move in department buildings, apartments and offices without problems. This navigation system provides the important information about the building for example stairs, ramps and slopes, and linking the routes of indoor and outdoor locations. It can be used not only for

N. Wattanavarangkul (✉) · T. Wakahara
Graduate School of Information and Communication Engineering, Fukuoka Institute of
Technology, 3-30-1 Wajiro-Higashi, Higashi-Ku Fukuoka 811-0295, Japan
e-mail: mgm12007@bene.fit.ac.jp

T. Wakahara
e-mail: wakahara@fit.ac.jp

people with disabilities but also for normal people, who can reach the destination by the optimal route.

We avoid using GPS signal, because in indoor environment, the GPS signal is weak and in may cause location errors and confusion. Instead, we use the information provided by the wheelchair sensor and smartphone's compass.

In order to use this information correctly, a user needs to download a detailed map of the location of interest. This map information will be available to download online (through web service) or onsite (through reading QR codes).

In our system, we use Java Open Street Map (JOSM) to create map databases for indoor and outdoor locations. Furthermore, A* algorithm and pgRouting are used to calculate the best route to destination. Then, we simulate two examples of movement in our department building. One representing indoor-to-indoor movement and the other one shows the best path for outdoor-to-indoor movement.

This paper is summarized as following. In [Sect. 2](#), we describe the purpose and motivation of our research. In [Sect. 3](#), we show the methods used in our system. In [Sect. 4](#), we introduce our navigation system. In [Sect. 5](#), we show results from simulations. And finally, we summarize the paper in [Sect. 6](#).

2 Purpose and Motivation of Research

2.1 Usage of Wheelchair

People with disabilities have many difficulties in moving alone if there is no assistant to show the way or help with directions. Especially when they do not know the location information, it is very difficult. The disabled people as well as healthy people need to be notified about the current position, in order to reach the destination safely. For this reason, a navigation system is introduced by using a sensor on the wheel of the wheelchair to calculate the moving direction and using compass in smartphone for displaying the direction of movement.

2.2 Indoor Navigation Techniques

As the power of GPS signal becomes small inside the buildings, this signal is hard to be utilized. Although various indoor navigation systems have been developed using different techniques, they often cannot navigate successfully because of the positioning errors. There are methods to measure the received power of the Bluetooth or Wi-Fi, and a method using an RFID sensor. Currently, the best method for indoor navigation is using the GPS repeater, but it has a very high cost.

2.3 Outdoor and Indoor Navigation

The disabled persons must select the location of the destination from the current position. They must also select and specify the location of the destination from indoor to outdoor or outdoor to indoor. Therefore it is necessary to find the optimal route between the outdoor and indoor.

3 Positioning System's Methods

3.1 Compass in Smartphone

The compass function is added recently in smartphones, and it can calculate the direction of the wheelchair movement. The compass of smartphone shows values from 0 to 359 degrees by measuring the Earth's magnetic field. It shows the direction of north at 0 degrees, east at 90 degrees, south at 180 degrees, and west at 270 degrees.

3.2 Wheel Sensor

A wheel sensor is used for measuring the speed of the wheel. The sensor is attached to the wheels of the wheelchair, and communicates with smartphone. In this paper, the smartphone collects data, such as speed, from the wheel sensor by using Bluetooth.

3.3 Map Database

For creating indoor map database, Java OpenStreetMap [1] editor called JOSM [2] is used. JOSM will be used to create the map database (a combination of map floor and floor information) and details about room, corridor, door, stairs, and elevators. Figure 1 shows the map of our department floor, which is saved in a file in the map database. This map database will be available to download (using QR codes) near the entrance of a building and in other possible locations, as well as available online.

For people with disabilities, it is important to know the route conditions, for example, the level of slope, stairs etc. By using map database, they can see all these information. In Fig. 2 we show the outdoor map of our school, near our department building.

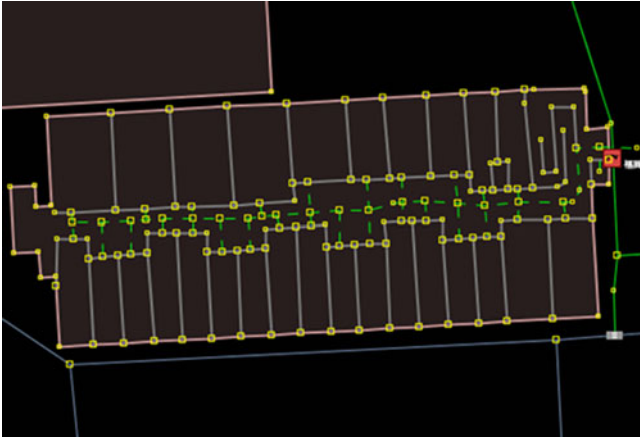


Fig. 1 Indoor map database

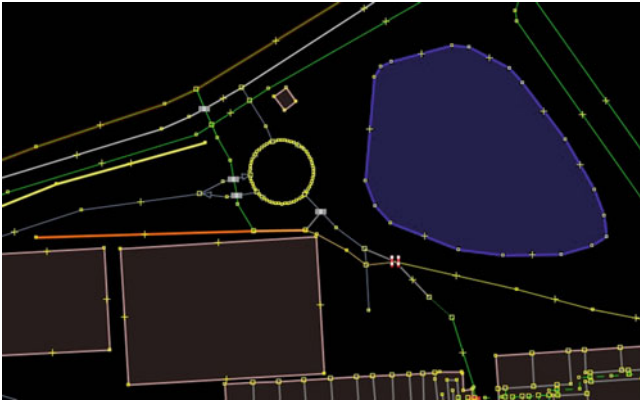


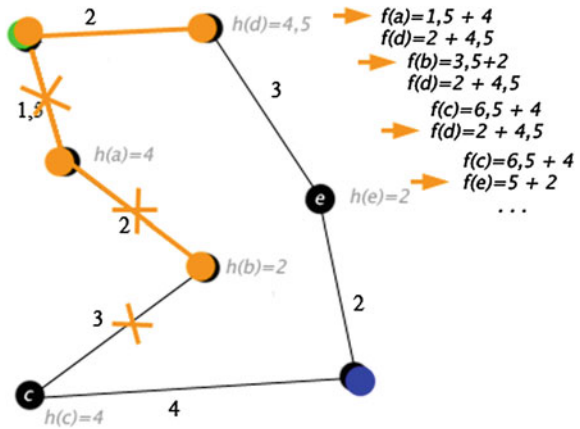
Fig. 2 Outdoor map database

4 Indoor Navigation System

4.1 A* Algorithm

In order to search for the shortest route to the destination, we use A* search algorithm [3]. In Fig. 3, is shown the calculation process of the algorithm. It calculates the shortest path from the start node to the goal node.

Fig. 3 A*Algorithm



4.2 pgRouting

Using an Open Source Software, called path selection pgRouting [4], we select and display the optimal trace passage to navigate from the current location to destination. There are two types of points in our simulation system: can pass points and cannot pass points. Taking in consideration these points, the pgRouting selects the optimal route from the map database.

4.3 An Example of Navigation

Figure 4 shows an example of a navigation route obtained by the method described above. The current position is shown with a green flag and the destination with a red flag. The optimal route is displayed by a red line from the current position to the destination.

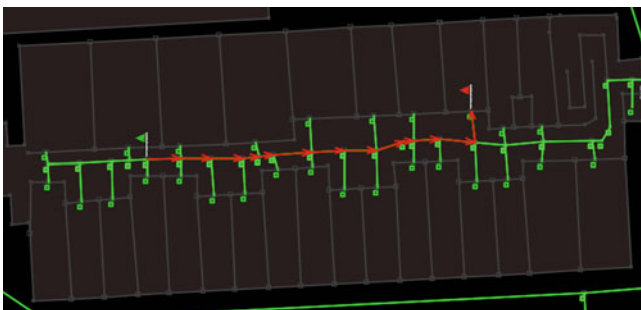


Fig. 4 Example of navigation

4.4 Procedure of Indoor Navigation System

When the disabled person is inside the building, he/she uses his/her smartphone to read QR [5] code on the walls in the entrance of the building and download the information from the map database. When the disabled is outside the building, first he/she can download the map data from the website. After downloading the map data on the smartphone, the disabled choose the destination. Our navigation system displays the route conditions and chooses the best route. After choosing the best route, it starts the navigation to the destination point. If there is a problem with this route, the system alerts the user and suggests a new route. The flow chart of this procedure is shown in Chart 1.

5 Simulation Results

In order to show the effectiveness of our system, we conduct simulations in our university for indoor and outdoor navigations.

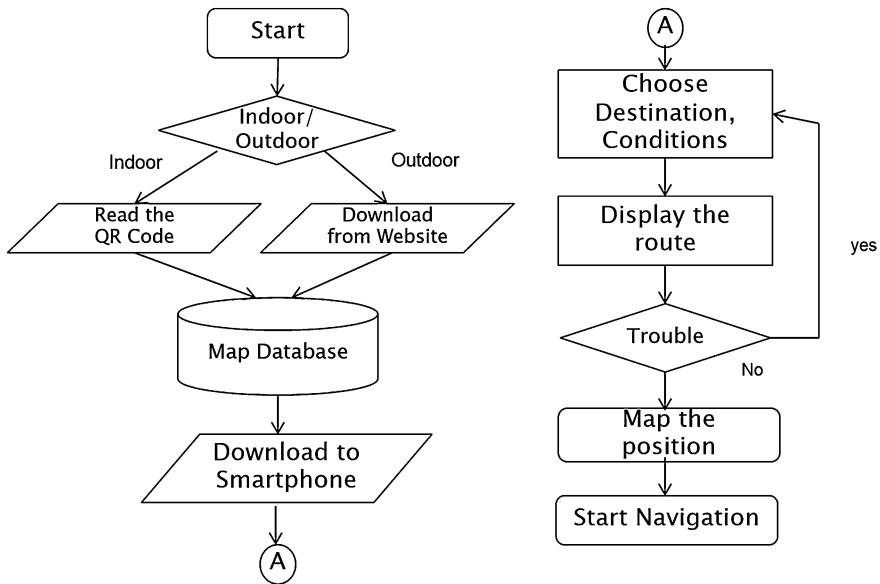


Chart 1 Procedure of indoor/outdoor navigation

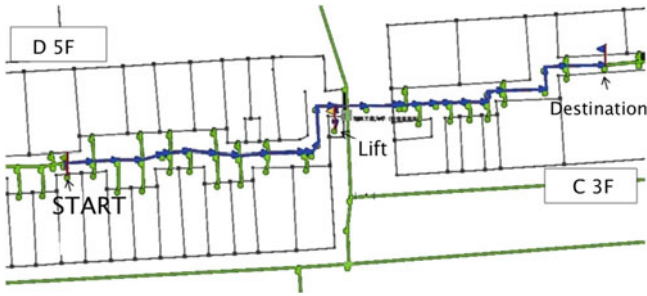


Fig. 5 Indoor-to-indoor navigation simulation

5.1 Indoor-to-Indoor Navigation Simulation

For indoor-to-indoor navigation, we assume that a user want to move from our laboratory, which is located in D building 5th floor, to the classroom in C building 3rd floor in the campus of Fukuoka Institute of Technology. Then we simulate the route search by choosing to use the elevator without using stairs. Figure 5 shows the selected route after simulations.

5.2 Outdoor-to-Indoor Navigation Simulation

For outdoor-to-indoor navigation, we suppose that a user wants to move from the entrance square of our university to the first floor of Building C. We use our simulation system to find the best route to destination. Assuming that the user is an unassisted person using a wheelchair, the high slope and stairs are avoided for reaching the destination (Fig. 6).

5.3 Distance Simulations

We also make outdoor measurements, using only one wheel sensor, without using GPS signal. We record the distance of three different routes: long route (A-route), short route (B-route), and curve route (C-route). We compare map results with measured results in the campus. The length of A-route from the map is 117.6 m and the distance measured is 116.6 m, so the error is 0.935 %. The length of the B-route from the map is 28.9 m and when measured is 28.6 m, so the error is 1.038 %. And the length of the C-route from the map is 24.3 m and measured in the campus is 24.1 m, so the error is 0.823 % (Fig. 7).



Fig. 6 Outdoor-to-indoor navigation simulation

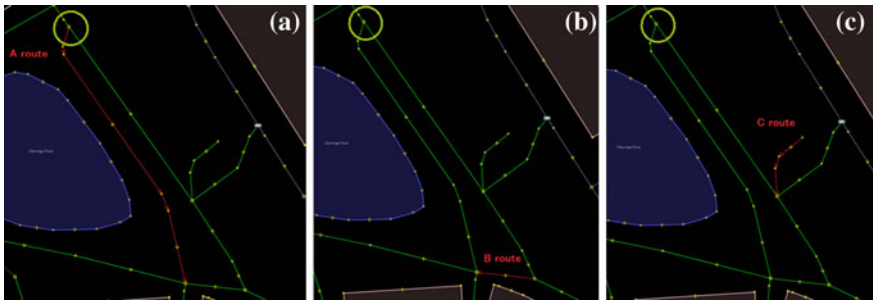


Fig. 7 Outdoor routes, a. Long route b. Short route c. Curve route

6 Conclusions

In this paper, we have developed an indoor and outdoor navigation system for disabled. In our system, we use a wheel sensor and digital compass of smartphone to find the best route for a disabled to reach the destination. The simulation results show a correct route for disabled people from the current position to the destination. The error of each route in the outdoor simulation was less than 1 %, in general.

In the future, we would like to make extensive experiments using both the wheel sensor and digital compass. Then we will consider new algorithms to optimize the search procedure.

References

1. OSM OpenStreetMap, <http://www.openstreetmap.org>
2. JOSM is an extensible editor for OpenStreetMap, <http://josm.openstreetmap.de>
3. A-Star Algorithm, http://en.wikipedia.org/wiki/A*_search_algorithm
4. pgRouting, <http://www.pgrouting.org/index.html>
5. QR Code, http://en.wikipedia.org/wiki/QR_code
6. Smith P, Viol N, Wehrle K (2011) FootPath: accurate map-based indoor navigation using smartphones. In: Proceedings of indoor positioning and indoor navigation (IPIN-2011), pp 1–8, Aachen, Germany
7. Nakajima M (2011) Path planning using indoor map data generated by the plan view of each floor. In: Proceedings of the 25th international cartographic conference, CO-103, Paris, France, 3–8 July 2011

Performance Comparison of Wireless Sensor Networks for Different Sink Speeds

Tao Yang, Elis Kulla, Leonard Barolli, Gjergji Mino
and Makoto Takizawa

Abstract Wireless Sensor Networks (WSNs) have become a hot research topic in academia as well as in industry in recent years due to its wide range of applications ranging from medical research to military. In this paper, we study the effect of mobile sink in WSN performance. The WSNs should allow a systematic deployment of sensor nodes including mobility among the sensor nodes. The disseminated data from the sensor nodes are gathered at the sink node. Data dissemination is the major source for energy consumption in WSNs. We consider as evaluation parameter goodput and depletion to evaluate the performance of WSNs considering different speeds of mobile sink. The simulation results show that, when the T_r is lower than 10 pps, the network is not congested and the goodput is higher when the sink node moves faster (20 m/s). When T_r is lower than 10, the depletion is higher when sink moves with lower speed (5 m/s). But, when T_r is larger than 10, the depletion is higher for higher values of the sink speed (20 m/s).

T. Yang · L. Barolli

Department of Information and Communication Engineering, Fukuoka Institute of Technology (FIT), 3-30-1 Wajiro-Higashi, Higashi-Ku, Fukuoka 811-0295, Japan
e-mail: taoyang.tou@gmail.com

L. Barolli

e-mail: barolli@fit.ac.jp

E. Kulla (✉)

Graduate School of Engineering, Fukuoka Institute of Technology (FIT),
3-30-1 Wajiro-Higashi, Higashi-Ku, Fukuoka 811-0295, Japan
e-mail: eliskulla@yahoo.com

G. Mino

Computer Technology Solution, 8B Industrial Way, Salem, NH 03079, USA
e-mail: gjmino@gmail.com

M. Takizawa

Department of Advanced Sciences, Hosei University, 3-7-2, Kajino-Machi,
Koganei-Shi, Tokyo 184-8584, Japan
e-mail: makoto.takizawa@computer.org

1 Introduction

Wireless Sensor Networks (WSNs) can be defined as a collection of wireless self-configuring programmable multihop tiny devices, which can bind to each other in an arbitrary manner, without the aid of any centralized administration, thereby dynamically sending the data to the intended recipient about the monitored phenomenon. By appropriately tuning the parameters of IEEE 802.15.4, WSNs can be applied to a variety of applications. Research on WSNs has been stimulated by the need of setting up the communication networks to gather information in situations where fixed infrastructure cannot be employed on the fly, as it occurs in the management of emergencies and disaster recovery. In a WSN, thousands of sensor nodes are deployed in a random fashion. The sensor nodes sense the phenomenon periodically and the sensed data is sent to the sink node. The information collected at the sink node is queried to extract the relevant information. By shortening the distance taken by the packets to reach the sink node, energy can be conserved. Mobility of sensor and sink may result in retrieving the data quickly [1–6].

In this paper, we present the analysis of the effect of IEEE 802.15.4 MAC protocol on the performance of AODV routing protocol in WSNs considering mobile sensor nodes, which move with different speeds. We consider goodput and depletion metrics to evaluate the performance of WSNs. The remainder of the paper is organized as follows. In Sect. 2, we present the related work. In Sect. 3, we explain the proposed network simulation model. In Sect. 4, we introduce AODV routing protocol. In Sect. 5, we discuss the metrics used for performance evaluation. In Sect. 6, we show the simulation results. Conclusions of the paper are given in Sect. 7.

2 Related Work

In our previous work [7], we implemented a simulation system for WSNs considering different protocols and different propagation radio models. The authors of [8] suggest a reinforcement learning algorithm for sensor nodes that they call Hybrid Learning-Enforced Time Domain Routing (HLETDR). Each node continuously learns the movement pattern of the mobile sink and statistically characterize it as a probability distribution function. Thus, sensor nodes always know in which direction they have to route messages to the sink at a given time instant. The advantage of the solution is that nodes do not need time synchronization, since they make forwarding decisions in their local time-domain.

In [9], the authors consider scenarios where sensors are deployed within a circle. The authors argue that in such cases the mobile sink should follow the periphery of the network in order to optimize the energy consumption of the nodes.

In our previous work [10], we obtained the simulation results for consumed energy in case of mobile sink. We found that the consumed energy was better than the stationary sink (about half of stationary in lattice topology). The goodput of random topology was better than lattice topology and the consumed energy of lattice topology was better than random topology.

In [11], we presented our simulation results of WSN for 4 cases of event movement. We used the goodput and consumed energy metrics to measure the performance. For the multi mobile sensors with TwoRayGround, the goodput was stable. Also, the goodput of Shadowing of mobile sensors was better than TwoRayGround. While, the consumed energy of mobile sensors using Shadowing was better than TwoRayGround.

3 Proposed Network Simulation Model

In our WSN, every node detects the physical phenomenon and sends back to the sink node the data packets. We suppose that the sink node is more powerful than sensor nodes. We analyze the performance of the WSN in a fixed time interval, which is the available time for the detection of the phenomenon and its value is application dependent. Proposed network simulation model is shown in Fig. 1. For simulation system implementation, we consider modeling and network stack. In this paper, we consider a scenario that 4 sensors are embedded in vehicles and they are moving randomly with 5 and 10 m/s speed in the WSN field.

Fig. 1 Network simulation model

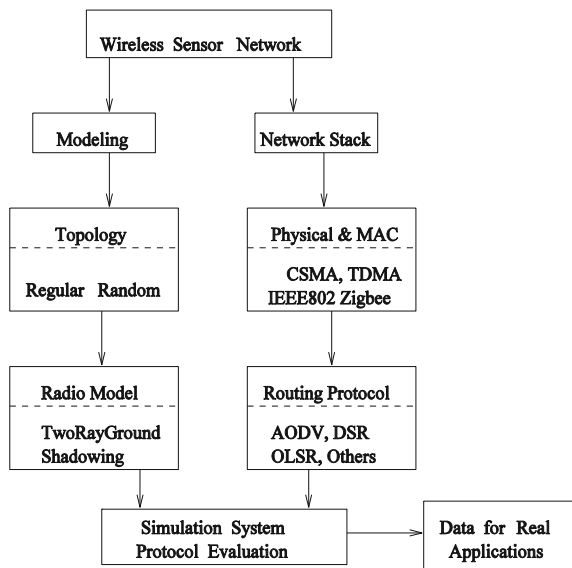
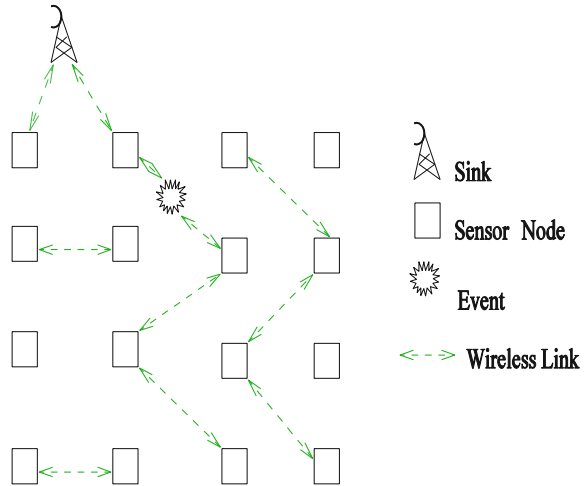


Fig. 2 An example of lattice network



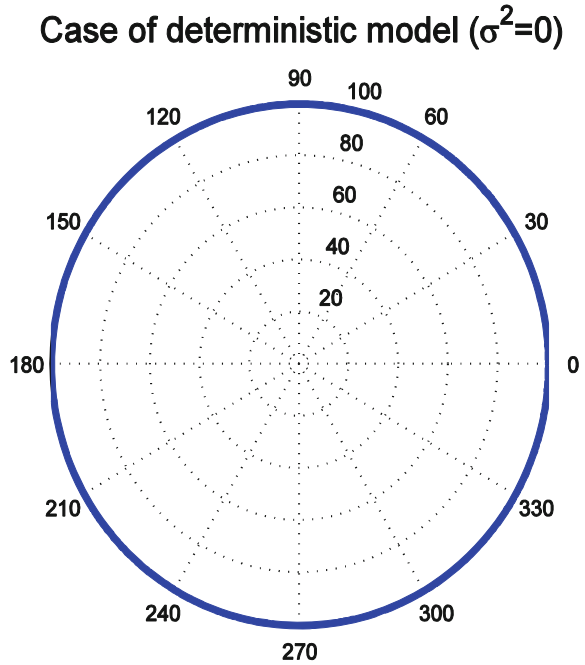
3.1 Topology

For the physical layout of the WSN, two types of deployment has been studied so far: the random and the lattice deployment. In the former, nodes are supposed to be uniformly distributed, while in the latter one nodes are vertexes of particular geometric shape, e.g. a square grid, as depicted in Fig. 2. In order to guarantee the connectivity of the network we should set the transmission range of every node to the step size, d , which is the minimum distance between two rows (or columns) of the grid. In fact, by this way the number of links that every node can establish (the node degree D) is 4. Nodes at the borders have $D = 2$.

3.2 Radio Models

In order to simulate the detection of a natural event, we used the libraries from Naval Research Laboratory (NRL) [12]. In this framework, a phenomenon is modeled as a wireless mobile node. The phenomenon node broadcasts packets with a tunable synchrony or pulse rate, which represents the period of occurrence of a generic event. As a consequence, this model is for discrete events. By setting a suitable value for the pulse rate, it is possible in turn to simulate the continuous signal detection such as temperature or pressure. These libraries provide the sensor node with an alarm variable. The alarm variable is a timer variable. It turns off the sensor if no event is sensed within an alarm interval. In addition to the sensing capabilities, every sensor can establish a multi-hop communication towards the Monitoring Node (MN) by means of a particular routing protocol. This case is the opposite of the polling scheme. Although not optimal for multi-hops WSNs, we assume that the MAC protocol is the IEEE 802.11 standard. This serves to us as a

Fig. 3 Transmission rang of TwoRay-Ground model



baseline of comparison to other contention resolution protocols. The receiver of every sensor node is supposed to receive correctly data bits if the received power exceeds the receiver threshold, τ . This threshold depends on the hardware. Other MAC factors affect the reception process, for example the Carrier Sensing Threshold (CST) and Capture Threshold (CP) of IEEE.802.11 used in ns-2. As reference, we select parameters values according to the features of a commercial device (MICA2 OEM). In particular, for this device, we found that for a carrier frequency of $f = 916$ MHz and a data rate of 34 KBaud, we have a threshold (or receiver sensitivity) $\tau_{dB} = -118$ dBm [13].

In Fig. 3 is shown the transmission range of TwoRayGround model [14]. TwoRayGround model considers both the direct path and a ground reflection path. It is applied in the environments which are like plains and have no obstacles. However, the transmission range of Shadowing model is random, this model is applied in the environments which have obstacles and are hardly to transmit data directly. In particular, the emitted power of the phenomenon is calculated according to a TwoRayGround propagation model. The received power at distance d is calculated by:

$$P_r(d) = \frac{P_t G_t G_r h_t^2 h_r^2}{d^4 L} \tag{1}$$

where G_t and G_r are the antenna gains of the transmitter and the receiver. h_t and h_r are the heights of the transmit and receive antennas respectively. L ($L \geq 1$) is the system loss.

3.3 Energy Model

The energy model concerns the dynamics of energy consumption of the sensor. A widely used model is presented in [15]. When the sensor transmits k bits, the radio circuitry consumes an energy of $kP_{Tx}T_B$, where P_{Tx} is the power required to transmit a bit which lasts T_B seconds. By adding the radiated power $P_t(d)$, we have:

$$E_{Tx}(k, d) = kT_B(P_{Tx} + P_t(d))$$

Since packet reception consumes energy, by following the same reasoning, we have:

$$E(k, d) = kP_{Tx}T_B + kT_B P_t(d) + kP_{Rx}T_B \quad (2)$$

where P_{Rx} is the power required to correctly receive (demodulate and decode) one bit.

3.4 Interference

In general, in every wireless network the electromagnetic interference of neighboring nodes is always present. The interference power decreases the Signal-to-Noise-Ratio (SNR) at the intended receiver, which will perceive a higher bit and/or packet error probability. Given a particular node, the interference power depends on how many transmitters are transmitting at the same time of the transmission of the given node. In a WSN, since the number of concurrent transmissions is low because of the low duty-cycle of sensors, we can neglect the interference. In other words, if we define duty-cycle as the fraction between the total time of all transmissions of sensor data and the total operational time of the network, we get always a value less than 0.5. In fact, the load of each sensor is $\ll 1$ because sensors transmit data only when an event is detected [15]. However, it is intuitive that in a more realistic scenario, where many phenomena trigger many events, the traffic load can be higher, and then the interference will worsen the performance.

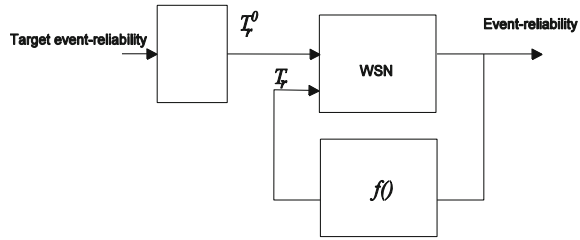
3.5 MAC Protocols

The Media Access Control (MAC) data communication protocol sub-layer, also known as the Medium Access Control, is a sublayer of the data link layer specified in the seven-layer OSI model (layer 2). It provides addressing and channel access control mechanisms that make it possible for several terminals or network nodes to communicate within a multiple access network that incorporates a shared medium, e.g. Ethernet. The hardware that implements the MAC is referred to as a medium access controller. The MAC sub-layer acts as an interface between the Logical Link Control (LLC) sublayer and the network's physical layer. The MAC layer emulates a full-duplex logical communication channel in a multi-point network. This channel may provide unicast, multicast or broadcast communication service.

3.6 Event Detection and Transport

We use the data-centric model similar to [16], where the end-to-end reliability is transformed into a bounded signal distortion concept. In this model, after sensing an event, every sensor node sends sensed data towards the MN. The transport used is a UDP-like transport, i.e. there is not any guarantee on the data delivery. While this approach reduces the complexity of the transport protocol and well fit the energy and computational constraints of sensor nodes, the event-reliability can be guaranteed to some extent because of the spatial redundancy. The sensor node transmits data packets reporting the details of the detected event at a certain transmission rate. The setting of this parameter, T_r , depends on several factors, as the quantization step of sensors, the type of phenomenon, and the desired level of distortion perceived at the MN. In [18], the authors used this T_r as a control parameter of the overall system. For example, if we refer to event-reliability as the minimum number of packets required at sink in order to reliably detect the event, then whenever the sink receives a number of packets less than the event-reliability, it can instruct sensor nodes to use a higher T_r . This instruction is piggy-backed in dedicated packets from the MN. This system can be considered as a control system, as shown in Fig. 4, with the target event-reliability as input variable and the actual event-reliability as output parameter. The target event-reliability is transformed into an initial T_r^o . The control loop has the output event-reliability as input, and on the basis of a particular non-linear function $f(\cdot)$, T_r is accordingly changed. We do not implement the entire control system, but only a simplified version of it. For instance, we vary T_r and observe the behavior of the system in terms of the mean number of received packets. In other words, we open the control loop and analyze the forward chain only.

Fig. 4 Representation of the transport based on the event-reliability



4 AODV

We are aware of many proposals of routing protocols for ad-hoc networks [17]. Here, we consider AODV protocol. The AODV is an improvement of DSDV to on-demand scheme. It minimizes the broadcast packet by creating route only when needed. Every node in network maintains the route information table and participates in routing table exchange. When source node wants to send data to the destination node, it first initiates route discovery process. In this process, source node broadcasts Route Request (RREQ) packet to its neighbors. Neighbor nodes which receive RREQ forward the packet to its neighbor nodes. This process continues until RREQ reaches to the destination or the node who knows the path to destination. When the intermediate nodes receive RREQ, they record in their tables the address of neighbors, thereby establishing a reverse path. When the node which knows the path to destination or destination node itself receive RREQ, it sends back Route Reply (RREP) packet to source node. This RREP packet is transmitted by using reverse path. When the source node receives RREP packet, it can know the path to destination node and it stores the discovered path information in its route table. This is the end of route discovery process. Then, AODV performs route maintenance process. In route maintenance process, each node periodically transmits Hello messages to detect link breakage.

5 Performance Metrics

In this paper, we evaluate the performance of the proposed model considering two metrics: goodput and depletion. The goodput is defined at the sink, and it is the received packet rate divided by the sent packets rate. Thus:

$$G(\tau) = \frac{N_r(\tau)}{N_s(\tau)} \tag{3}$$

where $N_r(\tau)$ is the number of received packet at the sink, and the $N_s(\tau)$ is the number of packets sent by sensor nodes which detected the phenomenon. Note that the event reliability is defined as $G_R = N_r(\tau)/R(\tau)$, where R is the required number of packets or data in a time interval of seconds.

As long as the WSN is being used, a certain amount of energy will be consumed. The energy consumption rate directly affects the life-time of the network, i.e. the time after which the WSN is unusable. The energy depletion is a function of the reporting rate as well as the density of the WSNs. It should be noted that the density of the network in the event-driven scenario correlates with the number of nodes that report their data. Accordingly, we define the depletion by the network in the detection interval τ as:

$$\bar{\Delta}(\tau) = \frac{NE_I - \sum_{i=1}^N e_i(\tau)}{N_\tau} \quad (4)$$

where $e_i(\tau)$ is the node energy and the means are computed over the number of nodes. The number of nodes N is set as power of integers in order to analyze the behaviour of the scaled versions of the network.

6 Simulation Results

In this section, we present the simulation results. We simulated the network by means of NS-2 simulator with the support of NRL libraries. Energy is uniformly distributed among all the sensor nodes. Sensor nodes nearby to the sink disperse large amount of data to the sink with less energy consumption while the nodes far away from the sink require more energy.

We consider the case when sensor nodes are deployed in the observation field. All sensor nodes are stationary. The sink moves randomly in the field and gathers the data from the sensor nodes.

We investigate the performance of WSNs when the sink move with different speeds. We have considered two mobile speeds: 5 m/s and 20 m/s.

In Table 1, we present the values of parameters used in our simulation system. Let us note that the power values concern the power required to transmit and receive one bit, respectively. They do not refer to the radiated power at all. This is also the energy model implemented in the widely used NS-2 simulator [16].

We carried out simulations considering AODV protocol and TwoRayGround radio model. For the simulations, the sample averages of Eqs. (3) and (4) are computed over 20 simulation runs and they are plotted in Figs. 5 and 6, respectively.

In Fig. 5 are shown the average values of goodput. We found that when the T_r is lower than 10 pps, the goodput is higher when the sink node moves faster (20 m/s). So, when the network is not congested, the goodput is higher for higher speeds of moving sink.

In Fig. 6 are shown the average values of depletion. From the simulation results, we found that, when T_r is lower than 10, the depletion is higher when sink moves with lower speed (5 m/s). But, when T_r is larger than 10, the depletion is higher for higher values of the sink speed.

Table 1 Radio model and system parameters

Radio model parameters	
Path loss coefficient	$\alpha = 2.7$
Variance	$\alpha_{db}^2 = 16 \text{ dB}$
Carrier frequency	916 MHz
Antenna	omni
Threshold (sensitivity)	$\gamma = -118 \text{ dB}$
<i>Other parameters</i>	
Reporting frequency	$T_r = [0.1, 1000] \text{ pps}^a$
Interface queue size	50 packets
UDP packet size	100 bytes
Detection interval	30 s
Routing protocol	AODV
Mobility model	Random Trip Mobility Model
Mobile sensor speed	5 m/s, 10 m/s
Number of sensor nodes	16
Simulation area	800 * 800
Simulation time (sec)	30

^a Packet per seconds

Fig. 5 Goodput for different speeds

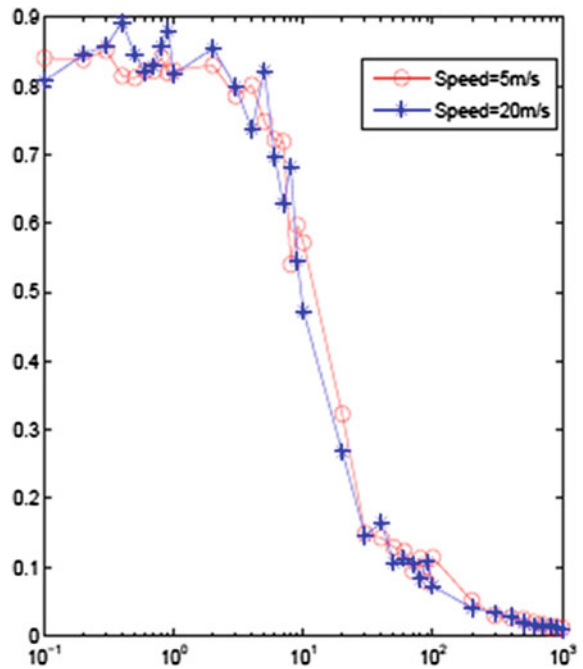
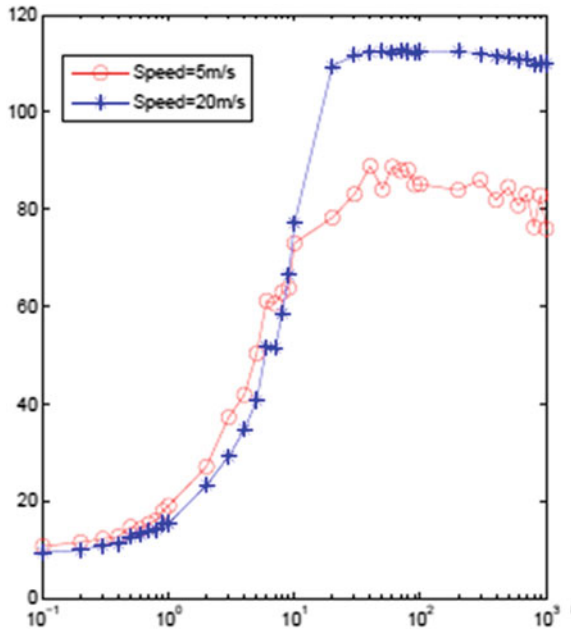


Fig. 6 Depletion for different speeds



7 Conclusions

In this paper, we presented our simulation system and discussed the simulation results of a WSN when sink node moves with different speeds considering Two-RayGround radio model and AODV protocol. We used the goodput and depletion to measure WSNs performance.

From the simulation results, we conclude as follows.

- When the T_r is lower than 10 pps, the network is not congested and the goodput is higher when the sink node moves faster (20 m/s).
- When T_r is lower than 10, the depletion is higher when sink moves with lower speed (5 m/s). But, when T_r is larger than 10, the depletion is higher for higher values of the sink speed (20 m/s).

In the future, we would like to carry out more extensive simulations for other MAC protocols, WSN topologies and different speed of mobile sensor nodes and sink together.

References

1. Giordano S, Rosenberg C (2006) Topics in ad hoc and sensor networks. *IEEE Commun Mag* 44(4):97–97
2. Hu W, Bulusu N, Jha S (2007) Overload traffic management for sensor networks. *ACM Trans Sens Networks* 3(4):18–38
3. Somasundara AA, Kansal A, Jea DD, Estrin D, Srivastava MB (2006) Controllably mobile infrastructure for low energy embedded networks. *IEEE Trans Mobile Comput* 5(8):958–973
4. Younis O, Fahmy S (2004) HEED: a hybrid, energy-efficient, distributed clustering approach for ad-hoc sensor networks. *IEEE Trans Mobile Comput* 3(4):366–379
5. Kulkarni SS (2004) TDMA services for sensor networks. In: Proceedings of the 24th international conference on distributed computing systems workshops. pp 604–609
6. Ye W, Heidemann J, Estrin D (2004) Medium access control with coordinated adaptive sleeping for wireless sensor networks. *IEEE/ACM Trans Networking* 12(3):493–506
7. Yang T, De Marco G, Ikeda M, Barolli L (2006) Impact of radio randomness on performances of lattice wireless sensor networks based on event-reliability concept. *Mobile Inform Syst (MIS)* 2(4):211–227
8. Baruah P, Urgaonkar R, Krishnamachari B (2004) Learning-enforced time domain routing to mobile sinks in wireless sensor fields. In: Proceedings of the 29th annual IEEE international conference on LCN-2004, pp 525–532
9. Luo J, Hubaux J-P (2005) Joint mobility and routing for lifetime elongation in wireless sensor networks. In: Proceedings of the INFOCOM-2005, pp 1735–1746
10. Yang T, Ikeda M, Mino G, Barolli L, Durresi A, Xhafa F (2010) Performance evaluation of wireless sensor networks for mobile sink considering consumed energy metric. In: Proceedings of the AINA-2010, pp 245–250
11. Yang T, Barolli L, Iwashige J, Durresi A, Xhafa F (2011) Comparison evaluation of static and mobile sensor nodes in wireless sensor networks consider packet-loss and delay metrics. In: Proceeding of the INCoS-2011, pp 196–202
12. Donward I (2004) NRL's sensor network extension to NS-2. <http://pf.itd.nrl.navy.mil/analysisnrlsensorsim/>
13. Crossbow Technology Inc., <http://www.xbow.com/>
14. Rappaport TS (2001) Wireless communications. Prentice Hall PTR, Upper Saddle River
15. Vincze Z, Fodor K, Vida R, Vidacs A (2006) Electrostatic modelling of multiple mobile sinks in wireless sensor networks. Proceedings of the IFIP networking workshop on performance control in wireless sensor networks (PWSN2006), pp 30–37
16. Akan OB, Akyildiz IF (2005) Event-to-sink reliable transport in wireless sensor networks. *IEEE/ACM Trans Networking* 13(5):1003–1016
17. Perkins C (ed) (2001) Ad hoc networks, Addison-Wesley, Reading

Induction Motor Drive Based Neural Network Direct Torque Control

Sy Yi Sim, Wahyu Mulyo Utomo, Zainal Alam Haron,
Azuwien Aida Bohari, Nooradzianie Muhd. Zin
and Roslina Mat Ariff

Abstract A neural network based direct torque control of an induction motor was presented in this paper. The paper trained a neural network for speed controller of the machine to use in the feed-back loop of the control system. The description of the control system, training procedure of the neural network is given in this paper. The complete neural network based direct torque control scheme of induction motor drive is simulated using MATLAB. The acquired results compared with the conventional direct torque control reveal the effectiveness of the neural network based direct torque control schemes of induction motor drives. The proposed scheme improved the performance of transient response by reduces the overshoot. The validity of the proposed method is verified by the simulation results.

Keywords Induction motor drive · Direct torque control · Neural network control

1 Introduction

Formerly, d.c. motors were used extensively in areas where variable-speed operation was required, since their flux and torque are inherent decoupled and could be controlled easily by the field and armature current, even though d.c. motors have several disadvantages, due to the existence of the commutator and the brushes, such as they required periodic maintenance, limited commutator capability under high-speed and they cannot be used in explosive or corrosive environment. These

S. Y. Sim (✉) · W. M. Utomo · Z. A. Haron · A. A. Bohari · N. Muhd. Zin
Electrical Power Department, Faculty of Electrical and Electronic Engineering, Universiti
Tun Hussein Onn Malaysia, 86400 Parit Raja, Batu Pahat, Johor, Malaysia
e-mail: syisim@hotmail.com

R. M. Ariff
Robotic and Mechatronic Department, Faculty of Electrical and Electronic Engineering,
Universiti Tun Hussein Onn Malaysia, 86400 Parit Raja, Batu Pahat, Johor, Malaysia

problems can be solved by the applicant of a.c. motors, which have simple and rugged structure, high maintainability and economy. The main drawback that makes a.c. motors retreat from the industry was the inherent coupling between torque and flux. However, this disadvantage was amend by the exits of vector control credit to the latter development in power electronic device that expand the use of AC electric machines instead of DC electric machines [1] and [2].

Vector control ensure dynamically decouples fast flux and torque control and belongs to high-performance control implemented in a closed-loop fashion [1], [3], [4], and [5]. The vector control can be implemented in many different ways but only several basic schemes that are offered in the market. The most popular strategies among are Field Oriented Control (FOC), Direct Torque Control (DTC) and Direct Torque Control-Space vector Modulation (DTC-SVM).

Due to the merit over the IM compare with other motor drives and the characteristic of fast torque response and high efficiency variable speed drives make it the best choice for electric vehicle driving motor since the EV drive system must have the following feature [6–8]. DTC provides a very quick and precise torque response excluding the complex field-oriented block and inner current regulation loop [4], in contrast to vector control. The Direct Torque Control was first introduced by Takahashi and has found great success with the notion to reduce the dependence on parameters of induction motor and increase the precision and the dynamic of flux and torque response [5].

In Sect.2, the Direct Torque Control system is described. Development of the proposed neural network DTC-SVM will be explained in Sect.3. Simulation result is given in Sect. 4. The last section will be a discussion and conclusion.

2 DTC System Control Description

The generic DTC-SVM scheme consists of two hysteresis controller namely the stator flux controller and torque. On the other hand, the DTC-SVM uses two errors to produce stator reference voltage vectors, and then modulated by the SVM algorithm [9] as illustrated in Fig. 1.

The induction model in the stator-fixed d-q reference frame is described by [10].

$$V_s = R_s i_s + \frac{d}{dt}(\Psi_s) . \quad (1)$$

$$V_r = 0 = R_r i_r + \frac{d}{dt}(\Psi_r) - j\omega_r \Psi_r . \quad (2)$$

$$\Psi_s = L_s i_s + L_m i_r . \quad (3)$$

$$\Psi_s = L_m i_s + L_r i_r . \quad (4)$$

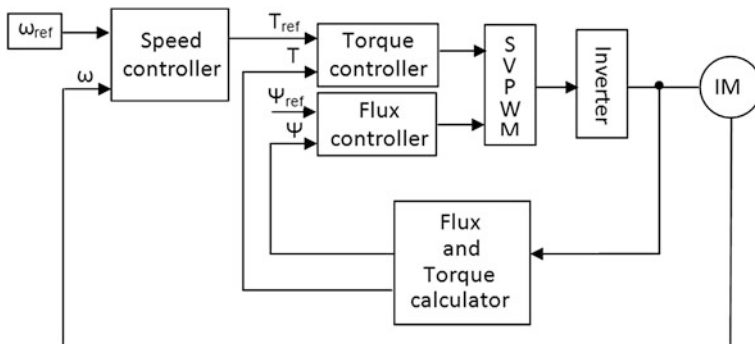


Fig. 1 DTC-SVM induction motor drive

Whereas the mechanical equation is given as below. The induction motor stator flux and torque are calculated in the flux and torque calculator as follows:

$$\Psi_{ds} = \int (V_{ds} - R_s i_{ds}) dt. \tag{5}$$

$$\Psi_{qs} = \int (V_{qs} - R_s i_{qs}) dt. \tag{6}$$

$$|\Psi_s| = \sqrt{\Psi_{ds}^2 + \Psi_{qs}^2}. \tag{7}$$

$$\theta_{\Psi_s} = \tan^{-1} \left(\frac{\Psi_{qs}}{\Psi_{ds}} \right). \tag{8}$$

Then, the electromagnetic torque is estimated as:

$$T_e = \frac{3p}{22} (\Psi_{ds} i_{qs} - \Psi_{qs} i_{ds}). \tag{9}$$

3 Neural Network DTC-SVM

Inspired by the successful function of the human brains, the artificial neural network (ANN) was developed for solving many large scale and complex problems. Based on ability to process some information and also to analyze the input and output simultaneously, it makes ANN suitable for dynamic and nonlinear system. The development of the structure and learning algorithm of the Neural Network Direct Torque Control (NNDTC) is explained as follows [11].

3.1 Proposed NN Speed Controller

This paper proposed a NN control method of DTC based on SVM to reduce the overshoot and torque ripple. The NN control is added to the speed controller to produce the torque reference. The block diagram of the proposed NN DTC-SVM of induction motor drive is shown in Fig. 2.

3.2 Structure of NNDTC

To design the neural network control some information about the plant is required. Basically, the numbers of input and output neuron at each layer are equal to the number of input and output signals of the system respectively. Based on the type of the task to be performed, the structure of the proposed NNDTC is as shown in Fig. 3.

The controller consists of input layer, hidden layer and output layer. Based on number of the neuron in the layers, the NNDTC is defined as a 1-3-1 network structure. The first neuron of the output layer is used as a torque reference signal ($a_1^2 = m_f$). The connections weight parameter between j th and i th neuron at m th layer is given by w_{ij}^m , while bias parameter of this layer at i th neuron is given by b_i^m . Transfer function of the network at i th neuron in m th layer is defined by:

$$n_i^m = \sum_{j=1}^{s^{m-1}} w_{ij}^m a_j^{m-1} + b_i^m . \tag{10}$$

The output function of neuron at m th layer is given by:

$$a_i^m = f^m(n_i^m) . \tag{11}$$

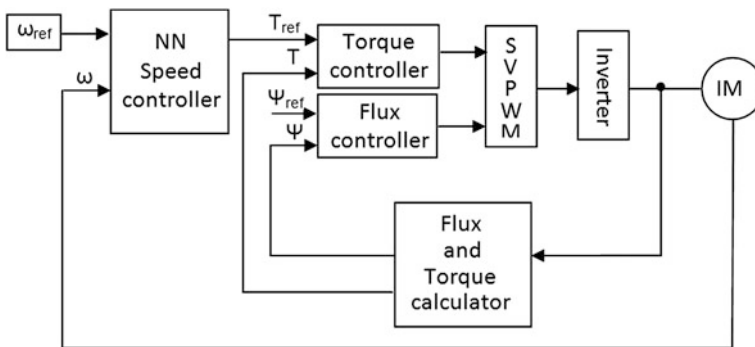


Fig. 2 Complete block diagram of proposed NN DTC-SVM

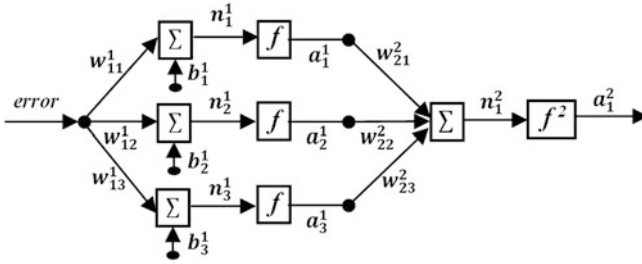


Fig. 3 Diagram block of neural network speed control for DTC induction motor drive

where f is activation function of the neuron. In this design the activation function of the output layer is unity and for the hidden layer is a tangent hyperbolic function given by:

$$f^m(n_i^m) = \frac{2}{1 + e^{-2n_i^m}} - 1 . \tag{12}$$

Updating of the connection weight and bias parameters are given by:

$$w_{ij}^m(k + 1) = w_{ij}^m(k) - \alpha \frac{\partial F(k)}{\partial w_{ij}^m} . \tag{13}$$

$$b_i^m(k + 1) = b_i^m(k) - \alpha \frac{\partial F(k)}{\partial b_i^m} . \tag{14}$$

where k is sampling time, α is learning rate, and F performance index function of the network.

4 Simulation and Results

Simulation was carried out to investigate the performance of the NNDC. In this section the dynamic model of a three-phase induction motor, space vector PWM and neural network control model have been developed. The simulation is developed using Borland C++, and then embedded as S-function in Simulink-Matlab. The parameters for the motor are given by:

- Frequency, $f = 50$ Hz.
- Pole, $p = 4$.
- Stator and rotor resistances, $R_s = 0.5\Omega$ and $R_r = 0.25\Omega$.
- Stator and rotor self inductances, $L_s = 0.0415H$ and $L_r = 0.0412H$
- Mutual inductance, $L_m = 0.0403H$.
- Combined of inertia, $J = 0.1$ kg – m².

To verify performance of the proposed NNDTC, the simulation results for a conventional DTC-SVM and the neural network (NN) DTC-SVM proposed controller are compared. With the same speed and load torque reference, the simulations of both methods are run simultaneously. The simulation is start at the speed on 80 rad/s with a constant load of 20 Nm applied. The startup response of both system is shown in Fig. 4, the improvement of the startup response by great reduce in overshoot as well as the settling time is observed.

Referring to Fig. 4, it shows that NN-controller have a start up response improved from the conventional PID controller. It is clearly explain that the startup response has a great improve by removed the overshoot from 94 rad/s. Besides that, the settling time also can be reduced.

The simulation testing is carry on by vary the speed reference from 80 to 120 rad/s. The performance of two system is observed. The speed trajectory of the motor when speed vary at the time of 1.5 s is shown in Fig. 5.

As illustrated in Fig. 5, with the constant load applied, the step up response of the speed trajectory again show the vast reduce in overshoot as well as the settling time. The overshoot is removed from 135 rad/s.

The simulation testing is continuing by step down the speed from 120 to 100 rad/s at the time of 3 s. The performance of two systems is observed. The speed trajectory of the motor when load is applied to the system at the time of 3 s is shown in Fig. 6.

As illustrated in Fig. 6, the overshoot of transient response is removed from 87 rad/s by apply of the proposed neural technique.

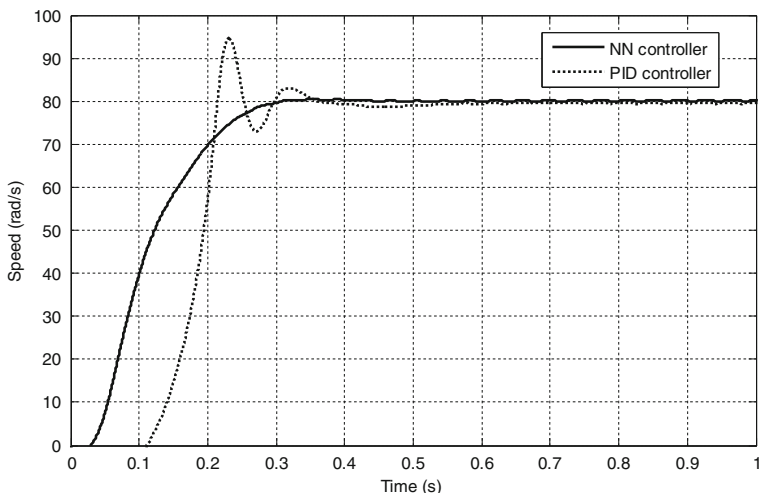


Fig. 4 Start up speed response comparison between conventional PID-DTC and NN-DTC controller

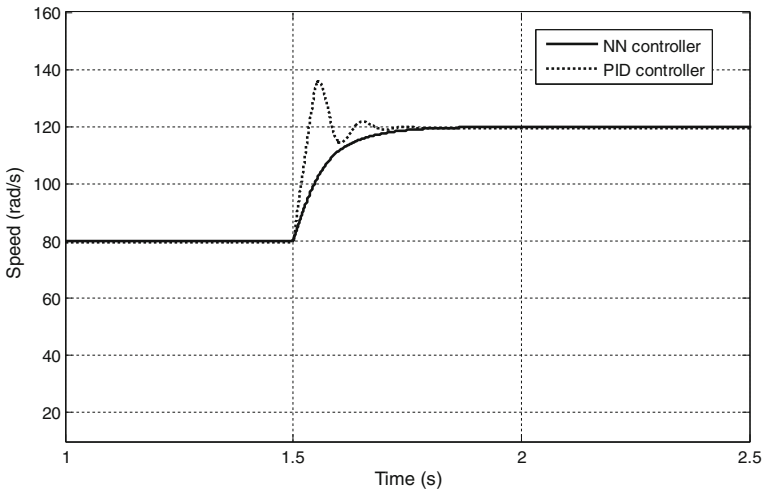


Fig. 5 Step up speed response comparison between conventional PID SVM and NN-SVM controller when the speed reference is varied from 80 to 120 rad/s

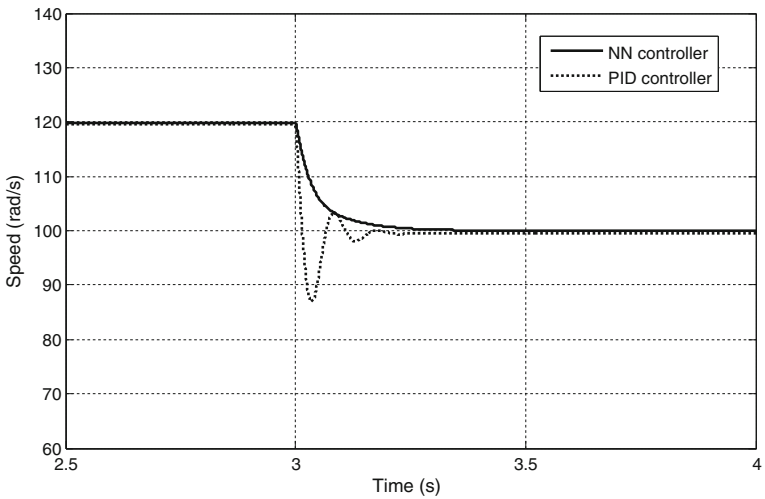


Fig. 6 Step down speed response comparison between conventional PID-DTC and NN-DTC controller when the speed reference is varied from 120 to 100 rad/s

5 Conclusion

The neural network controller for DTC-SVM speed controller induction motor drive system has been presented in this paper. The proposed method employs a single hidden layer neural network algorithm to generate the torque references.

The proposed controller is a nonlinear controller which can be employed without required any motor parameter data. Two control methods have been tested and compared: a conventional PID controlled DTC IM drive, and a NN controlled DTC IM drive. Proposed scheme shows good simulated result that improved the system performance. The improper transient response with high overshoot problem of the conventional PID-DTC can be solved. In addition, the results shows that the performance of transient response is improved by reduce the settling time.

6 Acknowledgments

The authors would like to gratitude University Tun Hussein Onn Malaysia for any valuable supports during conducting this research and in preparing this manuscript.

References

1. Boulghasoul Z, Elbacha A, Elwarraki E, Yousfi D (2011) Combined vector control and direct torque control an experimental review and evaluation. In: international conference on multimedia computing and systems (ICMCS), pp 1–6
2. Takahashi I, Ohmori Y (1989) High-performance direct torque control of an induction motor. *IEEE Trans Ind Appl* 25(2):257–264
3. Perron M, Hoang Le-Huy (2006) Full load range neural network efficiency optimization of an induction motor with vector control using discontinuous PWM. In: IEEE international symposium on industrial electronics, pp 166–170
4. Lin S-K, Fang C-H (2001) Sliding-mode direct torque control of an induction motor. In: the 27th annual conference of the IEEE industrial electronics society (IECON'01), vol 3, pp 2171–2177
5. Isao T, Toshihiko N (1986) A new quick-response and high-efficiency control strategy of an induction motor. *IEEE Trans Ind Appl* IA-22(5):820–827
6. Zhang X, Zuo H, Sun Z (2011) Efficiency optimization of direct torque controlled induction motor drives for electric vehicles. In: international conference on electrical machines and systems (ICEMS), pp 1–5
7. Haddoun A, Benbouzid MEH, Diallo D, Abdessemed R, Ghouili J, Srairi K (2005) A loss-minimization DTC scheme for EV induction motors. In: IEEE conference vehicle power and propulsion, pp 7
8. Bhim S, Pradeep J, Mittal AP, Gupta JRP (2006) Direct torque control: a practical approach to electric vehicle. In: IEEE power india conference, pp 4
9. Kaila SL, jani HB (2011) Direct torque control for induction motor using SVPWM technique. National conference on recent trend in engineering and technology
10. Wu J, Gao D, Zhao X, Lu Q (2008) An efficiency optimization strategy of induction motors for electric vehicles. In: IEEE vehicle power and propulsion conference, pp 1–5
11. Yatim AHM, Utomo WM (2004) Online optimal control of variable speed compressor motor drive system using neural control method. In: power and energy conference, pp 83–87

Adaptive Keyword Extraction System for the Hierarchical Category Search

Toshitaka Maki and Toshihiko Wakahara

Abstract As the Big Data is handled in the modern Internet, it needs various efficient search methods to retrieve the required information in the flood of information. In this paper, we propose a new Hierarchical Search Interface by Self-Organizing search method with a smartphone. The users can search the objective terms by pushing buttons for each adaptive hierarchical categories without any input of keyword. We describe the experimental results and the effectiveness of the proposed system is confirmed by the prototype simulation.

Keywords Big data · Morphological analysis · Complex network · Self-Organization · Category · Web mining · Keyword network

1 Introduction

In recent years, traditional concept of values has been diversified by the development of social media such as weblogs, bulletin board system and SNS (Social Networking Service). Therefore, the activity on the web, especially information retrieval has become indispensable and there is a need for techniques that can be searched efficiently from the explosively increased data.

Various data exists in the world of the Internet and the amount of information is countless. If you search for “politics” keyword in Google, you perhaps get the search results of approximately 600 million. If you add a “bulletin board” in the

T. Maki (✉) · T. Wakahara

Department of Information and Communication Engineering, Fukuoka Institute of Technology, 3-30-1 Wajirohigashi Higashi-ku, Fukuoka-shi 811-0295, Japan
e-mail: nce2015@gmail.com

T. Wakahara

e-mail: wakahara@fit.ac.jp

keyword, the search results will be reduced to about 38.4 million. In this way, you will be able to find the information quickly and accurately by entering more than one keyword in Yahoo! or Google search engine. However, smartphone users often cause troubles in entering keywords. In particular, for those who are not familiar with the manipulation of information, it requires complicated operation. In this case, by using the category search service such as Yahoo! Japan or goo, etc., you will be able to easily find useful information without entering any keyword. However, the category search service needs to be manually registered by the link information in advance. Therefore, it is difficult to register the latest or minor information. In another words, many link information cannot be registered in the category search service.

In this study, we propose an “Adaptive Hierarchical Category Search Interface [1]” and evaluate its effectiveness.

2 Related Work

Many studies about such as “Automatic extension of the dictionary” or “keyword extraction method” have been conducted so far. Here, we describe about morphological analysis and TF-IDF method.

2.1 Morphological analysis [2]

There are some engines of such as MeCab [3] or ChaSen [4] that can analyze Japanese sentences morphologically using a computer, and they are often used in natural language processing research.

e.g. “Fukuoka-ken is located in the northern part of the Kyushu region.”

=> Fukuoka (Noun), ken (Noun), is (Verb), located (Participle), in (Particle), ...

2.2 TF-IDF Method

The tf-idf method is a technique to extract important keywords from the text by weight rating. The tf-idf method uses two indices of “Term Frequency (TF Method)” and “Inverse Document Frequency (IDF Method)”.

2.2.1 TF Method: Definition of a high frequency keyword

Assumption: Words that appear repeatedly in the text are an important concept.

$$W_{td} = tf(t, d) \quad (1)$$

Weight value: W_{td} ; Word: t ; Text: d ;

2.2.2 IDF Method: Definition of a relatively high frequency keyword

Assumption: Keyword is a concept that the author has claimed.

$$idf(t) = \log \frac{N}{df(t)} + 1. \quad (2)$$

Number of documents in which the word exists: df

Total number of documents: N

2.2.3 TF-IDF Method: Keywords extraction method based on TF and IDF

Assumption: The important keyword does not exist in many documents.

$$W_{td} = tf(t, d) \times idf(t). \quad (3)$$

Problems: If there is a high frequency word, TF Method is effective. However, if there are many low frequency words, evaluation by TF Method may be constant values and it is valued at only IDF Method.

3 Proposed Hierarchical Category Search

We propose an adaptive Hierarchical Category Search Interface. By using this interface, users will be able to find the useful information easily without entering any keyword. To accomplish this, at first, we propose an adaptive keyword extraction system that composes the hierarchical category link.

3.1 Adaptive Keyword Extraction System

Adaptive Keyword Extraction System (AKES) evaluates the connectivity between keywords by weight rating, and this system excludes the thin relation keywords.

AKES in Fig. 1 performs the unsupervised learning in the following steps.

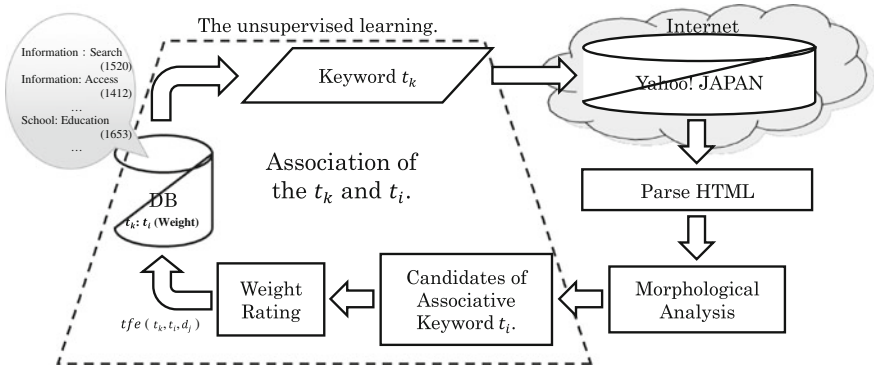


Fig. 1 A Schematic diagram of AKES

- (1) The keyword t_k is selected at randomly (1 from the database (DB)). 10 keywords have been registered in the DB in advance.
- (2) The new keyword t_k is searched by the Yahoo! JAPAN site.
- (3) The text data of title and description are extracted from the search results.
- (4) The candidates of associative keyword t_i . t_j are extracted by the morphological analysis. These are the noun or the adjective.
- (5) The keyword t_k is associated with t_i by weight rating and registered in the DB. If t_k and t_i are newly associated, weight rating of 100 points is added to the rating. If this term is again associated, 5 points are added. If it is not associated, one point is deducted. More information is described in Sect. 3.2.

The maladaptive keywords are culled by the repetitive steps shown in above steps. Accuracy of associative keyword extraction will continue to be improved.

3.2 Weight Rating Algorithm for AKES

There are many studies that attempt to extract keywords by TF-IDF Method or proprietary technique. In this study, we have built the AKES by proprietary TF method considering the category hierarchy. A weight rating method for the AKES is shown as below. We evaluate two types of accuracy by introducing bi-directional association of t_k and t_i .

- If t_k is associated with the t_i , w_m is set as the following Eq. (4).

$$w_m = \sum_j tfe(t_k, t_i, d_j). \tag{4}$$

$$tfe(t_k, t_i, d_j) = \begin{cases} 100; & \text{If the New registration} \\ W_m + 5; & \text{If } W_i \text{ is associated} \\ W_m - 1; & \text{If } W_i \text{ isn't associated} \end{cases} \quad (5)$$

- If t_i is associated with the t_k , w_n is set as the following Eq. (6).

$$W_n = \sum_j tfe(t_i, t_k, d_j). \quad (6)$$

$$tfe(t_i, t_k, d_j) = \begin{cases} 80; & \text{If the New registration} \\ W_n + 2; & \text{If } W_i \text{ is associated} \\ W_n; & \text{If } W_i \text{ isn't associated} \end{cases} \quad (7)$$

A connection between the keywords becomes clear by applying Eqs. (4), (5), (6) and (7) in AKES. Then the keyword network has been constructed as shown in Fig. 2. This network becomes suitable for a category search.

3.3 Hierarchical Category Search Interface

This time, a six layer model is tentatively defined. In addition, the number of keywords of each layer is set as 10. Keywords of the first layer and the second layer are fixed. A keyword from the third layer is replaced automatically by the user's selected keyword in the previous layer. By using this interface, it has become possible to extract the appropriate search terms from a million (10^6) words. Fig. 3 shows the system flow of the interface.

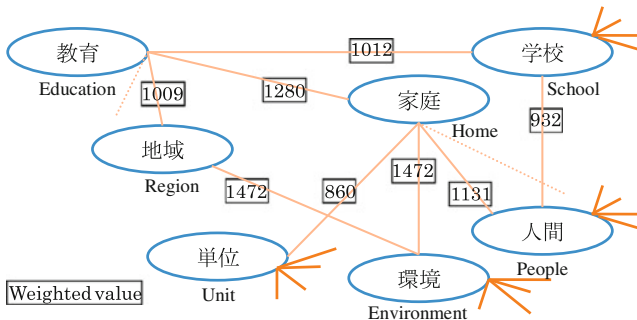
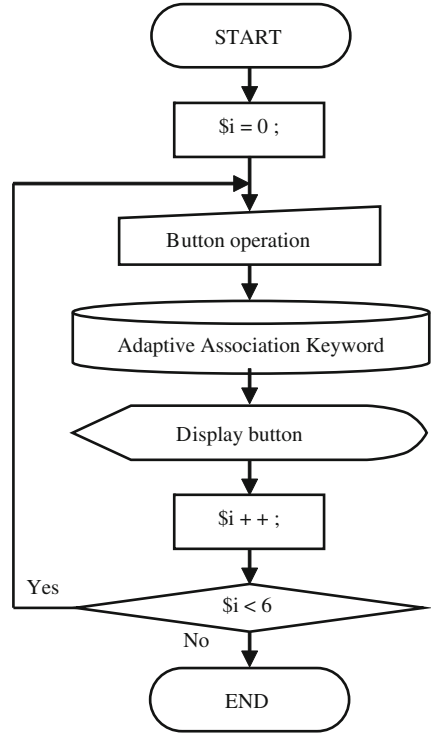


Fig. 2 Keyword network example

Fig. 3 System flow of the AKES Interface

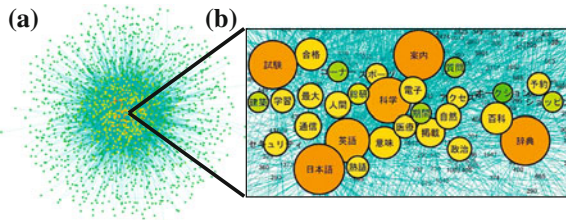


4 Experimental Results and Evaluation

4.1 Evaluation of Keyword Network

A keyword network of Fig. 4 has been constructed by AKES as shown in Fig. 1. After a million times trials are conducted, the number of top rating is 20,000, which is extracted in the keyword network. Other keyword network is culled as an incompatible. Initial 10 keywords was extended to about 5,000 words, and keyword network was formed about 550 thousand pieces.

Fig. 4 Keyword Network (a) Whole image; (b) Expanded central part



Looking at the keyword network of Fig. 4, it can be seen that most keywords are connected to each other. Figure 5 shows the results of analyzing the keyword network.

Figure 5a and 5 (b) shows a representation of Small-world characteristics of keyword network. It can be seen that the majority of keywords are connected by going through the three keywords, and all keywords are connected by through six keywords (Six degrees of separation).

Figure 5b shows a representation of a Scale-free [5] characteristics of keyword network. Keywords with a large number of connections are very few, and keywords with a small number of connections are abundant. This figure consists of both logarithmic basis. Equation (8) shows a representation of the power-law distribution and it is determined by the power approximation.

$$p(k) = 251.45 k^{-1.11}, \quad \gamma = 1.11 \tag{8}$$

A scale-free characteristic is expressed by the formula of power-law distribution ($P(k) \propto k^{-\gamma}, k \gg 1$). γ value of keyword network is calculated as 1.11. This value indicates that approximates the Zipf’s law ($\gamma = 1.0$). The Zipf’s law is the rule of thumb that frequency is proportional to $1/n$ of the n -th largest element ratio of the total. The Zipf’s law represents the access frequency of web pages or the word frequency “like”.

Keyword network and the Zipf’s law have similar properties. Therefore, we judged the keyword network shown in Fig. 4 has similar characteristics as the Zipf’s law and valid.

4.2 Evaluation of Interface

A hierarchical Categories Search Interface includes a function based on the keyword network. Fig. 6 shows an example of searching for videos of the bike. It shows six smartphone displays corresponding to each layer.

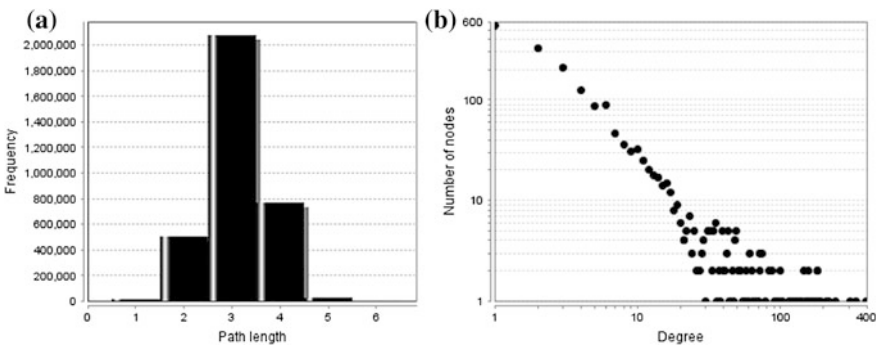


Fig. 5 The nature of the Keyword Network characteristics.(a) Small-word characteristics; (b) Scale-free characteristics

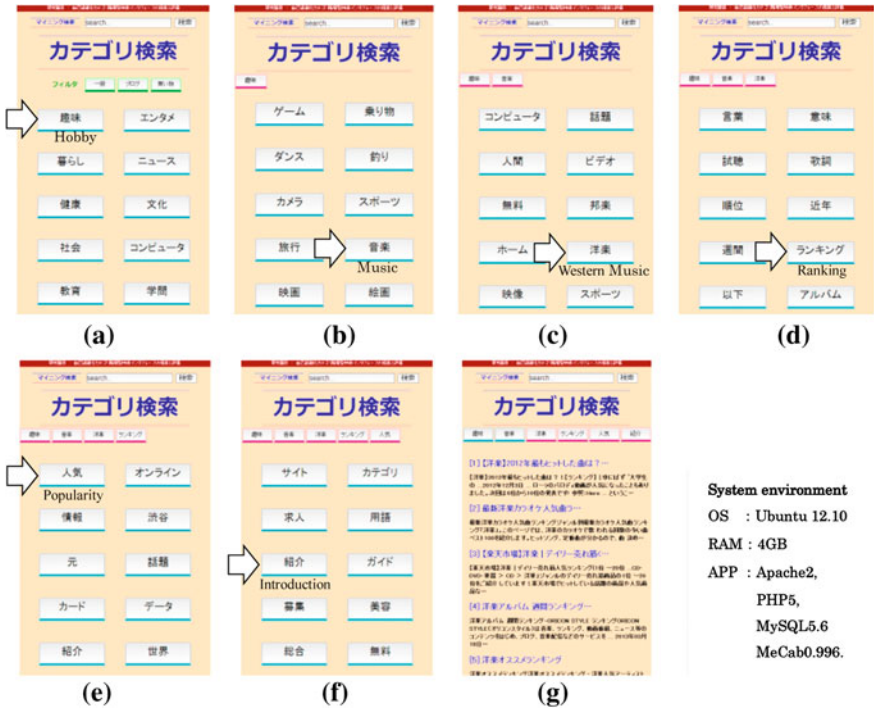


Fig. 6 Overview of the Interface. **a** First layer; **b** second layer; **c** third layer; **d** fourth layer; **e** fifth layer; **f** sixth layer; **g** search result

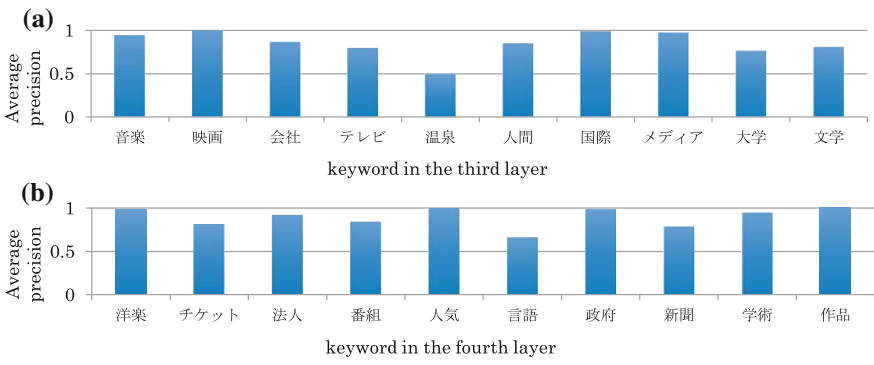


Fig. 7 Keyword categories of the KAES interface. **a** appropriate keyword categories in the second layer; **b** appropriate keyword categories in the third layer

The proposed interface is evaluated by the average precision. When a connectivity between keywords is weak, it is evaluated to be incongruent. Fig. 7 shows the evaluation results of the 400 keywords [6].

As shown in Fig. 7, the average precision is different for each keyword. Although the highest average precision is 1.0 (100 %), the lowest average precision is 0.49 (49 %). We think that it is because there is a bias connection in the keyword of the Web page. For example, as keywords of “information” exist in many Web pages, any other relational keywords are also hit and extracted together.

5 Conclusions

In this study, we propose a hierarchical category search interface for eliminating the complicated keyword entry in the smartphone. We make sure that users can only select to some extent in the words they want to search using the interface. However, it also contains a lot of noise. In the future, we intend to develop the ability to analyze the syntax appropriate for the category hierarchy in order to reduce the noise.

The main results of the study are described in the following:

- (1) The keyword weight rating algorithm by the unsupervised learning can extract the important candidate keywords. Hierarchical Category Search Interface by using the above algorithm is proposed and a six hierarchical and ten category model is also proposed.
- (2) The characteristics of the keyword network are similar as the ones of complicated network. Most keywords in the Web services are connected within six links.
- (3) Hierarchical category search algorithm is valid for obtaining the relational information without any keyword entry in the smartphone. The experimental results of the prototype show the effectiveness of the proposed interface.

References

1. Maki T, et al (2013) performance evaluation of a search interface by self-organizing hierarchical category. EIC 112,(379), LOIS2012-52, 29–34
2. Den Y (2009) A multi-purpose electric dictionary for morphological analyzers. JSAI 24(5)
3. Kenji K, Kunihiko K (2012) Keyword extraction rules to generate a keyword dictionary for japanese fishing web site ATISR
4. Kudo T, et al Applying conditional random fields to japanese morphological analysis
5. Osawa EI, Chinda K (2009) Extraction of structural information from complex network ICS-155, 23–29
6. Maki T, Wakahara T (2013) High accuracy of keyword extraction technique in hierarchical category search. EIC 112(466), LOIS2012-91, 125–130

Fuzzy Logic Control Design for Induction Motor Speed Control Improvement Through Field Oriented Control

Roslina Mat Ariff, Dirman Hanafi, Whayu Mulyo Utomo,
Kok Boon Ching, Nooradzianie Muhd Zin, Sy Yi Sim
and Azuwien Aida Bhoari

Abstract This paper focuses on improving induction motor performance by controlling its speed. The induction motor speed is controlled using field oriented control based structure associated with an induction motor. The field oriented control is implemented by combining with fuzzy logic control to reduce the uncertainties factors. The fuzzy logic control is developed based on Mamdani method. The inputs of fuzzy logic control are the error and derivative error between actual and reference speed of induction motor. The output of fuzzy logic control is the reference electric torque. The fuzzy logic control input output variables membership functions are chosen based on the parameters of the motor model. Motor state variables are identified indirect from induction motor model. The controller develops is implemented MATLAB Simulink. The simulation result shows that the fuzzy logic control is a suitable controller for improving induction motor performance with gives less settling time and steady state error than Proportional Integral Derivative control.

Keywords Induction Motor (IM) · Field Oriented Control (FOC) · Fuzzy Logic Control (FLC)

R. M. Ariff (✉) · D. Hanafi
Robotic and Mechatronic Department, Faculty of Electrical and Electronic Engineering,
Universiti Tun Hussein Onn Malaysia, Parit Raja 86400 Batu Pahat, Johor, Malaysia
e-mail: roslinamatariff@yahoo.com.my

W. M. Utomo · K. B. Ching · N. M. Zin · S. Y. Sim · A. A. Bhoari
Electrical Power Department, Faculty of Electrical and Electronic Engineering, Universiti
Tun Hussein Onn Malaysia, Parit Raja 86400 Batu Pahat, Johor, Malaysia

1 Introduction

Fuzzy Logic Control (FLC) as an Intelligent Control has widely applied for solving nonlinear systems problems like an electric motor drives [1]. As an intelligent control FLC does not depend on the system mathematical model [2–5] and has ability to handle nonlinearity of arbitrary complexity system.

Basic concept of an induction motor operates on the basis of interaction between induced rotor current and air gap field. In this condition often exists the motor's dynamic uncertainties like mechanical parameter uncertainty, external load disturbance, and unmodelled dynamics properties that all influenced the induction motor performance [6–8]. To solve this problem need to use the high performance controller.

Field-oriented control (FOC) of induction motor (IM) drives has been used in industrial applications [9]. High performance rotary machine drive required the field-oriented control technique, which is one of the most effective vector controls of IM due to the simplicity of designing and implementation [10]. Advent of high switching frequency PWM inverters has made it possible to apply for sophisticated control strategies to AC motor drives. The concept of the field oriented method is to use a separate controller to make the rotor's flux stabilizes to a desirable reference set point and motor independently control the speed through conventional linear control approaches. This technique makes variable speed drive with independent torque and flux control of induction motor possible implement, which also provides excellent dynamic response [11].

2 Induction Motor Model

The dynamic model of an induction motor is derived by first transformed to two-phase ones is the three-phase variables [12–15].

Voltage induced in a rotor bar of an induction motor depends on the speed of rotor relative to the magnetic field.

The magnetizing inductance of the motor Convenience or compatibility with the presentations of other network components is $d - q$ reference frames are usually selected on the basis form. The currents of the rotor are decomposed into $d - q$ coordinates, thus resulting into i_{dr} and i_{qr} . Since the frame $d - q$ of the rotor aligns with the frame $\alpha - \beta$ of the stator after rotation by an angle (θ) d it holds that:

$$\begin{pmatrix} i_{\alpha r} \\ i_{\beta r} \end{pmatrix} = \begin{pmatrix} \cos(\theta) & -\sin(\theta) \\ \sin(\theta) & \cos(\theta) \end{pmatrix} \begin{pmatrix} i_{dr} \\ i_{qr} \end{pmatrix} \quad (1)$$

Each of voltage variable, current or flux linkage in synchronous frame is stationary and fixed to a constant magnitude in steady state. The relationship is represented by Eq. 2.

$$\begin{pmatrix} V_{qs} \\ V_{ds} \\ 0 \\ 0 \end{pmatrix} = \begin{pmatrix} R_s + L_s P & \omega_e L_s & L_m P & \omega_e L_m \\ -\omega_e L_s & R_s + L_s P & -\omega_e L_m & L_m P \\ L_m P & \omega_r L_m & R_r + L_r P & \omega_r L_r \\ -\omega_r L_r & L_m P & -\omega_r L_r & R_r + L_r P \end{pmatrix} \begin{pmatrix} I_{qs} \\ I_{ds} \\ I_{qr} \\ I_{dr} \end{pmatrix} \quad (2)$$

Regardless of reference frame, the instantaneous input power (P_{in}) is:

$$P_{in} = (3/2)(V_{qs}I_{ds} + V_{ds}I_{qs}). \quad (3)$$

Electromagnetic torque defined as:

$$\begin{aligned} T_e &= (3/2)PL_m(I_{qs}I_{dr} - I_{ds}I_{qs}) \\ &= (3/2)(P/2)(L_m/L_x)\lambda_{dr}i_{qs} \end{aligned} \quad (4)$$

Speed of rotor defines as:

$$\omega_r = d\theta_r/dt. \quad (5)$$

where, V_{ds} and V_{qs} are d-q axis stator voltage, i_{ds} and i_{qs} are axis stator currents, i_{dr} and i_{qr} are d-q axis rotor currents. R_s and R_r are stator and rotor resistance per phase. L_s and L_r are the self-inductance of the stator and rotor respectively. L_m is the mutual inductance and T_e is electromagnetic torque. T_L is load torque and J_m is inertia. ω_e and ω_r are the speed of the rotating magnetic field and the speed of rotor respectively. P is the number of pole and θ_r is the rotor position.

3 Field Oriented Control Model

The electric motor position can be expressed as:

$$\theta_e = \int \omega_w dt = \int (\omega_r + \omega_{sl}) dt = \theta_r + \theta_{sl}. \quad (6)$$

where, ω_r is rotor speed and ω_{sl} is slip frequency. Then ω_e is electric motor speed formulated as Eq.7.

$$\omega_e = \omega_r + \omega_{sl}. \quad (7)$$

Slip speed define as:

$$\omega_{sl} = 2LrTe/3PT_r\lambda_{dr}^*. \quad (8)$$

For decoupling control, the rotor circuit equations are given as:

$$d\Psi_{dr}/dt + R_r i_{dr} - (\omega_e - \omega_r)\Psi_{qr} = 0. \quad (9)$$

Based on the induction motor model and FOC model, block diagram of induction motor driver can be developed as in Fig. 1.

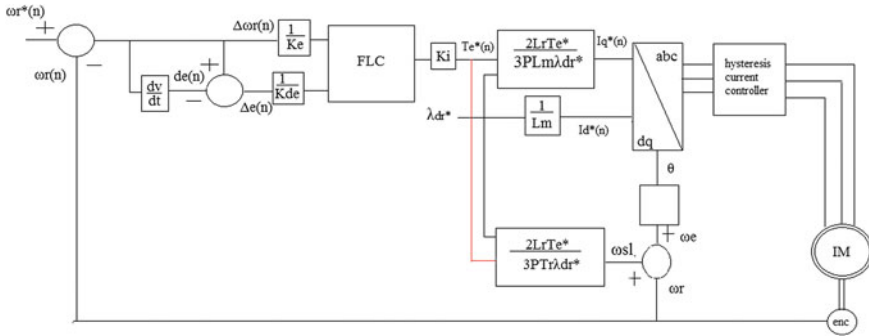


Fig. 1 The IM drive

The rotor time constant τ_r of IM is given by:

$$\tau_r = L_r/R_r. \tag{10}$$

The ω_r and λ_{dr} are determined using Eqs.11 and 12 respectively.

$$\omega_r = (L_m/\tau_r)(I_{qs}/\lambda_{dr}). \tag{11}$$

$$p\lambda_{dr} = (1/\tau_r)(-\lambda_{dr} + L_m I_{ds}). \tag{12}$$

4 Fuzzy Logic Control Design

In this paper, a Mamdani-type of FLC is developed for controlling the IM speed controller. The FLC input variables consist of the IM speed error and change of speed error and the output variable is the electrical torque. Each input variables have 5 membership functions and 7 membership functions as described in Figs. 2 and 3. Types of membership functions apply are triangular and trapezoidal functions. The functional relation between input and output of FLC are given by:

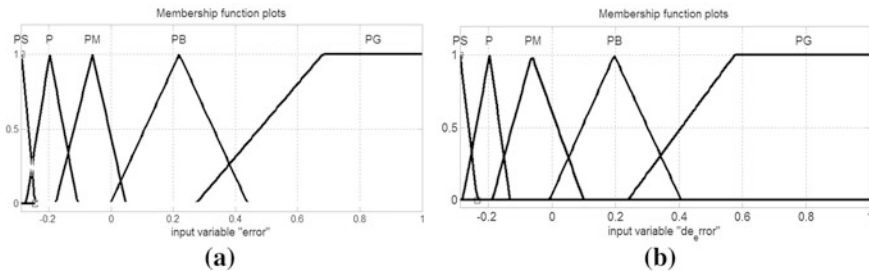


Fig. 2 The membership function for (a) error $\Delta\omega_r(n)$, b change in error $\Delta de(n)$

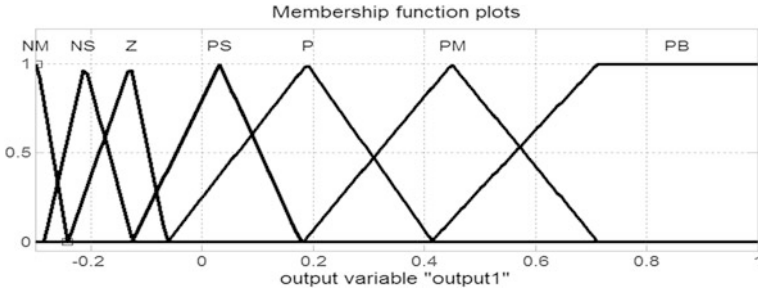


Fig. 3 The membership functions of output $T_e^*(n)$

$$T_e^*(n) = \int_{discrete} \Delta T_e^*(n) = f(\Delta e(n), \Delta \omega_r(n)). \tag{13}$$

where, $\Delta e(n)$ is the change of speed error and $\Delta \omega_r(n)$ is the sample of speed error. $T_e^*(n)$ is the electric torque reference and f is denotes the nonlinear function.

The data for rule of fuzzy logic control is show in table 1.

5 Result and Discussion

5.1 Result

The IM use as object of work has Frequency and Poles pairs are 50 Hz and 2, is stator resistance (Rs) is 0.3 Ω , rotor resistance (Rr) is 0.25 Ω , stator inductance (Ls) is 0.0415 mH, rotor inductance (Lr) 0.0412 mH, mutual inductance (Lm) is 0.0403 mH, Inertial moment and friction ceoficient are 0.1 and 0.02, and maximum torque (Tmax) is 250.

The test is started for constant speed 150 rad/s. The controllers responses comparison are represented in Fig. 4.

Based on graph responses above, FLC has steady state error and settling time are 0.13 % and 0.14 s respectively, while PID controller produces 0.53 % steady error and 0.5 s settling time.

Table 1 Rule of fuzzy logic control (FLC)

e	de				
	PS	P	PM	PB	PG
PS	NM	NM	NM	NM	NM
P	NM	NM	NM	NS	NS
PM	NM	NS	Z	PM	PB
PB	P	PM	PB	PB	PB
PG	PB	PB	PB	PB	PB

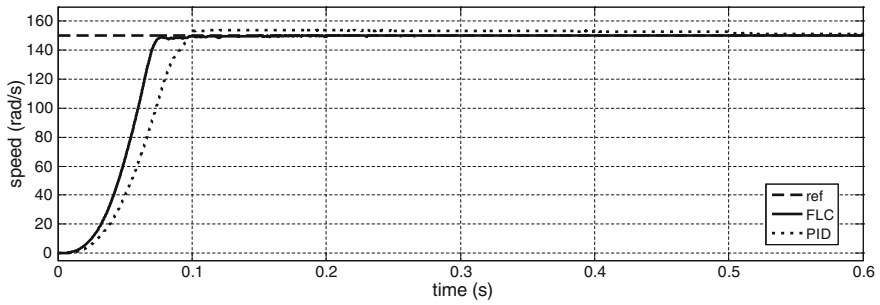


Fig. 4 Controller responses comparison for constant speed

The second test is done by increasing the IM speed from 100 rad/s to 150 rad/s and the result is shown by Fig. 5.

In this test FLC response has steady state error 0.13 % and settling time is 0.52 s. Then, PID controller response has steady state error and settling time are 0.87 % and 0.54 s respectively.

The final test is done by reducing the IM speed from 150 rad/s to 100 rad/s. The response of each controller is illustrated in Fig. 6.

For this kind of input signal, the steady state error of FLC and PID controller are 0.6 % and 0.22 % respectively.

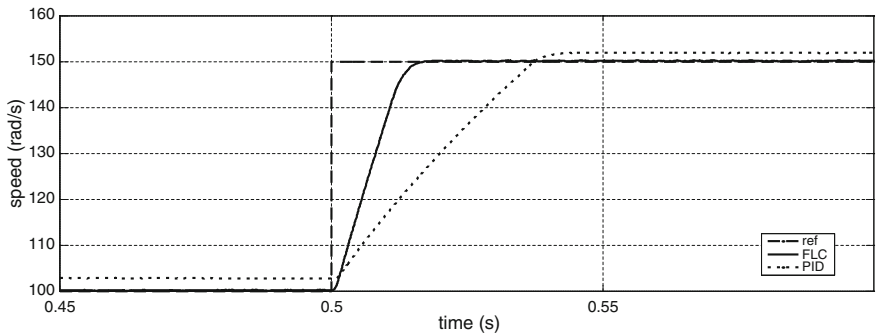


Fig. 5 simulation speed step up response of the drive of the FLC compare with the PID

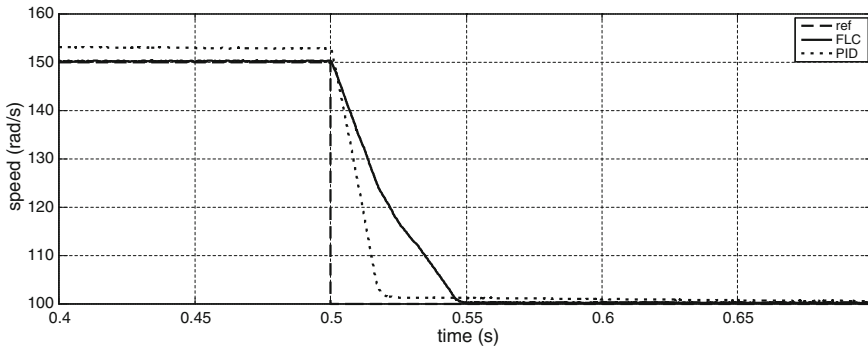


Fig. 6 simulation speed step down response of the drive of the FLC compare with the PID

6 Discussion

The IM speed control improvement has been representing. The improvement is done through control the FOC using FLC. The proposed method has been implemented using the MATLAB Simulink. Three kinds of input have applied to test and analyze the controller response.

7 Conclusion

This paper explains the method to improve the performance of the IM speed as a driver by control the FOC using FLC. Based on the test results for three types of input signals, FLC has better performance than PID controller. FLC has lower steady error and settling time. It means FLC is suitable controller for improve the IM speed performance.

Acknowledgments This work has been supported by Center of Graduate Studies Universiti Tun Hussein Onn Malaysia and Ministry of Higher Education.

References

1. Rathi MG (2010) Speed control of induction motor/: Fuzzy Logic Control v/s PI Control10:223–230
2. Lin CT, Lee CSG (1996) Neural Fuzzy Systems: A Neuro-Fuzzy Synergism to Intelligent Systems. Prentice-Hall, Upper Saddle River
3. Lai YS, Lin JC (2003) New hybrid fuzzy controller for direct torque control induction motor drives. IEEE Trans Power Electron 18:1211–1219
4. Youb LA, Craciunescu (2009) Direct torque control of induction motors with fuzzy minimization torque ripple. In: Proceeding WESCO, 2, pp 713–717

5. Uddin MN, Member S, Hafeez M (2012) FLC-Based DTC Scheme to Improve the Dynamic Performance of an IM Drive.48: 823–831
6. Wai RJ, Chang JM (2003) Implementation of robust wavelet neural network sliding mode control for induction servo motor drive. *IEEE Trans Ind Electron* 50:1317–1334
7. Wai RJ, Chang HH (2004) Backstepping wavelet neural network control for indirect field-oriented induction motor drive. *IEEE Trans Neural Netw* 15:367–382
8. Brdys MA, Kulowski GJ (1999) Dynamic neural controllers for induction motor. *IEEE Trans Neural Netw* 10:340–355
9. Ebrahim OS, Salem MF, Jain PK, Badr MA (2010) Application of linear quadratic regulator theory to the stator field-oriented control of induction motors. *IET Electr Power Appl* 4:637–646
10. Bose BK (2002) *Modern Power Electronics and AC Drives*. Prentice Hall, Knoxville
11. Vas P (1998) *Sensorless vector control and direct torque control*. Clarendon Press, Oxford
12. Bodson M, Chiasson J, Novotnak R (1994) High-performance induction motor control via input output linearization. In: *IEEE Control Syst Mag*, 24–33
13. Georges D, De WC, Ramirez J (1999) Nonlinear H2 and H1 optimal controllers for current-fed induction motors. *IEEE Trans Automat Control* 44:1430–1435
14. Marino R, Peresada S, Valigi P (1993) Adaptive input-output linearizing control of induction motors. *IEEE Trans Automat Control* 38:208–221
15. Marino R, Peresada S, Tomei P (1999) Global adaptive output feedback control of induction motors with uncertain rotor resistance. *IEEE Trans Automat Control* 44:967–983

Considering Lifetime of Sensors for Clusterhead Selection in WSN Using Fuzzy Logic

Qi Wang, Leonard Barolli, Elis Kulla, Gjergji Mino, Makoto Ikeda and Jiro Iwashige

Abstract In Wireless Sensor Networks (WSN), cluster formation and cluster head selection are critical issues. They can drastically affect the network's performance in different environments with different characteristics. In order to deal with this problem, we have proposed a fuzzy-based system for cluster-head selection and controlling sensor speed in Wireless Sensor Networks (WSNs). The proposed system is constructed by two Fuzzy Logic Controllers (FLC). We use four input linguistic parameters for evaluating lifetime of a sensor in FLC1. Then, we use the output of FLC1 and two other linguistic parameters as input parameters of FLC2 to control the probability of headcluster selection. By considering the moving speed of the sensor we are able to predict whether the node will leave or stay in the cluster. In this paper, we evaluate FLC1 and FLC2 by simulations and show that they have a good behavior.

Keywords Sensor speed · WSN · Feedback · Fuzzy-based · Cluster-head

Q. Wang · E. Kulla (✉)

Graduate School of Engineering, Fukuoka Institute of Technology (FIT),
3-30-1 Wajiro-Higashi, Higashi-Ku, Fukuoka 811-0295, Japan
e-mail: eliskulla@yahoo.com

Q. Wang

e-mail: wangqi19820707@gmail.com

L. Barolli · M. Ikeda · J. Iwashige

Department of Information and Communication Engineering, Fukuoka Institute of
Technology (FIT), 3-30-1 Wajiro-Higashi, Higashi-Ku, Fukuoka 811-0295, Japan
e-mail: barolli@fit.ac.jp

M. Ikeda

e-mail: makoto.ikd@acm.org

J. Iwashige

e-mail: iwashige@fit.ac.jp

G. Mino

Computer Technology Solution, 8B Industrial Way, Salem, NH 03079, USA
e-mail: gjmino@gmail.com

1 Introduction

Recent developments in technologies such as wireless communication and microelectronics have enabled Wireless Sensor Network (WSN) applications to be deployed for many applications such as battlefield surveillance and environment monitoring. An important aspect of such networks is that the nodes are unattended, resource-constrained, their energy cannot be replenished and network topology is unknown. The resource-constrained limitations make it essential for these sensor nodes to conserve energy to increase life-time of the WSN [1–4].

Recently, there are lot of research efforts towards the optimization of standard communication paradigms for such networks. In fact, the traditional Wireless Network (WN) design has never paid attention to constraints such as the limited or scarce energy of nodes and their computational power. Also, in WSN paths can change over time, because of time-varying characteristics of links, local contention level and nodes reliability. These problems are important especially in a multi-hop scenario, where nodes accomplish also the routing of other nodes' packets [4].

There are many fundamental problems that WSNs research have to address in order to ensure a reasonable degree of cost and system quality. Some of these problems include sensor node clustering, Cluster Head (CH) selection and energy dissipation. There are many research works that deal with these challenges [5–13].

The cluster based algorithms could be used for partitioning the sensor nodes into subgroups for task subdivision or energy management. Cluster formation is one of the most important problems in WSN applications and can drastically affect the network's communication energy dissipation. Clustering is performed by assigning each sensor node to a specific CH. All communication to (from) each sensor node is carried out through its corresponding CH node. Obviously one would like to have each sensor to communicate with the closest CH node to conserve its energy, however CH nodes can usually handle a specific number of communication channels. Therefore, there is a maximum number of sensors that each CH node can handle. This does not allow each sensor to communicate to its closest CH node, because the CH node might have already reached its service capacity. CHs can fuse data from sensors to minimize the amount of data to be sent to the sink. When network size increases, clusters can also be organized hierarchically.

In the conventional cluster architecture, clusters are formed statically at the time of network deployment. The attributes of each cluster, such as the size of a cluster, the area it covers, and the members it possesses, are static.

When a sensor with sufficient battery and computational power detects (with a high Signal-to-Noise Ratio: SNR) signals of interest, it volunteers to act as a CH. This is a simple method, because no explicit leader (CH) election is required and, hence, no excessive message exchanges are incurred. However, selecting of the CH in this way is not easy in different environments which may have different characteristics such as error rate, SNR, throughput and so on.

The heuristic approaches based on Fuzzy Logic (FL) and Genetic Algorithms (GA) can prove to be efficient for traffic control in wireless networks [14, 15].

In our recent works [16, 17], we proposed a fuzzy-based cluster selection method for WSNs, which used three parameters for CH selection: Distance of Cluster Centroid, Remaining Battery Power of Sensor and Number of Neighbor Nodes. We compared the performance with previous methods. The performance of our method was better than the previous methods. But, we found that for CH selection also sensor speed is very important. However, another important parameter in WSNs is the lifetime of sensors. In this work, we propose and implement a new Sensor Lifetime Fuzzy-based System (SLFS), which has two FLCs. We evaluate by computer simulations the performance of FLC1 and FLC2 and we show that the system has a good behavior.

The paper is organized as follows. In Sect. 2, we show some related work. In Sect. 3, we describe the proposed SLFS. In Sect. 4, we discuss the simulation results. Finally, conclusions are given in Sect. 5.

2 Related Work

In this section, we review related work in clustering algorithms. Several clustering methods such as weighted clustering [5], hierarchal clustering [6] and dynamic clustering [7] algorithms have been proposed to organize nodes as a cluster. Most algorithms elect CHs based on certain weights or iteratively optimize a cost function or use heuristic to generate minimum number of clusters. The Distributed Clustering Algorithm (DCA) [8] assumes quasi-stationary nodes with real-valued weights.

The Weighted Clustering Algorithm [5] selects a node based on the number of neighbors, transmission power and so on. The Max–Min d-Clustering Algorithm [9] generates dhop clusters with a run time of $O(d)$ rounds. This algorithm does not minimize the communicating complexity of sending information to the information center.

The hierarchical clustering scheme [6] uses spanning tree-based approach to produce cluster with certain properties. However, energy efficiency is not addressed in this work. In [10], the authors have proposed an emergent algorithm that iteratively tries to achieve high packing efficiency, however negotiation among nodes to be CH and join cluster based on degree and proximity leads to high amount of communication overhead, thus wastage energy.

LEACH [11, 12] uses two-layered architecture for data dissemination. In this scheme, sensors periodically elect themselves as CHs with some probability and broadcast an invitation message for nearby nodes to join the cluster. The nodes that do not intend to be CHs join the cluster based on the proximity of CH, thus minimizing the communicating cost. However, LEACH and PEGASIS [13] require the apriory knowledge of the network topology.

In [18], the authors propose a self-reconfiguring protocol for Wireless Personal Area Networks (WPAN) using an unsupervised clustering method. A fuzzy logic system is used to select the master/controller for each cluster. In our previous work

[19], we had shown by simulation results that the selection surface of our system was better than the system in [18]. But, we found that for CH selection the number of neighbor nodes is very important. For this reason, we proposed and implemented a CH system using FL and number of neighbor nodes [20, 21].

3 Proposed SLFS

The structure of the proposed SLFS is shown in Fig. 1. It consists of two Fuzzy Logic Controllers (FLCs). The FLC is the main part of SLFS and its basic elements are shown in Fig. 2. They are the fuzzifier, inference engine, Fuzzy Rule Base (FRB) and defuzzifier.

As shown in Fig. 3, we use triangular and trapezoidal membership functions for both FLCs, because they are suitable for real-time operation [22]. The x_0 in $f(x)$ is the center of triangular function, $x_0(x_1)$ in $g(x)$ is the left (right) edge of trapezoidal function, and $a_0(a_1)$ is the left (right) width of the triangular or trapezoidal function. We explain in details the design of FLC1 and FLC2 in following.

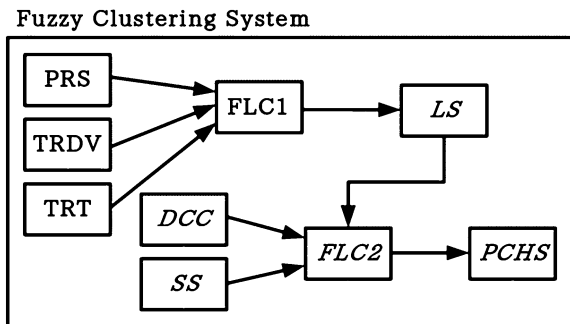
3.1 Description of FLC1

We use three input parameters for FLC1:

- Remaining Battery Power of Sensor (RPS);
- Transmission and Reception Data Volume of Sensor (TRDV);
- Transmission and Reception Time of Sensor (TRT).

The term sets for each input linguistic parameter are defined respectively as:

Fig. 1 Proposed SLFS scheme



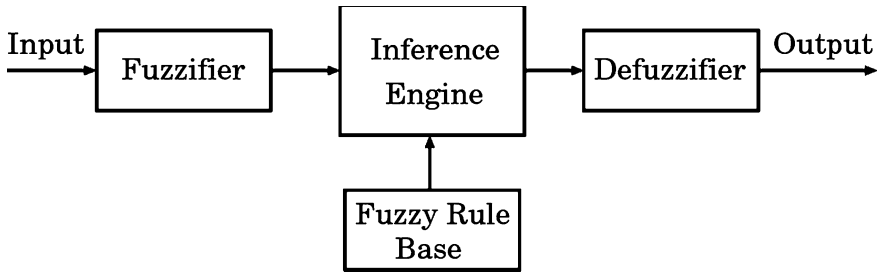


Fig. 2 FLC structure

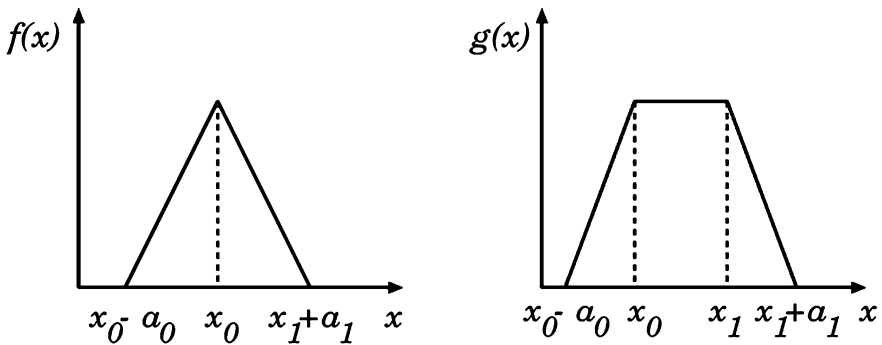


Fig. 3 Triangular and trapezoidal membership functions

$$\begin{aligned}
 T(RPS) &= \{Low(Lo), Middle(Mi), High(Hi)\}; \\
 T(TRDV) &= \{Light(Li), Moderate(Mo), Heavy(He)\}; \\
 T(TRT) &= \{Short(Sh), Moderate(Md), Long(Lg)\}.
 \end{aligned}$$

The output linguistic parameter is the Lifetime of sensor (LS). We define the term set of LS as: {Very Short (VS), Short (S), Little Short (LS), Medium (MD), Little Long (LL), Long (L), Very Long (VL)}.

The linguistic parameters and their term sets of proposed system are shown in Table 1. The fuzzy membership functions for input parameters are shown in Fig. 4.

The FRB is shown in Table 2 and forms a fuzzy set of dimensions $|T(RPS)| \times |T(TRDV)| \times |T(TRT)|$, where $|T(x)|$ is the number of terms on $T(x)$. The FRB has 27 rules. The control rules have the form: IF “conditions” THEN “control action”.

Table 1 Parameters and their term sets for FLC1

Parameters	Term sets
Remaining battery power of sensor (RPS)	Low, middle, high
Transmission and reception data volume of Sensor (TRDV)	Light, moderate, heavy
Transmission and reception time of sensor (TRT)	Short, moderate, long
Lifetime of sensor (LS)	Very short, short, little short, medium, little long, long, very long

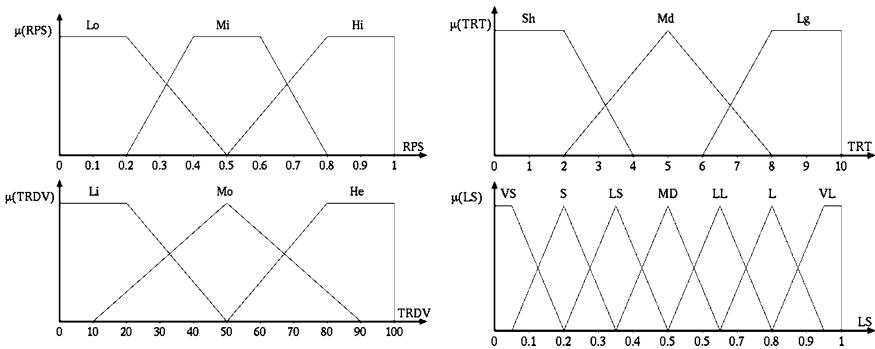


Fig. 4 Membership functions of FLC1

Table 2 FRB of FLC1

Rule	RPS	TRDV	TRT	LS	14	Mi	Mo	Md	LS
1	Lo	Li	Sh	VS	15	Mi	Mo	Lg	S
2	Lo	Li	Md	VS	16	Mi	He	Sh	LS
3	Lo	Li	Lg	VS	17	Mi	He	Md	S
4	Lo	Mo	Sh	VS	18	Mi	He	Lg	VS
5	Lo	Mo	Md	VS	19	Hi	Mo	Sh	VL
6	Lo	Mo	Lg	VS	20	Hi	Mo	Md	L
7	Lo	He	Sh	VS	21	Hi	Mo	Lg	MD
8	Lo	He	Md	VS	22	Hi	Mo	Sh	L
9	Lo	He	Lg	VS	23	Hi	Mo	Md	LL
10	Mi	Mo	Sh	LL	24	Hi	Mo	Lg	LS
11	Mi	Mo	Md	MD	25	Hi	He	Sh	LL
12	Mi	Mo	Lg	LS	26	Hi	He	Md	MD
13	Mi	Mo	Sh	MD	27	Hi	He	Lg	S

3.2 Description of FLC2

For FLC2, we use three input parameters:

- Lifetime of sensor (LS);
- Distance from Cluster Centroid (DCC);
- Sensor Speed (SS).

The term sets for each input linguistic parameter are defined respectively as:

$$\begin{aligned} T(LS) &= \{Short(Sh), Middle(Md), Long(Lo)\}; \\ T(DCC) &= \{Near(Ne), Moderate(Mo), Far(Fr)\}; \\ T(SS) &= \{Slow(Sl), Medium(Me), Fast(Fa)\}. \end{aligned}$$

The membership functions for input parameters of FLC2 are defined as:

$$\begin{aligned} \mu_{Sh}(LS) &= g(LS; Sh0, Sh1, Shw0, Shw1); \\ \mu_{Md}(LS) &= g(LS; Md0, Md1, Mdw0, Mdw1); \\ \mu_{Lo}(LS) &= g(LS; Lo0, Lo1, Low0, Low1); \\ \mu_{Ne}(DCC) &= g(DCC; Ne0, Ne1, New0, New1); \\ \mu_{Mo}(DCC) &= f(DCC; Mo0, Mow0, Mow1); \\ \mu_{Fr}(DCC) &= g(DCC; Fr0, Fr1, Frw0, Frw1); \\ \mu_{Sl}(SS) &= f(SS; Sl0, Slw0, Slw1); \\ \mu_{Me}(SS) &= f(SS; Me0, Mew0, Mew1); \\ \mu_{Fa}(SS) &= f(SS; Fa0, Faw0, Faw1). \end{aligned}$$

The output linguistic parameter is the Possibility of CH Selection (PCHS). We define the term set of PCHS as: {Very Weak (VW), Weak (W), Little Weak (LW), Medium (MD), Little Strong (LS), Strong (S), Very Strong (VS)}.

The membership functions for the output parameter PCHS are defined as:

$$\begin{aligned} \mu_{VW}(PCHS) &= g(PCHS; VW0, VW1, VWw0, VWw1); \\ \mu_W(PCHS) &= f(PCHS; W0, Ww0, Ww1); \\ \mu_{LW}(PCHS) &= f(PCHS; LW0, LWw0, LWw1); \\ \mu_{MD}(PCHS) &= f(PCHS; MD0, MDw0, MDw1); \\ \mu_{LS}(PCHS) &= f(PCHS; LS0, LSw0, LSw1); \\ \mu_S(PCHS) &= f(PCHS; S0, Sw0, Sw1); \\ \mu_{VS}(PCHS) &= g(PCHS; VS0, VS1, VS w0, VS w1). \end{aligned}$$

The linguistic parameters and their term sets of proposed system are shown in Table 3. The fuzzy membership functions are shown in Fig. 5. The FRB of FLC2 is shown in Table 4 and has 27 rules.

Table 3 Parameters and their term sets for FLC2

Parameters	Term sets
Lifetime of sensor (LS)	Short, medium, long
Distance from cluster centroid (DCC)	Near, moderate, far
Sensor speed (SS)	Slow, medium, fast
Probability (possibility) of CH selection (PCHS)	Very weak, weak, little weak, medium, little strong, strong, very strong

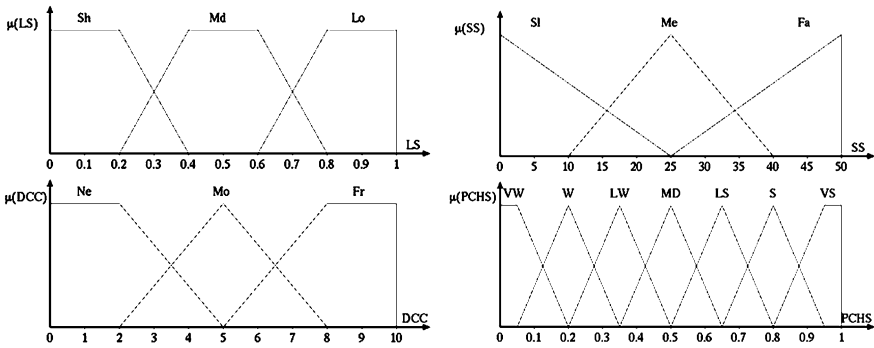


Fig. 5 Membership functions of FLC2

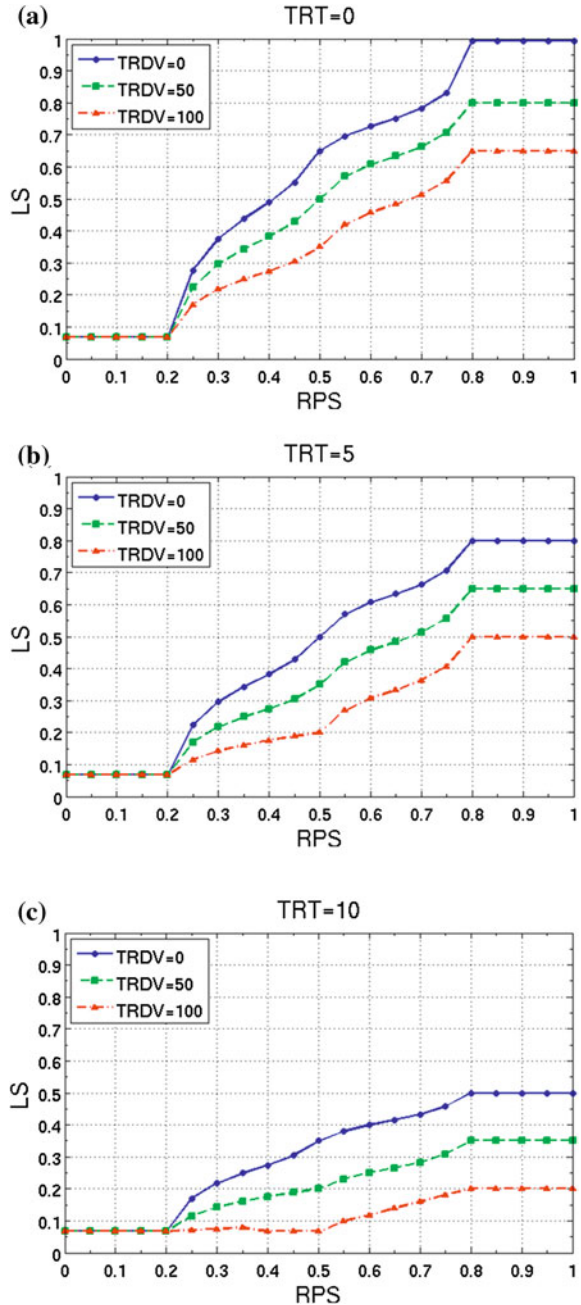
Table 4 FRB of FLC2

Rule	LS	DCC	SS	PCHS	14	Md	Mo	Me	LS
1	Sh	Ne	Sl	VS	15	Md	Fr	Lg	S
2	Sh	Mo	Me	VS	16	Md	Ne	Sl	LS
3	Sh	Fr	Lg	VS	17	Md	Mo	Me	S
4	Sh	Ne	Sl	VS	18	Md	Fr	Lg	VS
5	Sh	Mo	Me	VS	19	Lo	Ne	Sl	VL
6	Sh	Fr	Lg	VS	20	Lo	Mo	Me	L
7	Sh	Ne	Sl	VS	21	Lo	Fr	Lg	MD
8	Sh	Mo	Me	VS	22	Lo	Ne	Sl	L
9	Sh	Fr	Lg	VS	23	Lo	Mo	Me	LL
10	Md	Ne	Sl	LL	24	Lo	Fr	Lg	LS
11	Md	Mo	Me	MD	25	Lo	Ne	Sl	LL
12	Md	Fr	Lg	LS	26	Lo	Mo	Me	MD
13	Md	Ne	Sl	MD	27	Lo	Fr	Lg	S

4 Simulation Results

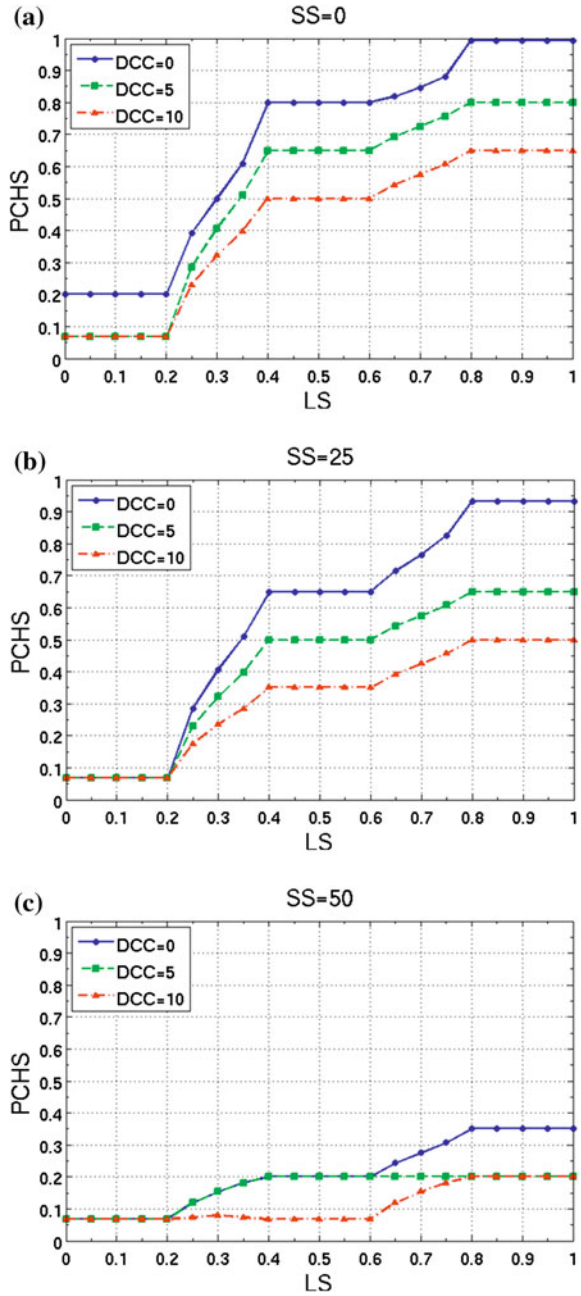
In our system, we decided the number of term sets by carrying out many simulations in MATLAB. We present the simulation results for SLFS, by showing the evaluation results for FLC1 and FLC2.

Fig. 6 FLC1 results for different TRT values



In Fig. 6, we show the results of LS (the output of FLC1), for different values of TRT. The results in each figure are shown as a relationship between RPS and LS,

Fig. 7 FLC2 results for different SS values



for different values of TRDV and TRT. We consider three values of TRT: 0, 5 and 10, which are for non active sensors, active sensors, and highly active users or cluster-head sensors, respectively. In general, when the TRT increases, the battery will be used more and the value of LS will be shorter, as we can see from Figs. 6a–c.

Let us consider Fig. 6b, where we consider an active sensor. The amount of data sent in the network is represented by the linguistic parameter TRDV. When TRDV is low the LS will be longer, as there will be less power used by the sensor. The same is true also for other values of TRT.

The LS is highly affected by the RPS. In the region where RPS is from 0.2 to 0.8 the relationship is almost linear and LS increases as the RPS increases. For RPS lower than 0.2, the LS will be near to zero for all values of TRT and TRDV. Otherwise, when RPS is higher than 0.8, LS will be higher value, depending on the values of TRT and TRDV.

In Fig. 7, we show the results of PCHS (the output of FLC2), for different values of SS and DCC. When the LS is lower than 0.2, the PCHS has the lowest value, because the cluster will not rely on a low-lifetime sensor as a CH. Then, for LS higher than 0.2, the PCHS tends to increase, because the sensors will be more reliable. On the other hand, PCHS will decrease when DCC is higher, because a sensor in the center of the centroid has higher probability to become a clusterhead.

Finally, the value of PCHS is also affected by SS. As the speed gets higher, PCHS will decrease. Especially, when SS is 50 PCHS decreases a lot, for all values of DCC and LS. Fast-moving sensors will jump from a cluster to another, so they should not be chosen as CHs.

5 Conclusions

In this paper, we proposed a simulation system based on FL for calculating lifetime of a sensor and cluster-head selection probability in WSNs. We implemented SLFS with two FLC: FLC1 and FLC2 and evaluated the performance by simulations.

From simulation results, we conclude as follows.

- When TRT increases, the value of LS will be shorter.
- When TRDV is low, the LS will increase for all values of TRT.
- For RPS lower than 0.2, LS will be near to zero. LS will increase linearly, as RPS increases from 0.2 to 0.8. When RPS is higher than 0.8, LS will be in its higher value, depending on TRT and TRDV.
- When the LS is lower than 0.2, the PCHS has the lowest value. For LS higher than 0.2, the PCHS increases.
- PCHS increases when DCC is lower, because sensors has higher probability to become a VH.

- As the speed gets higher, PCHS decreases. Fast-moving sensors will jump from a cluster to another, so they should not be chosen as CHs.

We have implemented the proposed system in MATLAB. We are working to implement it also in NS-2 in order to compare with other approaches. We would also like to use different input parameters, which will affect CH selection in different ways.

References

1. Akyildiz IF, Su W, Sankarasubramaniam Y, Cayirci E (2002) Wireless sensor networks: a survey. *Comput Netw* 38(4):393–442
2. Akyildiz IF, Kasimoglu IH (2004) Wireless sensor and actor networks: research challenges. *Ad Hoc Netw* 2(4):351–367
3. Giordano S, Rosenberg C (2006) Topics in ad hoc and sensor networks. *IEEE Commun Mag* 44(4):97
4. Al-Karaki JN, Kamal AE (2004) Routing techniques in wireless sensor networks: a survey. *IEEE Wirel Commun* 11(6):6–28
5. Chatterjee M, Das SK, Turgut D (2002) Wca: a weighted clustering algorithm for mobile ad hoc networks. *J Cluster Comput* 5(2):193–204
6. Banerjee S, Khuller S (2001) A clustering scheme for hierarchical control in multi-hop wireless networks. In: *Proceedings of IEEE INFOCOM-2001*, pp 1028–1037
7. Chen WP, How JC, Sha L (2004) Dynamic clustering for acoustic target tracking in wireless sensor networks. *IEEE Trans Mob Comput* 3(3):258–271
8. Basagni S (1999) Distributed clustering for ad hoc networks. In: *International symposium of parallel architectures, algorithms and networks (I-SPAN'99)*, pp 310–315
9. Amis AD, Prakash R, Vuong THP, Huynh DT (2000) Max–min d-cluster formation in wireless ad hoc networks. In: *Proceedings of IEEE INFOCOM-2000*, pp 32–41
10. Chan H, Perrig A (2004) Ace: an emergent algorithm for highly uniform cluster formation. In: *Proceedings of European workshop on wireless sensor networks (EWSN-2004)* pp 154–171
11. Heinzelman WB, Chandrakasan AP, Balakrishnan H (2004) An application-specific protocol architecture for wireless microsensor networks. *IEEE Trans Wireless Commun* 1(4):660–670
12. Heinzelman WR, Chandrakasan A, Balakrishnan H (2000) Energy-efficient communication protocol for wireless microsensor networks. In: *Proceedings of the 33rd annual Hawaii international conference on system sciences (HICSS)* pp 3005–3014
13. Lindsey S, Raghavendra C, Sivalingam KM (2002) Data gathering algorithms in sensor networks using energy metrics. *IEEE Trans Parallel Distrib Syst* 13(9):924–935
14. Chan PML, Sheriff RE, Hu Y, Conforto P, Tocci C (2001) Mobility management incorporating fuzzy logic for a heterogeneous ip environment. *IEEE Commun Mag* 39(12):42–51
15. Barolli L, Koyama A, Suganuma T, Shiratori N (2003) Gaman: a ga based qos routing method for mobile adhocnetworks. *J Interconnect Netw (JOIN)* 4(3):251–270
16. Wang Q, Ando H, Kulla E, Barolli L, Durresi A (2012) A fuzzy-based cluster-head selection system for WSNs considering different parameters. In: *Proceedings of the 26th international conference on advanced information networking and applications workshops (WAINA'12)*, pp 962–967
17. Wang Q, Barolli L, Kulla E, Durresi A, Biberaj A, Takizawa M (2012) A fuzzy-based simulation system for controlling sensor speed in wireless sensor networks. In: *Proceedings*

- of 15th international conference on network-based information systems (NBiS'12), pp 208–213
18. Liang Q (2003) A design methodology for wireless personal area networks with power efficiency. In: Proceedings of the wireless communications and networking (WCNC), vol 3, pp 1475–1480
 19. Anno J, Barolli L, Xhafa F, Durresi A (2007) A cluster head selection method for wireless sensor networks based on fuzzy logic. In: Proceedings of IEEE TENCON-2007, CD-ROM, 4 p
 20. Anno J, Barolli L, Durresi A, Xhafa F, Koyama A (2008) A cluster head decision system for sensor networks using fuzzy logic and number of neighbor nodes. In: Proceedings of IEEE Ubi-media 2008, pp 50–56
 21. Anno J, Barolli L, Xhafa F, Durresi A, Koyama A (2008) Performance evaluation of two-fuzzy based cluster head selection systems for wireless sensor networks. *J Mobile Inf Syst (MIS)* 4(4):297–312
 22. Mendel JM (1995) Fuzzy logic systems for engineering: a tutorial. *Proc IEEE* 83(3):345–377

Speed Control of Permanent Magnet Synchronous Motor Using FOC Neural Network

Nooradzianie Muhd. Zin, Wahyu Mulyo Utomo, Zainal Alam Haron, Azuwien Aida Bohari, Sy Yi Sim and Roslina Mat Ariff

Abstract This paper presents the performance analysis of the field oriented control for a permanent magnet synchronous motor drive with a proportional-integral-derivative and artificial neural network controller in closed loop operation. The mathematical model of permanent magnet synchronous motor and artificial neural network algorithm is derived. While, the current controlled voltage source inverter feeding power to the motor is powered from space vector pulse width modulation current controlled converter. The effectiveness of the proposed method is verified by develop simulation model in MATLAB-Simulink program. The simulation results prove the proposed artificial neural network controller produce significant improvement control performance compare to the proportional-integral-derivative controller for both condition controlling speed reference variations and constant load. It can conclude that by using proposed controller, the overshoot, steady state error and rise time can be reducing significantly.

Keywords: Permanent magnet synchronous motor drive · Field oriented control · Artificial neural network

1 Introduction

Permanent magnet synchronous motors (PMSM) are widely used in low and mid power applications such as computer peripheral equipment, robotics, adjustable speed drives and electric vehicles. Permanent magnet synchronous motor has the

N. Muhd. Zin (✉) · W. M. Utomo · Z. A. Haron · A. A. Bohari · S. Y. Sim
Electrical Power Department, Faculty of Electrical and Electronic Engineering,
Universiti Tun Hussein Onn Malaysia, Parit Raja, Batu Pahat 86400 Johor, Malaysia
e-mail: adzianie@gmail.com

R. M. Ariff
Robotic and Mechatronic Department, Faculty of Electrical and Electronic Engineering,
Universiti Tun Hussein Onn Malaysia, Parit Raja, Batu Pahat 86400 Johor, Malaysia

characteristics of high power density, free maintenances and high efficiency, which has been widespread application in the various electric drives applications [1]. In 1988 Pillay and Krishnan, R. presented PMSM drives and classified them into two types such as PMSM and brushless dc motor (BDCM) drives [2]. The PMSM has a sinusoidal back emf and requires sinusoidal stator currents to produce constant torque while the BDCM has a trapezoidal back emf and requires rectangular stator currents to produce constant torque. There are two methods to achieve zero steady state error: switching and integration. To eliminate steady state error, a Proportional-Integral-Derivative (PID) controller should be employed [3]. By using PID controller exact dq axis reactance parameters can be obtained. Moreover, to step change of command speed, parameter variations and load disturbances is very sensitive. Since it is slightly simple to implement, PID controller become most widely used for PMSM. So, a real time self-automated intelligent hardware implementation of PID controller as well as Field Oriented Control (FOC) is desired [4]. The PMSM can be used in Vector Control (VC) or so called FOC applications [5]. In FOC, motor stator currents & voltages are manipulated in the direct-quadrature (d-q) reference frame of the rotor. The inverter and motor is treated as one part in space vector pulse width modulation (SVPWM), and the algorithm has been extensively used, since it has superior features such as low pulsating torque, low current harmonic distortion and high voltage efficiency [6]. The artificial neural networks (ANN) are best suited for solving the problems that are nonlinear in nature. In ANN we can use parallel processing methods to solve some real-world problems where it is difficult to define a conventional algorithms. The ability of ANN to learn large classes of nonlinear functions is well known [8, 9]. It can be trained to emulate the unknown nonlinear plant dynamics by presenting a suitable set of input/output patterns generated by the plant [7]. In this paper, a model of closed-loop PMSM control system controlled by ANN develops and presents a comparative analysis of PID controller for speed performance in FOC PMSM drive. The effectiveness of the proposed method is verified by develop simulation model in MATLAB-Simulink.

2 Dynamic Modeling of PMSM

PMSM is essentially a three phase AC motor with sinusoidal back EMF driven by a DC source, which is converted to three-phase alternating currents supplying to the three stator windings of PMSM. The mathematic model of PMSM idq synchronous rotating reference frame can be obtained from synchronous machine model. Due to constant field produced by permanent magnets, the field variation is zero. It is also assumed that saturation and losses of core are negligible, the induced emf is sinusoidal and there is no damper winding on rotor. Using these assumptions, the voltage equations can write as follow:

$$v_d = R_s i_d + L_d \frac{d}{dt} i_d - L_q \omega_e \frac{d}{dt} i_q. \quad (1)$$

$$v_q = R_s i_q + L_q \frac{d}{dt} i_q - L_d \omega_e \frac{d}{dt} i_d + \omega_e \lambda_{PM}. \quad (2)$$

The produced torque of the machine can be presented as follow:

$$T_e = \frac{3}{2} P [\lambda_{PM} i_q + (L_d - L_q) i_d i_q]. \quad (3)$$

While, the maximum speed can be identified from the relationship:

$$T_e = T_L + K_f \omega_m + J \frac{d}{dt} \omega_m. \quad (4)$$

3 FOC System Description

Field oriented control also known as decoupling or vector control, came into the field of ac drives research in the late 1960s and was developed prominently in the 1980s to meet the challenges of oscillating flux and torque response in inverter fed induction and synchronous motor drive. The inexplicable dynamic behavior of large current transients and the resulting failure of inverters was a curse and barrier to the entry of inverter fed ac drives into the market. FOC is a control procedure for operating the motor that results in fast dynamic response and energy efficient operation at all speeds. It commutates the motor by calculating voltage and current vectors based on motor current feedback. It maintains high efficiency over a wide operating range and allows for precise dynamic control of speed and torque. The FOC controls the stator currents represented by a space vector. It transforms three-phase stator currents into a two-phase time variant system (α, β) . A two-coordinate time invariant system (dq) is obtained from that time variant system (α, β) . A two-coordinate time invariant system (dq) is obtained from that time variant system. In this structure the motor flux generating part is d (direct) and a torque generating part is q (quadrature). In FOC, motor stator currents and voltages are manipulated in the direct- quadrature (d-q) references frame of the rotor, which means must be mathematically transformed by using Park and Clarke transformation before they can be used for SVPWM output. Figure 1 is the diagram of velocity/current control loop using FOC technology based on PID controller.

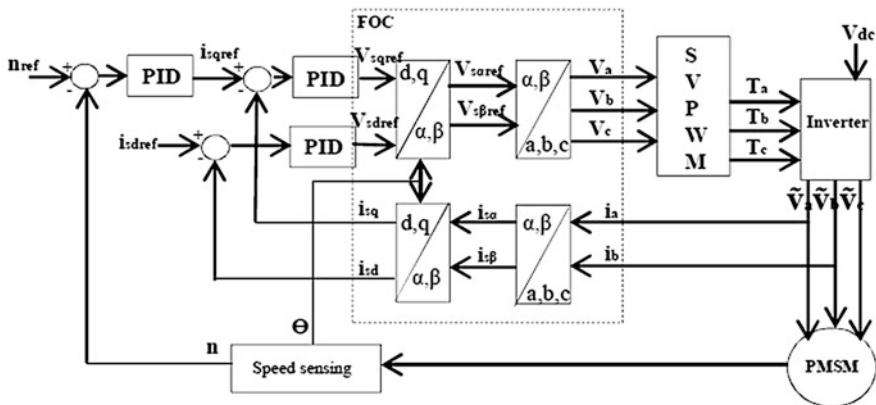


Fig. 1 A block diagram of PMSM drive based on PID controller

4 Proposed ANN Speed Controller

Inspired by the successful function of the human brains, the ANN was developed for solving many large scale and complex problems. Based on ability to process some information and also to analyze the input and output simultaneously, it makes ANN suitable for dynamic and nonlinear system.

4.1 Proposed ANN Speed Controller Description

The ANN control is added to the speed controller to produce the torque reference. The block diagram of the proposed ANN speed controller of FOC for PMSM drive is shown in Fig. 2.

4.2 Structure of ANN Speed Controller

To design the neural network control some information about the plant is required. Basically, the numbers of input and output neuron at each layer are equal to the number of input and output signals of the system respectively. Further the number of hidden layers and the total neurons is depended on the complexity of the system and the required training accuracy [10]. To implement search efficiency optimal control of PMSM drive, a multilayer perceptron neural network control is developed. Based on the type of the task to be performed, the structure of the proposed ANN speed controller is as shown in Fig. 3 [11].

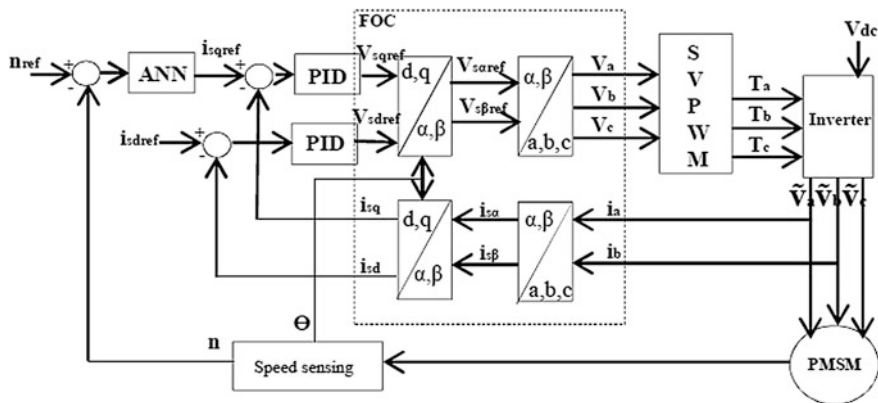


Fig. 2 The proposed block diagram of PMSM drive based on ANN speed controller

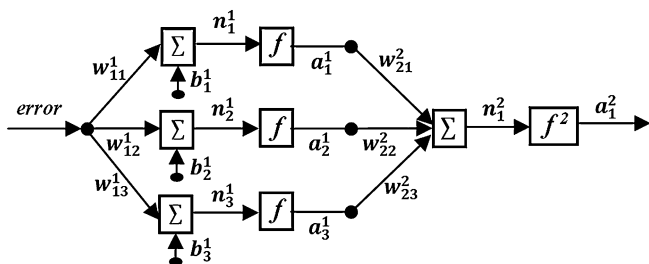


Fig. 3 Diagram block of ANN speed controller for FOC PMSM drive

The controller consists of input layer, hidden layer and output layer. Based on number of the neuron in the layers, the ANN is defined as a 1-3-1 network structure. The first neuron of the output layer is used as a torque reference signal ($a_1^2 = m_p$). The connections weight parameter between j^{th} and i^{th} neuron at m^{th} layer is given by w_{ij}^m , while bias parameter of this layer at i^{th} neuron is given by b_i^m . Transfer function of the network at i^{th} neuron in m^{th} layer and output function of neuron at m^{th} layer is defined by:

$$n_i^m = \sum_{j=1}^{S^{m-1}} w_{ij}^m a_j^{m-1} + b_i^m. \tag{5}$$

The output function of neuron at m^{th} layer is given by:

$$a_i^m = f^m(n_i^m). \tag{6}$$

where f is activation function of the neuron. In this design the activation function of the output layer is unity and for the hidden layer is a tangent hyperbolic function given by:

$$f^m(n_i^m) = \frac{2}{1 + e^{-2n_i^m}} - 1. \quad (7)$$

Updating of the connection weight and bias parameters are given by:

$$w_{ij}^m(k+1) = w_{ij}^m(k) - \alpha \frac{\partial F(k)}{\partial w_{ij}^m}. \quad (8)$$

$$b_i^m(k+1) = b_i^m(k) - \alpha \frac{\partial F(k)}{\partial b_i^m}. \quad (9)$$

where k is sampling time, α is learning rate, and F performance index function of the network.

5 Simulation Results and Discussions

To verify the feasibility of the proposed ANN speed controller of PMSM FOC method, some of the variations speed references and constant load has been observed. Both ANN and PID controller are run simultaneously. The simulation is developed in Simulink-Matlab. The parameters for the motor are 240 V, 50 Hz, Poles = 4, $R_s = 2.875\Omega$, $L_d = 0.0085H$, $L_q = 0.0085H$, Moment of inertia (J) = 0.0008 kgm^2 and Flux linkage (ψ) = $0.175Wb$. The simulation is testing by observe the system during start up response. The speed of the motor when a 7 Nm constant load is applied to the both system as show in Fig. 4.

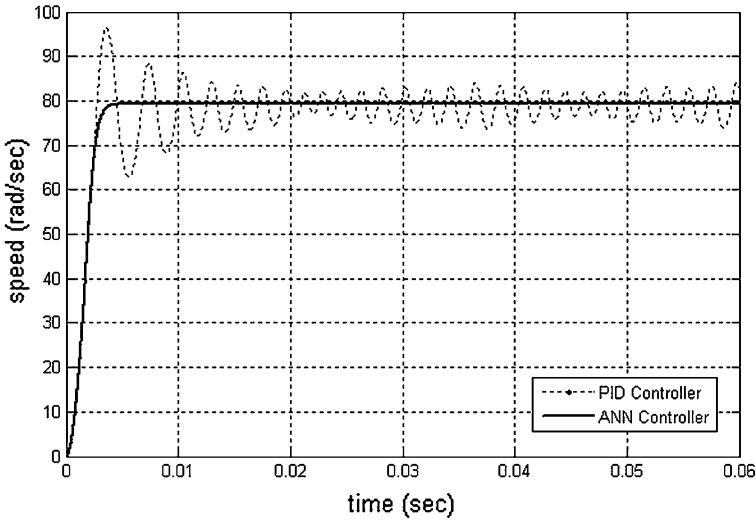


Fig. 4 Response comparison between conventional SVPWM and ANN speed controller when load is applied

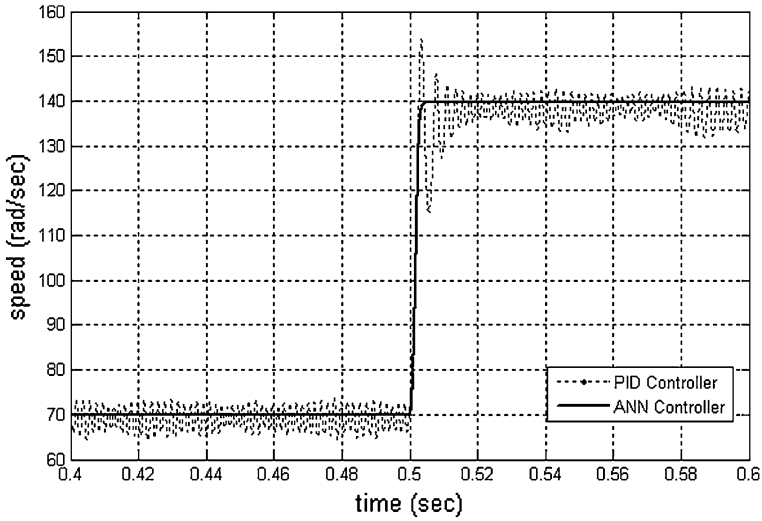


Fig. 5 Step up response comparison between conventional SVPWM and ANN speed controller

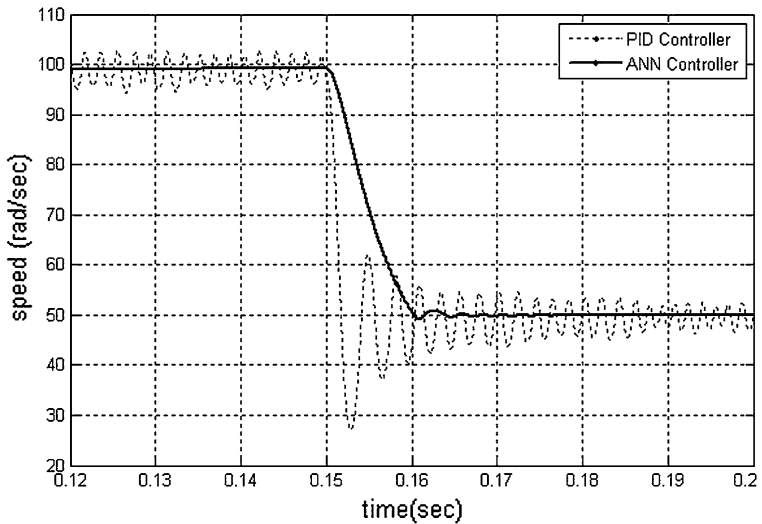


Fig. 6 Step down response comparison between conventional SVPWM and ANN speed controller

The simulation is continuing with constant 7 Nm load and the speed is vary from 70 rad/s to 140 rad/s at the time of 0.5 s for step up response for both systems as shown in Fig. 5.

While, for the step down response simulation, also start with constant 10 Nm load but the speed is vary from 100 rad/s to 50 rad/s at the time of 0.15 s for both systems as shown in Fig. 6.

The results show the overshoot of transient response is reduce and improved the settling time. As shown in figure above the improvement of both step responses by reduce in overshoot as well as the settling time. As illustrated in the figure, the settling time and the overshoot is also reduce by apply of the proposed neural technique, thus, improve the system performance at the same time.

6 Conclusion

This paper has presented the model of closed-loop PMSM control system controlled by ANN speed controller develops and presents a comparative analysis of PID controller for speed performance in FOC PMSM drive. The performance differences due to both ANN speed controller and PID controller were examined. The simulation results show that the ANN speed controller produce significant improvement control performance compare to the PID controller for both condition controlling speed reference variations and load disturbance variations. It can conclude that by using ANN speed controller, the overshoot, steady state error and rise time can be reducing significantly.

Acknowledgments All the authors would like to express a sincere acknowledgments to Universiti Tun Hussein Onn Malaysia for the valuable support during completion this research and manuscript.

References

1. Ke Song L, Liu W, Guangzhou L (2008) Fuzzy Logic Based Online Electromagnetic Loss Minimization of PMSM Drives. In: IEEE Vehicle Power and Propulsion Conference
2. Pillay P, Krishnan R (1989) Modeling, simulation, and analysis of permanent-magnet motor drives part 1: the permanent-magnet synchronous motor drive. *Ind Appl, IEEE Trans* 25:265–273
3. Wong LK, Bung FHF, Tam PKS (1998) Combination of sliding mode controller and PI controller using fuzzy logic controller. *IEEE Int Conf Fuzzy Syst* 1:296–301
4. Marufuzzaman M, Reaz MBI, Mohd. Ali MA (2010) FPGA implementation of an intelligent current dq PI controller for FOC PMSM drive. In: 2010 International conference on computer applications and industrial electronics (ICCAIE), Kuala Lumpur, p 602
5. Sergaki ES, Georgilakis PS, Kladas AG et al (2008) Fuzzy logic based online electromagnetic loss minimization of PMSM drives. In: Proceedings of the 2008 International Conference on Electrical Machines, Vilamoura, p 1
6. Weidong J, Qunjing W, Quan C et al (2009) SVPWM strategy for three-level inverter based on SVPWM strategy for two-level inverter. In: *Trans China Electrotechnical Soc* 24:108–114
7. Nguyen DH, Widrow B (1990) Neural network for self-learning control systems. *IEEE Control Syst Mag* 10:31–35

8. Yang Yi, Mahinda D, Rahman MA (2003) Implementation of an artificial neural network based real time adaptive controller for an interior PMSM. *IEEE Trans Ind Appl* 39:96–103
9. Narendra KS, Parthasarathy K (1990) Identification and control of dynamical systems using neural networks. In: *IEEE Trans Neural Network* 4–27
10. Choy I, Kwon SH, Choi JY, Kim JW et al (1996) On-line efficiency optimization control of a slip angular frequency controlled induction motor drive using neural networks. In: *IECON Proceedings 13 Annual Conference, Taipei*, pp 1216–1221
11. Yatim AHM, Utomo WM(2004) On line optimal control of variable speed compressor motor drive system using neural control model. In: *Power and Energy Conference, PECon 2004, Proceedings National*, pp 83–87

An Interactive Learning System Using Smartphone for Improving Students Learning Motivation

Noriyasu Yamamoto and Toshihiko Wakahara

Abstract The number of smartphones is increased exponentially and they are promising tools for interactive learning during lectures in the universities. However, when in a lecture room tens of sets of smartphones want to make simultaneous connection by Wi-Fi, the traffic will be increased and the network will be congested. In this study, we examined the effective use of the smartphones during the lectures. We considered a method of acquiring/utilizing the study records, which improves the students' learning motivation. In this research, we use smartphones as information terminals and carried out experiments in a real lecture room. The proposed method improves the degree of lecture understanding, thus improving students' learning motivation.

Keywords Learning Log · Life Log · Smartphone · Lecture System

1 Introduction

Recently, in many universities the information terminals such as note PC, workstations, servers and mobile phones are used successfully during the lectures. Also, there are many e-learning systems [1–7] that use these devices. The amount of information that a lecturer transmits to the participant during the lecture can be improved by using different information terminals. However, in a lecture, if participants' motivation for learning is low, the learning results are not good.

N. Yamamoto (✉) · T. Wakahara
Department of Information and Communication Engineering,
Fukuoka Institute of Technology, 3-30-1 Wajiro-higashi, Higashi-ku,
Fukuoka 811-0295, Japan
e-mail: nori@fit.ac.jp

T. Wakahara
e-mail: wakahara@fit.ac.jp

However, in universities is required to increase the learning motivation using information terminals.

Usage of the desk-top computers and notebook PCs for lecture may be inconvenient and they occupy a lot of space. Therefore, it will be better that students use small and lightweight terminals like Personal Digital Assistant (PDA) devices. Also, because of wireless networks are spread over university campuses, it is easy to connect mobile terminals to the Internet and now the students can use mobile terminals in many lecture rooms, without needing a large-scale network facility.

In this paper, we consider a method of acquiring/utilizing the study record, which improves students' motivation for learning. In this our research, we use smartphones as information terminals.

2 Learning System

In this section, we consider the learning systems in universities and investigate the problems they have during the lectures. As solution of these problems, we propose the use of lecture study records (logs).

2.1 Learning at Universities

During lectures in university, very often are used information terminals such as computers and projectors to display the distributed data in the Web and present the power point files or pdf files. Thus, the amount of information that a lecturer transmits to the participant in a lecture is improving by use of information terminals. In a lecture, if students' motivation for learning is low, their knowledge and learning ability will not be improved [8, 9]. However, in universities is required to increase the learning motivation using information terminals.

2.2 e-Learning System

In order to check the students' concentration, the lecturer carries out periodical tests. The lecturer can control the lecture by checking the tests results. These methods have been used in conventional learning systems, but we can also use them in e-Learning systems [1–5]. In fact, the tests do not require time and effort for implementation and processing of the results is easy. With the spread and miniaturization of an information terminal, the students can learn anywhere and anytime using smartphones [6, 7]. If a student utilizes an e-Learning system

positively, it will have a high learning efficiency. However, an e-learning system can't increase the learners' motivation.

2.3 Learning-Logs during a Lecture

In order that students can use the content of the lectures for learning in the future, the lectures are recorded. However, how the contents of a lecture are saved correctly is an important issue. Also, the mechanism that distributes lecture record efficiently is required. But, in such kind of system, the student motivation will influence the learning efficiency.

In this paper, we consider an interactive learning process in order to increase the motivation of the students for learning. Therefore, we save the students' active actions as study their records. A student is enforced to be in interactive learning status because the lecturer performs frequently actions during the lecture. Also, by using the recorded information, the lecturer can adjust the speed of a lecture. As a result, the learning process is more efficient.

3 Network Environment

In order to perform the study records, all students' smartphones need to connect to the network. In order to connect the smartphones to the network, the information outlet for each seat is required. It is difficult to install the information outlets in all lecture rooms. Moreover, maintenance and deployment of many information outlets require a lot of expenses.

However, now it is easy to make Wi-Fi connection with mobile terminals such smartphones. We installed the terminal adopter for Wi-Fi connection to improve the network environment for the lecture room. It should be noted that many devices can make Wi-Fi connection simultaneous during the lecture.

4 Smartphone Application Support for Lectures

In this section, we present the software configuration for lecture record. We install the server for performing the lecture records in a LAN environment. The records are recorded on the server database. Each student and the lecturer use their smartphones to connect with the server through the wireless network during the lecture and the lecturer can check the records and take appropriate actions.

4.1 Lecturer's Smartphone Application

The application software in the lecturer's smartphone terminal consists of the lecture control program that controls the lecture and the study record display program that displays the student's study record.

We show the function of a lecture control program below.

- (T1) The progress of a lecture can be checked by a "point" and a "selection type examination". The "point" describes the main point of the contents of a lecture.
- (T2) A lecturer can progress the lecture by moving the "point" or "selection type examination" to the next part. The lecturer can ask students about the lecture difficulty and speed of progress at the time of progress of the "point." The replies of the students for the lecture difficulty and lecture speed are recorded in the server as study records.

The study record display program consists of the following functions.

- (T3) The lecture difficulty and lecture speed of progress that the students select and the accuracy rate of the "selection type examination" are displayed on the screen of a lecturer's smartphone terminal in real time.
- (T4) After the end of a lecture, the displays of (T3) can be accessed by students.

4.2 Student's Smartphone Application

Using their smartphone terminals, the student can actively participate in the lecture by simple operations. The functions of the students' smartphone applications are as follows.

- (S1) The students login to the server through a wireless network at the time when the lecture starts.
- (S2) At the time when the lecture moves the "point" by his application to progress the lecture, the students reply for the lecture difficulty and the lecture speed of progress. The students can choose a reply operation at the time of selection test for making questions for the exam.

4.3 Lecture Flow

The flow of the lecturer's application, student's application, and the study record server described above are shown below.

- [Teacher01] The lecturer uses his smartphone application to connect to the server
- [Server01] The attendance registration for a student is started

- [Student01] The students use smartphone application and login to a server
- [Server02] A server notifies the attendance situation to the lecturer's smartphone application
- [Teacher02] After that the lecturer pushes the start button to start the lecture
- [Teacher03] The "point" shift to a student who makes questions for the exam of a selection type problem is directed to a server
- [Server03] Next "point" or selection type examination is transmitted to a student. Then, the "point" or a selection type examination is recorded
- [Student02] At the moment of "point" shift, for a defined period of time the student replies the lecture difficulty and lecture speed of progress. When a selection type examination is decided, the student answers in a defined period of time
- [Server04] The server collects the information of [Student02] and sends it to the lecturer's smartphone terminal application. The total information is saved as study record in the server
- [Teacher04] The total data of lecture difficulty and lecture speed of progress that the student answered is displayed. Then when the selection type examination is set by [Teacher03], the problem answer rate is displayed
- [Teacher05] When shifting to the next "point", it returns to [Teacher03]
- [Teacher06] In order to end the lecture, the lecturer connects to the server
- [Server05] The end of a lecture is transmitted to student application and the recording process is ended
- [Student03] Logoff. The end of a lecture is displayed

5 Evaluation Experiment

We performed experimental evaluation of the study record system. In the evaluation experiment, we used the lecture room with a capacity of 50 seats. We carried out two lectures of the same contents for two classes and the number of students was 40. We compared the learning effect by the case where it is not used with the case when a study record system is used.

One of the lectures was performed for 60 min. We carried out the quiz (ten-question full marks) for the degree of understanding and after that we checked the learning effect (See Table 1). In both classes, in those who students use the study record system, the average mark of the degree of understanding is ten percent - .5 premiums and the number of failures is decreased. Therefore, the study record system has good effects for improving students' motivation for learning.

Table 1 The degree of understanding test result after a lecture

	Lecture 1	Lecture 2
Class A [41 persons]	Used the Study Logs 91 (5)	Not Used 65 (18)
Class B [45 persons]	Not Used 80 (14)	Used the Study Logs 70 (9)

Average mark (the number of unsuccessful applicants)

6 Conclusions

In this paper, we presented the study record system to improve the students' motivation for learning. As information terminals are used smartphones. We carried experiments during real lectures. The results showed that the proposed study record system can improve degree of understanding the lecture. Therefore, the study record system has a good effect for improving students' motivation for learning. In our future work, we will carry out extensive experiments to evaluate the proposed system.

References

1. Underwood Jean, Szabo Attila (2003) Academic offences and e-learning: individual propensities in cheating. *Br J Educ Technol* 34(4):467–477
2. Harashima H (2004) Creating a blended learning environment using Moodle. The Proceedings of the 20th Annual Conference of Japan Society of Educational Technology, 23-25 September 2004, pp. 241–242
3. Brandl K (2005) Are you ready to “Moodle”? *Lang Learn Technol* 9(2):16–23
4. Dagger D, Connor A, Lawless S, Walsh E, Wade VP (2007) Service-oriented e-learning platforms: from monolithic systems to flexible services. *Internet Comput IEEE* 11(3):28–35
5. Patcharee B, Achmad B, Achmad HT et al (2013) Collaborating remote computer laboratory and distance learning approach for hands-on IT education. *IPSJ J* 54(1)
6. Emi K, Okuda S, Kawachi Y (2013) Building of an e-learning system with interactive whiteboard and with smartphones and/or tablets through electronic textbooks. *IPSJ SIG Notes* 118(3): 1–4
7. Yamaguchi S, Ohnichi Y, Nichino K (2013) An efficient high resolution video distribution system for the lecture using blackboard description. *Tech Rep IEICE* 112(190):115–119
8. Hirayama Y, Hirayama S (2001) An analysis of the two-factor model of learning motivation in university students. *Cult soc sci* 41:101–105
9. Ichihara M, Arai K (2006) Moderator effects of meta-cognition: A test in math of a motivational model. *Jpn J Educ Psychol* 54(2):199–210

Design and Implementation of H.264/AVC Reverse Biorthogonal Wavelet-Based Flexible Macroblock Ordering

Jing-Siang Wei, Zeng-Yao Lin and Chian C. Ho

Abstract Evolved from conventional Flexible Macroblock Ordering (FMO) that is coded out of raster sequence in spatial domain, this paper presents Wavelet-domain slice group partition and unequal error protection for H.264/AVC video communication. In detail, this paper develops Wavelet-based FMO (WFMO) algorithm to adaptively allocate macroblocks into 4 slice groups based on Reverse Biorthogonal (rbio) Wavelet transform, and then adopts unequal Reed-Solomon error correction to enhance the robustness of the packet carrying the slice group of most significance and psychovisual sensitivity. Experimental results show H.264/AVC codec with proposed Reverse Biorthogonal (rbio) WFMO can achieve better subjective and objective video quality under various packet loss conditions than that without FMO and that with conventional FMO. On the other hand, a DaVinci embedded platform implementation of H.264/AVC surveillance camera featuring rbio WFMO is accomplished. Implementation results demonstrate the video communication quality of H.264/AVC surveillance camera featuring rbio WFMO is superior under error-prone network environments and feasible for embedded real-time applications.

Keywords H.264/AVC · Flexible macroblock ordering · Reverse biorthogonal wavelet · DaVinci embedded platform

1 Introduction

The demand for low-bitrate and reliable video communication over error-prone wireless network has been growing dramatically. The latest block-based H.264/AVC video codec standard featuring high compression and error resilience can

J.-S. Wei · Z.-Y. Lin · C. C. Ho (✉)

Embedded SoC Laboratory, Department of Electrical Engineering, National Yunlin University of Science and Technology, Yunlin County, Douliou 64002, Taiwan, ROC
e-mail: futureho@yuntech.edu.tw

fulfill the demand and requirements smoothly, and it has popularly been applied to video conferencing, remote surveillance, distance learning, and streaming TV. However, since high-performance H.264/AVC standard emerged, all relevant researches have so far been focusing on redundancy of information in intra frames (spatial domain) or in inter frames (temporal domain). In the same way, researches on Flexible Macroblock Ordering (FMO) have so far been focusing on spatial-domain slice group partition or temporal-domain slice group partition.

FMO is one of the new error resilience methods involved in H.264/AVC [1–3]. With FMO, H.264/AVC can accomplish more robust transmission of compressed video than former video codec standards in the packet lossy environment. This is because FMO allocates macroblocks into slice groups in non-raster scan order and forms arbitrary-shaped slice groups when each frame is partitioned into more than one slice group. Once the packet loss is inevitably occurred, FMO can help H.264/AVC encoder disperse the distortion risk to anywhere spatially in the decoded frame in a number of flexible ways, and can help H.264/AVC decoder perform error concealment well and easily. With FMO, neighboring macroblocks in the encoded frame can be assigned to different self-contained slice groups and encapsulated to different corresponding packets so that lost macroblocks in the decoded frame can be scattered elsewhere or concealed by neighboring macroblocks.

In H.264/AVC standard, FMO provides several predefined MacroBlock Allocation map (MBAmapping) policies, e.g. well-known dispersed (checkerboard) type, foreground/background type, and explicit type, to adaptively specify which slice group each macroblock belongs to [4]. Figure 1a–c illustrates these three default MBAmapping policies of FMO in H.264/AVC standard. However, in fact, all MBAmapping policies of standardized or newly-released FMO methods in recent years can be merely summarized to two main categories.

One category is MBAmapping policy from spatial domain perspective, such as foreground/background type to divide each frame into a few regions of interest as a high-bitrate slice group and one remaining region of disinterest as a low-bitrate slice group [5], fully explicit type based on each macroblock's encoded bitrate [6], fully explicit type to individually assign each macroblock into three various-importance slice groups by means of each macroblock's reconstruction distortion extent in the decoder [7], foreground/background type to partition the frame into the foreground region as a basic-quality slice group and the background region as an enhancement slice group by motion activity evaluation [8], fully explicit type to classify each macroblock into two various-protection slice groups according to its influence on the decoded video quality after error concealment [9], and error-resilient scheme based on explicit spiral-interleaved-type FMO and dynamic redundant slice allocation depending on two wireless channel fading parameters [10]. The other category is MBAmapping policy from spatial and temporal domain perspective, such as 3D FMO MBAmapping to scatter the distortion effect in the current frame to the previous and next frames during packet loss [11]. Figure 1d illustrates MBAmapping policy of 3D FMO method.

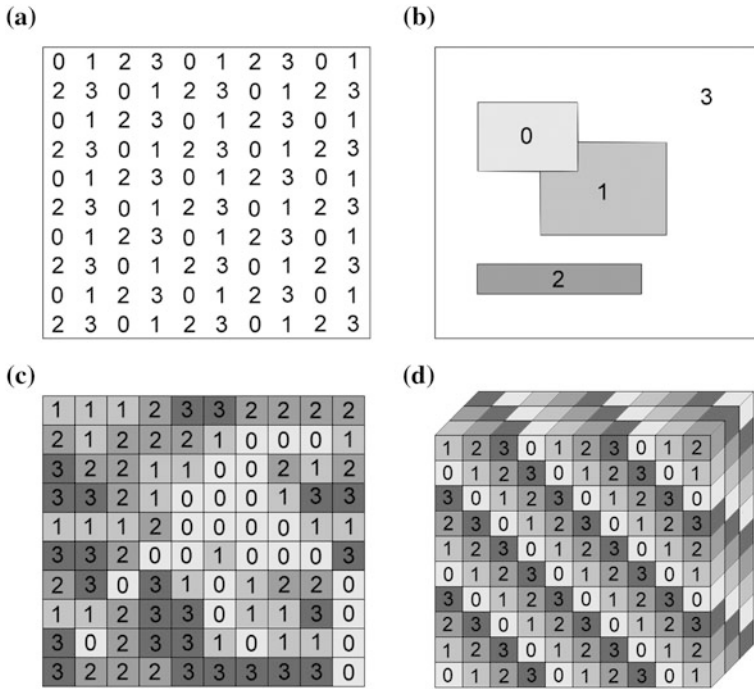


Fig. 1 MBAMap policies of conventional FMO methods

In this paper, a novel H.264/AVC FMO scheme is proposed from spatial-frequency domain perspective. It intends to extract the most psychovisually sensitive component from each frame as a significant slice group. In the proposed algorithm, each original frame is divided into 4 quarter-size slice groups by single-level two-dimensional Reverse Biorthogonal (rbio) Wavelet transform, and each slice group is encoded and packetized separately in the original H.264/AVC encoder. Then H.264/AVC encoder applies unequal Reed-Solomon error correction to enhance the robustness of the relatively significant and lowest-frequency slice group. So this proposed FMO algorithm is referred to as Wavelet-based FMO (WFMO).

2 Proposed rbio WFMO

In the last decade, Wavelet theory has developed itself as a versatile and promising tool for many fields, like modern signal processing, digital wireless communication, and interdisciplinary informatics. More technically, Wavelet theory has been playing an important role in time–frequency analysis techniques, like multi-resolution signal processing, multimedia subband coding, and Wavelet series

Table 1 Property comparison between Wavelet families

Wavelet Properties	Haar	Daubechies	Coiflet	Biorthogonal	Reverse biorthogonal
Compact support	○	○	○	○	○
Symmetry	○	×	×	○	○
Orthogonality	○	○	○	×	×
Smoothness	×	○	○	○	○

expansions. Despite there are lots of common Wavelet families eligible to perform frame-to-slice-group decomposition and slice-group-to-frame reconstruction for H.264/AVC codec, the following 4 key properties can be taken into account to make the best choice [12–15].

1. Compact support: This property determines if the filter length is finite so that the implementation is feasible.
2. Symmetry: This property is especially useful for linear-phase edge coding. In addition, human visual system is insensitive to the symmetric quantization error.
3. Orthogonality: This property preserves the lowest-dimensional representation and simplifies the computational complexity. But it is not necessarily essential for image decomposition and reconstruction.
4. Smoothness: This property brings image reconstruction a lower and smoother error. It is related to the filter length.

Table 1 compares pros and cons of 5 common Wavelet families, including Haar (haar), Daubechies (db), Coiflet (coif), Biorthogonal (bior), and Reverse Biorthogonal (rbio), on account of 4 aforementioned properties. Here, ○ represents the Wavelet family conforms to the requirement of the property, and × represents it does not. From Table 1, it reveals that bior and rbio Wavelet families are better at image decomposition and reconstruction for H.264/AVC codec. Because bior and rbio Wavelet families not only can accomplish all desired properties of compact support, symmetry, and smoothness by relaxing the orthogonal condition, but also can apply two sets of dual basis functions to image decomposition and reconstruction separately.

In the meanwhile, this paper runs a H.264/AVC multimedia communication simulation through an ideal packet lossless channel as shown in Fig. 2. It concentrates on determining which Wavelet family is the best method for frame-to-slice-group decomposition at the pre-state of H.264/AVC encoder and slice-group-to-frame reconstruction at the post-stage of H.264/AVC decoder. Figure 2 shows the architecture of H.264/AVC multimedia communication simulation with various Wavelet-based decomposition/reconstruction methods, and Table 2 lists all adopted simulation parameters of H.264/AVC JM Reference Software [16]. “Forman” video sequence with CIF resolution is used as a testing pattern. Figure 3a, b displays Peak Signal-to-Noise Ratio (PSNR) and bitrate comparison between H.264/AVC simulations with various Wavelet-based decomposition/

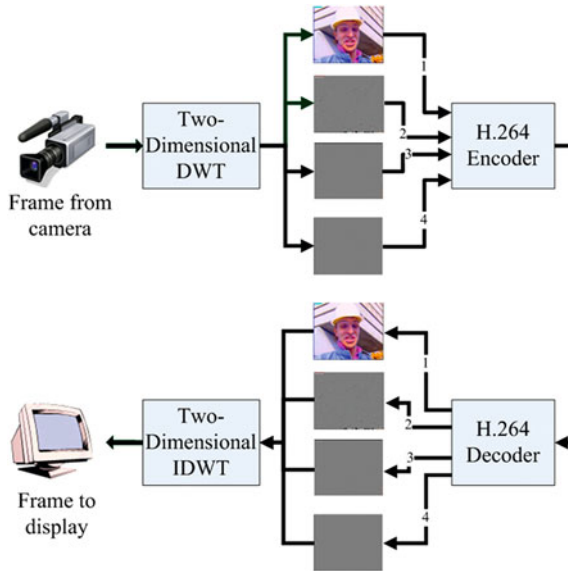


Fig. 2 Architecture of H.264/AVC codec simulation with various WFMO

reconstruction methods, in terms of Quantization Parameter (QP) values. In Fig. 3a, b the number appearing behind the short names of Wavelet families indicates the order of Wavelet filters. bior and rbio Wavelet families have two numbers separated by a dot because of two orders available for decomposition and reconstruction filters respectively. From Fig. 3a, b it is verified that the objective decoded video quality of H.264/AVC codec with rbio WFMO is the best among 5 common Wavelet families, despite its transmission bitrate is merely the second lowest. Therefore, this paper decides to apply “rbio1.3” Wavelet transform to the proposed WFMO algorithm for H.264/AVC codec.

Figure 4 illustrates the complete architecture and flowchart of H.264/AVC codec with proposed rbio WFMO and unequal error protection. Similar to conventional foreground/background-type FMO, in H.264/AVC encoder, the slice

Table 2 Simulation parameters of H.264/AVC with various WFMO

Reference software	JM 10.2
Profile	Baseline
Frame size	352 × 288 (CIF)
Frames to be encoded	20
Intra period	10
Frame rate	30 fps
Entropy coding	UVLC
Out file mode	RTP
Error concealment	Motion copy

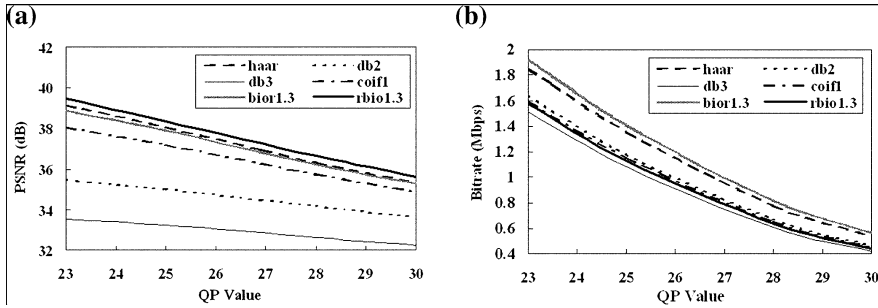
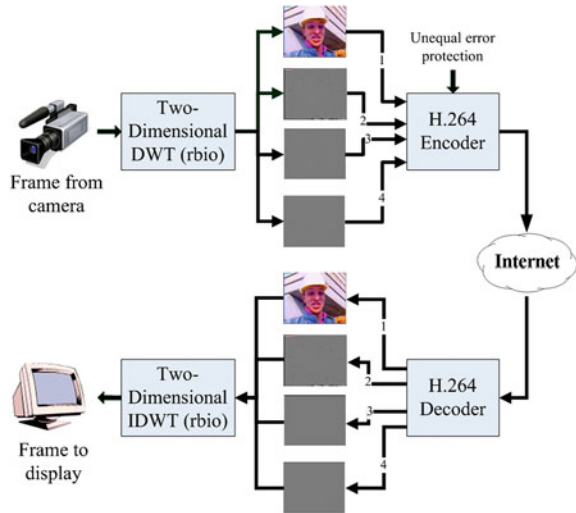


Fig. 3 **a** Objective video quality comparison and **b** transmission bitrate comparison, between H.264/AVC with various WFMO methods

Fig. 4 Architecture of H.264/AVC codec with proposed rbio WFMO



group of most significance and psychovisual sensitivity is encoded and packetized with stronger Reed-Solomon protection than all three other slice groups [17, 18]. Once the packet loss over the unreliable network is happened, H.264/AVC decoder utilizes Reed-Solomon protection as well as possible to correct the lowest-frequency slice group while working a simple error concealment on all three other slice groups with poor or even no error protection. Therefore, with the proposed rbio WFMO algorithm, packet loss effect does not destroy the lowest-frequency slice group seriously or produce block artifacts from imperfect error concealment, but just causes the high-frequency edges blurred.

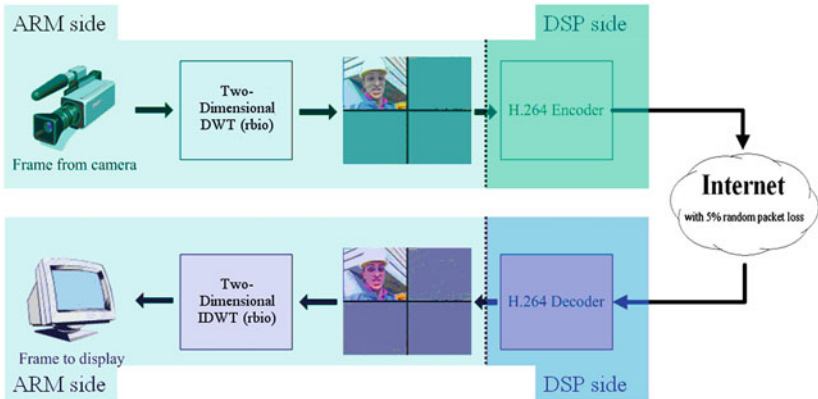
3 Implementation Methodology

Across most H.264/AVC video communication applications, not only rate-distortion optimization but also real-time processing is the fundamental requirement of H.264/AVC codec implementation. Especially, it definitely takes longer for H.264/AVC codec to run on the embedded platform. As a result, DaVinci, the asymmetric dual-core embedded platform composed of ARM general-purpose processor and TI digital signal processor, is rightly the best solution to the dilemma between frequently-updated protocol stacking and real-time codec computation [19]. In addition, DaVinci supports open-source embedded Linux operating system, and offers feature-rich video software development kit [20]. Comprehensive peripheral interfaces like Ethernet, camera, LCD, harddisk, and USB, are also available [21]. Thus, through high-performance and cost-effectiveness DaVinci embedded platform, H.264/AVC codec implementation can be extensively integrated and applied to video conferencing, remote surveillance, distance learning, and streaming TV.

Figure 5a illustrates the implementation architecture of H.264/AVC codec featuring proposed rbio WFMO on DaVinci embedded platform. In order to manifest the error-resilience effect of proposed rbio WFMO for H.264/AVC codec, H.264/AVC codec architecture with conventional dispersed-type FMO schemes as shown in Fig. 5b is also implemented for comparison. Here, both the network environments for Fig. 5a, b are simulated by SHUNRA\Cloud WAN Emulator with 5 % packet loss rate. Because FMO methods can work as a preprocessing operation before H.264/AVC encoder at the transmitter end, and work as a post-processing operation after H.264/AVC decoder at the receiver end. From Fig. 5a, it can be seen that the proposed WFMO algorithm can be easily implemented onto ARM general-purpose processor at the transmitter and receiver ends, and the original H.264/AVC codec must still be implemented onto TI digital signal processor at the transmitter and receiver ends. So the effort and complexity of the proposed WFMO implementation on DaVinci embedded platform is really insignificant. In Fig. 5a, each incoming frame from the camera is divided into four quarter-size slice groups by two-dimensional rbio Wavelet transform, and similarly, in Fig. 5b, each incoming frame from the camera is divided into four quarter-size slice groups by conventional FMO of dispersed (checkerboard) type.

Figure 6a, b randomly demonstrate four subsequent displayed frames at the H.264/AVC receiver with proposed rbio WFMO and with conventional dispersed-type FMO, respectively, under the network condition of 5 % packet loss rate. The subjective video quality comparison of the implementation results in

(a)



(b)

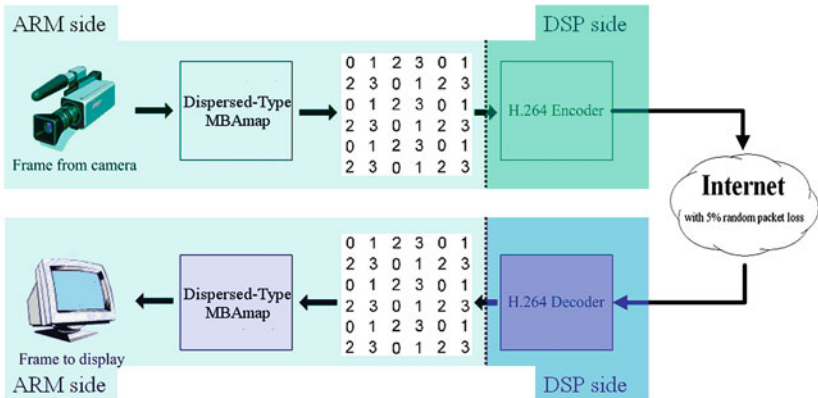


Fig. 5 Architecture of H.264/AVC codec implementation with a proposed rbio WFMO and b conventional dispersed-type FMO

Fig. 6 is quite similar to that of the simulation results. The proposed WFMO implementation indeed disperses the distortion effect to high-frequency band rather than elsewhere in spatial domain, so the decoded video quality of the proposed rbio WFMO is better than that of conventional dispersed-type FMO under packet loss condition.

(a)



(b)

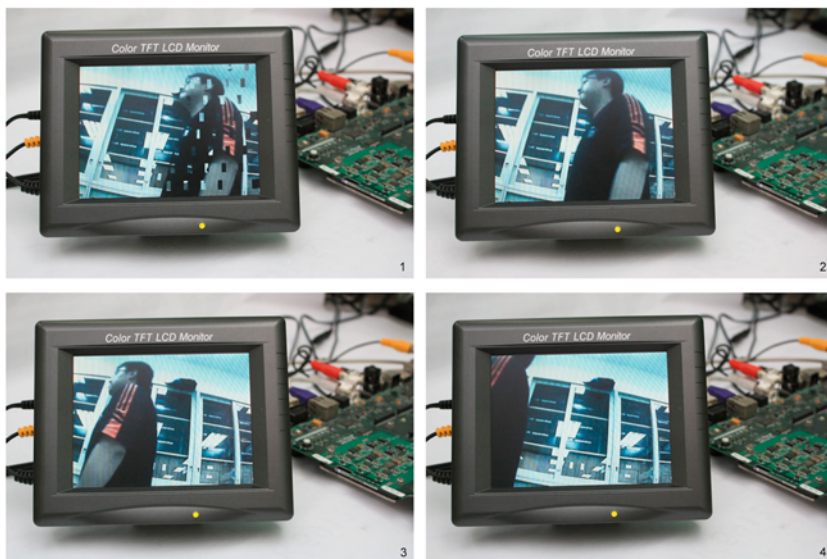


Fig. 6 Subjective video quality comparison at the H.264/AVC receiver with **a** proposed rbio WFMO and **b** conventional dispersed-type FMO

4 Conclusions

In the paper, rbio Wavelet-domain slice group unit is a brand-new concept for FMO methods in H.264/AVC standard, against conventional spatial domain or temporal domain slice group unit. The proposed rbio WFMO algorithm with unequal error protection scheme can help H.264/AVC encoder disperse the distortion risk to anywhere high-frequency in the decoded frame by rbio Wavelet transform, and can help H.264/AVC decoder perform unperceived error concealment. Once the packet loss effect is inevitably occurred, the proposed rbio WFMO algorithm sacrifices the high-frequency fidelity in the decoded frame. Moreover, through DaVinci embedded implementation, it is verified that the proposed rbio WFMO algorithm can perform well and can be smoothly integrated to H.264/AVC surveillance camera applications.

References

1. Wenger S (2003) H.264/AVC over IP. *IEEE Trans Circuits Syst Video Technol* 13:645–656
2. Wiegand T, Sullivan GJ, Bjntegaard G, Luthra A (2003) Overview of the H.264/AVC video coding standard. *IEEE Trans Circuits Syst Video Technol* 13:560–576
3. Wenger S, Horowitz M (2002) FMO: flexible macroblock ordering. *JVT-C089*
4. Richardson IEG (2003) H.264 and MPEG-4 video compression: video coding for next-generation multimedia. Wiley, Chichester
5. Dhondt Y, Lambert P, Notebaert S, de Walle RV (2005) Flexible macroblock ordering as a content adaptation tool in H.264/AVC. In: *Proceedings of SPIE*, pp 44–52
6. Hantanong W, Aramvith S (2005) Analysis of macroblock-to-slice group mapping for H.264 video transmission over packet-based wireless fading channel. In: *Proceedings of IEEE midwest symposium on circuits and systems*, vol 2. pp 1541–1544
7. Thomos N, Argyropoulos S, Boulgouris NV, Strintzis MG (2005) Error-resilient transmission of H.264/AVC streams using flexible macroblock ordering. In: *Proceedings of European workshop on the integration of knowledge, semantics and digital media technology*, pp 183–189
8. Benierbah S, Khamadja M (2005) A new technique for quality scalable video coding with H.264. *IEEE Trans Circuits Syst Video Technol* 15:1332–1340
9. Im SK, Pearmain AJ (2007) Error resilient video coding with priority data classification using H.264 flexible macroblock ordering. *IET Image Proc* 1:197–204
10. Katz B, Greenberg S, Yarkoni N, Blaunstien N, Giladi R (2007) New error-resilient scheme based on FMO and dynamic redundant slices allocation for wireless video transmission. *IEEE Trans Broadcast* 53:308–319
11. Ogunfunmi T, Huang WC (2005) A flexible macroblock ordering with 3D MBAMAP for H.264/AVC. In: *Proceedings of IEEE international symposium on circuits and systems*, vol 4. pp 3475–3478
12. Grgic S, Grgic M, Zovko-Cihlar B (2001) Performance analysis of image compression using wavelets. *IEEE Trans Industr Electron* 48:682–695
13. Zettler WR, Huffman J, Linden DCP (1990) Application of compactly supported wavelets to image compression. In: *Proceedings of SPIE image processing algorithms and techniques*, vol 1244, pp 150–160

14. Cohen A, Daubechies I, Feauveau JC (1992) Biorthogonal bases of compactly supported wavelets. *Commun Pure Appl Math* 45:485–500
15. Grgic M, Ravnjak M, Zovko-Cihlar B (1999) Filter comparison in wavelet transform of still images. In: *Proceedings of IEEE international symposium on industrial electronics*, vol 1, pp 105–110
16. H.264/AVC JM (2009) Reference software manual. <http://iphome.hhi.de/suehring/tml/>
17. Thomos N, Argyropoulos S, Boulgouris NV, Strintzis MG (2005) Error-resilient transmission of H.264/AVC streams using flexible macroblock ordering. In: *Proceedings of European workshop on the integration of knowledge, semantics and digital media technology*, pp 183–189
18. Wenger S (1999) Error patterns for internet experiments. In: *ITU-T Standardization sector*, document Q15-I-16r1
19. Texas Instruments Embedded Processors Wiki. Developer community for DaVinci and OMAP technology. http://wiki.davincidsp.com/index.php/Main_Page
20. Texas Instruments (2006) DVSDK getting started guide
21. Texas Instruments (2006) DVEVM getting started guide

Design and Characteristics of Two-Dimensional Color Code Editor with Dotted Images

Toshihiko Wakahara, Damri Samretwit, Toshitaka Maki
and Noriyasu Yamamoto

Abstract In recent years, QR code is widely used in the accessing to the Internet by cellular phones. As this code is a set symbol of simply black and white dots, it is very simple and insipid. In order to improve this weakness, a color two-dimensional color code editor with dotted images has been developed. This paper presents the design method and reading characteristics of the code editor. The experimental results show good performances of the decoding characteristics by the existing QR decoder and the effectiveness of the editor is also confirmed.

Keywords Two-dimensional code · QR code · Image processing · Color coding

1 Introduction

Recently Quick Response (QR) code [1] has been widely used in the accessing the various Internet services by mobile phones or smart phones. As it is standardized internationally by ISO/IEC [2] and is very convenient, it is widespread used globally in various services. But as the ordinary QR code is composed of simply

T. Wakahara (✉) · D. Samretwit · T. Maki · N. Yamamoto
Information and Communication Engineering, Fukuoka Institute of Technology, 3-30-1
Wajiro-higashi, Higashi-ku, Fukuoka-shi 811-0295, Japan
e-mail: wakahara@fit.ac.jp

D. Samretwit
e-mail: mgm100007@bene.fit.ac.jp

T. Maki
e-mail: s09b1046@bene.fit.ac.jp

N. Yamamoto
e-mail: nori@fit.ac.jp

black and white modules, the visibility is not good. The proposed two-dimensional color code editor provides a means to solve the above problems.

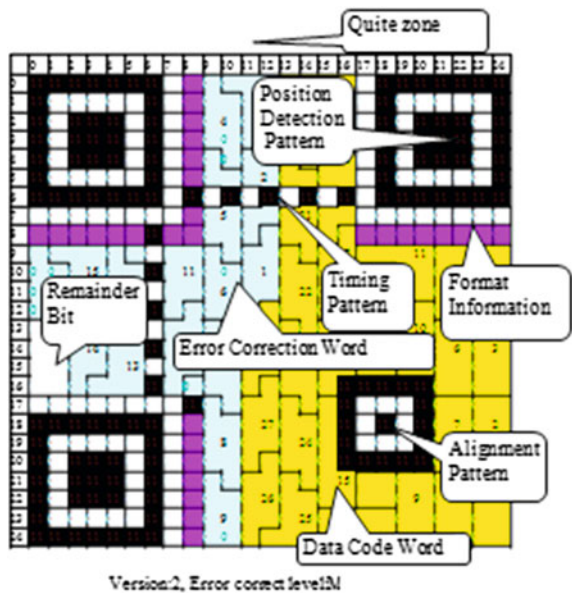
This paper presents a two-dimensional color code editor which can draw the colorful dotted image, its configuration and reading characteristics. The outline of QR code is described in Sect. 2. In Sect. 3, the configuration and characteristics of the editor is discussed. The experiments and their results are shown in Sect. 4. Finally, conclusions are described in Sect. 5.

2 QR Code Outline

2.1 Features of QR code

Figure 1 shows a QR code example of version 2, which consists of 25×25 modules and quite zone. In this figure, there are special marks, 3 position detection patterns and 1 alignment pattern and 28 data code words (yellow) and 16 error correcting words (light blue). There are 40 versions and a maximum size of QR code symbol is 177×177 modules, which becomes bigger 4 modules per one version. Each dot consists of a black (dark) or white (bright) module. Although there are 7 modules of a remainder bit in the left side, there is no pad codeword. This symbol is set at the optimal version and there is no redundancy codeword. If the version is selected more than 2, the pad codeword generates and a redundancy area becomes large. As the dotted image is inserted into the redundancy area of

Fig. 1 QR code example (version 2-M)



this QR code, this area is better to be large. There are some conditions for image insertion.

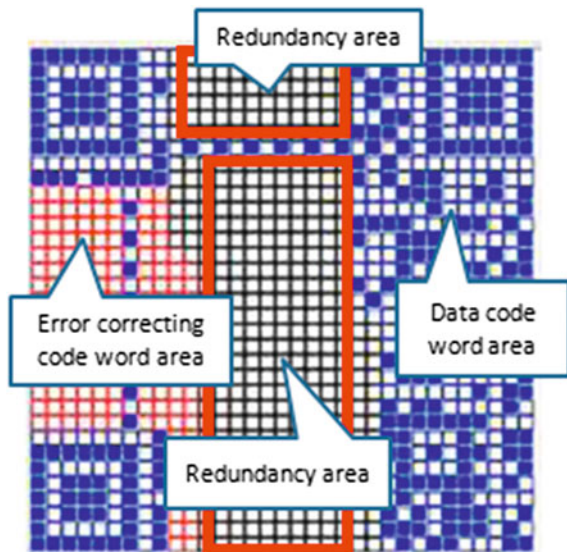
- (1) If the version number is larger than 6, the redundancy area becomes smaller because plural alignment patterns generate.
- (2) If the error correction level is high, there are many error correction code words and the redundancy area becomes small.
- (3) If RS (Reed Solomon) code are partitioned by the plural blocks, data code words are more complex arrangement and it's hard to draw the image.

The structure of the QR code is shown in Fig. 2. The main redundant modules are calculated as shown in Fig. 3.

2.2 Related Works

As the QR code is composed of simply black and white dots, design is not good

Fig. 2 Redundancy area



and it is very monotonous and innocent. In order to improve the appearance and design of the QR code, D-qr.net [3], QR-JAM [4] or LogoQ [5] have been developed. Then colorful MultifunctionQR [6] and colorful QR code [7] have also been developed. The Unitag [8] has also been developed in France. It can be inserted characters and logos. These examples are shown in Figs. 4 and 5.

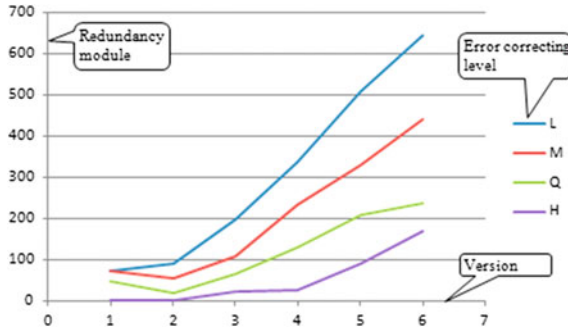
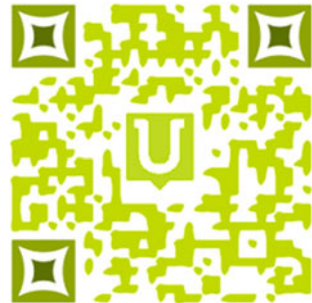


Fig. 3 Redundancy area capacity

Fig. 4 MultiFunctionQR



Fig. 5 Unitag



3 Two-Dimensional Color Code Editor

3.1 Color Characteristics and Monochrome Conversion

Black dots and white dots of QR code are corresponds to dark modules and bright modules, respectively. Although the existing QR decoder can read the color components, the reading characteristics are not clear and it may depend on the maker's decoding algorithms. The color of dark module can be read as black and the bright module can be read as white [9]. For example, the deep red, blue and

green colors are read as dark color. On the other hand, light blue, yellow, green are read as bright color. Figure 6 shows these characteristics.

The color is specified by RGB values or HSB (Hue, Saturation and Brightness). Although brightness and luminance show the similar brightness characteristics, luminance may include the human point of view. In this study, luminance value is used by monochrome conversion. Equation (1), which shows luminance value, can be obtained by converting from RGB signal values to the monochrome signal value.

$$Y = 0.299R + 0.587G + 0.114B$$

$$0 < R, G, B < 255. \tag{1}$$

The existing QR reader may usually be considered to be judged by the luminance value.

3.2 Two-Dimensional Color Code Editor

The two-dimensional color code editor can make not only usual QR code but also colorful two-dimensional code or colorful two-dimensional code with dotted images. The process flow of the code editor is shown in Fig. 7.

In Fig. 7, the feedback process is introduced if the dotted image cannot be drawn. In that case, by changing the parameters, such as the version and error correction level of QR code, the dotted images may able to be drawn. Any color of dots can be drawn in the redundancy area. But each color of dots in the data cord word area and error correction code word area can be changed by considering the above dark and bright luminance value. Figure 8 shows the interface of the two-dimensional color code editor. In this window, we can draw the dotted image again and again by pushing a pencil button and an eraser button. Then each color of any module can be changed in the interface of Fig. 9. In this interface, RGB value is

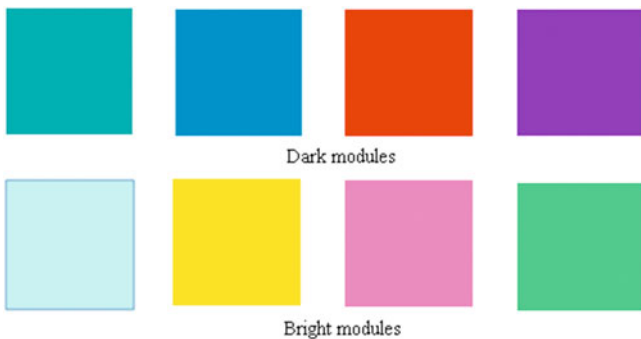


Fig. 6 Dark and bright modules

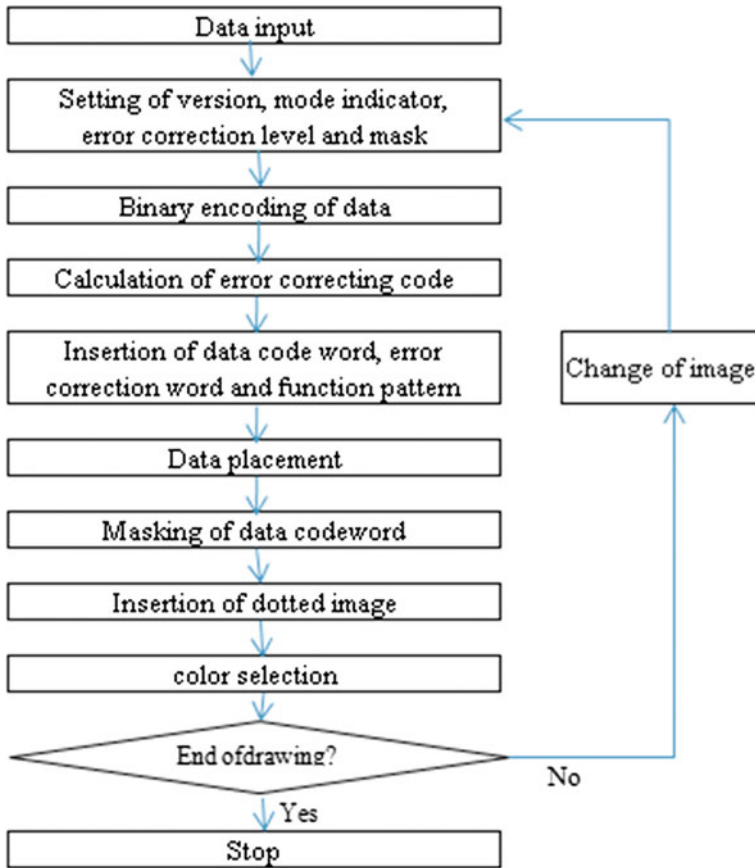


Fig. 7 Process flow of two-dimensional color code editor

shown and the luminance value is also shown in a red square box. If this luminance value is less than 50, the module color is judged to be dark and if the value is more than 90, the module is judged to be bright.

The colorization example of a two-dimensional code is described in the following:

- Step 1: At first, the data is inputted by setting the version and error correction level. A fundamental QR code is generated.
- Step 2: The dotted image is drawn in the vertical central part of the code with black and white dot.
- Step 3: The color of this two-dimensional code is converted to appropriate color considering the luminance of the color (Fig. 10).

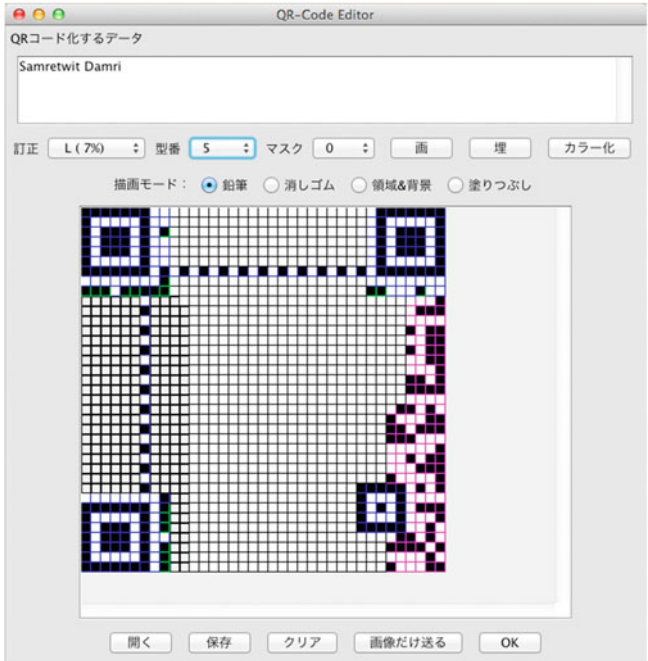


Fig. 8 Two-dimensional color code editor

Figure 11 shows the conversion of color and it can be read by the existing QR decoder.

4 Experiments and Results

The prototype system is configured and the experiments have been carried out. The experimental conditions are shown in Table 1.

The version is set at 5 and the error correction level is L. The reading characteristics by the existing QR decoder are shown in Fig. 12. This figure shows luminance values by change of hue values (from 0: red to 360: red). Bright or dark can be judged when the luminance value is more than 230(90 %). The luminance values of between 128(50 %) and 230 are judged bright or dark, which depends on the conditions. The luminance value of less than 128 is judged as dark. The luminance value is the highest when the hue value is 60, yellow, which is between red and green. This color can be read as bright most easily. On the other hand, the luminance value is the lowest when the hue value is 240, cyan. It is confirmed that the bright or dark is determined by the luminance value and the reference value is gained.



Fig. 9 Color indicator interface



Fig. 10 Typical example of colored two-dimensional code. a Dotted image is inserted, b two-dimensional code, c color conversion

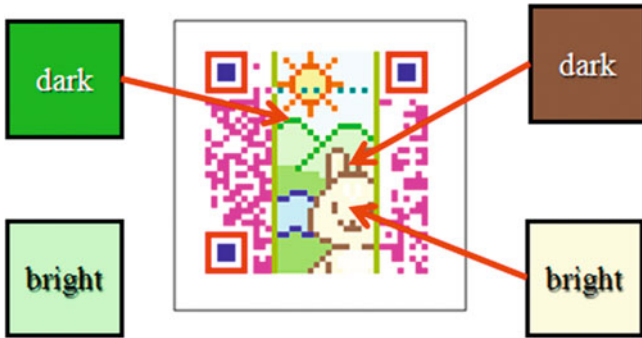


Fig. 11 Dark is converted to green and brown. Bright is converted to light green and light yellow

Table 1 Experimental conditions

Item	Specifications
QR code	Coding data Version Error correcting level 1
QR coding software	Two-dimensional color code editor
QR code display	MacBook Air (11 in.)
Lighting condition	Normal lighting (Fluorescent lamp)
Luminance conditions	80 % luminance
QR code reader	iPhone 4
QR decode software	i-nigma QRReader for iPhone Best barcode scanner

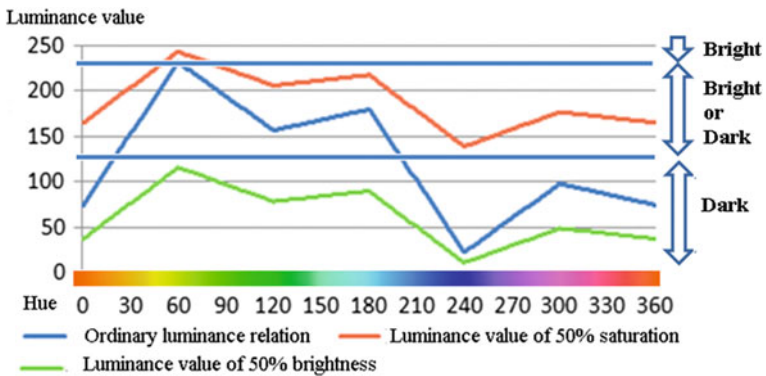


Fig. 12 Reading characteristics of the two-dimensional color code

5 Conclusions

We discussed about the architecture of the two-dimensional color code editor and evaluated the reading characteristics of the prototype by the experiments.

The following results become clear:

- (1) The QR code can be superimposed images in the redundancy area and also be changed colors from simple white and black patterns. The version of the QR code is selected to be less than 6 considering the alignment patterns. Then the error correction level is set to be low to ensure the area.
- (2) The redundant area of the QR code is longitudinal central portion. The colorful dotted images can be superimposed without affecting the error correction function.
- (3) In order to change colors by using the existing QR decoder as it is, the brightness of the color value is better to be set as follows:

Dark modules: less than 50 %

Bright modules: more than 90 %.

References

1. ISO/IEC 18004:2000 Information Technology: Automatic Identification and Data Capture Techniques (Barcode Symbology) QR Code (MOD), June (2000)
2. Japanese Industrial Standards: Two Dimensional Symbol-QR-Code-Basic Specification: JIS X 0510, October (2004)
3. D-qr.net, <http://d-qr.net/>
4. QR-JAM, <http://staff.aist.go.jp/hagiwara.hagiwara/qrjam/index.html>
5. LogoQ, http://logoq.net/logoq/logoq/01_logoq.html
6. MultiFuctionQR, <http://www.tech-jp.com/MultiFunctionQR>
7. colorfulQRcode, http://www.geocities.jp/japan_inf/DotNetBarcode/ColorfulQRCodeMaker/index.html
8. Unitag, <http://www.unitaglive.com/qrcode>
9. Hagiwara M (2011) Decorated 2D codes. J IEICE 94(4):341–343
10. case:MobileDesign, <http://case-mobile-design.com/>
11. Wakahara T, Yamamoto N, Ochi H (2012) Image processing of dotted pictures in the QR code of cellular phone: CSSE. Int J Comput Syst Sci Eng 27(1):73–81
12. QR code.com, Denso Wave Inc.<http://www.qrcode.com/en/codes/iqr.html>

Studies on Loss Evaluation of Bending in Post Wall Waveguide for Microwave Transmission

Hiroshi Maeda, Kazuya Tomiura, Huili Chen
and Kiyotoshi Yasumoto

Abstract Post wall waveguide is important structure for microwave transmission of integrated circuits with multi-layered substrates. It has simple periodic array of metallic or dielectric cylinders between parallel conducting plates. In this study, loss of bending part with the angle of 120° in post wall waveguide was evaluated both numerically and experimentally for microwave. We proposed the best configuration for bending part of the post wall waveguide.

Keywords Post wall waveguide · Bend · Loss · Microwave · Measurement · CIP method

1 Introduction

Post wall waveguides are attracting attentions as transmission line for microwave and millimeter wave. The structure is quite simple such as periodic array of dielectric or metallic cylinders, but shows good confinement of microwaves. As well-known similar periodic structure, photonic crystal (PC) waveguide [1] has intensively studied as substance of conventional metallic rectangular waveguides and optical waveguides using total internal reflection. The PC structure has photonic band gap (PBG) or electromagnetic band gap (EBG) for limited range of frequency band and direction. Authors' group has been investigated transmission characteristics of two dimensional photonic crystal waveguide by numerical method and confirmed the results by scale model in microwave frequency. The experiment by scale model [2, 3] is easily transformed to the post wall waveguide, because both structures consist of periodic array of dielectric or metallic cylinders

H. Maeda (✉) · K. Tomiura · H. Chen · K. Yasumoto
Department of Information and Communication Engineering, Fukuoka
Institute of Technology, Fukuoka 811-0295, Japan
e-mail: hiroshi@fit.ac.jp

[4–7]. In this paper, basic transmission characteristics of bending waveguides with post wall structure are reported. For the waveguide with metallic cylinders, experimental results and numerical results showed same tendency on transmission characteristics. These results are applicable for design of microwave and optical integrated circuits, especially for highly integrated circuits with many bending parts.

2 Setup of the Measurement

In Fig. 1, top view of unit triangular cell is illustrated, together with height of the cylinder. Diameter of the cylinder ϕ is 7.5 mm and the lattice period P is 26.5 mm, and height of the cylinder h is 29.5 mm, respectively. The coordinate axis is also shown in the figure. The longitudinal axis of the cylinder corresponds with polarization direction of electric field, as is shown in Fig. 2. Transverse electric (TE) mode with components (H_x, H_y, E_z) is excited in the input waveguide adapter.

To demonstrate two dimensional experiments, we put periodic metallic cylinders between two aluminum plates, as is depicted in Fig. 3. These aluminum plates were grounded to assume this structure is artificially two dimensional under ‘principle of mirror image’ in electromagnetic theory. These metallic rods were put periodically by using shallow guide holes, which were fabricated by mechanical mill machine with precision order of 1 μm . Material of the cylinder is also aluminum.

Measurements were done by using vector network analyzer Agilent Technologies E5071C after the calibration, which is illustrated in Fig. 4. Coaxial-to-waveguide adapters were used for input and output. Frequency range of the measurement is from 3.6 to 4.2 GHz, which corresponds to operation range of input and output waveguide adapters.

Schematic illustrations of two dimensional post wall waveguides were shown in Fig. 5. In Fig. 5a, fundamental single-layered post wall waveguide with two

Fig. 1 Illustration of unit cell of periodic triangular array

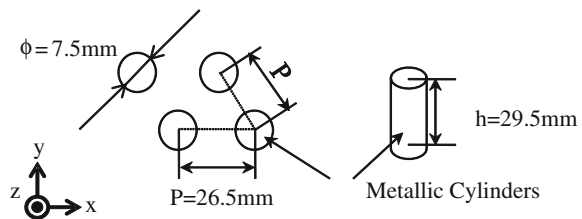
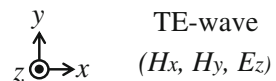


Fig. 2 Polarization of TE-wave and the coordinate system



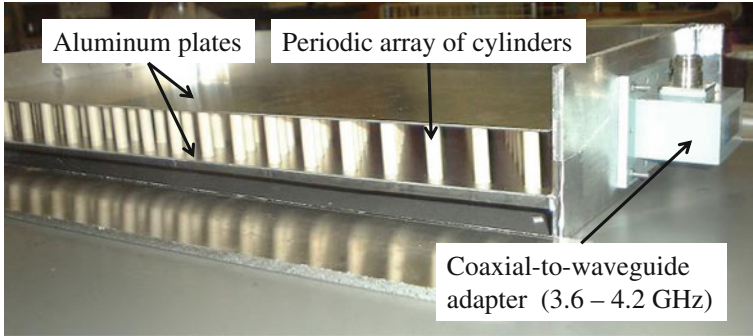


Fig. 3 Side view of a microwave experiment model of two dimensional photonic crystal structure. Through coaxial-to-waveguide adapter, microwave is excited and received

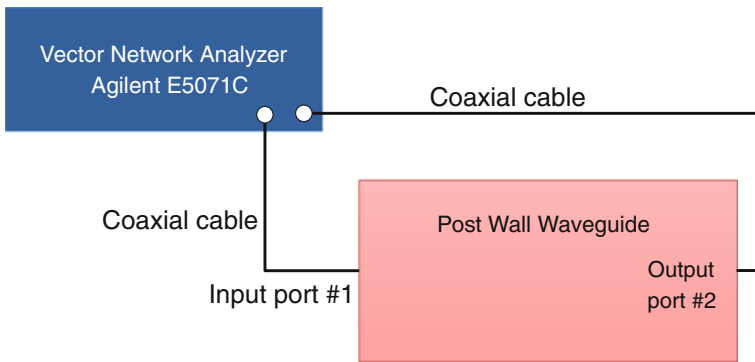


Fig. 4 Experimental setup of microwave measurement

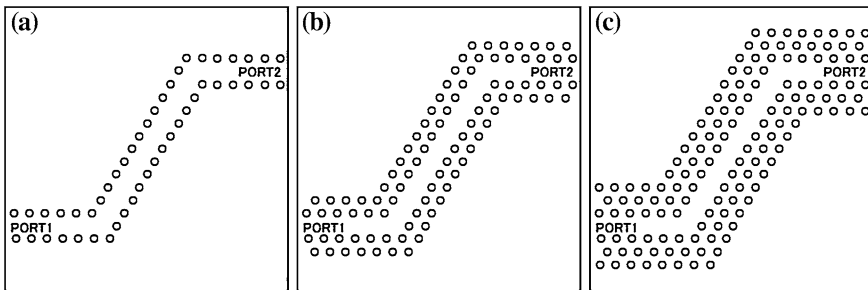


Fig. 5 Illustrations of post wall waveguide with periodic metallic cylinders. a Single-layered b Double-layered c Triple-layered

bending parts is situated, by making use of periodic triangular array in Fig. 1. In Fig. 5b, the waveguide was composed of post wall with double layers. In Fig. 5c, the waveguide is surrounded by triple layers of cylinders.

3 Results of Measurement and Simulation

3.1 Fundamental Results of Bending Waveguides

In Fig. 6, amount of measured transmission S_{21} is shown. The transmission of single-layered bending waveguide which is shown as blue line is the lowest among all of three types of structures. In Fig. 7, calculated results by CIP method [8–12] is shown for typical frequencies. From these results, radiation wave from bending point is expected in single-layered structure. The CIP method is a kind of finite difference scheme and the third order polynomials are used to express profiles. Compared with other conventional numerical technique, there exists a big

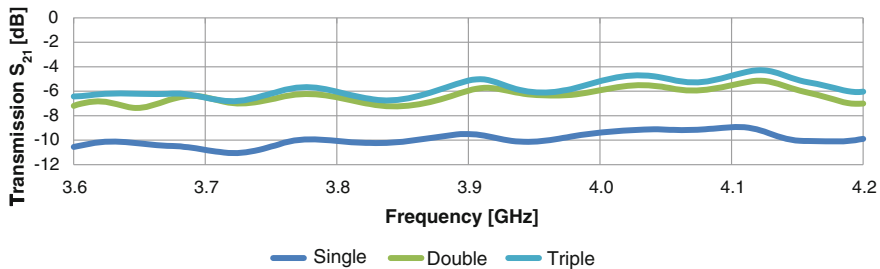


Fig. 6 Measured transmission characteristics of waveguides depicted in Fig. 5a–c

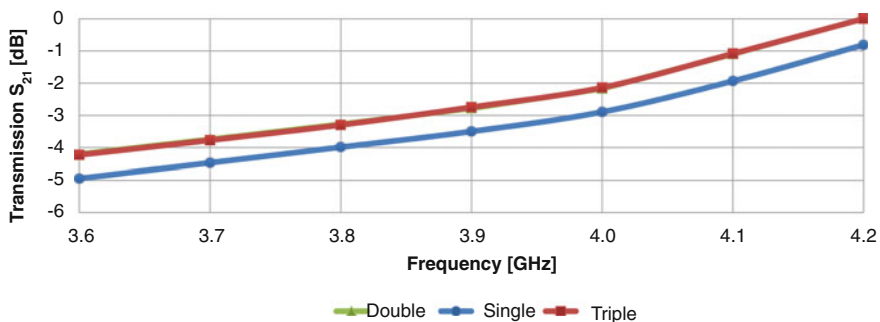


Fig. 7 Calculated transmission characteristics of waveguides depicted in Fig. 5a–c. The result of double-layered waveguide corresponded with that of triple-layered, and is completely hidden behind

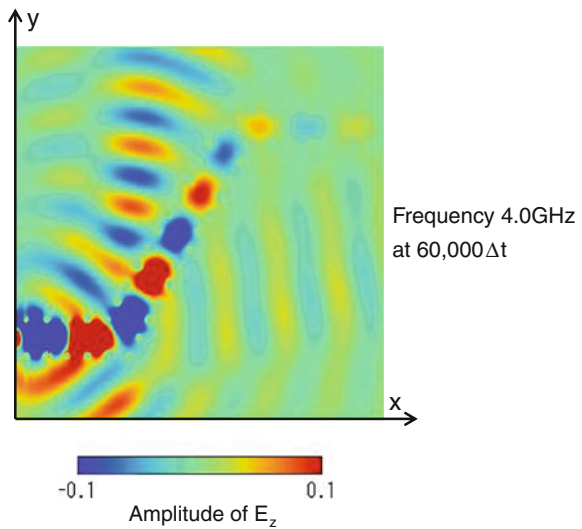
advantage in method to provide more precise result around material boundary. For computation by CIP method, the space grid size $\Delta x = \Delta y = 0.5 \text{ mm}$ and $\Delta t = 1.7 \times 10^{-13} \text{ s}$ was used.

In Fig. 8, the total electric field profile E_z in single-layered waveguide depicted in Fig. 5a is shown for frequency $f = 4.0 \text{ GHz}$ and time step $60,000\Delta t$ as a typical result. As is well observed from the figure, very strong radiation is clearly observed at the first bending point. To suppress this radiation, improvement of confinement around the bending point is required, for example, by adding other layers around the bending.

3.2 Improvement of Transmission S_{21}

To improve the transmission characteristics shown in Figs. 6 and 7, additional post wall layers were installed around bending. Here, four kinds of layers were examined as shown in Fig. 9a–d. The transmission characteristics S_{21} are shown in Fig. 10 as experimental results and in Fig. 11 as numerical results. Considering the radiation in Fig. 8, Type-I could not suppress it and showed poorest improvement. This is because additional layer was installed at outside of the bending points. It is similar for Type-II. For Type-III and Type-IV, additional layers could suppress the radiation, however, totally double layered at the bending was not sufficient. Consequently, Type-IV showed the best improvement on transmission.

Fig. 8 Electric field profile of E_z at typical time step and frequency for the structure depicted in Fig. 5a



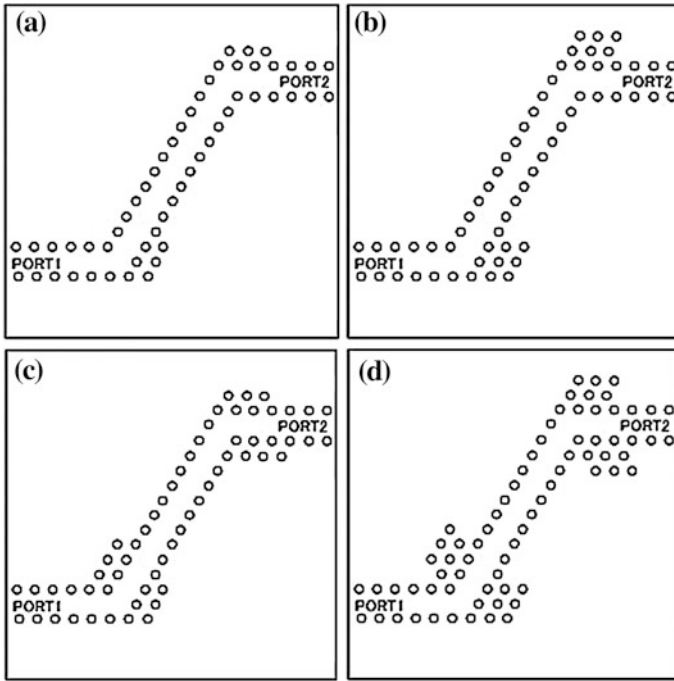


Fig. 9 Variation of single-layered post wall waveguide with guarding layers around bending point. **a** Type-I **b** Type-II **c** Type-III **d** Type-IV

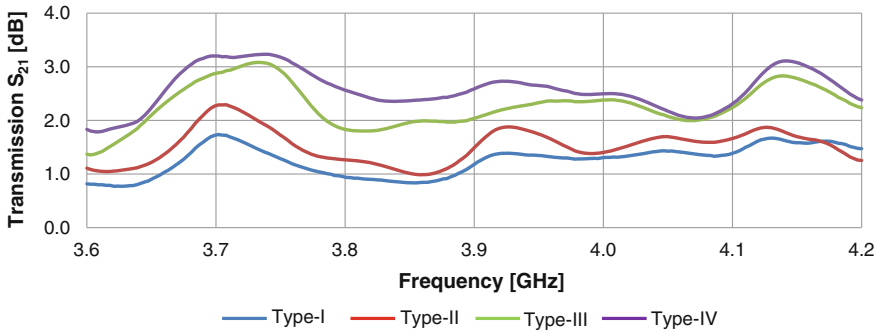


Fig. 10 Comparison of measured transmission characteristics S_{21} after the improvement as is shown in Fig. 9a–d

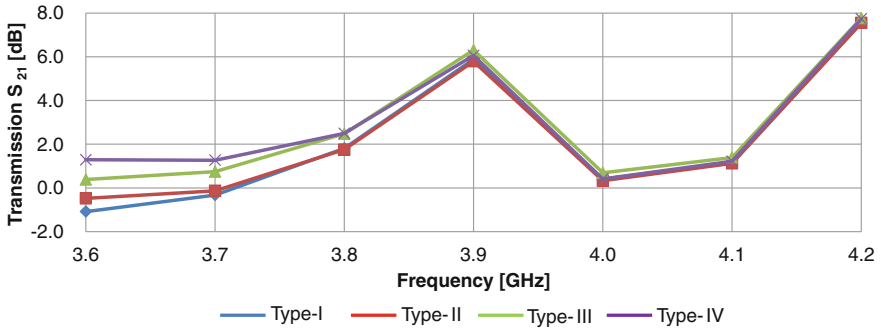


Fig. 11 Comparison of calculated transmission characteristics S_{21} after the improvement

4 Concluding Remarks

In this paper, experimental and numerical results of transmission in post wall waveguides with bending were demonstrated. It was found that periodic post wall with three layers is necessary for the confinement of electromagnetic field. Improvement of transmission characteristics for single-layered waveguide is achievable by adding posts around bending point. For the best confinement, we found that installing cylinders to be three layers at both sides of bending is effective. This result is applicable for integrated microwave and millimeter wave circuit. By applying scaling rule under holding the material parameters and normalized frequency to be constant, this circuit operates for optical frequency range. The result is expected to be applicable for optical integrated circuit.

Acknowledgments This work was financially supported by KAKENHI No. 24560430, Grant-in-Aid for Scientific Research (C) by Japan Society for the Promotion of Science (JSPS) in 2012. Also, authors express our thanks to D. Kunitake, K. Kosugi, K. Satoh, M. Maruyama, T. Izumi, and Y. Yano for their cooperation with measurement of post wall waveguide by scale model.

References

1. Yasumoto K (ed) (2006) Electromagnetic theory and applications for photonic crystals. CRC PRESS, Boca Raton
2. Temelkuran B, Ozbay E (1999) Experimental demonstration of photonic crystal based waveguides. *Appl Phys Lett* 74(4):486–488
3. Beaky M et al (1999) Two-dimensional photonic crystal Fabry-Perot resonators with lossy dielectrics. *IEEE Trans Microw Theor Tech* 47(11):2085–2091
4. Zhang Y, Terashima H, Ogata D, Maeda H (2011) Some trials to suppress unnecessary resonance in photonic crystal cavity structure. In: Proceedings of BWCCA 2011: 6th international conference on broadband, wireless computing, communication and applications, Oct 2011, pp 482–486

5. Maeda H, Chen H, Tomiura K, Shinohara T (2012) Numerical and experimental study on confinement of microwave in dielectric and metallic post array waveguide. In: Proceedings of INWC 2012: The 2nd international workshop on information networking and wireless communications in conjunction with NBiS 2012: The 15th international conference on network-based information systems, Sep 2012, pp 562–566
6. Maeda H, Zhang Y, Terashima H, Shinohara T (2011) Hexagonal resonator in two dimensional photonic crystal structure. In: Proceedings of IEEE INCoS 2011: 3rd IEEE international conference on intelligent networking and collaborative systems, Nov 2011, pp 537–540
7. Maeda H, Zhang Y, Terashima H, Maruyama T, Hironaka S (2011) Experimental study on four-branching waveguide in two dimensional photonic crystal structure with triangular lattice by scale model around 4 GHz. In: Proceedings of ISMOT-2011: 13th international symposium on microwave and optical technology, June 2011, pp 65–68
8. Yabe T, Feng X, Utsumi T (2001) The constrained interpolation profile method for multiphase analysis. *J Comput Phys* 169:556–593
9. Okubo K, Takeuchi N (2007) Analysis of an electromagnetic field created by line current using constrained interpolation profile method. *IEEE Trans Antennas Propag* 55(1):111–119
10. Maeda H, Terashima H, Maruyama T, Hironaka S (2010) Numerical analysis of scattered electromagnetic wave by a dielectric cylinder with high contrast by CIP method. In: Proceedings of MAPWC-2010: 1st international workshop on methods, analysis and protocols for wireless communication in conjunction with BWCCA-2010: 5th international conference on broadband and wireless computing, communication and applications, Nov 2010, pp 561–564
11. Maeda H, Zhang Y, Terashima H (2011) Numerical analysis of electromagnetic wave scattered by high-contrast dielectric cylinder using CIP method. In: Proceedings of INWC 2011: The 1st international workshop on information networking and wireless communications in conjunction with NBiS 2011: The 14th international conference on network-based information systems, Sep 2011, pp 491–496
12. Maeda H (2012) Numerical technique for electromagnetic field computation including high contrast composite material, chapter 3. In: Das N (ed) *Optical communications*. InTech (Open Access Publisher), Fijeka, pp 41–54. ISBN 978-953-51-0784-2

Resource Management for Hybrid 3.75G UMTS and 4G LTE Cellular Communications

Ben-Jye Chang, Ying-Hsin Liang and Kai-Xiang Cao

Abstract The UMTS and LTE/LTE-Advanced specifications have been proposed to offer high data rate for the forwarding link under high-mobility wireless communications. The keys include supporting multi-modes of various coding schemes (e.g., VSF-OFCDM, OFDM, OFDMA), multiple-input multiple-output, relay networks, etc. To balance loads among different communication interfaces is one of the most important issues that should be addressed for achieving efficient radio resource allocations. In a shared packet service, the 3GPP UMTS adopts the VSF-OFCDM interface to allocate orthogonal codes of an OVSF code tree in two-dimension (2D) spreading of the time and frequency domains. Conversely, although the LTE/LTE-Advanced interface offers a high data rate, it suffers from unbalanced loads and moderate reward. This paper thus proposes an adaptive radio resource allocation for balancing loads between the UMTS and LTE/LTE-Advanced interfaces according to various interference and mobility environments. Additionally, an adaptive multi-code allocation is proposed for the UMTS to

This research was supported in part by the National Science Council of Taiwan, under the contracts of NSC-101-2221-E-252 -008, NSC-101-2221-E-224-021-MY2, and NSC-101-2221-E-224-022-MY3.

B.-J. Chang (✉) · K.-X. Cao

Department of Computer Science and Information Engineering, National Yunlin University of Science and Technology, 123 University Road, Section 3, Douliou 64002 Yunlin, Taiwan (People's Republic of China)

e-mail: changb@yuntech.edu.tw

K.-X. Cao

e-mail: g9817709@yuntech.edu.tw

Y.-H. Liang

Department of Multimedia Animation and Application, Nan Kai University of Technology, Tianjin, Taiwan (People's Republic of China)

e-mail: t136@nkut.edu.tw

minimize the bandwidth waste rate while guaranteeing quality of service. Numerical results indicate that the proposed approach outperforms other approaches in fractional reward loss and system utilization.

Keywords Adaptive radio resource management · Adaptive modulation and coding · Load balancing · Resource block · 2D-spreading · Multiple input multiple output · Multicode · LTE-A

1 Introduction

As the extensively demanding of high bandwidth for real-time streaming transmissions in high-speed cloud-based applications increases, the fourth (4G) cellular communications [1, 2] are specified to offer high data rate for the shared packet service of the forward link. Moreover, NTT DoCoMo XG-PHS [3] proposes the Variable Spreading Factor-Orthogonal Frequency and Code Division Multiplexing (VSF-OFCDM) that spreads a single data bit with a two-dimensional (2D) spreading in the time and frequency domains. 3GPP [4] specifies the Long Term Evolution (LTE) [5, 6] in 3GPP release 8 as the 3.9th generation (3.9G) cellular communication. Several efficient techniques are extendedly adopted in LTE, including the multiple-input multiple-output (MIMO), the adaptive modulation and coding (AMC) mechanism, etc. [7]. To extend the service coverage by using a simple relay mechanism, 3GPP specifies the LTE-Advanced (LTE-A) specification [8–10], denoted by 3GPP Release 10, as the fourth generation (4G) standard. The relay node (RN) is adopted to extend the BS's service coverage, but not increases the BS deployment cost significantly. LTE-A adopts the 8×8 MIMO and three multiplexing modes are included: spatial diversity, spatial multiplexing, and beamforming.

Different modulation modes: UMTS's WCDMA, LTE's OFDMA, etc., are adopted and operated between the base station (BS) and a user-equipment (UE). An efficient radio resource management is required in a BS to balance loads among different modulation modes while maximizing the system reward. The related studies of the radio resource management and load balancing of UMTS/LTE are discussed as follows.

First, in UMTS, the novel OFCDM 2D spreading [11, 12] spreads a data symbol into the time and frequency domains to reduce the interference by using the orthogonal subcarriers. However, the VSF-OFCDM managed by an OVSF code tree needs an efficient algorithm to allocate codes to different arrival connections. The code allocation algorithms of the VSF-OFCDM scheme can be classified into three types: the allocations of 2D-based single code [13, 14], single code [15–21], and multicode [22–29] for a single connection request.

Although several different radio resource managements have been extensively proposed for UMTS cellular communications, a base station supporting various modulation modes for different-generation cellular communications requires to achieve balancing loads among the supported modulation modes and to consider the interference according to the location of the mobile node. Specifically, a mobile node located at the boundary of the serving BS uses a QPSK scheme for data transmission, and thus a higher data rate radio resource (or the channelization code) cannot be allocated to it. In addition, a mobile node with a very high mobility up to 300 km/h (i.e., in a high speed train) should use the LTE interface, rather than the UMTS one. Thus, to allocate the radio resources to different mobile nodes that are with different speeds and AMC schemes needs an efficient adaptive radio resource allocation approach. The objectives are to maximize system reward, to balance loads among different interfaces, and to increase network utilization.

This paper thus proposes an Adaptive Radio resource Allocation, namely ARA, for the LTE and UMTS interfaces according to the conditions of a mobile node. ARA consists of three phases: the conditions detection phase, the LTE and UMTS loads determination, and the radio resource allocation phase. Finally, the ARA approach can maximize reward, balance loads, and minimize bandwidth waste rate in 4G UMTS and LTE Communications.

This paper thus proposes an Adaptive Radio resource Allocation, namely ARA, for the LTE and UMTS interfaces according to the conditions of a mobile node. ARA consists of three phases: the conditions detection phase, the LTE and UMTS loads determination, and the radio resource allocation phase. Finally, the ARA approach can maximize reward, balance loads, and minimize bandwidth waste rate in 4G UMTS and LTE Communications.

The rest of this paper is organized as follows. [Section 2](#) defines the network model. Next, the proposed loads of UMTS and LTE Determination Phase (LDP) and the connection Admission control and Classification Phase (ACP) are described in [Sect. 3](#). The Dynamic resource Allocations of UMTS and LTE Phase (DAP) are detailed in [Sect. 3.3](#). [Section 4](#) presents the numerical results. Finally, conclusions and future works are given in [Sect. 5](#).

2 Network Model

In [Fig. 1](#), a 4G eNodeB consisting of two types of interfaces of UMTS and LTE is modeled as a system, $S_{Umts,Lte}^{id}$, where id represents the system's ID and $(Umts, Lte)$ are two-interface types offered by the eNodeB. The eNodeB dynamic allocates radio resource to different mobile nodes that are with different classes of traffic and different speeds, etc. In the UMTS interface, an OVSF code tree of eNodeB in VSF-OFCDM is modeled as a full binary tree, T , which has a maximum spreading factor, SF .

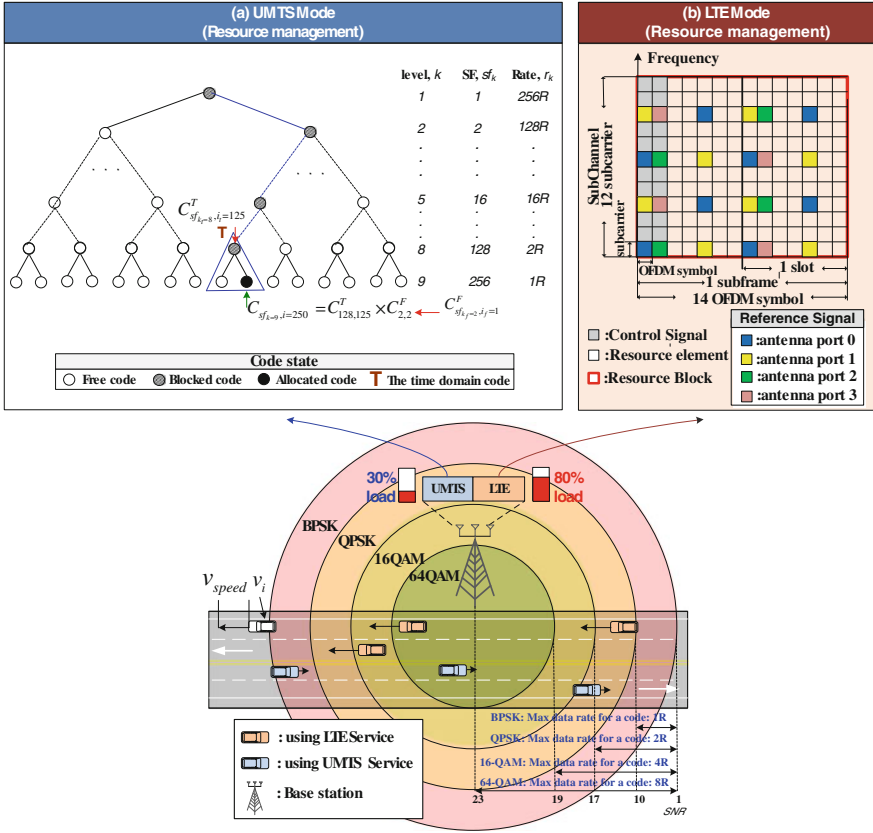


Fig. 1 Network model

As demonstrated in Fig. 1a, the OVSF code tree has height K , i.e., the number of levels, and the level index k , where $k = 1, \dots, K$. A channelization code of level k is denoted as $C_{sf_k, i}$, where sf_k is the spreading factor of level k , $sf_k = 2^{k-1}$, and i is the channelization code index of level k , $1 \leq i \leq sf_k$. The maximum spreading factor of the OVSF code tree is thus $SF = 2^{K-1}$. As a result, the total number of channelization codes of the OVSF code tree, N , is thus $N = \sum_{j=1}^{SF} j$ or $N = 2^K - 1$. A level k channelization code, $C_{sf_k, i}$, spread in the time and frequency domains. The time domain code is denoted as $C_{sf_{k_t}, i_t}^T$, where sf_{k_t} is the time domain spreading factor of level k_t , $sf_{k_t} = 2^{k_t-1}$, and i_t is the time domain code index of the level k_t , $1 \leq i_t \leq sf_{k_t}$. The frequency domain code is denoted as $C_{sf_{k_f}, i_f}^F$, where sf_{k_f} is the time domain spreading factor of the level k_f , $sf_{k_f} = 2^{k_f-1}$, and i_f is the time domain code index of the level k_f , $1 \leq i_f \leq sf_{k_f}$. For instance, same channelization codes, $C_{8,2}$ can be spread in different time and frequency domains as, $C_{8,2} = C_{2,1}^T C_{4,2}^F$, or $C_{4,1}^T C_{2,2}^F$, as demonstrated in Fig. 2.

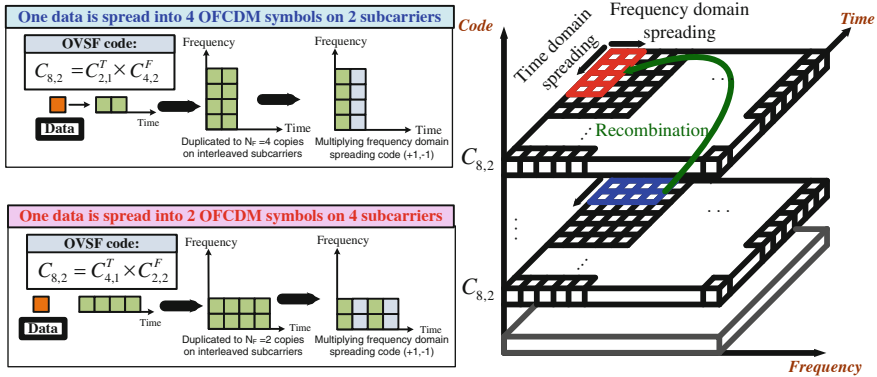


Fig. 2 Different combinations of 2D spreading in the time-frequency domain

In the LTE interface, a generic LTE PHY frame structure consists of 10 subframes in the time domain and each subframe consists of two slots. Each subframe can carry 14 OFDM symbols. A subchannel in the frequency domain consists of 12 subcarriers. Different bandwidth spectrums uses different numbers of subchannels, e.g., in a 1.4 MHz bandwidth spectrum, 1 channel consists of 6 subchannels.

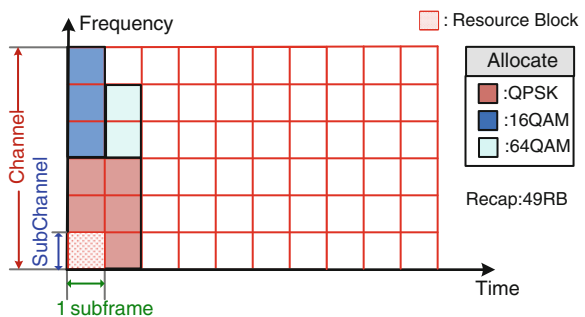
In LTE, the transmission unit for a user equipment (UE) is denoted as a Resource Block (RB) within a subframe (in time) and a subchannel (in frequency), as shown in Fig. 1b.

We assume that the system adopts Spatial multiplexing with four antennas, and the eNodeB uses individual Reference Signal symbol as the pilot symbol for every channel. The receiver channel can receive the data symbols correctly.

In the multiuser access case of OFDMA, all RBs of the same subframe can be allocated to different UEs. However, in the single user access case of OFDM, the RBs belonging to the same subframe only can be allocated to the same UE, rather than allocated to different UEs [30–33].

For any UEs, they can use different AMC as the modulation and coding scheme to communicate with the eNodeB. For instance, in Fig. 3 a UE requires a 12R bandwidth. Then, the eNodeB can allocate 6 RBs with the QPSK coding, 3 RBs with the 16QAM coding, or 2 RBs with 64QAM coding.

Fig. 3 Number of RBs of different AMC



In LTE's OFDMA, a UE is allocated at least one RB and the eNodeB can allocate various numbers of RBs to different UEs at the same subframe time. As a result, the access delay can be reduced. When the channel bandwidth is 1.4 MHz, the LTE can use 6 RBs within a subframe time. Conversely, when the channel bandwidth is 10 MHz, it can use 50 RBs instead.

Thus, the total data rate of the forwarding link offered by LTE in a PHY frame can be determined as shown below,

$$R_{DL} = (N_{RB}(N_{NSC}N_{NSS}N_{bit}^{AMC}))N_{TTI}, \quad (1)$$

where N_{RB} is the number of RBs can be supported within a subframe time; N_{NSC} is the number of subcarriers of a subchannel; N_{NSS} is the number of OFDM symbols of a subframe; N_{bit}^{AMC} is the number of data bits of a symbol, and N_{TTI} is the number of TTIs within a LTE PHY frame. Note that N_{bit}^{AMC} can be obtained, which is summarized from [34].

3 Adaptive Radio-Resource Allocation (ARA)

To adaptively allocate radio resource to mobile nodes with different velocities and channel quality indications (CQIs) and to balance loads between 3.5G's HSDPA and 4G's LTE, this paper proposes an Adaptive Radio-resource Allocation (ARA) approach for managing radio resource in the next generation high-speed cellular communication. The ARA approach consists of three phases: the Loads of UMTS and LTE Determination Phase (LDP), the connection Admission control and Classification Phase (ACP), and the Dynamic resource Allocations of UMTS and LTE Phase (DAP).

3.1 Phase 1: The Loads of UMTS and LTE Determination Phase (LDP)

The drawback of unbalanced loads among various supported communication modes (e.g., UMTS, LTE, etc.) significantly degrades the system utilization and reduces the network revenue because of rejecting the connections that can be accepted. Thus, LDP determines the loads of UMTS and LTE dynamically. The loads of any communication mode is changed and computed when a new incoming connection is accepted or an existing connection has been released completely. LDP is detailed as follows.

In UMTS, the radio resource of UMTS is coded and managed by the VSF-OVSF code tree. A channelization code is allocated to every accepted or carried connection. Note that the orthogonal characteristic of the VSF-OVSF code tree exhibits in two cases. First, the channelization codes at the same level are

orthogonal. Second, the orthogonal characteristic is met if the relationships of the codes are not ancestor descendant, because the code of the ancestor is the prefix of the descendant codes. Thus, the UMTS load, L_{UMTS} , is computed according to the allocated bandwidth and the total capacity supported by the UMTS mode, as indicated in Eq. (2)

$$L_{UMTS} = \frac{\sum_{k=1}^K (a_k \cdot 2^{k-1} R)}{2^{K-1} R} \cdot 100 \% \quad (2)$$

where a_k is the number of allocated channelization codes of level k and $2^{K-1}R$ denotes the total capacity of the VSF-OVSF code tree in UMTS.

Conversely, in LTE, the radio resource of LTE is coded and managed by the OFDMA Resource Blocks (RBs), and every RB is coded as shown in Fig. 3. In a multiuser MIMO LTE, the RBs of the same subframe can be allocated to different connections. Thus, in the multiuser MIMO LTE, the total number of RBs ($NRBs$) managed by an eNodeB in a frame time is determined by $NRB = N_{RB}N_{TTI}$, where N_{RB} is the number of RBs within a subframe time and N_{TTI} is the number of subframes (TTIs) within a PHY frame. Thus, the LTE load, L_{LTE} , is formulated according to the allocated RBs and the total number of RBs offered by the LTE mode, as shown in Eq. (3),

$$L_{LTE} = \frac{NRB_{Allocated}}{NRB} 100 \% \quad (3)$$

3.2 Phase 2: The Connection Admission Control and Classification Phase (ACP)

Connection Admission Control (CAC)

When a new class k connection arrives at an eNodeB, the eNodeB first adopts the capacity-based Connection Admission Control (CAC) to check whether the residual bandwidth is enough for the connection or not. In the capacity-based CAC, the eNodeB accepts an incoming connection, if the residual bandwidth is sufficient; otherwise, it rejects the connection.

Connection Classification (CC)

After the eNodeB accepts the connection, the eNodeB decides to allocate which mode of communication interface (i.e., UMTS or LTE) to the connection in terms of three factors:

- (1) the interface loads of the eNodeB (L_{UMTS} and L_{LTE}),
- (2) the reward (r_m) of the required traffic class (m), and
- (3) the velocity (v_i) of mobile node i .

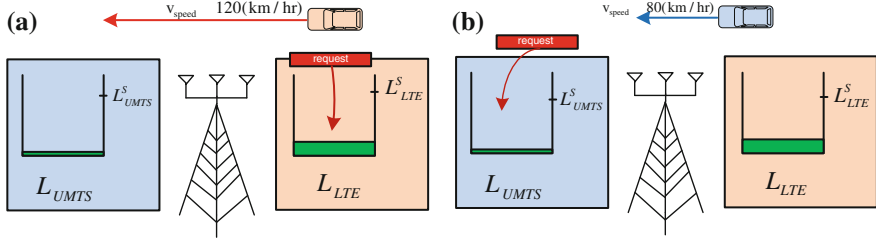


Fig. 4 Communication interface allocations while both loads are below the load thresholds

Based on the three impact factors, ACP proposes an interface determination algorithm that consists of two criteria to select the most proper one for the new incoming connection.

First, if both loads, L_{UMTS} and L_{LTE} , of the eNodeB are all below or all above their individual thresholds, i.e., $(L_{LTE} < L_{LTE}^S \text{ and } L_{UMTS} < L_{UMTS}^S)$ or $(L_{LTE} \geq L_{LTE}^S \text{ and } L_{UMTS} \geq L_{UMTS}^S)$, the eNodeB determines the communication interface by using the factors of mobile node velocity (v_i) and the carrying reward (r_m). ACP allocates LTE to a new connection if the carrying reward of using LTE is larger than that of using UMTS (i.e., $r_m^{LTE} > r_m^{UMTS}$), or the mobile node is with a high speed (e.g., $v_i \geq v^S$). Otherwise, ACP allocates UMTS to the new connection. Figure 4 demonstrates two different scenarios. Figure 4a allocates LTE to the incoming connection because $r_m^{LTE} > r_m^{UMTS}$ or $v_i \geq v^S$. Conversely, Fig. 4b allocates UMTS to the incoming connection because $r_m^{LTE} \leq r_m^{UMTS}$ or $v_i < v^S$.

Second, if only one mode exceeds its load threshold, i.e., in the cases of $(L_{LTE} < L_{LTE}^S \text{ and } L_{UMTS} \geq L_{UMTS}^S)$ and $(L_{LTE} \geq L_{LTE}^S \text{ and } L_{UMTS} < L_{UMTS}^S)$, ACP allocates the interface with a lower load to the new incoming connection.

Thus, ACP achieves the objectives of maximizing system reward and balancing loads between UMTS and LTE. After determining the interface mode for an incoming connection, the resource allocations of UMTS and LTE are proposed to maximize the interface reward and to minimize the interface overhead, as detailed in next section.

3.3 Phase 3: The Dynamic Resource Allocations of UMTS and LTE Phase (DAP)

This section details the Dynamic resource Allocation of UMTS and LTE Phase.

A. UMTS Resource Allocation

The UMTS resource allocation consists of four steps:

- (1) the AMC scheme (area) determination,
- (2) the multicode partition,
- (3) the determination of all 2D spreading combinations of all possible codes, and

(4) the cost-based code assignment.

Step 1. The AMC scheme (area) determination

The 4G communications support AMC [35] mechanism to dynamically use different modulation schemes when the distance or interference between the eNodeB and the mobile node are varied. For its simplicity, this paper considers four AMC schemes in UMTS: BPSK, QPSK, 16-QAM, and 64-QAM, according to the interference, in which 64-QAM can bring a higher data rate, but BPSK only brings the lowest data rate. The maximum data rate of a single channelization code used by different UMTS's AMC schemes is shown in Fig. 1c [36, 37].

Step 2. The multicode partition

This work adopts the multicode-based resource management for minimizing the bandwidth waste rate when the required data rate is not power of 2 of the basic rate ($1R$). Assume that a class m connection arrives at the system, the approach first maps the required data rate, mR , into a binary format by calling the function of $m2Bin(m)$. In addition, the partition procedure checks whether the data rate of the partitioned codes satisfy the maximum data rate supported by current AMC scheme or not.

If yes, the partitioned codes are obtained, $\vec{A} \leftarrow m2Bin(m)$, where \vec{A} is the assignment code set vector. If no, the un-satisfied codes, i.e., the data rate is larger than the maximum data rate offered by current AMC scheme, will be split into several smaller channelization codes by calling the function of $Split(\vec{A})$.

In UMTS, an antenna supports several rake-combiners [38] for transmitting multiple streaming via various channelization codes. Assume that the specified maximum number of rake-combiners is denoted as NCS. Thus, if $|\vec{A}| \leq NCS$, where $|\vec{A}|$ is the number of the partitioned codes, it will enter *Step 3* to assign every partitioned code. Otherwise, the multicode partition fails and the connection is rejected.

Step 3. To determine all 2D spreading combinations of all possible codes of $A\{\}$

After determining the multicode partition in *Step 2*, the required bandwidth of the incoming connection has been successfully mapped to a group of channelization codes. To do the code assignment of the group codes, *Step 3* is executed. The objectives of *Step 3* is to determine all 2D spreading combinations of all possible codes of $A\{\}$, i.e., $CAND\{\} \leftarrow A\{\}$.

Step 3 consists of four processes: (1) to determine all combinations of a free channelization code, (2) to check the number of candidates, (3) to check the channel load of the selected code, and (4) to recombine the 2D spreading of the selected code.

Step 4. Cost-based code assignment

In *Step 4*, several codes with the determined 2D spreading combinations exhibit in $CAND\{\}$, i.e., $|CAND\{\}| > 1$. The cost-based code assignment [14] is performed. Since the optimal selected channelization code requires the least carrying

Table 1 Number of RBs used for 16R under different AMC modulations

AMC modulation	The number of required RBs for a 16R data rate connection (RBs)
QPSK $\frac{1}{2}$	16
16QAM $\frac{1}{2}$	8
64QAM	3

cost that is computed based on sum of cost of all affected codes on the entire OVSF tree, the selected code can achieve a global optimal result.

B. LTE Resource Blocks Allocation

In LTE, the radio resource management unit is a Resource Block (RB) that is multiplexed by OFDMA and TDMA, as demonstrated in Fig. 3. All RBs in LTE are orthogonal and the RBs of the same subframe time can be allocated to different User Equipments (UEs), i.e., the case of multiuser access of OFDMA. We assume that the LTE system adopts 1.4 MHz channel bandwidth, and it has total 60 RBs within a PHY frame, in which a PHY frame consists of 10 subframes (i.e., TTIs).

As a result, we can determine the offered data rate of 1 RB for each AMC modulation, as indicated in Table 1. The minimum and maximum data rates of a RB are 144 Kbps (QPSK) and 3.456 Mbps (64-QAM), respectively. Thus, the number of RBs needed for a 16R required rate under different AMC modulations can be determined. For instance, the 16R required rate located at 64-QAM (with the single antenna case) needs 3 RBs, as determined as follows.

$$N_{RB} = \frac{16 \cdot 144 \text{ kbps}}{864 \text{ kbps}} = \frac{2304 \text{ kbps}}{864 \text{ kbps}} = 2.666 \simeq 3RBs \quad (4)$$

Although the eNodeB can allocate sufficient number of RBs for a 16R connection located in QPSK, it brings too much overhead and degrades the system reward and interface utilization. Thus, to maximize the system reward, the Maximum number of RBs (namely MRB) allocated for an incoming connection should be specified in LTE. In this paper, the eNodeB in LTE only can allocate maximum MRB RBs for an incoming connection. Otherwise, the eNodeB rejects the connection.

For instance, we assume that MRB is set to 4. If a vehicle located at the QPSK location requires 16R data rate, the incoming connection will be rejected. The reason is the number of required RBs is 16 that is more than MRB (i.e., 4). Conversely, if a vehicle located at the 64QAM location requires 16R data rate, the incoming connection can be accepted by the LTE interface. The reason is the number of required RBs is 3. That is smaller than MRB.

4 Numerical Results

This section evaluates the performance of the Adaptive Radio-resource Allocation (ARA) approach in the hybrid modes of UMTS and LTE in several important metrics: fairness, Fractional Reward Loss (FRL), utilization, etc. The compared

approaches include the 3GPP multicode specification (denoted by *3GPP_MS*) [39], the 2D spreading single code assignment (denoted by *2D_single*) [14], the crowded first multicode code assignment (denoted by *CF_MC*) [17] and the random multicode code assignment (denoted by *RAND_MC*) [17].

In the network model, the evaluated UMTS OVSF code tree, C_T , with the total capacity of 256R. This paper considers multiple classes of traffic arrival at the eNodeB and the required bandwidth of class m traffic, b_m , is normalized to the data rate of the leaf code, i.e., $b_m = m \cdot 1R$, where $1 \leq m \leq 16$. In the traffic model, the class m traffic arrives at an eNodeB with the arrival rate of $\lambda_m = \lambda/m$, where λ ranges from 2 to 22. The average holding time of all classes of traffic is exponentially distributed and the mean is normalized to one.

UMTS and LTE with considering the load balancing, in which the threshold is set to 0. That is, the eNodeB always allocates the incoming connection to the interface with a lower utilization. In Fig. 5, the LTE utilization (between 20 and 33 %) is higher than the UMTS utilization (between 18 and 23 %). The fairness is between 92 and 98 %, i.e., the utilizations of UMTS and LTE are fair.

Figure 6 evaluates FRL under various arrival rates ranging from 2 to 22. The FRLs of all approaches increase as the arrival rate increasing. ARA_NCS8 yields the lowest FRL, but CF and LM lead to the highest FRL. In addition, 3GPP_MS results in worse FRL because it neglects the 2D spreading, resource state, and load balancing. In Fig. 6, we can observe that the proposed ARA with different NCS can achieve lower FRL, because it simultaneously considers to maximize system reward and to balance loads of various interface-types. As a result, ARA avoids blocking the connection that can bring a high reward. In addition, AVCS_MAX and AVCS_MIN neglect the AMC modulation scheme, and thus yield a higher blocking probability and FRL.

Figure 7 compares total reward under various arrival rates, in which the total rewards of all approaches increase as the arrival rate increasing. ARA_NCS8 yields the highest reward. However, 2D_single yields the lowest reward. Clearly,

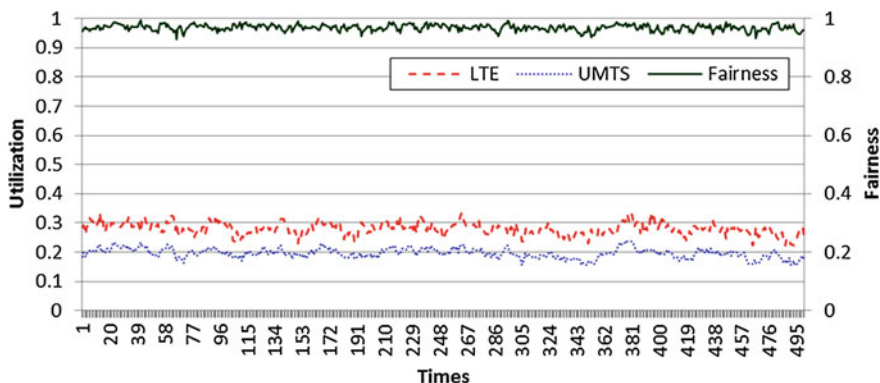


Fig. 5 Loads (Utilization) and fairness with considering load balancing of LTE and UMTS

Fig. 6 FRLs under different arrival rates and various NCS

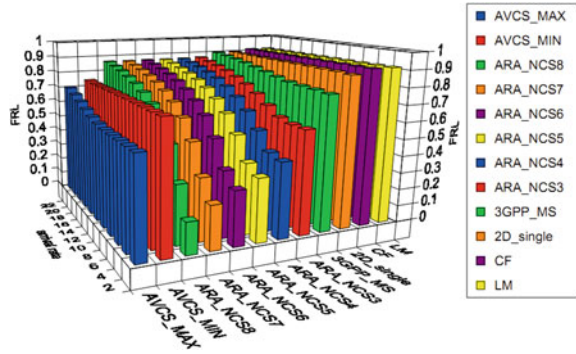
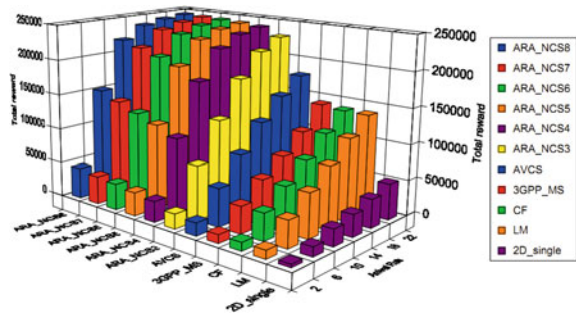


Fig. 7 Total reward under different arrival rates



since the single code approaches: 2D_single, LM and CF only allocate a single code for an incoming connection, the connection is easily to be rejected. As a result, the total reward of them are very low.

5 Conclusions

For balancing loads among different communication modes (UMTS/LTE/LTE-A, etc.) while maximizing system reward and to minimize bandwidth waste rate are the open issues that should be addressed in order to achieve high efficient radio resource management in high speed multimode cellular communications. This paper thus proposed the Adaptive Radio-resource Allocation (ARA) approach that consists of three phases: (1) the Loads of UMTS and LTE Determination Phase (LDP), (2) the connection Admission control and Classification Phase (ACP), and (3) the Dynamic resource Allocations of UMTS and LTE Phase (DAP). The first two phases: LDP and ACP efficiently achieve the load balancing feature. The DAP phase achieves the least bandwidth waste rate and increases network utilization and reward. Numerical results demonstrate that the proposed ARA approach outperforms the compared studies (3GPSS_MS, 2D_single, LF, and LM) in FRL, utilization, etc.

Acknowledgments This research was supported in part by the National Science Council of Taiwan, under the contracts of NSC-101-2221-E-252 -008, NSC-101-2221-E-224-021-MY2, and NSC-101-2221-E-224-022-MY3.

References

1. Meik K (2010) LTE-advanced technology introduction, White paper. Rohde & Schwarz, Munich, pp 3–22
2. TR 36.913 Version 10.0.0 (2011) Requirements for further advancements for Evolved Universal Terrestrial Radio Access (E-UTRA) (LTE-Advanced), 3GPP, pp 4–15
3. Maeda N, Kishiyama Y, Higuchi K, Atarashi H, Sawahashi M (2003) Experimental evaluation of throughput performance in broadband packet wireless access based on VSF-OFCDM and VSF-CDMA. *IEEE Proc Pers Indoor Mobile Radio Commun* 1:6–11
4. 3GPP, Online: <http://www.3gpp.org>
5. Daniel G-A, Iain S, Bob S (2010) LTE and LTE advanced. *Steepest Ascent*, pp 1–16
6. Abeta S (2010) Toward LTE commercial launch and future plan for LTE enhancements (LTE-advanced). 2010 IEEE International Conference on Communication Systems (ICCS), pp 146–150, Nov 2010
7. Shantha Kumar KN, Madhu K, Paruchuri C, Dinesh M (2009) LTE-advanced: future of mobile broadband. *TATA Consult Serv* 28(3):1380–1408
8. Gesbert D, Hanly S, Huang H, Shamai Shitz S, Simeone O, Wei Y (2010) Multi-cell MIMO cooperative networks: a new look at interference. *IEEE J Sel Areas Commun* 28(3):1380–1408
9. TR 36.912 Version 10.0.0 (2011) Feasibility study for further advancements for E-UTRA (LTE-Advanced), 3GPP, pp 6–61, March 2011
10. Qinghua L, Guangjie L, Wookbong L, Moon-il L, Mazzaresse D, Clerckx B, Zexian L (2010) MIMO techniques in WiMAX and LTE: a feature overview. *IEEE Commun Mag* 48(5):86–92
11. Zhou Y, Ng T-S, Wang J-Z, Higuchi K, Sawahashi M (2008) OFCDM: a promising broadband wireless access technique. *IEEE Commun Mag* 46(3):38–49
12. Kuo C-C, Sheen W-H, Chang C-J, Hsiao C-L (2008) On the transmitter-based preprocessing for 2-D OFDM-CDMA forward-link systems over time-varying Rayleigh Fading Channels. *IEEE Trans Veh Technol* 57(3):1968–1974
13. Zhou Y, Wang J, Ng T-S (2008) Downlink transmission of broadband OFCDM systems-Part V: Code assignment. *IEEE Trans Veh Technol* 7(11):4546–4557
14. Chang B-J, Wu C-H (2009) Adaptive load balancing MDP-based approach of two-dimensional spreading for VSF-OFCDM in 4G next-generation cellular communications. *IEEE Trans Veh Technol* 58(3):1143–1156
15. Hwang R-H, Chang B-J, Chen M-X, Tsai K-C (2006) An efficient adaptive grouping for single code assignment in WCDMA mobile networks. *Wirel Pers Commun* 39(1):41–61
16. Chang B-J, Chen M-X, Wang R-H, Tsai K-C (2006) Single code-based dynamic grouping with cycle interleaving algorithm for reducing waste rate in WCDMA cellular networks. *IEICE Trans Commun* 89(12):3306–3317
17. Tseng Y-C, Chao C-M (2002) Code placement and replacement strategies for wideband CDMA OVSF code tree management. *IEEE Trans Mob Comput* 1(4):293–302
18. Cheng S-T, Hsieh M-T (2005) Design and analysis of time-based code allocation schemes in W-CDMA systems. *IEEE Trans Mob Comput* 4(6):604–615
19. Chao C-M, Tseng Y-C, Wang L-C (2005) Dynamic bandwidth allocation for multimedia traffic with rate guarantee and fair access in WCDMA systems. *IEEE Trans Mob Comput* 4(5):420–429

20. Park J-S, Huang L, Kuo CCJ (2008) Computationally efficient Dynamic Code Assignment Schemes with Call Admission Control (DCA-CAC) for OVFSF-CDMA systems. *IEEE Trans Veh Technol* 57(1):286–296
21. Tsai Y-R, Lin L-C (2009) Quality-based OVFSF code assignment and reassignment strategies for WCDMA systems. *IEEE Trans Veh Technol* 50(2):1027–1031
22. Chang B-J, Chang P-S (2006) Multicode-based WCDMA for reducing waste rate and reassignments in mobile cellular communications. *Comput Commun* 29(11):1948–1958
23. Yang Y, Yum TSP (2005) Multicode multirate compact assignment of OVFSF codes for QoS differentiated terminals. *IEEE Trans Veh Technol* 54(6):2114–2124
24. Saini DS, Upadhyay M (2009) Multiple rake combiners and performance improvement in 3G and beyond WCDMA systems. *IEEE Trans Veh Technol* 58(7):3361–3370
25. Ferng HW, Chin H-L, Shiung D, Chen Y-T (2005) An OVFSF code tree partition policy for WCDMA systems based on the multi-code approach. 2005 IEEE 62nd vehicular technology conference, vol 2, pp 1212–1216, Sept 2005
26. Saini DS, Hastir V, Sood M (2009) Multi code assignment and reduction in code rate wastage for 3G and beyond WCDMA systems. *IEEE international advance computing conference*, pp 946–951, March 2009
27. Chang W-Y, Ouyang W, Wang C-Y, Liu M-T, Chang Y-W (2010) Graph model for OVFSF code placement. 2010 5th international conference on future information technology, pp 1–6, June 2010
28. Balyan V, Saini DS (2010) An efficient multi code assignment scheme to reduce call establishment delay for WCDMA networks. 2010 1st international conference on Parallel Distributed and Grid Computing (PDGC), pp 278–283, Oct 2010
29. Nemanja V, Jordi P-R, Oriol S, Ramon A (2011) Reinforcement learning for joint radio resource management in LTE-UMTS scenarios. *Comput Netw* 55(7):1487–1497
30. Amir S, Mohammad S-B (2010) Multi-user time-frequency downlink scheduling and resource allocation for LTE cellular systems. 2010 IEEE Wireless Communications and Networking Conference (WCNC), pp 1–6, April 2010
31. Ghosh A, Ratasuk R, Mondal B, Mangalvedhe N, Thomas T (2010) LTE-advanced: next-generation wireless broadband technology. *IEEE Wirel Commun* 17(3):10–22
32. Gessner C (2009) UMTS Long Term Evolution (LTE) technology introduction. Rohde & Schwarz, Munich, pp 3–53, Sept 2009
33. TS 36.221 Version 10.1.0 (2011) Physical channels and modulation, 3GPP, pp 6–101, March 2011
34. Belhouchet ML, Ebdelli MH (2010) LTE technology performance evaluation. ITU/BDT Arab regional workshop on 4G wireless systems, Jan 2010
35. TS 36.213 Version 10.1.0 (2011) Physical layer procedures, 3GPP, pp 5–112, March 2011
36. Huang J-S, Dou C. (2004) Adaptive modulation schemes for 3G WCDMA in multipath channels, pp 1–73, June 2004
37. Miki N, Kawai H, Taoka H, Higuchi K, Sawahashi M, Matsuno H, Nagasaka H (2009) MLD based MIMO-OFDM demodulation and decoding LSI with low power consumption for release 8 LTE. 2009 IEEE 70th Vehicular Technology Conference Fall (VTC 2009-Fall), pp 1–5, Sept 2009
38. TS 25.101 Version 10.1.0 (2011) User Equipment (UE) radio transmission and reception (FDD), 3GPP, pp 11–226, April 2011
39. TR 25.922 Version 7.1.0 (2007) Radio resource management strategies (Release 7), 3GPP, pp 7–91, March 2007

Automatic Travel Blog Generator Based on Intelligent Web Platform and Mobile Applications

Yi-Jiu Chen, Wei-Sheng Zeng and Shian-Hua Lin

Abstract It is very convenient to carry smartphones and take photos on the trip. With Apps installed in smartphones, users can easily share photos to friends on social networks. Huge amount of interesting photos are therefore accumulated through smartphones without facilities to manage these photos. We propose an integrated system that provides a mobile App for photographing on the trip, a desktop App for synchronizing photos with the web platform for sharing and organizing photos. While photographing, the web service recommends significant tags to photos and gets manual tags, the App transparently accumulates context-information for travel photos. Then, the desktop App facilitates users to collect and choose interesting photos for sharing and storing on the web platform. Finally, the system applies search engine and web mining techniques to extract textual sentences from pages that contain relevant information about photos for writing travel blogs easily and efficiently.

Keywords Mobile applications · Travel photo · Text mining · Social network

Y.-J. Chen (✉) · W.-S. Zeng · S.-H. Lin
Department of Computer Science and Information Engineering, National Chi Nan University, Puli, Nantou, Taiwan
e-mail: aa098123@gmail.com

W.-S. Zeng
e-mail: wilson7126@gmail.com

S.-H. Lin
e-mail: shlin@ncnu.edu.tw

1 Introduction

As the rapid development of smartphones, mobile network services and applications (Apps), users are familiar to take photos with smartphones on their trips and share photos to friends on social networks. With facilities provide mobile services and smartphone Apps, rich metadata information of a photo taken by the smartphone can be stored on the device and be uploaded to the website automatically. First, the Exchangeable Image File Format (EXIF) is a standard that specifies the formats for images, sound, and ancillary tags used by digital cameras (including smartphones) [7], so that the orientation, resolution, camera parameters, etc. of a photo are stored with the photo. Next, Based on Location-Based Services (LBS), the location information such as the position on the map, near attractions, or near friends on the social network, can be easily added into the photo through just one or two clicks on the App. Therefore, smartphones transparently help users to accumulate many interesting photos with location and textual information. Furthermore, many users write blog articles for recording their journey during or after the trip. However, writing travel blogs is still a tedious work that consists of collecting photos from several devices (smartphones or digital cameras), selecting interesting or valuable photos and uploading them to the blog site, thinking contents and stories for describing photos, finding references from the Web, decorating the article for readability, and designing template for presenting the blog article. Consequently, users frequently own many travel photos scattered on different devices, hard drives or web storages without generating nice contents. Based on aforementioned problems and motivations, we develop an intelligent web system for travelers to organizing travel photos and writing travel blogs easily and efficiently. The system consists of three parts of subsystems.

- Mobile App (*mApp*) for taking photos: By installing *mApp* on the smartphone, the photo with EXIF and location information is sent to *iTravel* and the web API returns *significant tags* [14] to the user for adding meaningful tags into photo.
- Synchronization App (*sApp*) for collecting interesting photos: By connecting smartphones and digital cameras, the *sApp* automatically extracts important photos from devices according to the space-time information near to those tagged photos. Consequently, *sApp* saves time for users by avoiding tedious manual selections for collecting photos from several devices.
- *iTravel* is an intelligent web platform for travel-related services that integrates social network services and blog services. First, *iTravel* partitions all photos into groups according to space-time information. Significant tags and the photo's metadata are employed to perform meta-search and fetch relevant pages from search engines. Applying information extraction techniques, relevant textual sentences are extracted for the photo. The traveler easily clicks relevant sentences as the title, annotation (caption, keywords or tags), and description. Consequently, writing travel blogs is easy on *iTravel*.

2 Related Works

The travel blog is composed of both travel photos and textual contents. Given a blog topic such as “two-day tour around the Sun Moon Lake”, we can obtain tens millions pages from search engines and tens thousands photos with tags from Flickr. Hence, the Web contains all materials for writing blogs, but how to write high-quality blogs efficiently by utilizing web resources? As for writing travel blogs, travelers surely want to use photos taken on the trip and mention stories and contents about objects in the photo. Web mining, including research topics of search engines, data mining, web information extraction, etc., provides key techniques for solving the problem. These and useful web resources techniques will be illustrated in the following sections.

However, to mining related information for a travel photo, some metadata like tags, location, time, etc. have to bind with the photo. Fortunately, the rapid development of mobile services and smartphones seal the gap by transparently storing photo metadata. Smartphones can manage acquisition, processing, transmission, and presentation of multiple modal data such as image, video, audio and text information, as well as rich contextual information like location and direction from the equipped sensors [13].

Research papers about computer-aided blog generators are not plentiful. In [3], authors proposed Travel Blog Assistant System (TBAS) that facilitates the travel blog writing by automatically selecting for each blog paragraph written by the user the most relevant images from an uploaded image set. By building relations between uploaded images and textual keywords, the system recommends images for the paragraph written by the user. The motivation is contrast to this paper that tagging photos on the trip with smartphone App, then applying tags and photos metadata to mine relevant contents for writing blogs. In [13], authors review blogging services based on manual efforts and categorize into three paradigms.

- *Manual mobile blogging* defines three steps to “choose photos”, “input texts”, and “publish or share”. Facebook App already carried out this approach.
- *Text-free automatic blogging* organizes photos by space–time order and presents photos on the map without using additional text. Nowadays, users take photos with iPhone and manage photos with iPhoto App installed in Mac OS.
- *Text-rich automatic blogging* provides a relatively friendly interface to help users create blogs in an automatic (or semi-automatic) manner.

3 The System

To provide travel-related information and knowledge for annotating the photo, search engine and data mining methods are applied to do following processes.

3.1 Domain Data Collection

In this paper, we focus on providing travel services in Taiwan. By querying keywords like “旅遊 (travel)” and “旅遊部落格 (travel blog)” to search engines, we collected tens thousands of pages from various websites. Based on the statistical information of page counts from individual sites, several important commercial travel sites and blog sites are discovered. Accordingly, the following DME module can extract travel objects with metadata from travel sites and find huge amount of textual sentences relevant to some travel objects from blog sites. To provide tag information for photos, the DDC module also crawls Flickr [8], the famous social network site for tagging landscapes. The photo tagged in Flickr consists of metadata: author’s ID (author may be associated to the quality), position (location), data and time, title, annotations, tags, albums, etc., as shown in Fig. 1. Therefore, DME is able to extract the metadata of travel objects from Flickr. Those tags extracted will be stored in a dictionary table and the Location-Based Search Engine (LBSE of our works in [14]) create inverted index (Location-Tag) to efficiently retrieve tags related to a position. We also collect pages from travel or blog sites for accumulating introductions to some travel objects, so that more sentences are extracted for decorating the photo while writing blogs, as examples shown in Fig. 2.

3.2 Domain Metadata Extraction

Many methods of Information Extraction [10–12, 15] were proposed for various purposes. In this paper, DME employs Cardie’s five pipe-lined processes, tokenization and tagging, sentence analysis, extraction, merging and template generation [4], to perform information extraction tasks that mine metadata of travel objects from aforementioned websites. First, tags and titles of landscapes are

Fig. 1 Photos with metadata can be collected from Flickr

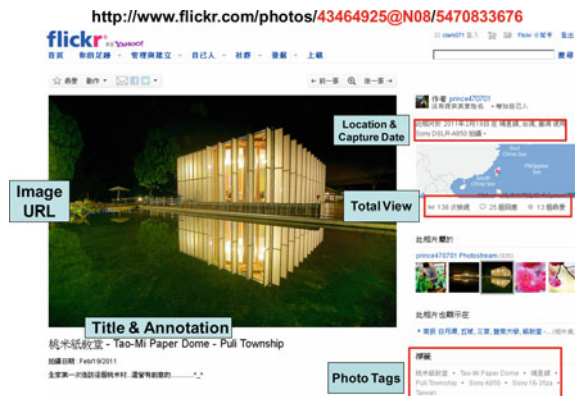


Fig. 2 Introductions and metadata of photos extractable from travel sites



extracted into the dictionary by crawler programs customized for Flickr, blog and travel sites. Next, relevant pages are parsed by the DOM [6] parser to elicit sentences to re-estimate the relevance based on tokens appearing in the dictionary. High-relevant sentences are analyzed for extracting novel phrases as new tags or titles. Statistics-based term-segmentation proposed in [5] is employed to explore new Chinese phrases. The DOM-tree node containing those sentences are applied to extract texts as the values of metadata attributes manually labeled and defined as templates of specific sites. Consequently, extracted metadata and objects are summarized in Table 1.

3.3 Significant Tag Recommendation

In the past study [14], we propose the Tag Recommendation System (*TRS*) for mining *significant tags* from Flickr’s photos. *TRS* consists of three modules. First, Location-Based Search Engine (*LBSE*) is designed to create inverted index [2, 9] of Location-Object for retrieving domain objects close to some location. Extracted metadata of domain objects are stored in the structured database. Tags and titles of domain objects are also merged into the dictionary table. Therefore, Tag Association Miner (*TAM*) applies the mining association method [1] to discover

Table 1 Travel-related objects with photos, tags, and itineraries extracted by DME

Object types	Counts	Relevant information
Tags for landscapes	73,846	Flick tags, titles, and extracted phrases
GPS data	33,148	Positions of photos, landscapes, restaurant, etc.
Landscape objects	3,315	Most photos are tagged with landscapes.
Restaurant objects	3,151	Frequently mentioned in blogs with landscapes
Accommodations objects	3,804	Frequently mentioned in blogs with landscapes
Photo objects	619,279	Many tags for camera parameters are useless.
Itinerary objects	686	The itinerary forms the framework of a blog.



Fig. 3 Photos and recommended tags (*red*: significant tags) returned by TRS

significant tags based on mining association rules between tags within the dictionary. Finally, TRS proposes ranking and scoring methods for recommending significant tags to photos with locations.

To facilitate the development of mobile applications and web services, we implement TRS services as Web API. Following examples show that the user took photos with our mApp, and click tags recommended from TRS API. These photos are taken around ChiChi, Nantou County, Taiwan (集集, 南投縣, 台灣), as shown in Fig. 3. The first photo received tags CheCheng (車埕) and huts (木屋). The former tags is corresponding to the location, the attraction may appear in Facebook “Where are you?” service; the latter is a significant tag applied to search valuable contents and stories by querying “車埕木屋” to Google. That’s why significant tags are more important than general tags like attractions while retrieving valuable information.

3.4 Photo Annotation Recommendation

Given a photo with some tags, photo annotation recommendation (PAR) rapidly retrieves relevant sentences based on the Tag-Sentence inverted index created in advanced. Then, PAR calculates scores of each sentence associated to the photo. Finally, high-score sentences are categorized into title, annotation (caption) and description according to score and length of the sentence. The result of a photo recommended by PAR is shown in Fig. 4. Given a photo (p) with several tags ($t \in p$), the score (S_{ip}) of a string (S_j) to the photo is derived from the product of the tag weight to the photo (w_t) and the weight of the tag to the string (w_{ti}). The length of tag and string in Equation (1) is for normalization that avoids the bias of short tag and long string. The remaining task is to assign strings as title, annotation or description of the photo.



Fig. 4 Textual sentences extracted and recommended as title, caption, or description that can be manually selected by clicking the check box

$$s_{ip} = \sum_{t \in p} \frac{|t| \times w_t \times w_{ti}}{|s_i|} \tag{1}$$

As we mentioned previously, sApp uploads travel photos to iTravel, re-ranks these photos according to date and time, and simply clusters them into several photo groups based on *space-time* information, in which photos were taken in near place and at close time. The data flow diagram of PAR is shown in Fig. 5. First, tags of a photo are employed to retrieve segments that are partitioned from the sentence according to punctuations. If some photos have no tags, tags of photos in the same group are applied. Obviously, shorter segments with high Photo-Segment scores will be categorized into annotations or titles. Then, adjacent segments are merged to extend to the whole sentence, and re-calculate the Photo-Sentence score. If we focus on sentence-level, titles or annotations are hard to be discovered due to lower score of the sentence. On the other hand, concentrating on the segment-level will obtain too many segments that cannot form a complete sentence for decorating the photo’s description. Finally, PAR categorizes strings (segments or sentences) into three classes: title, annotation, and description, based on following criteria.

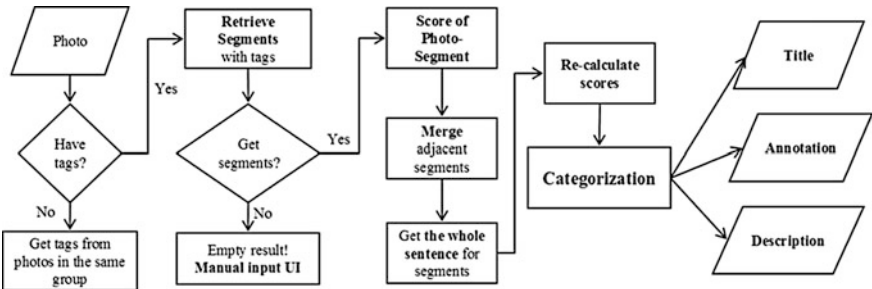


Fig. 5 Retrieving texts and recommending as title, caption, or description

- Title: matching with landscape tags, segment or short-length sentence and high Photo-String score.
- Annotation: segment or short-length sentence and high Photo-String score.
- Description: sentence and medium Photo-String score.

3.5 Travel Blog Generation

After selecting photos with sentences of titles, annotations and descriptions, the user can select templates and preview the blog results. By revising contents and decorating sentences and articles, the travel blog can be published on iTravel and other blog sites concurrently. Designing templates and implementing the web UI for manually revising contents is a tedious work and omitted in this paper. The system integrates iTravel, mApp, sApp and social network services and is summarized in Fig. 6.

4 Evaluation

To evaluate the performance of the proposed system, we actually take 12 photos around ChiChi as the test data and ask two users to write blogs on iTravel and Wretch (<http://www.wretch.cc/>, one of the most famous blog sites in Taiwan), respectively. Consequently, user A spends 510 s on writing 1,378 Chinese

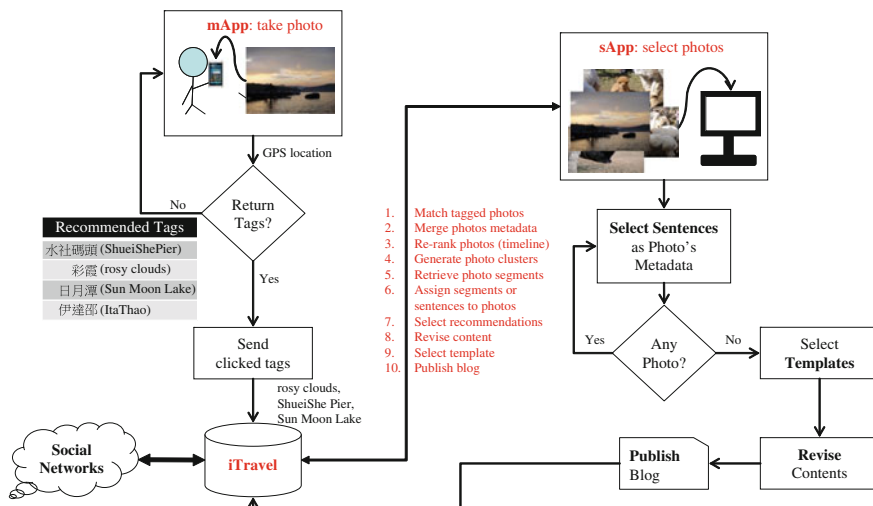


Fig. 6 The summarization of the integration on iTravel system, mApp and sApp



Fig. 7 The title, caption, and description with smart tags for specific strings is generated for the photo by manual clicks

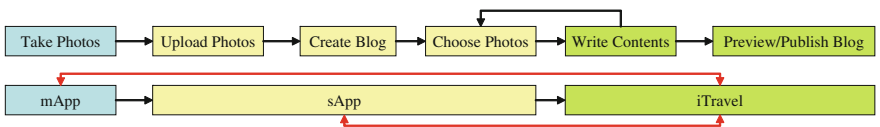


Fig. 8 Creating blogs: blog site versus this paper’s system

characters on iTravel; user B spends 3,605 s on writing 1,547 Chinese characters on Wretch. As the example shown in Fig. 7, each photo with title, caption, and description is generated by manual clicks on relevant photo sentences. The system also adds hyperlinks for strings covering specific terms appearing in the dictionary, like smart tags. By revising texts directly, set formats, and select various templates to present photos with different styles, the travel blog is generated easily and efficiently.

According to Fig. 8, the top/bottom DFD shows steps of writing blogs on Wretch/iTravel, respectively. Similar processes are mapped into the same color. Writing on traditional blog sites suffers from the cycle of (Choose Photos, Write Contents), each iteration spends a long time to think contents and type words. However, mApp and sApp communicate with iTravel based on smartphones and mobile services that would constantly accumulate metadata for guiding the mining process run on the backend of iTravel. Therefore, the system saves a lot of time for bloggers while thinking and writing.

5 Conclusion

In this paper, we carry out a system that seamlessly integrates mobile and desktop Apps with the proposed web platform, iTravel. Using smartphone App on the travel time, the traveler enjoys his or her trip by taking photos without efforts for

typing annotations into each photo. The desktop App automatically collects photos from not only smartphones installed with Apps but also other digital cameras that contains photos of the trip, and synchronizes those photos with iTravel. Based on search engine, web mining and information extraction techniques, iTravel automatically explores related metadata for the trip and recommend sentences for annotating photos. Consequently, writing travel blogs on iTravel is very simple and efficient.

References

1. Agrawal R, Imielinski T, Swami A (1993) Mining association rules between sets of items in large databases. In: ACM SIGMOD
2. Baeza-Yates R (1999) Modern information retrieval. Addison Wesley, New York
3. Bressan M, Csurka G, Hoppenot Y, Renders JM (2008) Travel Blog Assistant System (TBAS): an example scenario of how to enrich text with images and images with text using online multimedia repositories. In: VISAPP workshop on metadata mining for image understanding, 22 January, Funchal, Madeira, Portugal
4. Cardie C (1997) Empirical methods in information extraction. *AI Mag* 18(4):5–79
5. Chien LF (1997) PAT-tree-based keyword extraction for Chinese information retrieval. In: ACM SIGIR
6. DOM, Wikipedia, http://en.wikipedia.org/wiki/Document_Object_Model
7. EXIF, Wikipedia, http://en.wikipedia.org/wiki/Exchangeable_image_file_format
8. Flickr, <http://www.flickr.com/>
9. Frakes WB, Baeza-Yates R (1992) Information retrieval—data structures and algorithms. Prentice Hall, Upper Saddle River
10. Freitag D (1998) Machine learning for information extraction. PhD Dissertation of Computer Science Department, Carnegie Mellon University, Pittsburgh, PA
11. Hsu CN, Dung MT (1998) Generating finite-state transducers for semi-structured data extraction from the web. *Inform Syst* 23(8):521–538
12. Kushmerick N, Weld D, Doorenbos R (1997) Wrapper induction for information extraction. In: Proceedings of the 15th international joint conference on artificial intelligence
13. Li HZ, Hua XS (2010) Melog—Mobile experience sharing through automatic multimedia blogging. In: ACM multimedia workshop on mobile cloud media computing, pp 19–24
14. Wang JY, Chang YL, Zeng WS, Lin SH (2012) Recommend significant tags to travel photos based on web mining. In: 3rd international conference on mobile, ubiquitous, and intelligent computing, pp 84–89
15. Wang K, Liu H (2000) Discovering structural association of semistructured data. *IEEE Trans Knowl Data Eng* 12(3):353–371

Thai Wikipedia Link Suggestion Framework

Arnon Rungsawang, Sompop Siangkhio, Athasit Surarerk
and Bundit Manaskasemsak

Abstract The paper presents a framework that exploits the Thai Wikipedia articles as a knowledge source to train the machine learning classifier for link suggestion purpose. Given an input document, important concepts in the text have been automatically extracted, and the chosen corresponding Wikipedia pages have been determined and suggested to be the destination links for additional information. Preliminary experiments from the prototype running on a test set of Thai Wikipedia articles show that this automatic link suggestion framework provides reasonably up to 90 % link suggestion accuracy.

Keywords Thai Wikipedia · Wikify · Wikification · Sense disambiguation · Keyword extraction · Link suggestion · Machine learning

1 Introduction

Wikipedia, the most active and visited encyclopedia ever existence, has become one of the largest online repositories of knowledge with millions of articles available in number of languages. Terms in each Wikipedia article have been anchored to

A. Rungsawang (✉) · B. Manaskasemsak
Massive Information and Knowledge Engineering, Department of Computer Engineering,
Faculty of Engineering, Kasetsart University, Bangkok 10900, Thailand
e-mail: arnon@mikelab.net

B. Manaskasemsak
e-mail: un@mikelab.net

S. Siangkhio · A. Surarerk
Engineering Laboratory in Theoretical Enumerable System, Department of Computer
Engineering, Faculty of Engineering, Chulalongkorn University, Bangkok 10330, Thailand
e-mail: sompoptuck@gmail.com

A. Surarerk
e-mail: athasit.s@chula.ac.th

provide users with a quick way of an access to additional information. Those annotations have been done by Wikipedia contributors following the same guidelines concerning the selection of important concepts in the article, and assigning them with links to other related articles. Since each important concept in a page has been selected by human, many researchers have applied Wikipedia as a human crafted knowledge source in many natural language processing tasks [1–3, 6]. Here we interest in *wikification* process of Thai-language Wikipedia pages in which important concepts (or keywords) and their corresponding destination Wikipedia pages have been automatically identified.

Currently, Thai Wikipedia consists of around 79,000 pages [11] of which its size is only around one-fifth of the English Wikipedia volume. To promote the Thai Wikipedia usage and to facilitate Wikipedia contributors to easily create novel Thai-language based Wikipedia pages, an additional automatic utility is then required. To our knowledge, this work is the first attempt to explore the wikification process for Thai Wikipedia pages. Since Thai language attributes are different from the English ones, such that there is no separation between words, no inflected form for verb, no clearly form for a proper noun, etc., all methods reported and explored in the literatures [2, 3] that work with good performance in wikification processes are not suitable for Thai Wikipedia pages. Therefore, in this paper we propose a link suggestion framework especially for Thai wikification process.

Difference from the literature works [2, 3], our Thai Wikipedia *link suggestion* combines two main wikification processes, i.e., keyword extraction and link disambiguation, into one framework. Given an input document, features of the controlled vocabulary keywords have been extracted, and sent to a machine learning based classifier for identifying the proper destination Wikipedia pages. In case an ambiguity occurs, e.g., a polysemous word, other unambiguous keywords nearby will be examined, and their features will be extracted and used to determine the most appropriate sense for the considering ambiguous keyword. Our preliminary experiments that are based on a version of July 2012 Thai Wikipedia pages show a promising wikification performance in term of link suggestion accuracy.

In the following, we start by a brief overview on the state of the art in English wikification processes. We continue to our proposed link suggestion framework which describes how we pre-process the Thai Wikipedia data and extract features to train the machine learning classifier. We then provide the preliminary evaluation results. Finally, we conclude our findings, and recommend some interesting future research direction.

2 Related Work

Automatic link suggestion using Wikipedia as a knowledge source has been well explored in English language. Mihalcea and Csomai's Wikify work [2] seems to be one of the first proposals to use Wikipedia for wikification process. Their

system works in two separate phases. The first, *keyword extraction* involves identifying important words or phrases from which links should be made. This phase is divided into another two steps; candidate extraction, and keyword ranking. The candidate extraction step first parses the input document and extracts all possible n-grams that are also present in either Wikipedia titles or anchors (i.e., those words or phrases that have ever found to be linked to other Wikipedia articles.) Then the ranking step assigns a numerical value to each candidate, reflecting the *link probability* of a given candidate. Finally, candidate terms whose link probability exceeds a certain threshold will be selected as the keywords to be linked to other Wikipedia pages.

The second, *link (or sense) disambiguation* ensures that the extracted keywords found in the first phase are linked to the appropriate senses or articles. Since an anchor in Wikipedia can have more than one meaning, the correct sense can be selected based on the context where it occurs. To choose the appropriate destination, Mihalcea and Csomai [2] employ two disambiguation algorithms. The first one attempts to identify the most likely meaning for a word in a given context based on a measure of approximate contextual overlap calculated from the corresponding Wikipedia pages and the context where the ambiguous word occurs. The second one extracts features from the candidate term and its surrounding (the terms themselves and their parts of speech), and compares them to training examples obtained from the training data.

On the other hand, Milne and Witten [3] propose to use a machine learning based sense disambiguation in the first phase to inform keyword extraction in the second phase. They first select Wikipedia articles containing quite number of links as the training set, and divide the connection pair between an anchor term and its chosen Wikipedia article as a positive example, and the remaining possible pairs with other destinations as negative ones. Then two main features, i.e., commonness and relatedness, have been extracted. The commonness of a sense is defined as the number of times it is used as a destination in Wikipedia, while the relatedness of a sense compares the appropriate match between possible destination senses and other non-ambiguous keywords of the considering ambiguous word's context.

In contrast to Wikify's keyword extraction approach [2] that relies exclusively on link probability, Milne and Witten [3] propose to employ a machine learning based link detection (aka. keyword extraction.) The relatedness and disambiguation confidence features learned from Wikipedia articles in the previous disambiguation phase have been reused, including with the link probability value of Mihalcea and Csomai [2]. In addition, the generality feature of a topic which measures the minimum depth at which that topic is located in Wikipedia's category tree, and location/spread features which record the location of the first occurrence and the distance between the first and last occurrences of the considering candidate word have also been extracted to train the link detection classifier.

The key difference between our approach and the wikification processes proposed in [2, 3] is that we combine the keyword extraction and the link disambiguation into one shot. A candidate keyword is first detected, and then, when ambiguity occurs, the destination Wikipedia pages have been examined and

selected based on their semantic relatedness. Features extracted from pair of keywords and their destination pages are then used to train a machine learning classifier to learn how to suggest links in a new document.

3 Proposed Link Suggestion Framework

Link suggestion framework consists of four steps; pre-processing, feature extraction, training and testing the machine learning classifier.

3.1 Pre-Processing

All the experiments described in this paper are based on the 9th July, 2012 Thai Wikipedia version. Titles and contents of the whole Wikipedia have been parsed from the provided XML file [11]. Since Thai Wikipedia articles contain both English and Thai keywords, and the Thai language has no word boundary, we then first tokenize each word using Thai-English Lexitron (Lexeme Tokenizer, aka. Lexto) [8]. All words found once either in titles or anchor texts have been accumulated to build the controlled vocabulary set for later usage in both training and testing phases.

As we will treat each word in the controlled vocabulary as a candidate keyword for link suggestion, its term and document frequency, the number of times that term has and has not been used as keyword, type of that keyword (i.e., English or Thai, title or anchor), the list of destination Wikipedia articles, the list of articles that the keyword have been appeared, and the link probability, have been collected. In addition, other statistics such as article's length (i.e., the number of words), list of the incoming articles, the number of out-going links, and the type of article (i.e., either redirect or disambiguation page), have also been recorded for later usage in feature extraction process.

3.2 Feature Extraction

Given the controlled vocabulary setting, all controlled words and phrases (i.e., at least two consecutive tokens) found in a document will be treated as candidate terms. Since our link suggestion framework uses the machine learning classifier to determine whether the candidate term found in a document should be selected as link, we extract a training feature vector for each of its occurrence. The component features are explained as follows.

Link probability. As explained in [2], the link probability of a candidate term W to be selected as a keyword in a new document is defined as the number of

documents where that term has already been chosen as keyword ($\text{count}(D_{\text{key}})$) divided by the total number of documents in which the term appears ($\text{count}(D_W)$). This statistic can be collected from the Wikipedia articles.

$$LP(\text{keyword} \setminus W) \approx \frac{\text{count}(D_{\text{key}})}{\text{count}(D_W)}. \quad (1)$$

Semantic relatedness. The meaning of an appearing keyword in a document can be indirectly interpreted in term of its relatedness with the surrounding context [4]. For an ambiguous word, the appropriate destination sense can be determined by semantic relatedness between its candidate senses and context in which the word occurs. To calculate the relatedness between two articles A and B , here we employ the traditional cosine similarity measure [7] as follows:

$$\text{sim}(A, B) = \frac{A \cdot B}{\|A\| \cdot \|B\|} \quad (2)$$

where A and B represent two *tf.idf* based vectors [10] of the two articles of interest.

To disambiguate an ambiguous word, we consider senses of at most three unambiguous words on its left and right as the context. To select the most appropriate sense, we calculate the probability of which the candidate sense has already been chosen, and the similarity values between the input document and the candidate senses, using Eq. (3).

$$\text{Destination}(C, k) = \arg \max_{b_j \in B} [P(k, b_j) \cdot \text{sim}(C, b_j)] \quad (3)$$

where C is an input document, k is the keyword under consideration, B is the set of possible senses (i.e., destination Wikipedia pages) for k , and $P(k, b_j)$ is the probability that b_j is the destination page of k .

Position. To avoid the over-link problem, link to another Wikipedia page should be annotated only when clarification or context is needed. Here we let the machine to learn which position in a document (counting the first appearing keyword as one, the second as two, etc.) a keyword should be linked.

Title\English\Ambiguous\Redirect. These features record whether the keyword is found in a Wikipedia's title, or the keyword is written in English, or an ambiguous word, or the underlying article is a redirect page.

3.3 Training and Evaluating the Classifier

During the training phase, we extract the training features from pairs of keywords and their corresponding destinations found in a Wikipedia page. During the evaluation phase, a feature vector whose link is a pair of the controlled vocabulary term and its corresponding destination Wikipedia page is extracted and sent to the classifier to decide whether that link is appropriate to suggest. Both training and

```

1: @attribute link_prob numeric
2: @attribute left_sim3 numeric
3: @attribute left_sim2 numeric
4: @attribute left_sim1 numeric
5: @attribute this_sim numeric
6: @attribute right_sim1 numeric
7: @attribute right_sim2 numeric
8: @attribute right_sim3 numeric
9: @attribute position numeric
10: @attribute is_title {true,false}
11: @attribute is_english {true,false}
12: @attribute is_ambiguous {true,false}
13: @attribute is_redirect {true,false}
14: @attribute 'link' {Y,N}
15: @data
16: 0.0335,0,0,0,0.7864,0.6351,0.7123,0,1,true,false,false,false,Y

```

Fig. 1 An example record of a feature vector written in an ARFF

testing instances have been converted into an ARFF (Attribute-Relation File Format) [9], as an example record depicted in Fig. 1

In Fig. 1, line number 2-4, as well as 6-8, represent the semantic relatedness scores (calculated by Eq. (2)) between the sense (aka. the destination page chosen by Eq. (3)) of the keyword under consideration and the senses of other three context keywords on its left and right. Other lines provide the example of feature components as previously explained in Sect. 3.2.

4 Preliminary Results

We first pre-process the whole Thai Wikipedia version of July, 2012, as described in Sect. 3.1. Controlled vocabularies composing of around a hundred thousand terms of both Thai and English keywords have been extracted from both Wikipedia titles and anchors.

4.1 Training and Evaluation Data Set

To let the classifier learn how to suggest links in both training and evaluation phases, we randomly select Wikipedia articles containing at least 50 links. A total of 500 articles are chosen for training the classifier, and further 100 articles for evaluation.

A pair of anchor and their destination page can represent many training instances. For an ambiguous word, the connection between the anchor and its chosen destination Wikipedia page (i.e., the appropriate sense) provides a positive example, while the remaining possible pages provide negative ones. Since we

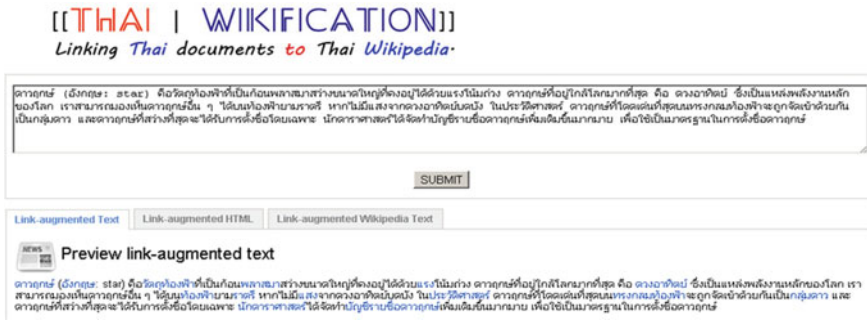


Fig. 2 A sample snapshot of a Thai Wikification system

normally annotate only once to a keyword in a Wikipedia page, then the same keyword that re-occurs (including with its intended sense) is also treated as a negative example. On average, a set of 500 training articles produces around 25,000 positive examples, and 80,000 negative ones.

4.2 Experimental Results

Though we here combine both keyword identification and disambiguation processes into one framework, we investigate and report them separately during the evaluation. For the first, precision and recall which depend on the number of correctly identified keywords are observed. For the later, accuracy that measures the number of correctly chosen destinations for all correct identified keywords is recorded.

We test our framework with the C4.5 decision tree classifier [5] using the WEKA machine learning toolkit [9]. Since each training and testing article has been selected randomly, we re-select them and repeatedly perform the experiments five times and average all the results. Finally, we obtain on average 72 % precision, 69 % recall, and 90 % link suggestion accuracy.

Figure 2 shows a sample snapshot of a Thai Wikification system¹ that can automatically suggest links for any Thai text to Thai Wikipedia pages. This interface allows the user to either paste the local text, or enter an URL of the web page. The system then processes the input provided by the user, automatically identifies the important keywords in that document, suggests the appropriate links, and finally returns and displays the link-augmented text as the result. In case that an URL is input into the system, the structure of the original web page is also maintained at the output with the wikified keywords.

¹ We have provided all data test and the Thai Wikification prototype to all interesting readers at <http://www.mikelab.net/ThWikify>.

5 Conclusion

In this paper, we present a framework that uses the Thai Wikipedia as a knowledge source for Thai-language based wikification process. We integrate both keyword extraction process that automatically identifies the important keywords from the input document, and disambiguation process that suggests appropriate destination Wikipedia pages as links, into one framework. Features extracted from all candidate keywords have been used to train a classifier to learn how to suggest the important links to other Wikipedia pages. Although we have obtained a reasonable wikification performance in terms of accuracy (90 %), the precision (72 %) and recall (69 %) are still not favorable when we compare them with those successes reported in the literature [2, 3]. We thus believe that there are still rooms to improve and investigate. Since the report here has only concluded from our preliminary experimental results, we still not explore the framework with other classifiers' setting. We also look forward to finding other additional relevant language features that are especially for Thai, and studying how to give more bias to the important features that have more classification power than the others. In addition, we plan to do further user study with our proposed framework.

Acknowledgement We would like to thank all anonymous reviewers for their comments and suggestions to improve the final version of the paper. We also would like to thank to both departments of computer engineering in Kasetsart University and Chulalongkorn University for the excellent research environment.

References

1. Kulkarni S, Singh A, Ramakrishnan G, Chakrabarti S (2009) Collective annotation on wikipedia entities in web text. In: Proceedings of the 15th ACM SIGKDD conference on knowledge discovery and data mining. ACM, New York, pp 457–465
2. Mihalcea R, Csomai A (2007) Wikify! Linking documents to encyclopedic knowledge. In: Proceedings of the 16th ACM conference on information and knowledge management. ACM, New York, pp 233–241
3. Milne D, Witten IH (2008) Learning to link with wikipedia. In: Proceedings of the 17th ACM conference on information and knowledge management. ACM, New York, pp. 509–518
4. Patwardhan S, Banerjee S, Paderson T (2003) Using measure of semantic relatedness for word sense disambiguation. In: Proceedings of the 4th international conference on computational linguistics and intelligent text processing, LNCS, vol 2588, pp 241–257
5. Quinlan JR (1993) C4.5: programs for machine learning. Morgan Kaufmann, San Francisco
6. Ratnov L, Roth D, Downey D, Anderson M (2011) Local and global algorithms for disambiguation to wikipedia. In: Proceedings of the 49th annual meeting on the association for computational linguistics. ACL, Oregon, pp. 1375–1384
7. Salton G, McGill MJ (1986) Introduction to modern information retrieval. McGraw-Hill, New York
8. Thai Lexitron (Lexto), <http://lexitron.nectec.or.th>

9. Witten IH, Frank E, Hall MA (2011) Data mining, practical machine learning tools and techniques. Morgan Kaufmann, San Francisco
10. Wu H, Luk R, Wong K, Kwok K (2008) Interpreting TF-IDF term weights as making relevance decision. ACM Trans Inform Syst 26(3):1-37
11. วิกิพีเดีย สารานุกรม, <http://th.wikipedia.org/wiki/หน้าหลัก>

Computing Personalized PageRank Based on Temporal-Biased Proximity

Bundit Manaskasemsak, Pramote Teerasetmanakul,
Kankamol Tongtip, Athasit Surarerks and Arnon Rungsawang

Abstract Dynamic behaviors of World Wide Web is one of the most important characteristics that challenge search engine administrators to manipulate their search collection. Web content and links are changed each day to provide up-to-date information. In addition, a fresh web page, like new news article, is often more interesting to web users than a stale one. Thus, an analysis of temporal activities of the Web can contribute to improve better search and result ranking. In this paper, we propose a web personalized link-based ranking scheme that incorporates temporal information extracted from historical page activities. We first quantify page modifications over time and design a time-proximity model used in calculating inverse propagation scores of web pages. These scores are then used as a bias of personalized PageRank for page authority assessment. We conduct the experiments on a real-world web collection gathered from the Internet Archive. The results show that our approach improves upon PageRank in ranking of search results with respect to human users' preference.

Keywords Temporal-biased personalized PageRank · Time-proximity model · Temporal analysis · PageRank computation · Web ranking algorithm

B. Manaskasemsak (✉) · P. Teerasetmanakul · A. Rungsawang
Massive Information and Knowledge Engineering Laboratory, Department of Computer Engineering, Kasetsart University, Bangkok 10900, Thailand
e-mail: un@mikelab.net

P. Teerasetmanakul
e-mail: boatblaster@gmail.com

A. Rungsawang
e-mail: arnon@mikelab.net

K. Tongtip · A. Surarerks
Engineering Laboratory in Theoretical Enumerable System, Department of Computer Engineering, Chulalongkorn University, Bangkok 10330, Thailand
e-mail: kankamto@gmail.com

A. Surarerks
e-mail: athasit.s@chula.ac.th

1 Introduction

Web link-based ranking schemes have been proved to play a successful role in ranking search results for years. The PageRank algorithm [18], for example, analyzes a web link structure in order to assess an authoritativeness of web pages. A page having many referrers (i.e., in-link pages) will implicitly be conveyed a high authority and thus should be ranked highly in the result list. However, one of the weakest point of the traditional PageRank scheme is that it computes an authoritative score for each web page based on only one crawled snapshot without incorporating temporal information concealed in pages and their connections. It is not surprising that PageRank prefers old pages and may bias against more recent ones [1, 6] since such recent pages have had less time to accumulate in-links in order to contribute their ranking. Therefore, some stale pages usually achieve high authorities than new fresh ones.

The Web is obviously dynamic. Page content and links are continually created, deleted, and changed over time. Moreover, web authors normally updated their pages to provide the recent and up-to-date information. Hence, it could be argued that in many situation a web user may be more interested in recently updated web pages rather than older ones. A new news article page is often more interesting than an old article; a web page for an upcoming conference is clearly more expected to be seen than a page for a past conference, for instance. In this case search engines indeed need a time-aware ranking technique for finding newer and more dynamic content.

In this work, we contribute a time-aware ranking that incorporate temporal aspects in the PageRank paradigm. The approach considers historical activities of web pages and extracts their modification timestamps. Then, we design a time-proximity model for estimating how much the closeness of each of two connected pages is, based on their modified times. To achieve this, we exploit five kernel functions, motivated by previous work [7, 8, 17, 19], to determine each of a weight for each linkage. All weights are then employed in the inverse propagation procedure in order to construct a temporal preference vector that is subsequently used as a bias in personalized PageRank computation to finally assess page authority. Experiments conducted on a real-world web data show a great improvement of our approach upon the traditional PageRank algorithm in term of relevance to the human users' preference.

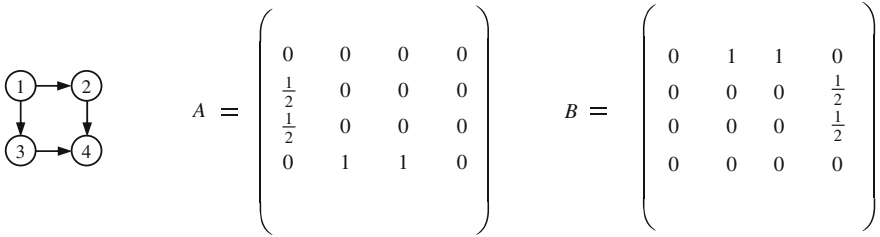


Fig. 1 An example of small web graph with two corresponding representations: the transition matrix A and the inverse transition matrix B

2 Background

2.1 Web Model and Representation

For a snapshot of the Web, we can model it as a directed graph $G = (V, E)$, with N web pages as a set of vertices V and their hyperlinks as a set of edges $E \subset V^2$ in which multiple edges (i.e., several hyperlinks pointing from the same source to the same target) are early unified by a single one. We also remove self hyperlinks. Figure 1 on the left-hand side illustrates a very simple web graph.

In practice, the web graph can simply be represented as a matrix. We first let $O(p)$ be the number of pages that are pointed by a page p , called *out-degree*; and $I(p)$ be the number of pages that point to a page p , called *in-degree*. Hence, we introduce here two versions of matrix representations. The first, a transition matrix A is defined as (also, depicted on the center of Fig. 1):

$$A(q, p) = \begin{cases} \frac{1}{O(p)} & \text{if } (p, q) \in E, \\ 0 & \text{otherwise.} \end{cases} \quad (1)$$

The second, an inverse transition matrix B is defined as (also, depicted on the right-hand side of Fig. 1):

$$B(p, q) = \begin{cases} \frac{1}{I(q)} & \text{if } (p, q) \in E, \\ 0 & \text{otherwise.} \end{cases} \quad (2)$$

2.2 PageRank

PageRank has been known as the most effective link-based ranking algorithm since the advent of Google [5, 18]. It analyzes the link structure, i.e., a web graph, to assess an authoritative score of web pages. Here, the basic concept behind PageRank is that if there is a hyperlink from a web page p to a web page q , then it

can be implied the author of p is interested in q and thus implicitly confers some authoritativeness to it. Furthermore, a page mostly referred by other authority pages has a high authority as well. The PageRank score of a page q , symbolized $r(q)$, is defined as:

$$r(q) = \alpha \sum_{p:(p,q)} \frac{r(p)}{O(p)} + (1 - \alpha) \frac{1}{N}, \quad (3)$$

where the coefficient α is a decay factor that in practice is usually set to 0.85 [11].

In addition, the PageRank computation is also equivalent to solving the principal eigenvector \bar{r} (i.e., representation of the PageRank scores of all web pages) of the problem $\bar{r} = \lambda A \bar{r}$ over the transition matrix A , defined in Eq. (1), with the dominant eigenvalue $\lambda = 1$ in an eigensystem [9]. Then, the equation can be expressed as:

$$\bar{r} = \alpha A \bar{r} + (1 - \alpha) \bar{d}, \quad (4)$$

where \bar{d} is a static score propagated over the whole pages. In a case of the traditional PageRank, this vector is defined by a uniform distribution $[\frac{1}{N}]_{N \times 1}$. However, many studies, including this work, attempt to employ a non-uniform one for determining a bias to some particular web pages [4, 12, 15], known as the personalized PageRank algorithm. Furthermore, the PageRank vector in Eq. (4) can be computed iteratively, for instance, by applying either the power method or Jacobi method [9].

2.3 Inverse PageRank

Inverse PageRank is a variation of PageRank that was introduced in [10]. In the opposite to PageRank, the inverse PageRank paradigm is a process of authority propagation backwards. That is, considering a hyperlink pointing from a page p to a page q , if the page q is supposed to have a high authoritative score, then the page p will also have high authoritative score. Therefore, this approach is to give preference to pages that can reach many other authority pages.

The computation of inverse PageRank is identical to that of the traditional PageRank algorithm, unless the inverse transition matrix B , defined in Eq. (2), is used instead of the regular transition matrix A . Let \bar{s} be a vector containing the inverse PageRank scores of all web pages. Then, the computation can be formulated as:

$$\bar{s} = \alpha B \bar{s} + (1 - \alpha) \bar{d}. \quad (5)$$

Similarly, α and \bar{d} are the decay factor and a static score distribution, respectively, and those also can be the same values used in the tradition PageRank.

3 Temporal-Biased Personalized PageRank

In this section, we present the proposed time-aware link-based ranking algorithm, named temporal-biased personalized PageRank (*TPPR*). Our scheme is composed of four consecutive steps: the first, modeling the Web with respect to historical page activities; the second, determining temporal information based on the time-proximity model; the third, determining temporal-biased vector using the inverse PageRank paradigm; and the last, assessing authoritative scores by employing the bias obtained from the previous step in the traditional PageRank algorithm.

3.1 Web Model Over the Time

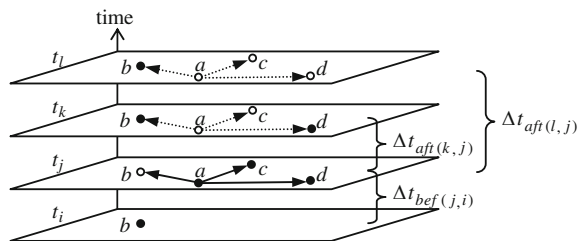
In our web model, the Web will be considered over time based on multiple snapshots at different time $\{t_0, t_1, \dots, t_n\}$. A change can be detected by considering difference in both page content and link connectivity from two consecutive snapshots. Figure 2 below shows a simple example of an archival web of four snapshots.

From the figure, a solid node and edge denote a page and a hyperlink having been changed, i.e., just creation or modification, at that time point; otherwise, they are symbolized by the transparent and dash ones, respectively. If a page (or a hyperlink) was deleted, it will not appear in that snapshot.

3.2 Time-Proximity Model

For any two pages, suppose that at time t_i , an author of a page p has created a link to a page q . One can argue that, at time t_i , p may be more interesting than q because of its recent up-to-dateness. However, since the Web is changing in an arbitrary time, it can possibly be that, at time $t_j > t_i$, the page q is modified to provide more up-to-date information while the author of p does not know and thus stales his/her page.

Fig. 2 An example of web model over the four snapshots



We introduce here the time-proximity model for determining temporal information, i.e., how much the closeness of modification timestamps is of any two web pages that have a link connectivity. Consider the web model depicted in Fig. 2, suppose that we would like to find the time-proximity between the page a and b at time t_i . Since the page a was created and had a link to b at time t_j after the creation of b , and afterwards b was modified without informing to the author of a , this time-proximity can be thus separately considered by two intervals: $\Delta t_{bef(j,i)}$ (i.e., the smallest gap before a was updated) and $\Delta t_{aft(l,j)}$ (i.e., the largest gap after a was updated). The former determines how much the page a is up-to-dateness comparing to the last version of b before being seen by the author of a . In opposite way, the latter determines how much the page a is outdated comparing to the last version of b that has never be seen by the author of a .

Let $w_{pq}(\Delta t_{bef}, \Delta t_{aft})$ be the weight representing the influence between two connected pages for a link $(p, q) \in E$, considering by the intervals Δt_{bef} and Δt_{aft} . Motivated by the previous work [7, 8, 17, 19] that used proximity-based methods, we modify five kernel functions and employ them in our time-proximity model: circle (Eq. (6)), cosine (Eq. (7)), gaussian (Eq. (8)), laplace (Eq. (9)), and triangle (Eq. (10)) kernels.

$$w_{circle_{pq}}(\Delta t_{bef(j,i)}, \Delta t_{aft(k,j)}) = \sqrt{1 - \left(\frac{\beta \Delta t_{bef(j,i)} + (1 - \beta) \Delta t_{aft(k,j)}}{|T|} \right)^2}. \quad (6)$$

$$w_{cosine_{pq}}(\Delta t_{bef(j,i)}, \Delta t_{aft(k,j)}) = \frac{1}{2} \left(1 + \cos \left(\frac{(\beta \Delta t_{bef(j,i)} + (1 - \beta) \Delta t_{aft(k,j)}) \pi}{|T|} \right) \right). \quad (7)$$

$$w_{gaussian_{pq}}(\Delta t_{bef(j,i)}, \Delta t_{aft(k,j)}) = \exp \left(- \frac{(\beta \Delta t_{bef(j,i)} + (1 - \beta) \Delta t_{aft(k,j)})^2}{2|T|^2} \right) \quad (8)$$

$$w_{laplace_{pq}}(\Delta t_{bef(j,i)}, \Delta t_{aft(k,j)}) = \exp \left(- \frac{\sqrt{2}(\beta \Delta t_{bef(j,i)} + (1 - \beta) \Delta t_{aft(k,j)})}{|T|} \right) \quad (9)$$

$$w_{triangle_{pq}}(\Delta t_{bef(j,i)}, \Delta t_{aft(k,j)}) = 1 - \frac{(\beta \Delta t_{bef(j,i)} + (1 - \beta) \Delta t_{aft(k,j)})}{|T|}. \quad (10)$$

Where $t_i < t_j < t_k$, $|T|$ is defined to the total number of snapshots, and β is determined the significance of before and after intervals. Since the larger the interval time is, the lower the weight is produced, we suggest the value of β should be in $[0,0.5]$. Finally, we normalize sum of all out-links of p to 1:

$$w'_{pq}(\Delta t_{bef}, \Delta t_{aft}) = \frac{w_{pq}(\Delta t_{bef}, \Delta t_{aft})}{\sum_{r:(p,r) \in E} w_{pr}(\Delta t_{bef}, \Delta t_{aft})} \quad (11)$$

3.3 Temporal-Biased Vector

We next employ the weights determined during the previous step in order to estimate a preference score (i.e., a bias) of web pages with respect to their historical activities. To achieve this, we hypothesize that when an author update his/her page, the author would completely inspect the entire page including up-to-dateness of content and relatedness of out-links. Thus, a page having many out-links can implicitly reflect activeness in itself since the author has to pay more effort in inspection. One approach to give more preference to that page is to exploit the inverse PageRank paradigm. However, instead of directly use the original inverse transition, we modify the Eq. (2) with incorporating temporal information, defined as:

$$B'(p, q) = \begin{cases} \frac{w'_{pq}(\Delta t_{bef}, \Delta t_{aft})}{\sum_{r:(r,q) \in E} w'_{rq}(\Delta t_{bef}, \Delta t_{aft})} & \text{if } (p, q) \in E, \\ 0 & \text{otherwise.} \end{cases} \quad (12)$$

We then compute temporal-biased vector \bar{s} followed Eq. (5), but replace B with B' .

3.4 Time-Aware Ranking

In the last step, we compute an authoritative score of web pages with respect to time-awareness based on the traditional PageRank defined in the Eq. (4). Motivated by the personalized PageRank concept [4], we therefore replace the static uniform vector \bar{d} with the temporal-biased one \bar{s} , obtained from the Sect. 3.3.

4 Experiments

4.1 Data Set Preparation

We defined a list of URLs selected from the ODP¹ and gathered them from the Internet Archive.² We started downloading snapshots provided from Feb.1996 until Dec.2012. Our web collection consists of around 65.6 Kpages and 194.6 Klinks in each snapshot.

To evaluate the performance of result ranking of our *TPPR* comparing to the traditional *PR*, we implemented a prototype Lucene-based searching system. For

¹ <http://www.dmoz.org/>

² <http://archive.org/>

the experiments, the last web snapshot was extracted the link structure for computing authoritative scores and the web pages were indexed for searching. We conducted the searching scenarios using a set of 35 sample queries, chosen from words frequently appearing in the title field of web pages in the data collection. For a given query, we excerpted top-twenty results ranking only by the *tf-idf* weight [2] and asked a number of volunteers to grade them. Each user can freely assign a score to each resulting page from 0 (unsatisfactory) to 4 (most satisfactory) based on his/her own preference.

4.2 Evaluation Metrics

We use the normalized discounted cumulative gain (*NDCG*), proposed in [13, 14], to measure ranking accuracies when there are multiple levels of relevance judgment. Given a query and a ranking τ , the *NDCG* computed at top- k document is given as:

$$NDCG_k(\tau) = Z_k \sum_{i=1}^k \frac{2^{r(i)} - 1}{\log_2(i + 1)}, \quad (13)$$

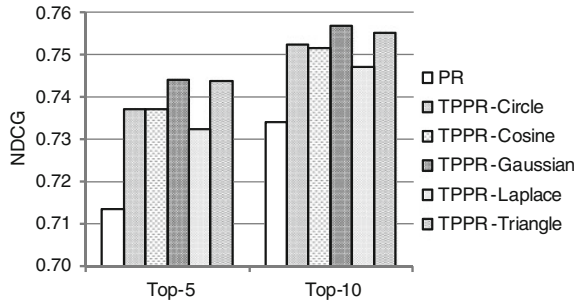
where $r(i)$ is the gain value associated with document at the i -th position of ranking and Z_k is a normalization factor to guarantee that a perfect of this top- k ranking will receive the score of one. Note that the gain value of a document is usually defined as a relevant score; however, in our experimental evaluation we define it as a users' preference score when seeing that document corresponding to a given query.

4.3 Results

To compare the quality of result ranking, we set the static parameter α used in the computation of both *TPPR* and *PR* to the same value of 0.85, and preliminarily set β used in *TPPR* to 0.2. Figure 3 below shows the results on average of *NDCG* over all queries produced at top-5 and 10 of the rankings, respectively.

It is clearly seen in Fig. 3 that all variations of *TPPR* achieve higher *NDCG* scores than does *PR*, indicating that temporal aspects can indeed influence authoritativeness in the ranking scheme. Moreover, by employing the Gaussian kernel function, we can obtain the highest values at top-10 of results, indicating that it can identify the pages most relevant to human users' preference within the top few results.

Fig. 3 Average *NDCG* scores at top-5 and 10 produced by *PR* and five variations of *TPPR*



4.4 Sensitivity Analysis

We now investigate the effect of parameter β specified in the time-proximity model of *TPPR*. We thus vary the value of 0.0 until 0.5 and then illustrate the results in Fig. 4.

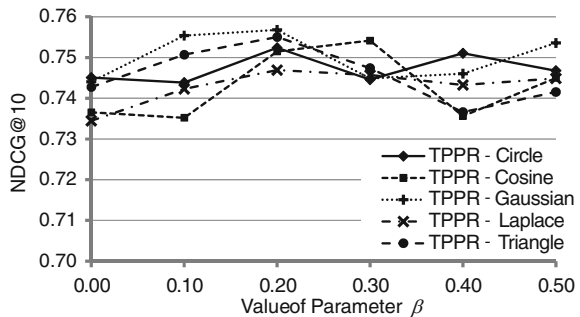
We can see the *NDCG* scores on average are increasing when varying β from 0 to 0.2. The reason is that when $\beta = 0$, *TPPR* does not consider recently updated target pages before a result page has a link pointing to. This may lead to loss of some valuable information. However, increasing β from 0.2 does not influence better the results (some decrease).

5 Related Work

Although the traditional PageRank [18] works well and has successfully been applied in several fields, many studies still attempt to improve it by incorporating various aspects: combining with topic of content [12], learning from users' behavior and log [16], and including other temporal features [3, 20], etc.

Our work differs from the priori study proposed in [3] in two aspects. First, we determine a temporal information based on the time-proximity model, instead of

Fig. 4 Average *NDCG* scores at top-10 produced by *TPPR* when varying the values of β



directly considering page and link freshness from observing their last modification. Second, we influence authoritative scores using a temporal-biased vector obtained from inverse PageRank paradigm, instead of incorporate temporal features in the page transition. In addition, our work differs from the work proposed in [20] in case that we propose the ranking scheme on web collection while that work is applied on scientific publication. Hence, some characteristics of both data are different.

6 Conclusions

One can conclude that recent information today is more probably interesting to most web users. In this paper, we present an alternative web link-based ranking scheme that incorporate temporal aspects in assessing web authoritativeness. The approach can be concluded by four steps. Firstly, we model the Web with respect to time based on web historical activities. Secondly, we propose a time-proximity model to determine the temporal information between two connected pages. Thirdly, we employ the concept of inverse PageRank in order to determine temporal biases to web pages. Lastly, we compute personalized PageRank using those biases to produce authoritative scores. The experiments conducted from real-world web historical data provided by the Internet Archive with a set of sample queries show the promising results with high improvement comparing to the traditional PageRank.

There are still some interesting experiments needed to be carried out. For instance, employing the time-proximity weights in between page transitions that we expect to achieve better improvement. In addition, we would further do more experiments on larger web data set.

References

1. Adamic LA, Huberman BA (2001) The web's hidden order. *Commun ACM* 44(9):55–59
2. Baeza-Yates RA, Ribeiro-Neto BA (1999) *Modern Information Retrieval*. ACM Press & Addison Wesley, New York
3. Berberich K, Vazirgiannis M, Weikum G (2006) Time-aware authority ranking. *Internet Math* 2(3):301–332
4. Brin S, Motwani R, Page L, Winograd T (1998) What can you do with a web in your pocket. *IEEE Data Eng Bull* 21(2):37–47
5. Brin S, Page L (1998) The anatomy of a large-scale hypertextual web search engine. *Comput Netw ISDN* 30(1–7):107–117
6. Cho J, Roy S.(2004) Impact of search engines on page popularity. In: *Proceeding of the 13th WWW Conf*
7. Dai N, Davison BD (2010) Freshness matters: In flowers, food, and web authority. In: *Proceeding of the 33th ACM SIGIR Conf*

8. Gerani S, Carman M, Crestani F (2012) Aggregation methods for proximity-based opinion retrieval. *ACM Trans. Inform. Syst.*, 30(4), article 26
9. Golub GH, Loan CFV (1996) *Matrix Computations*. Johns Hopkins University Press, Baltimore and London
10. Gyöngyi Z, Garcia-Molina H, Pederson J (2004) Combating web spam with TrustRank. In: *Proceeding of the 30th Conf. on VLDB*
11. Haveliwala TH (1999) Efficient computation of PageRank. Technical Report, Stanford InfoLab
12. Haveliwala TH (2003) Topic-sensitive pagerank: a context-sensitive ranking algorithm for web search. *IEEE Trans Knowl Data Eng* 15(4):784–796
13. Järvelin K, Kekäläinen J (2000) IR evaluation methods for retrieving highly relevant documents. In: *Proceeding of the 23rd ACM SIGIR Conf*
14. Järvelin K, Kekäläinen J (2002) Cumulated gain-based evaluation of IR techniques. *ACM Trans Inf Syst* 20(4):422–446
15. Jeh G, Widom J (2003) Scaling personalized web search. In: *Proceeding of the 12th WWW Conference*
16. Liu Y, Liu TY, Gao B, Ma Z, Li H (2010) A framework to compute page importance based on user behaviors. *Inf Retrieval* 13(1):22–45
17. Lv Y, Zhai C (2009) Positional language models for information retrieval. In: *Proceeding of the 32nd ACM SIGIR Conference*
18. Page L, Brin S, Motwani R, Winograd T (1999) The PageRank citation ranking: Bringing order to the web. Technical Report, Stanford InfoLab
19. Petkova D, Croft WB (2007) Proximity-based document representation for named entity retrieval. In: *Proceeding of the 16th ACM CIKM*
20. Yu PS, Li X, Liu B (2005) Adding the temporal dimension to search—A case study in publication search. In: *Proceeding of the International Conference on Web Intelligence*

KSVTs: Towards Knowledge-Based Self-Adaptive Vehicle Trajectory Service

Jin-Hong Kim and Eun-Seok Lee

Abstract The most of very large traffic system by growing the variety of services, the relationships between the vehicle network and the infrastructure are more complex. Moreover, intelligent transportation systems are getting more and more to develop a better combination of travel safety and efficiency since long time ago. Vehicle is being evolved and traffic environment is especially also organized well-defined schedules priorities, which is real time based wireless network traffic condition, variable traffic condition, and traffic pattern from the vehicle navigation system. Accordingly, we propose to Knowledge-based Self-adaptive Vehicle Trajectory Service using genetic algorithm in this paper.

Keywords Vehicle network · Intelligent transportation system (ITS) · Knowledge-based trajectory data (KTD) · Self-adaptive trajectory service (STS)

1 Introduction

Intelligent Transportation System (ITS) are getting more and more to develop a better combination of travel safety and efficiency from prehistoric times to the present. Vehicle is being evolved and traffic environment is especially also organized well-scheduled priorities, which is real time based network traffic condition, variable traffic condition, and traffic pattern for their destination, from

J.-H. Kim (✉)

Department of Computer Engineering, HanSung University,
116, Samseongyoro-16gil, Seongbuk-gu, Seoul, Korea
e-mail: jinhkm@hansung.ac.kr

E.-S. Lee

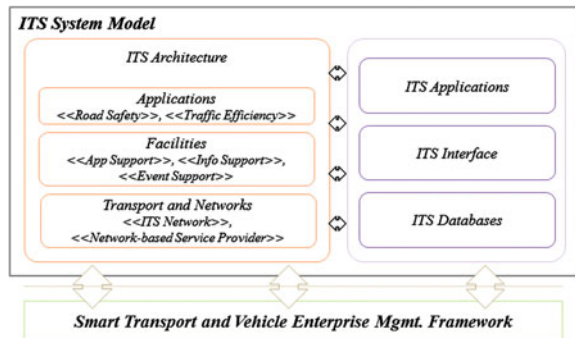
College of Information and Communication Engineering, SungKyunKwan University,
2066, Seobu-Ro, Jangan-Gu, Suown, Gyeonggi-Do, Korea
e-mail: leeess@skku.edu

the vehicle navigation system with GPS [1]. Namely, their remarkable evolution is strongly popularization of next generation wireless internet technology and stabilized the network platform. As these result, vehicle and transportation system are getting smart, they provide newly smart space and experience for drivers. However, intelligent vehicle (Smart vehicle) and transportation system are sadly to seek drivers which had road construction, collisions, debris in the roadway, and heavy traffic freeways particularly in a phenomenon known as traffic weaves [2]. Although, we have search navigation (general two trajectory with same destination at least) again or select the other way to avoid present situation, it is not good case with which occur another traffic jam, consume a great amount of fuel, and deteriorate the status of the vehicle and increase driver fatigue. To solve these problems exiguously, as we known that could a very difficult apply in real world, we propose Knowledge-based Self-adaptive Trajectory service (KSTs) model in intelligent vehicle and transport environment. The rest of the paper is organized as follows. Section 2 is intelligent transport system design, and Sect. 3 presents Knowledge-based Trajectory Data (KTD). Section 4 shows Self-adaptive Trajectory Service (STS). Finally, Sect. 5 is conclusion.

2 Intelligent Transport System Model

Generally, Intelligent Transport System encompasses the application of information and communication technologies to transport [3], as well as include standard-alone infrastructure applications such as traffic management system, and cooperative ITS application involving telematics, vehicle-infrastructure and vehicle to vehicle communications. These technologies cover private and public transport by road, expressway, as well as industrial way, together with application for cross model transport [4]. The focus of this design is on ITS as they are applied to road transport and to interactions between road transport and other transport modes. This ITS model is defined in Fig. 1 where the link between components of system is described.

Fig. 1 ITS system model. It presents transport telematics and intelligent transport systems that are based on the transport engineering to achieve better management framework of transport and processes by using the existing transport infrastructure



The management domain shown in Fig. 1 shows the framework of smart ITS design and maintenance with help of a significant model of an ITS system. We could suggest the basic management domain as follows: (1) *optimization of telecommunication environment between subsystems*; (2) *maximal exploitation of the existing ITS service*; (3) *unified implementation of aspect oriented software component*; (4) *recommendation of intelligent trajectory strategy*; (5) *protocol definitions for the whole set of ITS applications*.

3 Knowledge-Based Trajectory Data

Data collected for use in ITS basically includes information about vehicles, traffic, and events that affect them. Such as, the position, speed, and heading of individual vehicles could be monitored and recorded, or the flow and congestion of traffic in a network of roads could be stored along with any possibly related incidents or interruptions to traffic flow elsewhere in the network/vehicle network [5]. These can all then be correlated against events like accidents, network changes due to planned construction, or the dissemination of traffic data. For our research, the KTD to which the genetic algorithm is used [6–8], and our newly techniques are going to apply as part of CAAS Project at the SungKyunKwan University. KTD approach has potential for any search problem in which knowledge of good cases for sub-problems can be exploited to improve the case of the problem itself. The main idea is to use genetic algorithm to explore the space of problem subdivisions rather than the space of cases themselves, and thus capitalize on the near linear scaling qualities generally inherent in the divide and conquer approach [9–11]. In order to help operators in these problems of traffic trajectory, define decision-making with ITS system model-based approach. Namely, the goal was designed to a formal abstraction of the knowledge domain that we describe to come close to real-time traffic environment as possible. We assume that a case to a problem can be described by a finite number of parameters. Every parameter is coded into a number (for instance, a binary number is 0, 1, and so on.). *We could simply explained example if were either “Desired value = 0” or “Computing = $2x^2 + x - 1$ ”, it is possible to comparison computed value. But, if it were other case, that is “error” when the above problem has 2 cases, such as $x = -1$ or $x = 1/2$, we could not help modified of X .* Of course, for such a simple problem, these cases research loop is much less efficient than using a formal mathematical method that directly solves the problem. However, for ITS of real world, direct formal methods may be becomes a ITS model with a determine about equal to zero (we think that may be positive or negative). Accordingly, Generic algorithm for ITS is iterative loops of optimization, that is a fitness function measure the adaptation of a case to the problem needs. Every case is represented by a set of numbers that we call a set of “parameters” as shown in Fig. 2.

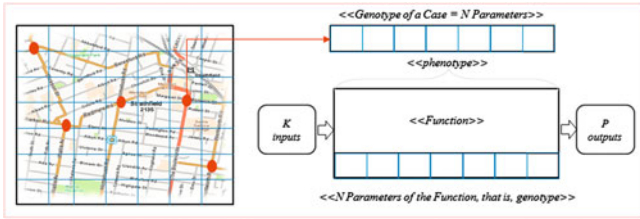


Fig. 2 ITS system model based genetic algorithm. It is shown that is going destination from Strathfield to Burwood in Australia. This shows a figure consisting of same red color of different each line, but we just consider fourth location in order to example

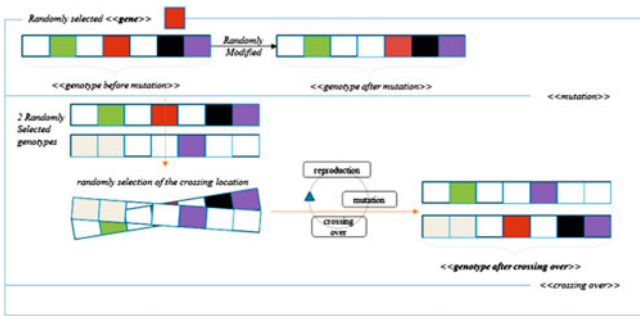


Fig. 3 This case is shown that phenotypes are modified through two ways. Firstly, it is mutation that it consists in moving one parameter through a random modification (*upper*). Secondly, it is crossing over from the two randomly selected genotypes (*lower*)

Phenotypes are filtered by the fitness function that reproduces the most adapted phenotypes. The more the adaptation is needed to the more the reproduction. Phenotypes are modified through two ways in Fig. 3 by genetic algorithm.

4 Self-Adaptive Trajectory Service

In this section, we explain how to compute the STS at an intersection, using an ITS system model. Suppose that an element at intersection i is delivered towards intersection j . Let m_{ij} be the link moving for edge e_{ij} , that is $M_{ij} = m_{ij} + E$. We note the expected shorten path STS at an intersection depends on the forwarding direction [12–14]. When we use this STS model to compute the STS at intersection i because of the traversal will be delivered with some probability to one of outgoing edges at intersection j . This means that when the carrier of this traversal arrives at intersection j , the next carrier on each outgoing edge towards intersection x will be met with probability P_{jx} . We suppose that as shown in Fig. 4 in this case,

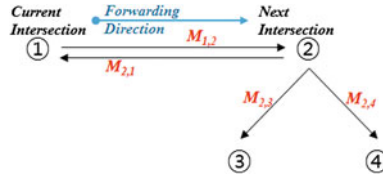


Fig. 4 STS computation for edges (e). First, it will take $m_{1,2}$ seconds to deliver a traversal to the intersection 2 via $e_{1,2}$. Once the traversal arrives at intersection 2, there are three possible cases to deliver the traversal. In other words, the traversal can be forwarded to one of three neighboring intersections of intersection 2 with some probability

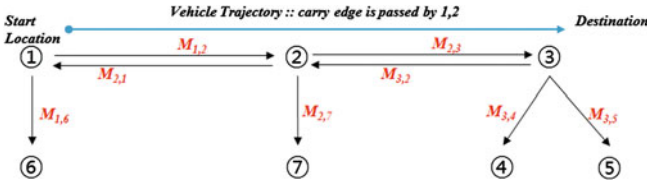


Fig. 5 The vehicle at intersection. First, the vehicle at intersection ① can try to forward the traversals to the neighboring intersections ② and ⑥. If it cannot forward the traversals at the intersection ①, it must carry them by the next intersection ②. When it arrives at intersection ②, it can try to forward again. If it cannot forward again, it will carry the traversal to the third intersection ③. At the destination, if the vehicle cannot forward, it discards the traversals

a traversal carried by a vehicle arrives at intersection ① and is sent towards intersection ②.

Contact Probability: Contact Probability is defined as the chance that a vehicle can encounter another vehicle at an intersection. Let R be communication range. Let v be the mean vehicle speed in the intersection area of intersection i which is a circle of radius R . Let T_i be the duration during which a vehicle is able to communicate with the vehicles around the intersection i . Clearly, T_i is affected by the vehicle speed, the communication range, the traffic signal pattern. *Forwarding Probability:* At an intersection, forwarding is to probabilistic in nature, therefore a traversal is forwarded with best-effort. Let's define the *forwarding probability* as the chance that a traversal carrier at intersection i can forward a traversal to another vehicle moving towards one of the neighboring intersections j_x for $x = 1 \dots m$. We note there is a clear distinction between the *contact probability* and *forwarding probability*, because a traversal will not be forwarded to a contacted vehicle that moves to a wrong direction. Accordingly, we are shown in Fig. 5, let the trajectory be ① \rightarrow ② \rightarrow ③ in the road traversal in ②.

5 Conclusions

This research paper has introduced the Knowledge-based Self-adaptive Vehicle Trajectory Service with the genetic algorithm. Our Self-adaptive vehicle trajectory service is good approaches using both KTD and STS. However, this limitation is resolved by simple prototype, as well as we don't have to easily apply by the restrict environment in real world. Nevertheless, our research is getting to more advantage, supporting the self-adaptive vehicle service of the aspect mechanism and the associating policies depending on adaptive traffic information variation especially. In our advanced future research, we will explore in-depth research on the KTD forwarding from vehicle network access points to moving vehicles for supporting the V2V/V2I infrastructure.

Acknowledgments This research was supported by Next-Generation Computing Development Program through the National Research Foundation of Korea (NRF) funded by the Ministry of Education, Science and Technology (No.2012033347).

References

1. Carter A (2005) The status of vehicle-to-vehicle communication as a means of improving crash prevention performance, Tech. Rep. 05-0264
2. Naumov V, Gross TR (2007) Connectivity-aware routing (CAR) in vehicular ad hoc networks. In: INFOCOM, IEEE
3. Zhao J, Cao G (2008) VADD: vehicle-assisted data delivery in vehicular ad hoc networks. *IEEE Trans Veh Technol* 57(3):1910–1922
4. Jeong J, Guo S, Gu Y, He T, Du D (2008) TBD: trajectory-based data forwarding for light-traffic vehicular networks, Tech. Rep. 08-040
5. Wu H, Fujimoto R, Guensler R, Hunter M (2004) MDDV: a mobility-centric data dissemination algorithm for vehicular networks. In: VANETACM
6. Michalewicz Z (1992) Genetic algorithms + data structures = evolutionary programs. Springer-Verlag, AI Series, New York
7. Spears W, DeJong K (1991) An analysis of multi-point crossover. In: Rawlins G (ed) *Foundations of genetic algorithms*. Morgan-Kaufmann, San Francisco
8. Starkweather T, Whitley D, Mathias K (1991) Optimization using distributed genetic algorithms. In: *Parallel problem solving from nature*. Springer Verlag, Berlin
9. Kim J-H, Kim S-C (2013) Toward hybrid model for architecture-oriented semantic schema of self-adaptive system. In: *International conference on green and human information technology (ICGHIT 2013)*, LNCS. Springer-Verlag
10. Navarro LDB, Sdholt M, Douence R, Menaud JM (2007) Invasive patterns for distributed applications. In *Proceedings of the 9th international symposium on distributed objects, middleware, and applications (DOA'07)*, LNCS. Springer Verlag
11. Grace P, Lagaisse B, Truyen E, Joosen W (2008) A reflective framework for fine-grained adaptation of aspect-oriented compositions. In: *7th international symposium on software composition (SC)*, LNCS, vol 4954, Budapest, Hungary. Springer Verlag, pp 215–230

12. Kim J-H, Kim S-C (2013) Design of architectural smart vehicle middleware. *Inform Int Interdiscipl J* (III), ISSN 1343-4500
13. Sharma PK, Loyall JP, Heineman GT, Schantz RE, Shapiro R, Duzan G (2004) Component-based dynamic QoS adaptations in distributed real-time and embedded systems. In: 6th international OTM conference on distributed objects and applications (DOA), LNCS, vol 3291, Larnaca, Cyprus. Springer, pp 1208–1224
14. Hoh B, Gruteser M, Xiong H, Alrabady A (2010) Achieving guaranteed anonymity in GPS traces via uncertainty-aware path cloaking. *IEEE Trans Mob Comput* 9(8):1089–1107

Part II
Secure and Trust Computing, Data
Management, and Applications

Secure and Reliable Transmission with Cooperative Relays in Two-Hop Wireless Networks

Yulong Shen, Xiaohong Jiang, Jianfeng Ma and Weisong Shi

Abstract This work considers the secure and reliable information transmission in two-hop relay wireless networks without the information of both eavesdropper channels and locations. This paper focuses on a more practical network with finite number of system nodes and explores the corresponding exact results on the number of eavesdroppers the network can tolerate to ensure a desired secrecy and reliability. For achieving secure and reliable information transmission in a finite network, two transmission protocols are considered in this paper, one adopts an optimal but complex relay selection process with less load balance capacity while the other adopts a random but simple relay selection process with good load balance capacity. Theoretical analysis is further provided to determine the exact and maximum number of independent and also uniformly distributed eavesdroppers one network can tolerate to satisfy a specified secrecy and reliability requirements.

Keywords Two-hop wireless networks · Physical layer secrecy · Relay cooperation · Transmission outage · Secrecy outage

Y. Shen (✉) · J. Ma

School of Computer Science and Technology, Xidian University, Xi'an 710071, China
e-mail: ylshen@mail.xidian.edu.cn

X. Jiang

School of Systems Information Science, Future University, Hakodate 418655, Japan

W. Shi

Department of Computer Science, Wayne State University, Detroit 48202 MI, USA

1 Introduction

Two-hop ad hoc wireless networks, where each packet travels at most two hops (source-relay-destination) to reach its destination, has been a class of basic and important networking scenarios [1]. Actually, the analysis of basic two-hop relay networks serves as the foundation for performance study of general multi-hop networks. Due to the promising applications of ad hoc wireless networks in many important scenarios (like battlefield networks, emergency networks, disaster recovery networks), the consideration of secrecy (and also reliability) in such networks is of great importance for ensuring the high confidentiality requirements of these applications. This paper focuses on the issue of secure and reliable information transmission in the basic two-hop ad hoc wireless networks.

Traditionally, the information security is provided by adopting the cryptography approach, where a plain message is encrypted through a cryptographic algorithm that is hard to break (decrypt) in practice by any adversary without the key. While the cryptography is acceptable for general applications with standard security requirement, it may not be sufficient for applications with a requirement of strong form of security (like military networks and emergency networks). That is because the cryptographic approach can hardly achieve everlasting secrecy, since the adversary can record the transmitted messages and try any way to break them [2]. That is why there is an increasing interest in applying signaling scheme in physical layer to provide a strong form of security, where a degraded signal at an eavesdropper is always ensured such that the original data can be hardly recovered regardless of how the signal is processed at the eavesdropper. We consider applying physical layer method to guarantee secure and reliable information transmission in the two-hop wireless networks.

By now, a lot of research efforts have been dedicated to providing security through physical layer methods. A power control scheme is proposed in [3] to ensure that an eavesdropper can never reach its desired signal-to-noise-plus-interference ratio ($SINR$). However, such scheme is not effective when the eavesdropper has a better channel than the receiver. The technique of artificial noise generation has also been widely explored to jam the eavesdroppers and provide secure transmission in the relay communications [4–7]. Recently, the cooperative jamming through node cooperation has been demonstrated to be efficient in ensuring physical layer security [8–10]. It is notable that these schemes generally rely on the knowledge of eavesdropper channels and locations to jam eavesdroppers. In practice, however, it is difficult to gain such information, specifically in untrusted network environment. To address this constraint, a cooperative protocol based on artificial noise generation and multi-user diversity has been proposed recently in [11] to achieve secure transmission in two-hop wireless networks without the knowledge of eavesdropper channels and locations. In particular, the asymptotic behavior of such cooperative protocol in a network has been reported there to illustrate how the number of eavesdroppers the network can tolerate scales as the number of system nodes there tends to infinite.

This paper focuses on applying the relay cooperation scheme to achieve secure and reliable information transmission in a more practical finite two-hop wireless network without the knowledge of both eavesdropper channels and locations.

The remainder of the paper is organized as follows. Section 2 introduces the system models and two cooperative transmission protocols considered in this paper. Section 3 provides theoretical analysis and also related discussions of the two protocols, and Sect. 4 concludes this paper.

2 System Models and Transmission Protocols

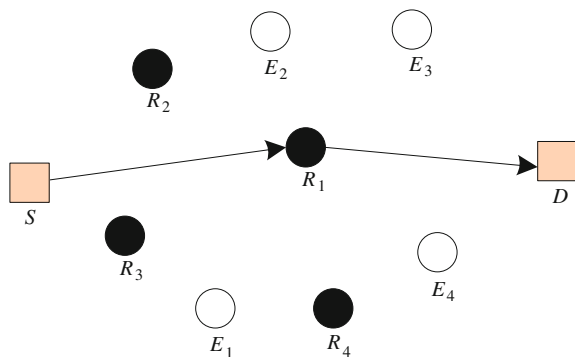
2.1 Network Model

As illustrated in Fig. 1 that we consider a network scenario where a source node S wishes to communicate securely with its destination node D with the help of multiple relay nodes R_1, R_2, \dots, R_n . In addition to these normal system nodes, there are also m eavesdroppers E_1, E_2, \dots, E_m that are independent and also uniformly distributed in the network. Our goal here is to ensure the secure and reliable information transmission from source S to destination D under the condition that no real time information is available about both eavesdropper channels and locations.

2.2 Transmission Model

Consider the transmission from a transmitter A to a receiver B , and denote by $x_i^{(A)}$ the i th symbol transmitted by A and denote by $y_i^{(B)}$ the i th signal received by B . We assume that all nodes transmit with the same power E_s , path loss between all pairs of nodes is equal and independent, and the frequency-nonselective multi-path

Fig. 1 System scenario



fading from A to B is a complex zero-mean Gaussian random variable. Under the condition that all nodes in a group of nodes, \mathcal{R} , are generating noises, the i th signal received at node B from node A is determined as:

$$y_i^{(B)} = h_{A,B} \sqrt{E_s} x_i^{(A)} + \sum_{A_j \in \mathcal{R}} h_{A_j,B} \sqrt{E_s} x_i^{(A_j)} + n_i^{(B)} \quad (1)$$

where the noise $\{n_i^{(B)}\}$ at receiver B is assumed to be i.i.d complex Gaussian random variables with $E\left[|n_i^{(B)}|^2\right] = N_0$, and $|h_{A,B}|^2$ is exponentially distributed with mean $E\left[|h_{A,B}|^2\right]$. Without loss of generality, we assume that $E\left[|h_{A,B}|^2\right] = 1$. The SINR $C_{A,B}$ from A to B is then given by

$$C_{A,B} = \frac{E_s |h_{A,B}|^2}{\sum_{A_j \in \mathcal{R}} E_s |h_{A_j,B}|^2 + N_0/2} \quad (2)$$

For a legitimate node and an eavesdropper, we use two separate SINR thresholds γ_R and γ_E to define the minimum SINR required to recover the transmitted messages for legitimate node and eavesdropper, respectively. Therefore, a system node (relay or destination) is able to decode a packet if and only if its SINR is greater than γ_R , while the transmitted message is secure if and only if the SINR at each eavesdropper is less than γ_E .

2.3 Transmission Protocols

We consider here two transmission protocols for secure and reliable information transmission in two-hop wireless networks. The first is optimal relay selection protocol, in which the optimal relay node with the best link condition to both source and destination is always selected for information relaying. The optimal relay selection protocol works as follows.

- (1) *Channel measurement between source S and relays:* The source S broadcasts a pilot signal to allow each relay to measure the channel from S to itself. The relays, which receive the pilot signal, can accurately calculate $h_{S,R_j}, j = 1, 2, \dots, n$.
- (2) *Channel measurement between destination D and relays:* Analogous to the step 1, the destination D broadcasts a pilot signal to allow each relay to measure the channel from D to itself. The relays, which receive the pilot signal, can accurately calculate $h_{D,R_j}, j = 1, 2, \dots, n$.
- (3) *Relay section:* The relay with the largest $\min\left(|h_{S,R_j}|^2, |h_{D,R_j}|^2\right), j = 1, 2, \dots, n$ is selected as relay, indexed by j^* . Using the same method with step 1 and step 2, each of the other relays $R_j, j = 1, 2, \dots, n, j \neq j^*$ exactly knows $h_{R_j,R_{j^*}}$.

- (4) *Message transmission from source S to the selected relay R_{j^*}* : The source S transmits the messages to R_{j^*} . Concurrently, the relay nodes in cooperative relay node set \mathcal{R}_1 , consists of cooperative nodes with the first t small $|h_{R_j, R_{j^*}}|^2, j = 1, 2, \dots, n, j \neq j^*$, transmit noise to generate interference at eavesdroppers.
- (5) *Message transmission from the selected relay R_{j^*} to destination D* : Similar to the Step 4, the relay R_{j^*} transmits the messages to destination D . Concurrently, the relay nodes in cooperative relay node set \mathcal{R}_2 , consists of cooperative nodes with the first t small $|h_{R_j, D}|^2, j = 1, 2, \dots, n, j \neq j^*$, transmit noise to generate interference at eavesdroppers.

The second is random relay selection protocol, in which the relay node is randomly selected. The random relay selection protocol works as follows.

- (1) *Relay selection*: A relay node, indexed by j^* , is selected randomly from candidate relay nodes $R_j, j = 1, 2, \dots, n$.
- (2) *Channel measurement between the selected relay and the other relays*: The selected relay j^* broadcasts a pilot signal to allow each of other relays to measure the channel from j^* to itself. Each of the other relays $R_j, j = 1, 2, \dots, n, j \neq j^*$ then knows the corresponding value of $h_{R_j, R_{j^*}}$.
- (3) *Channel measurement between destination D and the other relays*: The destination D broadcasts a pilot signal to allow each of other relays to measure the channel from D to itself. Each of the other relays $R_j, j = 1, 2, \dots, n, j \neq j^*$ then knows the corresponding value of $h_{R_j, D}$.
- (4) and (5) These two steps are same with that of the optimal relay selection protocol.

3 Theoretical Analysis

This section first defines the transmission outage and secrecy outage adopted in this paper to depict transmission reliability and transmission secrecy, and then provides theoretical analysis to determine the numbers of eavesdroppers a network can tolerate based on the proposed protocol.

The parameter t involved in the proposed protocol determines whether the relay and destination can receive the messages successfully and whether sufficient noise is generated to suppress eavesdroppers. For the analysis of the proposed protocol, we first determine the range for the parameter t to ensure both secrecy requirement and reliability requirement, based on which we then analyze the number of eavesdroppers a network can be tolerate by applying the protocol. There are two constants τ_1 and τ_2 , which satisfies $|h_{R_j, R_{j^*}}|^2 \leq \tau_1, R_j \in \mathcal{R}_1$ and $|h_{R_j, D}|^2 \leq \tau_2, R_j \in \mathcal{R}_2$.

3.1 Transmission Outage and Secrecy Outage

For a transmission from the source S to destination D , we call transmission outage happens if D cannot decode the transmitted packet, i.e., D received the packet with SINR less than the predefined threshold γ_R . The transmission outage probability, denoted as $P_{out}^{(T)}$, is then defined as the probability that transmission outage from S to D happens. For a predefined upper bound ε_t on $P_{out}^{(T)}$, we call the communication between S and D is reliable if $P_{out}^{(T)} \leq \varepsilon_t$. Notice that for the transmissions from S to the selected relay R_{j^*} and from R_{j^*} to D , the corresponding transmission outage can be defined in the similar way as that of from S to D . We use $O_{S \rightarrow R_{j^*}}^{(T)}$ and $O_{R_{j^*} \rightarrow D}^{(T)}$ to denote the events that transmission outage from source S to R_{j^*} happens and transmission outage from relay R_{j^*} to D happens, respectively. Due to the link independence assumption, we have

$$P_{out}^{(T)} = P\left(O_{S \rightarrow R_{j^*}}^{(T)}\right) + P\left(O_{R_{j^*} \rightarrow D}^{(T)}\right) - P\left(O_{S \rightarrow R_{j^*}}^{(T)}\right) \cdot P\left(O_{R_{j^*} \rightarrow D}^{(T)}\right) \quad (3)$$

Regarding the secrecy outage, we call secrecy outage happens for a transmission from S to D if at least one eavesdropper can recover the transmitted packets during the process of this two-hop transmission, i.e., at least one eavesdropper received the packet with SINR larger than the predefined threshold γ_E . The secrecy outage probability, denoted as $P_{out}^{(S)}$, is then defined as the probability that secrecy outage happens during the transmission from S to D . For a predefined upper bound ε_s on $P_{out}^{(S)}$, we call the communication between S and D is secure if $P_{out}^{(S)} \leq \varepsilon_s$. Notice that for the transmissions from S to the selected relay R_{j^*} and from R_{j^*} to D , the corresponding secrecy outage can be defined in the similar way as that of from S to D . We use $O_{S \rightarrow R_{j^*}}^{(S)}$ and $O_{R_{j^*} \rightarrow D}^{(S)}$ to denote the events that secrecy outage from source S to R_{j^*} happens and secrecy outage from relay R_{j^*} to D happens, respectively. Again, due to the link independence assumption, we have

$$P_{out}^{(S)} = P\left(O_{S \rightarrow R_{j^*}}^{(S)}\right) + P\left(O_{R_{j^*} \rightarrow D}^{(S)}\right) - P\left(O_{S \rightarrow R_{j^*}}^{(S)}\right) \cdot P\left(O_{R_{j^*} \rightarrow D}^{(S)}\right) \quad (4)$$

3.2 Analysis of the Optimal Relay Selection Protocol

We first establish the following two lemmas regarding some basic properties of $P_{out}^{(T)}$, $P_{out}^{(S)}$ and t , which will help us to derive the main result in Theorem 1.

Lemma 1 Consider the network scenario of Fig. 1 with equal path-loss between all pairs of nodes, under the optimal relay selection protocol the transmission

outage probability $P_{out}^{(T)}$ and secrecy outage probability $P_{out}^{(S)}$ there satisfy the following conditions.

$$P_{out}^{(T)} \leq 2 \left[1 - e^{-2\gamma_R t \max(\tau_1, \tau_2)} \right]^n - \left[1 - e^{-2\gamma_R t \max(\tau_1, \tau_2)} \right]^{2n} \quad (5)$$

$$P_{out}^{(S)} \leq 2m \cdot \left(\frac{1}{1 + \gamma_E} \right)^t - m^2 \cdot \left(\frac{1}{1 + \gamma_E} \right)^{2t} \quad (6)$$

Lemma 2 Consider the network scenario of Fig. 1 with equal path loss between all pairs of nodes, to ensure $P_{out}^{(T)} \leq \varepsilon_t$ and $P_{out}^{(S)} \leq \varepsilon_s$ by applying the proposed protocol, the parameter t must satisfy the following condition.

$$t \in \left[\frac{\log\left(\frac{m}{1 - \sqrt{1 - \varepsilon_s}}\right)}{\log(1 + \gamma_E)}, \frac{\log\left[1 - (1 - \sqrt{1 - \varepsilon_t})^{\frac{1}{n}}\right]}{-2\gamma_R \max(\tau_1, \tau_2)} \right] \quad (7)$$

The proof of Lemma 1 and Lemma 2 can be found in [12].

Based on the results of Lemma 2, we now can establish the following theorem about the performance of the proposed protocol.

Theorem 1 Consider the network scenario of Fig. 1 with equal path loss between all pairs of nodes. To guarantee $P_{out}^{(T)} \leq \varepsilon_t$ and $P_{out}^{(S)} \leq \varepsilon_s$ based on the optimal relay selection protocol, the number of eavesdroppers m in the network can tolerate must satisfy the following condition.

$$m \leq \left(1 - \sqrt{1 - \varepsilon_s} \right) \cdot (1 + \gamma_E)^{\frac{\log\left[1 - (1 - \sqrt{1 - \varepsilon_t})^{\frac{1}{n}}\right]}{2\gamma_R \max(\tau_1, \tau_2)}} \quad (8)$$

Proof From Lemma 2 we know that to ensure the reliability requirement, we have

$$t \leq \frac{\log\left[1 - (1 - \sqrt{1 - \varepsilon_t})^{\frac{1}{n}}\right]}{-2\gamma_R \max(\tau_1, \tau_2)} \quad (9)$$

To ensure the secrecy requirement, from Lemma 2 we know

$$m \leq \left(1 - \sqrt{1 - \varepsilon_s} \right) \cdot (1 + \gamma_E)^t \quad (10)$$

By letting t take its maximum value. Substituting (9) into (10), we get (8).

3.3 Analysis of the Random Relay Selection Protocol

We first establish the following two lemmas regarding some basic properties of $P_{out}^{(T)}$, $P_{out}^{(S)}$ and t , which will help us to derive the main result in Theorem 1.

Lemma 3 Consider the network scenario of Fig. 1 with equal path-loss between all pairs of nodes, under the random relay selection protocol the transmission outage probability $P_{out}^{(T)}$ and secrecy outage probability $P_{out}^{(S)}$ there satisfy the following conditions.

$$P_{out}^{(T)} \leq 1 - e^{-\gamma_R t(\tau_1 + \tau_2)} \quad (11)$$

$$P_{out}^{(S)} \leq 2m \cdot \left(\frac{1}{1 + \gamma_E} \right)^t - m^2 \cdot \left(\frac{1}{1 + \gamma_E} \right)^{2t} \quad (12)$$

The proof of Lemma 3 can be found in [12].

Lemma 4 Consider the network scenario of Fig. 1 with equal path loss between all pairs of nodes, to ensure $P_{out}^{(T)} \leq \varepsilon_t$ and $P_{out}^{(S)} \leq \varepsilon_s$ by applying the random relay selection protocol, the parameter t must satisfy the following condition.

$$t \in \left[\frac{\log\left(\frac{m}{1 - \sqrt{1 - \varepsilon_s}}\right)}{\log(1 + \gamma_E)}, \frac{\log\left(\frac{1}{1 - \varepsilon_t}\right)}{\gamma_R t(\tau_1 + \tau_2)} \right] \quad (13)$$

The proof of Lemma 4 can be found in [12].

Based on the results of Lemma 4, we now can establish the following theorem about the performance of the proposed protocol.

Theorem 2 Consider the network scenario of Fig. 1 with equal path loss between all pairs of nodes. To guarantee $P_{out}^{(T)} \leq \varepsilon_t$ and $P_{out}^{(S)} \leq \varepsilon_s$ based on the proposed protocol, the number of eavesdroppers m the network can tolerate must satisfy the following condition.

$$m \leq \left(1 - \sqrt{1 - \varepsilon_s}\right) \cdot (1 + \gamma_E)^{\frac{\log \log\left(\frac{1}{1 - \varepsilon_t}\right)}{\gamma_R t(\tau_1 + \tau_2)}} \quad (14)$$

Proof From Lemma 4 we know that to ensure the reliability requirement, we have

$$t \leq \frac{\log\left(\frac{1}{1 - \varepsilon_t}\right)}{\gamma_R t(\tau_1 + \tau_2)} \quad (15)$$

To ensure the secrecy requirement, from Lemma 3 we know

$$m \leq \left(1 - \sqrt{1 - \varepsilon_s}\right) \cdot (1 + \gamma_E)^t \quad (16)$$

By letting t take its maximum value, Substituting (15) into (16), we get (14)

4 Conclusion

This paper explores reliable and secure information transmission through multiple cooperative systems nodes in two-hop relay wireless network with passive eavesdroppers of unknown channels and locations, for which two transmission protocols are considered. For each protocol, theoretical analysis has been provided to show the number of eavesdroppers the network can tolerate subject to constraints on transmission outage probability and secrecy outage probability. These two protocols, each has different performance in terms of eavesdropper tolerance, load and energy consumption distribution among nodes, and also relay selection complexity, are suitable for different network scenarios depending on network scale and also energy consumption constraint there.

References

1. Narayanan S (2006) Two-hop forwarding in wireless networks. Dissertation for the degree of Doctor of philosophy, Polytechnic University
2. Talbot J, Welsh D (2006) Complexity and cryptography: an introduction. Cambridge University Press, Cambridge
3. Morrison K, Goeckel D (2011) Power allocation to noise-generating nodes for cooperative secrecy in the wireless environment. In: 45th Asilomar conference on signals, systems and computers (ASILOMAR), pp 275–279
4. Goel S, Negi R (2008) Guaranteeing secrecy using artificial noise. *IEEE Trans Wireless Commun* 7(6):2180–2189
5. Lai L, El Gamal H (2008) The relay-eavesdropper channel: cooperation for secrecy. *IEEE Trans Inform Theory* 54(9):4005–4019
6. Yuksel M, Erkip E (2007) Secure communication with a relay helping the wiretapper. In: Proceedings of 2007 IEEE information theory workshop, Lake Tahoe, CA
7. Negi R, Goelm S (2005) Secret communication using artificial noise. In: Proceedings of the IEEE Vehicular Tech. Conf, vol 3, Dallas TX, pp 1906–1910
8. Vasudevan S, Adams S, Geockel D, Ding Z, Towsley D, Leung K (2009) Multi-user diversity for secrecy in wireless networks. In: Information theorem and applications workshop
9. He X, Yener A (2008) Two-hop secure communication using an untrusted relay: a case for cooperative jamming. In: Proceedings of 2008 IEEE global telecommunications conference, New Orleans, LA
10. Dong L, Han Z, Petropulu A, Poor HV (2010) Improving wireless physical layer security via cooperating relays. *IEEE Trans Signal Proc* 58(3):1875–1888

11. Goeckel, Vasudevan S, Towsley D, Adams S, Ding Z, Leung K (2011) Artificial noise generation from cooperative relays for everlasting secrecy in two-hop wireless networks. *IEEE J Sel Areas Commun* 29(10):2067–2076
12. Shen Y, Jiang X, Ma J (2013) Generalized secure transmission protocol for flexible load-balance control with cooperative relays in two-hop wireless networks. CoRR abs/1301.1746

RC4 Stream Cipher with a Random Initial State

Maytham M. Hammood, Kenji Yoshigoe and Ali M. Sagheer

Abstract Rivest Cipher 4 (RC4) is one of the modern encryption techniques utilized in many real time security applications; however, it has several weaknesses including a correlation problem in the initially generated key sequences. In this paper, we propose RC4 stream cipher with a random initial state (RRC4) to solve the RC4's correlation problem between the public known outputs of the internal state. RRC4 solves the weak keys problem of the RC4 using random initialization of internal state S . Experimental results show that the output streams generated by RRC4 are more random than that generated by RC4. Moreover, RRC4's high resistivity protects against many attacks vulnerable to RC4 and solves several weaknesses of RC4 such as predictable first bytes of intermediate outputs by RC4.

Keywords Stream cipher · Random number generator · RC4

1 Introduction

Due to power limitation, low bandwidth, small storage, and limited computing capacity, cryptographic algorithms that can provide fast implementation, small size, low complexity and high security for resource-constrained devices such as

M. M. Hammood
Applied Science, University of Arkansas, Little Rock, USA
e-mail: mmhammood@ualr.edu

K. Yoshigoe (✉)
Computer Science, University of Arkansas, Little Rock, USA
e-mail: kxyoshigoe@ualr.edu

A. M. Sagheer
College of Computer, University of Anbar, Anbar, Iraq
e-mail: ali_makki@ieee.org

wireless sensor devices are imperative. Cryptographic algorithms are sequences of processes, or rules, used to encrypt or decrypt messages in a cryptographic system to provide security services. It includes symmetric and asymmetric key algorithms, but asymmetric key algorithms are inappropriate for resource-constrained devices for several reasons including the limited storage space and power [1]. Consequently, security systems should depend on a symmetric key cryptography in such cases. Stream ciphers can be classified as synchronous and asynchronous. In a synchronous stream cipher, a sequence of keys is generated independently from the plaintext and ciphertext. The drawback of synchronous is that both the sender and the receiver have to be synchronized for key usages. It can detect any deletion or insertion of bits by an active attack directly, yet such an attack can cause immediate loss of synchronization [2]. Asynchronous stream ciphers depend on the previously generated ciphertext in order to continue generating new ones, yet it cannot regenerate the same sequence of ciphertext. On the other hand, synchronous stream ciphers can regenerate a sequence of ciphertext because a key sequence is independent of the plaintext. This case is named self-synchronized because of the ability to re-synchronize after insertion or deletion of bits. Though, self-synchronization can be an important property, this type of stream cipher did not receive much interest [3].

Stream cipher relies on robustness of Pseudo Random Number Generator (PRNG) which has passes the statistical tests. Menezes et al. [4] considered one-time pad as a separate type of stream cipher. Consequently, the sequence key is truly random and not generated in a deterministic manner as it happens in other algorithms.

Rivest Cipher 4 (RC4) belongs to the stream cipher family which was developed in 1987 by Ron Rivest. RC4 is commonly used in security software based on stream cipher with communication protocols as in the encryption of traffic form-to secure web sites such as Secure Socket Layer (SSL), Wired Equivalent Privacy (WEP) and Transport Layer Security (TLS) implementations. RC4 has a simple design hardware implementation and it is fast, compared with other algorithms [5]. Furthermore, RC4 is fifteen times faster than Triple-DES and five times faster than Data Encryption Standard (DES) [3].

Sharif and Mansoor [6] provided comparisons between different encryption algorithms using different data sizes and key sizes. The simulation results clarify preponderance of RC4 algorithm over other algorithms in terms of speed and throughput.

The structures of stream ciphers are presented more than block ciphers. The security of the cryptographic algorithms can assess by cryptanalysis. Numerous weaknesses found in stream ciphers triggered by mathematical relations between the key, ciphertext, and plaintext. The main aim is to produce a random key asymptotic to the true random key [7]. Cryptanalyst refers to the theoretical knowledge and uses numerous statistical tools to find weaknesses in the ciphertext or cryptosystems.

The rest of the paper is organized as follows. [Section 2](#) reviews some related works. [Section 3](#) provided description of RC4, and [Sect. 4](#) describes some weaknesses of RC4. We present our algorithm to enhance randomness of RC4 in [Sect. 5](#), and evaluate it in [Sect. 6](#). [Section 7](#) is a conclusion.

2 Related Work

Many researchers tried to enhance the RC4 and create several algorithms. Variably Modified Permutation Composition (VMPC) presented by Zoltak [7] was designed to be efficient in software implementations to solve a weakness found in the RC4 Key Scheduling Algorithm (KSA) that was defined by Fluhrer et al. in [13]. The structure of Pseudo-Random Generation Algorithm (PRGA) in VMPC was more complex compared to RC4, which increased the resistant against attacks. In the same year, Paul and Preneel [9] presented RC4A as an enhancement over RC4 after finding out a new statistical weakness in the first two output bytes of the RC4 key stream generator. They presented that the number of outputs required for distinguishing the output of the RC4 random sequence with the presence of bias is 128, and they recommended to use 256 to overcome this bias. RC4A is considered to be robustness against most weaknesses of RC4, particularly its weakness of distribution in the first two output bytes. However, after one year, Maximov [8] proposed distinguishing attack on both VMPC and RC4A which can distinguish the cipher output from truly random number.

Mironov [11] presented a new model of RC4 and analyzed it by applying the theory of random permutation. Based on this analysis, he recommended to discard at least the first 512 bytes to avoid these weaknesses which have led to an increase in the execution time. Pardeep and Pateriya [14] presented PardeepCipher-RC4 (PC-RC4) as an extension to RC4 algorithm to improve randomness in KSA and PRGA, yet it increased the execution time.

Kamble and Meshram found that RC4 has weakness to differential attack, and showed how the plain text can be retrieved. In addition, the authors recommended how to avoid this attack using different sizes of key of greater than 32 bit [10]. Mousa and Hamad analyzed the effect of different parameters of the RC4 algorithm include the file size and the execution time, and concluded that the length of encryption key and the file size of influence the speed of encryption and decryption [15].

Chefranov and Mazurova [12] presented an extension of RC4 (RC4E) where they combined RC4 with a simple Heap's algorithm to provide enumeration of all potential permutations for periodic change of RC4 state. However, their algorithm requires additional memory to keep one more permutation compare with RC4. Hammood, et al. [16] presented an RC4 with two state tables (RC4-2S) which has improved the key generation time of the conventional RC4 while also outperforming randomness of the keys generated.

3 Description of RC4

Numerous stream cipher algorithms depend on Linear Feedback Shift Registers (LFSRs), especially in hardware. However, the RC4 design avoids the use of LFSRs. The algorithm involves KSA and PRGA which are implemented

sequentially. The idea of RC4 is to manipulate the elements by swapping them to achieve highest randomness. The RC4 algorithm has a variable key length which ranges between 0 and 255 bytes to initialize a 256-byte in initial state array by elements from $S[0]$ to $S[255]$. For secure RC4, it must use a key long at least 128 bytes [13]. The key of RC4 is initialized the KSA while the pseudo-random number is produced from PRGA part. The pseudo codes for the two parts of RC4 algorithm are shown in Algorithm 1 and Algorithm 2 where m is the message length of a plaintext, L is the length of the initial key in bytes, N is the size of the array or state S , and i and j are index pointers. The output of the second algorithm is a key sequence that will be XOR-ed with plaintext to get ciphertext or XOR-ed with ciphertext to get plaintext.

Algorithm 1. Key Scheduling for RC4

INPUT: $K [k_1, k_2, \dots, k_L], m$
OUTPUT: State $S=S_0, S_1, \dots, S_{255}$

1. $S[i] = i$, for $i=0, 1, 2, \dots, 255$
2. $j \leftarrow 0$;
3. For $i \leftarrow 0$ to 255 Do
 - 3.1. $j \leftarrow (j+S[i] + K[i \bmod L]) \bmod 256$
 - 3.2. Swap $S[i]$ with $S[j]$
4. Return (S)

Algorithm 2. Pseudo-Random Generation for RC4

INPUT: State S
OUTPUT: Key sequence $Kseq$

1. $j \leftarrow 0$
2. $i \leftarrow 0$
3. While not end of sequence Do
 - 3.1. $i \leftarrow (i+1) \bmod 256$
 - 3.2. $j \leftarrow (j+S[i]) \bmod 256$
 - 3.3. Swap $S[i]$ with $S[j]$
 - 3.4. $Kseq \leftarrow S [(S[i] + S[j]) \bmod 256]$
4. Return ($Kseq$)

4 The Weaknesses of RC4

After RC4 was exposed to public in 1994, the interest in the cryptanalysis of RC4 grew faster, especially after being used for the Wired Equivalent Privacy (WEP) implementations. Therefore, several weaknesses in RC4 were recognized including the one in KSA and the one in the relations between the S-box in different time. Some of these weaknesses are simple and can be resolved, but

others are serious because it can be exploited by attackers. Roos [17] studied the weaknesses of RC4 and found a significant correlation between the first few values in the state table and generated value. The main reason for that is the state table is first initialized to the sequence $(0, 1, 2, \dots, 255)$. For at least one out of every 256 possible keys, the initial byte of the key generated by RC4 is strongly correlated with a few bytes of the key. Occasionally, therefore, the keys allow prediction of the first bytes from the output of the PRGA. To eliminate this problem, it was suggested to ignore the first bytes of the output of the PRGA [11]. Our algorithm will address this problem without the need to neglect the first byte of output. The reason behind this weakness is the use of regular sequence of numbers from 0 to 255 as initial state. This gives the attacker a starting point to track numbers because the initial state has a regular sequence. Furthermore, there is a major statistical bias in the first output bytes which can be used to mount a ciphertext-only attack [13]. It has been recommended to reject at least the first 256 bytes of the key-stream output to discourage this attack [11]. Our algorithm with random initial state is resistant against these ciphertext-only attacks. There are many other attacks described in [13] such as subkey guessing attack, linear consistency attack, inversion attack, etc. In addition, an algebraic attack is a new type of higher order correlation attack. In order to protect from this attack, we will use a random initial state.

5 RC4 Stream Cipher with a Random Initial State

RC4 has a significant number of weaknesses in the phases of KSA and PRGA. One of the reasons which leads to these weaknesses is that the initialization process produces a deterministic sequence, $(0, 1, 2, \dots, 255)$ which gives the attacker an initial advantage. In this section, we present RRC4 as one of the RC4 stream cipher algorithm family to improve RC4 using random initialization of state table. Since the correlation among the publicly known outputs of the internal state depends on the randomness of the key sequence, RRC4 further tries to reduce the correlation problem in RC4 by resolving various RC4 attacks which exploit strong correlation among the publicly known outputs of the internal state.

The new algorithm consists of initialization phase (KSA) as shown in Algorithm 3 and output phase (PRGA) which is identical to the one used in RC4 as shown in Algorithm 2, respectively. All addition operations are carried out modulo N . KSA takes a key k consisting of 16 n -bit word. After the setup, the round algorithm is executed once for each word output. Indeed, all practical applications of the developed RC4 is implemented with $n = 8$, in which case, all entries of S along with i and j are bytes.

In the first phase of KSA, S is randomly generated by a sender from 0 to $N-1$ without duplication and initial S is shared with the receiver as an additional secret key. The input secret key k is used as a seed for the state S . In the systems or implementations which dynamically update k between a sender and a receiver,

S and k can be shared at the same time. Consequently, S becomes secret random inputs for the PRGA phase as shown in Algorithm 3.

S in PRGA is used to produce the sequence of output stream which will be XOR-ed with plaintext to get ciphertext or XORed with ciphertext to get plaintext. This technique solves the correlation between the public known outputs of the internal state with initial randomization of S .

Algorithm 3. Key Scheduling of RRC4

INPUT: k, m
OUTPUT: S

1. For $i \leftarrow 0$ to $N - 1$ Do
 $S[i] \leftarrow \text{Random}_i$
 Where $S \cap S = S \cup S = S = \{0, 1, 2, 3, 4 \dots N-1\}$
2. $j \leftarrow 0$
3. For $i \leftarrow 0$ to $N - 1$ Do {
 - 3.1. $j \leftarrow (j + S[i] + k [i \bmod L]) \bmod N$
 - 3.2. Swap $S[i]$ with $S[j]$ }
4. Return (S)

6 Evaluation

The generated output sequences are tested by NIST suite of statistical tests (National Institute of Standards and Technology) which is a randomness testing suite that consists of 16 statistical tests to measure the randomness of the output sequences of true random number generators or pseudorandom number generators as shown in Table 1. The design of the RRC4 was done using MATLAB and the tests of this PRNG were done by using NIST STS-1.6 [18]. We checked the produced binary sequence from RRC4 by NIST statistical tests. The probability of a good random number generator is represented by p value. Testing process compared p -value to 0.01. If the p -value is more than 0.01 then the sequence is accepted, else, the sequence is rejected because of the sequence non-randomness. However, some tests accepted large sizes of sequence and failed in the small size as well as other tests accepted both sizes. In our program, a large size, 134,000 bytes (1,072,000 bits), generated by each key and these sequences were tested, and subsequently calculated the average of the p -values result from these tests. As shown in Table 1, the p -values are acceptable when greater than 0.01, and the produced sequence can be deemed random, uniformly distributed, and suitable for cryptography.

If the tests give p -value asymptotically to 1, then the sequence appears to have perfect randomness. A p -value of zero indicates that the sequence appears to be completely nonrandom. The SUCCESS indicates the sequence is acceptable and has good randomness, where FAILURE means the sequence is not acceptable due to non-randomness.

Table 1 Result of running the NIST suite over the set data produced by the proposed RRC4 and standard RC4

Test No.	Statistical test name	RC4		RRC4	
		<i>p</i> -value	Conclusion	<i>p</i> -value	Conclusion
1	Approximate entropy	0.431137	SUCCESS	0.503525	SUCCESS
2	Block Frequency	0.398344	SUCCESS	0.461046	SUCCESS
3	Cumulative sums (forward)	0.558378	SUCCESS	0.552785	SUCCESS
4	Cumulative sum (reverse)	0.488489	SUCCESS	0.549893	SUCCESS
5	FFT	0.498602	SUCCESS	0.388331	SUCCESS
6	Frequency	0.524857	SUCCESS	0.614073	SUCCESS
7	Lempel–Ziv compression	1.000000	SUCCESS	1.000000	SUCCESS
8	Linear complexity	0.383646	SUCCESS	0.398958	SUCCESS
9	Longest runs	0.550414	SUCCESS	0.457552	SUCCESS
10	Non periodic templates	0.502847	SUCCESS	0.506389	SUCCESS
11	Overlapping template	0.476021	SUCCESS	0.426877	SUCCESS
12	Random excursions	0.480998	SUCCESS	0.495870	SUCCESS
13	Random excursions variant	0.519955	SUCCESS	0.539016	SUCCESS
14	Rank	0.547991	SUCCESS	0.600732	SUCCESS
15	Runs	0.472438	SUCCESS	0.522070	SUCCESS
16	Serial	0.562766	SUCCESS	0.576859	SUCCESS
17	Universal statistical	0.392082	SUCCESS	0.551906	SUCCESS

There are some statistical tests of PRBG that are very common and must be included in test suite such as *Runs* test, *Frequency* test, and *Universal* test (#15, #6, and #17 in Table 1) [19]. In these tests, the *p*-values of our algorithm are greater than the *p*-values of the standard RC4. Moreover, RRC4 is better than RC4 in most of the other tests.

7 Conclusion

Many security applications use stream cipher for data encryption, where the robustness of stream cipher depends on the strength of key stream generated. Rivest Cipher 4 (RC4) cipher system is an important encryption algorithm that can be used to protect the information on the common channel. The RC4 cipher shows some weaknesses including a correlation problem in the initially generated key sequences. The proposed RC4 with a random initial state (RRC4) solves the RC4's weak keys problem using a random initialization of internal state. The generated output sequences of the proposed RRC4 have passed the NIST suite of statistical tests. The RRC4 algorithm is not complicated one, thus it can be implemented in both hardware and software.

Acknowledgments This work is based in part, upon research supported by the National Science Foundation (under Grant Nos. CNS-0855248 and EPS-0918970). Any opinions, findings and

conclusions or recommendations expressed in this material are those of the author(s) and do not necessarily reflect the views of the funding agencies or those of the employers.

References

1. Wu Y, Ma D, Li T, Deng RH (2004) Classify encrypted data in wireless sensor networks. In: Proceedings of the vehicular technology conference, 2004. VTC2004-fall. 2004 IEEE 60th, vol.5, pp 3236–3239. Vol. 5, 26–29 Sept 2004
2. Turan MS, Doganaksoy A, Calik, C (2006) Statistical analysis of synchronous stream ciphers. In: Proceedings of the SASC 2006: Stream ciphers revisited
3. Ahmad S, Beg MR, Abbas Q, Ahmad J, Atif S (2010) Comparative study between stream cipher and block cipher using RC4 and hill cipher. In: Proceedings of the international journal of computer applications (0975–8887), vol 1(25)
4. Menezes AJ, Oorschot PC, Vanstone SA (2001) Handbook of applied cryptography. CRC Press, Boston, 2001
5. Gupta SS, Chattopadhyay A, Sinha K, Maitra S, Sinha B (2013) High-performance hardware implementation for RC4 stream cipher. IEEE Trans Comput 62(4):730–743
6. Sharif SO, Mansoor SP (2010) Performance analysis of stream and block cipher algorithms. In: Proceedings of the 3rd international conference on advanced computer theory and engineering (ICACTE), vol 1. IEEE, pp 522–525
7. Zoltak B (2004) VMPC one-way function and stream cipher. In: Fast software encryption, FSE 2004. LNCS 3017. Springer-Verlag, New York, pp 210–225
8. Maximov A (2005) Two linear distinguishing attacks on VMPC and RC4A and weakness of the RC4 family of stream ciphers. In: Fast software encryption, FSE 2005, vol 3557, Springer, pp 342–358
9. Paul S, Preneel B (2004) A new weakness in the RC4 keystream generator and an approach to improve the security of the cipher. In: Fast software encryption, FSE 2004. LNCS 3017. Springer-Verlag, New York, pp 245–259
10. Kamble BH, Meshram BB (2012) Robustness of RC4 against differential attack. Inter J Adv Res Comput Eng Technol 1(4), ISSN: 2278–1323
11. Mironov I (2002) (Not So) Random shuffles of RC4. In: Moti Y (ed) Advances in cryptology. Proceedings of the CRYPTO 2002, 22nd annual international cryptology conference. Lecture notes in computer science, vol 2442. Springer, pp 304–319
12. Chefranov AG, Mazurova TA (2006) Pseudo-random number generator RC4 period improvement. In: 2006 IEEE international conference on automation, quality and testing, robotics, vol 2, 25–28 May 2006, pp 38–41
13. Fluhrer S, Mantin I, Shamir A (2001) Weaknesses in the key scheduling algorithm of RC4. In: Proceedings of annual workshop on selected areas in cryptography, vol 2259, Springer, Toronto, pp 1–24
14. Pardeep, Pateriya, P (2012) PC-RC4 algorithm: an enhancement over standard RC4 algorithm. Inter J Comput Sci Net 1(3)
15. Mousa A, Hamad A (2006) Evaluation of the RC4 algorithm for data encryption. Inter J Comput Sci Appl 3(2)
16. Hammood MM, Yoshigoe K, Sagheer AM (2013) RC4-2S: RC4 stream ciphers with two state tables. In: Proceedings in the 5th FTIRA international conference on information technology convergence and services (ITCS'13). Lecture notes in electrical engineering, Springer
17. Roos A (1995) A class of weak keys in the RC4 stream cipher. In: Vironix Soft-ware Laboratories, Westville, South Africa
18. Rukhin A, Soto J, Nechvatal J, Smid M, Barker E, Leigh S, Levenson M, Vangel M, Banks D, Heckert A, Dray J, Vo S (2001) A statistical test suite for random and pseudorandom

- number generators for cryptographic applications. NIST special publication 800-22, National Institute of Standards and Technology (NIST), Gaithersburg. See <http://csrc.nist.gov/rng/>
19. Stallings W (2011) Cryptography and network security principles and practices, 5th edn. Prentice Hall, Pearson

Improved Redundant Power Consumption Laxity-Based (IRPCLB) Algorithm for Server Clusters

Tomoya Enokido, Ailixier Aikebaier and Makoto Takizawa

Abstract A client usually issues a request to one server in a cluster of servers and the server sends a reply to the client. Once the server stops by fault, the client is suspended to wait for a reply. In order to be tolerant of server faults, each request is redundantly performed on multiple servers. Here, the more number of servers a request process is redundantly performed, the more reliable but the more amount of electric energy is consumed. Thus, it is critical to discuss how to realize energy-aware, robust clusters of servers. In this paper, we newly propose the improved redundant power consumption laxity-based (IRPCLB) algorithm where once a process successfully terminates on one server, meaningless redundant processes are not performed on the other servers. We show the total power consumption of servers is reduced in the IRPCLB algorithm.

Keywords Green computing · Power consumption model · IRPCLB algorithm · Redundant execution · Reliable server cluster

T. Enokido (✉)
Rissho University, Tokyo, Japan
e-mail: eno@ris.ac.jp

A. Aikebaier
National Institute of Information and Communications Technology (NICT), Tokyo, Japan
e-mail: alisher@nict.go.jp

M. Takizawa
Seikei University, Tokyo, Japan
e-mail: makoto.takizawa@computer.org

1 Introduction

In information systems, a client issues a request and a server is selected for the request in a cluster of servers. A request process has to be redundantly performed on multiple servers to be tolerant of server faults [1, 2]. However, the total power consumption of a server cluster is increased to redundantly perform a process on multiple servers. In this paper, we discuss a reliable and energy-aware server cluster where a process is redundantly performed on multiple servers but the total electric power consumption can be reduced. Here, we consider computation type applications like scientific computation, where CPU resources are mainly consumed. In our previous studies [3–5], the *simple power consumption (SPC)* model and the *extended SPC (ESPC)* model are proposed to show how a server consumes the electric power to perform application processes of computation type. In the SPC model, the rotation speed of each fan is assumed to be fixed, i.e. the power consumption of each fan is constant. On the other hand, the total power consumption of a server depends on not only the power consumption of CPU but also cooling devices like fans in the ESPC model.

Suppose a request q_s is issued to a server s_r from a client but the server s_r stops by fault. The client c_s is suspended by waiting for a reply from the server s_r . Then, the client c_s issues the request q_s to another server. Thus, it takes time to recover from a server fault. Application requests have to be reliably performed in presence of server faults in a cluster. The *redundant power consumption laxity-based (RPCLB)* [6] algorithm to select multiple servers for redundantly and energy-efficiently performing an application process is proposed so that the total power consumption can be reduced in a cluster of servers. Here, a request q_s is sent to multiple servers in a cluster. As long as at least one server is operational, the request q_s is successfully performed. Since each application process is redundantly performed on multiple servers, the larger amount of electric power is consumed in a cluster. In this paper, we try to reduce the total power consumption of servers to redundantly perform a process. Suppose a process p_i is redundantly performed on a pair of servers s_r and s_u and terminates at times τ_{ri} and τ_{ui} on the servers s_r and s_u , respectively. If $\tau_{ri} < \tau_{ui}$, it is *meaningless* to perform the process p_i on the server s_u after time τ_{ri} . In this paper, once one process terminates on a server, meaningless processes on the other servers are forced to be terminated. This means, the power consumption to perform meaningless process is reduced. In this paper, we propose the *improved RPCLB (IRPCLB)* algorithm where meaningless redundant processes of each request are terminated. We evaluate the IRPCLB algorithm in terms of the total power consumption and the execution time compared with the RPCLB and round robin (RR) algorithms.

In Sects. 2 and 3, we present the computation model and the power consumption model of a server. In Sect. 4, we discuss the IRPCLB algorithm to reduce the total power consumption of servers. In Sect. 5, we evaluate the IRPCLB algorithm.

2 System Model

2.1 System Model

Let S be a cluster of multiple servers s_1, \dots, s_n ($n \geq 1$). We assume each server may stop by fault. Let N_{fault} be the maximum number of servers which stop by fault in the cluster S . Here, if $0 \leq N_{fault} < n$, the cluster S is tolerant of stop faults of servers. Let CS_s be a subset of servers in the cluster S , on each of which a request q_s from a client c_s is performed. Here, $N_{fault} + 1 \leq |CS_s| \leq n$. A client c_s first issues a request q_s to a load balancer K . The load balancer K selects a subset CS_s of servers in the cluster S and forwards the request q_s to every server s_t in the subset CS_s . On receipt of the request q_s , a process p_i is created for the request q_s and performed on the server s_t . Here, a notation p_i shows a process p_i performed on a server s_t . A term *process* means an *application process* for a request. Then, the server s_t sends a reply r_s to the client c_s . This means, each client c_s can receive at least one reply r_s from a server s_t even if the number N_{fault} of servers stop by fault in the cluster S . The client c_s takes only the first reply r_s and ignores the other replies after receiving the first reply r_s . Thus, we can redundantly perform even a non-deterministic process on multiple servers.

2.2 Simple Computation (SC) Model

We overview the *simple computation (SC)* model [5] with a multi-core CPU. Let nc_t be the number of cores in a CPU of a server s_t . Let $CP_t(\tau)$ be a set of current processes being performed on a server s_t at time τ and $NC_t(\tau)$ be $|CP_t(\tau)|$. Processes which are being performed and already terminate are *current* and *previous* at time τ , respectively. Let T_{ti} be total computation time of a process p_{ti} , i.e. a process p_i on a server s_t [sec]. $minT_{ti}$ is minimum computation time [sec] of a process p_i which is exclusively performed on a server s_t , where $minT_{ti} \leq T_{ti}$. $minT_i = \min(minT_{1i}, \dots, minT_{ni})$. The more number of processes are concurrently performed, the longer time it takes to perform each process on a server s_t . Let $\alpha_t(\tau)$ be the *computation degradation ratio* of a server s_t at time τ ($0 \leq \alpha_t(\tau) \leq 1$). $\alpha_t(\tau_1) \leq \alpha_t(\tau_2)$ if $NC_t(\tau_1) \geq NC_t(\tau_2)$. $\alpha_t(\tau) = 1$ if $NC_t(\tau) \leq 1$. In this paper, $\alpha_t(\tau)$ is assumed to be $\varepsilon_t^{NC_t(\tau)-1}$ where $0 \leq \varepsilon_t \leq 1$. If ε_t is 1, the elapse time lineally increases for the number $NC_t(\tau)$ of processes.

In this paper, the total amount of computation of a process p_i is defined to be $minT_i$ [sec], i.e. how long it takes to perform the process p_i without any other process on the fastest server in the cluster S . The *computation rate* $f_{ti}(\tau)$ [1/sec] (≤ 1) [5] gives the ratio of amount of computation of a process p_i to be done on a server s_t at time τ to the total amount of computation of the process p_i :

[Computation rate]

$$f_{ii}(\tau) = \begin{cases} \min T_i / \min T_{ii} & \text{if } NC_i(\tau) \leq nc_i. \\ \alpha_i(\tau) \cdot \min T_i / \min T_{ii} \cdot nc_i / NC_i(\tau), & \text{otherwise.} \end{cases} \quad (1)$$

The maximum computation rate $\max f_{ii}$ of a process p_i on a server s_t shows $\min T_i / \min T_{ii}$ where p_i is exclusively performed on one core. $0 \leq f_{ii}(\tau) \leq \max f_{ii} \leq 1$. The *simple computation (SC) model* [5] is defined in terms of the computation rate as follows:

[Simple computation (SC) model] $\max f_{ii} = \max f_{ij} = \text{Max} f_i$ for every pair of different processes p_i and p_j on a server s_t .

$\text{Max} f_i$ is the maximum computation rate of a server s_t , i.e. $\text{Max} f_i = \min T_i / \min T_{ii}$ for every process p_i .

Next, suppose that a process p_i starts and terminates on a server s_t at time st_{ii} and et_{ii} , respectively, i.e. $T_{ii} = et_{ii} - st_{ii}$ and $\int_{st_{ii}}^{et_{ii}} f_{ii}(\tau) d\tau = \min T_i$. Thus, $\min T_i$ shows the total amount of computation to be performed by a process p_i . The *computation laxity* $lc_{ii}(\tau)$ shows how much computation a server s_t has to spend to perform the process p_i at time τ , i.e. $lc_{ii}(\tau) = \min T_i - \int_{st_{ii}}^{\tau} f_{ii}(\tau) d\tau$.

3 Power Consumption Models

In our previous studies [3–5], the *simple power consumption (SPC) model* and the *extended simple power consumption (ESPC) model* to show how a server s_t consumes the electric power to perform processes are proposed. Let $\max E_t$ and $\min E_t$ be the maximum and minimum electric power consumption rates [W] of a server s_t , respectively. $E_t(\tau)$ shows the electric *power consumption rate* [W] of a server s_t at time τ . Here, $\min E_t \leq E_t(\tau) \leq \max E_t$. NFE_t ($\leq \max E_t$) shows the maximum power consumption rate where a rotation speed of each fan is minimum. In the SPC model [3], the power consumption rate $E_t(\tau)$ [W] is given as follows:

[Simple power consumption (SPC) model]

$$E_t(\tau) = \begin{cases} NFE_t & \text{if } NC_t(\tau) \geq 1. \\ \min E_t & \text{otherwise.} \end{cases} \quad (2)$$

If at least one process p_i is performed on a server s_t , the server s_t consumes electric power at fixed rate NFE_t . Otherwise, $E_t(\tau)$ is minimum, $\min E_t$. The power consumption rate $E_t(\tau)$ actually depends on the rotation speed of fans. The ESPC model [5] for a server s_t is given as follows:

[Extended simple power consumption (ESPC) model]

$$E_t(\tau) = \begin{cases} \min E_t & \text{if } NC_t(\tau) \geq M_t. \\ \rho_t \cdot (NC_t(\tau) - 1) + NFE_t & \text{if } 1 < NC_t(\tau) < M_t. \\ \min E_t & \text{otherwise} \end{cases} \quad (3)$$

Here, ρ_t is the increasing ratio of the power consumption rate on a server s_t . Here, $\rho_t \geq 0$ if $NC_t(\tau) > 1$ and $\rho_t = 0$ if $NC_t(\tau) = 1$. If $NC_t(\tau) = 0$, $E_t(\tau) = \min E_t$. M_t is the minimum number of concurrent processes where the server s_t consumes electric power at maximum rate. If $NC_t(\tau) \geq M_t$, $E_t(\tau) = \max E_t$. If $1 \leq NC_t(\tau) < M_t$, $E_t(\tau)$ linearly increases as the number $NC_t(\tau)$ of current processes.

4 A Server Selection Algorithm in a Cluster

4.1 Estimation of Power Consumption Laxity

The procedure **PLaxity**(s_t, τ) [5] is proposed to estimate the total power consumption laxity $lpc_t(\tau)$ [Ws] of a server s_t at time τ . The power consumption laxity $lpc_t(\tau)$ shows how much amount of power to be consumed to perform every current process at time τ on the server s_t . We assume the minimum computation time $\min T_i$ of each process p_i is a priori defined. If a new process p_{ti} is started on the server s_t at time τ , the process p_{ti} is added to a set $CP_t(\tau)$. If a process p_{ti} terminates, the process p_{ti} is removed in $CP_t(\tau)$. At time τ , a process p_{ti} starts on a server s_t , $lc_{ti}(\tau) = \min T_i$. The computation laxity $lc_{ti}(\tau)$ of each current process p_{ti} in $CP_t(\tau)$ is decremented by the computation rate $f_t(\tau)/NC_t(\tau)$ at time τ . $f_t(\tau)/NC_t(\tau)$ shows how much amount of computation the process p_{ti} does at time τ . If $lc_{ti}(\tau)$ gets 0, the process p_{ti} terminates. Given a process set $CP_t(\tau)$ at time τ , the power consumption laxity $lpc_t(\tau)$ of the server s_t is given by the following procedure **PLaxity**(s_t, τ):

```

PLaxity ( $s_t, \tau$ ) {
  if  $CP_t(\tau) = \phi$ , return (0);
   $laxity = E_t(\tau)$ ; /* formulas (2) and (3) */
  for each current process  $p_{ti}$  in  $CP_t(\tau)$ , {
     $lc_{ti}(\tau + 1) = lc_{ti}(\tau) - f_t(\tau) / NC_t(\tau)$ ;
    if  $lc_{ti}(\tau + 1) = 0$ ,  $CP_t(\tau + 1) = CP_t(\tau) - \{p_{ti}\}$ ;
  } return ( $laxity + \mathbf{PLaxity}(s_t, \tau + 1)$ );
}

```

4.2 The RPCLB Algorithm

In the *redundant power consumption laxity-based (RPCLB)* algorithm, a subset $CS_s (\subseteq S)$ of multiple servers in a cluster S is selected at time τ for a process p_i , where the total power consumption laxity $\sum_{s_t \in CS_s} lpc_t(\tau)$ is the minimum in the cluster S . Let rd_i be a *redundancy* of a process p_i , i.e. a number $|CS_s|$ of servers where a process p_i is redundantly performed. $N_{fault} + 1 \leq rd_i \leq n$. A subset CS_s of

the servers to perform a process p_i are selected at time τ by the following procedure **RPCLB_select**:

```

RPCLB_select( $S, p_i, rd_i, \tau$ ) {
   $CS_s = \phi$ ;
  while ( $rd_i > 0$ ) {
     $s_t =$  select a server where Plaxity( $s_t, \tau$ ) is minimum
      in  $S$ ;
     $S = S - \{s_t\}$ ;  $CS_s = CS_s \cup \{s_t\}$ ;  $rd_i = rd_i - 1$ ;
  } return ( $CS_s$ );
}

```

The load balancer K issues a request q_s of a process p_i to every server s_t in the subset CS_s . A process p_{it} is created and performed on each server s_t . Then, the reply r_s is sent to the client c_s . Once the client c_s receives a reply from a server, the request q_s commits. The client c_s then ignores a reply from every other server. Suppose a process p_i is redundantly performed on a pair of servers s_t and s_u in the subset CS_s . In the RPCLB algorithm, if the server s_u is operational, the process p_{ui} is still performed on the server s_u even if the process p_{it} had correctly terminated on another server s_t . Here, if the process p_{it} terminates on the server s_t at time τ and the server s_t has sent a reply to the client c_s , the process p_{ui} to be performed after time τ on the server s_u is *meaningless*. The server s_u just consumes the electric power for performing a meaningless process p_{ui} . In this paper, we improve the RPCLB algorithm by forcing meaningless processes to terminate to reduce the total power consumption of a cluster S .

4.3 Improved RPCLB (IRPCLB) Algorithm

In the IRPCLB algorithm, the load balancer K selects a subset CS_s of the servers to redundantly perform a process p_i by using the procedure **RPCLB_select**(S, p_i, rd_i, τ). If a process p_i terminates on one server s_t , meaningless processes on the other servers have to be terminated. Here, in order to force to terminate meaningless processes, a server s_t sends a termination notification $Tnotif(p_{it})$ of a process p_{it} to every other server in the subset CS_s . Suppose a server s_u in the subset CS_s receives a termination notification $Tnotif(p_{it})$ from a server s_t . If a process p_{ui} is still performed on the server s_u , the process p_{ui} is terminated, i.e. $CP_u(\tau) = CP_u(\tau) - \{p_{ui}\}$. If the process p_{ui} had been already terminated on the server s_u , the termination notification $Tnotif(p_{it})$ is ignored. Here, the client c_s might receive the replies of the process p_i from multiple servers. In this paper, once a client c_s receives a reply from a server in the subset CS_s , the client c_s commits. The client c_s then ignores the other replies.

By forcing meaningless processes to terminate, the electric power of each server can be reduced. The computation rate to be used to perform meaningless processes can be used for performing other processes on each server. As a result,

the computation time of each process on a server can be also shortened. Hence, the total power consumption in a cluster to redundantly perform each process can be more reduced in the IRPCLB algorithm than the RPCLB algorithm.

5 Evaluation of the IRPCLB Algorithm

We evaluate the IRPCLB algorithm in terms of the total power consumption and execution time compared with the RPCLB algorithm [6] and the basic round-robin (RR) algorithm [7]. There are nine heterogeneous servers s_1, \dots, s_9 as shown in Table 1, $S = \{s_1, \dots, s_9\}$. The parameters of each server s_t ($t = 1, \dots, 9$) are given based on the experimentations [5]. The rotation speed of each fan in the servers s_1, s_2 , and s_3 is changed to keep the temperature of devices and server’s case. Hence, the ESPC model holds for the servers s_1, s_2 , and s_3 . On the other hand, the rotation speed of every fan in other servers is fixed. Hence, the SPC model holds for other servers. The number m of processes are issued to the nine servers s_1, \dots, s_9 in the total simulation time 500 [sec]. The starting time of each process p_i is randomly selected between 1 and 500 [sec]. The minimum computation time $minT_i$ of each process p_i on the fastest server is randomly selected between 1 and 5 [sec] as a real number. In the evaluation, the IRPCLB, RPCLB, and RR algorithms are performed on the same traffic pattern. We assume the redundancy rd_i of each process p_i is the same rd . In this evaluation, IRPCLB(rd), RPCLB(rd), and RR(rd) stand for the IRPCLB, RPCLB, and RR algorithms with redundancy rd , respectively. The maximum communication delay time among every pair of servers in the cluster S is assumed to be one second.

Figure 1a shows the total power consumption [KW]s to perform the total number m of processes. The smaller amount of power consumption is spent in the RPCLB(1) algorithm than the other algorithms since each process is not redundantly performed. The smaller amount of power consumption is spent in the IRPCLB(rd) and RPCLB(rd) algorithms than the RR(rd) algorithm for $rd = 1, 2, 3$. In the IRPCLB algorithm, meaningless processes are terminated. Hence, total power consumption in the cluster S can be reduced in the IRPCLB(2) and

Table 1 Servers

Server s_t	s_1	s_2	s_3	s_4	s_5	s_6	s_7	s_8	s_9
<i>PC model</i>	<i>ESPC</i>	<i>ESPC</i>	<i>ESPC</i>	<i>SPC</i>	<i>SPC</i>	<i>SPC</i>	<i>SPC</i>	<i>SPC</i>	<i>SPC</i>
nc_t	2	2	2	4	4	4	1	1	1
$Maxf_t$	1.0	1.0	1.0	1.0	1.0	1.0	0.76	176	0.76
ε_t	1	1	1	1	1	1	1	1	1
$maxE_t$	224	224	224	–	–	–	–	–	–
NFE_t	175	175	175	155	155	155	142	142	142
$minE_t$	97	97	97	96	96	96	105	105	105
ρ_t	0.7	0.7	0.7	–	–	–	–	–	–
M_t	70	70	70	–	–	–	–	–	–

($1 \leq minTi \leq 5$ [sec])

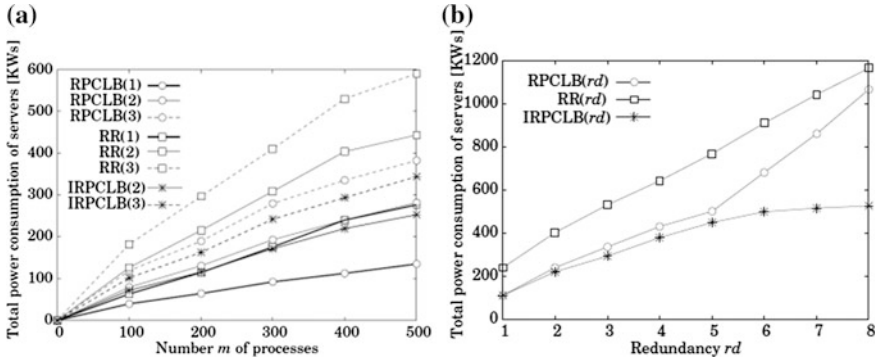


Fig. 1 Total power consumption. **a** Total power consumption for m . **b** Total power consumption for rd ($m = 400$)

IRPCLB(3) algorithms than the RPCLB(2) and RPCLB(3) algorithms, respectively. Figure 1b shows the total power consumption [KW's] for $rd = 1, \dots, 8$ where the total number 400 of processes are issued to the cluster S . In the RPCLB(rd) and RR(rd) algorithms, the total power consumption in the cluster S increases as the redundancy rd increases. The total power consumption in the IRPCLB algorithm is $O(\log rd)$ while the total power consumption in the RR and RPCLB algorithms is $O(rd)$. The smaller amount of power consumption is spent in the IRPCLB(rd) algorithm than the other algorithms. Especially, for $rd > 5$, the total power consumption to redundantly perform processes can be more reduced in the IRPCLB(rd) algorithm since the electric power to perform meaningless processes can be reduced and the computation rate to be used to perform meaningless processes can be used for performing other processes by forcing the meaningless processes to terminate.

Figure 2 shows the average increasing ratio of the execution time of each process in the IRPCLB(rd), RPCLB(rd), and RR(rd) algorithms for $rd = 1, 2, 3$ to the execution time of each process in the RPCLB(1) algorithm. Here, if $rd \geq 2$, there are multiple execution times for each process p_i since the process p_i is performed on multiple servers. The average increasing ratio of the RR algorithm is always larger than the IRPCLB and RPCLB algorithms. The average increasing ratios of the execution time in the RPCLB(2), IRPCLB(2), and IRPCLB(3) algorithms are almost 0. This means the execution time of each process in the RPCLB(2), IRPCLB(2), and IRPCLB(3) algorithms is almost the same as the RPCLB(1). The average increasing ratio of RPCLB(3) is higher than the RPCLB(2), IRPCLB(2), and IRPCLB(3) algorithms since meaningless processes are not terminated in the RPCLB algorithm for $m = 400$. The evaluation result shows the computation resource of servers is more efficiently used in the IRPCLB algorithm than the RPCLB and RR algorithms. From the evaluation results, we conclude the total power consumption and execution time of each process can be more reduced in the IRPCLB(rd) algorithm than the RPCLB(rd) and RR(rd) algorithms for each redundancy rd . Therefore, the IRPCLB algorithm is more useful than the RPCLB and RR algorithms.

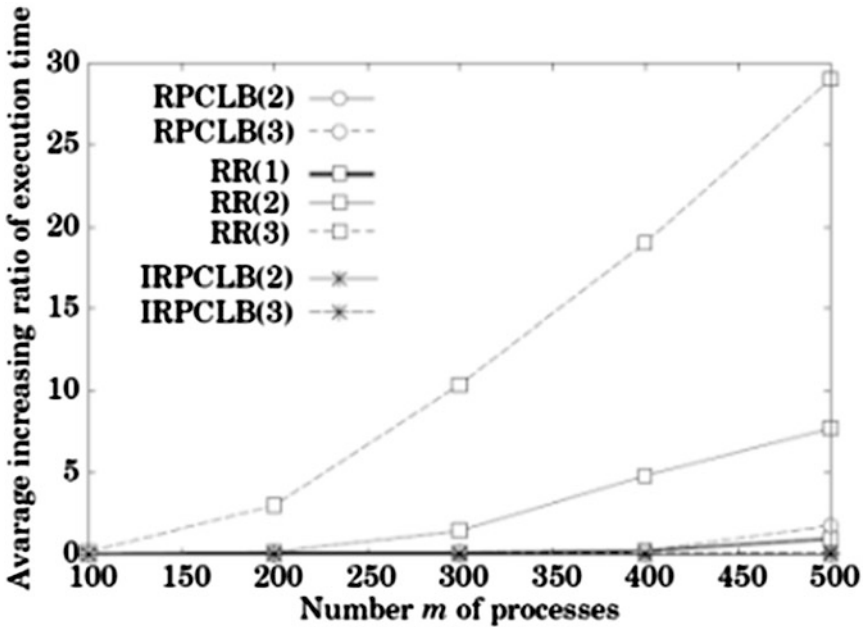


Fig. 2 Average increasing ratio of execution time

6 Concluding Remarks

In our previous studies [6], the RPCLB algorithm is proposed to select multiple servers for redundantly performing an application process so that not only processes can be reliably performed in presence of server faults but also the total power consumption in a server cluster can be reduced in computation type applications. In this paper, we proposed the IRPCLB algorithm where the meaningless processes are forced to be terminated. By forcing meaningless processes to terminate on servers, the total power consumption of a server cluster can be reduced in the IRPCLB algorithm than the RPCLB algorithm. We evaluated the IRPCLB algorithm with redundancy rd in terms of the total power consumption and the execution time compared with the RPCLB and RR algorithms. From the evaluation, the IRPCLB algorithm is more useful than the RPCLB and RR algorithms.

References

1. Hemmert S (2010) Green HPC: from nice to necessity. In: Proceeding of the computing in science and engineering, pp 8–10
2. Lamport R, Shostak R, Pease M (1982) The Byzantine generals problems. ACM Trans Program Lang Syst 4(3):382–401

3. Enokido T, Aikebaier A, Takizawa M (2010) A model for reducing power consumption in peer-to-peer systems. *IEEE Syst J* 4(2):221–229
4. Enokido T, Aikebaier A, Takizawa M (2011) Process allocation algorithms for saving power consumption in peer-to-peer systems. *IEEE Trans Ind Electron* 58(6):2097–2105
5. Enokido T, Takizawa M (2012) Energy-efficient server selection algorithms based on the extended simple power consumption model. In: *Proceedings of the 6th international conference on complex, intelligent and software intensive systems (CISIS-2012)*, pp 276–283
6. Enokido T, Aikebaier A, Takizawa M (2012) A redundant power consumption laxity-based (RPCLB) algorithm for computation type applications. In: *Proceedings of the 14th international symposium on multimedia network systems and applications (MNSA-2012)*, pp 562–567
7. Job Scheduling Algorithms in Linux Virtual Server, <http://www.linuxvirtualserver.org/docs/scheduling.html>

Security of Cognitive Information Systems

Marek R. Ogiela and Lidia Ogiela

Abstract In this publication will be described the most important security issues connected with a new generation of information systems focused on cognitive information systems (CIS). Such systems are mainly designed to perform a semantic analysis of complex visual structures, as well as human-being behavioral analysis. In our paper will be presented the ways of ensuring the secrecy of information processing in such systems, as well as some new opportunities of using semantic information processed by CIS to develop a new cryptographic protocol for personal authentication and secret information distribution. The paper will describe both CIS internal security features, and external possible application of authentication procedures along with intelligent information management.

Keywords Cryptographic protocols · Bio-inspired cryptography · System security

1 Introduction

Cognitive Information Systems were developed to support the complex visual data analysis (like a scene or context analysis), semantic interpretation of various situation, as well as supporting the decision-making processes [4]. The general idea of these systems is based on using cognitive resonance processes which imitate the natural human brain inference and understanding processes [1, 3]. There are

M. R. Ogiela (✉) · L. Ogiela
AGH University of Science and Technology, Al. Mickiewicza
30 PL-30-059 Krakow, Poland
e-mail: mogiela@agh.edu.pl

L. Ogiela
e-mail: logiela@agh.edu.pl

several types of Cognitive Information Systems developed for particular purposes or application areas [3, 4]. Most of them are dedicated for interpretation of visual patterns e.g. medical images or biometric patterns, or some numerical values e.g. economic data.

The most important class of Cognitive Information Systems is E-UBIAS class (Extended Understanding Based Image Analysis System) [4]. Such systems are constructed for performing an extended visual pattern semantic interpretation based on analysis of particular images or complex scene. As a result of such analysis it is possible to receive a very large information record which contains many global or local parameters describing the analyzed pattern or complex situation. This means that such cognitive information systems may play a great role in various application connected with security or safety. In this paper we try to describe some selected, and most important areas of application CIS for security purposes, connected with particular persons or users, as well as with global application e.g. in homeland security.

2 CIS Systems in Various Security Applications

As a result of cognitive resonance processes performed in CIS systems, it is possible to construct a very large information record which contain various numerical values and semantic information. Such information may be local (describing particular object or feature) or global (describing the complete image or several objects), but also may has form of semantic information, describing the meanings of the analysed pattern. All these form of information after collecting by CIS system may be used for many different purposes connected with security areas.

In particular we can try to use cognitive data analysis systems in the following important application:

- Application of CIS system for homeland security areas
- Application of CIS systems for personal characteristic and biometric extraction
- Various crypto-biometric application
- Secure information splitting and management

In the following section such possible application will be described more extensively.

3 Features of CIS Security Application

Having information connected with particular person or complex situation, we can try to use it in different manners, and develop some new security procedures, which allow to introduce a new systems for local (personal) or global application.

3.1 Cognitive Systems in Homeland Security

One of the areas of homeland security is wide possibilities of performing personal identification for particular bodies or citizens. For such purposes may be used the CIS system.

There are many circumstances in which state agencies should allow to perform a biometric identification e.g. airports transportation, banking systems or personal id infrastructure, forensic investigation at the crime scene or similar. All such task required to have abilities for quick and convenient acquisition of personal data, patterns or information. But having such personal information sometimes may generate some additional problems with management and proper selection of most important personal features which should be used for particular identification task, or even generate problems how can we used such personal information for another purposes beside straight identification. So the main theme of this paper will be connected with the latest achievements in the field of creation and application of cognitive information systems for analysis if personal data, and possible application of such patterns for identification purposes. This may be very important in future homeland security computer systems, and ambient intelligent systems allowing performing ubiquitous human monitoring tasks.

An identification analysis aimed at correctly recognising a given person, and in particular the assignment of the analysed characteristic features of a given individual to a specific person, are performed by correctly comparing traits with the set of data kept in knowledge bases. The personal data set of a given individual contains all the personal data that is available (i.e. is obtained during the data collection process). The personal data collected in the personal data set makes it possible to define characteristic traits of a given individual which will form the basis of the verification analysis. The verification of a person must be unambiguous, as it is not acceptable for the personal data collected in the system to point to more than one person characterised by specific traits. Thus the verification process must be unambiguous. If it is not, then the set of characteristic features must be supplemented with additional personal data which will make the identification process unambiguous.

Biometric analysis processes are conducted by a class of systems called Cognitive Personal Information Analysis and Identification Systems—CPIAIS. These systems represent one of classes of cognitive information systems whose operation is based on the cognitive resonance processes and inference.

3.2 CIS Systems in Personal and Biometric Analysis

A new technique of personal authentication and identification based on selected standard or non-standard biometric patterns was proposed using Cognitive Information Systems [5]. CIS systems carry out personal verification and identification

processes using some standard biometric patterns in the form of face images, fingerprints, DNA sequences, as well as using non-standard biometric patterns in the form of medical images presenting hand bones and heart arteries (Fig. 1).

Anatomical features play an important role in personal analysis processes. The former are subjected to complex analysis processes which are to produce an unambiguous identification of the person whose anatomical features were analyzed. The most widespread types of biometric analyses include analyses of the face, hand and voice. In the analysis of characteristic features of the face, it is important to describe and interpret parameters that can help describe a human face (e.g. the height face, the forehead height, the height nose etc.). The proposed CIS system has also been used to propose a formal description of the analysis of others biometric features [5, 6]. These features, with the added elements of the semantic data analysis, make an extended identification analysis possible. A formal solution based on defining a set of biometric characteristic features of the hand is proposed for analyzing the biometric features of hand bones [6].

In biometrics analysis also it's possible to analyze medical 3D images portraying lesions in large heart vessels—coronary arteries [6]. Images of this type are acquired, inter alia, in heart disease diagnostics used to assess the lesions of the cardiac muscle and also of coronary vessels.

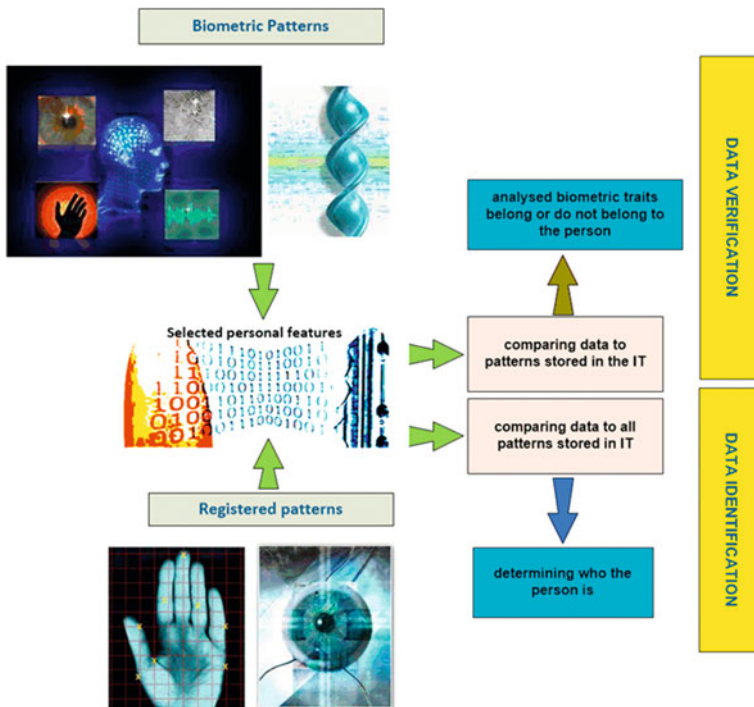


Fig. 1 Personal verification and identification processes

3.3 CIS in Crypto-Biometric Application

Personal information obtained using CIS systems can be used for various purposes, and also for authenticating parties in communication protocols or for generating cryptographic keys used in encrypted communications. Unique personal data extracted from selected biometric patterns can be used to create personalised cryptographic keys which can also be used to ensure the confidentiality of data stored or transmitted, and on the other, will contain biometric features allowing these keys to be assigned to a specific person. The general methodology demonstrating the opportunities for using personal information to create unique bit sequences that can be included in cryptographic keys has been described in [6].

The algorithm generating keys from biometric patterns works in two stages. At the first stage, it will use a CIS system which will analyse selected types of biometric images with a view to extracting a feature vector.

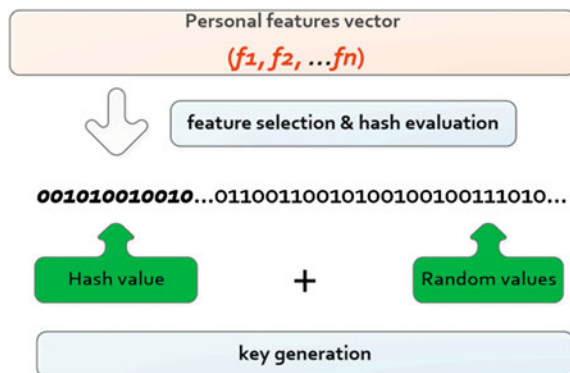
Such analysis, employing image pre-processing techniques, produces an information record containing many significant unique and personal parameters describing particular person.

In the second step, the keys are generated using selected personal characteristics and one of the hashing abbreviating functions. It is possible to generate any number of personalised keys in the following way:

- A hashing function must be selected to generate the keys
- For each personalised key a random set of several numerical features is selected
- For selected features a hash function are called
- The obtained hash value is entered as the sequence initiating a new key, while the random generation of bits allows supplementing it to the length required

The idea of crypto-biometric key generation is presented in Fig. 2.

Fig. 2 Key generation based on medical visualization



3.4 CIS in Secure Information Management

There are many types of methods for classifying information and protecting it from being accessed by unauthorized persons. They include threshold schemes and sharing techniques. In CIS system it is possible to use personal or biometric information to split or share important strategic data [7–10]. For such biometric sharing we can use any personal information e.g. features of the iris or coronary arteries layouts, which is material for the verification analysis while revealing secret information.

Using iris templates the melanin content can be a component for recognition processes executed as part of processes of information concealment (by splitting information into parts of the secret) after the stage of the proper personal verification. The same role may play the information record containing some personal information about coronary vessels conditions and spatial topology. Such information may be extracted using CIS system or during medical examination for particular person.

Information splitting algorithms dealing with concealing biometric information contained in the iris can be executed by two mutually independent ways of data splitting—both by a layer split and by a hierarchical split. The former means splitting the information between n secret holders and its reproduction by $n-m$ trustees of the secret. The latter case means that the secret is split between n holders of the secret, but the information can be reproduced by superior groups of secret holders within which the specific secret has been split into k parts ($k < n$). Thus the splitting methods depend on the purpose for which the information is split and concealed. In the case of personal identification systems or recognition systems, the methods of biometric data splitting most frequently used are layer splits. It plays a great role in modern information management models and systems.

4 Conclusion

Cognitive Information Systems were developed especially for performing semantic interpretation of visual patterns and complex data. As has been shown in this paper such systems play also a very important role in various aspect of secure computing. Such system allow to implement many biologically inspired algorithms, which are directed not only for semantic information extraction, but also for using such information, especially describing personal features, for implementing various security procedures important both from global and personal point of view. The most important areas of security features implementation using CIS systems are homeland defence information systems, personal and biometric identification, as well as intelligent and secure information management. It seems that in near future such systems due to theirs flexibility will have some other important applications in security areas.

References

1. Cohen H, Lefebvre C (eds) (2005) Handbook of categorization in cognitive science. Elsevier, The Netherlands
2. Ogiela L (2009) UBIAS systems for cognitive interpretation and analysis of medical images. *Opto-Electron Rev* 17(2):166–179
3. Ogiela L, Ogiela MR (2009) Cognitive techniques in visual data interpretation, studies in computational intelligence, vol 228, Springer-Verlag Berlin
4. Ogiela L, Ogiela MR (2012) Advances in cognitive information systems, cognitive systems monographs, vol 17, Springer-Verlag, Berlin
5. Ogiela L, Ogiela MR (2012) Visual image biometric identification in secure urban computing. In: Kim TH et al (eds) Computer applications for bio-technology, multimedia and ubiquitous city, CCIS 353. Springer, Heidelberg, pp 374–380
6. Ogiela MR, Ogiela L (2012) Medical visualizations in secure bio computing. In: 26th IEEE international conference on advanced information networking and applications workshops (WAINA-2012), Fukuoka, 26–29 March, pp 997–980. IEEE (2012)
7. Ogiela MR, Ogiela U (2012) DNA-like linguistic secret sharing for strategic information systems. *Int J Inf Manage* 32(2):175–181
8. Ogiela MR, Ogiela U (2012) Linguistic protocols for secure information management and sharing. *Comput Math Appl* 63(2):564–572
9. Ogiela MR, Ogiela U (2012) Information security management based on linguistic sharing techniques. In: Gupta M, Walp J, Sharman R (eds) threats, countermeasures and advances in applied information security. IGI Global, Hershey, pp 181–193
10. Ogiela MR, Ogiela U, Ogiela L (2012) Secure information sharing using personal biometric characteristics. In: Kim TH et al (eds) Computer applications for bio-technology, multimedia and ubiquitous city, CCIS 353. Springer, Heidelberg, pp 369–373

The Design of a Policy-Based Attack-Resilient Intrusion Tolerant System

Jungmin Lim, Yongjoo Shin, Seokjoo Doo and Hyunsoo Yoon

Abstract In order to identify and reduce the chance of vulnerability, a novel policy-based intrusion tolerant system (ITS) is studied in this paper. The suggested scheme quantifies the vulnerability level first, and then applies it to decide the candidate of the next rotation based on a policy. Experiments using CSIM 20 proved that it has enough capability to hide the VM rotation pattern which attackers are generally interested in and reduces the data leakage of the system greatly in spite of increasing the number of exposures.

Keywords Intrusion tolerant system (ITS) · Self-cleansing intrusion tolerance (SCIT) · Adaptive recovery

1 Introduction

In general, as most information systems are open to the public using online services, attackers are trying to intrude into those systems using their increased vulnerabilities. There are many popular defense mechanisms to malicious packet

J. Lim (✉) · Y. Shin · H. Yoon
Department of Computer Science, KAIST, 291 Daehak-ro, Yuseong-gu,
Daejeon, Republic of Korea
e-mail: jmlim@nslab.kaist.ac.kr

Y. Shin
e-mail: yj_shin@nslab.kaist.ac.kr

H. Yoon
e-mail: hyoon@nslab.kaist.ac.kr

S. Doo
Department of Electronic Engineering, Korea Army Academy at Yeong-cheon,
495 Hoguk-ro Gogyeong-myeon, Yeongcheon-si 770-849, South Korea
e-mail: doos.kr@gmail.com

attack: firewalls and intrusion detection systems (IDSs). However, it is not possible for those defense systems to shield our network from all attacks in reality. For these reasons, the capability to maintain good services under extremely threatening environment must be established, and intrusion tolerant systems (ITSs) are getting attention recently as one of the good solutions. They have been successfully applied in many huge projects such as MAFTIA [1] and OASIS [2]. Moreover, many research studies based on virtualization have been conducted these days [3, 4].

1.1 ITS Based on Virtualization

Most of virtual schemes focus on proactive recovery of each virtual machine (VM) as in the case of self-cleansing intrusion tolerance (SCIT) [3]. As shown in Fig. 1, the central controller has the responsibility of rotating each VM and each VM rotates its own state from online, grace, cleansing, and live spare in SCIT [4].

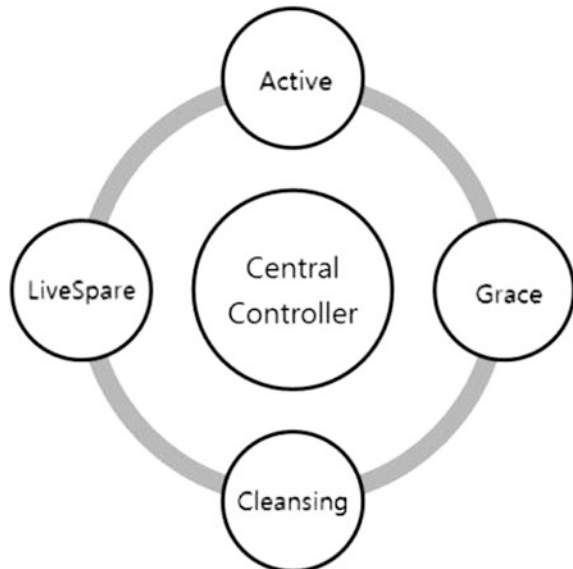
However, when a proactive recovery method based on virtual schemes is used simply, several weaknesses could be existed as follows.

Remark 1 Vulnerabilities of each VM might be repeatedly exposed to attackers because the system does not consider if VMs are contaminated from outside, or not.

Remark 2 The VM rotation pattern can be detected by attackers in case the system does not modify the VM rotation pattern while providing services.

Remark 3 According to the exposure of vulnerabilities and the VM rotation pattern, information leakage can be occurred.

Fig. 1 State rotation in SCIT



This paper presents a novel method for quantifying the degree of vulnerability through both file integrity monitoring and malicious code detection before entering the cleansing step. The calculated degree of vulnerability is applied to the selection of active VMs for the next rotation. By doing so, it is expected to hide the VM rotation pattern from attackers and to decrease data leakage. It should be noted that SCIT is based on random selection of VM.

Chapter 2 describes the architecture of the proposed system. Chapter 3 shows simulation results of the proposed scheme and compares them to SCIT. Finally, Chap. 4 concludes the study.

2 Policy-Based Intrusion Tolerant System Model

In our approach, the central controller has more responsibilities than SCIT in associated with selecting the next active VMs. Based on the degree of vulnerabilities, selecting less-vulnerable VMs is the main concern in this paper.

2.1 System Architecture

The proposed system architecture is illustrated in Fig. 2. The system consists of HW servers having several associated VMs, online VM group supplying services, and offline VM group preparing for the online state. It is assumed that all VMs provide the same web services with the same functionality to clients via the Internet even though they have different operating systems and applications one another.

After a VM supplies services during a certain designated period, the VM enters into the offline VM group. While the VM is on cleansing state, crucial files and memory integrity should be examined by the central controller. Through this process, the VM table is generated and stored in a secured database. The generated VM table is used to select the next online VMs which will be entered into the online VM group.

2.2 Algorithm

The detail process in the proposed scheme is explained in Fig. 3 and Algorithm 1. As shown in Fig. 3, file and memory analyses of every VM are executed after finishing online states. FileVerifier [5] is used for examining the integrity of crucial files and folders such as password, /usr/bin, and /usr/local/www. Basically, the initial hash values of the designated files and folders are stored in FileVerifier, and hash values after online state are investigated for the file integrity check. In addition, Yarascan-plugin in Volatility [6] is used for detecting main malicious codes from volatile memories such as RAM samples. The results from FileVerifier

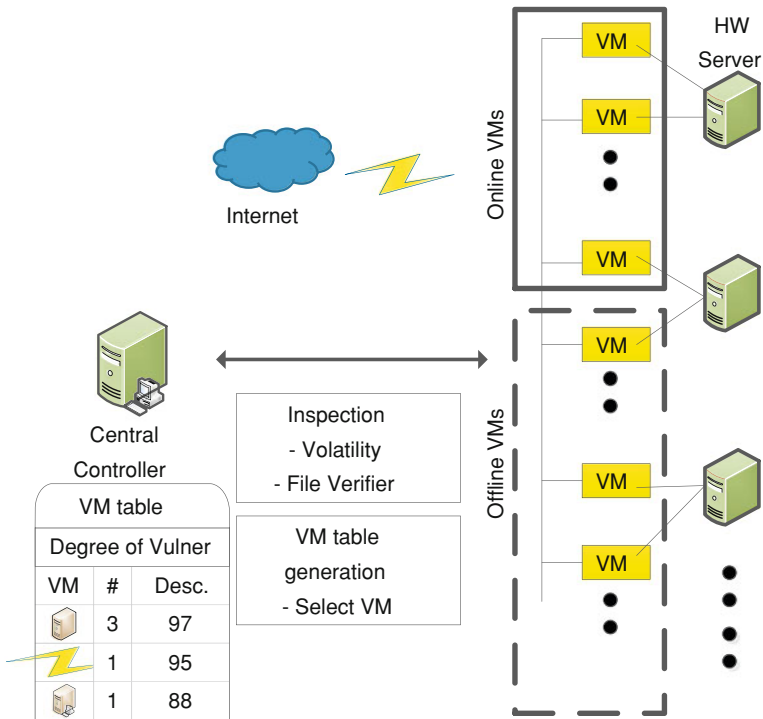


Fig. 2 Proposed system architecture

and Volatility are used to create a VM table by a certain policy which an operator designs. The VM table is used to select the next online VMs. Considerable policy will be introduced in [Chap. 2.4](#).

Algorithm 1 explains the decision process for selecting online VMs in brief. In order to include online VM group, the current score of each VM should be greater than the previous score stored in the table, or the current exposure time should be longer than the previous time value.

Algorithm 1 Decision Process

Parameters

VM_Group = [VM(0), VM(1), VM(2), VM(3), VM(4)]

temp_score {the score saved temporarily}

temp_time {the exposure time saved temporarily}

Decision Process

if VM (i) is on LiveSpare && score of VM(i) > temp_score

 then temp_score = score of VM(i)

 Exposure VM(i)

else if VM(i) is on LiveSpare && score of VM(i) == temp_score

```

&& time of VM(i) > temp_time
then
Exposure VM(i)
    
```

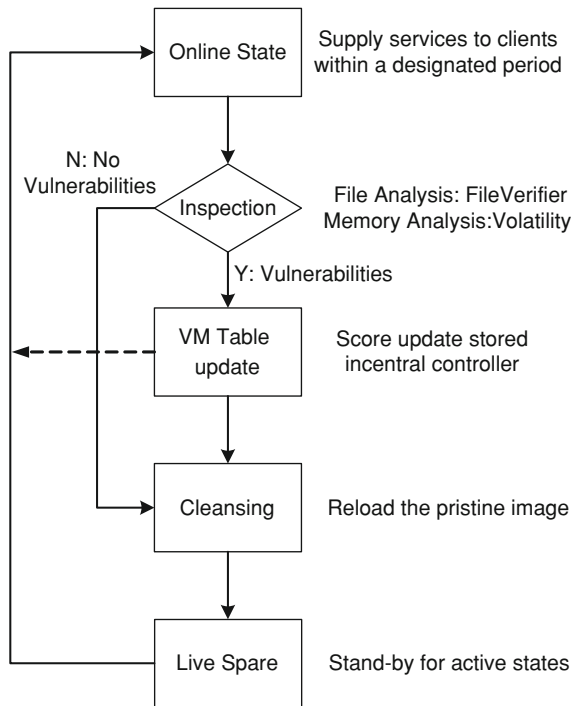
2.3 Availability Check

The following table describes the experiment environment for checking the availability of the suggested scheme.

Virtual image (web server)	Central controller
Windows XP(Service Pack 3), Windows 7 Apache 5, IIS	Intel Core i3 CPU 3.19 GHz, 4G RAM, 32bit Windows 7 VMware Workstation 7.0.0, Python

In order to measure time consuming taken by Volatility and FileVerifier, experiments with several compositions have been conducted 20 times. It was turned out that the average amount of time for FileVerifier was extremely short (about 0.67 s) because only hash values are checked. And the average time

Fig. 3 Flow chart for the proposed scheme



consuming taken by Volatility was about 24.27 s. After that, it was checked if the additional resources are needed due to the added time consuming, or not.

According to SCIT, the required number of VM images is calculated from (1) after adding time consumed by Volatility and FileVerifier [4].

$$N = \frac{W_{\text{grace}} + T_{\text{cleansing}} + T_{\text{inspection}}}{W_{\text{online}}} + 1 \quad (1)$$

W_{online} : OnlineWindow, W_{grace} : Grace period,

$T_{\text{cleansing}}$: Cleansingperiod, $T_{\text{inspection}}$: Integrity inspection

In connection with the minimal size of intrusion tolerant system consisting of 1 web server, 1 DB server and only 1 spare server (in case W_{online} is 120 s and $W_{\text{grace}} + T_{\text{cleansing}}$ is 300 s),

$$N = \frac{300 + 25}{120} + 1 = 3,$$

which is the same values as in SCIT. This means that additional resource is not needed for checking file integrity and memory analysis even in a larger system including more spare servers.

2.4 Example of a Policy

The following policy is applied to examine the proposed scheme

- All the scores are controlled by the central controller.
- All VMs have the same score of 100 initially and lose the score via a scoring policy. Also, exposure time of each VM is decreased depending on the following equation.

$W_{i_{\text{next}}}$: next online window, W_i : current online window

S_i : Score of VM(i), x : scoring variable

- The score of each VM is valid only for one round. (i.e. it is reset in the next round)
- Exposure time should not be reset.
- Exposure order is set by the score and exposure time (random if both are same)
- In case the decreased exposure time is exceed 10 % of the initial exposure time, overall exposure time is modified to normal distribution in order to prevent increasing the number of exposure of a specific VM.

As shown in Table 1, eight malicious codes referenced by 2012-AhnLab Report [7] are selected and the scores of CVEs are set by Common Vulnerability Scoring System (CVSS) of National Institute of Standards and Technology (NIST) [8].

Table 1 Scoring policy

Volatility				FileVerifier	
Yarascan	Score	Yarascan	Score	File integrity	Score
CVE-2011-2140	10	CVE-2010-0806	9.3	Passwd	15
CVE-2010-0754	4.3	CVE-2011-0611	9.3	/usr/bin	15
CVE-2012-0754	10	CVE-2011-3544	10	/usr/local/www	15
CVE-2012-0003	9.3	CVE-2009-0075	9.3		

Table 2 Example according to some events

Round	Event	VM1	VM2	VM3	VM4	Total
Initial	Start(score/exposure time)	100/500	100/500	100/500	100/500	2000
1	VM1: CVE-2012-2140, injected code	85/425	100/500	100/500	100/500	1925
2	VM3: Passwd,/usr/bin	100/425	100/500	70/350	100/500	1775
	Exposure time modification	100/500	100/500	70/300	100/700	2000
3	VM4: CVE-2012-0754	100/500	100/500	100/300	90/650	1950

Initially the score and exposure time for every VM are 100/500, respectively. Under scoring policy described in Table 1, the values can be changed depending on the events in Table 2.

3 Simulation and Results

3.1 Experiment Environment

To evaluate the performance of the suggested scheme, a series of simulations was done with CSIM 20 [9] which is useful in validating the feasibility of complex systems. Several experiment results in associated with expected information leakage of the suggested system were compared to the ones in SCIT.

For this, information leakage can be acquired by figuring out the area at a certain exposure time on information loss curve map suggested in several papers [10, 11]. For example, information leakage at the point A in Fig. 4 is the same as the area colored with black.

3.2 Performance Verification

To measure performance of proposed scheme, it is assumed that only one among 1000 packets is contaminated while VM is online state for 500 s. Then, the probability of successful attack is

$$P_{attack} = 0.001 * \frac{\exp(VM)}{500}, \text{ where } \exp(VM) \text{ is the exposure time of VM} \quad (2)$$

Fig. 4 Data leakage on information loss curve

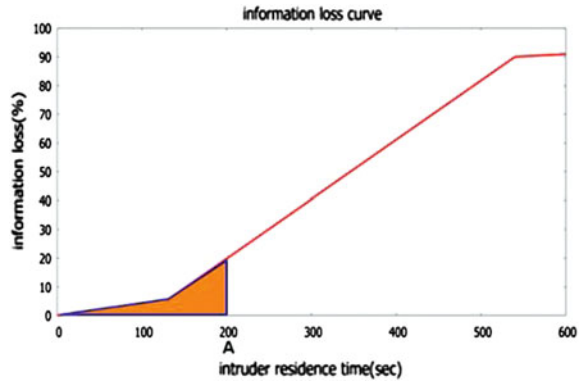


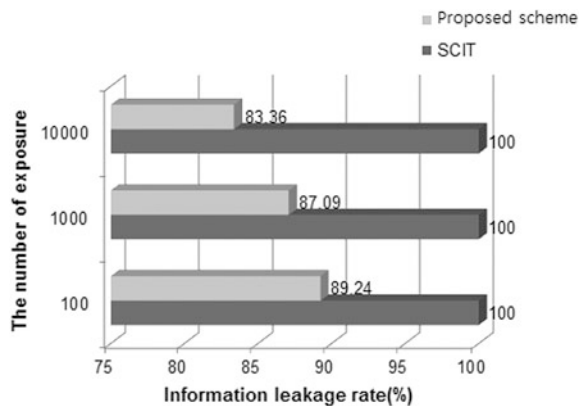
Table 3 Intruder’s residence time

Exposure time	300	400	450	500	600	650
Initial attack	273.8	273.8	273.8	273.8	273.8	273.8
Intruder residence time	26.2	126.2	176.2	226.2	326.2	376.2

Intruder’s residence time can be obtained by using (Exposure time—Initial attack time) where the initial attack time means the first attack launches based on P_{attack} . The intruder’s residence times are shown for each exposure time in Table 3.

By using the information loss curve in Fig. 4 and intruder’s residence time in Table 3, the information leakage rate were calculated. As shown in Fig. 5, as the number of exposure increases, the rate of information leakage for the proposed scheme is decreased, while the rate in SCIT keeps the same value of 100.

Fig. 5 The comparison of data leakage rate between the proposed scheme and SCIT



4 Conclusion

Recently, ITSs based on virtual schemes focusing on fast proactive recovery have been widely researched. As a result of first proactive recovery, however, VMs could be easily contaminated by attackers even for a short period of online state with uniform exposure pattern. In addition, the repeated pattern of rotation and the same exposure time of each VM with vulnerabilities can be targets for attackers. In this paper, in order to provide attack-resilient services, the suggested novel scheme quantifies the vulnerability of each VM and applies it to select the candidate of the online VM for the next rotation. This procedure is done with a series of policy prepared in advance. Experiment results clearly showed that the proposed scheme can reduce the data leakage rate remarkably compared to SCIT. Ultimately, it is expected that the proposed policy-based attack-resilient method complements the current existing ITS in that it not only hides the pattern of rotation but also reduces the exposure of vulnerabilities of the systems.

Acknowledgments This work was supported by the National Research Foundation of Korea (NRF) grant funded by the Korea Government (MEST) (No. 2012-0005390).

References

1. Miguel C, Paulo V, Nuno FN (2004) The architecture of a secure group communication system based on intrusion tolerance. In: Proceedings of the 2001 international conference on distributed computing systems workshop (ICDCS 2001), Arizona, USA, April 2001
2. Lala JH (2003) Organically assured & survivable information systems (OASIS): foundations of intrusion tolerant systems. IEEE Computer Society Press, <http://computer.org/cspres>, ISBN 0-7695-2057-X2003
3. Quyen N, Arun S (2010) Comparative analysis of intrusion-tolerant system architectures. In: IEEE security and privacy. Preprint. Accepted for publication, Aug
4. Quyen N (2010) Realizing S-reliability for services via recovery-driven intrusion tolerance mechanism. In: International conference on dependable systems and networks workshops (DSN-W)
5. <http://www.programmingunlimited.net/siteexec/content.cgi?page=fv>
6. <https://www.volatilesystems.com/default/volatility>
7. <http://www.ahnlab.com/kr/site/securitycenter/asec/asecReportView.do>
8. <http://www.first.org/cvss>
9. Schwetman H (2001) CSIM19: a powerful tool for building system models. In: Proceedings of the 2001 winter simulation conference, pp 250–255
10. David P, Arun KS (2010) An intrusion tolerance approach to enhance single sign on server protection. In: Proceedings of the third international conference on dependability (DEPEND 2010) Venice/Mestre, 18–25 July
11. Yih H, David A, Arun S (2006) Closing cluster attack windows through server redundancy and rotations. In: Proceedings of the second international workshop on cluster security (Cluster-Sec06), Singapore, May

Algorithms for Batch Scheduling to Maximize the Learning Profit with Learning Effect and Two Competing Agents

Jen-Ya Wang, Yu-Han Shih and Jr-Shian Chen

Abstract Due to the prevalence of e-learning and information technology, a wide choice of various learning styles is offered. So we might have multiple learning paths for a teaching material. However, learners differ from one another in their information literacy and cognitive load. These will influence the learning achievements greatly. Learners lacking information literacy are probably not able to determine their leaning paths easily. For example, obligatory courses, precedence relationship, time limit, and leaning effect should be taken into account. In light of these observations, we propose a genetic algorithm for determining leaning paths with many topics and a branch-and-bound algorithm for providing optimal learning paths of few learning topics.

Keywords Job scheduling · Learning path · Information literacy · Cognitive load · Learning effect

1 Introduction

Due to the prevalence of e-learning and information technology, a wide choice of learning styles is offered. In today's web-based learning environments, personalized curriculum sequencing is an important research issue [1, 2]. This is because

J.-Y. Wang · J.-S. Chen (✉)

Department of Computer Science and Information Management,
Hungkuang University, No. 34, Chung-Chie Road, Taichung 433,
Taiwan, Republic of China
e-mail: jschen@sunrise.hk.edu.tw

J.-Y. Wang

e-mail: jywang@sunrise.hk.edu.tw

Y.-H. Shih

Department of Computer Science and Engineering, National Chung-Hsing University,
No. 250, Guoguang Road, Taichung 402, Taiwan, Republic of China
e-mail: s99056009@cs.nchu.edu.tw

there is no single learning path which is suitable for everyone. Unlike traditional textbooks providing routine and fixed curriculum sequencing, web-based learning materials offer learners more flexible and complicated sequencing. Learners can determine their own learning paths according to their preferences. Especially for learners with different backgrounds, interests, and goals, different learning paths are thus called for. However, to decide a proper learn path for each learner is not easy. There are many things needed to be taken into account. That is, determining an on-line learning path for each individual is a very time-consuming process.

Information literacy and cognitive load will influence the learning achievements. As stated in [3], people may have different viewpoints on information literacy. However, the following definition is widely acceptable. Information literacy indicates the ability to identify when and what information is required and the ability to retrieve, evaluate, integrate, and utilize the information to solve problems [3–5]. Therefore, we learn that people with higher information literacy are easy to acquire new knowledge. Thus, we can conclude that people with lower information literacy cannot determine suitable learning paths efficiently. On the other hand, cognitive load is defined as the information load in the working memory. As long as the load is not beyond the capacity, people can process a specific amount of information. Therefore, the more difficult learners think the learning materials, the more intellectual efforts they need to make. It implies that the loads cannot exceed the amount that learners are able to take. When designing learning paths, overdoing is harmful to learning.

When designing learning paths, something need to be noticed first. There are compulsory topics and optional topics, course precedence exists, time limits need to reach, or learning effect is considered. Taking the data structure course as an example, array is basic and compulsory topic, whereas red–black tree belongs an advanced topic. For a given course, the compulsory topics need to be included in the learning paths. As for the optional topics, learners can choose some in order to increase their literacy and extra profits. Thus, we can design suitable learning paths by considering all the issues.

In typical scheduling problems, the processing time of a job is usually assumed to be a constant. However, in many realistic scheduling problems, workers and machines should be considered as a whole. If workers complete small and easy jobs first, the experiences can benefit the subsequent large jobs and workers can accelerate the processing times of these large jobs. Therefore, the position order of the jobs can influence the total completion time significantly. This phenomenon is called learning effect [6]. Therefore, we assume the large and difficult topics should be scheduled in the last parts of a learning path.

So far we have had many algorithms for generating learning paths, but few of them can provide suitable learning paths according to learners' backgrounds. In this study, we introduce two algorithms for batch scheduling to maximize the learning profit. Finally, the experimental results show the convergence speed and solution quality of the proposed algorithms. Using the proposed algorithms, an e-learning provider requires only a little run time to provide suitable learning paths.

2 Problem Definition

We consider n candidate jobs forming a partially ordered set $J = \{1, 2, \dots, n\}$. For each job j , both its profit and normal processing time are denoted by p_j . We must choose some subset for processing sequentially on a single machine within m K -length time intervals T_i 's. All jobs are from two agents AG_1 and AG_2 and available at time zero, where jobs from AG_1 are compulsory and jobs from AG_2 are optional. Furthermore, there are precedence relationships among jobs. e.g., job i may precede job j . Let $l(r) = \prod_{k=0}^r a(k)$ denote the learning effect, where $a(r)$ is a coefficient at position r , $a(0) = 1$, and $a(k) \leq 1$ for all k . The actual processing time of job j at position r is $p_{j[r]} = p_j l(r)$. Therefore, the objective function is defined as $\sum_{i=1}^m \sum_{j \in T_i \cap AG_2} p_j$ subject to

- (1) all jobs from AG_1 need to be chosen,
- (2) $\sum_{j \in T_i} p_{j[r]} \leq K$ for all i ,
- (3) all precedence constraints need to be satisfied,

where $j \in T_i \cap AG_2$ means job j is from AG_2 and scheduled within T_i .

3 Proposed Algorithms

In this section, we propose a genetic algorithm for obtaining near-optimal schedules and a branch-and-bound algorithm for obtaining optimal solutions.

3.1 Genetic Algorithm

We modify traditional genetic algorithms [7] by considering the following four issues: solution representation, population initialization, convergence speed, and solution quality.

Solution representation. Each solution, i.e., schedule, is denoted by a permutation of integers 1 to n . For example, a schedule [1–4] means that we assign job 3 to T_1 and subsequently assign job 2 to T_1 and so on. If T_1 is full, then we start to assign jobs to T_2 .

Population initialization. We use 100 random permutations of integers 1 to n as the first generation.

Selection. A standard roulette wheel is employed in this study [7]. The probability we select solution i is defined by $f_i / \sum_k f_k$, where f_i , the i th fitness or the profit gained schedule i .

Crossover. We use a PMX crossover operation [8]. First, two parent solutions are chosen according to the selection operation. Second, two distinct random numbers x and y are generated to form a substring for each parent. Without loss of

generality, we assume $x < y$. The relationship between the two corresponding jobs at the same position r are recorded, where $r = x, x + 1, \dots, y$. Third, we exchange the two substrings and obtain two new children. Finally, the two children are legalized according to the recorded relationships if there are duplicate jobs outside the substrings.

Mutation. A mutation operation based on the extraction and reinsertion is designed. We select two distinct random positions x and y and denote it by $x \rightarrow y$. Then we mutate it as follows. For example, a schedule of [1–6] is mutated to [1–6] if $2 \rightarrow 5$ and the schedule is mutated to [1–6] if $5 \rightarrow 2$.

3.2 Branch and Bound

A dominance property is developed in order to save unnecessary visits in a branch-and-bound tree. Suppose that $\pi = [\alpha, i, j, \beta]$ and $\pi' = [\alpha, j, i, \beta]$ are two schedules of jobs and the difference between them is a pairwise interchange of two adjacent jobs i and j , where α and β are two partial sequences.

Property 1 If $i \in T_i, j \in T_i$, and $i < j$, then π dominates π' .

The algorithm assigns jobs in a forward manner starting from the first position. The operations of the algorithm are described as follows.

Step 1 (Branching) By Property 1, we can eliminate the dominated nodes in the branch-and-bound tree. Therefore, we can reduce the run time greatly.

Step 2 (Bounding) For the non-dominated nodes, we utilize a simple upper bound to eliminate the nodes if their partial profits including their corresponding upper bounds are lower than current completed profits.

4 Experimental Results

This section shows the experimental results conducted on a Pentium IV, 3.2 GHz CPU, with 2 GB RAM. The results consist of two parts: one for smaller problems and the other one for larger problems.

In the first part, the numbers of jobs n are set at two levels, i.e., four and eight. The number of time intervals m is fixed at five and the time limit K is $1.5 \sum_{j=1}^n p_j / m$. For each T_i , we set the learning effect to $l(i) = \max\{0.975^i, 0.8\}$. The processing times (p_j) follow a uniform distribution $U(1, 100)$. The ratios of the numbers of jobs from AG_2 are set 0.25 and 0.5. Parameter $PRCD$ controls the number of precedence relationships, e.g., $PRCD = 0.5$ means there are $0.5n$

Table 1 The performance of GA for with small problem sizes

n	AG_1	PRCD	(BB-GA)/BB (100 %)		(UB-GA)/UB (100 %)	
			Mean	Stdv	Mean	Stdv
4	0.25	0.25	0.00000	0.00000	62.28054	10.22801
4	0.25	0.50	0.00000	0.00000	62.87234	8.42901
4	0.25	0.75	0.00000	0.00000	58.93599	9.31566
4	0.50	0.25	0.00000	0.00000	71.86231	11.21115
4	0.50	0.50	0.00000	0.00000	70.06278	10.10776
4	0.50	0.75	0.00000	0.00000	70.36109	9.22500
8	0.25	0.25	0.00000	0.00000	46.27574	3.92009
8	0.25	0.50	0.00000	0.00000	45.92407	3.72299
8	0.25	0.75	0.00000	0.00000	45.28478	3.37406
8	0.50	0.25	0.00000	0.00000	56.30509	5.59594
8	0.50	0.50	0.00000	0.00000	56.32860	6.57562
8	0.50	0.75	0.00000	0.00000	55.62817	4.94329

precedence relationships. Moreover, for GA, the evolutionary population size is 100 and the number of generations is 100. The crossover rate and mutation rate are 0.8 and 0.1, respectively. Finally, all the following experimental results are the averages of 20 trials. We report the means and the standard deviations of (BB-GA)/BB and (UB-GA)/UB, where GA denotes the profit value obtained by the genetic algorithm, BB denotes the optimal profit value obtained by the branch-and-bound algorithm, and UB denotes the profit value obtained by a simple upper bound. The run times are not reported since they are all smaller than 1 s. As seen from the ratios of (BB-GA)/BB, the genetic algorithm performs well since the error percentages are all 0s, which implies all suggested schedules are optimal. However, our upper bound is little overestimated. The maximal value of the (UB-GA)/UB is 71.86 %. Even for the worst case, all the solutions generated by the genetic algorithm are the optimal. It implies that the performance of the GA algorithm is good if $(UB-GA)/UB < 100\%$.

In the second part, we set $m = 10$ and $n = 100$ for testing larger problem instances. For GA, the evolutionary population size is 200 and the number of generations is 200. The other settings are the same to the settings of the first part. The results are summarized in Table 2. As seen from the ratios of (UB-GA)/UB, the performance of GA is still good for instances with a large number of jobs. The mean and the maximum ratios of (UB-GA)/UB are smaller than 100 %. According to the experiences of Table 1, the solutions generated by GA in Table 2 are still likely to be the optimal ones. A closer look at Table 2 reveals that (UB-GA)/UB slightly increases as the number of jobs from AG_1 increases. This is because the more we have jobs from AG_1 , the less free space we can accommodate the jobs from AG_2 .

Table 2 The performance of GA for with large problem sizes

AG_1	PRCD	Run time (sec)		(UB-GA)/UB (100 %)	
		Mean	Stdv	Mean	Stdv
0.25	0.25	3.68239	0.13048	56.27306	1.39912
0.25	0.50	3.78308	0.01543	56.37989	1.39687
0.25	0.75	3.96106	0.01758	56.48261	1.32747
0.50	0.25	3.62051	0.01497	70.95222	1.67111
0.50	0.50	3.79707	0.01692	71.27288	1.49233
0.50	0.75	3.98144	0.01589	71.45226	2.47213

5 Conclusion

In recent years, everyone knows that e-learning has been more prevalent and managing learning materials and providing suitable leaning paths have also become more important than ever. In this paper, we introduce a learning path scheduling problem where the objective is to maximize the total profit given a maximum time limit for each time interval. We propose a genetic algorithm and a branch-and-bound algorithm. Experimental results show that the proposed genetic algorithm performs well with average error percentages 0 % for small problem sizes. We hope that this study will encourage more discussion on scheduling problems related to learning path design.

Acknowledgments The authors would like to thank the National Science Council (NSC) of Taiwan for partially supporting this research under Contract NSC-101-2511-S-241-004.

References

1. Chen CM (2008) Intelligent web-based learning system with personalized learning path guidance. *Comput Educ* 51:787–814
2. Chen CM, Liu CY, Chang MH (2006) Personalized curriculum sequencing utilizing modified item response theory for web-based instruction. *Expert Syst Appl* 30:378–396
3. Probert E (2009) Information literacy skills: teacher understandings and practice. *Comput Educ* 53:24–33
4. Natalie EJ, Crowe KM (2013) Information literacy and communication research: a case study on interdisciplinary assessment. *Commun Educ* 62:97–104
5. Timmersa C, Veldkamp B (2011) Attention paid to feedback provided by a computer-based assessment for learning on information literacy. *Comput Educ* 56:923–930
6. Badiru AB (1992) Computational survey of univariate and multivariate learning curve models. *IEEE Trans Eng Manage* 39:176–188
7. Wang JY, Chang TP, Chen JS (2009) An enhanced genetic algorithm for bi-objective pump scheduling in water supply. *Expert Syst Appl* 36:3772–3790
8. Lopez EG, O’Neill M (2009) On the effects of locality in a permutation problem: the Sudoku puzzle. In: *Proceedings of the IEEE symposium on computational intelligence and games, Milano, Italy*, pp 80–87

A Fuzzy-Based System for Evaluation of Trustworthiness for P2P Communication in JXTA-Overlay

Kouhei Umezaki, Evjola Spaho, Keita Matsuo, Leonard Barolli, Fatos Xhafa and Jiro Iwashige

Abstract In this paper, we propose a new fuzzy-based trustworthiness system for P2P Communications in JXTA-Overlay. This system decides the Peer Reliability (PR) considering three parameters: Actual Behaviour Criterion (ABC), Reputation (R) and Peer Disconnections (PD). We evaluate the proposed system by computer simulations. The simulation results have shown that when there are too many peer disconnections, although the reputation and the ABC are improved, the peer reliability remains very low. For few peer disconnections, peer reliability is increased with the increasing of ABC, R and PD and the system have a good performance.

K. Umezaki (✉) · E. Spaho
Graduate School of Engineering, Fukuoka Institute of Technology (FIT),
3-30-1 Wajiro-Higashi, Higashi-Ku, Fukuoka 811-0295, Japan
e-mail: sannpei1@hotmail.co.jp

E. Spaho
e-mail: evjolaspaho@hotmail.com

K. Matsuo
Fukuoka Prefectural Kaho-Sogo High School, 1117-1 Haji, Keisen-machi, Kaho-gun,
Fukuoka 820-0607, Japan
e-mail: matuo-k7@fku.ed.jp

L. Barolli · J. Iwashige
Department of Information and Communication Engineering,
Fukuoka Institute of Technology (FIT), 3-30-1 Wajiro-Higashi, Higashi-Ku,
Fukuoka 811-0295, Japan
e-mail: barolli@fit.ac.jp

J. Iwashige
e-mail: iwashige@fit.ac.jp

F. Xhafa
Department of Languages and Informatics Systems, Technical University of Catalonia,
C/Jordi Girona 1-3 08034 Barcelona, Spain
e-mail: fatos@lsi.upc.edu

Keywords P2P · Fuzzy system · JXTA-overlay

1 Introduction

Peer-to-Peer (P2P) architectures will be very important for future distributed systems and applications. In such systems, the computational burden of the system can be distributed to peer nodes of the system. Therefore, in decentralized systems users become themselves actors by sharing, contributing and controlling the resources of the system. This characteristic makes P2P systems very interesting for the development of decentralized applications [1, 2].

JXTA-overlay is a middleware built on top of the JXTA specification, which defines a set of protocols that standardize how different devices may communicate and collaborate among them. It abstracts a new layer on the top of JXTA through a set of primitive operations and services that are commonly used in JXTA-based applications and provides a set of primitives that can be used by other applications, which will be built on top of the overlay, with complete independence.

In P2P networks, peers collaborate with each other by sending request services and providing services to other peers. As there is no central authority for identity and content authentication, selfish peers that do not share their resources and malicious peers that inject malicious contents can be connected in the network. These misbehaviors greatly reduce the overall performance of P2P systems. Therefore, it is critical to discuss how a peer can trust each of its neighbor peers [3, 4].

Fuzzy Logic (FL) is the logic underlying modes of reasoning which are approximate rather than exact. The importance of FL derives from the fact that most modes of human reasoning and especially common sense reasoning are approximate in nature. FL uses linguistic variables to describe the control parameters. The fuzzy set theory uses the membership function to encode a preference among the possible interpretations of the corresponding label. A fuzzy set can be defined by exemplification, ranking elements according to their typicality with respect to the concept underlying the fuzzy set.

In our previous work [5–7], we proposed and implemented a fuzzy-based trustworthiness system, which considered only positive effect parameters. In this paper, we propose a new fuzzy-based trustworthiness system for P2P communications in JXTA-overlay that decides the Peer Reliability (PR) considering three parameters: Actual Behaviour Criterion (ABC), Reputation (R) and Peer Disconnections (PD). We evaluate the proposed system by computer simulations. The simulation results has shown that the proposed system can effectively help peers to select reliable peers to download information.

The structure of this paper is as follows. In Sect. 2, we introduce FL used for control. In Sect. 3, we introduce the Project JXTA and JXTA-overlay. In Sect. 4, we present the proposed fuzzy-based peer trustworthiness system. In Sect. 5, we discuss the simulation results. Finally, conclusions and future work are given in Sect. 6.

2 Application of Fuzzy Logic for Control

The ability of fuzzy sets and possibility theory to model gradual properties or soft constraints whose satisfaction is matter of degree, as well as information pervaded with imprecision and uncertainty, makes them useful in a great variety of applications.

The most popular area of application is Fuzzy Control (FC), since the appearance, especially in Japan, of industrial applications in domestic appliances, process control, and automotive systems, among many other fields.

FC: In the FC systems, expert knowledge is encoded in the form of fuzzy rules, which describe recommended actions for different classes of situations represented by fuzzy sets.

In fact, any kind of control law can be modelled by the FC methodology, provided that this law is expressible in terms of “if... then...” rules, just like in the case of expert systems. However, FL diverges from the standard expert system approach by providing an interpolation mechanism from several rules. In the contents of complex processes, it may turn out to be more practical to get knowledge from an expert operator than to calculate an optimal control, due to modelling costs or because a model is out of reach.

Linguistic Variables: A concept that plays a central role in the application of FL is that of a linguistic variable. The linguistic variables may be viewed as a form of data compression. One linguistic variable may represent many numerical variables. It is suggestive to refer to this form of data compression as granulation [8].

The same effect can be achieved by conventional quantization, but in the case of quantization, the values are intervals, whereas in the case of granulation the values are overlapping fuzzy sets.

FC Rules: FC describes the algorithm for process control as a fuzzy relation between information about the conditions of the process to be controlled, x and y , and the output for the process z . The control algorithm is given in “if-then” expression, such as:

- If x is small and y is big, then z is medium;
- If x is big and y is medium, then z is big.

These rules are called FC rules. The “if” clause of the rules is called the antecedent and the “then” clause is called consequent. In general, variables x and y are called the input and z the output. The “small” and “big” are fuzzy values for x and y , and they are expressed by fuzzy sets.

Control Knowledge Base: There are two main tasks in designing the control knowledge base. First, a set of linguistic variables must be selected which describe the values of the main control parameters of the process. Both the input and output parameters must be linguistically defined in this stage using proper term sets. The selection of the level of granularity of a term set for an input variable or an output variable plays an important role in the smoothness of control. Second, a control knowledge base must be developed which uses the above linguistic description of

the input and output parameters. Four methods [9–12] have been suggested for doing this: expert’s experience and knowledge, modelling the operator’s control action, modelling a process, self organization.

Among the above methods, the first one is the most widely used. In the modeling of the human expert operator’s knowledge, fuzzy rules of the form “If error is small and change-in-error is small then the force is small” have been used in several studies [13, 14]. This method is effective when expert human operators can express the heuristics or the knowledge that they use in controlling a process in terms of rules of the above form.

3 JXTA Technology and JXTA-Overlay

JXTA Technology: JXTA technology is a generalized group of protocols that allow different devices to communicate and collaborate among them. JXTA offers a platform covering basic needs in developing P2P networks [15].

By using the JXTA framework, it is possible that a peer in a private network can be connected to a peer in the Internet by overcoming existing firewalls as shown in Fig. 1. In this figure, the most important entity is the router peer. A router peer is any peer which supports the peer endpoint protocol and routing messages between peer in the JXTA networks. The procedure to overcome the fire wall is as follows. In the Router Peer is stored the private address of Peer 1 by using the HTTP protocol pass the firewall from Peer 1. The Router Peer receives the data from Peer 2 and access the Private address of Peer 1 to transmit the data.

JXTA is an interesting alternative for developing P2P systems and group ware tools to support online teams of students in virtual campuses. In particular, it is appropriate for file sharing given that the protocols allow to develop either pure or mixed P2P networks. This last property is certainly important since pure P2P systems need not the presence of a server for managing the network.

JXTA-Overlay: JXTA-Overlay project is an effort to use JXTA technology for building an overlay on top of JXTA offering a set of basic primitives

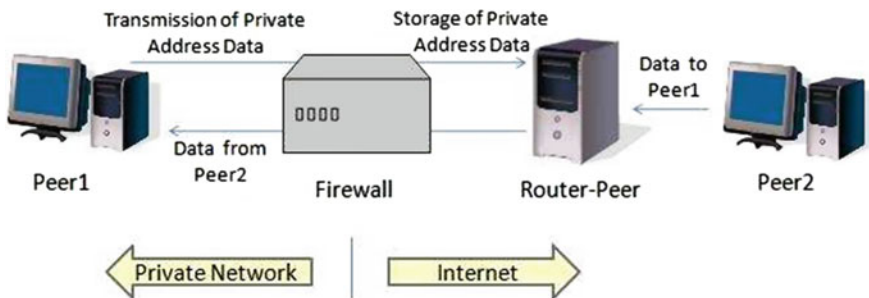
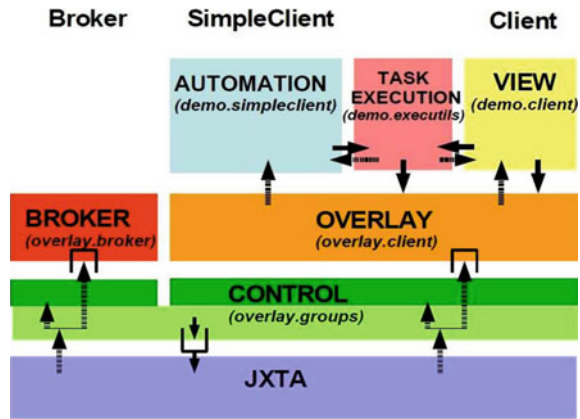


Fig. 1 P2P communication

Fig. 2 Internal architecture of JXTA-overlay



(functionalities) that are most commonly needed in JXTA-based applications. The proposed overlay comprises the following primitives: peer discovery, peer’s resources discovery, resource allocation, task submission and execution, file/data sharing, discovery and transmission, instant communication, peer group functionalities, monitoring of peers, groups and tasks.

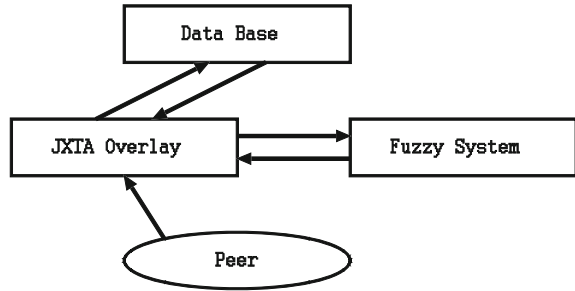
This set of basic functionalities is intended to be as complete as possible to satisfy the needs of JXTA-based applications. The overlay is built on top of JXTA layer and provides a set of primitives that can be used by other applications, which on their hand, will be built on top of the overlay, with complete independence. The JXTA-Overlay project has been developed using the ver-2.3 JXTA libraries. In fact, the project offers several improvements of the original JXTA protocols/ services in order to increase the reliability of JXTA-based distributed applications [16, 17] and to support group management and file sharing.

Except Broker and Client peers, the JXTA-Overlay has also Simple Client peers as shown in Fig. 2. The control layer interacts with the JXTA layer, and is divided into two parts: a lower part with functionality common to any kind of peer, and a higher part with functionality specific to Brokers and Clients.

4 Proposed Fuzzy-Based Trustworthiness System

We show our proposed system in Fig. 3. To complete a certain task in JXTA-Overlay network, we must select the most reliable peer. For peer reliability, we took in consideration three parameters: ABC, R and PD. Every time a peer joins JXTA-Overlay, these parameters are fuzzified using fuzzy system, and based on the decision of fuzzy system a reliable peer is selected. After peer selection, the data for this peer are saved in the database.

Fig. 3 Proposed trustworthiness system



The membership functions for our system are shown in Fig. 4. In Table 1, we show the Fuzzy Rule Base (FRB) of our proposed system, which consists of 36 rules.

The input parameters for peer-reliability assessment are: ABC, R and PD, while the output linguistic parameter is Peer Reliability (PR). The term sets of ABC, R and PD are defined respectively as:

$$\begin{aligned} \mu(ABC) &= \{\text{Bad, Partially Good, Good}\} \\ &= \{B, Pg, G\}. \\ \mu(R) &= \{\text{Bad, Minimally good, Partially good, Good}\} \\ &= \{Ba, Mg, P, Go\}. \\ \mu(PD) &= \{\text{Few, Many, Toomany}\} \\ &= \{F, Ma, Tm\}. \end{aligned}$$

and the term set for the output (PR) is defined as:

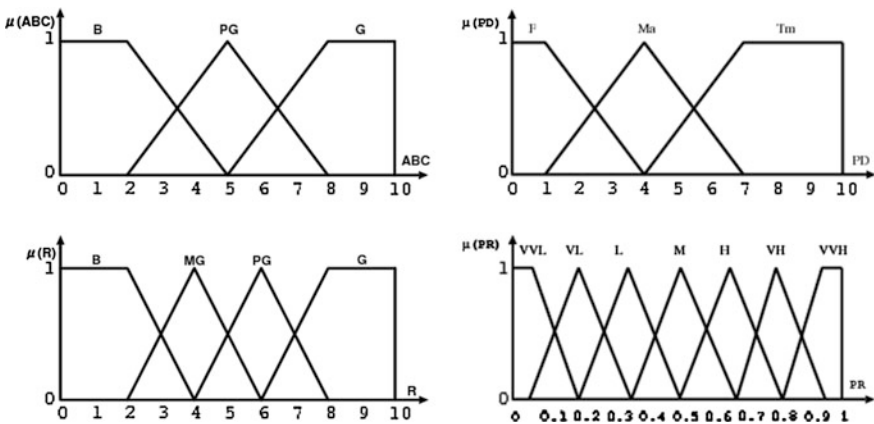


Fig. 4 Membership functions

Table 1 FRB

Rule	R	ABC	PD	PR
1	Ba	B	Tm	VVL
2	Ba	B	Ma	VVL
3	Ba	B	F	VVL
4	Ba	Pg	Tm	VVL
5	Ba	Pg	Ma	VL
6	Ba	Pg	F	L
7	Ba	G	Tm	VVL
8	Ba	G	Ma	L
9	Ba	G	F	M
10	Mg	B	Tm	VVL
11	Mg	B	Ma	VVL
12	Mg	B	F	VVL
13	Mg	Pg	Tm	VVL
14	Mg	Pg	Ma	L
15	Mg	Pg	F	M
16	Mg	G	Tm	VVL
17	Mg	G	Ma	M
18	Mg	G	F	H
19	P	B	Tm	VVL
20	P	B	Ma	VVL
21	P	B	F	VVL
22	P	Pg	Tm	VVL
23	P	Pg	Ma	M
24	P	Pg	F	H
25	P	G	Tm	VVL
26	P	G	Ma	H
27	P	G	F	VH
28	Go	B	Tm	VVL
29	Go	B	Ma	VVL
30	Go	B	F	VVL
31	Go	Pg	Tm	VVL
32	Go	Pg	Ma	H
33	Go	Pg	F	VH
34	Go	G	Tm	VVL
35	Go	G	Ma	VH
36	Go	G	F	VVH

$$\begin{aligned} \mu(\text{PR}) &= \{\text{Very Very Low, Very Low, Low, Middle, High,} \\ &\quad \text{Very High, Very Very High}\} \\ &= \{\text{VVL, VL, L, M, H, VH, VVH}\}. \end{aligned}$$

Fig. 5 Peer reliability for PD = 0

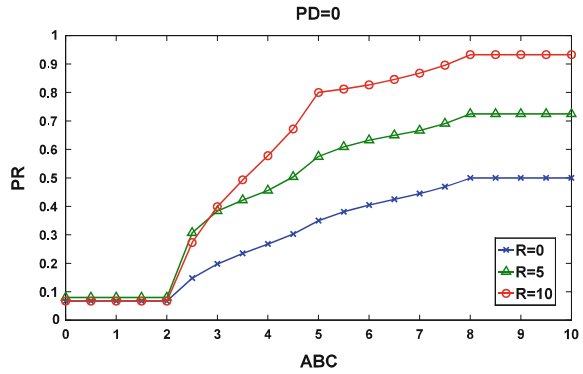
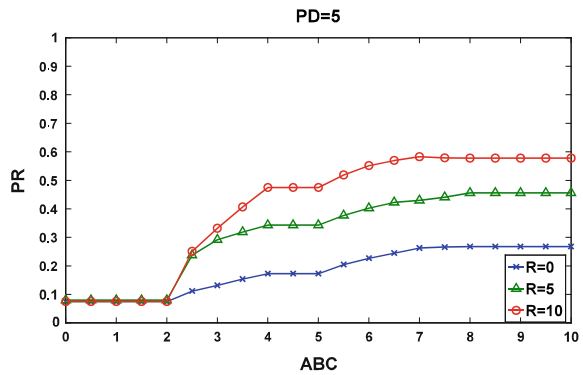


Fig. 6 Peer reliability for PD = 5

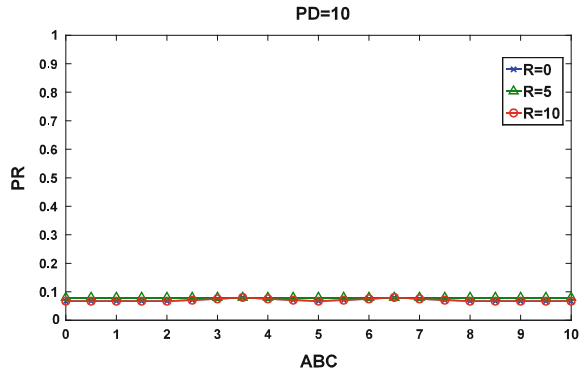


5 Simulation Results

In this section, we present the simulation results for the proposed system. The simulations are carried out using MATLAB. In Figs. 5, 6, 7 we show the performance of the system for three different values of PD: 0, 5, and 10, respectively. For each case, we keep the PD value constant and change the values of ABC and R and show the relation between PR with R, ABC and PD. In Fig. 5, are shown the simulation results for PD = 0. In this case, in the network there are only few peer disconnection and with the increasing of ABC and R, PR is increased. In Fig. 6, there are many peer disconnections. With the increasing of ABC and R, the performance in improved, but is decreased compared with the results for PD = 0 (see Fig. 5).

The results for PD = 10 are shown in Fig. 7. In this scenario there are too many peer disconnections and although the reputation and the ABC are improved, the peer reliability remains very low.

Fig. 7 Peer reliability for PD = 10



6 Conclusions and Future Work

In this paper, we proposed a fuzzy-based trustworthiness system for P2P Communications in JXTA-Overlay. This system decides the peer reliability considering three parameters: ABC, R and PD. We evaluate the proposed system by computer simulations.

The simulation results have shown that when there are too many peer disconnections, although the reputation and the ABC are improved, the peer reliability remains very low. For few peer disconnections, peer reliability is increased with the increasing of ABC, R and PD. The proposed system have a good behavior and can select reliable peers to download the information.

In the future work, we would like to make extensive simulations to evaluate the proposed system.

Acknowledgments This work is supported by a Grant-in-Aid for scientific research of Japan Society for the Promotion of Science (JSPS). The authors would like to thank JSPS for the financial support.

References

1. Xhafa F, Fernandez R, Daradoumis T, Barolli L, Caballe S (2007) Improvement of JXTA protocols for supporting reliable distributed applications in P2P systems. In: Proceedings of the NBS-2007 (Regensburg, Germany), LNCS 4658, Sep 2007, pp 345–354
2. Barolli L, Xhafa F, Durrresi A, De Marco G (2006) M3PS: A JXTA-based Multi-platform P2P System and Its Web Application Tools. *Int J Web Inform Syst* 2(3/4):187–196
3. Watanabe K, Nakajima Y, Enokido T, Takizawa M (2007) Ranking factors in peer-to-peer overlay networks. *ACM Trans Autonomouous and Adapt Syst (TAAS)* 2(3):1–26
4. Aikebaier A, Enokido T, Takizawa M (2010) Reliable message broadcast schemes in distributed agreement protocols. In: Proceedings of the BWCCA-2010, Fukuoka, Japan, Nov 2010, pp 242–249

5. Umezaki K, Spaho E, Ogata Y, Ando H, Barolli L, Xhafa F (2011) A fuzzy-based reliability system for JXTA-overlay P2P platform. In: Proceedings of the IMIS-2011, June–July 2011, pp 805–810
6. Umezaki K, Spaho E, Ogata Y, Barolli L, Xhafa F, Iwashige J (2011) A fuzzy-based trustworthiness system for JXTA-overlay P2P platform. In: Proceedings of the INCoS-2012, Nov–Dec 2011, pp 484–489
7. Umezaki K, Spaho E, Ogata Y, Barolli L, Xhafa F, Iwashige J (2012) A fuzzy-based trustworthiness system for JXTA-overlay P2P platform and its performance evaluation considering three parameters. In: Proceedings of the WAINA-2012, March 2012, pp 944–949
8. Kandel A (1992) Fuzzy expert systems. CRC Press, Boca Raton
9. Zimmermann HJ (1991) Fuzzy set theory and its applications, Second Revised Edition. Kluwer Academic Publishers, Boston
10. McNeill FM, Thro E (1994) Fuzzy logic: A practical approach. Academic Press, Inc., Boston
11. Zadeh LA, Kacprzyk J (1992) Fuzzy logic for the management of uncertainty. John Wiley and Sons, Inc., New York
12. Procyk TJ, Mamdani EH (1979) A linguistic self-organizing process controller. *Automatica* 15(1):15–30
13. Klir GJ, Folger TA (1988) Fuzzy sets, uncertainty, and information. Prentice Hall, Englewood Cliffs
14. Munakata T, Jani Y (1994) Fuzzy systems: an overview. *Commun ACM* 37(3):69–76
15. Brookshier D, Govoni D, Krishnan N, Soto JC (2002) JXTA: Java P2P programming. Sams Publishing, Indianapolis, 2002
16. IBM Corporation (2007) Making P2P interoperable: creating JXTA systems design P2P systems that extend beyond traditional network boundaries
17. Sun Microsystems (2007) JXTA java standard edition V2.5: programmers guide. June 2007

Applying Cluster Techniques of Data Mining to Analysis the Game-Based Digital Learning Work

Shu-Ling Shieh, Shu-Fen Chiou, Gwo-Haur Hwang
and Ying-Chi Yeh

Abstract Clustering is the most important task in unsupervised learning and applications is a major issue in cluster analysis. Digital learning, which arises in recent years, has become a trend of learning method in the future. The environment of digital learning may enable the learners work anytime and everywhere without the limitation of time and space. Another great improvement of digital learning is the ability of recording complete portfolio. These portfolios may be used to gain critical factors of learning if they are analyzed by data mining methods. Therefore, in this research will to analyze the records of students' portfolios of game-based homework by using Clustering Algorithm Based on Histogram Threshold (HTCA) method of data mining. The HTCA method combines a hierarchical clustering method and Otsu's method. The result indicates that the attributes or categories of impacting factors and to find conclusions of efficiency for the learning process.

Keywords Data mining · Clustering method · Game-based digital learning

S.-L. Shieh (✉) · G.-H. Hwang
Department of Information Networking and System Administration,
Ling Tung University, Taichung, Taiwan
e-mail: ltcc63@teamail.ltu.edu.tw

G.-H. Hwang
e-mail: ghhwang@mail.ltu.edu.tw

S.-F. Chiou
Department of Computer Science and Engineering, National Chung-Hsing University,
Taichung, Taiwan
e-mail: s9356055@cs.nchu.edu.tw

Y.-C. Yeh
The Graduate Institute of Applied Information Technology, Ling Tung University,
Taichung, Taiwan
e-mail: csgood30531@gmail.com

1 Introduction

Data mining technologies are usually used for anthropology, social science, biology and the others. The main mission of data mining is to excavate some unknown interesting information and behavior from these huge amount data. The e-learning becomes a new trend of learning in the near future [1]. By the aids of highly developing of information technology and tightly coupling of computer networks, e-learning improves the motivation and ability of the learners efficiently. Because e-learning uses the digital tutoring environment, the learning process of the students is also recorded in the same time. Therefore, these recorded learning data may be analyzed to know the learning efficiency of the learners [2]. Chang and Chen [3] have proposed that participants from Taiwan experienced increased in both content learning and engagement when using video game-based learning as resisted to text-based computer aided instruction. Huang [4] also applied some statistic methods to make comparison in a computer programming course by traditional learning and game-based digital learning. However, the analyzing report did not show the evidence of usage of the data generated by the learning process but only use the questionnaire of pre-test and post-test. There may be some losing to detect the learning process. Hence, the mission of this study will apply the Clustering Algorithm Based on Histogram Threshold (HTCA) [5] clustering method to analyze the data generated by traditional learning and game-based digital learning respectively. Then the goal of this study will to find the most influential attributes and to realize the effort of learning.

2 Related Work

2.1 *The Application of Data Mining in E-learning*

The main goal of data mining is to find useful knowledge or unknown valuable implicit information from a numerous collection of data. It may be used to make decisions or to forecast [6]. The application of data mining in education mainly locates in digital learning, since learners behaviors and portfolio of learning processes may be honestly and objectively recorded in the database. Researchers may easily apply data mining methods to achieve information about the learners [7]. Liu [8] applies Bayesian network software to assist teachers in efficiently deriving and utilizing the student model of activity performance from Web portfolios online. Liang et al. [2] analyzed all previous answering records of testers to find the association rules of inadequateness in course conceptions. In addition to providing the bases of off-school compensation lessons, the result of data mining may be used for the tutors as improvement and adjustment in the matters of teaching.

2.2 Hierarchical Thresholding Clustering Algorithm

The clustering technology is often used to discover the patterns and beneficial relations or hidden information in a data set [9–16]. A strategy called Hierarchical Thresholding Clustering Algorithm (HTCA) [5] is a dividing hierarchical clustering algorithm. HTCA consists of two steps: the first part is a dividing method. In this part the process will transfer the points in the data set into a finite number set of integers and then automatically find a threshold using Otsu's method. This step will separate the original data set into two sets. Then second part of HTCA is in a hierarchical structure. It will repeat the separating processes on the subsets until the number of subsets equals a default cluster number.

In the dividing process, to find a optimal separating point is the key operation. We suggest using the Otsu's method to find the separating point. First of all, choose an arbitrary separating point l , then collect those entries whose values are less than l as cluster C_1 , and the rest entries of the original data set as cluster C_2 . Calculate the probability p of values occur for every entry. Then suppose the distributing probabilities are ω , and compute the mean μ of cluster C_1 and C_2 . After all, we find the inter-clustering variance σ_b .

Test the separating point l from value 1 to r respectively, and write down the inter-cluster variances and intra-cluster variances. Find the point l^* which generates the largest inter-cluster variance.

Applying this dividing method continuously to every attributes of the data set, we find each optimal separating point l^* for each attribute respectively. Then we use these values to find the optimal separating vector L . Assume that the two central points of two clusters are m_1 and m_2 . By the means of nearest adjacent method, every entry point of the space will be assigned to the nearest cluster. This may accomplish a single separating process. Then repeat a hierarchical tree-constructing algorithm until the required k clusters has been generated.

$$\text{The optimal separating vector will be } L = \frac{(m_1 + m_2)}{2} \quad (1)$$

3 Applying HTCA Cluster Techniques to Analysis the Game-Based Digital Learning Work

3.1 The Data Set Used in Our Experiments

The system development tools include Adobe FLASH for the front-end interface design, PHP for Web page interconnection and MySql for the database management system. This game-based learning system provides to students with relative functions including chapter selection, learning profile, and individual score inquiry. The data set of this paper is a collection of quiz and assignment scores

obtained from a technical university in central Taiwan. These quizzes and assignments are designed both in traditional and game-based type. Students who take this course are arranged into 4 groups by the criteria of scores, H for high and L for low. Students who got both H scores are in group 1. Students who got H scores in game-based assignments and L scores in traditional assignments are in group 2. Students who got both L scores are in group 3. And students who got L scores in game-based assignments and H scores in traditional assignments are in group 4. The course in the experiment is a programming learning course based on both game-based homework and traditional homework. The data set contains 52 data points with 3 columns each in our experiments.

3.2 Research Flowchart

This paper uses HTCA clustering algorithm to classify if there is implicit information in data attributes from the portfolio of learning. First of all, we filter out the improper or inadequate data and save the data in the format we need. Then we use HTCA clustering algorithm to find groups among the attributes.

The algorithm of HTCA: (Fig. 1)

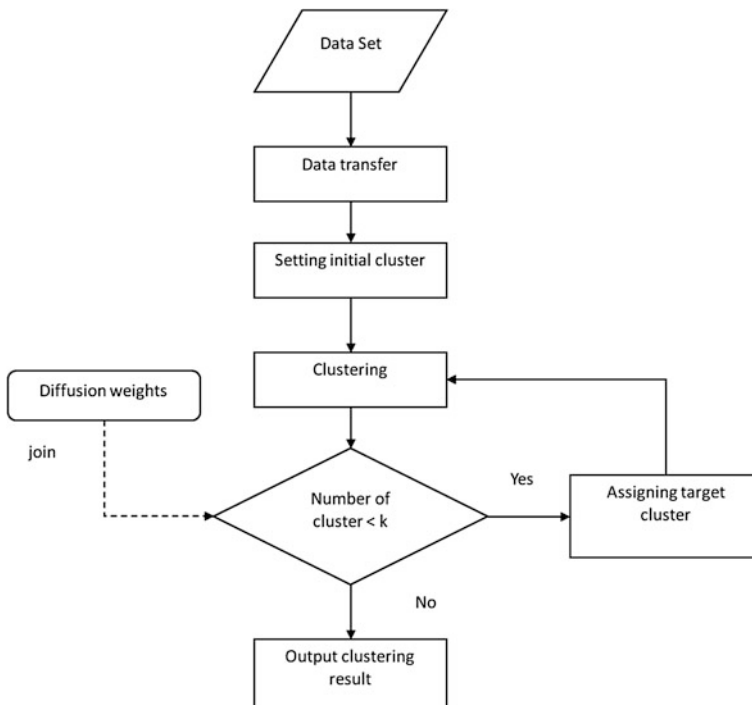


Fig. 1 The flowchart of the HTCA clustering algorithm

Table 1 Description of fields

Class	Identity
Score of traditional homework	A ₁ ,A ₂ ,A ₃ ,A ₄
Score of game-based homework	B ₁ ,B ₂ ,B ₃ ,B ₄
Score of midterm exam.	D ₁ ,D ₂ ,D ₃ ,D ₄

3.3 Experimental Procedure

(1) Collecting data

The data of this experiment is collected from a class of night division of a technical university in central Taiwan. When the tutor finished a chapter, there would be a homework left for the students to do further discussion and analyzing. The homework is given in two formats: game-based one and traditional one. The process of doing homework will be recorded in database.

(2) Transferring data

To find the key points that may influence the clustering results; we choose the game-based homework and traditional homework from five chapters. We build an effective data set by filtering out improper data and transferring the data into a required format.

The score given in a traditional homework is from 0 to 100. We conclude the score level into 4 parts: A₁ for 76–100, A₂ for 51–75, A₃ for 26–50 and A₄ for 0–25. The same scoring levels, B₁, B₂, B₃ and B₄ are also applied in homework that is in game-based format respectively in a range of 25. The score of midterm exams added with the operating achievement, which is from 0 to 140, is separated into four parts in a range of 35: D₁ for 106–140, D₂ for 71–105, A₃ for 36–70 and A₄ for 0–35 as shown in Table 1. Then save the transferred data into the experimental database.

3. Clustering using HTCA clustering algorithm

We apply the HTCA algorithm into the data set and find cluster for each data entry. First of all, data entries are mapped into finite sets of integers. Then use the Ostu’s method to search a threshold automatically, Repeat the dividing process continuously until the number of subsets equals a pre-defined amount.

4 Experimental Results

In this research, we use HTCA clustering algorithm to group the dataset into a pre-defined number of groups. The mining result is as follows.

The environment of experiment uses MATLAB R2010a as the platform of computation. HTCA clustering algorithm is implemented to be MATLAB programs that may be executed in the Windows 7 × 64 Home Advanced Service Pack 1. The CPU of computer is Intel(R) Core(TM) i7-2600 CPU @ 3.40 GHz, equipment is with 8.00 GB.

Table 2 Experiment gains in accurate

	Mean error rate	Mean run time
HTCA	0.27	0.21

The sampling data is collected from a part-timed studying program of a technical university in the central Taiwan. The number of data points is 52. The result of experiment shows that the accurate rate of clustering is 73 % using the HTCA clustering algorithm. Total executing will spend less than 1 s, as shown in Table 2. HTCA clustering algorithm do a practically fine job in accurate.

5 Conclusion

In this paper, we develop a methodology for applications of data clustering to find groups using HTCA clustering algorithm based on the data from the results of quizzes taken after both traditional exercises and game-based exercises. The clustered groups are used to realize the achievement of students in this class. The result of this experiment shows that the clustering accuracy is 73 % by applying the HTCA clustering algorithm. And the execution time is less than 1 s. In this paper will try to analyze the records of students' portfolios of game-based homework by using Clustering Algorithm Based on Histogram Threshold (HTCA) method of data mining. The result indicates that the attributes or categories of impacting factors and to find conclusions of efficiency for the learning process.

Acknowledgments This study is sponsored by the Science Council of Taiwan under the contract no. NSC 101-2221-E-275-006 and NSC99-2511-S-275-001-MY3.

References

1. Fayyad UM (1996) *Advances in knowledge discovery and data mining*. AAAI Press
2. Liang SC, Lin CC, Liou CH (2007) The study of an interactive mathematics teaching platform. In: *Proceedings of the 18th annual conference international information management association*
3. Chang T, Chen W (2009) Effects of computer-based video games on children: an experimental study. *Educ Technol Soc* 12(2):1–10
4. Hwang GH, Lee CY, Tseng WF (2012) Development and evaluation of an educational computer game for a certification examination. *J Educ Technol Develop Exch* 5(2):27–40
5. Shieh SL, Lin TC, Szu YC (2012) An efficient clustering algorithm based on histogram threshold, intelligent information and database systems. pp 32–39
6. Han J, Kamber M (2001) *Data mining: concepts and techniques*, Morgan Kaufmann, San Francisco
7. Chen YJ (2007) Data mining from a learning portfolio- a case of boolean logics inquiry course unit
8. Liu CC, Chen GD, Wang CY, Lu CF (2002) Student performance assessment using bayesian network and web portfolios. *J Educ Comput Res* 27(4):437–469

9. Agrawal R, Srikant R (1994) Fast algorithms for mining association rules. IBM Research Report RJ9839, IBM Almaden Research Center
10. Han J, Kamber M (2000) Data mining: concepts and techniques, Morgan Kaufmann, San Francisco
11. Hirschman L, Park JC, Tsujii J, Wong L, Wu CH (2002) Accomplishments and challenges in literature data mining for biology. *Bioinformatics* 18:1553–1561
12. Shieh SL, Liao IE, Hwang KF, Chen HY (2009) An efficient initialization scheme for SOM algorithm based on reference point and filter. *IEICE Trans Inform Syst*, E92-D(3):422–432
13. Shieh SL, Liao IE (2009) A new clustering validity index for cluster analysis based on a two-level SOM. *IEICE Trans Inform Syst* E92-D(9):1668–1674
14. Shieh SL, Liao IE (2012) A new approach for data clustering and visualization using self-organizing maps. *Expert Syst Appl* 39(15):11924–11933
15. Maulik U, Bandyopadhyay S (2002) Performance evaluation of some clustering algorithms and validity indices. *IEEE Trans Pattern Anal Mach Intell* 24(12):1650–1654
16. Perex HB, Nocetti FG (2007) Fault classification based upon self organizing feature maps and dynamic principal component analysis for inertial sensor drift. *Inter J Innovative Comput, Inform Control* 3(2):257–276

Design and Implementation of Social Networking System for Small Grouped Campus Networks

Jung Young Kim and Seung-Ho Lim

Abstract Recent rapid evolution of networking technologies and computing service technologies has lead a wide variety of Social Networking Services (SNS). In campus education environment, there are several specific social networking services for campus community members, which include teaching, class schedule, club activities, and practical use of campus buildings. In this paper, we have designed and implemented dedicated social network service systems for small grouped campus networks. The designed SNS systems, called *CamBook*, supports easy campus-based SNS services. It supports class management, club management, and augmented reality-based navigation services. With the services, campus members can use their campus lives efficiently.

Keywords Social network service · Campus education · Cambook

1 Introduction

Recent rapid evolution of networking technologies and computing service technologies has lead a wide variety of Social Networking Services (SNS). A Social Networking Service is an online service, platform, or site that focuses on facilitating the building of social networks or social relations among people who, for example, share interests, activities, backgrounds, or real-life connections [1]. Since their introduction in late 1990s, social network sites such as Facebook, MySpace

J. Y. Kim (✉) · S.-H. Lim
Department of Digital Information Engineering, Hankuk University
of Foreign Studies, Yongin-si, Korea
e-mail: permandos@naver.com

S.-H. Lim
e-mail: slim@hufs.ac.kr

have attracted billions of online users to interact with others with their daily lives and practices [2].

While supporting the social networking services, the main interests of users are their many kinds of daily lives surrounding the life environment, with the expression of text or pictures. The main services of current widely used SNSs are focused on communicating and sharing their usual life and public opinion in online network manner [3]. The SNS users communicate and share their public opinion within the socially connected group and to make consensus. However, these widely used SNSs have limitation in the aspect of professionalism. The functions of SNSs should be specialized to specific dedicated region. There are many specific social services in many specific social groups including education, political, economic, and health related grouped social system. The SNSs systems should be specialized to these specific small social groups, with specific services respectively.

Among these many small social groups we are interested in SNSs for social education systems. In case of campus education system, although the campus education deals with education for students, campuses encompass diverse works not only for teaching, but also varied works such as club, sports, meetings for small grouped social networks within campus members, with the diverse populations of students, administrators, and faculty. In addition to that, the campus members usually walk up and down from outsider the campus to inside, or vice versa. In that situation, the connected networked services are useful for more seamless and efficient social works. Therefore, the very specialized and dedicated social networking service systems should be required for the campus education systems.

In this paper, we design and implement the pilot SNS system for small grouped campus education system. The designed SNS system includes distinct services for students and faculty. Specifically, it supports class scheduling, study grouping, tutoring, communicating, and sharing lecture materials for inside campus social networks called intra-campus services. For outsider social network services, called inter-campus services, it supports augmented reality services for geometric and building information around campus, transportation services connecting outsider region and inside region of campus, and regional information around campus such as shopping and restaurant. With the designed SNS system, the campus users can easily access and enjoy superior campus lives.

2 Related Work

Social Network Service is widely used to support interactions among people that are related with each other. In general, there is not specific purpose for using SNS services, and their community formed naturally. However, the social situation surrounding some specific environment should make specific services that doesn't exist in general SNS systems. In campus education environment, there are several specific services for SNS system to serve for community members of campus, such

as teaching, class schedule, club activities, and practical use of campus buildings. Therefore, SNS system should be re-organized for campus education system.

There are several previous works for SNS services of campus education. J. Berg et al. [3] investigates the required SNS technologies and services for campus based education, in which, they summarized the core campus activities and services ideas, however, these are mainly focused on class education systems. K. Sagayama et al. [5] designed and implemented Campus SNS application based on the population of campus members. They analyzed characteristics and efficacy of a Campus SNS with the designed Campus SNS services, in the aspect of daily member activities.

The previous work mainly focused on the education systems based on the education class and individual experience and efficiency. The designed Campus SNS services in this paper deals with not only campus education SNS services such as sharing of class information, but also in-campus life activity and tour-like activities with intersection of outer campus systems.

3 CamBook: Campus SNS System

The overall architecture designed and implemented Campus SNS service system, called CamBook in this paper, is described in Fig. 1. As shown in the figure, our system consists of server and client systems. The servers are used for maintaining all the information and servicing key services to users, and the clients are devices used by campus members, which may include from mobile device to desktop computer. The servers are implemented with dynamic scripting language with javascript and PHP, and the data is maintained with Mysql database system. The Linux is For clients, we have implemented android framework-based mobile application for one representative example.

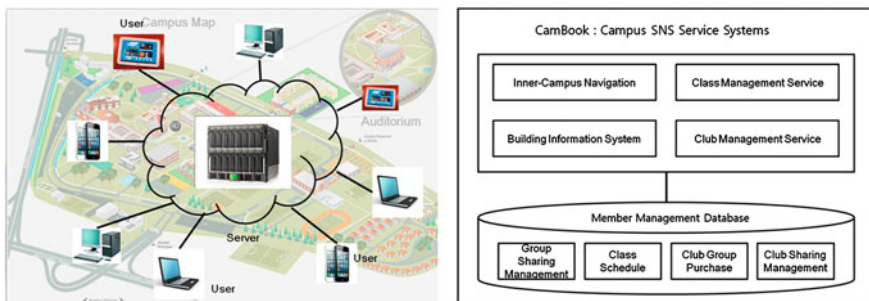


Fig. 1 Overall architecture and block diagram of CamBook SNS systems. It includes server managing all the Cambook service system and user database, and client users that have services of Cambook

3.1 Class and Club Management SNS Services

The designed SNS services for campus education system, CamBook, include intra-campus services and inter-campus services. For intra-campus education services, it supports inside activities for campus members, such as class management, club activity, and inner campus navigation and building information services. A student campus member makes setup his class schedule with CamBook, in which he can share the schedule with colleagues and discuss about that freely through CamBook system. After setup the schedule, small group-based blog is established for each class, and it is prolong until end of the semester. The class members can easily share and discuss anything about the class information with this group-based blog. Club activity service is similar to class management service except that club activity service is continued without regard to semester period and joining and withdrawal are possible. Also, club activity service is dedicated to its specific objective of the club, so dedicated services is also considered for each specific club. In current Cambook, only music and sports related clubs are supported for specific service supports. For music clubs, Cambook supports audio streaming services and group purchase services for watching show such as concert. For sports clubs, Cambook supports alert services for sports schedule and group purchase services for watching sports games.

3.2 Inner-Campus Navigation and Building Information SNS Services

In addition to class and club management services, Cambook give inner campus navigation service and building information services, which is based on the augmented reality. The Cambook's campus navigation services are described in Fig. 2. The details of navigation services are as follows. When a campus member enters in the campus with his mobile device, he can see his position in the campus map with his screen of mobile device. In the campus map visualized in his screen, the building locations are appeared, as shown in the first picture in Fig. 2. If a member would like to get building information, he can get the information by just staring the building with his mobile device. When he stares building with his device, the building information is depicted in this camera view of screen as overlay method, as shown in the second picture of Fig. 2, which is called augmented reality technology. In addition to the building information, he also can get his class information from the building information such as when the class is started in that building, if it is. The class information is based on the class management services of Cambook. Therefore, he can get class information as well as navigation information at the same time easily with Cambook's services.

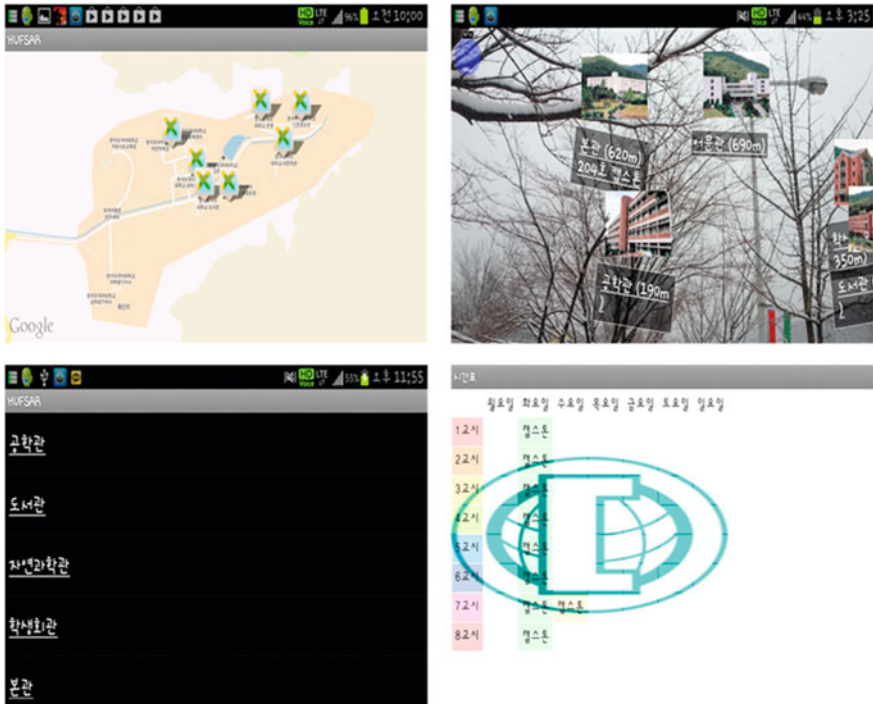


Fig. 2 Inner-campus navigation and building information service within Cambook. A campus member use this service with his class management and club management service to get in-time and in-place information

3.3 Inter-Campus SNS Services

In addition to the inner-campus SNS services, Cambook also gives a few services that would be used at outer the campus, or intersection between inner campus and outer campus; that is campus transportations and restaurant recommendation services near the campus. Many campus members come to campus with the synchronization of class schedule or meeting of other campus members, which is differ for every members and every semesters. The campus schedule is likely to be repeated with a weekly period, so Cambook supports weekly-based in-time transportation alert services, specifically, It give information about when and which transportation is suitable to the users that use inter-campus services.

The restaurant recommendation service is similar to other augmented reality-based restaurant recommendation service. Cambook gives restaurant information with GPS information and augmented reality view of user's screen and recommends best-effort restaurant for users.

4 Implementation and Analysis

The Cambook is mobile SNS applications running on mobile devices such as smartphone. Although it is based on mobile web application, the targeted system is android based mobile systems, since we use open android development systems and several open source code for SNS services including message passing and augmented reality. To use android internal API framework with mobile web app, hybrid web application is implanted with phonegap development environment. In addition, the server is also implemented for servicing server-side contents such as class group management, AR building information, class schedule, and message interfacing between users. The scalability of server is limited to under hundred users for each Cambook group, so if several Cambook group is added, another server systems should be added with the replication of server-side contents. The mobile applications running on android mobile device are connected to server system to interact and get service from server.

We have tested Cambook with the sample class within the department of university. For sample classes, about fifty class members are grouped for one Cambook SNS systems, and make SNS services that are supported by Cambook.

5 Conclusion

In campus education environment, there are several specific social networking services for campus community members, which include teaching, class schedule, club activities, and practical use of campus buildings. In this paper, we have designed and implemented dedicated social network service systems for small grouped campus networks. The designed SNS systems, called CamBook, supports easy campus-based SNS services. The server of Cambook is composed of class management, club management, and inner-campus augmented reality-based navigation and building information system. The cambook also supports inter-campus transportation service and restaurant commendation services. With the services, campus members can use their campus lives efficiently.

Acknowledgments This work was supported by Hankuk University of Foreign Studies Research Fund of 2013.

References

1. Social Network Service. http://en.wikipedia.org/wiki/Social_networking_service
2. Boyd DM, Ellison NB (2007) Social network sites: definition, history, and scholarship. *J Comput-Mediated Commun* 13(1):210–230
3. Berg J, Berquam L, Christoph K (2007) Social network technology: a “poke” for campus services, *Ecucause Rev* 42(2):32–44

4. Kanenishi K, Matsuura K, Sagayama K, Miyoshi Y, Minato J, Takagi T, Yano Y (2007) Progress of the federation for campus SNS using Shibboleth, In: ICCE2007 Supplementary Proceedings, vol 2. 309–311
5. Sagayama K, Kanenishi K, Matsuura K, Kume K, Miyoshi Y, Matsumoto J, Yano Y (2008) Application of campus SNS for supporting students and their behavior, Japan J Educ Technol 32:53–56
6. Okamoto T, Anma ZF (2010) The framework for e-learning 2.0 and its primary functions. In: Proceedings of the 13th IASTED international conference on computers and advanced technology in education, Aug. 23–25

Effective Searchable Symmetric Encryption System Using Conjunctive Keyword

Sun-Ho Lee and Im-Yeong Lee

Abstract Removable Storage provides excellent portability with lightweight and small size to fit into one's hand. Many users have turned their attention to high-capacity products. However, Removable Storage devices are frequently lost and stolen due to their easy portability. Many problems, such as the leaking of private information to the public, have occurred. The advent of remote storage services, where data is stored throughout the network, has allowed an increasing number of users to access data. The main data of many users is stored together on remote storage, but this has the problem of disclosure by an unethical administrator or attacker. Data encryption on the server is necessary to solve this problem. A searchable encryption system is needed for efficient retrieval of encrypted data. However, existing searchable encryption systems have low efficiency for data insert/delete operations and multi-keyword search. This paper proposes an efficient searchable encryption system.

Keywords Searchable symmetric encryption · Conjunctive keyword · Bloom filter

1 Introduction

Portable storage devices (e.g., USB memory, extended hard disk drive) are used to carry data. The disadvantage of such portable storage devices is the high risk that they will be lost or stolen; without the storage device, the data cannot be accessed.

S.-H. Lee · I.-Y. Lee (✉)

Department of Computer Software Engineering, Soonchunhyang University,
Chungcheongnam-do, Asan 336-745, Korea
e-mail: imylee@sch.ac.kr

S.-H. Lee

e-mail: sunho431@sch.ac.kr

Therefore, users demand a means to store and access their data via a secure network, where there is low risk that the storage will be compromised. The use of remote storage services, such as web hard drives, and cloud storage is surging. However, personal information and main data stored in remote storage can potentially be exposed. Therefore, a user needs to store encrypted data to reduce the issue of untrusted servers for data storage. In addition, there is an increasing need for a more secure searchable encryption system. In this paper, we proposed an efficient searchable encryption system.

2 Related Work

The Searchable Symmetric Encryption (SSE) [4] scheme by Curtmola et al. offers the most rapid service of existing symmetric searchable encryption systems. This scheme is implemented for data via a linked list with each keyword. However, this results in inefficient use of storage space, because each node contains the data addresses, and the next node's key and address. In addition, when adding data, a node first needs to perform decryption and change the link. This is a complex process. When deleting data, a complex process needs to be followed, where each keyword for the data is found and the node is deleted. This increases the load on the server. This scheme has inefficiencies in multi-keyword search. If users want to search data by multiple keywords, the server must repeat the search for each keyword [1–4].

3 Requirement

The searchable encryption system has the following requirements.

- **Confidentiality:** Only an authenticated entity can verify the communication data between the client and the remote storage server.
- **Efficient operation:** Data containing the keywords for search should be provided quickly.
- **Efficient usage of server storage space:** The capacity of the index to search for data should be limited.
- **Efficient traffic:** The network traffic between the client and server should be reduced.
- **Efficient data insert/delete operations:** An environment supporting frequent insertion/deletion of large amount of data provides efficient operations on the server.
- **Efficient data search:** If the search is not a single keyword search, efficient and flexible multiple keyword search should be provided.

4 Proposed Scheme

This paper suggests a scheme for efficient data insert/delete operations and conjunctive keyword search.

4.1 System Parameter

The system parameters in the proposed method are as follows.

k	Encryption key
m	Count of data
n	Number of whole keywords
j	Number of keywords per data ($j \leq n$)
q	Count of data, having specific keyword ($q \leq n$)
c	Number of one-way hash functions for bloom-filter
l	Length of bloom-filter bit stream ($l < n$)
d_i	i th data
w_i	i th keyword
$w_{i,j}$	j th keyword of i th data
W	Set of keywords
BF_*	Bloom-filter of *
$E_{*[]}[]$	Encryption by *
$D_{*[]}[]$	Decryption by *
$F_{*[]}[]$	Pseudo-random function by *
$P[]$	Pseudo-random permutation
$H[]$	Secure one-way hash function
DT_i	i th data table
T_*	Trapdoor for data with keyword *

4.2 Build Index

The system parameters in the proposed method are as follows. The indexes represent a keyword for encrypted data. Indexes are created as follows (refer Fig. 1).

Step 1. each m data that want to generate an index are encrypted by key k

$$E_k[d_1], E_k[d_2], \dots, E_k[d_m]$$

Step 2. key $k_1 - k_c$ that for a pseudo-random function are generated by pseudo-random permutation.

$$k_1 - k_c = P[k]$$

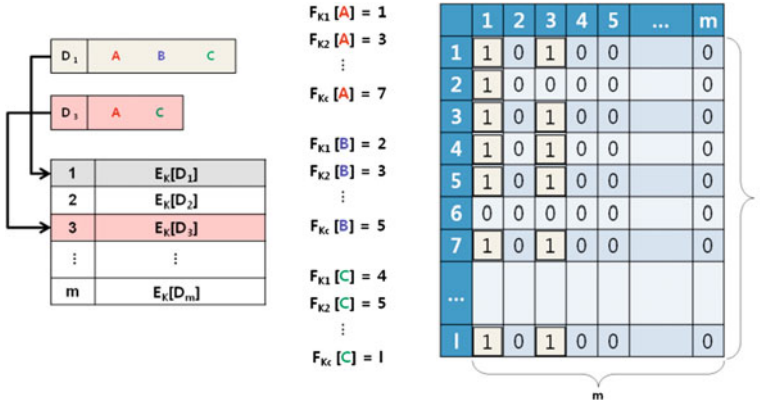


Fig. 1 Build index phase

Step 3. BF_{di} the representation for n keywords of d_i that are generated by pseudo-random function. BF_{di} are generated as follow and BF_{di} are represented by a 1-bit stream.

$$BF_{di} = [F_{k1}[w_{i,1}] || F_{k2}[w_{i,1}] || \dots || F_{kc}[w_{i,1}] || \dots || F_{kc}[w_{i,n}]]$$

Step 4. $BF_{d1} - BF_{dl}$ are generated for m data by repeating Step 3.

4.3 Generate Trapdoor

The indexes represent a keyword for encrypted data. Indexes are created as follows. The trap door to search for the data is generated by k, W from users (refer Fig. 2).

Step 1. key $k_1 - k_c$ that for the pseudo-random function are generated by pseudo-random permutation.

$$k_1 - k_c = P[k]$$

Step 2. The server searches for each keyword's index table using the trapdoor T_W .

$$T_W = T_{w1} \vee T_{w2} \vee \dots \vee T_{wj}$$

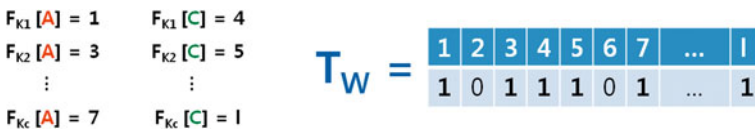


Fig. 2 Generate trapdoor phase

$$T_{wi} = [F_{k1}[w_i] || F_{k2}[w_i] || \dots || F_{kc}[w_i]]$$

4.4 Data Search

The server searches the data that have keyword set W by trapdoor T_W from the user (refer Fig. 3).

Step 1. Server gets BF_{di} ($i = 1-m$), representation of the data’s keyword information. Then, it performs the following operations, to determine if the data matches the keywords.

$$T_W = ? BF_{di} \oplus T_W(i = 1 - m)$$

Step 2. The server sends the matched data d_1-d_q to the user. The user can decrypt the encrypted data by its own key k .

5 Analysis of the Proposed Method

The proposed scheme satisfies the following requirements.

- **Confidentiality:** The proposed method encrypts the data and indexes. Therefore, it is difficult for an attacker to infer the communication content.
- **Efficient operation:** Data can be found via a single XOR and compare operation for the corresponding keywords.
- **Efficient usage of server storage space:** The proposed method use m bits per keyword.

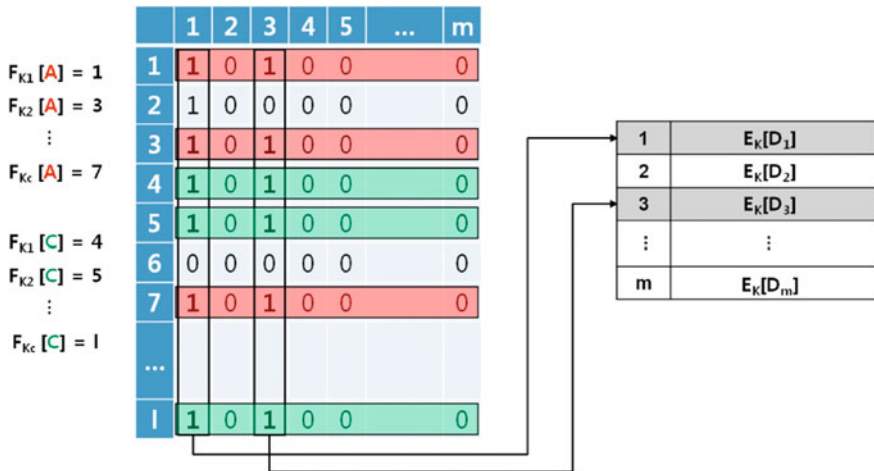


Fig. 3 Data search phase

Table 1 Analysis of calculation efficiency

	Song et al. [2]	Goh [3]	Curtmola et al. [1]	Proposed scheme
Calculation volume for compare	$J*m$	c	1	1
Size of index	$m*j*keyword$ <i>size</i>	l	$n*q*node$ <i>size</i>	$m*l$
Number of encryption for document insertion	2	0	3	0
Number of encryption for document deletion	$2e$	0	$2 \sim q + 1$	0
Communication round for search	n	n	n	1

- **Efficient traffic:** The proposed method will retrieve the data in one round of communication between the client and server.
- **Efficient data insert/delete operations:** The proposed method is efficient; it simply erases the data's bloom-filter bit stream on the index table, without encryption/decryption.
- **Efficient data search:** The proposed method provides multiple keyword searches in one round of communication (Table 1).

6 Conclusion

A searchable encryption system is required. The proposed scheme provides efficiency of storage and operation using bloom-filter. This scheme not requires an additional search operation for a multi-keyword search. Safety and security must be guaranteed to enhance the popularization of remote storage services. Therefore, studies of a searchable encryption system should be continued for remote storage environments.

References

1. Song D, Wagner D, Perrig A (2000) Practical techniques for searching on encrypted data. In: Proceedings of IEEE symposium on security and privacy, pp 44–55
2. Goh EJ (2003) Secure indexes, Technical Report, 2003/216, IACR ePrint Cryptography Archive
3. Chang YC, Mitzenmacher M (2005) Privacy preserving keyword searches on remote encrypted data. In: Applied cryptography and network security conference-ACNS, LNCS, vol 3531, pp 442–255
4. Curtmola R, Garay J, Kamara S, Ostrovsky R (2006) Searchable symmetric encryption: improved definitions and efficient constructions. In: Proceedings of the 13th ACM conference on computer and communication security-ACM-CCS, pp 79–88

5. Hwang YH, Lee PJ (2007) Public key encryption with conjunctive keyword search and its extension to a multi-user system. In: International conference on pairing-based cryptography, Pairing'07
6. Yang Y, Bao F, Ding X, Deng RH (2009) Int J Appl Crypt 1(4)

Secure Method for Data Storage and Sharing During Data Outsourcing

Sun-Ho Lee, Sung jong Go and Im-Yeong Lee

Abstract Data outsourcing services have emerged with the increasing use of digital information. They can be used to store data via networks and various devices, which are easy to access. Unlike existing removable storage systems, storage outsourcing is available to many users because it has no storage limit and does not require a storage medium. However, the reliability of storage outsourcing has become an important topic because many users employ it to store large volumes of data. To protect against unethical administrators and attackers, a variety of cryptography systems are used, such as searchable encryption and proxy re-encryption. However, existing searchable encryption technology is inconvenient for use in the storage outsourcing environments where users upload their data, which are shared with others as necessary. The users also change frequently. In addition, some existing methods are vulnerable to collusion attacks and have computing cost inefficiencies. In this paper, we propose a secure and efficient method for data storage and sharing during data outsourcing.

Keywords Searchable encryption · Proxy re-encryption · Data outsourcing · Outsourcing storage · Cloud storage · Distributed file system · Anti collusion

S.-H. Lee · S. j. Go · I.-Y. Lee (✉)

Department of Computer Software Engineering, Soonchunhyang University,
Asan-si, Chungcheongnam-do, Korea
e-mail: imylee@sch.ac.kr

S.-H. Lee
e-mail: sunho431@sch.ac.kr

S. j. Go
e-mail: sjgo@sch.ac.kr

1 Introduction

Network development has accelerated data communication and data outsourcing services have been developed to store data in distant storage media, which can be retrieved by a user with various devices. Many companies are now providing competitive high-capacity storage services. Thus, an increasing number of people are using storage outsourcing services to store their data. However, the storage of sensitive data such as body state information or financial information increases the development of the “big brother problem” and the risk of data disclosure by attackers and unethical administrators.

One method for protecting user data is data encryption on the data outsourcing server. However, this approach can cause difficulties during data access. Users must download all of their own data and decryption needs to be applied to the entire dataset before the data can be searched. This can be viewed as a major disadvantage of data outsourcing. Therefore, searchable encryption systems have been developed that can encrypt data indexes to allow index searching without exposing the data to attackers and unethical administrators [1–11]. However, this method is difficult to apply in a cloud environment where there is frequent data sharing among users. To address this problem, a searchable re-encryption (or proxy re-encryption with keyword search) system has been developed that re-encrypts encrypted indexes and allows users to search during safe storage outsourcing/data sharing without the need for a decryption process [12, 13].

However, some existing systems do not consider users who share data with other users, or the storage outsourcing structure, which means that they handle the indexes and data encryption as a single process. In reality, the indexes and data are stored separately during storage outsourcing. The indexes are stored on the master server and the data are split into chunks, which are then distributed to many chunk servers. Therefore, searchable re-encryption systems are difficult to apply to a real outsourcing storage system. In addition, some existing methods are vulnerable to collusion attack. Some existing schemes allow only one-hop data sharing. In reality, there is no longer any control after the data have been shared. If data need to be shared, the user has no choice other than to accept multi-hop re-encryption. Most searchable re-encryption schemes require large volumes of computing resources for data storage and sharing. Thus, this study proposes a technical scheme that allows the safe and free sharing of outsourced stored data, which considers the architecture of the data outsourcing system.

2 Preliminaries

In this section, we provide the necessary preliminary details.

2.1 Bilinear Maps

The bilinear map was proposed originally as a tool for attacking elliptical curve encryption by reducing the problem of discrete algebra on an elliptical curve to the problem of discrete algebra in a finite field, thereby reducing its complexity. However, this method has been used recently as an encryption tool for information protection, instead of an attacking tool. Bilinear pairing is equivalent to a bilinear map. These terms are defined and the theory is described below.

Definition 1 Characteristics that satisfy an admissible bilinear map are as follows.

- **Bilinear:** Define a map $e = G \times G \rightarrow G_T$ as bilinear if $e(aP, bP) = e(P, Q)^{ab}$ where all $P, Q \in G$, and all $a, b \in \mathbb{Z}$.
- **Non-degenerate:** The map does not relate all pairs in $G \times G$ to the identity in G_T . Note that G and G_T are groups of prime order, which implies that if P is a generator of G , $e(P, P)$ is a generator of G_T .
- **Computable:** There is an efficient algorithm to compute $e(P, Q)$ for any $P, Q \in G$. The following definition was constructed based on the bilinear map $e(aP, bQ) = e(P, bQ)^a = e(aP, Q)^b = e(P, Q)^{ab} = e(abP, Q) = e(P, abQ)$. With this map, the D-H decision problem can be solved readily for ellipses using the following equation: $e(aP, bQ) = e(cP, P) \Rightarrow ab = c$. Therefore, the following is the basis for resolving the difficulties of the bilinear map, which is used as an encryption tool by many encryption protocols.

Definition 2 When the elements G, P, aP, bP, cP (BDHP, Bilinear Diffie–Hellman Problem) are given, this relates to the $e(P, P)^{abc}$ calculation problem. In this study, the admissible bilinear map was used as the basis for secret number production during the key construction process between heterogeneous devices. This problem can be solved if the ellipse curve discrete mathematics problem can be solved. For example, a can be calculated from aP , so $e(P, P)^{abc}$ can be calculated using $e(bP, cP)^a$.

2.2 Requirements

The following requirements should be met to ensure safe search and sharing in a storage outsourcing environment.

- **Confidentiality:** Data transmitted between the storage outsourcing server and the client terminal should be identifiable only by validated users.
- **Search speed:** A client who has limited system resources should be able to search documents quickly, including word files, when they are stored in storage outsourcing systems.
- **Traffic efficiency:** The communication volume should be small to ensure network resource efficiency and energy efficiency between the client and server.

- **Calculation efficiency:** The calculation efficiency should be provided to facilitate index generation, search execution, and the safe sharing of data with other users.
- **Sharing efficiency among users:** The encrypted data must be retrieved from the saved remote data, which can be protected and shared safely and efficiently with users who are accessing an unreliable server. Cloud service providers need to guarantee the sharing of data only with permitted users.

3 Proposed Scheme

The proposed scheme satisfies the above requirements by applying the following detailed calculation.

3.1 System Parameters

- p : prime number
- G : cyclic additive group of order p
- G_T : cyclic multiplicative group of order p
- g : generator of G
- e : bilinear map, $G \times G \rightarrow G_T$
- sk_* : $*$'s private key in Z_p
- pk_* : $*$'s public key in G
- k : data encryption key
- $EC_k()$: symmetric key encryption by key k
- $DC_k()$: symmetric key decryption by key k
- w_* : $*$ th keyword of data
- W : set of w_*
- pd : plain data
- ed : encrypted data
- $H()$: hash function, $G_T \rightarrow Z_p$
- $H_1()$: hash function, $\{0,1\}^* \rightarrow G$
- $H_2()$: hash function, $G_1 \rightarrow G_1$
- T_* : trapdoor searching keyword $*$

3.2 Definition

The detailed steps performed by the proposed method are as follows.

- **KeyGen:** The storage outsourcing users generate public key pairs, which are created prior to using the service. The storage outsourcing server should not

know the user's private key. If the private key is leaked, the attacker can generate a trapdoor by acting as the owner of the private key. Thus, we generate a key pair based on the Discrete Logarithm Problem (DLP).

- **Enc**(sk, W, pd) $\rightarrow E, ed$: The data owner creates the encrypted index, E , and encrypted data, ed , which only the owner can search by inputting their own private key, sk , and set of keywords, W , which are sent to the master server.
- **TGen**(sk, w) $\rightarrow T_w$: To search the data safely, the user creates a trapdoor, T_w , which does not leak information related to the keyword w , which is being searched for using the private key sk . The trapdoor is sent to the master server. The storage outsourcing administrator should not be able to access information via a trapdoor.
- **Test**(E, T_w) \rightarrow "yes" or "no": Using the trapdoor generated by the user's private key and the search keyword, the server performs a test to confirm whether the encrypted data contain the keywords. If the cipher text contains the keyword specified, the server sends a "yes" to the user and a "no" if not. Thus, the server cannot learn anything about the keywords or the data.
- **REnc**(sk_a, pk_b, E_a) $\rightarrow E_b$: The data owner a creates a parameter to generate a data index for sharing that can be searched by b . This parameter is created using the data owner's private key sk_a , and the public key pk_b of the user who will be sharing the data. The master server creates a new index, E_b , which b can use to search via the trapdoor.
- **Dec**(sk, E, ed) $\rightarrow pd$: The rightful owner of the encrypted data uses their private key to decrypt the encrypted data.

3.3 Storage Scenario

The proposed method considers the storage outsourcing structure so an encrypting index used for sharing and searching is stored on the master server. We assume that each user has received a key pair before using the storage outsourcing service (refer to Step 1). The user encrypts the necessary keywords during data searching so they can perform their own search later and send this to the master server (refer to Step 2). The master server sends chunk information to the user for data storage, who then divides the data into chunks and stores it on the designated chunk server.

Step 1. Key generation (KeyGen). Each storage outsourcing service user generates a key pair

$$\begin{aligned} x &\in Z_p \text{ selection} \\ sk &= x \text{ setting up} \\ pk &= g^x \text{ setting up} \end{aligned}$$

Step 2. Index and data encryption (Enc). The data owner generates an encrypted index, which can be used for searching securely.

$$\begin{aligned} A &= pk_a^{hk} \quad (hk = H(k)) \\ b_i &= e(g, H_1(w_i))^{hk} \\ B &= \{b_1, b_2, \dots, b_n\} \end{aligned}$$

$$\begin{aligned}
C &= e(g, H_2(pk_a))^{hk} \cdot k \\
E_a &= (A, B, C) \text{ output encrypted index for the master server} \\
ed &= EC_k(pd) \text{ output encrypted data for the chunk server.}
\end{aligned}$$

3.4 Search and Reading Scenario

The user sends a trapdoor that can search data without exposing keyword information to the master server (refer to Step 1). The master server searches for the data with the keyword in the encrypted index using the trapdoor and then sends the chunk information that corresponds to the data to the user (refer to Step 2). The data retrieved is decrypted by the legitimate user (refer to Step 3). The user acquires the data by summing each chunk received from the chunk server that stores the data.

Step 1. Trapdoor generation (TGen). A user, a , who wants to search the data generates a trapdoor using the keywords and their secret key

$$T_w = H_1(w)^{-ska}$$

Step 2. Test. To confirm that the data contains the keywords sought by the user, the user performs the following tests with the public key, trapdoor, and crypt obtained from the server

$$\begin{aligned}
b_i &= ? H_2(e(A, T_w)) \\
&= H_2(e(pk_a^{hk}, H_1(w)^{-ska})) \\
&= H_2(e(g, H_1(w))^{hk})
\end{aligned}$$

Step 3. Decryption (Dec). The user can perform the following decryption using their private key and the crypt obtained from the server

$$\begin{aligned}
k &= C/e(A, H_2(pk_a)^{-ska}) \\
&= C/e(pk_a^{hk}, H_2(pk_a)^{-ska}) \\
&= C/e(g^{ska-hk}, H_2(pk_a)^{-ska}) \\
&= C/e(g, H_2(pk_a))^{hk} \\
&= (e(g, H_2(pk_a))^{hk} \cdot k) / (e(g, H_2(pk_a))^{hk}): \text{ output decryption key} \\
pd &= DC_k(ed): \text{ output decrypted data}
\end{aligned}$$

3.5 Sharing Scenario

To share data with the desired user and to allow the shared users to share data freely with another user, re-encryption needs to be performed to allow the shared users to search the encrypted index only.

Many parameters are required to implement proxy re-encryption and a separate searchable encryption scheme for secure data sharing in a storage outsourcing environment, which reduces the storage volume efficiency. Therefore, we propose an algorithm that provides both functions simultaneously. First, parameter A is

generated to allow index sharing with another user, which is sent to the storage outsourcing provider by the owner of the data (refer to Step 1). Next, the storage outsourcing provider changes the owner's index with respect to the data sharing target. Shared (re-encrypted) data searching is then possible, as shown in Steps 2–4. A user who acquires the data sharing index can always search for the corresponding data using keywords and download it.

Step 1. Re-encryption (REnc). If the data owner wants to share their data with other users, they generate keys for re-encryption. If user a wants to share their data with user b , a generates parameter A' using a 's secret key and b 's public key, as follows

$$A' = pk_b^{hk}$$

$$E_b = (A', B, C)$$

Step 2. Trapdoor generation (TGen). The user b who wants to search the data generates a trapdoor using the keywords and their secret key

$$T_w = H_I(w)^{-skb}$$

Step 3. Test. To confirm that the data contains the keywords the user seeks, the server performs the following tests using b 's trapdoor. It checks the equality $b_i = ? e(A', T_w)$. If this is true, the output is 'Yes' but 'No' if not,

$$b_i = ? e(A', T_w)$$

$$= e(pk_b^{hk}, H_I(w)^{-skb})$$

$$= e(g, H_I(w))^{hk}$$

Step 4. Decryption (Dec). The user can perform the following decryption with their private key

$$k = C/e(A', H_2(pk_a)^{-skb})$$

$$= C/e(pk_a^{hk}, H_2(pk_a)^{-ska})$$

$$= C/e(g^{ska-hk}, H_2(pk_a)^{-ska})$$

$$= C/e(g, H_2(pk_a))^{hk}$$

$$= (e(g, H_2(pk_a))^{hk} \cdot k)/(e(g, H_2(pk_a))^{hk}): \text{output decryption key}$$

$$pd = DC_k(ed): \text{output decrypted data}$$

4 Analysis

The proposed method satisfies the following requirements.

- **Confidentiality:** Using pairing, the proposed method makes it difficult for a malicious third party to decrypt communication contents, even if they eavesdrop on communications between the client and the server.
- **Search speed:** A user can check whether a document contains keywords by performing single pairing calculations, which increases the searching speed.
- **Traffic efficiency:** Keyword search and re-encryption requires only one round of communication, so the method increases the communication volume efficiency.

- **Calculation efficiency:** The relatively simple pairing calculation implies that the proposed method allows users to generate index and search documents, as well as perform re-encryption, which increases the calculation efficiency.
- **Sharing efficiency among users:** Our scheme allows encrypted and stored data on an unreliable distant storage outsourcing server to be shared safely and efficiently. In addition, our proposed method is different from existing methods because it does not require the shared subjects to be specified in advance, and no additional devices are required to manage the subjects who receive the shared data. Finally, if users want to re-share the data shared by the owner with other users, they only require one pairing calculation in an unreliable storage outsourcing environment.

5 Conclusion

The advent of storage outsourcing services has allowed many users to store and access data. Recent studies of the application of searchable encryption technologies to storage outsourcing have attempted to ensure the security of data. However, most available searchable encryption technologies are inefficient when adding data sharing objects because they are based on e-mail environments, which determine the objects with which data can be shared. In a storage outsourcing environment, users upload data on their own and share the data in a safe manner. Therefore, the indexes and data are separated so available technologies are compatible with data storage outsourcing systems. After considering the requirements of the data storage outsourcing environment, we specified the security requirements and proposed a method that provides both functions simultaneously: a proxy re-encryption function and a searchable encryption function. The proposed method provides a free sharing feature, which has the same calculation efficiency as existing methods. It appears that search methods based on multiple keywords will become important for ensuring flexibility and for facilitating search during data storage outsourcing. In the future, it will be necessary to develop a re-encryption system where an index containing multiple keywords with variable lengths can be encrypted and searched flexibly.

Acknowledgments This research was supported by the Basic Science Research Program through the National Research Foundation of Korea (NRF) funded by the Ministry of Education, Science, and Technology (2010-0022607). This research was supported by the MKE (The Ministry of Knowledge Economy), Korea, under the ITRC (Information Technology Research Center) support program (NIPA-2013-H0301-13-1003) supervised by the NIPA (National IT Industry Promotion Agency).

References

1. Song DX, Wagner D, Perrig A (2000) Practical techniques for searching on encrypted data. In: Symposium on security and privacy. California, USA
2. Goh EJ (2004) Secure indexes. Cryptography ePrint Archive
3. Curtmola R, Garay J, Kamara S, Ostrovsky R (2006) Searchable symmetric encryption: improved definitions and efficient constructions. In: Proceedings of the 13th ACM conference on computer and communications security. Virginia, USA
4. Boneh D, Crescenzo G, Ostrovsky R, Persiano G (2004) Public key encryption with keyword search. In: Proceedings of international conference on the theory and applications of cryptographic techniques. Interlaken, Switzerland
5. Boneh D, Waters B (2007) Conjunctive, subset and range queries on encrypted data. In: Proceedings of the 4th theory of cryptography conference. Amsterdam, The Netherlands
6. Hwang YH, Lee PJ (2007) Public key encryption with conjunctive keyword search and its extension to a multi-user system. In: Proceedings of the 1st international conference on pairing-based cryptography. Tokyo, Japan
7. Bao F, Deng RH, Ding X, Yang Y (2008) Private query on encrypted data in multi-user settings. In: Proceedings of the 4th international conference on information security practice and experience. Sydney, Australia
8. Kamara S, Lauter K (2010) Cryptographic outsourcing storage. In: Proceedings of Workshops on financial cryptography and data security. Canary Islands, Spain, pp 25–28
9. Ion M, Russello G, Crispo B (2011) Enforcing multi-user access policies to encrypted cloud databases. In: International symposium on policies for distributed systems and networks. Trento, Italy
10. Zhang B, Zhang F (2011) An efficient public key encryption with conjunctive-subset keywords search. *J Netw Comput Appl* 34:1
11. Yang Y (2011) Towards multi-user private keyword search for cloud computing. In: Proceeding of international conference on cloud computing. Singapore, Singapore
12. Chen X, Li Y (2011) Efficient proxy re-encryption with private keyword searching in untrusted storage. *Int J Comput Netw Inf Secur* 3:2
13. Wang XA, Huang X, Yang X, Liu L, Wu X (2011) Further observation on proxy re-encryption with keyword. *J Syst Softw* 85:643–654

Study on Wireless Intrusion Prevention System for Mobile Office

Jae Dong Lee, Ji Soo Park and Jong Hyuk Park

Abstract There has been an increase in the use of mobile devices. Further, the Internet environment has changed from a wired network to a wireless one. However, the existing wired security solutions are difficult to apply to the wireless network. In this paper, we propose a model for using enhanced mobile office service in a wireless network. This model also provides greater access control and a more secure mobile office.

Keywords WIPS · Wireless security · Wireless threat · Mobile office

1 Introduction

Recently, there has been an increase in the use of mobile devices such as smartphones and smart pads. At the same time, the working environment using mobile devices has also expanded. Earlier, the working environment was connected to the intranet through a wired network. However, the recent working environment has been modified to use both wired and wireless networks. Additionally, the increasing use of mobile devices has given rise to the need to enhance the efficiency and convenience of the business. However, the wireless network access faces new security threats. In a wired network, IPS, IDS, and Firewall can be used

J. D. Lee · J. S. Park · J. H. Park (✉)

Department of Computer Science and Engineering, Seoul National University of Science and Technology (SeoulTech), 172 Gongreung 2-dong, Nowon-gu, Seoul 139-743, Korea
e-mail: jhpark1@seoultech.ac.kr

J. D. Lee
e-mail: jdlee731@seoultech.ac.kr

J. S. Park
e-mail: jisoo08@seoultech.ac.kr

to block unauthorized access. However, this cannot be done so in a wireless network. Moreover, wireless networks are vulnerable to attacks (e.g., radio frequency jamming and deauthentication frame denial of service (DoS)) on the physical layer and data link layer of the OSI seven layer. Further, the existing wired solutions cannot effectively control an illegal access. Therefore, a wireless intrusion prevention system (WIPS) is used to strengthen the security of wireless networks. In this paper, we describe some of the WIPS research trends associated with the wireless security threats and countermeasures. In addition, we propose a WIPS service model for a more secure mobile office. The paper is organized as follows. [Section 2](#) discusses the related works, [Sect. 2.3](#) discusses the WIPS security threats and requirements, [Sect. 3.2](#) discusses the models and scenarios, and [Sect. 4](#) presents the conclusions.

2 Related Works

2.1 WIPS Concept and Construction

Wireless intrusion detection system (WIDS) monitors illegal AP and wireless attack tools. WIPS is an extension of WIDS. WIPS cuts off the security threat device after an automatic threat classification. In addition, the aim of WIPS is to prevent unauthorized access to internal information assets [1, 2].

WIPS consists of a server, database, sensor, and console. The server collects the raw data from the sensors and analyzes the collected data. The database is used to store the information from the server and sensors. The sensors monitor the wireless signal, and the sensed information is transmitted to the server. When the server or sensor information is required, the console establishes an interface between the administrators and the users [1, 2].

2.2 WIPS Research Trends

Wen-Chuan Hsieh and colleagues proposed a WIDS using the short message service (SMS) and Proactive for the detection of wireless attacks such as WEP cracking, MAC address spoofing, and wardriving. Dong Lijun and colleagues proposed a wireless-transport-layer-based IPS model, which can detect and intercept the traffic of the users through a single logical path between all the wireless devices and the destinations. Vartak and colleagues described over-the-air (OTA) wireless intrusion prevention techniques. They evaluated the performance of the testbed-based blocking technology, and the experimental results depending on the WIPS design were described. Jack Timofte described the countermeasures against wireless security threats with WIPS. Guanlin Chen and colleagues proposed a honeypot-based intelligent attack recognition engine for detecting and

blocking an attack beforehand, which attempts at minimizing the rate of misdiagnosis. Yujia Zhang and colleagues suggested a general framework for WIPS and discussed the use of core technology. Guanlin Chen and colleagues proposed a model that can block or predict the behavior of the attacker by applying specific rules. This model uses the specific device information and reduces the rate of misdiagnosis [2–7].

2.3 WIPS Security Requirements

The security requirements of WIPS can be classified by the security elements of confidentiality, integrity, and availability.

- **Confidentiality:** The wireless signal can be propagated to a large number of unspecified devices, which implies that important information (such as personal information and billing data stored on the wireless terminal) can be leaked. These devices are more vulnerable to attacks (e.g., sniffing and evil twin) when compared with the wired devices.
- **Integrity:** System confusion can be caused by a man-in-the-middle attack (e.g., unauthorized change, deletion, and insertion of data). WIPS is necessary to integrity the assurance methods during data transfer.
- **Availability:** DoS attacks undermine the system availability and productivity and reduce the system resources and ability to access information. Wireless networks are vulnerable to attacks (e.g., RF jamming and deauthentication frame DoS) on the physical layer and data link layer of the OSI seven layer. Therefore, certain technical mechanisms to prevent these attacks are required.

3 WIPS for Mobile Office Service Model

3.1 System Architecture

It is difficult to perform access control with respect to the user position and to grant permission. The existing WIPS has the ability to completely block the access or permit access to specific wireless devices. By considering the security threats and difficulty in control faced by the existing WIPS, we propose a service model. In this service model, after loading the positioning module, the sensors measure the signal to determine the user position and save the user permission data profile. Through the above-mentioned aspects, the proposed model attempts to solve the access control and security issues (Fig. 1).

The proposed model consists of a WIPS mobile office agent, WIPS mobile office AP, WIPS mobile office sensor, WIPS mobile office server, and WIPS mobile office database. A WIPS mobile office agent in the user smartphone saves

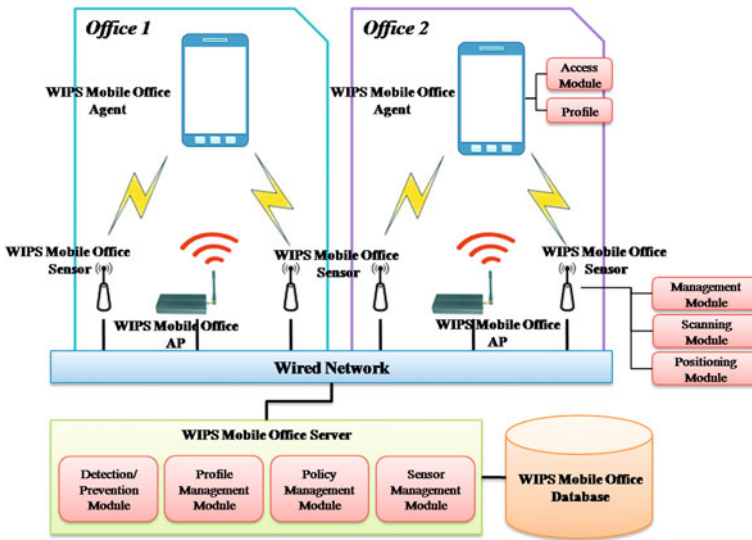


Fig. 1 WIPS architecture for mobile office service model

in the profile of the device information and network access permission controlled by the access module. The WIPS AP performs a part of the communication function of the WIPS mobile office agent. When the WIPS mobile office agent connects to a wireless network, the device location is measured by the WIPS mobile office sensor with the positioning module. With the information received from the server, the WIPS mobile office agent is controlled by the management module. The WIPS mobile office server stores the profiles of the users and devices after access to the wireless network is requested by the WIPS mobile office agent. When the stored profiles match with those in the WIPS mobile office database, the server permits the device communication (Table 1).

3.2 Use Case Scenario

Figure 2 shows the use case scenario of the service model. For the wireless network connection and certification, the server should compare profile A in the

Table 1 Definitions of numerical formulas

Sign	Meaning
WIPS-MO_Agnt	WIPS mobile office agent
WIPS-MO_AP	WIPS mobile office AP
WIPS-MO_Sensor	WIPS mobile office sensor
WIPS-MO_Svr	WIPS mobile office server
WIPS-MO_DB	WIPS mobile office database

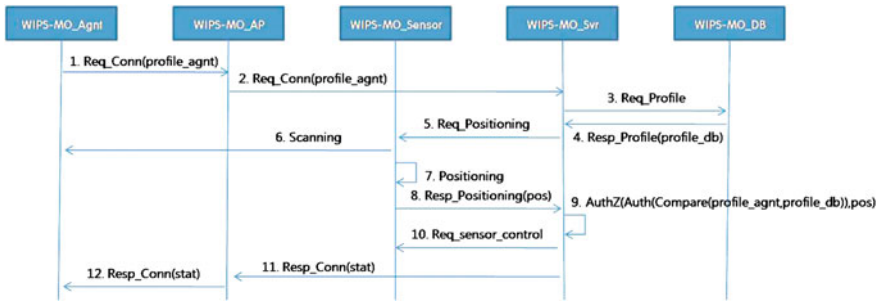


Fig. 2 Use case scenario

WIPS mobile office agent with profile B in the WIPS mobile office database The server transmits the information about the WIPS Mobile office agent location to the WIPS mobile office sensor. After gaining authority, the WIPS mobile office agent is available in the wireless network.

The specific operation process is as follows:

- (1) WIPS-MO_Agnt → WIPS-MO_AP: Req_Conn(profile_agnt)
 WIPS-MO_AP → WIPS-MO_Svr: Req_Conn (profile_agnt)
 Through WIPS-MO_AP, WIPS-MO_Angt transmits the information about profile_agnt to WIPS-MO_Svr.
- (2) WIPS-MO_Svr → WIPS-MO_DB: Req_Profile
 WIPS-MO_DB → WIPS-MO_Svr: Resp_Profile(profile_db)
 For detecting the user profile, “WIPS-MO_DB” is requested by “WIPS-MO-Svr” to receive profile_db.
- (3) WIPS-MO_Svr → WIPS-MO_Sensor: Req_Positioning
 For detecting the WIPS-MO_Agnt position, WIPS-MO_Sensor requests WIPS-MO_Svr for the information about the positioning action.
- (4) WIPS-MO_Sensor: Scanning and positioning
 WIPS-MO_Sensor detects WIPS-MO_Agnt location.
- (5) WIPS-MO_Sensor → WIPS-MO_Svr: Resp_Positioning(pos)
 WIPS-MO_Sensor transmits information about WIPS-MO_Agnt position to WIPS-MO_Svr.
- (6) WIPS-MO_Svr: AuthZ(Auth(Compare(profile_agnt,profile_db)), pos)
 After the server compares profile_agnt with profile_db, it executes Authentication Auth(). Using the WIPS-MO_Agnt position information, it executes Authorization AuthZ().
- (7) WIPS-MO_Svr → WIPS-MO_Sensor: Req_sensor_control
 Through the authorization status, WIPS-MO_Svr requests WIPS-MO_Sensor for the information about the WIPS-MO_Agnt signal limitation.
- (8) WIPS-MO_Svr → WIPS-MO_AP: Resp_Conn(stat)
 WIPS-MO_AP → WIPS-MO_Agnt: Resp_Conn(stat)
 Through WIPS-MO_AP, WIPS-MO_Svr transmits the connection information to WIPS-MO_Agnt.

4 Conclusion

A WIPS is developed to ensure safe use of the mobile office both in the wired environment and in the wireless environment; however, currently, it is highly vulnerable to various elements.

Researchers have been studying the secure technology with regard to the devices and wireless network in order to solve the vulnerability issue. The following are the techniques to solve this issue: clean the automatic connecting profile, prevent from connecting the disproved AP in public, set the permission and password for self-access control, and classify and block the disproved AP/client, thereby blocking the complex threats and attacks. The following are the techniques for secure technology management: through real-time wireless network monitoring, monitor the secure status of the devices such as smartphones, tablets, and laptops.

In this paper, we have discussed the WIPS concept, architecture, threats, requirements, and WIPS mobile office service model. In the existing devices, the service model provides access control not only to detect the user profile but also to determine the user location while using the mobile office. As only the Wireless AP environment has been considered in this study, research on the access via Bluetooth, 3G, and LTE is required. In addition, studies should be conducted on new wireless technologies and in the political field.

Acknowledgments This research was supported by the Basic Science Research Program through the National Research Foundation of Korea (NRF) funded by the Ministry of Education, Science and Technology (2012-0008296), Republic of Korea.

References

1. Jack TIMOFTE (2008) Wireless intrusion prevention system. *Revista Informatica Economica* 47:129–132
2. Zhang Y, Chen G, Weng W, Wang Z (2010) An overview of wireless intrusion prevention systems. In: 2nd International conference on communication systems networks and applications
3. Hsieh WC, Lo CC, Lee JC, Huang LT (2004) The implementation of a proactive wireless intrusion detection system. In: Proceedings of the 4th international conference on computer and information technology, IEEE Press, 2004, pp 581–586
4. Lijun D, Yu S, Xia T, Liao R (2007) WBIPS: a lightweight wtls-based intrusion prevention scheme. In: Proceedings of the International conference on wireless communications, networking and mobile computing, IEEE Press, 2007, pp 2298–2301
5. Vartak V, Ahmad S, Gopinath KN (2007) An experimental evaluation of over-the-air (OTA) wireless intrusion prevention techniques. In: Proceedings of the 2nd international conference on communication systems software and middleware, IEEE Computer Society, 2007, pp 1–7
6. Chen G, Yao H, Wang Z (2009) Research of wireless intrusion prevention systems based on plan recognition and honeypot. In: Proceedings of the international conference on wireless communications and signal processing, IEEE Computer Society, 2009, pp 1–5
7. Chen G, Yao H, Wang Z (2010) An intelligent WLAN intrusion prevention system based on signature detection and plan recognition. In: 2nd International conference on future networks

A Component Model for Manufacturing System in Cloud Computing

HwaYoung Jeong and JongHyuk Park

Abstract Cloud computing is a new trend that is expected to reshape the information technology landscape. It can provide a new process to user such as software, infrastructure and platforms as a service over the Internet. In this trend, traditional way for manufacturing system has been changed from set up the system software in the machine to access internet and use it at anytime. Manufacturing system has process consists of many production parts and stages. And control and operate status is necessary to monitor, observe and manage the system very often. In this paper, we propose component model for manufacturing system in cloud computing environment. This model consists of three layers; manufacturing cloud, service cloud and user cloud. And each layer relate their role to other factor in the cloud.

Keywords Manufacturing system · Cloud computing · Cloud manufacturing system · Component model for manufacturing

1 Introduction

Under the traditional model, the enterprises need to purchase not only infrastructure such as hardware but also software licenses to establish an IT system, and need specialized personnel to maintain. It needs to upgrade various facilities including hardware and software to meet the demands when the scale of business extends.

H. Jeong

Humanitas College of Kyunghee University, Hoegi-dong, Seoul 130-701, Korea
e-mail: hyjeong@khu.ac.kr

J. Park (✉)

Department of Computer Science and Engineering,
Seoul National University of Science and Technology,
Seoul, Korea
e-mail: parkjonghyuk1@hotmail.com

For the enterprises, what they really need is only the tool which can complete the work and improve efficiency but the hardware and software themselves [1]. Cloud computing is a new technology trend that is expected to reshape the information technology landscape. It is a way to deliver software, infrastructure and platforms as a service to remote customers over the Internet. Cloud computing reduces the cost of managing hardware and software resources by shifting the location of the infrastructure to the network. It offers high availability, scalability and cost-effectiveness since it is particularly associated with the provision of computing resources on-demand and with a pay-as-you-use model [2].

“The world of manufacturing of this century is a networking information world—inside and outside of enterprises and linked to all participants of markets. The fast and global transfer of information and open markets is beside of economic aspects the main driver of changing the global structure of manufacturing.” With these statements Westkämper characterizes in short the new paradigm of manufacturing [1]. The left side of Fig. 1 depicts four major drivers that influence the economy of all industrial nations, whereas the right side highlights the fields in which a dynamic adaptation of industrial production has to take place for a sustainable competitiveness [3].

In this trend, manufacturing system has changing from traditional ways to cloud computing service. That is, product life cycles are reduced in the continuously changing marketplace, modern manufacturing systems must have sufficient responsiveness to adapt their behaviors efficiently to a wide range of circumstances. To respond to these demands, including high productivity and production flexibility [3], the application of cloud computing environment to manufacturing system has been necessary.

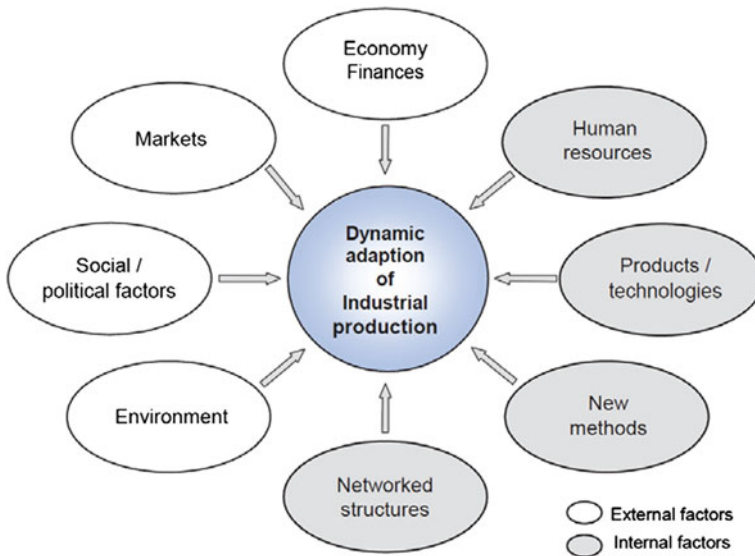


Fig. 1 Turbulent influences—dynamic adaptation of manufacturing structures (Westkämper)

In this paper, we propose a component model for manufacturing system considering in cloud computing environment. A proposal model has to apply cloud computing layers. Therefore we separated three layers; manufacturing cloud, service cloud and user cloud. The rest of the paper is organized as follows: [Sect. 2](#) describe the cloud computing environment and manufacturing system, [Sect. 3](#) describes the proposal model with cloud computing, and [Sect. 4](#) discusses about the Conclusion.

2 Cloud Computing and Manufacturing System

2.1 Cloud Computing

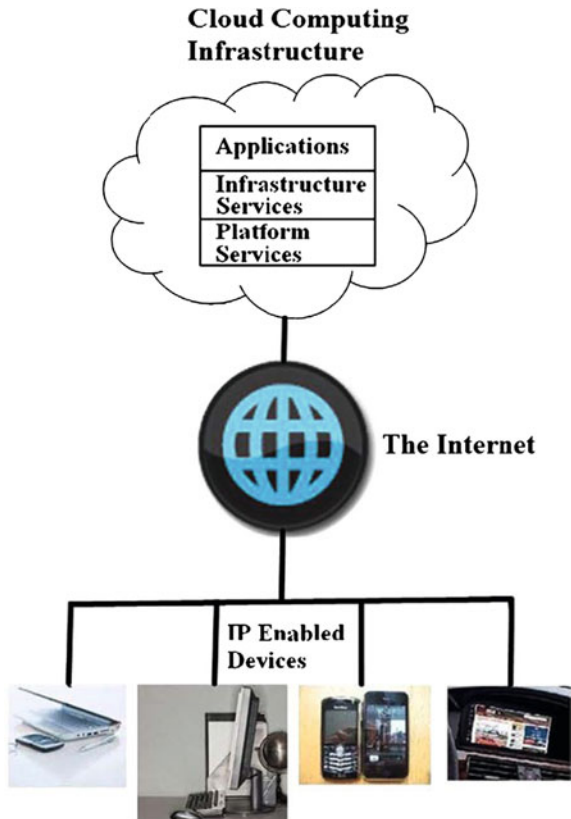
The word ‘cloud’, in cloud computing, is a fairly accurate description of the ephemeral nature of the structure by which the services are offered. Just as a cloud might appear and disappear rapidly, and the forces of air, heat and water vapour will change the internal dynamic of the cloud, so the services offered over the Internet by providers of software can be as equally as transitory [4]. Cloud computing refers to both the applications delivered as services over the Internet and the hardware and systems software in the data centers that provide those services. Services can be: Software (SaaS), Platform (PaaS), or Infrastructure (IaaS) [2]. The factors are as below [5].

- Infrastructure as a Service (IaaS): Products offered via this mode include the remote delivery (through the Internet) of a full computer infrastructure (e.g., virtual computers, servers, storage devices, etc.);
- Platform as a Service (PaaS): To understand this cloud computing layer one needs to remember the traditional computing model where each application managed locally required hardware, an operating system, a database, middleware, Web servers, and other software. One also needs to remember the team of network, database, and system management experts that are needed to keep everything up and running. With cloud computing, these services are now provided remotely by cloud providers under this layer;
- Software as a Service (SaaS): Under this layer, applications are delivered through the medium of the Internet as a service. Instead of installing and maintaining software, you simply access it via the Internet, freeing yourself from complex software and hardware management. This type of cloud service offers a complete application functionality that ranges from productivity (e.g., office-type) applications to programs such as those for Customer Relationship Management (CRM) or enterprise-resource management.

And Cloud computing represents a convergence of two major trends in information technology—(a) IT efficiency, whereby the power of modern computers is utilized more efficiently through highly scalable hardware and software resources

and (b) business agility, whereby IT can be used as a competitive tool through rapid deployment, parallel batch processing, use of compute-intensive business analytics and mobile interactive applications that respond in real time to user requirements. The concept of IT efficiency also embraces the ideas encapsulated in green computing, since not only are the computing resources used more efficiently, but further, the computers can be physically located in geographical areas that have access to cheap electricity while their computing power can be accessed long distances away over the Internet. However, as the term business agility implies, cloud computing is not just about cheap computing—it is also about businesses being able to use computational tools that can be deployed and scaled rapidly, even as it reduces the need for huge upfront investments that characterize enterprise IT setups today. Fig. 2 shows cloud computing infrastructure [6].

Fig. 2 Cloud computing infrastructure



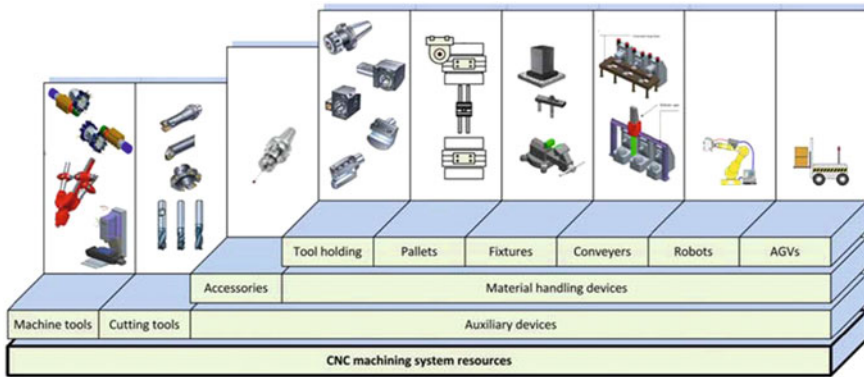


Fig. 3 Element of CNC manufacturing system

2.2 Manufacturing System

Generally, a manufacturing process consists of many production stages. A product usually undergoes a production line that progressively alters the nature of the incoming material until it reaches the consumer in the form of a finished good. Every stage produces a proportion of items that fail to meet the necessary requirements imposed by more manufacturing operation, the consumer, government regulations or some combinations of these. Control of every stage is necessary to verify that specific quality level is being maintained [7]. Example is, a computer numerical controlled (CNC) machining system consists of a number of elements such as CNC machining centers, automated material handling systems, loading and unloading stations, tool storage and other auxiliary devices as shown in Fig. 3. CNC manufacturing can be defined as the combination of machining and supporting activities for a range of multi-purpose machine tools capable of performing subtractive or additive processes in converting raw material into finished products. In the automated environments material handling systems such as robotic arms, gantry and pallet changing systems carry work pieces or cutting tools to different CNC manufacturing workstations. Typically at the loading and unloading station, each part is clamped on a fixture which is mounted on a pallet. The part is then processed on the machines while loaded on the pallet. When operations are complete, the part is unloaded at the loading and unloading station [8].

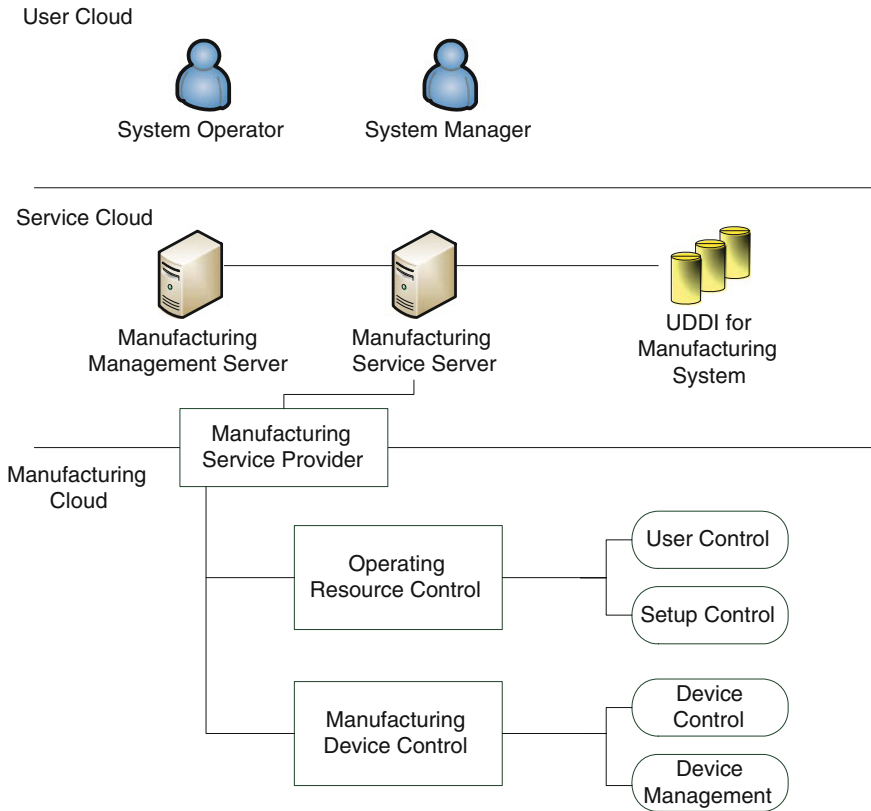


Fig. 4 The structure of manufacturing system in the cloud computing

3 The Component Model for Manufacturing System in Cloud Computing Environment

In order to make model for manufacturing system in cloud computing environment, we make a structure as shown in Fig. 4. It has three layers; Manufacturing cloud, Service Cloud and User cloud. Manufacturing cloud has two process, Operating Resource Control and Manufacturing Device Control. The Operating Resource Control is deal with the process for control and manage between the machine and user. The Manufacturing Device Control has process for device operation and control. They also serve to their process logic to Manufacturing service server by Manufacturing service provider. All the processes provide to user as a service. So it use UDDI and SOAP. UDDI for Manufacturing System has much information of service for manufacturing system control and management. And Manufacturing Management Server handle to process between the user and

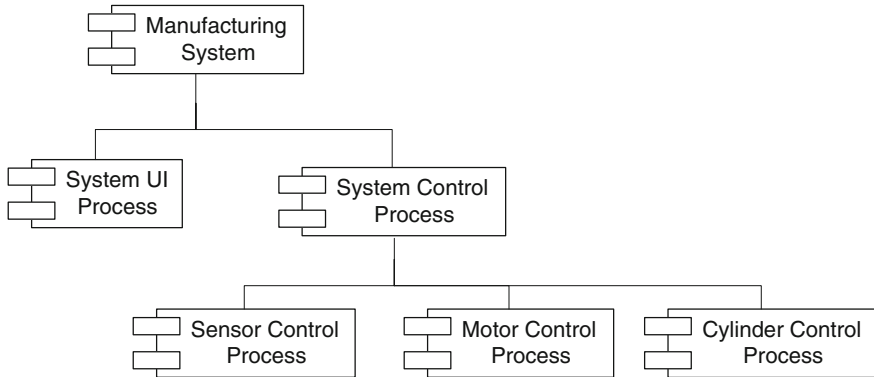


Fig. 5 The component model for manufacturing system

manufacturing system services. The component model for this system is shown in Fig. 5. In this model, System control process consists of sensor, motor and cylinder control process. They are include management system units.

4 Conclusion

In this research, we propose a component model for manufacturing system in cloud computing environment. It has three layers; Manufacturing cloud, Service Cloud and User cloud. Manufacturing cloud has two process, Operating Resource Control and Manufacturing Device Control. All the processes provide to user as a service. So it use UDDI and SOAP. UDDI for Manufacturing System has much information of service for manufacturing system control and management. In the component model consists of System UI Process and System Control Process. This system provide all the process for manufacturing system to system operator and engineer.

References

1. Zhang S, Yan H, Chen X (2012) Research on key technologies of cloud computing. *Phys Procedia* 33:1791–1797
2. Bourguiba M, Haddadou K, Pierre G (2012) Packet aggregation based network I/O virtualization for cloud computing. *Comput Commun* 35:309–319
3. Wiendahl HP, ElMaraghy HA, Nyhuis P, Zäh MF, Wiendahl HH, Duffie N, Brieke M (2007) Changeable manufacturing—classification, design and operation. *Ann CIRP* 56(2):581–836. doi:10.1016/j.cirp.2007.10.003
4. Mason S, George E (2011) Digital evidence and ‘cloud’ computing. *Comput Law Secur Rev* 27:524–528

5. Sultan N (2010) Cloud computing for education: a new dawn? *Int J Inf Manag* 30:109–116
6. Marston S, Li Z, Bandyopadhyay S, Zhang J, Ghalsasi A (2011) Cloud computing—the business perspective. *Decis Support Syst* 51:176–189
7. Kaya I, Engin O (2007) A new approach to define sample size at attributes control chart in multistage processes: an application in engine piston manufacturing process. *J Mater Process Technol* 183:38–48
8. Vichare P, Nassehi A, Kumar S, Newman ST (2009) A unified manufacturing resource model for representing CNC machining systems. *Robot Comput Interg Manuf* 25:999–1007
9. Park SC (2005) A methodology for creating a virtual model for a flexible manufacturing system. *Comput Ind* 56:734–746

Traditional Culture Learning System for Korean Folk Literature, Pansori

Dong-Keon Kim and Woon-Ho Choi

Abstract This research aims to develop Korean traditional culture's learning system. This system was processed using internet. And the target is folk literature, Pansori. Actually, in spite of Pansori is one of famous folk literature, it is not familiarly area on peoples due to difficult learning and understanding them. Our system attempt to provide Pansori's learning materials to user very easily and conveniently. The learning materials were managed by learning meta data in LCMS and learning process data was controlled by LMS.

Keywords Folk literature · Traditional culture · Pansori · E-learning system · LMS · LCMS

1 Introduction

Max Weber characterized the shift from traditional (often religious) values to modern ones as the 'pervasive rationalization' of all spheres of society, and the process of modernization as the 'institutionalization of purposive-rational economic and administrative action' [1]. Subsequent theorists have stylized modernity into a general model of evolutionary social development [2] in which the core societal goal is economic growth rather than survival in harmony with natural surroundings, and the dominant individual goal is achievement through income and consumption rather than through moral standing. An inevitable characteristic

D.-K. Kim

Humanitas College, Kyung Hee University, 1 Hoegi-dong, Dongdaemun-gu, Seoul, Korea
e-mail: dehi@khu.ac.kr

W.-H. Choi (✉)

Department of Linguistics, Seoul National University, Gwanak 1, Gwanak-ro, Gwanak-gu, Seoul, Korea
e-mail: woonhochoi@gmail.com

of modernization for both Weber and his successors is the dramatic devaluation of tradition through universalisation of norms of action, generalization of values, and individual-based patterns of socialization. Tradition has become, at best, a way of presenting the past as an increasingly scarce non-renewable resource and, at worst, an impediment to progress [3]. Cultural environment is an important factor influencing human sexual behaviors [4]. Traditional culture, folk literature, educators have become concerned about preschoolers in Korea who seem to prefer reading about Disney's movie characters to traditional folk literature. Especially since the learning of English and globalization have become critical parts of Korean early childhood education, teachers and parents use popular books, songs, movies, and websites published in the United States to teach English. These American teaching materials contain beliefs and behavior generally acceptable in western culture. However, they are often in conflict with Korean traditional teachings. Researchers [5, 6] suggest that when preschool children devote a significant amount of time and effort to learning English, they learn not only the foreign language but also new cultural beliefs and ways of life. For example, when children learn to say, "hello" to their teacher in English, they also grasp the accompanying action of waving their hand. This is considered inappropriate in Korean society where children are expected to bow their head when greeting their teachers. When children read stories and watch media programs created for students in the United States, they are exposed to westernized beliefs which tend to affect their behavior. If these trends continue, educators predict that Korea's traditional values will gradually disappear and Korea will lose many of its authentic traditional beliefs [7].

In the context, traditional culture's (about folk literature) learning system for children was need. This paper aims to develop folk literature's learning system to easily understand them. The target topic is Pansori, one of the folk literatures of Korea. And the learning system is based on online system. For this system, we consider to use LMS (Learning Management System) and LCMS (Learning Contents Management System) with learning materials.

2 Related Works

2.1 Folk Literature

Folk Literature is highly instructive and can therefore be well utilized for children's value education. It contains useful lessons to help young children grow into moral and responsible adults, capable of making sound judgments. Folk tales usually conclude with rewards for virtuous characters who have exhibited traditional values. Reading traditional folk literature allows children to experience an emotional catharsis and internalize social values through personal connections made with characters. Folk literature can inspire children with morality and help

them develop into well-rounded members of society. Thus, Korean educators believe the use of folk literature is a culturally and developmentally appropriate method of teaching values which reflects the thoughts that have guided the lives of Korean people for thousands of years [7].

2.2 E-Learning System

Along with the advancement of information technology, the electronic learning (e-learning) has played an important role in teaching and learning, which has become more and more popular not only in different levels of schools but also in various commercial or industrial companies [8]. E-learning refers to the use of electronic devices for learning, including the delivery of content via electronic media such as Internet/Intranet/Extranet, audio or video tape, satellite broadcast, interactive TV, CD-ROM, and so on. This type of learning moves the traditional instruction paradigm to a learning paradigm, thereby relinquishing much control over planning and selection to the learners. In addition, it is capable of bringing the following advantages to learners: cost-effectiveness, timely content, and access flexibility [9].

Additionally, E-learning in the workplace offers special benefits. First, a robust early education and initial occupational preparation will no longer be sufficient for a long working life. Ongoing learning through working life is a necessity for most workers, and essential for those engaged in transitions across work and occupational boundaries. In this context, e-learning provides an effective approach for ongoing learning by virtue of its flexibility to access, just-in-time delivery, and cost-effectiveness. Second, while company product, structure, and policies become more volatile in today's dynamic environment, e-learning enables companies to adjust learning requirements and update knowledge resources in a more efficient way. Third, e-learning enables employees to build enduring community of practice when they come together to share knowledge and experience; it is important to improve individual and organizational performance by knowledge sharing and dissemination. Recent research has motivated the integration of e-learning with knowledge management for organizational strategic development [10]. Figure 1 shows a sample of e-learning system. E-learning is the use of technologies in learning opportunities, with an aim to automate education and develop self-paced learning. To achieve this, a number of studies have made effort on intelligent tutoring techniques, such as personalized learning assistance; recommendation of learning objects based on individual preference; and adaptive learning path guidance. In doing so, ontology and semantic Web technologies have been applied in e-learning development with the purpose to model, represent, and manage learning resources in a more explicit and effective way [10].



Fig. 1 Example of e-learning system

3 Folk Literature’s Learning System

In order to provide learning materials for folk literature, we develop learning system. The system has a topic, Pansori. This chapter was described the learning system process and environment.

3.1 Pansori

Pansori is one of the art forms that represent Korean vocal music. Pansori is a musical drama in which a solo singer, holding a fan in one hand, delivers a long story by the means of sori (song), aniri (narration), and ballim (mimetic gestures). In a pansori performance the singer is accompanied only by a gosu (drummer) [11]. Figure 2 shows Pansori.

‘Pansori,’ often referred to as Korean Opera, is a type of traditional Korean music which tells a themed story in the form of music theater, with two musicians sharing the spotlight—a singer (‘sorikkun’) and a ‘gosu’. The singer plays the central role through his singing, words, and body language while the drummer plays an accompanying role by providing the rhythm and shouting words of encouragement to add to the passion of the performance. With a distinct, inimitable sound, rhythm, and singing technique, Pansori is truly representative of



Fig. 2 Example of Pansori

Korea’s unique cultural landscape. Pansori first emerged during the mid-Joseon era (1392–1910), when common culture began to evolve. The scribes of Pansori and the year of their origin are hard to pinpoint—it began as an oral tradition that was continued by professional entertainers. During the Joseon era, entertainers were regarded as lowly peasants, which explains why Pansori remained mostly in commoners’ circles. But towards the end of the Joseon era, aristocrats took notice—and the audience for Pansori operas increased. Originally a collection of 12 operas, there are now regrettably only five that have been passed down to us today—Chunhyangga, Simcheongga, Heungbuga, Jeokbyeokga, and Sugungga. A Pansori performance is lengthy, some even taking up to 4–5 h to complete. In 2003, Pansori was officially recognized by UNESCO as an important piece of world culture [12].

3.2 Pansori’s 5 ‘Madang’

The 5 Pansori operas are called ‘madang,’ a word which literally means courtyard, but carries strong ties to traditional and folk games. In short, Pansori was considered a form of traditional play. The suffix of ‘ga’ at the end of each ‘madang’ name means ‘song’ [12].

- Chunhyangga: The old novel ‘Chunhyangjeon’ in opera form. The love story of Sung Chunhyang, the daughter of a courtesan, and Lee Mongyong, the son of an aristocrat. Of the five Pansori ‘madang,’ it is valued the greatest in terms of musical and literary achievement. Famed portions of the opera include ‘Sarangga’ (love song), ‘Ibyeolga’ (farewell song), and ‘Okjungga’ (prison cell song).

- Simcheongga: The old story of ‘Simcheongjeon’ in opera form. Simcheong, the daughter of a blind man who sought to regain her father’s vision by offering rice at a temple, she sold herself to a boatman as a sacrifice to the ocean in exchange for the rice. The Dragon King of the sea, however, was touched by her love and rescued her, reuniting her with her beloved father. A child’s love for their parent is the central theme of this story.
- Heungbuga: The old story of ‘Heungbujeon’ in opera form. There are two brothers, Nolbu and Heungbu. Nolbu is older and wealthy, with a wicked heart. The younger brother, Heungbu, is poor but is a kind soul. When Heungbu comes into fortune by helping a swallow with a broken leg, the envious Nolbu purposely breaks the leg of a swallow and fixes it before setting it free in the hopes that he will be likewise awarded. The simple moral kernel of the tale is that kindness is rewarded and wickedness is punished.
- Jeokbyeokga: A portion of the Chinese tale ‘Samgukjijeon’ transferred into opera form. Famous songs include the ‘Samgochoryeo’ and ‘Jeokbyeokgang River Battle.’

Sugungga: The old story ‘Tokkijeon’ in opera form. When the underwater Dragon King falls ill, he sends a sea turtle to land in order to find the liver of a hare to use as medicine. The opera contains much humorous banter between the characters.



Fig. 3 Learning activity for Pansori



Fig. 4 Sample screen shot of Pansori e-learning system. The system is prototype

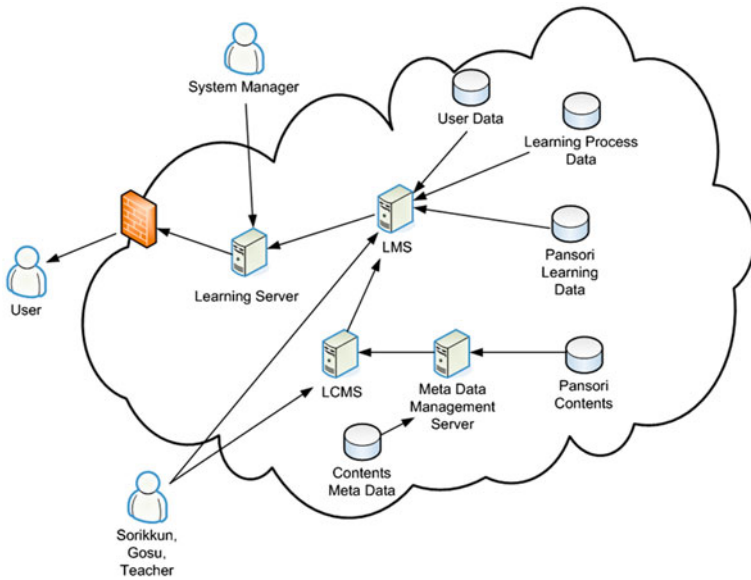


Fig. 5 Pansori e-learning system's structure with LMS and LCMS

3.3 Folk Literature's Learning System, Pansori

Traditional way for Pansori learning is only face to face learning process. Figure 3 shows the learning activity for Pansori. Unfortunately, the way has limit to easily understand and get a chance to know about Pansori. Also it has limitation of location area to get a class for Pansori. Therefore, we develop the online based Pansori's learning system. Figure 4 shows a prototype of Pansori's learning system. It can display lecture movie and text at the same time. Therefore user is able to study to sing following the contents using two materials, movie and text. Figure 5 shows an environment for Pansori's learning system. In this system, LMS was used to management learning process and provide learning materials efficiently to user. Furthermore, LCMS which is to control and manage the Pansori's contents was used. Therefore user is able to access Pansori's learning system when he/she wants to know Pansori.

4 Conclusion

In this research, we design the folk literature, Pansori's learning system. In spite of Pansori is Korean traditional culture and song, many Koreans are not familiar due to difficult learning and understanding them. This research attempts to overcome their burden and to reduce their rejection filling. This system is on online process. Therefore user is able to access when he/she wants to know and study Pansori. Then he/she is able to get various learning materials for Pansori from LMS and LCMS.

References

1. Habermas J (1987) The philosophical discourse of modernity. Polity Press, Cambridge
2. Coleman J (1968) Modernization. In: International encyclopedia of the social sciences, vol 10. Macmillan Free Press, New York
3. Jenkins TN (2000) Putting postmodernity into practice: endogenous development and the role of traditional cultures in the rural development of marginal regions. *Ecol Econ* 34:301–314
4. Gao E, Zuo X, Wang L, Lou C, Cheng Y, Zabin LS (2012) How does traditional confucian culture influence adolescents' sexual behavior in three asian cities? *J Adolesc Health* 50(3):S12–S17
5. Cromdal J (2004) Building bilingual oppositions: code-switching in children's disputes. *Lang Soc* 33(1):33–58
6. Cummins J (1991) Language development and academic learning. In: Malave L, Duquette G (eds) *Language, culture and cognition: a collection of studies in first and second language acquisition*. Multilingual Matters, Clevedon, pp 161–175
7. Lee GL (2011) Best practices of teaching traditional beliefs using Korean folk literature. *Procedia Soc Behav Sci* 15:417–421

8. Chao R-J, Chen Y-H (2009) Evaluation of the criteria and effectiveness of distance e-learning with consistent fuzzy preference relations. *Expert Syst Appl* 36:10657–10662
9. Shee Daniel Y, Wang Y-S (2008) Multi-criteria evaluation of the web-based e-learning system: a methodology based on learner satisfaction and its applications. *Comput Educ* 50:894–905
10. Jia H et al (2010) Design of a performance-oriented workplace e-learning system using ontology. *Expert Syst Appl*. doi:[10.1016/j.eswa.2010.08.122](https://doi.org/10.1016/j.eswa.2010.08.122)
11. What is Pansori? (2012) http://www.chungnam.net/mediaMain.do?article_no=MD0000363460&med_action=view&mnu_cd=CNMMENU01096&orderby=REG_DATE
12. Intangible Heritage of Humanity List—The Pansori Epic Chant (2012) http://english.visitkorea.or.kr/enu/CU/CU_EN_8_5_7_2.jsp

Auction Based Ticket Selling Schemes with Multiple Demand from the Agents in Static Environment

Sajal Mukhopadhyay, D. Ghosh, Narayan C. Debnath
and N. RamTeja

Abstract First-come-first-serve (FCFS) scheme is used for selling the tickets in ticket market that is a multi-million dollar industry for any popular event. But in a competitive environment is this FCFS efficient? In earlier literature it has been shown that the auction based alternative solutions using the framework of mechanism design, a sub field of game theory, can provide better results against FCFS in terms of profit making and efficiency in allocation. However the solution proposed in the earlier literature can address the ticket selling environment where an agent can give demand for a single ticket in static environment. In many situations a single agent can give demand for multiple tickets in static environment. In this paper, with the use of mechanism design framework some elegant solutions are proposed in static environment where an agent can give demand for multiple tickets.

Keywords Ticket market · Static environment · Mechanism design · Multiple demand

S. Mukhopadhyay (✉) · N. RamTeja
Department of Information Technology, National Institute of Technology, Durgapur,
West Bengal, India
e-mail: sajmure@gmail.com

N. RamTeja
e-mail: teja48@gmail.com

D. Ghosh
Department of Computer Science and Engineering, National Institute of Technology,
Durgapur, West Bengal, India
e-mail: profdg@yahoo.com

N. C. Debnath
Department of Computer Science, Winona State University, Winona, USA
e-mail: Ndebnath@winona.edu

1 Introduction

When the available tickets of any event is sold by the event organizers, huge market is created in terms of selling the available tickets against a huge demand of tickets. This market is termed as TM or Ticket Industry (TI) [1–3]. One can buy a ticket at a ticket window or counter by appearing physically or can buy a ticket online. The ticket booking options mentioned in the literature constitute two big markets for selling tickets for entertainment industries namely *Primary Market, and Secondary Market*. When the organizer of the entertainment event directly sells the tickets, the market created by that situation is called the primary market [2, 11]. Sometimes the tickets are sold to the third parties and then those third parties resale the tickets. The market created via the third parties is called secondary market [2, 6, 11]. One does not see or hear the same way from two different seats in the premises. Based on the quality of the seats different categories of seats are available in the premises [2, 7, 10]. In this paper 4 categories of seats are considered. In the primary and secondary markets tickets are sold at present mainly with *first come first serve* (FCFS) basis. In this scheme whoever comes first get the ticket(s) and ticket is sold with a fixed price. For different categories of seats different fixed price is set for the FCFS scheme. Even though the FCFS scheme is the most popular one but *it doesn't provide equal opportunity* for everybody purchasing the tickets. Recently in [8, 12, 13] alternative solutions are proposed using the MD framework against the FCFS scheme when a single ticket is demanded from each agent in static environment. In static environment the participating agents wait up to a stipulated time set by the event organizers. In this paper the total stipulated time is divided into three slots. However it can be a single slot only. The three slots are considered as this will provide the opportunity for the agents coming earlier for their journey or admission to the arena if they are allocated the ticket(s). For further details of mechanism design one can see [5, 9] and for auctions and its applications refer [9, 15, 17].

In selling tickets the most realistic situation is to allow multiple bids from a single agent. In this multiunit demand environment multiple persons (agents, bidders synonymously will be used) are in a competitive environment and they can give the demand for at most k tickets that are available for sale. The bids can be given either coming to the centre directly or through any e-environment. The bids given by the agents are collected up to the stipulated time and then an auction is run to allocate the tickets to the competing agents participating in the auction. If there is m number of tickets available to the event organizers, the available tickets are distributed in three different slots proportionately. In each of the proposed algorithms, three times the auction are run. However, how many rounds the auction will be run depends on the auctioneer. In this paper three has been chosen heuristically. It can be any small constant.

Rest of the paper is organized as follows. Characterization of the problem is given in Sect. 2 that will be helpful to clarify the notations that are used in subsequent sections. In Sect. 3 the existing scheme is discussed. The proposed

mechanisms are explored in Sect. 4. In Sect. 5 the proposed schemes are compared with the existing schemes with stylized experiments and data sets. In Sect. 6 conclusions and future works have been given.

2 Characterization of the Problem

Each customer of the tickets is represented by an agent or a bidder and they can give demand for the multiple tickets. Let $I = \{1, 2, \dots, n\}$ denote the set of all agents. The agents may reveal their true valuation or may misreport. The type of an agent is described by $\hat{\theta}_i = (\hat{v}_i)$. Here \hat{v}_i is the marginal valuation vector and formally the valuation vector could be defined as $\hat{v}_i = \langle \hat{v}_{i,1}, \hat{v}_{i,2}, \dots, \hat{v}_{i,m_i} \rangle$ where $\hat{v}_{i,j}$ denotes the marginal value of agent i for the j th unit and m_i is the maximum demand from agent i that is $\hat{v}_{i,k} = 0$ for $k > m_i$. Here $\hat{\theta}_i$ is introduced with the fact in mind that the agents can misreport their valuations. Here $\hat{\theta} = \{\hat{\theta}_1, \dots, \hat{\theta}_n\}$ denotes the reported type of all agents and $\hat{\theta}_{-i}$ is the types of all agents except i . Winners will be selected from all of the feasible outputs \mathcal{O} . The valuation function of an agent $i \in I$ is given by $\hat{\theta}_i : \mathcal{O} \rightarrow \Re$. Here $\hat{\theta}_i = \theta_i$ indicates the fact that the agent reports its type truthfully. The utility of an agent is denoted by u_i and is given by

$$u_i(o) = \theta_i(o) - p_i \tag{1}$$

where $\theta_i(o)$ is an agent's valuation given its *true type (not its declaration)* Loser pay zero and its utility is also zero. Top allocation as chosen by the auctioneer is given as

$$x^* = \operatorname{argmax}_{o \in \mathcal{O}} \sum_{i=1}^n \hat{\theta}_i(o) \tag{2}$$

Top allocation as chosen by the auctioneer if agent i were not present in the auction

$$x^*_{-i} = \operatorname{argmax}_{o \in \mathcal{O}_{-i}} \sum_{i=1}^n \hat{\theta}_i(o) \tag{3}$$

3 Existing Scheme

The main existing scheme that is prevailing in the ticket market for selling multiple tickets against the multiunit demand by the agents is FCFS. In FCFS scheme the agents line up in a queue in front of a counter and get the tickets if the tickets

are not exhausted when their turn has come. In e-environment the demand is given with some electronic medium (such as Internet) and the tickets are allocated instantly until exhausted. An agent may purchase multiple tickets.

4 Proposed Algorithms

To the best of our knowledge in TM, the main algorithm that is used is FCFS when multiple demands for the tickets are allowed. In this paper three algorithms have been tried in one place against the FCFSM and comparisons are made accordingly. The three algorithms proposed here are: (1) Multiunit First Price Auction for multiple demands (MFPAM), (2) Multiunit Second Price Auction for multiple demands (MSPAM), (3) Multiunit VCG Mechanism for multiple demands (MVCGM).

4.1 Multiunit First Price Auction for Multiple Demand

The MFPAM algorithm for TM allocates the tickets to the top most m' bidders in each round if m' tickets are available for sale. MFPAM charges each bidder their own bid price $\hat{v}_{i,j}$ if they are selected as winners' for its j th bid according to Eq. 4. The Overall time complexity of MFPAM is $O(n^2)$ as $m \leq n$.

$$p_i(\hat{\theta}_1, \dots, \hat{\theta}_n) = \begin{cases} \hat{v}_{i,j}, & \text{if } i \text{ wins for } j\text{th bid} \\ 0, & \text{Otherwise} \end{cases} \quad (4)$$

4.2 Multiunit Second Price Auction for Multiple Demand

It can be shown easily with a counter example that the MFPAM mechanism is vulnerable to manipulation and hence truth-telling is not an equilibrium bidding strategy for the agents. This fact leads to instability in the system, which in turn leads to inefficient investments on behalf of the agents. However in MSPAM some incentives are given to the winning bidders and because of that it is less prone to manipulation.

4.2.1 Algorithm

The MSPAM algorithm for ticket market allocates the tickets to the topmost bidders and each winning bidder is charged to the next highest bidder's bid price

(other than this agent) if they are selected as winners according to Eq. 5. Here $Ext_{j \neq i}(\cdot)$ is an operator that extracts the valuations of the other agents whose valuation is just below that agent's valuation for whom the payment is calculated. Say for example the payment of agent i is to be calculated and say it has given demand for two tickets. Further assume that apart from this agent another two agents are participating and each of them has given one unit demand for the tickets. After sorting say, agent i is at first and third position according to the allocation rule. So in this case $Ext_{j \neq i}(\cdot)$ will extract the bid price of second and fourth agent and agent i will pay this two agent's bid price. Here l is the number of tickets an agent being allocated. The symbol \in is denoting the fact that an agent winning the ticket(s) will pay \in plus the valuations of the other agents whose bid price is just below him. In this paper the payment is considered with $\in = 0$. The overall time complexity of MSPAM is $O(n^2)$ as $m = O(n)$.

$$p_i(\theta_1, \dots, \theta_n) = \begin{cases} Ext_{j \neq i}(\theta_1, \dots, \theta_n) + l * \in & \\ 0, & \text{Otherwise} \end{cases} \tag{5}$$

4.3 Multiunit Vickery-Clarke-Groves Mechanism for Multiple Demands

The algorithm stated in MSPAM is not dominant strategy incentive compatible (DSIC) as it can be shown that by manipulation an agent can gain. In this section an algorithm motivated by the celebrated VCG mechanism is proposed that is DSIC i.e. in this mechanism an agent can't gain by manipulation. In this scheme Vickery auction with *Clarke's pivot rule* is used [4, 14, 16]. The proposed algorithm is named as Multiunit Vickery-Clarke-Groves Mechanism for multiple demands (MVCGM).

$$p_i(\theta_1, \dots, \theta_n) = \sum_{i \neq j} \theta_j(x_{-i}^*) - \sum_{i \neq j} \theta_j(x^*) \tag{6}$$

4.3.1 Algorithm

In each round MVCGM algorithm for ticket market allocate the tickets to the top m' bidders and charges each of them the damage he has done to the system, if they are selected as winners according to Eq. 6 (formed by combining Eqs. 2 and 3). Here $\sum_{i \neq j} \theta_j(x_{-i}^*)$ represents the total valuation when agent i is *not participating* in the auction and $\sum_{i \neq j} \theta_j(x^*)$ represents the total valuation of all other agents except i when agent i is *participating* in the auction. However the losers pay 0. In the

MVCGM algorithm the central idea is that an agent’s bids are considered in the subsequent rounds with the *available bids*, even if his bids are allocated in the earlier rounds. In each round except the first, two auctions are run: In the first auction the allocation is done for the currently available bids that are yet to be allocated. The winner’s payment is stored in an appropriate data structure called the payment vector in this paper. In the second auction the agents already allocated are checked with the current available bids. This auction is termed as a *dummy auction* (DA) in this paper. Whatever payment is calculated in this dummy auction is stored as the element of the payment vector so far created. This idea of the dummy auction ensures that an agent’s payment can be updated and he can’t gain by misreporting its type. After running all the auctions, the payment of each winning agent is finalized. The extra amount, if any, is repaid to the winning agents. The overall time complexity of the MVCGM is $O(n^3)$. Algorithm MVCGM can be better illustrated with an example given in Fig. 1. Here six tickets are available for sell. 3 tickets are kept in the first round and one is kept in second and two are in third round. In this example the payment calculation and its corresponding payment vector is shown for agent 1. In the payment vector, (1, 5) is indicating that the agent 1 has to pay 5 and so on for others. The payment and its corresponding payment vector for the other agents can be shown similarly.

4.3.2 The Proof of DSIC of MVCGM

We can claim the MVCGM algorithm is DSIC. The DSIC mechanism indicates that truth telling is the best response from the agents.

Theorem 1 The 3-round MVCGM algorithm is dominant strategy incentive compatible.

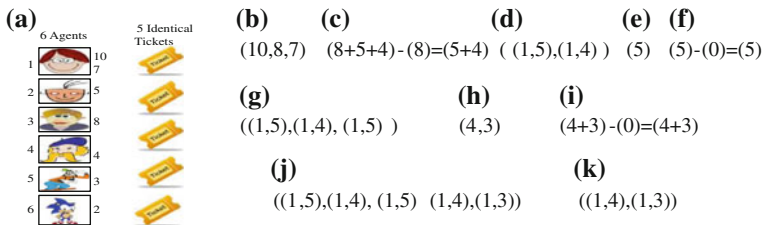


Fig. 1 Illustrative example for MVCGM. **a** Multiple demands from six agents. **b** Valuation of the winners at $t = 1$ when three tickets available. **c** Payment of the 1st agent at $t = 1$. **d** Payment vector showing only of 1st agent **e** winners at $t = 2$ when one ticket available. **f** Payment of the 1st agent after the DA at $t = 2$. **g** Payment vector showing only of 1st agent at $t = 2$. **h** winners at $t = 3$ when two tickets available. **i** Payment of the 1st agent after the DA at $t = 3$. **j** Payment vector showing only of 1st agent at $t = 3$. **k** The final payment vector of the 1st agent

Before going to the proof let us define the utility function again by considering Eq. 1. $u_i(o) = \theta_i(o) - p_{i,j}^r$, where $p_{i,j}^r$ is the payment of the winning bidder i in some particular round r for j th ticket allocated.

Proof The proof is divided into two parts:

(a) *In the particular round where the bidder wins:*

Case 1: Suppose his true bid is $v_{i,j}$ and he wins. His utility is $u_{i,j} = \hat{\theta}_i(o) - p_{i,j}^r \geq 0$. Now, for an attempted manipulation $v'_{i,j} \geq p_{i,j}^r$, i will still win and would still pay $p_{i,j}^r$. Hence $u'_{i,j} = u_{i,j}$, that is evident from the definition of the utility. We can say no gain is achieved as long as he is winning. However for $v'_{i,j} \leq p_{i,j}^r$, i would lose, so $u'_i = 0 < u_i$. Similar logic can be given if an agent deviates by more than one bid price.

Case 2: If i loses by bidding $v_{i,j}$, then $u_i = 0$. Let j be the last bidder who is in the winning set x^* (the set is considered sorted in descending order of the bid values without loss of generality). Further assume that his true bid is $v_{j,j}$, thus $v_{j,j} \geq v_{i,j}$. For an attempted manipulation, $v'_{i,j} \leq v_{j,j}$, i would still lose and so, $u'_i = 0 = u_i$. The bidder i would win, if $v'_{i,j} \geq v_{j,j}$. But he would pay $v_{j,j}$. Thus his utility would be $u'_i = v_{i,j} - v_{j,j} \leq 0 = u_i$. In this case instead of gaining, he is paying more than his true valuation. In the similar line of argument we can say that if j be any arbitrary bidder in the winning set, the same negative utility will be achieved by misreporting the value. This logic is true for part or full deviation from the losers.

(b) *Considering all the 3-rounds:* In this case the question is: any bidder i , winning at any round r , is it possible for him to achieve some gain by deviating from his true value v_i or reporting his value v_i and participating in later rounds? The claim is no. Why? By reporting the true value v_i at that round his utility will be $u_i = v_i - p_i^r$. We have already seen attempted manipulation in the same round will not increase his utility. Now, if he decides to participate in the next round by reporting his true value v_i and he wins, his utility $u'_i = v_i - p_i^{r'}$ where $p_i^{r'}$ is the payment made by the bidder i at some later round r' . In this case utility increased is $u'_i - u_i = (v_i - p_i^{r'}) - (v_i - p_i^r) = p_i^r - p_i^{r'}$. Now if $p_i^r - p_i^{r'} \leq 0$, then $u'_i < u_i$. Hence no gain is achieved. If $p_i^r - p_i^{r'} \geq 0$, then $u'_i \geq u_i$. In this case gain can be achieved, but from the payment rule of the algorithm it is clear that if $p_i^r - p_i^{r'} \geq 0$ then, this extra amount is repaid to the bidder based on the updated payment vector at the end of the last round. Hence by participating in the next round by reporting his true value will not increase his gain. By deviating from his true value will not achieve any gain can be proved in the similar line of argument in Case 1 and Case 2.

5 Comparisons of the Proposed Schemes

Here all algorithms are compared for the Gumbel (left skewed) distribution and Gumbel (right skewed) distribution with several cases. In each distribution 1000 values are considered with mean 1000 and standard deviation 50. The bid valuations of the agents are assumed to follow the close interval (b, c) where $b = FCFS$ price and $c = 4 * FCFSprice$. The unit of the bid valuations is considered as \$. In the x axis the total available tickets are shown. The interpretation is that, the range of the total number of tickets available is 100 – 400 depending on the number of seats available in the event or the number of tickets to be sold in terms of auction. In y axis the income is shown against the available tickets and scaled down to 1000. The income is considered after selling all the categories of tickets. For the experiments the income is interpreted as the total amount earned after selling the tickets. The left skewed data has been chosen to get substantial data to be less than the mean. The right skewed data has been chosen to get substantial data to be more than the mean. A simple probabilistic calculation can show that 1/2 of the bidders can deviate in expectation. The medium and large amount of deviation is taken heuristically. In this paper 1/6 amount of bid price is taken as the large amount of deviation and 1/8 amount of bid price is taken as medium deviation (Figs. 2 and 3).

5.1 For Gumbel (left skewed) Distribution and Gumbel (right skewed) Distribution

In the case of medium deviation by half of the bidders it is shown that the income from the truthful auction (MVCGM) coming close to the MSPAM and MFPAM. It is shown in Figs. 4 and 5. However for large GR distribution MVCGM is slightly better. But for the case large large deviation by half of the bidders it is shown that the income from MVCGM is a good choice compared to MFPAM and MSPAM. It is

Fig. 2 Half of the agents deviating large in GL

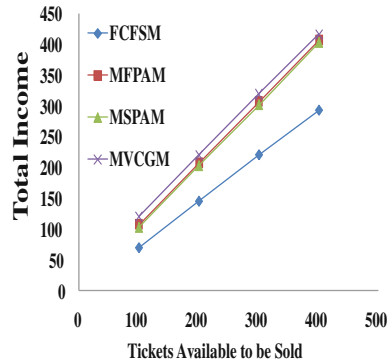


Fig. 3 Half of the agents deviating large in GR

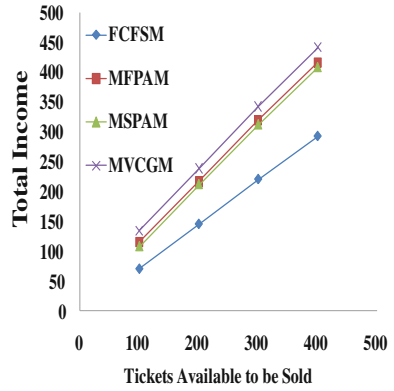
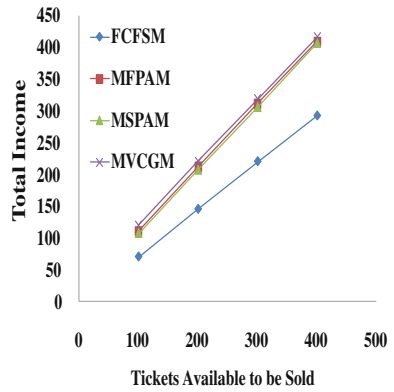


Fig. 4 Half of the agents deviating medium in GR



depicted in Figs. 2 and 3. In Fig. 6 social efficiency is considered. The social efficiency signifies the fact that how many agents will deviate from their true value in MFPAM and MSPAM compared to MVCGM. The less will be the deviation the more will be their social efficiency. As some incentives are given to MSPAM, it

Fig. 5 Half of the agents deviating medium in GR

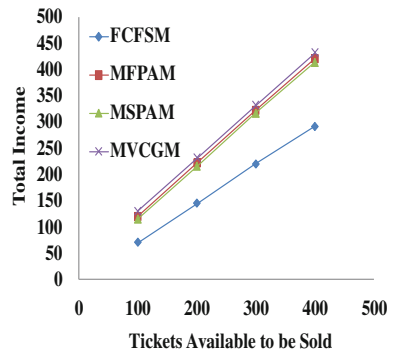
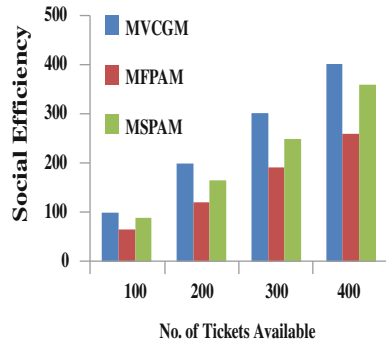


Fig. 6 Social efficiency when half of the agents deviate



will be less prone to deviation that is simulated in the graphs. The social efficiency of MVCGM is 100 % as it is DSIC.

6 Conclusions and Future Works

In this paper alternative solutions are proposed in selling tickets for the TM where a single agent can give demand for multiple tickets in static environment. Both DSIC and non-DSIC mechanisms were proposed in the current paper. In this paper a reservation price is set below which an agent's bid(s) will not be accepted. However what could be the optimal reservation price is not mathematically justified. What should be the optimal reservation price, in this environment, so that the optimal profit and social efficiency can be achieved, could be an interesting future work.

References

1. Courty P, Paglioreo M (2012) The pricing of art and art of pricing. In Thorsby EV (ed) The hand book of economics of art and culture, vol 2
2. Courty P (2000) An economic guide to ticket pricing in the entertainment industry. *Louvain Econ Rev* 66(2):167–192
3. Courty P (2003) Some economics of ticket resale. *J Econ Perspect* 17(2):85–97
4. Clarke E (1971) Multipart pricing of public goods. *Public Choice* 11:17–23
5. Arrow K (1951) *Social Choice and Individual Values*. Yale University Press, New Haven
6. Krueger AB (2005) The economics of real superstars: the market for concerts in the material world. *J Labour Econ* 23(1):1–30
7. Leslie P (2004) Price discrimination in boardway theatre. *RAND J Econ* 35(3):520–541
8. Mukhopadhyay S, Singh RK, Ghosh D, Bhattacharjee J et al (2010) An efficient auction based ticket booking scheme for indian cinemas. In: International conference on recent trends in Business Administration and Information Processing (BAIP), pp 376–381
9. Nisan N, Roughgarden T, Tardos E, Vazirani VV (2007) *Algorithmic game theory*. Cambridge University Press, New York

10. Rosen S, Rosenfield AM (1997) Ticket pricing. *J Law Econ* 40(2):351–76
11. Happel S, Jennings M (2002) Creating a future markets for major events tickets: problems and prospect. *CATO J* 21(3):443–461
12. Mukhopadhyay S, Ghosh D, Debnath NC (2012) A new framework for an efficient ticket booking scheme based on mechanism design. *J Comput Methods Sci Eng* 12:13–27
13. Mukhopadhyay S, Jose M, Debnath NC, Ghosh D (2013) An efficient multiunit VCG mechanism for ticket booking scheme of J-league football tournament. In: 8th IEEE international conference on industrial informatics, INDIN, pp 704–707
14. Groves T (1973) Incentives in teams. *Econometrica* 41:617–631
15. Vries de S, Vohra RV (2003) Combinatorial auctions: a survey. *inform. J Comput* 15(1):284–309
16. Vickery W (1961) Counterspeculation, auctions and competitive sealed tenders. *J Finan* 16(1):837
17. RamaSuri N, Narahari Y, Garg D, Prakash H (2009) Advanced information and knowledge processing series in game theoretic problems in network economics and mechanism design solutions. Springer, London

A Decision Tree-Based Classification Model for Crime Prediction

Aziz Nasridinov, Sun-Young Ihm and Young-Ho Park

Abstract The growing availability of information technologies has enabled law enforcement agencies to collect detailed data about various crimes. Classification techniques can be applied to these data to build decision-aid tools and facilitate investigations of law enforcement agencies. In this paper, we propose an approach for constructing a decision tree based classification model for a crime prediction. Proposed model assists law enforcement agencies in discovering crime patterns and predicting future trends. We provide an implementation and analysis of our proposed method.

Keywords Crime prediction · Classification · Decision tree user experience

1 Introduction

The growing availability of information technologies has enabled law enforcement agencies to collect detailed data about various crimes [1]. Criminologists and statisticians have been using their skills and knowledge trying to analyze these data, with varying degrees of success. However, the volume of crime and the greater awareness of modern criminals have made the process of analyzing the crime data difficult, because human reasoning fails when he is presented with

A. Nasridinov (✉) · S.-Y. Ihm · Y.-H. Park
Department of Multimedia Science, Sookmyung Women's University,
Cheongpa-ro 47-gil 100, Yongsan-Ku, Seoul 140-742, Korea
e-mail: aziz@sookmyung.ac.kr

S.-Y. Ihm
e-mail: sunnyihm@sookmyung.ac.kr

Y.-H. Park
e-mail: yhpark@sookmyung.ac.kr

millions of records. Therefore, there is a requirement for a technique to assist in analyzing the crime data. Data mining techniques can be applied to facilitate this task.

Data mining is a process concerned with uncovering patterns, associations, anomalies, and statistically significant structures and events in data. It is defined as the process of discovering meaningful new correlations, patterns and trends, often previously unknown, by sifting through large amounts of data, using pattern recognition, statistical and mathematical techniques [2]. It can help us not only in knowledge discovery, that is, the identification of new phenomena, but also it is useful in enhancing our understanding of known phenomena. One of the key steps in data mining is a classification task. Classification is the procedure to build a rule using the pre-defined classes and their features in dataset and apply this rule to a new data for discriminating each observation [3]. Classification techniques can be applied to the crime data to build decision-aid tools and facilitate investigations of law enforcement agencies.

In this paper, we propose an approach for constructing a decision tree based classification model for a crime prediction. The decision trees represent a supervised method to classification. It is a tree structure, where non-terminal nodes represent tests on one or more attributes and terminal nodes reflect decision outcomes. In the context of our proposed approach, the decision tree classification model assists law enforcement agencies in discovering crime patterns and predicting future trends. We also provide an implementation and analysis of our proposed method.

The rest of the paper proceeds as follows. In [Chap. 2](#) we present related work. In [Chap. 3](#) we describe our proposed method. [Chapter 4](#) shows our implementation. [Chapter 5](#) highlights conclusion.

2 Related Work

Data mining is a powerful tool, which enables law enforcement agencies to discover patterns and predict the future crimes. There have been numerous research on applying data mining techniques to crime data.

Chen et al. [4] categorized different crime types and proposed some techniques to mine crime data such as entity extraction and association rule mining. They also developed a framework that identifies the relationships between crime types and data mining techniques applied in crime data analysis. The developed framework helps investigators to find associations and identify patterns to make predictions. They implemented some case studies and showed their developed framework can help increase efficiency and reduce errors.

Liu et al. [5] proposed a STT (spatio-temporal-textual) search engine for extracting, indexing, querying and visualizing crime information. They give scores to each of the data factors (spatial, temporal, and textual) and use the score to rank the data. This tool helps crime detection for investigators, identification of crime

trends and patterns for decision makers and researchers, and security of city life for residents and journalists. Shah et al. [6] proposed CROWDSAFE, a novel convergence of Internet crowd sourcing and portable smart devices to enable real time, location based crime incident searching and reporting. It is targeted to users who are interested in crime information. The system leverages crowd sourced data to provide novel features such as a Safety Router and value added crime analytics. In addition to the demonstration of hotspots, CROWDSAGE also provides crime clusters, historical crime statistics to the users in a dashboard interface.

3 Proposed Method

In this chapter, we will describe the proposed approach in details. Our approach is to construct a decision tree based classification model for a crime prediction. Proposed model assists law enforcement agencies in discovering crime patterns and predicting future trends. Overall design of proposed approach is shown in Fig. 1.

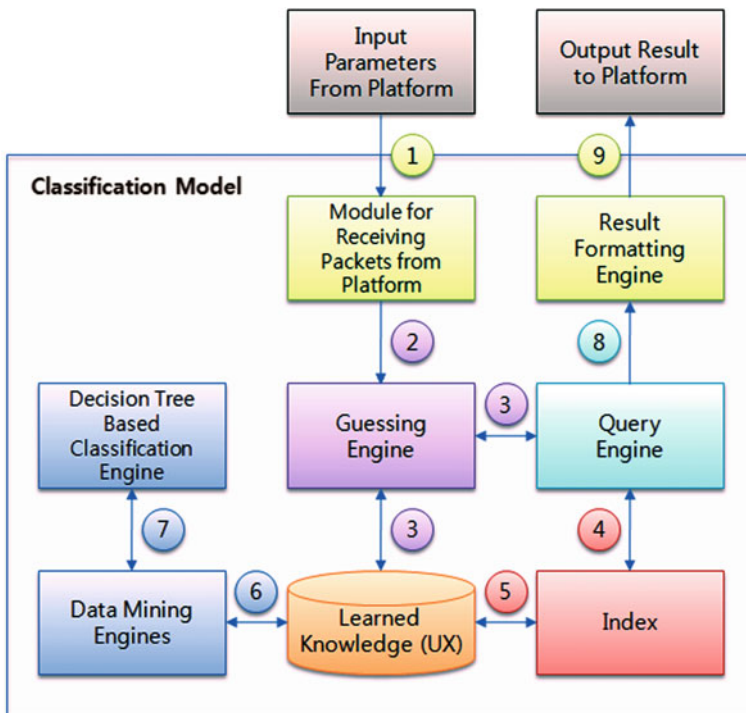


Fig. 1 Overall design of proposed method

Detailed description of proposed method is given through the following steps:

Step 1. As a part of a global platform, classification model receives input parameters from the platform as packets. Input parameters could be captures of facial emotion, heartbeat rate, voice tone and so on.

Step 2. There could be situations, where there is no result from the data mining engine and approximate answer is needed to be replied. Guessing engine is responsible to do this action using the some abbreviated clues.

Step 3. Guessing engine seeks a potential result in a database of learned knowledge (user experiences, UX). The learned knowledge module is responsible for storing data on a database. Guessing engine can directly access to the database or in order to speed up the lookup process, it may access to the database through the query engine.

Steps 4 and 5. Database is indexed and queried using a query engine. The query engine is responsible for query processing, distributing the queries to underlying data sources for execution, and collecting the query results. The index technique is used for implementing a faster lookup within a database.

Step 6. Discovering crime patterns and predicting future trends through the data stored in the database is performed. In this step, the data mining engines are responsible to do this task.

Step 7. The observations made in the data mining engine are carefully examined, crime patterns are discovered, and future trends are predicted. The classification engine is responsible for the maintenance of a standard classifier. It employs the decision tree learning algorithm so that the performance of the data mining engines can be improved. This engine will be explained in details in the [Sect. 3.1](#).

Step 8. The obtained results are formatted according to the format requested by a platform.

Step 9. Formatted results are returned to the platform.

3.1 Classification using Decision Tree

One of the key steps in data mining is classification task. Classification is the procedure to build a rule using the pre-defined classes and their features in dataset and apply this rule to a new data for discriminating each observation. When classification is used, existing dataset can easily be understood and it will help to predict how new events will behave based on the classification criteria.

Decision tree is one of the well-known classification techniques. It builds classification in the form of a tree structure and divides a dataset into smaller subsets. At the same time an associated decision tree is incrementally developed. The final result is a tree with decision nodes and leaf nodes. A decision node has two or more branches. Leaf node represents a classification or decision. The topmost decision node in a tree, which corresponds to the best predictor called root node [7]. Decision algorithm used in our approach is shown in [Fig. 2](#).

Algorithm decisionTree(D, A, T)⁴
Input: Crime attributes (UX attributes)⁴Output: Decision tree on the bases of UX attributes⁴

```

1  if  $D$  contains only training examples of the same class  $c_j \in C$  then
2    make  $T$  a leaf node labeled with class  $c_j$ 
3  elseif  $A = \emptyset$  then
4    make  $T$  a leaf node labeled with  $c_j$ , which is the most frequent class in  $D$ 
5  else //  $D$  contains examples belonging to a mixture of classes. We select a single
6    // attribute to partition  $D$  into subsets so that each subset is purer
7     $p_0 = \text{impurityEval} - 1(D)$ ;
8    for each attribute  $A_i \in \{A_1, A_2, \dots, A_k\}$  do
9       $p_i = \text{impurityEval} - 2(A_i, D)$ ;
10   end
11   Select  $A_g \in \{A_1, A_2, \dots, A_k\}$  that gives the biggest impurity reduction,
      computed using  $p_0 - p_g$ 
12   if  $p_0 - p_g < \text{threshold}$  then //  $A_g$  does not significantly reduce impurity  $p_0$ 
13     make  $T$  a leaf node labeled with  $c_j$ , the most frequent class in  $D$ 
14   else
15     Make  $T$  a decision node on  $A_g$ 
16     Let the possible values of  $A_g$  be  $v_1, v_2, \dots, v_m$ . Partition  $D$  into  $m$ 
      disjoint subsets  $D_1, D_2, \dots, D_m$  based on the  $m$  values of  $A_g$ .
17     for each  $D_j$  in  $\{D_1, D_2, \dots, D_m\}$  do
18       if  $D_j \neq \emptyset$  then
19         create a branch (edge) node  $T_j$  for  $v_j$  as a child node of  $T$ ;
20         decisionTree( $D_j, A - \{A_g\}, T_j$ ) //  $A_g$  is removed
21       end
22     end
23   end
24 end

```

Fig. 2 Decision tree algorithm used in proposed method

In this algorithm, D is the set of input attributes; A is the output attributes; T is a set of training data. In lines 1 and 2, if D contains only training examples of the same class then we assign T as a leaf node. In the lines 3 and 4, if A does not have any output attributes then we make T a leaf node, which is the most frequent class in D . In lines 5 and 6, if D contains examples belonging to a mixture of class, we select a single attribute to partition D into subsets. In this case, the key to building a decision tree is which attribute to choose in order to branch. The objective is to reduce impurity or uncertainty in data as much as possible. This is performed in line 7.

In this algorithm, we use a measure called Information Gain, which calculates the reduction in Entropy that would result on splitting the data on attribute, A . So given a set of example D , we first calculate its Entropy as following:

$$entropy(D) = - \sum_{j=1}^{|c|} Pr(c_j) \log_2 Pr(c_j) \quad (1)$$

where $Pr(c_j)$ is the probability of class c_j in dataset D . If we make attribute A_i , with v values, the root of current tree, this will partition D into v subsets D_1, D_2, \dots, D_v . Lines 8, 9, 10 perform this action. The expected entropy of A_i is used as the current root:

$$entropy_{A_i}(D) = \sum_{j=1}^v \frac{|D_j|}{|D|} * entropy(D_j) \quad (2)$$

Information gained by selecting attribute A_i to branch or to partition the data is as following:

$$gain(D, A_i) = entropy(D) - entropy_{A_i}(D) \quad (3)$$

We choose the attribute with the highest gain to branch/split the current tree, which is line 11 of the algorithm. In lines 12 and 13, if gain does not significantly reduce impurity then make T a leaf node, which is the most frequent class in D . In lines 14, 15 and 16, if gain is able to reduce impurity then we make T a decision node. In lines 17, 18, 19, if subsets attributes are not empty then we create a branch (edge) node for leaf node. In line 20, we repeat lines 1 to 20 without selected leaf node.

4 Implementation

In this chapter, we demonstrate how to apply the decision tree algorithm described in [Chap. 3](#) on a real life example. Attribute selection is the fundamental step to construct a decision tree. We used attributes shown in [Table 1](#). These attributes indicate various UX-based crime situations in the past. In [Table 1](#), Facial Emotion, Heartbeat Rate, Voice Tone and State denotes attributes. Among these attributes State attribute refers as a class or classifier. Because based on Facial Emotion, Heartbeat Rate, Voice Tone, we need to decide whether state is dangerous or neutral, therefore State is a classifier to make a decision.

We implemented proposed approach, which is described in [Sect. 3](#). We used Java language and NetBeans 6.5 IDE. We classify crime data using decision tree into two classes, such as danger and neutral. Using this method, we have obtained a classifier tree shown in [Fig. 3](#).

In this tree, nodes belong to the crime data attributes. Tracing these nodes, we could reach leave nodes, which represent the classification of the crime. For example, if the body sensors indicate low heartbeat then there is no reason to see

Table 1 Dataset used in decision tree

Heartbeat rate	Voice tone	Facial emotion	State
Low	Loud	Fear	Neutral
Low	Loud	Anger	Neutral
Low	Loud	Surprise	Neutral
High	Loud	Fear	Danger
High	Loud	Anger	Danger
High	Loud	Surprise	Neutral
Low	Low	Fear	Neutral
Low	Low	Anger	Neutral
Low	Low	Surprise	Neutral
High	Low	Fear	Neutral

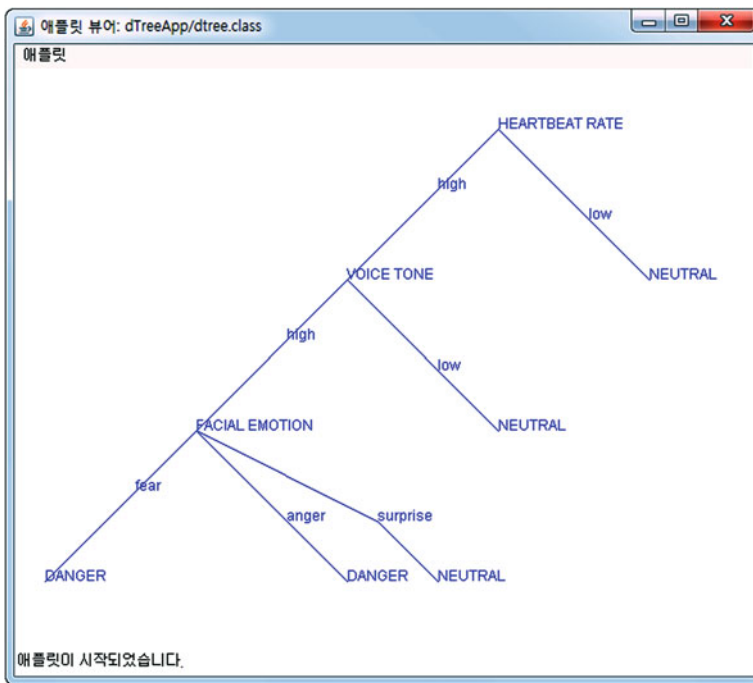


Fig. 3 Decision tree generated by a dataset in Table 1

the parameters. If heartbeat is low then the situation is neutral. If body sensors demonstrate the high heartbeat and there is no noise by the victim it is a neutral case too. However, it is dangerous situation when heartbeat rate is high, voice tone is high and facial emotion is fear or anger. Using our implementation, we could discover crime patterns and predict future trends.

5 Conclusion

In this paper, we have proposed a methodology for constructing a decision tree model of crimes on the basis of the user experiences. The decision tree can infer the characteristics of an unknown crime, and helps police in discovering patterns and predicting future crimes. We provided an implementation and analysis of our proposed method using a real life example in crime situation. The result of implementation has resulted in a decision tree, which classifies crime cases into two classes such as danger and neutral. Results of our implementation and analyses are good enough to motivate us to use decision tree in order to discover patterns and predicting the future crimes.

Acknowledgments This work was supported by the IT R&D program of MKE/KEIT. [10041854, Development of a smart home service platform with real-time danger prediction and prevention for safety residential environments].

References

1. Baumgartner K, Ferrari S, Palermo G (2008) Constructing Bayesian networks for criminal profiling from limited data. *Knowl Based Syst* 21(7):563–572
2. Fayyad UM, Piatetsky-Shapiro G, Smyth P (1996) The KDD process for extracting useful knowledge from volumes of data. *Commun ACM (Special Issue on Data mining)* 39(11):27–34
3. Lim N (2007) Classification by ensembles from random partitions using logistic regression models. Dissertation
4. Chen H, Chung W, Xu JJ, Wang G, Qin Y, Chau M (2004) Crime data mining: a general framework and some examples. *The Comp* 37(4):50–56
5. Liu X, Jian C, Lu CT (2010) A spatio-temporal-texture crime search engine. In: *Proceeding of the 18th SIGSPATIAL international conference on advances in geographical information systems*, pp 528–529
6. Shah S, Boa F, Lu CT, Chen IR. (2011) CROWDSAFE: Crowd sourcing of crime incidents and safe routing on mobile devices. In: *Proceedings of the 18th SIGSPATIAL international conference on advances in geographical information systems*, pp 521–524
7. Wang B, Dong H, Boedihardjo AP, Lu CT, Yu H, Chen IR, Dai J (2012) An integrated framework for spatio-temporal-textual search and mining. In: *Proceeding of the 20th SIGSPATIAL international conference on advances in geographical information systems*, pp 570–573
8. Yousef M, Najami N, Khalifa WA (2010) A comparison study between one-class and two-class machine learning for MicroRNA target detection. *J. Biomed. Sci. Eng.* 247–252

Part III
Artificial Intelligence Applications
for E-Services

Innovation Performance on Digital Versatile Disc (DVD) 3C Patent Pool Formation

Yu-Hui Wang

Abstract Theoretical suggestions are inconsistent with empirical findings about whether patent pools encourage innovation domain. This paper empirically examines the firm-level innovation on patent pool formation. In order to empirically investigate the variance of the innovation performance of patent pool, this paper proposes hypothesis for post-formation innovation performance in comparison to pre-formation one in the DVD (Digital Versatile or Digital Video Discs) 3C pool members. This paper employs well-used patent quality indicator- forward citation count as patent quality measurement. To further test the hypothesis, this paper will apply one-sample *t*-test to conclude whether the mean of the post-formation forward citation count significantly declines comparing with the pre-formation one. Based on the result, this paper aims to verify whether patent pools formation slow down patent innovation performance from firm-level perspective and contribute to the growing literature on the effect of institutional innovations on the follow-on innovation.

Keywords Innovation • Patent pool • DVD 3C • Patent quality • Forward citation

1 Introduction

Federal Trade Commission (FTC) report noted that in certain industries the large number of issued patents makes it virtually impossible to identify all the potentially relevant patents, review their claims and evaluate the infringement risk or the need for a license [1]. Company may encounter overlapping or fragmented intellectual property rights owned by different companies that must be combined

Y.-H. Wang (✉)
National Taipei University of Technology, Taipei City,
Taiwan
e-mail: isecho@ntut.edu.tw

before technology commercialization [2]. Patent pools which involve patents from multiple patentees for the purpose of pooling a group of patents into a single licensing package is a readily available tool used for overcoming the potentially harmful effects of overlapping or blocking patent rights [3].

Many of the economic analysis of patent pools to date has focused on their role in economy effect and competition policy [4]. Recent work by Hall and Ziedonis [5] and Joshi and Nerkar [6] demonstrated whether patent pools encourage innovation domain. While prevailing theories generally suggest that modern pools would boost firms' innovative performance, recent empirical works have raised some serious implications about the intricacies of patent tools at the micro level [7]. Theoretical models of patent pools suggest that pools encourage innovation for the reason that lower risks of litigation and improved licensing schemes increase expected profits for participating firms, and thus it increases firms' incentives to invest in R&D.

However, Farrell and Katz [8] stated a patent pool aggregates fragmented IP rights into a single package for licensees and the innovation incentives of all of the firms in the industry change substantially subsequent to the pool formation. Lampe and Moser [9] find a significant decline in the innovation rate of both groups in the sewing machine industry after the formation of the Sewing Machine Combination. Similarly, studying three modern pools in the optical disk industry, Joshi and Nerkar [6] find once a patent pool is formed; the pool licensors generate less and lower quality patents in the technology field relating to the patent pool relative to those of nonparticipants.

In order to identify the inconsistent theoretical predictions and empirical findings, this paper proposes to empirically examine the firm-level innovation on patent pool formation. This paper empirically investigates the variance of the innovation performance of DVD 3C pool members. The innovation performance of each licensor will be separately analyzed. This paper aims to provide a better understanding of how formation of patent pools affects the innovation performance from firm-level perspective.

2 Institutional Background: DVD 3C Patent Pool

The massive global optical disc industry is made possible by the systemic innovation of digital audio-visual technology and it represents a market in which multiple patent pools have been formed by competing firms [6]. During a two-year period, from June 1997 to June 1999, the DOJ approved the formation of three patent pools closely related to systemic innovation in digital video technology.

The main benefit of the Moving Picture Experts Group 2 (MPEG-2) standard is the efficient coding of images, video, and audio into a compressed digital format that enables storage in a small file size with high quality [6]. In June 1997, the MPEG-2 pool became the first patent pool to receive the DOJ's approval. DVDs are used for the storage of high-quality audio and video information, such as

movies, and can also be used for data storage. DVDs are formatted differently from CDs, and store information at a higher density [10]. In December 1998, the DOJ approved the DVD3C pool which is organized by Philips, Sony and Pioneer three founding members contributing to DVD Forum’s Digital Video Disc (Video and Read Only Memory ROM) standards. LG has recently joined. In June 1999, DVD6C, another pool comprised of six members of DVD Forum that contributed to the DVD-Video and -ROM standards was also approved by the DOJ. There is no overlap in membership between DVD3C and DVD 6C, although both pools support the same standards. The DOJ decided that it was preferable for potential licensees to deal with two pools rather than with the ten companies on an individual basis [11].

3 Research Design and Sample

The research framework is described in Fig. 1. In order to identify the inconsistent theoretical suggestions and empirical findings, this paper empirically examines the firm-level innovation on patent pool formation. Joshi, and Nerkar [6] stated after a patent pool is formed, the quantity and quality of related patents filed by licensors decrease for several main reasons: (1) From a licensor’s perspective, not pursuing follow-on innovation based on the pool enables all licensors to maximize revenues by not introducing unwanted competition; (2) Not continuing to pursue innovation based on the pool may decrease the risks and costs associated with patent

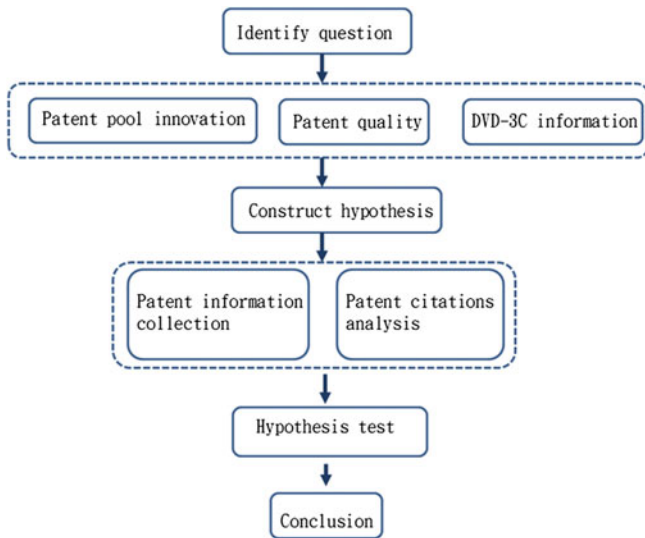


Fig. 1 Research framework

litigation. Thus, this paper proposes the following hypothesis for post-formation innovation performance in comparison to pre-formation one in the pool:

Hypothesis: Patent pool formation leads to patents with lower quality being incorporated into the patent pool. Next, this paper generates DVD 3C patent data for each company. DVD 3C lists patents included in the pool in its website (<http://www.ip.philips.com/licensing/program/42/dvd-r-rw-recorder-philips-only>). For each patent listed as included in the pool, this paper also collect data includes the USPTO patent number, apply date, forward citations received from the USPTO.

In order to further test the hypothesis, this paper employs patent well-used patent quality indicator- forward citation count. The forward citation count of a patent measures how often a patent has been cited by future patents and it is indicative of a high-impact innovation [12]. In order to eliminate the bias from patent age, this paper will divide the average forward citation per patent for a given year by the number of years lapsed between the grant year of the patent and the present in order to arrive at an adjusted average. This paper will apply one-sample t-test, used for determining whether there is sufficient evidence to conclude that the mean of the population from which the sample is taken is different from the specified value, to examine the proposed hypothesis.

4 Result and Implications

This paper generates DVD 3C patent data for each member. There are five licensors: Philips, Sony, Pioneer, LG and HP. However, HP and LG were ignored for the reason that they have only 3 and 9 patents and most of patents were filed before the end of 1998 (the critical year of pool formation). 248 patents which

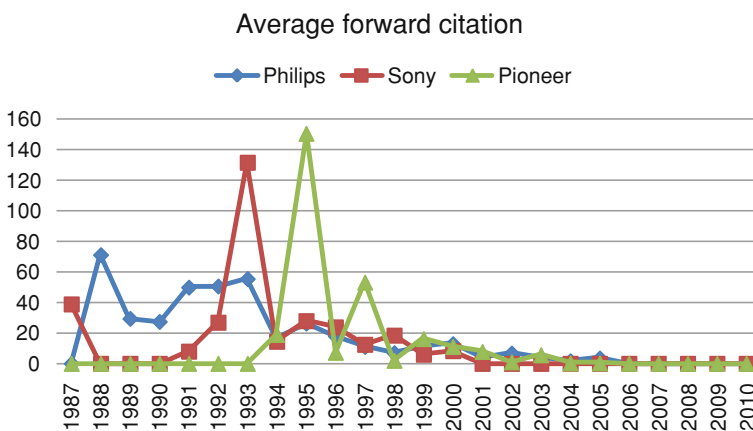


Fig. 2 Average forward citation of each major licensor in DVD 3C

were filed by Philips (99), Sony (47), Pioneer (102) are analyzed as the study sample. This paper calculates and illustrates the average forward citation of each major licensor as shown in Fig. 2.

Average forward citation analysis shows a general downward trend over time, consistent with the manner that an older patent is more likely to have been cited than a more recent patent, all else being equal. Thus, in order to eliminate the bias from patent age, this paper needs to further divide the average forward citation per patent for a given year by the number of years lapsed between the grant year of the patent and the present in order to arrive at an adjusted average. Through using one-sample t-test to test adjusted average annualized citations, this paper aims to verify whether patent pools formation slow down patent innovation performance from firm-level perspective and contribute to the growing literature on the effect of institutional innovations on the follow-on innovation.

Acknowledgments The author thanks the National Science Council of Taiwan for supporting this research under the grant of NSC 101-2221-E-027 -080 -. The author also thanks Pei-Chi Chang's (master student at National Taipei University of Technology) efforts in generating data.

References

1. Federal Trade Commission (2003) To promote innovation: the proper balance of competition and patent law and policy.
2. Clarkson G, Dekorte D (2006) The problem of patent thickets in convergent technologies. *Ann N Y Acad Sci* 1093:180–200
3. Shapiro C. (2001) Navigating the patent thicket: cross licenses, patent pools, and standard-setting. In: Jaffe A, Lerner J, Stern S (eds) *Innovation policy and the economy*, vol. 1, p 119–150
4. Teece D, Sherry E (2003) Standards setting and antitrust. *Minnesota Law Rev* 87:1913–1994
5. Hall BH, Ziedonis RH (2001) The patent paradox revisited: an empirical study of patenting in the U.S. semiconductor industry, 1979–1995. *Rand J Econ* 32(1):101–128
6. Joshi M, Nerkar A (2011) When do strategic alliances inhibit innovation by firms? Evidence from patent pools in the global optical disc industry. *Strat Mgmt J* 32:1139–1160
7. Vakili K (2012) Competitive effects of modern patent pools: the effect of the MPEG-2 Pool on incumbents? *Inovative performance*
8. Farrell J, Katz ML (2000) Innovation, rent extraction, and integration in systems markets. *Economics Working Papers E00-286*, University of California, Berkeley
9. Lampe RL, Moser P (2010) Patent pools and the direction of innovation: evidence from the 19th-century sewing machine industry. *NBER Working Papers 17573*, National Bureau of Economic Research, Inc.
10. Vangie Beal, DVD Formats Explained, http://www.webopedia.com/DidYouKnow/Hardware_Software/DVDFormatsExplained.asp, (2009)
11. Serafino D (2007) Survey of patent pools demonstrates variety of purposes and management structures. *Knowledge Ecology Int'l*
12. Trappey JC, Wang YH, Lin TH, Peng HY (2012) Empirical analysis of patent cross-licensing for light-emitting diode industry. 21th International association for management of technology, Hsinchu, Taiwan, March, pp 18–22
13. Ma TC (2010) Competition authority independence, antitrust effectiveness, and institutions. *Rev Law Econ* 30(3):226–235

Top-k Monitoring Queries for Wireless Sensor Database Systems: Design and Implementation

Chi-Chung Lee and Yang Xia

Abstract A wireless sensor database differs from a relational database, in that it is comprised of a wireless sensor network (WSN), not disks. Nevertheless, the sensing data in the wireless sensor database still are represented as tables. Abstracting the sensing data as the table, end users are able to use SQL to retrieve the required sensing data and do not become aware of the WSN. In the wireless sensor database, top-k monitoring query is an important application and has received much attention in the research community. This research builds on an existing wireless sensor database, TinyDB, and equips TinyDB with the function of performing top-k monitoring queries. The end users finally are able to submit a top-k SQL statement to the wireless sensor database and indeed retrieve the required top-k sensing readings from the WSN.

Keywords Top-k monitoring query · Wireless sensor network · Wireless sensor database system

1 Introduction

With the advance of communication, embedded computing, and sensing technologies, wireless sensor networks (WSNs) have been applied in our daily life [1]. These applications of WSN may be to find the largest temperature values in a building, the driest area in a farm, or the points of most intense vibration in a bridge, etc. A WSN consists of a sink and several sensor nodes. Each sensor node

C.-C. Lee (✉) · Y. Xia

Department of Information Management, Chung Hua University, Hsinchu, Taiwan
e-mail: leecc@chu.edu.tw

Y. Xia

e-mail: m09410025@chu.edu.tw

is equipped with a transmission module and several sensors. The sensors monitor the environment and collect the readings, such as temperature, humidity, luminosity, pressure, carbon dioxide concentration, etc. The transmission module then sends or forwards the readings to the sink, using ad hoc networking. The sink then sends the collected sensing data to the task manager through the internet or a satellite network. The task manager node analyzes these sensing data and finally provides the analyzed result to the end users for decision making [2].

In the database research community, several studies [3–6] treat a WSN as a database for the convenience of the accessing of sensing data. These researches refer to these systems as *sensor database systems* or *sensor network database systems* [3]. Treating a WSN as a database benefits the end user's focus on how to use sensing data to solve daily life problems and helps the end users to ignore the instructions of the WSN. The sensor network database system abstracts the sensing data as tables and therefore the end users are able to use SQL to retrieve the required sensing data from the WSN. The end users finally complete their jobs. The most two well-known sensor database system projects in academia are the COUGAR project [3] and the TinyDB project [6]. In research on sensor database systems, advancing top-k monitoring queries is one of the current issues [7–12]. These studies proposed several approaches to perform top-k monitoring efficiency. The simplest way to implement the top-k monitoring query was centralization approach [7]. In this approach, all raw data sensing by the sensor nodes was sent to the task manager and then generated the top-k monitoring results. The drawback of the centralized approach was the data transmissions consumed mass bandwidth and energy of the WSN. To overcome this drawback, two other approaches were proposed. The first approach aggregated the raw sensing data with a small size during the time that the sensing data were transmitted [7]. The second approach set filters to reduce or delete that sensing data which did not contribute to the result of the top-k monitoring in the sensing data transmission [7, 10–12].

Upon careful surveying, we find the existing research on the top-k monitoring query only focus on how to use the aggregation technique, the filtering technique and reading statistics to conserve the energy of the WSN. There is no work to implement the top-k monitoring query in the wireless sensor database system. This research stands on TinyDB [6] and equips it with the function of performing the top-k monitoring query. To achieve this goal, we revise the syntax and re-write the compiler modules of the TinySQL. The top-k SQL statement finally can be run on TinyDB.

The rest of this paper is organized as follows: In Sect. 2, the state-of-the-art of the wireless sensor database system is introduced. Sections 3 and 4 present the design and the implementation of the top-k monitoring query respectively. Section 5 concludes this paper.

2 Wireless Sensor Database System

We give a brief introduction of the wireless sensor database system in this section. The data model and the query language are described in sequence.

2.1 Data Model

Sensing data in the wireless sensor database systems are logically represented as a table and are referred to as *sensors* [6]. Every sensing datum is represented as a record in the sensors table. The attributes of the sensors table include the identifier of the sensor node and in addition some sensor observations. Depending on the sensor function, the observations may be temperature, humidity, luminosity, pressure, carbon dioxide concentration, etc. In addition to the above attributes, the sensors table also has a dummy attribute, epoch, which shows the number of the round for receiving the sensing data in current top-k monitoring query. The schema of the sensors table can be given by

sensors(epoch, nodeid, temp, light, ...),

where epoch stands for the number of the rounds for receiving the sensing data in current top-k monitoring query, nodeid stands for the identifier of the sensor node, temp stands for the temperature reading, and light stands for the light reading.

2.2 Query Language

Most of the query languages in existing sensor database systems were based on SQL. For example, TinySQL [6], the query language of TinyDB, keeps original SQL operations, such as selection, projection, join, grouping, and aggregation etc. However, in the wireless sensor database, the sensing data are an unbound data stream. TinySQL therefore introduces a sampling operation to adopt the unbound data stream. The unbound data stream may cause a sensing data flood on the WSN and finally hurt the performance if the sensing data are not filtered by the sampling operation. The syntax after the extension of the sampling operation in original SQL can be written as

SELECT select-list
FROM tablename

...

[SAMPLE PERIOD epoch [FOR period]].

In the SAMPLE PERIOD clause, the epoch literal stands for the interval which the sensing data are reported once in every interval and the period literal stands for a specific time period which the query is limited to run. Except for the SAMPLE PERIOD clause, the syntax of the other clauses in TinySQL are the same as those

of their corresponding clauses in the original SQL. For example, the SQL statement for requesting the light and temperature readings and the sensor node identifiers once per second for five seconds can be written as

```
SELECT sensorid, light, temp
FROM sensors
SAMPLE PERIOD 1s FOR 5s.
```

3 Design of Top-k Monitoring Query

We introduce of the top-k monitoring query design in this section. The syntax of the top-k monitoring SQL and the design of its compiler are described.

3.1 Syntax

The semantic of typical top-k monitoring queries is “Finding the top k values of the specific observation.” Following this semantic, there are two concerns when we code the SQL statements of these top-k monitoring queries. The first concern is which observation do the end users want to rank, and the second concern is of how much value is the end users interest in the first concern. Writing a top-k SQL statement, we give the end user interest ranking observation in the ORDER BY clause and extend the SELECT clause to specify the number of the ranked values of the end user’s interest. The syntax of the top-k monitoring query SQL statement is given by

```
SELECT [TOP integer] select-list
FROM sensors
[WHERE where-clause]
...
[ORDER BY orderby-list]
[SAMPLE PERIOD epoch [FOR period]].
```

In the SELECT clause, the TOP keyword and the integer literal are used to specify the number of the end user’s interest ranked readings. Therefore, the SQL statement of the top-k monitoring query “Reporting the top two light readings and their corresponding node identifiers once per second for five seconds” can be written as

```
SELECT TOP 2 nodeid, light
FROM sensors
ORDER BY light
SAMPLE PERIOD 1 FOR 5
```

In the SELECT clause of this SQL statement, “TOP 2” indicates that the end user only is interested in the two highest light readings. In the ORDER BY clause, “ORDER BY light” indicates that the required sensing data are ranked by the light observation.

3.2 Compiler Design

A compiler is a program which converts source codes to object codes. Therefore, the top-k monitoring query compiler converts top-k SQL statements to a series of sensor instructions. The SQL compiler employs the scanner to identify tokens in the lexical analysis and the parser to construct the relationships among the tokens in the syntax analysis [13]. This research amends the scanner and the parser of TinySQL to equip TinySQL with the function of performing top-k monitoring. Note that the other parts of the TinySQL compiler are still employed unchanged.

Lexical analysis. To identify the tokens of the top-k SQL statement, lexical analysis is performed by the scanner. The scanner is enhanced and can identify tokens “TOP” and “ORDER BY”. The token expressions are given as the following.

```
TOP=“TOP”|“top”;
ORDER_BY=“ORDER BY”|“order by”;
```

Syntax analysis. The syntax analysis constructs the relationships among the tokens which are identified by the scanner. The relationships of these tokens are represented as grammar by Backus Normal Form (BNF). The BNF expression of the grammar is listed as follows.

```
sql_stat ::=select_stat from_stat | select_stat from_stat where_stat
          | select_stat from_stat order_by_stat
          | select_stat from_stat where_stat order_by_stat;
select_stat ::=SELECT top_stat select_stat_list;
top_stat ::=TOP CONSTANT;
select_stat_list ::=select_stat_list COMMA attr | attr;
from_stat ::=FROM from_stat_list;
from_stat_list ::=from_stat_list COMMA source | source;
source ::=QUERY_STRING CONSTANT | NAME | NAME AS NAME;
where_stat ::=WHERE condition | WHERE condition more_conditions;
condition ::=arith_expr rel_op CONSTANT | arith_expr rel_op NAME;
more_conditions ::=bool_op condition | bool_op condition more_conditions;
bool_op ::=AND | OR;
order_by_stat ::=ORDER BY NAME;
```

In the above expressions, the terminal tokens are uppercase while the non-terminal tokens are lowercase.

4 Implementation of Top-k Monitoring Query

We describe the development environment, the system architecture, the program modules and the result to introduce the implementation of the top-k monitoring query.

4.1 Development Environment

We used the wireless sensor network developing toolkit produced by Crossbow Cooperation to implement the system. The toolkit consists of several sensors, a gateway and a software development toolkit. The program modules were implemented by JAVA and used Eclipse as the development tool.

4.2 System Architecture

The components in the hardware architecture are distinguished as the server end and the sensor end. The server end has a PC equipped with a gateway as a data sink. The device of the gateway is the MB510 gateway of Crossbow. The sensor end consists of several sensor nodes, each having a process unit and a sensor unit. We use MICAz of Crossbow as the process unit and MTS300 of Crossbow as the sensor unit. MTS300 can sense light and temperature, etc.

Similar with the hardware architecture, the software architecture is divided into the server and the sensor programs which are run on the server and the sensors respectively. The software architecture is shown in Fig. 1. The server program consists of user interface, query processing, instruction transmission, data receiving and network interface modules. The sensor program consists of data acquisition, data aggregation, instruction receiving, data transmission, and network interface modules.

4.3 Modules

To extend TinySQL with the ability of performing top-k monitoring queries, this research re-codes four modules of the server program. These four modules are the user interface, the query processing, the command transmission and the data receiving modules. The tools and libraries for developing these modules are listed in Table 1.

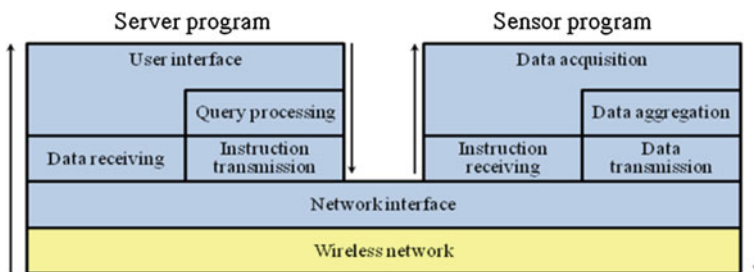


Fig. 1 Software module architecture

Table 1 Tools and library for developing server module

Module	Tools and library
User interface	Java, Eclipse
Query processing	JLex, CUP
Command sending	TinyOS, Java, Java comm API
Data receiving	TinyOS, Java, Java comm API

The user interface module provides a command-line interface to let an end user submit the top-k monitoring SQL statement and then forward this statement to the query processing module to complete the data retrieving. After the required sensing data are transmitted back, the required sensing data also are displayed on this command-line interface.

The query processing module is the most critical module in the system programs. It accepts the top-k monitoring SQL from the user interface module. The module then scans and parses the accepted top-k monitoring SQL and stores the parsing result to the query expression data structure. The query processing module finally executes the query based on the query expression data structure and generates requests which are passed to the instruction transmission module. We use JLex and CUP to code the scanner and the parser of the top-k monitoring query compiler.

The instruction transmission module accepts the requests from the query processing module, translates the requests into the instructions of sensors and sends these instructions to the sensors by the network interface module. On the other hand, the data receiving module receives the sensing data from the WSN and further passes these sensing data to the user interface module. The instruction transmission module and the data receiving module are implemented by JAVA and the connection between the PC and the gateway is established by Java communications API.

5 Result

The implemented system has been deployed in the sensor field. However, we only deployed four sensor nodes due to the restriction of our limited resource. Consider the following top k monitoring SQL statement which monitors the readings of the two highest illumination nodes in the sensor field.

```
SELECT TOP 2 nodeid, light
FROM sensors
ORDER BY light
SAMPLE PERIOD 2048
```

The result of this query is shown in Fig. 2. In the period from epoch 1 to epoch 4, the two highest illumination nodes are node 1 and node 3. In order to confirm that the implemented system is indeed functioning, we use a shelter to


```

/opt/tinyos-1.x/tools/java
GreatExpuser-86b92dcf /opt/tinyos-1.x/tools/java
$ java net/tinyos.tinydb.TopK
請輸入要查詢的 SQL 指令 =>
SELECT TOP 2 nodeid,light FROM sensors ORDER BY light SAMPLE PERIOD 2048
Catalog file in use: net/tinyos/tinydb/catalog.xml
Creating PhoenixSource with serial@COM3:57600
serial@COM3:57600: resynchronising
TOP Number ->2
Order By Name ->light
送出查詢！建置結果表格！
| Epoch | nodeid | light |
-----|-----|-----|
1 | | |
1 | | |
2 | 1 | 722 |
2 | 3 | 762 |
3 | 1 | 725 |
3 | 3 | 758 |
4 | 1 | 738 |
4 | 3 | 758 |
5 | 4 | 712 |
5 | 3 | 759 |
6 | 4 | 719 |
6 | 3 | 765 |
7 | 4 | 719 |
7 | 3 | 768 |
8 | 4 | 713 |
8 | 3 | 766 |
9 | 4 | 707 |
9 | 3 | 761 |
10 | 4 | 704 |
10 | 3 | 758 |
11 | 1 | 741 |
11 | 3 | 756 |
12 | 1 | 743 |
12 | 3 | 760 |
13 | 1 | 694 |
13 | 3 | 764 |
14 | 2 | 691 |
14 | 3 | 765 |
15 | 2 | 688 |
15 | 3 | 758 |

```

Fig. 2 An example of a top-k monitoring query

mask node 1 in the period from epoch 5 to epoch 10. In this period, node 4 replaces node 1 among the two highest illumination nodes. When the shelter of node 1 is removed at epoch 11, node 4 leaves and node 1 again returns to the two highest illumination nodes. This result shows that the implemented system is functioning effectively.

6 Conclusion

The top-k monitoring query retrieves the top-k sensor readings from the wireless sensor network in every epoch of the user specific period. This research builds on TinyDB and equips TinySQL with the top-k monitoring functionality. We report our design and implementation works in this paper. The result shows that end users

finally are able to submit an easy SQL statement to the wireless sensor database and acquire the required top-k readings from the WSN.

Acknowledgments Benjamin Fiscman is appreciated for his editorial assistance.

References

1. Ho L, Walker Z, Moh M (2005) A prototype on RFID and sensor networks for elder healthcare. In: 2005 ACM SIGCOMM workshop on experimental approaches to wireless network design and analysis. ACM New York, NY, USA, pp 70–75
2. Tilak S, Abu-Ghazaleh NB, Heinzelman W (2002) A taxonomy of wireless micro-sensor network models. *Mobile Comput Commun Rev* 1(2):1–8
3. Bonnet P, Gehrke JE, Seshadri P (2001) Towards sensor database systems. In: 2nd international conference on mobile data management, Springer, pp 3–14
4. Kempe D, Dobra A, Gehrke JE (2003) Gossip-based computation of aggregate information. In: 44th annual IEEE symposium on foundations of computer science. IEEE Press, New York, pp 482–491
5. Yao Y, Gehrke JE (2003) Query processing for sensor networks. In: First biennial conference on innovative data systems research, IEEE Press, New York
6. Madden S, Franklin MJ, Hellerstein JM, Hong W (2005) TinyDB: an acquisitional query processing system for sensor Networks. *ACM TODS* 30(1):122–173
7. Wu M, Xu J, Tang X, Lee W (2007) Monitoring top-k query in wireless sensor networks. *IEEE Trans Knowl Data Eng* 19(7):962–976
8. Malhotra B, Nascimento MA, Nikolaidis I (2011) Exact top-K queries in wireless sensor networks. *IEEE Trans Knowl Data Eng* (23)10:1513–1525
9. Chen B, Liang W, Yu JX (2010) Online time interval top-k queries in wireless sensor networks. In: Eleventh international conference on mobile data management, IEEE Press, New York, pp 177–182
10. Zeinalipour-Yazti D, Andreou P, Chrysanthis KP, Samaras G (2007) MINT views: materialized in-network top-k views in sensor networks. In: 7th international conference on mobile data management, IEEE Press, Washington, DC, pp 182–189
11. Wu M, Xu J, Tang X (2006) Processing precision-constrained approximate queries in wireless sensor networks. In: 7th international conference on mobile data management, IEEE Press, New York, pp 31–36
12. Mouratidis K, Bakiras S, Papadias D (2006) Continuous monitoring of top-k queries over sliding windows. In: 2006 ACM SIGMOD international conference on management of data, pp 635–646
13. Aho AV, Sethi R, Ullman JD (2007) *Compilers: principles, techniques, and tools*, 2nd edn. Addison-Wesley

Protection Management of Enterprise Endpoint Based on the ITIL Management Framework

Mei-Yu Wu, Shih-Fang Chang and Wei-Chiang Li

Abstract There are many endpoints such as notebooks and desktop computers in the internal environment of modern enterprise. However, convenient network applications accompanied by the threat of various forms of information, such as computer viruses, spyware, operating system vulnerabilities, a malicious web site, attack of malware. The endpoints are the largest number of the subject in the corporate computer environment. If information threats affect the endpoint operation, the business operations and revenue will suffer the loss. The main purpose of this study is focus on the endpoint protection for enterprises. The research adopts ITIL management framework approach to provide endpoint protection management and assessment methodology of effectiveness. The proposed approach could be regarded as planning reference for information department during endpoint protection management. Besides, the proposed approach provides protection mechanisms for enterprise endpoint to reduce the impact from information threats.

Keywords Information technology infrastructure library (ITIL) · Information threats · Endpoint protection

M.-Y. Wu (✉) · W.-C. Li

Department of Information Management, Chung Hua University, Hsinchu, Taiwan, ROC
e-mail: mywu@chu.edu.tw

W.-C. Li

e-mail: e09910017@chu.edu.tw

S.-F. Chang

Department of Internet Security, Information and Communications Research Laboratories,
Industrial Technology Research Institute, Hsinchu, Taiwan, ROC
e-mail: finney@itri.org.tw

1 Introduction

As the continuing development and progress of information technology (IT), enterprises adopt IT equipment that is already not unusual situations. For example, using network connection and the universal serial bus (USB) portable device brought fast and convenient operating environment for the enterprise. However, convenient IT equipment hidden countless crises. The convenient IT not only enhances the productivity of enterprises for development, but also brings serious problems and challenges for information security management. Different endpoint user has different information literacy and security awareness level. If there is not comprehensive management, information threats might easy to spread within the enterprise and then becomes hazards and financial loss.

According to Internet security threat report issued by Symantec, there are 5.5 billion malicious attacks are detected and intercepted in 2011 that was more than 81 % increase over the previous year [1]. There were a variety of industries of multinational organizations have suffered huge losses due to network attacks. The report pointed out the total cost of data leakage losses caused by malicious threats in 2011 reached 3.01 million U.S. dollars. Most of the attacks locked the nature of the work as sales, human resources, assistants of executives, and media and public relations populations. Targeted attacks caused the destruction of network and loss of intellectual property right of many enterprises. In addition, half of the targeted attacks in 2011 focused on SMEs. Therefore, companies need more comprehensive protection management to resist information threats.

Information technology infrastructure library (ITIL) is considered a framework of best practice guidance for IT service management and it is widely used in the business world [2, 3]. There are many information services applied in enterprise. According to the key principles of ITIL, i.e. service strategy, service design, service transition, service operation and continual service improvement, these applications are regarded as information service for users; in contrast, they are management issue for service provider. Using ITIL framework, IT department will effectively master and reduce the impact of threats and improve management efficiency [4].

Therefore, this research proposes a management mechanism to protect enterprise endpoint based on the ITIL management framework. The proposed approach provides endpoint protection management and assessment methodology of effectiveness, and in addition reduces the impact from information threats. The remainder of this paper is organized as follows. [Section 2](#) reviews related works on overview of ITIL management framework, overview of information threat, and protection mechanisms. [Section 3](#) introduces the proposed protection management of enterprise endpoint based on ITIL management framework. A complete effectiveness assessment for endpoint protection is offered in [Sect. 4](#). Finally, [Sect. 5](#) presents our conclusions.

2 Related Work

Computerization in enterprises today is extensively spread. Therefore, the risk management of information threats is discussed constantly in relevant literature. Endpoint protection management is a troublesome for many enterprises. As the enterprise is continually expanding more and more numbers of endpoints, comprehensive management has become an important topic. In the past, IT department invested most resources on the technical management of system. In contrast, today IT management focuses on service management due to the increasing dependence on information technology.

The comparison between traditional IT management and IT service management is shown in Table 1 [4, 5].

2.1 The Overview of ITIL

Information technology infrastructure library (ITIL) was published between 1989 and 1995 by Her Majesty’s Stationery Office (HMSO) in the UK on behalf of the Central Communications and Telecommunications Agency (CCTA) – now subsumed within the Office of Government Commerce (OGC). A second version of ITIL was published as a set of revised books between 2000 and 2004. In 2007, ITIL V2 was superseded by an enhanced and consolidated third version of ITIL [3].

ITIL defines service management as a set of specialized organizational capabilities for providing value to customers in the form of service. ITIL contains a set of five publications, the ITIL Core, which provide structure, stability, and strength to an IT organization’s service management capabilities [6–8]. The management framework of ITIL V3 is illustrated in Fig. 1.

The management framework of ITIL V3 contains one core, i.e. service strategy, and four phases, i.e. service design, service transition, service operation and continual service improvement. The core of ITIL management framework and each phase are separate, independent and not dependency. Enterprise could introduce different phase depending on needs.

Table 1 The comparison between traditional IT management and IT service management

Topic	Traditional IT management	IT service management
Position	Technical-oriented	Service-oriented
Management model	Passive and afterwards management	Proactive and plan management
Management method	Centralized and completed within the enterprise	Distributed and outsourced
Management viewpoint	Isolated department perspective	Integrated view of enterprise
Management practice	One-time problem solving as target	Clear responsibility and repeatability
Management process	Informal process	Optimized operation
Thinking point	From the internal of IT department	From the perspective of service

Fig. 1 The management framework of ITIL V3 [7]



2.2 The Overview of Information Threats

There are a number of risks in the enterprise operation. The intrusion and attack of information threat is very important for risk management. If there is no adequate management, it will affect the operation of enterprise.

Different types of classifications for information security threats have been suggested [9]. For example, according to the national institute of standards and technology (NIST) classification, information threats contain errors and omissions, fraud and theft, employee sabotage, loss of infrastructure that supports the system, malicious hackers, and malicious code [10]. Malicious codes are virus, Trojan horses, worms, spyware, grayware and etc. [11–14]. Enterprise should identify the vulnerabilities that might be exploited by the threats [15]. Enterprise should implement protect mechanism to prevent security failure occurring in the light of prevailing threats and vulnerabilities.

2.3 Protection Mechanisms

Endpoint security protection and control is an important issue for IT department. There are many existing literatures that discuss endpoint protected mechanism, such as malware protect function, cloud antivirus, web reputation services, file reputation services, e-mail protection, software firewall and device control. In malware protect function, many approaches are proposed, such as opcode-sequence-based malware detection [16], semi-supervised learning for unknown malware detection [17, 18], and intelligent PE-malware detection system based on association mining [19].

Some related work discussed risk management based on ITIL [20]. The ITIL framework stated that risk should be identified, measured and mitigated. Appropriate protect mechanism should be specified as desired in the actual business scenario.

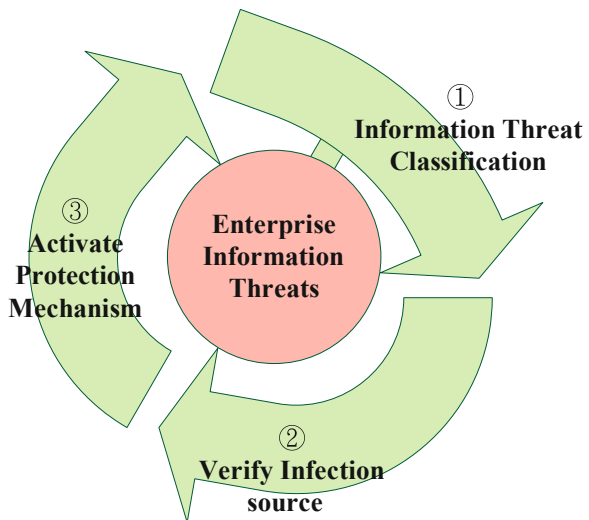
3 Endpoint Protection Management Based on ITIL Management Framework

The research applied ITIL V3 management framework to protect endpoint. Possible information threat of endpoint is not only from external, but also need to beware of diffusion of the internal environment. We propose three main protection steps to achieve endpoint protection that is information threat classification, verify infection source, and activate suitable protection mechanism. The core management steps of endpoint management are illustrated in Fig. 2.

Three treatment actions against the information threat are monitor, block, and analysis. At first, monitoring various information of endpoint and then verify the classification of information threat. Then endpoint management system should implement information security policy to block vulnerabilities of internal system, such as distributing hot-fix and applying password rule. Finally regular report should be issued to evaluate the effectiveness, such as continuous attacked or infected endpoints should be classified as abnormal event.

ITIL management framework contains one core and four phases. Each approach is separate, independent and no order of implementation. Enterprise could introduce different approach depending on needs. Endpoint protection management approach mentioned in this study is the same. Enterprise could decide the needed approach to implement according to the manpower, resource, and budget of practical situation.

Fig. 2 The core management steps of endpoint management framework



3.1 Strategy Management of Endpoint Protection

Service strategy is the core of ITIL. The meaning of service strategy is to confirm the factors affecting the demand and progressively implement related approach to achieve goals. In strategy management of endpoint protection, IT department should verify the factors affecting the demand and plan the budget to procure endpoint protection solution. Besides, IT department should adjust and enable the combination of related functions according to the protection needs, such as web reputation services and e-mail protection. The detail operation of ITIL service strategy and strategy management of endpoint protection is described in Table 2.

3.2 Design Management of Endpoint Protection

There are seven approaches in design management of endpoint protection. They are capacity, availability, service level, information security, service continuity, and supplier management, and service catalogue. The detail operation of ITIL service design and design management of endpoint protection is described in Table 3.

Table 2 The operation of ITIL service strategy and strategy management of endpoint protection

ITIL management framework		Implementation of endpoint protection management
Phase	Approach	
Service strategy	1. Demand management	Confirm the factors that affect the endpoint protection. The factors are classified into endpoint protection operation management of information department and repair service of users.
	2. IT financial management	(i). Formula of budget Endpoint budget = each endpoint protect costs * total endpoint numbers * purchase sufficient rate (ii). Enterprise evaluates the cost-benefit analysis according to the invested resources and service assessment definition.
	3. Service portfolio	Manage the hardware and software services for endpoint protection and adjust the combinations based on needs.
	4. Strategy generation	(i). Define the treatment strategy of each information threat. (ii). Implementing security strategy of operating system. (iii). Implementing treatment strategy of internal infection source. (iv). Implementing deployment strategy of update and hot fix of endpoint protection.

Table 3 The operation of ITIL service design and design management of endpoint protection

ITIL management framework		Implementation of endpoint protection management
Phase	Approach	
Service design	1. Capacity management	Define the agreed service level according to the IT infrastructure cost-benefit, and time considerations.
	2. Availability management	With different sources of infection, related protection approach should be implemented.
	3. Service level management	Negotiating the endpoint protection standard and process that agreed by users and ensure they are actually carried out.
	4. Service catalogue	Services that could be publicly available should be announced to users.
	5. Information security management	Protection server must be stored in a protected place and the configuration information should be aware by only authorized internal personnel.
	6. Service continuity management	Develop the disaster recovery measures of endpoint protection including backup.
	7. Supplier management	Select the qualified supplier according to the request for proposal (RFP).

Table 4 The operation of ITIL continuous service improvement and effectiveness assessment of endpoint protection

ITIL management framework		Implementation of endpoint protection management
Phase	Approach	
Continuous service improvement	1. Service measurement	The study proposes various indicators to calculate the protection rate of information threat.
	2. Service reporting	Using regular weekly report to measure the performance and efficiency.
	3. Service improvement	When encountering to be improved operation of endpoint protect, defining the improving steps according to the order of importance.

4 Effectiveness Assessment for Endpoint Protection

The last phase of endpoint protection is to verify the effectiveness. Continual service improvement of ITIL management framework is effectiveness assessment of service management. This phase includes service measurement, service reporting and service improvement. The detail operation of ITIL continuous service improvement and effectiveness assessment of endpoint protection is described in Table 4.

5 Conclusions and Future Works

In the design concept of enterprise endpoint protection product, IT department usually has flexible to adjust the setting because the diversity of endpoint environment. However, adjustment improperly may cause protective excessive or protective lack and affecting the operation of enterprise. The research proposed an endpoint protect management mechanism based on ITIL management framework. The proposed strategy, design, and assessment of protection could be adjusted according to the needs, budget, and manpower of enterprise. The proposed approach provides effective protection mechanisms for enterprise endpoints to reduce the impact from information threats.

Endpoint security mechanism must have faster reaction in response to rapidly changing of threat attack. In future work, we will implement the endpoint protection management system and performance evaluation system. If the system can be successfully developed, the cost of management will be reduced and the effectiveness of management will be apparent.

References

1. Symantec: Internet Security Threat Report (ISTR). vol. 17(2011)
2. Jelliti M, Sibilla M, Jamoussi Y, Ghezala HB (2010) A model based framework supporting ITIL service IT management. In: Bider, et al. (eds) BPMDS 2010 and EMMSAD 2010. LNBP, vol. 50. Springer-Verlag, Berlin Heidelberg, p 208–219
3. The IT Service Management Forum, An introductory overview of ITIL V3, http://www.best-management-practice.com/gempdf/itsmf_an_introduutory_overview_of_itilv3.pdf
4. Marrone M, Kolbe LM (2011) Impact of IT service management frameworks on the IT organization: an empirical study on benefits, challenges, and processes. *Bus Inform Syst Eng* 3(1)
5. McFarlane I, Dugmore J (2006) IT service management self assessment workbook, 2nd edn. British Standards Institute, London
6. APM Group Ltd, ITIL Management, <http://www.itil-officialsite.com>
7. Computer Aid, Inc, ITIL V3 Service Life Cycle, <http://www.itservicemanagement-itil.com/category/it-service-management-cat/itil-v3-life-cycle/>
8. WisdomFish.ORG, ITIL V3 Structure, <http://java.wisdomfish.org/soa/soa-design-patterns/itil-v3>
9. Alhabeeb M, Almuhaideb A, Le PD, Srinivasan B (2010) Information security threats classification pyramid. In: 2010 IEEE 24th international conference on advanced information networking and applications workshops, p 208–213
10. Guttman B, Roback E (1995) An introduction to computer security: the NIST handbook. Diane Pub Co
11. Morales JA, Al-Bataineh A, Xu S, Sandhu R (2010) Analyzing and exploiting network behaviors of malware. In: Jajodia S, Zhou J (eds) SecureComm 2010. LNCS, vol. 50. Springer, Berlin, Heidelberg, p 20–34
12. Sinchai C (2008) Multiple logs analysis for detecting zero-day backdoor trojans. Cleveland State University, Cleveland
13. Wagener G, State R, Dulaunoy A (2008) Malware behaviour analysis. *J Comput Virol* 4:279–287

14. Zhang Y, Song L, He Y (2011) A novel immune-inspired method for malicious code extraction and detection. In: Zhang J (ed) ICAIC 2011. CCIS, vol. 226. Springer-Verlag, Berlin, Heidelberg, p 501–509
15. ISO/IEC 27001. (2005) Information Technology—Security Techniques—Information Security Management Systems—Requirements
16. Santos I, Brezo F, Nieves J, Peña YK, Sanz B, Laorden C, Bringas PG (2010) Idea: opcode-sequence-based malware detection. In: Massacci F, Wallach D, Zannone N (eds) ESSoS 2010. LNCS, vol. 5965. Springer-Verlag, Berlin, Heidelberg, p 35–43
17. Santos I, Nieves J, Bringas PG (2011) Semi-supervised learning for unknown malware detection. In Abraham A, Corchado JM, Rodríguez González S, de Paz Santana, JF (eds) International symposium on DCAI. AISC, vol. 91. Springer-Verlag, Berlin, Heidelberg, p 415–422
18. Santos I, Sanz B, Laorden C, Brezo F, Bringas PG (2011) Opcode-sequence-based semi-supervised unknown malware detection. In Herrero A, Corchado E (eds.) CISIS 2011. LNCS, vol. 6694. Springer-Verlag, Berlin, Heidelberg, p 50–57
19. Ye Y, Wang D, Li T, Ye D, Jiang Q (2008) An intelligent PE-malware detection system based on association mining. *J Comput Virol* 4:323–334
20. Vilarinho S (2003) Miguel Mira da Silva: risk management model in ITIL. *Commun Comp Inform Sci* 220:306–314

Adaptive Content Recommendation by Mobile Apps Mash-Up in the Ubiquitous Environment

Chih-Kun Ke, Yi-Jen Yeh, Chang-Yu Jen and Ssu-Wei Tang

Abstract Traditionally, e-services are composed to assist the enterprise business process. In recent years, Software as a Service (SaaS) model in cloud computing enriches the mobile commerce. Mobile commerce promotes the service providers building an application market platform to serve customers. However, an application market platform may collect a huge number of mobile application services (mobile Apps) and each App is usually designed with little functionality. A customer may fetch a number of Apps to mash up in order to satisfy his/her comprehensive requirements. How to mash up the Apps to provide a feature-rich composition for a customer becomes an interest research issue. In this work, we explore an approach of Apps mash-up composition in a service platform for adaptive content recommendation. A user profile conducts the service level agreements in evaluating the service quality. An Apps mash-up composition is recommended to the customer an adaptive content in a ubiquitous environment.

C.-K. Ke (✉) · C.-Y. Jen · S.-W. Tang
Department of Information Management,
National Taichung University of Science and Technology,
Taichung 40401, Taiwan, Republic of China
e-mail: ckk@nutc.edu.tw

C.-Y. Jen
e-mail: s1801B104@nutc.edu.tw

S.-W. Tang
e-mail: s13003011@nutc.edu.tw

Y.-J. Yeh
Department of Division for Mobile Internet Software Technology,
Network Services and System Technology,
Information and Communications Research Laboratories,
Industrial Technology Research Institute,
Hsinchu 31040,
Taiwan, Republic of China
e-mail: EthanYeh@itri.org.tw

Keywords Software as a service · Service level agreement · Apps mash-up · Content filtering · Adaptive content recommendation

1 Introduction

In service-oriented computing paradigm, e-services can be described, published, located, discovered, programmed, and configured using XML-based technologies over a network. E-services are self-aware, self-contained modules and perform functions that can range from answering simple requests to executing business processes [1]. The loose coupling property makes the e-services to compose a comprehensive e-service with various functionalities. The composite e-service is used to accomplish specific business tasks in enterprise application integration (EAI), e.g., the broker or auction mechanism over internet is a kind of composite e-service in the ubiquitous environment. The simple object access protocol (SOAP), web service description language (WSDL), universal description, discovery, and integration infrastructure (UDDI), web services business process execution language (BPEL) techniques and Internet standards, e.g., hypertext transfer protocol (HTTP), are enforced to reconstruct an integrated e-service system from non-network-based systems or deployed e-services over standard middleware platforms [2].

In recent, cloud computing performs a new e-service style for customers. The service models of cloud computing include software as a service (SaaS), platform as a service (PaaS), and infrastructure as a service (IaaS). SaaS model enriches the electronic commerce in the ubiquitous environment (also known as mobile commerce) which promotes the service providers to build an application market platform or portal. Various software service portals, e.g., Apple stores and Google Play, provide channels for the customer to acquire software services from a service provider [3, 4]. The software service in software service portals is also called as an App. A customer uses lightweight mobile devices to acquire Apps and customize the personal requirements. However, an application market platform may collect a huge number of mobile application services (mobile Apps) and each App is usually designed with little functionality. A customer may fetch a number of Apps to mash up in order to satisfy his/her comprehensive requirements. How to mash up the apps to provide a feature-rich composition for the customer becomes an interest research issue.

In a service-oriented environment, quality of service (QoS) is an important significant requirement in evaluating a software service [5], especially a composite e-service. Organization uses service level agreement (SLA) to coordinate the service providers and users [6]. User personal and operational data forms the user profile [7]. Information retrieval techniques [8] are used to extract key terms from a user personal data. The extracted key terms form a profile to represent the information needs of users for acquiring the services. Moreover, the profile can be

generated according to the context of the user operation, e.g., searching, selecting and rating to services. According to certain context, the key terms also recorded in a user profile. The user profile reflects the satisfaction a user observes after consuming a service [7]. Therefore, how to enforce the SLAs in various Apps convergence is a service quality consideration. In this work, we try to use the SLAs to coordinate the fetched Apps and mash up the Apps in evaluating the composite service quality. The SLAs are designed according to a user profile. The various contents of Apps are configured based on meeting the different service requirements in SLAs.

In this work, we explore the approach of mobile Apps mash-up processing in a service platform for adaptive content recommendation. The functionality of the proposal approach include: collect the mobile Apps provided by an application market platform as the candidate services; analyze a customer's comprehensive requirements to build a user profile and conduct the service level agreement (SLA) in evaluating the service quality; based on SLAs and summary descriptions of Apps, mash up the composite services; keep the content satisfying user requirements during mash-up processing; recommend the adaptive content to the user in the ubiquitous environment; collect user feedback to improve the proposed approach for mobile Apps mash-up processing in a service platform. The remainder of this paper is organized as follows. Section II introduces the proposed approach and its functionality based on a software development view in a mobile device for ubiquitous computing. In Sect. 3, we present our conclusions and indicate a direction for future work.

2 System Approach and Functionality

This section introduces the approach and its functionality of a mobile Apps mash up processing in the ubiquitous environment, including the user requirement analysis, mobile apps mash-up, content filtering, and adaptive content recommendation modules, is shown in Fig. 1.

User Requirement Analysis Module collects key terms from the personal, operational data and the context of the user operation. The extracted key terms form a profile to represent the information needs of users for acquiring the Apps. The SLAs are constructed according to a user profile for QoS evaluating. **Mobile Apps Mash-up Module** is used to fetch the Apps from the application market platforms over the internet (in the ubiquitous environment). Then the module identifies the Apps' communicate interface in order to mash up the collected Apps. **Content Filtering Module** fetches relevant contents of the mash-up composite Apps from the cloud storages or central databases. According to predefined SLAs in user requirement analysis module, content filtering module adaptive evaluates and filters out the irrelevant Apps' contents from the user requirements. **Adaptive Content Recommendation Module** presents the evaluated contents in a service platform interface and adaptive recommend to the user. User can rate or give a

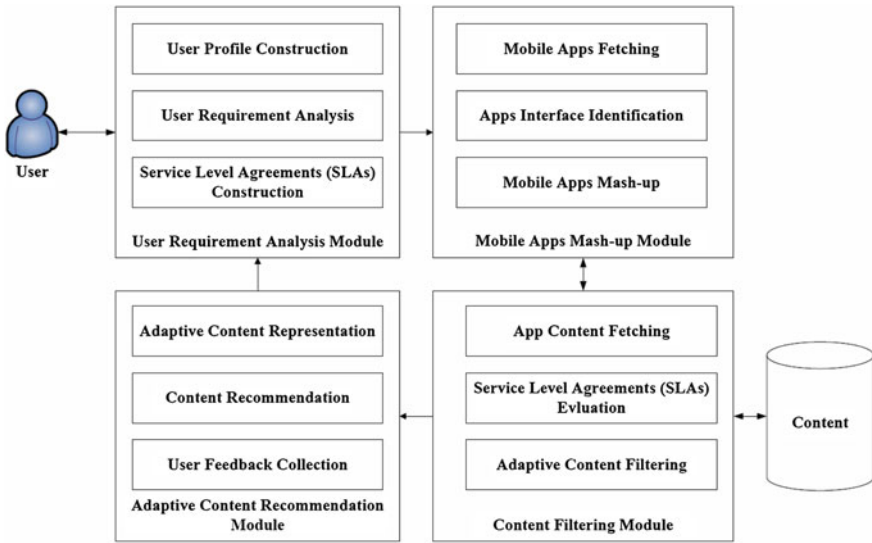


Fig. 1 An approach for a mobile Apps mash-up processing in the ubiquitous environment

score in a service platform interface about the quality of the recommend contents. This work's functionality is demonstrated by an implementation in a mobile device. We use a tablet as an experimental service platform which is running on an Android-based operation system. The Android SDK [9] function calls are also used to explain the proposed approach's modules working.

2.1 Functionalities of the Proposed Approach

The system initialization process is presented as three steps, including initialize, produce a tag, and produce a block operations.

- (1) **Initialize an App bar:** The Android SDK's `slidingDrawer` component is used to construct an App bar and put in a designed App box. Then the system calls the Android SDK's `setOnDrawerOpenListener` component to initial an App bar.
- (2) **Produce an App tag:** The system produces a unique App tag as the identification for user fetching.
- (3) **Produce an App block:** The system check the current App blocks, and produce a new App block.

The App fetching process is presented as three steps, including fetch, drag, and put operations.

- (1) **An App fetching:** The user executes the “on Long Click” mode to fetch an App, and inherit Android SDK’s **View.DragShadowBuilder** component to produce a shadow which size is the same as an App box to receive the drag operation to a position.
- (2) **Start drag:** Inherit Android SDK’s **View.OnDragListener** component to enforce a drag operation to move an App shadow to a position. The system uses the **getAction()** component to check the life cycle of drag operation starting or not.
- (3) **Put in an accepted object:** The accepted object indicates that the system dynamically produces an App block. The life cycle of drag operation decides to put a shadow in an accepted block or not.

The operations of initialization and App fetching processes are shown in Fig. 2.



Fig. 2 The operational steps of the initialization and App fetching processes

The Apps mash-up process is presented as four steps, including mash up, get, filter, and close operations.

- (1) **Mash up an App:** When an App's shadow is successful put in an accepted object, the system decides to mash up the contents in its App block according to its tag (App identification). Besides, the system also sets up the content filtering criteria for this App and deletes the App box at the same time.
- (2) **Get the content filtering criteria:** The system bases current App(s) deployment and historical records to get the content filtering criteria from a javabean.
- (3) **Content filter:** In an App fragment's life cycle onStart() operation, the system uses `getActivity().findViewById` method to get the current Apps and relevant content filtering criteria to enforce SQL commands to filter the relevant contents.
- (4) **Close an App bar:** After finishing the drag operation of an App, the system uses `setOnDrawerCloseListener` component to close an App bar.



Fig. 3 The operational steps of Apps mash-up and adaptive content recommendation processes

The adaptive content recommendation process is presented as three steps, including store, adjust, and usage operations.

- (1) **Store the Composite mash-up Apps:** After each drag and mash-up Apps composition operations, the filtered contents are stored in a repository.
- (2) **Adjust the App:** If the user want delete some App, he/she can use “**on Long Click**” mode to remove the App. This operation uses Android SDK fragment’s life cycle **onDestroyView()** to remove the object. At this time, the system enforces the content filtering to update the composite mash-up Apps relevant information again. The final results of the contents are updated to in a repository.
- (3) **Usage of an App:** User can use drag operation to get an App in a single system interface. Beside, a user also can use **onDoubleClick** mode to use the App.

The operations of Apps mash-up and adaptive content recommendation processes are shown in Fig. 3.

3 Conclusions

This work proposed an approach of mobile Apps mash-up process in a service platform for adaptive content recommendation. We collect the mobile Apps from an application market platform as the candidate services. A customer’s comprehensive requirement is analyzed to build a user profile and conduct the service level agreements (SLAs) in evaluating the service quality. In mash-up process, we base on the SLAs to compose Apps and recommend the adaptive content to the user. User feedback is collected to improve the proposed approach for mobile Apps mash-up processing in a service platform.

Future direction of this work includes having the real case experiments and relevant discussions. Some intelligent techniques, e.g., case-based reasoning and fuzzy theory, will be used to reinforce the proposed approach. The user feedback will provide valuable information to help us improve this approach more effective.

Acknowledgments This research was supported in part by the Industrial Technology Research Institute and the National Science Council of Taiwan (Republic of China) with an NSC grant 101-2410-H-025-006.

References

1. Papazoglou MP (2007) Web services: principles and technology. Prentice-Hall, Reihe
2. Liu DR, Ke CK, Lee JY, Lee CF (2008) Knowledge maps for composite e-services: a mining-based system platform coupling with recommendations. *Expert Syst Appl* 34(1):700–716
3. Candan KS, Li WS, Phan T, Zhou M (2009) Frontiers in information and software as service. In: *Proceeding of IEEE international conference on data engineering, ICDE 2009*, pp 1761–1768

4. Chang SF (2011) A reference architecture for application marketplace service based on SaaS. *Int J Grid Util Comput* 2(4):243–252
5. Goscinski A, Brock M (2010) Toward dynamic and attribute based publication, discovery and selection for cloud computing. *Future Gener Comput Syst* 26:947–970
6. Silaghi GC, Şerban LD, Litan CM (2010) A framework for building intelligent SLA negotiation strategies under time constraints, economics of grids, clouds, systems, and services. *Lect Notes Comput Sci* 6296:48–61
7. Ke CK, Chang SF, Lin ZH (2013) An adaptive e-service for bridging the cloud services by an optimal selection approach. *J Softw*, in press
8. Richrdo BY, Berthier RN (1999) *Modern information retrieval*. The ACM Press, New York
9. Android SDK, <http://developer.android.com/sdk/index.html>

A Real-Time Indoor Positioning System Based on RFID and Kinect

Ching-Sheng Wang, Chien-Liang Chen and You-Ming Guo

Abstract Global navigation satellite system is fully well developed in outdoor positioning nowadays; however, it cannot be applied in indoor positioning. The research of indoor positioning is rapidly increasing in recent years, and most researchers have paid much attention to RFID technology in indoor positioning; however, RFID is restricted by hardware characteristics and the disturbance of wireless signals. It is difficult to deal with the RFID positioning method. Therefore, this paper proposed an indoor real-time location system combined with active RFID and Kinect. Based on the identification and positioning functions of RFID, and the effective object extraction ability of Kinect, the proposed system can analyze the identification and position of persons accurately and effectively.

Keywords RFID · Kinect · Indoor · Positioning · Localization

1 Introduction

Location-based service (LBS) has received considerable attention in recent years. Taking the popular outdoor positioning system, GPS, as an example, many practical positioning applications have been developed. However, GPS performs too poorly inside buildings to provide usable indoor positioning, thus, studies on indoor positioning systems have also received considerable attention. A comparison of the common indoor positioning systems using the methods of RFID, WiFi,

C.-S. Wang (✉) · C.-L. Chen · Y.-M. Guo
Department of Computer Science and Information Engineering, Aletheia University,
Taipei, Taiwan, ROC
e-mail: Cswang@mail.au.edu.tw

C.-L. Chen
e-mail: au5199@mail.au.edu.tw

Ultrasounds, Bluetooth, and WIMAX, [1] found that RFID is the best choice for indoor positioning in consideration of accuracy and cost.

The research of RFID indoor positioning is increasingly in recent years. For example, The SpotON system first applied the positioning concept of GPS to indoor positioning and used the principle of Received Signal Strength Indication (RSSI) to calculate distance [2]. And Ni et al. proposed the famous LANDMARC positioning system [3]. Then, the VIRE, as proposed by Zhao et al. [4], the LEMT, as proposed by Yin et al. [5], are RFID positioning systems that aim to improve the positioning effect of LANDMARC. Besides, Wang et al. [6, 7] have proposed different positioning improvement mechanisms. However, even RFID is applicable to the indoor positioning, due its hardware characteristics, namely, wireless signals are likely to be disturbed by indoor environments and furnishings, the positioning accuracy limits of the RFID positioning system are difficult to address.

Therefore, this paper implemented an accurate indoor real-time location system using the motion-sensing function of Kinect released by Microsoft. As the Kinect can accurately extract persons, even for different heights, body types, and skin colors, it is very applicable to indoor real-time location positioning. Although Kinect is limited by infrared detection distance, the proposed system is complemented by the embedded Kinect RGB color camera; thus, it still can implement dynamic tracking of remote persons. It is also integrated with the ID function of RFID, and a precise person positioning and identification system is completely implemented.

The remainder of this paper is organized as follows. [Section 2](#) reviews past works on indoor positioning, including RFID positioning, video tracking, and Kinect positioning; [Sect. 3](#) introduces the overall architecture and positioning mechanisms of the proposed positioning system; [Sect. 4](#) describes the implementation and experimental results of the proposed system; [Sect. 5](#) gives conclusions.

2 Related Works

The research on dynamic video tracking has become more mature in recent years. Furthermore, some positioning studies have combined RFID and video tracking. Germa et al. [8] proposed a system for identifying persons using RFID and video tracking. They validated the feasibility of combining images with RFID techniques, and designed a system for tracking and identifying persons. However, this system requires a functionally complicated mobile robot and RFID reader equipped with multidirectional antenna, which has high cost. Mandeljc et al. [9] proposed a system using UWB (ultra-wideband) and video for indoor person positioning. Although this system has good positioning effect, multiple UWB equipment and cameras are required to be installed at the scene, thus, the system construction cost is very high.

Wang et al. [10, 11] have designed a system for real-time tracking and positioning of indoor persons by successfully combining image with RFID technologies.

However, it is found in experimental experience that there remain person overlapping and shielding problems, and the results of positioning are likely to be influenced by body height and type, thus, the implementation effect requires improvement. The occurrence of Kinect solves the aforesaid problems. As Kinect can accurately extract persons, it will not have failed identification resulted from different heights, body types, and skin colors, and the image processing chip embedded in Kinect can greatly increase the efficiency image processing, which renders it very applicable to the implementation of an indoor person positioning system.

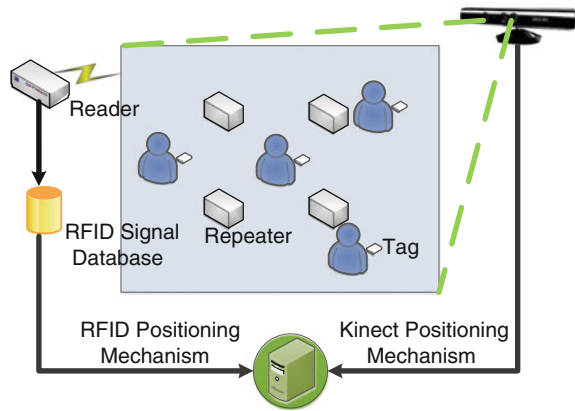
Some studies have used Kinect to design person positioning systems. Schindhelm [12] proved that the Kinect was very applicable to indoor positioning of public buildings. Nakano et al. [13] also proposed using Kinect for indoor person positioning. However, the aforesaid systems lack the function of person identification. This paper combines the accurate person positioning ability of Kinect with the person identification function of RFID to complete an indoor positioning system for accurate positioning and person identification.

3 System Architecture and Positioning Mechanisms

The positioning system proposed in this paper is consisted of two parts, including an active RFID positioning mechanism and a Kinect positioning mechanism (system architecture is as shown in Fig. 1). For the RFID positioning part, we placed multiple active RFID Repeaters in the scene in advance, and then the tester carried the active Tag while moving among the various blocks, meanwhile, the Reader integrated the Tag signals forwarded by all the Repeaters, and analyzed the signal strength scales of the Tag signals. Afterwards, the system defined the signal strength reference values of various positioning blocks according to the collected signal strength information, and stored related data in the database to complete the initialization analysis of a positioning environment. Through immediate addressing, the preliminary positioning of RFID can be completed by analyzing the Tag signals collected by all the Repeaters and matching the signal strength reference values in the database.

In the Kinect positioning system part, provided that Kinect is mounted high in the positioning area, the position information of moving persons can be instantly extracted by means of the accurate person detection function of Kinect, and then the actual positions of persons in the scene are determined by coordinate transformation equation. Finally, the preliminary positioning result of the RFID positioning system is compared with the positioning result of the Kinect positioning system, and pairing is completed on the principle of minimum distance, meaning the personal information in RFID is perfectly integrated with the precise positioning result of Kinect.

Fig. 1 Schematic diagram of system architecture



3.1 RFID Positioning Mechanism

When the Repeaters are denser in the RFID positioning system the positioning accuracy is higher; however, this increases cost and signal collision. Therefore, the proposed system only adopts appropriate RFID equipment that considers both accuracy and construction costs, uniformly places equipment within the positioning environment, and first conducts preliminary person positioning. Afterwards, the positioning system for accurate positioning and identification is completed by the precise positioning ability of Kinect. The main mechanisms of RFID positioning in this paper include a signal classification mechanism and a sensing overlap area analysis mechanism, as described below:

Signal Classification Most RFID positioning systems directly use signal strength as the basis of positioning; however, this method sometimes neglects the differences among the signal strengths of various Tags, whereas, the signal classification mechanism proposed in this paper can set appropriate signal strength intervals according to the individual differences among environments and Tag signal strengths, thus, effectively enhancing the stability of the positioning system.

The proposed system classifies signal strength into four levels according to the distance between RFID Repeater and Tag, and the signal strength values received by various Tags at 0.5 m, 1.5 m, and 3 m equidistance, are tested in the positioning field (as shown in Fig. 2). According to the data in Fig. 2, the signal strength value of individual Tags have a different RSSI value due to the differences in Tag and in environment; therefore, using fixed signal strength as the standard to estimate distance often results in considerable positioning errors.

Therefore, the proposed system receives the signal strength of different Tags at different distances, and filters occasional too strong or too weak unstable signals as an effective reference frame. When the signal strengths of all the Tags are collected and analyzed, the appropriate signal strength interval for each Tag can be set (as shown in Table 1) as a reference for subsequent determination of sensing range, thus, enhancing the stability of RFID positioning.

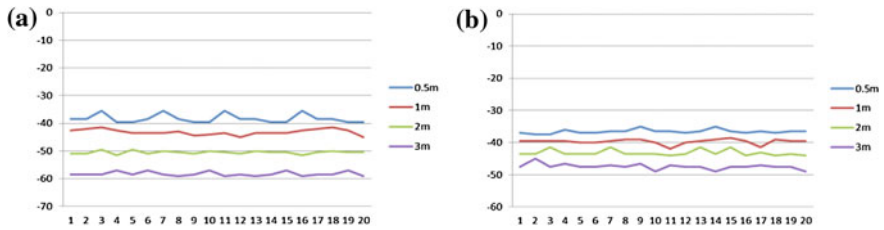


Fig. 2 Records of signal strengths of different tags at different distances. (a) Tag1 signal strength (b) Tag2 signal strength

Table 1 Signal strength intervals corresponding to signal levels of individual tags

Signal level	Distance between repeater and Tag	RSS of Tag1 (dBm)	RSS of Tag2 (dBm)	RSS of Tag3 (dBm)
L0	<0.5 m	-40	-45	-45
L1	0.5–1.5 m	-58	-50	-55
L2	1.5–3 m	-65	-58	-60
L3	>3 m	-68	-65	-70

Sensing Overlap Area Analysis Figure 3 shows the schematic diagram of the overlapped sensing areas of the proposed system, with an active RFID Repeater laid at intervals of 3 m within the positioning space, where the circular area in a radius of 3 m centered in the position of Repeater is the sensing range, and the positioning space is divided into multiple independent sensing overlapped areas. Afterwards, the positioning of the sensing overlap areas is completed by analyzing and matching the signal strength scales received by adjacent Repeaters. When the system locates sensing overlap areas, the centers of various blocks will be used as locating points to complete the preliminary positioning of relative positions, which are then integrated with the results of Kinect to determine the final locating points. There are five types of sensing overlapped areas in the proposed system, as described below.

Red block. It means the position is very close to a certain Repeater, thus, the signal strength detected by the Repeater is level L0;

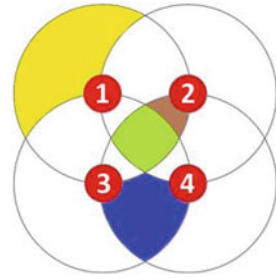
Brown block. It means the signal strength detected by Repeater2 has not reached level L0, but has reached level L1; the signal strength detected by Repeater1 and Repeater4 is level L2; while that detected by Repeater3 is level L3;

Green block. It means the signal strength detected by Repeater1, Repeater2, Repeater3, and Repeater4 is level L2.

Blue block. It means the signal strength detected by Repeater3 and Repeater4 is level L2; the other Repeaters have not detected signals above level L2.

Yellow block. It means the signal strength detected by Repeater1 is level L2; the other Repeaters have not detected signals above level L2.

Fig. 3 Schematic diagram of sensing overlap areas of RFID positioning



3.2 Kinect Positioning Mechanism

Microsoft Kinect has three lenses, the middle lens is an RGB color camera, with an infrared transmitter and an infrared camera placed on both sides, forming a depth sensor. In terms of the Kinect positioning mechanism in this paper, a Kinect is mounted in the positioning scene to instantly extract the position information of moving persons, and then, the actual positions of persons in the scene are calculated by the coordinate transformation equation, matched with the preliminary positioning result of the RFID positioning system, finally, personal ID is integrated with accurate positioning. The proposed system divides Kinect positioning into three positioning modes, as based on the operating characteristics of Kinect, as described below:

Within 4.5 m from Kinect (Including Skeleton Information) When a person enters into the 4.5 m sensing range of Kinect, the proposed system uses Kinect SDK to efficiently extract the skeleton information of the person, and uses the Ankle Left of skeleton as the positioning coordinates. When person positioning is completed, the system marks it with a blue frame (as shown in Fig. 4a).

Within 4.5 m from Kinect (Excluding Skeleton Information, Including Depth Information) Since the officially released SDK of Kinect only extracts the skeleton information of two persons, when there are more than two persons in the 4.5 m sensing range of Kinect, the proposed system uses the depth information extracted by Kinect to determine the lowest left endpoint of the persons as the positioning coordinates. When person positioning is completed, the system marks it with a green frame (as shown in Fig. 4b).

Beyond 4.5 m from Kinect (Excluding Skeleton and Depth Information) When a person is beyond the 4.5 m sensing range of Kinect, the proposed system uses the RGB color camera embedded in Kinect for person positioning by image processing. Traditional image processing modes often require complex and time consuming calculations, while the proposed system excludes the aforesaid two kinds of located persons before image processing-based positioning, which can effectively enhance system effectiveness. When person positioning is completed, the system marks it with a yellow frame, and the center point of the lower margin of the frame is used as the positioning coordinates (as shown in Fig. 4c). When the

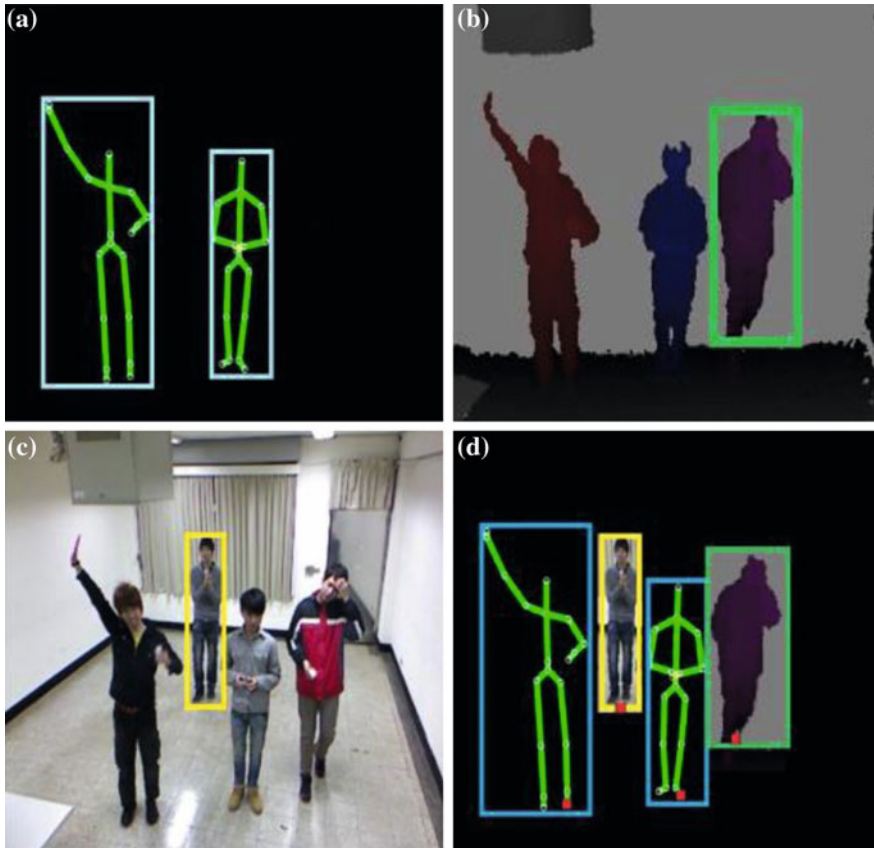


Fig. 4 Schematic diagram of Kinect positioning result. (a) Skel information (b) Depth information eton (c) RGB video (d) Integration result

three modes of positioning are completed, the system will automatically integrate all the positioning information (as shown in Fig. 4d).

4 Experimental Results

The implementation environment for the proposed system is an $8M \times 5M$ laboratory (as shown in Fig. 4a). The experimental equipment includes a notebook computer equipped with an active RFID Reader, four RFID Repeaters mounted within the scene, several RFID Tags carried by users, and one Kinect. The RFID equipment of the proposed system adopts the RFID chip module of Texas Instruments, and indoor layout and signal loss tolerance must be tested and set before implementing positioning (including signal collision, attenuation model,

interference of electromagnetic wave, etc.). The Kinect positioning system is composed by WPF (Windows Presentation Foundation).

First, the proposed system uses the RFID positioning mechanism proposed in this paper to obtain the ID information of persons and preliminary positioning results. Afterwards, the accurate positions of persons are obtained by the Kinect positioning mechanism, and the result of Kinect positioning is used as the final positioning coordinates. Finally, the pairing is completed on the principle of minimum distance, where the personal information in RFID is perfectly integrated with the precise positioning result of Kinect. The steps and experimental results of combining RFID positioning with Kinect positioning are as described below:

Step 1: RFID positioning: Fig. 5a shows the actual positioning scene, Fig. 5b shows the positioning result of RFID. The blue squares in Fig. 5b are the positioning results calculated by the RFID positioning system (including ID information). It is found in Fig. 5 that, the positioning results of RFID are slightly different from the actual positions, thus, the proposed system integrates the positioning results of RFID with the positioning results of Kinect in order to improve positioning accuracy.

Step 2: Kinect positioning: Fig. 6b shows the positioning results of Kinect. The red squares in Fig. 6b are the positioning results calculated by the Kinect positioning system (excluding ID information). The proposed system uses Kinect SDK to effectively extract the skeletons of persons, depth information, and RGB video in the scene, and determines the actual positions of persons in the scene by coordinate transformation. When person positioning is completed, the system uses green, blue, and yellow frames to mark the persons identified by the three kinds of Kinect positioning modes (as shown in Fig. 6a).

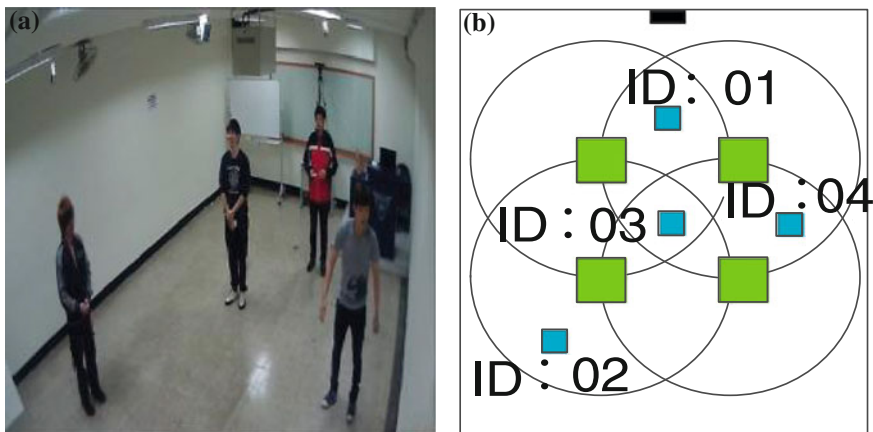


Fig. 5 Schematic diagram of RFID positioning results

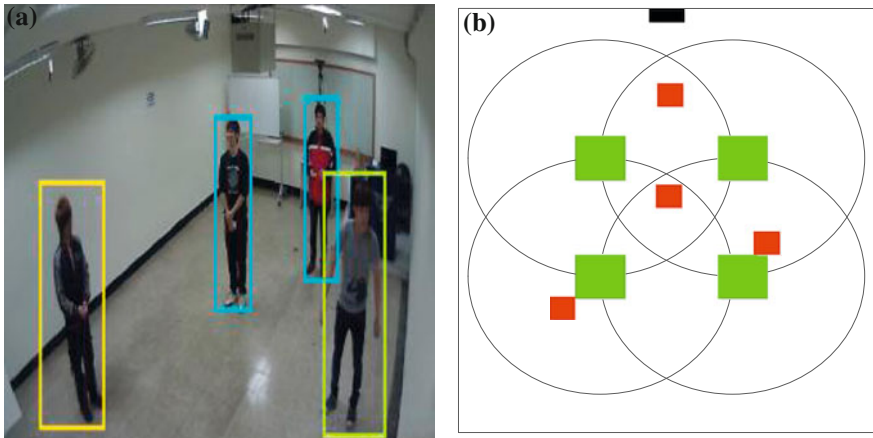


Fig. 6 Schematic diagram of Kinect positioning results

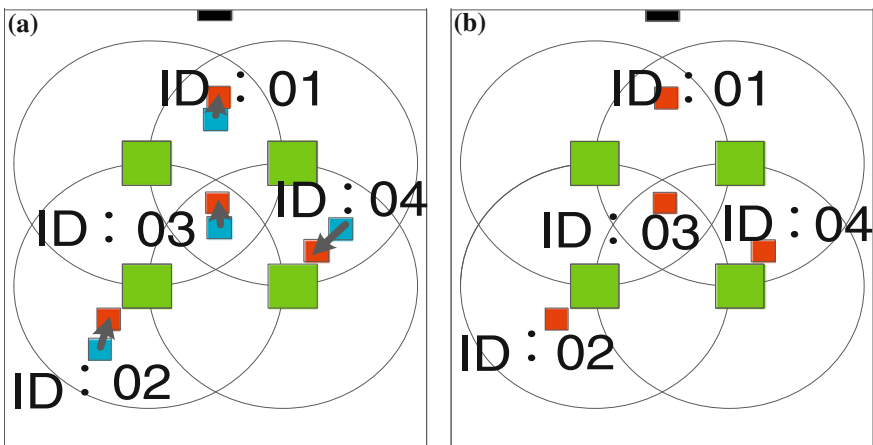


Fig. 7 Schematic diagram of pairing and integration result

Step 3: Integration of positioning results: Fig. 7 a shows the pairing process of RFID and Kinect positioning. The proposed system completes the pairing of RFID positioning results (blue squares) on the principle of minimum distance, as based on the positioning results of Kinect (red squares), and integrates the corresponding ID information. After pairing, the final positions displayed by the system are the coordinates calculated by Kinect positioning and the corresponding ID information (as shown in Fig. 7 (b)).

5 Conclusions

This paper proposed an indoor real-time location system combined with active RFID and Kinect. RFID signal classification and sensing overlap area mechanisms were used to complete the preliminary positioning of persons, combined with the stable and accurate person extraction ability of Kinect, in order to implement accurate personal identification and positioning. The experimental results proved that, in addition to implementing real-time personal identification, the proposed system can effectively enhance the accuracy and stability of person positioning. In addition, the proposed system only uses one Kinect, one RFID Reader, and several Repeaters and Tags, thus, effectively reducing the construction costs of an indoor positioning system.

Acknowledgments The authors would like to thank the National Science Council of the Republic of China, Taiwan for financially supporting this research under Contract No. NSC-101-2221-E-156-013 and NSC-99-2632-H-156-001-MY3.

References

1. Benavente-Peces C, Moracho-Oliva VM, Dominguez-Garcia A, Lugalde-Rodriguez M (2009) Global system for location and guidance of disabled people: indoor and outdoor technologies integration. In: The fifth international conference on networking and services, IEEE Press, Valencia, p 370–375.
2. Hightower J, Want R, Borriello G (2000) SpotON: an indoor 3D location sensing technology based on RF signal strength. UW CSE Technical Report (2000)
3. Ni LM, Liu Y, Patil AP (2003) LANDMARC: indoor location sensing using active RFID. In: The first IEEE international conference on pervasive computing and communications, Texas, pp 407–415
4. Zhao Y, Liu Y, Ni LM (2007) VIRE: active RFID-based localization using virtual reference elimination. In: The 2007 international conference on parallel processing, Xian, China
5. Yin J, Yang Q, Ni LM (2008) Learning adaptive temporal radio maps for signal-strength-based location estimation. *IEEE Trans Mob Comput* 7(7):869–883
6. Wang CS, Huang CH, Chen YS, Zheng LJ (2009) An implementation of positioning system in indoor environment based on active RFID. In: The second IEEE international conference on Ubi-media computing, Taipei, Taiwan, p 71–76
7. Wang CS, Huang XM, Hung MY (2010) Adaptive RFID positioning system using signal level matrix. *World Acad Sci Eng Technol* 46(135):746–752
8. Germa T, Lerasle F, Ouadah N, Cadenat V (2010) Vision and RFID data fusion for tracking people in crowds by a mobile robot. In: The computer vision and image understanding, vol 114, no. 6. Elsevier, New York, pp 641–651
9. Mandeljc R, Kovačić S, Kristan M, Perš J (2013) Tracking by identification using computer vision and radio. *Sensors* 13(1):241–273
10. Wang CS, Chen CC (2011) Flexible localization and identification system based on RFID and vision tracking technologies. In: 2011 international symposium on computer science and society, Kota Kinabalu, Malaysia, p 356–360
11. Wang CS, Cheng LC (2011) RFID & vision based indoor positioning and identification system. In: The third IEEE international conference on communication software and networks, Xian, China, pp 506–510

12. Schindhelm CK (2012) Evaluating SLAM approaches for Microsoft Kinect. In: The eighth international conference on wireless and mobile communications, Venice, Italia, p 402–407
13. Nakano Y, Kai K, Izutsu K, Tatsumi T, Tajitsu K (2012) Kinect positioning system (KPS) and its potential applications, 2012. In: International conference on indoor positioning and indoor navigation, Montbeliard-Belfort, France

Intuitional 3D Museum Navigation System Using Kinect

Ching-Sheng Wang, Ding-Jung Chiang and Yu-Chia Wei

Abstract Most of the museum navigation systems lack the function of user interaction. Even the small number of systems with user interaction functions, but required special and expensive devices, or may use non-intuitional operation methods. This paper used popular and economic Microsoft Kinect devices to establish an interactive 3D museum navigation system that supports intuitional commands. The users are allowed to intuitively control the 3D navigation system by physical motions and voice commands without wearing any additional appliances. The experiments show that the proposed system improves the effect of navigation satisfactorily.

Keywords Kinect · Intuitional · Museum · Navigation · Virtual reality

1 Introduction

In recent years, with rapid hardware and software development, the PC computing capability in 3D mode has greatly improved. With the appropriate hardware, 3D virtual reality can be displayed vividly. The 3D navigation system previously requiring high-end equipment for development can now be established by a PC. At present, most of the 3D navigation systems lack the functions of user interactions, while some navigation systems with interaction functions mostly use expensive

C.-S. Wang (✉) · Y.-C. Wei

Department of Computer Science and Information Engineering, Aletheia University,
Taipei, Taiwan, People's Republic of China
e-mail: cswang@mail.au.edu.tw

D.-J. Chiang

Department of Digital Multimedia Design, Taipei Chengshih University of Science
and Technology, Taipei, Taiwan, People's Republic of China
e-mail: dingjung.chiang@gmail.com

Table 1 Comparison of interactive devices

	Kinect	Wii remote	VICON	5DT glove
Cost	Low	Low	Extremely high	High
Wearing equipment	Not needed	Needed	Needed	Needed
Spatial requirements	Medium	Medium	High	Low
Accuracy	Medium	Low	High	High

interactive devices, or their operations are non-intuitional and need time to learn [1–3].

Currently, the common interactive devices used in navigation systems include VICON, 5DT Glove, Wii Remote, and Kinect. The comparison of those devices is shown in Table 1. The VICON system has accurate motion capture capability, but requires setting up multiple cameras and installing positioning marks on the users, thus, the overall cost is very high. The 5DT Glove induction glove is expensive and can only capture hand movement information, thus, its application is limited. Wii Remote, introduced by Nintendo in 2006, is one of the emerging interactive devices in recent years. Compared with other interactive equipment, Wii Remote has the advantages in cost and installation environment, thus, it is applied in human–machine interactive systems. However, Wii Remote is handheld, rendering it inconvenient and with poor positioning accuracy [4, 5].

In November 2010, Microsoft officially introduced the Kinect game controller. Microsoft Kinect has a RGB color camera and a depth sensor that consisting of an infrared transmitter and an infrared camera. Compared with Wii Remote, Kinect is not handheld, does not require wearing any auxiliary equipment, and has relatively better performance in spatial requirements and capture motion accuracy. Therefore, this paper used the Kinect device to capture user motion and voice data, and developed an interactive 3D museum navigation system that supports intuitional commands.

The remainder of this paper is organized as follows. Section 2 describes the recent research results in Kinect-related human–machine interaction; Sect. 3 introduces the system architecture and three types of interactive commands; Sect. 4 discusses the implementation environment and test results; finally, the conclusion is given in Sect. 5.

2 Related Works

At present, Kinect has been used as the interactive device in some systems. These systems, according to whether the recognition method involves human skeleton information, can be divided into two types. One does not require the use of skeleton information, and is mainly based on the depth image for analysis of the user’s hand positions and motion trajectory in order to determine the different interactive commands [6–8]. The second type is mainly based on the user’s

skeleton information to determine the user's body motions to implement the various types of interactive commands [9–11].

Regarding studies on Kinect without using skeleton information, Wilson and Benko proposed an interactive projection system consisting of three projectors and Kinect [6]. The system uses Kinect to obtain the depth image in order to analyze user position and allow the users to interact with the virtual objects in the projected screen. Schlatter et al. used depth information to analyze the user's hand position and hand movements to allow the user to interact with the virtual scenes [7]. Gallagher captured the user's hand image by image recognition and analyzed the fingers' movement trajectory to establish an intuitional gesture interactive system [8].

Regarding studies on Kinect using skeleton information, Kammergruber et al. used the relative position of the human skeleton to determine the corresponding operational commands, and applied it in virtual environment navigation operations [9]. The relative position between the joints was used as the basis for the determination of operational commands, rather than intuitional motions; therefore, it is less likely to meet the demand for intuitional operation commands. Sakai et al. used human skeleton information to analyze the user's physical motions to determine the corresponding interactive commands [10]. Based on the physical motion, the operation is fairly intuitive. However, the various motions cannot be mixed for application, thus, interaction is very limited. Freitas et al. used human skeleton information to prepare a set of rehabilitation interactive games [11]. The system can identify the various joint groups and analyze specific body motions.

As discussed above, the object detail level of the depth image captured by the depth sensor of Kinect decreases with increasing distance from Kinect, thus, the operational distance should be at least 3 m, if using the depth image to identify detailed hand commands. On the other hand, when the distance between user and Kinect is at least 3 m, Kinect cannot capture the user's full body image, thus, it cannot identify body motions. As a result, the intuitiveness and variety of interactive commands are very limited. Moreover, if users manipulate the interactive system with both hands in the air, they will easily tire.

The system proposed in this paper allows the user to stand in an area at a distance of about 3.5 m from Kinect in order to facilitate skeleton identification and analyze the characteristics of the various joints, including angle and direction, before determining and implementing the corresponding physical commands, including turnaround, moving, and view. Although it is difficult to identify detailed hand movements at such a distance, the system can determine and implement the corresponding hand interaction commands, including scaling, rotation, and moving, according to the relative positions of both hands in the space. Moreover, the proposed system can combine intuitional body motions and hand interactive command.

Dam et al. summarized the common somatosensory operational methods used in virtual environments, and compared the advantages and disadvantages of various methods [12]. This paper categorizes somatosensory operations into Selection and Navigation. The operational methods in the Selection category can be divided into three types, including Hover, Push, and Hold. The operational methods in the

Navigation category can be divided into Virtual Foot DPad + Body Turn, Virtual Button, and Virtual Circle + Body Turn. The method and principle of selecting objects, as proposed in this paper, is similar to the Hover method, as analyzed in the above mentioned paper. It has the advantages of high intuitiveness and operational simplicity. The navigation command, as proposed in this paper, is similar to the method of Virtual Foot DPad + Body Turn, as analyzed in the above mentioned paper. The method can control movement directions according to the direction the body is facing, and determine backward or forward movements by stepping forward or backward. This method is regarded as having some advantages, including high intuitiveness and operational simplicity.

3 System Architecture and Commands

The system architecture is as shown in Fig. 1, which is consisted of the interaction interface component, command analysis component, and an immersive 3D display component. Regarding the interaction interface, the proposed system uses Microsoft Kinect for Windows SDK to connect Kinect in order to capture the information of the skeleton coordinates and sounds of the user. The angles of the various joints are analyzed to obtain the motion characteristics of the user. Microsoft Speech API is applied to analyze the voice content of the user. The command analysis component is responsible for comparison and implementation of various motion commands, hand commands, and voice commands. Besides, the 3D display component used the nVIDIA 3D Vision and 3D projector to generate the immersive 3D environment. The proposed system supports three types of intuitional commands as described below.

3.1 Motion Commands

Body motion command is based on motion characteristics, such as angle and direction of body joints, as the identification conditions. The relevant commands are designed by intuitional motion characteristics, include turnaround command, moving command, and view command. The functions of various commands are illustrated as follows:

Turnaround Command. The proposed system calculates the desired angle of rotation of the user according to the rotational vector of the shoulders, and the display scene of the navigation system is rotated according to the rotational direction of the user (as shown in Fig. 2).

Moving Command. The proposed system determines the user's step by analyzing the skeleton information of the feet of the user. When the user moves forward one step, it implements the command of moving forward. When the user moves backward one step, it implements the backward motion command.

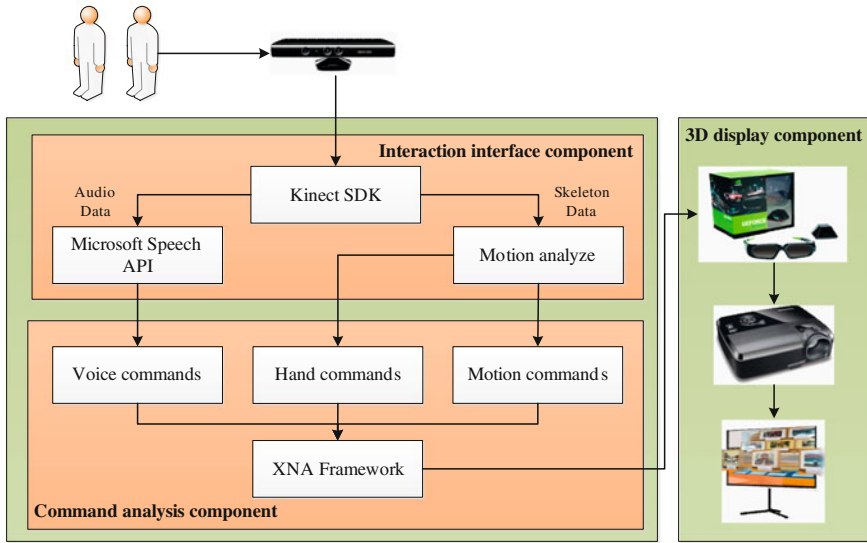
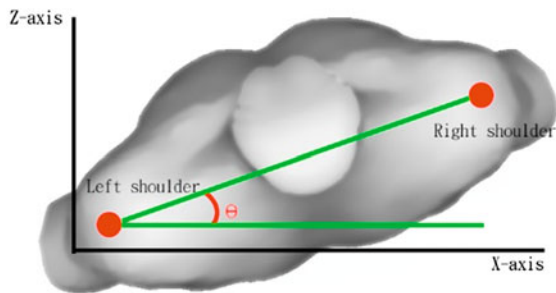


Fig. 1 Schema diagram of system architecture

Fig. 2 The angle computation of turnaround command

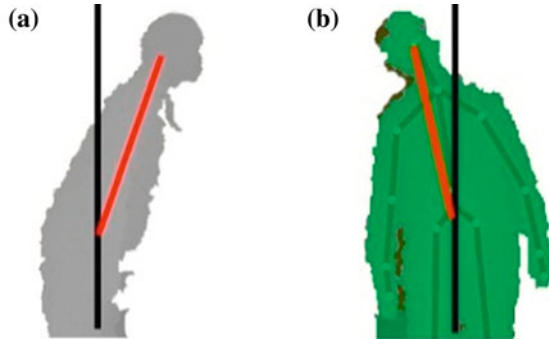


View Command. The system determines the user’s browsing motion by analyzing the user’s spine skeleton information. When the user bends forward or backward, the display image is zoomed in or out (motions are as shown on the left of Fig. 3). When the user’s head moves left or right, the display image will be rotated anti-clockwise or clockwise simultaneously (as shown in Fig. 3).

3.2 Hand Commands

The hand commands are the most common interactive commands. However, if the user is not standing in the center, the coordinate conversion in the virtual space will often be affected, thus, the interaction effect is affected accordingly. In this

Fig. 3 Schematic diagram of view commands **a** the user's bending forward, **b** the head is right-skewed



paper, user's chest position is used as the relative coordinated center. By calculating the relative position of the chest and hand, it is converted into the absolute position in the interaction system. This conversion method regards the individual user as the center of the coordinate system. In addition to avoiding the impact of the standing position, it can simultaneously support the operation of multiple persons to effectively enhance system flexibility and variety. The hand-related commands of this system are illustrated as follows:

Selection Command. The proposed system analyzes the hovering time of the hand coordinate on the object. When the time is more than certain seconds, it implements selection commands similar to a left button mouse click (using left hand) or right button (using right hand).

Scaling Command. When an object is selected, if it is a display object that can be adjusted in size, the system can implement the corresponding zoom commands of enlarging or reducing the object according to the analysis of the change in distance of both hands.

Rotation Command. When an object is selected, if it is a rotational display object, the system can implement the various directional rotation commands by analyzing the information of the vectors of both hands in space.

Shift Command. When an object is selected, if it is a movable interaction object, the system can shift the position of the object in the virtual space according to the user hand position.

3.3 Voice Commands

Voice recognition technology has become considerably mature and has been gradually applied in general life, such as Siri of iOS. In a PC, there are many development kits, including Microsoft Speech API, IBM Via Voice, and Toshiba LaLaVoice. The Microsoft-developed Speech Application Program Interface (Speech API) is a free software package. Its compatibility in the Windows operating system is extremely high, and the recognition effect is satisfactory.

Therefore, this paper used Microsoft Speech API as the major voice recognition software package.

In Microsoft Speech API, the language with the highest rate of voice recognition is English. Hence, the proposed system designs the simple voice commands in English. The main commands for navigation scenes include, move forward, move backward, turn left, turn right, look up, and look down. Moreover, the commands for object operation include, select, zoom in, and zoom out. In addition, the voice commands could be integrated with motion and head commands to enhance the flexibility of navigation control.

4 Implementation and Result

The proposed system’s configuration environment is shown in Fig. 4. First, in a 5×8 m space, this paper used nVIDIA 3D Vision equipment and a ViewSonic PJD-64213D projector to establish an immersive 3D navigation scene, and placed a Microsoft Kinect under the projection screen. The system hardware includes a PC with an Intel Core i5 CPU; the system development environment uses C# and Kinect for Windows SDK. The virtual scene for testing is the “3D Virtual Oxford college Museum” established using 3Ds Max and XNA Framework 4.0.

During the system test, 1–2 users stood on the left and right at a distance of 3.5 m before Kinect to facilitate the system obtaining the full body skeleton information and capture voice commands. Various body motion commands, hand interactive commands, and voice commands were alternately used to operate the 3D museum navigation system. The implementation results are shown in Fig. 5. The various tests and analysis results are shown in Table 2, and discussed below.

Using Hand Commands Only. When using hand movements for the operation of the interaction system, some operations, such as object selection and scaling, and rotation and movement, can be rapidly and intuitively completed. However, regarding moving, turnaround, and other operations of scenes, as it usually takes a

Fig. 4 Schema diagram of system environment



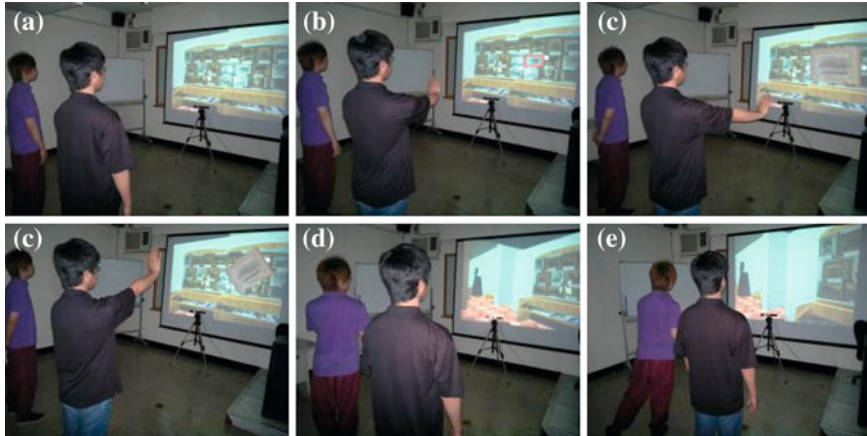


Fig. 5 Schema diagram of implementation results (a) Original image (b) Selection commands (c) Scaling command (d) Rotation command (e) Turnaround command (f) Moving command

Table 2 Comparison of interaction commands

	Hand commands [6, 7]	Body commands [9, 10]	Our system
Selection and scaling commands	Rapid operation and highly intuitive	Hard to operate	Rapid operation and highly intuitive
Rotation and moving commands	Rapid operation and highly intuitive	Hard to operate	Rapid operation and highly intuitive
Moving, turnaround and view commands	Tires easily, and poor intuitiveness	Easy to operate, highly intuitive	Easy to operate, highly intuitive
Multi-user operation	No	No	Yes
Voice commands	No	No	Yes

longer time to raise the hands, the operation is relatively more tiring, and thus, is less intuitive.

Using Body Commands Only. When using body motions for the operation of the interaction system, it is very difficult to complete some operations, including object selection and scaling, and rotation and moving. However, regarding the operations of moving and turnaround of scenes, it is very easy and highly intuitive to complete by stepping or turning the body.

Using Hand and Body Commands. The proposed system can use hand and body motions for operation. Therefore, operations including object selection, scaling, rotation, and moving, or operations of scene moving and turnaround, can be intuitively and rapidly completed. Moreover, it can allow two users to use the system simultaneously to increase the fun of interaction. In addition, the proposed system has voice commands. It can use simple English words to implement multiple types of commands to effectively enhance the flexibility of the system and improve the problem of fatigue.

5 Conclusions

This paper adopted economic Microsoft Kinect to successfully develop an interactive 3D museum navigation system supporting intuitional commands. The proposed system can support intuitional motion, hand, and voice commands, which can be combined alternately in application to realize more diversified interactive functions. Compared to other interactive systems, the proposed system has advantages of ease and rapid operation, high intuitiveness, and multiple-user accessibility, which can enhance the impression and performance of navigation effectively. Our future research will integrate the popular mobile devices in order to realize more diversified applications of 3D navigation system.

Acknowledgments The authors would like to thank the National Science Council of the Republic of China, Taiwan for financially supporting this research under Contract No. NSC-101-2221-E-156-013 and NSC-99-2632-H-156-001-MY3.

References

1. Kulik A, Blach R, Frohlich B (2006) “Two - 4—six”—a handheld device for 3D-presentations. In: IEEE symposium on 3D user interfaces, Virginia, pp 167–171
2. Jeong S, Choi W, Hashimoto N, Sato M (2005) Reactive virtual human system with haptic sensation and adaptive function. In: The 2005 international conference on cyberworlds, Yokohama, Japan, pp 461–466
3. Benko H, Feiner S (2007) Balloon selection: a multi-finger technique for accurate low-fatigue 3D selection. In: IEEE symposium on 3D user interfaces 2007, North Carolina, pp 79–86
4. Schlömer T, Poppinga B, Henze N, Boll S (2008) Gesture recognition with a Wii controller. In: The 2nd international conference on tangible and embedded interaction, Bonn, Germany, pp 11–14
5. Wang CS, Kao SS (2008) An intuitional 3D virtual navigation system supporting motion and voice commands. In: The IASTED international conference on internet and multimedia systems and applications 2008, Hawaii, pp 18–20
6. Wilson A, Benko H (2010) Combining multiple depth cameras and projectors for interactions on, above and between surfaces. In: The 23rd annual ACM symposium on user interface software and technology, New York, pp 273–282
7. Schlatter O, Migge B, Kunz A (2012) User-aware content orientation on interactive tabletop surfaces. In: 2012 international conference on cyberworlds, Darmstadt, Germany, pp 246–250
8. Gallagher G (2010) CSAIL brings ‘minority report’ technology alive. MIT CSAIL News. <http://www.csail.mit.edu/node/1362>
9. Kammergruber F, Ebner A, Günthner PW (2012) Navigation in virtual reality using Microsoft Kinect. In: 12th international conference on construction application of virtual reality, Taipei, Taiwan, pp 350–359
10. Sakai T, Fujimura W, Robert S, Kosaka T, Shirai A (2012) AccuMotion: intuitive recognition algorithm for new interactions and experiences for the post-PC era. In: The 14th virtual reality international conference, Laval, France

11. Freitas DQ, Da Gama AEF, Figueiredo L, Alves T, Marques-Oliveira D, Teichrieb V, Araújo C (2012) Development and evaluation of a Kinect based motor rehabilitation game. In: Brazilian symposium on computer games and digital entertainment, Brasília, Brazil, pp 144–153
12. Dam PF, Loaiza M, Soares LP, Raposo AB (2012) A study of selection and navigation techniques using Kinect in VR. In: The 14 symposium on virtual and augmented reality, Niteroi, Brazil

Application of QR-Code Steganography Using Data Embedding Technique

Wen-Chuan Wu, Zi-Wei Lin and Wei-Teng Wong

Abstract Quick response (QR) code is a convenient product for mobile phone user. People can use the Smartphone camera to capture the code, and then decode it through dedicated reader application. Usually the code stands for text, contact information, or a web hyperlink. Users scan the image of QR code to display information or open a website page in the phone's browser. QR codes appear everywhere on posters, publicity flyers, TV advertisements, and even business cards. Since QR code looks like random noise, its existence may hurt the picture of commodities. In this paper, we propose a data embedding scheme to camouflage the existence of QR code. Experimental results showed that the proposed scheme hides the QR code successfully. Moreover, the quality of stego-images is nearly to 30 dB.

Keywords Quick response (QR) code · Data embedding · Vector quantization · Codebook clustering

1 Introduction

Recently, Internet has gradually become an important means of communication over human daily life. People can receive the news and information easily by using various mobile devices to browse the web pages anywhere and anytime. Before linking to the website, a designated Uniform Resource Locator (URL) must be inputted in advance. As we all know, it is more difficult and time-consuming to type by using phone keypad than keyboard [1, 2]. To solve this issue, the quick response code [2–4], QR code for short, is introduced in recent years.

W.-C. Wu (✉) · Z.-W. Lin · W.-T. Wong
Department of Computer Science and Information Engineering, Aletheia University,
Tamsui, Taipei 25103 Taiwan, Republic of China
e-mail: au4387@au.edu.tw

QR code, which consists of black and white square dots, is a 2-dimensional barcode in a square shape. Mobile phone users can read the code easily by using an app with a QR-code scanner. And, data of any format such as text, emails, URL, phone number, and more can be translated as a QR code through code generator. As a result, QR codes have become common in consumer advertising and personal trademark. More and more products and goods attach to the relevant QR code. However, its existence hurts the picture of commodities because QR codes look like random noise.

In this paper, we aim at solving the mentioned problem. We utilize the data hiding technique to camouflage the appearance of QR code. Data hiding is an information security way to protect the secrets by embedding it into an unimportant cover media, so that the data cannot be perceptible [5]. Overall speaking, the quality of the stego-media carried with secrets is rather high and acceptable. Therefore, this paper employs this advantage of data hiding to cover the QR code. The rest of this paper is organized as follows. Section 2 introduces the popular QR code and the basic concepts of VQ compression technique. Section 3 describes the proposed data embedding algorithm in detail. Section 4 gives some experimental results for proving the proposed algorithm. Finally, conclusions are drawn in Sect. 5.

2 Related Works

2.1 Quick Response (QR) Code

Quick response code [2–4], is a variation and evolution of standard barcode, first designed in Japan. Traditional barcodes attached to items are optical machine-readable labels that record items' information. Different from that, QR code is a 2-dimensional barcode that can contain more information including number, character, English, Japanese or Chinese language. Up to now, more and more goods and items are attached to QR code, poster and business card for example.

Figure 1 shows a QR code for the website of URL “<http://yahoo.com.tw>”. The code is a square which consists of black square dots arranged on a white background [1]. In particular, there are special square patterns in three corners. These three patterns are helpful to image orientation and alignment. Therefore, users can

Fig. 1 QR code for the URL “<http://yahoo.com.tw>”



Table 1 Error correction capability of QR code

Level	Recovered codewords
Low (L)	7 % of codewords to be recovered
Medium (M)	15 % of codewords to be recovered
Quartile (Q)	25 % of codewords to be recovered
High (H)	30 % of codewords to be recovered

scan the QR code quickly whether any angle, and then decode the information correctly. The major purpose of QR codes is for Smartphone users to link the website quickly or acquire the related data immediately without any typing. Because of its fast readability and greater storage capacity, recently, QR code has become popular outside and widely applied to applications of commercial tracking, transport ticketing, product labeling, personal contact information, and so on [2, 4].

Since the image of a QR code is captured by Smartphone cameras, some mistakes might be induced in the decoding phase. Hence, a QR reader must be provided with the capability of error correction. Even though few of damages appeared in it, the QR code can still be decoded correctly. As shown in Table 1, there are four error correction levels by using Reed Solomon algorithm [4]. The higher the error correction level, the less storage capacity will be. It is suggested commonly to adopt medium level to correct 15 % of codewords. Although it is easy and fast to decode instead of traditional typing, the existence of QR code will hurt the picture of commodities, posters and advertisements especially.

2.2 Vector Quantization

Vector quantization [6], VQ for short, is an efficient and simple technique for lossy data compression. This technique works by replacing small original blocks with indices into a codebook [7]. Take grayscale images as an example of VQ compression. Initially, it is necessary to design a set of representative image blocks beforehand to form a codebook $CB = \{C_0, C_1, \dots, C_{N-1}\}$, in which each element C_i is a k -dimensional codeword. The literature in [7] utilizes vectors clustering and training approach, namely LBG algorithm, on a few testing images, where each of them is divided into a pile of $n \times n$ blocks (i.e. $k = n^2$). A good codebook is able to reduce block redundancies and minimize the distortion between the original image and the reconstructed image.

Secondly, an image to be compressed is performed on the VQ encoding procedure. As the name implies, the image needs to be divided into non-overlapping blocks of $n \times n$ pixels and then transformed into a k -dimensional vector. In order to minimize the visual distortion, each vector must seek the VQ codebook CB to find out its reproduction vector. Certainly, the reproduction is the most similar than other codewords in CB . The corresponding index of the found codeword is

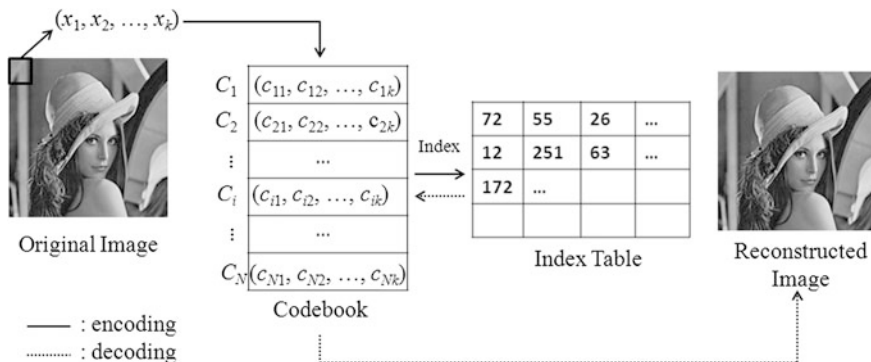


Fig. 2 The illustration of VQ encoding and decoding procedure

subsequently collected in an index table. That table is the product of the encoding procedure and its volume is far less than that of the original image indeed. During the decoding procedure, the identical codebook is employed to translate the index back to its corresponding codeword for the reconstructed image.

Table look-up operation in the decoding procedure can accelerate the index decoding process. For this reason, VQ has the advantage of fast decoding and low bit rate in practice [8]. Figure 2 shows the illustration of encoding and decoding an image by VQ. In which, the solid line means the vector encoding process and the dotted line means the index decoding process. Suppose that each image vector is $X = (x_1, x_2, \dots, x_k)$ and the i th codeword is $C_i = (c_{i1}, c_{i2}, \dots, c_{ik})$. For each X , the most similar codeword C_w is the best-matched difference vector with the least Euclidean distance as shown in Eq. (1). Note that w is the index of winner C_w and its bit size is $\log_2|CBI|$. When in the decoding phase, the vector of index w is used to reconstruct the corresponding image block.

$$d(C_w) = \underset{\forall i}{\text{Min}}\{d(C_i)|d(C_i) = \sqrt{\sum_{j=1}^k (c_{ij} - x_j)^2}, i = 1, 2, \dots, N\}. \quad (1)$$

3 The Proposed Scheme

In order to reduce the destruction of appearance, we attempt camouflaging the existence of QR code in a poster or picture. Here, the techniques of edge detection [9] and VQ compression [8, 10, 11], are adopted to embed a 2-dimensional QR code as invisible secret data. The situational diagram of QR code for mobile users is shown in Fig. 3. When mobile users capture a picture, the QR code embedded into it can be extracted easily, and then decode the code by using dedicated QR reading devices to open the website through browser.

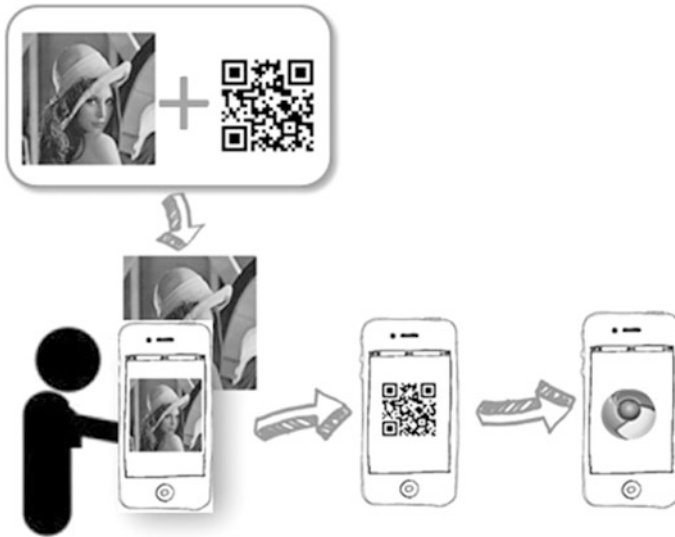


Fig. 3 Situational diagram for mobile users

Edge detection [9] is one of morphology operations, which aims at identifying the apparently edge or contour of images. These edge points whose vertical and horizontal gradient values exceed a predefined threshold TH are usually situated at which image brightness changes sharply. If the pixels at these edge points are slightly modified, we cannot perceive any difference between images before and after. For this reason, we utilize edge detection to embed QR code into these edge points. In addition, considering that fast decoding of VQ, the proposed scheme also introduces it during the data embedding procedure. Our scheme includes two parts: the data embedding procedure and the extraction procedure.

Figure 4 shows the flowchart of the proposed scheme. In embedding procedure, first of all, only partial pixels in the original image are reserved as the region of interest (ROI). That is to say, the proposed scheme embeds a QR code in ROI merely. And then, we perform Sobel's edge detector on ROI to obtain an edge map. According to this map, we will select complex areas out for data embedding. If there are four edge points in a $n \times n$ block of the edge map, it is regarded as a complex block; otherwise, it is regarded as a non-complex block. Here, only complex blocks will be taken into account for the next embedding process. The detailed steps for the data embedding are stated below.

Step 1: Prepare a VQ complicated codebook CB of size N by using LBG training algorithm. Note that, only the complex blocks in test images are chosen to be training data.

Step 2: Cluster the codewords in CB according to the criterion of the Euclidean distance to obtain $N/2$ pairs almost [8]. Each pair holds only two codewords C_i and C_j , where $Alt(C_i) = C_j$ represents the alternative codeword

of vector C_i is C_j . Finally, CB will be partitioned into three sub-codebooks such that $CB = \{SC_0, SC_1, SC_x\}$ [10].

Step 3: Convert a QR code into a binary bit stream $S = \{s_i \mid s_i \in [0,1]\}$.

Step 4: Search the most similar codeword C_w from CB for each complex block.

- (1) C_w in SC_0 : If bit s_i is 0, the block will be replaced by codeword C_w .
Otherwise, It will be replaced by codeword $Alt(C_w)$ if bit s_i is 1.
- (2) C_w in SC_1 : If bit s_i is 1, the block will be replaced by codeword C_w .
Otherwise, It will be replaced by codeword $Alt(C_w)$ if bit s_i is 0.
- (3) C_w in SC_x : None of binary bit is embedded into the complex block.

Step 5: Repeat Step 4 above again and again until all the bits in S have been processed.

After the data embedding steps as illustrated above, the proposed scheme will output a new stego-image, which looks almost the same as the original image without any noticeable distortion. When users want to acquire the embedded QR code out of stego-image, he/she needs to adopt the same complicated codebook CB and pair it into three sub-codebooks $SC_0, SC_1,$ and SC_x . The following is the data extraction algorithm as shown in Fig. 4b.

Step 1: Derive the ROI region just the same as the embedding above.

Step 2: Divide ROI region into several and non-overlapping $n \times n$ blocks.

Step 3: Search the same codeword C_w from CB for each codeword.

- (1) If C_w in SC_0 , it means the block carries the binary bit ‘0’ of QR code.
- (2) If C_w in SC_1 , it means the block carries the binary bit ‘1’ of QR code.
- (3) If C_w in SC_x or C_w not found, it means the block does not hide any data of QR code.

Step 4: Repeat Step 3 mentioned above again and again until all the blocks have been processed.

Step 5: Convert a series of binary bits into a QR code. Then, decode it by using the dedicated QR reader to obtain specific text, URL, or other information.

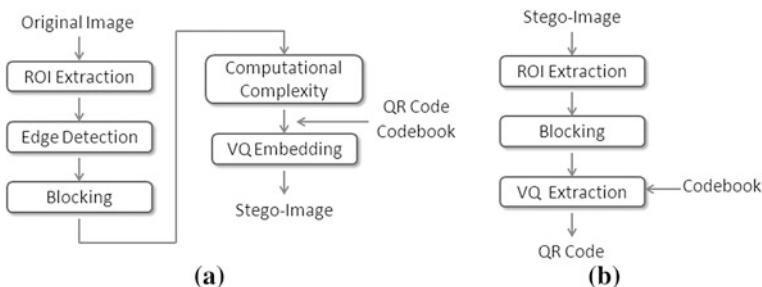


Fig. 4 Flowchart of the proposed scheme. **a** Embedding procedure. **b** Extraction Procedure

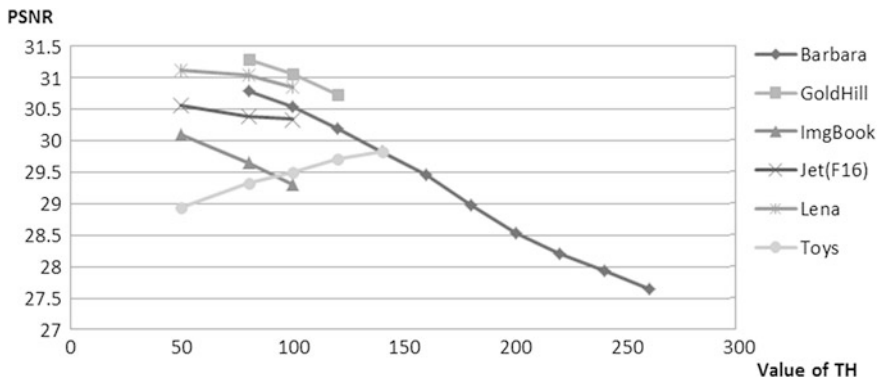


Fig. 5 PSNR results at different thresholds under codebook (N = 512)

4 Experimental Results

In our experiment, six images (512 × 512 pixels), including “Lena”, “Jet (F16)”, “Toys”, “Barbara”, “GoldHill”, and “ImgBook”, were taken as the cover carriers. Each of which was drawn out the ROI region of 488 × 488 pixels to embed the QR code as shown in Fig. 1. In addition, two codebooks of sizes 256 and 512 were acquired by performing the LBG training algorithm on five standard images “Jet (F16)”, “Lena”, “Toys”, “Boat”, “Baboon”. Figure 5 shows the quality results in PSNR at different thresholds (TH), where the codebook size is 512. It can be obviously seen that the resulted quality is degraded mostly when the value of TH rises. The reason is that the higher threshold value TH is, the more complex codewords collected in CB but the more degraded quality will be. Therefore, it is suggested to adopt the thresholds TH ranged between [100, 120].

Table 2 presents the performance of the six test images under different codebooks and thresholds, in which N/E means that the image cannot embed the QR code under the assigned condition. In addition, Fig. 6 shows the visual results of the proposed scheme for subjective evaluation. The embedded results for the “Lena”, “Jet (F16)”, and “Barbara” images are still acceptable. Such a visual quality, over 30 dB, cannot easily notice the appearance of QR code.

Table 2 Performance (PSNR, dB) of different test images under various variables

Images	N = 256, TH = 100	N = 512, TH = 100	N = 256, TH = 120	N = 512, TH = 120
Barbara	29.56	30.54	29.13	30.19
GoldHill	30.57	31.07	30.35	30.73
ImgBook	29.01	29.30	N/E	N/E
Jet (F16)	29.75	30.34	N/E	N/E
Lena	30.11	30.85	N/E	N/E
Toys	N/E	29.50	N/E	29.71

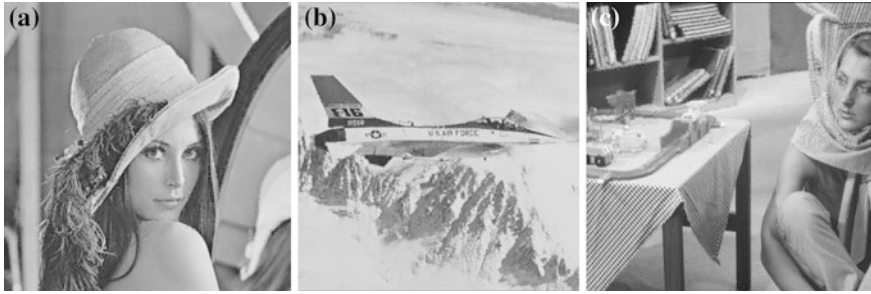


Fig. 6 The embedded results under $N = 512$ and $TH = 100$. **a** Lena (PSNR = 30.85 dB). **b** Jet (F16) (PSNR = 30.34 dB) **c** Barbara (PSNR = 30.54 dB)

5 Conclusions

A simple and efficient QR-code steganographic scheme is proposed in this paper. We combine the advantages of edge detection and vector quantization to camouflage the appearance of a QR code. First is to extract the ROI region out of the original image. Next, an edge map is generated in order to find out complicated image blocks. Merely these blocks are hidden into the bit stream of QR code by using VQ coding. As shown in the experiments, the performance of the proposed scheme in both quality and efficiency is quite satisfactory. In the future, we intend to investigate the extension of our proposed scheme to bear some image processing attacks in stego-images.

Acknowledgments This work was supported by National Science Council, Taiwan, Republic of China, under the Grant NSC 101-2221-E-156-011 and NSC 99-2632-H-156-001-MY3.

References

1. Deshmukh O, Sonavane S (2013) Multi-share crypt-stego authentication system. *Int J Comput Sci Mobile Comput* 2(2):80–90
2. Huang HC, Chang FC, Fang WC (2009) Applications of reversible data hiding techniques with the quick response codes. *Commun Comput Inf Sci* 58:1–8
3. Kieseberg P, Leithner M, Mulazzani M, Munroe L, Schrittwieser S, Sinha M, Weippl E (2010) QR code security. In: 4th international workshop on trustworthy ubiquitous computing, Paris, France, pp 1–6
4. Rungraungsilp S, Ketcham M, Kosolvijak V, Vongpradhip S (2012) Data hiding method for QR code based on watermark by compare DCT with DFT domain. In: 3rd international conference on computer and communication technologies, India, pp 144–148
5. Wu WC, Wu YC (2012) Improved reversible data hiding based on residue histogram shifting. In: 6th international conference on genetic and evolutionary computing, Kitakyushu, Japan, pp 23–26
6. Gray RM (1984) Vector quantization. *IEEE ASSP Mag* 1(2):4–29

7. Linde Y, Buzo A, Gray RM (1980) An algorithm for vector quantizer design. *IEEE Trans Commun* 28:84–95
8. Chang CC, Wu WC, Chen YH (2008) Joint coding and embedding techniques for multimedia images. *Inf Sci* 178:3543–3556
9. Shrivakshan GT, Chandrasekar C (2012) A comparison of various edge detection techniques used in image processing. *Int J Comput Sci Issues* 9(1):269–276
10. Chang CC, Wu WC (2005) A steganographic method for hiding secret data using side match vector quantization. *IEICE Trans Inf Syst* E99-D(9):2159–2167
11. Qin C, Chang CC, Chen KN (2013) Adaptive self-recovery for tampered images Based on VQ indexing and inpainting. *Signal Process* 93(4):933–946

Combining FAHP with MDS to Analyze the Key Factors of Different Consumer Groups for Tablet PC Purchasing

Chen-Shu Wang, Shiang-Lin Lin and Heng-Li Yang

Abstract People living become highly informationized, resulting in Tablet PC has developed vigorously in recent years. To understand the consideration of the customers when purchasing Tablet PC is getting important. This study applies Fuzzy Analytic Hierarchy Process (FAHP) to find out the key factors affecting the consumer's purchasing of Tablet PC. Further, combining Multidimensional Scaling (MDS), decision maker can realize that the similarity and difference among the consumer groups. Through literature review and expert interview, we select appropriate evaluation components to construct the hierarchical structure of evaluation and conduct the AHP questionnaire on 15 experts. The FAHP analysis results show that the importance of evaluation criteria in following order: operating system, color and hardware while customer intend to buy a Tablet PC. Furthermore, through the perceptual map of MDS, we could be find out the consumer groups of Businessman and Officer, as well as Student and Housewife, have similar demands when purchasing Tablet PC.

Keywords Fuzzy analytic hierarchy process (FAHP) • Multidimensional scaling (MDS) • Tablet PC

C.-S. Wang · S.-L. Lin (✉)
Graduate Institute of Information and Logistics Management, National Taipei University of Technology, Taipei, Taiwan, China
e-mail: t9938015@ntut.edu.tw

C.-S. Wang
e-mail: wangcs@ntut.edu.tw

H.-L. Yang
Department of Management Information Systems, National Chengchi University, Taipei, Taiwan, China
e-mail: yanh@nccu.edu.tw

1 Introduction

Thanks to the advancement of the electronic technology and the mobile networks, people living become highly informationized, resulting in e-Book, Smartphone and Tablet PC start to develop vigorously in recent years. Moreover, with the progress of the multimedia technology, the communication, entertainment, word processing and e-commerce, can be now integrated into one platform through seamless integration of Computer, Communication and Consumer Electronics (3C) industries. Via different mobile devices, consumers can browse web pages, receive or send e-mails, trade stocks online, wirelessly communicate with other people, and get the latest information anytime and anywhere. Many studies even indicate the application of Tablet PCs to education would enable largely improved teaching quality [1–3].

Early in 2010, Apple Inc. released the first generation of Tablet PC, named iPad, which brought a new wave to the market, and resulted in great shock to the IT industry. This wave makes more major IT industrial companies, such as ASUS, Acer, Samsung, Amazon, Sony, etc., invest in development of Tablet PC successively. In the International Consumer Electronics Show (CES) held in 2011, Tablet PC was granted as the most potential consumer electronics as expected.¹ Some experts also point out that the Tablet PC will become an indispensable device for the consumer as well as the smartphone. It seems to become a new tendency.

Tablet PC equipped with complete OS, touch screen and powerful hardware. Moreover, it also added with Bluetooth, Wi-Fi and 3G, which makes Tablet PC differentiate from the unmovable desktop and more convenient to consumers [4]. However, with the high elimination ratio of consumer electronics, in order to maintain high competitiveness, the market positioning of product and the acceptance degree of consumer is the most critical factor for Tablet PC. Due to the powerful functionality and wide applicability resulted in the expensive price and unclear market positioning of the Tablet PC.

Being faced with the state-of-the-art high-tech products of Tablet PCs, this study intends to analyze the degree of acceptance of the Tablet PC products by customers and the customer preference towards the Tablet PC products. Further, finding out the principal influence on consumer's purchasing. In this study, through literature review and expert interview, we select appropriate evaluation components to construct the hierarchical structure of evaluation. The Fuzzy Analytic Hierarchy Process (FAHP) is employed in this study to find out the key factors affecting the consumer's purchasing of the Tablet PC. Further, the Multidimensional Scaling (MDS) is also used in combination with FAHP to assist the manufacturers in more accurate and efficient selection of the optimal target consumer groups in the process of making decision on the target products. Moreover, perceptual maps are constructed for the decision makers to realize the

¹ International Consumer Electronics Show (CES), 2011, <http://www.cesweb.org/>

similarity and variance in different consumer groups' preference for Tablet PCs. Finally, this study provides some corresponding marketing plans and promotion strategies to the manufacturers and the researchers in the related industries, so that the manufacturers can use these plans and strategies as a basis for building their own strategy of entering the Tablet PC market.

2 Literature Review

2.1 Fuzzy Analytical Hierarchy Process

Among various decision making methods, Analytic Hierarchy Process (AHP) proposed by Saaty is a Multiple Attribute Decision Making (MADM) which is most used [5, 6]. It could structuralize the complicated decision making issues and provide decision maker with the important weight of decision and the priority of alternative solution. The consistency for each criterion is further verified [7], and a hierarchical decision-making system is then established [8]. In 1985, Buckley proposed the Fuzzy Analytic Hierarchy Process (FAHP) method that integrated the Fuzzy theory with AHP [9]. FAHP can improve the disadvantage of fuzziness and subjective opinion brought by the component pairwise comparison when conducting the AHP expert questionnaire survey, which might result in the deviation of the analytic results. Compared with the traditional AHP, FAHP requires more complicated calculation steps, which are detailed as below:

- (1) Build the hierarchical structure of evaluation.
- (2) Conduct pairwise comparison: After the hierarchical structure of evaluation is built, adopt the 9-level pairwise comparison scale between the components.
- (3) Build pairwise comparison matrix: On the upper triangular part of the pairwise comparison matrix A , place the evaluation value of the comparison result for a group of components made up of $A_1, A_2, A_3, \dots, A_n$. While put the reciprocal number of the value for the relative position on the lower triangular part, namely, $a_{ij} = 1/a_{ji}$, where a_{ij} represents the relative priority of Component i to component j .
- (4) Translate the matrix value into the triangular fuzzy numbers (\tilde{M}_{ij}), where $\tilde{M}_{ij} = (L_{ij}, M_{ij}, R_{ij})$ is the fuzzy number of component i to component j [10].
- (5) Calculate fuzzy weights: Obtain the overall triangular fuzzy numbers $M_i = (L_i, M_i, R_i)$ of all components based on the triangular fuzzy numbers of the component and by using the calculation of geometric mean. And sum up the triangular fuzzy numbers of n components, to obtain the sum L_i'', M_i'' and R_i'' of the fuzzy numbers. Finally, calculate the triangular fuzzy weights (W_i) based on the ratio between these two numbers.
- (6) Best Non-fuzzy Performance value (BNP) and Normalization.
- (7) Series of hierarchical and priority.

2.2 Multidimensional Scaling

Multidimensional Scaling (MDS) was proposed by Torgerson in 1952, which provides a visualized presentation of the complicated relation between components, in a perceptual map [11]. It could conduct pairwise comparison between n different components, and set up these components in low-dimension [12]. This study adopts Non-MDS, which inputs the attribute data, but could obtain the results of variable data. The basic steps are detailed as below:

- (1) Obtain the similarity (distance) between the data: Take the similarity between the data as the basic input of MDS. If there are n data, it will obtain the similarity for m pairs of data, in which $m = n(n-1)/2$. Assume there is no event with equal distance among the data, the similarity of the objects could be ranked as $S_{ij(1)} < S_{ij(2)} < S_{ij(3)} < S_{ij(4)} < \dots < S_{ij(m)}$.
- (2) Find out the distance of the data pairs in dimension: Set $S_{ij}^{(q)}$ as the distance between the data pair (i,j) in dimension q after rotation, and $S_{ij(1)}^{(q)} < S_{ij(2)}^{(q)} < S_{ij(3)}^{(q)} < S_{ij(4)}^{(q)} < \dots < S_{ij(m)}^{(q)}$.
- (3) Calculate stress coefficient: The stress ($S(q)$) is used to evaluate the goodness of fit of dimension (q) to the data. Generally, it is better smaller than 0.1 [13]. Based on the relation between the number of dimensions and stress, it will determine the appropriate dimensions in perceptual map. Through this map could show the hidden structure or spatial relation between the data, and achieve the classification result through the spatial difference.

3 Study Design and Architecture

This study proposes an assessment method combining FAHP and MDS, in order to evaluate the Key factors of purchase Tablet PC for different consumer Groups.

3.1 Build the Hierarchical Structure of Evaluation

Via expert interview, this study classifies the factors of consumer's purchasing of Tablet PC into three dimensions. Besides, selecting nine appropriate criteria in total and five consumer groups as alternatives respectively, which as shown in Fig. 1.

Based on the selected components via the expert interview, Table 1 shows the explanation of each criterion.

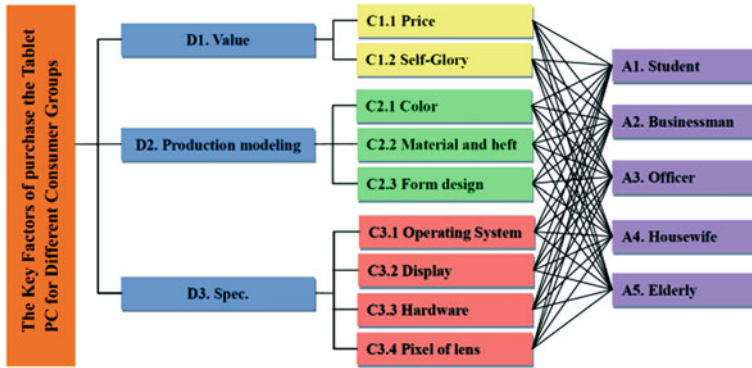


Fig. 1 Hierarchical structure of evaluation for Tablet PC’s consumer groups

Table 1 The explanation of each evaluation criteria

Criteria	Description
C1.1 Price	When buying Tablet PC, the consumer’s attention degree of price level
C1.2 Self-glory	When buying Tablet PC, the sense of self-glory brings to consumers form product
C2.1 Color	When buying Tablet PC, the consumer’s attention degree of the product’s color
C2.2 Material and heft	When buying Tablet PC, the consumer’s attention degree of product’s material and heft
C2.3 Form design	When buying Tablet PC, the consumer’s attention degree of form design
C3.1 Operating system	When buying Tablet PC, the consumer’s attention degree of operating system
C3.2 Display	When buying Tablet PC, the consumer’s attention degree of screen size
C3.3 Hardware	When buying Tablet PC, the consumer’s attention degree of hardware efficacy (e.g., CPU, RAM, VGA, battery, etc.)
C3.4 Pixel of lens	When buying Tablet PC, the consumer’s attention degree of camera’s pixel of lens

3.2 AHP Questionnaire Design and Analysis

The established hierarchical structure of evaluation as the foundation to design the AHP expert-questionnaire. In this study, the vendors of Tablet PC are regarded as subjects for the expert interview and conducted the pairwise comparison between components. We have received 15 expert questionnaires, and applies professional AHP software-Super Decisions to calculate the relative weight of the components in each questionnaire. Subsequently, we could obtain the relative weights of each component, and further verify the inconsistency of the questionnaire.

3.3 The Relative Fuzzy-Weight and Series of Hierarchical

After the consistency verification, the pairwise comparison matrixes for each layer of evaluation are obtained. Through converting fuzzy pairwise comparison matrix, the triangular fuzzy number requires the calculation of its geometric mean first. Finally, via BNP and normalization, it could get the relative fuzzy-weight between components, as shown in Table 2.

After getting the relative fuzzy-weight between the components, it will get the overall absolute weights and the priority of entire hierarchical structure of evaluation through series of hierarchical. In Table 3, we realize that the top three criteria are 「Operating System」 (0.344), 「Color」 (0.207) and 「Hardware」 (0.202).

3.4 Multidimensional Scaling Analysis

Through FAHP, the relative fuzzy-weight of all components can be achieved. Further, this study prioritizes the importance of each criterion with consumer groups, as shown in Table 4.

Table 2 The relative weight of each components

Components	Weight of triangular fuzzy numbers	BNP	Relative fuzzy-weight
D1 Value	(0.043, 0.063, 0.121)	0.076	0.066
C1.1 Price	(0.649, 0.875, 1.168)	0.897	0.872
C1.2 Self-glory	(0.097, 0.125, 0.174)	0.132	0.128
D2 Production modeling	(0.145, 0.265, 0.636)	0.349	0.303
C2.1 Color	(0.447, 0.747, 1.202)	0.799	0.734
C2.2 Material and heft	(0.087, 0.119, 0.255)	0.154	0.141
C2.3 Form design	(0.066, 0.134, 0.210)	0.136	0.125
D3 Spec	(0.328, 0.672, 1.183)	0.727	0.632
C3.1 Operating system	(0.257, 0.557, 1.060)	0.625	0.525
C3.2 Display	(0.065, 0.124, 0.311)	0.167	0.140
C3.3 Hardware	(0.131, 0.283, 0.652)	0.355	0.298
C3.4 Pixel of lens	(0.025, 0.036, 0.072)	0.044	0.037

Table 3 The weight and priority of each criteria

Criteria	Weight of triangular fuzzy numbers	BNP	Absolute weight	Priority
C1.1 Price	(0.028, 0.055, 0.141)	0.075	0.045	5
C1.2 Self-glory	(0.004, 0.008, 0.021)	0.011	0.007	9
C2.1 Color	(0.065, 0.198, 0.765)	0.343	0.207	2
C2.2 Material and heft	(0.013, 0.032, 0.162)	0.069	0.041	6
C2.3 Form design	(0.010, 0.035, 0.133)	0.059	0.036	7
C3.1 Operating system	(0.084, 0.374, 1.254)	0.571	0.344	1
C3.2 Display	(0.021, 0.083, 0.368)	0.157	0.095	4
C3.3 Hardware	(0.043, 0.190, 0.771)	0.334	0.202	3
C3.4 Pixel of lens	(0.008, 0.024, 0.085)	0.039	0.024	8

Table 4 The weight and priority of each criteria with consumer groups

Criteria		Student	Businessman	Officer	Housewife	Elderly
D1	C1.1	0.473(1)	0.059(4)	0.036(5)	0.149(3)	0.283(2)
	C1.2	0.170(3)	0.055(5)	0.117(4)	0.396(1)	0.262(2)
D2	C2.1	0.111(4)	0.423(1)	0.162(3)	0.271(2)	0.033(5)
	C2.2	0.134(3)	0.095(4)	0.043(5)	0.480(1)	0.249(2)
	C2.3	0.554(1)	0.102(3)	0.231(2)	0.064(4)	0.048(5)
D3	C3.1	0.278(3)	0.298(2)	0.307(1)	0.084(4)	0.033(5)
	C3.2	0.066(4)	0.040(5)	0.311(2)	0.174(3)	0.408(1)
	C3.3	0.063(4)	0.474(1)	0.320(2)	0.085(3)	0.058(5)
	C3.4	0.403(1)	0.349(2)	0.069(4)	0.044(5)	0.134(3)

Table 5 Perceived values

Dimension	Student	Businessman	Officer	Housewife	Elderly
D1	0.643	0.113	0.152	0.546	0.546
D2	0.799	0.620	0.437	0.815	0.329
D3	0.810	1.162	1.007	0.388	0.633

Table 6 Euclidean distances and coordinate for each consumer groups

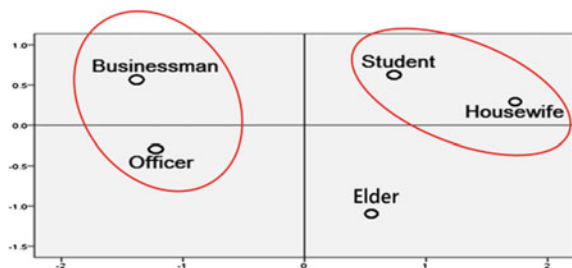
Alternatives	A1	A2	A3	A4	A5
A1. Student	0	-	-	-	-
A2. Businessman	0.661	0	-	-	-
A3. Officer	0.641	0.243	0	-	-
A4. Housewife	0.434	0.908	0.826	0	-
A5. Elderly	0.511	0.742	0.553	0.545	0

Through calculating the sum of weight for each component, the perceived values are obtained, as shown in Table 5.

Via the perceived values, the Euclidean distances (d_{AB}) between two consumer groups is calculated, and build the Euclidean distance matrix, as shown in Table 6.

By the Euclidean distance matrix, this study applies the SPSS statistic software and generates a perceptual map, as shown in Fig. 2.

Fig. 2 Perceptual map of two dimension space



Through this map, decision maker can realize that the “Businessmen” and “Officer” can be grouped together; as well as the “Students” and “Housewives” are rather similar.

4 Data Analysis and Results

4.1 Analysis of Evaluation Factors

In this study, the results from the analysis performed with FAHP indicate that the “Operating System” is the evaluation factor most emphasized by the consumers when purchasing the Tablet PC. Due to the increasing prevalence of smartphones among consumers, most manufacturers developing the Tablet PCs select to use the same smartphone operating system for the Tablet PCs. As a result, the consumers are not willing to invest a lot of money and time in using the Tablet PC that has operating system and operation interface different from what they are familiar with in using a smartphone. Therefore, the consumers, when purchasing a Tablet PC, would first consider choosing one that has an operating system platform familiar to them.

The second factor most concerned is the “Color” of the Tablet PC. As a matter of fact, the technology of multi-touch screen is now quite mature, and the Tablet PCs developed and sold by different manufacturers at very close selling prices have only small difference in their hardware specifications and functions. Hence, the color of the product is also one of the important considerations for consumers when they purchase Tablet PC. Moreover, the “Hardware” is also a crucial factor being considered by consumers. When using the Tablet PC, the consumers have high requirements for the operational smoothness and sensitivity. In consequence, the specifications of hardware for the Tablet PC are extremely important.

4.2 Analysis of Consumer Groups

By variance analysis of consumer groups, the mostly valued by “Students” is “Price” factor. Since most of students could not have incomes to support themselves, when purchasing a relatively expensive product, the primarily consideration is the price. In addition, the “self-glory” factor is relatively valued by “Housewives”. This group has simple life and small social circles, thus most of them wish to show off to the people surrounding and gain the identification with others when they purchasing a new Tablet PC. Furthermore, the group of “Elderly” attaches great importance to “Display” factor when purchasing Tablet PC, due to it is harder for the elder to watch screen than other consumer groups. Regarding “Businessman” and “Officer”, both of two consumer groups are

emphasize the factors with “Operating system” and “Hardware” when purchasing Tablet PC.

From the perceptual map created in MDS, it can be found that the consumer groups of “Businessmen” and “Officers” have similar demands when they purchase Tablet PCs, and so do the customer groups of “Students” and “Housewives”. Therefore, when promoting products to different target consumer groups, the Tablet PC manufacturers may set the consumer groups having similar requirements as the same target consumers, so as to secure increased market share.

5 Conclusions and Future Prospects

In this study, FAHP is applied to analyze the key factors being taken into consideration by different consumer groups when they purchase the Tablet PCs. Furthermore, in this study, MDS is used in combination with FAHP, and the similarity and variance in different consumer groups’ preference for the Tablet PCs are represented using Perceptual Maps, which serve as a useful reference for the Tablet PC manufacturers in making marketing plans aimed at different consumer groups. In the future, the combined decision-making method proposed in this study can be applied to various fields, such as SCM, BPM and so on. It is also possible to use the method proposed in this study in diverse explorations and researches to analyze the marketing strategies for other technological products, including but not limited to Smartphones and Notebook.

References

1. Anderson JE, Schwager PH, Kerns RL (2006) The drivers for acceptance of tablet PCs by faculty in a college of business. *JISE* 17(4):429
2. Barton C, Collura K (2003) Catalyst for change. *The J* 31(4):39–41
3. Lomas C, Rauch U (2003) Learning with tablet PCs: true learning tools or trendy devices. *Syllabus* 17(2):19–20
4. McCloskey P (2002) Tablet PCs stake out higher ed. *Syllabus* 16(5):18–20
5. Saaty TL (1977) A scaling method for priorities in hierarchical structures. *J Math Psychol* 15(3):231–281
6. Saaty TL (1980) Analytic hierarchy process. *Encyclopedia of biostatistics*. Wiley, Chichester
7. Mahdavi I, Fazlollahtabar H, Heidarzade A, Mahdavi-Amiri N, Rooshan YI (2008) A heuristic methodology for multi-criteria evaluation of web-based e-learning systems based on user satisfaction. *J Appl Sci* 8(24):4603–4609
8. Shee DY, Tzeng GH, Tang TI (2003) AHP, fuzzy measure and fuzzy integral approaches for the appraisal of information service providers in Taiwan. *J Glob Inf Technol Manag* 6(1):8–30
9. Buckley JJ (1985) Fuzzy hierarchical analysis. *Fuzzy Sets Syst* 17(3):233–247
10. Chiou HK, Tzeng GH, Cheng DC (2005) Evaluating sustainable fishing development strategies using fuzzy MCDM approach. *Omega* 33(3):223–234

11. Torgerson WS (1952) Multidimensional scaling: I. Theory and method. *Psychometrika* 17(4):401–419
12. Chen MF, Tzeng GH, Ding CG (2008) Combining fuzzy AHP with MDS in identifying the preference similarity of alternatives. *Appl Soft Comput* 8(1):110–117
13. Kruskal JB, Wish M (1978) *Multidimensional Scaling*. Sage, Newbury Park

Game-Based History Ubiquitous Learning Environment Through Cognitive Apprenticeship

Wen-Chih Chang, Chiung-sui Chang, Hsuan-Che Yang
and Ming-Ren Jheng

Abstract Game based learning involves interesting story, interaction and competition elements which promote the imagination, interest, concentration and creativity of the learner. Besides, ubiquitous learning integrates location-aware and context-aware technology in our living environment. Learners are motivated by firsthand or second historical relics. Visiting and interview activities with old people also promote learners have history thinking. Combining the u-learning environment and cognitive apprenticeship which reveals the solving problem inner progress from the expert, learners observe, learn, scaffold and exploration in the proposed system. The game-based history ubiquitous learning environment integrated into cognitive apprenticeship theory. The learners can challenge the game tasks by their own group or compete with other teams or collaborate with other teams.

Keywords Game based learning · History learning · Mobile learning · Social network analysis

W.-C. Chang · M.-R. Jheng (✉)
Department of Information Management, Chung Hua University, Hsinchu City,
Republic of China
e-mail: JhengMingRen@gmail.com

C. Chang
Department of Educational Technology, Tamkang University, New Taipei City,
Republic of China

H.-C. Yang
Department of Business Administration, Tunghan University, New Taipei City,
Republic of China

1 Introduction

With the rapid development of new information technology and multiple teaching and teaching system through the game presents teaching materials, learners learning arrangements by the story, or a set of steps and rules. Computer games used in digital learning more and more widely possessed effectiveness as [1] describes the game can improve listening, speaking, reading and writing ability, [14] for the physical concept of import games ingredient learners through the game type easier to understand physical abstraction, and through simulation game operation physics experiments. Addition, the game allows learner Poly precision will God to focus on the face of the game prompt lifting tasks and problems, improve learning motivation and interest, appropriate arrangements more can enhance learning efficiency.

2 Related Works

2.1 *Game Element and Learning Theories*

Explore the teaching of the game for the game on the teaching and research of the subsequent design, great benefit, following the concept of game design and game education curriculum design related even to explore. Prensky [13] pointed out that the Games can promote the players active play environment, and you can explore in the game, observation, trial and error and solve the problem.

Prensky [13], Malone [8, 9] research can be found in the game by providing task challenge, task feedback and a variety of fantasy form and content, and enhance the intrinsic motivation of players play. Owen [11] study, the game itself plays a significant role in the history of human development which points out, many of the people's behavior activities can be presented through games. He asked the six points for the game composed architecture contains the goal of the game, the game takes place, the game participants, the game steps the specification language restrictions and playtime.

Schlechy [16] mentioned that immersive learning mode (engage) include the following elements: (1) the desire to focus learning objectives, (2) the challenge task, (3) clear and convincing assessment standards, and (4) learning protective mechanism for the negative results of the initial failure, (5) the outcome of the performance certainly mode, (6) contact with other people, and (7) novelty and diversity, (8) selectivity, (9) trustworthiness. The learning mode mainly focus on the task challenges, higher and longer focus on the learning ability and time needed to complete the task, this task requires the learner to expand their learning cognitive and Community interpersonal skills.

2.2 Learning Design Theories

Game-based action learning for teaching a considerable extent helpful, the following behavioral learning and cognitive the theory supplemented motivation theory to explore action learning design should pay attention to the breakdown of parts to increase the learners' learning outcomes.

Behavioral learning theory, Hopson (2001) study mentioned within the fixed time intervals, give positive encouragement to achieve operational constraints. Cognitive learning theory focused to put the memory of how to interpret memory how to keep and how to recall the memory elements.

Reldman [15] explained information processing, storage, and recall the mentioned memory program. Sensory temporary, short-term memory and long-term memory, feeling temporary accept the information and the very short time maintained, short-term memory to store a limited amount of information for a few minutes, long-term memory to store large amounts of information to last a long time period.

How learners can enhance learning efficiency?

NTL Institute (2006) development of "learning pyramid", this chart type description learners through active learning, for example, to teach another person to learn a concept, the learning can learn 90 % and applied immediately.

Learners practice in an instance or things you can learn 75 %. Learners integrate into the group discussions can learn 50 %. Learners see test paradigm or the drill can learn 30 %. Learners learn through sound image, 20 % are able to learn. Learners are able to learn through reading to 10 %. In this study, the learning pyramid to emphasize active learning, and focus on learning in the real environment.

2.3 Mobile-Learning

Action learning all the time learners to achieve the purpose of learning through mobile devices. People over a computer network to learn anytime, anywhere, to obtain the latest knowledge and learning resources, learning to become more flexible and diversified [6], through mobile devices and wireless network the combination of road communications technology to obtain information called action learning.

After treatment with embedded sensing technology innovation, associative capability of the computer into the living environment, aware of the situations and the state of the people, to get useful information, based on the individual needs active assistance, which is ubiquitous computing the basic concept.

Context-aware action learning to use context-aware sensing technology combined with good mobility, facilitate the action of high-profit vehicles for learning aids learners during learning at the same time for interaction with the real-life

situation. Context-aware action learning to use context-aware sensing technology combined with good mobility, facilitate the action of high-profit vehicles for learning aids learners during learning at the same time for interaction with the real-life situation. Mobile devices device with a wireless network communications and sensor technology learning activities is called context-aware ubiquitous learning activities, the learning system more good understanding of learner behavior and environmental parameters number of real-time rendering in real life [6].

2.4 Cognitive Apprenticeship

“Apprenticeship” long teaching methods, “cognitive apprenticeship” is a further evolution of the outcome, the level of more structured, covering a wider teaching theory. The following details the research and application of teaching mode—“cognitive apprenticeship” meaning and dimension.

Many as the theoretical framework of cognitive apprenticeship began in the 10 years after Collins et al. [3] propose a cognitive apprenticeship. Domestic and foreign research are found the cognitive apprenticeship production for teaching mode architecture can promote learners have better learning outcomes and micro thinking ability ([2, 10]; Rogoff 1990).

The study design based on cognitive apprenticeship teaching model teaching activities or critical thinking tools software [17], can be used for the development of cognitive skills and reasoning ability ([5, 12]; Rogoff 1990); same time, study the cognitive apprenticeship used to solve complex technical training courses [7, 18], for example, the basic training of nursing clinical courses, to help care the Department the learners successfully become nurse practitioners [4], and to promote interest in the motivation of the learner work.

Further, the study is the use of cognitive apprenticeship teacher–student interaction patterns—demonstration they use professional teachers to teach and scaffolding curriculum for learners to learn science through real participation.

The above study, the use of the cognitive apprenticeship certain steps, such as the “scaffolding” or “reflection”, included in the instructional design considerations, some of these teaching research design cognitive function from the contextual learning and social constructivism explore cognitive apprenticeship promote learners’ comprehension ability, cognitive thinking skills, complex problem-solving ability and the knowledge and skills of learning.

Table 1 presents the outcome of the action learning at home and abroad in recent years. Based on the above analysis of the literature, it is not difficult to understand the effectiveness of teaching and learning, cognitive apprenticeship Therefore, in this study, further research will the cognitive apprenticeship integrate into the history of game-based learning system, to facilitate more effective instructional design and promotion.

Table 1 Adapting cognitive apprenticeship in game design

Levels	Five levels of cognitive apprenticeship teaching methods
Demonstration	Game-based learning system with the first volume of a high school history courses, in addition to the history of game-based learning systems use to the teacher in the classroom curriculum and campus demonstration, the system provides learning resources for learners queries. The teacher first recording for some demonstration of problem-solving mode (approximately 2–3 tasks), through demonstration animation, learners first understand how the game learning environment problem solving, providing learners learning and thinking about the problem solving process. Shown in Fig. 1, the game tasks first inform freshwater Town Development Profile, content to provide examples, demonstrations checkpoints way, and then expand the task
Training	<p>First the arrangements simple game tasks so that learners first practice. Verify that the learners are familiar with the actual operation of the task to solve process through training game task checkpoints. The training hurdle of training</p> <ol style="list-style-type: none"> (1) The use of communication tools: learners use mobile carrier communication includes file sharing, text messaging, instant call (2) QR code sensing operation: An exercise activity actually utilized mobile carrier sensing operation to answer questions and operation (3) Photography operation: learners learn to use the mobile carrier to take pictures, and photos uploaded to the server to complete the game tasks (4) Google map operation: learners learn through Google map to find their place and position to move forward (5) Learning resource utilization: the learner action vehicle to view learning resources, query, and use of learning resources to complete the task
Scaffolding	<p>The game-based history learning system provides the following four functions:</p> <ol style="list-style-type: none"> (1) In this study, with the QR code to provide the text perception GPS signal support location-aware task checkpoints provide learners reminded learning on interactive conditions, such as checkpoints moving in the wrong direction, the current position does not match with the task location, learners suspected get lost, provide prompt information. Figure 2 indicates the actual checkpoints task attributes (generally, cooperation, competition) (2) Learning interactive, less text perceive design game-history the checkpoints textbooks, learners will collect historical information and tasks prompted combination to guide students to solve puzzles in order (3) Provide learning materials at any time to provide relevant historical background, historical time chart, character names and location information (4) The learner group a total of 3–5 people, divided into team leader and team members, the team is led by better academic performance of students who learn through each learner the ability of different composition, learners can learn from each other and assist reach scaffolding learning
Clarify	<p>When learners into the mission, the first describes the historical background, tell learners living in locations, historical background, learners into the historical events, and then challenge the task</p> <p>Challenge process, learners interact with QR code support situational awareness, if the answer is wrong, give advice and tips. If answered correctly, the further the whole story of the historical events and development (Fig. 3)</p>

(continued)

Table 1 (continued)

Levels	Five levels of cognitive apprenticeship teaching methods
Reflection	Group of collaborative learning tools to provide learners with other learners group together to unlock the game-historical task, collected in the two study groups, discuss the historical evidence, the background of the times may change. Students can imitate each other and to learn the history of the other students thinking and discussion skills, game-based action learning communication functions to communicate with each other or distress through text messaging, instant voice communication with face-to-face group discussion (Fig. 4)
Explore	Learners can design their own game style historical challenge tasks (see Fig. 5) and map, the test of the other students how to use the Historical Cognition and thinking through the game levels. To ensure that the educational game levels will be teacher certification

Fig. 1 Historic building tasks

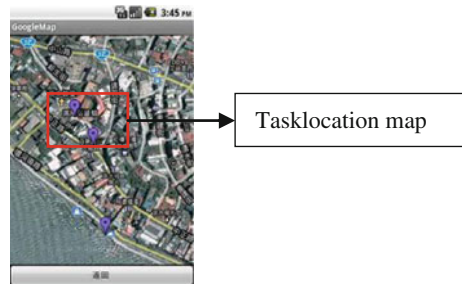


Fig. 2 Actual game tasks

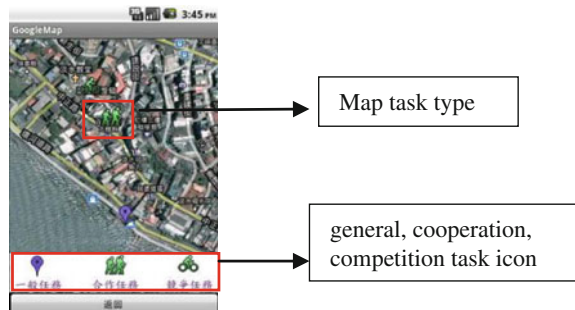


Fig. 3 Content resources show



Fig. 4 Joint working group for help



Fig. 5 Edit the new task



3 System Design

Cognitive apprenticeship aimed at promoting learner self-learning and the transfer of knowledge to the practical application level; use of cognitive apprenticeship teaching methods need to be experts to deal with the problems of the inner process explicit, and let the learners by observation the explicit process further learning and thinking; learners start learning through expert demonstration teaching mode, can promote learner future to show more of the learning strategies [10].

Cognitive apprenticeship teaching methods, including the following levels [3, 10]:

- (1) Demonstration: presented expert to perform tasks, learners observe and build a conceptual model to understand the tasks required to process.
- (2) Training: learner’s learning behavior contains observation further timely provide learners implied, feedback and reminders.
- (3) Scaffolding: contains instructional assessment to support learners to learn specific tasks.
- (4) Clarify: use any kind of way for learners to learn how to converge their knowledge in problem-solving reasoning process.
- (5) Reflection: learners’ experts’ or other students to compare the process with their own problems to solve.

- (6) Explore: let learners learn to own architecture they are interested, and the problem can be solved.

Cognitive apprenticeship teaching method focuses on the initiative through expert mode and teaching behavior so that learners construct their own knowledge, at the same time, the teaching methods emphasize the use of a real-life situation starting point for learning as learners, thereby promoting effective learning, through a the context of cooperation mechanisms to stimulate learners' intrinsic motivation [10].

4 Conclusion

Game-based learning is mainly hoping to trigger the learners' interest and motivation for learning objectives as packaging and interactive way through the game, and the research reference of Prensky scholars [13] 12 game elements to construct. The interaction between the learners have a friendly competition and cooperation to help enhance the learning speed and learning outcomes, cultivate the relationship between the people in the process at the same time maintaining a good attitude.

References

1. Brownfield S, Vik G (1983) Teaching basic skills with computer games. *Train Dev J* 37(12):53–56
2. Chiu MH, Chou CC, Liu CJ (2002) Dynamic processes of conceptual change: analysis of constructing mental models of chemical equilibrium. *J Res Sci Teach* 39(8):688–712
3. Collins A, Brown JS, Newman SE (1989) Cognitive apprenticeship: teaching the crafts of reading, writing, and mathematics. In: Resnick LB (ed) *Knowing, learning, and instruction: essays in honor of Robert Glaser*. Lawrence Erlbaum, Hillsdale, pp 453–494
4. DeBourgh GA (2001) Using web technology in a clinical nursing course. *Nurse Educator* 26(5):227–233
5. Hendricks CC (2001) Teaching causal reasoning through cognitive apprenticeship: what are results from situated learning? *J Educ Res* 94(5):302–311
6. Hwang GJ, Tsai CC, Yang SJH (2008) Criteria, strategies and research issues of context-aware ubiquitous learning. *Educ Technol Soc* 11(2):81–91
7. Jarveka S, Bonk CJ, Lehtinen E (1999) A theoretical analysis of social interactions in computer-based learning environments: evidence for reciprocal understandings. *J Educ Comput Res* 20(3):363–388
8. Malone T (1980) What makes things fun to learn? A study of intrinsically motivating computer games. Xerox, Palo Alto
9. Malone TW, Lepper MR (1987) Making learning fun: a taxonomy of intrinsic motivations for learning. In: Snow RE, Farr MJ (eds) *Aptitude, learning, and instruction, III: cognitive and affective process analysis*. Lawrence Erlbaum Associates, Hillsdale, pp 223–253

10. Neumann A, Gräber W, Tergan S-O (2005) Paris—visualizing ideas and information in a resource-based learning scenario. In: Tergan S-O, Keller T (eds) Knowledge and information visualization. Springer-Verlag Berlin, Heidelberg, pp 256–281
11. Owen M (2004) *An Anatomy of Games*. Futurelab Series, Bristol
12. Patel A, Kinshuk K, Russell D. (1999) Designing life-long learning systems for numeric domains. *Educ Technol* 39(5):8–11
13. Prensky M (2001) *Digital game-based learning*. McGraw-Hill, New York
14. Ravenscroft A (2002) Developing and evaluative dialogue games for collaborative elearning. *J Comput Assist Learn* 18(1):93–101
15. Reldman RS (1996) *Understanding psychology*. McGraw Hill, India
16. Schlechty PC (1997) *Inventing better schools: an action plan for educational reform*. Jossey-Bass, San Francisco
17. Stockhausen LJ, Zimitat C (2002) New learning: re-apprenticing the learner. *Educ Media Int* 39(3/4):331–338
18. Tilley CL (2001) Cognitive apprenticeship. *Sch Libr Media Activities Monthly* 18(3):37–38

The Behavioral Patterns of an Online Discussion Activity in Business Data Communication Class

Chiu Jui-Yu and Chang Wen-Chih

Abstract According to the empirical observation that group decision making can not only provides people much comprehensive information and knowledge to face the rapid development of modern sciences and technologies, but also provides people much different and various point of view. Participants are 106, belong to two classes of undergraduate students, to discuss sharing of content online for corporate communications issues, web content, text to speech acts to quantify the qualitative coding analysis, sequence analysis of the behavior of the conversion, is used explore discuss the generation of behavior patterns. The study looked at students' learning to the corporate communications knowledge sharing activities online, so its contents and recommendations of the results thus affecting the limit.

Keywords Behavior coding · Content analysis · Sequence analysis and discuss patterns of behavior

1 Introduction

In recent years, updated with the advances in technology and teaching methods, learning activities become more complex. Knowledge sharing on the internet can help people solve problems. Group decision-making is not only able to provide more complete information and knowledge to face the rapid development of modern science and technology issues, but also to provide a more different view point of reference diversity [12].

C. Jui-Yu (✉) · C. Wen-Chih
Chung Hua University, Hsinchu, Taiwan
e-mail: lances5512@hotmail.com

C. Wen-Chih
e-mail: earnest@chu.edu.tw

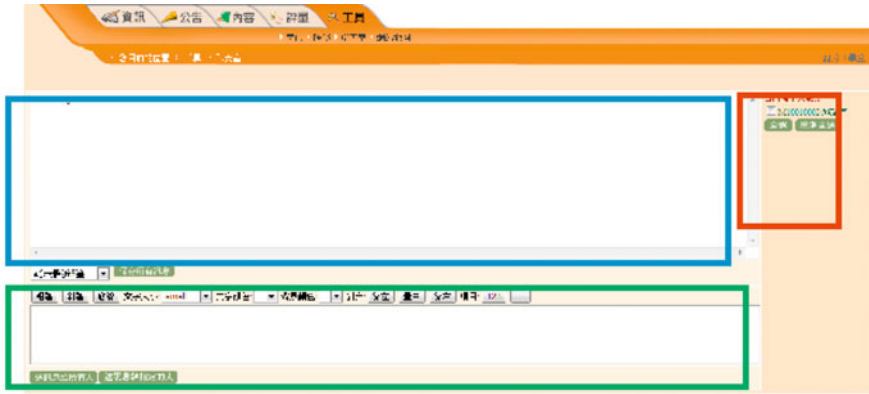


Fig. 1 In *red* part, it shows who now is on the internet. In *blue* part, it shows that all the chat history. In *green* part, it shows that the message who is editing

We select online forum through Business Data Communications course of study and quantify the qualitative content analysis and sequence analysis as a tool for exploring behavioral patterns discussed. Business Data Communications courses mainly in the basic concepts of Information Science and Information Management, Introduction to computer and telecommunications network, computer network and wireless communications professional basis.

There are agreements to deepen the network structure and network introduced effective application of network development courses. Regardless of the communication taken encoding, it usually via a different communication path desired to communicate the message to the recipient. Communication media, including: verbal communication (face-to-face conversation, telephone, etc.), written communication (e-mail, official documents, bulletins, letters, etc.) and non-verbal communication (body language, facial expressions, eyes, etc.).

Use some kind of media to communicate a certain message is not only a technical problem, in fact, most likely effect of communication have a significant impact, and with the use of different media, the recipient of the message will produce different decoding methods (Besides 1994).

Reference to “Exploring the behavioral patterns of an online knowledge-sharing discussion activity among teachers with problem-solving strategy” (Hou et al. 2009) the individuals similar range of community and communication tools used in corporate communications for the content range whether there are differences of interpretation of the results are interested in doing research, and to provide a reference for the contribution.

There are many studies to solve the problems of knowledge sharing, focusing on the process of the knowledge of the interaction between the community members. This analysis including exploring the “internal” and “explicit” knowledge (Hendriks 1999). Organization or community can come up with all kinds of knowledge sharing strategy, in order to achieve innovative knowledge

conversion between members of restructuring for (Davenport and Prusak 1998; Gilbert and Gordey Hayes 1996).

Many studies of knowledge sharing, also discussed to motivate the members to share and innovative combination of knowledge. Many studies have also tried to order to solution of non-synchronous discuss theoretical teaching aid beneficiary, the use of non-synchronous discuss theory to conduct cooperative learning, also has become today's digital learning trend one [3, 7, 14]

If you can combine online discussion and problem solve, ask students to respect teachers a learning theme, in line with each other questions and solve each other's problems, should be achieved by the interaction under the influence of the social environment by sharing knowledge and learning (Leach and Scott 2000). To cultivate the student's ability to solve complex problems more efficiently, and to clarify the synergistic conduct this type of teaching and learning activities, data collection, discussion and advice.

Clarify the order depth teaching activities in synergy conduct, data collection, discussion and comments integrated online discussion behavior interaction, using sequence analysis [1].

Behavior can be tested for the encoding indirect continuity of significant resistance, In order solution is not similar do not discuss the theoretical behavior as between the serial trends, explore its online discussion interactive dynamic mode, the way has been gradual in some studies using (Hou et al. 2008, 2009; Jeong 2003 [5]; King and Roblyer 1984).

Therefore, the purpose of this study by serial analysis of calculus, based on knowledge building content analysis coding system to analyze the behavior of students online collaborative problem-solving knowledge building mode (Gunawardena, Lowe and Anderson [6]).

With the coding, analysis of the behavior patterns of knowledge building its discussion to a similar range of community and communication tools, used in the enterprise data communications courses, and am interested in doing research whether there are differences of interpretation of the results, and to provide a reference to the contribution.

2 Related Works

2.1 The Patters of Communication

The problem solving strategy is a cooperative study for (Gagne and Briggs 1979) procedure often used. Strategy on the use of online problem-solving method, has many different scholars define the research "to solve the problem in a different way" (Gagne 1980; incubation 1988; Meyer 1985; Sternberg 1996). Gagne (1980) will be combined with previous knowledge and solve problems in the process of understanding a new problem.

Sternberg (1996) is the process of removing barriers to seeking solutions to solve the problem. Many studies have also raised the problem-solving process and models (henna, Porter, Hagaman 1995; Isaksen and Parnes, in 1985; Sternberg 1996). The above scholars pointed out that, “solve the problem” focused on the past experience and knowledge, thinking, and the use of cognitive skills, profound solve new problems.

This process not only helps solve the problem, but also encourages student interaction/discussion with their peers, and the development of their cognitive abilities in “cooperative learning”. This is why to solve the problem has long been as a teaching strategy (Gagne and Briggs 1979; Duch, Groh and Allen 2001). This strategy can also be applied to teacher education, discussion activities, to promote the teaching of knowledge interaction (Xu 2004).

2.2 The Analysis Method

In the research record, we can put all kinds of “events” Encoding a random theoretical and mathematical statistics studied chaos digital sequence statistics law characteristics to predict, control or solve practical problems. By the majority of the problem, the random number is chronologically arranged in sequence, and then you can get a series of event sequences observed sample.

In this study, to Interaction analysis model coding systems (Gunawardena, Lowe and Anderson [6]), this coding system has been repeatedly used in online discussion coding analysis (Jeong 2003; Sing and Khine 2006). The study also found that the coding system is divided into five knowledge to construct Phases (as shown in Table 2.2), will help enhance the content analysis and validity (Rourke and Anderson 2004).

Encoding based on the topic (questions) as a unit. Each question will have a number of discussion messages. Coders will be in chronological order from the first. And then encoded each message content, if the same message posted multiple coding. Ex: previous paragraphs is C1 paragraphs is C3, the article message coding sequence C1C3 (as shown in Table 1). All topics after a total of two groups of coding then encoded data to sequence analysis.

2.3 On-Line Discussion for Students

Due to the face-to-face community interaction space and time constraints, the growing body of research has begun to use the online forum to create online learning communities (The Dana Yendol-Silva 2003; Hobson and Simolin 2001; star and Kane 2006).

Network Learning Community (Web-Based Learning Community) refers to a group of people in similar learning goals and objectives that drives through the

Table 1 Interaction Analysis Model (Gunawardena, Lowe and Anderson’s 1997)

Code	Phase	Content
C1	Sharing or comparing of information about discussion topics	Statement of observation or opinion; statement of agreement between participants
C2	Discovery and exploration of dissonance or inconsistency among participants	Identifying areas of disagreement, asking, or answering questions to clarify disagreement
C3	Negotiation of meaning or construction of	Negotiating the meaning of terms and knowledge negotiation of the relative weight to be used for various agreement
C4	Testing and modification of proposed synthesis or co-construction	Testing the proposed new knowledge against existing cognitive schema, personal experience, or other sources
C5	Agreement statement(s) or application of newly constructed meaning	Summarizing agreement and metacognitive statements that show new knowledge construction

discussion, communication, interaction, feedback, share, provide, exchange, cooperation, or search process knowledge creation, experience exchange and flow of information, knowledge sharing activities and thus common by the interaction of the different knowledge background of individuals, gradually construct and create virtual learning environment, learning to grow in order to create a knowledge community (Ji-Cheng Zhang 2002).

Network Learning Community is by someone else’s point of view through the novice and expert discussion and stimulates promote self-reflection, and gradually establish their own knowledge systems and concepts [9]. Internet learning communities can enhance learners actively construct knowledge through interpersonal interaction so that learners get participation and identity. Therefore, empirical analysis of a large number of samples in this study explores the potential limitations and solutions.

3 Research Method

3.1 Participants

The study participants were 106 belonging to the Information Management Department of the Chinese University of two classes of undergraduate students published web content for corporate communications. The study participants attend the course “Management Information Systems” taught the basic theories about information management, enterprise electronic import of practical case.

In this study, the use of network learning environment platform the system can provide various types of discussion forums to discuss teaching activities to implement various network router. Participants can be in the discussion forum Post

a new topic and watch all been published topics tap into each topic page for the relative topic published discussion respond (Houhui Ze Zhang Guoen and Song Yao-ting 2008; Chang, Sung and Hou 2006).

The network learning system for academic discussion platform of campus closed learning environment students can check the real name of the speaker, and also to avoid external interference and considerations for experimental validity. In addition to the declaration of the issues discussed, teachers try not to speak into guide impact experiments effectiveness.

3.2 Data Analysis

In this study, it will conduct a 93-day teaching activities. Term of teaching activities require students to discuss whether District published a specific inquiry topic to share problems or ideas. Other peers published a response to that discussion and answers through online discussion in into the behavior known intellectual construct integration. Avoid subjective guide teachers of teachers not conducted intervention, discuss the records are complete automatically recorded in the system.

In this study, a total of 93 days the 212 topic has been to respond to a total of 2506 discussion behavior coding completed. The way of coding a statement posted in chronological order according to each message in the statement. Reliability in accordance with the chronological coding conducted to ensure that the encoded content.

We randomly selected 1253 message (about total message volume half), handed over to another officer to conduct code analysis. Kappa reliability 0.669 ($Z = 8.073$, $p < 0.01$), to achieve a significant degree of 0.01 level. The encoded data were conducted serial analysis of knowledge building content analysis.

4 Discussions

Quantitative content analysis and sequence analysis results indicate that the C1 (recommendations or clarify issues) and C2 (solutions or related information), which triggered C3 (based on the existing solutions are compared and discussed) the probability.

In the total number of C1 and C2 appear total behavior in 60 % (C1: C2) is (28 %: 32 %), wherein the (C1/C3, C2/C3) is (57 %, 50 %).

Irrelevant messages (C5), meaning is not relevant to the discussion or off-topic discussion in the previous emphasis on learner rarely mentioned (Hou, Zhang and Song 2007).

This indicates that there is a certain degree of problem-solving behavior continued interaction, knowledge sharing behavior may vary from one type of

organization to another deviation from the discussion (discussion topics unrelated to those) rarely see significant (Bock and other people. In 2005, Yang 2007; Yang and Chen 2007).

This also shows that, although most have not been established learning related knowledge exchange culture (Baraboo, etc.; Tyack and Cuban 1995), after the application to solve the problem of knowledge sharing discussion activity in continuous mode and sequence analysis of the process of in-depth discussions (between C1 and C2 close interaction C1/C2, C2/C1) certain additional benefits prone to lead to C3 (based on existing solutions are compared and discussed) and subsequent integration of the C4 (recommendations summarize the conclusions) this problem solving sequence mode, significant in the data presented.

On the other hand, C2/C3 the probability is not low (C2/C3 behavior sequence transition probability of about 57 %) than C1/C2 (29 %) and C2/C1 (13 %) of the high, participants often proposed their own solutions or opinions, rather than remain in the external asked questions (C1) or answer the problem (C2), based on knowledge sharing (C1/C3, 50 %; C2/C3, 57 %) of them to a certain proportion of in-depth discussion or comparison (C3), discuss the difficulty of learning through external knowledge to solve problems, help to break the problem. (Carroll 2003).

From behavior coding conversion probability rationale can be observed by the method of implementation experience the difference go to discuss the high proportion of learning to achieve the depth effect (C2/C3, 57 %) stay in the text itself C1 (recommendations or clarify issues) external level. There is very few of the proportion of (1 C1/C1, 5 %).

It shows that the application of the forum for thinkers answer the broader approach is not limited to a specific answer mode (C2/C2, 8 %) (C3/C3), (C4/C4, 0 %) (C5/C5, 15 %).

Many speak proportion is worth noting that perhaps the attribute differences considerations theme (creative needs), C5 (independent of the other main topic of discussion), and by the significant difference (C3) may also high (C5/C3, 56 %)

This may indicate that the differences caused by the ethnic cultures, most of the learning community to pursue the examination system is the correct answer, and other community is more or less a little personal color banter style learning.

The sharing of knowledge that we all know do doubt compare discussion answer, the face of new knowledge will be used to explore mode (C1/C3, 50 %), most people still view to reflect on what the difference (C3) go back also a lot of good practice (C2) (C3/C2, 44 %) or reading the conclusions and summary (C4) after thinking defined interpretation of correctness (C1) (C4/C1, 44 %).

5 Conclusion

To explore to solve the problem based on the sharing of knowledge in this empirical study, we observed that online communities to discuss and resolve the problem. Through content analysis and sequence analysis, we conducted empirical

observation and analysis of the patterns of behavior so that we can see how sharing and knowledge between partial restrictions.

In addition, the depth and enthusiasm to promote interaction and motivation appropriate combination of virtual community reward online communities, and more mixed design interactive mechanism, which also deserves to be analyzed. These future studies can help us understand how to more effectively share knowledge online and determined to help them share their teaching knowledge.

References

1. Bakeman R, Gottman JM (1997) *Observing interaction: An introduction to sequential analysis*, 2nd edn. Cambridge University Press, UK
2. Basadur M (1994) *Managing the creative process*. In: Runco MA (ed) *Problem finding, problem solving, and creativity*. Norwood, New Jersey, Blex
3. Bodzin AM, Park JC (2000) Dialogue patterns on the world wide web. *J Comput Math Sci Teach* 19(2):161–194
4. D’Zurilla TJ, Goldfried MR (1971) Problem solving behavior modification. *J Normal Psychol* 78(1):112–119
5. England E (1985) Interactional analysis: The missing factor in computer-aided learning design and evaluation. *Educ Technol* 25(9):24–28
6. Gunawardena C, Lowe C, Anderson T (1997) Analysis of global online debate and the development of an interaction analysis model for examining social construction of knowledge in computer conferencing. *J Educ Comput Res* 17(4):397–431
7. Henri F (1992) computer conferencing and content analysis. In: A. R. Kaye (Ed.), *Collaborative learning through computer conferencing: the Najaden papers* New York: Springer, pp.117(136)
8. Hewitt J (2005) Toward an understanding of how threads die in asynchronous computer conference. *J Learn Sci* 14(4):567–589
9. Lave J, Wenger E (1991) *Situated learning: Legitimate peripheral participation*, New York: Cambridge University Press
10. Lin X, et al. CTGV, *Instructional design and the development of learning communities*, In: B.G. Wilson (Ed.), *Constructivist learning environments case studies instructional design*, NJ: Educational technology publications, pp. 203–220
11. Mayer RE (1992) *Thinking, problem solving, cognition*. W. H. Freeman and Company, New York
12. McShane and Von Glinow (2005). *Organizational behavior*. publisher: McGraw-Hill/Irwin; 4 (Ed) (March 20, 2008)
13. Schoenfeld AH (1992). *Learning to think mathematically problem solving, metacognition, and sense making in mathematics*. In groups (Ed). *handbook of research on mathematics teaching and learning*. Maxwell Macmillan Canada: Macmillan Publishing Company
14. Vonderwell S (2003) An examination of asynchronous communication experiences and perspectives of students in an online course: a case study. *Internet High Educ* 6(1):77–90

Integration of a Prototype Strategical Tool on LMS for Concept Learning

David Tawei Ku and Chi-Jie Lin

Abstract From the perspective of instructional design, when facing the different knowledge domains, the instructional strategies and activities should be matched for the different contents. It is equally important when using LMS as a delivering platform for the web-based learning. However, regardless the popular mutual functions, most of LMSs do not provide teaching supporting tools or activities in particular knowledge domains for instructor to use. Therefore, LMS is only working as a better looking FTP, but not able to help instructors to deliver better instruction. In order to tackle this issue, this study first employed content analysis to induce the teaching strategies of conceptual knowledge domain and analyze the basic functions of LMSs on market. Then, following the content analysis, based on the open source code LMS Moodle, a plug in, strategical learning tool “concept pointer” has been designed and developed. Via the formative evaluation from experts, instructors and students, its advantage and usage have been discussed. According to the formative evaluation, the “concept pointer” could help instructors to highlight the learning content and inspire learners’ understanding. As the results, the strategical learning tool “concept pointer” provided the positive effects to teaching and learning in the conceptual knowledge domain.

Keywords Conceptual knowledge · Learning management system · Strategical tool · Conceptual knowledge

D. T. Ku (✉) · C.-J. Lin

Department Educational Technology, Tamkang University, New Taipei City, Taiwan
e-mail: dtk@mail.tku.edu.com

C.-J. Lin

e-mail: gill19841017@gmail.com

1 Introduction

Since the strong development of Internet technology, the domestic organizations from the government, industrial and commercial enterprises to major institutions are beginning to build the network teaching environment as the main target. In the craze of teaching and learning in the digital network, Yue (1999) mentioned Regardless media, all teaching required via purposeful, prudent advance planning and design, in order to effectively deliver teaching and promote learning. Every teaching (content) is required through a rigorous instructional design process, on the one hand it can control the teaching process output in full of all sorts of variables and conditions, on the other hand it can be appropriate way to provide the teaching aids.

About the instructional design process, Morrison, Ross and Kemp (2001) pointed out that the task analysis is one of the most critical steps. Through task analysis can further the learning content by attribute characteristics to be classified, to link the teaching objectives, strategies, methods, and final evaluation standards, and these four tend to consistency. Wang (2004) also said that how according to the nature of the learning content, at the right time to choose the appropriate method to provide learners with learning, the key factors of learning outcomes virtue or vice. Therefore, instructional design task analysis, learning content-based classification, will be important considerations based on teaching strategies and activities designed.

In online teaching, Govindasamy (2002) mentioned that most of the vendors to provide a digital network teaching are only the technology provider. Yet, for the instructional design, development, teaching guide has been overlooked. The result of technology-led instruction, tend to ignore the original intent of the Web-based learning. Yue (1999) pointed out that online teaching is not the answer to teaching or learning, but under the proper use, can help improve the quality of teaching, and the proper teaching aids can also enhance the learning outcomes. Therefore, “the aids” will not a leading role, and the functions have to bring help to the main purpose. Back to the basic teaching strategies should therefore be re-thinking network tools how best to assist the teaching and learning activities.

In the network environment, unlike the traditional classroom face-to-face teaching, teachers do not have full control when facing the students. Besides to enhance their own capacity for information technology, teachers must also be able to utilize instructional strategies for teaching which is an undoubtedly burden for them. Therefore, it is so critical to build a convenient teaching situation in the network platform to provide an integrated support teaching tool to assist teachers in online teaching application. Currently, most functions of the network teaching platform design, although the diverse and constantly strengthen the tools, in-depth examining, no one has been built from the view point of learning content itself. So in the past, even the network platform is very popular, yet because of the limitations of the functions, these Learning Management Systems provide virtually no help for the course content and teaching activities design. Moreover, in order to

promote so called “e-learning” as asked, many of them created online courses just cut the corner by converting paper handouts to digital formats. It does not only ignore the advantages of the multimedia and Internet technology, more important it hindered learning.

The consolidated above, this study would like to think from the perspective of the learning content direction, especially the conceptual foundation for language learning content to be summarized and finishing belong teaching strategies and methods through literature analysis, combined with interactive design principles, design for the appropriate aids open source network platform, look forward to the positive for the use and design of future LMS.

2 Related Studies

2.1 Conceptual Knowledge and the Related Teaching Strategies

Concept is constantly to be defined since the term has been coined. Merrill, Tennyson and Posey (1992) pointed out that the concept is a set of objects with the same attributes, signal events combination, but has a particular symbol or name. Simple, the generic name of the concept is the same kind of things (Bell 1990). The Zhang (1999) is based on the human angle to define the concept of the word, think the concept is a learner who has a broad understanding of things with common attributes. Therefore, from the definition of the scholars of the concept itself has established attributes and characteristics, to understand the concept, it is necessary to understand these properties.

On the teaching in concept content, learners’ cognitive processes must undergo three stages, abstraction, classification and identification. abstraction abstract way to understand the concept of attribute characteristics, such as the concept of “building blocks” that can be used abstract nature such as “shape” to describe; classification of similar properties to be classified as the same concept, such as all different models of vehicles; in addition, identification is the difference between the cognitive concept properties, such as the swallow is bird, not fish (Wen 1987). Therefore, for the teaching of the conceptual content first need to understand the concept itself of properties and characteristics.

Fleming and Levie (1993), cited in addition to learning strategies, rendering the concept of teaching can still include the manipulation of a few teaching elements, such as

1. Listed in the definition of the concept and properties. The Newby and Stepich (1987) more accurate to think, to teach the concept of teaching strategies must be placed in the key attributes of the concept.

2. Use the concept in different contexts. Such as the use of this concept in the game, or in the use of the dialogue between teachers and students, through different scenarios in use, help produce the transfer of learning.
3. Example and non-examples. “Paradigm” is related to the concept of learning things; “non-example” refers to things that are not associated with the concept itself. Examples and the selection and use of non-example, the use of the concept of teaching is quite necessary, in addition to help learners at first to face the new concept, easy to understand, can outline the concept of critical properties (Smith and Ragan 2005).
4. Classification practice. Through the presentation of different concepts and practice by the learner in the classification.

In addition to the above, and integrate your scholars proposed different strategies and methods for teaching and learning of the concept.

2.2 Consideration of Interactive Design in Web-Based Learning

Interactive is a necessary and shall be considered a major factor in e-learning. Compared to traditional classroom teaching and web-based learning both synchronous and asynchronous, for teachers, the control of students are relatively lower which required proper strategies to attract learners’ attention to last learning events. So the design of interactive teaching activities, flexibility in the use of materials and tools are very important issue (Ku 2005).

As web interactivity, Moore (1989) mentioned three main types, distance learning including Learner-content interaction. It also is regarded as the basic teaching strategy, teachers must help learners interact with the content and learners can learn new knowledge into existing cognitive structure.

Ji (2003) pointed out that when learners interact with the content, learners will be obtained based on cognition to perform on external behavior. When individuals external interaction feedback messages and expect feedback within the existing cognitive structure is different, the moment will produce cognitive conflict and learners will try to take into account the new message. Therefore, in interactive design, web-based learning environment should provide opportunities for external manipulation which in order to bring out the reflection, to reach learners’ cognitive interaction. So web interactivity design has to interact with the teaching materials and also re-vitalized the teaching contents. The learners can have an opportunity from passive reading to join to real learning activities, explore learning and thinking (Chung 2001).

The Internet interactive design allows the web-based learning is not only simply presenting the materials, but also allows learning truly to occur. Using some of the traditional application exercises, including fill in the blank, drag and drop, etc. Through these activities guide learners into the teaching materials, and will focus

on the content, practice (Jolliffe Ritter and Stevens 2001). Wu (2005) is also mentioned the user control that contains a selection of the content, sequence, speed, rendering control message symbol presents also the basic interactive tools, timely provision of learning aids.

Summarized the scholars for interactive design and teaching materials, which may include the following principles:

1. Interaction must cause learners to become active learning and participate in the activities.
2. Interaction must be able to stimulate the learners, trigger learners immanence thinking.
3. Interaction must provide learners opportunity to manipulate which allows learners to thinking and understanding from the process of learning.
4. Users can learn the powers of self-control.

2.3 LMS Development and Instructional Design

LMS (Learning Management System), as the name suggested is to construct on the Internet, integrated network functions to simulate the traditional teaching environment, and provide support for teaching and management platform. In this study, in order to understand the current LMS available, teaching function or tool design profile, so the functional analysis focused on the most popular brand around the field of education and industry. The LMS can be roughly divided into two categories: software copyright registered by the manufacturer and the open source free software. According to the comparison of two major name brand copyright software, Blackboard and Wisdom Master from Ku (2005), and also add other open source free software platform Moodle and Atutor.

Be able to understand these LMS with the current status of the teaching support and interactive features through the Table 2. To observe the angle of teaching content delivery, four LMS tools generally have web access, such as upload and download teaching materials, web pages, and other basic functions. In the interactive considerations, they focus on human interaction such as synchronous and asynchronous design. Yet, actual teaching content to interact with the game is only in the quiz functional design and whiteboard in Blackboard. It shows that the real direct and interactive learning content tools are still somehow limited.

3 System Prototype Desing

Teaching strategies and methods based on the conceptual content type belongs, this study attempted to design a LMS assisted teaching tools, and integrated into the web-based learning and content of interactive design principles, described as follows:

3.1 Introduction of the Tool: Concept Pointer

The idea for teachers by different objects text randomly presented in small circles or boxes, requirements the topic learners according to their requirements, be thinking Click. While the other is named “Concept Pointer” has two points meaning content in accordance with the teaching arrangements, one for learners think Click, to help learners click activity content theme more clearly; when learners confused when faced with the click activity, teaching activities provide tips the learners after pointing it better proficient understood. Teachers in the use of teaching, if teaching is a concept type, you can content design through all sorts of positive and negative cases, create a text project presented interesting ways, by learners using mouse clicks. “Concept Pointer” itself belongs to the generic nature of the tool that takes teachers to be applied flexibly according to their design.

3.2 Conceptual Teaching Strategies and Interactive Design Principle

“Concept Pointer” reference in the planning and design teaching strategies and methods to be able to support the positive and negative cases practice, classified and summarized the contents of exercises, as well as memory after learning exercises, interactive elements considerations, expectations “Concept Pointer” learners thinking can trigger, causing challenges with fun, allows learners to content manipulation respond, and provide content prompts help learners to learn in the game activities will think alike that aids contained teaching strategies, methods, and interactive elements of consideration, structured presentation. (Fig. 1)

3.3 User Interface for Teachers and Students

“Concept Pointer” is to design architecture in the open source network teaching platform Moodle, Moodle has a teaching module characteristics, this study will also think alike packaged into a single module, for teachers to demand the use of platform installation. “Concept Pointer” can be roughly divided into the end of teachers and students end the two interfaces. At the end of the part of teachers, the main function is to provide teachers in producing teaching content as the main interface to the Flash component step of the way by teachers based on step editing teaching content, where teachers can set the game level, time, correct and non-right content, etc. set finished, press the release button to generate learning activities for students to learn to use.

Students use “Concept Pointer” by login students end interface, by time, life-loving, scores, sound effects, and error-free challenges vitality factor in the game,

challenge students to learn and generate interest, and students through activities presented to slide the mouse symbol of boxing gloves, click on his view that the right content, and pause to read the content on activities suggest that in order to achieve the learning function.

To understand the achievement of the students’ exercises, and accepted level of “Concept Pointer”, teachers end to read student outcomes. Read the results screen, teachers can select the record to be read Which learners, and in the top of the record of the learner, through mouse clicks can read the details according to the topic of the breakdown of personal and answer questions, including the use of the number of occurrences of all content items alike during the learner reached ratios, etc.

4 Formative Evaluation and Finding

The “Concept Pointer” design and development process and the actual formative evaluation include a total of four dimensions: (a) expert evaluation of the results of the design and development stage; (b) tool test results and modification; (c) students evaluation; (d) teachers evaluation are described as follows:

4.1 Interface Design and Expert Evaluation

In a four points Likert scale questionnaire, the average scale is 3.20 points. Except question 4 (2.90), 6 (2.50) and 14 (2.30), others are more than Three points which shows the overall student satisfaction with this learning system is high (Table 1). Independent sample t test and examine the satisfaction of differences between male and female found higher overall satisfaction, no significant difference ($t > 0.05$), expressed satisfaction no significant differences between male and female.

4.2 Teacher Interview

Single factor analysis of variance results shown that the males time to complete the task ($M = 149.8$) is significantly more than females ($M = 71.2$), $F = 12.198$,

Table. 1 Performance (Completed Time) One-way ANOVA

	SS	df	MS	F	Significant
BG	15444.90	1	15444.90	12.19	0.008*
WG	10129.60	8	1266.20		
Total	25574.50	9			

*p < 0.05

$p = 0.08$. In face the significant differences in average scores between male and female, and the performance of females is better than males, this results reflecting attitudes questionnaire, males have lower learning attitude than female on Chinese language learning (see Table 1).

4.3 User Satisfaction Questionnaire

Student satisfaction questionnaire based on the six-point scale, six points students are most satisfied and 5 is very satisfied, 4 are satisfied, contrary 1 is very dissatisfied, very dissatisfied, 3, sub-is not satisfied.

Student satisfaction questionnaire showed that satisfaction mostly dropped in between satisfied and very satisfied.

Further, through open-ended questions, summarized finishing students alike advantage of the top three most mentioned are such as can 1. Learning in the game, lively and interesting, so learning improve with power and effectiveness; 2 “Concept Pointer” presents clear, easy to understand, and very easy to learn, and 3. Bright and rich color design, the layout is attractive for learners. The most mentioned need to be modified and improved is content project design, see Table 2.

It has been found to support and integrate into the design concept of principled teaching activities through formative evaluation and the actual teaching process, and from students and teachers to use after the reaction, most of them felt strange, satisfaction and convenience. Student user questionnaire score, average only in the satisfaction and are satisfied between, yet to reach a very satisfactory, showing that there is a need to revise. Through the recommendations of experts and users are most of the contents are alike diagram board can tend to be more comprehensive in the future, more in line to meet the teaching needs.

Table 2 Descriptive Statistics Type Styles

Question Item	Gender	Mean.
4. It is too fact. I have hear several time to understand it	M	2.40
	F	3.40
	Total	2.90
6. I like to use handheld device to learning. It is very convenient	M	2.20
	F	2.80
	Total	2.50
14. I think the questions are too easy	M	1.60
	F	3.00
	Total	2.30

5 Conclusion and Discussion

5.1 Strategic Teaching Tools Indeed Necessary to Support Learning Content in LMS

Analysis of the literature of the course of the study, found that the network teaching platform as a teaching and learning environment, but the face of different learning content type cannot provide the teaching tool support, that affect the design of teaching activities; In this study, the actual departure from the perspective of learning content selection belongs to the content itself desirable teaching strategies and methods, design network teaching platform development support tools. Can be learned from the evaluation of the results, and indeed be able to help the teachers to the content type of teaching strategies, taking into consideration the network teaching activities; Also attracted the interest on the student use thinking and review for content learning, so the net the functional design of the road teaching platform do need to think about the Content Type strategic teaching tool support.

5.2 “Concept Pointer” Can Support the Concept of Content Belongs to the Part of the Teaching Strategies and Methods

From the significance of the teaching strategies and activities at the same time you want to design a teaching tool, can be found in a single network teaching tool does not fully support and meet all of the teaching strategies and methods in the study and Content Type. The research on conceptual learning Content Type, selection of appropriate teaching strategies and methods for teaching activities blueprint planning, further R & D in network teaching platform able to support the activities of strategic teaching tool: “Made Easy”. Through the teaching of the the actual curriculum unit development, alike have been able to part of the teaching strategies and methods for conceptual content belongs practical learning activities

5.3 Teaching Strategies With Web Learning Content, and Interactive Principle Combination are Very Critical for Web-Based Learning Design

Network content interaction considerations of principle, allows the activities of students during the learning content can more easily enter the learning situation, with two-way interaction between the students and the content and guide students

deeper thinking and understanding of the learning content. Through experts, users, teachers and users of student evaluation results can be found in the Internet content for interactive consideration indeed cause interest in learning, also allows the students for the inherent thinking and manipulation of content in order to respond to so that students learning content in the network, from passive to active. Therefore, while thinking from the perspective of learning content design a strategic teaching tool, consider the principles of interaction with the content network really necessary.

5.4 Teaching Support Tools Just Media, Instructional Design and Teaching Activities Arrangement are the Key Points

The users teacher and student evaluation results, found that the content, the key to the design of the project or topics proposed amendments focus more, it can be learned teaching tool is only a medium to convey the content of the key to the quality of teaching is good or bad remains to learning content design, choreography and teaching activities. In addition to the need to understand the learning content type belongs to which classification the teachers have to consider the students' familiarity with the content, teaching activities have a clear blueprint for, and then pick enough to support the activities of teaching tools, content expedient decomposition design, set into the tool, to achieve a more appropriate learning.

References

1. Chen P-S (2007) New career selection-chinese language teaching, *Economical daily*, Fed. 5, retrieved from <http://www.udn.com/2007/1/19/NEWS/FINANCE/FIN11/3694588.shtml>
2. Tal K (2009) <http://www.krysstal.com/spoken.html> Accessed 1 Oct 2009
3. Ministry of Education (2009)
4. Ye M-T (1999) *Chinese language teaching norm and theoretical basic*. Taipei, Taiwan
5. Kynaslahti H (2003) Search of elements of mobility in the context of education. In: Kynaslahti H, Seppala P (ed) *Mobile learning* pp 41–48
5. E-campus project (2005) On the Asian-pacific counties promote the policy of the ubiquitous network society, Retrieved from http://www.nici.nat.gov.tw/content/application/nici/generala/guest-cnt-browse.php?cntgrp_ordinal=1002006100110003&cnt_id=758
6. O'Malley JM (1987), The effects of training in the use of learning strategies on learning english as a second language. In: Wenden A, Rubin J (ed) *Learner strategies in language learning*, Prentice Hall, New York pp 13–144
7. Oxford RL (1990) *Language learning strategies: what every teacher should know*. Heinle & Heinle, Boston
9. Mayer RE (1988) Learning strategies: an overview. In: Weinstein CE, Goetz ET, Alexander PA (eds) *Learning and study strategies*. Academic Press, New York, pp 11–22

10. Rigney JW (1987) Learning strategies: theoretical perspective. In: O'Neil HF Jr (ed) Learning strategies. Academic Press, New York
11. Smith LP, Ragan LP, Ragan TJ (2005) Instructional design , 3rd edn. New York
12. Jiang JL (2008) Vietnamese immigrants cross-cultural study of language learning strategies. Taipei, WS
13. Chamot AU, Kupper L (1989) Learning strategies in foreign language instruction. Foreign Lang Annual 22:13–14
14. Vann RJ, Abraham RG (1990) Strategies of unsuccessful learners. TESOL Q. 24:177–198
15. Mullins PY (1992) Successful english language learning strategies of students enrolled at the faculty of arts. Chulalongkorn University, Bangkok, Thailand. Diss, United States International University
16. Schön DA (1987) Educating the reflective practitioner: toward a new design for teaching and learning in the professions. Jossey-Bass higher education series, Jossey-Bass, San Francisco, US
17. Scribner S (1984) Studying working intelligence. In: Rogoff B, Lave J, Everyday Cognition : Its development in social context, MA : Harvard University Press , Cambridge, pp 9–40
18. Suchman LA (1987) Plans and situated action : the problem of human-machine communication. Cambridge University Press, New York
19. Lave J (1988) Cognition in practice. Cambridge University Press, UK
20. Brown JS, Collins A, Duguid P (1989) Situated cognition and the culture of learning. Educ Researcher 18(1):32–42
21. Collins A, Brown JS, Newman SE (1989). Cognitive apprenticeship: teaching the craft of reading, writing and mathematics. In: Resnick LB (ed) Knowing, learning and instruction: essays in honor of robert glaser hillsdale, NJ: Erlbaum pp 453–494
22. McLellan H (ed) (1996) Situated learning perspectives. Educational technology publications, NJ
23. Schilit WN (1995) A system architecture for context-aware mobile computing. Unpublished doctoral thesis, Columbia University
24. Schilit B, Theimer M (1994) Disseminating active map information to mobile hosts. IEEE Network 8(5):22–32
25. Dey AK, Abowd GD (1999) Towards a better understanding of context and context-awareness. (GVU Technical Report GITGVU-99-22)
26. Liu T-Y, Tan T-H, Chu Y-L (2009) Outdoor natural science learning with an RFID-supported immersive ubiquitous learning environment. Educ Technol Soc 12(4):161–175
27. Tseng JCR, Hsu SYY, Hwang G-J (2009) A collaborative ubiquitous learning platform for computer science education. In: Proceeding of the 14th annual ACM SIGCSE conference on innovation and technology in computer science education
28. Huang Y-M, Hsu S-H, Cheng S-C (2009) The experience of adopting game-based learning in library instruction, Lecture notes in computer science, pp 571–576
29. Horng C-F, Hourg G-J, Sun C-S (2007) Mobile learning combined with RFID for technical and vocational education and training, In: Proceeding of the 3rd international conference on Mobile multimedia communications, Nafpaktos, Greece
30. Ogata H, Yano H (2003) How ubiquitous computing can support language learning. In Proceeding of KEST, pp 1–6

Part IV
Advanced Social Network Technologies

Application-Driven Approach for Web Site Development

Chun-Hsiung Tseng

Abstract Some Web sites, such as google bookmark, evernote, or online calendar provides, are actually Web-based tools helping users complete their tasks and are regarded to as application-oriented Web sites. Today, the infrastructure support for building such Web sites is poor. What is the best approach to construct application-oriented Web sites? Perhaps some paradigms and generic guidelines will be helpful. In this paper, the researcher proposes preliminary results on some guidelines and infrastructure supports of application-oriented Web sites construction. The proposed solution is based on VWBE, which is the author's previous research result. Several issues such as application interface definition and application state management are addressed in this paper.

Keywords Web application · Framework · Mashup · Design pattern

1 Introduction

Today, the number of existing Web sites is huge. What is the role played by these Web sites? What do these Web sites provide to end users? Although a large portion of Web sites are document-oriented, that is, they are actually electronic documents delivering information to target users, some are not. Some Web sites, such as google bookmark, evernote, or online calendar provides, are actually Web-based tools helping users complete their tasks. These Web sites are application-oriented rather than document-oriented. Additionally, if carefully designed, functionalities provided by application-oriented Web sites can be integrated to

C.-H. Tseng (✉)

Department of Computer Information and Network Engineering,
Lunghwa University of Science and Technology,
Taoyuan, Taiwan
e-mail: lendle_tseng@seed.net.tw

complete more complex jobs. Compared with the power provided by application-oriented Web sites, the infrastructure support today is in fact very poor. To utilize the information delivered by document-oriented Web sites, there are various information extraction mechanisms and algorithms. To construct document-oriented Web sites, there is tons of HTML authoring tools. However, to the best of the author's knowledge, there are no globally-adoptable tools and platforms for building application-oriented Web sites, not to mention proven mechanisms and paradigms. The lack of infrastructure support results in poor compatibility and low reusability between application-oriented Web sites.

What is the best approach to construct application-oriented Web sites? Perhaps some paradigms and generic guidelines will be helpful. Considering how a normal desktop application is built, one will find that the object-oriented paradigm is the most popular. The core concepts of the object-oriented paradigm are modularization and reusability. Therefore, the goal of this research is to develop a sound framework for designing reusable application-oriented Web components. The goal is not easy to achieve since both syntax and platform supports will be needed.

The remaining of the paper is as the following: first, the result of the survey of existing works will be listed. Then, the core concept will be explained and a prototype implementation will be introduced. After that, some discussions about the current implementation will be presented, and finally, the conclusions and future works.

2 Related Works

2.1 Web Application Development

According to Jazayeri [1], in just one decade, the Web has evolved from being a repository of pages used primarily for accessing static, mostly scientific, information to a powerful platform for application development and deployment. The evolving of usage scenarios of Web applications results in the evolving of design principles for them. As shown in his survey, there was a continuing "desktop-to-Web" trend, which refers to the observation that there was a trend to move desktop applications to Web. Since the distinctions between desktop-based and Web-based applications have been getting blurred, the trend to apply existing software engineering approaches, which were mainly developed for desktop-based applications, to the development of Web-based applications appears reasonable and needed.

The research of Wang and Zahadat [2] emphasized that most Web applications and Web sites have emerged and transpired over recent years and the newly emerged Web applications are fundamentally different from traditional Web applications. The authors also mentioned that a new type of software development life cycle had emerged and promised to affect Web design and development. As stated in the paper, the Web had changed from a medium to a platform for delivering software. Different

from traditional Web site designers, what Web developers do today is developing Web applications instead of authoring simple Web contents.

In [3], the concept of “Web native interactive applications” was proposed. The paper stated that the initial design of Web technologies which was based on “Web of documents” did not accommodate the requirements today. The paper also proposed AgentWeb, which was an environment for building Web-based interactive computer games. The environment was built following the Model-View-Controller (MVC) architecture. The authors emphasized that current open Web standards were sufficient to support sophisticated interactive applications.

2.2 Object-Oriented Web

“Object-Oriented Web” is not a brand-new terminology. In [4], object-oriented Web is viewed as the next step of the semantic Web and is depicted with the following example:

Look at the blogs for instance, they usually have a “comment” feature and it would be interesting if this feature was available wherever the posts appear, whether it is on the original blog, a RSS aggregator like Google Reader, or a social network. Just consider the blog articles as objects capable of ubiquity composed of data (properties) as well as actions (methods) and you’ll start to envision what I mean by the Object Oriented Web.

The term is also mentioned in [5], and the article also viewed object-oriented Web as the extension of the semantic Web. None of these articles gave a formal definition of the object-oriented Web. Despite of the missing of a formal definition, however, the blueprint of the object-oriented Web had already been sketched by several earlier research works. For example, Gaedke and Rehse developed a component-based Web engineering methodology [6] based on the object-oriented concept. In their research, a WebComposition repository system was proposed for maintaining Web components and a markup language, WCML, was used as a convenient way to define the representation of components. WCML was introduced in [7] for defining reusable Web components. The definition of a “component” in the research was almost identical with the definition of an “object” today. In [8], the author tried to improve the “Web object model” by providing a richer base representation than HTML, an API to the state of components, and an enhanced ability to define relationships between state and behaviour.

2.3 Cloud Computing

Cloud computing is internet-based computing, whereby shared servers provide resources, software, and data to computers and other devices on demand, as with the electricity grid. Although by most standards, cloud computing is still in the

early stages of adoption by midsize and larger organizations, but the pace is increasing as users look for additional cost savings and technology perks, such as scalability [9]. Cloud computing technologies have shifted people's concentration on computer technology from single machine to the internet centering on Web by using storage and services from Web [10]. Cloud computing can be viewed as the evolution of distributed computing, however, due to the mature of virtualization technologies, cloud computing appears more adaptable [11].

3 Application-Oriented Web Sites

An application-oriented Web site is a Web site which acts like an application. Rather than simply reading information presented on them, people execute functionalities provided by application-oriented Web sites to complete their tasks. Typical application-oriented Web sites are online-dictionaries, online calendars, and online office applications, etc. These Web sites are valuable, however, since there is almost no infrastructure and tool support for building such type of Web sites, creating application-oriented Web sites today is not easy. A lot of technologies such as AJAX, DHTML, and JSON etc. are involved. Furthermore, the lack of infrastructure support makes it even more difficult to integrate application-oriented Web sites. Imagine that how can the functionalities provided by two application-oriented Web sites be integrated. Nowadays, there is in fact no promising approach to achieve that unless all involved Web sites provide standard-compliant application interfaces such as SOAP or Restful. Otherwise, most solutions depend on page scraping, which suffers from instability. In this paper, the researcher proposes preliminary results on some guidelines and infrastructure supports of application-oriented Web sites construction.

There are several aspects to consider if developers are building interoperable application interfaces for their Web sites:

1. Object definition versus object instances.
2. How to define application interfaces?
3. Which functionalities are included in the application interface?
4. How to interpret results returned from function invocations?
5. How to manage instances of applications?

In this and later sections, we propose our solutions to these questions followed by some discussions.

3.1 *Object Definition versus Object Instances*

In this research, we consider Web pages and javascript functions associated with them. A Web page contains information. Thinking of a Web page as an object in

the object-oriented paradigm, for application-oriented Web sites, the information can be regarded to as member data of an object. On the other hand, javascript functions form the functional layer and can be regarded to as member functions. During execution, member functions can definitely have access to member data and client applications access member data through member functions, so this definition fits the object-oriented paradigm well. One thing to be noted is that we have to distinguish between object definitions and object instances. Conceptually, the set of static files, i.e., Web pages, external javascript files, embedded javascript functions, etc., forms the definition of an object. At runtime, what client applications interact with are object instances. These instances are created based on the specified Web resources and there can be more than one instance for one definition. The current implementation handles constructions of object instances and manages mappings between instances and definitions but does not handle instance sharing between client applications.

3.2 How to Define Application Interfaces?

Interoperability can only be achieved if application interfaces that can be understood by involved applications do exist. Today, to access functionalities provided by a Web site, no matter it is application-oriented or not, the most commonly used tool will be Web browsers. However, Web browsers are interfaces between human beings and Web sites and can hardly be regarded to as application interfaces. Only few Web sites provide application interfaces. Examples are google docs and delicious bookmarking services. These Web sites typically provide application interfaces compliant with protocols such as SOAP or Restful. To “invoke” functionalities exposed by these Web sites is easy since one simply builds applications that can exchange messages with these Web sites (or more specifically, the servers hosting them) according to the protocols. The problem is, for most Web sites that do not follow these protocols, one can simply rely on ad-hoc solutions that thus the resulting applications will be unstable and rarely usable.

To address the issue, the researcher’s previous research result, the virtual Web browsing environment (VWBE [12]), is adopted and extended. Originally, VWBE simply simulates the behavior of a real Web browser. Accepting a URL as the input, VWBE loads the targeted Web resource and related resources into it, constructs a document object model (DOM) reflecting the Web page, and wraps javascript functions declared in the Web resource as Web services adopting the SOAP protocol. After that, client applications can access exposed javascript functions through Web service calls. This architecture suffers from several problems: first, many javascript functions declared on Web pages are used for presentation only and it will not be reasonable to expose these javascript functions. Second, in some cases, exposing only javascript functions declared on Web pages is not enough. To meet requirements of client applications, some additional functions may be needed. As a result, enhancing the original VWBE is needed.

In this research, we extend the original VWBE by allowing the injection of external javascript functions at runtime. This version of VWBE accepts a URL (the main Web page) and a set of javascript files as input parameters. At runtime, VWBE automatically merge these files. During execution, these augmented javascript files have a reference to the DOM of the main Web page and thus can access the full functionalities provided by the original Web sites. These javascript files form the application interface and will be exposed through VWBE's Web service interface.

3.3 Which Functionalities Are Included in the Application Interface?

As stated above, many javascript functions declared on Web pages are used for presentation only. These functions should not be included in the application interface. As a result, this version of VWBE uses annotations to specify needed javascript functions. Annotations are small pieces of information that can be attached to javascript functions and are used as meta-information of the attached function. To prevent interfere with execution of normal javascript functions, VWBE annotations are written in javascript comments. For example,

```
/*
 * @export()
 */
function multiply(a, b){
  return a*b;
}
```

VWBE looks for the “@export()” annotation to determine javascript functions to be exported. Note that/* ... */is ordinary comment syntax of javascript and thus will not cause interference.

3.4 How to Interpret Results Returned from Function Invocations?

Executing a JavaScript function has two different types of returns. One of them is normal function return. The other is reflecting the result in the DOM. The former is simple to deal with. VWBE simply transforms returned javascript objects into corresponding SOAP objects. However, due to the fact that a Web page itself can be viewed as an information source, it is possible that the execution of a javascript function results in modification in the Web page hosting it. In such scenario, the Web page itself should be included in the returning results. For simplicity, VWBE allows a javascript function to return a DOM node. In case data on the hosting Web

page should be included in the returned result, one simply returns the DOM node containing the result. During the transmission across the Internet, the DOM node is serialized into string representation and will be reconstructed in the invoker's memory space. The returned DOM result can be messy since there are data nodes mixed with presentation nodes. A possible solution is to apply transformation technologies such as XSLT or H2X to the returned DOM node but this is beyond the scope of this paper.

3.5 How to Manage Instances of Applications?

Managing instances and states of applications is a further issue. Considering Web pages and associated javascript functions as definitions of applications, what VWBE manages are actually instances of these applications. As stated in previous sub sections, execution of javascript functions can result in modifications in DOM. Hence, we have to distinguish between different application instances and manage their states separately. By assigning ids to client sessions, this can be easily achieved. However, things can be even more complicated if the execution of javascript functions results in page transition. Navigating to a new URL causes the loading of new Web pages, associated resources, javascript functions, and hence the instantiating of a new application instance. Page transitions happen in several different forms:

1. through anchor links
2. through javascript manipulation (e.g. `window.location.href`)
3. through form submission.

VWBE thus intercepts these events, instantiates new application instances, and puts application instances into the execution context of client applications.

Another issue will be how to switch between application instances involved in a client session. In this version of VWBE, the concept of client context is introduced. Before accessing a Web application, client program has to acquire a client context in advance. From the client context object, references to involved Web application instances can be accessed.

4 Discussions

4.1 Annotations on JavaScript Functions

The annotation functionality deserves more discussions. For now, it is only used for specifying javascript functions to be exported. However, the functionality is generic and thus can be used in other scenarios. For instance, parameters of

javascript functions are weakly-typed but SOAP-based Web services are strongly-typed and annotations can be used to overcome the incompatibility. Furthermore, annotations can be used for associating semantic information with application interfaces. Such information will be useful if automatic discovery of suitable functions is desired.

4.2 Complex Web Application Modularization

Current implementation of VWBE only allows one-to-one mappings between Web pages and Web applications. Such granularity can be overly rough. There are cases in which a Web page contains more than one Web applications. For example, a Web page can contain both a calendar component and a notebook component. It appears reasonable to create two Web applications based on such Web page. On the other hand, some complex Web applications require more than one Web page or even more than one Web site. Due to the diversity of design patterns for Web applications, current implementation of VWBE can hardly support these scenarios directly. However, if meta-information is available, supporting complex Web applications is still possible.

5 Conclusions and Future Works

In this paper, a framework and a tool set supporting the development of application-oriented Web sites are proposed. The solution shown in this paper is based on an enhanced version of VWBE, the virtual Web browsing environment. The environment is capable of wrapping existing Web pages into Web applications. With some extensions, VWBE becomes a suitable framework for Web application development.

The capability of creating Web applications based on existing Web sites is convenient, but there are certainly limitations. Perhaps an important issue that has to be solved is the lacking of commonly-adoptable module system for development of application-oriented Web sites. The very popular template-based mechanisms are good for modularization of document-oriented Web sites but not for application-oriented Web sites. In the future, the goal is to develop a more complete module system that can be used to search modules, manage modules, and perhaps orchestrate modules. With the system, better design patterns for developing application-oriented Web sites can be developed.

References

1. Jazayeri M (2007) Some trends in web application development. In: Proceedings of the 2007 future of software engineering, 2007, pp 199–213
2. Wang J, Lochovsky F (2003) Data extraction and label assignment for web databases. In: Proceedings of the 12th international conference on world wide web, 2003, pp 187–196
3. Jazayeri M, Ahmadi N (2011) End-user programming of web-native interactive applications. In: Proceedings of the 12th international conference on computer systems and technologies, 2011, pp 11–16
4. Kindalab (2007) Le web orienté objet. Available at <http://frenchblog.kindalab.com/2007/10/21/le-Web-orienté-objet/>
5. Vila M (2007) The object oriented Web
6. Chang C, Lui S (2001) IEPAD: information extraction based on pattern discovery. In: Proceedings of the 10th international conference on world wide Web, 2001, pp 223–231
7. Gaedke M, Schempff D, Gellersen HW (1999) WCML: an enabling technology for the reuse in object-oriented web engineering. In: Proceedings of the 8th international world wide web conference, 1999
8. Manola F (1999) Technologies for a web object model. *IEEE Internet Comput* 3(1999):38–47
9. Schneiderman R (2011) For cloud computing, the sky is the limit. *Signal Process Mag* 28
10. Zhang X, Dong G (2010) A new architecture of online trading platform based on cloud computing. In: Proceedings of the 2010 Asia-Pacific conference on wearable computing systems, 2010, p 32
11. Kim I, Kim, T, Eom Y (2010) NHVM: design and implementation of linux server virtual machine using hybrid virtualization technology. In: Proceedings of the 2010 international conference on computational science and its applications, 2010, pp 171–175
12. Tseng CH (2011) Virtual browsing environment for mashups. In: Proceedings of the 2011 international conference on advanced information technologies, 2011, p 154

The Analysis of the Participants' Personality for the Contestants of the National Skills Competition

Kung-Huang Lin, You-Syun Jheng, Lawrence Y. Deng
and Jiung-Yao Huang

Abstract The article aims to analyze the personality traits between the winners from the Golden Hands Award of National Skills Competition and the other students under the Industry-Related, Agriculture-Related, and Marine Fisheries-Related. This paper undergoes the Independent Samples *t* Test and One-Way ANOVA on the data by using SPSS. The experiment results showed that there are a number of variations in personality traits for different vocational categories. The forward personality of skills competition award winners are significantly higher than the student without participating in the skills competition training. Moreover, the profile data on gender under different vocational categories, family background, and birth order, were also observed with several personality traits showing significant differences. Hence, this study aims to find out the personality traits of the previous award winners and recommend suitable students to participate in the National Skills Competition.

Keywords Golden hands award · Personality traits · Background variables · Statistical analysis · National skills competition

K.-H. Lin
Graduate Institute of Human Resource Management,
National Changhua University of Education,
Changhua, Taiwan

Y.-S. Jheng · J.-Y. Huang
Department of Computer Science and Information Engineering, National Taipei University,
Taipei, Taiwan

L. Y. Deng (✉)
Department of CSIE, St. John's University, New York, USA
e-mail: lawrence@mail.sju.edu.tw

1 Introduction

The National Skills Competition of high school students is the most important contest for senior and vocational high school students in Taiwan. This competition is held annually once whereby the categories differ as they are different departments in school. The schools in Taiwan are actively nominating their students to participate in this competition as it prepares the students with hands-on experience, practical skills other than professional knowledge. However, there is a lack of extensive discussion on how to select suitable students to participate in skill competitions based on the personality trait differences among students, so that students can undergo a better effective education.

This paper presents the questionnaire survey for the Mini-Makers (Big-Five Personality) [10]. This study adopted the Chinese version of the Mini-Markers questionnaire [7, 8]. This study is conducted on senior and vocational high school students. In order to understand the reliability and validity of the Chinese version of the questionnaire, reliability analysis is conducted. In the Chinese version of the Mini-Markers questionnaire, the Cronbach's alpha value is 0.86, meaning it has high reliability and good internal consistency. The questionnaire was distributed to students from three vocational departments, namely Industry-Related (IR), Agriculture-Related (AR), and Marine Fisheries-Related (MFR). By using the Big-Five personality analysis, statistical analysis was conducted on all data attained while finding out the personality traits with significant difference [4, 11]. Meanwhile, the characteristics will undergo data forecast to specifically recommend students who have the ability to be award winners.

This paper is organized as follows: [Sect. 2](#) describes the related works with research design, research assumption, and the complete details of research process. [Section 3](#) presents research assumptions and the methods. [Section 4](#) describes results that include the difference description of personality traits under the different background variables. [Section 5](#) concludes discussion results.

2 Related Work

Personality traits refers to the exceptional personality exhibited by individuals while facing people, incidents, matters and even the entire environment adaptability of an individual [1]. These traits can be used for studying human personality from the dimension of psychology [5]. Moreover, the personality is also exhibited in the physical and mental characteristic compositions under the interaction between factors such as individual gender, family background and growing environment. These characteristics often come with considerable representative significance while the formation of personality is a series of cumulative growth and development in psychological dimension, which also determines the unique pattern of individual thinking and behaviors. Hence, students of different departments often exhibit different characteristics in personality traits.

This paper look into the personality traits from the research perspective and the Big-Five proposed by this study is based on the Big-Five personality proposed by Goldberg [3], with over 100 groups of descriptive words. Gerard Saucier (1994) selected 40 groups of strong and powerful description and prepared into the Mini-Markers [10]. The Mini-Markers questionnaire is a small list that contains impressive words for describing human personality. The personality study under the testing framework contains five scopes that summarize personality traits, namely Extraversion (Factor I), Agreeableness (Factor II), Conscientiousness (Factor III), Emotional Stability (Factor IV), and Intellect or Openness (Factor V) [2, 9]. Each construct contains 8 descriptive words which we have organized in more detailed explanations, as shown in Table 1. The descriptive words labeled with * indicate them as reverse questions, whereas each group of descriptions are coordinated with situational interpretations so that students can comprehend the implications of each group of descriptions better when filling out the questionnaires.

For example, students of IR often prefer hands-on operation and are usually good at mathematics and logistics. Students of AR prefer the nature, animal and plants also pay particularly interest in natural gardening with continuous innovation and invention. Students of MFR generally prefer the oceanic and marine work

Table 1 Correspondence and interpretation of the Big-Five personality traits (Mini-Markers)

Big-Five Factor	Significance	Term	
Factor I	<i>Extraversion</i> —The term refers to the degree of personal adjustment in interpersonal relationship, whereas outgoing people usually have more positive emotion with self-affirmation	<i>Bold</i> <i>Energetic</i> <i>Extraverted</i> <i>Talkative</i>	<i>Bashful*</i> <i>Quiet*</i> <i>Shy*</i> <i>Withdrawn*</i>
Factor II	<i>Agreeableness</i> —The term refers to the degree of obedience to others, whereas team people show strong cooperation, friendliness, and easily trust others	<i>Cooperative</i> <i>Kind</i> <i>Sympathetic</i> <i>Warm</i>	<i>Cold*</i> <i>Harsh*</i> <i>Rude*</i> <i>Unsympathetic*</i>
Factor III	<i>Conscientiousness</i> —Persons with high conscientiousness often are equipped with rational personality traits, fulfilling their duties in order to realize their plans	<i>Efficient</i> <i>Organized</i> <i>Practical</i> <i>Systematic</i>	<i>Careless*</i> <i>Disorganized*</i> <i>Inefficient*</i> <i>Sloppy*</i>
Factor IV	<i>Emotional Stability</i> —The term refers to stable emotion and the degree of impulse control. It is the characteristic of emotional stability	<i>Relaxed</i> <i>Unenvious</i> <i>Envious*</i> <i>Fretful*</i>	<i>Jealous*</i> <i>Moody*</i> <i>Temperamental*</i> <i>Touchy*</i>
Factor V	<i>Intellect or Openness</i> —The term indicates the quantity and depth of individuals for object interests. Their rationality and openness indicate novel imagination and full of curiosity for the intrinsic and extrinsic world	<i>Complex</i> <i>Creative</i> <i>Deep</i> <i>Imaginative</i>	<i>Intellectual</i> <i>Philosophical</i> <i>Uncreative*</i> <i>Unintellectual*</i>

* negation terms

with diligence, endurance and challenging spirit. In this view, the personality traits for students in different departments also vary [12]. Therefore, this paper conducted a survey on the personality traits for students in the IR, AR, and MFR. Our elementary results showed that the different departments would render significantly different personality in the statistical analysis for personality traits. The Sect. 4 will elaborate on comparison and description for the different categories.

In sum of the aforementioned, the emphasis is on look for personality traits with influence indicators from the research experiment. This paper using personality traits analysis and recommend to the suitable participants to the school. Additionally, for students with different gender, family background and birth order, the testing result of personality traits will help them understand their strengths and weaknesses in addition to providing relevant data and aspects of personality traits as reference to choosing the departments suitable for them.

3 Method

The factors affect the personality traits of vocational students could generally be divided into two dimensions: intrinsic factors of students and extrinsic factors such as the impact from different departments and environment. The study offers specific recommendation for schools and students by discussing the scope. While limiting to the controllable factors related to the students excluding intelligence and the impact from extrinsic factors to learning effectiveness. The overall research framework is shown in Fig. 1.

The study issued questionnaires to the senior occupations high schools nationwide with the objects of questionnaire methods comprising Gold Hand Award winners and students not participating in the skills competition training. The number of valid samples undergone statistical analysis was 356 and the valid recovery rate was 95.7 %.

Moreover, the questionnaire object include students of three vocational departments, namely IR (accounting for 249 questionnaires), AR (58 questionnaires), and MFR (49 questionnaires). This paper deals with a case analysis of the Big-Five personality for each IR, AR, and MFR.

This paper verifies on the following assumptions based on the survey on the Big-Five personality questionnaires:

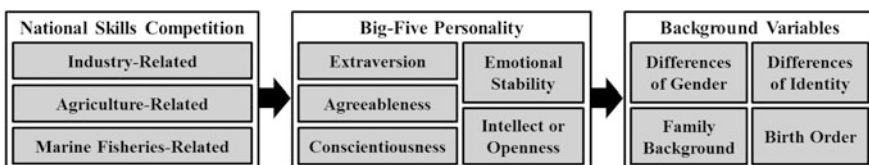


Fig. 1 Research framework

- (1) The gender of different department for any significant difference in personality traits.
- (2) Whether if there is significant difference in personality traits for the golden award winners of different departments and the students without participating in skills competition training.
- (3) Whether if there is significant difference in personality traits for family backgrounds with different departments.
- (4) Whether if there is significant difference in personality traits for the birth order of different departments.

The study adopted the Big-Five personality from the questionnaire survey, Mini-Makers [10], whereas the representative description for the personality trait for each question adopts the 7-point Likert scale [6]. The valid questionnaires are organized and undergo statistical analysis for data analysis using SPSS. In order to search for the difference of the difference background variables on the 40 personalities based on the Independent Samples t-Test and One-Way ANOVA statistical method.

4 Experimental Results and Discussion

The preliminary results illustrated that the personality traits of different departments show several differences while the forward personality of winners of skill championship indeed were significantly higher than students without participation in the skill competition training. Moreover, under the different profile data of gender, family background and birth order for different departments, this paper also discover several personality traits with significant difference.

According to the statistical results of the Independent Samples t-Test, testing on the significant different of gender, Male Students (M) and Female Students (F), and personality traits under the 95 % confidence level showed that there are several projects with the average means of significance. In which, the testing result was not significant for M (91 %) and F (9 %) from the IR with. The testing results for M (47 %) and F (53 %) from AR showed significant difference in the personality traits for Bold and Imaginative with an average mean indicating higher score for male than for female. The testing results for M (59 %) and F (41 %) from MFR showed significant difference in the personality traits for Organized, Practical and Touchy with an average mean indicating higher score for F than for M. The above results are shown in Table 2.

Next, for testing on the significant different in difference of identity, students of industry department who are Award Winners (AW) and students Without Participation in training (WP), and personality traits under the 95 % confidence level showed that there are several projects with the average means of significance. Among which, students of IR, AW (55 %) and WP (45 %) showed significant difference in personality traits for Imaginative and Systematic with an average

Table 2 Independent samples t-test—differences of gender

Term <i>*negation</i> terms	IR (Industry-related)		AR (Agriculture-related)		MFR (Marine fisheries-related)	
	Mean (SD)		Mean (SD)		Mean (SD)	
	M	F	M	F	M	F
Bold			5(1.21)	4.16(1.64)	2.24*	
Imaginative			5.48(1.34)	4.58(1.34)	2.56*	
Organized					4.28(1.16)	4.95(0.89) -2.19*
Practical					4.66(1.05)	5.5(1.05) -2.78**
Touchy*					3.52(1.81)	4.55(1.70) -2.01*

* $P < 0.05$ (significant); ** $P < 0.01$ (highly significant)

means indicating that AW scoring higher than WP. The aforementioned students also showed significant difference in Moody, Sloppy, Touchy and Withdrawn with an average means indicating than WP scoring higher than AW. Students of AR, AW (59 %) and WP (41 %) showed significant difference in personality traits for Complex, Philosophical and Systematic with an average means indicating that AW scoring higher than WP. Students of MFR, AW (51 %) and WP (49 %) showed significant difference in personality traits for Efficient with an average means indicating that that AW scoring higher than WP. The above testing results are shown in Table 3.

Finally, the testing on the significant different in difference of family background, whose parents work in Related areas (R) and parents Not engaged in Related work (NR), and personality traits under the 95 % confidence level showed that there are several projects with the average means of significance. Among which, students of MFR, R (10 %) and NR (90 %) did not show significance for testing results. Students of IR, R (12 %) and NR (88 %) showed significant difference in personality traits for Careless, Extraverted and Sloppy with the average means indicating the NR scoring higher than R. Students of AR, R (12 %) and NR (88 %) showed significant difference in personality traits for Complex and Deep with the average means indicating the R scoring higher than NR. The testing results are shown in Table 4.

According to the statistical results of One-Way ANOVA, the testing on the significant different in difference of birth order, First Born (1stB), Second Born (2ndB), Third Born (3rdB), Last Born (LB) and Only Children (OC), and personality traits under the 95 % confidence level showed that there are several projects with the average means of significance. Among which, AR competition consisted of 1stB (29 %), 2ndB (31 %), 3rdB (9 %), LB (29 %), and OC (2 %) both received insignificant testing results. Students taking IR competition consisted of 1stB (41 %), 2ndB (33 %), 3rdB (10 %), LB (12 %), and OC (4 %) showed significant difference in the personality traits for Creative and Talkative which underwent LSD Post Hoc. Both Creative and Talkative showed 1stB > 2ndB.

Table 3 Independent Samples t-test—differences of identity

Term *negation terms	IR (Industry-related)			AR (Agriculture-related)			MFR (Marine fisheries-related)		
	Mean (SD)		t	Mean (SD)		t	Mean (SD)		t
	AW	WP		AW	WP		AW	WP	
Imaginative	5.37(1.17)	5.04(1.38)	2.08*						
Systematic	5.08(1.13)	4.73(1.20)	2.36*	4.97(1.29)	4.13(0.85)	3.01**			
Moody*	3.4(1.69)	4.03(1.62)	-2.96**						
Sloppy*	2.86(1.53)	3.33(1.52)	-2.42*						
Touchy*	2.72(1.65)	3.24(1.51)	-2.56*						
Withdrawn*	2.48(1.40)	2.94(1.41)	-2.55*						
Complex				4.06(1.59)	2.96(1.08)	2.93**			
Philosophical				4.53(1.24)	3.88(1.12)	2.07*			
Efficient							5.32(0.90)	4.71(1.16)	-1.83*

* $P < 0.05$ (significant); ** $P < 0.01$ (highly significant)

Table 4 Independent samples t-test—family background

Term *negation terms	IR (Industry-related)		AR (Agriculture-related)		MFR (Marine fisheries-related)	
	Mean (SD)		Mean (SD)		Mean (SD)	
	t		t		t	
	R	NR	R	NR	R	NR
Careless*	3.45(1.80)	4.1(1.63)				-2.03*
Extraverted	3.74(1.84)	4.53(1.34)				-2.29*
Sloppy*	2.52(1.61)	3.15(1.52)				-2.17*
Complex			4.29(0.76)	3.51(1.56)	2.16*	
Deep			5.43(0.98)	4.37(1.23)	2.17*	

* $P < 0.05$ (significant); ** $P < 0.01$ (highly significant)

Table 5 One-way ANOVA—Birth order

Term *negation terms	IR (industry-related)		AR (Agriculture-related)		MFR (Marine fisheries-related)	
	F	Post Hoc (LSD)	F	Post Hoc (LSD)	F	Post Hoc (LSD)
	Creative	2.64*	1stB > 2ndB			
Talkative	2.55*	1stB > 2ndB				
Complex					2.99*	LB > 1stB > 2ndB > 3rdB
Inefficient*					3.18*	LB > 1stB > 2ndB

1stB First Born; 2ndB Second Born; 3rdB Third Born; LB Last Born; OC Only Children

* $P < 0.05$ (significant)

Students taking MFR competition consisted of 1stB (39 %), 2ndB (33 %), 3rdB (6 %), LB (18 %), and OC (4 %) showed significant difference in the personality traits for Complex and Inefficient which underwent LSD Post Hoc. The results showed that significant difference for Complex was LB > 1stB > 2ndB > 3rdB and for Inefficient was LB > 1stB > 2ndB. The above testing results are shown in Table 5.

In this report, we emphasized on finding students with potential personality traits of winners. This paper strongly emphasizes discovered several significant personality traits with differences from the constructs of the Big-Five personality, whereas the distribution of traits was inclined towards Conscientiousness and Intellect or Openness for all departments, as shown in Table 3.

5 Conclusion

The results showed the statistical analysis of different departments under the background variables including gender, difference of identity, family background, and birth order indicated that there were several personality traits containing

difference. The preliminary testing proved the assumptions this paper proposed. The difference in personality traits varies following the variation in departments, which suggests that students of different departments will have different personality traits. In sum of the aforementioned chapters, the study proposes two specific contributions. First, this paper improve the traditional selection of skill competition winners as traditional selection only selected students with better academic performance while highly likely neglecting students with potential traits for skills. The analysis of personality traits can more specifically recommend students with personality traits of winners. Second, the testing results for personality traits for students with different gender, family background and birth order help students understand their strengths and weaknesses as well as providing students with relevant data on the suitable departments for them from the aspect of personality traits.

This paper proposes closer look into the personality trait difference for different departments because past studies have not conducted in-depth discussion on the different departments while the population quantity we acquired was considerably enormous compared to past studies. Hence, we must take deliberation in the interpretation to the difference characteristics of personality traits. We attain several implications of personality trait difference for different departments while providing assumptions and analysis on the different background variables, as well as sufficient interpretation for the personality trait difference of all background variables. Such discoveries emphasize the importance of understanding the significant personality traits of departments. Apart from the personality trait difference in the difference of identity, we also tested the background variables including gender, family background and birth order in several personality traits. The data can be provided as reference for students as career planning or aptitudes.

References

1. Allport GW (1961) *Pattern and growth in personality*. Holt, Rinehart & Winston, New York
2. Digman JM (1990) Personality structure: emergence of the five-factor model. *Annu Rev Psychol* 41:417–440
3. Goldberg LR (1992) The development of markers for the Big-five factor structure. *Psychol Assess* 4(1):26–42
4. Husin LIBA, Zaidi NA (2011) The correlation effects between big five personality traits and job satisfaction among support staff in an organization. *Humanities, science and engineering (CHUSER)*, pp 883–887
5. Kassir S (2003) *Psychology*. Prentice-Hall, Inc, USA
6. Likert R (1932) A technique for the measurement of attitudes. *Arch Psychol* 22(140):1–55
7. Lin SC (2008) The relationships between humor styles, ridicule styles and big-5 personality traits of high school students. Master's theses, National Digital Library of Theses and Dissertations in Taiwan: 097NTNU5328030
8. Lin NP, Chiu HC (1999) A study of service quality—the effects and applications of service providers' personality traits. *J Manag* 16(2):175–200

9. O'Connor BP (2002) A quantitative review of the comprehensiveness of the five-factor model in relation to popular personality inventories. *Assessment* 9:188–203
10. Saucier G (1994) Mini-markers: a brief version of goldberg's unipolar big-five markers. *J Pers Assess* 63(3):506–516
11. Shi M, Li X, Zhu T, Shi K (2010) The relationship between regulatory emotional self-efficacy, big-five personality and internet events attitude. *Web Society (SWS)*, pp. 61–65
12. Xie J, Lin R, Jeng YC, Li J (2010) How different personality types are related to perception of professional ethics. *IET international conference*, pp 241–246

Ontology-Based Multimedia Adaptive Learning System for U-Learning

Lawrence Y. Deng, Yi-Jen Liu, Dong-Liang Lee and Yung-Hui Chen

Abstract More and more video streaming technologies supporting for E-learning systems are popular among distributed network environment. The Web's Information Seeking System as the main provider of information is indisputable. How to provide multimedia Information seeking support E-learning system is becoming more and imperative. In this paper, we provided a multimedia information system for e-learning. This system requires adaptable and reusable support for the modeling of multimedia content models and also supports possible interactive, transfer of streams multimedia data such as audio, video, text and annotations using with network facilities. However, we investigated these existed standards and applications for multimedia documents models such as HTML, MHEG, SMIL, HyTime, RealPlay and MS Windows Media that let us to find that these standards and applications models do not provide adequate support for advanced reuse and adaptation. Consequently, we proposed a new approach for the modeling of reusable and adaptable multimedia content. We developed a comprehensive system for advanced multimedia content production: support for recording the presentation, retrieving the content, summarizing the presentation, weaving the presentation and customizing the representation. This approach significantly impacts and supports the multimedia presentation authoring processes in terms of methodology and commercial aspects.

Keywords: Ontology · Distance learning · Content tree · Adaptive learning system

L. Y. Deng (✉) · D.-L. Lee
Department CSIE, IM, St. John's University, New York, USA
e-mail: Lawrence@mail.sju.edu.tw

Y.-J. Liu
Department of Computer Science and Information Engineering, Tamkang University,
New Taipei, Taiwan

Y.-H. Chen
Department of Computer Information and Network Engineering,
Lunghwa University of Science and Technology, Taoyuan County, Taiwan

1 Introduction

In past decade, the distributed network environment is growing rapidly. Any web-based application system must consider the user's various demands, such as the different cultural context, the learning environment as well as the professional field; For past few years, we had aimed at the multimedia's main characteristics and the adaptively operations to develop the video-based multimedia information seeking system for distance learning [1–4].

Figure 1 depicted a conceptual framework for media retrieval for learning. This conceptual framework for information seeking prompts a learner with an information need to reconfigure it as a query to media course content management system, that in turn seeks multimedia learning objects whose media object representation best match the query [5].

There were two major scenarios for operating the multimedia information seeking system. The first scenario was the recording and editing the course contents. Lecturer interface provide functions as the media recorder. We should record the time information (from video device, audio device, power point... etc.) for media synchronizing. In the editing period, lecturer can configure the importance degrees and the keywords for course content object. These importance degrees in course contents addressed the difference significance from lecturer cognitive. When learner accessed the course contents, they have the reference in accordance with the lecturer cognitive or the user's own reference feedback. Therefore, the media adaptive weaving and summarization could be extracted by referencing the attributes of time period, keywords and importance degrees. The attributes of the course content will be stored in the concept object ontology module.

There were five sections in this paper. First above section introduced the video-based multimedia information seeking system. Some significant concepts presented our approaches and discussed the adaptation operation evaluations, this paragraph discuss our approach that try to work steadily and make solid progress. [Chapter 2](#) discussed the related fundamental theories. [Chapter 3](#) gives the formal framework and the related adaptation operation for a detailed understanding of the multimedia content model. [Chapter 4](#) summarizes our work and gives an outlook to ongoing and future work.

2 Background Knowledge on Ontology-Based Information Representation

Ontology was one theory in philosophy and primarily to explore knowledge characteristics of life and real objects; in artificial intelligent field it was used to define the content of domain knowledge, express knowledge, solve communication, and commonly share problems; in information technology field it offered much assistant for research and development of E-commerce and Knowledge

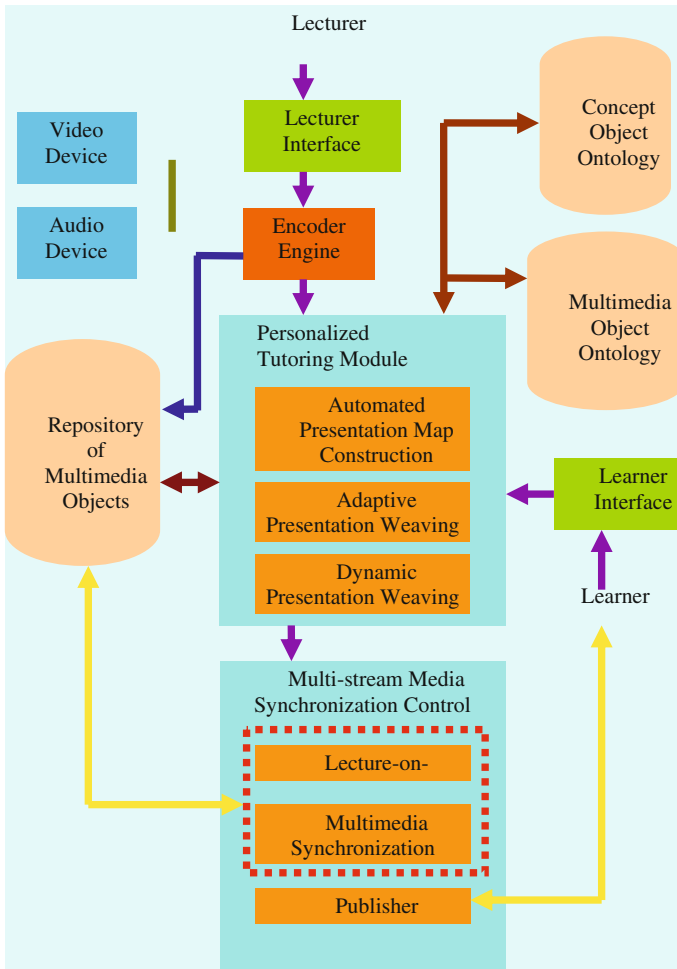


Fig. 1 Ontology-based multimedia information seeking system architecture

Management [6]. Ontology provides complete semantic models, that means in specified domain all related entities, attributes and base knowledge among entities have sharing and reuse characteristics which could used solving the problems of common sharing and communication. To describe the structure of the knowledge content through ontology can accomplish the knowledge core in a specified domain and automatically learn related information, communication, accessing and even induce new knowledge, so, ontology is a powerful tool to construct and maintain an information system.

The Adaptive Learning System is the system that performs the regulation/adaptation for learner, and to confirm the student preference for learning. Adaptive Learning System is derived from Intelligent Tutoring Systems (ITSs) and contains:

Table 1 Learning features analysis about adaptive/dynamic/time limitation for related research and our approach

	Adaptive	Dynamic	Time limitation
Karampiperis and Sampson 2004	Yes	Yes	No
Chen et al. 2007	Yes	No	No
Tsai et al. 2007	Yes	No	No
Our approach	Yes	Yes	Yes

learning material, characteristic of learner, and teaching strategy to support the adaptive learning approach [7]. There are many research issues in ALS, for example: course planning, intelligent Q &A analysis, interactive problem solving support, collaborative learning support, adaptive presentation, and adaptive navigation support [8].

Table 1 presented the compare results of learning features analysis about Adaptive/Dynamic/Time Limitation for Related Researches with our approach.

3 Ontology-Based Adaptive Multimedia Information Seeking System

In the section, we assume that multimedia content model must offer the possibility to represent alternatives and categorically to conform to the dynamic user-context.

Table 2 is an example of labeled concept and keywords for slide item. As row of Concept shown, S1 and S2 are the first and outline slide respectively, and from S3 to S10 represent the subchapters' slides. As row of K1 shown, Keyword K1 appears in S5 and S10, Keyword K2 appears in S8 and S9, Keyword K3 appears in S8 and S10, and Keyword K4 appears in S3, S4 and S6. As given above information in Table 2 that represents the respective hierarchical relationship among learning object as well as Fig. 2 shown. Concept Ontology represents Hierarchical Relationship among Concepts Objects. Hierarchical Relationship among Concepts Objects consists of concept objects (labeled as table of content) and arcs (relationships:1. ConsistsOf, 2. References, 3. IsBasedOn and 4. Requires).

According to the hierarchical relationship among learning object, we can derive a Multimedia Presentation Map, as shown in Fig. 3. Multimedia Presentation Map consists of multimedia objects (slides:s1 ~ s10), concept objects(labeled as table

Table 2 An example of labeled concept and keywords for slide item

Slide item	S1	S2	S3	S4	S5	S6	S7	S8	S9	S10
Concept	First	Outline	Ch1	1-1	1-2	1-2	Ch2	2-1	2-1	2-2
K1					⊙					⊙
K2								⊙	⊙	
K3								⊙		⊙
K4			⊙	⊙		⊙				

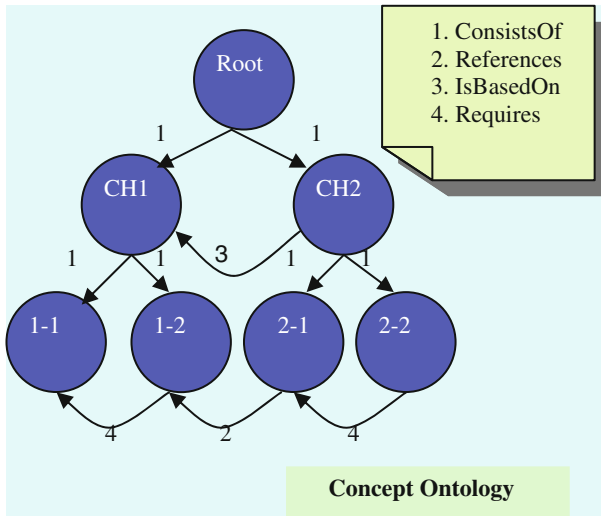


Fig. 2 Hierarchical relationship among concepts objects

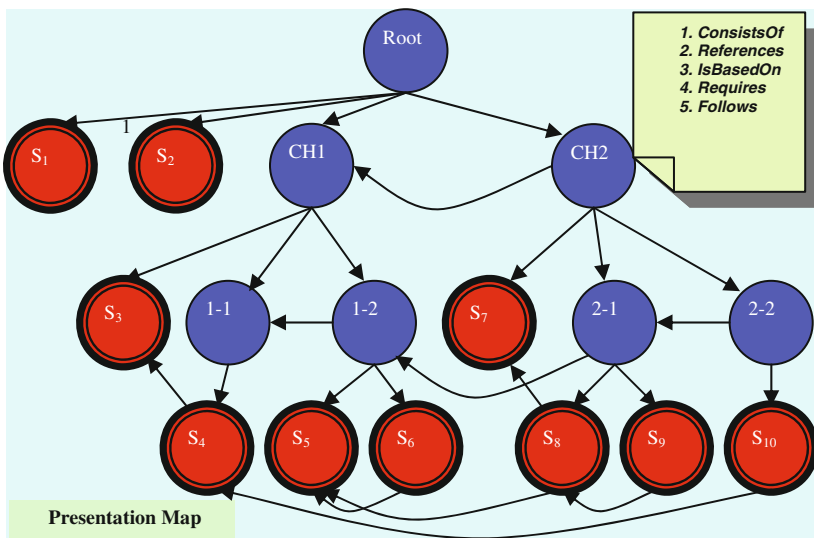


Fig. 3 Multimedia presentation map

of content) and arcs (relationships:1. ConsistsOf, 2. References, 3. IsBasedOn, 4. Requires and 5. Follows).

According to Multimedia Presentation Map and the keywords assigned by the user, each presentation object will be equipped with a reasonable weight value.

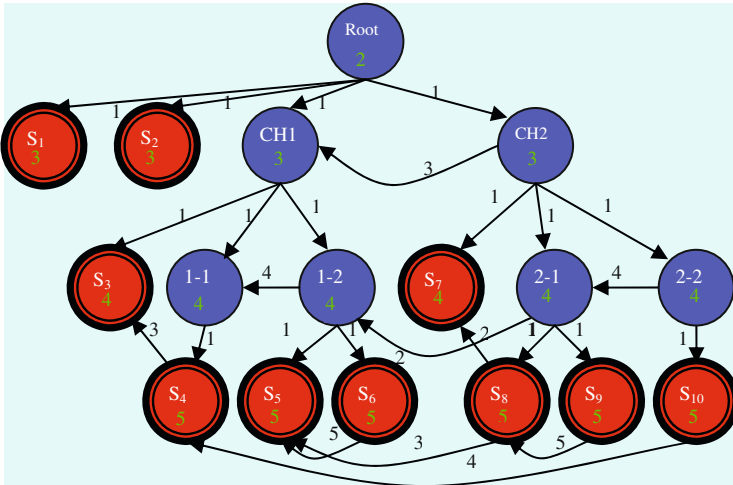


Fig. 4 Initialize weight value

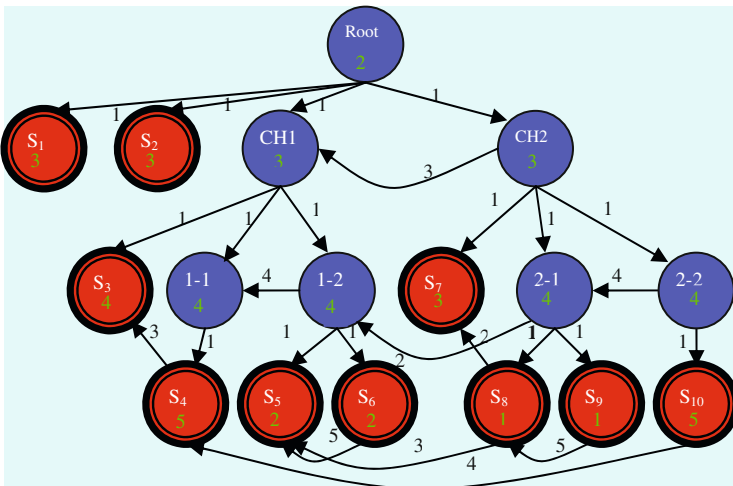


Fig. 5 Set weight value according to user query

First, all presentation objects' weight values are initialized on the basis of Multimedia Presentation Map, as shown in Algorithm 1 and Fig. 4. The concept objects, which have no parent node, are taken as root nodes. The weight values of root nodes are initialized as initialValue. The weight value that represents highest priority. Function setWeightValueOfChild is used to initialize the weight values of root nodes' descendant nodes recursively. The rule of initialization is as follow:

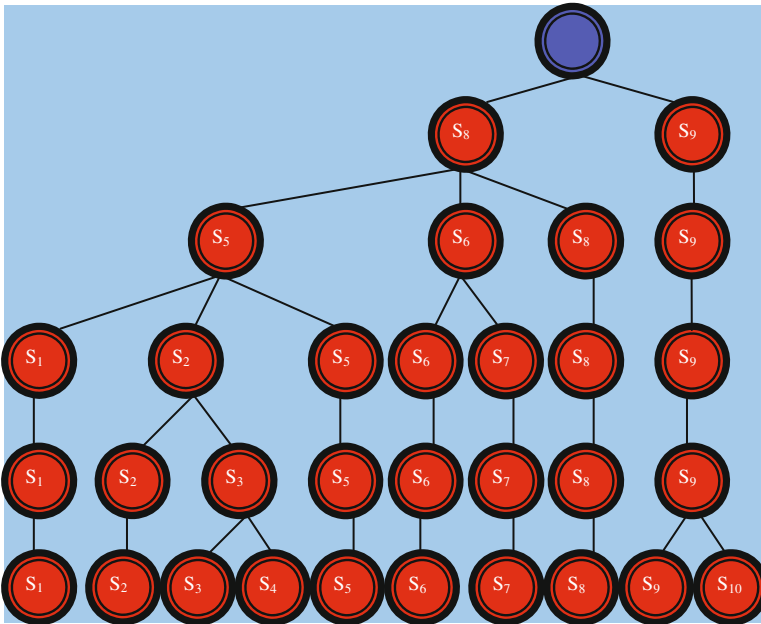


Fig. 6 Multimedia content tree

$Weight_value_of_child = weight_value_of_parent + 1.$ (The bigger weight value represents the higher priority.)

Then, the weight values are modified according to the keywords assigned by the user, as shown in Fig. 5. According to the weight values of all presentation objects, a Multimedia Content Tree can be generated, as shown in Fig. 6. The adaptive presentation would be generated according to Multimedia Content Tree and the limitation of time. The level, whose length is closer and not longer than the limitation of time, would be chosen to weaving new lecture. According to the learning condition of the learner, the content of the lecture would be adapted dynamically. During user’s taking lessons in lecture, his progress would be observed. If his performance does not meet the expectations, system would find the keywords that user needs most and re-builds the content tree. According to the new Content Tree, the content of the lecture would be adapted dynamically.

4 Conclusion and Future Work

In this article, we not only proposed an ontology-based well-defined description multimedia content model for adaptive multimedia content but also offered a framework of web-based multimedia information seeking support system for learning. In order to model the fundamental multimedia course content requirements

clearly, we began to use the ontology technology to describe the multimedia learning object and formalized definitions for user-concerned adaptive adaptation operation. Building metadata for learning object (video-based) representation matched classic information-retrieval model that crested with the searching engine technologies now pervasive on the web.

Thus, the configuration and the operation steps of the multimedia information seeking support system are clear and definite. Finally, we considered the generated presentation with different operations for learning context. The final goal of our approach was to provide a feasible multimedia content model and the unequivocal framework to developer as guiding principle or policy. We hope that our approach can be used to the general purposed multimedia information seeking support system for distance learning, enterprise training, commercial advertisement, and others.

In this dissertation, a multimedia information seeking support system was introduced and the ways of constructing the multimedia information seeking support system for distance learning was addressed. The main contributions of this research can be summarized as follows.

References

1. Deng LY, Chen Y-H, Liu Y-J, Chang Y-C (2009) Ontology-oriented SCJP learning and assessing system design. *J. Softw* 4(2):159–166
2. Chen Y-H, Deng LY, Liu Y-J (2008) Trust development and relevance feedback in activity understanding based on advanced petri net model for virtual university. *Int J Inf Technol* 2(2):96–109
3. Ontology-based adaptive presentation for course management system. In: Special session on E-learning infrastructure and applications in conjunction with the 2008 international computer symposium (ICS 2008), pp 437–443
4. Adaptive content model for distance education. In: 3rd international conference on information technology: research and education (ITRE 2005), pp 333–337
5. Pirolli P (2009) Powers of 10: modeling complex information seeking systems at multiple scales. *IEEE Comput* 42(3):33–41
6. Using rule mining and behavior prediction techniques in web information query processing. In: Proceedings of the 6th conference on artificial intelligence and applications, Kaohsiung, pp 574–579
7. Burns HL, Capps CG (1988) Foundations of intelligent tutoring systems: an introduction. In: Polson MC, Richardson JJ (eds) Foundations of intelligent tutoring systems. Lawrence Erlbaum Associates, Hillsdale, pp 1–19
8. Brusilovsky P (1996) Methods and techniques of adaptive hypermedia. In: Brusilovsky P, Vassileva J (eds), Special issue on adaptive hypertext and hypermedia, user modeling and user-adapted interaction 6(2-3):87–129
9. Yu Z, Nakamura Y, Zhang D, Kajita S, Mase K (2008) Content provisioning for ubiquitous learning. *J Pervasive Comput* 7(4):62–70

The Taguchi System-Neural Network for Dynamic Sensor Product Design

Ching-Lien Huang, Tian-Long John Wan, Lung-Cheng Wang and Chih-Jen Hung

Abstract The key successful factor of the new product design (NPD) of sensor manufacturing industry is the selections of the best parameter level. For above reasons, the selection of best parameter level sometimes causes more cost increasing and job reworking. Previous studies focus on try and error test and structured approach for the replacement and management of selection of the parameter level in product design, but rarely on a dynamic environment. Therefore, this work presents a novel algorithm, the Taguchi System-two steps optimal algorithm, which combines the Taguchi System (TS) with neural network (NN) method, which is shown how product adjusted under a dynamic environment in product design. From the results, the proposed method might possibly be useful for our problem by selecting of parameter level size and adjusting the parameters by NN in the DSPDS is observed in this study.

Keywords Taguchi system (TS) · Dynamic product design system (DPDS) · Dynamic sensor product design system (DSPDS) · Neural network (NN) · New product design (NPD)

C.-L. Huang (✉) · C.-J. Hung

Department of Industrial Management, Lunghwa University of Science and Technology, 300, Sector 1, Wanshou Road, Guishan, Taoyuan County 33306, Taiwan, People's Republic of China
e-mail: lynne.line@msa.hinet.net

T.-L. J. Wan

Department of Information Management, Lunghwa University of Science and Technology, Guishan, Taoyuan County, Taiwan, People's Republic of China

L.-C. Wang

Department of Component BG, Lunghwa University of Science and Technology, Guishan, Taoyuan County, Taiwan, People's Republic of China

1 Introduction

The selection of best parameter level is the most important job in sensor product design areas. From previous papers, the TS method has been successfully combination of various kinds of other's method and tools by adjusting the parameters and parameter levels [1–10] (Kun et al. 2011). Besides, the NN has been successfully provided in dynamic environments [11, 12].

Therefore, this work presents a novel algorithm, the Taguchi System-neural network, which combines the Taguchi System (TS) with the NN method, which is shown how product adjusted under the dynamic environment in product design. The remainder of this paper is organized as follows. Section 2 describes the TS algorithmic process for selecting of parameter level and presents the NN method in a dynamic environment. Section 3 illustrates the algorithm's effectiveness and shows the analysis. Section 4 discusses the results. Conclusions are finally drawn in Sect. 4, along with recommendations for future research.

2 The Taguchi System-Neural Network Algorithm

The process of TS-NN algorithm will be generated in this section. Besides, the results which will be discussed in the later part of this section. And, the proposed algorithm starts with the following. First, to establish the TS model, one set of data is chosen from a system. The parameters of the original data are selected to calculate the signal-to-noise (SN) ratios. The most important task is to determine which parameter levels are selected. Second step, the NN algorithm is applied, which is completed using the next two detail steps. First, establish the structure, which is form by the formula $Y_i = \beta M_i$ is applied to a DSPDS.

In sum, the algorithmic procedure has the following three steps.

Step 1. Construct the Taguchi System

First, the levels of the important parameter of the product are chosen based on the SN ratios, which is shown in Eq. (1).

$$\eta = 10 \log_{10} \frac{\bar{Y}^2}{S^2} \quad (1)$$

The process is as follows.

- (1) **Estimate the parameters of product:** Assess the parameters.
- (2) **Decide parameter level number of product:** Set and select the parameter level number of product from the data set as control parameters. For example, there is a product, which parameter may have three levels. The number “1” denotes level 1, which is defined the level 1 of the parameter, the number “2” denotes

level 2, which is defined the level 2 of the parameter, the number “3” denotes level 3, which is defined the level 3 of the parameter.

- (3) **Compute the SN ratios of product:**
 Compute the SN ratios of parameters.

Step 2. Establish the dynamic system

- (4) **Construct the dynamic system:**
 The NN algorithm is utilized to construct and verify the DSPDS.

Figure 1 presents the TS-NN algorithm.

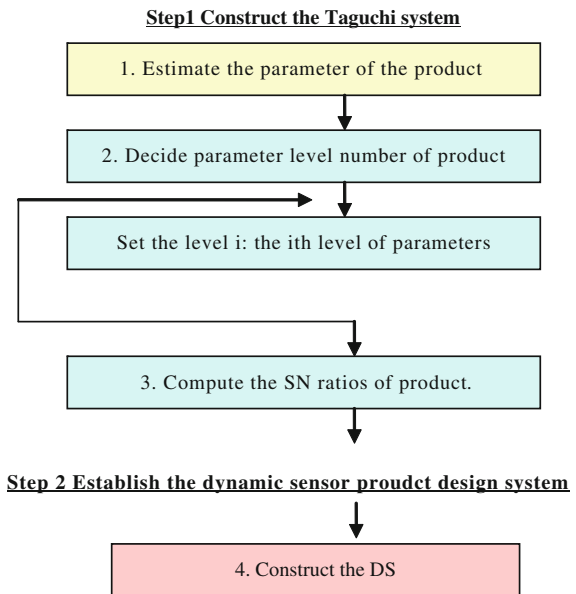
3 Verification

The procedure of TS and NN will be verified and discussed in this section by a speed sensor of winding machine.

3.1 Establish the Taguchi System

The proposed case is a company that produces speed sensor of winding machine. It is the important part in many kinds of machine. For establishing the TS model, the

Fig. 1 Taguchi System-NNalgorithm



parameters, the level numbers of parameter, and the observation values are collected and coded from v_1 to v_4 , L_1 to L_3 and y_1 to y_3 .

In total, 27 data are selected from the data set. The TS-NN algorithm is applied as follows.

At first, the original data and the SN ratios of these parameters are calculated (Table 1).

Consequently, the levels of the parameters are selected form the data set. The expected value of the SN ratios is an optimal state.

3.2 Modeling the Dynamic System

The process of NN will be generated and discussed in this section.

3.3 Establish the Dynamic System

The NN algorithm is applied to determine whether the DS is good. The processes are as follows.

Step 1. Modeling the DS

The NN algorithm is used to create a DS. Thus, the second set of input and output data is selected, and a neural network model is constructed to map the model.

Step 2. Training and testing the NN algorithm

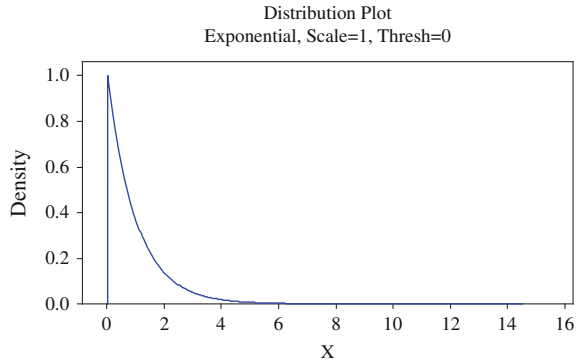
The relationship model between parameters and responses is developed using an NN, in which 16 inspection data are used for training and 11 lots are used for testing. The model structure is selected using 4-4-4 (input-hidden-output) (Table 1). Then, to determine the options of the NN structure, the architecture 4-4-4 is chosen to get the convergent performance. Restated, the RMSE of training error is 0.01, and the testing error is 0.01.

These two RMSE values for training and testing are convergent (Fig. 2).

Table 1 The SN ratios of experiment results

Level	v_1	v_2	v_3	v_4
1	43	40	42	48
2	42	52	48	52
3	48	52	53	44
Delta	11	10	9	8
Rank	2	1	3	4

Fig. 2 The testing values of the 4-4-4 RMSE structure



According to data for the confirmation set, the formula for desirable functions is $Y_{ij} = F(v_1, v_2, v_3, v_4)$, which is applied for a DSPDS can map in 4-4-4 (input-hidden-output) NN structure successfully.

4 Conclusion

In above analysis, the levels of parameters which based on SN ratios are successfully selected. In another word, the TS algorithm is successful applied to a product design in the selection of parameter level. In modeling a DS, the NN algorithm shows that the 4-4-4 structure is the optimal architecture, and the RMSE value for training and testing are converge at 0.01. However, the methodology of the TS can easily solve the selection of parameter level in PD problems, and is computationally efficient.

We conclude that the propose algorithm can be applied successfully to dynamic environments for solving the PD problems.

References

1. Ozelik B (2011) Optimization of injection parameters for mechanical properties of specimens with weld line of polypropylene using Taguchi method. *Int Commun Heat Mass Transf* 38:1067–1072
2. Lin CH, Shih SJ, Lu AT, Hung SS, Chiu CC (2012) The quality improvement of PI coating process of TFT-LCD panels with Taguchi methods. *Optik* 123:703–710
3. Liao CN, Kao HP (2011) Supplier selection model using Taguchi loss function, analytical hierarchy process and multi-choice goal programming. *Comput Ind Eng* 58:571–577
4. Yiamsawas D, Boonpavanitchakul K, Kangwansupamonkon W (2011) Optimization of experimental parameters based on the Taguchi robust design for the formation of zinc oxide nanocrystals by solvothermal method. *Mater Res Bull* 46:639–642

5. Cheah ELC, Heng PWS, Chan LW (2010) Optimization of supercritical fluid extraction and pressurized liquid extraction of active principles from *Magnolia officinalis* using the Taguchi design. *Sep Purif Technol* 71:293–301
6. Boothroyd G, Dewhurst P, Knight WA (2002) *Product design for manufacture and assembly*. Marcel Dekker, New York
7. Davila JA, Machuca F, Marianga N (2011) Treatment of vinasses by electrocoagulation–electroflotation using the Taguchi method. *Electrochim Acta* 56:7433–7436
8. Villafañe JFM, Ocampo CM (2011) Optimisation of energy consumption in arsenic electro-removal from groundwater by the Taguchi method. *Sep Purif Technol* 70:302–305
9. Rouzbeigi R, Edrissi M (2011) Modification and optimization of nano-crystalline Al_2O_3 combustion synthesis using Taguchi L16 array. *Mater Res Bull* 46:1615–1624
10. Liu WL, Chien WT, Jiang MH, Chen WJ (2010) Study of Nd:YAG laser annealing of electroless Ni–P film on spiegel-iron plate by Taguchi method and grey system theory. *J Alloy Compd* 495:97–103
11. Huang CL, Hsu TS, Liu CM (2010) Modeling a dynamic design system using the Mahalanobis Taguchi system—two-step optimal based neural network. *J Stat Manag Syst* 13(3):675–688
12. Huang CL, Lin CI, Tai SH (2012) The component search—two-steps optimal algorithm for data-mining in dynamic environments. *J Stat Manag Syst* 15(2 and 3):249–260
13. Su CT, Yeh CJ (2011) Optimization of the Cu wire bonding process for IC assembly using Taguchi methods. *Microelectron Reliab* 51:53–59
14. Mukherjee I, Ray PK (2010) Optimal process design of two-stage multiple responses grinding processes using desirability functions and metaheuristic technique. *Appl Soft Comput* 8:402–421
15. Solehati N, Bae J, Sasmito AP (2012) Optimization of operating parameters for liquid-cooled PEM fuel cell stacks using Taguchi method. *J Ind Eng* 18:1039–1050

Using Decision Tree Analysis for Personality to Decisions of the National Skills Competition Participants

Dong-Liang Lee, Lawrence Y. Deng, Kung-Huang Lin, You-Syun Jheng, Yung-Hui Chen, Chih-Yang Chao and Jiung-Yao Huang

Abstract The article aims to find the pivotal personality traits which can influence on winning a prize, compare the difference between the winning participants and the non-winning participants, and finally construct decision trees to achieve classification and prediction by using the Big Five personality traits to analyze the performance of senior and vocational high school students in Taiwan in National Skills Competition. The research utilizes t-Test and C4.5 Decision Tree to analyze commerce-related and home economics-related students. The experiment results showed that it has statistical significances on several personalities in statistical analysis between commerce-related and home economics-related students. However, because the personalities which have statistical significances are the key factor to affect whether a participant can win a prize, I go one step further to construct decision trees to predict the winner of National Skills Competition effectively in the future.

Keywords Big Five personality traits · National skills competition · Statistical significance · Statistical analysis · Decision tree

D.-L. Lee · L. Y. Deng (✉) · Y.-S. Jheng
Departments of IM, CSIE, St. John's University, Newyork, USA
e-mail: lawrence@mail.sju.edu.tw

K.-H. Lin · C.-Y. Chao
Graduate Institute of Human Resource Management,
National Changhua University of Education,
Changhua, Taiwan

J.-Y. Huang
Department of Computer Science and Information Engineering, National Taipei University,
New Taipei, Taiwan

Y.-H. Chen
Department of Computer Information and Network Engineering,
Lunghwa University of Science and Technology,
Guishan, Taoyuan

1 Introduction

Personality traits are related to the attitude and behaviors of students, with particular significant relationship in all aspects or learning performance of the educational environment [2, 5]. Although there are no evidences supporting that one's personality can determine his or her thinking approach, we can apply personality traits to predict the personal learning attitudes based on the research on the Big Five personality traits, because learning attitude is a persistent learning and thinking pattern. Such habits are developed over long-term accumulation and we can obtain the individual advantage and flaws at learning through a comprehensive analysis of tests on personality traits, in order to effectively enhance the learning achievement of students.

Based on the Big Five personality traits, the study applies Mini-Markers questionnaire as tools for personality trait questionnaire survey [3, 4, 12]. The questionnaire survey was partially commissioned to New Taipei Municipal TamShui Commercial Industrial Vocational Senior High School Principal Kung-Huang Lin to assist issuing the issuing and testing of questionnaires to various schools. The objects include Winner participants (W^P) of Commerce-Related (CR) and Home Economics-Related (HER) from vocational senior high schools in Taiwan (Gold Hand Award winners) and the Non-winning participants (N^P) (including students without participation in training). Moreover, the process of questionnaire issuing was provided with explanation from the counselor. The questionnaire recovered underwent data processing before storing into the database, which was applied with reliability analysis to validate the true conformance of the overall questionnaire to reliability standards. After the compiling the questionnaire, the valid samples were applied with data reasoning including statistical analysis and decision tree.

This paper is organized as follows: [Sect. 2](#) describes the related works with research design, research assumption, and the complete details of research process. [Section 3](#) presents research assumptions and the methods. [Section 4](#) describes results that include the difference description of personality traits under the different background variables. [Section 5](#) concludes discussion results.

2 Related Work

Some studies from Taiwan have conducted inductive analysis on the key factors for National Skills Competition participants in terms of technical performance.

Liu [9] mentioned three important conclusions to the participant training course from his study on the important and relevance of factors related to the National Skills Competition participant training course: 1. Participant skill performance related factors. 2. Participant learning course. 3. Teaching strategies of instructors [9]. For the factors related to participant technical performance, the study suggested several

main factors for participants to receive good performance from the skills competition, including professional skills, ambition, willpower, concentration, resistance to stress, and good working attitudes and habits. Next, the study referred the learning course of participants to as the preliminary thinking on skill implementation to repeated skill operational practices in addition to further discovering problems and solving problems. Finally, the study referred the teaching strategies of instructor to as the participants repeatedly correcting and improving through the instructors planning and training [9].

Chao [1] suggested from his study on the selection and training for National Skills Competition participants that the control over participant personality is also one of the effective educational strategies. Every participating student has different personalities. It will make students show their real capability more easily in the contest hall if instructors can grasp and understand the personality of every student and therefore to improve participants' weaknesses, establish their confidence, and enhance their on-site response capacity [1].

In sum of the aforementioned literatures collected, it is revealed that the influence of personality traits and skill competition are strongly correlated. Personality traits involve various factors of psychological dimensions extensively and the study applied the Big Five personality traits to analyze the CR and HER, from the vocational senior high schools, with in-depth analysis on the personality trait difference between the W^P and N^P for use as the screening and training for various vocational departments in the forecast of National Skills Competition participants.

3 Method

The study analyzed the study process of whether students can win by participating in the National Skills Competition. The overall framework is shown in Fig. 1. The study applies Mini-Markers [12] personality trait questionnaire to conduct the questionnaire survey [8, 12]. The valid samples of recovered questionnaires were saved in the database and undergone SPSS analysis. The t-Test was used the main statistics analysis method to test significant difference between the W^P and N^P before building the C4.5 Decision Tree [10] for predicting the winning personality traits for future skills competition [10].

The Mini-Marker is a small list that contains impressive words for describing human personality. The personality study under the testing framework contains

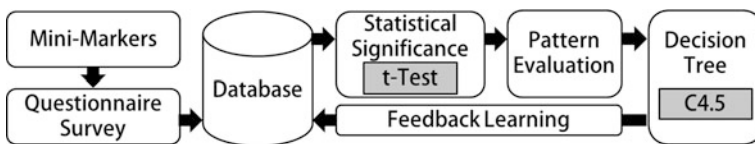


Fig. 1 Research framework

five scopes that summarize personality traits, namely Extraversion, Agreeableness, Conscientiousness, Emotional Stability, and Intellect or Openness, as shown in Table 1 [12].

The study applied Mini-Markers questionnaire incorporate with the 7-point Likert Scale to effectively implement the testing of the Big Five personality traits on students [6, 7]. The implementation of the questionnaires was issued by the counselor while providing explanations for students beforehand. The counselor will provide instructions for any student not understanding the content of Mini-Markers questions during the testing process. The number of valid samples undergone statistical analysis was 310 and the questionnaire object include students of two vocational departments, namely CR (accounting for 205 questionnaires), and HER (105 questionnaires). This paper deals with a case analysis of the Big Five personality for each CR, and HER.

4 Experiment Independent Samples t-Test

According to the statistical results of the Independent Samples t-Test, testing on the significant different in difference of identity and personality traits under the 95 % confidence level showed that there are several projects with the average means of significance. Among which, students of CR, W^P (53 %) and N^P (47 %) showed significant difference in personality traits for Fretful, Sloppy, Talkative, Uncreative, Unsympathetic and Withdrawn with an average means indicating that N^P scoring higher than W^P. Students of HER, W^P (52 %) and N^P (48 %) showed significant difference in personality traits for Creative, Deep, Efficient, Philosophical, Systematic and Unenvious with an average means indicating that W^P scoring higher than N^P; as well as showing significant difference in Uncreative with the average means indicating that N^P scoring higher than W^P. The above testing results are shown in Table 2.

Table 1 Correspondence the Big Five factors in Mini-Markers

Extraversion	Agreeableness	Conscientiousness	Emotional stability	Intellect or openness
Bashful ^a	Cold ^a	Careless ^a	Envious ^a	Complex
Bold	Cooperative	Disorganized ^a	Fretful ^a	Creative
Energetic	Harsh ^a	Efficient	Jealous ^a	Deep
Extraverted	Kind	Inefficient ^a	Moody ^a	Imaginative
Quiet ^a	Rude ^a	Organized	Relaxed	Intellectual
Shy ^a	Sympathetic	Practical	Temperamental ^a	Philosophical
Talkative	Unsympathetic ^a	Sloppy ^a	Touchy ^a	Uncreative ^a
Withdrawn ^a	Warm	Systematic	Unenvious	Unintellectual ^a

^a Negation terms

Table 2 Independent samples t-Test—differences of identity

Term	CR (Commerce-related)		t-value	HER (Home economics-related)		
	Mean (SD)			Mean (SD)		t-value
	W ^P	N ^P	W ^P	N ^P		
Fretful ^a	3.37 (1.32)	3.84 (1.46)	-2.45*			
Sloppy ^a	2.82 (1.34)	3.25 (1.62)	-2.09*			
Talkative	5.00 (1.13)	5.41 (1.22)	-2.46*			
Uncreative ^a	2.63 (1.19)	3.16 (1.41)	-2.89**	2.73 (1.04)	3.34 (1.36)	-2.6*
Unsympathetic ^a	2.62 (1.17)	3.15 (1.54)	-2.71**			
Withdrawn ^a	2.75 (1.36)	3.23 (1.59)	-2.32*			
Creative				5.42 (1.13)	4.78 (1.17)	2.84**
Deep				5.07 (1.02)	4.36 (1.10)	3.45***
Efficient				5.40 (1.18)	4.90 (1.18)	2.17*
Philosophical				4.36 (0.91)	3.86 (1.28)	2.34*
Systematic				5.25 (0.91)	4.34 (1.14)	4.58***
Unenvious				4.56 (1.05)	3.82 (1.26)	3.3**

*: $P < 0.05$ (significant); **: $P < 0.01$ (highly significant); ***: $P < 0.001$ (extremely significant)

^a Negation terms

In this section, we emphasized on finding students with potential personality traits of winners. This paper strongly emphasizes discovered several significant personality traits with differences from the constructs of the Big Five personality.

5 Experiment C4.5 Decision Tree and Discussion

The personality difference between the W^P and N^P from the National Skills Competition underwent t-Test analysis to discover the personality traits tested with statistical significance, as shown in Table 2. There are six projects in CR and seven projects in HER. To further validate the different level of priority accounted by personality traits, the study adopted C4.5 Decision Tree classification on personality traits with statistical significance. Figure 2a shows the decision tree results of CR and Fig. 2b shows the decision tree result of HER.

Figure 2 shows the classification results of decision tree for the CR and HER. The experiment mainly classifies the decisions based on the “Winning participants” and “Non-winning participants” from the CR and HER. In particular, the decision tree for CR randomly divided the 205 primitive sample data into trained samples (2/3) and tested samples (1/3), whereas the results of decision-tree in Fig. 2a yielded a prediction accuracy of 67.4 % according to the inference rules of trained samples and the prediction accuracy of 52.2 % according to the inference rules of tested samples. Table 3 shows the description for the decision tree rules. Additionally, the decision tree for HER randomly divided the 105 primitive sample data into trained samples (2/3) and tested samples (1/3), whereas the results

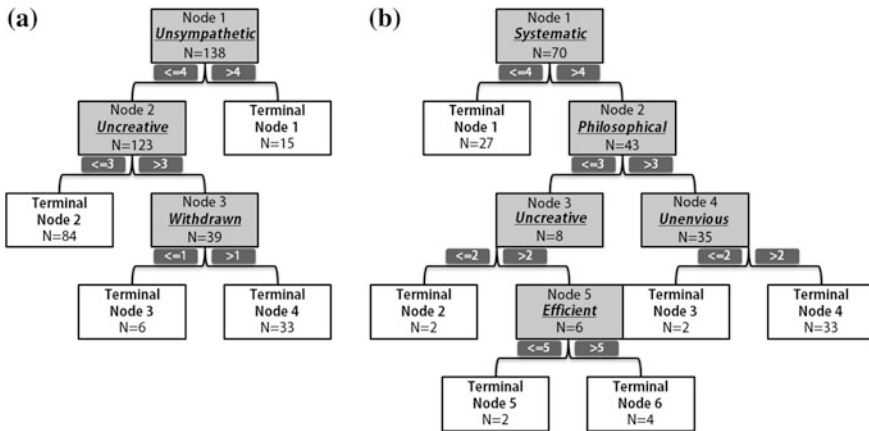


Fig. 2 Decision tree model **a** Commerce-related; **b** Home economics-related

of decision tree in Fig. 2b yielded a prediction accuracy of 80 % according to the inference rules of trained samples and the prediction accuracy of 68.6 % according to the inference rules of tested samples. The description for the decision-tree rules for CR in Table 3, HER in Table 4.

The “Yes” in Table 3 and Table 4 shows the classification results of winning participants while the “No” indicates the classification results of non-winning participants. Moreover, to avoid the problem with overfitting (overly meticulous data description that could result in poor efficiency and the possibly worse results for the actual data, despite of the high matching degree for training), only 15 matched terminal node complying with the rules with accuracy of over 65 % were discussed.

Terminal Node 1: Non-winning participants, Unsympathetic >4

The trait of Unsympathetic received relatively higher score in the CR, indicating the participants care more about their own perception and would not easily work with others. They are likely to be taken advantage by others. The instructor must pay attention while set an example to assist students from the CR with solving problems in this aspect.

Table 3 Classification rules—decision tree for commerce-related

Terminal node	Rule description	Data amount	True	False	Accuracy (%)
1	No Unsympathetic > 4	15	12	3	80
2	Yes Unsympathetic <= 4 and uncreative <= 3	84	56	28	66.67
3	Yes Unsympathetic <= 4, uncreative > 3 and withdrawn <= 1	6	4	2	66.67
4	No Unsympathetic <= 4, uncreative > 3 and withdrawn > 1	33	21	12	63.64

Terminal node 1 and 2 is the best in rule description

Table 4 Classification rules—Decision tree for home economics-related

Terminal node	Rule description	Data amount	True	False	Accuracy (%)
1	No Systematic ≤ 4	27	20	7	74.1
2	No Systematic > 4 , philosophical ≤ 3 and uncreative ≤ 2	2	2	0	100
3	No Systematic > 4 , philosophical > 3 and unenvious ≤ 2	2	2	0	100
4	Yes Systematic > 4 , philosophical > 3 and unenvious > 2	33	27	6	81.8
5	No Systematic > 4 , philosophical ≤ 3 , uncreative > 2 and efficient ≤ 5	2	2	0	100
6	Yes Systematic > 4 , philosophical ≤ 3 , uncreative > 2 and efficient > 5	4	3	1	75

Terminal node 1 and 4 is the best in rule description

Terminal Node 2: Winning participants, Unsympathetic ≤ 4 and Uncreative ≤ 3

The participants from the CR scoring lower in the trait of Unsympathetic and Uncreative show that they can think for others while come with reflection, implying that the respondents have more mature state of mind with capability to reflect and progress; they are the ideal candidate for the Gold Hand Award winners in CR.

Terminal Node 1: Non-winning participants, Systematic ≤ 4

In HER category, students with lower score in personality trait of Systematic indicate their inability to formulate objectives and implementation. They lack the logics and rationality in doing things or effectively control home economics administration. The instructors must pay attention while setting an example to assist the HER students to solve such problems.

Terminal Node 4: Winning participants, Systematic > 4 , Philosophical > 3 and Unenvious > 2

In HER category, students with higher score in personality trait of Systematic indicate their ability in planning objectives and following the rules. The students with high score in Philosophical and Unenvious personality trait reveal the respondents' ability to comprehend new principles or concepts with susceptibility to offer innovative ideas, who do not panic and are calm, usually retaining more stable performance in competition. In sum of the above, the students with the personality traits mentioned are the ideal candidate for the Gold Hand Award winner in HER.

6 Conclusion

One of the effective educational strategies is to control students' personality, applying adaptive learning with their talents, so that the students will achieve more outstanding performance in routine learning and skills competition. The

personality traits required for participants in commerce-related and home economics-related are describe in the following conclusions:

1. **Commerce-Related**

Participant in commerce-related need to pay attention to unsympathetic personality, open their mind and treat people, incident and things with objectivity. If they are overly objective about their professionalism and ideas, they are setting drawbacks on their progress. Moreover, pay attention to Uncreative and Withdrawn personality, more positively explore and think at routine basis and attempt to solve rather than escape from encountering of problems. Pay attention to these personality traits, the participants for commerce-related will be increase winning likelihood in the National Skills Competition.

2. **Home Economics-Related**

The participants in home economics-related need to pay attention to Systematic, Philosophical, Unenvious, and Efficient in order to learn step by step and with rationality, comprehending new principles or concepts while coming up with innovative ideas. Participants with calmness are less likely to panic at operating skills and thereby maintaining more stable performance at the competition. The participants in home economics-related will increase the winning likelihood in National Skills Competition with these personality traits equipped.

The study makes the following contribution: First, the study analyzed the difference of personality traits between the winning participants and non-winning participants in the commerce-related and home economics-related students in vocational senior high schools in Taiwan. The experiment results can be used to help students understand the impact of personality traits on the National Skills Competition, in addition to providing relevant data as reference to students. Secondly, the study tested the statistical significance from the winning participants and non-winning participants from the commerce-related and home economics-related National Skills Competition. In addition to conducting statistical analysis, the study also further conducted the decision tree experience while the results promote the understanding on the relationship between the personality traits and the performance of National Skills Competition participants.

References

1. Chao CY, Huang CL, Chang CC (2012) Skill learning in lathe operations: strategies for selecting and training national skill competition participants. *Int J Soc Sci Educ* 2(4):833–840
2. Conard MA (2005) Aptitude is not enough: how personality and behavior predict academic performance. *J Res Pers* 40(3):339–346
3. Goldberg LR (1990) An alternative “description of personality”: the big-five factor structure. *J Pers Soc Psychol* 59(6) 1216–1229.(American Psychological Association)

4. Goldberg LR (1992) The development of markers for the big-five factor structure. *Psychol Assess* 4(1):26–42
5. Komaraju M, Karau SJ, Schmeck RR, Avdic A (2011) The big five personality traits, learning styles, and academic achievement. *Pers Individ Differ* 51(4):472–477
6. Likert R (1932) A technique for the measurement of attitudes. *Arch Psychol* 22(140):1–55
7. Lin SC (2008) The relationships between humor styles, ridicule styles and big-5 personality Traits of high school students. Master's Theses, National Digital Library of Theses and Dissertations in Taiwan: 097NTNU5328030
8. Lin NP, Chiu HC (1999) A study of service quality: the effects and applications of service providers' personality traits. *J Manag* 16(2):175–200
9. Liu CW, Chen YM (2012) An analysis on the training course for the national skills competition participants. Department of Industrial Education and Technology, National Changhua University of Education, Master Program
10. Quinlan JR (1993) C4.5: programs for machine learning, Morgan Kaufmann Publishers Inc., San Francisco
11. Santos R, Marreiros G, Ramos C, Neves J, Bulas-Cruz J (2011) Personality, emotion, and mood in agent-based group decision making. *IEEE Intell Syst* 26(6):58–66
12. Saucier G (1994) Mini-markers: a brief version of goldberg's unipolar big-five markers. *J Pers Assess* 63(3):506–516

Intelligent Reminder System of Having Medicine for Chronic Patients

Dong-Liang Lee and Chun-Liang Hsu

Abstract This research is originally creative research, and already applied patent under authority of Patent Bureau of Taiwan (applying case number: 095121418). People living in modern society are full of much pressure from all kinds of environment everyday and with the great change of dining habit people easily have many chronic diseases. In addition to causing huge damage to individual health, it also cost much society medical resource. Most chronic diseases need special care from nursing staff to remind of when to have the correct medicine. It is naturally proceeding in wards but patients usually forget to punctually have medicine once they leave the hospital and get back home, and this situation neglecting or forgetting to have medicine according to doctors' instruction often causes many unfortunate deaths of patients resulting in offsetting-less for individual and family. Owing to the speedy development of communication technology and semiconductor, GSM communication module can be integrated and embedded into single chip and let GSM be carried into many products to increase the added-value of products. So how to combine microprocessor with communication module to construct a safe, intelligent, and full-purpose monitoring system for individual to have medicine to solve the problem mentioned above becomes an interesting issue for us. The research category of this study are including a medicine box as the main part of product which includes GSM module, speech-functional DSP, control panel displaying all information for patients, medicine detecting function, and a single chip microprocessor to operate the monitoring function. On the other hand,

D.-L. Lee (✉)

Department of Information Management, St. John's University, No. 499, Sec. 4, Tang-kin Rd, Taipei County, Taiwan, ROC
e-mail: lianglee@mail.sju.edu.tw

C.-L. Hsu

Department of Electrical Engineering, St. John's University, No. 499, Sec. 4, Tang-kin Rd, Taipei County, Taiwan, ROC
e-mail: liang@mail.sju.edu.tw

the interface of the commander terminal PC in nursing center, instructing all information for patients to punctually have medicine, is developed by us programming with VB language. The system function was verified completed successful and could be published for commercials for its creativity and practical purpose.

Keywords GSM communication module · Speech-functional DSP · Intelligent monitoring · Microprocessor · Interface

1 Study Motivation

People living in modern society are full of much pressure from all kinds of environment everyday and with the great change of dining habit people easily have many chronic diseases. In addition to causing huge damage to individual health, it also cost much society medical resource. Most chronic diseases need special care from nursing staff to remind of when to have the correct medicine. Owing to the speedy development of communication technology and semiconductor, GSM communication module can be integrated and embedded into single chip and let GSM be carried into many products to increase the added-value of products. So how to combine microprocessor with communication module to construct a safe, intelligent, and full-purpose monitoring system for individual to have medicine to solve the problem mentioned above becomes an interesting issue for us.

Base on the study motivation mentioned above, The research category of this study are including a medicine box as the main part of product, including GSM module, speech-functional DSP, control panel displaying all information for patients, medicine detecting function, and a single chip microprocessor to operate the monitoring function. On the other hand, the interface of the commander terminal PC in nursing center, instructing all information for patients to punctually have medicine, is developed by us programming with VB language. The monitoring system has dynamic monitoring screens, auto-oral -notifying system, alarm system, timing and procedure management for having medicine, and auto-tracing patients system by GSM system to deal with all kinds of patients without punctually having medicine.

The whole system has superiorities such as bi-direction communication-interface being able to real-time manage all emergency, and notify close friends or family of the patients whether they having medicine according to planed schedule punctually or not so as to further protect their health.

2 Importance of the Research

It is wonderful to concrete the conception “implementing knowledge into real life” and try to lead automation conception into daily life; furthermore, let people feel the convenience and practical function of technology.

This system make it significant that the mission of simple but not being neglected for having medicine of patients is taken over by hospital through auto-detecting and monitoring on servo computer in nursing center and can insure patients’ having medicine according doctor’s prescription punctually as well as their health. This invention also provided records of chronic patients to make patients having medicine simple, informational, and systemic. Furthermore, in this system, combining computer communication function, GSM wireless system, and serial communication technique of microprocessor to becoming local communication system not only obtain a complete communication system but also enrich the extra-value of unique system.

3 Software and Hardware Structure

The whole system-structure of the medicine box for certain individual patient, in which an intelligent monitoring system was designed and whole circuits was PCB-layout in the box, was shown in Fig. 1. The system included GSM communication module that collected patient’s information of having medicine and transmitted the information to the nursing center in hospital as well as collected the response information from center for being indicated on medicine box to correctly decoding the echo code as to control alarm-system, oral-message and LCD displayer to remind patient to have medicine punctually.

The embedded system chip was responsible to real-time detect the condition of medicine in the box and send the coding message to nursing center dealing with the condition through GSM communication module. Meanwhile, control the flushing lights on the box to apparently notify the patient the time ought to take the

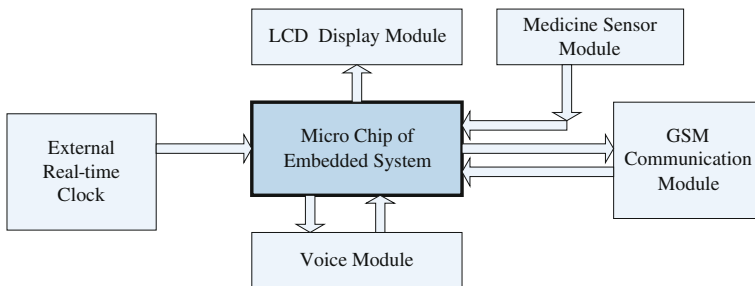


Fig. 1 Patient’s medicine box system structure

medicine. LCD display module indicated the present condition of medicine in the box, the message from nursing center, the ID of the patient, the time having medicine, the name of the medicine, and the meal-time of having medicine.

4 Research Design

There were five sub-system of the intelligent medicine-box as following:

- (1) The medicine condition corresponding to the scanned result and its coding.
- (2) Full-function and bi-direction of the networking communication system.
- (3) Dot-matrix Chinese-text LCD displayer system.
- (4) Sensors and detecting system of medicine.
- (5) Speech broadcasting system.

All the sub-system was described as following sections.

4.1 System Structure

The main control center interface were set up both in the computer of the patients' home and the PC of the nursing center in the hospital, and could be easily input every meal-time of having medicine of the patient. When the time of having medicine is up, the main control center would send related message to SMS module in Slave PC of patient home by COM PORT. Slave PC would decode the message and proceed to the proper action (Fig. 2).

4.2 The Main Tasks for Slave PC (Patient's Home)

- (1) Receiving the SMS control message from main servo PC in hospital to indicate all information.
- (2) Scanning the condition of the medicine in the box when receiving message.
- (3) Judging whether the patient was properly having the medicine according to the doctor's order, and then response the result to nursing center.
- (4) If there was no medicine, the system indicate normal, otherwise, displaying the warning message on the screen and send the warning message to the patient as well as reminding speech.

The procedure of operating reminding system of the intelligent medicine-box and its control software flowchart was shown in Fig. 3.

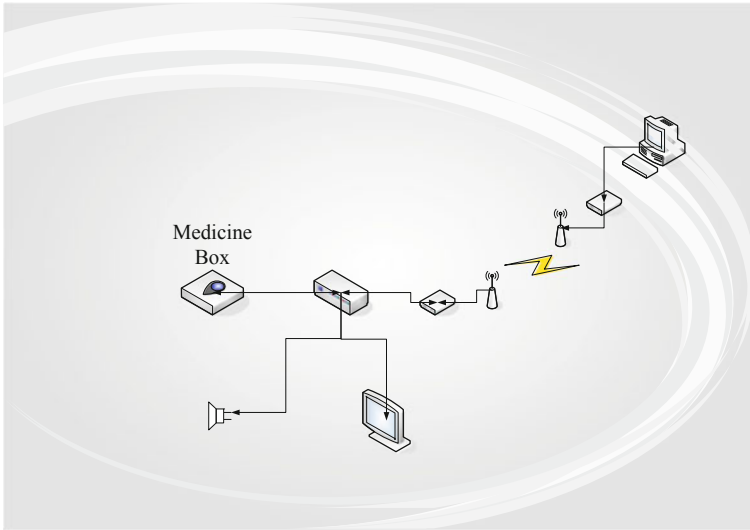


Fig. 2 The conception of system communication structure

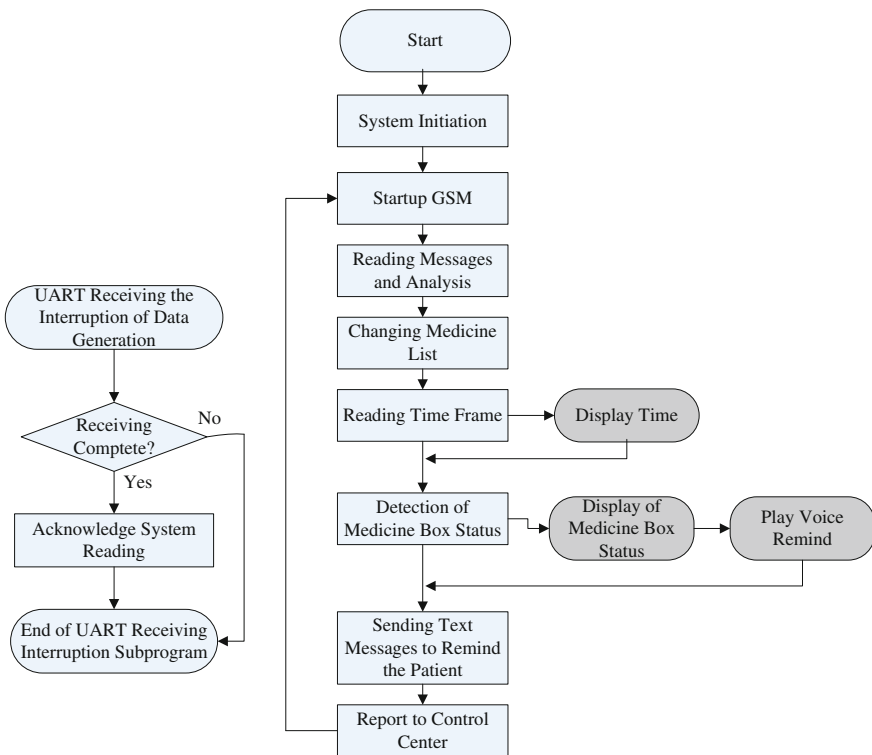


Fig. 3 Control flowchart of medicine box

4.3 The Communication Interface Design of the Medicine Box

The development platform in the study was GSM phone-set as the reminder for having medicine. There were control codes set at the end of the information to indicate the true location of the box and provide all the information of the patient having medicine to guarantee the right time to having right medicine.

4.4 Protocols of Communication

4.4.1 Nursing Center to Medicine Box

Table 1 Communication protocol of nursing center

Command bit (3)	Patient's number (8)	Medicine sheet (8)	Time (6)	The first time having medicine (2)	No. of tablets (28)
-----------------	----------------------	--------------------	----------	------------------------------------	---------------------

Command bit: CTB —> center to box (Table 1)

Patient No.: 00 00 00 00

Medicine Sheet No.: 00 00 00 01

Time: 0 6 0 0 8 1 4 (Year/Month/Date)

First Having Time: The first Checked Having Time

Coding Number: Coding No. of Having Medicine according to the location in Table 2

Table 2 Coding number of having medicine

Time	Mon	Tue	Wed	Thu	Fri	Sat	Sun
Morning	1	5	9	13	17	21	25
Noon	2	6	10	14	18	22	26
Evening	3	7	11	15	19	23	27
Night	4	8	12	16	20	24	28

4.4.2 Medicine Box To Hospital Nursing Center

Table 3 Communication protocols of medicine-box

Command bit (3)	No. of medicine Sheet (8)	Time of having Medicine (2)	Status of having Medicine (1)
-----------------	---------------------------	-----------------------------	-------------------------------

Command Bit: BTC —> Medicine-box to Nursing center

No. of Medicine Sheet: 00 00 00 01

Time of Having Medicine: Echo Status of Time of Having Medicine

Status of Having Medicine: 1:Not Having Medicine 2: Delaying Having Medicine

4.5 The Procedure of Nursing Center Designed with VB

Figure 8 showed the monitoring screen of the main-server in the nursing center, the main function of the screen was the entrance to all of the sub-function and response the action message to the medicine box. The monitoring system would recall the phone-set every 3 s and check whether there was any message of having medicine sending in as shown in Fig. 4. If there was related message sent in, and

Fig. 4 Control flowchart of monitoring in nursing center (1)

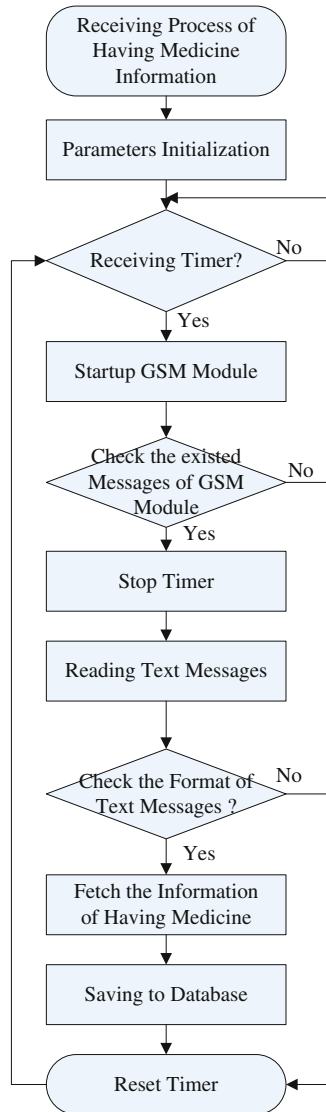
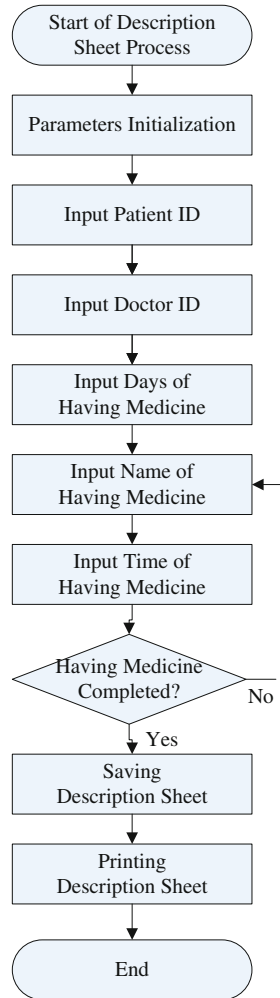


Fig. 5 Control flowchart of monitoring in nursing center (2)



then justified whether the content was the string led by CTB, if the answer was right, then decoded the number of description sheet, meal-time, and information of having medicine and recorded into database after verifying as shown in Fig. 5.

Figure 6 showed the screen in which the doctor assigned the description sheet. First of all, input the ID No. of the doctor and patient, then input the total days of having medicine, the name of the medicine, and finally input the meal-time for each medicine, Finally the system would double check the information stored into database was correct and give one copy to the patient as the direction for having medicine.

Fig. 6 Control flowchart of monitoring in nursing center (3)

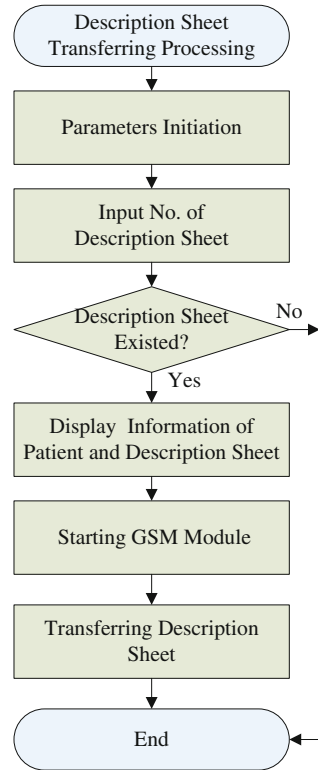


Figure 7 showed the description sheet would be sent to medicine box in patient’s home through GSM module, but the system must check whether there was the sheet in the database before sending to the patient, and then the patient’s name and the content of the description sheet. All the data was complete correct, the information would be coded and sent to the medicine box far away in the patient’s home through GSM module.

In order to let the doctor to learn the condition of patient’s having medicine, we designed the inquire system of having medicine of patients. First of all, input the ID NO. of the patient, the system would list all of the description sheet, after we selected one of them, the system would fetch the list from the database and transfer it into screen picture information easily to be read by people (Figs. 8, 9).

Fig. 7 Control flowchart of monitoring in nursing center (4)

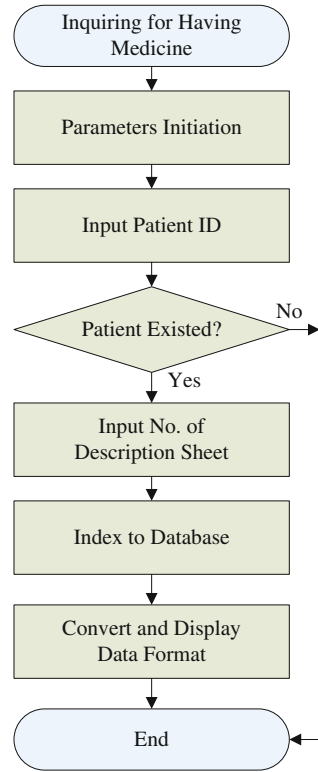


Fig. 8 Initial monitoring and controlling screen of the main servo of nursing center

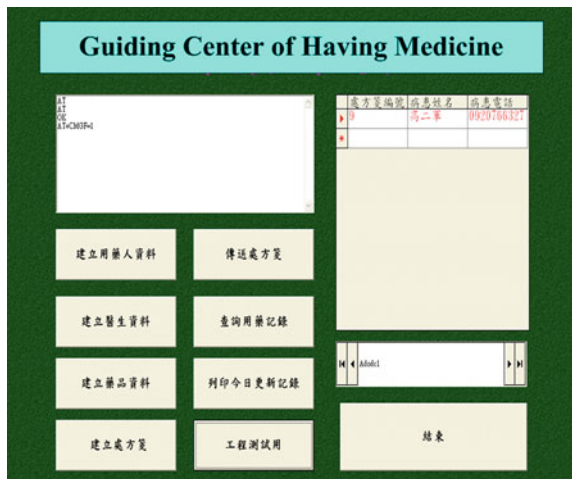
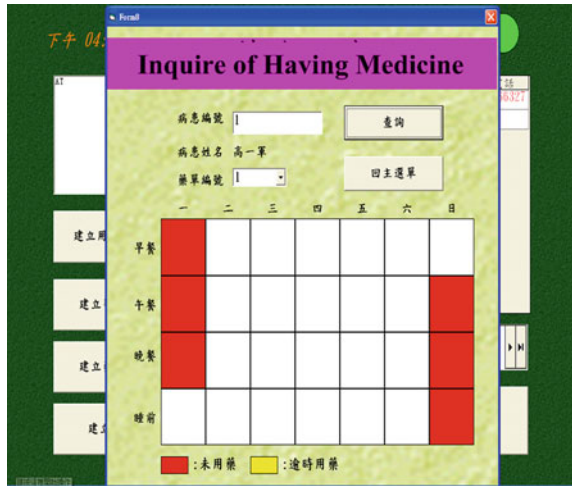


Fig. 9 The screen shown the condition of having medicine of some patient under monitoring in nursing center



4.6 The Finished Remote Monitoring and Controlling Human-Machine Interface Screen on the Servo of Nursing Center

See Figs. 8 and 9.

5 Conclusion

In the research paper, we tried to combine local communication concept with auto-control and implemented the methodology on the management system for developing patient's having medicine system. As for the reason we adopted the local communication network designed by ourselves is that although we could get better effect for hospital uses PC as the main monitoring tools, but the cost was too high, not easy to maintain, and it was difficult for any patient to use the PC. Local communication system was designed with Single chip microprocessor and it was easy design and lower cost, and easily learns for the usage of the control interface for the patients, therefore the creativity of the project was quite practical and precious.

References

1. Hwa-hen Technology Corp. (2006) XSBBase270 WinCE/Linux Data book
2. Hwa-hen Technology Corp.(2006) XSBBase270 Experiment Manual

3. Wang K-R (2007) VisualBasic 6.0 and Windows API, Flag Bookstore
4. Wang K-R (2007) VisualBasic6.0 database design, Flag Bookstore
5. Ko-nan (2003) :Circuits design with computer and analysis. Taiker-Da
6. Fan I-C (2007) Visual Basic and RS232 serial communication control, Wen-Kwei Bookstore

Part V
Data Management for Future
Information Technology

A Skewed Spatial Index for Continuous Window Queries in the Wireless Broadcast Environments

Jun-Hong Shen, Ching-Ta Lu, Ming-Shen Jian and Tien-Chi Huang

Abstract Location-based services (LBSs) via wireless data broadcast can provide a huge number of mobile clients for simultaneously accessing spatial data according to their current locations. A continuous window query is one of the important spatial queries for LBSs. It retrieves spatial objects in a fixed window region of every point on a line segment and indicates the valid segments of them. In this paper, we propose a skewed spatial index for continuous window queries considering skewed access patterns in the wireless broadcast environments.

Keywords Continuous window queries · Skewed access patterns · Spatial index · Wireless data broadcast

1 Introduction

Due to its high scalability, wireless data broadcast enables a huge number of mobile clients simultaneously access data at anytime and anywhere. With the advances in positioning systems, e.g., GPS, location-based services (LBSs) via wireless data broadcast provide the mobile clients with applications according to their current locations. A continuous window query is one of important spatial queries for such applications. It retrieves spatial objects in a fixed window region

J.-H. Shen (✉) · C.-T. Lu
Department of Information Communication, Asia University, Taichung, Taiwan
e-mail: shenjh@asia.edu.tw

M.-S. Jian
Department of Computer Science and Information Engineering,
National Formosa University, Yunlin County, Taiwan

T.-C. Huang
Department of Information Management, National Taichung University
of Science and Technology, Taichung, Taiwan

of every point on a line segment and indicates the valid segments of them. For example, a tourist issues a query asking attractions within one mile according to his location when driving. Since the tourist is moving, the answered result should contain attractions within the query region and indicate their valid segments.

Due to the limited battery life of mobile devices, energy conservation is a crucial issue for lengthening the recharging period of the devices. Spatial indexes are interleaved with spatial objects to save energy consumption. In this case, the mobile devices can skip unwanted data by slipping into the doze mode, and stay in the active mode to listen the wireless channel only when the desirable data is arrived [5, 7].

In real life applications, a few hot attractions are frequently visited than the others, i.e., skewed access patterns. Under such the scenario, more popular data should appear more times in a broadcast cycle than less popular ones, resulting in the decrease of the average client waiting time, i.e., a nonuniform broadcast [6, 8]. In this paper, we focus on the design of the spatial index for supporting continuous window queries in the nonuniform broadcast.

In the literature, many spatial indexes are proposed to support the efficient query processing of spatial queries in the wireless broadcast systems. Distributed spatial index [9] and the neighbor-index method [7] were proposed to support continuous window queries over wireless data broadcast. Considering skewed access patterns, a grid-based distributed index (GDIN) [2] was developed for window queries in the nonuniform broadcast by using a regular space partition. Multi-leveled air index scheme (MLAIN) [3] was developed to improve the disadvantage occurred in GDIN by using a multi-level space partition. These methods were designed for broadcasting data on the one wireless channel. A grid-based indexing scheme on multiple channels (GRIM) [4] was proposed to support window queries considering skewed access patterns on the multiple-channel broadcast.

To the best of our knowledge, there is no existing work on spatial indexes for supporting the continuous window queries with skewed access patterns. In this paper, we propose a skewed spatial index for efficiently processing continuous window queries according to the clients' skewed access patterns in the wireless broadcast systems. To keep a good spatial locality, our proposed method partitions a data space into cells and allocates them in the one-dimensional space according to the Hilbert curve. Then, our proposed method applies Acharya et al. [1] Broadcast Disks to allocate popular spatial objects contained in the cells more times on the wireless channel than regular ones, resulting in quick access for the popular objects. The cell indexes considering the nonuniform broadcast are interleaved with the spatial objects on the wireless channel to support efficient access.

The rest of this paper is organized as follows. In Sect. 2, we give a brief description of the related techniques applied in our proposed method. In Sect. 3, we present our proposed skewed spatial index. Finally, a conclusion is presented in Sect. 4.

2 Background

In this paper, we apply Acharya et al.'s Broadcast Disks [1] to organize spatial objects into a popularity hierarchy which results in a skewed transmission of objects and quicker access to more popular objects. To preserve the spatial locality of objects, we allocate spatial objects into the wireless channel in the order of the Hilbert curve. Broadcast Disks and the Hilbert curve are briefly described in this section.

2.1 Broadcast Disks

Acharya et al. [1] have proposed the use of a periodic dissemination architecture in the context of wireless mobile systems, called Broadcast Disks (*BD*). The algorithm has the following steps:

1. Order data items ($=N$) from the hottest (most popular) to the coldest.
2. Partition the list of the data items ($=N$) into multiple disks ($=S$ disks), where each disk D_i , $1 \leq i \leq S$, contains pages ($=K_i$) with similar access probabilities. That is, $N = \sum_{i=1}^S K_i$.
3. Choose the relative frequency λ_i of broadcast for each disk D_i , $1 \leq i \leq S$.
4. Split each disk into a number of smaller units, called chunks C_{ij} , where C_{ij} denotes the j th chunk in disk D_i . First, calculate L as the LCM (Least Common Multiple) of the relative frequencies. Then, split each disk D_i into $NC_i = L/\lambda_i$ chunks, $1 \leq i \leq S$, where NC_i denotes the number of chunks in disk D_i .
5. Create the broadcast program by interleaving the chunks of each disk in the following manner:

```

for  $i := 1$  to  $L$  do
begin
  for  $j := 1$  to  $S$  do
  begin
     $k := ((i - 1) \bmod NC_j) + 1$ ;
    Broadcast chunk  $CK_{j,k}$ ;
  end;
end.

```

2.2 Hilbert Curve

The Hilbert curve is a continuous path which passes through every point in a multi-dimensional space once to form a one-one correspondence between the coordinates of the points and the one-dimensional sequence numbers of the points on the

curve [7]. It can preserve the spatial locality of points. The spatial locality means that points that are close to each other in a multi-dimensional space are remained to close to each other in a one-dimensional space. The Hilbert curve of order n recursively divides the space into four equal-sized cells and gives each cell a sequence number from 0 to $(2^{n*2} - 1)$. Figure 1a shows the Hilbert curve of order 1. The curve can keep growing recursively by following the same rotation and reflection pattern at each cell of the basic curve. Figure 1b shows the Hilbert curve of order 2.

3 The Proposed Skewed Spatial Index

In our proposed method, a data space containing N spatial objects is recursively partitioned to $2^n \times 2^n$ cells according to the Hilbert curve of order n ; that is, the data space is processed by an n -level partition. Moreover, each cell contains η spatial objects. The cell containing popular objects is called the hot cell. We apply Acharya et al.'s BD [1] to allocate the spatial objects on the wireless channel. The spatial objects are sorted in the descending order of their access probabilities, and partitioned into S disks, D_1-D_s . In each disk, the sequence of the spatial objects is following the sequence of the Hilbert curve.

Take spatial objects shown in Fig. 2 for example. In the figure, object $O8$ is the most popular object, objects $O4$, $O10$ and $O11$ are popular objects, and the rest are regular objects. The data space is processed by a two-level partition and partitioned into $2^2 \times 2^2$ cells according to the Hilbert curve of order 2. Each cell contains one spatial object, i.e., $\eta = 1$. A cell of the Hilbert curve of order i is denoted by $C(i,j)$, where i is the order of the Hilbert curve, and j is the sequence number of the Hilbert curve of order i , $0 \leq j \leq 2^{i*2} - 1$. The parent cell of the Hilbert curve of order $(i-1)$ of $C(i,j)$ can be easily derived, i.e., $C(i-1, \lfloor j/4 \rfloor)$. For example, object $O1$ is contained in cell $C(2,0)$ of the Hilbert curve of order 2. The parent cell of the Hilbert curve of order 1 of $C(2,0)$ is $C(2-1, \lfloor 0/4 \rfloor) = C(1,0)$.

Assume that the spatial objects are partitioned to 3 disks according to their access probabilities, i.e., $S = 3$, as shown in Fig. 3a. In each disk, the spatial

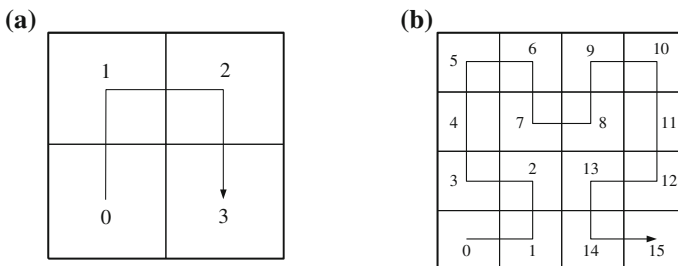


Fig. 1 The Hilbert curve: a order 1; b order 2

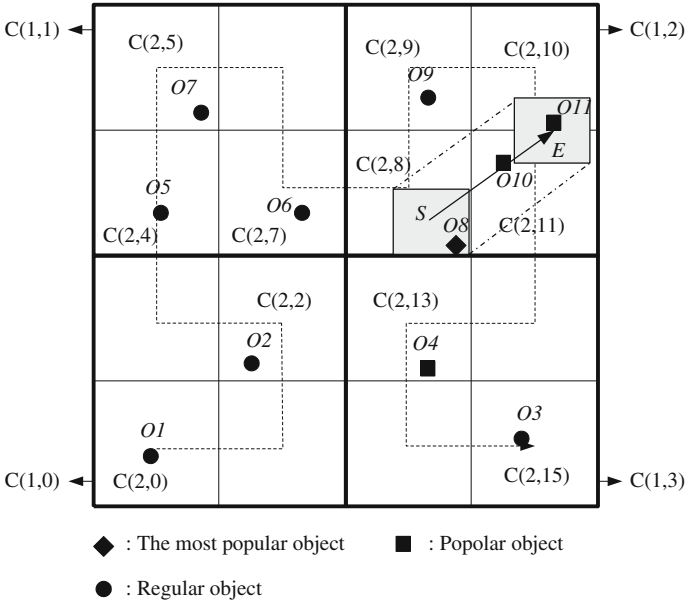


Fig. 2 Spatial objects allocated in the order of the Hilbert curve

objects are allocated in the sequence of the Hilbert curve of order 2. The relative frequencies of disks D_1 , D_2 , and D_3 are set to $\lambda_1 = 4$, $\lambda_2 = 2$, and $\lambda_3 = 1$, respectively. In this case, the least common multiple of the relative frequencies, L , is 4. Then, D_1 has $NC_1 = L/\lambda_1 = 4/4 = 1$ chunk, D_2 has $NC_2 = L/\lambda_2 = 4/2 = 2$ chunks, and D_3 has $NC_3 = L/\lambda_3 = 4/1 = 4$ chunks, as shown in Fig. 3b. For example, D_2 has 3 objects partitioned to 2 chunks, $CK_{2,1}$ and $CK_{2,2}$. The chunks are interleaved to the wireless channel according to Step 5 of Broadcast Disks mentioned in Sect. 2.1. Figure 3c shows the interleaved result consisting of 4 minor cycles, m_1 - m_4 , which contain one chunk from each disk. Each minor cycle has a hot cell group containing hot cells. This broadcast result produces a three-level memory hierarchy in which D_1 is the smallest and fastest level and D_3 is the largest and slowest level.

3.1 Index Structure

Similar to MLAIN, our proposed skewed spatial index has two kinds of indexes: the hot cell index and the cell index. The hot cell index is interleaved before each hot cell group. The cell indexes of the Hilbert curve from order 1 to order $(n-1)$ are interleaved before the first element of the Hilbert curve of the next order. Moreover, the cell index of the Hilbert curve of order n is interleaved before each cell of the Hilbert curve of order n . Figure 4 shows the index allocation of the broadcast

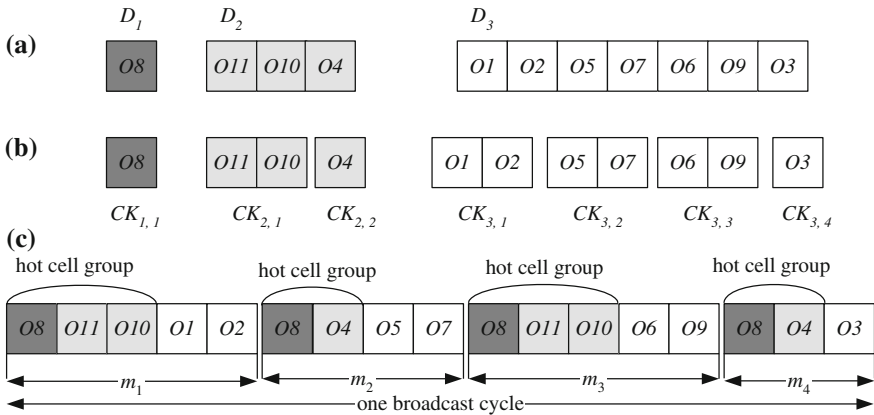


Fig. 3 The allocation of spatial objects: **a** three disks with the corresponding objects; **b** chunks for each disk; **c** the allocation of the spatial objects

spatial objects shown in Fig. 3c. Take object $O1$ for example. It is the first element contained in $C(1,0)$ via the first-level partition. Moreover, it is contained in $C(2,0)$ via the second partition. Therefore, the sequence of the index allocation for $O1$ is the cell index of $C(1,0)$ followed by the cell index of $C(2,0)$. In Fig. 4, a hot cell index is interleaved before each hot cell group.

The hot cell index contains the arrival time of the nearest cell index of the Hilbert curve of order 1 that will be broadcast on the channel (NR), and the hot cell information (HCI). HCI contains the arrival time of the cell indexes for all hot cells. The entries in HCI are of form $\langle C(i,j), t \rangle$, where $C(i,j)$ is the cell identifier and t is the arrival time of the cell index for that cell. Take the first hot cell index shown in Fig. 4 for example. NR stores the arrival time, $t4$, of the nearest cell index for cell $C(1,0)$, which is of the Hilbert curve of order 1. HCI stores the information about the hot cells, $C(2,8)$, $C(2,10)$, $C(2,11)$ and $C(2,13)$.

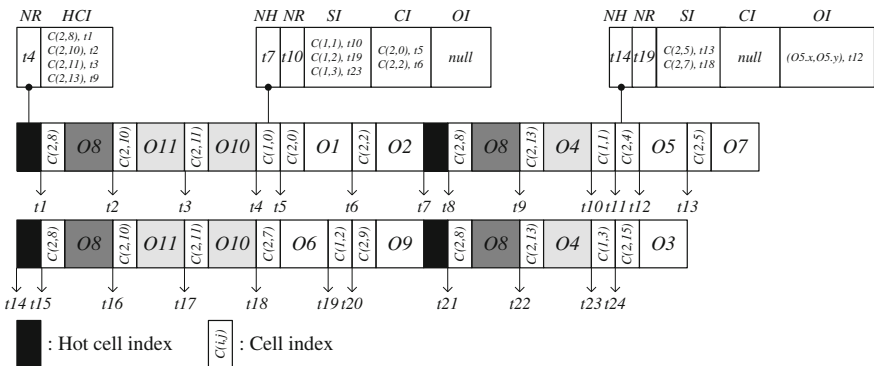


Fig. 4 The index information interleaved with the spatial objects

The cell index contains the arrival time of the nearest hot cell index that will be broadcast on the channel (NH), NR , sibling information (SI), child information (CI) and object information (OI). OI stores the coordinates of the objects in that cell, and their corresponding arrival time. This enables that the query process can check if the objects are within the query region before accessing them. Take the cell index for cell $C(1,0)$ for example. NH stores the arrival time, $t7$, of the nearest hot cell. NR stores the arrival time, $t10$, of the cell index for the cell of the Hilbert curve of order 1, $C(1,1)$. SI stores sibling information about the cells of the Hilbert curve of the same order, $C(1,1)$, $C(1,2)$ and $C(1,3)$. CI stores child information about the cells of the Hilbert curve of the next order, $C(2,0)$ and $C(2,2)$. Since cell $C(1,0)$ does not contain object information, OI is null in this case. Take the cell index for cell $C(2,4)$ for another example. NH stores the arrival time, $t14$, of the nearest hot cell. NR stores the arrival time, $t10$, of the cell index for the cell of the Hilbert curve of order 1, $C(1,2)$. SI stores sibling information about the cells of the Hilbert curve of the same order, $C(2,5)$ and $C(2,7)$. Since cell $C(2,4)$ is not further partitioned, it does not contain any child, i.e., $CI = \text{null}$. OI stores object information in cell $C(2,4)$, i.e., the coordinates of object $O5$ and its arrival time, $t12$.

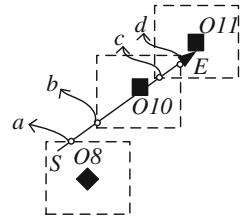
3.2 Continuous Window Queries

For a continuous window query, the cells of the Hilbert curve of order n overlapped with the query region of the continuous window query should be examined. Those cells are recorded in candidate cell set CCS , and their corresponding cell indexes are further examined to check if the spatial objects are within the query region via their coordinates stored in OI before accessing them. The access protocol is as follows.

1. Tune into the wireless channel to get the arrival time of the following nearest hot cell index, and proceed to it.
2. Examine entries in the hot cell index to get the arrival time of the cell indexes overlapped with the query region, and put the arrival time into queue CQ in the ascending order. Note that CQ is a queue storing the arrival time of the next visited index or object in the ascending order.
3. If all information about the cells in CCS can be found out in the hot cell index, follow the arrival time in CQ to retrieve the cell indexes to get the corresponding objects.
4. Otherwise, put the arrival time in NR into CQ in the ascending order. Find out the rest cells in CCS and put their arrival time into CQ by using SI and CI stored in the visited cell indexes. Follow the arrival time in CQ to retrieve the cell indexes to get the corresponding objects.

Take the continuous window query for segment \overline{SE} shown in Fig. 1 for example. In Fig. 1, all the objects covered by the polygon region should be retrieved. Therefore, cells $C(2,8)$, $C(2,10)$ and $C(2,11)$ overlapped with the query region

Fig. 5 Minkowski regions



should be examined, i.e., $CCS = \{C(2,8), C(2,10), C(2,11)\}$. Assume that the client tunes into the broadcast channel at the beginning of the first hot cell index shown in Fig. 4. After examining HCI in this hot cell index, the client has the arrival time of the cell indexes of $C(2,8)$, $C(2,10)$ and $C(2,11)$, i.e., $CQ = [t1, t2, t3]$. In this case, since all cell indexes for the cells in CCS are found out via the hot cell index, the client does not need to visit other cell indexes to process the query process. Following the sequence in CQ , the client checks OI in these cell indexes to determine if the spatial objects are within the query region and then retrieves them from the wireless channel. The answered spatial objects for this query are $O8$, $O10$ and $O11$.

For a continuous window query, the answered objects are only valid along part of the query line segment, i.e., validity segments [9]. Therefore, the answered objects should be assigned with their corresponding validity segment. The validity segment of each answered object can be determined by its Minkowski region [9]. The Minkowski region (Fig. 5) has the same size as the query window and centers at the answered object. The validity segment of the answered object is the intersection of the query line segment with its Minkowski region. In Fig. 1, the answered objects for query line segment \overline{SE} are objects $O8$, $O10$ and $O11$. Their corresponding Minkowski regions are shown in Fig. 4. The validity segments of objects $O8$, $O10$ and $O11$ are \overline{Sa} , \overline{ba} and \overline{ca} , respectively.

4 Conclusion

In this paper, we have addressed the problem of processing continuous window queries for skewed access patterns in the wireless data broadcast environments. We have proposed a skewed spatial index for efficient processing such queries. In our proposed method, popular spatial objects are broadcast more often than regular ones, resulting in quick access of the popular objects.

Acknowledgments This research was supported in part by the National Science Council of Republic of China under Grant No. NSC 99-2221-E-468-019 and Grant No. NSC 100-2511-S-025-002-MY2.

References

1. Acharya S, Franklin M, Zdonik S, Alongso R (1995) Broadcast disks: data management for asymmetric communications environments. In: Proceedings of the 1995 ACM SIGMOD international conference on management of data, pp 199–210
2. Im S, Youn HY, Choi J, Ouyang J (2011) A novel air indexing scheme for window query in non-flat wireless spatial data broadcast. *J Commun Netw* 13(4):400–407
3. Im S, Choi J (2012) MLAIN: multi-leveled air indexing scheme in non-flat wireless data broadcast for efficient window query processing. *Comput Math Appl* 64:1242–1251
4. Im, S Choi J (2012) Quick data access on multiple channels in non-flat wireless spatial data broadcasting. *IEICE Trans Commun E95-B(9)*:3042–3046
5. Shen JH, Chang YI (2007) A skewed distributed indexing for skewed access patterns on the wireless broadcast. *J Syst Softw* 80(5):711–723
6. Shen JH, Chang YI (2008) An efficient nonuniform index in the wireless broadcast environments. *J Syst Softw* 81(11):2091–2103
7. Shen JH, Lu CT, Jian MS (2013) Neighbor-index method for continuous window queries over wireless data broadcast. *Appl Mech Mater* 284–287:3295–3299
8. Yee WG, Navathe SB, Omiecinski E (2002) Efficient data allocation over multiple channels at broadcast servers. *IEEE Trans Comput* 51(10):1231–1236
9. Zheng B, Lee WC, Lee CK, Lee DL, Shao M (2009) A distributed spatial index for error-prone wireless data broadcast. *VLDB J* 18(4):959–986

Advancing Collaborative Learning with Cloud Service

Yong-Ming Huang, Chia-Sui Wang, Jia-Ze Guo, Huan-Yu Shih and Yong-Sheng Chen

Abstract Cloud computing has become one of the most important information technologies due to the development of Internet technologies. Accordingly, cloud computing has been applied to various fields, in which many researchers have also tried to apply cloud computing to education field. Despite much research on cloud to education, little effort has been devoted to applying them to a course in programming. Programming is a subtle and serious work, which requires a lot time to think, design, implement, testing and debugging. Hence, teachers often teach students to collaboratively engage in programming. Among the applications of cloud computing, collaborative service is the most potential applications for achieving collaborative learning, in which they can be used to assist students in collaboratively accomplishing a learning task. Accordingly, we explore how to use such services to assist students in learning programming. Three collaborative services are used in this study, in which Simplenote is used to support students in discussing; Google Docs is used to support students in designing; CodeRun is used to support students in programming.

Keywords Cloud computing · Collaborative learning · Programming

Y.-M. Huang (✉) · J.-Z. Guo · H.-Y. Shih · Y.-S. Chen
Department of Applied Informatics and Multimedia, Chia Nan University
of Pharmacy and Science, Tainan City, Taiwan
e-mail: ymhuang@mail.chna.edu.tw

J.-Z. Guo
e-mail: ejiru8yk6@gmail.com

H.-Y. Shih
e-mail: a8754123@yahoo.com.tw

Y.-S. Chen
e-mail: qwerasfd007@yahoo.com.tw

C.-S. Wang
Department of General Education, Chia Nan University
of Pharmacy and Science, Tainan City, Taiwan
e-mail: didijayjay@gmail.com

1 Introduction

In recent years, cloud computing has been regarded as most promising information technology to realize a variety of innovative applications. Cloud computing is a network-based computing model, in which various hardware and software resources are viewed as cloud to provide users with different kinds of services [1]. If the cloud is accessible to everyone, it is called public cloud; if the cloud is accessible to an internal organization, it is called private cloud [1]. By using cloud computing, developers do not need to spend time and effort to build their own information technology infrastructure [2]. On the contrary, they can concentrate their attention on the development of innovative applications. Accordingly, users can enjoy the convenience of cloud computing.

So far many researchers have noticed that cloud service is helpful to achieve the educational innovative applications. For example, some researchers noticed that cloud computing provides much richer services over the Internet than before, such as Google Apps for Education and Google Docs. These cloud services are tailored to provide a platform for educational organizations to develop their own educational application [3, 4]. In this manner, some cash-strapped educational institutions can directly rent cloud service to develop their own educational services, while do not need to spend time to maintain their own information technology infrastructure [5]. Overall, such cloud services can provide students and teachers with free or low-cost schemes to supersede expensive proprietary productivity tools.

Among cloud services, collaborative service is the most potential service for realizing collaborative learning [6, 7]. The collaborative service can be used to assist users in easily accomplishing real-time collaboration and adding social capabilities when they are engaged in teamwork. That is to say, such collaborative services are innately useful for achieving collaborative learning activities such as collaborative writing [7]. For example, Calvo et al. used Google Docs service to develop a cloud-based learning tool to assist students in achieving the collaborative writing and support teacher manage collaborative and individual writing assignments in large cohorts [6]. Accordingly, collaborative service enables students to engage in collaborative learning.

Despite much research on cloud to education, little effort has been devoted to explore the application of cloud service to collaborative learning. To this end, we intend to unveil the potential application and see to how collaborative learning can be benefited by cloud service.

2 Cloud Computing Overview

Cloud computing intrinsically provides massive computing and storage capacities, enabling the delivery of a variety of service [5]. By its intrinsic features, although some researchers have interpreted it in different perspectives [2, 8], most of them

state four basic characteristics of it: (1) it is applicable to massive storage and massive calculation; (2) its payment mode is pay-as-you-go, the users only need to pay for actually used resources; (3) it is a computing mode providing services according to requirements, the required resources may not be allocated beforehand; (4) it is a service-oriented architecture, the service scale can be set and provided dynamically according to requirements [2, 8]. Fundamentally, cloud computing provides three levels of service: infrastructure as a service (IaaS), platform as a service (PaaS), and software as a service (SaaS), as summarized in the following.

IaaS offers hardware infrastructure such as computing power and storage space as services. It enables users to directly rent the hardware infrastructure rather than spending time and budget to build their own [2, 8, 9], with the advantage of the infrastructure being scaled easily to accommodate the future demand [9, 10]. Two well-known examples in this service are Amazon EC2 (Elastic Cloud Computing) for supplying computing power service and Amazon S3 (Simple Storage Service) for supplying storage space service.

PaaS offers software development platform as services. This service enables users to directly design, implement, debug, test, deploy and operate their software in cloud [10]. Unlike IaaS, the users of PaaS do not need to address hardware configurations or software installations, instead, they can utilize PaaS to directly create their own software in cloud. Two well-known examples in this service are Google App Engine and Microsoft Azure that allow users to develop software in cloud without dealing with hardware and software configurations.

SaaS mainly offers software on the Internet as services. This service enables users to directly access software by using the Internet instead of installing special software on their computer [8]. Unlike PaaS, SaaS only hosts completed software whereas PaaS offers a development platform that hosts both completed and in-progress software [9]. Examples of Google Apps for Education and Google Docs belong to this category, which provide web-based educational and office software applications.

3 Application of Cloud Service to Collaborative Learning

This study is to explore the use of cloud service in collaborative learning, in which a programming course is used as an example. To this end, we collect a number of collaborative services that can be used to support the programming course, as described below.

3.1 *Simplenote*

Simplenote [11] is a cloudalized note service. It enables users to easily keep notes, lists, and ideas on the mobile device and desktop computer, so that users can keep notes seamlessly. In addition, it is different from other note services, Simplenote provides students with several functions to achieve collaborative learning. “Share notes” function, students can decide that note is private or public. “Collaborative editing” function, students can invite others to collaboratively edit your note. “Sync save” function, the notes are automatically synchronized with different devices. “Go back in time” function, students can access multiple backups of their notes, in which they just drag the version slider to go back in time. Accordingly, when students want to discuss how to design a system, they can use Simplenote to support students in achieving brainstorming.

3.2 *Google Docs*

Google Docs is a cloudalized word processing service [12]. It enables students to directly draw diagrams and create documents on cloud, so that they can collaboratively edit their files. By using this service, students can collaboratively design the flow chart or architecture diagram of a system when they finished the discussion of system design. Once students accomplished the system design, they also can use this service to collaboratively write the system design document that describes the system requirements, operating environment, system architecture, and so on. During collaboration, students can use instant messaging function of this service to discuss how to edit their files concurrently. Moreover, students also can use track changes function to track who made the change and compare the difference between different versions.

3.3 *CodeRun*

CodeRun is a cloudalized integrated development environment (IDE) service [13]. CodeRun is a cross-platform IDE and designed for the cloud, in which students can easily use it to develop, debug and deploy application through browser. By using CodeRun, students can program their system in the cloud and they can easily share their code with their students, as shown in Fig. 1. As owner of a shared project, the owner can control read/write permissions of the people you choose to invite. When students share code with CodeRun, their project is assigned with a unique URL that they can send to others. Anyone who navigates to their link receives a separate, fully modifiable and runnable version of their code. More importantly,

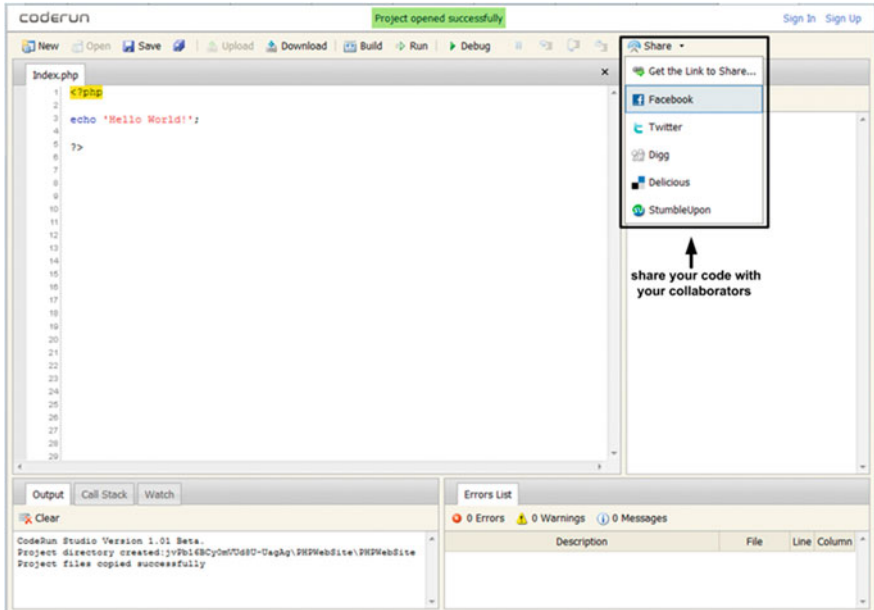


Fig. 1 The CodeRun

students can save a lot of time for developing system, because they can invite others to debug their code. Overall, students can use CodeRun to collaboratively program their system in the cloud.

4 Discussion and Conclusion

Cloud computing provides people with a whole new experience, in which collaborative service is a great innovative applications and useful to realize collaboration. With the rapid growth of information and the increase in the amount of information exchanged, individuals have been unable to handle a lot of information. On the contrary, people should adopt the collaboration to accomplish tasks, in which everyone brings their talents into full play respectively. Thus, it is a vital issue to develop a sound approach to train students to be able to collaboratively carry out tasks. Although in school teachers often ask students who need to adopt the collaboration to accomplish assignments, students are still working alone. For example, teachers ask students to collaboratively write a report, but students may be limited by what tools do not well support collaboration such as early Microsoft Office. However, with the development of cloud services, teachers can use collaborative service to assist students in realizing collaboration. By using such services, students can collaboratively carry out brainstorming, design, and

implement their ideas. More importantly, students can learn the spirit of teamwork during the period of collaboration.

Collaborative service is one of the most important cloud services, which can be used to assist students in engaging in collaborative learning. In this study, we showed that three collaborative services are used to support students in programming, in which Simplenote is used to support students' brainstorming, Google Docs is used to support students' design, and CodeRun is used to support students' implement. Hence, students can use these collaborative services to collaboratively engage in programming. To further explore students' perspectives on these services, in future work, we will construct an experiment based on the technology acceptance model to explore their perceptions of collaborative service for programming.

Acknowledgments The authors would like to thank the National Science Council of the Republic of China for financially supporting this research under Contract No. NSC 102-2511-S-041-001.

References

1. Armbrust M, Fox A, Griffith R, Joseph AD, Katz R, Konwinski A, Lee G, Patterson D, Rabkin A, Stoica I, Zaharia M (2010) A view of cloud computing. *Commun ACM* 53(4):50–58
2. Foster I, Zhao Y, Raicu I, Lu S (2008) Cloud computing and grid computing 360-degree compared. In: *Proceedings of the grid computing environments workshop*, Austin
3. Wheeler B, Waggener S (2009) Above-campus services: shaping the promise of cloud computing for higher education. *EDUCAUSE Rev* 44(6):52–67
4. Wen JR, Chen CP (2011) The strategy of implementing the internet and cloud computing in teaching. *Int J Res Rev Comput Sci* 2(1):83–87
5. Sultan N (2010) Cloud computing for education: a new dawn? *Int J Inf Manage* 30(2):109–116
6. Calvo RA, O'Rourke ST, Jones J, Yacef K, Reimann P (2011) Collaborative writing support tools on the cloud. *IEEE Trans Learn Technol* 4(1):88–97
7. Siegle D (2010) Cloud computing: a free technology option to promote collaborative learning. *Gift Child Today* 33(4):41–45
8. Vaquero LM (in press) Educloud: paas versus Iaas cloud usage for an advanced computer science course. *IEEE Trans Edu*. doi: [10.1109/TE.2010.2100097](https://doi.org/10.1109/TE.2010.2100097)
9. Dillon T, Wu C, Chang E (2010). Cloud computing: issues and challenges. In: *Proceedings of the 24th IEEE international conference on advanced information networking and applications*, Perth
10. Weber AS (2011) Cloud computing in education in the Middle East and North Africa (Mena) region: can barriers be overcome? In: *Proceedings of the 7th international scientific conference eLSE—elearning and software for education*, Bucuresti
11. Simplenote (2013) Simplenote. <http://simplenote.com/>
12. Google Docs (2013) Google Docs. <http://docs.google.com/>
13. CodeRun (2013) Google Docs. <http://coderun.com/>

Using MapReduce Framework for Mining Association Rules

Shih-Ying Chen, Jia-Hong Li, Ke-Chung Lin, Hung-Ming Chen
and Tung-Shou Chen

Abstract Data mining in knowledge discovery helps people discover unknown patterns from the collected data. PIETM (Principle of Inclusion–Exclusion and Transaction Mapping) algorithm is a novel frequent item sets mining algorithm, which scans database twice. To cope with big transaction database in the cloud, this paper proposes a method that parallelizes PIETM by the MapReduce framework. The method has three modules. Module I counts the supports of frequent 1-item sets. Module II constructs transaction interval lists. Module III discovers all the frequent item sets iteratively.

Keywords Frequent itemsets · Association rules · Data mining · MapReduce

This research is supported in part by NSC in Taiwan under Grant No. NSC-101-2221-E-025-014.

S.-Y. Chen (✉) · J.-H. Li · H.-M. Chen · T.-S. Chen
Department of Computer Science and Information Engineering, National Taichung
University of Science and Technology, Taichung, Taiwan
e-mail: sychen@nutc.edu.tw

J.-H. Li
e-mail: s18003103@nutc.edu.tw

H.-M. Chen
e-mail: hmchen@nutc.edu.tw

T.-S. Chen
e-mail: tschen@nutc.edu.tw

K.-C. Lin
Department of Computer Science and Engineering, National Chung-Hsing University,
Taichung, Taiwan
e-mail: phd9212@cs.nchu.edu.tw

1 Introduction

Data mining [1] in knowledge discovery helps people discover unknown patterns from the collected data. Association rule mining is one of the most important mining techniques. It generates implication rules among commodities. The generated rules can be used further for strategy decisions.

The association rule mining problem is to discover all the association rules that exceed the values of *minimum support* and *minimum confidence* [2]. Suppose that there are a set I of n items, a_1, \dots, a_n , and a database D of m transactions, T_1, \dots, T_m , over the items. A set X of k items of I is called a k -itemset of I . The *support* of the itemset X , denoted by $sup(X)$, is defined as the fraction of transactions where X occurs. X is termed *frequent* if $sup(X)$ exceeds a user-specified *minimum support*. On the other hand, the *confidence* of an association rule XUY is defined as $sup(XUY)/sup(X)$, which means the fraction of all transactions containing X that also contain Y .

Apriori [2, 3] is one of the most important association rule mining algorithms. In the algorithm, the frequent k -item sets are permuted to generate the candidate $(k + 1)$ -itemsets. The $(k + 1)$ -candidate itemsets whose supports exceed the minimum supports become the frequent $(k + 1)$ -item sets. The process goes on iteratively till no more candidate itemsets are generated.

Principle of Inclusion–Exclusion and Transaction Mapping (PIETM) [4] improves Apriori by introducing the Inclusion–Exclusion Principle [5] and the idea of transaction intervals. PIETM constructs transaction intervals for mapping and storing the transaction IDs of each item, and uses the Inclusion-Exclusion-Principle to count the supports of itemsets. In this way, PIETM scans the transaction database twice only.

Due to the cost of database scans, association rule mining algorithms become ineffective if the transaction database grows much bigger. In this paper, we propose a method that parallelizes PIETM by the MapReduce framework to solve the problem.

MapReduce [6] provides a high-efficiency programming framework for processing big data in parallel on the Hadoop file system (HDFS) [7]. The framework is composed of the Map and Reduce phases. During the Map phase, the mappers obtain data from the HDFS and compute them. The results of the mappers are passed to the Reducers to generate the final result in the Reduce phase.

For processing data, the input data of the mappers is a set of $\langle key_1, value_1 \rangle$ pairs. Each Mapper processes the data and generates another set of $\langle key_2, value_2 \rangle$ pairs. $\langle key_2, value_2 \rangle$ pairs of a Mapper are hashed into region files by a hash function of key_2 . Therefore, the pairs of the same value of the field key_2 are hashed into the same region file. A Reducer then reads the hashed pairs from its region files. By sorting the hashed pairs in the order of key_2 , the Reducer merges the pairs and generates a set of $\langle key_2, list(value_2) \rangle$ pairs. Every $list(value_2)$ s on each Reducer are collected as the final result.

The paper is organized as follows. Section 2 reviews the related research. Section 3 proposes our method to parallelize PIETM, and Sect. 4 illustrates the proposed method by an example. Section 5 concludes our work.

2 Related Work

Apriori [3] is the most popular frequent itemset mining algorithms. Apriori finds the frequent 1-itemsets by scanning the database first. Then, candidate 2-itemsets are generated by joining each pair of the frequent 1-itemsets. By scanning the database again, the candidate 2-itemsets whose supports exceed the minimum support become the frequent 2-itemsets. The process goes on to discover higher order frequent itemsets. It terminates when no more candidate itemsets are generated. The cost of Apriori is high since it scans database in each iteration.

Based on Apriori, PIETM [4] introduces the Inclusion–Exclusion Principle [5] and the idea of transaction intervals [8]. In this way, PIETM reduces the number of database scans to two times.

PIETM uses the Inclusion–Exclusion Principle, as shown in Eq. (1), to count the supports of itemsets. In Eq. (1), A_i denotes a set. $|A_i|$ denotes its cardinality.

$$\begin{aligned}
 \left| \bigcup_{i=1}^n A_i \right| &= \sum_{i=1}^n |A_i| - \sum_{1 \leq i < j \leq n} |A_i \cap A_j| \\
 &+ \sum_{1 \leq i < j < k \leq n} |A_i \cap A_j \cap A_k| + \dots + (-1)^{n-1} |A_1 \cap A_2 \dots \cap A_n| \quad (1)
 \end{aligned}$$

PIETM artfully redefines the meanings of the terms in Eq. (1) to count the supports of itemsets. In PIETM, A_i denotes the set of transaction IDs in which item a_i occurs. Accordingly, $|A_i|$ denotes the number of transactions containing a_i ; that is, $|A_i|$ is equal to $sup(a_i)$. The intersection of sets, $A_1 \cap A_2 \cap \dots \cap A_k$, is called a k -intersection term. It indicates the transaction IDs in which the k -itemset $\{a_1, a_2, \dots, a_k\}$ occurs. $|A_1 \cap A_2 \cap \dots \cap A_k|$ is equal to the support of this k -itemset, denoted by $sup(a_1 a_2 \dots a_k)$ for clarity. On the other hand, $A_1 \cup A_2 \cup \dots \cup A_k$ is called a k -union term, which indicates the transaction IDs in which any one of the items a_1, a_2, \dots , and a_k occurs. PIETM counts the support of a k -itemset by counting in advance the supports of $(k-1)$ -itemsets and support of the k -union term. For example, $|A_1 \cup A_2 \cup A_3| = |A_1| + |A_2| + |A_3| - (|A_1 \cap A_2| + |A_1 \cap A_3| + |A_2 \cap A_3|) + |A_1 \cap A_2 \cap A_3| = sup(a_1) + sup(a_2) + sup(a_3) - (sup(a_1 a_2) + sup(a_1 a_3) + sup(a_2 a_3)) + sup(a_1 a_2 a_3)$. Clearly, $sup(a_1 a_2 a_3)$ are derived if $sup(a_1), sup(a_2), sup(a_3), sup(a_1 a_2), sup(a_1 a_3), sup(a_2 a_3)$ and the 3-union term $|A_1 \cup A_2 \cup A_3|$ are known.

To count the support of the k -union term, PIETM takes advantage of transaction interval lists [8], where the number of transactions containing an item is represented as intervals. The support of the k -union term is the length of the union of the intervals.

3 Proposed Method

We propose a method using MapReduce to parallelize PIETM. The method parallelizes the structure construction process and the mining process in PIETM by three modules. Module I counts the supports of frequent 1-itemsets. Module II constructs transaction interval lists. Module III discovers all the frequent itemsets iteratively.

The Map and Reduce functions in Module I are illustrated in pseudo codes in Figs. 1 and 2, respectively. A Mapper reads the database and emits $\langle a_i, 1 \rangle$ for each item a_i in every transaction. Later, a Reducer sums up the 1 s for each item a_i in Line 3, and emits item a_i together with its support if it is frequent in Line 4.

Module II constructs the transaction interval lists. In Fig. 3, a Mapper writes frequent 1-itemsets into a Distributed Cache [7] in HDFS. It also creates a list, namely a group list, to collect the frequent 1-itemset. The group list is further divided into r groups, where r is a user-specified value. In fact, the value of r depends on the number of Reducers for various degrees of parallelism.

A Mapper in Module II reads the prime transaction database and emits $\langle \text{goupid}, \langle \text{ID_of_}T_x, \text{frequent_1_items_in_}T_x \rangle \rangle$ for each transaction T_x . During the process, Line 10 checks if an item is frequent. In Lines 11–21, a list of frequent 1-items with the same group id is constructed. The pair $\langle \text{goupid}, \langle \text{ID_of_}T_x, \text{frequent_1_items_in_}T_x \rangle \rangle$ is emitted in Line 18.

```

Input: <key, transaction  $T_x$ >
Output: <item $a_i$ , 1>
1.      Map class {
2.      Map function {
3.          for each item  $a_i$  in  $T_x$ 
           output < $a_i$ , 1>;
4.      }
5.      }

```

Fig. 1 Map class of module I

```

Input: <item $a_i$ , list<1s>>
Output: <item $a_i$ , support of  $a_i$ >
1.      Reduce class {
2.      Reduce function {
3.          for each value 1 in list
           support += 1;
4.          if (support >= minimum_support)
           output < $a_i$ , support>;
5.      }
6.      }

```

Fig. 2 Reduce class of module I

```

Input: <key, transaction  $T_x$ >
Output: <groupid, <ID_of_  $T_x$ , frequent_1_items_in_  $T_x$ >
1. Map class {
2.   setup function {
3.     Write frequent 1-itemsets  $F_1$  into distributed cache;
4.     Create group list  $GL$  from  $F_1$ ;
5.   }
6.   Map function {
7.     frequentitems=the set of item names in  $GL$ ;
8.     for j = 0 to  $T_x$ .length-1{
9.       item= $T_x[j]$ ;
10.      if (item  $\notin$  frequentitems) break;
11.      if (j==0){
12.        Gv=group id of  $T_x[0]$  in  $GL$ ;
13.        break;
14.      };
15.      gid=Gv;
16.      Gv= group id of  $T_x[j]$  in  $GL$ ;
17.      if (gid!=Gv) {
18.        Output <gid, <x, items>>;
19.        items = "";
20.      }
21.      items+= item;
22.    }
23.  }
24.}

```

Fig. 3 Map class of module II

```

Input: <groupid, list(< $T_{id}$ , items>>)
Output: <item, interval>
1. Reduce class {
2.   Reduce function {
3.     for i=0 to list.length-1 { //each list
4.       for j=0 to list[i].items.length-1 { //each item in  $T_{id}$ 
5.         a=list[i].items[j];
6.         TList= $\emptyset$ ;
7.         for k=i+1 to list.length-1
8.           if (a $\in$ list[k].items) TList=TList $\cup$ list[k]. $T_{id}$ ;
9.         sort elements in TList in the increasing order;
10.        separate TList into contiguous intervals: [ $s_1, e_1$ ] [ $s_2,$ 
11.           $e_2$ ]... [ $s_n, e_n$ ];
12.        output <a, [ $s_1, e_1$ ] [ $s_2, e_2$ ]... [ $s_n, e_n$ ]>;
13.      }
14.    }

```

Fig. 4 Reduce class of module II

In Fig. 4, a Reducer in Module II constructs transaction intervals. Nested loops in Lines 3 and 4 iterate for every item in every input list ($\langle T_{id}, \text{items} \rangle$). In each iteration, a list of transaction T_{id} containing item a (assigned in Line 5), namely

```

Input: <key, candidates>
Output: <itemsets, support>
1.Map class {
2.  setup function {
3.    write frequent 1 to (k-1)-itemsets and interval list
    intoDistributed Cache;
4.  }
5.  Map function {
6.    calculate sup(candidates)by the inclusion-exclusion
    principle;
7.    if (sup(candidates)>= minimum support)
        output <candidates, sup(candidates)>;
8.  }
9.}

```

Fig. 5 Map class of module III

TList, is constructed in Line 7. *TList* is sorted in the increasing order in Line 8, and is separated into several contiguous intervals in Line 9. The pair that is composed of the item *a* and the intervals of *TList* is emitted in Line 10 (Fig. 5).

Module III discovers the frequent *k*-itemsets. Note that higher order frequent itemsets are discovered by chaining multiple MapReduce jobs of Module III. In the Map function in Module III, Line 3 sets up the supports of frequent 1 to (*k*-1)-itemsets and the transaction interval lists. Line 6 calculates the supports of candidate *k*-itemsets. If an itemset is frequent, it is emitted together with its supports. On the other hand, Fig. 6 illustrates the Reduce function of Module III, which simply emits the outputs of the Mappers of the module.

4 Illustrated Example

We illustrate how the parallelized PIETM algorithm works by an example. Table 1 shows the original database. Suppose that the minimum support is 3. In Module I, a Mapper reads the transaction database and emits $\langle a_i, 1 \rangle$ for each item a_i in every

```

Input: <itemsets, support>
Output: <itemsets, support>
1.Reduce class {
2.  Reduce function {
3.    output <itemsets, support>;
4.    collect all itemsets;
5.  }
6.  Create_candidate function {
7.    compute candidate (k+1)-itemsets;
8.    writecandidate (k+1)-itemsets into a HDFS file;
9.  }
10.}

```

Fig. 6 Reduce class of module III

Table 1 Transaction database

T _{id}	Items of T _{id}
1	A, B, C, D, E
2	A, C, D, G
3	A, B, H
4	B, C, D, I, J
5	B, D, K, L

transaction. As a result, $\langle A, 1 \rangle, \langle B, 1 \rangle, \langle C, 1 \rangle, \langle D, 1 \rangle, \langle E, 1 \rangle, \langle G, 1 \rangle, \langle H, 1 \rangle, \langle I, 1 \rangle, \langle J, 1 \rangle, \langle K, 1 \rangle, \langle L, 1 \rangle$ are emitted for 3, 4, 3, 4, 1, 1, 1, 1, 1, 1, and 1 times, respectively. A Reducer in the module sums up the ones for each item and emits the frequent items if they exceed the minimum support. Table 2 shows the result. This requires scanning database once.

In Module II, transaction interval lists are created. Table 3 illustrates the frequent 1-itemsets of transactions, while Table 4 illustrates the group list used in the Mappers in the module. The group list is divided into 2 groups, with group IDs are 1 and 2, in the example. Items A and B belong to group 1, while items C and D belong to group 2. Based on the structures of the frequent 1-itemsets and the group list, a Mapper in the module scans database the last time and emits $\langle \text{groupid}, \langle \text{ID_of_}T_x, \text{frequent_1-items_in_}T_x \rangle \rangle$ for each transaction T_x . For example, for

Table 2 Output of the reducers in module I

Frequent 1-items	Times
A	3
B	4
C	3
D	4

Table 3 Frequent 1-itemsets of transactions in module II

T _{id}	Items of T _{id}	Frequent 1-itemsets of T _{id}
1	A, B, C, D, E	A, B, C, D
2	A, C, D, G	A, C, D
3	A, B, H	A, B
4	B, C, D, I, J	B, C, D
5	B, D, K, L	B, D

Table 4 Group list in module II

Item	Group id
A	1
B	1
C	2
D	2

Table 5 Output of the mappers in module II

Key	Value
1	$\langle 1, AB \rangle$
1	$\langle 2, A \rangle$
1	$\langle 3, AB \rangle$
1	$\langle 4, B \rangle$
1	$\langle 5, B \rangle$
2	$\langle 1, CD \rangle$
2	$\langle 2, CD \rangle$
2	$\langle 3, \text{null} \rangle$
2	$\langle 4, CD \rangle$
2	$\langle 5, D \rangle$

transaction T_1 , $\langle 1, \langle 1, AB \rangle \rangle$ and $\langle 2, \langle 1, CD \rangle \rangle$ are emitted. Table 5 illustrates the output of the Mappers in Module II.

In Table 5, the records with the same key value (i.e., group id) are shuffled to the same Reducer to create the transaction intervals of items. The transaction intervals constructed after the Reducers of Module II are shown in Table 6. Take item B as an example, since item B appears in transactions $T_1, T-3, T-4, T-5$ in Table 5, the transaction intervals of item B are [1, 1] and [3, 5]. Note that each interval should be contiguous.

In Module III, frequent 2-itemsets to higher order frequent itemsets are discovered by executing multiple MapReduce jobs iteratively. Table 7 lists the supports of candidate 2-itemsets, which are calculated with the Inclusion-Exclusion Principle. Take $sup(A \cup B)$ as an example. To count $sup(A \cup B)$ requires $sup(A), sup(B)$ and $sup(A \cap B)$. The support of $A \cup B$ can be counted from transaction intervals of items A and B. In Table 6, A's interval is [1, 3] and B's interval is [1, 1] and [3, 5]. Therefore, the interval of $A \cup B$ is [1, 5], which means that items A or B occur in T_1-T_5 . Then, we have $sup(A \cup B) = 5$. As a result, $sup(A \cap B) = sup(A) + sup(B) - sup(A \cup B) = 3 + 4 - 5 = 2$. In Table 7, the candidate 2-itemsets BD and CD are frequent as their supports exceed the minimum support, which is 3 in the example.

Table 6 Transaction intervals of the transaction database

Item	Transaction intervals
A	[1, 3]
B	[1, 1] [3, 5]
C	[1, 2] [4, 4]
D	[1, 2] [4, 5]

Table 7 Support of candidate 2-itemsets

Candidate 2-itemsets	Support	Frequent
AB	$ A \cap B = A + B - A \cup B = 3 + 4 - 5 = 2$	–
AC	$ A \cap C = A + C - A \cup C = 3 + 3 - 4 = 2$	–
AD	$ A \cap D = A + D - A \cup D = 3 + 4 - 5 = 2$	–
BC	$ B \cap C = B + C - B \cup C = 4 + 3 - 5 = 2$	–
BD	$ B \cap D = B + D - B \cup D = 4 + 4 - 5 = 3$	Yes
CD	$ C \cap D = C + D - C \cup D = 3 + 4 - 4 = 3$	Yes

5 Conclusions

In this paper, we propose a method to parallelize PIETM, which discovers frequent itemsets from a database, by the MapReduce framework. The method keeps the features in PIETM: constructing structures for counting supports and adopting the Inclusion–Exclusion principle. To parallelize the structure construction process and the mining processes, three modules are designed. Module I counts the supports of frequent 1-itemsets. Module II constructs transaction interval lists. Module III discovers the frequent itemsets. However, the bottleneck of the method is the construction of interval lists in Module II. Therefore, our future work includes how to design faster solutions and measure their performance.

References

1. Han J, Kamber M, Pei J (2011) Data mining: concepts and techniques. Morgan Kaufmann, San Francisco
2. Agrawal R, Srikant R (1994) Fast algorithm for mining association rules in large database. In: Bocca JB, Jarke, M, Zaniolo C (eds.) VLDB'94. In: Proceeding of the 20th international conference on VLDB. pp 487–499, Santiago
3. Agrawal R, Imielinski T, Swami A (1993) Mining association rules between sets of items in large databases, In: the ACM SIGMOD conference on management of data, pp 207–216
4. Lin KC, Liao IE, Lin SF, Chang TP. A frequent itemset mining algorithm base on the inclusion–exclusion principle and transaction mapping. information. Science. accepted with minor revision
5. Liu CL (1968) Introduction to combinatorial mathematics. McGraw-Hill, New York
6. Dean J, Ghemawat S (2004) MapReduce: simplified data processing on large clusters. In: Proceedings of the 6th symposium on operating systems design and implementation (OSDI), pp 137–150
7. Apache hadoop. <http://hadoop.apache.org>
8. Song M, Rajasekaran S (2006) A transaction mapping algorithm for frequent itemsets mining. in. IEEE Trans Knowl Data Eng 18(4):472–481

Cloud Feedback Assistance Based Hybrid Evolution Algorithm for Optimal Data Solution

Ming-Shen Jian, Fu-Jie Jhan, Kuan-Wei Lee and Jun-Hong Shen

Abstract This paper develops a cloud based parallel and distributed evolutionary hybrid algorithm with feedback assistance to help planners solve the data optimal problems such as travel salesman problems. Each step and type of evolution algorithm is established via various virtual machines in cloud. The proposed feedback assistance is based on the fitness evaluation result and survival ratio of evolution algorithm. The feedback assistance can interact with the evolution algorithm and emphasize the process with more survival individuals in the next generation of evolution algorithm. Taking the advantage of cloud and the proposed feedback assistance, system users can take less effort on deploying both computation power and storage space. The convergency of optimal solution can be enhanced.

Keywords Evolution algorithm · Cloud · Optimal solution · Feedback · Hybrid

1 Introduction

Evolution algorithms or genetic algorithms were proposed based on natural evolution selection “survival of the fittest.” Evolution algorithms are flexible to solve a variety of problems if the encoding models and evaluation functions of these problems can be well-defined. In recent decades, evolution algorithms are widely used in many fields for solving optimal solution which are usually proved

M.-S. Jian (✉) · F.-J. Jhan · K.-W. Lee
Department of Computer Science and Information Engineering,
National Formosa University, 632 Yunlin County, Taiwan
e-mail: jianms@nfu.edu.tw

J.-H. Shen
Department of Information Communication, Asia University,
413 Taichung City, Taiwan

to be NP-complete problems, such as traveling salesman problem (TSP), graph coloring problem (GCP), and vehicle routing problem [1–3] etc. Hence to enhance the performance of simple GA, becomes an active research.

The major factors hiding behind the structure of evolution algorithm are selection pressure and population diversity. These two factors control the convergence speed and the robustness of solution. The selection pressure influences the fitness and the relations between chromosomes of the offspring and the parents. Jian [4] proposed that the evolution algorithm including sexual and asexual production can converge faster and perform better than the traditional or classical evolution algorithm. It means that to control the selective pressure and diversification is an important issue.

Typically, VRP indicates a closed route and with once visit constraint. According to the model presented by Özdamar et al. [5], generates sets of “broken” routes and vehicles that do not need to return to depots. There are also many types of solutions such as dynamic integer linear programming [5–11], Dijkstra algorithm [12–14], metaheuristic algorithms as ant colony and genetic algorithms [12, 14–18], immune intelligence [19], greedy method [20], game theory [21], fuzzy multi-objective program [6, 17, 22–24], etc. Yi and Özdamar [11] proposed an integrated capacitated location-routing model (LRP) with a multi-depot network flow based routing formulation for coordinating logistics support and evacuation operations. Özdamar and Yi [20] applied the greedy neighborhood search method to build path. Kanoh and Hara [14] designed the hybrid genetic algorithm and Dijkstra algorithm to use three objectives of route length, travel time, and ease of driving to choose a favorite route from the Pareto-optimal set. However, the data or searching space for solution finding may be huge. In other words, to find the optimal solution corresponding to the dynamic state in time is needed. Therefore, to adopt the cloud computing can be a solution fir huge data management.

By using the virtual implementation of hardware and operating systems, cloud computing provides users the ability to create or deploy their own applications with huge computing resources. Many services [24] including Amazon’s EC2, IBM’s Smart Business cloud offerings, Microsoft’s Azure, and Google’s AppEngine, etc. are based on cloud computing. According to the structure of cloud computing, users’ application can be established individually on virtual machines. Based on the concept of distributed system and parallel processing, the evolution algorithm can be partially divided into procedures to effectively find the optimal solution via adapting cloud computing.

The rest of this paper is organized as follows. Section 2 introduces the related work and the problem statement. Section 3 presents the proposed algorithm. Performance evaluation is given in Sect. 4. At last, conclusion is drawn in Sect. 5.

2 Related Works and Problem Statement

In this section, the related concept of evolution algorithm and the problem statement for the proposed *Cloud Feedback Assistance Based Hybrid Evolution Algorithm* will be introduced.

2.1 Related Works and Concepts of Evolution Algorithm

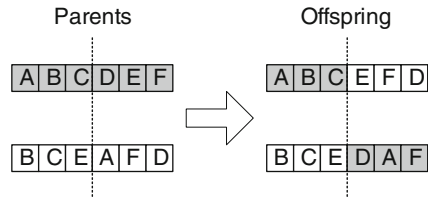
The basic evolution algorithm such as genetic algorithm (GA) has its standard procedures as in the following to search the best solution iteratively.

- Step 1. Representation: The first step is to transform all candidate solutions to the genotype form for describing the possible candidate solutions of the problem. Then, the objective function (also called the fitness function) is also assigned to map each candidate (chromosome) a value.
- Step 2. Initialization: Generate (often in random) the population of the first generation for being the parents of the second generation.
- Step 3. Selection: This procedure selects the proper individuals as parents to reproduce the newborn offspring.
- Step 4. Crossover: This procedure would mix parents' chromosomes and pass to children. The chromosomes of offspring consist of the partial chromosomes from its parents. Crossover rate is also a topic researches because a proper crossover rate gains a better performance [11].
- Step 5. Mutation: This procedure would simulate accidents happening in reproduction and vary gene in random way. The mutation operation can increase diversity and improve the probability of overcoming local optima during the search process.
- Step 6. Survival: According to Darwin's "survival of the fittest" rule, this step is to drop some individuals to maintain the same population size. As so, those remaining chromosomes passing this step are better in the fitness evaluation function than those dropped chromosomes. In another way, the adaptive population size is also a method of improving performance [12].
- Step 7. Checking: If the stop criteria are satisfied, then stop. Otherwise, go to Step 3.

The goal of the traveling salesman problem (TSP) is to find the minimum trip of cities. The general presentation is to encode the permutation of cities which are visited sequentially.

In addition to representation, crossover takes an important role for generating good sibling. In this paper, Partially mapped crossover (PMX), which is developed by Goldberg and Lingle, is the most popular and well-known two-parent crossover for combinatorial optimization problems and used in this paper (Fig. 1).

Fig. 1 Partial-mapped crossover



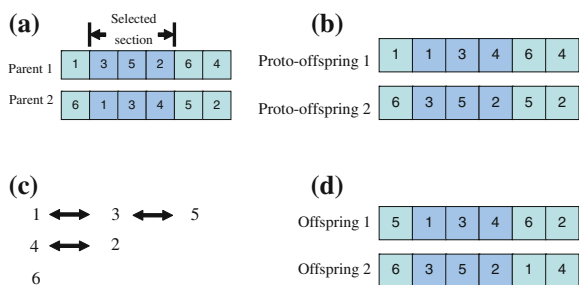
Furthermore, in this paper, two different PMX methods are adopted. In addition to one point (one cut) PMX method above, two-point (two cuts) PMX method is also implemented. Similar to one point (one cut) PMX, two-point (two cuts) PMX will select the partial section of the chromosome randomly for exchanging as Fig. 2. However, no matter which types of PMX methods is used, fixing the offspring chromosome is needed. For example, Fig. 2b shows that there will be several genes of the chromosome identical or repeatedly appeared after crossover. By establishing the relationship between the genes exchanged between chromosomes of parent, the exchanging relationship can be found such as 1-3-5 which means the replacing method to fix the repeated gene from original chromosome. At last, the

Yi and Kumar [18] developed genetic local search operators incorporating domain knowledge into a genetic algorithm which would almost lead fitness to the best answer. However, they mentioned that additional local search operators can decrease the efficiency of evolution algorithm. In addition, fast convergence speed usually does not lead to the best answer. In other words, the disadvantage of local search is the quick premature convergence of population. Although evolution algorithm is recognized as a powerful and heuristic algorithm, efficiency is still an important issue.

2.2 Problem Statement

When disasters occur, suppose the rescuing processes are held by an emergency center, or a rescuing center, the two main goals are to rescue the injured persons and deliver the relief materials. Here, we focus on the process of relief materials

Fig. 2 Example of two-point PMX **a** Select a section randomly to be exchanged. **b** Exchange the section to the offspring. **c** Establish the relationship. **d** Correct the reminders of the offspring



delivering. In general, there are several stages in relief materials delivering, such as information gathering, relief planning, rescuing resource gathering, and rescuing process. Suppose there are multiple disaster points and one supply point. All relief materials are collected in one supply point for delivering to the disaster points.

The highlighted problem here is to determine the exact number and the routing schedule of all vehicles from the supply point to all disaster points within their limited time periods. Suppose that the set of the disaster points P can be denoted as $P = \{p_i \mid 1 \leq i \leq \gamma\}$ where γ indicates the total number of disaster points. The location of each disaster point can be represented as $p_i = (x_i, y_i)$. Then, the distance between two disaster points p_i and p_j can be denoted as $dist_{i,j}(p_i, p_j)$. Since the relief materials should be delivered within their time period, the successful delivering can be evaluated by the following equation.

$$\begin{aligned}
 f(s) &= \sum_{i=1}^r x_i && \text{and} \\
 x_i &= \begin{cases} 0 & rcvt_i \leq \text{exp } t_i \\ rcvt_i - \text{exp } t_i & \text{otherwise} \end{cases} && (1)
 \end{aligned}$$

where $rcvt_i$ indicates the practical receiving time of i th disaster point and $\text{exp } t_i$ is the expiration time of the i th disaster point. In other words, the objective is to minimize the $f(s)$. If the velocities of the vehicles are the same, then the total practical receiving time can be calculated according to the total distance of delivering. In other words, since the objective described here is a small-the-best objective, the objective function of the emergency problem can be reduced as the traveling salesman problem.

3 Proposed System

To solve the emergency logistic problem, some steps of evolution algorithm for optimal solution searching are improved. The flowchart of the proposed evolution algorithm with feedback control algorithm is shown as Fig. 3.

The feedback control is added and provides the probabilities for activating different types of crossover methods based on cloud virtual machine. The value of probability controls the amount of virtual machines with the specific crossover procedure activated. The feedback control algorithm evaluates the probability value according to the function as follows:

$$C_k = \frac{|ch_k|}{|\text{Total Individuals}|} \tag{2}$$

where ch_k indicates the survived chromosome created by the k th type of crossover method. In other words, the crossover method with better performance (high survival rate) may be further executed according to the probability C_k . In

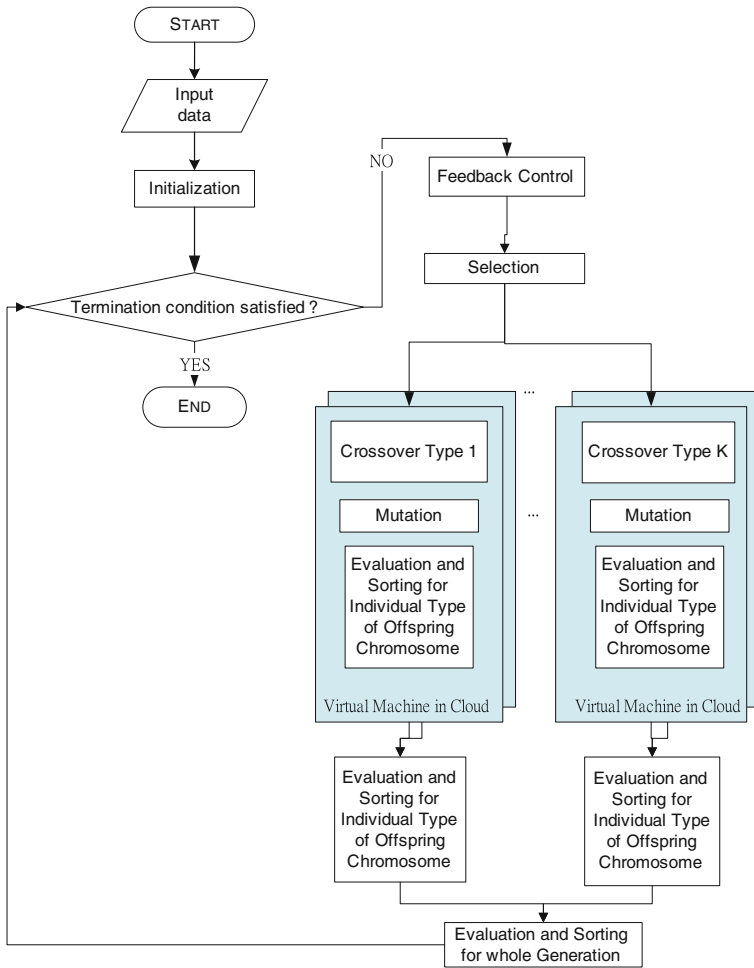


Fig. 3 The flowchart of the proposed system

the beginning, the value of C_k is set zero at the first generation of evolution algorithm. The total number of offspring chromosome can be averagely created from each crossover method according to the crossover rate, $\beta\%$ ($<100\%$). In other words, there will be at most $\beta\%$ offspring chromosome survived in the beginning of the every next generation or each new generation. In addition, the total percentage of offspring chromosome from the k th type of crossover method will be set as $\beta/k\%$.

However, due to the fitness result and the total amount of survived offspring chromosome in the next generation, the probability value, C_k , to active the k th type of crossover method may be changed. Therefore, the probability of crossover

method with better performance (high survival rate) for further executing will be dynamically changed during each generation. Then, according to the probability value C_k , the proposed system can further execute the k th type of crossover method once. In other words, the k th type of crossover method may be executed once or twice. Since the total percentage of offspring chromosome from the k th type of crossover method is already set as β/k %, the total amount of offspring chromosome may be $2\beta/k$ % if the crossover method is executed twice. Therefore, the fitness and competition in the k th type of crossover method will be needed. Only the total 1/2 amount of the offspring chromosome from the best can be reserved and passed for sorting of whole population.

4 Simulation Result

To verify the proposed algorithm, benchmark: kroA200 type TSP problem: 200-city problem A is used. The population size is 100. Crossover rate is set to 0.8 (80 %), and mutation rate is 0.01. According to the experimental results shown in Fig. 4, the objective value of shortest routing path can be reduced more quickly. Comparing with one point (one cut) PMX and two-point (two cuts) PMX, the hybrid crossover method based on the feedback control algorithm can converge more quickly and about 28–30 % faster than other two types of crossover procedure.

Furthermore, the total times of crossover method executed including the further execution according to the probability C_k can be only 72–74 % (after 30000 generations). In other words, during the optimal solution searching, the computing workload of evaluation and sorting can be reduced if the temporary optimal solutions between three different types of crossover methods are the same. In other word the total summation of three different types crossover methods can be shown as Fig. 5. Figure 5 presents the division result of single crossover method and the proposed system according to follows:

$$R = \frac{\sum \text{Times of Single Crossover Method executed}}{\sum \text{Times of Proposed Hybrid Crossover Method executed}}$$

The value R can be presented in Fig. 6. If the value R closes to 1, it means the total times of crossover method between single one or two points and the proposed hybrid method are more the same. In other words, the value should close to 1 as near as possible. The trend line shows that the division value tends to value 1.

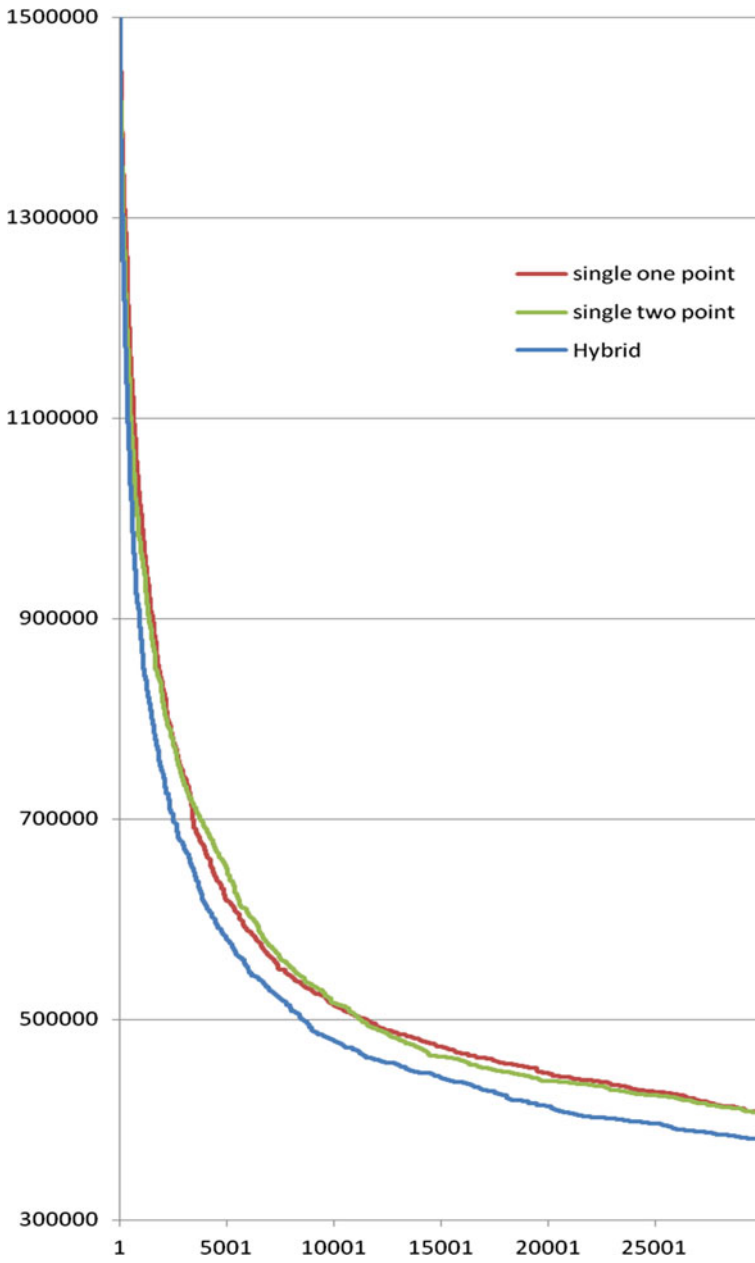


Fig. 4 The convergency trend of three different crossover method

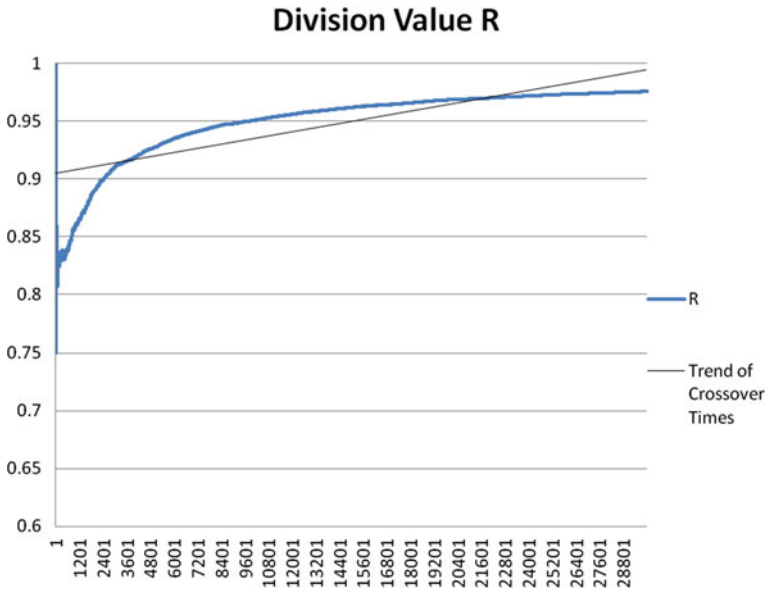


Fig. 5 The division result of single crossover method and the proposed system

5 Conclusion

In this paper, we develop a Cloud Feedback Assistance Based Hybrid Evolution Algorithm for Optimal Data Solution to solve the emergency logistic problem. Via the proposed feedback control algorithm, the whole convergence process can be enhanced more efficiently and effectively. The suitable crossover procedure which can obtain the better results can be further adopted according the evaluation result of feedback control algorithm. In addition, the total times of crossover and evaluation between different crossover procedures can be still under controlled.

References

1. Eksioglu B, Vural AV, Reisman A (2009) The vehicle routing problem: a taxonomic review. *Comput Ind Eng* 57:1472–1483
2. Golden BL, Assad A (1988) *Vehicle routing: methods and studies*. Elsevier Science Publishing Company, Amsterdam
3. Toth P, Vigo D (2001) *The vehicle routing problem*. Society for Industrial and Applied Mathematics, Philadelphia
4. Jian MS et al (2009) Life-Cycle and Viability based Paramecium-Imitated Evolutionary Algorithm. *WSEAS Trans Comput* 8(8)
5. Özdamar L, Ekinci E, Küçükyazici B (2004) Emergency logistics planning in natural disasters. *Ann Oper Res* 129:217–245

6. Sheu J (2007) An emergency logistics distribution approach for quick response to urgent relief demand in disasters. *Transport Res E: Logist Transport Rev* 43:687–709
7. Castro J (2003) Solving difficult multicommodity problems with a specialized interior-point algorithm. *Ann Oper Res* 124:35–48
8. Chiu Y, Zheng H (2007) Real-time mobilization decisions for multi-priority emergency response resources and evacuation groups: Model formulation and solution. *Transport Res E: Logist Transport Rev* 43:710–736
9. Haghani, Oh S (1996) Formulation and solution of a multi-commodity, multi-modal network flow model for disaster relief operations. *Transport Res A: Pol Pract* 30:231–250
10. Yan S, Shih Y (2009) Optimal scheduling of emergency roadway repair and subsequent relief distribution. *Comput Oper Res* 36:2049–2065
11. Yi W, Özdamar L (2007) A dynamic logistics coordination model for evacuation and support in disaster response activities. *Eur J Oper Res* 179:1177–1193
12. Yuan Y, Wang D (2009) Path selection model and algorithm for emergency logistics management. *Comput Ind Eng* 56:1081–1094
13. Zografos KG et al (2002) A real-time decision support system for roadway network incident response logistics. *Transport Res C: Emerg Technol* 10:1–18
14. Kanoh H, Hara K (2008) Hybrid genetic algorithm for dynamic multi-objective route planning with predicted traffic in a real-world road network. In: *Proceedings of the 10th annual conference on genetic and evolutionary computation, GECCO 2008*, pp 657–664
15. Fan HM, Zhao T, Zhao XY, Jang MB, Dong GS (2008) Research on emergency relief goods distribution after regional natural disaster occurring. In: *International conference on information management, innovation management and industrial engineering, ICIII '08*, vol 3 (3), pp 156–161
16. Peng JZ, Xu WS, Yang JJ (2009) A hybrid heuristic algorithm for large scale emergency logistics. In: *Second international conference on intelligent computation technology and automation, ICICTA '09*, vol 3 (3) pp 899–902
17. Yang L, Jones BF, Yang S (2007) A fuzzy multi-objective programming for optimization of fire station locations through genetic algorithms. *Eur J Oper Res* 181:903–915
18. Yi W, Kumar A (2007) Ant colony optimization for disaster relief operations. *Transport Res E: Logist Transport Rev* 43:660–672
19. Hu Z (2009) A network for emergency logistics management inspired by immune multi-affinity model In: *International conference on information management, innovation management and industrial engineering*, vol 4 (4) pp 22–25
20. Ozdamar L, Yi W (2008) Greedy neighborhood search for disaster relief and evacuation logistics. *Intell Sys IEEE* 23(23):14–23
21. Reyes PM (2005) Logistics networks: a game theory application for solving the transshipment problem. *Appl Math Comp* 168:1419–1431
22. Tzeng G, Cheng H, Huang TD (2007) Multi-objective optimal planning for designing relief delivery systems. *Transport Res E: Logist Transport Rev* 43:673–686
23. Sheu J (2010) Dynamic relief-demand management for emergency logistics operations under large-scale disasters. *Transport Res E: Logist Transport Rev* 46:1–17
24. Christensen JH (2009) Using RESTful web-services and cloud computing to create next generation mobile applications. In: *OOPSLA 2009*, pp 627–633

Molecular Simulation Methods for Selecting Thrombin-Binding Aptamers

Jangam Vikram Kumar, Wen-Yih Chen, Jeffrey J. P. Tsai
and Wen-Pin Hu

Abstract To study and compare the simulation methods on the different scoring functions to analyze the consistency of the Docking score between the aptamers and protein. Thrombin is well characterized and has been studied with the thrombin binding aptamer (TBA) and mutated TBA sequences in a previous report, which finds three representative aptamers have best, medium, and worst binding interactions with thrombin. Discovery Studio 3.5 is a useful modeling and simulation software. The ZDOCK in this package incorporates a simple and novel scoring function: Pairwise Shape Complementarity. By using ZDOCK, we also can evaluate the differences in the binding ability between the interactions of the thrombin and aptamers. Basically, our results are consistent with the previous report. From this study, we make sure that the ZDOCK can provide reliable results and able to be used as an alternative method in performing *in silico* selection of aptamer.

Keywords Molecular simulation · Aptamers · Pairwise shape complementarity · Thrombin · Selection

J. V. Kumar · J. J. P. Tsai · W.-P. Hu (✉)

Department of Biomedical Informatics, Asia University, 41354 Taichung City, Taiwan
e-mail: wenpinhu@asia.edu.tw

J. V. Kumar
e-mail: vikramkumar.bioinf@gmail.com

J. J. P. Tsai
e-mail: president@asia.edu.tw

W.-Y. Chen
Department of Chemical and Materials Engineering, National Central University, 32001
Jhong-Li City, Taiwan
e-mail: wychen@ncu.edu.tw

1 Introduction

The protein-protein docking problem has interested biophysicists and computational biologists for decades, since it is important to the computational determination of 3D structure assemblies as well as drug design.

Computational approaches are usually applied to identify candidate compounds for new drugs using information obtained from the target structure to identify lead compounds with low time and cost [1].

A number of algorithms have been developed to address the initial stage of unbound protein-protein docking, such as FTDock, DOT, and GRAMM [2–5]. Accelrys Discovery Studio® (DS) software provides comprehensive modeling and simulation capabilities for computational chemists, computational biologists, and other scientists engaged in small molecule and biotherapeutics-based research. The latest version 3.5 is a comprehensive portfolio of small molecule drug design and market-leading biological simulation tools.

DS protein docking predicts protein-protein structure interactions of novel targets rapidly and accurately by performing rigid body docking with the well-published ZDOCK algorithm [6, 7]. ZDOCK algorithm employs an FFT-based method using a Pairwise Shape Complementarity (PSC) function for identifying docked conformations and scores hits based on atomic contact energies.

ZDOCK is a rigid-body docking program that requires minimal information about the binding site and is targeted at initial-stage unbound docking. The program uses individual protein structures determined by experimental or computational methods as inputs and predicts the structure of a number of protein complexes (i.e., the top 2000 complexes). ZDOCK uses a simple shape complementarity method called PSC. The PSC method is optionally augmented with desolvation (DE) and electrostatic (ELEC) energy terms to rank the docked poses [8]. PSC is not based explicitly on protein surface curvature or surface area, but rather rewards all close atomic contacts between the protein receptor and the protein ligand within a specific cutoff distance.

However, there are several issues when dealing with protein-protein docking—the large size of the system, the conformation changes of the proteins upon binding, and the availability of the individual 3D structures, or lack thereof. The large system size makes sampling conformational space prohibitively expensive, so to reduce the search space, fast Fourier transform (FFT) methods, geometric hashing, and bit mapping, are used to speed up calculations [9]. ZDOCK is a kind of initial stage algorithm for studying molecular interactions [8]. In the initial stage, the protein receptor and protein ligand are treated as rigid bodies and all six rotational and translational degrees of freedom are fully explored with scoring functions that are tolerant to conformational changes, also known as soft docking functions.

Fifteen-mer TBA that binds to thrombin was selected as a model, as it had been well characterized. Its structure has been determined [10]. The TBA and three other mutated oligonucleotides, selected on the basis of their binding score (best,

medium, worst) were collected [11]. In this study, the TBA and three mutated oligonucleotides were sketched in discovery studio and simulations were performed with thrombin to evaluate the potential of using ZDOCK for selecting aptamers by utilizing and comparing with the data confirmed by simulation and experimental approaches [11]. Even though the method used for simulation is different to previous report, we compared the results of binding affinity in selection of aptamers.

2 Materials and Methods

The DNA aptamers collected from a literature were designed using Discovery studio, and this single software package was used as a platform for simulations. All the computational experiments were performed using Pentium(R) Dual-Core CPU, 3.20 GHz with RAM of 4 GB supported by Windows 7 Professional OS.

2.1 Setting up Aptamers

Fifteen-mer TBA and other 3' mutated oligonucleotide sequences are collected from a literature [11], which have the binding ability to thrombin. The sequences for TBA and other three mutated oligonucleotides are:

- TBA: 5'-GGT TGG TGT GGT TGG-3'
- “Best” aptamer: 5'-GGT TTG TGT GGT TAG-3'
- “Medium” aptamer: 5'-GGC TGG TGT GAT TGG-3'
- “Worst” aptamer: 5'-GGT AGG TGT GGT TGC-3'

The 15-mer TBA along with best, medium and worst binding score sequences were drawn as a single strand in α -helix conformation by Discovery Studio 3.5 with the options for building and editing nucleic acid tools. The molecular weights of the constructed molecules were also taken into consideration.

2.2 Setting up a ZDOCK Run

The aptamer-thrombin complex NMR structure (PDB code, 1HAO), in which the 15-mer TBA was present was downloaded from PDB. It was taken on to the platform of Discovery Studio. Water molecules along with nucleotide sequence were removed from the protein (1HAO) (Fig. 1).

ZDOCK which is a rigid-body protein-protein docking algorithm based on the fast Fourier transform correlation technique that is used to explore the rotational

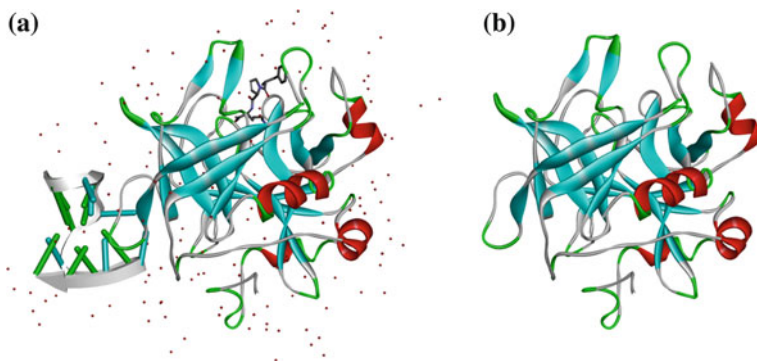


Fig. 1 **a** The 1HAO which was downloaded from PDB and was prepared for simulation by cleaning it. The red dots are water molecules. The ligand and nucleotide group present in the 1HAO are removed and resulted as **(b)**

and translational space of a protein-protein system is taken into account, with the cleaned thrombin along with TBA.

In ZDOCK, the angular step size for rotational sampling of ligand orientations was kept to 6 degrees which performs finer conformational sampling and thus typically results in more accurate predictions. The tools in the RMSD group are used to calculate the RMSD between different docked poses or between docked poses and an experimental structure. The RMSD cutoff and interface cutoff were set to 10 Å. The same ZDOCK procedure was followed for the other three mutated oligonucleotides with thrombin individually to compare the consistency of the docking results with other researchers [11].

3 Results and Discussions

The complex NMR structure of thrombin was downloaded from PDB (PDB Code: 1HAO). With the resources of Discovery Studio 3.5, 15-mer TBA along with other three mutated aptamer sequences reported in literature were drawn in single strand, α -helix conformation. There was a consistency between the molecular weight obtained by sketching with Discovery Studio and the molecular weights of the oligonucleotides drawn with Hyperchem 7.5 [12] (Fig. 2).

ZDOCK was performed for protein docking to analyze docked poses. For computing thrombin with worst sequence it took 9 h and 33 min for computing, 9 h and 17 min for medium sequence, 8 h and 38 min for best sequence and 9 h and 14 min for 15-mer TBA. The ZDOCK scores for the computed aptamers were in the range of 21.76–23.48.

The top poses are reported with the poses clustered into groups according to their spatial proximity (Fig. 3) and poses are ranked according to the ZDOCK scores. Top poses are determined by the PSC scoring function used in the

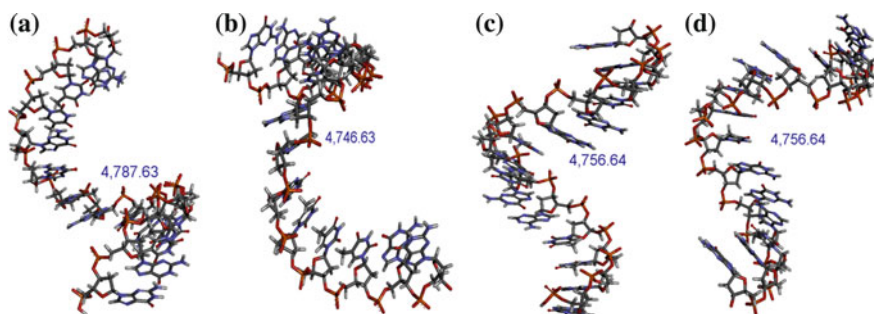


Fig. 2 The oligonucleotide sequences sketched using Discovery Studio 3.5. The molecular weights are mentioned along with the structure **a** TBA structure. **b** The “Best” mutated TBA sequence. **c** The “Medium” mutated TBA sequence. **d** The “Worst” mutated TBA Sequence

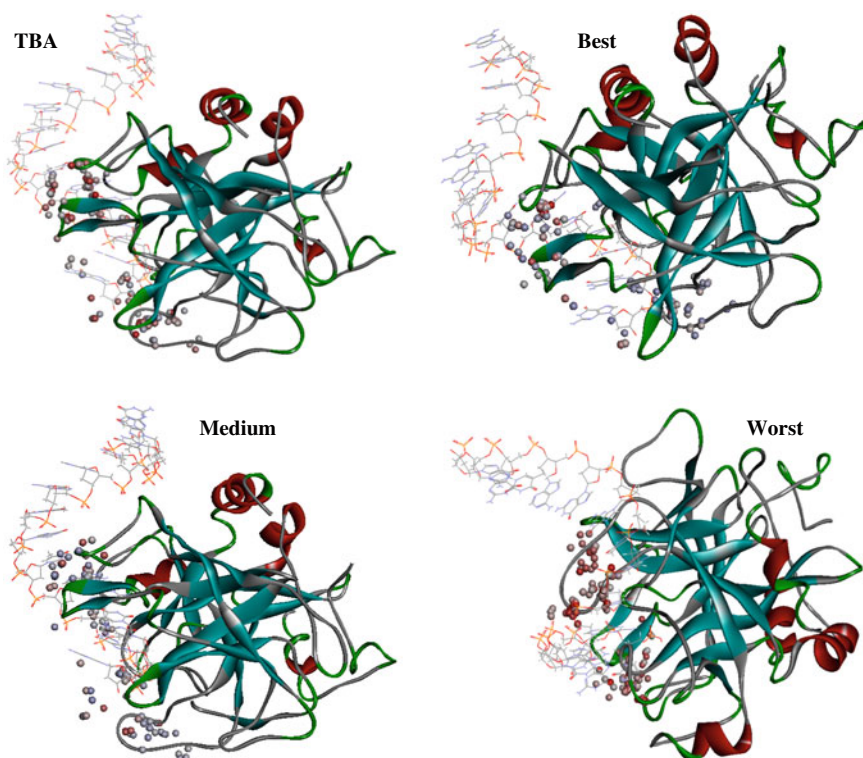


Fig. 3 The input structures of ligand and receptor protein are shown after the docking Except for the thrombin and aptamer are shown in the figure, the dots with different colors around the protein are the poses. Red color dots in these figures indicate better poses. These dots in the figures are the top poses in large clusters for the aptamers

Table 1 The simulation results obtained from the ZDOCK used in this study and shapegauss [11] as scoring function

Name	ZDOCK		Shapegauss scoring function	
	Cluster size	ZDOCK score	Score for heparin-binding exosite	Score for fibrinogen-binding exosite
TBA	156	22.48	−982	−1422
Best	155	23.46	−1364	−1748
Medium	148	22.98	−1256	−1209
Worst	91	21.76	−404	−667

protocols. The information about cluster, cluster size and density are also given in the end of simulation. The meanings of these three values are: Cluster—contains the cluster group number for each pose; Cluster Size—reports the size (number of poses) of a cluster; Density—represents the number of neighboring poses within the Clustering | RMSD Cutoff distance.

Each pose has its ZDOCK score (calculated by PSC scoring function), and pose 1 has the highest (best) ZDOCK score. The ZDOCK Score 23.46 was highest for the “Best” sequence, and the next best was TBA with a score of 22.48. The ZDOCK score for “medium” and “worst” oligonucleotides were 22.98 and 21.76, respectively.

The dock results of thrombin with TBA and mutated TBA obtained from previous report were from shapegauss scoring function with fast rigid exhaustive docking (FRED) by using the protein-ligand docking program called as OpenEye. In the OpenEye software, a specific binding site can be chosen for performing docking simulation. Both heparin-binding exosite and fibrinogen-binding exosite are studied in the previous study [11], and different binding scores are obtained in these two exosites. In this study, we are not able to choose any specific binding site for docking by using the ZDOCK method. However, ZDOCK method calculates many possible interaction poses between the aptamer and thrombin. The pose with the highest ZDOCK score in each simulation means this pose is the best pose for the aptamer and thrombin. In comparison, the “Best” aptamer could get highest binding scores no matter what kinds of methods were used or binding exosites were selected (shown in Table 1). Besides, “Worst” aptamer got the least binding scores in both methods. Concerning about the ranking for these four aptamer sequences in the simulation, our results with ZDOCK were consistent to the results obtained by shapegauss scoring function in heparin-binding exosite. According to these results, the ZDOCK method shows its potential of using in the selection of aptamer, which is demonstrated by utilizing the well characterized aptamers and Thrombin.

4 Conclusions

We performed ZDOCK to analyze the interaction between human alpha-thrombin and its best aptamer along with medium and worst binding ability oligonucleotides, based on the findings obtained from other researchers. This simulation

approach has the potential to select best aptamers in a competition. Our docking results were compared with the results which were obtained from OpenEye software by other researchers. The comparative results showed that there is a consistency in results between these simulation methods. In this study, we evidences that the ZDOCK method also can be used in the computational selection of aptamer. Besides, the whole simulation procedures in our study are finished with single software package.

Acknowledgments The authors gratefully acknowledge the financial support provided by Asia University (Taiwan) under contract number 101-asia-23.

References

1. Brown CJ, Dastidar SG, See HY, Coomber DW, Ortiz-Lombardia M, Verma C, Lane DP (2010) Rational design and biophysical characterization of thioredoxin-based aptamers: insights into peptide grafting. *J Mol Biol* 395:871–883
2. Gabb HA, Jackson RM, Sternberg MJE (1997) Modeling protein docking using shape complementarity, electrostatics and biochemical information. *J Molec Bio* 272:106–120
3. Mandell JG, Roberts VA, Pique ME, Kotlovyy V, Mitchell JC, Nelson E, Tsigelny I, Ten Eyck LF (2001) Protein docking using continuum electrostatics and geometric fit. *Prot Eng* 14:105–113
4. Vakser IA (1997) Evaluation of GRAMM low-resolution docking methodology on the hemagglutinin-antibody complex. *Proteins* 31:226–230
5. Chen R, Mintseris J, Janin J, Weng Z (2003) A protein-protein docking benchmark. *Proteins* 52:88–91
6. Pierce B, Weng Z (2008) A combination of rescoring and refinement significantly improves protein docking performance. *Proteins* 72:270–279
7. Chen R, Weng Z (2003) ZDOCK: an Initial-stage protein-docking algorithm. *Proteins* 52:80–87
8. Chen R, Weng Z (2003) A novel shape complementarity scoring function for protein-protein docking. *Proteins* 51:397–408
9. Vajda S, Camacho CJ (2004) Protein-protein docking: is the glass half-full or half-empty? *Trends Biotech* 22:110–116
10. Macaya RF, Schultze P, Smith FW, Roe JA, Feigon J (1993) Thrombin-binding DNA aptamer forms a unimolecular quadruplex structure in solution. *Proc Natl Acad Sci USA* 90:3745–3749
11. Bini A, Mascini M, Mascini M, Turner AP (2011) Selection of thrombin-binding aptamers by using computational approach for aptasensor application. *Biosens Bioelectron* 26:4411–4416

An Efficient Group Key Management Scheme for Web-Based Collaborative Systems

Yung-Feng Lu, Rong-Sheng Wang and Shih-Chun Chou

Abstract Web 2.0 describes a collection of web-based technologies which share a user-focused approach to design and functionality. Under the supporting of Web 2.0 technologies (e.g., HTML5), there are many applications, e.g., seamless reader over equipment, collaborative editing with multiple members, portable multimedia over devices, on browsers become feasible. In one of our previous works, we proposed a two-factor authentication with key agreement scheme for web-based collaborative systems. This paper further extends it to have secure group communication for web-based collaborative systems. With the proposed mechanism, members of the collaborative work could be share their messages easily and co-work securely. In order to provide high efficiency and data confidentiality, this paper presents an efficient group key agreement scheme for group members. The group members can join/leave the group easily.

Keywords Web-based applications · Collaborative systems · Key management

1 Introduction

New technologies such as DHTML, Adobe Flex, Ajax, and HTML5 [1], have witnessed the emergence and rapid development of many Web-based applications. This type of Web-based applications have the benefits of wide accessibility,

Y.-F. Lu (✉)

Department of Computer Science and Information Engineering, National Taichung University of Science and Technology, Taichung, Taiwan
e-mail: yflu@nutc.edu.tw

R.-S. Wang · S.-C. Chou

Innovative Digttech-Enabled Application and Services Institute,
Institute for Information Industry, Taipei, Taiwan
e-mail: benchou@iii.org.tw

platform independence, no installation or upgrading, rich user experience, dynamic content, high scalability easy-to-share, and easy-to-use. HTML5 is the next generation markup language for structuring and presenting content for the World Wide Web, many new features are supported to explore multimedia and to interact with user on a browser. Using HTML5 could create richer user experiences in a standardized way; web applications have seen increased usage where they are more favorable than desktop applications. The rise in the prevalence of HTML5 can be attributed to their flexibility, which enables web-based application designers to go beyond the limitation of conventional desktop applications. Under the supporting of HTML5, there are many applications, e.g., seamless reader over equipments, collaborative editing [2, 3] with multiple members, portable multimedia over devices, on browsers become feasible.

To have good access control, many excellent authentication mechanisms, e.g., password authentication [4], ID-based authentication [5, 6], were developed. In our previous work, we proposed a two-factor authentication with key agreement scheme for web-based collaborative systems. This approach integrates URI fragment identifier with secure email token and identity-based remote mutual authentication scheme on ECC. However, it did not provide a feasible group key management while a set of group members might changes.

In this paper, we are interested in the providing of secure group communication for web-based collaborative systems. With the proposed mechanism, members of the collaborative work could be share their messages easily and co-work securely. In order to provide high efficiency and data confidentiality, we proposed a group key management that inspired by [7] and integrate it with our previous work [8].

The rest of this paper is organized as follows: [Section 2](#) summaries bilinear Diffie-Hellman problem, scenario, and the system setup. [Section 3](#) presents an ID-based group key management scheme of web-based collaborative systems. [Section 4](#) provides a brief analysis. [Section 5](#) is the conclusion.

2 Preliminaries

2.1 Bilinear Diffie-Hellman Problem

Many researchers have been proposed excellent identity-based cryptography schemes. To hold the computationally efficient, many of them are based on mathematical functions called bilinear non-degenerate maps. A bilinear non-degenerate map is a function pairing elements from one cyclic group to another of the same prime order, where the discrete log problem is hard in the first group [9]. The security of identity-based cryptography is based on the assumption that the particular bilinear maps chosen are one-way functions. Thus, it is easy to calculate the result from a given a pair of operands, but hard to calculate the inverse.

This property is the Bilinear Diffie-Hellman Assumption, since the Bilinear Diffie-Hellman problem is reducible to the discrete-log or inverse operation for these bilinear maps [10]. In simplified notation, a bilinear map is a pairing that has the property:

$$Pair(a \cdot X, b \cdot Y) = Pair(b \cdot X, a \cdot Y)$$

In several mechanisms, the the \bullet operator above refers to multiplication of a point on an elliptic curve by integers [11].

2.2 Scenario

This paper is an extension of our previous work [8]. As shown in Fig. 1, a member can join a collaborative editing after a strong mutual authentication process. Each member wish to join the joint work, he must pass the mutual authentication process. After this process, the collaborative server and he will keep a session authentication key. Since this scheme did not provide a feasible group key management while a set of group members might changes, we need further extend it to have a group key agreement for secure group collaboration.

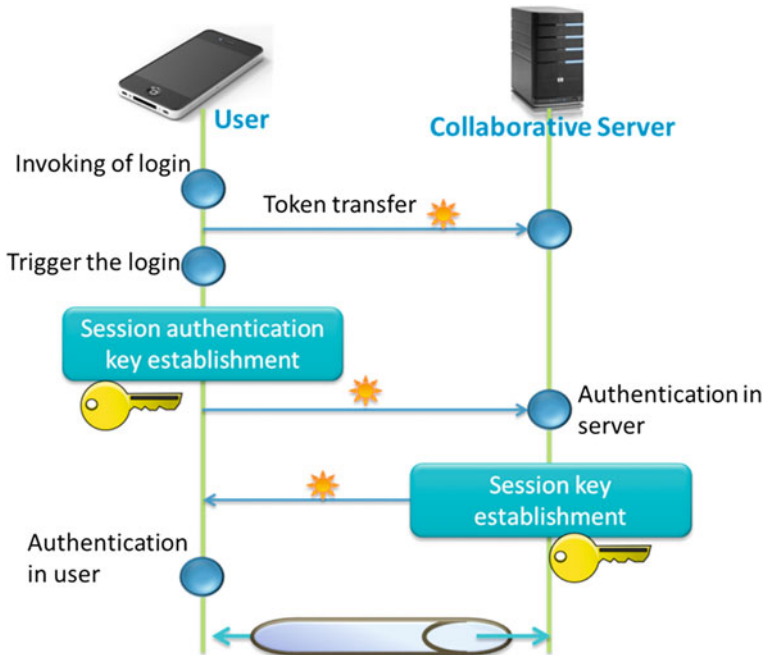


Fig. 1 The overview of a session authentication key establishment process that proposed in [8]

2.3 System Setup

We assume a trusted collaborative server U_1 is responsible for private key generation for members in the system. The collaborative server selects two groups $G1$ and $G2$ of order q for some large prime q .

A bilinear mapping $\hat{e}: G1 \times G1 \rightarrow G2$ maps a pair from $G1$ to $G2$. The bilinear mapping satisfies the following properties:

- Bilinear: $\hat{e}: G1 \times G1 \rightarrow G2$ is bilinear if $\hat{e}(aP, bQ)^{ab}$ for all $P, Q \in G1$ and all $a, b \in \mathbb{Z}$.
- Non-degenerate: There exists a pair $P, Q \in G1$ such that $\hat{e}(P, Q) \neq 1$.
- Computable: An efficient algorithm to compute $\hat{e}(P, Q)$ exists for any $P, Q \in G1$.

A generator $P \in G1$ and a master secret $s \in \mathbb{Z}^*_q$ are also randomly chosen by the collaborative server. The server computes a public value $P_{pub} = sP$, and publishes the public parameters $\langle q, G1, G2, \hat{e}, P, P_{pub}, H1 \rangle$ to all members in the system, where $H1$ is a hash function. The private key generated by the server for a member with identity ID_i is $sH_1(ID_i)$. In the system, we assume the hardness of bilinear Diffie-Hellman problem:

Given $\langle P, aP, bP, cP \rangle$ for some $a, b, c \in \mathbb{Z}^*_q$, to compute $W = \hat{e}(P, P)^{abc} \in G2$.

A number of notations used in this work are listed in Table 1.

3 The ID-based Group Key Agreement Scheme with the Collaborative Server

3.1 The ID-based Group Key Agreement

Suppose the collaborative server U_1 , that initiates the protocol, knows a set of members U_2, U_3, \dots, U_n and wants to have a private session for a joint work with them. Since the collaborative server has been done a mutual authentication with all

Table 1 Notations and Abbreviations

U_i	The i^{th} member
ID_i	ID of member U_i
U_1	The first member, in this work is the collaborative server
$E_i(*)$	Encryption with the session authentication key SK_i of U_i
$E_k(*)$	Symmetric encryption with K
Nym_i	Pseudonym for member U_i
r_i	Random number selected by U_i
Sig_i	Signature computed over the corresponding message by U_i
h	A hash function mapping from $G2 \times G1 \rightarrow \{0, 1\}^k$, where k is the security parameter

members, she knows all members' session authentication key, i.e. SK_i , she knows all the members' identities as well. So she starts the session in the following steps:

- (1) The collaborative server as the session initiator chooses a pseudonyms Nym_i for member U_i and a random number r_1 . Then, the collaborative server encrypts a concatenation of all members' identities and pseudonyms with their session authentication keys, i.e., SK_i , respectively. At the end, she sends each member the following request:

$$U_1 \rightarrow U_i : E_i(ID_i || ID_1 || \dots || ID_n || Nym_1 || Nym_2 || \dots || Nym_n || Sig_1), r_1 P$$

The signature Sig_1 is computed over the respective message by the collaborative server with its private key.

- (2) After member U_i , ($i \neq 1$) receives the request from the collaborative server, he does a series decryption trial using his session authentication key to check if he is one of the members requested by the collaborative server. If he successfully decrypts this cipher text and finds out his identity is in the ID list, then he looks for his Nym_i and sends the following message to U_{i-1} and U_{i+1} :

$$U_i \rightarrow U_{i-1}, U_{i+1} : Nym_i, r_i P$$

where r_i is a random number chosen by member U_i .

- (3) When U_i receives the above messages from U_{i-1} and U_{i+1} , he first verifies that these are U_{i-1} and U_{i+1} 's pseudonyms according to the pseudonym list he decrypted in message of step (1). If the verification is successful, he calculates two keys using his private key $sH_1(ID_i)$ as follows:

$$k_i = h(\hat{e}(H_1(ID_{i+1}), sH_1(ID_i)) || r_i r_{i+1} P)$$

$$k_{i-1} = h(\hat{e}(H_1(ID_{i-1}), sH_1(ID_i)) || r_i r_{i-1} P)$$

Then U_i computes $X_i = k_i / k_{i-1}$ and broadcast the following message to all the other members:

$$U_i \rightarrow * : Nym_i, X_i$$

Otherwise, he just ignores the message.

- (4) U_i waits until he receives all $X_{j(j \neq i)}$, and checks the pseudonyms $Nym_{j(j \neq i)}$ are valid. After that, he computes

$$k_{i+1} = k_i X_{i+1}, k_{i+2} = k_{i+1} X_{i+2}, \dots, k_{i+n-1} = k_{i+n-2} X_{i+n-1}$$

Then U_i computes the group session key as $K = H(k_1 || k_2 || \dots || k_n)$, where H is defined from $\{0, 1\}^*$ to $\{0, 1\}^k$. After computing the session group key K , $U_{i(i \neq 1)}$ sends $K = H(K || ID_1 || ID_2 || \dots || ID_n)$ to the collaborative server, Then the collaborative server verifies whether all the other group members computed the same key or not.

3.2 Group Member Join

Suppose the collaborative server U_1 , and members U_2, \dots, U_n are having a private joint work. And the messages of this collaborative editing were protected via session group keys using the protocol described above. Assume U_1 , the collaborative server, wants another member U_{n+1} to join the collaborative editing. U_1 can start the group member joining process as follows:

- (1) The collaborative server (i.e., U_1) tells U_n and U_{n+1} about U'_{n+1} 's joining. He sends the following messages to U_n and U_{n+1} respectively:

$$U_1 \rightarrow U_n : E_n(ID_{n+1} || Nym_{n+1} || Sig_1),$$

$$U_1 \rightarrow U_{n+1} : E_{n+1}(ID_1 || Nym_1 || r_1 P || ID_n || Nym_n || r_n P || ID_{n+1} || Nym_{n+1} || Sig_1)$$

- (2) After U_{n+1} receives the invitation from U_1 , he decrypts the message using his session authentication key SK_{n+1} to retrieve his pseudonym selected by U_1 . After that, he chooses a random number r_{n+1} , and computes

$$k_{n+1} = h(\hat{e}(H_1(ID_1), sH_1(ID_{n+1})) || r_{n+1} r_1 P),$$

$$k'_n = h(\hat{e}(H_1(ID_n), sH_1(ID_{n+1})) || r_{n+1} r_n P)$$

He calculates $X_{n+1} = k_{n+1}/k'_n$ and sends the following message to both U_1 and U_n :

$$U_{n+1} \rightarrow U_1, U_n : Nym_{n+1}, r_{n+1} P, X_{n+1}$$

- (3) After U_1 and U_n receives the above message from U_{n+1} , they can compute

$$k_{n+1} = h(\hat{e}(H_1(ID_{n+1}), sH_1(ID_1)) || r_1 r_{n+1} P),$$

$$k'_n = h(\hat{e}(H_1(ID_{n+1}), sH_1(ID_n)) || r_n r_{n+1} P)$$

Then, they compute $X'_1 = k_1/k_{n+1}$ and $X'_n = k'_n/k_{n-1}$.

U_n sends X'_n to

$$U_1 : U_n \rightarrow U_1 : X'_n$$

and U_1 sends the following message to U_{n+1} :

$$U_1 \rightarrow U_{n+1} : E_{n+1}(X'_1 || X_2 || \dots || X_{n-1} || X'_n)$$

Then, U_1 also broadcast the following message to all other members:

$$U_1 \rightarrow * : E_K(X'_1 || X_{n+1} || X'_n || Sig_1).$$

3.3 Group Member Leave

Now we discuss how to deal with group member leaving. If a group member leaves the private collaborative editing, and he should not access the conference content after that, then the group key should be updated accordingly.

Assume a member U_i is leaving the group and the group key should be updated for the remaining $n - 1$ members. The protocol runs as follows to update the group key:

- (1) The collaborative server U_1 informs U_{n-1} and U_{n+1} that U_i is leaving, and they should recomputed their k_{i-1} and k_i respectively.

$$\begin{aligned}
 U_1 &\rightarrow U_{i-1}, U_{i+1} : E_K(ID_i || Nym_i || Leave || Sig_1), \\
 U_1 &\rightarrow U_{i-1} : E_{i-1} \left(ID_i || Nym_i || ID_{i-1} || Nym'_{i-1} || ID_{i+1} || Nym'_{i+1} || Sig_1 \right), \\
 U_1 &\rightarrow U_{i+1} : E_{i+1} \left(ID_i || Nym_i || ID_{i-1} || Nym'_{i-1} || ID_{i+1} || Nym'_{i+1} || Sig_1 \right)
 \end{aligned}$$

This message is encrypted with the old group key, and the message is signed by the collaborative server U_1 .

- (2) U_{i-1} and U_{i+1} receive the message from U_1 and verify the signature's validity. If the verification is successful, U_{i-1} and U_{i+1} exchange their random value r'_{i-1} and r'_{i+1} .

$$\begin{aligned}
 U_{i-1} &\rightarrow U_{i+1} : Nym'_{i-1}, r'_{i-1}P, \\
 U_{i+1} &\rightarrow U_{i-1} : Nym'_{i+1}, r'_{i+1}P
 \end{aligned}$$

Then they calculate the new k'_{i-1} and k'_{i+1} respectively:

$$\begin{aligned}
 k'_{i-1} &= h(\hat{e}(H_1(ID_{i+1}), sH_1(ID_{i-1})) || r'_{i-1}r'_{i+1}P), \\
 k'_i &= h(\hat{e}(H_1(ID_{i-1}), sH_1(ID_{i+1})) || r'_{i+1}r'_{i-1}P)
 \end{aligned}$$

In above equations, $k'_{i-1} = k'_i$ since U_i leaves the group.

- (3) Then they calculate $X'_{i-1} = k'_{i-1}/k'_{i-2}$, $X'_{i+1} = k_{i+1}/k'_i$, then they send X'_{i-1} and X'_{i+1} to U_1 .

$$\begin{aligned}
 U_{i-1} &\rightarrow U_1 : X'_{i-1}, \\
 U_{i+1} &\rightarrow U_1 : X'_{i+1}
 \end{aligned}$$

- (4) The collaborative server U_1 broadcasts X'_{i-1} and X'_{i+1} to all other members, and they compute the new group key.

$$U_1 \rightarrow * : E_K \left(U_i || U_{i-1} || U_{i+1} || X'_{i-1} || X'_{i+1} || Sig_1 \right)$$

The new group key is computed as $K' = H(k_1 || k_2 || \dots || k'_{i-1} || k'_{i+1} || \dots || k_n)$.

4 Discussion

In this section, we present a brief analysis on the security and privacy of the protocol. Specifically, we discuss the anonymity and group key secrecy of the protocol.

4.1 Anonymity

In the group key agreement protocol, the message firstly sent from the collaborative server is encrypted using the session authentication key of each member, and only the legitimate group members can decrypt this message and get the pseudonyms. Even though an outside attacker obtains all the pseudonyms from the transcript, the attacker cannot match them to the real identities of members unless he can decrypt the message using the session authentication key.

4.2 Group Key Secrecy

In the group key agreement protocol, the group key K is generated by concatenating all the k_i 's. Because the k_i 's are obtained sequentially with one k_i and all the other X_j , attackers should have at least one k_i to compute the session group key. However, when computing k_i , since it did not have ID_i and without the master secret key s , it is difficult to compute $k_i = h(\hat{e}(H_1(ID_{i+1}), sH_1(ID_i)) \| r_i r_{i+1} P)$. Therefore, the passive adversary cannot compute the group key K .

5 Conclusion and Future Work

This paper presents a study of the providing of secure group communication for web-based collaborative systems. With the proposed mechanism, members of the collaborative work could be share their messages easily and co-work securely. This paper is based on our previous work that have been provide strong mutual authentication to provide efficient and secure group communications. The proposed scheme achieves anonymity, group key secrecy for the group session key. It also supports dynamic membership, and group members can join/leave the group.

For future research, we shall further explore the security properties of the proposed mechanism. We shall also integrate the proposed scheme with ECC to provide stronger security. Some wireless communication technologies, e.g., NFC, would discuss to provide user flexibility.

Acknowledgments This study is conducted under the “Digital Convergence Service Open Platform” of the Institute for Information Industry which is subsidized by the Ministry of Economy Affairs of the Republic of China. This work was also supported by National Science Council, NSC101-2218-E-025-001.

References

1. Harjono J, Ng G, Kong D, Lo J (2010) building smarter web applications with html5. In: CASCON NJ, USA, p 402–403
2. Lu YF, Lin PH, Chou SC, Wang RS (2012) Multimedia support framework for distributed web-based collaborative editing. IEEE ISIC, In
3. Lautamaki J, Nieminen A, Koskinen J, Aho T, Mikkonen T, Englund M (2012) cored: browser-based collaborative real-time editor for java web applications. In: CSCW, New York, NY, USA, p 1307–1316
4. Yang Y, Zhou J, Wong JW, Bao F (2010) towards practical anonymous password authentication. In: ACMACSAC, New York, NY, USA, p 59–68
5. Yang JH, Chang CC (2009) An id-based remotemutual authentication with key agreement scheme for mobile devices on elliptic curve cryptosystem. *Comput Secur* 28(3–4):138–143
6. Kim HS, Lee SW, Yoo KY (2003) Id-based password authentication scheme using smart cards and fingerprints. *SIGOPS Oper Syst Rev.* 37(4):32–41
7. Wan Z, Ren K, Lou W, Preneel B (2008) Anonymous id-based group key agreement for wireless networks. *IEEE WCNC, Netw Track*, In
8. Lu YF, Lin PH, Ye SS, Wang RS, Chou SC (2012) A strong authentication with key agreement scheme for web-based collaborative systems. *IEEE ISPACS*, In
9. Bilinear Pairings <http://rooster.stanford.edu/~ben/math/ep/pairing.php>
10. Yacobi Yacov (2002) A note on the bi-linear diffie-hellman assumption. *Cryptology ePrint Archive*, Report
11. Identity-based-encryption <http://www.voltage.com/technology/ibe.htm>

The Diagnosis of Mental Stress by Using Data Mining Technologies

Hsiu-Sen Chiang, Liang-Chi Liu and Chien-Yuan Lai

Abstract In today's fast-paced and competitive environment, mental stress has become a part and parcel of our daily life. However, mental stress can have serious effects on both our psychological and physical health. People under long-term stress can cause mental disorders, and cardiovascular disease. Moreover, people often ignore the symptoms of stress from their own bodies. Therefore, many chronic disease and mental illness are more and more serious gradually and damaging their body. The prior studies are interest in the diagnosis of metal stress. Some physiological parameters are used for the diagnosis of mental stress. However, these parameters pattern recognition is a difficult problem due to they have a time varying morphology subject to physiological conditions and the presence of noise. Therefore, how to capture and analyze personal physiological signals to assessment of mental stress under different conditions is a recurrent issue in many engineering and medicine fields. In addition, it is also important how to provide appropriate ways for stress relief under different the mental stress level. This study will evaluate different classification methods and understand which one is appropriate to detect the mental stress. Three data mining technologies are used to detect the mental stress level and have an experiment to evaluate the performance of the mental stress diagnosis. The heart rate, blood pressure, heart rate variability and autonomic nervous system are used to assess the level of mental stress. It might be helpful to assess mental condition in clinical practice.

Keywords Mental stress · Heart rate variability · Data mining

H.-S. Chiang (✉) · L.-C. Liu

Department of Information Management, National Taichung University of Science and Technology, No. 129, Sect. 3, Sanmin road, Taichung city 404, Taiwan
e-mail: hschiang@nutc.edu.tw

C.-Y. Lai

Dong Wu Vocational High School, Chiayi, Taiwan

1 Introduction

Nowadays, competitive and fast-paced environment has affected many people health and made stress become a part of our daily life. However, stress can be positive for improve study and work efficiency, there are also negative could materially physical and psychological impact. The medical report pointed out that the long-term excessive stress will be directly or indirectly caused inattention, memory loss and manic spirit, such as cardiovascular and gastrointestinal diseases, are more likely to harm the body's immunologic functions. In addition, the excessive mental stress is also one of the major factors that lead to emotional instability or suicide [2]. Therefore, it is impossible to avoid mental stress because people are too busy or accustomed and ignore some mental stress in daily working environment. Although they know that mental stress adjustment and management is important. However, people become taking some preemptive actions to reduce stress if they informed of their stress levels (Sanches et al. 2010).

Electrocardiogram (ECG), recording the contraction and expansion of the heart tissue movement to generate a graph of the voltage change, its important physiological parameters. Therefore, through the ECG can obtain important information in heart function and cardiovascular. Heart rate variability (HRV) refers in sinus rhythm, successive cardiac cycle small differences, reflecting the pulsatile rhythm continuity moment is the heartbeat spacing tiny cyclical changes. HRV is the physiological phenomenon of variation in the time interval between heartbeats by Autonomic Nervous System (ANS). The ANS will adjustment physiological parameters for prompting the body to process any situations. Today, ECG, HRV and ANS have become one of the ways to prevent method. Moreover, they are many studies used to measure disease, including heart, cardiovascular disease and mental stress. However, physiological signals are severely contaminated by different types of noises and other interferences [4]. Therefore, we notice that how to obtain and filter signals will improve diagnosis of mental stress in this research. This study want to understand which one data mining methods are used to assess the level of mental stress and suggestion stress relief for users appropriately.

2 Related Work

Mental stress is a physiological reaction to suit the external environment change. When people feel something has changed around their environment or something just happen suddenly, their body will release chemicals in the blood. These chemicals give people more energy and power to suit this changes or possible danger. However, if people sustain too much stress or under stress for a long time, in this process, their body will keep consumption their energy, the body will send alert messages to remind people. If we do not confront this problem, our mental and immune system will be weakened continuously and caused many diseases,

such as cardiovascular disease, depression, apoplexy and so on. Mental health seems to be the most obvious and direct health and social stress will be generated by the impact (Williams and Mohammed 2009). Electrocardiography (ECG) is a transthoracic interpretation of the electrical activity of the heart over a period of time, as detected by electrodes attached to the surface of the skin and recorded by a device external to the body.

In prior research, the diagnosis of mental stress were adapted ECG to analysis different physiological characteristics, and combined with data mining, neural network and fuzzy theory to automatically diagnose the level of mental stress. The time domain analysis and frequency domain analysis is the mainly method in ECG, Heart rate variability (HRV) and Autonomic Nervous system (ANS) is adopted to analysis the parameters of physiological characteristics. The time domain analysis in HRV is based on time to calculate the difference between heart beating rates and standard deviation to generate different standard value, including Standard Deviation of all Normal to Normal intervals (SDNN) and Root Mean Square of the Successive Differences (RMSSD), and using these methods to estimate the level of mental stress. The frequency analysis using algorithm to calculate the spectrum of heart rate, the spectrum of different frequencies shows the sum of the power of the heartbeat fluctuation. ANS reaction in the part of frequency of cardiac electrical signals is divided into three frequency bands, including the regulation of peripheral vasomotor tension and the Very Low Frequency (VLF) of temperature regulate, the Low Frequency (LF) of the stress receptors reflex in stress sensor and blood pressure regulation, as well as the High Frequency (HF) of breath. To this end, we use three band energy changes to estimate the situation of ANS regulation ([1] Saul 1990). Pagni et al. (1991) use the short-term R-R interval and cardiovascular systolic blood pressure as spectrum analysis to research how the mental stress influences ANS and circulatory system. They detected VLF energy is higher than usual when participants' stress focused. Satish et al. (1998) describe that change the temperature of hand and the listening test to control physical stress and mental stress environment to investigate the large intestine activity status and cardiovascular changes pressure.

3 Methods

3.1 Naïve Bayes

Naïve Bayes (NB), or Naïve Bayesian Classifier, is one of most effective, good performance and very simple classification algorithms in many applications [3]. Which is a statistical learning technique based on Bayes' theorem and classifier assumes that under the given condition of the classification characteristics the attribute values are independent of each other [5]. Bayes' theorem is a theorem

with two distinct interpretations in probability theory and statistics. A Bayes' theorem is defined in (1):

$$P(A|B) = \frac{P(B|A)P(A)}{P(B)} \quad (1)$$

Mathematically, Bayes' theorem gives the relationship between the probabilities of event A and B. However, the probability model for a classifier is a conditional model $P(C|F_1, \dots, F_n)$. Using Bayes' theorem then writes (2):

$$P(C|F_1, \dots, F_n) = \frac{P(C)P(F_1, \dots, F_n|C)}{P(F_1, \dots, F_n)} \quad (2)$$

Now assume that each feature F_i is conditionally independent of other feature F_j for $j \neq i$ give the class C . For that, the model can be expressed as:

$$P(C) \prod_{i=1}^n P(F_i|C) \quad (3)$$

According to Eq. (3), the conditional distribution over the class variable C is expressed like this:

$$P(C|F_1, \dots, F_n) = \frac{1}{Z} P(C) \prod_{i=1}^n P(F_i|C). \quad (4)$$

Finally, the corresponding classifier is defined as follows:

$$\text{classify}(f_1, \dots, f_n) = \arg \max_c P(C = c) \prod_{i=1}^n P(F_i|C) \quad (5)$$

3.2 Decision Tree

The decision tree (DT) is a decision support method for classification, which has uses a tree-like graph or model of decisions. It has been widely used and popularity because of its simplicity and easy comprehensible as a classification rule. Decision tree have several advantages, such as simple to understand and interpret, have value even with little data, robustness to noise and ability to deal with redundant attributes.

A classification and regression trees (CART) is a technique that generates a binary decision tree. As with ID3, entropy is used as a measure to choose the best splitting attribute and criterion. However, where a child is created for each sub-category, only two children are created (splits a node into two). At each step, an exhaustive search is used to determine the best split and only one criterion is chosen as the best over all possible criteria. If CART detects no met pre-set

stopping rules or further gain can be made. The splitting will stop. Each observation falls into one terminal node and uniquely defined by a set of rules.

3.3 Support Vector Machine

Support vector machines (SVM) are used for classification and regression analysis by supervised learning with associated learning algorithms. More formally, SVM constructs a hyper-plane in a multi-dimensional space, which can be used for classification and regression. A SVM can be briefly described as follows:

Let given training data, a set of n points of the form:

$$(x_1, y_1), \dots, (x_m, y_m) \in X \times \{\pm 1\} \tag{6}$$

X is nonempty set form the patterns x_i and the y_j are labels, targets or outputs. It attempts to identify a hyper-plane in a multi-dimensional space and this hyper-plane is used to data classification. Any hyper-plane can be written as the set of points x satisfying:

$$((w \times x) + b) = 0 \tag{7}$$

A hyper-plane satisfying Eq. (7), if the training data are linearly separable, we can select two hyper-plane to separate data and there no point between them. We can be described as:

$$((w \times x) + b) = 1, ((w \times x) + b) = -1 \tag{8}$$

We can find the distance between these two hyper-planes $2/||w||$ by using geometry. However, we have to prevent data points from falling into the margin, for each i we add the following constraint and get the optimization problem:

$$((w \times x) + b) \geq 1, ((w \times x) + b) \leq -1, \text{Minimize}(w, b) ||w|| \tag{9}$$

It is difficult to solve the optimization problem because it depends on $||w||$ and it involves a square root to the norm of w . The constrained problem can be expressed by introducing Lagrange multipliers:

$$\min_{w, b} \max_{a \geq 0} \left\{ \frac{1}{2} ||w||^2 - \sum_{i=1}^n a_i [y_i (w \times x - b) - 1] \right\} \tag{10}$$

These problems are used standard quadratic programming techniques and programs for solved. Nevertheless, the SVM is a local search method and vulnerable to local optima [6].

4 Experiment Design

The detection of mental stress experiment is divided into the data preprocessing phase and conduct experiment. Data preprocessing phase has two parts in the physiological signal no stress/stress, as follows: (1) decomposes the signal, (2) removes the noise of the signal. We use singular value decomposition (SVD) to decompose the physiological signal of noise and use Butterworth high pass filter (BHPF) to remove the baseline wander phenomenon of external factors (such as skin resistance, instrument current), and acquire clean physiological signal. This study take advantage of [7] rules to identify the peak of each heartbeat, and calculate indicators of relevant characteristics.

4.1 Description of Data Set

The data set is provided by Physionet which is not only an open source platform, but also provides clinical ECG data, the algorithm of ECG signal analysis and research achievements. Therefore, this research adopts PhysioNet to progress the experiment. We use stress recognition in automobile drivers which provides by PhysioNet. There are 16 health volunteers as participants to participate the stress test to obtain the physiological data, including ECG, Electromyography (EMG), galvanic skin response (GSR) and breathe ratio, the sampling frequency is 496 Hz, the experiment time is about 60–90 min which depends on traffic conditions.

4.2 Experiment Processing

First of all, we have to extract 5 min no stress/stress two phases from 16 continuous physiological records. In order to assure the validity of the two phases, we start to extract the middle of the phase which starts from 300 to 600 s, and the high stress of the stress phase which starts from 1,100 to 1,400 s. After extracted the signal, there will be 32 samples which have 16 no stress phases and 16 stress phases when all phases are intercepted. In this study, diagnosis of mental stress experimental procedures is divided into the following steps: filter the ECG signal, extract the physiological characteristics from ECG and mental stress detection.

4.2.1 ECG Signal Filtering

The original signal of ECG has too much noise. This research adopts the SVD to separate the noise and decomposition of the characteristic values of the signal eigenvectors and singular values. At this time, we remove the singular values

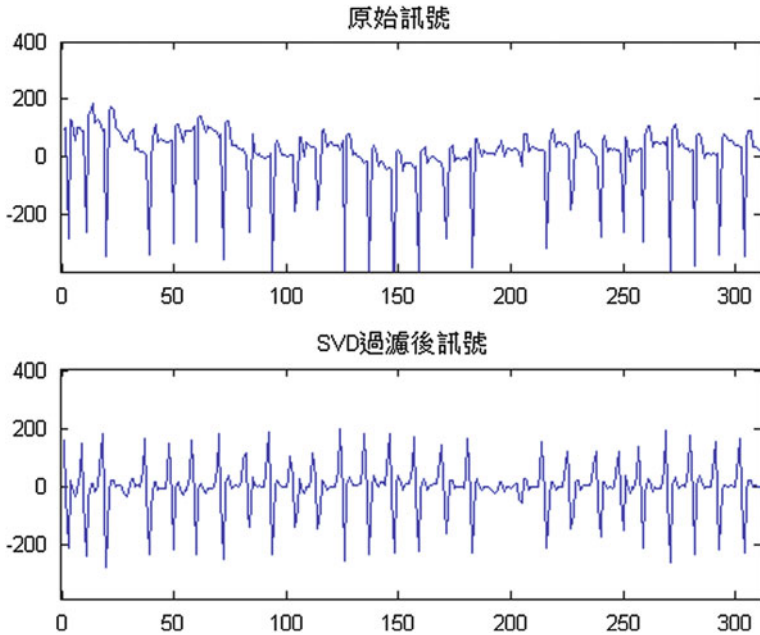


Fig. 1 The original signal and after filtering signal

which lower than average and use the SVD to recombination the signal. It will be a new signal phase after filter the noise which shows in Fig. 1, and we can see the signal after filtered is clearer than before filtered. We also used the BHPF to smooth out the baseline wander phenomenon that external factors caused. Briefly, BHPF can make the original level of volatility shocks turn into the volatility of average height, in order to enhance the accuracy of detect the r-peak.

4.2.2 Extracting the Characteristics

We used the r-peak detection to find the r-peak of ECG after the filter is preprocessed which originally proposed by [7]. At first, we use first derivative test to find the slope of every signal point and lower the P wave and T wave, and then use 250 maximum of slope as a basic initial value. We take the So and Chan [7] suggestion to use the 0.7 as a threshold value. If there have two continuous slope values, we can look forward to find the maximum value as r-peak. The red point on this picture is the actual position. When r-peak is detected, we use the interval value of r-peak as characteristic values. The characteristic values are used to calculate the Mean, SDNN, RMSSD, NN50 and differ value over 50 ms (pNN50).

4.3 The Evaluation of Classification Methods

This study adopted some methods and machine learning classification methods to verify for the mental stress detection based on ECG signals. In addition, these methods are evaluation and to understand which methods have the most effectiveness in diagnosis of the mental stress. In the mental stress detection test, this study uses the Naïve Bayes (NB), decision tree (CART) and support vector machine (SVM) as models, and use the software named Statistica10 to analyze the characteristics of mental stress so as to find some associated rule from the characteristics, and expect the possibility of no stress/stress further.

We let the ECG data set to 7:3 ways to divide into training set and testing set, and using every kind of algorithm to analyze and expect that described in last paragraph. In decision tree, we use CART to build decision tree; we also use the Eqs. (1–4) to build the probability tables for Naïve Bayes; the calculation kernel function of SVM use the polynomial function to calculate.

False Negatives (FN): That means the value of stress phase has stumbled into no stress phase; False Positive Rate: $FP/(TN + FP)$; Overall Accuracy: $TP + TN / (TP + FP + FN + TN)$, the performance has shown in Table 1.

The experimental results show that the combination with the minimum information entropy and APN which has used by this study has the best performance in Detection Rate, False Positive Rate and Overall Accuracy. NB not only has the high Detection Rate, but also has the high False Positive Rate. DT has the highest Detection Rate, relatively, also has high False Positive Rate as NB. Comparing with SVM and BN, the decision tree has the high performance in Detection Rate and Overall Accuracy.

In this study, we used some classification methods that had the best performance than different data mining classification methods in the diagnosis of mental stress with these 32 samples. It is suitable to assist in clinical diagnosis of mental stress as show in Table 1.

Table 1 The estimate comparison of different classification method in mental stress

Method of classification	TP	TN	FP	FN	Detection rate (%)	False positive rate (%)	Overall accuracy (%)
Naïve bayes	10	14	6	2	83.33	30.00	75.00
Decision tree (CART)	9	15	7	1	90.00	31.82	75.00
Support vector machine	8	11	8	5	61.54	42.11	59.38

5 Conclusion

These researches gives the combination method with minimize entropy principle approach and APNs to diagnosis mental stress for users. Experimental results showed that the assessment of mental stress can effective diagnosis level and accurately determine the users mental stress through NB, DT and SVM to comparisons.

Therefore, this study will develop assessment system to mental stress assessment and suggestion stress relief base on decision tree (CART) in the future. And, we expect that the system have significant effectiveness in terms of mental stress assessment, auxiliary diagnosis, adaptation and management of mental stress and avoid immune disorder and reduce the probability of chronic diseases.

Acknowledgments The authors would like to thank the National Science Council of Taiwan for Grants NSC 100–2410-H-025–005 which supported this research.

References

1. Electronics M (1992) Heart rate variability physician's guide. In: West Tower Avenue Milwaukee
2. Freeman JB, Garcia AM, Fucci C, Karitani M, Miler L, Leonard HL (2003) Family-based treatment of early-onset obsessive-compulsive disorder. *J Child Adolesc Psychopharmacol* 13:71–80
3. Ji Y, Yu S, Zhang Y (2011) A novel naive bayes model packaged hidden naive bayes. In: IEEE international conference on information technology and artificial intelligence, vol 2, pp 151–487
4. Karthikeyan P, Murugappan M, Yaacob S (2011) ECG signals based mental stress assessment using wavelet transform. In: IEEE international conference on control system, computing and engineering, pp 258–262
5. Lin J, Yu J (2011) Weighted naive bayes classification algorithm based on particle swarm optimization. In: IEEE international conference on communication software and networks, pp 444–447
6. Lin SW, Shiue YR, Chen SC, Cheng HM (2009) Applying enhanced data mining approaches in predicting bank performance: a case of taiwanese commercial banks. *Exp Syst Appl* 36:11543–11551
7. So HH, Chan KL (1997) Development of QRS detection method for real-time ambulatory cardiac monitor. In: 19th International conference, vol 2, pp 289–292

Part VI
Intelligent Agent System and Its
Applications

Intelligent Rainfall Monitoring System for Efficient Electric Power Transmission

Rong-Chi Chang, Teng-Shih Tsai and Leehter Yao

Abstract Global climate change has given rise to disastrous heavy rainfall during typhoon seasons, wreaking havoc on our living environments. The electric power transmission lines in Taiwan are spread throughout the island, while some towers are located in high-altitude mountains, calling for good early warning and monitoring mechanisms in the face of natural disasters. This study integrates the QPESUMS radar echo system adopted by the Central Weather Bureau to develop an automatic real-time rainfall estimation and monitoring system, which takes advantage of intelligent agents to handle the massive volume of rainfall information for analysis. Rainfall estimation using adaptive algorithms monitoring the rainfall fluctuations at remote towers can provide maintenance crews with real-time information for timely repairs.

Keywords Intelligent agent · Monitoring · Rainfall estimation · Electric power transmission

1 Introduction

The power system is the combination of power generation, transmission and distribution, where the transmission system acts as a bridge between the power plant and the user, akin to the vein of a power system connecting all the substations

R.-C. Chang (✉)

Department of Digital Media Design, Asia University, Taichung, Taiwan ROC
e-mail: roger@asia.edu.tw

T.-S. Tsai · L. Yao

Department of Electrical Engineering, National Taipei University of Technology,
Taipei, Taiwan ROC
e-mail: tst05106@gmail.com

L. Yao

e-mail: ltyao@ntut.edu.tw

in the transmission network. The global climate change in recent years has had disastrous impact on our living environment, such as the extreme heavy rainfall during typhoons. Taiwan is characterized as a hazardous area, with active faults lining the island, while a majority of the electricity transmission towers are located in hilly areas. Real-time tower monitoring and maintenance, particularly during the typhoon season with heavy rainfall, can minimize possible devastating damage [1].

Since a greater part of Taiwan's power transmission towers are stationed in the mountains or highlands, the single-point rainfall information gathered from ground stations cannot possibly supply a comprehensive hydrological model for a given area. The latest addition to improving rainfall estimation is remote sensing imagery, such as radar and satellite image data. The main advantage of telemetry technology lies in the effective detection of spatial variations in rainfall on a wider scale. In terms of quantitative rainfall estimates, telemetry image information can offer a broader perspective on the actual catchment rainfall than ground rainfall stations. The Central Weather Bureau has been utilizing QPESUMS (Quantitative Precipitation Estimation and Segregation Using Multiple Sensor) since 2002 to integrate multiple observations with geographic information as its system providing real-time severe weather monitoring information.

This study aims to apply the QPESUMS system and automatically intercept and gather radar rainfall information through intelligent agents for further interpretation and analysis. Together with the use of spatial interpolation algorithm, the proposed system analyzes rainfall spatial distribution and gauges the rainfall changes in areas where power transmission towers are located, which can then serve as a frame of reference for decision-makers in relevant units to take precautionary or contingency measures or dispatch personnel for timely maintenance. This system also integrates GIS information in the construction a visually robust real-time warning notification system.

2 Related Work

The Central Weather Bureau completed the Doppler radar observation network at the end of 2001 in Taiwan, and introduced the QPESUMS system to enable effective use of radar, satellite and rain estimation information, upgrading the monitoring, analysis and early warning capability for violent or mutational weather. Quantitative radar rainfall estimation technology has matured which provides more uniform and higher resolution of spatial rainfall distribution information on a bigger scale, securing itself as the most effective way to improving rainfall estimation accuracy.

According to Brands [2] and Wilson [3], radar rainfall estimation application in hydrologic model making use of ground stations to calibrate radar rainfall estimates can reduce the error to approximately 20–30 %. Yu et al. [4] established the GBDM (Grid-Based Distributed rainfall-runoff Model) and obtained good results in flood forecasting models using radar rainfall data. Collier [5] suggested that

most of the variables in the hydrological cycle have substantial spatial variability, which gives rise to the characteristic of chronicling temporal rapid variations. Meanwhile, precipitation plays an important role in the hydrologic process research, thus it is imperative to have a continuous record of rainfall in as many as locations as possible. Relying solely on the sporadic network of ground rainfall stations, the rainfall data are insufficient to meet the needs of a sound distributed hydrological model. Now, radar technology allows high-resolution spatial and temporal information, effectively improving the accuracy of flood forecasting. Bell and Moore [6] integrated grid-based distributed rainfall-runoff model and radar rainfall estimation with good simulation results. Corral et al. [7] used radar rainfall estimation in semi-distributed hydrological model, in which the catchment grid-scale was split into square hydrological $1 \times 1 \text{ Km}^2$ cells and TOPMODEL was applied to grid computing. Compared with the distributed precipitation inputs from this lumped model, the simulation from the radar-integrated semi-distributed hydrological model showed more promising results, evidencing that meteorological radar information on precipitation may be a favorable hydrological application for further developments. Philip et al. [8] utilized geographic information systems (GIS), Next Generation Weather Radar (NEXRAD) and the Internet to establish an urban flood warning system, where real-time cumulative rainfall information can be collected by the radar system for effective disaster prevention and early warning.

Burrough and Mcdonnell [9] tested objective quantitative precipitation forecasting (QPF) test data for objective rainfall patterns, and compared that with the findings from the National Weather Service, in which Common factor analysis (CFA) and Bayesian Correlation Score (BCS) were used to analyze simulated variability. The results showed that the QPF model obtained a higher BCS, but the simulation performance for intense rainfall events was lower. Carter et al. [10] pointed out Taiwan's QPESUMS system is designed to integrate radar information to construct a quantitative precipitation estimates (QPE), with the ultimate task of providing 0–2 h of short-term quantitative precipitation forecast (QPF) in disastrous typhoon weather; and suggested reasonable QPE/QPF information will in turn benefit disaster mitigation, hydrological applications and dam water resource management.

In recent years, spatial interpolation technique has been implemented in a wide range of applications in underground mineral deposit, hydrologic runoff, topography simulation, and climate modeling [11, 12], and its main purpose is to explore unknown spatial information from known spatial data. There are different standards for various interpolation techniques in different areas of research; generally, they can be divided into deterministic interpolation and stochastic interpolation, wherein the former adopts an estimation with no estimates of errors, e.g. nearest-neighbor and inverse-distance weighting (IDW), and the latter provides an estimate variable to indicate the estimation of error estimates, e.g. Kriging and minimum curvature [13, 14].

3 The Proposed Method

Intelligent agents are extensively used in automation systems, since they are capable of performing specific tasks repeatedly, where they use built-in or learnt knowledge database to complete given tasks or make decisions on behalf of the user. This study aims to develop a rainfall estimation and monitoring system that exploits intelligent agents to connect to the Central Weather Bureau’s QPESUMS system to get real-time updated information on extreme weather information at 10-minute intervals; the monitoring design also delivers high-resolution quantitative precipitation estimations for the past 24 h, where the locations of power transmission towers are subjected to inverse-distance weighting calculation to gauge to real-time rainfall estimates at respective towers as a crucial reference information for timely tower maintenance or disaster analysis.

Figure 1 shows the structure of the whole system. In this figure, it mainly consists of an acquisition agent, an operation agent and a presentation agent. The scheme first obtains the radar data and the rainfall station information from Central Weather Bureau (CWB) and then detects whether those data are existent. After decoding, an inverse-distance weighting operation is employed to calculate the rainfall in each transmission tower. In data generating part, it has five cumulative rainfall data will be computed in storage layer: 1 h rainfall, 24 h rainfall, daily rainfall, 30 days rainfall and monthly rainfall. When user inquires the rainfall information passed by web

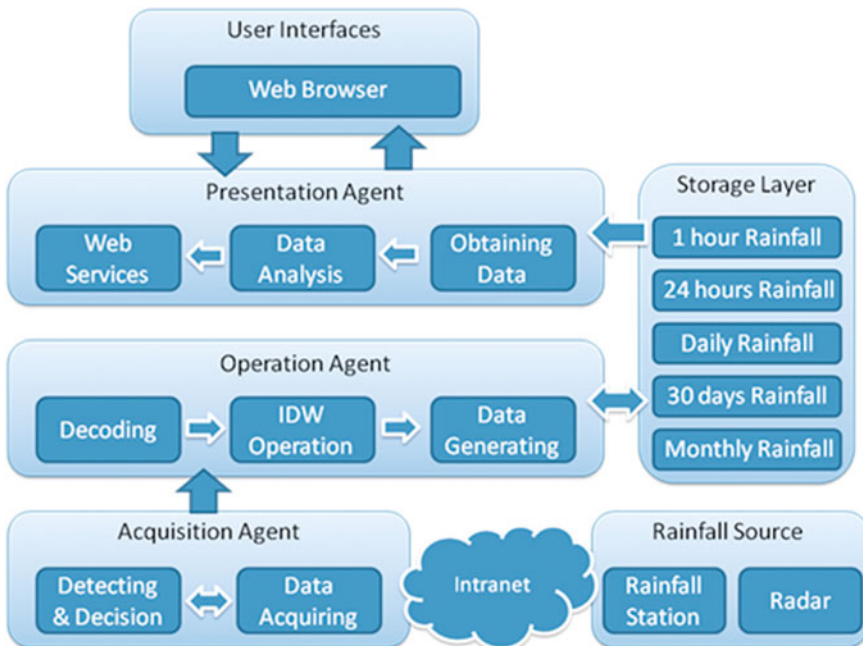


Fig. 1 The structure of the intelligent rainfall monitoring system

services, the corresponding rainfall data will be obtained to perform the disaster analysis with each transmission tower. Finally, the results after performing the disaster analysis are shown in browser to provide user inquiring.

3.1 Inverse-Distance Weighting Method

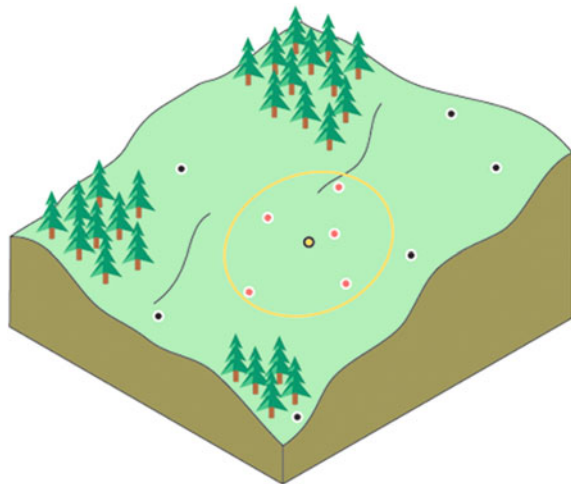
The IDW [15] method is a straightforward and noncomputationally intensive method. It has been regarded as one of the standard spatial interpolation procedures in geographic information science and has been implemented in many GIS software packages [16]. As shown in Fig. 2, many GIS users without much background in spatial statistics and geostatistics will use IDW as a default method to generate a surface when attribute values are available only at sampled locations. The IDW method is used to estimate the unknown value in location, given the observed values at sampled locations, which can be expressed as S_0 , given the observed values at sampled locations, which can be expressed as

$$\hat{y}(S_0) = \sum_{i=1}^n \lambda_i y(S_i) \tag{1}$$

where $\hat{y}(S_0)$ is estimated value in location S_0 which is a linear combination of the weighting value λ_i and observed values $y(S_i)$ in location S_i , where λ_i is defined as following:

$$\lambda_i = \frac{d_{oi}^{-\alpha}}{\sum_i^n d_{oi}^{-\alpha}} \tag{2}$$

Fig. 2 An illustrate of IDW method



with

$$\sum_i^n \lambda_i = 1 \tag{3}$$

here $d_{oi}^{-\alpha}$ is the distance between S_o and S_i with a power. The parameter α is expressed as a geometric form which is a positive real number. The specification implies that if $\alpha > 1$, the distance-decay effect will be more than proportional to an increase in distance, and vice versa. Thus, small α tends to yield estimated values as averages of S_i , while large α tends to give larger weights to the nearest points and increasingly down-weights points farther away. Therefore, when $\alpha = 0$ with $\lambda_i = 1/n$, then

$$\hat{y}(S_o) = \sum_{i=1}^n \lambda_i y(S_i) = \sum_{i=1}^n \frac{1}{n} y(S_i) \tag{4}$$

From above equation, estimated value is average of all sampled values. When $\alpha = \infty$, the weighting value λ_i will be expressed as

$$\lambda_i = \begin{cases} 1 & i = j \\ 0 & i \neq j \end{cases} \tag{5}$$

and

$$\hat{y}(S_o) = \sum_{i=1}^n \lambda_i y(S_i) = y(S_j) \tag{6}$$

in this case, the estimated value $\hat{y}(S_o)$ will be the same as the observed value in the nearest sampled location S_j .

3.2 QPESUMS Data

Quantitative Precipitation Estimation and Segregation Using Multiple Sensors (QPESUMS) is a total system integration incorporating data from multiple radars, numerical models, satellite, lightning and surface sensors. All data are mosaiced to a common grid providing a one-stop radar analysis tool. The QPESUMS systems produce quantitative precipitation estimates mainly including three parts: (1) Determining Z-R relation where Z and R are reflectivity factor and rainfall intensity, respectively. (2) The rainfall obtained by radar observing. (3) Compute precipitation rates and distributions using appropriate Z-R relations, where Z-R relation is computed from the raindrop density function, which can be expressed as

$$Z = 32.5R^{1.65} \tag{7}$$

where the units of Z and R are mm^6/m^3 and mm/h , respectively. Presently, the grid ranges of QPESUMS system in Taiwan are latitude $20 \sim 27^\circ\text{N}$ and longitude $118 \sim 123.5^\circ\text{E}$, that the overall grid is 561×441 and resolution is $1.25 \times 1.25 \text{ km}$. While so far the QPESUMS system still need to improve the exactitude of rainfall prediction, but the spatial rainfall analysis based on high resolution is of great value for reference (Fig. 3).

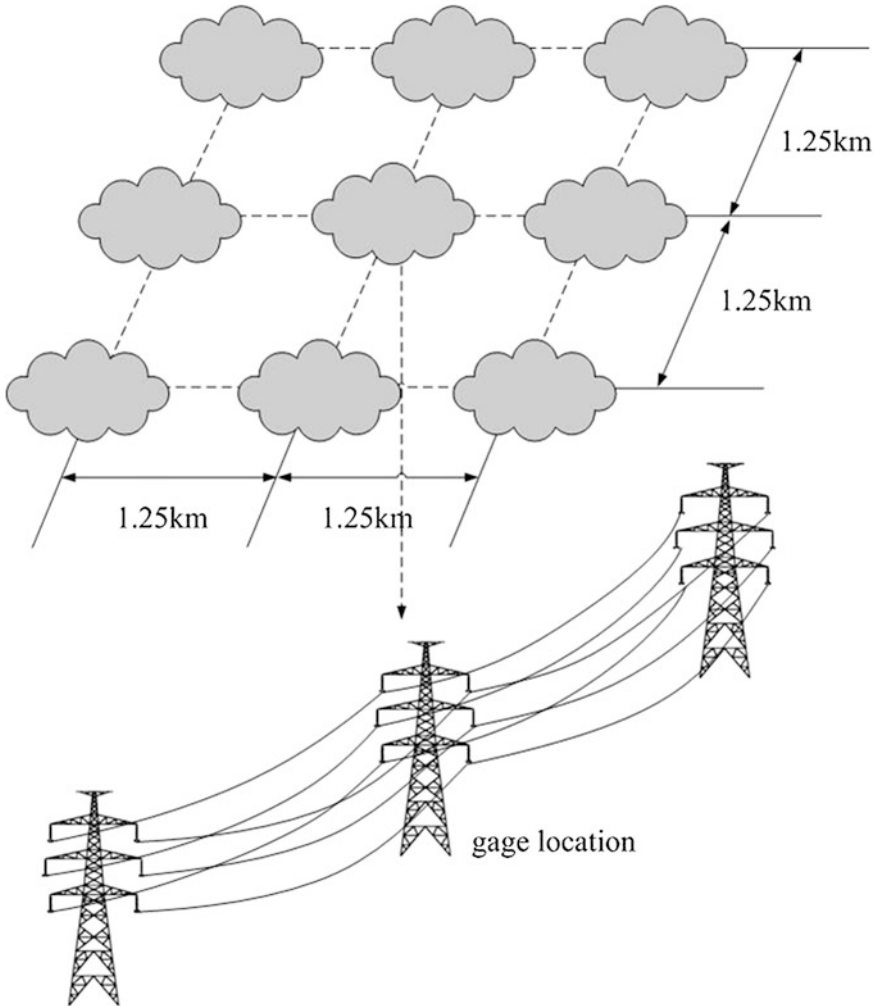


Fig. 3 Structure of the QPESUMS on electric power transmission

4 Experimental Results

Table 1 lists, respectively, the cumulative rainfall of 2013/01/10, 2013/01/11 and 2013/01/12. Regarding the cumulative rainfall of three days, it is shown that the total rainfall of 2013/01/12 is much more than other days since the front staying on Taiwan. To calculate exactly the estimated error, a cross validation method is used to evaluate the IDW prediction results. The cross validation method is based on percent error, which is define as

$$PE = \frac{RMSE}{\frac{1}{N} \sum_{i=1}^N P_i^*} \times 100 \% \tag{8}$$

where

$$RMSE = \sqrt{\frac{1}{N} \sum_{i=1}^N (P_i - P_i^*)^2} \tag{9}$$

and the root mean square error (RMSE) is the mean of the squared difference between the observed value and predicted value P_i , and N is the number of observations.

The RMSE comparison between the calculating results of IDW method and the actual precipitation of 566 rainfall stations are shown in Table 2. In spite of the estimated errors have slight difference at these three days, the calculating results of IDW method are applied to rainfall estimation still of great value for reference. Table 3 lists the comparison of estimated value and observed value on three rainfall stations. At 2013/01/11, the estimated error is increased slightly due to less rainfall. On the contrary, when rainfall is plentiful, the estimated error is decreased gradually. Thus, it can be seen that the IDW method would be more exactly to calculate rainfall when precipitation is increased. By the way, most landslide disasters usually occurred on larger rainfall events.

Table 1 The cumulative rainfall of three days in Taiwan

Date	24 h cumulative rainfall		Total cumulative rainfall (mm)
	Maximum rainfall (mm)	Station	
2013/01/11	45.0	#1	1022.81
2013/01/10	122.5	#2	3231.88
2013/01/12	199.0	#3	6345.32

Table 2 The RMSE comparison of three days

Date	2013/01/11	2013/01/10	2013/01/12
RMSE (mm)	0.07	0.18	0.24
PE (%)	4.04	3.29	2.18

Table 3 The comparison of estimated value and observed value on three rainfall stations

Date	2013/01/11	2013/01/10	2013/01/12
Station	#1	#2	#3
Observed value (mm)	45.0	122.5	199.0
Estimated value (mm)	25.4	119.3	206.4
Error (mm)	19.6	3.2	7.4

5 Conclusions

This study proposes an intelligent rainfall estimation system powered by the Central Weather Bureau's QPESUMS system, using intelligent agents to automatically gather and analyze radar echo data and provide rainfall estimates at respective power transmission towers through inverse-distance weighting calculation. Actual experiment findings in comparison with 566 ground rainfall stations showed that rainfall estimates by using inverse-distance weighting calculations offer better informational value and shorten computing time, particularly for towers located in remote mountainous areas. In addition, this GIS-integrated system offers visualized real-time rainfall information that will contribute to the swift maintenance and safety management of transmission towers.

References

1. Beehler ME (1997) Reliability centered maintenance for transmission systems. *IEEE Trans Power Delivery*:1023–1028
2. Brands E (1974) Radar rainfall pattern optimizing technique. NOAA Teach, Memo, ERL NSSL-67, Oklahoma, pp 16
3. Wilson JW (1970) Integration of radar and raingague data for improved rainfall measurement. *J Appl Meteor* 9:189–497
4. Yu PS (1987) Real-time grid based distributed rainfall-runoff model for flood forecasting with weather radar. Ph.D. Thesis, University of Birmingham
5. Collier CG (1996) Weather radar precipitation data and their use in hydrological modeling. In: Abbott MB, Refsgaard JC (eds) *Distributed hydrological modeling*. Kluwer Academic Publishers, Dordrecht, Chap. 8, pp 143–163
6. Bell VA, Moore RJ (1998) A grid-based distributed flood forecasting model for use weather radar data. Part 2: case studies, hydrology and earth system sciences, vol 2. (2–3), pp 283–298
7. Corral C, Sempere-Torres D, Revilla M, Berenguer M (2000) A semi-distributed hydrological model using rainfall estimates by radar, application to Mediterranean basins. Part B: Physics and Chemistry of the Earth
8. Bedient Philip B, Holder Anthony, Benavides Jude A, Vieux Baxter E (2003) Radar-based flood warning system applied to tropical storm allison. *J Hydrol Eng* 8(6):308–318
9. Burrough PA, McDonnell RA (1998) *Principles of geographical information systems*. Oxford University Press, New York
10. Carter MM, Elsner JB, Bennett SP (2000) A quantitative precipitation forecast experiment for Puerto Rico. *J Hydrol* 239:162–178

11. Chiou TK, Chen CR, Chang PL (2005) Status and outlook of a quantitative rainfall estimation technique in central weather bureau. Taiwan, Geophysical Research Abstracts, vol 7, 10637
12. Goovaerts P (2000) Geostatistical approaches for incorporating elevation into the spatial interpolation of rainfall. *J Hydrol* 228:113–129
13. George YL, Wong DW (2008) An adaptive inverse-distance weighting spatial interpolation technique. *J Comput Geosci* 34:1044–1055
14. Buytaert W, Celleri R, Willems P, Bievre BD, Wyseure G (2006) Spatial and temporal rainfall variability in mountainous areas: a case study from the south Ecuadorian Andes. *J Hydrol* 329:413–421

A Computational Data Model of Intelligent Agents with Time-Varying Resources

Anthony Y. Chang

Abstract This paper aims to develop a generic and complete computation model toward scheduling, resource allocation, and action model of agents and to design the relevant simulated intelligent agent framework for agent applications. We propose a computation model and development tools to deal with dynamic data, translation of data models, qualitative information, time quantity, uncertainty, functionality, and semantic analysis. We also develop the relevant grammar and algebra system to locate resources and maintain constrains. The system allow user to define percepts and actions of agents. Script language with percept lists are integrated with scheduling and resource allocations. Several computation algorithms and operation tables which include a set of complete temporal logics are proposed. The combined temporal data models are generalized by composing point and interval algebra with qualitative and quantitative functions. The table look-up mechanism has the advantages for computation and realization.

Keywords Intelligent agents • Scheduling • Resource allocation • Wireless sensor networks • Semantic analysis

1 Introduction

It is necessary to communicate between the master agent and the other worker agent when several agent work together in multiagent systems. To synchronize the various types of agents is the major challenge for a coordination system. The coordination of actions is the set of supplementary activities, which need to be carried out in a multi-agent environment. When accessing common resources, it is

A. Y. Chang (✉)
Department of Information Technology, Overseas Chinese University,
Taichung, Taiwan Republic of China
e-mail: achang@ocu.edu.tw

necessary to guarantee that the system remains in a coherent state, and the actions have to be synchronized by computing procedures [1]. Biniaris present key issues related to the distributed implementation of a Finite-Difference Time Domain (FDTD) code using java mobile agents, and special agent communication and synchronisation aspects related to FDTD are presented in Biniaris et al. [2]. Conservative and optimistic approaches for resolving distributed simulation of multi-agent hybrid systems are presented in Hur and Lee [3] provided a collaborative agent interaction and synchronization system for ensuring effective structuring and control of a distributed conference. Mishra and Xie [4] design an interagent communication and synchronization model in the DaAgent mobile-agent-based computing system.

Protocols for multiagent resource allocation provide a general framework for realizing resource allocation problems among agents and settings. Anshul Rai et al. [5] present a novel approach Wrasse to resource allocation that could solve specific allocation problems in cloud environments. Palden Lama and Xiaobo Zhou [6] propose AROMA, a system that automates the allocation of heterogeneous Cloud resources and configurations. Resource allocation is widely used in real life and corporate. A distributed resource allocation mechanism with fairness for cognitive radios in wireless mobile ad hoc networks is presented in [7]. An improved approximation algorithm deal with fixed interval of time and given amount of the resources for resource allocation proposed in [8].

This paper proposes an intelligent methodology to analyze and verify time requirements with resources from the agent systems. It also develops a temporal algebra system as a computational data model to maintain temporal constraints and to generate consistent scheduling. It eliminates conflict relation specification and reduces redundant relations to obtain minimal essential structural relations between coordinating agents efficiently. In addition, it reasons about not only definite information but also uncertain knowledge. The resulting model integrates the structural relation indexes, object attributes, quality class, and quantities for time-varying resource allocation of agents.

2 Computation Data Model about Time

Constraint satisfaction techniques play an important role in current computer science. Many difficult problems involving search from areas such as machine vision, scheduling, graph algorithms, machine design, and manufacturing can be considered to be the cases of the constraint satisfaction problem. In our previous work [9], an Interval Transitive closure Table and constraint propagation algorithms are proposed for temporal reasoning.

Definition 2.1 (*Well-defined Interval*)

If P is the set of points and \leq is the usual ordering on P , then $[P; \leq]$ is partially ordered. Let $a, b \in P$ such that $a \leq b$. The set $\{x \mid a \leq x \leq b\}$ is called

a well-defined interval of P and denoted as $[a, b]$. The set $\{x \mid a < x < b\}$ is called a pure interval, which is the subset of well-defined interval.

Definition 2.2 (*Endpoint Relations*)

If P is the set of points, a binary relation \diamond of two points based on point relations $\{<, =, >\}$. Let $A:[a, b]$ and $B:[c, d]$ are two intervals, where $a, b, c, d \in P$. The binary relations $a \otimes b$ and $c \otimes d$ are the duration relations. And the binary relations $a \otimes c, a \otimes d, b \otimes c,$ and $b \otimes d$ are called *endpoint relations*. These relations are denoted as $A_s \otimes B_s, A_s \otimes B_e, A_e \otimes B_s,$ and $A_e \otimes B_e$ respectively.

Based on qualitative point relations, we use an encoding method to generalize and prove the 13 interval exclusion relations. Suppose A_s and A_e are the starting and ending points of the line segment A . And, B_s and B_e are those of B . We define a binary relation, \otimes , (either $<, =,$ or $>$ for “ A is before B ”, “ A is the same as B ”, or “ A is after B ”) of two points. The 13 *interval relations* introduced by Allen [10] make the binary relations hold in the first part of the Table 1.

The second part of the table has five special cases for bounded relations. The extended interval relations allow start point and end point of one interval is equal. For instance, we use $A \text{ ols } B$ to represent A is a non-divided atom interval (i.e., the starting and the ending points are located at the same position) and B is a interval that could contain other sub-intervals. Where A and B meets at the starting point of A . These five special cases were not considered in [10].

We develop an $O(n)$ -time algorithm [9] for propagation temporal constraint between two time events.

$$\text{TemporalTuple} = \text{Name} \times 29\text{Relset} \times \text{Name}$$

Table 1 Relations between endpoints of two intervals

$A_s \otimes B_s$	$A_s \otimes B_e$	$A_e \otimes B_s$	$A_e \otimes B_e$	ID	Point-interval relations	Simplified conditions
<	<	<	<	1	{<}	$A_e < B_b$
>	>	>	>	2	{>}	$A_b > B_e$
>	<	>	<	3	{d}	$A_b > B_b \wedge A_e < B_e$
<	<	>	>	4	{di}	$A_b < B_b \wedge A_e > B_e$
<	<	>	<	5	{o}	$A_b < B_b \wedge A_e < B_e$
>	<	>	>	6	{oi}	$A_b > B_b \wedge A_e > B_e$
<	<	=	<	7	{m}	$A_e = B_b$
>	=	>	>	8	{mi}	$A_b = B_e$
=	<	>	<	9	{s}	$A_b = B_b \wedge A_e < B_e$
=	<	>	>	10	{si}	$A_b = B_b \wedge A_e > B_e$
>	<	>	=	11	{f}	$A_b > B_b \wedge A_e = B_e$
<	<	>	=	12	{fi}	$A_b < B_b \wedge A_e = B_e$
=	<	>	=	13	{e}	$A_b = B_b \wedge A_e = B_e$
=	=	>	>	14	{los}	$A_b = B_b = B_e < A_e$
<	<	=	=	15	{loe}	$A_b > A_e = B_b = B_e$
=	<	=	<	16	{ols}	$A_b = A_e = B_b < B_e$
>	=	>	=	17	{ole}	$B_b > A_b = A_e = B_e$
=	=	=	=	18	{oo}	$A_b = A_e = B_b = B_e$

$\forall tt: \text{TemporalTuple} \bullet tt = (A, rs, B) \Leftrightarrow tt-1 = (B, rs-1, A)$

$O: \text{TemporalTuple} \times \text{TemporalTuple} \rightarrow \text{TemporalTuple}$

For solving point/interval algebra networks, we develop an algorithm for finding all pairs of feasible relations.

Definition 2.3 *Formal Endpoint Relations with Quantity*

A formal endpoint relation $Q_E = (E_R, V_E)$ is a quantitative-qualitative valuable.

Where E_R , is an endpoint relation based on the point space $\{<, =, >\}$, and V_E is a quantity which expresses a quantitative value associated with E_R between two endpoints.

Let (R_1, v_1) and (R_2, v_2) denote two formal endpoint relations, R_1 and R_2 are two qualitative temporal variables, v_1 and v_2 are two quantity associated with quality. The meaning of some quantitative-qualitative calculus operators and equalities are defined as follows (Table 2).

3 Qualitative Time States and Transformations

Relations are similar to each other in certain degree. For example, “during” and “starts” are similar since the only difference is the starting points of the two intervals are different. However, “before” and the inverse of “meets” are not quite the same.

In Table 1, each of the 13 interval relations and 5 point-interval relations are defined by four “ \otimes ” relations. These relations can be used as a base of our evaluation criterion. A *relational-distance* of two “ \otimes ” relations belong to two different temporal relations occurs if those two temporal relations hold different relations in the same column of Table 1.

Definition 3.1 *Point relation states*

(PRS) defined with respect to a point relation r of index n have n incompatible differences from r . The following table gives a definition of point relation distance: (Table 3)

Table 2 Addition of qualitative-quantitative relations

(R_2, v_2)	$<_{v_2}$	=	$>_{v_2}$
(R_1, v_1)			
$<_{v_1}$	$<_{v_1+v_2}$	$<_{v_1}$	$<_{v_1-v_2}$, if $(v_1 > v_2)$ =, if $(v_1 = v_2)$ $>_{v_2-v_1}$, if $(v_1 < v_2)$
=	$<_{v_2}$	=	$>_{v_2}$
$>_{v_1}$	$>_{v_1-v_2}$, if $(v_1 > v_2)$ =, if $(v_1 = v_2)$ $<_{v_2-v_1}$, if $(v_1 < v_2)$	$>_{v_1}$	$>_{v_1+v_2}$

Table 3 Point relation states (PRS)

PRS	>	=	<
>	0	1	2
=	1	0	1
<	2	1	0

Definition 3.2 An extended point-interval relation states

(EPIRS) defined with respect to a point-interval or interval relation r of index n have n incompatible differences from r . Let R and R' are two interval relations or point-interval relations. The encoding point relation of R (see Table 1) is R_{AsBs} , R_{AsBe} , R_{AcBs} , R_{AcBe} , and the encoding point relation of R' is R'_{AsBs} , R'_{AsBe} , R'_{AcBs} , R'_{AcBe} . We have a EPIRS formula:

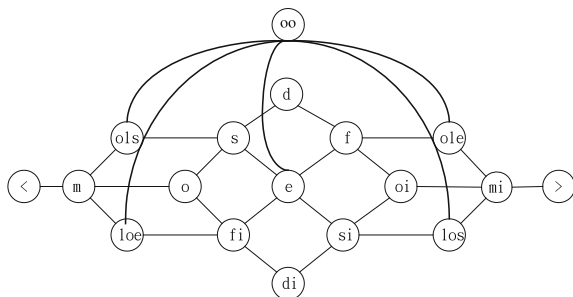
$$EPIRS(R, R') = PRS(R_{As\otimes Bs}, R'_{As\otimes Bs}) + PRS(R_{As\otimes Be}, R'_{As\otimes Be}) + PRS(R_{Ac\otimes Bs}, R'_{Ac\otimes Bs}) + PRS(R_{Ac\otimes Be}, R'_{Ac\otimes Be})$$

The index of EPIRS with respect to each temporal relation in Table 1 can also be retrieved from the length of a shortest path in a *distance graph* (see Fig. 1).

We have developed a fast computation mechanism to representation the varying of temporal relations. Using a bit-slicing representation of the relations, the index of image similarity can be computed in a few operations.

According to Raghavan [11] representation, the Binary temporal relations, OCPN (object composition Petri nets) and PACFG (probabilistic, attributed context free grammar) could be traslated each other. Agents may indicate their interest in one or more resources and time specifications in computational setting. We could derive the qualitative relations and quantitative values by closure table efficiently, then translate to Petri nets repreasentations as basis of designs of user interface. Also, we can maintain the states constraints and resources in varying time series.

Fig. 1 States of well-defined interval relations



4 Resource Allocating for Actions with Time

The resources could be defined as time-dependent objects and time-independent objects. The time-dependent resources combined with many consecutive units when assigned to agents. Allocation of each unit have it time constraints. It may be a single action or a group of actions with time branching. Time-independent objects are static resources that are not to change the state during the setting to agents. We can define the conditions for the resource allocator with selection criteria the obtains many attribute to be defined, such as durations, costs, variations.

The purpose of the *ComputeRDI* algorithm is to add an assigned node or a relation to the allocations. If there is a conflict cycle in the original reduced relation domain, the algorithm eliminates that conflict first by altering the user to select a reasonable relation to replace the original one. The *ComputeRDI* algorithm starts from taking each path of user edges of length 2, and computes a derived edge from that path. The insertion of edge $e = (a, b)$ results a cycle, but no conflict. The reasonable set of edge e (i.e., $e.rs$) is computed from two edges, (a, n_{k-1}) and (n_{k-1}, b) , which are user edges or derived edges. Since we increase the path length, pl , of the path of user edges one by one. The derived edge (a, n_{k-1}) (or user edge, if $pl = 2$) must have been computed in a previous interaction. The algorithm repeats until all edges are added to the complete graph K_n , which contains $n * (n-1)/2$ edges.

Algorithm : *ComputeRDI*

Input : $G = (GV, GE)$

Output: $K_n = (K_nV, K_nE)$

Preconditions : true

Postconditions : $GV = K_nV \wedge GE \setminus UE \cup UE' \subseteq K_nE$

Steps :

1 : $G = \text{EliminateConflicts}(G)$

2 : $K_n = G \wedge pl = 2$

3 : repeat until $|K_nE| = |K_nV| * (|K_nV| - 1) / 2$

3.1 : for each $e = (a, b) \wedge e \notin K_nE \wedge a \in K_nV \wedge b \in K_nV \bullet$

there is a path of user edges from a to b , with path length = pl

3.2 : suppose $((n_1, n_2), (n_2, n_3), \dots, (n_{k-1}, n_k))$

is a path with $a = n_1 \wedge b = n_k \wedge k = pl + 1$

3.3 : set $e.rs = \text{Table29}((a, n_{k-1}).rs, (n_{k-1}, b).rs)$

3.4 : $K_nE = K_nE \cup \{e\}$

3.5 : $pl = pl + 1$

In order to express more precise relations without losing qualitative information, the temporal relations extended with qualitative mechanisms for handling quantitative information. To give a concrete form to the topic of temporal representation, consider the following variable and equations with quantitative and qualitative information.

Definition 4.1 An integrated temporal algebra or is defined by the 6-tuple

$$T = (d_1, d_2, R_{ss}, R_{se}, R_{es}, R_{ee})$$

where $d_1, d_2 \in Q_E$ called the duration. It contains a fixed quality $\{<\}$ and a quantity to label the quantitative value between starting point and ending point.

$R_{ss}, R_{se}, R_{es}, R_{ee} \in Q_E$ contains the endpoint relation $A_b \diamond B_b, A_b \diamond B_e, A_e \diamond B_b, A_e \diamond B_e$ between A and B respectively, and a quantity associating with the endpoint relations.

Definition 4.2 Given a nonempty set $T = (d_1, d_2, R_{ss}, R_{se}, R_{es}, R_{ee})$, \otimes is a binary operation on T , $\otimes : T \times T \rightarrow T$ is the quantitative-qualitative composition function.

Theorem 4.1 (Quantitative-Qualitative Composition Functions)

$$\text{Let } (d_A, d_B, A_bB_b, A_bB_e, A_eB_b, A_eB_e) \otimes (d_C, d_D, B_bC_b, B_bC_e, B_eC_b, B_eC_e) \\ = (d_A, d_C, A_bC_b, A_bC_e, A_eC_b, A_eC_e)$$

$$\text{then } [A_bC_b] = [A_bB_b] + [B_bC_b] = [A_bB_e] + [B_eC_b]; \quad [A_bC_e] = [A_bB_b] + [B_bC_e] \\ = [A_bB_e] + [B_eC_e]; \quad [A_eC_b] = [A_eB_b] + [B_bC_b] = [A_eB_e] + [B_eC_b]; \\ [A_eC_e] = [A_eB_b] + [B_bC_e] = [A_eB_e] + [B_eC_e] \blacksquare$$

In addition, a quantitative-qualitative equation correctly expresses both qualitative equation and quantitative equations by formal endpoint variables and operators. We give a set of equations, for an example:

- Given $[d_A], [d_B]$ and $[A_eB_s]$

$$[A_bB_b] = [d_A] + [A_eB_b]$$

$$[A_bB_e] = [d_A] + [A_eB_b] + [d_B]$$

$$[A_eB_e] = [A_eB_s] + [d_B]$$

where $[d_A], [d_B], [A_b], [B_b], [A_e],$ and $[B_e]$ are expressing duration of A, duration of B, begin of A, begin of B, end of A, and end of B respectively. ■

Example 4.1 Considering the user defines a presentation scenario with three temporal intervals of actions, following requirements are known:

- A during B: $A \{d\}_{4,6} B$
- End of A is before beginning of C for 3 sec.
- The duration of A is 8 sec.
- The duration of C is 12 sec.
- The scenario starting with B.

In integrated temporal algebra, the information could be denoted as:

$$A \{d\}_{4,6} B \rightarrow [A_bB_b] = >_4, [A_eB_e] = <_6$$

$$A \{<\}_3 C \rightarrow [A_eC_b] = <_3$$

$$[d_A] = 8 \rightarrow [A_bA_e] = <_8$$

$$[d_C] = 12 \rightarrow [C_bC_e] = <_{12}$$

The temporal algebra system is proved as an algebraic group, with associative and transitive relations. We could compute timing from serial specifications.

$$[B_c B_b] = [B_c A_e] + [A_e A_b] + [A_b B_b] = >_6 + >_8 + >_4 = >_{18} \rightarrow [B_c] >_{18} [B_b]$$

$$[A_b B_b] = >_4 \rightarrow [A_b] >_4 [B_b]$$

$$[A_e B_b] = [A_e B_c] + [B_c B_b] = <_6 + >_{18} = >_{12} \rightarrow [A_e] >_{12} [B_b]$$

$$[C_b B_b] = [C_b A_e] + [A_e A_b] + [A_b B_b] = >_3 + >_8 + >_4 = >_{15} \rightarrow [C_b] >_{15} [B_b]$$

$$[C_e B_b] = [C_e C_b] + [C_b B_b] = >_{12} + >_{15} = >_{27} \rightarrow [C_e] >_{27} [B_b]$$

If the scenario beginning at 20th seconds of the presentation, then $[B_b] = 20$, $[B_c] = 38$, $[A_b] = 24$, $[A_e] = 32$, $[C_b] = 35$, $[C_e] = 47$ respectively.

Also we could define multiple tuples and functions such as

Action(A1, A2, T, R, S)

Where A1, A2 are agents, T and R are Integrated Temporal Variable and Integrated Resource Variable, and S could be a returned values by sensor.

5 Conclusions

This paper develops a general, theoretical computational model for discussing scheduling, resource allocation, and action model of agents. We develop algorithms to analyze constraints between resources in database by computational data model. The computed schedules and constraints are stored in database after encoding. We also develop the relevant grammar and algebra system to locate resources and maintain constrains. The intelligent agent development models could be used in many related applications, and we apply the technology to mobile agent communication, web agent and interactive multimedia as cases study. We believe that the architecture could benefit other interesting researches and applications such as job scheduling, automatic searching, robotics, data mining, wireless sensor networks, decision supported systems etc.

Acknowledgments This work is supported by the National Science Council of Taiwan, under Grant NSC-101-2221-E-240-003.

References

1. Ferber J (1999) Multi-agent systems: an introduction to distributed artificial intelligence. Addison Wesley Longman Inc, New York
2. Biniaris CG, Antonis IK, Dimitra IK, Iakovos SV (2002) Implementing distributed FDTD codes with java mobile agents. IEEE Antennas Propag Mag 44(6):115–119.
3. Hur Y, Lee I (2002) Distributed simulation of multi-agent hybrid systems. In: Proceedings of fifth IEEE international symposium on object-oriented real-time distributed computing, (ISORC 2002), 29 April–1 May, Washington, pp 356–364
4. Mishra S, Xie P (2001) Interagent communication and synchronization in DaAgent. In: Proceedings of 21st international conference on distributed computing systems, 16–19 April 2001, Mesa, pp 699–702
5. Rai A, Bhagwan R, Guha S (2012) Generalized Resource Allocation for the Cloud. In: Proceedings of the third ACM symposium on cloud computing, SoCC '12, Oct 2012

6. Lama P, Zhou X (2012) AROMA: automated resource allocation and configuration of MapReduce environment in the cloud. In: Proceedings of the 9th international conference on Autonomic computing, ICAC'12, Sept 2012, pp 63–72
7. Wang W, Shin KG, Wang W (2012) Distributed resource allocation based on queue balancing in multihop cognitive radio networks. *IEEE/ACM Trans Netw (TON)* 20(3):1493–1512
8. Calinescu G, Chakrabarti A, Karloff H, Rabani Y (2011) An improved approximation algorithm for resource allocation. *Trans Algor (TALG)* 7(4) Article 48
9. Shih TK, Chang AY (1998) The algebra of spatio-temporal intervals. In: Proceedings of the 12th international conference on information networking, Jan 21–23, 1998
10. Allen JF (1983) Maintaining knowledge about temporal intervals. *Commun ACM* 26(11)
11. Raghavan SV, Prabhakaran B, Tripathi SK (1996) Synchronization representation and traffic source modeling in orchestrated presentation. *IEEE J Sel Areas Commun* 14(1):104–113

An Intelligent Energy-Saving Information Interface Agent with Web Service Techniques

Sheng-Yuan Yang, Dong-Liang Lee, Kune-Yao Chen
and Chun-Liang Hsu

Abstract This paper focuses on developing an intelligent energy-saving information interface agent system with Web service techniques in cloud environments. This system contains two main portions: an information processing and decision-making platform, and a cloud information interface. The proposed system architecture not only satisfies a lot of interface system designs, but also presents unique functions of interface agents, and then shows that the decision-making precision, system reliability and system validity yield excellent system qualities. In terms of user satisfaction according to Quesenbery and Nielsen, the proposed system can score as high as 73 %.

Keywords Web services · Cloud interface agents · Energy-saving information systems

S.-Y. Yang (✉)

Department of Computer and Communication Engineering, St. John's University,
New Taipei City, Taiwan
e-mail: ysy@mail.sju.edu.tw

D.-L. Lee · K.-Y. Chen

Department of Information Management, St. John's University, New Taipei City, Taiwan
e-mail: lianglee@mail.sju.edu.tw

K.-Y. Chen

e-mail: kychen@mail.sju.edu.tw

C.-L. Hsu

Department of Electrical Engineering, St. John's University, Taiwan 499, TamKing Rd.,
Sec. 4, Tamsui District, New Taipei City, Taiwan, ROC
e-mail: liang@mail.sju.edu.tw

1 Introduction

The growing popularity of computers, and constant network technology improvements are two significant features related to the rapid advancement of Internet applications. Web Services principally provide services for application programs on the Internet and enable the use of programs in other machines; they are equipped with powerful inter-communication and extendibility. Related standards include: XML (Extensible Markup Language), SOAP (Simple Object Access Protocol), WSDL (Web Services Description Language), and UDDI (Universal Description, Discovery and Integration) [1]. In the cloud epoch, cloud services, one after another, seem to be becoming part of our daily lives. Cloud computing is an Internet- (“cloud-”) based development technique and use of computer technology. In other words, it sets up the necessary operating resources and related data on the Internet so that users can directly use them when they access the Internet. Furthermore, this study also investigates a means of constructing a cloud computing interaction diagram for extensively and seamlessly entering related Web information agent systems through Web service techniques.

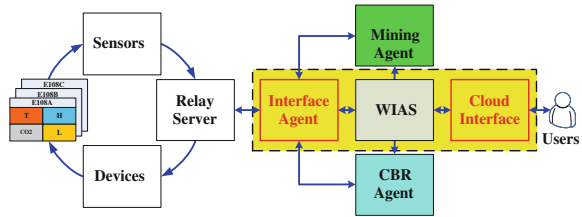
Taiwan is a small, densely populated country, with scarce resources, that relies on imports for 97 % of its energy. According to the 2008 Year-Book of the Energy Bureau of Economy Ministry, the total consumption of electrical power in Taiwan was 23,195 billion kWh, and the growth rate is 10 % per year [2]. The consulting cases of energy-saving in official organizations indicated that if energy-saving programs were put into practice, such as power system management, luminance facilities, air-conditioning management, regarding parameters of temperature, humidity, illuminance, and CO₂, 20 % electrical energy saving could be effectively achieved [3]. Therefore, a means of constructing an energy-saving information system concurrently with monitoring and feedback control has become necessary.

In summary, this paper focuses on developing an intelligent energy-saving information interface agent system with Web service techniques in cloud environments. This system contains two main parts: an information processing and decision-making platform, and a cloud information interface. The proposed system architecture not only satisfies a number of interface system designs, but also presents unique functions of interface agents, and shows that the decision-making precision, system reliability and system validity yield excellent system qualities. In terms of user satisfaction according to Quesenberry and Nielsen, the proposed system can score as high as 73 %.

2 Energy-Saving Information Systems

Figure 1 shows the diagram of an example of the energy-saving and multi-agent system [4]. This system not only gives consideration to more of the traditional concerns, but also integrates Web service technology to efficiently employ each

Fig. 1 Diagram of an example of the energy-saving and multi-agent system



part of the information in the system. Its operation processes are briefly described below. First, the sensors in the system collect each sensor’s data in the monitoring space, such as temperature, humidity, etc. The system then goes through the middle-way server to send those data back to the Interface Agent on the server end, and to storage in the cloud databases in the WIAS (Web-Service-Based Information Agent System) [5], to be used in training the intelligent decisions of the Data Mining Agent [6] and the CBR Agent [7]. The Interface Agent can trigger the decision-making process, the three-stage intelligent decision, at the same time as the sensor data is received, including the prediction solutions, the CBR solutions or the solutions predefined by the Predefined Rules (constructed by experts in the energy-saving domain). The system then sends the final decision results back to the monitoring end to carry out the corresponding control. The process and data change mentioned above can go through the Cloud Interface on the server end in order to proceed to the data browsing, to achieve the study goal of energy saving and feedback control.

3 Proposed System Architecture

The proposed system contains two main portions: an information processing and decision-making platform, and a cloud information interface, as shown in Fig. 2. The former is responsible for decision making, receiving data packets and returning decision results. It is composed of three sub-systems: Receiver/Transmitter, Decision Maker, and WSI (WIAS Service Interface). The cloud information interface is made up of several sub-systems, which respectively take on individual sub-web pages of the cloud webpage. Each of them can independently operate and employ each function, including: real-time information browsing, historical information queries, dynamic decision-making process, WIAS service interface, data mining process, CBR process, and system homepage.

3.1 Information Processing and Decision Making Platform

This platform contains the three sub-systems mentioned above and a system initiation interface for developing the example of the energy-saving multi-agent

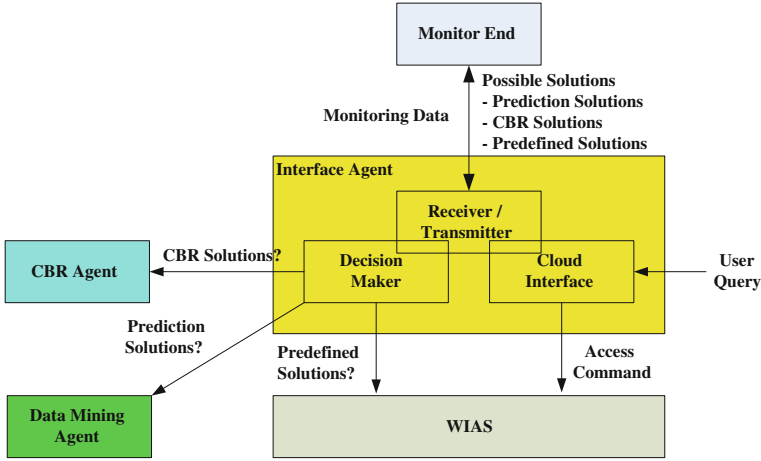


Fig. 2 Architecture of the intelligent cloud energy-saving information interface agent system

system [4]. The Receiver/Transmitter is responsible for receiving sensor data, filing duplicate information and depositing processed information into the cloud database with the help of Web services: Share_ViewDBSDT, Share_ViewSensorInfo and IA_InsRawData [5].

The Decision Maker employs the three-stage intelligent decision processing to provide corresponding possible solutions of feedback control with the help of Web services DM_Solutions, CBR_Solutions and IA_Solutions [5]. In other words, the Decision Maker can ask the Data Mining Agent (through Web service DM_Solutions) and the CBR Agent (through Web service CBR_Solutions) whether corresponding possible solutions exist based on the monitoring data. A detailed flowchart of this process is shown in Fig. 3. The successful energy-saving processing procedures can reflect upon monitoring data at the monitor end in real-time. The data can be periodically fed back into the stable energy-saving process case base, and can influence the Data Mining Agent in order to modify corresponding prediction rules and modules with the help of WIAS [5]. The chaining process enhances the system robustness by aiming at energy-saving monitor data processes, and actually obtaining the three-stage intelligent decision processing.

The WSI is a Java communication interface to the WIAS. Because Java cannot directly use WIAS's services, the system must pre-load the dedicated function library before using those services. This approach not only wastes system resources, but is also very inconvenient; the critical point is that each procedure with WIAS's network services acts as an individual user, which is very expensive in terms of the number of network connections on the backend system. However, the number is usually a limited value. For this reason, a specific communication interface was pre-constructed for the proposed system: WSI, as shown in Fig. 4, which collects all necessary functions of the proposed system and loads those functions one at a time, acting as the only communication pathway to WIAS, thereby easily solving the above mentioned problem.

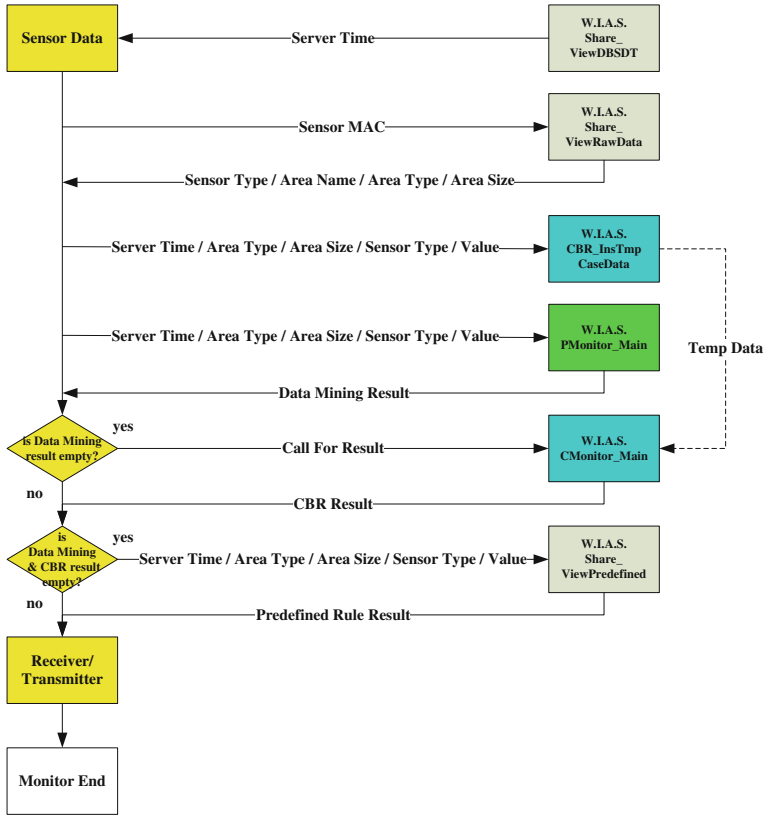


Fig. 3 Processing flowchart of decision maker

Fig. 4 Interface class of the WSI

```

    Package ESAS6_2 Time Deprecated Index Help
    File ESAS6_2_WIAS_Service_Interface.java
    File ESAS6_2_WIAS_Service_Interface.java

    Class ESAS6_2_WIAS_Service_Interface
    java.lang.Object
    ↳ ESAS6_2_WIAS_Service_Interface
    ↳ ESAS6_2_WIAS_Service_Interface
    ↳ ESAS6_2_WIAS_Service_Interface
    ↳ ESAS6_2_WIAS_Service_Interface

    Package ESAS6_2
    ↳ ESAS6_2_WIAS_Service_Interface
    ↳ ESAS6_2_WIAS_Service_Interface
    ↳ ESAS6_2_WIAS_Service_Interface
    ↳ ESAS6_2_WIAS_Service_Interface

    Nested Class Summary
    ESAS6_2_WIAS_Service_Interface.InnerClass
    ESAS6_2_WIAS_Service_Interface.InnerClass
    ESAS6_2_WIAS_Service_Interface.InnerClass
    ESAS6_2_WIAS_Service_Interface.InnerClass

    Field Summary
    ESAS6_2_WIAS_Service_Interface.InnerClass
    ESAS6_2_WIAS_Service_Interface.InnerClass
    ESAS6_2_WIAS_Service_Interface.InnerClass
    ESAS6_2_WIAS_Service_Interface.InnerClass

    Constructor Summary
    ESAS6_2_WIAS_Service_Interface.InnerClass
    ESAS6_2_WIAS_Service_Interface.InnerClass
    ESAS6_2_WIAS_Service_Interface.InnerClass
    ESAS6_2_WIAS_Service_Interface.InnerClass

    Method Summary
    Methods inherited from class java.lang.Object
    clone, equals, hashCode, getClass, notify, notifyAll, toString, wait, wait, wait
    
```

3.2 Cloud Information Interface

The Cloud Interface is responsible for providing the complete browsing functions of the energy-saving information to users. It contains system homepage, real-time browsing, historical queries, decision-making process, data-mining process, CBR process and WIAS services.

The real-time browsing page allows users to browse the real-time data of each sensor. Its interface consists of a hierarchical data table arranged in order from left to right, and hierarchical permutations based on their corresponding data sizes. Due to this structure, users can easily understand the corresponding information at a glance. The hierarchical structure was constructed by WIAS services *Share_ViewSensorInfo* and *Share_ViewRawData*. Finally, this page was automatically refreshed periodically (every 10 s at present), in order to dynamically display information.

The historical query page allows users to query all variations in historical monitored data and represent corresponding variations as line charts and data tables, making those monitored data user friendly, with the help of the WIAS Web service *Share_ViewRawData*, fully showing corresponding charts or tables after the user enters query conditions.

When users want to identify the information decision-making process, they can use the decision-making process page to get the corresponding processing procedure. The method involves reading the system log file in a fixed unit time (currently 10 s), and representing corresponding results. Figure 5 illustrates the content of the system log files that were periodically entered by the receiver, parser, transmitter and decision maker in their corresponding processes, with their own procedure names as tags. Based on these tags, the cloud information interface then displays their data in the corresponding data fields.

The WIAS service page is responsible for providing, testing and displaying the bottom layer of operation on WIAS Web services supporting the system. The data-mining process page and CBR process page are responsible for providing detailed information of data-mining process and CBR process respectively. The system homepage is the cloud information system interface itself, which becomes the system webportal to provide entry to the system with menus of all system functions.

4 System Demonstrations, Evaluations and Comparisons

4.1 Information Processing and Decision Making Interface Platform

As mentioned above, the system processing procedure of the proposed system is as shown in Fig. 6. The left-hand side is responsible for displaying the dynamic decision-making process that consists of decision-making process information

Fig. 5 Part of the system log file

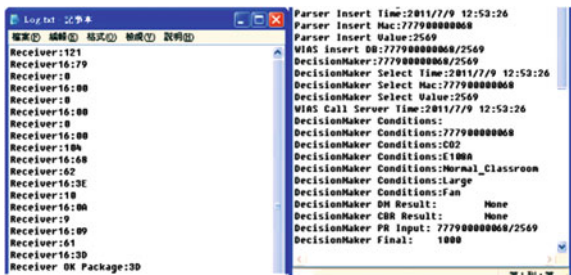


Fig. 6 Interface platform of the proposed system

The screenshot shows a web-based interface with a table of data. The table has columns for '数据源' (Data Source), '传输结果' (Transfer Result), '决策结果' (Decision Result), and '数据大小' (Data Size). The data is organized into sections: Receiver Process, 传输数据 (Transfer Data), 数据包源 (Data Packet Source), 验证数据 (Validation Data), 分析结果 (Analysis Results), Decision Process, and W.I.A.S. Sensor Data. The table contains multiple rows of data with timestamps and numerical values.

coming from the Receiver/Transmitter and Decision Maker, including information ranging from sensor data to decision-making results. The right-hand side is responsible for showing the integration list that merges with the packet information of the Receiver/Transmitter, the corresponding transferred results, and the decision-making results of the Decision Maker.

4.2 Cloud Information System Interface

The Cloud Information system Interface is responsible for providing the complete browsing functions of energy-saving information to users, which consist of many independent pages with individual information display functions constructed by PHP (Personal Home Page). It contains the system homepage, real-time browsing, historical queries, decision-making process and WIAS services [8]. Here are the data-ming process page (Fig. 7) and CBR process page (Fig. 8).

Fig. 7 Data-ming process page



Fig. 8 CBR process page



4.3 System Evaluations

The information decision making means that the optimal results are chosen from a group of related candidate sets. Finding specific and/or useful information on the Internet is similar to picking a random sample from a huge amount of data. In the sampling survey domain, reliability was usually employed to measure the degree of precision of the sampling system itself, while validity testing emphasized whether it could correctly reflect the properties of the appearance of things. This study employed the aid of a mathematical model, provided by Peter [9] in 1979 and cited in several papers, to represent the definitions of reliability and validity. The experimental outcomes are shown in Table 1. The average reliability and validity values were 0.989687 and 0.996558, respectively. From the technical literature [10], we know that the regular-level values of reliability and validity were 0.7 and 0.5, respectively, which verify and validate our experiment results with high-level outcomes of information decision-making.

The satisfaction evaluation of our system interface is very important. For example, we conduct a “usability” analysis on the system content, and an “Easy-to-use” analysis on the system operation. This study employed the 5E function

Table 1 Overall reliabilities and validities of the proposed system

	Reliability	Validity
Humidity	0.994276	0.998102
Temperature	0.996089	0.99927
Illuminance	0.990592	0.995771
CO ₂	0.977792	0.99309
Average	0.989687	0.996558

proposed by Quesenbery [11] for true analysis of the usability of the proposed system. In order to evaluate usability, this study employs the ten basic principles of user interface design suggested by Nielsen [12]. The decision-making interface and cloud information interface of the proposed system are a twin system, and they can be evaluated as a single system; when evaluated with a combination of Quesenbery and Nielsen, the satisfaction degree of the decision-making interface is 53 %, while the cloud information interface scores 60 %. When one of the two above standards can be reached, it appears to meet the satisfaction requirement; the overall satisfaction degree can be improved, up to 73 %, detailed as shown in Table 2.

Table 2 Whole user satisfaction analysis of the proposed system

Standards	Items	System decision-making interface	Cloud information interface	Whole system interface
Usability Quesenbery 5E	Efficient	O	O	O
	Effective	O	O	O
	Engaging	O	O	O
	Error Tolerant	X	X	X
	Easy to Learn	X	O	O
Easy-to-use Nielsen	Visibility of system status	O	X	O
	Match between system and the real world	O	O	O
	User control and freedom	X	X	X
	Consistency and standards	O	O	O
	Error prevention	X	O	O
	Recognition rather than recall	X	O	O
	Flexibility and efficiency of use	O	O	O
	Aesthetic and minimalist design	O	O	O
	Help users recognize, diagnose, and recover from errors	X	X	X
Help and documentation	X	X	X	
Total comparisons		53 %	66 %	73 %

Legend: 「O」 means to have this function, while 「X」 means none

Fig. 9 Monitor system interface of energy-saving information of ITRI



4.4 System Comparisons

Figure 9 is the monitor system interface of the energy-saving information of the Industrial Technology Research Institute, ITRI, in Taiwan. Figure 10 is the energy-saving website display of Providence University in Taiwan. Its display function of the maximum contract electrical capacity will become the focus of one of our future investigations. The most important point is that the two systems mentioned above do not have the true control function of energy-saving feedback. That is a unique advantage of our prototype system. Table 3 summarizes all differences among the three systems mentioned above.

Fig. 10 Energy-saving website display of providence university



Table 3 Comparisons between the proposed system and the two related systems in Taiwan

Systems functions	The proposed system	ITRI's monitor system	Website of providence university
Dynamic curve diagram	O	O	O
Data table	O	X	O
Graphic user interface	O	O	O
Data refresh time	O	O	O
On-line browsing	O	X	O
Data query function	O	X	O
Visitor guidance	O	X	X
Dynamic decision process	O	X	X
Intelligent decision making	O	X	X
Feedback control	O	X	X

Legend: 「O」 means to have this function, while 「X」 means none

5 Conclusions and Discussions

This study developed an intelligent energy-saving information interface agent system with Web service techniques in cloud environments; it shows that the decision-making precision, system reliability and system validity yield excellent system qualities. In terms of user satisfaction according to Quesenbery and Nielsen, the proposed system can score as high as 73 %. There are still a number of necessary additions to be made to the system in future work, including: completing necessary support functions to the data mining agent and case-based reasoning agent, adding the calculation and display function of the maximum contract electrical capacity, operating through the cloud information interface to control electrical facilities. In terms of the combined Quesenbery and Nielsen user satisfaction analysis, the proposed system still has about 27 % to be investigated, including: Error Tolerance, User control and freedom; Help users recognize, diagnose and recover from errors; and Help documentation. In addition, with the use of JavaScript and Ajax, the proposed system's performance can be enhanced and optimized to provide still more artistic, colorful, interactive and varied information services.

Acknowledgement The authors would like to thank Hung-Chun Chiang, Ming-Yu Tsai and Guo-Jui Wu for their assistance in system implementation and experiments. This partial work was supported by the National Science Council, ROC, under Grants NSC-101-2221-E-129-001 and NSC-101-2632-E-129-001, and the Ministry of Education, Taiwan, R.O.C., under Grant Skill of Taiwan (1) Word No. 1010046558P.

References

1. Wu HH (2013) Introduction to Web Service Techniques. Report of academia sinica, academic institution in the Republic of China. <http://www.ascsc.sinica.edu.tw/nl/93/2023/02.txt>, Accessed 20 Jan 2013
2. Bureau of Energy of Ministry of Economic Affairs (2008) Electric power consuming statistics in energy statistics year book of Taiwan in 2008. Taipei, Taiwan
3. Energy Center of China Technical Consultants, Inc. (2007) Industry energy-saving service report. Taipei, Taiwan
4. Yang SY, Chiang HC, Wu GJ (2010) Developing an intelligent energy-saving information processing and decision supporting system. In: Proceedings of 2010 symposium on constructing industrial and academic park of green energy science and technology and intelligent energy-saving techniques and project achievement lunching ceremony, Taipei, Taiwan, pp 41–47
5. Yang SY (2013) A novel cloud information agent system with web service techniques: example of an energy-saving multi-agent system. *Expert Syst Appl* 40(5):1758–1785
6. Yang SY, Wu GJ (2011) Cloud data-mining agent system with web services—example on an energy-saving information system. In: Proceedings of 2011 joint conference on Taiwan software engineering and object-oriented technology and applications, Taipei, Taiwan, pp 396–400
7. Yang SY, Tsai MY (2011) Cloud case-based reasoning agent system with web services—example on an energy-saving information system. In: Proceedings of 2011 symposium on digital life technologies, Yunlin, Taiwan, pp H2-5
8. Yang SY, Lee DL (2012) Developing a cloud intelligent and energy-saving information interface agent with web services. In: Proceedings of the 26th IEEE international conference on advanced information networking and applications, Fukuoka, Japan, pp 1310–1315
9. Peter JP (1979) Reliability: a review of psychometric basics and recent marketing practices. *J Mark Res* 16:6–17
10. Wu TX (1985) The reliability and validity of attitude and behavior research: theory, application, and self-examination. *Public opinion monthly*, pp 29–53
11. Quesenbery W (2011) WQ Usability. <http://www.wqusability.com/>, Visited on Jan. 20, 2013
12. Nielsen J, Pernice K (2010) *Eyetracking web usability*, 1st edn, Chap 5. Peachpit Press, Pearson Education, San Francisco. ISBN 0-321-49836-4

Part VII
Intelligent Robotics, Automations,
Telecommunication Facilities,
and Applications

3D Trajectory Planning for a 6R Manipulator Robot Using BA and ADAMS

P. Masajedi, Kouroshe Heidari Shirazi
and Afshin Ghanbarzadeh

Abstract In this article we will study the end effector motion control for a series robot with 6 rotational joints to move on a predetermined 3-dimensional trajectory. Since for any end effector there are more than a single set of answers regarding to robot parts orientation, finding a method which gives designer all existing states will lead to more freedom of action. Two different methods were used to solve robot inverse kinematic. In the first method ADAMS software was considered, which one of the common software is in order to solve inverse kinematic problems. Then bee algorithm (BA) is used which is an intelligent method. This method is the one of the fastest and most efficient method among existing method for solving non-linear problems. Hence problem of inverse kinematic solution is transformed into an affair of optimization. Comparison of results from both models shows the reasonable performance of BA method in solution of robot inverse kinematic because of its capability in providing the answer from all existing states along with the privilege of no need to 3D modeling.

Keywords Manipulator robots · Bee algorithm · Inverse kinematic

The original version of the chapter has been revised: The author name “A Gün” have been added in the reference 7. A correction to the chapter can be found at

https://doi.org/10.1007/978-94-007-6996-0_114

P. Masajedi (✉) · K. H. Shirazi · A. Ghanbarzadeh Mechanical Engineering Department,
Shahid Chamran University of Ahvaz, Ahvaz, Iran
e-mail: p-masajedi@mscstu.scu.ac.ir

1 Introduction

Conducted researches in the field of robotics include a wide range of theoretical and practical topics like motion planning [1], intelligent control [2, 3], and motion control on predetermined 3-dimensional trajectories [4]. Trajectory design for robot arms is usually performed in Cartesian space and determination of robot joint movements by having the location and orientation of end effector is called robot inverse kinematics.

There are different methods for solving inverse kinematic problem including algebraic, geometrical, and trial and error methods which are both time consuming and difficult to be solved numerically [5]. In recent years there have been numerous efforts to use new methods in reverse kinematics solutions. KOKER et al. [6] considered a multi-layer neural network design for a robot with 3 degrees of freedom in 2004. DURMUS et al. [7] solved inverse kinematic for a robot with 6 degrees of freedom using BA algorithm in 2011.

The main aim of this research is investigating a novel method for solving inverse kinematic problem. The necessity for introducing a new method refer to the weakness of previous methods such as time-consumption and 3D modeling that not only need an exact simulated model but also in order to change the problem from a specific model to another one, simulated robot needs to be fully rebuild. Another downside is that using simulating software just evaluates one possible solution, while accessing to all possible answers is accessible using numerical methods. Because of difficulties in solving complex nonlinear equations of motion of robot, Bee algorithm, as an optimization method, is considered. The results obtained in this essay strongly demonstrate the reliability of this method along with no need to 3D modeling and consequently no more time need to be spent for changing the model. In addition, all possible solution can be acquired regarding to motion constraint of joints.

2 Inverse Kinematic

Figure 1 illustrates the KR16 robot specification which has been studied in this research.

For a robot with n degrees of freedom, relation between joints is given by (1).

$$x(t) = f(\theta(t)) \quad (1)$$

where $x(t)$ is the position of end effector, $\theta(t)$ is the vector of robot joints angles, and f is a nonlinear continuous function that connects joint variables to work environment coordination. This equation has only a unique answer solvable by analytical methods [8]. In the other hand, it is possible to solve the inverse kinematic problem by solving of the following equation.

$$\theta(t) = f^{-1}(x(t)) \quad (2)$$

Unlike direct kinematic, this equation does not have a unique answer. In order to solve it, Denavit-Hartenberg characteristics need to be defined for a robot firstly.

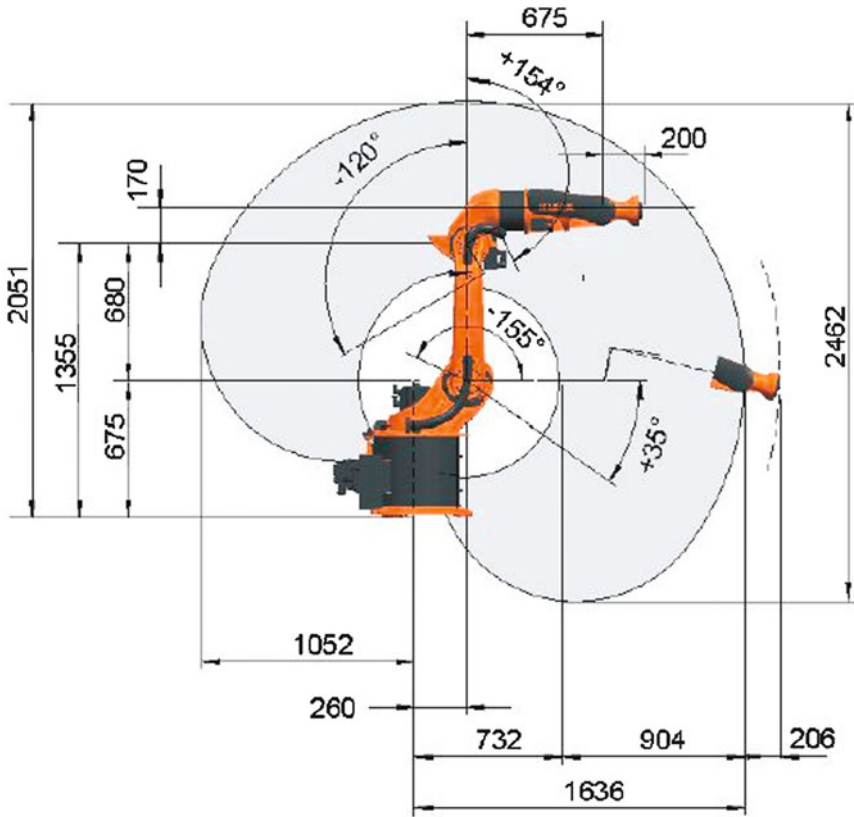


Fig. 1 Specification of KOKA KR16

3 Denavit-Hartenberg System

To explain the relevant motion of the end effector from fixed joint, a matrix needs to be defined which includes relative rotation and replacement of determined coordinate system from fixed coordinate system. For this purpose, Denavit-Hartenberg system is considered for each joint. According to definition, a rotational matrix that describes each joint relative to the previous joint is given by (3).

$${}^{n-1}T_n = \begin{bmatrix} \cos \theta_n & -\sin \theta_n \cos \alpha_n & \sin \theta_n \sin \alpha_n & a_n \cos \theta_n \\ \sin \theta_n & \cos \theta_n \cos \alpha_n & -\cos \theta_n \sin \alpha_n & a_n \sin \theta_n \\ 0 & \sin \alpha_n & \cos \alpha_n & d_n \\ 0 & 0 & 0 & 1 \end{bmatrix} \quad (3)$$

Finally, the matrix determining orientation and position of end effector is derived by multiplying matrices obtained from (3) for each joint.

$${}^6T_0 = {}^0T_1 {}^1T_2 {}^2T_3 {}^3T_4 {}^4T_5 {}^5T_6 = \begin{bmatrix} n_x & s_x & a_x & p_x \\ n_y & s_y & a_y & p_y \\ n_z & s_z & a_z & p_z \\ 0 & 0 & 0 & 1 \end{bmatrix}. \tag{4}$$

4 Analytical Solution

According to definition, a robot arm will have redundancy if for same end effector state there is more than a set of joint angles [8]. As it is mentioned in KOKA company tutorial file, for a specific position of end effector, there are 8 possible states presented in Fig. 2.

4.1 Possible Joints Orientation

Regarding to Fig. 2, 8 possible solutions for the same position of end effector will be evaluable through (5) for joints 1–6 respectively. The aim of this essay is finding specific set of joints variables which conduct the end effector motion on desired path.

According to Fig. 3, all possible solutions for joint variables are evaluable by (5).

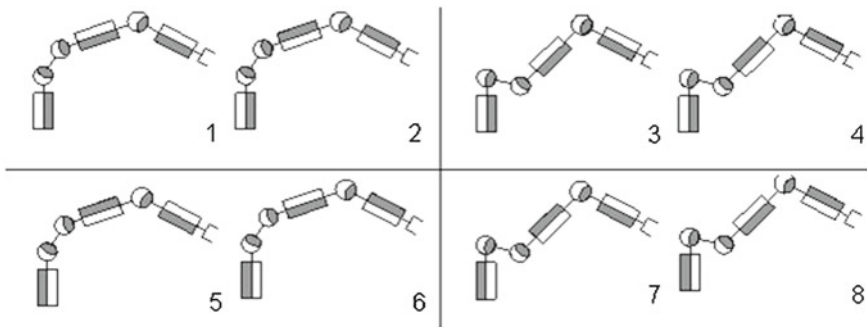


Fig. 2 Possible solution for KR16 robot inverse kinematic problem

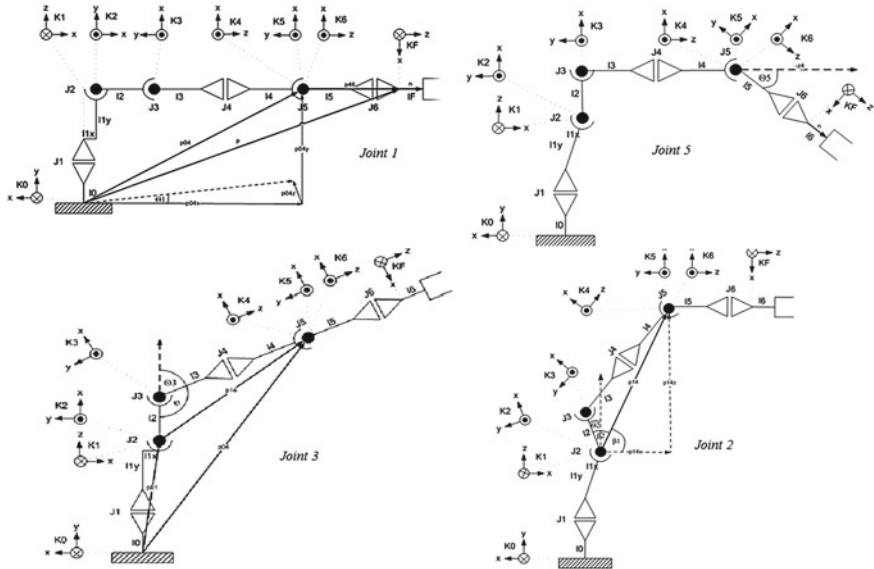


Fig. 3 Joints orientation for different positions of end effector

$$\left\{ \begin{array}{l}
 \theta_{1,1} = \theta_{1,2} = \theta_{1,3} = \theta_{1,4} = \arctan 2(-p_{04,z}, p_{04,x}) \\
 \theta_{1,5} = \theta_{1,6} = \theta_{1,7} = \theta_{1,8} = \arctan 2(-p_{04,z}, p_{04,x}) + \pi \\
 \Theta_{2,1} = \Theta_{2,2} = -(\beta_1 + \beta_2), \Theta_{2,3} = \theta_{2,4} = -(\beta_1 - \beta_2) \\
 \Theta_{2,5} = \Theta_{2,6} = (\beta_1 + \beta_2), \Theta_{2,7} = \Theta_{2,8} = (\beta_1 - \beta_2) \\
 \Theta_{3,1} = \Theta_{3,2} = \pi - \phi, \Theta_{3,3} = \Theta_{3,4} = \pi + \phi \\
 \Theta_{3,5} = \Theta_{3,6} = -(\pi - \phi), \Theta_{3,7} = \Theta_{3,8} = -(\pi + \phi) \\
 \Theta_{4,1} = \Theta_{4,6} = a \tan 2(r_{23,A}, r_{13,A}), \Theta_{4,2} = \Theta_{4,5} = a \tan 2(r_{23,A}, r_{13,A}) + \pi \\
 \Theta_{4,3} = \Theta_{4,8} = a \tan 2(r_{23,B}, r_{13,B}), \Theta_{4,4} = \Theta_{4,7} = a \tan 2(r_{23,B}, r_{13,B}) + \pi \\
 \Theta_{5,1} = \Theta_{5,2} = \arccos(z_{4A}.n), \theta_{5,3} = \Theta_{5,4} = -\arccos(z_{4A}.n) \\
 \Theta_{5,5} = \Theta_{5,6} = \arccos(z_{4B}.n), \Theta_{5,7} = \Theta_{5,8} = -\arccos(z_{4B}.n) \\
 \Theta_{6,1} = \Theta_{6,5} = a \tan 2(-r_{32,A}, r_{31,A}), \Theta_{6,2} = \Theta_{6,6} = a \tan 2(-r_{32,A}, r_{31,A}) + \pi \\
 \Theta_{6,3} = \Theta_{6,7} = a \tan 2(-r_{32,B}, r_{31,B}), \Theta_{6,4} = \Theta_{6,8} = a \tan 2(-r_{32,B}, r_{31,B}) + \pi
 \end{array} \right. \quad (5)$$

5 BA Based Optimization

Imitating the interesting foraging behaviors of honeybees, Pham et al. [9] proposed bees' algorithm (BA) to solve the optimization problems. In BA methodology,

N random solutions are constructed, in which, N_1 solutions, with higher fitness values, are considered as the best solutions. Among the best solutions, N_2 solutions with greater fitness values are chosen as the elite ones. To reach better solutions, neighborhood searches around the best and elite solutions are performed. n_1 and n_2 are the number of exploitations around the best and elite solutions, respectively, while n_2 is greater than n_1 . Besides, the remaining $N-N_1$ solutions are chosen randomly. Note that, the random solution, x_{rand} , is calculated by (6).

$$x_{rand} = x_{min} + \alpha(x_{max} - x_{min}) \quad (6)$$

where α is a random vector which its elements are between 0 and 1. x_{min} and x_{max} are the lower and upper bounds for the solution vector, respectively. The neighborhood searching around each element of the solution vector (i.e. x_i) is performed using

$$xp_i = (x_i - r) + 2\alpha_i \cdot r \quad (7)$$

where xp_i is the i th element of the new solution vector obtained from a neighborhood search around x_i with the radius equal to r . The iteration continues until the stopping criterion is met. The optimization target is to find the best solution of the problem. In this paper, we are searching for the best selection of joint angles to control the end effector in desired path, hence objective function will be defined as (8).

$$Error = (x - x_{desired})^2 + (y - y_{desired})^2 + (z - z_{desired})^2 \quad (8)$$

The number of scout bees using in optimization with BA is 50, number of best selected patches is 3, number of elite selected patches is 1, number of recruited bees around best selected patches is 4, and patch radius for neighborhood search is selected 0.02.

6 Simulation Results

In this section results evaluated by ADAMS and BA will be illustrated. In order to obtain Adams results, the robot is simulated in ADAMS environment and then it has been constrained by the end effector to move on predetermined path. Subsequently, corresponding joints variations are measured through the path.

To evaluate the BA results, 21 accuracy points are defined as a presumed trajectory to be followed by the end effector and then a set of joint angles will be calculated from (8) according to BA process. By accounting motion limitation of each joint, 8 possible answers are accessible for a specific target.

By using interpolation method between driven angles for each joint, related spline could be obtained. Then these splines are assumed as the motor input for

each joint in ADAMS. Consequently, end effector movement according to joints input evaluated by BA is compared with predetermined trajectory in order to test its reliability. Figure 4 shows 2 different set of joint angles obtained by BA (blue dot) and ADAMS (red line) for same end effector predetermined trajectory.

According to Fig. 4, the green curve exhibits calculated joint angles via BA which are connected to each other using 6th order interpolation and in order to move on desired trajectory.

By inserting calculated values for each joint, based on selected accuracy points, and using Eqs. (3) and (4), p_x, p_y, p_z will be evaluated. Figure 5 shows these amounts (black dot) which are connected to each other using sixth-order interpolation.

In order to study the calculated joint angles more precisely, estimated values through BA (Fig. 4) are imported as motor inputs in ADAMS. Figure 6 shows that how robot moves in ADAMS environment regarding imported amounts for each joint.

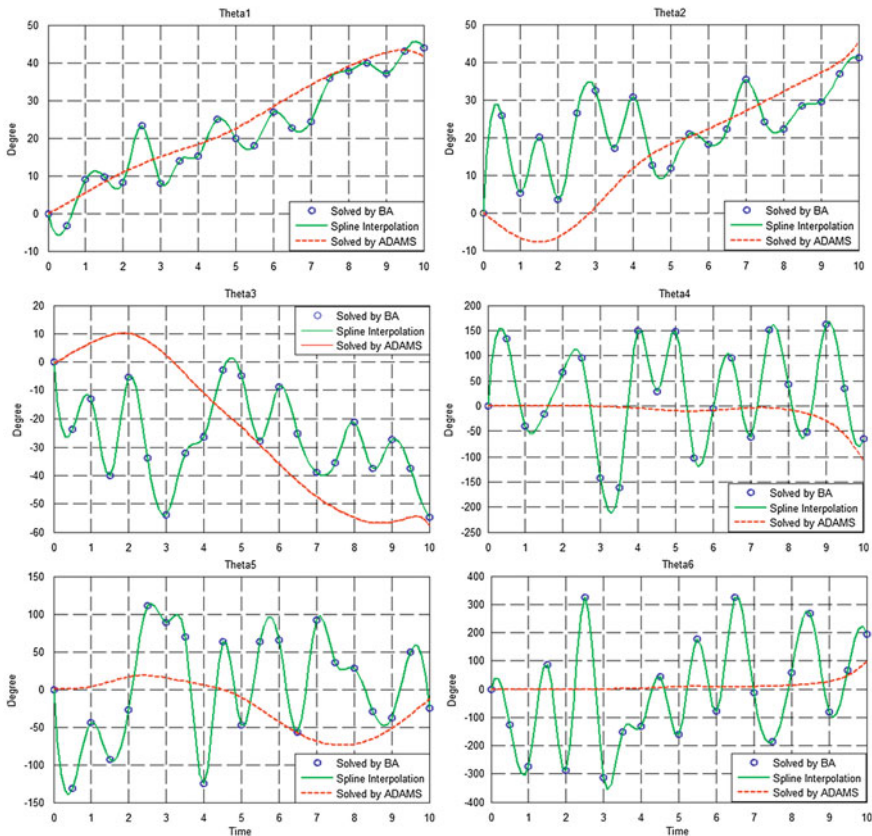


Fig. 4 Joints variation evaluated by ADAMS and BA

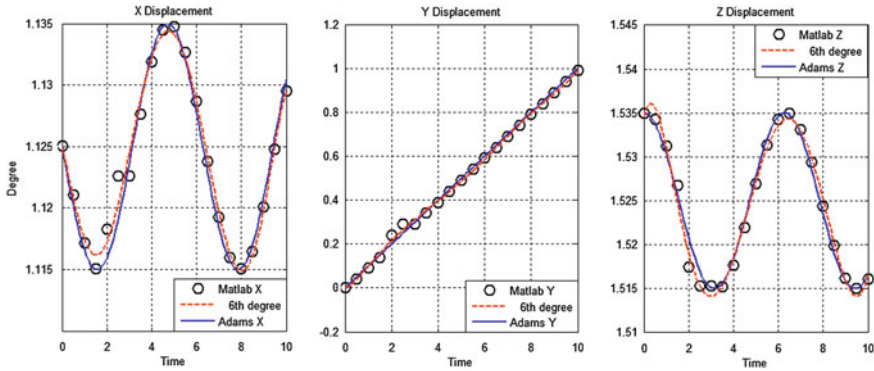


Fig. 5 The end effector trajectory for components X, Y and Z

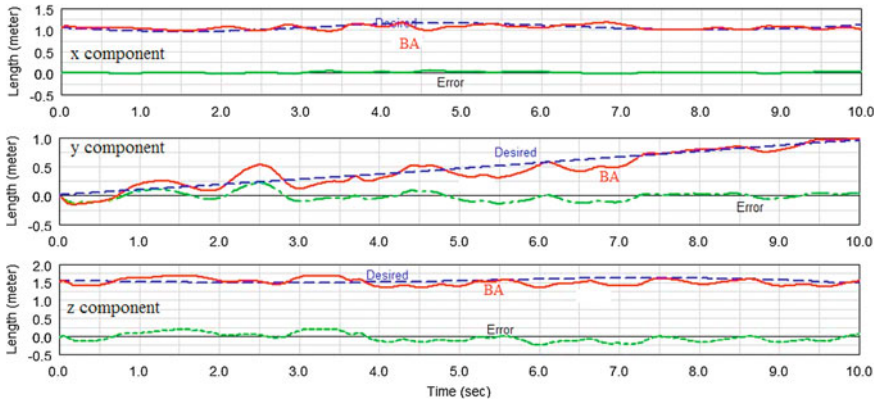


Fig. 6 End effector components variation comparison

In Fig. 6, green curve shows the difference between traversed trajectory and desired one. As it is depicted in figure, end effector follows the desired path while created error is close to zero. Undoubtedly, using more accuracy points will increase the precision of tracking.

According to Fig. 7, forces tolerated by joints in a situation in which values calculated by ADAMS are used have a more uniform trend, while the magnitude of these forces are greater than values calculated by BA method.

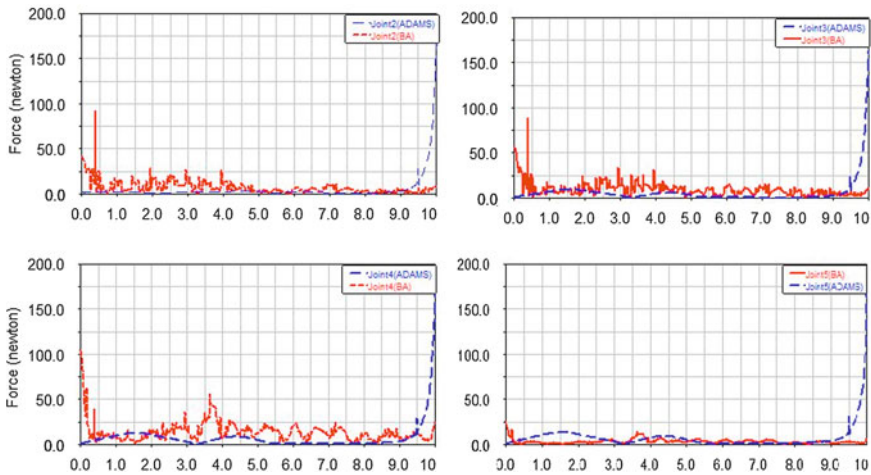


Fig. 7 Comparison of force created in joints by ADAMS and BA

7 Conclusion

In this article inverse kinematic problem is studied for a 6R manipulator robot using ADAMS and BA intelligent optimization method. For this purpose both linear and curved trajectories were considered to evaluate the reliability of mentioned methods.

According to simulation results, ADAMS software exhibited very high precision in predicting joint angles to conduct a robot on a predetermined trajectory, but a precise 3D model will be required and there with, only one of 8 possible states are calculated. To point out some advantages of optimization methods, we could refer to its capability of calculating all possible states for joint angles without need to 3D simulation of robot, in a very short time and with a high level of precision. Hence, the designer will have more freedom of action in dealing with physical obstacles for a given state by using other states. Also, in order to increase precision, number of accuracy points can be increased so that satisfies the criteria.

References

1. Smith KB, Zheng Y (2001) Optimal path planning for helical gear profile inspection with point laser triangulation probes. *J Manuf Sci Eng* 123:90–98
2. Hu H, Ang MH, Krishnan H (2000) Neural network controller for constrained robot manipulators. In: *International conference on robotics and automation*, San Francisco, pp 1906–1911
3. Jiang P, Li Z, Chen Y (2001) Iterative learning neural network control for robot learning from demonstration. *J Control Theory Appl* 21:447–452

4. Ou Y, Xu Y, Krishnan H (2004) Tracking control of a gyroscopically stabilized robot. *Int J Robot Autom* 19:125–133
5. Küçük S, Bingül Z (2005) The Inverse kinematics solutions of fundamental robot manipulators with offset wrist. In: *IEEE international conference on mechatronics, Taipei*, p 19–205
6. Köker R, Öz C, Cakar T, Ekiz H (2004) A study of neural network based inverse kinematics solution for a three-joint robot. *J Robotics Auton Syst* 49:227–234
7. Durmus B, Temurtas H, Gün A (2011) An inverse kinematics solution using particle swarm optimization. In: *11th international advanced technologies symposium, Elazığ*, pp 194–197
8. Hashiguchi H, Arimoto S, Ozawa R (2004) A sensory feedback method for control of a handwriting robot with D.O.F-redundancy. In: *International conference on intelligent robots and systems, Sendai*, pp 3918–3923
9. Pham D, Ghanbarzadeh A (2005) The bees algorithm. technical report, manufacturing engineering centre, Cardiff University, UK
10. Xu J, Wang W, Sun Y (2010) Two optimization algorithms for solving robotics inverse kinematics with redundancy. *J Control Theory Appl* 8:166–175

Performance Improvement of Human Detection Using Thermal Imaging Cameras Based on Mahalanobis Distance and Edge Orientation Histogram

Ahra Jo, Gil-Jin Jang, Yongho Seo and Jeong-Sik Park

Abstract In the thermal imaging, human object detection is difficult when the temperatures of surrounding objects are similar to or higher than human's. In this paper, we propose a novel algorithm suitable to those environments. The proposed method first compute a mean and variance of each pixel value from the initial several frames, assuming that there is no object in those frames. Then for each frame after the initial frames, the Mahalanobis distance is computed between the mean value and the current frame at each pixel, and the region of interest (ROI) is estimated. Finally, using the aspect ratio and edge orientation histogram, we determine if the ROI is human or not. The experimental results show that the proposed method is effective in both summer and autumn.

Keywords Thermal imaging · Surveillance system · Human detection · Mahalanobis distance · Edge orientation histogram

A. Jo (✉) · G.-J. Jang
Ulsan National Institute of Science and Technology, School of ECE, UNIST-gil 50,
Ulsan 689-798, Republic of Korea
e-mail: araya23@unist.ac.kr

G.-J. Jang
e-mail: gjang@unist.ac.kr

Y. Seo · J.-S. Park
Department of Intelligent Robot Engineering, Mokwon University, 88 Doanbuk-ro, Seo-gu,
Dajeon 302-729, Republic of Korea
e-mail: yhseo@mokwon.ac.kr

J.-S. Park
e-mail: parkjs@mokwon.ac.kr

1 Introduction

Most surveillance-system researches use a visible-light camera. However, it is hard to detect human activities at night or rainy weather with the visible-light cameras. Unfortunately, almost all crimes occur in those environments. To solve this problem, nowadays some researchers proposed using a thermal imaging camera. It is independent to lighting conditions because it measures the infrared radiation emitted by the object to capture the images.

Under the observation that, in thermal imaging at low temperatures, human is usually brighter than background objects such as buildings, trees, etc., we can easily extract human regions using statistical confidence measures in the gray-level, brightness histogram [1]. On the other hand, at high temperatures, human is darker than or very similar to backgrounds brightness hence histogram method is not suitable to those cases.

In this paper, we propose an efficient human detection method using thermal imaging cameras in summer and autumn. First, we propose a novel background-subtraction technique using the Mahalanobis distance [2] and its edge information to detect the region of interest (ROI) of the target human. Second, we propose a human classification technique using Bhattacharyya distance between the edge orientation histogram for the known template and the ROI.

The remainder of this paper is described as follows. We begin with characteristics of thermal images in the daytime and describe the main components of the object detection and person classification algorithms (Sect. 2). We then present experimental results (Sect. 3). Lastly, we conclude with a summary of our proposed method.

2 Human Object Detection in Thermal Images

James and Vinay proposed a method of classifying foreground and background regions using Mahalanobis distance [2]. However, it is difficult when the difference between background and foreground pixel values is small. Therefore, we propose a technique for background using the edges in the Mahalanobis distance images. To detect human regions, we use the edge orientation histogram method.

2.1 Characteristics of Thermal Images in the Daytime

The thermal imaging camera captures the infrared radiation emitted by objects. In the resulting image, each pixels in the (x, y) -plane is expressed by integer numbers from 0 to 255 according to the temperature of the corresponding pixel location.



Fig. 1 Thermal images in summer and autumn afternoons

As shown in Fig. 1, if the temperature of the background is higher or equal to the human's, it is hard to distinguish the human object from the background due to similar measurements.

Moreover, in the case of capturing the thermal images from a long distance, the measurement may contain time-varying noises because the radiated heat is absorbed by the air or other obstacles in the way. Figure 2 shows the measurement at a single pixel from a long distance, and the value fluctuates a lot along the time axis due to the additive measurement noise. Therefore, reliable foreground detection is very hard in such circumstance with simple background subtraction methods [1–3].

2.2 Construction of the Mahalanobis Distance Images

As shown in Fig. 2, the background image is not fixed and time-varying. If we assume that the additive noise in each pixel is a Gaussian random variable with zero mean, the variance is the only necessary parameter to describe its statistical behavior. We further assume that there is no moving object in the initial several frames, and compute the mean and the variance of those samples. The optimal estimate for the background is the sample mean, and the noise variance is the sample variance. The distance from the background image is computed by Mahalanobis distance [2], which is defined by the Euclidean distance normalized by a known variance, such that

$$D(x, y) = \frac{(I(x, y) - \mu(x, y))^2}{\sigma(x, y)^2} \quad (1)$$

where (x, y) is the pixel coordinate, $I(x, y)$ is the intensity at the pixel of the current image frame, and $\mu(x, y)$ and $\sigma(x, y)^2$ are the sample mean and the sample variance of the background. The 2-dimensional, Mahalanobis distance map whose elements

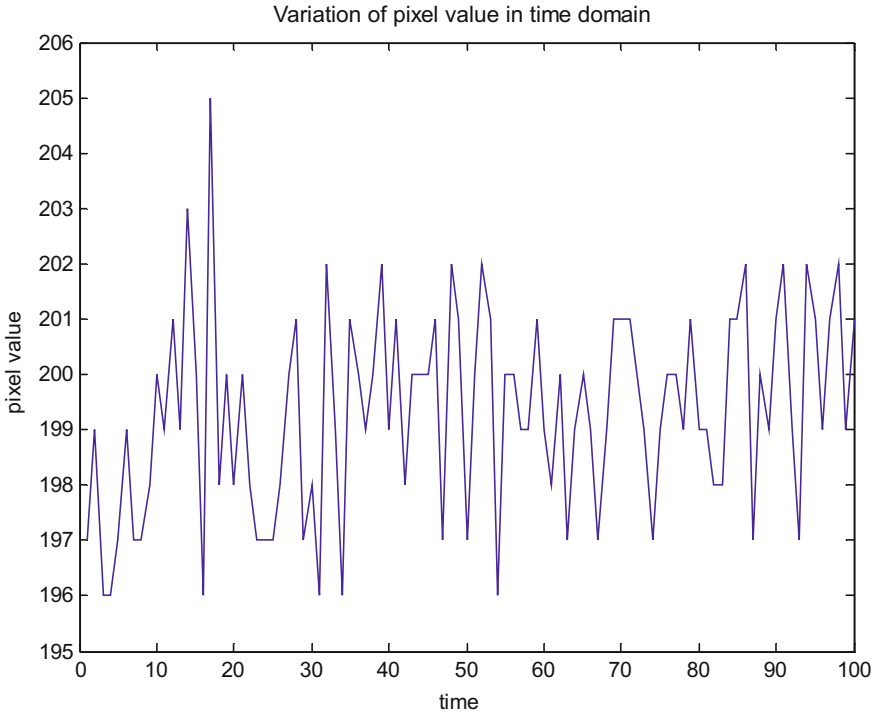


Fig. 2 Variation of pixel value in time domain

are $D(x, y)$, which is the difference from the initial background statistics, and used for detecting foreground objects from the current frame.

2.3 Edge Detection

We perform canny edge detection in the Mahalanobis distance map to find the existence of the foreground, moving objects in the current frame. Figure 3 is the Canny edge detection results when moving objects exist, and Fig. 4 is the result when there is no moving object.

As shown in Fig. 3, when there are moving objects, the difference from the background in the region containing the moving objects is much larger than the remaining region, so the edges around the moving objects become more distinctive. In Fig. 4, when there is no moving object, the difference from the background represented by the Mahalanobis distance map is all similar for all of the pixels, so a lot of false edges are generated. We classify those cases by comparing the variance of the edge map to the predefined threshold: if the variance of the edge map is larger than the threshold, the current image is determined to have no

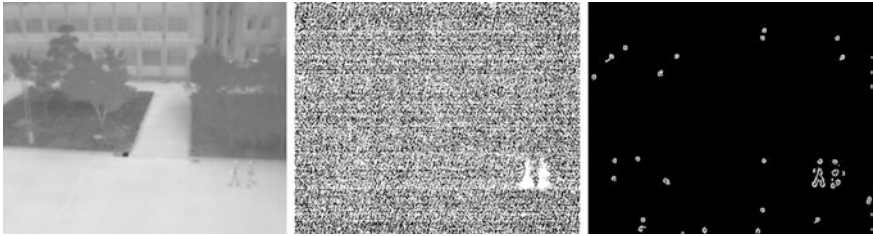


Fig. 3 An example of a moving object case. *Left* Input image. *Middle* Mahalanobis distance map. *Right* Canny edge detection results



Fig. 4 An example of no moving object case. *Left* Input image. *Middle* Mahalanobis distance map. *Right* Canny edge detection results

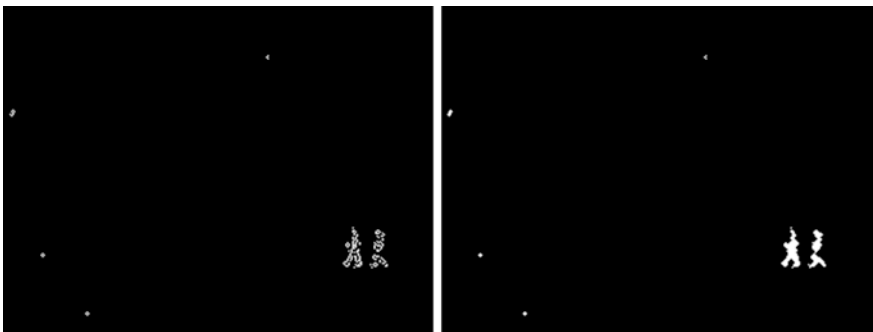


Fig. 5 Result of Sobel edge detection and morphologically close operation

moving object. Otherwise, we refine the object detection results by applying Sobel edge detectors followed by a morphologically close operation to fill inside the edge. The final object detection result is shown in Fig. 5.

2.4 Blob Grouping

Thermal camera measures the infrared radiation emitted by the object to capture the images. When the camera captures a human object, its image is highly affected by the thickness of the clothes and the carrying stuffs. This may make the region of a single person split into a number of sub-regions, i.e., in many separate parts. To handle such cases, we apply a blob grouping technique to find a reliable region of a human object.

We use grouping algorithm presented formerly [1]. Among detected blobs, the ones with smaller area than a given threshold are regarded as noises, and they are excluded in the grouping process. Blobs with enough area size are grouped by the distance between the centers of blob pair with considerations on the variance of the pixel locations in the blobs, and an example result is shown in Fig. 6.

2.5 Human Region Identification

Because the human walks upright, the aspect ratio of the detected object can be used to identify if the object is human or not. Simply speaking, if the height is shorter than the width, it is less likely to be a human object. More specifically, the edge orientation histogram (EOH) [4] is calculated for the current ROI and the template of the human object, and their dissimilarity is measured by the Bhattacharyya distance. The human classification using edge orientation histogram is described as follows: first, Canny edge detector is applied to the ROI as shown in Fig. 7.

Second, we measure the gradient of edges [4], and construct the histogram, with their relative frequencies to make it independent to the size of the ROIs (Fig. 8).

Fig. 6 Result of Blob grouping





Fig. 7 Left ROI. Right Canny edge detection of result

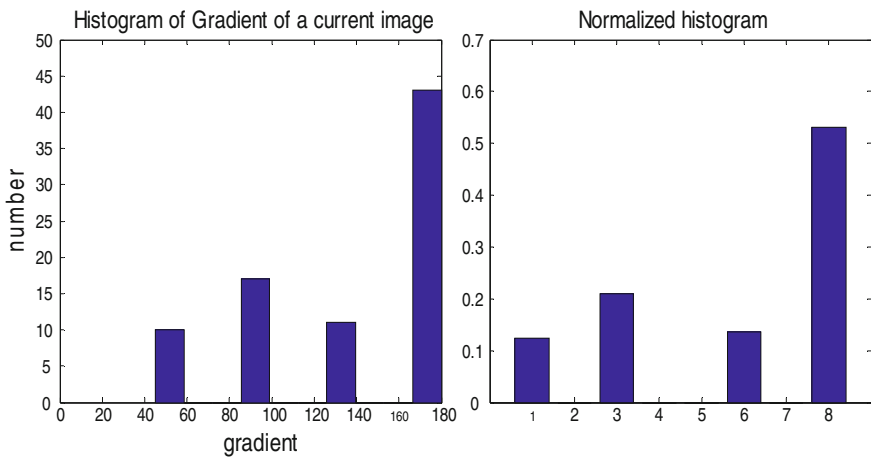
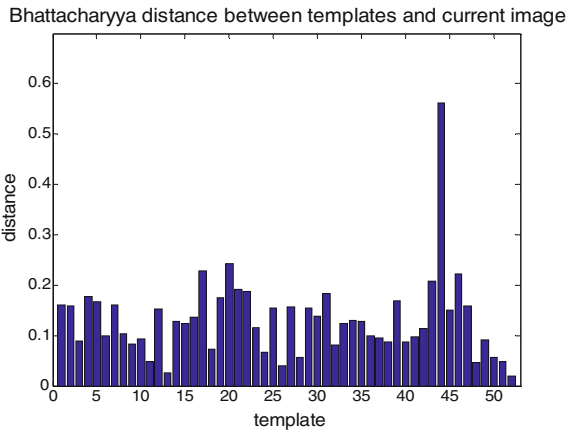


Fig. 8 Left Edge orientation histogram of a ROI. Right Histogram of relative frequencies of the edge orientations

Third, we measure Bhattacharyya distances between the histograms of the current ROI and pre-selected human templates. Then, find the minimum, and, if it is smaller than the predefined threshold, we determine that the ROI contains a human object (Fig. 9).

Fig. 9 Bhattacharyya distance between templates and current image



3 Experimental Results

The experimental results of the proposed method are shown in Fig. 10. The first row is experimental result in summer and other rows are results in autumn. Each image is arranged in a chronological order. As a result, the proposed method is effective in both summer and autumn.

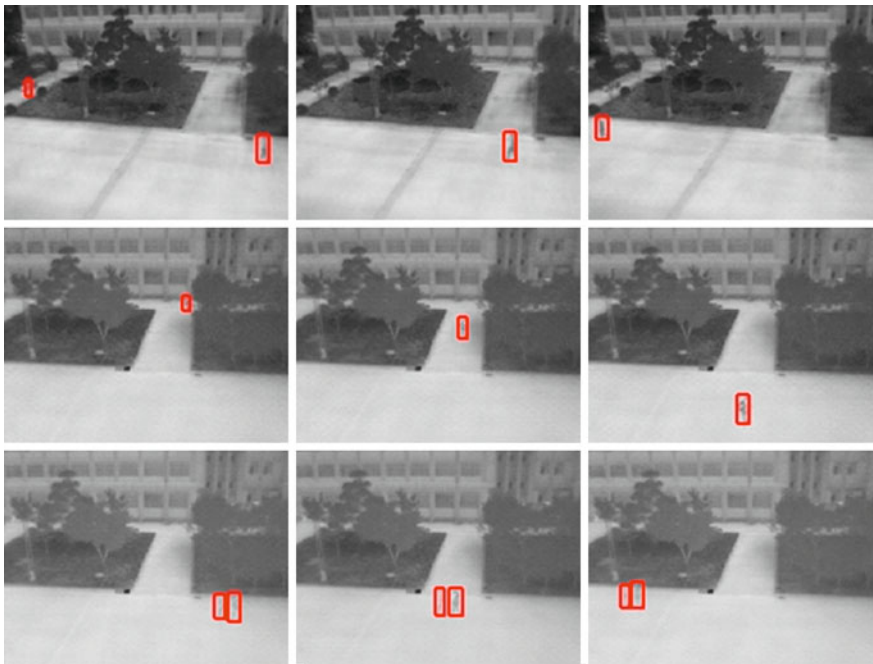


Fig. 10 Experimental results

The previously proposed methods are focused on winter and night. Therefore, we are not able to compare between ours and their methods.

4 Conclusion

We present a two-stage method to detect human objects in thermal imagery using a thermal-based background-subtraction and identification using aspect ratios of the ROIs. First, we check that if there exists a moving object in the current frame using the edge distribution of the Mahalanobis distance map. If found, we construct edge orientation histogram and compute the Bhattacharyya distances between the histograms of the current ROI and the known templates. Using the computed distances, we decide if the ROI is human or not. The experimental results show that the proposed method is effective at daytime.

Future work includes automatic adjustment of edge strength threshold for robust identification of human object in daytime to eliminate the need for visible light camera.

Acknowledgments This work was supported by the Basic Science Research Program through the National Research Foundation of Korea (NRF) funded by the Ministry of Education, Science and Technology (no. 2012-0008090) and the Basic Science Research Program through the National Research Foundation of Korea (NRF) funded by the Ministry of Education, Science and Technology (MEST) (2011-0013776).

References

1. Jo A, Seo Y, Park J-S, Jang G-J, Choi M-Y (2012) Person detection method using thermal imaging camera for outdoor surveillance system. The Institute of Webcasting: Internet and Telecommunication, Seoul
2. James WD, Vinay S (2004) Robust background-subtraction for person detection in thermal imagery. In: IEEE workshop on object tracking and classification beyond the visible spectrum
3. Han J, Bhanu B (2005) Human activity recognition in thermal infrared imagery. In: IEEE computer society conference on computer vision and pattern recognition
4. Weijin L, Zhang, Y-J (2007) Real time object tracking using fused color and edge cues. In: 9th international symposium on signal processing and its applications, pp 1–4, 12–15

Sensibility to Muscular Arrangement of Feedforward Position Control for Non-Pulley-Musculoskeletal System

Hitoshi Kino, Shiro Kikuchi, Yuki Matsutani and Kenji Tahara

Abstract This paper studies the feedforward position control induced by the redundancy in a non-pulley-musculoskeletal system. Targeting a planar two-link musculoskeletal system with six muscles as a case study, the motion convergence depending on the muscular arrangement is examined. The results indicate that the motion convergence is extremely sensitive to the muscular arrangement and that adding small offsets for the points of muscle connection can remarkably improve the positioning performance.

Keywords Tendon · Manipulator · Non-pulley model · Internal force

1 Introduction

Focusing attention on the dexterity of an actual human, the human system is characterised by two significant points: structural features and signal-processing features. The former connotes that the human body possesses a musculoskeletal structure; muscles create motion by transmitting muscular force through tendons. Because muscles can only transmit tension, redundant actuation is necessary.

H. Kino (✉) · S. Kikuchi
Fukuoka Institute of Technology, Wajiro-higasi, Higashi-ku, Fukuoka 811-0295, Japan
e-mail: kino@fit.ac.jp

S. Kikuchi
e-mail: mcm08003@bene.fit.ac.jp

Y. Matsutani · K. Tahara
Kyushu University, 744 Motoooka Nishi-ku, Fukuoka 819-0395, Japan
e-mail: matsutani@hcr.mech.kyushu-u.ac.jp

K. Tahara
e-mail: tahara@mech.kyushu-u.ac.jp

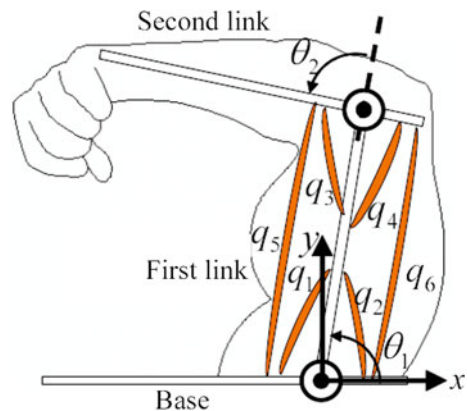
Consequently, the redundant actuation yields an internal force between muscles. To date, several humanoid robots with a musculoskeletal structure have been developed [1, 2]. Regarding the signal-processing aspect, many hypotheses have been advanced to elucidate the principles of human motion generation [3–6]. Consequently, by incorporating knowledge obtained from physiological findings into actual mechanical systems, manipulator systems that are more flexible and dexterous and thus more humanlike can be realised.

Turning now to robotics, the features of wire-driven (or ‘cable-driven’) systems appear similar to the human mechanical structure in terms of the drive of unidirectional force. Namely, these wire-driven systems use wire cables that can only transmit tension. Kino et al. reported that the internal force of a parallel-wire-driven system produces a particular potential energy field; sensorless position control can thereby be achieved by inputting the constant internal force balancing at a desired position [7].

In this paper, expanding on the feedforward positioning of a parallel-wire-driven system, the motion convergence of the musculoskeletal system modelled after a human arm is investigated when constant internal force balancing at a desired posture is inputted to the muscles. The target system has two links consisting of two joints (shoulder and elbow joints) and six muscles (two biarticular muscles and four simple joint muscles) under the zero-gravity condition, as presented in Fig. 1. Note that this system has no pulleys in the joints for the transmission of muscular tension. Each muscle is approximated as a straight muscle directly attached to limbs. This non-pulley-musculoskeletal model has a particular non-flat potential field generated by the internal force. Taking advantage of the constant internal force, the non-pulley-musculoskeletal model enables feedforward positioning.

The potential energy generated by the internal force is strongly governed by both the values of the internal force and the muscular arrangement. Therefore, the motion convergence might depend similarly on both. The dependency of the motion convergence on the muscular arrangement is then demonstrated through a

Fig. 1 Two-link non-pulley-musculoskeletal system



case example. The result indicates that the motion convergence of the feedforward positioning is extremely sensitive to the muscular arrangement and that adding small offsets for the muscular connected points on the links can specifically improve the work space in this case.

2 Feedforward Position Control

2.1 Problem Setting

To simplify the discussion, the following are assumed:

- The term “*muscle*” denotes as the mechanical parts of an actuator unit and wire cables in a wire-driven system.
- The muscles are regarded as massless rigid cables with variable length and can only transmit tension.
- The target system has no static/Coulomb friction and is under a non-gravity condition but have adequate viscosity in the joints.
- Each muscle is arranged to be straight.
- The target system guarantees non-singularity, defined as “vector closure [8]” during a motion.
- A sufficiently large internal force can be produced at any time to prevent the muscles from slackening.

2.2 Target System

This section expands the feedforward positioning to a planar two-link system with two joints (shoulder and elbow joints) and six muscles (two biarticular muscles and four simple joint muscles). In Fig. 1, q_i depicts the length of the i -th muscle and θ_1 and θ_2 indicate the shoulder and elbow angles respectively. The muscles labelled as $i = 1 \dots 4$ are simple joint muscles, and the others ($i = 5, 6$) are biarticular muscles. The joint angular vector is $\theta = (\theta_1, \theta_2)^T$ and the position of the hand is $x = (x, y)^T$. It is presumed that the joint angles are limited to $0 < \theta_i < \pi$ and that the relations among these displacement vectors are calculable analytically through inverse/forward kinematics.

The relation between the muscular tension vector $\alpha = (\alpha_1 \dots \alpha_6)^T$ and the resultant torque vector $\tau = (\tau_1, \tau_2)^T$ is expressed as $\tau = W(\theta)\alpha$, where $W(\theta)$ is a Jacobian matrix (2×6). Consider inputting the constant internal force v_d balancing at a desired angular vector, θ_d , to the muscular tension α of the two-link system. The generated torque τ can be rewritten as

$$\tau = W(\theta)v_d, \quad (1)$$

where

$$v_d = (I - W(\theta_d)^+ W(\theta_d))k_e. \quad (2)$$

The vector k_e can be selected arbitrarily as long as each element of v_d is positive.

From Eq. (1), the value of v_d is determined according to k_e and $W(\theta_d)$ which is determined uniquely by the muscular arrangement and the joint angle. Because this system has six DOFs with respect to the muscular lengths, which are constrained to the two DOFs of the joint angles, the internal force v_d belongs to the four-DOF null space of $W(\theta_d)$. Therefore, the internal force v_d cannot be determined uniquely. Thus, not only the design of the muscular arrangement but also the selection of the internal force is extremely important in applying feedforward positioning for musculoskeletal systems.

The resultant motion can be converged quasi-statically at the desired posture if the generated potential energy is minimised at the desired posture. In this case, the potential energy P generated by inputting v_d can be expressed as follows in the muscular length coordinates:

$$P = \sum_{i=1}^6 (q_i - q_{di})v_{di}. \quad (3)$$

Therein, $q_d = (q_{d1} \dots q_{d6})^T$ is defined as the desired muscular length corresponding to the desired position θ_d .

2.3 Inputting Internal Force

The analysis described herein uses the following internal force to obtain the simplest v_d :

$$v_d = \gamma(I - W(\theta_d)^+ W(\theta_d))(1, 1, 1, 1, 1, 1)^T, \quad (4)$$

where γ is a positive coefficient. Although this choice is one of the simplest selections for $k_e = (1, 1, 1, 1, 1, 1)^T$, it indicates an optimisation minimising the Euclidean norm of v_d under the condition that $\sum_{i=1}^6 v_{di}$ is constant.

This section investigates the motion convergence of the two-link system depending on muscle arrangement. Figure 2 presents the parameters of the arrangement. In this section, two samples of the muscle arrangement are prepared as a case study. The prepared arrangements differ in terms of the fixture points on the base and the second link as shown in Fig. 3a, b. The arrangement (a) has offsets for both simple joint muscles and biarticular muscles. This arrangement is

Fig. 2 Symbols for muscular arrangement

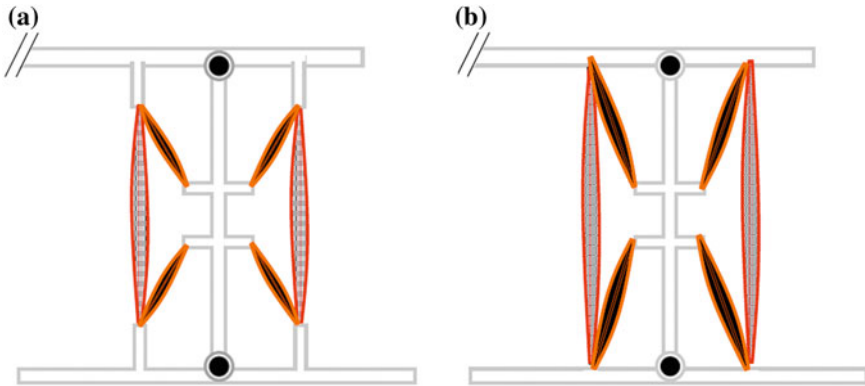
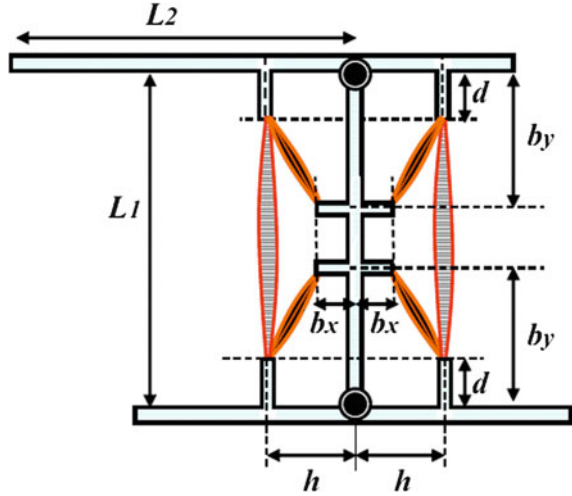


Fig. 3 Two samples of muscular arrangements. **a** OF-OFF arrangement. **b** D-D arrangement

defined as “OF–OF”. The arrangement (b) does not have any offsets for the muscular fixed points. This arrangement is defined as “D–D”. These configurations are symmetrical. The difference between D and OF configurations is simply $d = 0$ or $d > 0$. Next, giving Eq. (4) into the two-link system as the feedforward input, the work space and the motion convergence of the two samples are investigated. Here, *work space* is defined as the set of quasi-statically feasible desired points for the feedforward positioning. In other words, it is the set of desired positions for which motion can quasi-statically converge at each desired x_d corresponding to θ_d when the internal force balancing at each x_d is given. To reveal the motion convergence and the work space quasi-statically, it must be determined whether the potential energy P is minimised at each desired position. The

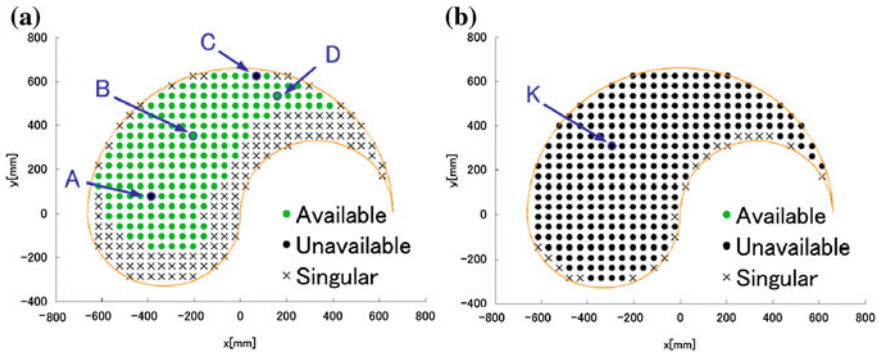


Fig. 4 Work space of two-link musculoskeletal system. **a** OF-OFF arrangement. **b** D-D arrangement

minimisation of the potential P at a desired position x_d allows for quasi-static feedforward positioning.

3 Result of Case Study

3.1 Work Space

Figure 4 shows the resultant work space of the two sample arrangements, the specifications of which are $h = 50$, $d = 20$, $b_x = 10$, $b_y = 120$, $L_1 = 330$, $L_2 = 330$ mm and $\gamma = 100$. To derive this work space, the potential energy of each desired point must be calculated numerically and checked for the location of the minimum point. In this case example, the desired points x_d are discretely varied in steps of 46 mm. According to the resultant motions, the desired points are classified into the following groups:

- The desired point equal to the minimum point of the potential energy is defined as an *available* desired point of the feedforward positioning.
- The point not corresponding to the minimum point is defined as an *unavailable* desired point.
- At some desired points, the balancing internal force delivered derived from Eq. (4) can have negative values. These points are termed *singular* points.

In Fig. 4, the green points show the available desired points and the black points are unavailable. The remaining black crosses are the singular points.

The OF-OFF arrangement widely spreads the available points in Fig. 4a such that it can achieve the feedforward positioning almost entirely throughout except through singular points. The singular points, however, are most numerous. There are two unavailable points: A and C in Fig. 4a. The potential gradient of the points

A and C is almost zero in the vicinity of each desired point. Therefore, the difference might be attributable to numerical error.

The D–D arrangement has unavailable points throughout the entire range of motion except for a few singular points, as depicted in Fig. 4b. Feedforward position control is impossible for this arrangement. This feature is opposite that of the OF–OF arrangement.

4 Conclusion

This paper described feedforward position control using muscular redundancy for (a musculoskeletal system and presented an investigation of the motion) convergence.

The feedforward position control was quasi-statically examined based on muscular arrangement. As a case example, giving small offsets for the muscular fixture points, this paper investigated the work space for two sample arrangements. Consequently, it was confirmed that the motion convergence is extremely sensitive to small changes in the muscular arrangement and that the tiny offsets improve the positioning performance in this case.

This case example treated only the offsets of the muscular arrangement. More detailed analysis, however, should be conducted based on quantitative evaluation. This topic will be the subject of our future works.

References

1. Mizuuchi I, Tajima R, Yoshikai T, Sato D, Nagashima K, Inaba M, Kuniyoshi Y, Inoue H (2002) The design and control of the flexible spine of a fully tendon-driven humanoid “Kenta”. In: Proceedings of the IEEE/RSJ international conference intelligent robots and systems, vol 3. pp 2527–2532
2. Mizuuchi I, Nakanishi Y, Sodeyama Y, Namiki Y, Nishino T, Muramatsu N, Urata J, Hongo K, Yoshikai T, Inaba M (2007) An advanced musculoskeletal humanoid Kojiro. In: Proceedings of the 7th IEEE-RAS international conference on humanoid robots, pp 294–299
3. Feldman AG (1986) Once more on the equilibrium point hypothesis (λ model) for motor control. *J Motor Behav* 18(1):17–54
4. Hogan N (1984) An organizing principle for a class of voluntary movements. *J Neurosci* 4(11):2745–2754
5. Kawato M, Furukawa K, Suzuki R (1982) A hierarchical neural-network model for control and learning of voluntary movement. *Biol Cybern* 57:169–185
6. Arimoto S, Sekimoto M (2006) Human-like movements of robotic arms with redundant DOFs: virtual spring-damper hypothesis to tackle the Bernstein problem. In: Proceedings of the IEEE international conference on robotics and automation, pp 1860–1866
7. Kino H, Yahiro T, Taniguchi S, Tahara K (2009) Sensorless position control using feedforward internal force for completely restrained parallel-wire driven systems. *IEEE Trans Robotics* 25(2):467–474
8. Kino H, Yahiro T, Takemura F, Morizono T (2007) Robust PD control using adaptive compensation for completely restrained parallel-wire driven robots: translational systems using the minimum number of wires under zero-gravity condition. *IEEE Trans Robotics* 23(4):803–812

Mobile Sensing-Based Localization Method for Illegal Electricity Usage by Using Inspection Robot

Bat-Erdene Byambasuren, Mandakh Oyun-Erdene
and Dong-Han Kim

Abstract Detection and localization of illegal electricity usage are important issue for power delivery companies of power system. In order to detect illegal electricity usage, network current-based methods using smart meter were mostly used in previous researches. Two main disadvantages of these methods are that they are unable to detect the exact location of illegal electricity usage. The latter is all users must be disconnected from the power system to detect the location. In this research, inspection robot can be used for detecting of illegal electricity usage. The inspection robot can define location of illegal electricity usage on the air transmission line without disconnection. In addition, this method can indicate fault location of transmission line. This paper presents a novel mobile sensing-based localization method for illegal electricity usage by using inspection robot, and it is verified through simulation results.

Keywords Illegal electricity usage · Localization method of illegal electricity usage · Inspection robot · Remote detection of illegal electricity usage

1 Introduction

In this era of technology, electricity is most useful part of our life, where the amount of consumption is steadily increasing. As this increasing, illegal electricity usage is stagnantly existed on the power delivery system. Detecting and localizing

B.-E. Byambasuren (✉) · M. Oyun-Erdene · D.-H. Kim
Department of Electrical Engineering, Kyung Hee University, Seoul, Korea
e-mail: baterdene@khu.ac.kr

M. Oyun-Erdene
e-mail: mandakh@khu.ac.kr

D.-H. Kim
e-mail: donghani@khu.ac.kr

illegal electricity usage is the most important issue for power delivery companies [1].

Illegal electricity usage can be detected by the current difference between two energy meter, which are installed on the start and end section of transmission branch [2, 3]. However, the main disadvantage of this method is the usage of additional energy meter, which has to be installed on every transmission branch of users.

Illegal electricity usage can be detected by measuring the line impedance when the power delivery system of all users are disconnected and then a low voltage signal having high frequency component is transmitted to the power delivery system [4]. However, the power delivery system of all users must be disconnected to detect illegal electricity usage.

However, sometimes, the illegal electricity usage on the power delivery system may be occurring on a low voltage of air transmission line [5]. In this paper, a novel method is proposed to detect and to define the location of illegal electricity usage on the air transmission line. The proposed method measures the current value of illegal electricity usage under the transmission line by using inspection robot. Once the illegal current value is calculated, then it can define the location of illegal electricity usage. The proposed method does not necessary to install additional energy meters on the transmission branch of electrical users. Significantly, the proposed method can detect illegal electricity usage in real-time without disconnecting the electricity on users side. This research presents a new trend of inspection robot for smart grid system as well as robot navigation using air electrical transmission line. Furthermore, the proposed method can be extended to detect the fault location for power system.

2 Mobile Sensing-Based Localization Method for Illegal Electricity Usage by Using Inspection Robot

Detection and Localization Method for Illegal Electricity Usage. We assume that power delivery system has infrastructure as shown in Fig. 1a. The structure of TSM is shown in Fig. 1b.

As shown in Fig. 1a, the main energy meter (MEM) and terminal smart meter (TSM) are installed on the starting node and on the final end of each electrical user, respectively. MEM measures the total energy of all electrical users, whereas TSM measures the energy usage of each user and transmits the measured value through a power line when the detection system does not detect illegal electricity usage. If an illegal electricity usage is occurred on the power delivery system, the measured value of MEM and the summation of each TSM measurements will not be equivalent. In this case, the proposed method begins the detection process by switching the status of TSMs. Note that the switches of TSM can be either turned

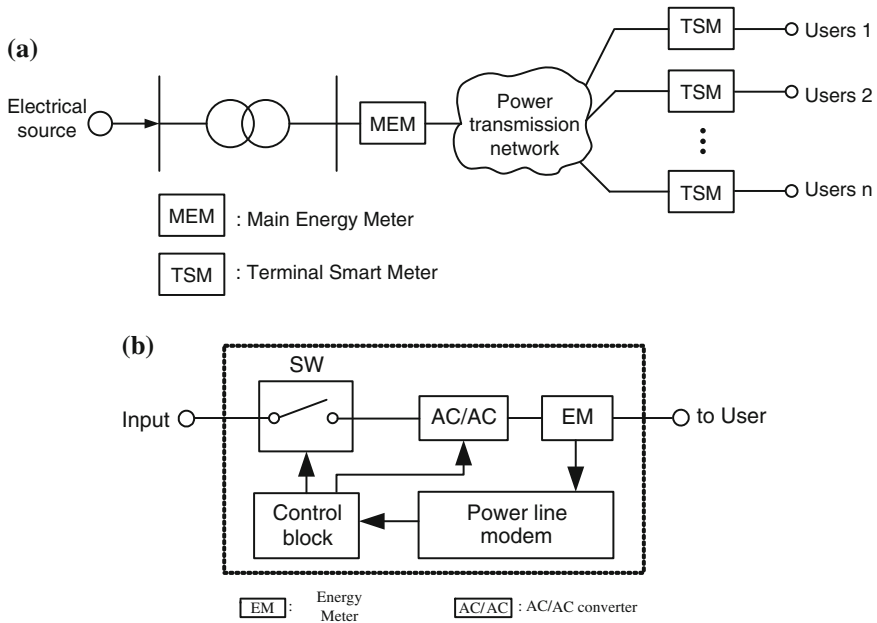


Fig. 1 Structures: a Proposed power delivery system, b Terminal smart meter

on or off simultaneously by the control command of control block with a high frequency component.

Voltage sag is converted to a normal by AC/AC converter, which is created by the switching frequency. Then, the normal voltage is delivered to an electrical user and the energy meter can measure user voltage as a normal condition. In this case, the main current is measured by MEM, which only expresses illegal electricity current when user’s currents are switched off by TSMs. However, when user’s currents are switched on by TSMs, the measured current of MEM represents the total current of power delivery system. In the proposed method, inspection robot is used to measure the current of transmission line for power system. The inspection robot can crawl under the transmission line and detect obstacle using CCD camera and other sensors. When the robot detects an obstacle, it can pass through by the obstacle [6–8]. In this research, the inspection robot should sense an illegal current by remote current sensor [9, 10], which is filtered from the measured line current when user’s currents are switched off by TSMs.

Separation Process of Illegal Current. To detect and localize of illegal electricity usage, the illegal current should be separated from measured current using the inspection robot. Figure 2 shows the signal process to separate the illegal current.

When the measured current from the inspection robot is multiplied by an impulse signal, the illegal current section can be extracted. In this case, the impulse signal becomes active when users are disconnected by TSMs. In addition,

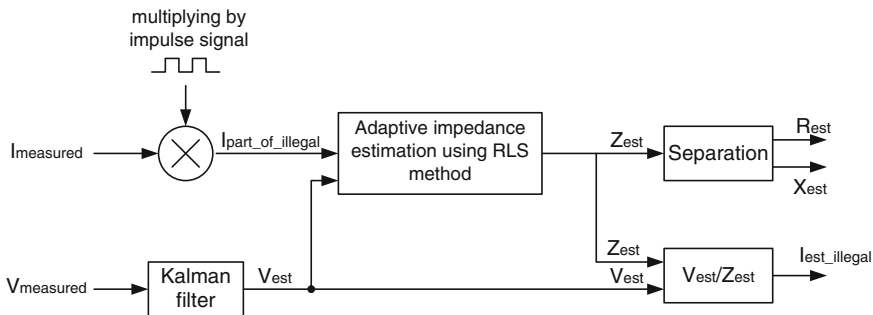


Fig. 2 Separation process of illegal current

the measured current can be multiplied by another active impulse signal when users are connected by TSMs. In this condition, multiplied current represents the total component of current.

Furthermore, the measured voltage from power delivery system is filtered by Kalman filter (KF) from the noise of measurement equipment [11]. Because KF generates efficiency response for sinusoid signals with constant frequency. After that, the adaptive impedance estimation is estimated by values of multiplied illegal current section and filtered voltage using Recursive Least Square (RLS) method.

To explain adaptive impedance estimation for separation process, let’s consider one of example. Figure 3a shows an example of extracted illegal current section. Multiplied current by another active impulse signal is shown in Fig. 3b.

From the Fig. 3a, when the impulse signal is active, the multiplied values of extracted current will be represented original illegal current value. However, the multiplied values of extracted illegal current will be equal to zero when the impulse signal is inactive which is called focusing section. In the focusing section, original illegal current values will be disappeared. Therefore, an estimation of original illegal current values is necessary in focusing section. To estimation, impedance values of illegal electricity usage should be calculated using measured current and filtered voltage when impulse signal is active. There is assumed that

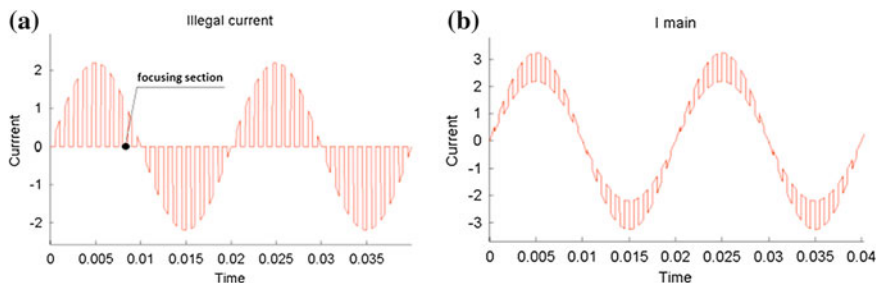


Fig. 3 Extracted current sections: **a** Extracted illegal current, **b** Extracted total current

illegal electricity usage is not changed and constant. Then, calculation of the illegal current is possible using estimated impedance and filtered voltage. According to Ohm's law, impedance is expressed as follows:

$$\begin{aligned} \dot{Z}_{est_illegal} &= \frac{\dot{V}_{est}}{\dot{I}_{meas}} \\ \dot{Z}_{est_illegal} &= R_{est_illegal} + jX_{est_illegal}, \\ \dot{V}_{est} &= V_{estR} + jV_{estI}, \\ \dot{I}_{meas} &= I_{measR} + jI_{measI} \end{aligned} \tag{1}$$

where $\dot{Z}_{est_illegal}$ is estimated impedance, $R_{est_illegal}$ is estimated resistance, $X_{est_illegal}$ is estimated reactance, \dot{V}_{est} is filtered voltage using KF, V_{estR} , V_{estI} are real and imaginary part of voltage, \dot{I}_{meas} is measured current of during active impulse signal, I_{measR} , I_{measI} are real and imaginary part of current.

Measured current using remote sensing method has measurement noise. Therefore, when there is used remotely measured current, accuracy of the estimated impedance will be decreased. In this case, RLS method can be used to increase the calculation accuracy and to reduce the measurement noise for estimated impedance [12, 13]. The calculation model can be represented as follows:

$$\begin{aligned} y_t &= \mathbf{h}_t^T \mathbf{X}_t \\ y_t &= \begin{bmatrix} I_{measR}^t \\ I_{measI}^t \end{bmatrix}, \mathbf{h}_t^T = \begin{bmatrix} V_{estR}^t & 0 \\ 0 & V_{estI}^t \end{bmatrix}, \mathbf{X}_t = \begin{bmatrix} \frac{1}{R_{est_illegal}^t} \\ \frac{1}{X_{est_illegal}^t} \end{bmatrix} \end{aligned} \tag{2}$$

The objective of least square method is to determine parameters such that the parameter error is minimized. It is possible to determine that the minimum error is obtained as:

$$\mathbf{X} = (\mathbf{h}^T \mathbf{h})^{-1} \mathbf{h}^T \mathbf{y} \tag{3}$$

The RLS method is iteratively used to calculate the parameter vector \mathbf{X} as follows:

$$\mathbf{X}_t = \mathbf{X}_{t-1} + \mathbf{G}_t [\mathbf{y}_t - \mathbf{h}_t^T \mathbf{X}_{t-1}] \tag{4}$$

$$\mathbf{G}_t = \frac{\mathbf{P}_{t-1} \mathbf{h}_t}{\mathbf{I} \lambda + \mathbf{h}_t^T \mathbf{P}_{t-1} \mathbf{h}_t} \tag{5}$$

$$\mathbf{P}_t = \frac{[\mathbf{I} - \mathbf{G}_t \mathbf{h}_t^T]}{\lambda} \mathbf{P}_{t-1} \tag{6}$$

where \mathbf{G} is the weight of matrix, \mathbf{P} is the degree of precision of the measurement, \mathbf{I} is the identity matrix, and λ is the forgetting factor.

Now, calculation of impedance is possible using RLS method. After the calculation of impedance, illegal current can be plotted by to estimated impedance and filtered voltage in focusing section. In addition, resistance and reactance can be defined from estimated impedance.

Localization Algorithm for Illegal Electricity Usage. The proposed working environment of inspection robot to detect the location of illegal electricity usage is shown in Fig. 4. The robot starts to move away from MEM and its motion is continued even if an illegal current is measured. Circle and triangle markers are placed on every node of power delivery system and on every branch of users, respectively. Note that the marker is not placed if the branch is continued and connected to a node.

Finite state diagram of inspection robot is shown in Fig. 5. If the measured current from robot has an illegal current section, the robot continues its motion towards a node marker. If the robot has arrived to the node marker, it detects all of triangle branch markers and moves to the most right side of branch by using CCD camera. The value of illegal current is calculated on the triangle marker of passed branch. If the illegal current is detected, the robot continues its motion to pass this branch until the exact location of illegal electricity usage. In this way, the exact detected location of illegal electricity usage can be transmitted by the robot. After transmission, the robot goes back to the node and checks the next branch. If the illegal current is not detected on the triangle marker of passed branch, the robot goes back to the node and checks the next branch. When all branches with triangle marker are examined, the robot goes to non-marker branch and repeats its process.

The proposed detection process gets terminated when there is no branch having any markers, which is equivalent to inspecting all power delivery system.

3 Simulation Results

Regulator simulation of voltage sag. Switching noise of TSM generates voltage sag and it can be compensated using AC/AC regulator. Note that buck-boost AC/

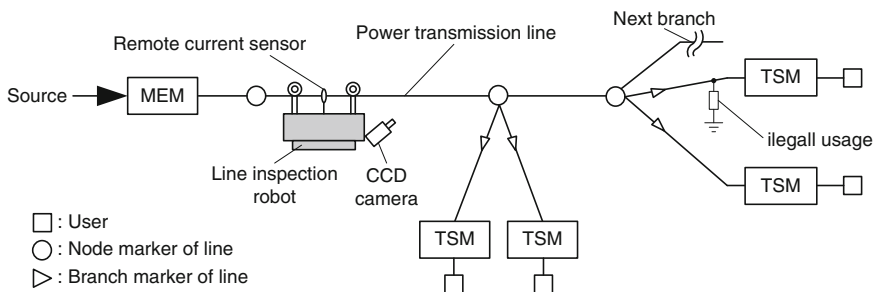


Fig. 4 Working environment of inspection robot

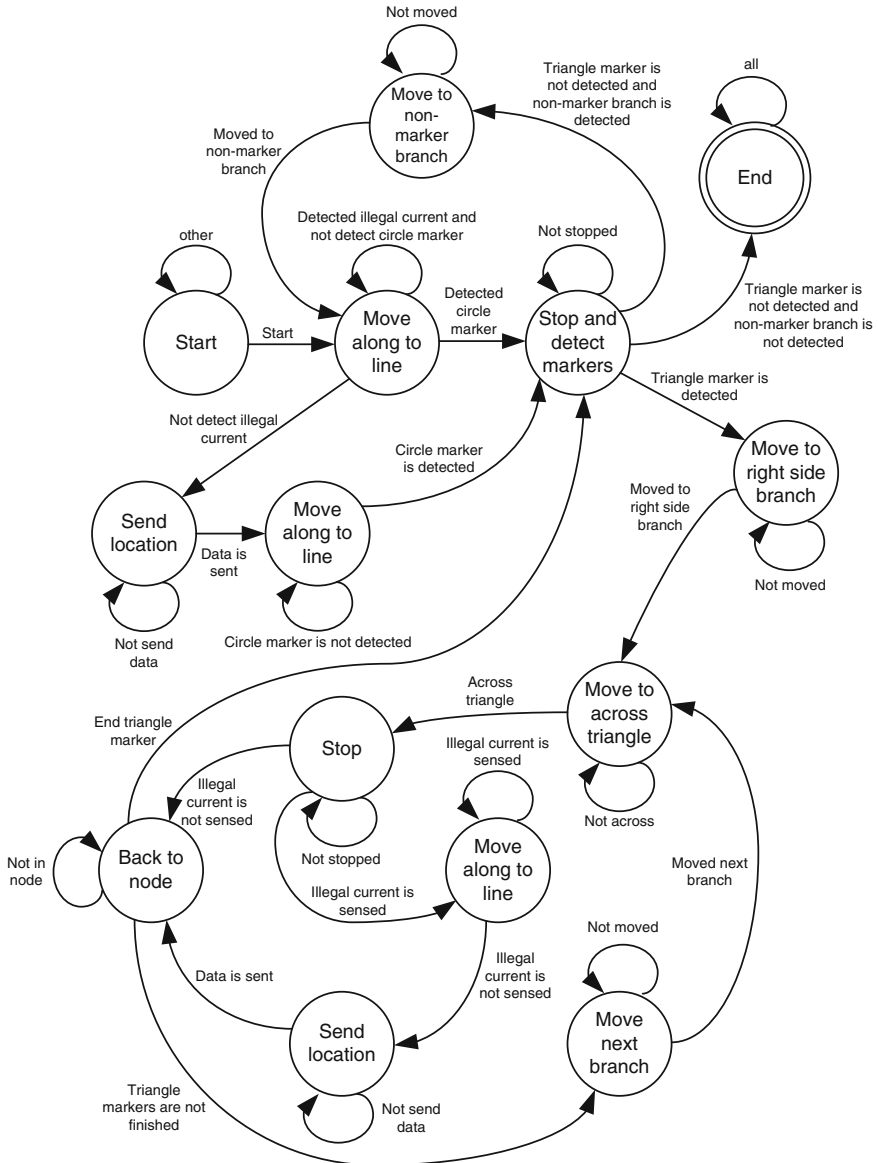


Fig. 5 Finite state diagram of inspection robot

AC convertor was used in the regulator simulation of voltage sag [14]. Figure 6 shows the result of regulator simulation. In the simulation the results of separation of illegal current, illegal electricity usage was connected in the power delivery line. From the result, we can see that the proposed method was able to regulate the user's output voltage level to the normal value.

Fig. 6 Output voltage on the user

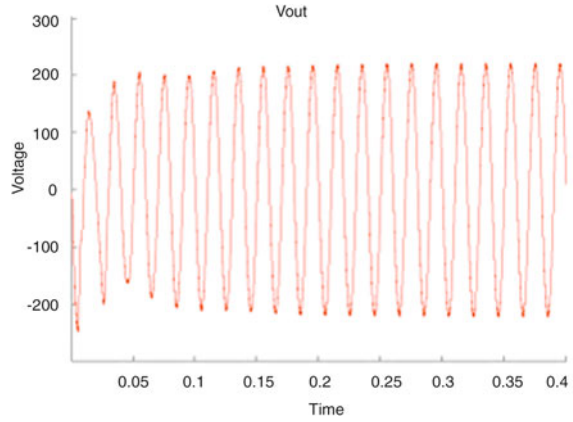
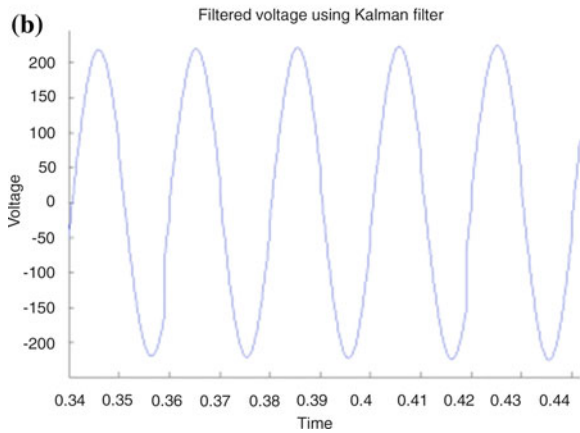
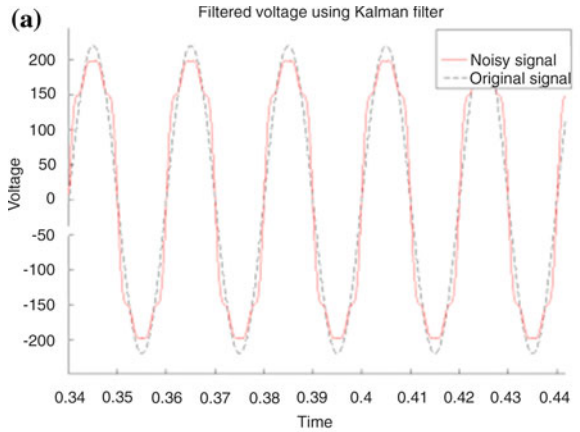


Fig. 7 Simulation results of filtering for measured voltage: **a** Noisy and original signal, **b** Filtered signal using KF



Simulation of filtering for measured voltage. A noise source is generated in voltage measurement, which depends on error of measurement equipment and statistical factor. KF can be used to decrease the noise source, which is simulated in this section. To implement simulation of filtering for measured voltage, noise sources are generated by Gaussian white noise with signal noise ratio (SNR) 20 dB, 15 % third harmonic, 10 % fifth harmonic, and 5 % seventh harmonic. After that, filtered signal is plotted using KF. The simulation results are shown in Fig. 7. From Fig. 7, noisy signal was successfully filtered, and filtered signal could be successfully used to separation process of illegal current.

Simulation of separation process for illegal current. According to structure as shown in Fig. 2, separation process was simulated. In the simulation results of separation of illegal current, illegal electricity usage was connected in the power delivery line model.

The parameters used in this line model are as follows: $V_{source} = 220 \text{ V}$, $f_{line} = 50 \text{ Hz}$, $R_{illegal} = 100 \text{ } \Omega$, $L_{illegal} = 500 \text{ mH}$ ($X_{illegal} = 2\pi f_{line} L_{illegal}$), $R_{load} = 200 \text{ } \Omega$, $F_{pwm \text{ of } TSM} = 1 \text{ kHz}$, duty ratio of switches $D = 0.5$. In addition, time period of simulation was 0.8 s, number of iteration was 8, and time periods of the each iteration were 0.1 s.

Figure 8 shows simulation results of separation process for illegal current. From the results of estimated resistance and reactance, estimated values were compensated to original values from third iteration. Real and imaginary parts of illegal

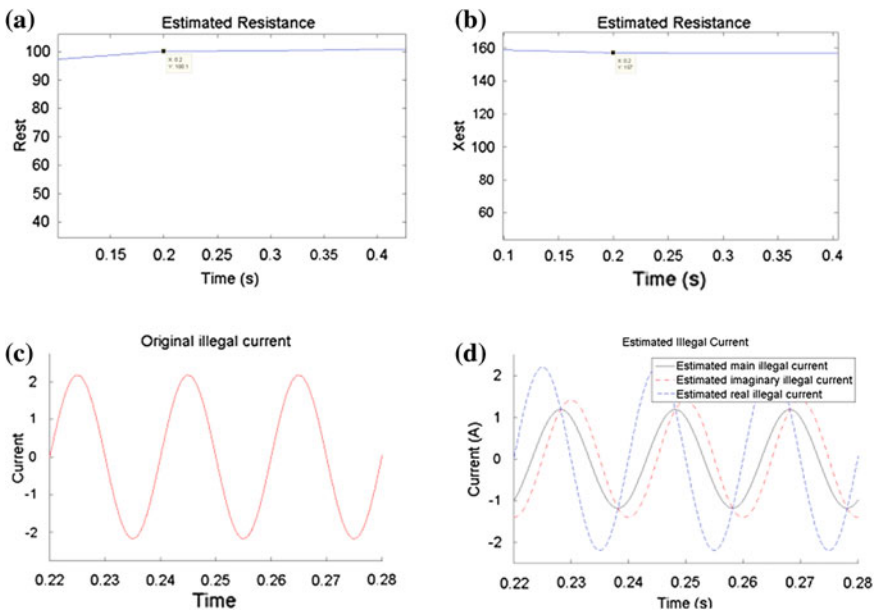


Fig. 8 Simulation results of separation process for illegal current: **a** Estimated resistance, **b** Estimated reactance, **c** Original illegal current, **d** Estimated illegal current

current and estimated illegal current were calculated using estimated resistance and reactance, which are plotted in Fig. 8d. From the results, we can see that illegal current was successfully separated.

4 Conclusion

The proposed method was implemented and the simulation results showed that the location of illegal electricity usage could be detected by the mobile sensing-based localization method. It was more efficient and useful way than installing the energy meter chip on every user's branch. Note that the proposed method became a consistent method for the new trend of smart grid system and conformed for the non-fixed power transmission line. Through the proposed method, the location and user of non-fixed power transmission line may be changed by the power delivery companies.

Acknowledgments This work was supported by a grant from the Basic Science Research Program through the National Research Foundation of Korea(NRF) funded by the Ministry of Education, Science and Technology (2012R1A1A2043822) and the Technology Innovation Program of the Knowledge economy (No. 10041834) funded by the Ministry of Knowledge Economy (MKE, Korea). In addition, it was supported by MKE (Ministry of Knowledge Economy), NIPA (National IT Industry Promotion Agency), and KOFST (The Korean Federation of Science and Technology Societies, 2012 Science and Technical Support specialists Supporters (H5701-12-1002)).

References

1. Bat-Erdene B, Sang-Yep N, Dong-Han K (2011) A novel remote detection method of illegal electricity usage based on smart resistance. *Futur Inf Technol Commun Comput Inf Sci* 185:214–223
2. Cavdar H (2004) A solution to remote detection of illegal electricity usage via power line communications. *IEEE Trans Power Deliv* 19(4):1663–1667
3. Deaver BJ, Radtke WO (2008) Power theft detection system and method. United States Patent, May 2008, No. US 2008/0109387 A1
4. Pasdar A, Mirzakuchaki S (2007) A solution to remote detecting of illegal electricity usage based on smart metering. In: *Proceedings of the IEEE international workshop soft computing applications*, pp 163–167
5. Depuru S, Wang L, Devabhaktuni V, Gudi N (2010) Measures and setbacks for controlling electricity theft. In: *North American Power symposium, 2010*, pp 1–8
6. Fu S, Liang Z, Hou Z, Tan M (2008) Vision based navigation for power transmission line inspection robot. In: *Proceedings of the 7th IEEE international conference on cognitive informatics, 2008*, pp 411–417
7. Guo R, Han L, Sun Y, Wang M (2010) A mobile robot for inspection of substation equipments. In: *Proceedings of the 1st international conference on applied robotics for the power industry, Oct 2010*, pp 1–5

8. Katrasnik J, Pernus F, Likar B (2010) A survey of mobile robots for distribution power line inspection. *IEEE Trans Power Deliv* 25(1):485–493
9. Tobin NP, McCormack M, O'Loughlin E, Tobin K (2001) Remote current sensing on overhead power lines. In: *CIRE2001*, June 2001, Conference Publication No. 482
10. Durand M (1998) Remote current sensor. In: *United States Patent*, June 1998, No. 5767668
11. Magnus D (2012) Power grid integration using Kalman filtering. Thesis of Master, Uppsala University, Uppsala
12. Zoran V (2000) A tutorial an adaptive control: the self-tuning approach. University of Zagreb, Croatia
13. Astrom KJ (1995) *Adaptive control*. Addison-Wesley, Boston
14. Jin N, Tang HJ, Liu W, Ye PS (2009) Analysis and control of buck-boost chopper type AC voltage regulator. In: *IPEMC*, pp 1019–1023

Development Age Groups Estimation Method Using Pressure Sensors Array

Junjirou Hasegawa, Takuya Tajima, Takehiko Abe
and Haruhiko Kimura

Abstract This paper aims to estimate age groups by walking data using pressure sensors array. Techniques of the age groups estimation in many retail businesses (for example, convenience stores, supermarkets, shopping malls, etc.) are marketable. There are many researches of the age estimation using face images, walking silhouette data, etc. However, there are some problems too. One of problem is that the estimation classes are a few. Moreover, many age estimation systems use some video cameras. Therefore, these systems may invade surveyed person's privacy by taking one's face images. In this study, this fact is one of merit in using the pressure sensors. The pressure sensors array gets feature quantity including center of gravity, pressure value, etc. In this study, our system classifies surveyed persons to 7 age groups as each decade. Here, surveyed persons are 20–80 s. Average estimation accuracy of all age groups is 72.86 %. The highest estimation accuracy is 86.67 % at 70 s.

Keywords Marketing · Age estimation · Walking data · Pressure sensors

1 Introduction

According to white paper on aging society, edition 2012, Japan, the population of elderly people 65 and over is 23.3 % of the total population of Japan. Japan will be undoubtedly the real aged society in the future. The ratio of the elderly people has

J. Hasegawa (✉) · T. Tajima
3-30-1 Wajiro-higashi, Higashiku, Fukuoka 811-0295, Japan
e-mail: mdm12006@bene.fit.ac.jp

T. Abe
1-1 Machihata-cho, Toyohashi-shi, Aichi 441-8522, Japan

H. Kimura
Kakuma-machi, Kanazawa, Ishikawa 920-1192, Japan

been increasing every year. Moreover, it will be 26.8 % in 2015, 33.4 % in 2035, and 39.9 % in 2060 [1]. As seen from the above, the aging society which no country in the world has experienced until now is coming. Meanwhile, the marketing deployment for elderly people is considering it as important problem by many retail businesses.

In the retail business, the targeting customers and area marketing for a given marketing strategy need to grasp these characteristics. Until now, in order to understand customers characteristics and behaviors in the retail business, historical data on customers, like point-of-sale data (POS data) has traditionally be used. Using such data, one can determine which customer purchased what and where, and that data can be analyzed in greater depth. For example, in the field of marketing, customer purchasing behavior models using such data [2, 3]. More recently, in order to handle large volumes of data, data mining was conducted in many industries [4], and this was helpful for improving sales promotion activities and brand strength. While customer purchasing history data is able to record the purchasing results for a given customer, it is difficult to grasp the purchase age groups of goods and market area. Therefore, techniques of the age groups estimation in many retail businesses (for example, convenience stores, supermarkets, shopping malls, etc.) are marketable techniques. Because those techniques are applicable for market research and customer analysis. In the convenience store, a customer's age classification is manually estimate by the staff. This estimation includes dispersion for each staffs. Thus, this method is not efficiently for collecting of customer's age groups. Here, in Japan, Tertiary industry is an important industry for nearly 70 % of the Japanese economy (in terms of GDP and employment). However, Japanese labour productivity in tertiary industry is about 40 % as compared with the U.S. Moreover, Japanese labour productivity in tertiary industry is bottom among advanced nations. These labour productivity is regarded as weakness from a standpoint of global competitiveness. In future, if this system helps labour productivity by market research, this Japanese weakness will be resolved. The purpose of this study is the age groups estimation by walking data using a pressure sensors array. This fact is one of merit in using the pressure sensors. The pressure sensors array gets feature quantity including weighted center, pressure value, area of foot, etc. Thus, pressure sensor obtains values data only. Obviously the footprint which consists of numerical values is not invasion privacy.

2 Related Work

We briefly review related work on face image based and gait based age estimation.

The face image based age classification problem is usually defined as a multi-class classification problem and is solved by using various classifiers such as a neural network classifier and nearest neighbor classifier [5]. Face image based age estimation is formulated as a regression problem from face features to age, and estimation approaches mainly fall into global model based approaches and personal model based approaches. Face image based age estimation has already

been installed in adult authentication system for automatic vending machines of cigarettes in several countries. Gait based age estimation, a learning method of an age-ordinary preserving discriminant subspace and a multi-label guided subspace [6], classified children (3–5 years old) and adults (30–52 years old) [7], classified younger people (average 28.4 years old, standard deviation 6.4 years) and the elderly (average 69.2 years old, standard deviation 5.1 years) [8], and classified four groups: children (under 15 years old), adult male, adult female, and the elderly (over 65 years old). Moreover, analysis of walking silhouette using 25 synchronous cameras (2 layers of 12 encircling cameras and an overhead camera with a mirror), and six screens surrounding the treadmill [9]. Therefore, there are the estimation classes a few on gait based age group estimation and age estimation than face image based studies. Adult authentication system has false recognition of adult authentication. Moreover, one of problems is that many age estimation systems use some video cameras. Therefore, these systems may invade surveyed person's privacy by taking one's face images.

3 Measurement System

3.1 Pressure Sensor

This measurement system uses an array consisting of three pressure sensors. This pressure sensor is developed by Xiroku Inc. [10] and they are called LL sensor. This sensor consists of orthogonal coil pattern and thin aluminum sheet. Using the cameras result an invasion of privacy. Also, the camera system inflicts discomfort and stress for the person being watched. Unfortunately, this situation may cause an unnatural walking. This is the conflicted system. Thus, this system cannot use cameras. Therefore, pressure sensors are used in this study. This pressure sensor does not cause an invasion of privacy. Because, this sensor do not have personally identifiable information (e.g. fingerprint). Additionally, these sensors are entirely unaffected by environment (e.g. lighting, camera focus and range). Consequently, this system can measure easily and stably. And, the user of this system does not feel any stress. Table 1 shows the specifications of the pressure sensor. Figure 1 shows the structure of pressure sensor. Figure 2 shows output of the footprints from the pressure sensor.

Table 1 Specification of pressure sensor

Sensor type	Electromagnetic induction
Size	600 mm × 600 mm
Thickness	1 mm
Resolution	10 mm
Sensing point	3600 points per sheet
Sampling period	120 frame per second
Element separation	10 mm

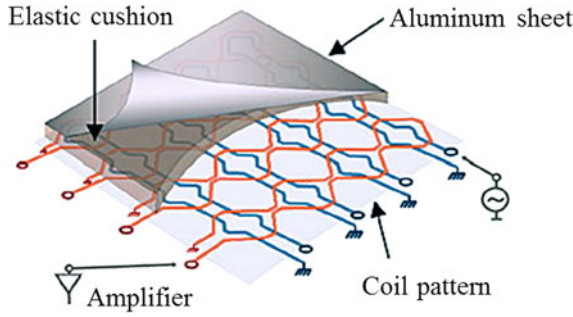


Fig. 1 Structure of pressure sensor [11]

3.2 Measurement Method

This system starts obtaining pressure value data, and these data are changed to point data of weighted center. An obtaining time is 1 s. 1 obtained data has 30frames, because the sampling period is 30frame per second. 1 frame data has person's pressure value, a step taken walking, 2 points of data of the weighted center and fluctuation of weighted center. In other words, the 2 point data is weighted center of x axis and y axis. We attached some conditions to measurement examinees. Some conditions are walking without shoes, as usual walking speed of each person, and fill out a questionnaire. The questionnaire has age, gender, experience of sports. We obtained 42 subjects with ages ranging from 20 to over 80 s. Figure 3 is shown installation of pressure sensors array. The detail of measurement method as follows.

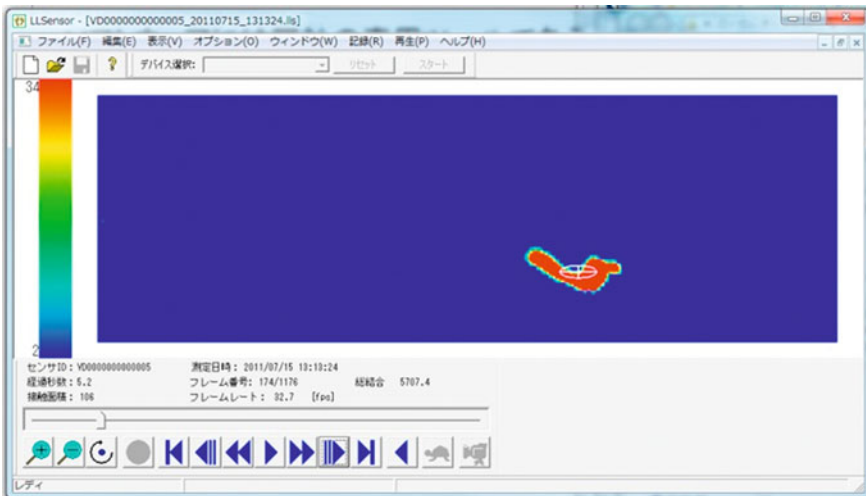


Fig. 2 Output of footprints from pressure sensor

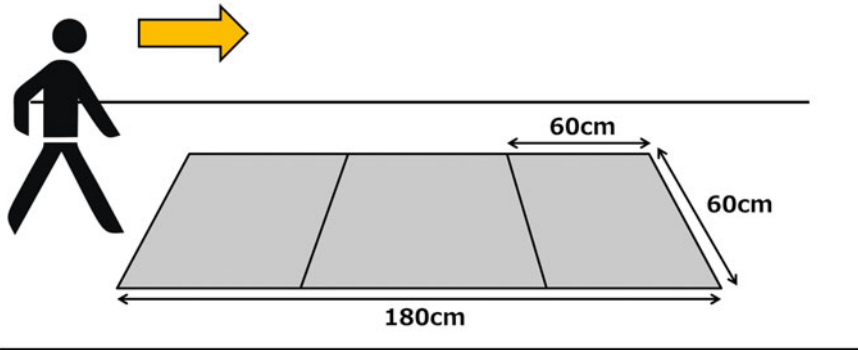


Fig. 3 Sensor installation

- (1) 1 examinee walking on sensor array.
- (2) Sensor starts record data when examinee's foot is on sensor.
- (3) Sensor records data during on sensor.
- (4) (1)–(3) repeats 10 times.
- (5) Answer a questionnaire.
- (6) (4)–(5) repeats next examinees.

4 Experiment

In this section, we explain to support vector machine, 10-fold cross validation, estimation method and experimental result.

4.1 Support Vector Machine

We use the support vector machine (SVM) [12–15] to estimate the age groups of a person. It uses a margin between hyper plane and training samples as an evaluation function. This study requires binary classification. Therefore, we use a single SVM. When the SVM is unable to separate the observation data into linear space, it realize the linear separation by mapping data to a higher dimensional space through nonlinear conversion. The method to greatly reduce the amount of calculation is called the kernel trick. There are some kernel functions such as linear, polynomial, sigmoid, and Gaussian. Although the SVM performance is affected by the kernel selection and parameters, the effective method for selecting the kernel has not yet been established [12]. In this study, we used the Gaussian kernel because the number of parameters of the Gaussian kernel is small. In Eq. 1, the Gaussian kernel is described. $K(x, x')$ is the kernel function, x and x' are input data, and γ is the dimensionality of the data.

$$K(x, x') = \exp\left(-\gamma|x - x'|^2\right). \quad (1)$$

4.2 10-Fold Cross Validation

If the number of calculations of estimation accuracy is 1 time, this result may be higher or lower contingently by biased data etc. We should check the average estimation accuracy. Thus, we calculated the average of estimation accuracy by 10-fold cross validation. The 10-fold cross validation is the method that divides original data into 10 equal parts. These parts are treated as 9 training data sets and 1 testing data set. Next, SVM learns with 9 training data sets. And, 1 testing data set is estimated by SVM. These estimation processes are executed 10 times. Therefore, 1 testing data set is changed 10 times in the calculation processes of average estimation accuracy. Finally, the average estimation accuracy is calculated from these results.

4.3 Walking Data-Based Age Groups Estimation

The coordinate of weighted center is shown by 2 point data that are the x axis and y axis. The range of x axis is 1–180 and the range of y axis is 1–60, because resolution of the pressure sensor is 1 cm, and a side is 60 or 180 cm. In Table 2, coordinate of the upper left corner is (1, 1) and the coordinate of the lower right corner is (180, 60). Moreover, the coordinate of total pressure value of sensor area, area of footprints, step length and interval between the both foots. This system obtains a coordinate of x axis enter of gravity(x), total pressure value of sensor area (w) per 30 frame per second. Additionally, area of foot(s), step length (l) and interval between the both foots (b) is not depend on the frame. We use walking data of 1 s. Because, it is not influenced by a customer's irregular motion. However, it will have high flexibility to a setting position. Figure 4 shows example of the obtained walking data. In addition, the walking data are different walk time each. Thus, we modify to walking data of 1 s. We gave 1 instruction signal to obtained data of Table 2. The instruction signals are the names of the person's age

Table 2 The coordinate walking data

Frame no.	1	2	3	...	29	30	More frame
Coord x	5	9	11	...	53	53	...
Coord w	935	2895	3486	...	6113	6220	...
Coord s	21	44	58	...	102	104	...
Coord l	70						
Coord b	20						

Fig. 4 The obtained walking data

groups in this study. For example, the instruction signals are 20–80 s. This process is for estimation using support vector machine (SVM). SVM is a type of supervised learning method. Therefore, SVM needs the instruction signal. Moreover, we processed 1 obtained data of 30frame to 1 record with the instruction signal. Table 2 shows example of records. In Table 2, “f1” means frame no. 1, “f30” means frame no. 30, and “No.” means record number. We obtained 10 experimental records per each person. Therefore, the number of records is 420.

4.4 Experimental Result

Table 3 shows experimental results of the average estimation accuracy of the age groups. The Average estimation accuracy of all age groups is 72.86 %. The highest estimation accuracy is 86.67 % at 70 s.

5 Consideration

The average estimation accuracy is subtle estimation. We can explain these results as follows. The 50 and 70 s classification are exceeded over 80.0 %. This means effective feature quantity of the age groups estimation. However, all age groups incorrect estimated. From the result of the experience of sports in the questionnaire, we think that each examinee’s walking data has dispersion. Therefore, we think enough reliability is not provided statistically.

Table 3 The average estimation accuracy of age groups (%)

	20 s	30 s	40 s	50 s	60 s	70 s	80 s
20 s	75.0	8.3	6.7	1.7	3.3	1.7	3.3
30 s	3.3	55.0	3.3	3.3	1.7	1.7	3.3
40 s	13.3	10.0	75.0	1.7	10.0	3.3	3.3
50 s	3.3	3.3	5.0	81.7	6.7	0.0	3.3
60 s	3.3	1.7	3.3	1.7	66.7	1.7	1.7
70 s	1.7	3.3	6.7	5.0	8.3	86.7	15.0
80 s	0	18.3	0.0	5.0	3.3	5.0	70.0
Total average accuracy					72.86		

6 Conclusion

We purpose to estimation system of the age groups using pressure sensors array in this study. This system has one of merit in using pressure sensor. Moreover, the average estimation accuracy is 72.86 % by result of experimentation of 7 age groups. As for future policy, we intend to increase the examinees of each age group in order to improve the system with higher reliability. Moreover, we will improve feature quantity with higher accuracy.

References

1. Cabinet Office in Japan (2012) White paper on aging society (in Japanese)
2. Guadagni PM, Little JDC (1983) A logit model of brand choice calibrated on scanner data. *Mark Sci* 2:203–238
3. Gupta S (1988) Impact sales promotions on when, what, and how much to buy. *J Mark Res* 25:342–355
4. Hamuro et al (1998) Mining pharmacy data helps to make profits. *Data Min Knowl Discov* 2:391–398
5. Lantis A, Draganova C, Christodoulou C (2004) Comparing different classifiers for automatic age estimation. *IEEE Trans Syst Man Cybern B* 34(1):621–628
6. Lu J, Tan Y-P (2010) Ordinary preserving manifold analysis for human age estimation. In: IEEE computer society and IEEE biometrics council workshop on biometrics 2010, San Francisco, CA, USA, pp 1–6
7. Davis J (2001) Visual categorization of children and adult walking style. In: Proceedings of the international conference on audio- and video- based biometric Pearson authentication, pp 295–300
8. Begg R (2005) Support vector machine for automated gait classification. *IEEE Trans Biomed Eng* 52(5):828–839
9. Mannami H, Makihara Y, Yagi Y (2010) Gait analysis of gender and age using a large-scale multi-view gait database. In: Proceedings of the 10th Asian conference on computer vision, Queenstown, New Zealand, Nov 2010, pp 975–986
10. Xiroku Inc. <http://www.xiroku.com/>
11. LL sensor. <http://www.llsensor.com/>
12. Cristianini N, Shawe-Taylor J (2000) An introduction to support vector machine and other kernel based learning methods. Cambridge University Press, New York
13. Tsuda K (2000) What is support vector machine. *IEICE Trans* 83(6):460–466
14. Pontil M (1998) Support vector machines for 3D object recognition. *IEEE Trans PAMI* 20(6):637–646
15. Vapnik V (1995) The nature of statistical learning theory, statistics for engineering and information science. Springer, New York

Bio Rapid Prototyping Project: Development of Spheroid Formation System for Regenerative Medicine

**Takeshi Shimoto, Nozomi Hidaka, Hiromichi Sasaki,
Koichi Nakayama, Shizuka Akieda, Shuichi Matsuda,
Hiromasa Miura and Yukihide Iwamoto**

Abstract Cells construct is made by spheroid-culturing the cells and collecting the spheroids. The spheroids are manufactured by dispensing cell turbid liquid into a special multiwell plate. If there is a difference in the number of cells when dispensing the cells turbid liquid, spheroids in different sizes are generated. Moreover, spheroids are not generated if the number of cells is extremely small, and if large, spheroids in distorted shapes are generated. Therefore, this study was aimed to develop a system that generates similar spheroids. In result, all the spheroids generated using developed system came in a pure spherical shape, and generation of spheroids is confirmed on all the wells.

Keywords Tissue engineering · Rapid prototyping system · Cell construct · Spheroid

T. Shimoto (✉) · N. Hidaka · H. Sasaki
Department of Information and Systems Engineering, Fukuoka Institute of Technology,
3-30-1 Wajiro higashi, Fukuoka, Japan
e-mail: simoto@fit.ac.jp

K. Nakayama
Department of Advanced Technology Fusion, Graduate School of Science
and Engineering, Saga University, Saga, Japan

S. Akieda
Cyfuse Biomedical K.K, Chiyoda-ku, Japan

S. Matsuda
Department of Orthopaedic Surgery, Kyoto University, Kyoto, Japan

H. Miura
Department of Bone and Joint Surgery, Graduate School of Medicine,
Ehime University, Matsuyama, Japan

Y. Iwamoto
Department of Orthopaedic Surgery, Graduate School of Medical Sciences,
Kyushu University, Fukuoka, Japan

1 Introduction

In the field of regenerative medicine, three-dimensional tissue engineering, which intends to regenerate lost tissues and organs, is focused. Formation of a three-dimensional construct outside the body has already been attempted by using combination of three elements, i.e., cells, growth factors/genes, and scaffold. Reports have been made on the technique to create a construct by overlaying cell sheets [1–3] or the technique to overlay cells while seeding them at arbitrary positions [4–7]. However, all of them use a scaffold such as biodegradable polymer and hydrogel, thereby leaving concerns over the necessary cost and side effects when implanting to live organs. There are some literatures that mention scaffold-free but have not reached the stage of clinical experiments [8].

We have already established a technique to make a three-dimensional construct only with cells. In fact, we have successfully made high-density mesenchymal stem cell autologous constructs, HD MACs with the diameter of about 10.0 mm and the height of about 6.0 mm only with cells. However, these constructs are usually made by skilled technicians who are familiar with cells, reagents, and cells culture methods. This means only a limited number of people can make the HD MACs, and moreover, the larger the implant constructs made for regenerative medicine become, the longer the work hours become. As a result, there may rise possibilities of contamination risks to spread and variation in quality of the cells construct to occur. Therefore, there is a need for automatization of the process using robotics technology. And with the intention of make a cells construct, we are developing a cell processing robot for regenerative medicine.

Cells construct is made by spheroid-culturing the cells and collecting the spheroids. The spheroids are manufactured by dispensing cell turbid liquid into a special multiwell plate. If there is a difference in the number of cells when dispensing the cells turbid liquid, spheroids in different sizes are generated. Moreover, spheroids are not generated if the number of cells is extremely small (Fig. 1a), and if large, spheroids in distorted shapes are generated (Fig. 1b).

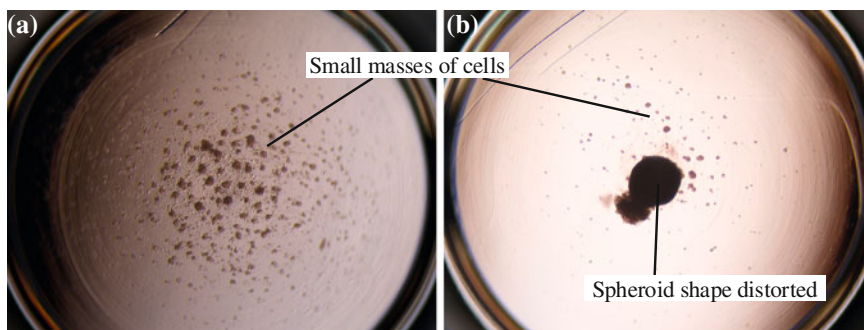


Fig. 1 Spheroids on a special multiwell plate that has been manufactured. **a** Spheroids are not generated if the number of cells is extremely small. **b** Spheroids in distorted shapes are generated if the number of cells is extremely large

Therefore, this study was aimed to develop a system that generates similar spheroids.

2 Materials and Methods

2.1 Development of Spheroid Formation System for Regenerative Medicine

An overview and a schematic view of the spheroid formation system for regenerative medicine are presented in Figs. 2 and 3 respectively. Basic operations such as attachment of tips are carried out using a cleanroom SCARA robot (E2C, EPSON) and suction and discharge of cells are carried out using an electric cylinder (CPL28T2B-06KD, Orientalmotor). Members used for the device are made of autoclavable or ethanol-sterilizable material. The whole device is installed in a clean bench to be kept clean and ultraviolet sterilization can be done when out of service. The control software is operated with a touch screen in view of the clean environment, with an easy-to-operate program screen.

A tip-removable pipette of 2 × 2 channel is attached to the fourth articular of end of the SCARA robot and a sterilized tip is fixed to handle cells. The tip is made of resin and it requires a delicate force to attach. It was securely attached as failing to do so not only can affect all the works but also can cause an error in a

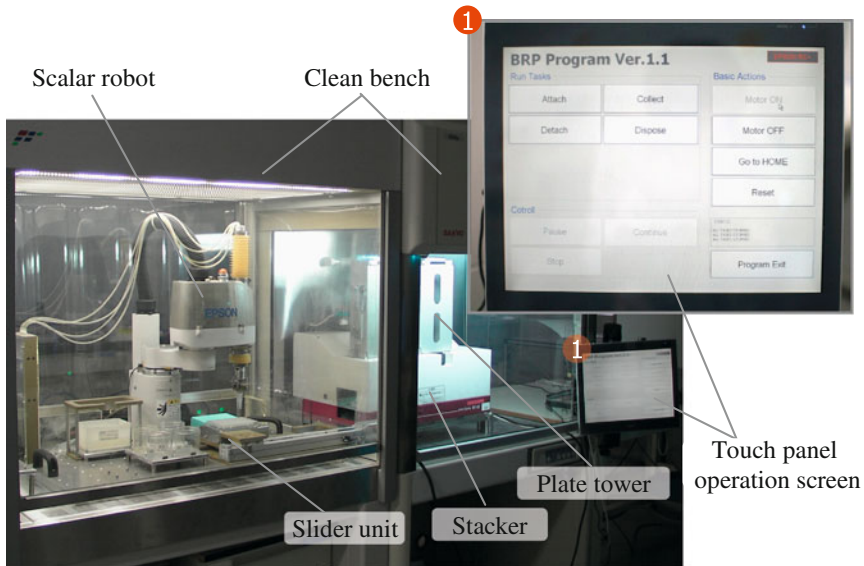


Fig. 2 The spheroid formation system for regenerative medicine

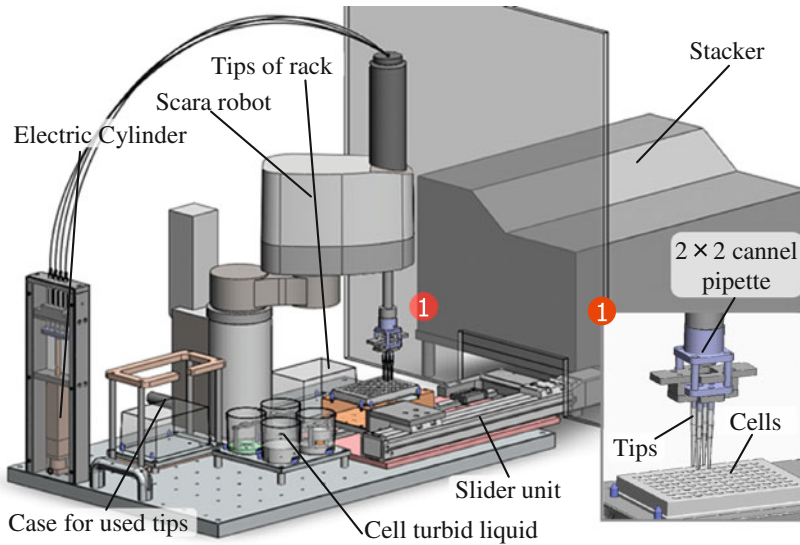


Fig. 3 Schema of the spheroid formation system for cartilage regeneration

relative coordinate system at the tip end and damages the cells. Since the tip is discarded after sterilized with high-pressure steam when the work is finished, it was made removable in a container to which it is discarded.

As a function evaluation of spheroid formation system, we conducted a research on the generation of contamination by falling bacteria test and measured the length of time required to dispense cell turbid liquid. The falling bacterium test was conducted by statically placing culture dishes filled with culture fluid used in this research at the four corners of the clean bench on which the device is installed, and releasing the lid of the culture dishes while the system is in operation. Static culture was performed for a week, and then a skilled technician observed the culture fluid by a microscope to investigate the presence or absence of contamination. As for the time required to make spheroids, we compared the time required to dispense the cell turbid liquid with this system and by handwork. The handwork was performed by one skilled technician.

2.2 Creation of Spheroid

In this study, cells construct is made by spheroid-culturing the cells and collecting the spheroids. The spheroids are manufactured by dispensing cell turbid liquid into a special multiwell plate. The multiwell plate for forming spheroids can generate 96 spheroids per plate. To make cells construct using mold, ten plates are required when knee joint of a Japanese white rabbit is targeted. More multiwell plates are required to make cells constructs for human. So, a stacker and a slider unit that

conveys multiwell plates to a fixed position are used to automatically feed the multiwell plates. When a system was first developed, multiwell plates were manually replaced. Now, the multiwell plate automatic feeding module reduces factors such as impacts on cells and contamination, thereby enabling operations in a clean environment. A plate tower of the stacker can be incubated as it is and can be easily managed.

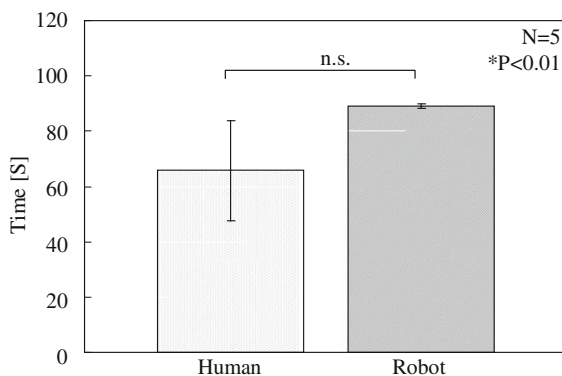
We used MSC (Mesenchymal Stem Cell) harvested from a Japanese white rabbit. MSC passage was carried out on a culture dish (Φ 150 mm, H25 mm, CORNING) and for the culture fluid for passage, we used DMEM (dulbecco's modified eagle medium, Nissui) to which 10 % FBS (fetal bovine serum, HyClone), 4.4 mM sodium hydrogen carbonate (WaKo), 9.9 mM HEPES (2-[4-(2-hydroxyethyl)-1-piperazinyl] ethanesulfonic acid, DOjinDO), and 1.2 % antibiotics (penicillin and streptomycin, Meiji) were added. Upon reaching the required number of cells, they were dispensed into a multiwell plate (multiwell plate, SUMILON), and after a two-day spheroid culture, we took out the manufactured spheroids and conducted a macroscopic evaluation. We performed dispensing works using a system developed.

3 Results

Once contamination occurs, cells need to be discarded regardless of the level of progression. A skilled technician observed the results of the falling bacterium test with a microscope. According to him, no occurrence of contamination was confirmed and the clean status was maintained in the system.

The lengths of time per multiwell plate to dispense cell turbid liquid are presented in Fig. 4. The spheroid formation system used a pipette of 2×2 channels whereas a pipette of 1×8 channels was used for the handwork. There was variation in the results by handwork because the procedure depended on the operator's physical conditions and concentration. When dispensing the cell turbid

Fig. 4 Dispensing time to a multiwell plate of 96 well format



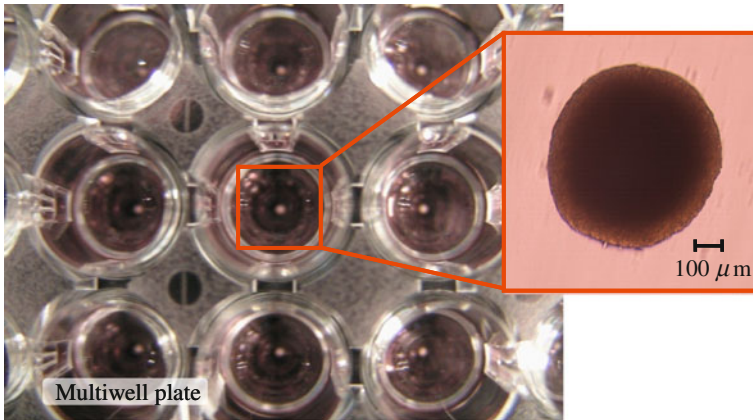


Fig. 5 Spheroids generated on the multiwell plate using the spheroid formation system

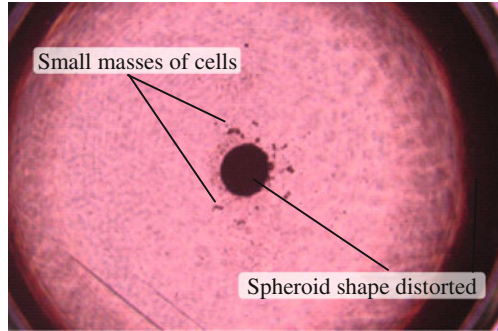
liquid, a certain number of cells need to be seeded into the multiwell plate. However, since cells in the cell turbid liquid precipitate rapidly, sufficient stirring is necessary. Procedures by hand are as follows; a motion of sucking the cell turbid liquid from the bottom of a V-shaped rectangular container specially made for a pipette of 1×8 channels and discharging it at the upper part is repeated and seeding the cells by stirring thoroughly. Cell processing robot uses a pipette of 2×2 channels and accordingly a container of frustum of a cone was made for the cells turbid liquid. Because it is a frustum of a cone, an extra motion of stirring the cells turbid liquid to the shape of the frustum was added to the motion of sucking the cells turbid liquid from the bottom and discharging it at the upper part that caused processing by the robot to take more time. However, no significant difference was found.

The spheroids generated by using the cell processing robot are presented in Fig. 5. If there is a difference in the number of cells when dispensing the cells turbid liquid, spheroids in different sizes are generated. Moreover, spheroids are not generated if the number of cells is extremely small, and if large, spheroids in distorted shapes are generated. All the spheroids generated by this system came in a pure spherical shape, and generation of spheroids is confirmed on all the wells.

4 Discussions

When building a cells construct for the rabbit femoral cartilage regeneration, the number of cells necessary is about 4.0×10^7 and the number of spheroids are as many as about 800. In addition, if human is targeted, a large cells construct needs to be made that requires long working hours, thus a system like this device is considered effective.

Fig. 6 Example of spheroids formation by a non-skilled technician



In this experiment, the handwork was conducted by a skilled technician and there was no failure in the spheroid generation. However, when it was conducted by a non-skilled technician, it took longer time for the work and sometimes resulted in failure (Fig. 6). This could have been because the cells were exposed to the external air for a long time or the pipettes were erroneously operated and resulted in the occurrence of contamination, death cells, or nonuniform works. When spheroids were made using this system, there were no failures such as occurrence of contamination.

Since cells are handed in this research, in spheroid exfoliation by pipetting or stirring of cells turbid liquid, it is necessary to reconstruct the motions of skilled technicians with specialist knowledge and technique so as not to damage the cells. There is no significant difference between the lengths of time in dispensing cells turbid liquid by this system and that by the handwork carried out by a skilled technician, similar to spheroids made by handwork, reproducible spheroid were successfully made though macroscopically evaluated. In addition, the clean bench used in this system does not have specifications that are vulnerable to dynamic actions such as vibrations of SCARA robot when it is operated at the maximum speed, and hence the work speed is moderated to 50–70 % consequently, providing the clean bench with rigidity can increase the work speed to achieve further efficiency.

In this research, a macroscopic evaluation on the results of the generated spheroids has been made and the effectiveness of the system was discussed. When clinical application is taken into account, a quantitative evaluation is required in order to confirm quality control and compatibility of spheroids. From quantitative evaluation, we will perform reproducibility confirmation and feedback to spheroids generation protocol and intend to achieve realization of products for regenerative medicine.

5 Conclusions

This purpose of this study is to develop the cell processing robot for cartilage regeneration. In this paper, we have performed the development and evaluation of a spheroid formation system. When regenerative medicine develops and cells

constructs for implantation grow in size, automatization will be required inevitably. Moreover, the field of tissue engineering such as regenerative medicine requires skilled technicians that have specialist knowledge and technique which will result in imposing them a big load. This system that reproduced the techniques of skilled technicians and could successfully make spheroids similar to the those made by handwork can keep uniformity in work and can greatly contribute to clinical application of the regenerative medical technology. This research group has also established a method to place multiple types of spheroids in arbitrary spatial positions and is developing a device to which a manipulator is applied. Therefore, this system will be able to contribute to make constructs of organs and tissues that have complicated shapes or constructs.

Acknowledgments This research was supported by Computer Science Laboratory in Fukuoka Institute of Technology.

References

1. Harimoto M, Yamato M, Hirose M, Takahashi C, Isoi Y, Kikuchi A, Okano T (2002) Novel approach for achieving double-layered cell sheets co-culture: overlaying endothelial cell sheets onto monolayer hepatocytes utilizing temperature-responsive culture dishes. *J. Biomed Mater Res* 62(3):464–470
2. Shiroyanagi Y, Yamato M, Yamazaki Y, Toma H, Okano T (2003) Transplantable urothelial cell sheets harvested noninvasively from temperature-responsive culture surfaces by reducing temperature. *Tissue Eng* 9(5):1005–1012
3. Sasagawa T, Shimizu T, Sekiya S, Haraguchi Y, Yamato M, Sawa Y, Okano T (2010) Design of prevascularized three-dimensional cell-dense tissues using a cell sheet stacking manipulation technology. *Biomaterials* 31(7):1646–1654
4. Nakamura M, Kobayashi A, Takagi F, Watanabe A, Hiruma Y, Ohuchi K, Iwasaki Y, Horie M, Morita I, Takatani S (2005) Biocompatible inkjet printing technique for designed seeding of individual living cells. *Tissue Eng* 11(11–12):1658–1666
5. Tsang VL, Chen AA, Cho LM, Jadin KD, Sah RL, DeLong S, West JL, Bhatia SN (2006) Fabrication of 3D hepatic tissues by additive photo patterning of cellular hydrogels. *FASEB J* 21(3):790–801
6. Rago AP, Dean DM, Morgan JR (2009) Controlling cell position in complex heterotypic 3D microtissues by tissue fusion. *Biotechnol Bioeng* 102(4):1231–1241
7. Miller ED, Fisher GW, Weiss LE, Walker LM, Campbell PG (2006) Dose-dependent cell growth in response to concentration modulated patterns of FGF-2 printed on fibrin. *Biomaterials* 27(10):2213–2221
8. Norotte C, Marga FS, Niklason LE, Forgace G (2009) Scaffold-Free vascular tissue engineering using bioprinting. *Biomaterials* 30(30):5910–5917

Robot Control Architectures: A Survey

Evjola Spaho, Keita Matsuo, Leonard Barolli and Fatos Xhafa

Abstract This paper surveys and analyzes the relevant literature on robot control architectures. The design of an efficient collaborative multi-robot framework that ensures the autonomy and the individual requirements of the involved robots is a very challenging task. This requires designing an efficient platform for inter-robot communication. P2P is a good approach to achieve this goal. P2P aims at making the communication ubiquitous thereby crossing the communication boundary and has many attractive features to use it as a platform for collaborative multi-robot environments.

Keywords Robot control • Survey • P2P architectures

E. Spaho (✉)

Graduate School of Engineering, Fukuoka Institute of Technology (FIT), 3-30-1
Wajiro-Higashi, Higashi-Ku, Fukuoka 811-0295, Japan
e-mail: evjolaspaho@hotmail.com

K. Matsuo

Fukuoka Prefectural Kaho-Sogo High School, 1117-1 Haji, Keisen-machi Kaho-gun,
Fukuoka 820-0607, Japan
e-mail: matuo-k7@fku.ed.jp

L. Barolli

Department of Information and Communication Engineering, Fukuoka Institute
of Technology (FIT), 3-30-1 Wajiro-Higashi, Higashi-Ku, Fukuoka 811-0295, Japan
e-mail: barolli@fit.ac.jp

F. Xhafa

Department of Languages and Informatics Systems, Technical University of Catalonia,
C/Jordi Girona 1-3, 08034 Barcelona, Spain
e-mail: fatos@lsi.upc.edu

1 Introduction

Robots are being steadily introduced into modern everyday life and are expected to play a key role in the near future. Typically, the robots are deployed in situations where it is too dangerous, expensive, tedious, and complex for humans to operate. Although many of the real-life applications may only need a single robot, a large number of them require the cooperation of a team of robots to accomplish a certain task. The use of multiple robots of overlapping capabilities offers a cost-effective and more robust solution. This redundancy in the robots' capabilities makes the overall system more flexible and fault-tolerant.

There are many research works for the control of single mobile robots, but not much has been done for cooperative mobile robots. The design of an efficient collaborative multi-robot framework that ensures the autonomy and the individual requirements of the involved robots is a very challenging task. This requires designing an efficient platform for inter-robot communication. P2P is a good approach to achieve this goal. P2P aims at making the communication ubiquitous thereby crossing the communication boundary. It is network independent, scalable and can operate over TCP/IP, Bluetooth, and other wired and wireless technologies. It also facilitates creating any overlay network which provides an automatic and efficient abstraction of the physical network implementation details. As a result, P2P technology shows many attractive features to use it as a platform for collaborative multi-robot environments [1].

The rest of the paper is organized as follows. In [Sect. 2](#), we give an overview of the various current and past researches of architectures for robot control. We give an introduction of P2P robot control and JXTA-Overlay Platform in [Sect. 3](#). In [Sect. 4](#), we discuss the implications of the developmental approach for robotics research. In [Sect. 5](#), we give future research directions and conclusions.

2 Architectures for Robot Control

Developing a multi-robot control architecture has been the subject of several studies. Asama et al. proposed ACTor-based Robot and Equipments Synthetic System (ACTRESS) [2]. The ACTRESS architecture tackles the issues of communication protocols with different abstraction levels, path planning, and task assignment through multi-stage communication protocols. The architecture was tested on heterogeneous mobile robots performing complex object pushing tasks that cannot be accomplished with a single robot.

In [3] is proposed a biologically inspired CELLular rOBOTics system (CEBOT). Robots within the CEBOT architecture are tightly coupled and can dynamically reconfigure their physical structure in response to different environment changes. The CEBOT hierarchy is based on the selection of a cluster of master cells to coordinate subtasks by communicating with other master cells.

Efficient communication protocols among CEBOT agents have also been discussed in several studies. Reducing the communication requirements, estimating the volume of information exchange between the involved robots, and effective solutions for choosing the master cells, were among the addressed issues [4].

GOFER is another distributed multi-robot problem solving architecture [5, 6]. It is based on a centralized task planning and scheduling module, which keeps track of the task allocation and the availability of all the robots through direct communication with them. The system also uses conventional artificial intelligence and task allocation algorithms, such as Contract Net Protocol to dispatch the subtasks to be performed by individual robots. Despite its satisfactory performance in applications, like following a wall and pushing objects, most of the GOFER implementations involved no more than three robots. In addition, GOFER is designed for indoor environments only and its dependence on a centralized task planning and scheduling module represents a major limitation from a flexibility and fault-tolerance perspective. In order to alleviate the naturally inherited problems in most of the aforementioned frameworks, the ALLIANCE architecture was introduced [7]. It is a behavior-based architecture incorporating with mathematically modeled motivations to deal with task allocation for multi-robot cooperation with fault tolerance. The architecture is designed for small to medium-sized teams of loosely coupled heterogeneous mobile robots operating in dynamic environments to perform tasks with possible ordering dependencies. The ALLIANCE architecture also assumes that the robots are probabilistically capable of assessing the performance of their actions as well as those of others through perception and broadcast communication.

In [8] the authors describe an open and modular approach to design and implement a real-time robot control system using Open Source Software (OSS) which includes a Linux-based Real-Time Operating System Xenomai, real-time IEEE 1394 device driver and other middleware components.

There are some other research works that deal with the autonomous distributed robot systems. In these systems, many autonomous mobile robots cooperate together to carry out complicated tasks [9–13].

In [14] is proposed an Adaptive Reservation-Time Division Multiple Access (AR-TDMA) medium access control protocol which can realise a real-time communication among robots in a heterogeneous environment by using a reservation mechanism. Also, by using an adaptive time slot allocation method, the protocol has a flexible behaviour and can deal with the changes of number of robots.

Furthermore, the proposed protocol can reduce the packet collision probability.

However, all these research works deal with different communication protocols for robot communication.

In [15–17], the authors proposed and implemented a humanoid robot control platform. In this platform, the control components are implemented as CORBA servers and behave as agents. The platform allows easy addition, deletion and updating of new devices. The authors carried out many experiments and confirmed

the effectiveness of the proposed platform. However, this platform is based on C/S approach.

There are other works [18–20], which deal with biped robots. However, most of them deal with robot architecture, walking generation or robot tracking.

3 A P2P Robot Control System

Our proposed platform includes a set of protocols that are able for robot communication and control. The proposed platform is based on JXTA architecture [21–23] and is implemented by Java Language. Thus, it is platform independent (does not depend on the OS).

In our proposed system, we combine P2P communication and robot technology. The robot size is 450 (W) × 1200 (H) × 250 (D) mm and the robot weight is 24 kg. The biped walking robot has 19 motors (V-SERVO). The robot is shown in Fig. 1. We implemented the computer Interface (ETC-A013) in the robot. The mounted computer is equipped with Z520PT processor, two serial ports (RS-232C), four USB devices, LAN device and Controller Area Network (CAN).

Fig. 1 Biped walking robot used for experiments

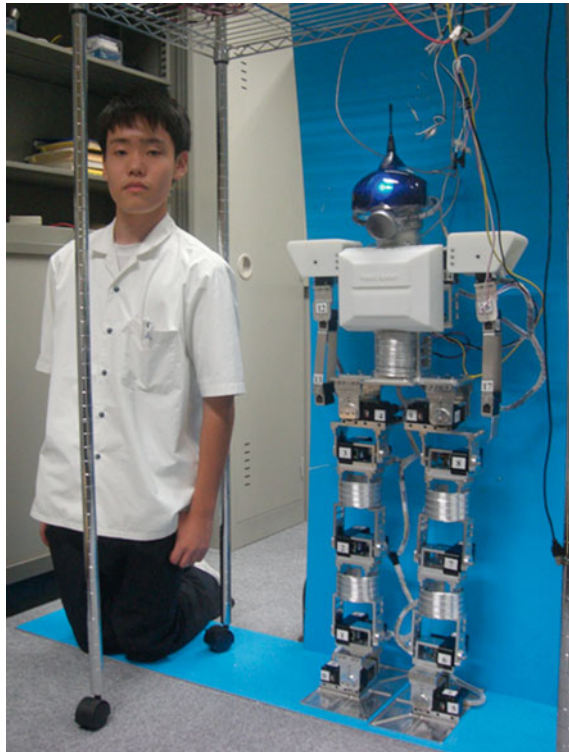




Fig. 2 ETC-A013 computer mounted in biped robot

The computer size is 210 (W) × 29 (H) × 150(D) mm. We implemented the computer in the back side of our robot as shown in Fig. 2.

Our goal is not only to control the robots in a WAN but also to overcome the firewalls and other security devices. This is why we use the JXTA-Overlay P2P platform. The system image for the control of biped robots by P2P system is shown in Fig. 5.

The P2P robot control system is shown in Fig. 3 and a snapshot of the robot control system interface is shown in Fig. 4. We will consider the biped robots as peers. We developed now a knowledge sharing system for biped robots as shown in Fig. 6.

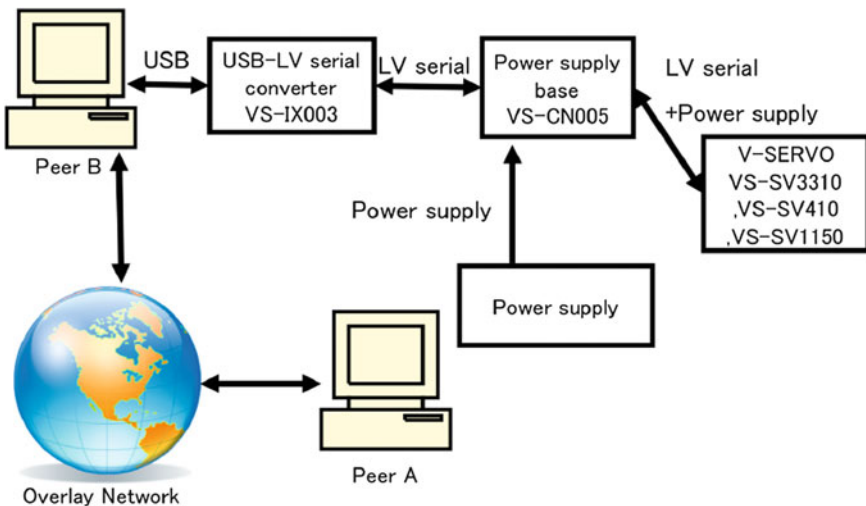


Fig. 3 P2P robot control system

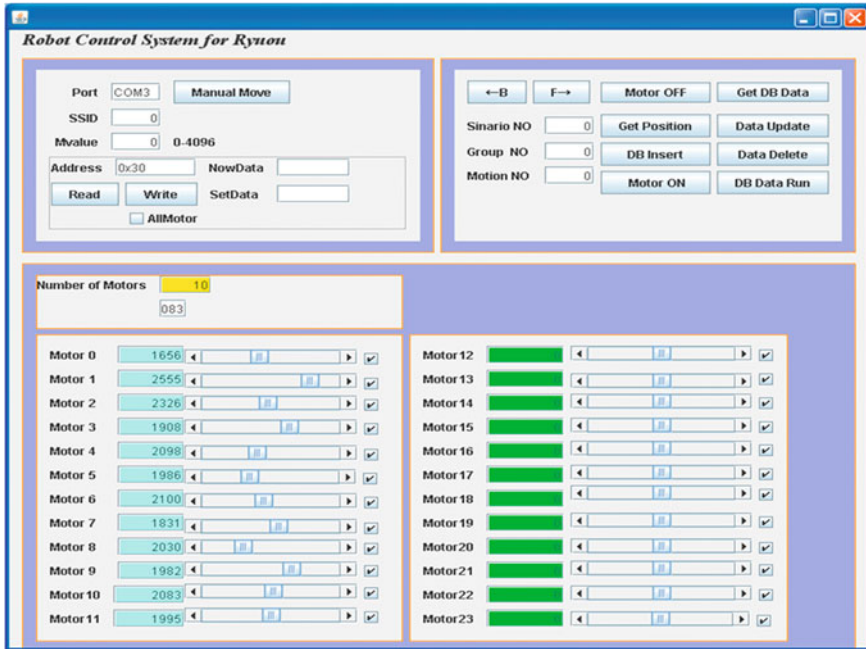


Fig. 4 A snapshot of robot control system interface

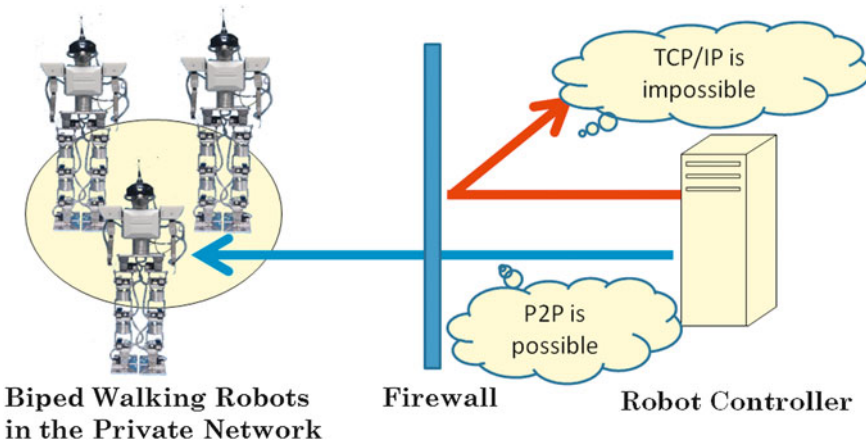


Fig. 5 Overcome of security devices by P2P technology

The Motors of robot are controlled via JXTA-Overlay P2P system. Experiments are carried out in real environment and we confirmed the effectiveness of JXTA-Overlay.

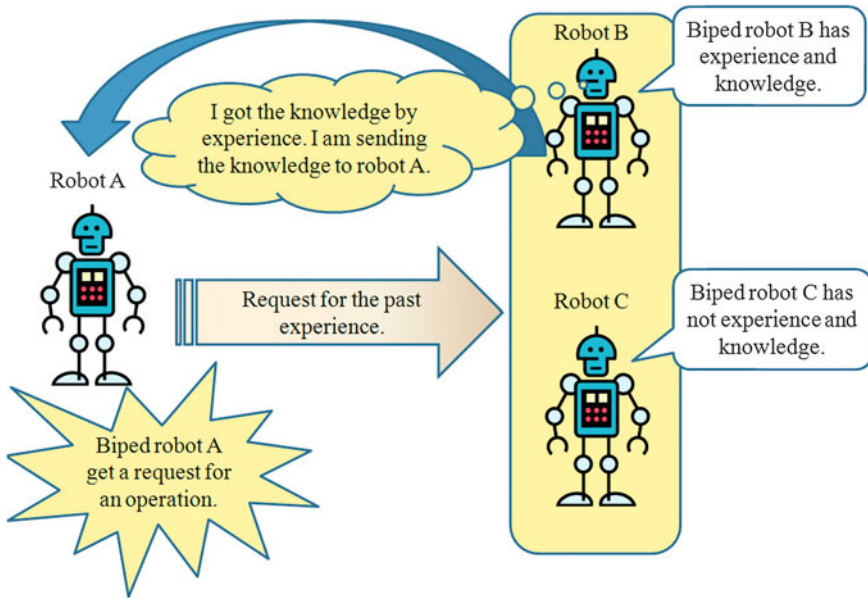


Fig. 6 Proposed knowledge sharing system for biped robot

4 Discussion and Future Prospects

By using many robots in a distributed way, the robot functions can be simplified and the system cost, fault tolerance and flexibility can be improved. In the case, where there are many robots and if one robot has a problem, the other robots can cooperate to finish a requested task. Therefore, the distributed robot systems are better than single robots. However, in distributed robot systems, to realise a common task, the robots should cooperate together and consider not only their own task but also the complete task (Figs. 5 and 6).

Robots offer many advantages to accomplishing a wide variety of tasks given their strength, speed, precision, repeatability, and ability even in extreme environments. Most robots perform these tasks in an isolated manner, and the interest is growing in the use of tightly interacting multi-robot systems to improve performance in current applications and to enable new capabilities. Potential advantages of multi-robot systems include redundancy, increased coverage and throughput, flexible reconfigurability and functionality.

Controlling and programming cooperative multi-robot systems is a highly complicated task that requires a flexible control architecture and programming environment that are able to handle the distributed nature of multi-robot systems.

Robot architectures are distinguished from other software architectures because of the special needs of robot systems. Cooperation among multiple robots working as a team needs a very high level of control. The success of mobile robots control

architectures depends on satisfying characteristics such as safety, security, reliability and availability.

The control system of robots should be modular (divided into smaller subsystems) that can be separately and incrementally designed, implemented, debugged and maintained. As the field of robotics is rapidly changing, the future work should be focused on the design of open and modular system so they can quickly adopt a new promising technology by just replacing the corresponding module of the system not redesign the entire system for adopting some small changes in hardware or software.

Reliable inter-robot communication is crucial for dangerous applications for this reason new protocols should be built.

5 Conclusions

In this paper is provided a brief review of robot control architectures. As the field of robotics is rapidly changing, the future work should be focused on the design of open and modular system so they can quickly adopt a new promising technology by just replacing the corresponding module of the system not redesign the entire system for adopting some small changes in hardware or software. By using many robots in a distributed way, the robot functions can be simplified and the system cost, fault tolerance and flexibility can be improved. The integration of system infrastructure with the development of intelligent robotic architectures will lead to robots that display ever greater levels of autonomy. During the literature review work, we found that P2P aims at making the communication ubiquitous thereby crossing the communication boundary and has many attractive features to use it as a platform for collaborative multi-robot environments.

Acknowledgments This work is supported by a Grant-in-Aid for Scientific Research from Japanese Society for the Promotion of Science (JSPS). The authors would like to thank JSPS for the financial support.

References

1. Asama H (2002) Distributed adaptive robotics for co-sustainable engineering. *J Rob Soc Jpn* 20(6):577–578
2. Asama H, Ozaki K, Matsumoto A, Ishida Y, Endo I (1992) Development of task assignment system using communication for multiple autonomous robots. *J Rob Mechatron* 4(2):122–127
3. Fukuda T, Iritani G (1995) Construction mechanism of group behaviour with cooperation, In: *Proceedings of the IEEE/RSJ IROS-95*, pp 535–542
4. Fukuda T, Kawauchi Y, Asama H (1990) Analysis and evaluation of cellular robotics (CEBOT) as a distributed intelligent system by communication information amount. *Proceedings of the IEEE/RSJ IROS-90*, pp 827–834

5. Caloud P, Choi W, Latombe JC, Pape CL, Yim M (1990) Indoor automation with many mobile robots. In: Proceedings of the IEEE international workshop on intelligent robots and systems, pp 67–72
6. Pape CL (1990) A combination of centralized and distributed methods for multiagent planning and scheduling. In: Proceedings of the IEEE international conference on robotics and automation, pp 488–493
7. Parker LE (1998) Alliance: an architecture for fault tolerant multirobot cooperation. *IEEE Trans Rob Autom* 14(2):220–240
8. Sarker MO, Kim C, Cho J, You B (2006) Development of a network-based real-time robot control system over IEEE 1394: using open source software platform. In: Proceedings of IEEE international conference on mechatronics, pp 563–568
9. Chaimowicz L, Sugar T, Kumar V, Campos MFM (2001) An architecture for tightly coupled multi-robot cooperation. In: Proceedings of IEEE international conference on robotics and automation, pp 2992–2997
10. Inoue L, Nakajima T (2001) Cooperative object transportation by multiple robots with their own objective tasks. *J Rob Soc Jpn* 19(7):888–896
11. Ozaki K, Asama H, Ishida Y, Matsumoto A, Endo I (1996) collision avoidance using communication between autonomous mobile robot. *J Rob Soc Jpn* 14(7):961–967
12. Parnichkun M, Ozono S (1998) CDCSMA-cd communication method for cooperative robot systems. *Adv Rob* 11(7):669–694
13. Rybski PE, Stoeter SA, Gini M, Hougen DF, Papanikolopoulos NP (2002) Performance of a distributed robotic system using shared communications channels. *IEEE Trans Rob Autom* 18(5):713–727
14. Arai J, Koyama A, Barolli L (2008) AR-TDMA: an adaptive reservation time division multiple access control protocol for robot inter-communication. *Inter J Wireless Mob Comput (IJWMC)* 3(1/2):4–11
15. Takeda K, Nasu Y, Capi G, Mitobe K, Yanakawa S (2000) A multi-layer client/server robot control platform based on corba. In: Proceedings of world automation congress (WAC-2000), vol 10, Hawaii, USA, pp 585–591
16. Takeda K, Nasu Y, Barolli L, Capi G, Mitobe K (2001) A new humanoid control architecture based on corba. In: Proceedings of international conference on production engineering, design and control PEDAC-2001, vol 2, Alexandria, Egypt, Feb 2001, pp 925–934
17. Takeda K, Nasu Y, Capi G, Yamano M, Barolli L, Mitobe K (2001) A CORBA-based approach for humanoid robot control. *Ind Rob Inter J* 28(3):242–250
18. Lim HO, Takanishi A (2007) Biped walking robots created at Waseda University: WL and WABIAN family. *Philos Trans Royal Soc* 365(1850):49–64
19. Liu T, Inoue Y, Shibata K (2010) Imitation control for biped robot using wearable motion sensor. *J Mechan Rob* 2(024501):1–5
20. Verrelst B, Vanderborght B, Vermeulen J, Van Ham R, Naudet J, Lefeber D (2005) Control architecture for the pneumatically actuated dynamic walking biped lucy. *Mechatron* 15(6):703–729
21. Brookshier D, Govoni D, Krishnan N, Soto JC (2002) JXTA: Java P2P programming. Sams Publishing, Indianapolis
22. IBM Corporation (2007) Making P2P interoperable: creating JXTA systems design P2P systems that extend beyond traditional network boundaries
23. Sun Microsystems (2007) JXTA java standard edition V2.5: programmers guide. June 2007

Experiment Verification of Position Measurement for Underwater Mobile Robot Using Monocular Camera

Natsuki Uechi, Fumiaki Takemura, Kuniaki Kawabata
and Shinichi Sagara

Abstract Authors have been developing the underwater robot that can be used for environmental protection work in the sea near Okinawa. It is difficult to get the position of underwater robot, because it cannot use GPS in sea. Authors have been developing the underwater robot to work in the sea near Okinawa with a high radree of transparency, so we try to develop the inexpensive measurement for underwater robot using a monocular camera. In this paper, we illustrate the measurement method and the basic experiment on land and underwater.

1 Introduction

Recently, the activity concerning the environmental sustainability and conservation is recommended by the change in the global environment. Especially, the coral reefs that are present in Okinawa etc., is a base of the ecosystem, and important existence for human beings to live [1]. However, it has been reported that about 1/3 of the reef-building corals in the world is a threatened species in report by World Conservation Union (IUCN) [2]. Therefore, it is pressing needs to conservation and protection of the coral reef based on the analysis of the influence that the habitat factor gives the ecosystem.

All these work is done by the hand work though the vegetation of coral reef and capture of Crown-of-thorns-starfish is being done as a protection activity of the coral reef by the diver. Therefore, the removal of the physical burden and danger is

N. Uechi · F. Takemura (✉)
Okinawa National College of Technology, Okinawa, Japan
e-mail: takemura@okinawa.ct.ac.jp

K. Kawabata
RIKEN, Saitama, Japan

S. Sagara
Kyushu Institute of Technology, Kyushu, Japan

hoped for. Because the number of coral decreases rapidly when the coral exceeds 20 [m] in depth from living by depth that sunlight reaches [3], it be able to act by about 20 [m] in depth as underwater robot that done the protection activity of the coral reef. Then, authors develop the underwater robot that can work by 20 [m] in depth and are researching [4].

A coral investigation, the research, and the protection activity are often done periodically. In order to determine the cause of the decline of coral, time and location information is important information. However, the underwater robot cannot grasp “positional information” because GPS cannot use at undersea. The expensive apparatus is needed in obtaining enough accuracy though a positional measurement that uses the sound wave and the supersonic wave is chiefly done in underwater. In this study, we develop the system that acquires the location information of the underwater robot. There is no applied example from poor visibility in water to a positional measurement of on underwater object though positional measurement by monocular camera is researched at land [5]. The underwater robot that authors are developing has aimed at the coral maintenance activity in the Okinawa neighboring waters. It is thought that a positional measurement with a monocular camera is quite possible because of a positional measurement of the underwater robot that acts in depth and the sea area where the transparency is high. Figure 1 shows an image of a blue coral that was taken in Oura Bay (Nago city, Okinawa prefecture, Japan). Figure 1 was taken a blue coral from below about 5 [m] in surface of the sea. Even if depth is about 5 [m], a blue coral can be confirmed clearly from Fig. 1.

Moreover, it is possible to use it also for the operational support of the underwater robot by offering image obtained by monocular camera image to the operator of the underwater robot.

Here we proposes the positional measurement method of the underwater robot with a monocular camera, and describes about the system. Moreover, it reports on the basic experiment in land and underwater.

Fig. 1 *Blue coral in Oura Bay—depth: approx. 5 m*



2 Method of Positional Measurement

2.1 Outline of Positional Measurement

The underwater robot that uses it in this study is having cable, and operator PC in the sea (land) is teleoperated robot (ROV) connected by LAN cable. The following apparatus are installed in the underwater robot.

Equipment to be mounted on the underwater robot

- LED marker
- Depth sensor

Depth information of the underwater robot by the depth sensor is assumed to be already-known through LAN cable.

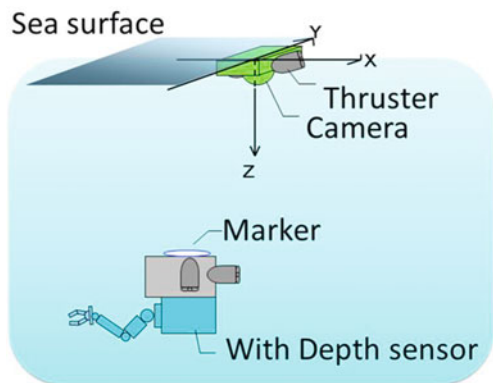
The positional measurement method is shown in Fig. 2. The sea movable body with the thruster is floated on the sea, and the downward monocular camera is installed in the sea movable body. The following apparatus are installed in the sea movable body.

Equipment to be mounted on a sea floating body.

- GPS
- Attitude sensor (acceleration sensor and gyro sensor)
- Thruster

The state to float the monocular camera on the surface of the sea is assumed to be parallel to the surface of the sea. The depth of the underwater robot is enabled to be measured by the depth sensor. The LED marker is equipped in the underwater robot and the position on the image is measuring by the image processing. And the conversion formula of the size for each 1 pixel (length) in depth in made by correcting the swerve. Thus, an actual position is understood from counting the number of pixel from the starting point to the marker, and combining conversion formula of a real position with depth information on the underwater robot.

Fig. 2 Position measurement method



Here, there is actually no such situation though the monocular camera is assumed to become parallel to the surface of the sea. Then, it is system that acquires the global coordinate of the underwater robot by correcting attitude based on information on the installed attitude sensor, and GPS information and integrating it. Moreover, it is supposed to move the sea floating body to locate the underwater robot at the image center by installing the thruster.

2.2 1 Pixel and Real Distance Conversation in Depth Information

In this position measurement method, the location information is shown by the pixel value in monocular camera. Therefore, it is necessary to convert pixel value into real position [m]. Figure 3 shows the position of the camera and the underwater robot of the sea. Depth D [m] is already-known from a depth sensor of the underwater robot. H [pixel] is the vertical size, a_w [rad] is the vertical angle, W [pixel] is the horizontal size, and a_H [rad] is horizontal angle of the picture. If the transform coefficient to the actual position to vertical direction is C_W and horizontal direction is C_H , the following equation is established relationship.

$$C_W = \frac{2 \cdot D \cdot \tan(a_w/2)}{W} \text{ [m/pixel]} \tag{1}$$

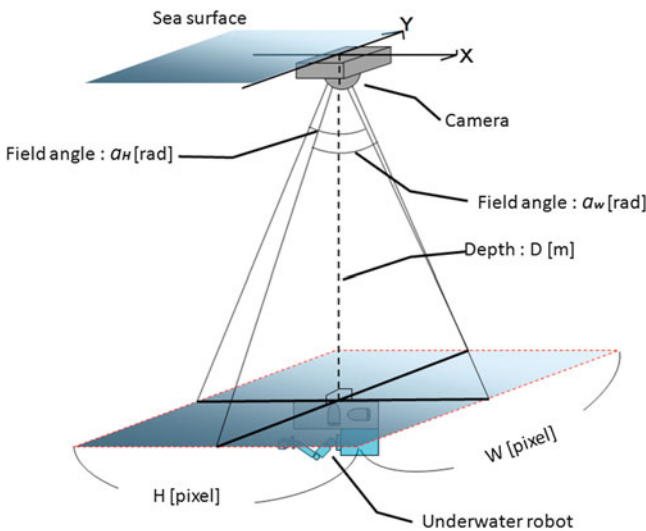


Fig. 3 Relation of between pixel and real-distance

Table 1 Camera specification

Picture size	W:1280 × H:960 [pixel]
Field angle—vertical	$a_H:80.9$ [rad]
Field angle—horizontal	$a_W:66.3$ [rad]

$$C_H = \frac{2 \cdot D \cdot \tan(a_H/2)}{H} \text{ [m/pixel]} \tag{2}$$

The spacing error is contained when using it for the position tracking as it is because the swerve is caused in the camera. Pixel the swerve correction then real distance transform coefficient C_H and C_W are obtained. The image size, the horizontal angle of view, and the vertical picture corner after the swerve is corrected are shown in Table 1.

Thus, real position (R_H, R_W) can be requested by using the conversion formula of the next expression from the pixel value (position P_H of the vertical direction, horizontal direction, and position P_W) in the image.

$$R_W = C_W \cdot P_W = 0.00136D \cdot P_W \text{ [m]} \tag{3}$$

$$R_H = C_H \cdot P_H = 0.00133D \cdot P_H \text{ [m]} \tag{4}$$

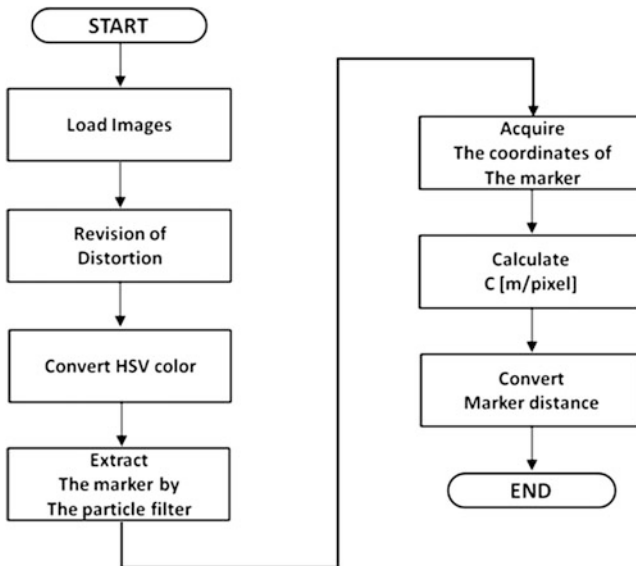


Fig. 4 Flow chart

2.3 Method of Image Processing

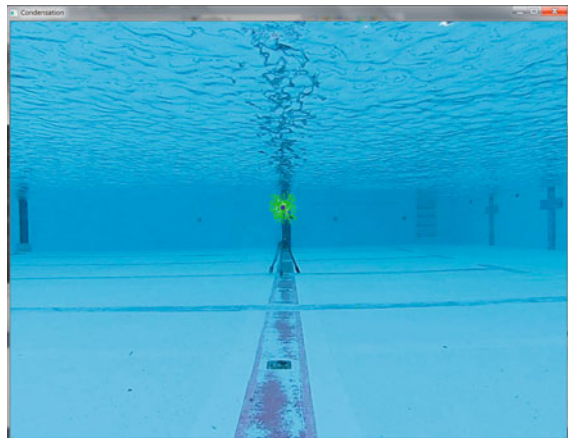
The image processing program uses Microsoft Visual C++ 2010 Express Edition, and the image processing library uses OpenCV1.0 that is open source.

Figure 3 shows the flow of the image processing. HSV is converted after the image is corrected, and the marker is detected with the particle filter. The mean value at the position of the particle is adjusted to the position in the image. A real position is requested from the center position of the particle based on expression (3) and (4) (Fig. 4).

Fig. 5 Result of the image processing (*land*)



Fig. 6 Result of the image processing (*underwater*)



3 Basic Experiment

Carry out basic experiments used a monocular camera at outdoor, whether the marker can be recognized by the particle filter. At this time, the LED light is adopted in the marker. The distance of the monocular camera and the marker is 5 [m].

Shows Fig. 5 that is processing the distortion correction. And shows Fig. 6 that is the particle filter.

Blue point is the position of the center of gravity of the particle. The marker was able to detect by using the particle filter in both land and underwater.

4 Conclusion

Authors are trying the development of the position measurement system of the underwater robot using a monocular camera from the development of the underwater robot that works in the sea off Okinawa where the transparency is high.

In this paper, it reported on the basic experiment by the positional measurement method and land.

The parameter of the particle filter is adjusting now. From now, we are going to test the accuracy of the position measurement. In the future, we aim to build a position measurement system integrated to GPS information and attitude sensor information.

Acknowledgments This study received The Telecommunications Advancement Foundation in 2012 fiscal year and was done.

References

1. Ministry of the Environment (2009) White paper on the environment, the sound material-cycle society and the biodiversity in Japan incorporate Japan's economy into the sound global environment, p 47 (in Japanese)
2. Carpenter KE et al (2008) One-third of reef-building corals face elevated extinction risk from climate change and local impact. *Science* 321:560–563
3. Motokawa T (2008) Story of coral and coral reef. Chukoshinsho (in Japanese)
4. Takemura F, Shiroku RT (2010) Development of the actuator concentration type removable underwater manipulator. In: The 11th international conference on control, automation, robotics and vision (ICARCV2010), pp 2124–2128
5. Zhang T, Li W, Kuhnlenz K and Buss M (2011) Multi-sensory motion estimation and control of an autonomous quadrotor. *Adv Robotics* 25:1493–1514

Emergency Detection Based on Motion History Image and AdaBoost for an Intelligent Surveillance System

Jun Lee, Jeong-Sik Park and Yong-Ho Seo

Abstract This paper proposes a method to detect emergency situations in a video stream using a Motion History Image (MHI) and AdaBoost for a video-based intelligent surveillance system. The proposed method creates a MHI of each human object through an image processing technique entailing background removal based on Gaussian Mixture Model (GMM) followed by labeling and accumulating the foreground images. The obtained MHI is then compared with the existing MHI templates to detect emergency situations. To evaluate the proposed emergency detection method, a set of experiments on a dataset of video clips captured from a surveillance camera were conducted. The results show that we successfully detected emergency situations using the proposed method.

Keywords Gaussian mixture model · Motion history image · Video-based surveillance system · AdaBoost

1 Introduction

Currently there is strong demand for intelligent emergency detection techniques that automatically analyze situations recorded in a live video stream captured from a surveillance camera. This paper proposes a method to detect emergency situations for a video-based intelligent surveillance system [1].

J. Lee · J.-S. Park · Y.-H. Seo (✉)
Department of Intelligent Robot Engineering, Mokwon University,
Mokwon Gil 21, Seo-gu, Daejeon, Republic of Korea
e-mail: yhseo@mokwon.ac.kr

J.-S. Park
e-mail: parkjs@mokwon.ac.kr

The proposed method traces a human object in the field of view of a surveillance camera after separating the foreground from the background in the image using conventional image processing techniques including a Gaussian Mixture Model (GMM) and labeling.

We also develop a vision-based surveillance system based on the proposed method to record images captured from an IP camera installed under the ceiling of an indoor environment, similar to existing CCTV surveillance systems.

This paper is organized as follows. The proposed emergency detection method is described in [Sect. 2](#). Experimental results are presented in [Sect. 3](#) and a conclusion is finally given in [Sect. 4](#).

2 Emergency Detection Method Using Motion History Image

The proposed method first extracts the foreground, which is assumed to be a human object, from the input image. Human object tracking is then conducted to create a Motion History Image (MHI) of the current object from sequential images in a given duration triggered by using a similarity threshold between the current and the next foreground human object.

2.1 Foreground Extraction and Human Object Tracking

For detection of a human object, separation of the foreground from the background is necessarily required. The conventional approach for foreground extraction requires modeling of the background in a video stream.

Therefore, we employ a GMM-based approach, which is a robust and widely used method for background modeling. The suggested method uses multi-Gaussian distributions in order to prevent the regular Gaussian distribution from falling into the maximum local point by using average and standard deviations of distributed values. A mixture of Gaussians is maintained for the underlying distribution for each pixel's color values. For each new frame, the mean and covariance of each component in the mixture are updated to reflect the change of the pixel values. If a new value is far enough from the mixture in a new image, the current background model is updated. The foreground can be extracted by calculating the difference between the entire image and the current background model [2].

The following parameters of each Gaussian component need to be learned dynamically. Equation (1) gives the average, Eq. (2) gives the variance, and Eq. (3) gives the weight parameter of each Gaussian component.

$$\hat{\mu}_j = \frac{\sum_{n=1}^N P(\omega_j | x_n, \theta) x_n}{\sum_{n=1}^N P(\omega_j | x_n, \theta)} \tag{1}$$

$$\hat{\sigma}_j^2 = \frac{\sum_{n=1}^N P(\omega_j | X_n) \|X_n - \hat{\mu}_j\|^2}{\sum_{n=1}^N P(\omega_j | X_n)} \tag{2}$$

$$\hat{\omega}_j = \frac{1}{N} \sum_{n=1}^N P(\omega_j | X_n) \tag{3}$$

After extracting the foreground binary image, noise is removed by applying dilation and erosion operation prior to the labeling process.

Human object tracking is conducted after foreground extraction. Labeling is a process to obtain blobs from the foreground image. For this process, we apply a

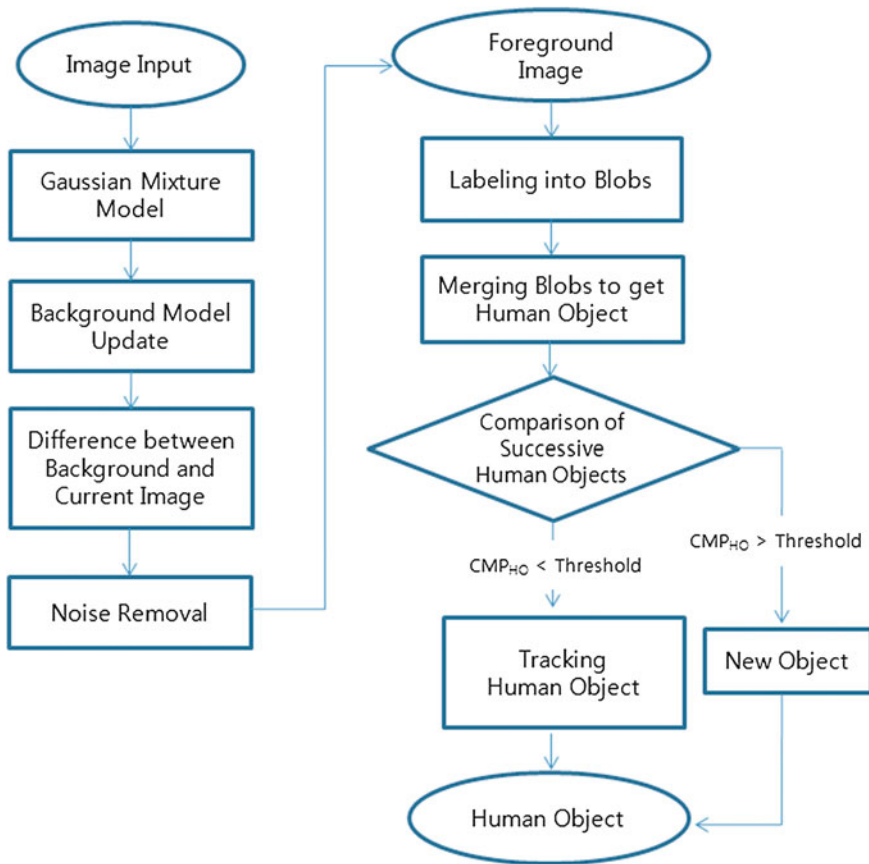


Fig. 1 Flowchart of foreground extraction and human object tracking

well-known blob labeling algorithm [3]. The near blobs then need to be merged because they can form a candidate of the human object.

The tracking process also includes a comparison of two human objects in successive image frames to determine whether the current human object is the same object as either the previous one or a new one. This can be calculated by measuring the Euclidian distance of the center of masses and the difference of sizes of two objects. In this study, we simply use a correlation-based approach, by which the sum of pixel differences between two objects is calculated and a threshold value is defined to recognize a new human object.

Figure 1 shows a flowchart of the foreground extraction and the human object tracking steps, which are used as preprocessing techniques in our emergency detection method. In Fig. 1, CMP_{HO} and Threshold denote the correlation value of two successive human objects and the predefined threshold value, respectively.

2.2 Emergency Detection Using MHI

Unlike posture recognition, which uses a single image frame, a sequence of images should be considered to recognize human action. Given a sequence of images, we adapt a representation of the MHI to a model of human action. The MHI accumulates an image sequence into a single image that captures spatial and temporal information about motion [4]. The MHI has advantages of fast processing speed and the ability to represent short-duration movement.

It is possible to apply various types of MHIs. In this study, we identify each human object by giving higher weight to recent frames rather than previous frames when accumulating the human object [5]. Examples of MHI templates for emergency situations are shown in Fig. 2.

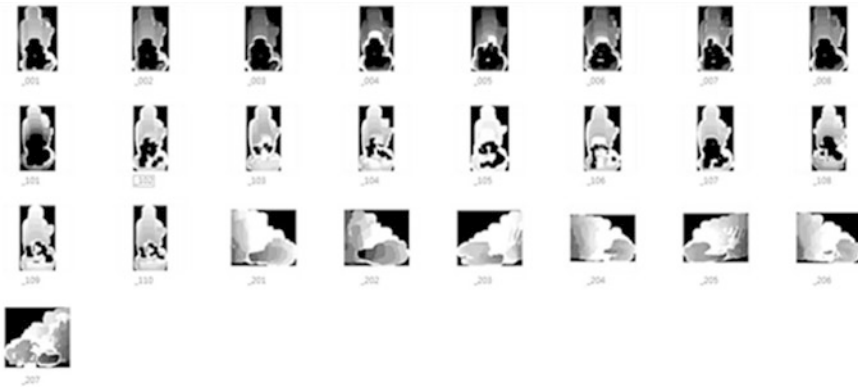


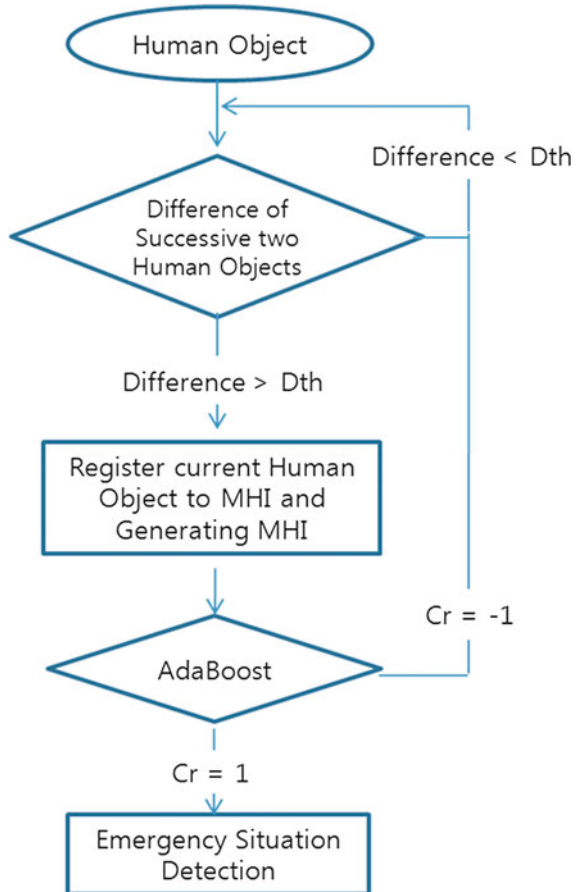
Fig. 2 Examples of MHI templates of positive samples for emergency situations

AdaBoost is used to detect behaviors of emergency situations. AdaBoost was proposed in 1995 as a general method for generating a strong classifier out of a set of weak classifiers [6, 7]. It works even when the classifiers are taken from a continuum of potential classifiers such as neural networks and LDA. However, for the sake of simplicity, it assume that the pool of experts is finite, that it contains L classifiers, and that it is provided as input to AdaBoost. This is the case, for example, with the well-known method of face recognition introduced by Viola and Jones [8].

A strong classifier $f(x)$ can detect emergency situations by combining a set of weak classifiers $h_i(x)$ as in the following Eq. (4). The output of the strong classifier, $Cr(x)$, is given by the following Eq. (5).

$$f(x) = \sum_{t=1}^T a_t h_t(x) \tag{4}$$

Fig. 3 Flowchart of emergency detection using MHI and AdaBoost



$$Cr(x) = \text{sign}\left(\sum_{t=1}^T a_t h_t(x)\right) \tag{5}$$

If the MHI of the current situation is identical to one of the Adaboost classifiers that we trained using the MHI templates of the given emergency situation, the output $Cr(x)$ of the Adaboost classifier will be close to 1. In this study, the detection result of the emergency situation is satisfied when we trained the AdaBoost with positive samples and negative samples at a ratio of 1–3. Figure 3 shows a flowchart of the emergency detection using MHI. In Fig. 3, D_{th} represents the predefined threshold value for accumulating successive human objects.

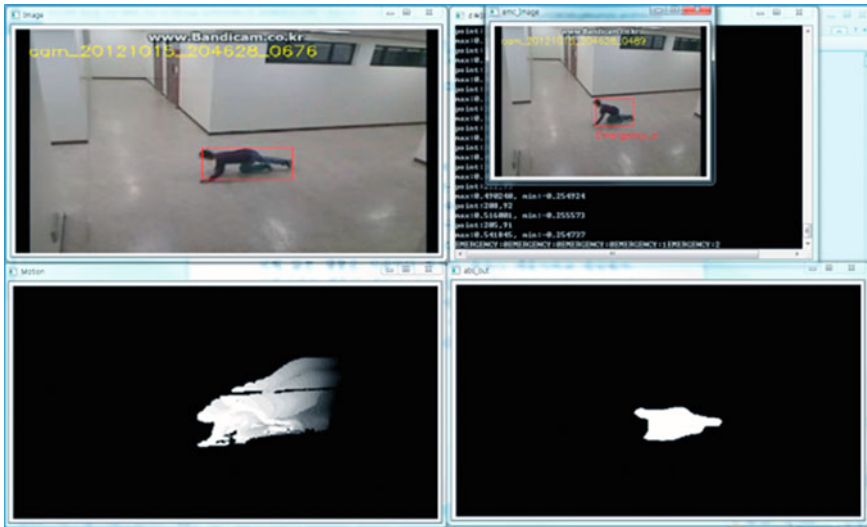


Fig. 4 Result of emergency situation detection and MHI template of falling

Table 1 Experimental results of emergency detection

Emergency case	Detection results	
	Using AdaBoost (%)	Using template matching (%)
Squatting down	65	40
Falling down	75	45
Walking	90	80
Total	76	55

3 Experimental Results

We installed the IP camera under the ceiling of a corridor with a height of 2.5 m and a width of 1.5 m for our experiments. We reproduced the situations of falling down and squatting down as emergency cases. Figure 4 represents a result of emergency situation detection and a MHI template of falling down.

The experimental results of emergency detection are represented in Table 1 for three emergency situations: squatting down, falling down, and walking.

4 Conclusion

This paper proposes an emergency detection method using a MHI for a video-based intelligent surveillance system. The proposed system can detect emergency situations automatically, and thus could deliver notification of the current emergency to a surveillance manager. The proposed method consists of three fundamental processes for detecting an emergency situation: foreground extraction, human object tracking to create a proper MHI, and emergency classification using AdaBoost.

The feasibility and effectiveness of the proposed method were successfully verified by conducting several experiments involving emergency detection for squatting down and falling down cases under an indoor environment, similar to a conventional CCTV surveillance system.

For future work, we will enhance the quality of the foreground by considering external factors such as the light an the angle and walking speed of a human object, and also will enhance the emergency detection accuracy.

Acknowledgments This work was supported by the Basic Science Research Program through the National Research Foundation of Korea (NRF) funded by the Ministry of Education, Science and Technology (MEST) (2011-0013776). This work was also supported by the NAP (National Agenda Project) of the Korea Research Council of Fundamental Science & Technology.

References

1. Jeong IW, Choi J, Cho K, Seo YH, Yang HS (2010) A vision-based emergency response system with a paramedic mobile robot. *IEICE Trans Inf Syst* E93-D(7):1745–1753
2. Samet H, Tamminen M (1988) Efficient component labeling of images of arbitrary dimension represented by linear bintrees. *IEEE Trans Patt Anal Mach Intell* 10(4):579–586
3. Stauffer C, Grimson WEL (1999) Adaptive background mixture models for real-time tracking. In: *Proceedings of IEEE computer society conference on computer vision and pattern recognition*, vol 2, pp 246–252
4. Bobick AF, Davis J (2001) The recognition of human movement using temporal templates. *IEEE Trans Patt Anal Mach Intell* 23(3):257–267

5. Han T-W, Seo Y-H (2009) Emergency situation detection using images from surveillance camera and mobile robot tracking system. *J Inst Webcasting Internet Telecommun (IWIT)* 9(5):101–107
6. Freund Y, Shapire R (1995) A decision-theoretic generalization of on-line learning and an application to boosting. In: *Proceedings of the second European conference on computational learning theory*, pp 23–37
7. Hastie T, Tibshirani R, Friedman J (2001) *The elements of statistical learning*. Springer, New York
8. Viola PA, Jones MJ (2001) Robust real-time face detection. *ICCV* 2:747

Marker Tracking for Indirect Positioning During Fabric Manipulation

Mizuho Shibata

Abstract We describe here a marker tracking algorithm for indirect positioning during planar fabric manipulation. Indirect positioning is a unique problem during manipulations of deformable objects. Improving the tracking of position by a robotic system contributes to the dexterous manipulation of deformable objects. To formulate this algorithm, we assessed the movement of a single robotic finger moving one manipulated point on a fabric to one positioned point or marker, to the desired point on a floor. To select an appropriate algorithm, we classified disturbances during the positioning of fabrics. To precisely detect the position of the marker during these disturbances, we applied the combination of a particle filter and a labeling processing to the algorithm. Experimental evidence showed that, due to its precision in detecting position, this algorithm was suitable for indirect positioning.

Keywords Fabric manipulation • Non-collocated manipulation • Marker tracking

1 Introduction

In this manuscript, we discuss image processing for the manipulation of deformable objects, in this case fabrics. Fabric manipulations are required in many industrial fields, including apparel and linen supply services, but most are performed by hand. Automation of fabric manipulation can enhance its efficiency. Several methods of fabric manipulation have been described [1–3]. Mechanical grippers, with pins [4] and rollers [5] to grasp fabrics, have been developed to handle fabric. Sensory systems, utilizing visual and tactile information, have been

M. Shibata (✉)

Department of Robotics, Kinki University, 1 Takaya-Umenobe,
Higashi-hiroshima, Hiroshima, Japan
e-mail: shibata@hiro.kindai.ac.jp

developed to sense or recognize fabric manipulations [6, 7]. Models of fabrics have been developed to analyze their manipulation, with most models using a spring-mass-damper system to reduce computation time [8, 9]. Several strategies have also been introduced for fabric manipulation [10, 11], including systems that integrate various techniques in their working strategies [12, 13]. We have developed a robotic system that can manipulate a fabric such as a handkerchief [13]. We have classified these manipulations into their basic motions, including grasping, wiping [14], unfolding [15], and placing [16] motions, and integrated these motions in series [13].

Wiping motion using a deformable object is defined as a task in which there is contact, but no relative movement, between the manipulator and the object, while there is both contact and relative movement between the object and a floor during the displacement of the object. We applied contacts with the fabric and the environment, including the fingertips of the robotic hand, to the sequence. These contacts adequately constrained movement and deformation of the fabric, realizing this sequence utilizing an open-loop control law for a one-handed robot with two grippers [14]. Similarly, utilizing contact with fabrics and an environment can result in easy manipulations to handle deformable objects. In this manuscript, we discuss the indirect positioning of fabrics (Fig. 1). Indirect positioning, or non-collocated control, is a positioning problem, in which a positioned point on a deformable object is moved to a desired point, as determined by coordinates or a floor, by moving a manipulated point that differs from the positioned point (Fig. 1). This positioning problem is unique to manipulations of deformable objects due to the dynamics of the object. Among studies of indirect positioning are those involving vibration suppression control of a flexible structure such as a flexible arm [17, 18]. The concept of indirect positioning has been applied to fabric manipulation [8, 19]. Modeling of a deformable object can affect a control law during indirect positioning [8]. Our group analyzed the effects of the viscosity of a linear deformable object on indirect positioning [19]. In this manuscript, we discuss planar indirect positioning, in which a single robotic finger moves a manipulated point on a flat floor (Fig. 1). We considered the indirect positioning as a type of wiping slide motion. Utilizing contact with fabrics and an environment, the

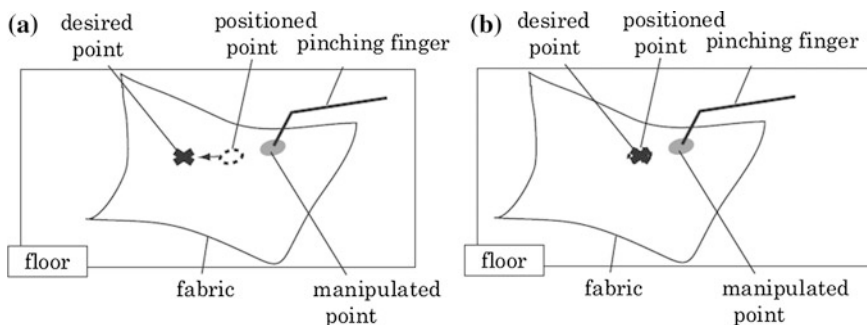


Fig. 1 Indirect positioning for fabric manipulation. **a** Initial condition. **b** Convergent condition

fabrics can be easily replaced. We utilized one marker to measure the positioning point. Precise positioning, however, may require visual feedback, and a visual feedback system requires the marker to be measured robustly and accurately, even during disturbances. In this manuscript, we consider the effects of disturbances on the indirect positioning of fabrics. To develop marker tracking for the indirect positioning of fabrics, we applied the combination of a particle filter and a labeling method to image processing.

2 Problem Settings

In this section, we describe the setting of the problem underlying the indirect positioning of fabrics. Based on this problem setting, we selected an image processing algorithm. As described in Sect. 1, the system consists of a single manipulator or robotic finger moving one positioning point to the desired point on a fabric placed on a flat floor. This high-precision algorithm can track the marker in a short computation time. We assumed that there was no slippage between the robotic fingertip and the fabric during this manipulation. The positioned point on the fabric was indicated with a black mark, and the position of the marker was determined using an image obtained by a camera.

To select an adequate algorithm for the problem, we classified disturbances that may occur during indirect positioning (Fig. 2). One major disturbance during this manipulation arises from the manipulator itself. The manipulator should be placed as close to the marker as possible to reduce the effects of the fabric’s dynamics.

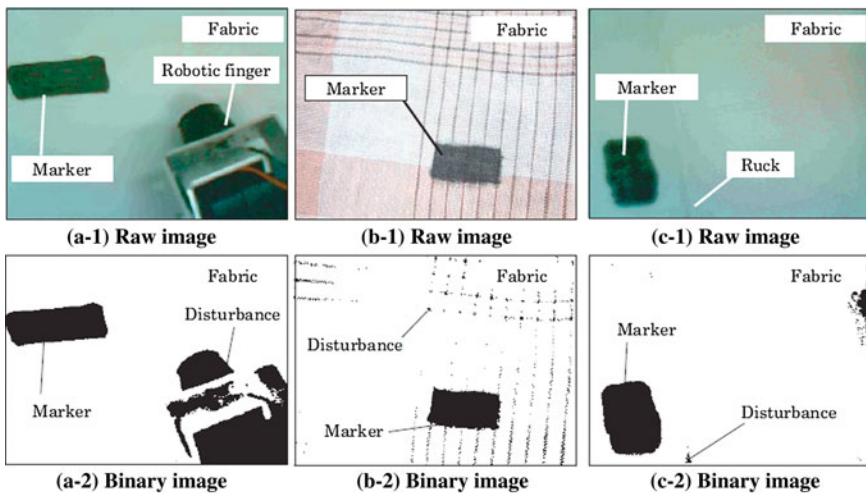


Fig. 2 Disturbances during planar indirect positioning of fabric manipulation. **a** Robotic finger. **b** Design of fabrics. **c** Ruck on fabrics

This is indicated by the photograph of the robotic finger (Fig. 2a-1). The disturbance by the manipulator may be large relative to the area occupied by the marker (Fig. 2a-2), emphasizing the need to select an algorithm with robustness for such a large disturbance.

We should also consider the characteristic disturbances of a fabric. One of these disturbance is the design on the fabric (Fig. 2b-1). For example, a fabric with a waffle pattern can generate many small disturbances (Fig. 2b-2), suggesting the need to select an algorithm with robustness for these disturbances.

Another disturbance is due to rucks on the fabric (Fig. 2c-1). Fabrics can buckle in response to compression, with buckling generating rucks on the fabric, which may account for a considerable degree of disturbance during manipulations (Fig. 2c-2). Rucks are generated by mechanical conditions, such as the relative movements of the robotic finger, the fabric and the floor. Therefore, these rucks will not be generated if the manipulator moves the fabric in an adequate configuration. In this manuscript, we do not consider rucks on the fabric.

3 Proposed Algorithm

In this section, we introduce an image processing algorithm for the indirect positioning of fabrics based on the problem settings described above. Image processing based on a particle filter was applied to the algorithm to track a marker on the fabric. Particle filter tracking is a type of time series filter such as a Kalman filter [20]. Distributions dealt with by particle filters are nonlinear and nongaussian, allowing their application to various tracking problems. The particle filter algorithm generates several particles around the target stochastically, followed by the elimination of some of these particles based on predefined criteria. The position of the target was calculated as the average position of all surviving particles so that the tracking based on particle filters has robustness for disturbances such as noises and occlusions in short-time. The position determined by the algorithm can move partially and randomly because the positions of the particles are generate stochastically. Therefore, the precision of the position after the calculation must be somewhat low to utilize the input signals of positioning problems. For example, the average position of particles may move randomly even if the marker does not move, because of the principle of the algorithm. To overcome this difficulty, we applied the combination of a particle filter and a labeling processing to the algorithm. This proposed algorithm consists of following processes or steps, shown in detail in Fig. 3.

- (a) image capturing: the camera in this system captures a raw image,
- (b) initializing: the initial positions of the particles are determined relative to the marker for preprocessing,
- (c) binary processing: the raw image is converted to a binary image,

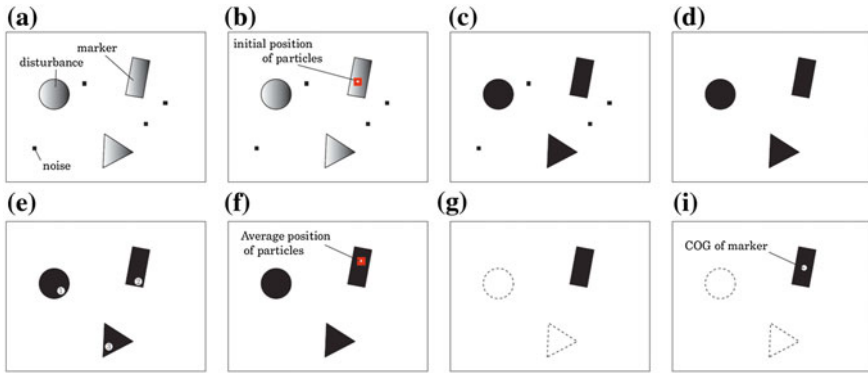


Fig. 3 Overview of the steps of the proposed algorithm. **a** Image capturing. **b** Initialization. **c** Binarization. **d** Erosion. **e** Labeling. **f** Particle filter. **g** Recognition. **h** Calculating COG

- (d) erosion process: the binary value of the target pixel is inverted depending on the conditions of pixels near the target pixel,
- (e) labeling process: clusters of black pixels are labeled based on a labeling method,
- (f) calculations: particles are generated/eliminated based on the criteria of a particle method. The average position of the particles is calculated,
- (g) recognition: the labeling data obtained in Step (e) were compared with the average positions in Step (f). The label area, including the average position of particles as the marker, and the target area were determined,
- (h) calculating center of gravity; the center of gravity (COG) of the target area was calculated and defined as the position of the marker.

Using this algorithm, we dealt with a grayscale image in Step (a), allowing erosion and labeling. In Step (b), we set the initial position of the image using a mouse. In Step (c), the threshold of the binary process was determined adequately using a manual. The white noises in the image are reduced through erosion (Step (d)), using a four-neighbor erosion process [21] to the step. A 4-neighbor labeling method [21] was utilized for this image (Step (e)). During this step, all clusters, including disturbances, were labeled. In Step (f), we applied the CONDENSATION method [20] to the algorithm of the particle filter. The label number of the marker may change during Step (e), depending on the relative positions of the marker and the disturbances. Even if the label number changes during the manipulation, however, the particles track the area of the marker. That is, we obtained the current labeling number of the marker (Step (g)), directly utilizing the COG of the marker directly, allowing the proposed algorithm to more precisely determine the position of the marker than when using the particle filter alone (Step (g)). The single loop of the proposed algorithm consists of capturing one image and processes from Step (c) to Step (h). After Step (h), the camera captures the next image.

4 Experiments

In this section, we implement the proposed algorithm, and then verify its validity experimentally. We utilized three conditions in order to verify the validity of this algorithm (Fig. 4). We first checked the path on a plain white fabric of a black rectangular marker, measuring 20×10 mm, moved from its initial position 20 mm to the right in a straight path for approximately 3 s (Fig. 4a). Here, the manipulating point is on the right of the figure to avoid rucking the fabric during manipulation. This manipulating point is not observed in the images obtained during the experiment. The distance between the fabric and the floor was approximately 165 mm. The spatial resolution of each pixel was approximately 0.4 mm. The origin in the task coordinate is at the upper left corner of the image. To investigate the relative merits of the proposed algorithm, we compared it with a tracking algorithm using only a particle filter. Figure 4b confirms the influence of a single large disturbance on the marker for the proposed algorithm, with the area of disturbance larger than that of the marker. In Fig. 4c, we utilized a fabric with a waffle pattern as a model of many disturbances during movement of a fabric. In all experiments, we utilized the same experimental setup. Figure 5 shows the paths of the markers obtained during these experiments. The proposed algorithm was able to determine the straight path (Fig. 5a-1). Although the particle filter alone could track the marker, the path was not straight because of statistical elements (Fig. 5a-2). These results indicate the superiority of the proposed algorithm, which can be utilized to track an indirectly positioned marker.

One advantage of the proposed algorithm is the computation time, which is independent of the number of disturbances (Table 1). These times were determined from the average of 40 samplings and include the image capture time. This algorithm requires that only the COG of the objective area, or marker, is calculated. The COGs of other areas, including disturbances and noises, are not calculated because the objective area can be adequately determined based on tracking of the particle filter.

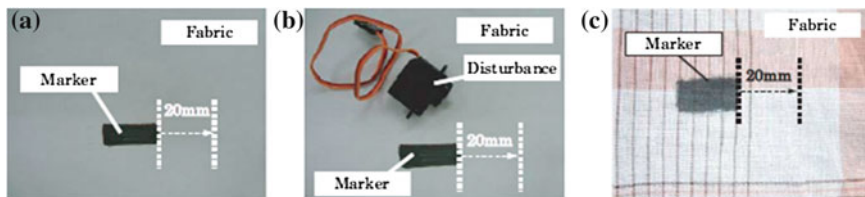


Fig. 4 Experimental setup. **a** Without disturbance. **b** With one disturbance. **c** With disturbances (Fabric designs)

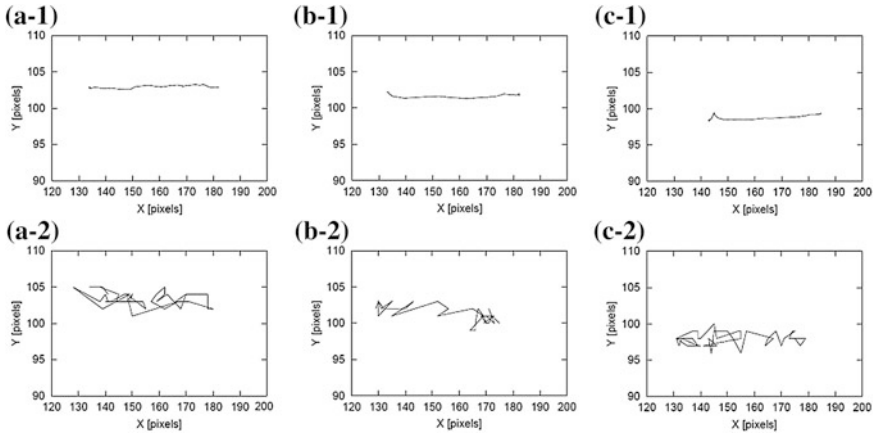


Fig. 5 Experimental results. **a-1** Proposed algorithm without disturbances. **a-2** Particle filter without disturbances. **b-1** Proposed algorithm with one disturbance. **b-2** Particle filter with one disturbance. **c-1** The proposed algorithm with disturbances. **c-2** The particle filter alone with disturbances

Table 1 Computation times for steps in the proposed algorithm

Experiment	Ave. time (ms)	Standard deviation (ms)
(a-1) in Fig. 5	73.0	7.4
(b-1) in Fig. 5	75.8	8.2
(c-1) in Fig. 5	73.1	7.3

5 Summary

This manuscript has described a marker tracking algorithm for indirect positioning of planar fabric manipulation. We considered the scenario in which one robotic finger moved one manipulated point on a fabric, such that the positioned point, or marker, corresponds with the desired point on a floor. In order to select an adequate algorithm, we showed typical disturbances by (a) the manipulator (b) the design of the fabrics and (c) the rucks of the fabric. We applied the combination of a particle filter and a labeling process to the algorithm to detect the marker precisely under these disturbances. We checked the validity of this algorithm through several experiments. Our experimental results showed that the algorithm was more robust than an algorithm based solely on a particle filter.

Acknowledgments This research was partially supported by The Furukawa Foundation for promotion of technical science.

References

1. Taylor PM (1990) Sensory robotics for the handling of limp materials. Springer Verlag, Berlin
2. Taylor PM, Pollet DM, Abbott PJW (1998) The Influence of environmental conditions on automated fabric handling. *J Rob Mechatron* 10(3):258–263
3. Parker JK, Dubey R, Paul FW, Becker RJ (1983) Robotic fabric handling for automation garment manufacturing. *J Eng Ind* 105:21–26
4. Fahantidis N, Doulgeri Z (2000) A gripper for grasping non-rigid material pieces out of a bundle. In: Proceedings of the IEEE international conference on intelligent robots and systems, pp 2145–2150
5. Kabaya T, Kakikura M (1998) Service robot for housekeeping? Clothing handling? *J Rob Mechatron* 10(3):252–257
6. Torgerson E, Paul FW (1987) Vision guided robotic fabric manipulation for apparel manufacturing. In: Proceedings of 1987 IEEE international conference on robotics and automation, pp 1196–1202
7. Ono E, Kita N, Sakane S (1995) Strategy for unfolding a fabric piece by cooperative sensing of touch and vision. In: Proceedings of the IEEE international conference on intelligent robots and systems, pp 441–445
8. Hirai S, Wada T (2000) Indirect simultaneous positioning of deformable objects with multi pinching fingers based on uncertain model. *Robotica* 18(1):3–11
9. Kita Y, Saito F, Kita N (2004) A deformable model driven visual method for handling clothes. In: Proceedings of the international conference on robotics and automation, pp 3889–3895
10. Paraschidis K, Fahantidis N, Vassiliadis V, Petridis V, Doulgeri Z, Petrou L, Hasapis G (1995) A robotic system for handling textile materials. In: Proceedings of 1995 IEEE international conference on robotics and automation, pp 1769–1774
11. Hamajima K, Kakikura M (1998) Planning strategy for task untangling laundry? Isolating clothes from a washed mass? *J Rob Mechatron* 10(3):244–251
12. Hata S, Hojoh H, Toda M, Hamada T (2011) Cloth handling system for linen supply industry. In: Proceedings of the international conference on mechatronics and automation, pp 864–869
13. Shibata M, Ota T, Endo Y, Hirai S (2008) Handling of hemmed fabrics by a single-armed robot. In: Proceedings of the 4th IEEE conference on automation science and engineering, pp 882–887
14. Shibata M, Ota T, Hirai S (2009) Wiping motion for deformable object handling. In: Proceedings of the IEEE international conference on robotics and automation, pp 134–139
15. Shibata M, Ohta T, Hirai S (2010) Robotic unfolding of hemmed fabric using pinching slip motion. In: Proceedings of the international conference on advanced mechatronics, pp 392–397
16. Shibata M, Hirai S (2012) A fabric manipulation utilizing contacts with environments. In: Proceedings of the IEEE conference on automation science and engineering, pp 438–443
17. Smith RS, Cheng-Chih C, Fanson JL (1994) The design of hinf controllers for an experimental non-collocated flexible structure problem. *IEEE Trans Control Syst Technol* 2(2):101–109
18. Matsuno F, Ohno T, Orlov YV (2002) Proportional derivative and strain (PDS) boundary feedback control of a flexible space structure with a closed-loop chain mechanism. *Automatica* 38(7):1201–1211
19. Shibata M, Hirai S (2006) Soft object manipulation by simultaneous control of motion and deformation. In: Proceedings of the 2006 IEEE international conference on robotics and automation, pp 2460–2465
20. Isard M, Blake A (1998) Condensation-conditional density propagation for visual tracking. *Int J Comput Vis* 29(1):5–29
21. Burger W, Burge MJ (2007) Digital image processing: an algorithmic introduction using java. Springer

Vision-Based Human Following Method for a Mobile Robot Using Human and Face Detection

Se-Jun Park, Tae-Kyu Yang and Yong-Ho Seo

Abstract This paper presents a method of vision based human following for a mobile robot to trace a given human in an indoor environment. For a mobile robot to perform vision based human tracing reliably, we combined a silhouette based human detection and two-stage face detection technique. In this paper, the human detection uses a Histogram of Oriented Gradient (HOG). The face detection is composed of two stages, face detection using a Haar-like wavelet feature and AdaBoost and face detection using skin color with motion information and validation of contour shape. Finally, the performance of the proposed system is verified by conducting experiments where a mobile robot follows a human successfully in a real indoor environment.

Keywords Mobile robot · Human following · Face and human detection · AdaBoost · HOG

1 Introduction

Robust object detection and tracking technology for autonomous navigation of mobile robots is a very important issue in robotics research. In particular, it is critical when both the mobile robot and human are moving [1]. Difficulty in vision-

S.-J. Park · T.-K. Yang · Y.-H. Seo (✉)
Department of Intelligent Robot Engineering, Mokwon University,
Mokwon Gil 21, Seo-gu, Daejeon, Republic of Korea
e-mail: yhseo@mokwon.ac.kr

S.-J. Park
e-mail: sjpark@mokwon.ac.kr

T.-K. Yang
e-mail: tkyang@mokwon.ac.kr

based real-time object detection and tracking technology depends on the kind of target object to be tracked and its surrounding environment.

Face detection to find the position and size of a face that exists in a given image captured from a camera attached on a robot is an important step to perform human following. Therefore, we propose a method of vision-based human following in a dynamic environment using the contour information detection of a human as well as a face detector.

In this paper, we present a cascaded method that combines three detectors including one human detector and two face detectors to perform reliable human target tracking. First, the human detection uses contour information of a human based on a Histogram of Oriented Gradient (HOG). When the image captured from the camera of a robot does not contain all contour information, it fails to detect a human, and dual-stage face detection is then activated. The first stage of the face detection method uses Haar-like wavelet features and AdaBoost, well-known methods included in OpenCV [2]. For the second stage of face detection, we use skin color with motion information and validation of the face contour shape.

The proposed method should deal with robust object following of a mobile robot while the mobile robot and human are moving in a dynamic environment with obstacles by combining the output results of human and face detection. Finally, we verified the feasibility and performance of the suggested method by conducting autonomous navigation experiments where a mobile robot should follow a human while avoiding obstacles in a complex indoor environment by applying the proposed method.

2 Related Works

Object tracking methods can be classified into color-based approaches, template-based approaches, and motion-based approaches according to the characteristics of the target object.

First, color-based methods use the color distribution of the object as a characteristic value. These methods are widely used because they are based on a simple and fast algorithm. The color distribution variations of each object can be expressed by generating a Gaussian Mixture Model based on a color histogram of the object after converting a RGB color model into a HSV or YUV color model. This method can easily extract a moving object from the background [3].

Second, template-based methods usually register the template of an object in various forms prior to tracking. These methods show more stable performance than the motion-based methods. However, the conventional template-based methods cannot effectively deal with size change and rotation of object. Papageorgiou proposed a pedestrian detection method using wavelet template creation and SVM [4].

Third, the motion information is an important cue for object tracking. The motion-based tracking methods can be represented as a set of motion parameters expressed as a Parametric Motion Model for the motion information of an object.

These methods can be applied to a moving camera by using the background motion model and independent object motion model creation. The optical flow method is a representative algorithm [5].

In this paper, we use a template-based method to detect a human and face detection. We use a Histogram of Oriented Gradient as a template in the human detection stage and Haar-wavelet features in the face detection stage. We also use AdaBoost as a classifier of these two templates. Finally, we add another face detector that combines a skin color-based detector with motion information and validation of contour shape as a second technique when the first face detector fails to find a face.

3 Vision-Based Human Following Method

3.1 Vision-Based Human Tracker Based on Human and Face Detection

The set of image features used for human detection is based on duplicated encoding and high density of image area using histogram gradient descriptors. Here, descriptors can be classified into static HOG and motion HOG. The static HOG is calculated through individual images and the appearance features, and it includes R-HOG, C-HOG, Bar HOG, and Centre-Surround. The motion HOG is calculated by a set of continuous video and motion channel, and is used for video detection.

The static HOG and motion HOG are based on an oriented histogram [6]. Figure 1 shows the static HOG encoding process. For human detection, we use a method based on HOG and AdaBoost proposed by Laptev [7].

In this study, we use a well-known face detection algorithm based on AdaBoost proposed by Viola and Jones. This detector is an excellent algorithm in terms of its speed and detection performance [8]. The Haar-wavelet feature expresses edges or lines in an image and it contains two or more rectangular areas. In a given sub-window, the Haar-wavelet feature can be defined as the weighted subtraction of the brightness sum of two rectangular areas.

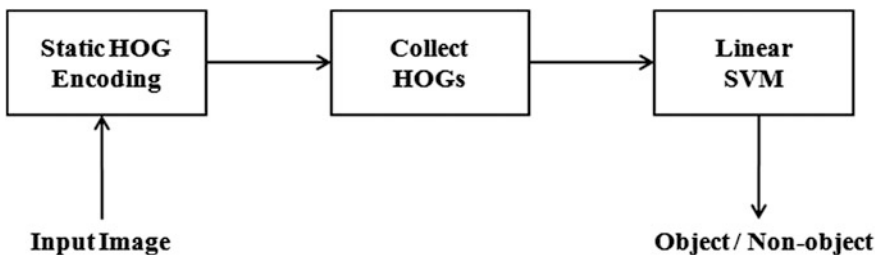


Fig. 1 Static HOG encoding process

In order to deal with detection failure of the human detector and the face detector mentioned above, we propose another face detector based on skin color filtering with motion information and contour shape validation. This face detector works well on small size faces even if the described two detectors do not work, but false alarms of this detector are relatively higher. The skin color filtering method is widely used due to fast computation time and simple operation. However, if the background color is similar to the skin color, it does not work well, and it is also sensitive to illumination changes [9].

Therefore, we combined the skin color filtering with motion information and contour shape validation to minimize the impact of the background or lighting problems to reduce the risk of incorrect detection with the use of skin color only. The proposed face detection method calculates the difference of successive two images: the result is called a motion map. It then selects candidate regions of a face by using skin color filtering merged with the motion map. Finally, it detects a face by verifying that the contour shape is close to an ellipse.

Figure 2 shows a human detection result using HOG and AdaBoost and Fig. 3 shows results from the two different face detectors. The left figure of Fig. 4 shows the face detection result using a Haar-wavelet and AdaBoost and the right two figures show the face detection result and its internal process using skin color filtering with motion and validation of the contour shape. These figures show that the implemented human detector and two face detectors works relatively well.

Figure 4 shows a flow chart of our vision-based human following based on human and face detection. First, the proposed following method tries to detect a human. When this stage fails, it usually means that the current image does not contain an entire outline of the human, and therefore it activates the first face detection using the Haar-wavelet and AdaBoost. If this stage fails to find a face, then the second face detection based on skin color with motion and validation of the contour shape is activated lastly. The mobile robot can follow a moving human in dynamic indoor environments according to this cascaded detection method with the simple following algorithm described in the next section.

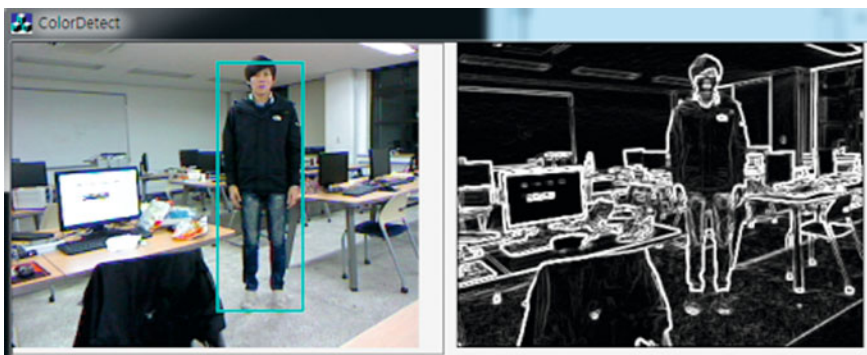


Fig. 2 Result from the HOG based human detector



Fig. 3 Results from the two different face detectors

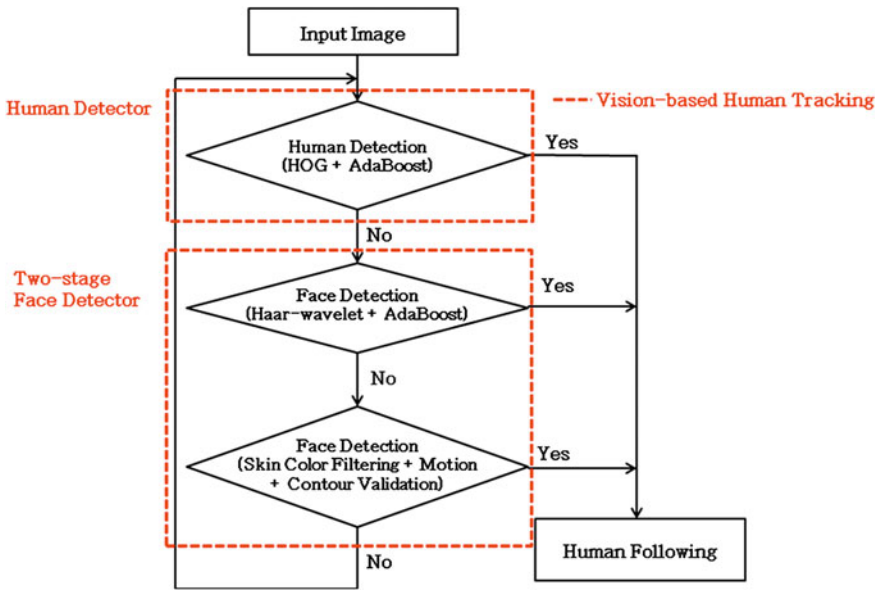


Fig. 4 Flow chart of vision-based human tracker based on human and face detection

3.2 Human Following of Mobile Robot

In this study, we implement a simple human following algorithm where a mobile robot traces a human path autonomously based on the 2D position of a human target from a vision-based human tracker. If the human target is detected by the vision-based human tracker, we need to decide the robot movement according to the horizontal displacement of the robot and the human target. Usually a camera is installed at the front of the mobile robot, and we can hence assume that the center of the horizontal axis of the image plane is the center of the robot. Therefore, the horizontal displacement of the robot and the human can be simplified to the

horizontal position of the 2D position of the detected human target, and we can easily convert this horizontal displacement to the target heading angle.

If the heading angle is within a given range defined as the angle threshold, the mobile robot will move forward, and if the heading angle is beyond the threshold, the robot will turn left or right according to the sign of the heading angle. If the human target is not detected during vision-based tracking in the short term, the mobile will keep the previous movement, and finally if the target is lost in the long term, the robot will rotate or step forward randomly to find the target. The human following algorithm of the mobile robot is shown below.

Human Following Algorithm of Mobile Robot

```

While Human Following is activated
  If Human tracking success
    if (Heading Angle >= Angle Threshold
      && Heading Angle < Angle Threshold)
      Move Forward;
    else if (heading angle <= - Angle Threshold)
      Left Turn;
    else Right Turn;
  Else if Human tracking fail in short term
    Keep Previous Movement;
  Else if Human tracking fail in long term
    Random Turn and Step Forward;
EndWhile

```

4 Experimental Results

For the experiment, we developed our own mobile robot. The robot has two differential driving wheels and two auxiliary caster wheels. It also has two PSD sensors and five ultrasonic sensors located on its front that can detect ranges for obstacle avoidance. Table 1 shows the specifications of the mobile robot.

Also, the robot has a webcam for a vision-based human tracker. The camera is mounted at the front of the robot. Figure 5 shows photographs of the human following experiment.

Figure 6 shows experimental results of the proposed vision-based human following scheme. In this figure, ■ represents the trajectory of human movement and

Table 1 Specifications of mobile robot

Item	Specification
Body dimensions	W550 x D900 x H1100 [mm]
Body weight	30 kg
Driving way	2 Wheel Differential Drive
Driving speed	Max. 1.5 m/sec



Fig. 5 Human following experiment

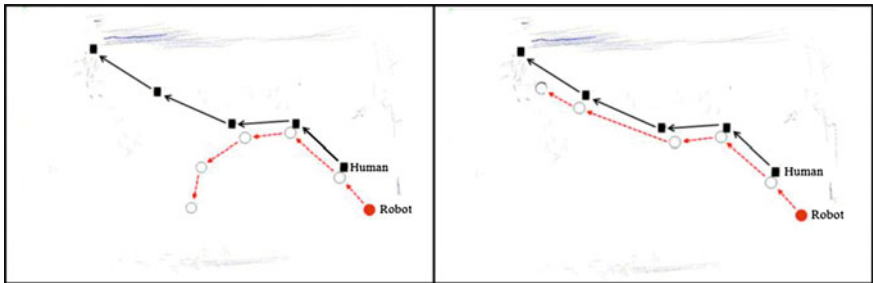


Fig. 6 Experiment for human tracking

○ represents the trajectory of the mobile robot. The left side of Fig. 6 shows the experimental result of the human following using human detection only and the right side of Fig. 6 shows the experimental result using the proposed tracker using face and human detection. When we use human detection only, the robot can easily fail to detect the human target. In contrast, when we use the proposed tracker, the robot can follow the human stably.

5 Conclusion

In this paper, we present a method of vision-based human following for a mobile robot using cascaded human and face detectors. The proposed vision-based tracker detects a human using HOG and AdaBoost. It also has a two-stage face detector, which uses a Haar-wavelet based AdaBoost method and skin color filtering with motion and validation of the contour shape of a face. If the tracker does not find a

human, it tries to find a face in captured images successively to enhance the human detection rate.

Through the experiment, we confirm that the mobile robot can follow a human successfully in a complex indoor environment using the proposed vision-based tracker and simple human following algorithm. For further work, we are planning to extend this method so that it can perform human following in an outdoor environment. Also, we will continue to improve the performance of the vision-based tracker and human following algorithm for the purpose of an autonomous mobile robot carrying luggage at airports and hotels as a public service robot.

Acknowledgments This work was supported by the Basic Science Research Program through the National Research Foundation of Korea (NRF) funded by the Ministry of Education, Science and Technology (MEST) (2011-0013776).

References

1. Schlegel C, Illmann J, Jaberg H, Schuster M (1998) Vision based person tracking with a mobile robot. In: Ninth British machine vision conference, BMVC '98, Southampton, pp 418–427
2. Viola Paul A, Jones Michael J (2001) Robust real-time face detection. *ICCV* 2:747
3. Senior A (2002) Tracking people with probabilistic appearance models, *IEEE*. In: International workshop on performance evaluation of tracking and surveillance, pp 48–55
4. Papageorgiou C, Oren M, Poggio T (1998) A general framework for object detection. In: International conference on computer vision, pp 555–562
5. Barron JI, Fleet DJ, Beauchemin SS (1992) Performance of optical flow techniques, *IEEE*. In: conference on computer Vision and pattern recognition, pp 236–242
6. Dalal N, Triggs B, (2005) Histograms of oriented gradients for human detection, *IEEE*. In: *CVPR*, vol 1, pp 886–893
7. Laptev I (2006) Improvements of object detection using boosted histograms, In: *Proceeding of British machine vision conference*, Edinburgh, UK
8. Viola P, Jones M (2001) Rapid object detection using a boosted cascade of simple features, In: *proceeding of IEEE. CVPR*, Kauai, Hawaii, pp 12–14
9. Jang Heejun, Ko Hyesun, Choi Youngwoo, Han Youngjoon, Hahn Hernsoo (2005) A new face tracking method using block difference image and kalman filter in moving picture. *J Fuzzy Log Intell Syst* 15(2):163–172

Precise Location Estimation Method Using a Localization Sensor for Goal Point Tracking of an Indoor Mobile Robot

Se-Jun Park and Tae-Kyu Yang

Abstract Simultaneous localization is the most important research topic in mobile robotics. In this study, we propose a precise location estimation algorithm for a mobile robot based on a localization sensor and artificial landmarks in the ceiling in order to achieve point tracking. The proposed technique estimates the location of landmarks in the ceiling, generates the global ceiling and the global ceiling map for landmarks, and estimates the location of a mobile robot based on the ceiling map. The localization algorithm effectively removes incorrectly recognized landmarks using a histogram. In addition, the algorithm removes the measurement noise based on a Kalman filter. In order to evaluate the performance of the proposed precise localization technique, we performed several experiments using a mobile robot. The experimental results demonstrated the feasibility of the proposed localization algorithm.

Keywords Location estimation · Localization sensor · Mobile robot · Goal point tracking

1 Introduction

Fundamental studies on mobile robotics can be divided into five main research topics: obstacle avoidance, self localization, mapping, path maintenance and comeback [1–4]. The mobile robot should steadily recognize its current location to perform duties. The main line of research on location-awareness is self-recognition

S.-J. Park · T.-K. Yang (✉)

Department of Intelligent Robot Engineering, Mokwon University,
88 Doanbuk-ro, Seo-gu, Daejeon, Republic of Korea
e-mail: tkyang@mokwon.ac.kr

S.-J. Park
e-mail: sjpark@mokwon.ac.kr

of location coordinates and obstacles through odometer information obtained from an encoder, infrared and ultrasonic sensors [5, 6]. However, it is difficult to recognize global coordinates due to the low precision and poor accuracy of odometer information. Therefore, a method for calculation of the exact global coordinates is required to achieve efficient mapping and route recognition. In some cases, determination of a relative position rather than an absolute position is important.

Sensor-based methods for recognition of absolute position include use of an ultrasonic active beacon, RFID tags and near-infrared camera [7]. However, the methods cannot guarantee the absolute error because they are sensitive to environment changes, and they also present installation difficulties. Several methods to take advantage of a robot's global localization sensor have been introduced [8, 9]. The methods employ a system for self-recognition of robot location using artificial landmarks and near-infrared emitters. The robot localization method using landmarks on the ceiling recognizes incorrect landmarks from the dead-zone and overlap-zone in the landmark array process. Therefore, an incorrect landmark produces a large number of position errors in the ceiling image processing procedure. In addition, position measurement errors occur by shaking or vibration while a robot navigates.

To solve these problems, this paper removes position errors by eliminating the uncertain landmarks using a threshold in the histogram. We also propose a precise location estimation algorithm to remove the measurement noise using a Kalman filter.

2 Ceiling Artificial Landmark Localization

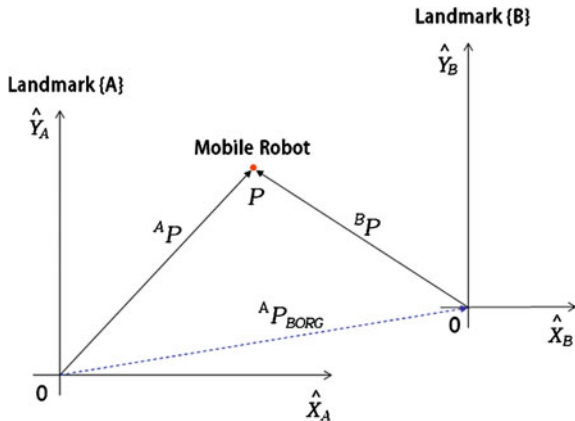
To estimate location of landmarks and explain how to create a ceiling map, we make some assumptions and define the environment. First, we assume that the ceiling attached landmark is a flat surface. Second, we assume that the robot's moving ground is a flat surface. Finally, we assume that the robot estimates its absolute position in relation to the corresponding landmark coordinate system through recognition of one or two landmarks from a ceiling image in real-time. Figure 1 shows position estimation of landmarks.

In Fig. 1, the coordinate system $\{B\}$ has a same compass as the coordinate system $\{A\}$ and has a different translation. The position of the mobile robot is defined as vector ${}^A P$ in coordinate system $\{A\}$ and vector ${}^B P$ in coordinate system $\{B\}$. Because the two vectors are defined by the coordinate system with the same orientation, a translation vector ${}^A P_{BORG}$ can be represented as given in Eq. (1).

$${}^A P_{BORG} = {}^A P - {}^B P \quad (1)$$

The robot recognizes the landmark during navigation. In such a case, because the robot recognizes the same landmark several times, we can calculate a more accurate origin coordinate through an average value ($Mark_{local}$). The average value ($Mark_{local}$) is obtained by Eq. (2).

Fig. 1 Position estimation of landmarks



$$Mark_{local} = \frac{1}{d} \sum_{i=1}^d A_P_{BORG} \tag{2}$$

Here, d is the number of continuous landmarks. The ceiling global map can be expressed as Eq. (3). In Eq. (3), m is the number of ceiling landmarks.

$$Mark_{world}(m) = \sum_{i=1}^m \sum_{k=1}^i Mark_{local}(i). \tag{3}$$

3 Precise Location Estimation of Mobile Robot for Goal Point Tracking

3.1 Error Removal of an Incorrectly Recognized Landmark

The mobile robot recognizes landmarks through image processing after attaching landmarks under the ceiling at constant intervals. The landmark recognition rate is low despite the landmark arrangement and inaccuracy due to image processing problems. However, if the landmark is recognized incorrectly, we cannot obtain the robot’s position.

Therefore, we propose a method to remove position errors caused by incorrectly recognized landmarks. The robot estimates its position by recognizing the nearest ceiling landmark while it is navigates. At this time, incorrect recognition of landmarks occurs by dead-zone or overlap-zone navigation, unexpected turns and inaccurate image processing. The occurrence probability ($p(r_k)$) for continuous landmarks (r_k) is defined as Eq. (4).

$$p(r_k) = \frac{n_k}{n} \quad k = 1, 2, 3, \dots, L \tag{4}$$

where, n is the total number of landmarks, n_k is the number of k th landmarks and L is the number of continuous landmarks. Therefore, we can remove the position error caused by incorrectly recognized landmarks by removing landmarks (r_k) below the threshold, as given in Eq. (5).

$$p(r_k) \geq \text{Threshold} \quad k = 1, 2, 3, \dots, L. \quad (5)$$

3.2 Measurement Error Removal by Kalman Filter

Position measurement error can occur by shaking or vibration despite removal of the position error caused by incorrectly recognized landmarks while the robot is navigating. Thus, we estimate the state variable value of the dynamic system as input with incoming noise through the sensor using a Kalman filter [10], and estimate the precise position of the mobile robot. We require the system model, given as Eq. (6) for system modeling using a Kalman filter.

$$\begin{aligned} x_{k+1} &= Ax_k + Bu_k \\ z_k &= Hx_k + v_k \end{aligned} \quad (6)$$

Here, $A = 1$, $B = 0.2$, $H = 1$, $Q = 0$, $R = 4$. Equation (6) can then be expressed as Eq. (7).

$$\begin{aligned} x_{k+1} &= x_k + 0.2u_k \\ z_k &= x_k + v_k \end{aligned} \quad (7)$$

In Eq. (7), x_{k+1} represents the present position of the mobile robot. z_k represents the measured position value of the mobile robot including noise ($v_k = N(0, 2^2)$).

4 Experimental Results

In order to evaluate the location estimation performance of the mobile robot, we built an experiment environment by attaching 12 landmarks on a ceiling (7.45 × 6.07 m × 2.4 m). Table 1 shows the main specifications of StarGazerTM.

As in Table 1, StarGazerTM recognizes one or two landmarks and recognizes the absolute position of the robot (10 times/sec). Table 2 shows the actual values

Table 1 Main specifications of StarGazerTM

Item	Specification
Product	HAGISONIC CO., LTD.
Model	StarGazer TM (HSG-A-02)
Landmark recognition	Max. two
Measurable time	10 times/sec

Table 2 Landmark location for reference coordinate

Landmark ID	Actual		Estimation		Distance error (m)
	X (m)	Y (m)	X (m)	Y (m)	
544	0.0	0.0	0.0	0.0	0.0
64	0.0	1.825	-0.0153	1.9059	0.0823
50	0.0	3.645	-0.0090	3.7420	0.0974
576	1.820	3.635	1.8440	3.7689	0.1360
2	1.820	1.820	1.8343	1.8809	0.0626
18	1.820	0.0	1.8199	0.0188	0.0188
80	3.640	0.0	3.6839	0.0750	0.0869
562	3.640	1.815	3.6719	1.9468	0.1356
112	3.640	3.640	3.6844	3.8100	0.1757
578	5.460	3.645	5.5932	3.7748	0.1860
546	5.460	1.825	5.5659	1.8644	0.1130
66	5.460	0.0	5.5571	-0.0113	0.0978

and estimated values of the ceiling landmarks and the distance error for each landmark ID. The average distance error is relatively low at less than 10 cm (0.0993 m).

Figure 2 (left) shows the measured position of the mobile robot, indicating that large location error occurs by incorrectly recognized landmarks. Also, Fig. 2 (right) shows the position of the mobile robot using a threshold (3) in the histogram. However, measurement noise remains due to shaking or vibration of the mobile robot while the robot is navigating. Therefore, we removed measurement noise using a Kalman filter as seen in Fig. 3. In Fig. 3, the noise of locations X and Y has a relatively large value of $-0.27 \sim 0.27$ m because large measurement error occurs by shaking when the robot is turning.

Table 3 shows the average and standard deviation of the position noise and distance noise of the mobile robot. Therefore, this paper obtains more accurate position estimate values by removing distance noise (approximately 0.08 m) using the proposed algorithm.

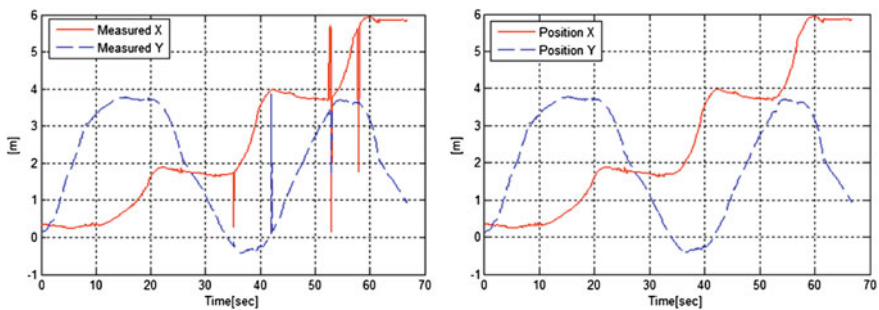


Fig. 2 Measured position of mobile robot (*left* incorrectly recognized ID, *right* processing of incorrectly recognized ID)

Fig. 3 Position errors of mobile robot

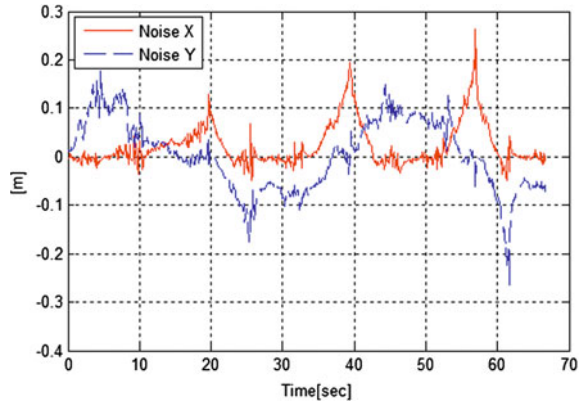


Figure 4 shows experimental results of goal point autonomous navigation. Here, the red circle shows the starting point and the goal point, and the black rectangle shows obstacles used in the experiment. In Fig. 4, the mobile robot navigates toward the goal point, avoiding obstacles relatively accurately through precise position estimation.

Table 3 Position and distance noise of mobile robot

	X (m)	X (m)	Distance (m)
Average	0.0301	0.0599	0.0794
Standard deviation	0.0490	0.0727	0.0876

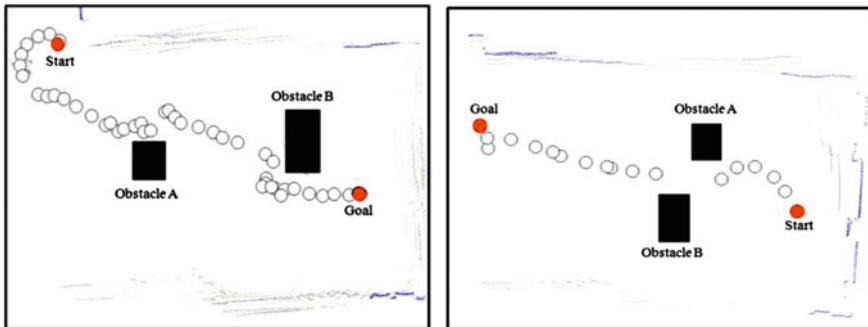


Fig. 4 Experiment for goal point tracking

5 Conclusion

In this paper, we estimated the position of ceiling landmark for precise position estimation of a mobile robot, and built a global map of ceiling landmarks. We removed large error caused by incorrectly recognized landmarks using a threshold in a histogram on the basis of the global map. Also, we proposed a precise location estimation algorithm to remove the measurement noise using a Kalman filter.

In experiments, we created a global map of a ceiling and the average distance error between actual landmarks and estimation landmarks was less than 0.1 m. We also removed large error caused by incorrectly recognized landmarks using the proposed histogram based method. In our measurement, the significant noise occurred when the robot was turning, with an average value of approximately 0.08 m. We removed the distance noise through robot position estimation using the proposed algorithm in this paper, and obtained a precise location estimation value. Also, we observed that the mobile robot navigates toward the goal point accurately through precise position estimation while avoiding obstacles.

References

1. Karlsson N, Bernardo ED, Ostrowski J, Goncalves L, Pirjanian P, Munich ME (2005) The vSLAM algorithm for robust localization and mapping. In: Proceedings of the IEEE Interference Conference on Robotics and Automation, pp 24–29
2. Montemerlo M (2003) Fast SLAM: A factored solution to the simultaneous localization and mapping problem with unknown data association. PhD thesis, Robotics Institute, Carnegie Mellon University
3. Dissanayake M, Newman P, Clark S, Durrant-Whyte H, Csorba M (2001) A solution to the simultaneous localization and map building (SLAM) problem. *IEEE Trans Robotics Autom* 17(3):229–241
4. Thrun S, Burgard W, Fox D (2005) Probabilistic robotics. MIT Press, Cambridge
5. Borenstein J, Feng L (1996) Measurement and correction of systematic odometry errors in mobile robots. *IEEE Trans Robotics Autom* 12(6):869–880
6. Pahlavan K, Li X, Makela J (2002) Indoor geolocation science and technology. *IEEE Commun Mag* 40(2):112–118
7. Liu J, Po Y (2007) A localization algorithm for mobile robots in RFID system. In: WiCon 2007 international conference on wireless communications, networking and mobile computing, pp 2109–2112
8. Lee S, Song J-B (2007) Mobile robot localization using infrared light-reflecting landmark. In: ICCAS '07 international conference on control, automation and system, pp 674–677
9. Wang H, Yu H, Kong L (2007) Ceiling light landmarks based localization and motion control for a mobile robot. *IEEE International Conference on Networking, Sensing and Control*, MonA01, pp 285–290
10. Welch G, Bishop G (2006) An introduction to the Kalman filter, UNC-Chapel Hill, TR 95-041

Motion Capture Based Dual Arm Control of a Humanoid Robot Using Kinect

Kyo-Min Koo, Young Joon Kim and Yong-Ho Seo

Abstract This paper proposes a Motion Capture Based Dual Arm Control Method for a humanoid robot using a Microsoft depth camera called Kinect. A system that controls a humanoid robot by imitating a human's motion can be applied to various areas of tele-robotic applications due to its intuitive operation and convenience. Therefore, we developed a remote dual arm control system to process data captured from a depth camera and to control the joint angles of motors of dual arms of a humanoid robot using a human gesture based non-contacting motion capture method. In experiments, we successfully demonstrated dual arm control of a robot using the proposed motion capture based method using Kinect.

Keywords Motion capture · Robot arm control · Humanoid robot · Depth camera

1 Introduction

With the development of robot-related technologies, the use of robots has been widely extended to healthcare, entertainment, and industries. In addition, studies on Human-Robot Interaction (HRI) technology that enable robots and humans to communicate and cooperate are actively being carried out in the field of robotics research. A system to control robots more conveniently and intuitively for various areas of application and the resulting various demands of users is thus required [1]. However, the current robot control methods are basically limited in their manipulation methods, and suffer from resultant inconveniences; e.g., users have to learn new interfaces for operating robots.

K.-M. Koo · Y. J. Kim · Y.-H. Seo (✉)
Department of Intelligent Robot Engineering, Mokwon University,
Mokwon Gil 21, Seo-gu, Daejeon, Republic of Korea
e-mail: yhseo@mokwon.ac.kr

Thus, we propose a control method for existing complex robots and develop a robot remote dual arm control system employing the user's arm gestures as an interface. As a way to improve the existing control methods, a contactless motion capture method is proposed for convenient and intuitive control by the user's physical actions instead of a separate controller.

2 Humanoid Dual Arm Robot Control System

A dual arm control system for a humanoid robot is configured as shown in Fig. 1. The system carries out joint value extraction from user skeleton data captured from a Kinect. The system then controls the motors of the dual arms of a humanoid robot in a Windows application. The processing flow of flow of the proposed dual arm control system is shown in Fig. 2.

In this research, we used the Microsoft depth camera Kinect for XBOX 360 as a camera and a depth sensor of a humanoid robot as shown in Fig. 3. Table 1 shows its specifications [2].

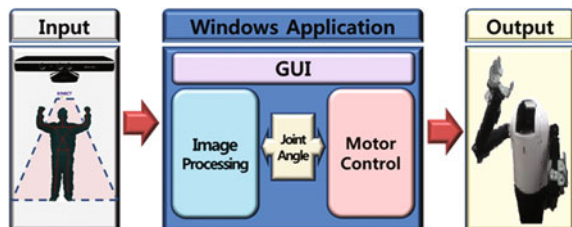
We used a humanoid robot called Mokwoni, developed by the Department of Intelligent Robot Engineering in Mokwon University, as a test bed to apply and test the proposed method [3].

Figure 3 shows the appearance of the humanoid robot Mokwoni (left) and its arm DOF alignment. The robot has two arms that have 7 servo motors each from shoulders to grippers. Thus, each arm of the humanoid robot has 7 degrees of freedom in total including the gripper. We used DYNAMIXEL EX-106 + , RX-64 and AX-12A from Robotis to develop servo motors of the humanoid robot's arms [4]. Table 2 shows the specifications of the humanoid robot.

3 Development of Application Software for Dual Arm Control of a Humanoid Robot

We developed application software to process the depth data captured from Kinect and to control the robot's joint motor. The software consists of a window form monitor to set each joint angle value of the robot arm and a window that displays

Fig. 1 Configuration of a dual arm control system for a humanoid robot



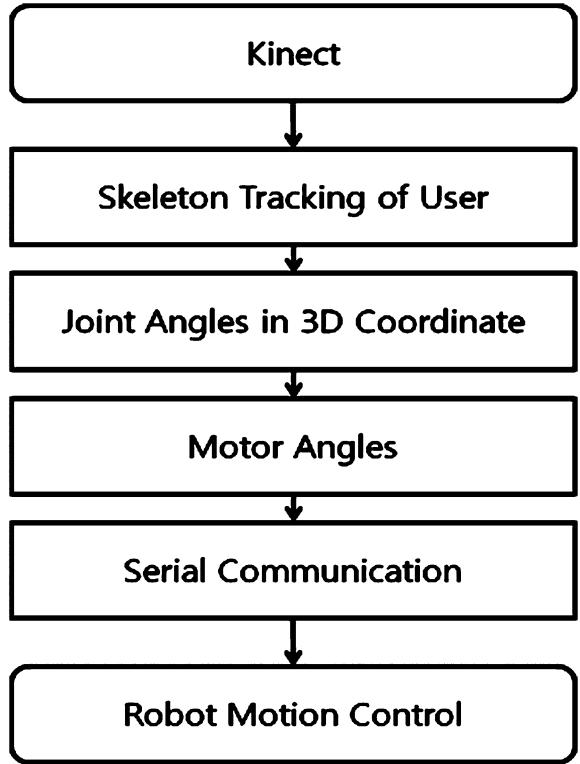


Fig. 2 Processing flow of a dual arm control system for a humanoid robot

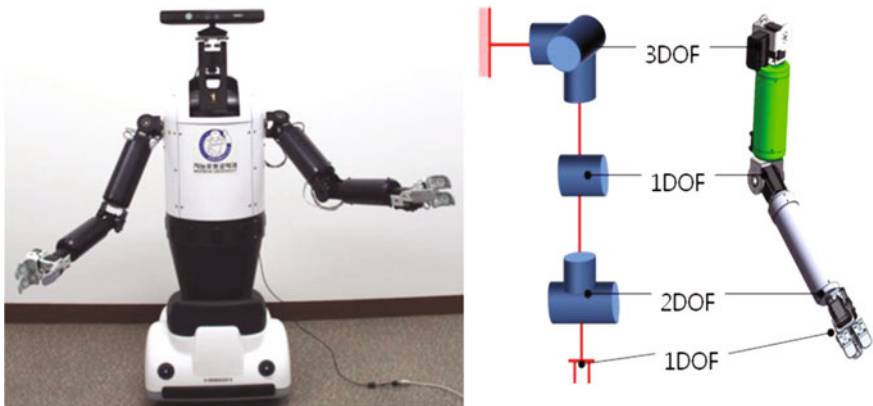


Fig. 3 Appearance of a humanoid robot, Mokwoni (left), and its Arm DOF alignment (right)

Table 1 Specifications of Microsoft Kinect for XBOX 360

Type	Specifications
Sensor	Color and depth sensor Microphone array
Viewing angle	43° vertical by 57° horizontal field of view
Frame rate	30 frames per second
Default resolution	Depth: VGA (640 × 480) Color: VGA (640 × 480)
Skeletal Tracking	Tracks 20 joints per active player

Table 2 Specifications of a humanoid robot, Mokwoni

Type	Spec
Size	Height: 120 cm Width: 80 cm
Weight	30 kg
Degree of freedom	Head 1DOF Arm 7 DOF (6 DOF arm with 1 DOF gripper) Waist 1 DOF Mobile 2DOF
Servo Motors at Arm	DYNAMIXEL EX-106+ Minimum control angle: About 0.06° × 4,096 Joint operating range: 251° Communication method: RS-485 DYNAMIXEL RX-64 HN05-N1 Type Minimum control angle: About 0.29° × 1,024 Joint operating range: 300° Communication method: RS-485
Servo Motors at Gripper and Head	DYNAMIXEL AX-12A Minimum control angle: About 0.29° × 1,024 Joint operating range: 300° Communication method: RS-232 TTL
Servo Motors at Mobile and Waist	DC servo motor with Encoder

the current angle of the motor based on a.NET Framework 4.0, as shown in Fig. 4. It was developed using Microsoft Visual Studio 2010 and runs on a Windows PC.

At the upper left corner in Fig. 4, the Kinect sensor connected to the PC is found and marked and at the bottom, an interface is made to select the user image data value to be output with a radio button. On the right side of Fig. 4, depth data and skeleton data captured from Kinect are displayed in one screen.

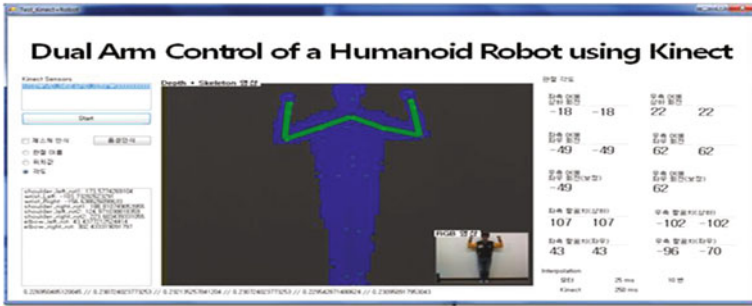


Fig. 4 Windows application software for dual arm control of a humanoid robot

3.1 Joint Value on 3-D Spatial Coordinates

To implement movement of the robot arms in real three-dimensional space, a program to find the angle value in the 3-D spatial coordinates of the user’s arm should be implemented. If the positional values of the joint point are obtained through Kinect SDK, the values on the three-dimensional coordinates can be obtained, based on which the angle values should be calculated. For this calculation, the joint vector of the relevant position is projected to a plane, as shown in the left side of Fig. 5; then, using Eq. (1), through the inner product of the two vectors, the angle between the two is found [5].

For the shoulders, 2 degrees of freedom should be extracted, 2 planes in pivot directions are respectively set, and the projected angle between the vector and the joint vector is calculated.

$$\vec{a} \cdot \vec{b} = |\vec{a}| |\vec{b}| \cos \theta$$

$$\theta = \cos^{-1} \left(\frac{|\vec{a}| |\vec{b}|}{(\vec{a} \cdot \vec{b})} \right) \tag{1}$$

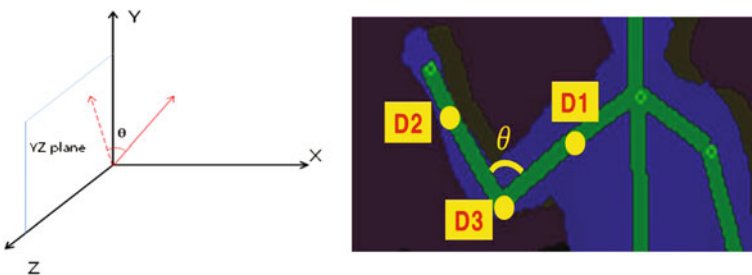


Fig. 5 Script for Definition of Environment (left) and 3D Modeling Mesh (right)

For the elbow angle, the positions of joint points among the shoulder, elbow, and wrist are obtained as D1, D2, D3 in the right side of Fig. 5 through Kinect SDK, and the angle θ is found using Eq. (2).

$$\theta = \cos^{-1}\left(\frac{a^2 + b^2 - c^2}{2ab}\right)$$

$$a = \sqrt{(D2_x - D1_x)^2 + (D2_y - D1_y)^2}$$

$$b = \sqrt{(D3_x - D2_x)^2 + (D3_y - D2_y)^2}$$

$$c = \sqrt{(D1_x - D3_x)^2 + (D1_y - D3_y)^2}$$
(2)

3.2 Motor Control Using Cosine Interpolation

For smooth control of the robot motion, a unit interval should be given to send motor angles periodically. The target angle is then divided into angles between the initial angle and target angle by using interpolation technique [6].

In this study, we set 20 ms as a unit interval for interpolation. We also use cosine interpolation to get the smooth trajectory of each joint angle. As seen in Fig. 6, when the motor turns from the initial angle to the target angle, using Eq. (3), a point connecting the two angle points smoothly is generated using cosine function. We can get the intermediate angle at any interval of x between the initial angle and target angle by simply applying Eq. (4) [7].

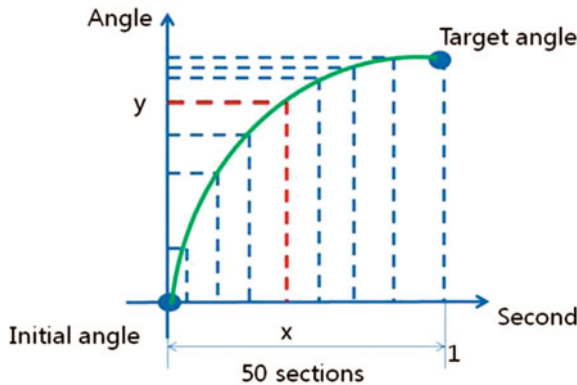


Fig. 6 Example of cosine interpolation



Fig. 7 Experimental environment for the proposed Motion Capture Based Dual Arm Control System

$$\text{tempInterp} = \frac{1 - \cos(\text{interval of } x * \pi)}{2} \tag{3}$$

$$y = \text{initial value} * (1 - \text{tempInter}) + \text{target value} * \text{tempInterp} \tag{4}$$

4 Experimental Results

The rotational angle for each joint of axes X, Y, Z of the user’s arm is set to the angle of the motor corresponding to the human joint, and in the Windows application program developed in this study, a system that controls the motor was implemented in RS-485 and RS-232 serial communication.



Fig. 8 Test using humanoid robot dual arms

Figure 7 shows the experimental environment for the proposed motion capture based dual arm control system with the humanoid robot.

From the results of the test, the angle value of the user joint was calculated and displayed with the positional values of each joint point of the user read from Kinect through the Window application program developed in this study, and using cosine interpolation, each joint of the robot was controlled and the humanoid robot dual arm was successfully controlled, as seen in Fig. 8.

5 Conclusion

This study used the three-dimensional camera feature of a depth camera, Kinect, to implement a contactless motion capture based humanoid robot dual arm control technology and its usefulness was verified through tests.

Realistically, multiple constraints follow the implementation of a robot arm that moves in the same manner as that of a human by extracting the three-dimensional human joint value. The robot's arm and the user's arm have different length, and there is a limit to produce the same position of the motor, that is, a robot joint, in correspondence to human motion. Thus, for more precise control, studies on feedback of the robot joint angle value using kinematics and the resulting posture correction have been performed, and research on the human arm and the hardware design structure of robot arms should follow. Therefore, future studies should carry out research on methods of adjusting postures by supplementing this problem. Nonetheless, this study is significant in that it proposes a contactless motion capture based humanoid robot dual arm control technology using Kinect and has demonstrated its usefulness.

The three-dimensional camera motion capture technique proposed in this study can be applied to various areas such as medical manipulator robot, entertainment including gaming, remote control, etc., and will help users control robots conveniently and intuitively by becoming controllers themselves instead of employing controllers with complex functions.

Acknowledgments This work was supported by the Basic Science Research Program through the National Research Foundation of Korea (NRF) funded by the Ministry of Education, Science and Technology (MEST) (2011-0013776). This work was also supported by the NAP (National Agenda Project) of the Korea Research Council of Fundamental Science & Technology.

References

1. Goodrich MA, Schultz AC (2007) Human-Robot Interaction: A Survey. *Foundations and trends in human-computer interaction* 1(3):203–275
2. Microsoft Kinect for XBOX 360, <http://msdn.microsoft.com>
3. Dept. of Intelligent Robot Eng., Mokwon Univ., <http://robot.mokwon.ac.kr>

4. ROBOTIS DYNAMIXEL, <http://www.robotis.com>
5. Seo Y, Jeong I, Yang H (2007) Motion capture-based wearable interaction system and its application to a humanoid robot. *AMIO. Adv Robot* 21(15):1725–1741
6. Kim C, Kim S, Ra S, You B (2007) Regenerating human-like arm motions of humanoid robots for a movable object. In: *SICE Annual Conference* pp 1081–1086
7. Yang H, Seo Y, Chae Y, Jeong I, Kang W, Lee J (2006) Design and development of a biped humanoid robot, AMI2, for Social Interaction with Humans. In: *IEEE-RAS International conference on humanoid robots*, pp 352–357

Scalable Building Facade Recognition and Tracking for Outdoor Augmented Reality

Suwon Lee, Yong-Ho Seo and Hyun S. Yang

Abstract This paper proposes a scalable building facade recognition and tracking system for outdoor augmented reality enabling real time augmentation of various information onto the facade. The system is composed of three modules: recognition and tracking module, server-client module and GPS module. In the recognition and tracking module, Generic Random Forest was used for real time recognition and three-dimensional pose estimation of facades. For scalable recognition, global region is divided into multiple local regions and then, same regional buildings are trained separately into a forest. In the server-client module, client maintains own travel map in order to choose proper forest by employing GPS sensor, and server transmits a new forest when client detects never visited regions. This makes our system scalable and also expansible to new regions.

Keywords Outdoor augmented reality · Building facade recognition · Generic random forest

S. Lee · H. S. Yang
Department of Computer Science, Korea Advanced Institute of Science and Technology,
Daejeon, Republic of Korea
e-mail: swlee@kaist.ac.kr

H. S. Yang
e-mail: hsyang@kaist.ac.kr

Y.-H. Seo (✉)
Department of Intelligent Robot Engineering, Mokwon University, Mokwon Gil 21, Seo-gu,
Daejeon, Republic of Korea
e-mail: yhseo@mokwon.ac.kr

1 Introduction

Augmented reality (AR) is a kind of human–computer interaction that enhances our perception and helps us to see, hear, and feel our environments by providing local virtuality [1, 2]. AR technology gives us a better quality of education, directions to find our way, instructions in an assembly, and new experiences or enjoyments that we otherwise could not [3].

Recently, there has been a lot of augmented reality systems developed for outdoor activities ranging from pure sensor based, to pure vision based, to hybrid approaches. Traditional systems rely on location based sensors like GPS for position measurements with the assistance of magnetic compasses for orientation estimations [4–8]. While GPS provides reliable accuracy in open spaces, the accuracy deteriorates significantly in urban environments since there are many other signals in urban environments which jam the transmissions of GPS signal and also reflection from buildings is one of the reasons. As a result, the performance of the position measurements depends severely on the location. Pure vision based approaches such as [9–12] perform image based object recognition to localize and track the users in outdoor environments. The user context in these approaches is acquired by querying the image to database of labeled objects. Hybrid approaches fuse data from different sensors such as camera, GPS and gyroscopes [13–15]. In these hybrid approaches, successive approximation of GPS data and edge tracking information from the three-dimensional geo referenced graphical models are combined for better localization and robustness against environmental influences. In this way, most of them are focused on better accuracy but not on scalability issue.

In this paper, we propose a scalable building facade recognition and tracking system for outdoor augmented reality that can augment various information onto the facade in real time. In our system, global region is divided into multiple local regions and each local regional buildings train a Generic Random Forest separately. Each forest performs real time recognition and three-dimensional pose estimation of facades in own region. GPS sensor is employed for choosing proper forest in order to limit the recognition scope of target buildings, and server transmits a new forest to a client when new local region is detected. As a result, our system becomes scalable and expandable.

The rest of the paper is organized as follows. In [Sect. 2](#), we first describe recognition and tracking process. We then present scalable model in [Sect. 3](#). [Section 4](#) gives the experimental results. Finally, we conclude with a brief summary and discussion in [Sect. 5](#).

2 Recognition and Tracking

In this section, we describe recognition and tracking module which can recognize and track multiple building facades in real time. In this module, recognition and tracking are performed repeatedly for an input frame as shown in [Fig. 1](#).

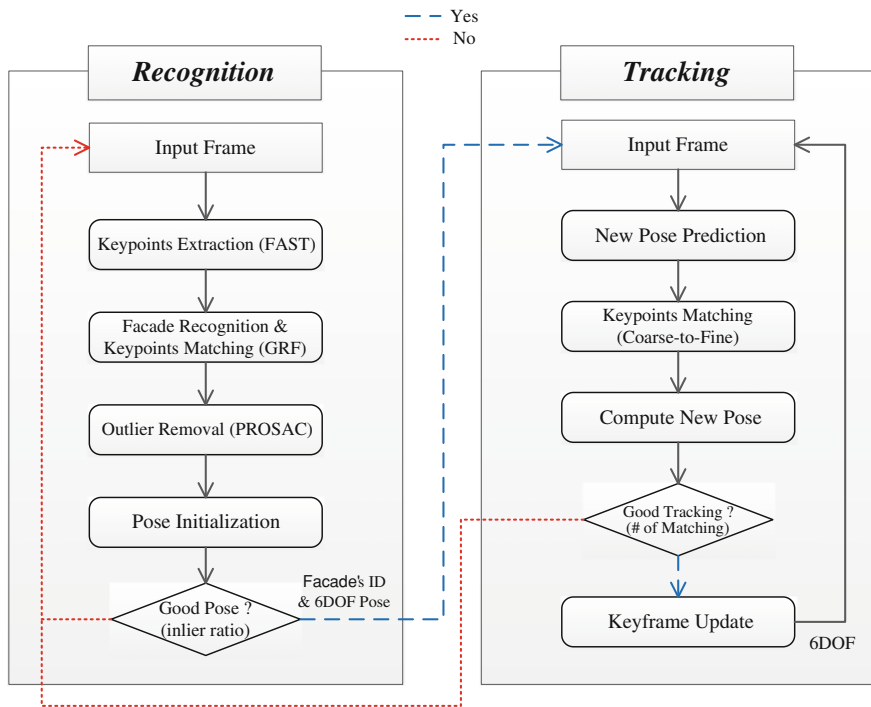


Fig. 1 Recognition and tracking module

Initially, the recognition process is performed for every frame captured by the camera. For real time multiple building facades recognition with their three-dimensional pose estimation, we adopted Generic Random Forest (GRF) [16], designed to be capable of simultaneous object recognition and keypoints matching through one pass over the original Random Forest [17]. As shown in Fig. 2, a GRF consists of N_T random trees, and each tree performs D binary tests comparing the intensities of two random pixel locations of the input image patch surrounding a keypoint. Through D binary tests, an image patch reaches a leaf node among 2^D leaf nodes. Every leaf node of each tree has $n + 1$ posterior probability distributions: 1 distribution is to decide where the image patch comes from n building facades, and each of the n distributions is for the corresponding building facade's keypoints matching. As a result, the GRF is capable of simultaneously both building facade recognition and its three-dimensional pose estimation by keypoints matching. Every image patch surrounding a keypoint is passed through the GRF and the candidate facade is predicted with matching pairs between current input frame and candidate facade's training image. We used FAST corner detector [18] as a keypoint extractor in our implementation. To calculate its three-dimensional pose from matching pairs, we eliminated outliers by computation of a homography between current input frame and candidate facade's training image using PROSAC [19]. In this way, only inliers are remained and used to calculate the initial three-dimensional pose:

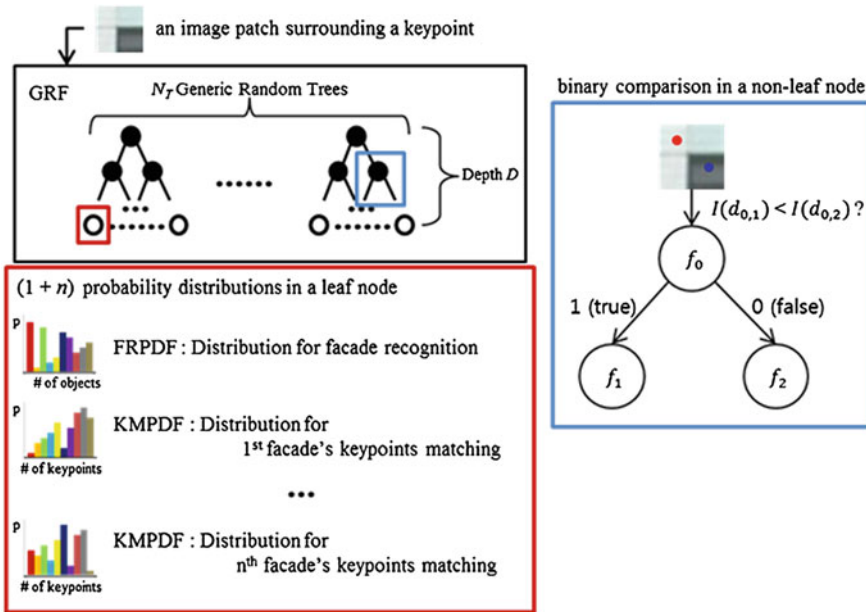


Fig. 2 Generic random forest

six-degree-of-freedom (6 DOF) pose is estimated only if inlier ratio is larger than a threshold; otherwise, the candidate facade is rejected to be recognized [20].

Once the recognition process is done, ID of building facade and its three-dimensional pose are estimated, and then the tracking process is started using training image of the building facade as an initial keyframe. For every frame, tracking process predicts a new pose of the facade using the previous three-dimensional pose and the current camera motions. For the prediction of new pose, coarse-to-fine matching is conducted, and the opportunity to update the keyframe is given only in the case of good tracking. More detailed tracking process is described in [21], and our tracking process is performed in the same manner as the work.

The aforementioned recognition and tracking process is performed in a local region in order to limit the number of target facades to a certain number. This regional restriction is overcome by scalable model in which local region is expanded to global region. The details are described in the following Section.

3 Scalable model

For scalability, we present scalable model in this Section. Key idea of the scalable model is to limit the recognition scope of target buildings. For this, we first divide global region into multiple local regions as shown in Fig. 4, and each local

regional buildings train GRF separately. After that, the system activates proper GRF according to currently visited region using location information measured by GPS in real time. As a result, the recognition scope of target buildings in a moment is reduced to the buildings located in currently visited local region.

As shown in Fig. 3, we designed server-client module for transmission of GRF. Every GRF has $n + 1$ probability distribution and each distribution is stored separately in a independent file, called FRPDF(facade recognition probability distribution file) and KMPDF(keypoints matching probability distribution file) as shown in Fig. 2. In server-client module, the PDF files are transmitted only when the need arises. For FRPDF, client maintains own travel map updated in GPS module in real time. Each region in the travel map has one of the following four states: currently visited region, newly detected region, detected region and never detected region (Fig. 4). In a moment, client activates currently visited regional FRPDF for recognition among detected regional FRPDFs. The detected regions are expanded by accumulating adjacent regions of currently visited region, and the client receives newly detected regional FRPDF from server to prepare next movement. As shown in Fig. 4, the region's states are changed depending on movement of currently visited region (A to B). In this case, client activates B's regional FRPDF for recognition and receives three new FRPDFs from server.

Similarly, KMPDF is updated only when the need arises. After recognition process in recognition and tracking module using the activated FRPDF, a facade ID is predicted as a candidate result and waits for verification by keypoints

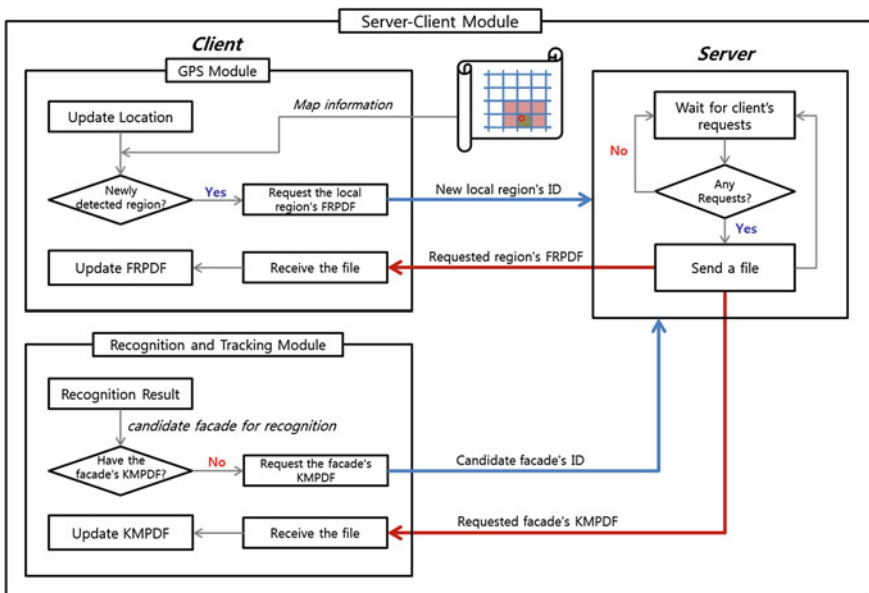


Fig. 3 Scalable model

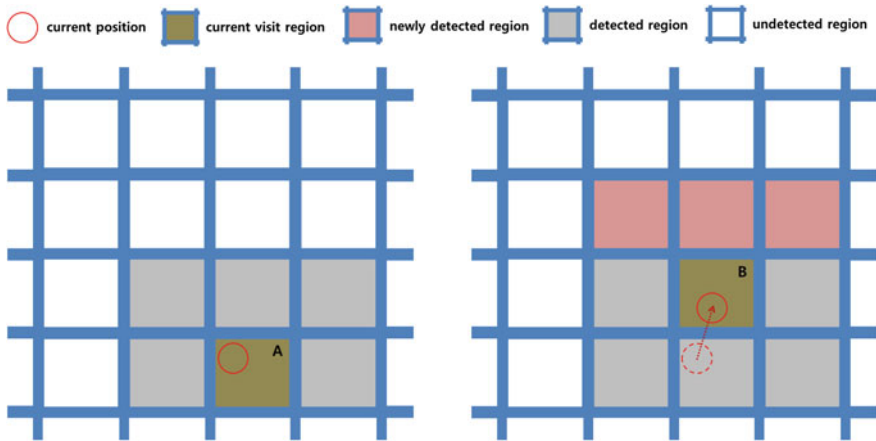


Fig. 4 Travel map

matching using the proper KMPDF, the candidate facade's one. At this point, the module checks whether the KMPDF already exists or not. If the module does not have the KMPDF, the module requests the file to server and wait for transmission; otherwise, performs keypoints matching immediately. All of the aforementioned processes of scalable model are shown in Fig. 3.

4 Experimental Results

For implementation, we used our system on a laptop with a 2.10 GHz dual-core processor and 2 GB of memory, and tested the system in KAIST campus. We divided KAIST into 12 local regions in order that the number of facades in a region is less than 30. Every facade in a local region is used to train a GRF which consists of 50 trees of 10 depths as mentioned in Sect. 2. Figure 5 shows the demonstration of the system. For an input image, 250 keypoints are extracted on a facade using FAST corner detector. At runtime, our system recognizes multiple facades and augments their pose on each of them.

For experiments, we first measured the recognition rate under different tree depth and different number of facades. We randomly synthesized 100 new facades per a facade, and they were used as a query image to measure the average recognition rate. The results are shown in Fig. 6.

We then measured the computational time under different number of tracked facades using four test movies. Each test movie has 500 frames and includes various events with tilts, scale variations, rotation, and fast movement. The result was that the number of tracked facades has entirely effect on tracking process. However, it neither has effect on keypoints extraction nor recognition process as

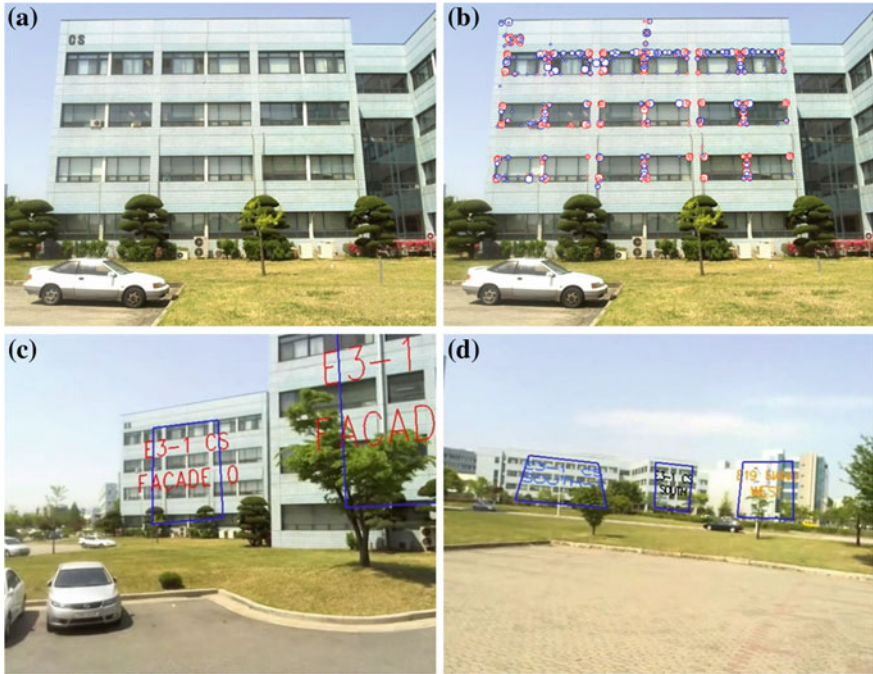


Fig. 5 (a) an input image for train (b) extracted keypoints on a facade (c) multiple facades tracking on same building (d) multiple facades tracking on other buildings

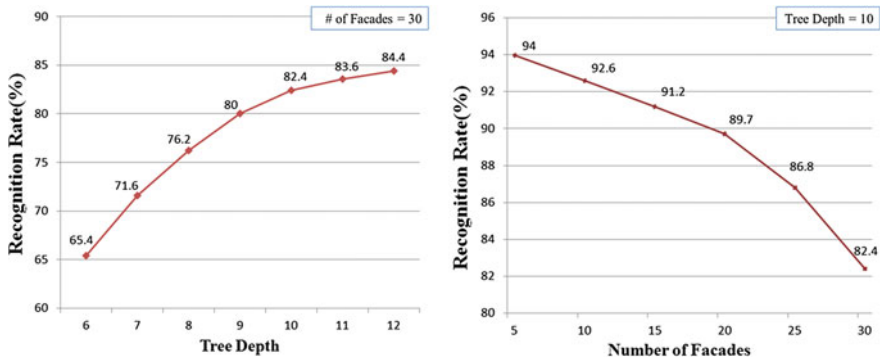


Fig. 6 Recognition rate

shown in Fig. 7. In case of tracking four buildings at once, our system spends 35.12 ms that achieves approximately 30 fps. This result demonstrates that our system is fast enough for frame rate performance.

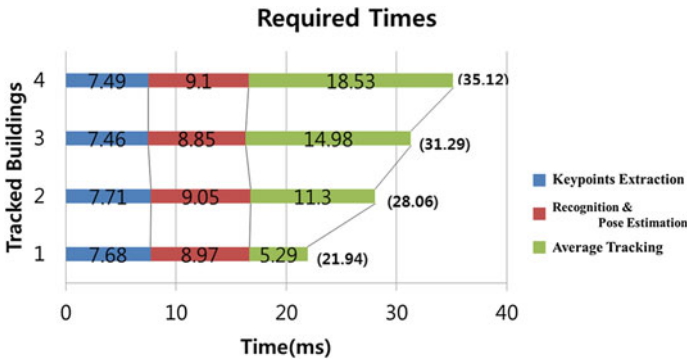


Fig. 7 Computational time

5 Conclusion

In this paper, we presented scalable building facade recognition and tracking methods. For recognition and tracking facades, we adopted GRF, designed for simultaneous object recognition and keypoints matching. By using GRF method, our system was able to recognize and track multiple facades in real time. Through the proposed scalable model, we were able to make our system scalable and expandible. The scalable model is theoretically perfect on the assumption that network and GPS performance are reliable. The scalable model is expected to be applied to other outdoor AR applications which have scalability issue.

However, our recognition and tracking module is vulnerable to various variations caused by both external and internal reasons: occlusion, lighting conditions, weather or season changes and repetitive patterns of facade itself. The main reason is the recognition and tracking process entirely depends on texture based vision algorithm. The problems are very challenging but some trials like sensor fusion or learning techniques may be possible. We have plans to attempt the trials as a future works.

Acknowledgments This work was supported by the IT R&D program of MKE/MCST/IITA, [10039165, Development of learner-participational and interactive 3D Virtual learning contents technology]. This work was also supported by the Basic Science Research Program through the National Research Foundation of Korea (NRF) funded by the Ministry of Education, Science and Technology (MEST) (2011-0013776).

References

1. Azuma R, Baillot Y, Behringer R, Feiner S, Julier S, MacIntyre B (2001) Recent Advances in Augmented Reality. *IEEE Comput Graphics Appl* 21(6):34–47
2. Krevelen DWF, van Poelman R (2010) A survey of augmented reality technologies, applications and limitations. *Int. J. of Virtual Reality* 9(2):1–20
3. Lee S, Jung J, Hong J, Ryu J, Yang H. (2012) :AR paint: A fusion system of a paint tool and AR. *ICEC 2012. LNCS, vol 7522. Springer, Heidelberg* pp 122–129
4. Azuma R, Hoff B, Neely H, Sarfaty R (1999) A motion-stabilized outdoor augmented reality system. In *Proc. IEEE, Virtual Reality*, pp 252–259
5. Hollerer T, Feiner S, Terauchi T, Rashid G, Hallaway D (1999) Exploring MARS: developing indoor and outdoor user interfaces to a mobile augmented reality system. *Computer & Graphics* 23(6):779–785
6. Baillot Y, Brown D, Julier S (2001) Authoring of physical models using mobile computers. In: *Proceedings international symposium on wearable computers*, pp 39–46
7. Thomas B, Demczuk V, Piekarski W, Hepworth D, Gunther B (1998) A wearable computer system with augmented reality to support terrestrial navigation. In: *Proceedings international symposium on wearable computers*, pp 168–171
8. Piekarski W, Thomas B (2001) Tinmith-metro: New outdoor techniques for creating city models with an augmented reality wearable computer. In: *proceedings international symposium on wearable computers*, pp 31–38
9. Arth C, Wagner D, Klopschitz, M, Irschara A, Schmalstieg D (2009) Wide area localization on mobile phones. In: *proceedings international symposium on mixed and augmented reality*, pp 73–82
10. Gordon I, Lowe D (2004) Scene modeling, recognition and tracking with invariant image features. In: *proceedings international symposium on mixed and augmented reality*, pp 110–119
11. Irschara A, Zach C, Frahm J, Bischof H (2009) From structure-from-motion point clouds to fast location recognition. In: *proceedings IEEE conference on computer vision and pattern recognition*, pp 2599–2606
12. Ta D, Chen W, Gelfand N, Pulli K (2009) Surftrac: Efficient tracking and continuous object recognition using local feature descriptors. In: *proceedings IEEE conference on computer vision and pattern recognition*, pp 2937–2944
13. Satoh K, Anabuki M, Yamamoto H, Tamura H (2001) A hybrid registration method for outdoor augmented reality. In: *proceedings international symposium on augmented reality*, pp 67–76
14. Reitmayr G, Drummond TW (2007) Initialisation for visual tracking in urban environments. In: *proceedings international symposium on mixed and augmented reality*, pp 161–172
15. Reitmayr G, Drummond TW (2006) Going out: Robust tracking for outdoor augmented reality. In: *proceedings international symposium on mixed and augmented reality*, pp 109–118
16. Cho K, Yoo J, Yang H (2009) Markerless visual tracking for augmented books. In: *proceedings joint virtual reality conference of EGVE-ICAT-EuroVR*, pp 13–20
17. Lepetit V, Fua P (2006) Going out: Keypoint recognition using randomized trees. *IEEE Trans Pattern Anal Mach Intell* 28(9):1465–1479
18. Rosten E, Drummond TW (2006) Machine learning for high-speed corner detection. In: *Proceedings European conference on computer vision*, pp 430–443
19. Chum O, Matas J (2005) Going out: Matching with PROSAC-progressive sample consensus. In: *proceedings IEEE conference on computer vision and pattern recognition*, pp 220–226
20. Schweighofer G, Pinz A (2006) Robust Pose Estimation from a Planar Target. *IEEE Trans Pattern Anal Mach Intell* 28(12):2024–2030
21. Cho K, Jung J, Lee S, Lim S, Yang H (2011) Real-time recognition and tracking for augmented reality books. *Computer Animation and Virtual Worlds* 22(6):529–541

Head Pose Estimation Based on Image Abstraction for Multiclass Classification

ByungOk Han, Yeong Nam Chae, Yong-Ho Seo and Hyun S. Yang

Abstract We address the problem of head pose estimation from a facial RGB image as a multiclass classification problem. Head pose estimation continues to be a challenge for computer vision systems due to extraneous characteristics and factors that do not contain pose information and affect changing pixel values in a facial image. To achieve robustness against variations in identity, illumination condition, and facial expression, we propose an image abstraction method that can reduce unnecessary information and emphasize important information for facial pose classification. Experiments are conducted to verify that our head pose estimation algorithm is robust against variations in the input images.

Keywords Head pose estimation · Image abstraction · Multiclass classification

1 Introduction

Significant attention has been shown to the question of how people naturally interact with computers. This is called Natural User Interface (NUI). An NUI is a human-machine interface that does not use devices for input; that is, it is a natural

B. Han · Y. N. Chae · H. S. Yang
Department of Computer Science, Korea Advanced Institute of Science and Technology,
Daejeon, Republic of Korea
e-mail: ByungOk.Han@kaist.ac.kr

Y. N. Chae
e-mail: ynchae@kaist.ac.kr

H. S. Yang
e-mail: hsyang@kaist.ac.kr

Y.-H. Seo (✉)
Department of Intelligent Robot Engineering, Mokwon University, Mokwon Gil 21,
Seo-gu, Daejeon, Republic of Korea
e-mail: yhseo@mokwon.ac.kr

interaction method between a human and a computer that is similar to effective communication between people. In order to achieve non-intrusive and natural human–computer interaction (HCI), recognition technologies, such as face recognition, facial expression recognition, activity recognition, and gesture recognition, are important.

In addition to these techniques, it is also crucial to improve the estimation process for human head poses for the NUI. Head pose estimation is a technology designed to obtain three-dimensional (3D) orientation properties from an image of a human head; that is, it is designed to extract head angle information from an image in terms of roll, pitch, and yaw rotations. Among various 3D object properties in 6 degrees of freedom, pitch and yaw are more difficult to estimate than the other properties, such as roll angle, two-dimensional (2D) translation, and scale, which can be calculated easily using 2D face detection techniques. However, it is difficult to estimate the pitch and yaw angles because of occlusions due to features such as glasses, beards, hair, and angular changes of the head. Differences in illumination and facial expression also pose problems during the extraction process for these angular properties of head images.

2 Related Works

In recent years, numerous studies have attempted to estimate 3D human head poses using facial RGB images. These studies can be divided into methods based on classification and those based on regression using machine learning methods. They can also be divided based on whether the pose space is discrete or continuous. The advantage of the classification approach is that the training datasets that are used in a training session can be expanded to a larger set at any time [1]. Moreover, the training data requires only human head images and corresponding labels with head angle information. However, this approach is only capable of estimating designated, discrete poses of the head. The regression methods for human head pose estimation, on the other hand, can obtain information about continuous poses of the head. It is difficult to design a robust estimation process for head pose though, due to variations in identity, illumination, and facial expression. These techniques attempt to find non-linear or linear mapping functions that connect head images and pose labels.

From the point of view of image representation, head pose estimation can be categorized into two types: appearance-based methods and geometric-feature-based methods. They can be classified by the characteristics of the description vectors that are used to train; the appearance-based approach uses texture information from a facial image, whereas the geometric-feature-based approach manipulates positional information of the facial features such as eyes, eyebrows, nose, and mouth. Because the first method exploits pixel values in the facial image as it is, it has to include an effective noise removal algorithm such as face alignment. The second method finds facial features using model-based algorithms

such as the Active Shape Model (ASM) [2], the Active Appearance Model (AAM) [3], or the Constrained Local Model (CLM) [4]. Feature vectors can be composed of location information obtained using several facial feature detectors trained with another training set for 2D location detection. The feature vectors, which are composed of the positional information, can be used as a supervised learning framework. Furthermore, they can be employed directly to estimate facial poses. For instance, a triangle obtained from three points, comprised of two eyes and one nose, can be utilized for pose estimation by simply calculating a projected triangle on the image plane. The geometric approach can be tedious because facial feature locations in all facial images should be labeled manually for composition of training data. On the other hand, it can be an intuitive way to estimate head pose because it uses location information.

Our approach in this paper is based on concepts from multiclass classification and an appearance-based method. For noise reduction, we propose a novel approach that is based on image abstraction. Image abstraction was originally developed for artistic purposes with automatic stylization. In addition, it was also employed to communicate information in [5]. In other words, it provides important perceptual information for the recognition process by simplifying the visual contents. A related study [6] addresses the image abstraction methods for coarse head pose estimation algorithms that are simple and accurate. It is, to my knowledge, the first study in head pose estimation that uses image abstraction. However, it only considers the estimation process for various head poses in terms of variations in identity; it does not consider variations of illumination or facial expression. This paper examines the problems of removing unnecessary information for head pose estimation. We focus on an image abstraction method that uses a facial sketch image obtained from a contour image and a cartoon-like effect. Then, we evaluate the effectiveness of the noise removal algorithm through various experiments.

The remainder of this paper is organized as follows. [Section 3](#) provides an overview of the framework of our system. [Section 4](#) contains details about the image abstraction method used for noise reduction. We present our research results in [Sect. 5](#) and conclude this paper in [Sect. 6](#).

3 System Overview

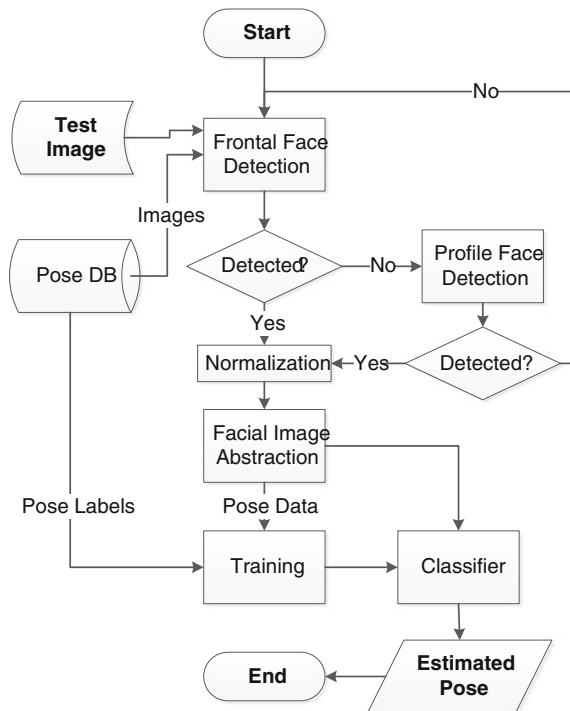
Humans can easily recognize head poses by detecting simple sets of edges like cartoon faces. Because people can intuitively abstract the features of faces, they are capable of simply identifying head poses. In particular, people have trained-in shapes or configurations of contours of features such as eyes, noses, mouths, eyebrows, foreheads, and chins. Using this, they can remember abstracted images of heads by inference from the trained data. Our system is designed and implemented from this perspective.

The overall process of our system is described in Fig. 1. To classify facial poses, a classifier comprising facial pose data has to be created to learn facial poses and corresponding labels from the Pose database (Pose DB) during the training session. First, the Adaboost face detection algorithm is used to detect coarse frontal and profile faces from images in the Pose DB. If there is no face in an image, then it is removed from the training data. Then, the pose data is normalized after the exception handling process and described using our image abstraction method. Using the vectors from the image abstraction algorithm, a classifier is trained by performing the Support Vector Machine method for a multiclass classification. After the training session, a test image is vectorized to a contour image as above and the resulting pose is estimated as the outcome.

4 Image Abstraction

Image abstraction removes unnecessary information and emphasizes the main contents by reinterpreting scene information. This process can help viewers to catch visual information that has been specifically adapted. We use an image abstraction method to interpret facial images. Our image abstraction method is

Fig. 1 Overall process of our system



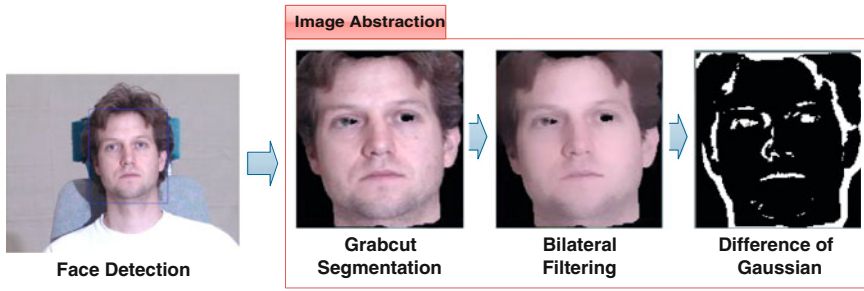


Fig. 2 Image abstraction pipeline

described in Fig. 2. The proposed algorithm performs the Grabcut segmentation [7] after the rectangular area of a face is provided by face detection. Then, for a cartoon-like effect, the bilateral filtering [8] removes some noise and the Difference of Gaussian (DoG) method [9] extracts contours from the face.

4.1 Grabcut Algorithm

Grabcut is a method for performing segmentation in an image. The only input is a rough segmentation between the foreground and the background. This is achieved by using the Graph Cut algorithm and the Gaussian Mixture Model (GMM). The basic procedure of the Grabcut algorithm is as follows.

- (1) A user input comprising a face region, background region, and unknown region is obtained. The unknown region can contain either face or background information.
- (2) The pixels are modeled from the background and face regions using the GMM.
- (3) Each face and background GMM component is selected by choosing the most probable components. Then, every pixel is assigned to the corresponding GMM component.
- (4) Two new GMMs are trained from the pixel sets that were created in the previous step.
- (5) A graph is built and the Graph Cut is used to determine the segmentation of face and background pixels.
- (6) Steps 4–6 are repeated until the segmentation converges.

4.2 Bilateral Filtering

The bilateral filter is a smoothing filter that preserves edges. This filter is based on a Gaussian filter and the weights of the Gaussian are influenced by the spatial

location in an image and the corresponding intensity value, to be exact, a spatial filter and a range filter. This approach is non-iterative, local, and simple. After a face image is obtained from the Grabcut method, noise in the foreground region is reduced and the facial contours, which provide visual cues for the identification of the head pose, are extracted using this method.

4.3 Difference of Gaussian

DoG utilizes the differences between the two Gaussian images and extracts the edges. A convolution operation is conducted using two Gaussian masks, which have different standard deviations. The DoG algorithm is similar in function to the retina, which reads information from an image. The thickness of edges can be controlled by adjusting the two standard deviations of the Gaussian. Our approach employs this algorithm to emphasize facial contours and create a binary image composed of edges.

5 Experiment

We evaluated our method using the Multi-PIE face dataset [10]. The dataset contains 750,000 images of 337 people from 15 viewpoints, 19 illumination conditions, and a range of facial expressions. We used implementations of the face detection, Grabcut, and bilateral filtering algorithms from the OpenCV library [11]. Final contour images from the proposed method are shown in Fig. 3. As can be seen, these images have similar patterns according to pose variation. If these patterns are regular regardless of the other variations, we can ignore the slight alignment error that is crucial for the recognition process. To verify the

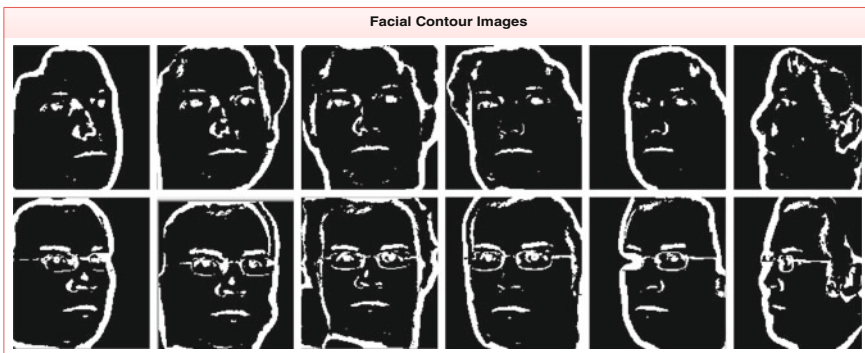


Fig. 3 Facial contour images obtained using our image abstraction algorithm

Table 1 Head pose classification results with corresponding datasets composed of variations in identity, illumination, and facial expression

Variation	Average recognition rate (%)
Identity	83.3
Identity (small set)	98.3
Illumination	83.4
Facial expression	90.4

The dataset for identity variation contains 15 viewpoints whereas the small set with identity variation has 7 viewpoints

effectiveness of our method, we conducted several experiments with variations in identity, illumination, and facial expression. Table 1 shows the results of our framework for the different variations. It shows that the proposed method can remove noise effectively and emphasize pose information, especially contours.

6 Conclusion and Future Work

This study demonstrated that the image abstraction for head pose estimation can be successfully applied to the multiclass classification problem. Cartoon-like facial contour images can be used to abstract the characteristics of common facial poses quickly. These images can reduce noise due to variations in identity, illumination condition, and facial expression. In addition, experimental results show that the edges of a facial image can significantly affect visual communication between humans and computers. In the future, face detection algorithms should be modified to incorporate effective head pose estimation processes so that they can detect faces that are rotated by a tilt angle. We plan to expand this work to allow for batch alignment of faces using image abstraction.

Acknowledgments This work was supported by the IT R&D program of MKE & KEIT (10041610, The development of the recognition technology for user identity, behavior and location that has a performance approaching recognition rates of 99 % on 30 people by using perception sensor network in the real environment). This work was also supported by the Basic Science Research Program through the National Research Foundation of Korea (NRF) funded by the Ministry of Education, Science and Technology (MEST) (2011-0013776).

References

1. Erik, MC, Mohan MT (2009) Head pose estimation in computer vision. *A Surv IEEE Trans Pattern Anal Mach Intell* 31(4):607–626
2. Cootes TF, Taylor CJ, Cooper DH, Graham J (1995) Active Shape Models-Their Training and Application. *Comput Vis Image Underst* 61(1):38–59
3. Cootes TF (2001) Active Appearance Models. *IEEE Trans Pattern Anal Mach Intell* 23(6):681–685

4. David C, Cootes TF (2008) Automatic feature localisation with constrained local models. *Pattern Recogn* 41(10):3054–3067
5. Holger W, Sven CO, Bruce G (2006) Real-time video abstraction, *ACM SIGGRAPH*, pp 1221–1226
6. Anant VP, Brejesh L (2012) Exploiting perception for face analysis: image abstraction for head pose estimation, *computer vision—ECCV 2012. Workshops and Demonstrations LNCS* 7584:319–329
7. Carsten R, Vladimir K, Andrew B (2004) GrabCut—interactive foreground extraction using iterated graph cuts, *ACM SIGGRAPH*, pp 309–314
8. Tomasi C (1998) Bilateral filtering for gray and color images, *International conference on computer vision (ICCV)*, pp 839–846
9. Lowe DG (1999) Object recognition from local scale-invariant features. *International Conference on Computer Vision (ICCV)* 2:1150–1157
10. Ralph G, Iain M, Jeffrey C, Takeo K, Simon B (2010) Multi-PIE, *Image Vision Comput* 28:807–813
11. Open Source Computer Vision, <http://opencv.org/>

Recovering Human-Like Drawing Order from Static Handwritten Images with Double-Traced Lines

Takayuki Nagoya and Hiroyuki Fujioka

Abstract This paper focuses on an ill-posed problem of recovering a human-like drawing order from static handwritten images with double-traced lines. The problem is analyzed and solved by employing a method based on the graph theoretic approach. Then, a main issue is to obtain the smoothest path of stroke from a graph model corresponding to input image. First, we develop an index on double-traced lines “D-line index” by employing the spline curves. Then, it is shown that the graph is transformed to a semi-Eulerian graph. The restoration problem reduces to maximum weight matching problem and is solved by a probabilistic tabu search. We examine the effectiveness and usefulness by some experimental studies.

Keywords Human-like drawing recovery · Graph theory · Handwritten images

1 Introduction

Recovering human handwriting motion from static handwritten images (e.g. signature, etc.) is a challenging problem in the various fields—such as forensic sciences, biomimetics and character recognition, etc. An effective approach for such an ill-posed problem may be the graph theoretic approach and various types of recovery algorithm based on the graph theory have been developed (see e.g.

T. Nagoya
Humanities Center, Tottori University of Environmental Studies,
Wakaba-Kita, Tottori 689-1111, Japan
e-mail: nagoya@kankyo-u.ac.jp

H. Fujioka (✉)
Department of System Management, Fukuoka Institute of Technology,
3-30-1, Wajiro-higashi, Higashiku, Fukuoka 811-0295, Japan
e-mail: fujioka@fit.ac.jp

[1–3]). For example, Yasuhara et al. (e.g. [4]) have developed the hybrid approach which is merged both of local tracing and global graph searching methods. In the method, the types of each edge and vertex are determined by locally analyzing the structure of the graph model corresponding to the character stroke. Then, the labeling information of stroke is obtained. By globally searching the graph based on the labeling information, we thus can recover some dynamic information of stroke. Similar work has been presented in our work [5, 6]. But, since the drawing order is determined at each vertex by employing only the local structure of graph, the recovered drawing order may not correspond to a human-like smoothest path of the possible ones.

In this study, we develop a new method for recovering human-like drawing order from static handwritten images. We here analyze and solve such a recovery problem by employing the graph theoretic approach in [5, 6]. Then, our concern is to derive the smoothest path from the graph model corresponding to input handwriting image. First, we constitute the graph model from the input image by employing thinning algorithm. Then, we locally analyze the structure of graph at each vertex. Here, supposing that the input image includes some double-traced lines (D-lines) on the stroke, the identification method of D-lines is developed by introducing “D-line index” based on spline curves [7]. Such a method may enable us to transform any graph models including D-lines to semi-Eulerian graph models. Thus, the restoration problem reduces to maximum weight perfect matching problem of graph. For such a matching problem, we finally present a probabilistic tabu search algorithm. A recovery example for human handwritten images includes.

In the sequel, we assume that an undirected graph G with vertex set $V(G) = \{v_1, v_2, \dots, v_n\}$ and edge set $E(G) = \{e_1, e_2, \dots, e_m\}$ is already constructed from an input I . Each edge of G corresponds to a part of stroke in the skeleton and each vertex of G corresponds to a geometrical feature point at which an edge terminates and multiple edges are connected.

2 Detection and Removing of Double-Traced Lines on Stroke

Let us consider the case where a graph G is semi-Eulerian. Then, there exists a walk on G which traverses all of the edges exactly once from a vertex with degree one (i.e. start vertex) to another one (i.e. end vertex). Such a walk is called as ‘Euler path’. The problem of finding a Euler path in a semi-Eulerian graph can be computed in polynomial time. But, we often face a case where some stroke is drawn twice. We refer such a stroke traversed twice as “double-traced line (D-line)”. In such a case, the graph G obtained from input I never become semi-Eulerian. We thus need to detect all the D-lines in order to construct a semi-Eulerian graph from G .

In Fig. 1, a set of possible D-lines on the stroke is shown. We readily see that all the types of D-lines except to Fig. 1a, say Fig. 1b–f, are represented as the graph with same structure. The fact may yield difficulties to distinguish the differences among their D-lines from only local structure information on G . We therefore introduce an index called as “D-line index” using the spline curves in order to identify D-lines (Sect. 2.1). Then, a method for transforming graph G with D-lines into semi-Eulerian one is developed (Sect. 2.2). Note here that the differentiation on the types of D-line will be achieved by global analysis presented in later section.

2.1 D-Line Index

We may notice that all the types of D-lines in Fig. 1 do not only consist of an edge between two vertices with odd degree, but the length of edge is generally small. When D-line is given as a path between two vertices $v_{D1}, v_{D2} \in V(G)$, the path P_D is written as

$$P_D = \langle (v_{D1}, v_{D2}) \rangle \tag{1}$$

with $v_{ki} \in V(G), i = 1, 2, \dots, l$, where (v_p, v_q) denotes an unordered pair of adjacent vertices v_p and v_q , hence an edge between v_p and v_q . In order to determine whether a path P_D is D-line, we introduce the following D-line index.

Specifically, we define D-line index based on the straightness and smoothness between the path P_D and the incident edges to P_D . Let $DLI(P_D) \in \mathbf{R}^+$ be index of D-lines for the path P_D , $DLI(P_D)$ is defined as

$$DLI(P_D) = ST(P_D) + \lambda SM(P_D) \tag{2}$$

with a weighted parameter $\lambda \in \mathbf{R}^+$.

Here, $ST(P_D)$ and $SM(P_D)$ denote the ratios on straightness and smoothness respectively for P_D as follows.

The straightness ratio $ST(P_D)$ is evaluated by

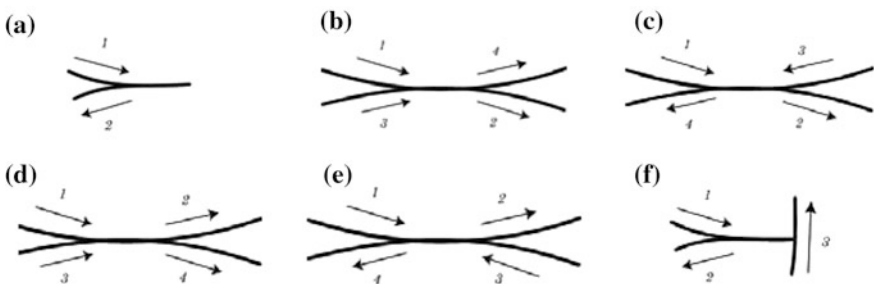


Fig. 1 Double traced lines (D-lines)

$$ST(P_D) = d(P_D)/l(P_D), \tag{3}$$

where $d(P_D)$ is Euclidean distance between two vertices v_{D1} and v_{D2} in (1) and $l(P_D)$ is the total number of pixels on P_D . Note here that it holds that $ST(P_D) \geq 1$ with upper bound being achieved when the path becomes exactly straight line. Thus, $ST(P_D)$ approaches to 0 as the straightness of path P_D decreases.

On the other hand, the smoothness ratio $SM(P_D)$ in (2) is defined as

$$SM(P_D) = \min \left\{ \sum_{i=1,2} S(e_D, e_i^{v_{D1}}), \sum_{i=1,2} S(e_D, e_i^{v_{D2}}) \right\} \tag{4}$$

with

$$S(e_d, e_i^{v_{Dj}}) = \int_0^1 \left\| \frac{d^2 x_{[e_d, e_i^{v_{Dj}}]}(s)}{ds^2} \right\|^2 ds / \int_0^1 \left\| \frac{dx_{[e_d, e_i^{v_{Dj}}]}(s)}{ds} \right\| ds. \tag{5}$$

Here, $e_i^{v_{Dj}}$ denotes an edge $(v_{Dj}, v_i^{v_{Dj}})$ for $i, j = 1, 2$, where $v_i^{v_{Dj}}$ is an adjacent vertex to v_{Dj} . e_D denotes the edge that is obtained by merging all edges of P_D to one. Also, $x_{[e_d, e_i^{v_{Dj}}]}(s)$, $s \in [0, 1]$ denotes some approximated spline curve constructed from a set of sequential pixel data on the path $(e_D, e_i^{v_{Dj}})$.

2.2 Construction of Semi-Eulerian Graph

We next present a method for transforming the graph G with D-lines to a semi-Eulerian graph. Then, our task may be detection of all the D-lines by using D-line index and remove the all the odd-degree vertices.

If some D-lines exist on the stroke, the odd-degree vertices of graph G must be either D-line or terminal point on stroke (i.e. the start and end points). Now, let $V_I \subseteq V(G)$ be a set of vertex with degree one. Then each vertex $v_i \in V_I$ is either a terminal point of stroke or a degree one vertex of a D-line. In other words, there exist exactly two vertices, denoted by $v_s, v_t \in V_I$, which correspond to start and end points of stroke. We then identify v_s and v_t by using the D-line index DLI in (2) as follows.

For each $v_i \in V_I$, we find the nearest vertex $v_j \in V(G) (i \neq j)$ from v_i whose degree is odd greater than or equal to three. Let $P(v_i, v_j)$ be the shortest path in G between v_i and v_j . Then, the vertex v_i with the smallest $DLI(P(v_i, v_j))$ may not be a terminal of D-line. Hence, two vertices with smallest DLI may be regarded as the terminal vertices v_s and v_t .

Next, let V_D be the set of every odd degree vertices of G , where $v_s, v_t \in V_I$ are omitted. Then, it is easy to see that $|V_D|$ is even. Moreover, any D-lines are the shortest path between a pair of vertices of V_D , because the path length corresponding to D-line must be very short. According to the fact that any D-line does not connect two vertices both of which have degree one, all the D-lines are identified as follows.

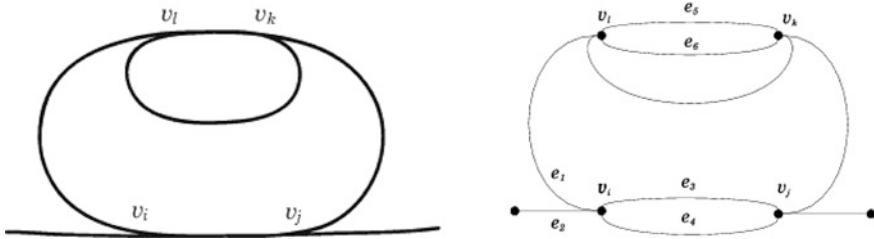


Fig. 2 An example of input I (left) and the constructed semi-Eulerian graph G_{eul} (right)

Let G_{odd} be an edge weighted graph with a set of vertex $V(G_{odd})$,

$$V(G_{odd}) = V_D \tag{6}$$

and a set of edge $E(G_{odd})$,

$$E(G_{odd}) = (V_D \times V_D) / \{(v_i, v_j) | \deg(v_i) = \deg(v_j) = 1\}, \tag{7}$$

where $A \times A$ is the Cartesian product of A with itself.

Also, we introduce the weight function $w: E(G_{odd}) \rightarrow \mathbf{R}^+$ defined as

$$w(v_i, v_j) = \text{DLI}(P(v_i, v_j)) \tag{8}$$

for each $(v_i, v_j) \in E(G_{odd})$. Then, the detection of D-lines can be regarded as the maximum weighted matching problem on G_{odd} . As is well known, the maximum weighted matching problem can be solved in polynomial time. If we detect the terminal vertices and D-lines, we readily transform the graph G into a semi-Eulerian graph G_{eul} . For example, when we are given a input I as illustrated in Fig. 2, we get *semi-Eulerian graph* G_{eul} as shown in Fig. 2b.

From the above results, we can get the following lemma.

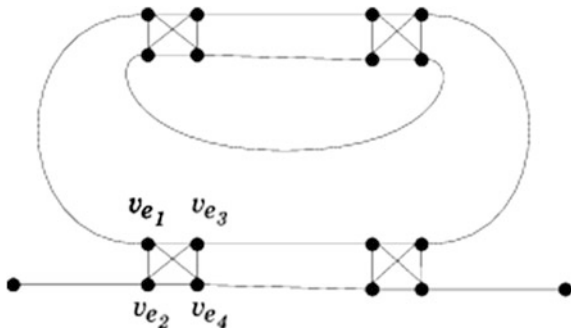
Lemma 1 G_{eul} is a semi-Eulerian graph. Furthermore, Euler paths of G_{eul} corresponds one-to-one with strokes of the given image.

Remark 1 By the path duplication method, it can be shown that the above results are readily extended to the case where some stroke intersects with D-lines.

3 Construction of Optimal Euler Path

We here develop a method for recovering the smoothest drawing order, which may correspond human handwriting motion, from input image I . Specifically, we find the smoothest Euler path from the semi-Eulerian graph G_{eul} . First we construct continuity graph from semi-Eulerian graph G_{eul} obtained in the previous method (Sect. 3.1). Then, the smoothest Euler path is approximated by employing probabilistic tabu search algorithm (Sect. 3.2).

Fig. 3 A continuity graph obtained from the semi-Eulerian graph G_{eul} in Fig. 2



3.1 Construction of Continuity Graph

Let v_i be even degree vertex of G_{eul} and let $\{e_1, \dots, e_d\}$ be a set of adjacent edges of v_i . For each v_i , we create a complete graph C_{v_i} whose vertices are $\{v_{e_1}, \dots, v_{e_d}\}$. Then, v_i is replaced by C_{v_i} and we connect v_{e_i} to e_i for $i = 1, \dots, d$. Moreover, the weight $S(e_i, e_j)$ is assigned for each edge (v_{e_i}, v_{e_j}) . Note that the graph G_{con} is no longer Eulerian.

By using a perfect matching of C_{v_i} , a path of graph G_{con} may reduce to a path corresponding to an Euler path of G_{eul} as follows. Let M_p be a set of perfect matchings defined as

$$M_p = \{M_{v_i}\}_{v_i \in V(G_{eul})}, \tag{9}$$

where $M_{v_i} \in M_p$ is a perfect matching of C_{v_i} . Then, the graph G'_{con} defined as

$$G'_{con} = (V(G_{con}), (E(G_{con}) - \cup_{v \in V(G_{eul})} E(C_v)) \cup M_p) \tag{10}$$

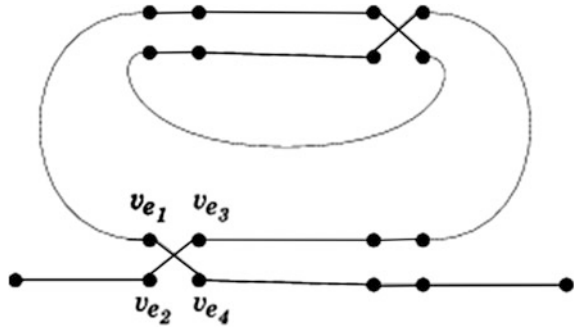
is a path that correspond to an Euler path of G_{eul} whenever G'_{con} is connected. Then, the following theorem holds.

Theorem 1 For a set of perfect matchings M_p in (9), G'_{con} is a path corresponding to an Euler path of G_{eul} whenever G'_{con} is connected. Conversely, for every Euler path P of G_{eul} , there exists a perfect matching M_p such that G'_{con} corresponds to P (Fig. 3).

3.2 Probabilistic Tabu Search

From the results in Sect. 3.1, we see that the problem of computing optimum Eulerian path in G_{eul} reduces to one of computing a set of perfect matching $M_p = \{M_{v_i}\}_{v_i \in V(G_{eul})}$. Here, M_{v_i} denotes a perfect matching of C_{v_i} such that G'_{con} is connected. Also, the total weight of M_p represents smoothness of a corresponding Euler path. For computing such M_p such that G'_{con} is connected, we here use a probabilistic tabu search algorithm as follows.

Fig. 4 A graph G'_{con} obtained from the continuity graph G_{con} in Fig. 3



First, we compute an Euler path P_e of G_{eul} . Then, a set of perfect matching of complete graph $\{C_{vi} \mid vi \in v(G_{eul})\}$ corresponding to P_e is given as M_p in (9). Here, M_p is set as initial feasible solution of probabilistic tabu search. In the probabilistic tabu search, an optimal solution is iteratively obtained by modifying the initial feasible solution to better one. Then, a tabu list T of feasible solutions is used to avoid modifying to feasible solution that have been visited in the recent past. Here, an initial setting of T is set as $T = \{M_p\}$. Then, the algorithm may find better feasible solution M'_p of which the weight is larger than that of previously visited feasible solutions by repeating the following local change: First, we choose C_{vi} randomly from $\{C_{vi} \mid vi \in v(G_{eul})\}$ with probability proportional to the weight of $M_{vi} \in M_p$. Then, two edges $e_1 = (v_1, v_2)$ and $e_2 = (v_3, v_4)$ of M_{vi} are chosen uniformly at random. Moreover, we set $E_1 = \{(v_1, v_2), (v_3, v_4)\}$, $E_2 = \{(v_1, v_3), (v_2, v_4)\}$, and $E_3 = \{(v_1, v_4), (v_2, v_3)\}$. If there exists $i \in \{2, 3\}$ such that $w(E_i) \leq w(E_1)$ and $M'_p = M_p/E_1 \cup E_i$ is a feasible solution unlisted in T , then we update T and M_p as $T = T \cup \{M'_p\}$ and $M_p = M'_p$ respectively. The process is iteratively carried out for new M_p and T until a predefined time limit N is exceeded. Finally, the algorithm outputs M_p that is the best feasible solution found so far as the desired drawing order of input handwritten image I (Fig. 4).

4 Experimental Studies

We examine the effectiveness and usefulness by some experimental studies. In Fig. 5, we show some recovering results for human handwriting images, where each images were written by pen tablet device. In these figures, the written order is

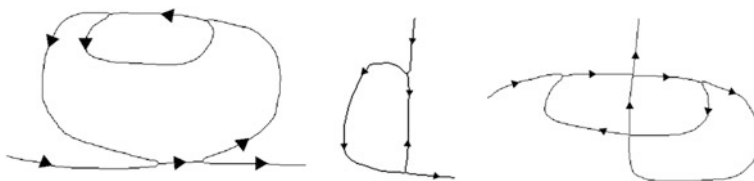


Fig. 5 Experimental results

illustrated by arrow marks. From the results, we may observe that our method can correctly recover the human-like drawing order of handwritten image even when the double-traced lines are included.

References

1. Plamondon R (2000) Online and off-line handwriting recognition: a comprehensive survey. *IEEE Trans Pattern Anal Mach Intell* 22(1):63–84
2. Lee S, Pan JC (1992) Offline Tracing and Representation of Signatures, *IEEE Trans. Systems, Man, and Cybernetics* 22(4):755–771
3. Jager S (1996) Recovering writing traces in off-line handwriting recognition: using a global optimization technique. In: *Proceedings of 13th international conference on pattern recognition*, pp 931–935, Vienna, 25–29 Aug 1996
4. Kato Y, Yasuhara M (2000) Recovery of drawing order from single-stroke handwriting images, *IEEE Trans. on Pattern Analysis and Machine Intelligence* 22(9):938–949
5. Fujioka H, Nagoya T (2011) Recovering stroke order from multi-stroke character images. In: *Proceedings of the 2011 2nd international conference on innovative computing and communication, and 2011 2nd Asia-Pacific Conference on information technology and ocean engineering*, pp 34–37, Macao, 5–6 March (2011)
6. Nagoya T, Fujioka H (2012) Recovering dynamic stroke information of multi-stroke handwritten characters with complex patterns. In: *Proceedings of the 2012 international conference on frontiers in handwriting recognition*, pp 718–723, Bari, Italy, 18–20 Sept (2012)
7. Fujioka H, Kano H (2012) Optimal vector smoothing splines with coupled constraints. *Transactions of the Institute of Systems, Control and Information* 25(11):299–307

Noise Reduction Scheme for Speech Recognition in Mobile Devices

Jeong-Sik Park, Gil-Jin Jang and Ji-Hwan Kim

Abstract This paper proposes an efficient noise reduction scheme for speech recognition in mobile devices. Due to the limited capacity of mobile devices, the speech recognition system requires a noise reduction module processed with low computational intensity. For noise reduction in mobile devices, the proposed approach directly utilizes packet data estimated by a speech coder. In particular, we apply pitch information for comb filtering, a well-known noise reduction method.

Keywords Noise reduction • Speech recognition • Mobile device • Comb filtering

1 Introduction

As mobile devices such as smartphones and tablet PCs have become very popular, an importance of voice as a convenient and reliable man–machine interface has been increased [1]. Accordingly, the research on Automatic Speech Recognition (ASR) has been varied from on-line telecommunication network to mobile environments. Particularly, in mobile environments, it needs to be considered by low computational power and memory as well as limited capacity of mobile devices.

J.-S. Park (✉)

Department of Intelligent Robot Engineering, Mokwon University,
Daejeon, South Korea
e-mail: parkjs@mokwon.ac.kr

G.-J. Jang

School of Electrical and Computer Engineering, Ulsan National Institute
of Science and Technology (UNIST), Ulsan, South Korea
e-mail: gjang@unist.ac.kr

J.-H. Kim

Department of Computer Science and Engineering, Sogang University,
Seoul, South Korea
e-mail: kimjihwan@sogang.ac.kr

The research works, especially related to extracting feature parameters used for ASR system in mobile environments, can be classified into three categories: (a) extraction from the input speech of the speech coder, (b) extraction from the packets generated after encoding process, and (c) extraction from the output speech of the coder [2]. Method (a), in which ASR system is located inside a device, gives high recognition performance, but has limitations on applying intensive algorithms over the device capacity. Bitstream-based method (b), which uses coding parameters such as Line Spectral Frequency (LSF) directly for recognition, gives good recognition rate while it requires no feature extraction processes. On the other hand, method (c), in which ASR system exists in the server side, gives lower performance due to the distortion of the output speech caused by speech coding and decoding process while any algorithms can be applied to ASR.

In this paper, a method applying the comb filtering technique, which is a well-known noise reduction method, to the output speech is proposed and it is related to the extraction method (c). In Sect. 2, we present the details of the proposed method. Experiments and results are shown in Sect. 3. And Sect. 4 concludes this paper.

2 Proposed Noise Reduction in a Mobile Device

Most of noise reduction methods such as spectral subtraction detect the non-speech frames from the speech signals, then estimate the noise components in the frames, and use the estimate to reduce the noise components included in the speech frames. However, it is not possible to estimate the correct noise components for output speech of the speech coder embedded in mobile devices since energy of the non-speech frames is decreased by the coder. As a result, it has limitations on reducing noise components in the speech frames. Accordingly, methods that do not require noise estimation in non-speech frames are applicable to the output speech. One of the methods maintaining this property is the comb filtering, which reduces noise components, using the fundamental frequency, in other words, the pitch period, of the speech signals [3, 4].

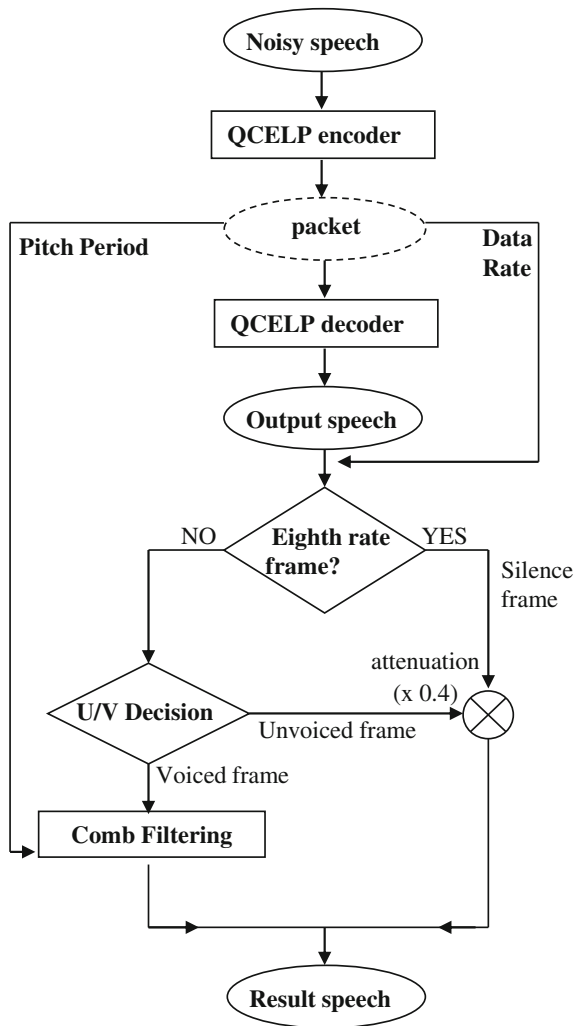
The comb filtering is based on the property that waveforms of the voiced sound are periodic with a period that corresponds to the pitch period, or the fundamental frequency, and its principle is as follows. The noisy voiced sound has noise components within speech harmonics. The components can be reduced by passing harmonics of speech, using a comb filter constructed with the frequency response corresponding to the fundamental frequency.

2.1 Proposed Process for Noise Reduction

Proposed noise reduction process employing the comb filtering technique is described in Fig. 1. This process consists of two stages, one of which is to select voiced frames and the other is to apply comb filtering to the selected voiced frames.

The comb filtering utilizes the pitch period of the speech signals, and therefore the filtering process should be applied to only the frames containing the pitch period, that is, the voiced frames. For this reason, a process for selection of the voiced frames must be preceded by comb filtering. For this process, we extract and use the data rate information from the packets generated by the speech coder

Fig. 1 Proposed noise reduction process based on comb filtering



embedded in mobile devices. We give further details about this process, using the QCELP coder as a representative speech coder.

The QCELP coder is a variable bit-rate speech coder that dynamically selects one of four kinds of data rates for each frame, depending on the speech activity [5]. Four kinds of data rates are called: full rate (8 kbps), half rate (4 kbps), quarter rate (2 kbps), and eighth rate (1 kbps). In general, silence and background noise are encoded at the eighth rate, whereas active speech is encoded at the upper rates. In consideration of this property, all frames designated as the eighth rate are excluded in the next steps.

Frames excepting the eighth rate frames can be designated as speech frames. But among the speech frames, only the voiced frames possess a periodic property of signals, that is, the pitch period. Hence, the unvoiced speech frames cannot be submitted to the comb filtering process. For the selection of the unvoiced frames, Unvoiced/Voiced (UV) decision is required. In this study, we employ the U/V decision technique using autocorrelation coefficient [6].

The second stage of proposed process is applying comb filtering to the voiced frames. To obtain a reliable result from comb filtering process, estimation of correct pitch information is necessarily required. Previous researches introduced various techniques for pitch estimation such as cepstral-based and LPC-based approaches. However, it is quite difficult to estimate the correct pitch period from noisy speech. In particular, this task may require intensive computational power in mobile devices.

To overcome these problems, we extract the pitch period information directly from the speech packets. The pitch period estimated by the Qualcomm Code-Excited Linear Prediction (QCELP) coder is relatively correct, especially for the voiced frames. In particular, the pitch information is used for generation of output speech, and thus, the comb filtering for the output speech provides more reliable result. Finally, direct use of pitch information excludes the pitch estimation process.

Figure 2 provides further description of comb filtering process applied to the voiced frames. As shown in this figure, a comb filter is constructed per sub-frame since the number of the pitch data in each frame is different according to the data rate. In this figure, a 'full rate' frame, in which the pitch is updated four times, is divided by four sub-frames. And four comb filters are constructed using respective pitch periods ($T_1 \sim T_4$), and applied to each sub-frame.

After the comb filtering process, the signal energy of the voiced frames is degraded due to reduction of noise components. In order to balance the energy of the voiced frames and that of other frames, a simple attenuation is performed on frames corresponding to silence and unvoiced speech frames.

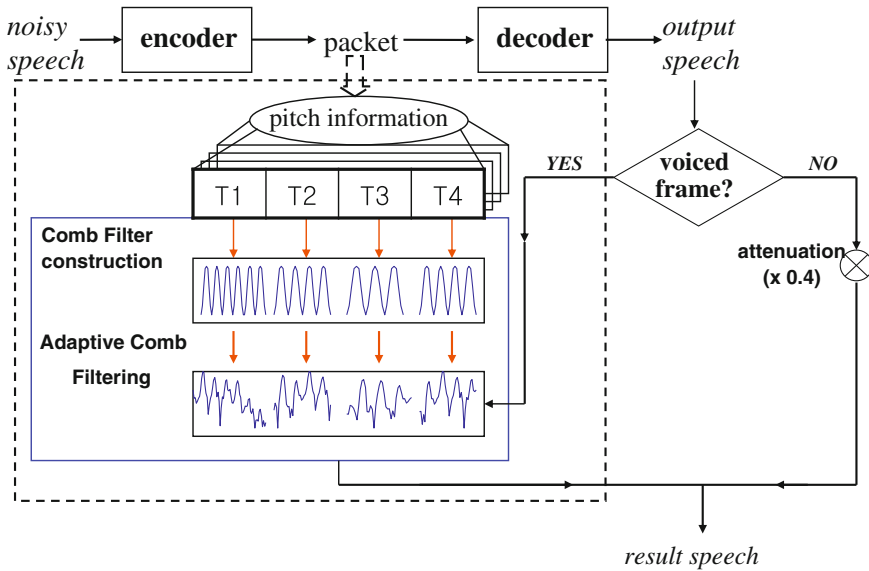


Fig. 2 Further description of comb filtering process

3 Experiments and Results

To evaluate the efficiency of the proposed approach, we performed speech recognition experiments on output speech of the QCELP speech coder.

3.1 Experimental Environments

Recognition experiments were performed on the Aurora 2 database, a noise-contaminated version of the TI-DIGITS database. Our recognition system has the same structure as the baseline system provided by Aurora 2 task, using Hidden Markov Model (HMM) to train acoustic models and using 39 dimensional Mel-Frequency Cepstral Coefficients (MFCCs) as a feature parameter. This feature set consists of 12 dimensional MFCCs and log energy with their first and second derivatives. The HMM models were trained with noiseless speech data. Training and testing follow the steps specified in [7]. For testing, we used a test set that consists of three types of noise conditions, that is, subway, babble, and car.

Table 1 Word recognition accuracy for feature parameters extracted from output speech and noise-reduced speech

dB	Output speech (baseline)				Noise-reduced speech (proposed)			
	subway	babble	car	Av.	subway	babble	car	Av.
Clean	98.1	98.5	98.2	98.3	98.3	98.3	98.1	98.2
10	61.8	75.7	72.7	70.1	78.2	84.3	87.8	83.4
5	42.2	49.8	45.6	45.9	54.5	64.2	66.7	61.8
0	21.2	17.5	19.2	19.3	24.2	27.5	31.8	27.8
Avg.	55.8	60.4	58.9	58.4	63.8	68.6	71.1	67.8

3.2 Recognition Results

The experimental results are presented in Table 1. This table provides the word recognition accuracy for two kinds of feature parameters extracted from: (1) the output speech and (2) the output speech processed by the proposed noise reduction procedure.

It is observed that the noise-reduced output speech provides superior performance to the original output speech over all types of noise conditions and noise levels. As a whole, the average accuracy of the baseline system and the proposed system were 58.4 % and 67.8 %. From this result, the proposed approach presented about 30 % of relative performance improvement to the baseline system. The efficiency of the proposed system is more significant on the noise conditions rather than a clean condition. The experimental results demonstrate that the noise components included in the output speech of a mobile device are effectively reduced by the proposed noise reduction scheme.

4 Conclusion

In this paper, we proposed a process to reduce the noise components effectively, by applying comb filtering to the output speech of the speech coder in a mobile device. The proposed approach utilizes useful information from packet data estimated by the speech coder. In particular, direct use of pitch information improves the comb filtering performance and reduces computational time consumption.

The results of speech recognition experiments performed on the Aurora 2 database demonstrated that the proposed approach effectively removes noise components, deteriorating the recognition error rate. However, in clean speech environment, the proposed approach showed poor performance compared to the baseline. This is due to the distortion of speech signal caused by comb filtering. In the future work, we will investigate a method to minimize the distortion.

Acknowledgments This research was supported by the Converging Research Center Program funded by the Ministry of Education, Science and Technology (2012K001341).

References

1. Lim MJ, Lee ES, Kwon YM (2012) Implementing Mobile Interface Based Voice Recognition System. *Computer Applications for Database, Education, and Ubiquitous Computing*, 352:150–157
2. Kim HK (2000) Bitstream-based feature extraction for wireless speech recognition. In: *International conference on ASSP*, pp 1607–1610
3. Frazier RH (1975) An adaptive filtering approach toward speech enhancement. S.M.thesis, M.I.T., Cambridge
4. Frazier RH, Samsam S (1976) Enhancement of speech by adaptive filtering. In: *International conference on ASSP*, pp 251–253
5. Gardner W (1993) QCELP: a variable rate speech coder for CDMA digital cellular. *Speech and audio coding for wireless and network applications*. Kluwer Academic Pub., Dordrecht pp 77–84
6. Atal BS, Rabiner LR (1976) A Pattern Recognition Approach to Voiced-Unvoiced-Silence Classification with Applications to Speech Recognition. *IEEE Trans Acoust Speech Signal Process* 24:201–212
7. Hirsch HG, Pearce D (2000) The AURORA Experimental Framework for the Performance Evaluations of Speech Recognition Systems under Noisy Conditions. In: *ISCA Tutorial and Research Workshop*

Implementation of a Large-Scale Language Model in a Cloud Environment for Human–Robot Interaction

Dae-Young Jung, Hyuk-Jun Lee, Sung-Yong Park,
Myoung-Wan Koo, Ji-Hwan Kim, Jeong-sik Park,
Hyung-Bae Jeon and Yun-Keun Lee

Abstract This paper presents a large-scale language model for daily-generated large-size text corpora using Hadoop in a cloud environment for improving the performance of a human–robot interaction system. Our large-scale trigram language model, consisting of 800 million trigram counts, was successfully implemented through a new approach using a representative cloud service (Amazon EC2), and a representative distributed processing framework (Hadoop). We performed trigram count extraction using Hadoop MapReduce to adapt our large-scale language model. Three hours are estimated on six servers to extract trigram counts for a large text corpus of 200 million word Twitter texts, which is the approximate number of daily-generated Twitter texts.

D.-Y. Jung · H.-J. Lee · S.-Y. Park · M.-W. Koo · J.-H. Kim (✉)
Department of Computer Science and Engineering, Sogang University, Seoul, South Korea
e-mail: kimjihwan@sogang.ac.kr

D.-Y. Jung
e-mail: dyjung@sogang.ac.kr

H.-J. Lee
e-mail: hyukjunl@sogang.ac.kr

S.-Y. Park
e-mail: parksy@sogang.ac.kr

M.-W. Koo
e-mail: mwkoo@sogang.ac.kr

J. Park
Department of Intelligent Robot Engineering, Mokwon University, Daejeon, South Korea
e-mail: parkjs@mokwon.ac.kr

H.-B. Jeon · Y.-K. Lee
Electronics and Telecommunications Research Institute, Electronics and
Telecommunications Research Institute, Daejeon, South Korea
e-mail: hbjeon@etri.re.kr

Y.-K. Lee
e-mail: yklee@etri.re.kr

Keywords Language model · Large-scale · Cloud · Human–robot interaction

1 Introduction

Service robots operate autonomously to perform services useful to the well-being of humans. Unlike industrial robots, which are typically found in manufacturing environments, service robots interact with a large number of users in a variety of places including hospitals, homes, restaurants, and offices. In order to coexist with humans in their daily lives and fulfill their requests, service robots should be able to understand human communication.

Speech recognition aims to find the most likely word sequence, \hat{W} , which maximizes the product of $P(O|W)$ and $P(W)$ provided by an acoustic model (AM) and a language model (LM), respectively. The standard approach in an LM requires a word-based n -gram [1]. If all histories with the same most recent $n-1$ words are treated as equivalent, the word-based n -gram probability is approximated as below:

$$P(w_i|w_1, \dots, w_{i-1}) \approx P(w_i|w_{i-n+1}, \dots, w_{i-1}) \quad (1)$$

In general, the word-based n -gram LM is easy and efficient for training from a corpus of millions of words.

However, building an LM gives rise to two problems: excessive memory requirement and data sparsity. For a trigram with a 65 k word vocabulary, we must be able to produce probabilities for $2.2 * 10^{14}$ possible different sequences. If the probability for each sequence requires 4 bytes, then the total required memory for the trigram LM would be $8.8 * 10^{14} = 880$ TB. Such a large amount of data cannot be stored in a single server. The other key issue concerns handling data sparsity while maintaining accurate word predictions. An hour-long English broadcast news program contains approximately 10 k words. If all the words from one channel are transcribed for one year, 24 h a day, we obtain $10 \text{ k} * 24 * 365 = 8.7 * 10^7$ trigram sequences. It is impossible to collect such a large amount of data for training a text corpus. As a result, the vast majority of trigram sequences are not observed in training the text corpus.

One way to solve this problem is through LM adaptation. In LM adaptation, a background LM is adapted to a domain-specific model so that the adapted model can match the lexical information in the test data [1]. Advances in social networking services have led to the generation of large text corpora. For example, Twitter creates 200 million texts every day [2]. For such a large text corpus, it is impossible to adapt an LM within 24 h on a single server. Thus, we focus on cloud computing, which has successfully performed large-data processing.

In this study, we build a large-scale language model for daily-generated large-size text corpora using Hadoop in a cloud environment and performed trigram

count extraction using Hadoop MapReduce to adapt our large-scale language model.

The paper is organized as follows: Sect. 2 discusses studies related to LM adaptation methods. In Sect. 3, we describe a method of implementing a large-scale LM and trigram count extraction for LM adaptation. In Sect. 4, we evaluate our system in a cloud environment, and in Sect. 5, we conclude this paper.

2 Related Works

LM adaptation methods have been explored to resolve domain mismatch problems. In LM adaptation, a background LM is adapted to a domain-specific model so that the adapted model can match the lexical information in the test data.

Figure 1 shows the general framework of LM adaptation. In Fig. 1, Co_B is a large background corpus and Co_A is the small-size domain corpus. LM_A is the adapted LM and LM_B is the background LM. The fundamental concept of LM adaptation is based on the maximum a posteriori (MAP) estimation and involves combining Co_B and Co_A at the frequency count level rather than the model level [3]. The goal of minimum discrimination information (MDI) adaptation is to find an LM_A whose probability distribution satisfies the specific constraints derived from a small domain corpus and that has the minimal discrimination information with the background LM [4]. However, previous research has focused on LM adaptation performed on a single server.

Conventionally, an n -gram LM is represented by a flat text format (e.g., the ARPA format) or a tree-bucket format. Because the typical sizes of the above two file formats are very large, LM compression has received considerable attention from the speech recognition community. In general, LM compression is carried out by pruning and quantizing the floating-point components of the LM.

As cloud services become more affordable, it is better to implement an LM over multiple servers rather than on a single server with LM compression. However, to the best of our knowledge, the implementation details for LM over multiple servers have not yet been published.

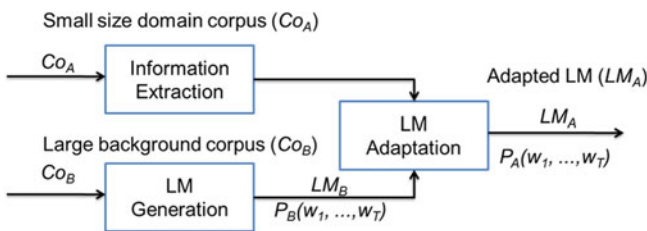


Fig. 1 General framework of LM adaptation

3 System Design

This section presents the design of the system of a large-scale LM and trigram count extraction which is a part of LM adaptation.

3.1 Design of a Large-Scale Language Model Using a Distributed Storage System

This section describes our proposed approach for the implementation of a large-scale n -gram LM using a distributed storage system. The design should meet the following objectives:

- Scalability over increasing training data size: Our training corpus for the background LM is 1 trillion word tokens of text from publicly accessible web data collected by Google. We use Twitter texts as LM adaptation data—200 million texts are created in a day. The size of the LM training corpus increases whenever an LM adaptation is performed.
- Time complexity for search and update operations: An efficient data structure, such as search or update from the perspective of metadata for the entire table, should be devised and implemented for main operations. A representative data structure is a B+ tree.
- Data sparsity characteristic of LM: One of the most representative speech recognition systems, hub4, has a 65 k word vocabulary. This vocabulary generates $2.7 * 10^{14}$ different word sequences, out of which only 0.00001 % of the different word sequences are observed in the training data.

The above three aspects match well with the design objectives of BigTable [5], which was developed by Google for the management of structured data that are too massive to be stored on a single server. BigTable is a distributed storage where a big table is split into small tables, which are stored on multiple servers.

BigTable has a general master–slave configuration, where slaves are called tablet servers. The master server manages tablet servers using Chubby. Each tablet server has its own UserTable. The location of this table is maintained as a three-level hierarchy analogous to that of a B+ tree. In a B+ tree, insertion, deletion, search operations are accomplished at $O(\log n)$ time.

The root tablet contains the location of all tablets in a special METADATA table. Each METADATA tablet contains the location of a set of user tablets. The METADATA table stores the location of a tablet under a row key, which is an encoding of the tablet's table identifier and its end row. When a row key is searched by a user request, BigTable first seeks the location of the ROOT tablet on a Chubby file. Then, BigTable detects the location of the METADATA tablet from the root tablet, whose range corresponds to the requested row key. Similarly, BigTable finds the location of UserTable containing the row key from the

METADATA tablet. Next, BigTable returns the value associated with the row key within UserTable.

During data insertion of a pair of (row key, value), the location of UserTable is determined by the same procedure as for the search of the row key. Next, a node with the pair is added at the location of UserTable. Each pair of (row key, value) is stored in a node of a linked list. All nodes in this linked list are sorted according to the row key.

Since BigTable supports distributed storages and data insertion within $O(\log n)$ time, BigTable satisfies the first two design objectives: scalability over increasing training data size and time complexity for search and update operations.

Compared to relational databases, BigTable has a simple schema, which consists of only a row key and column family. BigTable is referred to as a non-relational database. Non-relational databases do not have the features of relational databases, such as data integrity and reliability. In a relational database, the storage overhead increases owing to the complex schema required to ensure data integrity and reliability in sparse data processing. As data become sparser, the ratio of the schema storage overhead to LM data storage increases rapidly. Missing an element in an LM adversely affects the generation of a word and the consecutive words. Therefore, it is unnecessary to use such an excessive storage in LM to ensure data integrity and reliability. For this reason, the BigTable is suitable for the structure of an LM having a data sparsity characteristic.

Our large-scale LM was implemented on the Amazon Elastic Compute Cloud (Amazon EC2) [6] service with the use of Hbase [7], which is an open-source project of BigTable. Amazon EC2 is a platform as a service that provides scalable computing capacity in a cloud environment. In Hbase, our large-scale LM was implemented as a table which uses a trigram tuple as a key and a trigram count as a value. These counts are extracted from 800 million trigram tuples in ‘Web 1T 5-gram Version 1’ [8]. The implementation details are described in [Sect. 4](#).

3.2 Trigram Count Extraction Using MapReduce

In order to extract trigram counts from daily generated large size texts within a limited amount of time, distributed processing on a cloud environment is required. One of the most representative distributed processing methods is MapReduce [9]. MapReduce is a simple programming model for processing massive numbers of datasets on a commodity server cluster using a distributed computing framework. we performed trigram count extraction using MapReduce.

Figure 2 presents the concept diagram of MapReduce for trigram count extraction. The first step is to split the entire domain corpus into DataNodes. The next step is to run the map function on each DataNode. Several map functions can be run concurrently on a DataNode. A map function reads one text line from the part of the domain corpus dedicated to the corresponding DataNode. The map function finds all the trigrams generated from the text line and displays their

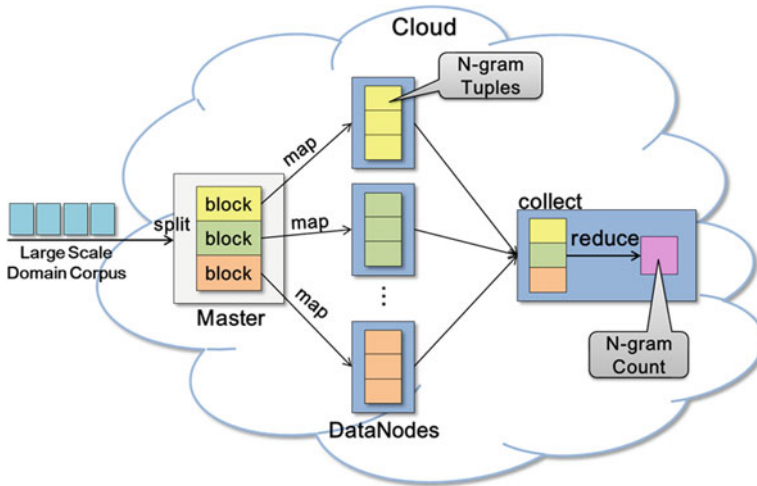


Fig. 2 Conceptual diagram of mapreduce in trigram count extraction

counts. The key is a group of three words in a trigram, and the value is the trigram count. In the final step, the MapReduce framework collects the outputs of all the map functions. The reduce function adds all values related to the same key, and creates a new pair with the key and the sum of values, which is the corresponding n -gram count for the entire domain corpus. We implemented the above of Map and Reduce functions on Hadoop [10] MapReduce framework. Hadoop is an open-source project by Apache for providing distributed computing infrastructure.

4 Evaluation

We implemented our large-scale LM and trigram count extraction on the Amazon EC2 service. Amazon EC2 is a platform as a service that provides scalable computing capacity in a cloud environment. Amazon EC2 has two main advantages. First, it reduces the time required to obtain and boot new server instances to a couple of minutes, allowing a system to quickly scale up or down its capacity according to the computing requirements. Second, it provides a reference testing environment for LM adaptation.

In our evaluation, we used high-CPU extra-large instances. Each instance utilized 7 GB of memory, 20 EC2 compute units, and 1.69 TB of storage. One EC2 compute unit provides an equivalent CPU capacity of a 1.0–1.2 GHz 2007 Opteron or 2007 Xeon processor. This type of instance is a recommended configuration for running an Hbase. Evaluations were carried out using Hadoop-1.0.1 and Hbase-0.92.1 on Ubuntu 11.10 on each Amazon EC2 instance. The setup

parameters for Hadoop MapReduce were assigned according to the default configuration, except for the maximum number of map tasks per node, which was set to four based on the limit of the computation power of an instance.

4.1 Performance Evaluation

Ultimate goal of our research find the optimal number of amazon EC2 instances in the LM adaptation under the time constraint that the Twitter text data generated daily should be processed within one day. The processes in LM adaptation are divided into trigram count extraction and model update. This paper focuses on the analysis of the required amount of processing time in trigram count extraction according to the size of the Twitter text and the number of Amazon EC2 instances.

The size of available Twitter texts was about 6.8 GB, which is approximately 30 % of the Twitter texts (21 GB) generated daily. Hence, we analyzed the correlation between the amount of data and the processing time in trigram count extraction with a fixed number of instances for the available data. Then, the processing time was estimated for the entire amount of daily-generated Twitter texts.

Figure 3 shows the results of our analysis. The diamond-shaped points depict the pairs of (amount of data, processing time) when the number of instances is two. Although the diamond points in Fig. 3 are sparse, it appears that the processing time increases linearly with increasing amount of data. The upper line with diamond-shaped points in Fig. 3 is the line-of-best-fit for the results at two instances, as estimated by the least-squares method (LSM). This line fits the data very well. The R square value is calculated to be 0.998. It appears that the processing time increases by about 732 s per 1 GB of additional Twitter texts. This positive correlation is also observed for different numbers of instances. If the horizontal scalability is guaranteed according to the number of instances in the distributed processing for trigram count extraction, then the slope of the line-of-best-fit is inversely proportional to the number of corresponding instances.

According to Fig. 3, as the number of instances increases, the slope of each line-of-best-fit is decreased. However, they are not inversely proportional. When the number of instances is four (second upper line with square-shaped points), the processing time increases by about 601 s per 1 GB of additional Twitter texts. This is due to that map functions are executed on multiple instances by maintaining data locality, but network overhead is incurred during the reduce phase when one instance collects the results of the map functions. Consequently, the advantages of distributed processing are diminished as the number of instances increases.

Based on the linear correlation between the amount of data and the processing time derived from Fig. 4, we estimated the required time to process 21 GB of data by varying the number of instances between 2 and 16. Figure 4 presents the estimated amount of time according to number of instances. We found that fewer than 3 h are required to process 21 GB when the number of instances is six. Even when the number of instances is two, it is expected that 4 h are sufficient to process 21 GB.

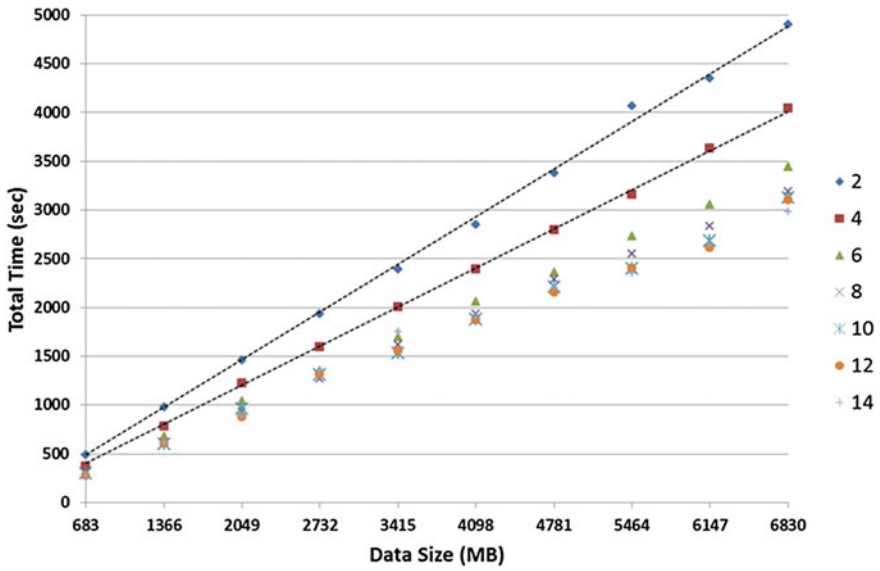


Fig. 3 Processing time of trigram count extraction according to twitter texts data size

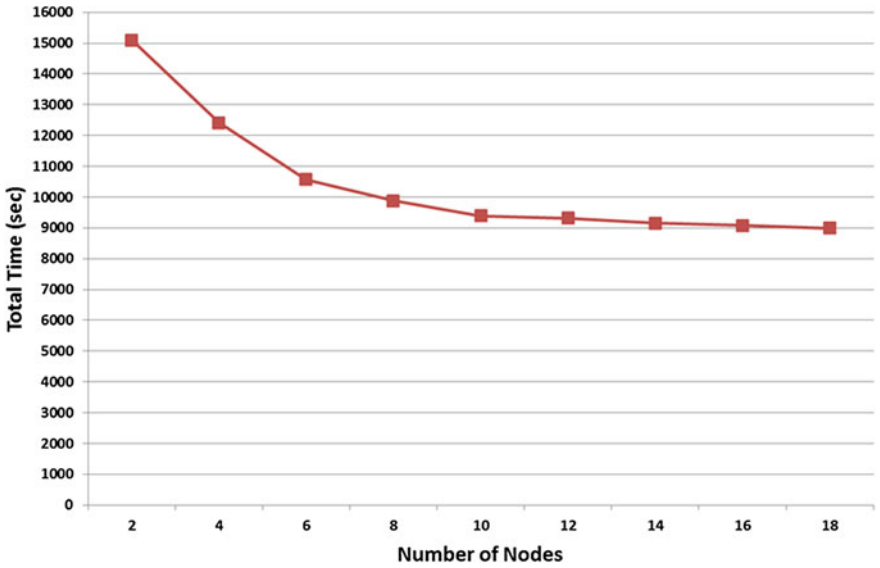


Fig. 4 Forecasted processing time of trigram count extraction for 21 GB twitter texts by using LSM

Considering the time constraint (24 h) for completing LM adaptation, the time required for trigram count extraction does not constitute a substantial portion. Therefore, the optimal number of instances should be determined by considering the required time in model update according to the number of instances.

5 Conclusion

In this paper, we presented a large-scale language model, consisting of 800 million trigram counts, using Hbase in Amazon EC2 and performed trigram count extraction using Hadoop MapReduce to adapt our large-scale LM.

For trigram count extraction, we found that fewer than 3 h are required to process daily-generated Twitter texts when the number of instances is six. Considering the time constraint for completing LM adaptation, the time required for trigram count extraction does not constitute a substantial portion.

The optimal number of instances should be determined by considering the required time in model update. This optimal number will be investigated as a future work.

References

1. Bellegarda J (2004) Statistical Language Model Adaptation Review and Perspectives. *Journal of Speech Communication* 42:93–108
2. Million tweets per day (2011). <http://blog.twitter.com/2011/06/200-million-tweets-per-day.html>
3. Masataki H, Sagisaka Y, Tawahara T (1997) Task adaptation using MAP estimation in N-gram language model. In: *Proceedings of international conference on acoustics, speech, and signal processing*, pp 783–786
4. Pietra S, Pietra V, Mercer R, Roukos S (1992) Adaptive language modeling using minimum discriminant estimation. In: *Proceedings of international conference on acoustics, speech, and signal processing*, pp 633–636
5. Chang F, Dean J, Ghemawat S, Hsieh W, Deborah A, Wallach B, Chandra T, Fikes A, Gruber R (2006) BigTable: A distributed storage system for structured data, *operating systems design and implementation'06*, Seattle
6. Amazon Elastic Compute Cloud (Amazon EC2), <http://aws.amazon.com/ec2/>
7. Welcome To Apache HBase, <http://Hbase.apache.org>
8. Web 1T 5-gram Version 1, <http://www ldc.upenn.edu/Catalog/CatalogEntry.jsp?catalogId=LDC2006T13>
9. Dean J, Ghemawa S (2004) MapReduce: Simplified data processing on large clusters, *operating systems design and implementation'04*, Google labs pp 137–150
10. Shvachko K, Kuang H, Radia S, Chansler R (2010) The hadoop distributed file system, *mass storage systems and technologies*

Speed Control Using a PID Algorithm for an Educational Mobile Robot

Se-Young Jung, Se-Jun Park, Yong-Ho Seo and Tae-Kyu Yang

Abstract In this paper, we propose a new method using the PID controller gain value from rotation of wheels according to rotation momentum characteristics for an educational mobile robot. P-Gain, I-gain and D-gain have been changed from the mobile robot via wireless remote control in a real-time basis. The transmitted gain value is calculated by real-time operation of embedded software in the robot. Experiments are carried out to find the optimized gain value of two conditions, maximum speed and minimum speed. The gain of intermediate velocity region is calculated from this gain value using primary curve fitting. The intermediate region gain value is calculated by real-time transmission of the mobile robot. Successful results are demonstrated with PID control using the calculated intermediate region gain value.

Keywords PID control · Variable PID gain tuning · Educational mobile robot

1 Introduction

Many mobile robots use a PID-control algorithm for position control or velocity control. These are important algorithms in mobile robots for travelling to a desired location and for desired velocity control. The PID-control algorithm is a traditional

S.-Y. Jung · S.-J. Park · Y.-H. Seo · T.-K. Yang (✉)
Department of Intelligent Robot Engineering, Mokwon University,
Mokwon Gil 21, Seo-gu, Daejeon, Republic of Korea
e-mail: tkyang@mokwon.ac.kr

S.-J. Park
e-mail: sjpark@mokwon.ac.kr

Y.-H. Seo
e-mail: yhseo@mokwon.ac.kr

control algorithm [1]. Many robots use PID-control algorithms in various fields such as industry, medicine, and automation systems. The reliability of PID-control depends on how the PID set gain value is selected [2, 3].

A PID-control algorithm that is tuned by an inaccurate gain value does not converge to the goal point. For this reason, many research groups have sought methods to find a stable gain value [4]. But it is not easy to find the stable gain. For example, physical movement momentum is not stable while velocity is changing.

In this paper, we define the values of both the maximum and minimum speed. An intermediate value is also calculated by primary curve fitting on two different gains. The intermediate gain value is obtained by experiments using a PID-controller on a mobile robot, CRX10. The mobile robot can consequently move with precise accuracy by the variable PID gain value. The variable PID gain value can be configured by a PC or smart-phone through wireless communication. The gain value will be reflected in real-time on a mobile robot in a PID control loop and controlled. The software used in the experiment was created on Visual Studio C# language base in .Net Frameworks 3.0 [5]. The mobile robot used in the experiments is CNROBOT's CRX10. Connection between the mobile robot and PC is by Bluetooth [6].

2 Mobile Robot Platform

2.1 General Feature CRX10

CRX10 of CNRobot uses Bluetooth communication as a wireless interface with an Android-based smart-phone, smart pad, or desktop. It sends sensor information and receives a set value on a real-time basis. The communication speed between the mobile robot and the PC is 119600 bps and the signal of the mobile robot is transmitted at a speed of 30 ms per packet. In addition, two-way communication is possible within 100 m. The appearance of the mobile robot platform is shown in Fig. 1 and its key specifications are listed in Table 1.

Fig. 1 Appearance of the mobile robot platform, CRX10



Table 1 Hardware specifications of the mobile robot platform, CRX10

H/W item	Specification
Microcontroller	ATmega128 (main), ATmega88 (sensor)
Wheel	Four wheels driven by two DC motors
Display	8 × 8 LED dot-matrix
Sensor	PSD sensor—3EA Flower IR sensor—7EA Magnetic encoder—2EA Bumper sensor—3EA
Communication	Bluetooth 2.4Gh/Serial RS232
Transport speed	MAX. 1 m/s
Battery/Run time	Li-ion cell 11.1 V 2600 mA/up to 4 h
Charging time	2.5 h

2.2 Hall Sensor Signal and Microcontroller Interrupt Connection

CRX10 has two brush type motors and a magnet hall sensor type encoder. Signals A and B are generated from the magnetic hall sensor by motor rotation. Channel A is higher than channel B when the motor rotation is in the forward direction. In contrast, the channel B signal becomes higher than that of channel A when the motor is moving in the reverse direction. Sixteen square wave outputs are generated by motor rotation and the magnet hall sensor for each channel.

The magnet hall sensor signal output timing chart is shown in Fig. 2. Equation (1) is used to compute the hall sensor output according to the position of the motor phase difference.

$$\Delta\Phi = \left| 90^\circ - \frac{\Phi}{P} \times 180^\circ \right| \leq 45^\circ \tag{1}$$

Microcontroller interrupt 0~3 is connected to the hall sensor output and is shown in Fig. 3. The decision of forward or backward direction status is decided from the input 4 channel.

Fig. 2 Magnet hall sensor signal output timing chart

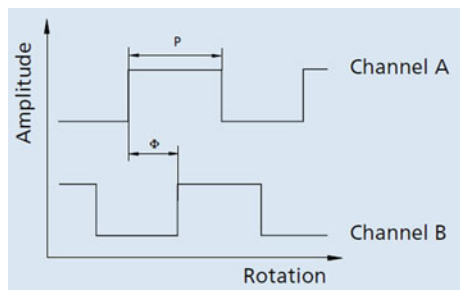
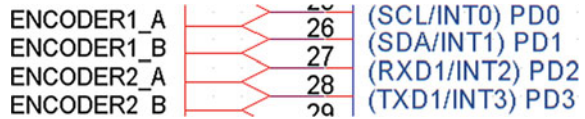


Fig. 3 Connection circuit of between magnet hall sensor output and microcontroller



3 User Interface Design and Variable PID-Control

3.1 Console Software

Figure 4 shows the screen of the main menu of the application to choose the output functions and control types of the mobile robot through real-time Bluetooth data communication after data acquisition.

This program is operated based on .Net Frameworks 3.0. The graph in the middle of the main window displays the current RPM, PID control gain value, RPM error value and the target goal. We can see the value in the PID gain setting scrollbar and change the motor speed for text input to the left in the main graph. Value of various input sensors are displayed at the bottom of the graph and a Dot-matrix setting box and communication setting box are provided for communication connections.

3.2 PID Control Loop in Mobile Robot

A traditional control algorithm [7] is applied to the PID controller. It is delineated by Eq. (2).

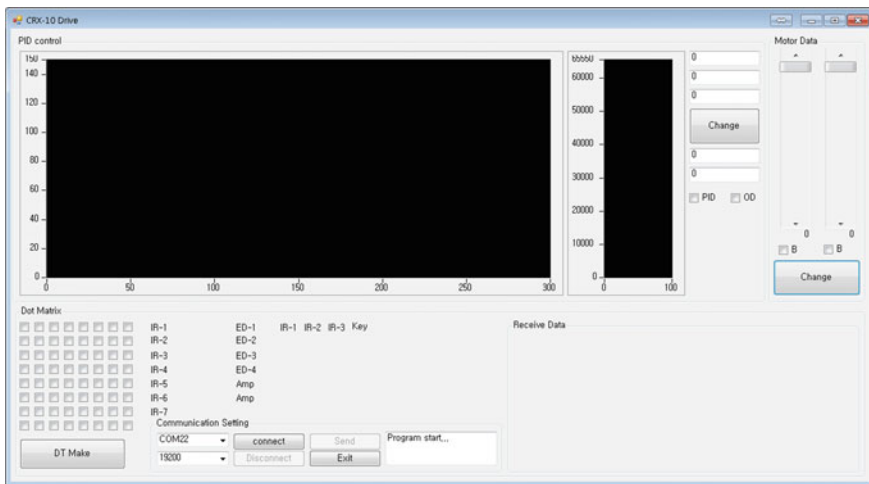


Fig. 4 Console software of mobile robot application for information output and control

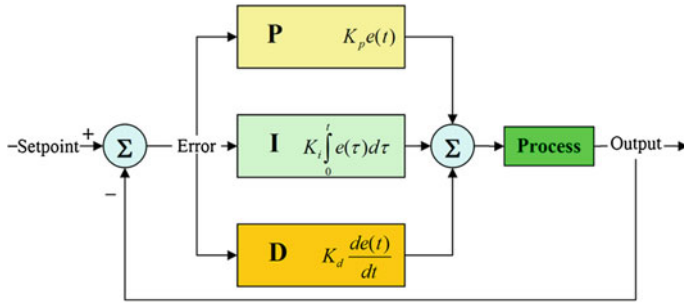


Fig. 5 PID control block diagram

$$MV(t) = K_p e(t) + k_i \int_0^t e(\tau) d\tau + K_d \frac{de}{dt} \tag{2}$$

The goal of the PID control loop is configuration of the number of encoder pulses according to the rotational speed of the motor. The PID controller of the mobile robot is equipped with embedded software. The gain value is transferred to the controller through real-time communication. Gain is applied to the PID controller in mobile robot embedded software. A block diagram illustrating PID control is shown in Fig. 5.

3.3 Variable PID Control Loop in Mobile Robot

Traditional PID control after gain tuning has an inaccurate response due to load change or mechanical characteristics. In this paper, we change the gain value obtained from the traditional PID to improve the accuracy of the PID control while a mobile robot operates. This approach can be summarized as Eq. (3).

$$MV(t) = K'_p e(t) + K''_i \int_0^t e(\tau) d\tau + K'''_d \frac{de}{dt} \tag{3}$$

The PID control loop cycle and update for the error value are controlled in 30 ms. We calculate the mid-point value using first order curve fitting by PID gain tuning. The result is divided into minimum speed and maximum speed.

Table 2 PID gain table for variable gain

Gain	Maximum speed	Minimum speed
K_p	0	0.1
K_i	0.001	0.2
K_d	0.001	0.1

4 Experimental Results

4.1 Tuning for Variable PID Gain Value

We divided the speed into low and high level for PID gain tuning, and calculated a mid-point value using primary curve fitting. CRX-10 has a maximum speed at 112 pulse output of 30 ms, and the wheel output pulse tuning has a minimum speed at 12 pulse output of 30 ms. The optimized gain values ' K_p , K_i , K_d ' are '0, 0.001, 0.001' and 0.01, 0.2, 0.1, respectively, where the highest speed is obtained at the optimized gain value, as shown in Table 2.

4.2 Experiments at the Gain Change

This experiment yields different results due to different gain values. In this case of maximum speed tuning, the gain value did not converge on the minimum speed. The minimum speed tuning gain also similarly did not converge at maximum speed as shown in Table 3.

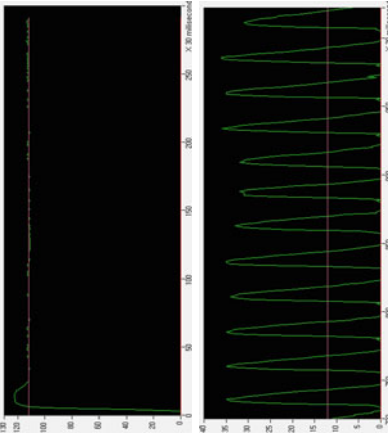
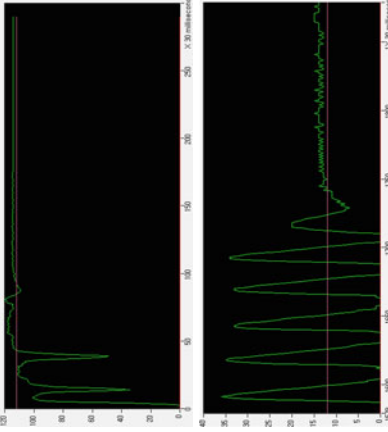
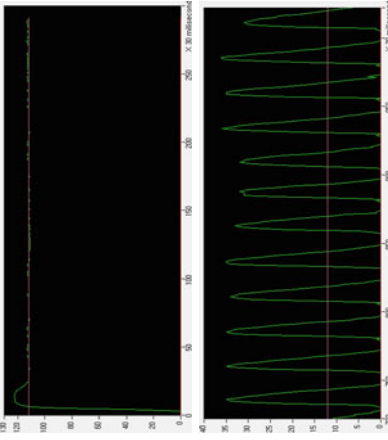
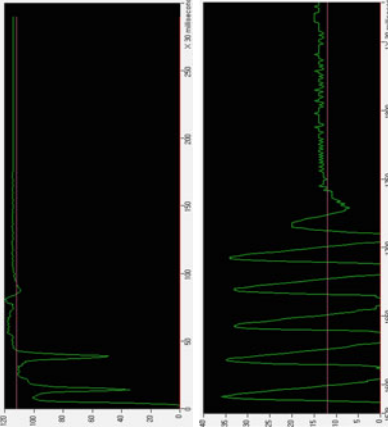
Calculated for gain by the primary curve fitting, the mid-setpoint gain shows better performance than the maximum and minimum tuning gain values. This setpoint is 55 pulse per 30 ms and ' K_p , K_i , and K_d ' are calculated as '0.05, 0.1, and 0.5,' as shown in Fig. 6

4.3 Result

In the experimental result, there was a deviation of PID control. The gain tuned at maximum speed does not converge in the minimum speed set. Similarly, the gain tuned at minimum speed does not converge in the maximum speed set.

From these results, the mobile robot requires different gain for different goal speeds. Stable control is confirmed when using an intermediate value for PID-control in the mobile robot obtained by the results calculated from the first order fitting curve.

Table 3 Results according to speed and gain

Gain value target speed	Maximum speed tuning gain	Minimum speed tuning gain
112 pulse per 30 ms		
12 pulse per 30 ms		

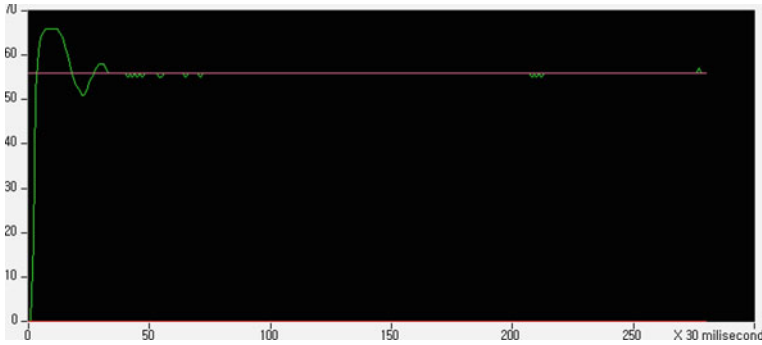


Fig. 6 Console software of mobile robot application for information output and control

As a result, as shown in these experiments, the PID controller has problem because of fixed gain. However, we demonstrated that using more than a PID gain can provide more accurate control.

5 Conclusion

We proposed a method to remotely turn PID gain by using a desktop computer, and calculated an intermediate value for PID-control. The intermediate value was calculated from two gains. The first gain value was tuned at maximum velocity. And the other gain value was tuned at minimum velocity. The intermediate value was calculated from the first order curve fitting method. We performed experiments to obtain accurate gain for PID-control.

We can apply variable PID-control to the mobile robot. In addition, we conducted an actual experiment using CRX10 to evaluate the performance of the proposed control method. Variable PID-control was applied for mobile robot control. The obtained results confirmed that it is possible to control a mobile robot by the variable PID-controller.

Lastly, the PID results differed according to the various situations in our experiment. Therefore, to obtain better performance, it would be effective to use intermediate values computed by a different control algorithm such as adaptive control or a neural networks.

Acknowledgments This work was supported by the Basic Science Research Program through the National Research Foundation of Korea (NRF) funded by the Ministry of Education, Science and Technology (MEST) (2011-0013776). This work was also supported by the Prevention of Disaster with Information Technology Center of Mokwon University through the Regional Innovation Center Program (RIC) funded by SMBA of Republic of Korea.

References

1. Isaksson AJ, Graebe SF (1999) Analytical PID parameter expressions for higher order systems. *Automatica* 35:1121
2. Chen D, Seborg DE (2002) PI/PID controller design based on direct synthesis and disturbance rejection. *Ind Eng Chem Res* 41:4807–4822
3. Skogestad S (2003) Simple analytic rules for model reduction and PID controller tuning. *J Process Control* 13:291–309
4. Ryu J-C, Agrawal S, Franch J (2008) Motion planning and control of a tractor with a steerable trailer using differential flatness. *ASME Trans J Comput Nonlinear Dyn* 3(3):031 003.1–8
5. Microsoft Developer network. <http://msdn.microsoft.com/en-en/vstudio/hh341490>
6. CNRobot Inc. <http://www.cnrobot.co.kr>
7. Bonvin D, Srinivasan B, Hunkeler D (2006) Control and optimization of batch processes. *IEEE Control Syst Mag* 26:34–45

Performance Analysis of Noise Robust Audio Hashing in Music Identification for Entertainment Robot

Namhyun Cho, Donghoon Shin, Donghyun Lee, Kwang-Ho Kim,
Jeong-Sik Park, Myoung-Wan Koo and Ji-Hwan Kim

Abstract Many technical papers have been published related to music identification. However, most of these papers have focused on describing their algorithms and their overall performance. When music identification is applied to embedded devices, the performance is affected by the level of frame boundary desynchronization, environmental noise, and channel noise. This paper presents an empirical performance analysis of music identification, in terms of its Peak Point Hit Ratio (PPHR). In theory, music identification systems guarantee a 100 % accurate PPHR between the queried music and its reference. However, PPHR falls to 40.8 % by desynchronization when a frame boundary is desynchronized by half the frame shift. In addition, due to environmental noise, PPHR decreases to 69.6, 59.4, 46.1, and 24.3 % at SNR 15 dB, 10 dB, 5 dB, and 0 dB, respectively. For music clips recorded in an office environment, PPHR is 58.7 % due to environmental and channel noise.

N. Cho · D. Shin · D. Lee · K.-H. Kim · M.-W. Koo · J.-H. Kim (✉)
Department of Computer Science and Engineering, Sogang University, Seoul, South Korea
e-mail: kimjihwan@sogang.ac.kr

N. Cho
e-mail: cnh2769@sogang.ac.kr

D. Shin
e-mail: donghoon@sogang.ac.kr

D. Lee
e-mail: redizard@sogang.ac.kr

K.-H. Kim
e-mail: kimkwangho@sogang.ac.kr

M.-W. Koo
e-mail: mwkoo@sogang.ac.kr

J.-S. Park
Department of Intelligent Robot Engineering, Mokwon University, Daejeon, South Korea
e-mail: parkjs@mokwon.ac.kr

Keywords Music identification · Performance analysis · Audio hashing · Desynchronization · Environmental noise · Channel noise

1 Introduction

Interest in music recognition has been growing dramatically after successful releases of embedded applications. The representative applications such as Shazam and Gracenote are based on audio fingerprinting [1]. These types of music recognition applications work in several ways either based on an audio fingerprint generated by changes in energy across consecutive bands [2, 3] or based on hash keys generated by peak points [4]. The latter is more robust and able to withstand environmental noise [5].

The latter system successfully recognizes the queried music file if hash key accuracy of the queried music compared with the reference music is greater than that compared with the best candidate.

According to our experiments, the average of the hash key accuracy of the queried music file compared with the best candidate is measured at about 3.3 %. This 3.3 % of hash key accuracy can be converted to 18.2 % of peak point accuracy ($3.3 \% = (18.2 \%)^2$), because a hash key consists of two peak points and an exact match of a hash key requires an exact match of two peak points. In theory, Music Identification System (MIS) guarantees 100 % accuracy in identifying the peak points of a queried music and its reference. However, when MIS is applied to embedded devices, performance deteriorates due to (1) desynchronization of the frame starting point, (2) environmental noise, (3) channel noise (the queried music is played on a speaker and recorded using a mobile phone's internal microphone).

In this paper, we examine the amount of degradation caused by the above three factors. In Sect. 2, the MIS algorithm based on hash key generation between peak points is summarized. In Sect. 3, each factor is described and analyzed. In Sect. 4, we conclude this paper.

2 Related Works

This paper introduces the music-identification algorithm described in [4]. This algorithm is based on hash key generation at peak points.

2.1 Peak Point Generation

Overlapping frames are generated by segmenting audio signals. Spectrogram is created by performing a Fourier transform on every frame. A point in a spectrogram is a candidate for comparison if it has more energy than any of its neighbors. Generated peak points are robust in the presence of noise that is linearly superimposed [6]. In this paper, 1,024 sample-length frames are generated with an overlap of 160 samples, 1,024 FFT points are used, and the size of region is configured as 9×9 .

2.2 Strategy to Reduce the Number of Peak Point Combinations

In order to reduce the number of combinations, only a part of peak points are allowed to be combined with the peak points in their corresponding target zones. These are called anchor points. In this paper, top N peak points with high energy every second are chosen as anchor points. Each anchor point has a unique target zone. A target zone is defined as a square area, whose width is TL and height is FL . TD is the distance from an anchor point to a target zone. Hence, the total number of combinations of peak points is reduced into the multiplication of the total number of anchor points and the average number of peak points in their corresponding target zones. In our experiment, 100, 1, 100, and 25 are assigned for N , TD , TL , and FL , respectively.

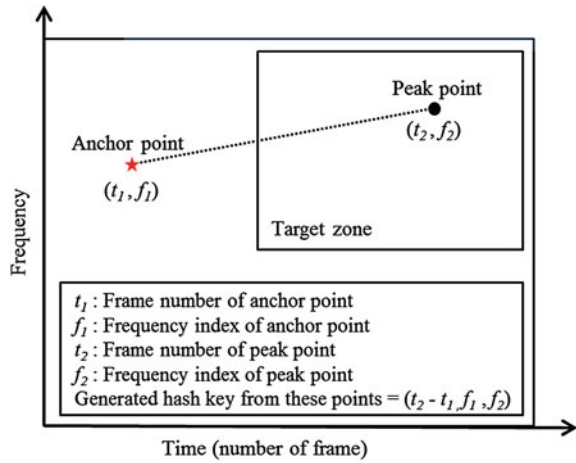
2.3 Hash Key Generation

A hash key is generated from each pair of anchor points and peak points in their corresponding target zone. A hash key contains three components: the time difference between the two points, and the frequencies of two points. Figure 1 shows the concept diagram of a hash key generated from an anchor point (t_1, f_1) and a peak point (t_2, f_2) . From these points, a hash key $(t_2 - t_1, f_1, f_2)$ is generated.

2.4 Searching and Scoring

For a queried music clip, hash keys are generated according to the processes described in Sect. 2.1–2.3. These hash keys are compared with the hash keys generated from each music file in a music database. For each music file, the number of hash key hits is counted. If the reference music file is one of the music

Fig. 1 Concept diagram of a hash key generated from an anchor point and a peak point



files in the database, a significant number of counts appear on the reference music file. The music that receives the largest counts is deemed to be the result of music identification.

3 Experiments

Ten thousand music MP3 files were purchased from www.bugs.co.kr, which is one of the most famous online music providers in Korea. Table 1 shows the statistics of the music files according to genre. The music database consists of hash keys generated from the 16 kHz sampled 10,000 PCM music files.

To analyze the system’s performance, we collected two sets of 300 queried music clips. Three hundred music files were randomly chosen from the set of 10,000 music files. The first set consists of 3-second-long clips taken from 1/4 position of each music file. The second set consisted of 10-second-long clips at the same position were recorded in quite office.

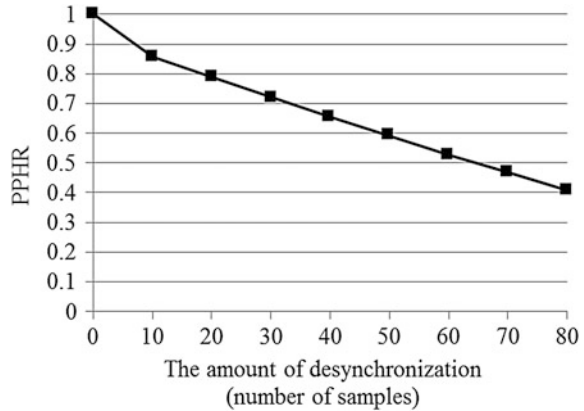
3.1 Desynchronization

Even in the absence of noise distortion, it is unlikely that the frame alignment of the input signal will correspond exactly to the one used to compute the original hash, which is stored in a reference database [7].

Table 1 Statistics of music files according to genre

Genre	K-pop	Pop	Sound-tracks	Classical and jazz	Total
Number of music files	2,900	2,700	2,200	2,200	10,000

Fig. 2 PPHR according to the amount of desynchronization



In order to examine the distortion of the peak point caused by desynchronization, we used the first set of 300 music query files and simulated the amount of desynchronization by shifting the frames up to 80 samples with the increment of ten samples. Figure 2 shows Peak Point Hit Ratio (PPHR) according to the amount of desynchronization. It appears that PPHR degrades linearly as the number of desynchronized samples increases up to 80. The worst case takes place when a clip is desynchronized with a shift of half a frame. In this case, PPHR surprisingly plunges 40.8 %.

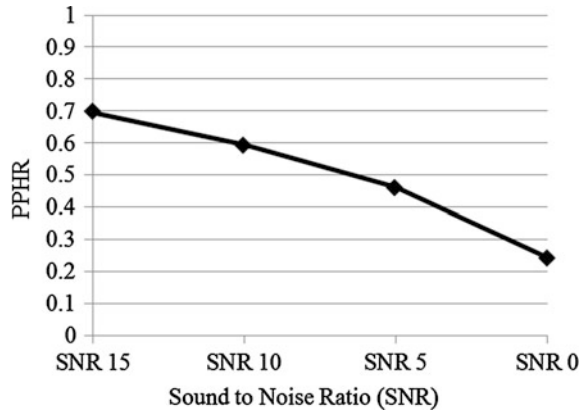
3.2 Environmental Noise

In our study, environmental noise is defined as unpleasant or unwanted ambient sound. In order to examine the effect of environmental noise, we recorded the babble noise at a cafe using an embedded device (iPhone 3GS). We controlled the level of noise in terms of Signal to Noise Ratio (SNR) by mixing the recorded noise with clean music clips. We used the first set of 300 music query files as clean music clips. Figure 3 shows PPHR according to the level of environmental noise. Although the points in Fig. 3 are sparse, it shows that PPHR degrades linearly as the level of noise increases.

3.3 Channel Noise+Environmental Noise

When propagated through a channel, signals are shaped and distorted by the channel's frequency response and attenuating characteristics. In order to examine the effect of channel noise, we used a second set of recorded music clips. These music clips contain three types of noise: channel noise, environmental noise, and

Fig. 3 PPHR according to the level of environmental noise



desynchronization. If the exact amount of desynchronization is known, it can be removed from the clip by shifting the clip by the amount of desynchronization. For all of the recorded music clips in the second set, the best starting point where PPHR is at a maximum is determined and PPHR is measured between each clip and its reference music file. The average PPHR is 58.7 %. This amount of degradation in PPHR is caused by channel and environmental noise. These clips were recorded at SNR 15 dB, and channel noise decreased PPHR by around 10 %.

4 Conclusion

The performance of music identification is empirically analyzed. De-synchronization, environmental noise, and channel noise are addressed as the main factors that affect performance.

According to experiments, PPHR is 58.7 % for music clips recorded in an office environment (environmental noise + channel noise). In addition, PPHR falls to 40.8 % when the frame boundary is desynchronized by as much as half the frame shift. If all of these factors affect the system together, the peak point accuracy between the queried music and its reference drops to 23.9 %, which only differs by 5.7 % from 18.2 % (the average of peak point accuracy between the queried music and the best reference, explained in Sect. 1). If the system is used in a situation with extreme environmental noise (such as SNR 0 dB), the performance of the system becomes unreliable.

Acknowledgments This work was supported by the National Research Foundation of Korea (NRF) grant funded by the Korea Government (MEST) (2010-0004522).

References

1. Cano P, Batlle E, Kalker T, Haitsma J (2005) A review of audio fingerprinting. *J Signal Process Syst* 41:271–284
2. Haitsma J, Kalker T (2002) A highly robust audio fingerprinting system. In: *Proceedings of the international symposium on music information retrieval (ISMIR)*, pp 144–148
3. Haitsma J, Kalker T, Oostveen J (2001) Robust audio hashing for content identification. In: *Proceedings of the content-based multimedia indexing*, pp 19–21
4. Wang A (2003) An industrial strength audio search algorithm. In: *Proceedings of the international symposium on music information retrieval (ISMIR)*, pp 7–13
5. Wang Q, Liu G, Guo Z, Guo J, Chen X (2011) Structural fingerprint based hierarchical filtering in song identification. In: *Proceedings of the international conference on multimedia and expo*, pp 1–4
6. Jalabert E, Fabacher E, Guy N, Lizy-Destrez S, Rappin W, Rivier G (2011) Optimization of star search algorithm for ESMO star tracker. In: *Proceedings of the international ESA conference of guidance, navigation and control systems*, pp 1–21
7. Balado F, Hurley N, McCarthy E, Silvestr G (2007) Performance analysis of robust audio hashing. In: *Proceedings of the informational forensics and security*, pp 254–266

Preliminary Experiments of Dynamic Buoyancy Adjusting Device with an Assist Spring

Norimitsu Sakagami, Amira Shazanna Binti Abdul Rahim
and Satoshi Ishikawa

Abstract In this paper, we propose a dynamic buoyancy adjusting device with an assist spring for underwater robot survey. The purpose of this device is to prevent underwater robots from agitating the water and sand during underwater survey and sampling. The proposed buoyancy adjusting device is actuated by an electric motor with a passive spring that provides some assistance to the motor. The assist spring supports actuator torque and allows low gear. As a result, the proposed device would achieve better energy efficiency and higher speed for dynamic control. To evaluate the performance of the proposed device, we designed and developed a dynamic buoyancy adjusting device as a prototype. Preliminary experiments indicate that the proposed device could be used for dynamic control of underwater robots.

Keywords Underwater robot · Dynamic buoyancy control · Assist system

1 Introduction

Small underwater robots are occasionally used for biological and archaeological surveys. In these surveys, it is necessary for underwater robots to move closer to target objects for observation or sampling. In general, thrusters are used for underwater robot locomotion. Thrusters are one of the useful tools for underwater robots to move

N. Sakagami (✉) · A. S. B. A. Rahim
Department of Navigation and Ocean Engineering, Tokai University,
3-20-1, Orido, Shimizu-ku, Shizuoka 424-8610, Japan
e-mail: sakagami@scc.u-tokai.ac.jp

A. S. B. A. Rahim
e-mail: 9aku1116@mail.tokai-u.jp

S. Ishikawa
Research Institute for Humanity and Nature, 457-4, Kamigamo-motoyama,
Kita-ku, Kyoto 603-8047, Japan
e-mail: oounagi@chikyu.ac.jp

efficiently. Therefore, a lot of Remotely Operated Vehicles (ROVs) and Autonomous Underwater Vehicles (AUVs) employ thrusters as a locomotion device. Thrusters are useful for positioning underwater robots [1, 2]. Several researchers also use thrusters to change the robot's attitude [3, 4] as well as locomotion.

On the other hand, other researchers proposed and developed other locomotion devices for underwater robots based on volume change (buoyancy control). Shibuya et al. developed a biology-inspired underwater robot that installs buoyancy control devices inspired by the sperm whale hypothesis [5]. These devices include paraffin wax that changes the volume by heating or cooling. Wasserman et al. [6] developed a dynamic buoyancy system using a variable ballast tank. Buoyancy control devices are also used for underwater gliders [7, 8] and disk-type underwater robot [9].

In this paper, we developed a mechanical piston cylinder that changes its volume by an electric motor. Generally, mechanical piston cylinders have simple structures that consist of actuators, high ratio gearboxes, and waterproof cylinders. The high ratio gearboxes are used to counter the force applied by high water pressure. However, the high ratio gearbox makes it difficult for the buoyancy control device to move quickly. To overcome such difficulty, we propose a dynamic buoyancy adjusting device (DBAD) that is actuated by an electric motor with an assist spring. The assist spring allows a lower gear ratio, because the spring provides some assistance to the motor. To evaluate the performance of the proposed device, we developed a DBAD as a prototype in this paper.

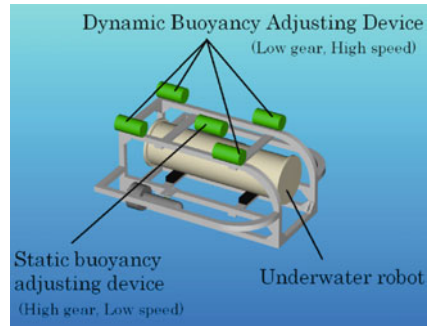
The outline of this paper is the following: the motivation and concept in this paper is described in Sect. 2. In Sect. 3, the design and development of a prototype DBAD is presented briefly. The specifications of the developed DBAD are also described. Section 4 presents a description of several preliminary experiments that were conducted to assess the performance of the developed DBAD. The experimental results indicate that the developed device is promising for dynamic control of underwater robots.

2 Motivation and Concept

Frequent use of thrusters during underwater observations sometimes causes the stirring up of sand from the sea bottom. In such cases, an operator cannot see anything except for sand during observations. In seaweed beds, thrusters may get entangled with seaweed. In some water sampling studies, it is undesirable for thrusters to agitate the water during the sampling. Because of these reasons, we designed and developed a buoyancy adjusting device for dynamic control in this paper.

The proposed DBAD can dynamically change its volume. We aim to use the DBAD to control an underwater robot dynamically. Several buoyancy adjusting devices are attached to an underwater robot, as seen in Fig. 1. This robot has two types of buoyancy adjusting device. One type is a set of the proposed DBADs with a low ratio gearbox and an assist spring. The other buoyancy adjusting device has a

Fig. 1 Concept of use of dynamic buoyancy adjusting device



high ratio gearbox that is required to support the DBADs, because the DBAD which has a low ratio gearbox compresses and works around an equilibrium point where the spring force balances the force due to water pressure acting on the DBAD.

Each device independently changes its volume, and controls the center of buoyancy of the robot and varies the buoyancy force. As the result, the robot can silently move close to target objects without use of thrusters. The proposed device can avoid stirring up sand from the sea bottom, agitating the water during the water sampling, and getting entangled with seaweed.

3 Design and Development of DBAD

We designed and developed a prototype DBAD in order to study its characteristics and potential use. The prototype is to be used in a water tank. Figure 2 presents the three-dimensional design and the developed DBAD. Table 1 shows the principal dimensions of the DBAD.

In the prototype, a servo actuator (Kondo Kagaku Co., Ltd. KRS 786 ICS) drives the DBAD. The output shaft of the actuator is connected to a slide screw (Misumi Co., Ltd., MSSRA824-55-S10-Q6) which transfers reciprocating motion of the

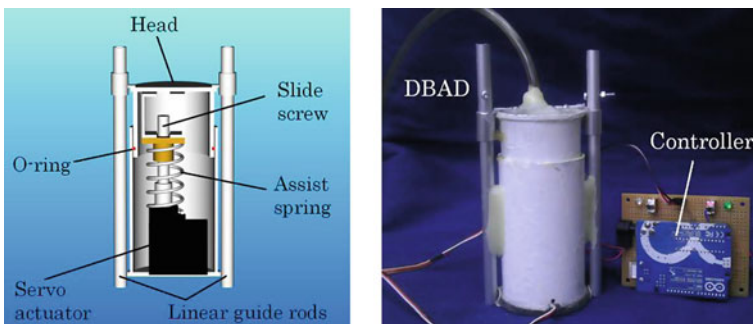
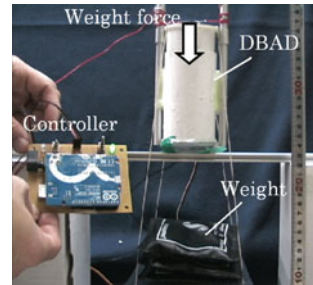


Fig. 2 Design and development of the prototype DBAD

Table 1 Principal dimensions of the prototype DBAD

Dry weight	0.240 kg
Diameter of the head	55 mm
Height	175 mm
Actuator torque	0.8526 Nm
Spring constant	4,600 N/m

Fig. 3 Experimental setup for measuring generative force, speed and electric energy consumption

DBAD head. Though the rotational angle of the actuator was limited from 0 to 180°, we changed the electric and mechanical parts to allow it to rotate unlimitedly. A spring (Accurate Co., Ltd., C280) is located between the servo actuator and the DBAD head to support the actuator. The spring constant is 4,600 N/m. In this prototype, the spring directly counters the force applied by water pressure. The main body of the DBAD is made from polyvinyl chloride pipe and acrylic plate. The electric and mechanical parts are sealed with an O-ring and adhesives. An air hole is placed on the top of the head to allow the DBAD to change its volume easier. The maximum motion distance of the head is set at 25 mm. In terms of volume, it is possible to change its volume of approximately 60 cm³.

The DBAD can be manually or automatically controlled by using a controller which includes a 16-MHz micro-controller, as seen in Fig. 2.

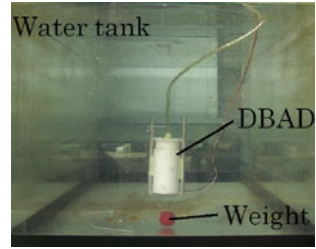
4 Preliminary Experiments

This section presents several experiments that show the performance of the developed DBAD. Here, we present results, comparing the performance of the DBAD with and without the assist spring based on the following aspects: generative force, speed, and electric energy consumption.

4.1 Experimental Setups

Figures 3 and 4 present the overviews of the experimental setups. Figure 3 shows the setup for measuring generative force, speed and electrical energy consumption.

Fig. 4 Experimental setup in a tank



In these experiments, weight forces were applied to the DBAD head instead of static water pressure. A weight force can be converted to a water pressure or a water depth using the head area of the DBAD. Figure 4 presents the experimental setup for underwater testing. An air tube was connected to the air hole on the top of the head to change the volume easily, as seen in Fig. 4.

4.2 Measurement of Generative Force

First, we measured the maximum force generated by the DBAD with and without the assist spring. In the case with the spring, the DBAD was able to lift 8.1-kg of weight which is converted to the water pressure of approximately 0.034 MPa and the water depth of 3.4 m. In comparison, the device without the spring was able to lift 6.3-kg of weight which is converted to the pressure of approximately 0.027 MPa and the depth of 2.7 m. This result indicates that the assist spring supported the servo actuator and increased the generative force by approximately 29 %.

4.3 Measurement of Speed and Energy Efficiency

We also measured the speed and electrical energy consumption of the DBAD to compare the performance with the assist spring to that without the spring. In these experiments, the DBAD moved in a reciprocating motion with amplitude of 0.011 m, and weight forces were applied to the DBAD head instead of static water pressure.

Figures 5 and 6 respectively show the average speeds of the DBAD head when the DBAD expanded in the case with or without the assist spring. The x-axis represents the depth, which is converted from the weight force. The y-axis is the average speed. Each value is the average of five measurements and the error bars indicate the maximum and minimum measured values. The average speeds with the spring were higher than those without the spring. Therefore, these results indicate that the spring supported the actuator when the DBAD expanded.

Figures 7 and 8 show the average speeds of the head when the DBAD compressed. The speeds with the spring were lower than those without the spring,

Fig. 5 Average speed during expansion with the assist spring

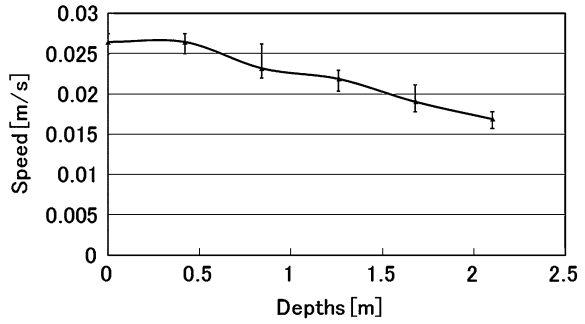
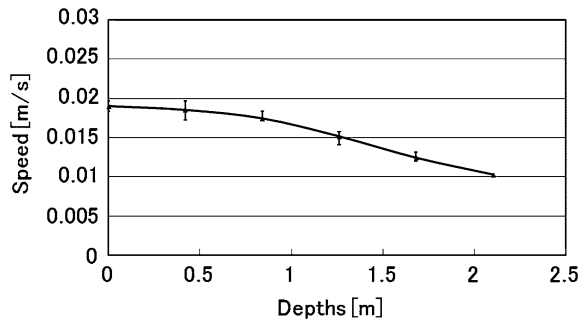


Fig. 6 Average speed during expansion without the assist spring



because the DBAD compressed against the spring force. However, as the depth increased, the speed with the spring also increased. For the dynamic buoyancy control, both expansion and compression must be fast. Therefore, the performance of the DBAD is desirable when the depth increases.

Figures 9 and 10 respectively illustrate the electric energy consumption of the DBAD with and without the assist spring. These results show the DBAD with the spring was more efficient than that without the spring as the depth increased. When the depth was over 2.0 m, the electric energy consumption of the DBAD with the spring was 3 times higher than that without the spring.

Fig. 7 Average speed during compression with the assist spring

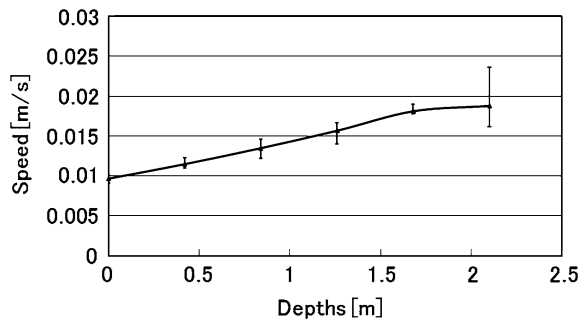


Fig. 8 Average speed during compression without the assist spring

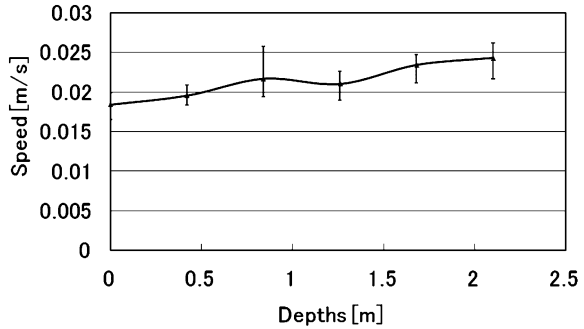


Fig. 9 Electric energy consumption with the assist spring

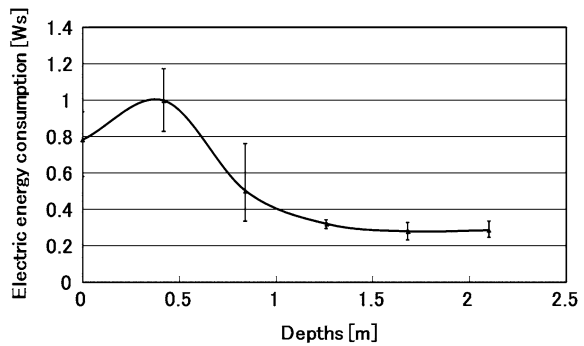
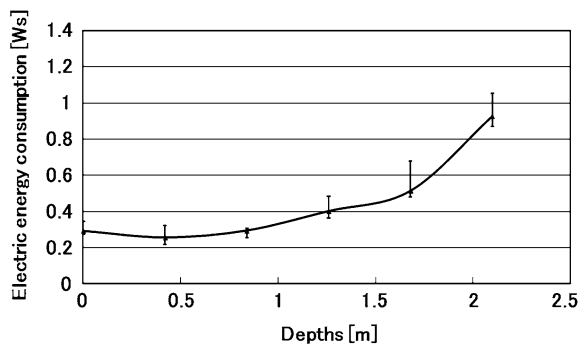


Fig. 10 Electric energy consumption without the assist spring



4.4 Tank Test

We also tested the motion performance of the DBAD in a water tank which has a depth of 0.45 m. The red object in the figure is a weight to immerse the DBAD which has positive buoyancy. Figure 11 illustrates the successive pictures during the motion. The DBAD changed its volume and could repeat the up and down motion in the tank. The average motion speed was approximately 0.1 m/s.

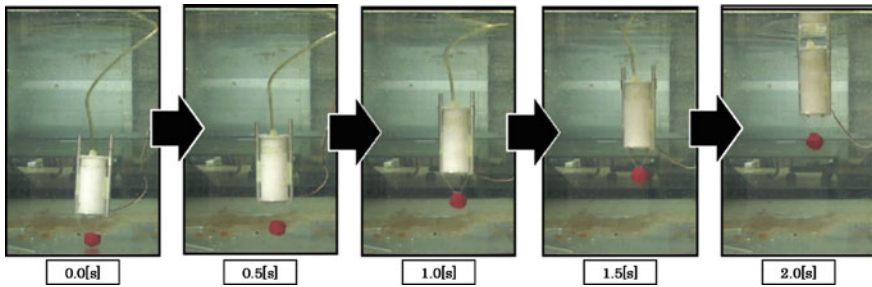


Fig. 11 Motion performance of the DBAD in a test tank

These results demonstrate that the DBAD would be useful for dynamic control of underwater robots.

5 Conclusion

From the experimental results of the developed DBAD, we were able to conclude the following:

- (1) The DBAD with the assist spring as a prototype has been designed and developed.
- (2) The DBAD increased the maximum generative force by 29 % compared with the buoyancy adjusting device without the assist spring.
- (3) The speed of the DBAD head was increased, and the electric energy consumption was reduced by using the assist spring.
- (4) The developed DBAD could change its volume and move up and down dynamically in a water tank. Therefore, we will use the DBAD to implement a dynamic control of underwater robots.

References

1. Riedel JS (2000) Shallow water stationkeeping of an autonomous underwater vehicle: the experimental results of a disturbance compensation controller. In: OCEANS 2000 MTS/IEEE conference and exhibition, vol 2, pp 1017–1028
2. van der Zwaan S, Santos-Victor JDA (2001) Real-time vision-based station keeping for underwater robots. In: OCEANS 2001 MTS/IEEE conference and exhibition, vol 2, pp 1058–1065
3. Whitcomb LL, Smallwood DA (2001) Toward model based dynamic positioning of underwater robotic vehicles. In: OCEANS 2001, MTS/IEEE conference and exhibition, vol 2, pp 1106–1114

4. Doniec M, Vasilescu I, Detweiler C, Rus D (2010) Complete SE³ underwater robot control with arbitrary thruster configurations. In: 2010 IEEE international conference on robotics and automation, pp 5295–5301
5. Shibuya K, Kawai K (2009) Development of a new buoyancy control device for underwater vehicles inspired by the sperm whale hypothesis. *Adv Robot* 23:831–846
6. Wasserman KS, Mathicu JL, Wolf MI, Hathi A, Fried SE, Baker AK (2003) Dynamic buoyancy control of an ROV using a variable ballast tank. In: *Oceans 2003*, vol 5, pp SP2888–SP2893
7. Eriksen CC, Osse TJ, Light RD, Wen T, Lehman TW, Sabin PL, Ballard JW, Chiodi AM (2001) Seaglider: a long-range autonomous underwater vehicle for oceanographic research. *IEEE J Oceanic Eng* 26(4):424–436
8. Arima M, Ishii K, Nassiraei AAF (2011) Development of the ocean-going underwater glider with independently controllable main wings, SOARER. In: 2011 international offshore and polar engineering conference, vol 2, pp 274–278
9. Nakamura M, Koterayama W, Inada M, Marubayashi K, Fukuoka K, Hyodo T (2009) Disk-type underwater glider for virtual mooring and field experiment. *Int J Offshore Polar Eng* 19(1):66–70

Optimization of a Cart Capacity Using the Three-Dimensional Single Bin Packing Problem for a Serving Robot

Ara Khil and Kang-Hee Lee

Abstract Given a set of rectangular-shaped items such as dishes, cups, saucers, or forks and a rectangular tray of a cart, the three-dimensional single bin packing problem (3D-BPP) involves orthogonally packing a subset of the items within the tray. If the value of an item is given by its volume, the objective is to maximize the covered volume of the tray. Thus, this paper aims to optimize the transport capacity of a serving robot carrying a cart. This experiment, the first of its type, proves the feasibility of this endeavor efficiently.

Keywords Three-dimensional single bin packing problem • Three-dimensional knapsack problem • Serving robot • Cart • Tray • Optimization

1 Introduction

James Kuffner at Google introduced the term “Cloud Robotics” to describe a new approach to robotics that takes advantage of the Internet as a resource for massively parallel computation and sharing of vast data resources [1]. The robot specialized company, Willow Garage, is funded from Google, has received attention to introduce “Cloud Robotics”, is exploiting the cloud resource of Google, for the services such as the context-awareness and the object manipulation that are required to process enormous data. This paper, based on the concept of

A. Khil (✉)

School of Computer Science and Engineering, College of Information Technology,
Soongsil University, 511 Sangdo-Dong, Dongjak-Gu, Seoul, Republic of Korea
e-mail: ara@ssu.ac.kr

K.-H. Lee

Global School of Media, College of Information Technology,
Soongsil University, 511 Sangdo-Dong, Dongjak-Gu, Seoul, Republic of Korea
e-mail: kanghee.lee@ssu.ac.kr

Cloud Robotics, would rather focus on optimizing the task planning in order to serve effectively dishes by using a cart or tray than do simple motion planning [2].

Thus, this paper formulates this problem as a three-dimensional finite bin packing problem (3D-BPP) and aims to optimize the amount of a dish cart capacity which the serving robot can carry at one time. The rest of the paper is composed as follows. In Sect. 2, we formulate the optimization problem of a cart storage using the 3D-BPP. Section 3 describes the structure of the ONEBIN algorithm [3–5] for finding possible positions for placing items. The experiments in Sect. 4 are performed to demonstrate the feasibility of the proposed scheme in Sects. 2 and 3. The empirical and theoretical analyses follow to investigate its characteristics. Concluding remarks follow in Sect. 5.

2 Modeling a Dish Cart Problem with a 3D-BPP

We model a dish cart capacity filing problem (DCCP) with a three-dimensional single bin packing problem (3D-BPP) [5] (Fig. 1). This 3D-BPP consists of orthogonally packing into one bin as many items as possible. The aim is to find a feasible packing of a subset of the items on the cart (tray) that maximizes the total volume of the packed items. We assume that the origin of the coordinate system is in the left-bottom-back corner of the bin. We are given a set of n rectangular-shaped items, each characterized by width $w_j \leq W$, height $h_j \leq H$, and depth $d_j \leq D$ ($j \in J = \{1, \dots, n\}$), and one three-dimensional bin (container) having width W , height H , and depth D . The items such as dishes, cups, forks, and knives are different from shapes, styles, and materials as listed in Table 1.

In this study, we use an enumerative algorithm for the exact solution of 3D-BPP that Martello et al. [5] proposed. Therefore, the parameters including lower bounds, in Table 2 [3] can be followed directly. The detailed theorems and proofs can be referred in Ref. [5].

Fig. 1 A serving robot PR2 carrying a dish cart. The depth of the tallest item(s) becomes D

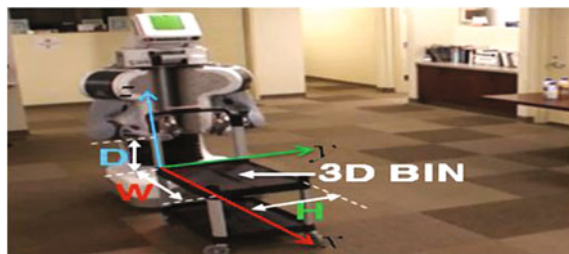





Table 1 Item list

j	3D shape	w_j	h_j	d_j	Description
1		5	32	99	Fork
2		25	25	5	Plate
3		4	22	99	Knife
4		16	16	99	Saucer and cup
5		3	12	99	Teaspoon
6		10	7	99	Bowl
7		7	7	99	Can
8		6	6	99	Cocktail glass
9		8	8	99	Cola cup

3 ONEBIN: An Exact Algorithm for Filling a Single Bin

This section describes the algorithm called ONEBIN [5] for finding the best filling of a single bin using items from a given set \bar{J} . Initially, no item is placed, so $C(0) = \{(0, 0, 0)\}$. At each iteration, given the set $I \subset \bar{J}$, currently packed items, set $C(I)$ is determined through 3D-CORNERS together with the corresponding volume $V(I)$. If F is the total volume achieved by the current best filling, we may backtrack whenever.

Table 2 Parameters and lower bounds for 3D-BPP

Index	Parameter	Description
1	I	Instance defined by item j and all the pieces currently assigned to bin i
2	i	Bin index
3	n	Number of items or rectangular pieces
4	J	$\{1, \dots, n\}$ A set of items
5	j	Item index or item name
6	W	Bin (tray) width
7	H	Bin (tray) height
8	D	Bin (tray) depth
9	w_j	Width of item j
10	h_j	Height of item j
11	d_j	Depth of item j
12	I'	Instance defined by the unassigned items and all the pieces currently assigned to active bins
13	c	Number of currently closed bins
14	L_0	$L_0 = \left\lceil \frac{\sum_{j=1}^n h_j w_j d_j}{HWD} \right\rceil$
15	L^{WH_1}	Refer to [5]
16	L^{WH_2}	Refer to [5]
17	L_1	$\max\{L^{WH_1}, L^{WD_1}, L^{HD_1}\}$
18	L_2	$\max\{L^{WH_2}, L^{WD_2}, L^{HD_2}\}$
19	z^*	Best incumbent solution value
20	$C(I)$	Resulting corner points
21	$\hat{C}(I)$	Set of corner points of the envelope
22	$S(I)$	$\{(x, y, z) : \forall i \in I, x \geq x_i + w_i \text{ or } y \geq y_i + h_i \text{ or } z \geq z_i + d_i\}$
23	$\hat{S}(I)$	Feasible $S(I)$

$$\sum_{i \in I} v_i + (B - V(I)) \leq F$$

If no more items fit into the bin (i.e., if $C(I) = 0$), we possibly update F and backtrack. Otherwise, for each position $(x_j, y_j, z_j) \in C(I)$ and for each item $j \in \bar{J} \setminus I$, we assign the item to this position and call the procedure recursively.

3.1 Algorithm 2D-CORNERS: Determining the Corner Points in 2D Single Bin

Given an item set I , it is quite easy to find, in two dimensions, the set $\hat{C}(I)$ of corner points of the envelope associated with the feasible region $\hat{S}(I)$ defined by the $x - y$ faces of the items in I . Following Property 2, let us order the items according to their end points $(x_j + w_j, y_j + h_j)$, so that the values of $y_j + h_j$ are

nonincreasing, breaking ties by the largest value of $x_j + w_j$. The following algorithm for determining the corner points set consists of three phases.

Algorithm 2D-CORNERS:

begin

if $I = 0$ **then** $\hat{C}(I) := \{(0, 0)\}$ **and return;**

comment: Phase 1 (identify the extreme items e_1, \dots, e_m);

$\bar{x} := m := 0$;

for $j := 1$ **to** $|I|$ **do**

if $x_j + w_j > \bar{x}$

then $m := m + 1$; $e_m := j$; $\bar{x} := x_j + w_j$;

comment: Phase 2 (determine the corner points);

$\hat{C}(I) = \{(0, y_{e_1} + h_{e_1})\}$;

for $j := 2$ **to** m **do**

$\hat{C}(I) := \hat{C}(I) \cup \{(x_{e_{j-1}} + w_{e_{j-1}}, y_{e_j} + h_{e_j})\}$;

$\hat{C}(I) := \hat{C}(I) \cup \{(x_{e_m} + w_{e_m}, 0)\}$;

comment: Phase 3 (remove infeasible corner points);

for each $(x'_j, y'_j) \in \hat{C}(I)$ **do**

if $x'_j + \min_{i \in \bar{J} \setminus I} \{w_i\} > W$ **or** $y'_j + \min_{i \in \bar{J} \setminus I} \{h_i\} > H$

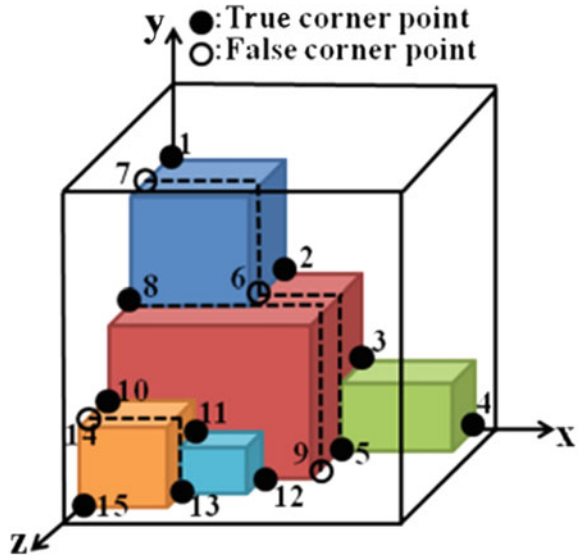
then $\hat{C}(I) := \hat{C}(I) \setminus \{(x'_j, y'_j)\}$

end.

3.2 Algorithm 3D-CORNERS: Finding Possible Positions for Placing an Item

Algorithm 2D-CORNERS set $C(I)$ of corner points in three dimensions, where I is the set of three-dimensional items currently packed into the bin. One may apply the algorithm for $z = 0$ and for each distinct z coordinate where an item of I ends, by increasing two values. For each such coordinate z' , 2D-CORNERS can be applied to the subset of those items $i \in I$ that end after z' , i.e., such that $z_i + d_i > z'$ adding the resulting corner points to $C(I)$. However, as shown in Fig. 2, some false corner points like 6, 7, 9, 13, and 14 can be obtained because they are corner points in the two-dimensional cases. To remove such points, the following 3D-CORNER

Fig. 2 Three-dimensional single bin filling (Corner points $C(I)$ are found by applying algorithm 2D-CORNERS six times on for each value of z'_k i.e., such that (1, 2, 3, 4) \rightarrow (5, 6, 7) \rightarrow (8, 9) \rightarrow (10, 11, 12) \rightarrow (13, 14) \rightarrow (15).)



algorithm is used such that no corner point will be generated inside the three-dimensional envelope.

Algorithm 3D-CORNERS:
begin

```

if  $I = 0$  then  $\hat{C}(I) = \{(0, 0, 0)\}$  and return;
 $T := \{0\} \cup \{z_i + d_i : i \in I\}$  (comment: do not duplicate equal values in  $T$ );
sort  $T$  by increasing values, and let  $T = \{z'_1, \dots, z'_r\}$ ;
 $C(I) := \hat{C}(I_0) := 0$ ;  $k := 1$ ;
while  $k \leq r$  and  $z'_k + \min_{i \in \bar{I}} \{d_i\} \leq D$  do
  begin
     $I_k := \{i \in I : z_i + d_i > z'_k\}$ ;
    apply 2D-CORNERS to  $I_k$  yielding  $\hat{C}(I_k)$ ;
    comment: add true corner points to  $C(I)$ 
    for each  $(x'_j, y'_j) \in \hat{C}(I_k)$  do
      if  $(x'_j, y'_j) \notin \hat{C}(I_{k-1})$ 
        then  $C(I) := C(I) \cup \{(x'_j, y'_j, z'_k)\}$ 
     $k^* := k$ ;  $k = k + 1$ ;
  end

```

end
end.

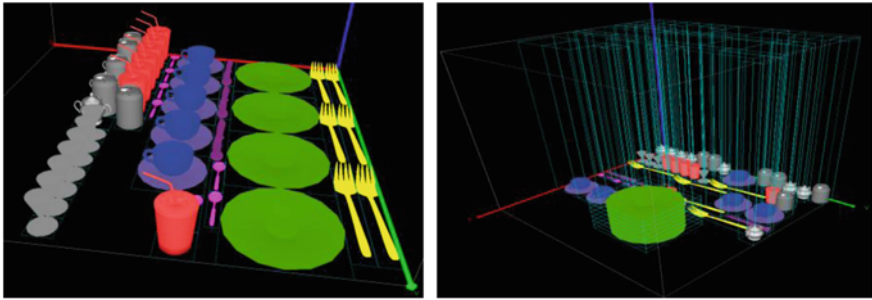


Fig. 3 Maximum packing for *left side*: 40 items-2D-BPP and *right side*: 48-items 3D-BPP

The volume $V(I)$ occupied by the envelope associated with I is

$$V(I) = \sum_{k=2}^{k^*} (z'_k - z'_{k-1})A(I_{k-1}) + (D - z'_{k^*})A(I_{k^*})$$

where the last term is nonzero whenever $k^* < r$.

4 Experiment

The experiments are performed to demonstrate the feasibility of the proposed scheme. In these test problems, the sizes of the pieces to be packed were varied and the bin sizes (tray) were always same as $W \times H \times D = 1 \times 1 \times 1 = 1$. The experiment was implemented in visual C++ 2008, OpenGL 2.0, and WinXP. It works well on an Intel PC with core i7 3.0 GHZ CPU and 8 GB RAM.

Figure 3 shows general cases of randomly generated problem instances having different combinations of items. Compared to the 2D-BPP result, the 3D-BPP result shows less covered area of the tray in spite of larger numbers of items because PLATEs were stacked.

5 Concluding Remarks

We presented the world’s first 3D-BPP applied to the situation of the maximization of the capacity of a cart for a serving robot. By using this concept, more effective service can be offered by various types of serving robots.

Acknowledgments This research was supported by Basic Science Research Program through the National Research Foundation of Korea (NRF) funded by the Ministry of Education, Science and Technology (grant No. 2012-0003583).

References

1. Kufner JJ (2010) Cloud-enabled robots. In: IEEE-RAS international conference on humanoid robots, Nashville, TN
2. PR2 Cleans Up with a Cart, <http://www.willowgarage.com/pages/pr2/overview>
3. Berkey JO, Wang PY (1987) Two dimensional finite bin packing algorithms. *J Oper Res Soc* 38:423–429
4. Martello S, Vigo D (1998) Exact solution of the two-dimensional finite bin packing problem. *Manag Sci* 44:388
5. Martello S, Pisinger D, Vigo D (2000) The three-dimensional bin packing problem. *Oper Res* 48:256–267

A Study on Splitting LPC Synthesis Filter

Kwang-Bock You and Kang-Hee Lee

Abstract In this study, for analysis speech signal the 10th order LPC synthesis filter is split into five 2nd order filters to avoid the nonlinear interactions of the poles. This novel algorithm allows us to reconstruct the wideband speech signal from the narrowband one by using the relationship between AR coefficients and its corresponding analog poles. The relationships between AR parameters and the continuous poles are presented.

Keywords LPC synthesis filter · AR parameter · Wideband speech signal · Sampling rate

1 Introduction

Many operations of a robot need to be ready for sensing the signals around its environments even though it is in the idle state. Hence, usually, it may be required a heavy bit-budget. If the enhanced algorithm in this study may be applied to the speech synthesis with the minimum number of bits, then the remaining bits can be assigned to other operations of the robot.

Generally, a speech Formant is characterized by a pole frequency and its bandwidth of the transfer function of filter in the Linear Predictive Coding (LPC) model. However, it is difficult to synthesize a speech Formant structure by just

K.-B. You (✉)

School of Electronic Engineering, College of Information, Soongsil University,
511 Sangdo-Dong, Dongjak-Gu, Seoul, Korea (Rep.)
e-mail: kwangbockyou@ssu.ac.kr

K.-H. Lee

Global School of Media, College of Information, Soongsil University,
511 Sangdo-Dong, Dongjak-Gu, Seoul, Korea (Rep.)
e-mail: kanghee.lee@ssu.ac.kr

pole modification. The major problem is pole interaction [1, 2]. Model parameters such as LPC coefficients, however, can be expressed as products form of highly nonlinear interactions of all the poles of the model. Hence, the change of sampling rate results in a set of complicated relationships among model parameters. Therefore, in this paper, first, the relationships between AR parameters α_k and the corresponding continuous poles s_k are derived. Second, the new enhancement algorithm that deals with the separation of the 10th order LPC synthesis filter into five 2nd order filters to avoid the aforementioned nonlinear interactions of the poles is suggested. Then, the simulation and its results are followed. Finally, in the conclusion some possible applications of the proposed enhancement algorithm are introduced and the future works are discussed.

2 The AR Parameters α_k and the Corresponding Poles s_k

Consider a real wide-sense stationary (WSS) process $X_a(t)$ of finite order as the response of a minimum-phase system $H_a(s)$ with input a white-noise process $v(t)$ [3, 4]. The power spectrum of this system can be expressed as

$$S_a(s) = \sigma_v^2 H_a(s) H_a(-s) \quad (1)$$

where $\sigma_v^2 = E\{v(t)v(t)\}$.

The autocorrelation function of this process is able to be found as following:

$$R_a(\tau) = \sigma_v^2 \sum_{k=1}^N C_k e^{s_k |\tau|} \quad (2)$$

where N represents the order of $S_a(s)$ and the coefficients C_k can be determined from the initial value theorem.

On the other hand, the transfer function of the Autoregressive (AR) process of N th order can be expressed as

$$H(z) = \frac{G}{1 + \sum_{k=1}^N \alpha_k z^{-k}} \quad (3)$$

where the coefficients $\{\alpha_k\}$ are real and G is a constant.

The power spectrum for this system can be expressed as

$$S(z) = \sigma_v^2 H(z) H(z^{-1}) \quad (4)$$

where $\sigma_v^2 = E\{v(t)v(t)\}$

Since the power spectrum is the Fourier transform of the autocorrelation function, we can express the power spectrum as

$$S(e^{j\omega}) = \sum_{m=-\infty}^{\infty} R(m)e^{-j\omega m}, \quad -\frac{\pi}{T} \leq \omega \leq \frac{\pi}{T} \quad (5)$$

where $R(m) = E\{X(m)X(n - m)\}$ and T represent the autocorrelation function and the sampling interval, respectively. We assume here that the aliasing does not occur. Since $X(n) = X_a(nT)$, the autocorrelation function $R(m)$ can be described as

$$R(m) = E\{X(m)X(n - m)\} = R_a(mT) = \sigma_v^2 \sum_{k=1}^N C_k e^{s_k |mT|} \quad (6)$$

Inserting Eq. (6) into (5), we obtain the power spectrum in a product form,

$$S(z) = \sigma_v^2 \frac{N(z)}{\prod_{k=1}^N (z - e^{s_k T}) \prod_{k=1}^N (z^{-1} - e^{s_k T})} \quad (7)$$

Rewriting the Eq. (4) by inserting (3)

$$\begin{aligned} S(z) &= \sigma_v^2 \frac{G}{1 + \sum_{k=1}^N \alpha_k z^{-k}} \cdot \frac{G}{1 + \sum_{k=1}^N \alpha_k z^k} \\ &= \sigma_v^2 \frac{G}{\sum_{k=0}^N \alpha_k z^{N-k}} \cdot \frac{G}{\sum_{k=0}^N \alpha_k z^{k-N}} (\alpha_0 = 1) \end{aligned} \quad (8)$$

Since denominators of Eqs. (7) and (8) can be regarded as the characteristic polynomials for this system, we conclude that [5]

$$\sum_{k=0}^N \alpha_k z^{N-k} = \prod_{k=1}^N (z - e^{s_k T}) \quad (9)$$

This Equation shows the relationships between the coefficients of AR process and its corresponding analog poles. In general, we can describe this relationship as shown below:

$$\begin{aligned} \alpha_{(m,0)} &= 1 \quad \text{for } m = 1, 2, \dots, N \\ \alpha_{(m+1,k)} &= \alpha_{(m,k)} - e^{(s_{(m+1)}T)} \alpha_{(m,k-1)} \quad \text{for } m = 1, 2, \dots, N-1 \text{ and } k = 1, 2, \dots, m \\ \alpha_{(m+1,m+1)} &= -e^{(s_{(m+1)}T)} \alpha_{(m,m)} \quad \text{for } m = 1, 2, \dots, N-1 \\ \alpha_{N,N} &= (-1)^N e^{\sum_{k=1}^N s_k T} \end{aligned} \quad (10)$$

when $N = 2$, the numerator $N(z)$ in Eq. (7) is expressed as

$$\begin{aligned} N(z) &= C_1 (1 - e^{2s_1 T}) (1 + e^{2s_2 T}) + C_2 (1 - e^{2s_2 T}) (1 + e^{2s_1 T}) \\ &\quad - \{C_1 (1 - e^{2s_1 T}) e^{s_2 T} + C_2 (1 - e^{2s_2 T}) e^{s_1 T}\} (z + z^{-1}) \end{aligned} \quad (11)$$

After calculating the coefficients of $(z + z^{-1})$ term and the constant term with $R(1) = R(-1) = C_1 e^{s_1 T} + C_2 e^{s_2 T}$, $R(0) = C_1 + C_2$ and $R(2) = C_1 e^{2s_1 T} + C_2 e^{2s_2 T}$, we can find the power spectrum for 2nd order model:

$$S(z) = \sigma_v^2 \frac{\{R(0) - R(2)\} (1 - e^{2(s_1+s_2)T})}{\prod_{k=1}^2 (z - e^{s_k T}) \prod_{k=1}^2 (z^{-1} - e^{s_k T})} \tag{12}$$

3 Splitting the LPC Synthesis Filter

The wideband speech signal would not be reconstructed by the pole modification with changing the sampling rate due to the pole interaction of the transfer function of the LPC synthesis filter, $H(z) = \frac{1}{A(z)}$. Thus, the 10th order LPC synthesis filter is split into five filters of 2nd order to avoid the pole interaction. The transfer function of the 10th order LPC synthesis filter can be expressed as

$$H(z) = \frac{1}{A(z)} = \frac{1}{1 + \sum_{k=1}^{10} \alpha_k z^{-k}} = \frac{1}{\prod_{k=1}^5 (1 - p_k z^{-1})(1 - p_k^* z^{-1})} \tag{13}$$

where α'_i s are prediction coefficients and p'_i s and $p_i^{*'}s$ are roots and complex conjugate roots of $A(z)$, respectively. Rewrite Eq. (13) as five equations of 2nd order. That is,

$$H(z) = \frac{1}{(1 - p_1 z^{-1})(1 - p_1^* z^{-1})} \cdots \frac{1}{(1 - p_5 z^{-1})(1 - p_5^* z^{-1})} = \prod_{k=1}^5 H_k(z) \tag{14}$$

where $H_k(z) = \frac{1}{1 + \alpha_{k,1} z^{-1} + \alpha_{k,2} z^{-2}} = \frac{1}{(1 - p_1 z^{-1})(1 - p_1^* z^{-1})}$.

In Sect. 2, the relationships between the parameters of AR model and its corresponding analog poles were shown. By using Eq. (9) we can describe the relationships between model parameters of the 2nd order filter and corresponding analog poles,

$$\begin{aligned} \alpha_{(k,1)} &= -e^{(s_k T + s_k^* T)} \\ \alpha_{(k,2)} &= e^{(s_k + s_k^*) T} \end{aligned} \tag{15}$$

where the complex poles $s_k = \sigma_k + j\omega_k$. Then, we can calculate σ_k and ω_k .

$$\begin{aligned} \sigma_k &= \frac{1}{2T} \ln(\alpha_{k,2}) \\ \omega_k &= \frac{1}{T} \cos^{-1} \left(\frac{-\alpha_{k,1}}{2\sqrt{\alpha_{k,2}}} \right) \end{aligned} \tag{16}$$

Now, applying new sampling interval $T_0 (= \frac{T}{2})$ to Eq. (16), new model parameters with respect to T_0 are obtained

$$\begin{aligned}\beta_{k,1} &= -e^{(s_k T_0 + s_k^* T_0)} \\ \beta_{k,2} &= e^{(s_k + s_k^*) T_0}\end{aligned}\quad (17)$$

Therefore, we can find new transfer function of LPC synthesis filter for the wideband signal:

$$\begin{aligned}G_k(z) &= \prod_{k=1}^5 \frac{1}{1 + \beta_{k,1} z^{-1} + \beta_{k,2} z^{-2}} \\ &= \prod_{k=1}^5 \frac{1}{(1 - q_k z^{-1})(1 - q_k^* z^{-1})}\end{aligned}\quad (18)$$

where q_k 's and q_k^* 's are new poles and complex conjugate poles for new sampling interval, respectively. It is important notice that Eq. (18) for the wideband speech signal model is obtained by changing only the sampling interval from T to T_0 .

The LPC parameters cannot ensure the stability of the synthesis filter due to their dynamic range. For practical purposes, Line Spectral Frequencies (LSFs) should be used in systems since their ordering property ensures the stability of the synthesis filter [6–8].

4 The Simulation and its Results

Now, the new enhancement algorithm which is described by Eq. (13) through (18) is examined by the simulation. Our data which is sampled by 16 kHz is the sentence—“Don’t ask me to carry an oily rag like that”—spoken by a female. We take 480 samples which is the length of 30 ms as a processing frame. Then, we normalize the 16 kHz sampled speech data as follows [9]:

$$\begin{aligned}SampleMean : \mu_s &= \frac{\sum_{n=1}^N s(n)}{N} \\ SampleVariance : \sigma_s^2 &= \frac{\sum_{n=1}^N \{s(n) - \mu_s\}^2}{N} \\ NormalizedData : \widehat{s(n)} &= \frac{s(n) - \mu_s}{\sigma_s}\end{aligned}\quad (19)$$

where $s(n)$ and N represent the 16 kHz sampled speech data and the total number of samples in a frame, respectively.

The 8 kHz sampled speech data to be processed through the proposed enhancement algorithm in this study are generated by downsampled the 16 kHz speech data. The following figures are the results of the simulation. Figure 1 shows the normalized 16 kHz sampled speech data. The 8 kHz sampled speech data,

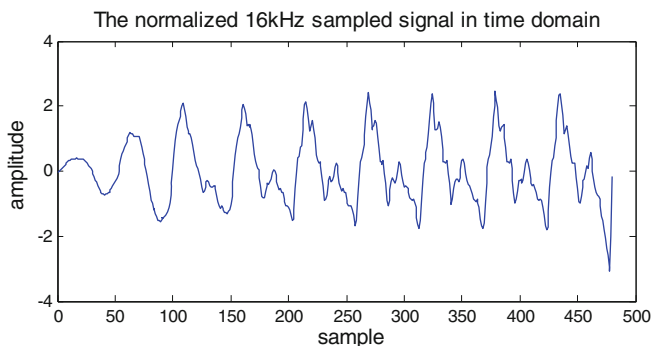


Fig. 1 The normalized 16 kHz sampled signal in time domain

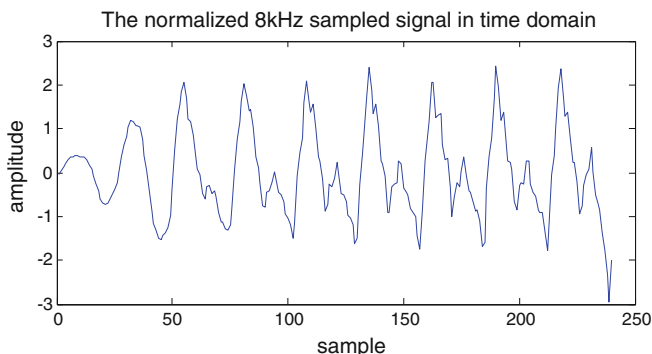


Fig. 2 The normalized 8 kHz sampled signal in time domain

which are the input signal to the proposed enhancement system, are presented in Fig. 2. The reconstructed 16 kHz sampled speech data, of course, by the splitting LPC synthesis filter are shown in Fig. 3.

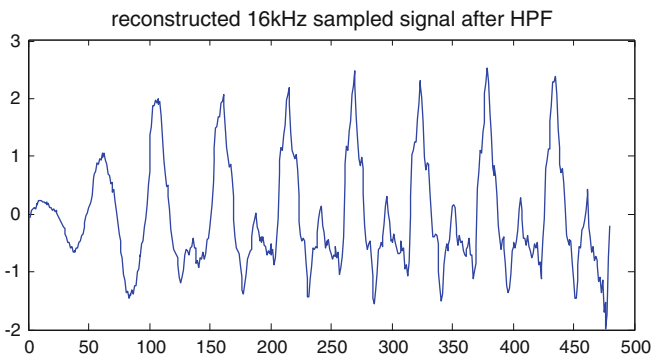


Fig. 3 Reconstructed 16 kHz sampled signal after HPF

5 Conclusion

The novel enhancement algorithm is to reconstruct the wideband speech signal from the information contained in the narrow band one.

The interaction between poles does not exist in the model parameters because of the 2nd order model.

As we have stated in Sect. 1, the proposed algorithm can be valuable to use for the housekeeping robot and the ubiquitous environmental monitoring system [10].

This suggested enhancement algorithm addresses the speech reproduction issue. When the speech is to be heard through loudspeakers in some applications such as videophones and video conferencing systems, speech quality often becomes a major concern. Wideband speech processing offers one way of improving the speech quality [11]. Image quality degradation occurs due to the shortage of bit budget in videophone and video conferencing systems. Since the proposed algorithm can reconstruct the wideband speech signal from the spectral information of narrowband one, at the encoding end there will be some remaining bits which can be allocated to the image.

Acknowledgments This research was supported by Basic Science Research Program through the National Research Foundation of Korea (NRF) funded by the Ministry of Education, Science and Technology (Grant No. 2012-0003583).

References

1. Mizuno H, Abe M, Hirokawa T (1993) Waveform-based speech synthesis approach with a formant frequency modification. In: Proceedings of ICASSP'93, pp II,195–198
2. Kondoz AM (1994) Digital speech (coding for low bit rate communications systems). Wiley, Chichester
3. Papoulis A, Pillai SU (2002) Probability, random variables, and stochastic Processes, 4th edn. McGraw-Hill, Inc., Punta Gorda
4. Haykin S (1991) Adaptive filter theory, 2nd edn. Prentice-Hall Inc., Upper Saddle River
5. Schroeder MR (1981) Direct (nonrecursive) relations between cepstrum and predictor coefficients. IEEE Trans ASSP ASSP-29(2):291
6. Soong FK, Juang B (1993) Optimal quantization of LSP parameters. Trans Speech Audio Process IEEE 1(1):15–24
7. de Marca JRB (1994) An LSF quantizer for the North-America half-rate speech coder. Trans Veh Technol IEEE 43(3):413–419
8. Mian GA, Riccardi G (1994) A localization property of line spectral frequencies. Trans Speech Audio Process IEEE 2(4):536–538
9. Leon-Garcia A (2009) Probability, statistics, and random processes for electrical engineering, 3rd edn. Prentice Hall, Upper Saddle River
10. Martin KD (1999) Sound-source recognition: a theory and computational model. Ph.D, Dissertation, MIT
11. Roy G, Kabal P (1991) Wideband CELP speech coding at 16 Kbits/Sec. In: Proceedings of ICASSP'91, pp 17–20

Teleoperation of a Master–Slave Pneumatic Robot Arm System Over the Internet: Consideration of Delay Between Oregon and Fukuoka

Shunta Honda, Tomonori Kato, Hiromi Masuda
and Ittirattana Jullakarn

Abstract Teleoperation of pneumatic robots is desired in the fields of rescue, surgery, and rehabilitation therapy. In the present study, teleoperation control of a four-DOF robot arm system incorporating pneumatic artificial rubber muscles is proposed. In the experiment of the present study, the distance between the master and the slave systems is approximately 8600 km. Signals and images from the master controller side are sent over the Internet using user datagram protocol (UDP). The effectiveness of the proposed system is discussed by the experimental results.

Keywords Teleoperation · Robot arm · Pneumatic artificial rubber muscle · User datagram protocol

1 Introduction

A pneumatic system has a high weight-power ratio and compliance. In addition, the air is a clean substance to drive actuators. Therefore, teleoperation of pneumatic robot systems that incorporate pneumatic actuators have been applied in a number of fields. For example, teleoperation control of construction machinery is applied at disaster sites in order to minimize injuries and the loss of workers during rescue operations. For this purpose, a remote control system using pneumatic artificial rubber muscle (PARM) as the actuator of a robot system was developed and applied to the tasks of manipulating construction machinery [1]. Surgical operations and rehabilitation therapies are other examples of tasks that can be performed using teleoperation control of pneumatic systems [2, 3].

S. Honda · T. Kato (✉) · H. Masuda · I. Jullakarn
Fukuoka Institute of Technology, 3-30-1, Wajiro-higashi, Higashi-ku,
Fukuoka 811-0295, Japan
e-mail: t-kato@fit.ac.jp

In the present study, we have developed a four-degree-of-freedom (DOF) pneumatic robot arm, which incorporates two two-DOF modules as the slave system. The arm has a manipulator module as a gripper. In addition, we developed a master controller system so that the operator can control the master/slave system intuitively.

Two web cameras are attached to the pneumatic robot system (slave system). Images from the camera are transported to the master side over the Internet using Skype™ and are displayed on a laptop computer. Normally, the signals from the master controller would be transported over the Internet using user datagram protocol (UDP). Since UDP uses a simple transmission model without implicit hand-shaking dialogues for guaranteeing reliability or data integrity, time-sensitive applications, such as real-time robot teleoperations, often use UDP because dropping packets is preferable to waiting for delayed packets. However, in order to avoid the effects of signal losses associated with UDP, interoperable telesurgical protocol (ITP) is used in the present study.

The teleoperation experiments were conducted between two universities separated by approximately 30 km. The effectiveness of the proposed system was confirmed by the experimental results.

2 Development of a Robot Arm System

2.1 Pneumatic Robot Arm (Slave System)

Pneumatic artificial rubber muscle (PARM) is a novel actuator that has a high weight-power ratio [4]. As shown in Fig. 1(Left), PARM is composed of a rubber tube impregnated with fibers. The PARM that was selected as the actuator for the robot arm (slave system) is the Fluidic Muscle (MXAM-20-AA) manufactured by FESTO. According to its specifications, the maximum contraction over the

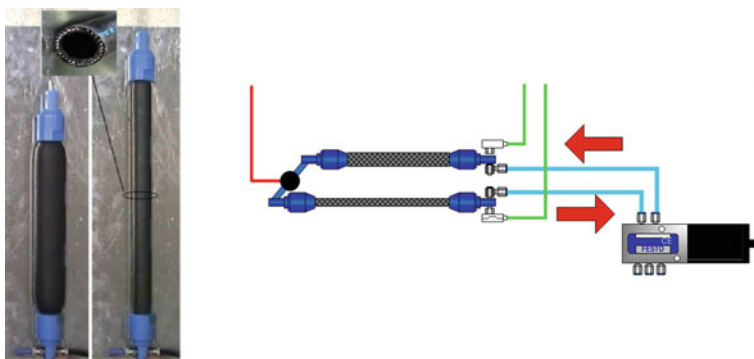


Fig. 1 Pneumatic artificial rubber muscle (*Left*) and Antagonistic drive (*Right*)

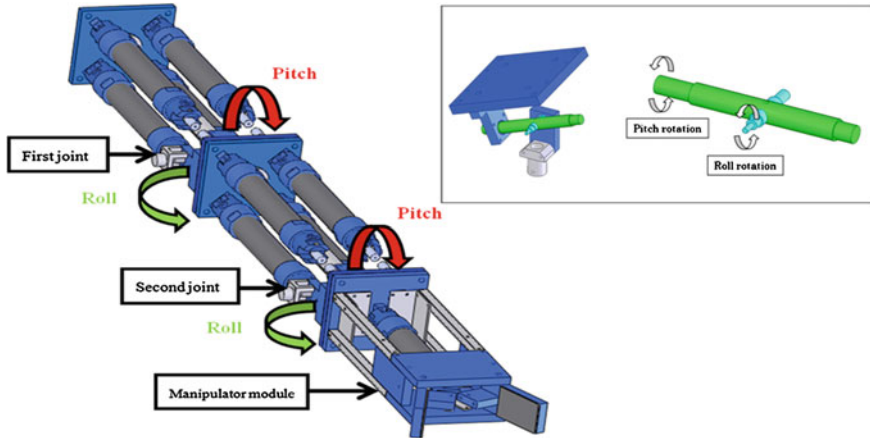


Fig. 2 Robot arm (slave system) (CAD image)

nominal length is 20 %. The driving system of a single joint using PARMs is shown in Fig. 1(Right). Two PARMs are connected in parallel to a link. A five-port pneumatic servo valve (MPYE-5-M5-B:FESTO) controls supply and exhaust air to the PARMs. The difference in contraction between the two PARMs creates joint torque. A potentiometer was attached to each joint, and the rotation angle was measured and controlled. We have developed a two-DOF module using four PARMs (two joint driving systems). The length of the two-DOF module is approximately 350 mm. By coupling two two-DOF modules, a four-DOF robot arm was designed and fabricated, as shown in Fig. 2. The weight of the arm is approximately 3 kg. Since each module is controlled with two five-port servo valves, the arm is controlled with five servo valves (including the servo valve for the manipulator module). Potentiometers were attached to each joint, and the rotation angles were measured.

2.2 Master Controller

A master control system was developed so that the operator can control the master/slave system intuitively. The newly developed master control system consists of a master manipulator, an electric power source, and a laptop computer. The skeletal structure of the master manipulator is similar to that of the slave system (robot arm). Four potentiometers are attached to the each angles of the master manipulator, and a switch button to activate the manipulator module as a gripper is incorporated into the master manipulator.

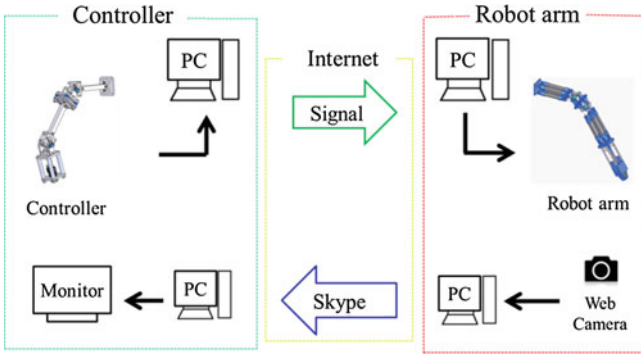


Fig. 3 Diagram of teleoperation control (master/slave system)

3 Tel-Operation Experiment Between Fukuoka and Oregon

3.1 Teleoperation Control System

Figure 3 shows a schematic diagram of the teleoperation control of the master/slave system. An operator controls the master controller while viewing the image captured by the camera at the slave side, which is sent to the master side over the Internet using Skype™. The signals from the potentiometers of the master controller are sent to a laptop computer through an AD converter. In the laptop computer, coordinate transformations are performed for each joint. The transformed angle values are then transported over the Internet using User Datagram Protocol/Internet Protocol (UDP/IP).

On a computer located at the slave side, coordinate transformations are performed on each joint (same as the master side). After the signals are transported from the master side to the computer of the slave side, the set angle values are calculated and the control signals are transported to the servo valves through a DA converter. Since response and stability are preferable to positioning, simple P (proportional) control was applied in the experiment. The sampling time of both the master and slave computers is 2.0 ms. The motion vision is captured by web camera(s) in slave robot side. Images from the camera are transported to the master side over the Internet using Skype™.

3.2 Experimental Procedures

In teleoperation experiments, the master controller system was located at Oregon State University (1500 SW Jefferson Way, Corvallis, Oregon, USA), and the slave system was located at Fukuoka Institute of Technology (3-30-1 Wajiro-higashi,

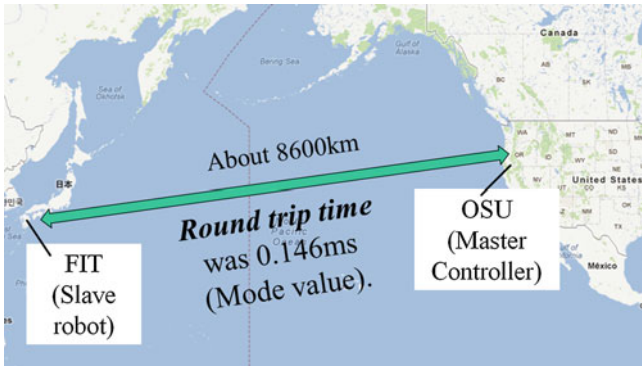


Fig. 4 Map of experiment

Higashi-ku, Fukuoka, Japan) as Fig. 4. The distance between the master controller system and the slave system is approximately 8600 km. The round trip time (RTT) through the Internet communication was measured for 20 times in the experiment, and the mode value of RTT was 0.146 ms.

The experimental setup is shown in Fig. 5 (master side) and Fig. 6 (slave side). There are two tables in front of the robot arm. An empty PET bottle is placed on the left-hand table. The experimental procedures are as follows:

- (1) The robot starts from its original position, shown in Fig. 5.
- (2) The empty PET bottle on the left-hand table is grasped using the gripper (manipulating module).
- (3) The PET bottle is moved to the right-hand table. (The gripper is opened to release the bottle.)

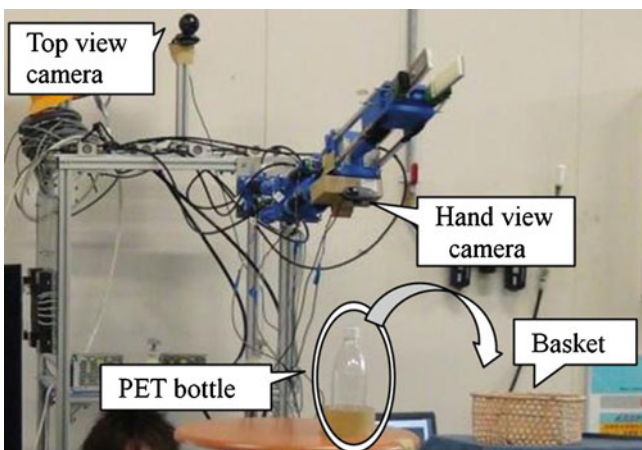


Fig. 5 Photograph of experimental site (slave robot side, Fukuoka)

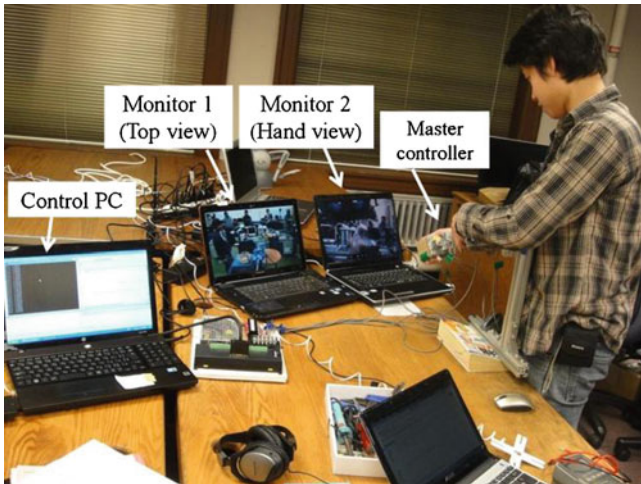


Fig. 6 Photograph of experimental site (master controller side, Oregon)

The time required for the task is measured in each experiment.

As shown in Fig. 5, there are two cameras attached to the robot arm. One is for “Top view” as a main camera, and the other is for “Hand view” as a sub camera. In order to ensure the effectiveness of the sub view, the experiments were conducted under the conditions of with and without the sub camera.

The experiments were conducted for three people. Each person tried the experiment “with” and “without” using the sub camera alternatively for five times each. The number of mistake (Failure in grasping, Falling the bottle) was counted for each experiment.

3.3 Experimental Results

Teleoperation of robot system itself was successfully conducted. The experimental results for each person are shown in Table 1 and the summary of experimental results is shown in Table 2. By the results of the number of mistake, it seems that using the sub camera contributes to improve the accuracy of controllability. However, with the case of using the sub camera, the more time is required compared with the case without using the sub camera. One of the cause that can be thought is the movement of sight when using the sub camera, since in that case there are two monitors to be checked.

Table 1 Experimental results for each person

Number of trial	Time required (s) (with sub camera)	Number of mistake (with sub camera)	Time required (s) (without sub camera)	Number of mistake (without sub camera)
<i>Subject number 1</i>				
1st	13.99	0	12.99	0
2nd	26.04	0	32.93	1
3rd	43	1	16.93	0
4th	18.85	0	11.25	0
5th	11.94	0	37.19	1
	22.76 s (Average)	1 (Total)	22.26 s (Average)	2 (Total)
<i>Subject number 2</i>				
1st	58.5	2	18.59	0
2nd	18.59	0	13.45	0
3rd	29.31	1	23.43	0
4th	19.22	0	20.28	0
5th	42.34	1	17.8	0
	33.59 s (Average)	4 (Total)	18.71 s (Average)	0 (Total)
<i>Subject number 3</i>				
1st	20.62	0	18.35	0
2nd	15.43	0	22.93	1
3rd	17.88	0	12.12	0
4th	12.99	0	11.34	0
5th	9.71	0	9.94	0
	15.33 s (Average)	0 (Total)	14.94 s (Average)	1 (Total)

Table 2 Summary of experimental results

	Time required (s) (Average)	Number of mistake (Total)
With sub camera	23.89	5
Without sub camera	18.63	3

4 Conclusion

In the present study, we developed a four-DOF pneumatic robot arm that incorporates two two-DOF modules as the slave system. The robot arm has a manipulator module that can be used as a gripper. In addition, we developed a master controller system so that the operator can control the master/slave system intuitively. A web camera is attached to the pneumatic robot system, and images captured by the camera are transported to the master side over the Internet using Skype™ and are displayed on a laptop computer. The signals from the master controller are transported over the Internet using UDP. Master/slave teleoperation control experiments were conducted between two universities in Fukuoka and Oregon that are separated by a distance of approximately 8600 km.

Teleoperation of robot system itself was successfully conducted. By the experimental results. It seems that using the sub camera contributes to improve the accuracy of controllability. However, with the case of using the sub camera, the more time is required compared with the case without using the sub camera. Though one of the cause that can be thought is the movement of sight when using the sub camera, since in that case there are two monitors to be checked, Further investigation is needed on this matter.

References

1. Sasaki T, Kawashima K (2008) Remote control of backhoe at construction site with a pneumatic robot system. *Autom Constr* 17:907–914
2. Tadano K, Kawashima K (2007) Development of a master slave manipulator with force display using pneumatic servo system for laparoscopic surgery. *Int J Assist Robot Mechatron* 8(4):6–13
3. Takaiwa M, Noritsugu T (2009) Development of wrist rehabilitation equipment using pneumatic parallel manipulator-acquisition of P.T.'s motion and its execution for patient-.In: *Proceedings of IEEE 11th international conference on rehabilitation robotics*, CD-ROM
4. Chou C, Hannaford B (1996) Measurement and Modeling of Mckibben pneumatic artificial muscles. *IEEE Transa Robot Autom* 12:90–103
5. Kato T, Higashi T, Shimizu K (2010) Teleoperation of a robot arm system using pneumatic artificial rubber muscles -teleoperation over the internet using UDP and a web camera-. In: *Proceedings of fifth international conference on broadband, wireless computing, communication and applications*, pp 714–718

Fundamental Study of a Virtual Training System for Maxillofacial Palpation

Tatsushi Tokuyasu, Erina Maeda, Takuya Okamoto, Hiromu Akita, Kazuhiko Toshimitsu, Kazutoshi Okamura and Kazunori Yoshiura

Abstract Maxillofacial palpation is a physical examination technique where face or jaw are touched with fingers to determine their shape, consistency and location. Dentists utilizes palpation to diagnose pathological condition of a patient suffered from maxillofacial diseases. This paper proposes a virtual training system for maxillofacial palpation. To provide a virtual palpation system, a basic patient model is constructed based on linear elastic finite element method. Finally the simulation results and the remained issues making the system more practical are discussed.

Keywords Virtual reality · Haptic system · Finite element method · Maxillofacial palpation

1 Introduction

Maxillofacial palpation has been considered as one of the essential diagnostic methods for dentists to diagnose patient's pathological condition. A number of palpation methods have been proposed according to the cases of patient [1, 2]. Regardless of the importance of maxillofacial palpation, however this is mostly neglected in medical training simulators [3, 4]. Meanwhile, students of dental

T. Tokuyasu (✉) · E. Maeda · T. Okamoto · H. Akita
Department of Information and Systems Engineering, Fukuoka Institute of Technology,
3-30-1 Wajiro higashi, Fukuoka, Japan
e-mail: tokuyasu@fit.ac.jp

K. Toshimitsu
Department of Mechanical Engineering, Oita National College of Technology, Oita, Japan

K. Okamura · K. Yoshiura
Faculty of Dental Science, Department of Oral and Maxillofacial Radiology, Kyushu
University, Fukuoka, Japan

school have become dentists without practical training about maxillofacial palpation before finishing their dental school. Though the palpation diagnosis, the diseased region and its stage have to be known in order to enhance the quality of life (QOL) of a patient. Therefore, accurate skills of maxillofacial palpation of dentists leads to early detection of the diseases. The reason why of lacking practical training with a patient in dental school, there is some concerns of that dental students endanger the safety of a patient. Against the background of this dental education, a training simulator has been highly desired by the coauthor dentists.

The accuracy of palpation skill depends on the sense and/or the experience of a dentist, so the deftness is needed to accurately diagnose a patient. Additionally, it is difficult to cultivate common objectivity in the skill of palpation among dentists because, even in dentists, personal difference in the feeling of fingertip must be lying hidden among them.

It has assumed that the reliability of palpation skill improves through the training with palpation score that is based on synthesizing palpation data of several regions of a patient [5, 6]. But, even though the reliability of palpation score is high, the diagnosis accuracy of palpation might not be ensured. Because there is no ensured that the reliability of basic palpation data is good. Then, Ohmura et al. clarified finger pressure in palpation by using their developed palpation simulator as shown in Fig. 1, in which a head mannequin model was built and force sensors are embedded in its maxillofacial surface [5, 6]. According to their investigations, the contribution factors generating pressure force in palpation diagnosis lie on either side of doctor and patient. This implies that dentists have to accumulate the experience of palpation diagnosis with a patient to enhance the reliability of palpation.

Actually, Ohmura's simulator enables us to experimentally contact the maxillofacial shape of a human, in which trainees learn how to not only approach a patient but also evaluate the feelings of touching the patient objectively. With respect to use this simulator in the case of practical training in dental education facilities, it is desired to have the patient model various symptomatic states. In order to answer this request, the physical patient model has to be reconstructed.

Fig. 1 Scene of palpation training in Ohmura's simulation model [5]



Then, this study began to develop a virtual system for maxillofacial palpation training, in which functional specifications of a patient model changes corresponding to a variety of conditions of a patient.

This study firstly builds a virtual patient model based on linear finite element method in this paper. The technical issues necessary to provide the virtual training environment of maxillofacial palpation with computer graphics and haptic hardware are described in the following sections. After the experimental result will be written, the remained technical issues to enhance the quality of our system are discussed.

2 Materials and Methods

2.1 System Structure

Figure 2 shows a schematic diagram of the system we would like to develop, where one desktop computer controls a haptic device and processes a virtual patient model. A trainee operates a pen stylus end-effector of the haptic device to virtually touch the patient model in the computer display. The computer calculates the reaction force to the contact of a virtual finger with the patient model with expressing the deformation of maxillofacial surface without time delay.

The computer, used in this paper, is running on Windows 7 64 bit OS. Visual studio 2010 has been adopted as the development environment. Additionally, Intel C++ Composer XE2011 that supports parallel computing of Intel multi-core processor, has been installed in this computer to implement parallel processing of the virtual patient model.

PHANToM Omni produced by Sensable inc. will be used as a haptic device in earlier stage of this study, because this device has convenient functions to reflect the operation of trainee and to transmit the reaction force to the trainee via a pen stylus of end-effector of PHANToM.

Fig. 2 Schematic diagram of a maxillofacial palpation training system



2.2 Virtual Maxillofacial Model

In the field of medical engineering, finite element method (FEM) has been used often to simulate the behavior of a patient model in a surgical training system [7, 8]. This study also applies FEM to make the patient model of a maxillofacial shape.

On trial basis of this study, CT image data of a mannequin model, in which a human skull bone was embedded in, is taken as a patient data. Figure 3a shows a slice data of CT image taken from a mannequin, and Fig. 3b is the visualized image drawn with a free medical image processing software, Osirix.

The most important request for the patient model is to deform against external force without time delay. Of course the reaction force has to be computed in real time. It has been well known that the computation cost increases in FEM computation, and this has become the reasons of that researchers avoided to use FEM in building their patient model [8].

By the way, the displacement occurred in actual palpation for maxillofacial surface is not large, so that linear type of FEM computation might fill our requests to the maxillofacial palpation system. Then, linear elastic FEM model is used in this study. In order to make the FEM model of a head from CT image of a mannequin, the following steps are performed; (i) infilling hollow portions of all slices of CT image by manually operations, (ii) converting the operated CT images to binary, (iii) extracting the volume data from the image data, and (iv) meshing the volume data into tetrahedral elements.

For (iii) and (iv) procedures, a volume data can be easily constructed by using Image J and a commercially available meshing software, GiD 10, where front advanced method has been used to process of meshing. Figure 4 shows the image of a head composed of tetrahedral elements (15718 elements of 4010 node points).

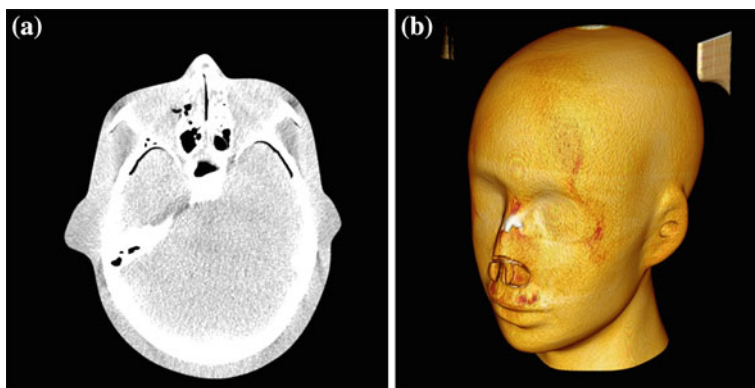
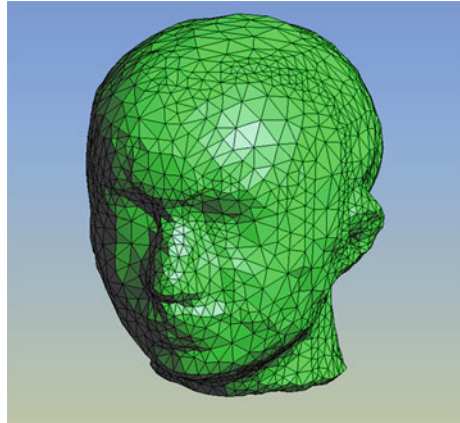


Fig. 3 Example images of the source CT data for maxillofacial model, **a** A slice of CT, **b** 3D graphic visualized with Osirix

Fig. 4 The developed tetrahedral mesh model



2.3 Computation of Reaction Force with FEM Model

Physical properties of human organs are nonlinear. Though several researches attempted to make a virtual organ by using nonlinear FEM in a surgical simulator, the complexity of nonlinear FEM computation algorithm and its computation cost had become the bottleneck. Hence, this study also avoided to apply nonlinear FEM computation to make a patient model and decided to use linear FEM computation.

In the computation of linear FEM model, basically Hooke’s law described in the Eq. (1) governs the relationship between external force and the displacement of an elastic model, where f is nodal force vector, u is nodal displacement vector, and K is stiffness matrix. In general, the model obeying the Eq. (1) has been called as elastic body.

$$f = Ku \tag{1}$$

By using the inverse matrix K^{-1} of the stiffness matrix K , the displacement of an elastic body due to the external force f is derived by the Eq. (2).

$$u = K^{-1}f \tag{2}$$

The position of virtual finger is expressed as the point. This is determined by a trainee through the operation of haptic device. As a consequence, we ignore the posture of end-effector in this paper. The movement of trainee’s finger is considered as the enforced displacement δ in the FEM computation, and then the reaction force f_r generated by the enforced displacement δ can be derived as shown in the Eq. (3).

$$f_r = K\delta \tag{3}$$

The resultant displacement depicting deformation of the maxillofacial surface due to the palpation can be calculated by the Eq. (4).

$$\delta = K^{-1}f_r \quad (4)$$

The mentioned computation method certainly reduces the computation cost, because only once computation of the inverse matrix K^{-1} of a stiffness matrix K is necessary to continue the reaction of the patient model against the palpation during training.

3 Results

This study underwent deformation simulations of the developed maxillofacial model, where the nodes under the neck region are fixed as the boundary condition. By using Open GL graphic library, the FEM model has been visualized on the computer display. Figure 5 show the scenes of deformation, where the small sphere indicates the point of a virtual finger and the node of operational object. Pressing a node of the cheek region is shown in Fig. 5a. And Fig. 5b is the appearance where a node of the cheek region is pulled with a small displacement.

The enforced displacements given to simulate the press and the pull operations against the virtual model were given computationally in order to add the deformation perpendicularly for the maxillofacial surface. And then, the time-series data was simulated as shown in Fig. 6. For one sequence of FEM computation, it takes less than approximately eight milliseconds. No time delay was confirmed in this experiment.

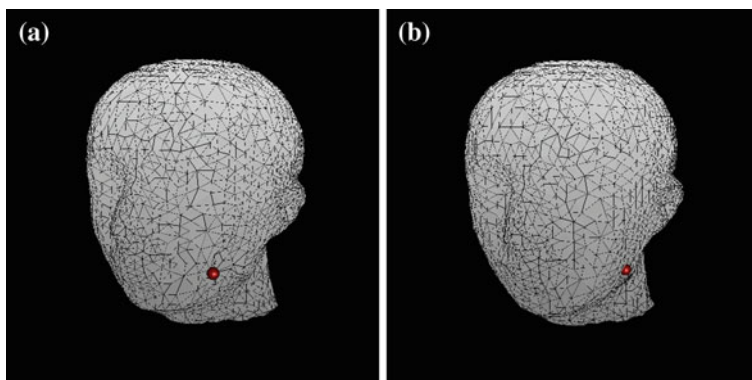
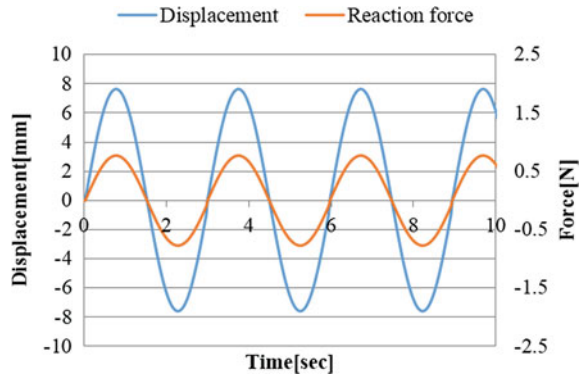


Fig. 5 Simulation results for deformation against pressing and pulling a node of cheek region of the virtual patient model. **a** Pressing on cheek, **b** Pulling a node of cheek surface

Fig. 6 Time-series of displacement and reaction force



4 Discussions

In the phase of constructing the volume data from CT image, firstly all inside region of head is high contrast. Consequently the volume data had become dense more than necessary to construct a maxillofacial model. This brought the increment of the numbers of element and node. By the way, the appearance of maxillofacial surface is too rough to depict the impression of human maxillofacial surface. This issue can be overcome with making the size of element outside the cranial bone smaller with hollowing the region inside cranial bone. Or, the use of spline compensation would be effect to enhance the appearance of the patient model.

Figure 6 shows the relationship between the pressure force and the deformation against the region of cheek surface of the patient model. The stiffness matrix K of the FEM computation for the patient model was tentatively given uniformly, so the calculated reaction force became not realistic. To determine the elastic coefficient of stiffness matrix K is one of the most important tasks to complete the patient model. Because physical properties of organ tissue are nonlinear and it can be considered tissue structures chance substantially due to the influence of diseases. As the traditional method to determine the elastic coefficient of stiffness matrix K , the parameters are adjusted by referencing to the feelings of a skilled doctors [8]. But this was impractical method, doctors have a full schedule for the number of parameter should be adjusted.

Recently, ultrasound elastography has been produced. This measurement system enables us to estimate three dimensional elastic data of organ tissue noninvasively. The authors have been entertaining to use this measurement instrument in the construction of our patient model.

5 Conclusions

This study aims to develop a training system for maxillofacial palpation. This paper firstly introduced how to build the patient model in our system, where linear FEM computation applied to the volume data model extracted from the CT image data of a mannequin. The deformation simulation resulted successively for the first trial of the developed system, in which there were no time delay in the reaction of the patient model against the enforced displacement given computationally. For future work, the external reality of the patient model will be improved with reducing the number of elements. And the practical test of palpation will be done after the system links to the haptic device.

References

1. Okeson JP (1989) Management of temporomandibular disorders and occlusion. C.V. Mosby, ST. Louis, pp 209–274
2. Schwartz L (1959) Disorders of the temporomandibular joint. W. B. Saunders, Philadelphia, pp 1–471
3. Ullrich S, Kuhlen T (2009) Haptic palpation for medical simulation in virtual environments. *IEEE Trans Vis Comput Graph* 18(4):617–625
4. Zhang Y, Phillips R, Ward J, Pisharody S (2009) A survey of simulators for palpation training. *Studies Health Technol Inf* 142:444–446
5. Ohmura T, Morita O (2001) Pressing pain exploration for maxillofacial palpation. *Odontology* 88:500–504 (In Japanese)
6. Akimoto S, Ohmura T, Shimizu K, Sawaguchi M, Koji T, Morita O (1996) Study on the training effect of palpation force. *Prosthodontic* 40:255–259
7. Adachi K, Fujita A, Kohmura E, Kanzaki H (1996) A study on cerebellar retraction simulation using three-dimensional finite element brain model. *J JSCAS* 9(3):258–259
8. Tokuyasu T, Kitamura T, Sakaguchi G, Komeda M (2005) Development of a training support system for cardiac muscle palpation. In: *Proceedings of the first international conference on complex medical engineering*, pp 146–150

Design of a 2-DOF Wearable Mechanism for Support of Human Elbow and Forearm

Tetsuya Morizono and Motoki Suzuki

Abstract A 2-DOF wearable mechanism for support of human elbow and forearm is proposed in this paper. An advantage of the mechanism is easy attachment to a human arm: rigorous adjustment of attachment positions is unnecessary when the mechanism is attached. This paper firstly illustrates design and a model of the mechanism, and then derives kinematics. A supporting method applicable to the mechanism is secondly described. Thirdly, a mockup for future design of a prototype is shown. An issue for future development of the mechanism is finally discussed.

Keywords Wearable robot · Easy attachment · Elbow · Forearm · Braking support

1 Introduction

Wearable mechanical devices are still an attractive field of study, and many mechanical designs have been proposed. Development of the devices for a human arm is considered to be especially important for assist of human activities and rehabilitation. Recent developments of the devices are surveyed in [1].

This paper focuses on motion support of human elbow and forearm. Combination of elbow rotational motion and forearm pronation-supination motion generates 2-DOF motion. An idea of supporting the motion is applying two mechanical rotational joints independently to each motion [2–6]. However, this

T. Morizono (✉) · M. Suzuki
Fukuoka Institute of Technology, 3-30-1, Wajiro-Higashi, Higashi-ku,
Fukuoka 811-0295, Japan
e-mail: morizono@fit.ac.jp

M. Suzuki
e-mail: s09c2024@bene.fit.ac.jp

idea may cause a problem. From kinematic viewpoint, rotational axes of the mechanical joints must be exactly arranged on those of human elbow and forearm, but this is considered to be a difficult task because the exact arrangement of the mechanical joints requires rigorous and careful adjustment of attachment position(s) when a wearable device is placed on a human arm. Flexibility of human skin enables motion of a human arm even in the case that the adjustment of attachment position is inaccurate, however, the inaccurate adjustment causes kinematic mismatch between a human arm and the device. The kinematic mismatch generates force exerted on a human arm, and a safety problem may occur as a result.

An idea of avoiding the attachment problem described above is using a device actuated with flexible material ([7] for example), however, the flexibility generally causes another difficulty in modeling of the device for analysis. Using a parallel mechanism seems to be an idea of overcoming the problem [8], however, a complex mechanism may make realization of a portable device more difficult.

The authors think that a key idea of overcoming the problem is redundancy of the mechanism, as also discussed in the study of [9]. Based on this idea, one of the authors was developed a mechanism suitable for a portable device [10]. The purpose of the study was realizing a 1-DOF wearable mechanism for support of human elbow motion, and the mechanism was designed so that rigorous adjustment was unnecessary when it was attached on a human arm.

The design concept of the study [10] can be extended for supporting 2-DOF motion by both human elbow and forearm; therefore, this paper proposes a design of a wearable mechanism for supporting the 2-DOF motion. This paper is organized as follows: Sect. 2 describes a model of the mechanism. Section. 3 derives kinematics of the mechanism based on the model in Sect. 2. Section. 4 describes an idea of “braking support” with a braking device, and statics necessary for further analysis is given. A mockup for future manufacturing of a prototype is shown in Sect. 5. Section. 6 discusses an issue for future development of the mechanism. Finally, Sect. 7 describes conclusion.

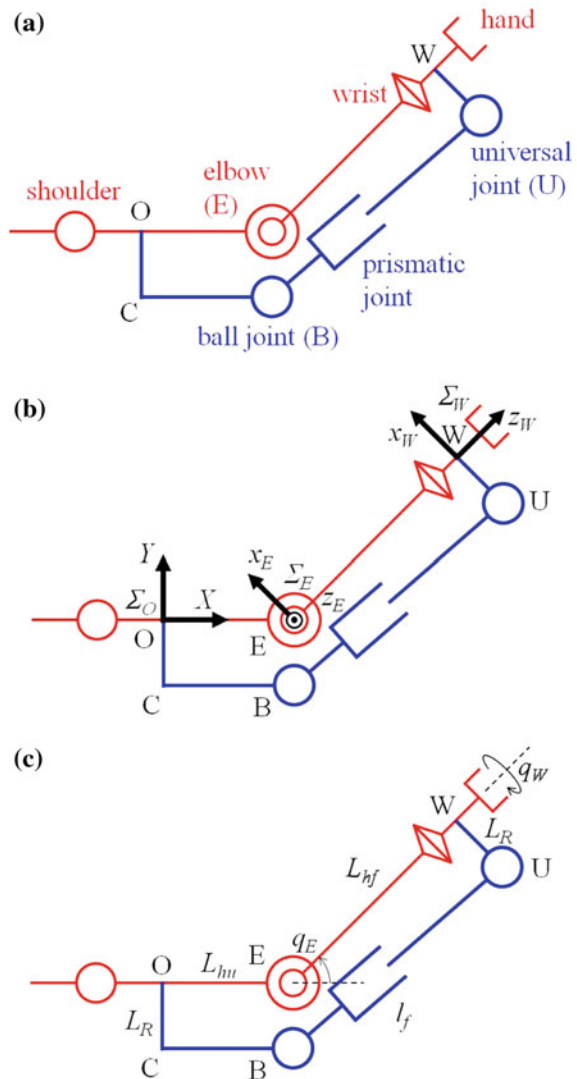
2 Model

This paper considers a model shown in Fig. 1. The model includes both a human arm (illustrated by the red color) and the wearable mechanism attached to the human arm (illustrated by the blue color). The model of a human arm considers elbow and wrist joints as shown in Fig. 1a. The elbow joint is referred to as the joint E hereafter. The points O and W denote attachment points of the wearable mechanism, and it is assumed that they locate on the upper arm and the forearm, respectively. The wearable mechanism is a 6-DOF mechanism assembled by a ball joint B (3-DOF), a prismatic joint (1-DOF) and a universal joint U (2-DOF). The point C is a kinking point of a link and no joint is installed in that point. It is assumed that the angles BCO, COE and UWE are kept perpendicular while the

wearable mechanism is on the human arm. Although the wearable mechanism itself is 6-DOF, its motion becomes 2-DOF in combination with the human arm. This is verified by the formula calculating DOF of a robotic mechanism, and also by kinematics shown in Sect. 3.

Fig. 1b depicts coordinate systems for deriving kinematics. Σ_O is the reference coordinate system and its origin locates on the point O. Σ_E and Σ_W are the coordinate systems for the joint E and the point W. The z_E axis is on the rotational axis of the joint E, and the z_W axis is on the rotational axis of the wrist joint. The x_E axis is perpendicular to both z_E and z_W axes.

Fig. 1 The kinematic model including a human arm and the wearable mechanism: **a** models of a human arm (red color) and the wearable mechanism (blue color), **b** coordinate systems for deriving kinematics, and **c** constants and variables for expressing kinematics



Some constants necessary for expressing kinematics are shown in Fig. 1c. L_R denotes the distance between the points O and C. It is assumed that the segment WU also has the same distance. L_{hu} denotes the distance between the points E and O. It is assumed that the segment BC has the same distance. Here, it is noted that L_{hu} is assumed to be constant *once* the wearable mechanism has been attached to the human arm; however, it is possible to take any value when the mechanism is attached

(provided that the segment BC is adjustable). The distance L_{hf} between the joint E and the point W is similarly defined and has the same feature of attachment; therefore, rigorous adjustment of the attachment points O and W are unnecessary when wearing the mechanism.

Fig. 1c also shows variables for expressing kinematics. The angle q_E denotes the flexion angle of the elbow, and its extended posture is expressed by $q_E = 0$. The angle q_W denotes the rotational angle of the forearm, here, $q_W = 0$ means that the axes x_E and x_W are parallel. The length l_f is defined as the distance between the joints B and U, and denotes the displacement of the prismatic joint.

3 Kinematics

The goal of this section is expressing the length l_f by a function of q_E , q_W , L_R , L_{hu} and L_{hf} . Firstly, DH parameters between Σ_O and Σ_E are $a_{OE} = L_{hu}$ (the length of a link), $\alpha_{OE} = 0$ (the twist angle), $d_{OE} = 0$ (the link offset) and $\theta_{OE} = \pi/2 + q_E$ (the joint angle). They yield the following homogeneous transformation matrix ${}^O T_E$:

$$\begin{aligned} {}^O T_E &= \begin{bmatrix} \cos(\frac{\pi}{2} + q_E) & -\sin(\frac{\pi}{2} + q_E) & 0 & L_{hu} \\ \sin(\frac{\pi}{2} + q_E) & \cos(\frac{\pi}{2} + q_E) & 0 & 0 \\ 0 & 0 & 1 & 0 \\ 0 & 0 & 0 & 1 \end{bmatrix} \\ &= \begin{bmatrix} -\sin q_E & -\cos q_E & 0 & L_{hu} \\ \cos q_E & -\sin q_E & 0 & 0 \\ 0 & 0 & 1 & 0 \\ 0 & 0 & 0 & 1 \end{bmatrix}. \end{aligned} \quad (1)$$

Similarly, DH parameters between Σ_E and Σ_W are $a_{EW} = 0$, $\alpha_{EW} = \pi/2$, $d_{EW} = L_{hf}$ and $\theta_{EW} = q_W$. Therefore, the transformation matrix ${}^E T_W$ between Σ_E and Σ_W is

$${}^E T_W = \begin{bmatrix} \cos q_W & -\sin q_W & 0 & 0 \\ 0 & 0 & -1 & -L_{hf} \\ \sin q_W & \cos q_W & 0 & 0 \\ 0 & 0 & 0 & 1 \end{bmatrix}. \quad (2)$$

The position vector ${}^W p_U$ of the point U on Σ_W is obtained from Fig. 1b, c

$${}^W p_U = [-L_R \quad 0 \quad 0 \quad 1]^T. \tag{3}$$

Therefore, the position vector ${}^O p_U$ of the point U on Σ_O is calculated as follows:

$$\begin{aligned} {}^O p_U &= {}^O T_E^E T_W^W p_U = [X_U \quad Y_U \quad Z_U \quad 1]^T \\ &= \begin{bmatrix} L_R \sin q_E \cos q_W + L_{hf} E + L_{hu} \\ -L_R \cos q_E \cos q_W + L_{hf} E \\ -L_R \sin q_W \\ 1 \end{bmatrix}. \end{aligned} \tag{4}$$

The coordinates of the joint B on Σ_O is also obtained from Fig. 1b, c:

$${}^O p_B = [X_B \quad Y_B \quad Z_B \quad 1]^T = [L_{hu} \quad -L_R \quad 0 \quad 1]^T. \tag{5}$$

The length l_f is defined as the distance between the joints B and U, therefore,

$$\begin{aligned} l_f &= \sqrt{(X_U - X_B)^2 + (Y_U - Y_B)^2 + (Z_U - Z_B)^2} \\ &= \left\{ (L_R \sin q_E \cos q_W + L_{hf} \cos q_E)^2 + (-L_R \cos q_E \cos q_W + L_{hf} \sin q_E + L_R)^2 \right. \\ &\quad \left. + L_R^2 \sin^2 q_W \right\}^{1/2}. \end{aligned} \tag{6}$$

Mathematical operation for Eq. (6) derives the following equation:

$$l_f = \sqrt{L_{hf}^2 + 2L_R L_{hf} \sin q_E + 2L_R^2 (1 - \cos q_E \cos q_W)}. \tag{7}$$

4 Support of Motion

4.1 Idea of “Braking Support”

We can see from Eq. (7) that the displacement l_f of the prismatic joint is related to the two angles of q_E and q_W . From this fact, we can understand that support by power assist with installing an actuator on the prismatic joint is impossible because those angles cannot be independently controlled.

However, it is considered that many situations exist in our daily life where support by power assist is not necessarily needed, for example, carrying a heavy object such as a massive shopping bag. In that case, it is considered that fatigue of a human arm can be decreased by constraining human elbow and forearm with the wearable mechanism. Again, Eq. (7) shows that l_f is related to both q_E and q_W .

Therefore, they can be fixed to certain values if l_f is fixed to a certain value (here, remember that motion ranges of human elbow and forearm are limited to π [rad] at most). This brings an idea of introducing a braking device into the prismatic joint for fixing its length.

4.2 Statics

For further inspection of the above idea (this is a part of future work, unfortunately), deriving statics of the wearable mechanism is helpful. With referring to Fig. 1c, we assume that brake force f_f acts on the prismatic joint, and the brake force brings brake torques τ_E and τ_W on human elbow and forearm. The virtual displacements Δl_f , Δq_E and Δq_W are also assumed for the prismatic joint, the elbow and the forearm. The principle of virtual work derives the following equation:

$$f_f \Delta l_f = \tau_E \Delta q_E + \tau_W \Delta q_W \quad (8)$$

From Eq. (7),

$$\Delta l_f = \frac{\partial l_f}{\partial q_E} \Delta q_E + \frac{\partial l_f}{\partial q_W} \Delta q_W. \quad (9)$$

Substituting Eq. (9) into Eq. (8) yields

$$f_f \left(\frac{\partial l_f}{\partial q_E} \Delta q_E + \frac{\partial l_f}{\partial q_W} \Delta q_W \right) = \tau_E \Delta q_E + \tau_W \Delta q_W. \quad (10)$$

Comparison of both sides of Eq. (10) obtains the following equations:

$$\tau_E = f_f \frac{\partial l_f}{\partial q_E}, \quad \tau_W = f_f \frac{\partial l_f}{\partial q_W}. \quad (11)$$

Substituting partial differentials calculated from Eq. (7) into Eq. (11) finally yields

$$\tau_E = f_f \frac{L_R (L_{hf} \cos q_E + L_R \sin q_E \cos q_W)}{\sqrt{L_{hf}^2 + 2L_R L_{hf} \sin q_E + 2L_R^2 (1 - \cos q_E \cos q_W)}}, \quad (12)$$

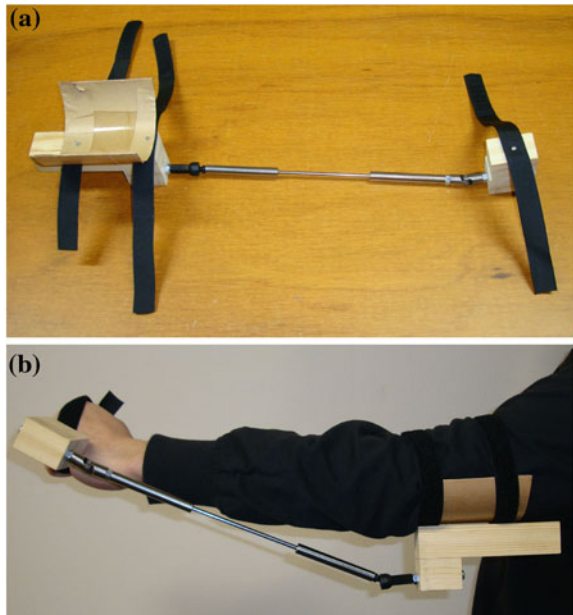
$$\tau_W = f_f \frac{L_R^2 \cos q_E \sin q_W}{\sqrt{L_{hf}^2 + 2L_R L_{hf} \sin q_E + 2L_R^2 (1 - \cos q_E \cos q_W)}}. \quad (13)$$

5 Mockup

For the purpose of designing a prototype in future, a mockup of the mechanism was assembled as shown in Fig. 2a. The left side component including a ball joint (igus AGRM-06LC) is the attachment for a human upper arm, and the right side component including a universal joint (SANYU K-6) is the attachment for a human forearm. Two pipes and a rod connect the components and constitute a prismatic joint.

The view of the mockup mounted on a human arm is shown in Fig. 2b. From this figure, it is verified that the wearable mechanism proposed in this paper is capable of following 2-DOF motion of elbow and forearm. However, the current mockup has some problems. The main problem is assembling of a ball joint. The considerably limited tilt angle of a ball joint makes full range motion of a human elbow impossible. For overcoming this problem, the mounting angle of the ball joint to the upper arm attachment must be carefully considered. This requires mathematical analysis based on the kinematics, and this is a part of future work. Development of the attachments is also needed so that they can satisfy the assumption for three attachment angles (BCO, COE and UWE) depicted in Fig. 1.

Fig. 2 A mockup of the wearable mechanism: **a** full view, **b** view of the mechanism mounted on a human arm



6 Discussion on an Issue for Future Development

Besides the issues found from the mockup, the study in this paper has an issue for future development. It is briefly discussed in this section.

The length L_R shown in Fig. 1c greatly associates with compactness of the mechanism, that is, a smaller L_R is more desirable from a viewpoint of compactness because it realizes a mechanism closer to a human arm. However, we also need to pay our attention to the brake torques τ_E and τ_W , because they are also concerned with L_R .

This paper considers this issue through some examples of the torques calculated under a special angle condition of $q_E = 0$ and $q_W = \pi/2$ [rad]. Substituting those angles into Eqs. (12) and (13) yields

$$\tau_E = f_f \frac{L_R L_{hf}}{\sqrt{L_{hf}^2 + 2L_R^2}}, \quad \tau_W = f_f \frac{L_R^2}{\sqrt{L_{hf}^2 + 2L_R^2}} \quad (14)$$

From a related study [10], we assume that $L_R = 0.034$ m and $f_f = 16.7$ N. In addition, we choose the value of L_{hf} to be 0.2 m because the length of a human forearm can be assumed to be approximately 0.25 m (in the case of Japanese people [11]). The calculation results of the torques are $\tau_E = 0.55$ nm and $\tau_W = 0.094$ nm. If L_R can be stretched to the double length (0.068 m), the brake torques become $\tau_E = 1.0$ nm and $\tau_W = 0.35$ nm.

If we focus on τ_E , its magnitude 1.0 nm is capable of supporting a force of 4 N acting on a human hand. This is obtained by dividing the torque (1.0 nm) by the length of the human forearm (assumed to be 0.25 m) (under the assumption that the long axis of the forearm is perpendicular to the direction of gravitational force). The force of 4 N corresponds to a load of which mass is only 0.4 kg, therefore, it is necessary to improve supporting capacity of the mechanism.

As shown in the above, the brake torques can be increased by increasing L_R , however, a problem is that compactness of the mechanism is vitiated as L_R is increased. Another method of increasing the brake torques is increasing the magnitude of the brake force f_f , as suggested by Eq. (14). For example, it is expected that using an air gripper as a braking device and activating it with highly compressed air increase f_f . Using a pneumatic actuator contributes to maintaining portability of the mechanism, and less controllability of a pneumatic actuator will not become a problem because an air gripper considered here is statically actuated only for generating the brake force. However, the brake force cannot be infinitely increased because it is the frictional force acting between an air gripper and a link of the prismatic joint. Therefore, improving mechanical design of the mechanism will be also necessary. For example, using two or more prismatic joints with braking devices in parallel is a method of increasing the magnitude of f_f .

7 Conclusion

This paper proposed a wearable mechanism for 2-DOF motion generated by human elbow and forearm. An advantage of the proposed mechanism was that rigorous adjustment of attachment positions was unnecessary when the wearable mechanism was attached to a human arm. This paper firstly derived kinematics of the mechanism based on a model including both a human arm and the mechanism. The mechanism proposed in this paper is impossible to support human elbow and forearm by power assist due to lack of DOF of the prismatic joint, however, this paper described that “braking support” constraining the human elbow and forearm was applicable by introducing a braking device into the prismatic joint. The mockup for future design of a prototype suggested that the mounting angle of a ball joint should be improved for realizing full range motion of a human elbow.

This paper finally discussed an issue for future development of the mechanism. Some examples of calculation for the brake torques suggested that capacity of the “braking support” was not satisfactory; however, the discussion also suggested that the capacity can be increased by improving mechanical design of the mechanism.

References

1. Gopura RARC, Kiguchi K (2009) Mechanical designs of active upper-limb exoskeleton robots. IEEE 11th international conference on rehabilitation robotics. 178–187
2. Perry JC, Rosen J et al (2007) Upper-limb powered exoskeleton design. IEEE/ASME Trans Mechatron 12(4):408–417
3. Gopura RARC, Kiguchi K (2009) SUEFUL-7: A 7DOF upper-limb exoskeleton robot with muscle-model-oriented EMG-based control. Proceedings of IEEE/RSJ international conference on intelligent robots and systems. 1126–1131
4. Johnson GR, Carus DA et al (2001) The design of a five-degree-of-freedom powered orthosis for the upper limb. Proc Inst Mech Eng [H] 215:275–284
5. Mihelj M, Tobias N et al (2007) ARMin II – 7 DoF rehabilitation robot: mechanics and kinematics. IEEE international conference on robotics and automation. 4120–4125
6. Rahman MH, Ouimet TK et al (2010) Development and control of a wearable robot for rehabilitation of elbow and shoulder joint movements. Proceedings of 26th annual conference on IEEE industrial electronics society. 1506–1511
7. Noritsugu T, Takaiwa M et al (2011) Development of power assist wear using pneumatic rubber artificial muscles. J Rob Mechatron 21(5):607–613
8. Gupta A, O’Malley MK (2006) Design of a haptic arm exoskeleton for training and rehabilitation. IEEE/ASME Trans Mechatron 11(3):280–289
9. Amigo LE, Casals A et al (2011) Design of a 3-DoF joint system with dynamic servo-adaptation in orthotic applications, Proceedings of IEEE international conference on robotics and automation 2011. Shanghai, China, 3700–3705
10. Morizono T (2012): Design and preliminary evaluation of a wearable elbow joint, Proceedings of IEEE/SICE international symposium on system integration, 13–18
11. Kouchi M, Mochimaru M (2005) AIST Anthropometric Database, National Institute of Advanced Industrial Science and Technology, H16PRO 287 <http://riodb.ibase.aist.go.jp/dhbodydb/91-92/> (in Japanese)

Variable Quantile Level Based Noise Suppression for Robust Speech Recognition

Kangyeoul Lee, Gil-Jin Jang, Jeong-Sik Park and Ji-Hwan Kim

Abstract This paper addresses the issues of single microphone based noise estimation technique for speech recognition in noisy environments. Many researches have been performed on the environmental noise estimation; however, most of them require voice activity detection (VAD) for accurate estimation of noise characteristics. We propose an approach for efficient noise estimation without VAD, aiming at improving the conventional quantile-based noise estimation (QBNE). We fostered the QBNE by adjusting the quantile level according to the relative amount of added noise to the target speech. From the observation that the power spectral density (PSD) of noise is close to the Gaussian distribution, while that of speech is more narrowly populated, the level of additive noise is measured by the selected Gaussianity functions. We compared the proposed method with the conventional QBNE and minimum statistics based method on a simple speech recognition task in various SNR levels. The experimental results show that the proposed method is superior to the conventional methods.

Keywords Quantile-based noise estimation · Speech recognition · Gaussianity

K. Lee (✉) · G.-J. Jang

School of Electrical and Computer Engineering, Ulsan National Institute of Science and Technology, Ulsan, Republic of Korea
e-mail: leeky985@unist.ac.kr

G.-J. Jang
e-mail: gjang@unist.ac.kr

J.-S. Park
Department of Intelligent Robot Engineering, Mokwon University,
Taejon, Republic of Korea
e-mail: parkjs@mokwon.ac.kr

J.-H. Kim
Department of Computer Science and Engineering, Sogang University,
Seoul, Republic of Korea
e-mail: kimjihwan@sogang.ac.kr

1 Introduction

Due to recent advances in technology, the use of automatic speech recognition (ASR) is extremely increased by spread of using smart devices. Although there are several important factors to enhance speech recognition rate, purity of speech is regarded as most crucial one. Unfortunately, the speech is always exposed to numerous acoustic background noises in recording environment as shown in Fig. 1. The service suppliers such as wireless telecommunication companies or application providers for smart devices should take care of handling various background noises, since we commonly use the devices in outdoors.

So far, a lot of noise suppress algorithms are proposed, and they are mostly based on spectral subtraction that is first introduced by Boll in 1979 [1]. It assumes that additive noise changes slowly over time and uncorrelated with speech and approximates the power spectral density (PSD) of the noise signal by an average in non-voice periods. Most conventional methods depend on voice activity detection (VAD) which detects the presence of speech. However, it is not easy to distinguish speech or noise, its performance varies a lot in accordance with types and the amount of additive noises.

Several methods based on spectral subtraction are proposed to eliminate VAD. Minimum statistics-based noise estimation is notable for VAD independent method [2]. It tracks noise power spectrum through taking minimum value of smoothed PSDs of noisy speech. Quantile-based noise estimation (QBNE) is another wide use method that is not required VAD [3]. The basic concept of QBNE succeeded to MS-based method but it assumes that the noise PSD is contained for significant percentage of noisy speech PSD instead taking minimum value. However, due to intrinsic assumptions of the noise characteristics, both methods suffer from performance variation in different noise conditions. The proposed method not only remedies the shortcomings of conventional methods, but also eliminates the need for VAD. Based on observed log PSD of stationary

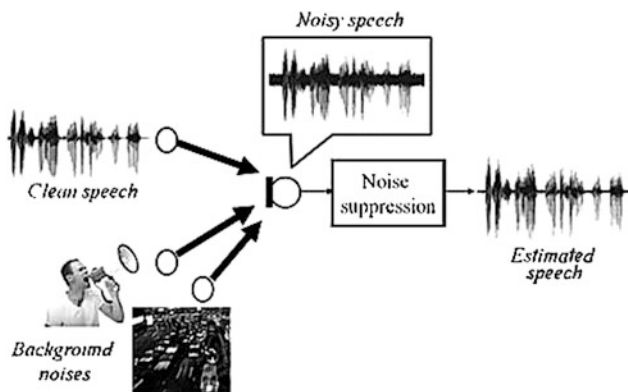


Fig. 1 Single microphone based noise suppression system

noise and speech, we can aware that the distribution of a stationary noise is close or peakier than Gaussian (super-Gaussian), while a speech signal is spreader than Gaussian (sub-Gaussian). Therefore, we impose variable quantile levels according to the measured statistical moments of the log PSD at each frequency. A contrast function is used to classify the super-Gaussian (positive) and the sub-Gaussian (negative) by distance of the given distribution [4], and we adjusted higher quantile level when the distribution is Gaussian or super-Gaussian.

After the estimation, a time-domain Wiener filter suppressing the found noise PSD is derived from the noise estimate and applied to the input noisy speech signal. ASR experiments are carried out on speech separation challenge database [5] to verify improvement of proposed methods. The proposed method shows stable performance over various SNR conditions, while the conventional methods show degraded performance in high or low SNRs.

2 Conventional Qantile-Based Noise Estimation

Spectral subtraction based noise suppression techniques need good noise power spectrum estimator. Most conventional noise estimation methods use VAD to estimate background noise. The VAD updates estimated noise whenever speech is absent. However short pause detection is difficult and the performance of the VAD varies according to the kinds and conditions of noise [6]. On the other hand, [2, 3] and [8] proposed noise estimators that continuously track noise power spectrum for each frequency band regardless of existence of speech. These methods have advantage for reducing errors from VAD.

Usually the noisy signal $y(n)$ is processed frame by frame for STFT, and each frame length is proper to set 10–30 ms for processing. It is assumed that for the duration of a frame, $s(n)$ and $v(n)$ can be considered WSS process. We represent the additive noise to the speech in the PSD domain as follows:

$$|Y(\omega, t)|^2 = |S(\omega, t)|^2 + |V(\omega, t)|^2, \quad (1)$$

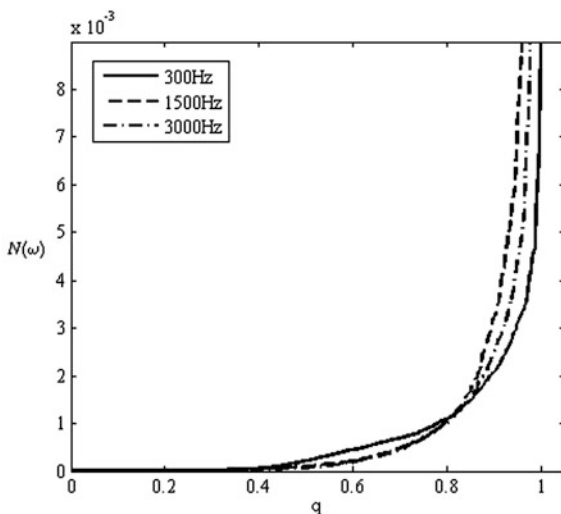
where t is current time index and $Y(\omega, t)$, $S(\omega, t)$ and $V(\omega, t)$ are STFT versions of $y(n)$, $s(n)$, and $v(n)$ respectively.

Stahl proposed QBNE which takes q th quantile of the noisy speech spectrum. QBNE assumes that the noise power for each frequency band is contained for significant percentage of noisy speech segment. In order to estimate noise power spectrum, firstly, observed power spectrum frames $|Y(\omega, t_m)|^2, m = 0, \dots, D$ are sorted for a frequency band ω as below equation where D is fixed window length.

$$|Y(\omega, t_0)|^2 \leq |Y(\omega, t_1)|^2 \leq \dots \leq |Y(\omega, t_D)|^2. \quad (2)$$

The noise power spectrum at each frequency band is estimated by taking q th quantile as follows.

Fig. 2 Quantiles of PSD at 300 Hz, 1.5 kHz and 3 kHz in speech signal of the TIMIT corpus



$$|\hat{V}(\omega, t)|^2 = |Y(\omega, t_{[qD]})|^2 \tag{3}$$

For instance, $q = 1$ yields the maximum, $q = 0$ the minimum, and $q = 0.5$ the median. It is found that $q \approx 0.5$ is optimal empirically, as shown in Fig. 2. The QBNE method has very simple concept and can track noise power spectrum without reference to speech presence as MS based method. However estimated noise power will be close to speech power component when little amount of noise is added. In that case, speech can be eliminated as well as additive noise when performing Wiener filtering. As a result, overestimation of noise power spectrum may distort the output signal and it leads low recognition rate.

3 Variable Quantile Level Estimation Using Negentropy

In high SNR condition, speech power can be presumed as noise power and it leads to increase distortion of output signal. One of the representative characteristics of stationary noise is that its power spectrum does not vary too much along time [8]. For example, Fig. 3a, b and c show the histograms for 2 kHz log-scale power spectrum of the airport, babble and restaurant noise from AURORA-2 database, respectively. As shapes of distributions, the histograms of noises are near to Gaussian distribution or super-Gaussian. On the other hand, as we discussed [4], speech varies much faster than noise and power is spread broadly. This phenomenon makes a shape of log scale histogram deviate from Gaussian. Figure 3d shows such shape of log-scale histogram which is much broader than Gaussian.

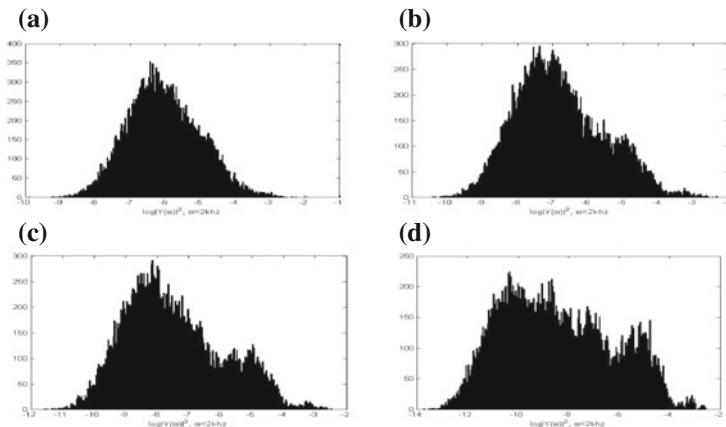


Fig. 3 Histogram of log-scale PSD for various noises and clean speech at 2 kHz: **a** SNR: 0 dB, **b** SNR: 5 dB, **c** SNR: 10 dB and **d** SNR: 20 dB

In noisy speech problem, we could expect that the more the environment is noisy, the more a distribution of logarithm power spectrum nears to super-Gaussian. If a distribution is getting sharp, SNR of a frequency band is getting low. In this case, QL had to be adjusted to higher level. On the other hand, a distribution is getting obtuse means that SNR of input signal is getting high, so we need to choose low QL. So Gaussianity is the key factor for measuring degree of contamination of the noisy speech as well as selecting the optimal quantile levels.

For example, let $\mathbf{b}(\omega, t)$ logarithm power spectrum buffer at current time t .

$$\mathbf{b}(\omega, t) = \left[\log\left(|Y(\omega, t - D)|^2\right), \log\left(|Y(\omega, t - D + 1)|^2\right), \dots, \log\left(|Y(\omega, t)|^2\right) \right], \tag{4}$$

where D is the buffer length. We define \hat{r} which represents Gaussianity and segment SNR indirectly as Eq. (33). Input buffer $b(\omega, t)$ needs to force zero mean with unit variance before function $f(\cdot)$ which estimates Gaussianity of the distribution is performed.

$$\hat{r} = f\left(\frac{\mathbf{b}(\omega, t) - E(\mathbf{b}(\omega, t))}{\sigma_b}\right), \tag{5}$$

where σ_b is standard deviation of $\mathbf{b}(\omega, t)$. And then we need to map \hat{r} to $q_{\hat{r}}$ which is optimal quantile level for estimating noise power of segment $\mathbf{b}(\omega, t)$ according to the function $f(\cdot)$. Finally, noise power spectrum can be estimated as following equation.

$$|\hat{V}(\omega, t)|^2 = |Y(\omega, t_{[q_{\hat{r}}T]})|^2. \tag{6}$$

To measure the Gaussianity exactly, Hyvärinen proposed the negentropy based method which estimates non-Gaussianity of a random variable without suffering outlier effect [9]. The entropy of a random variable \mathbf{x} with probability density $f(\mathbf{x})$ is defined as

$$H(\mathbf{x}) = - \int f(\mathbf{x}) \log f(\mathbf{x}) dx. \quad (7)$$

An important property of Gaussian distribution is that it has the maximum entropy among all distribution over the entire real axis $[-\infty, \infty]$. The uniform distribution has the maximum entropy among all distributions over a finite range. Based on this property, the negentropy is defined as

$$J(\mathbf{x}) = H(\mathbf{x}_G) - H(\mathbf{x}), \quad (8)$$

where \mathbf{x}_G is Gaussian random variable of the same mean and variance with \mathbf{x} . Since entropy of Gaussian is the largest over all random variable, negentropy is always greater than zero, and it is zero if and only if \mathbf{x} follows Gaussian random variable. The problem for using negentropy is that it is very difficult for computation hence approximations of negentropy are needed. An approximation is proposed by Hyvärinen as

$$J(\mathbf{u}) \approx \sum_{i=1}^p k_i [E\{G_i(\mathbf{u})\} - E\{G_i(\mathbf{g})\}]^2 \propto [E\{G(\mathbf{u})\} - E\{G(\mathbf{g})\}]^2, \quad (9)$$

where k_i are some positive constants, and \mathbf{g} is a normal distribution. Although this approximation may be not accurate, Eq. (9) can be used to construct a measure of non-Gaussianity that is consistent in the sense that it is always non-negative, and equal to zero if \mathbf{u} follows Gaussian distribution. G_i are some non-quadratic functions such as

$$G_1(\mathbf{u}) = \frac{1}{a} \log(\cosh(a\mathbf{u})), \quad G_2(\mathbf{u}) = - \exp\left(-\frac{\mathbf{u}^2}{2}\right), \quad (10)$$

where $1 \leq a \leq 2$ is suitable constant. Since results of $E\{G(\mathbf{u})\}$ indicates that how \mathbf{u} is close to Gaussian distribution, we can use it for estimating the Gaussianity. In this manner, function $G(\cdot)$ is useful for setting QL instead of kurtosis. If distribution \mathbf{u} is getting sharp, the result of function $G(\mathbf{u})$ gets small. It means that SNR of a frequency band is getting low, thus we need to set high QL. While increasing output value of function $G(\mathbf{u})$, distribution \mathbf{u} is getting obtuse. In other words, if SNR of input signal is getting high, we need to choose low QL. We define \hat{r}_i which can estimate Gaussianity and segment SNR indirectly as follow,

$$\hat{r}_i^N = E\left\{G_i\left(\frac{\mathbf{b}(\omega, t) - E\{\mathbf{b}(\omega, t)\}}{\sigma_{\mathbf{b}}}\right)\right\}, \quad i = \{1, 2\}, \quad (11)$$

where, i is a type of quadratic function and $\sigma_{\mathbf{b}}$ is standard deviation of $\mathbf{b}(\omega, t)$. Basically, QBNE works well in very noisy condition. As mentioned before,

\hat{r}_i which is smaller than or equal to some threshold means that the distribution of log scale power spectrum is close to Gaussian, therefore the signal is low SNR. Optimal quantile level corresponding to \hat{r}_i is experimentally found as below equation.

$$q_r^N = \begin{cases} 0.5; & \hat{r}_1 < 0.447 \text{ or } \hat{r}_2 < -0.692 \\ 0.1; & \text{otherwise} \end{cases} \quad (12)$$

Finally, estimated noise power for each frequency band can be obtained as follows,

$$|\hat{V}(\omega, t)|^2 = |Y(\omega, t_{[q_r^N T]})|^2. \quad (13)$$

4 Experimental Results

To verify improvement, we compared the two types of proposed methods to the QBNE and MS based method separately, by automatic speech recognition experiments on the Speech Separation Challenge (SSC) database [5]. The SSC database has clean speech set of 17,000 utterances for training, spoken by 34 different speakers. The training set is recorded in quiet condition without any background noise. Each utterance consists of 6 words in the format, such as “command-color-preposition-letter-number-adverb”. For example, “bin-blue-on-A-5-soon”.

The acoustic models of the words are built by the HTK. The features are extracted by 39-dimensional vectors consisting of 12 MFCCs plus log energy, plus their velocities and accelerations at every 10 ms. We also employ separate testing set of 600 utterances which is exclusive with training set.

The proposed methods are evaluated on 8 different noise environments, “airport, babble, car, exhibition, restaurant, street, subway and train”, from the AURORA-2 database and noises are added to clean speeches. We simulated in 6 different SNR conditions, such as 20, 16, 12, 8, 4 dBs and clean speech. All HMMs are trained by clean speech to verify degree of noise reduction.

In Table 1, “None” column lists the performance results without noise suppression. Each row is the average recognition rates over all noise types in specific SNRs. The proposed methods are about 6.0 and 5.9 % better than “None”, whereas QBNE and MS are 4.4 and 3.2 % better. QBNE performed quite well under severe noisy conditions; on the contrary, the performance of MS becomes better as SNR increases, and best in clean condition. The variable quantile level based approaches take both advantages of QBNE and MS. In 12 dB SNR, the performances of the proposed methods are similar to MS on the average; in 8 dB SNR, they are slightly better and QBNE, and much better than the others.

Table 1 Results of speech recognition experiments

SNR	None (%)	MS (%)	QBNE (%)	Proposed	
				Neg-1 (%)	Neg-2 (%)
Clean	97.56	97.61	95.39	96.00	96.00
20 dB	94.14	94.83	92.45	94.61	94.48
16 dB	89.94	91.70	90.19	92.19	91.99
12 dB	80.46	84.26	85.42	87.40	87.28
8 dB	64.62	70.47	75.83	77.65	77.33
4 dB	45.30	52.08	59.33	60.40	60.31
Average	78.67	81.82	83.10	84.71	84.57

5 Conclusion

This paper proposed a novel noise estimation technique without VAD. The MS based method and QBNE are conventional VAD-free methods, however they have some shortcoming for various SNR environments. To overcome it, we proposed a noise estimation method regarding to adjusting QL for each frequency band according to estimated SNR. The shape of the log power spectral densities at individual frequency band is compared to Gaussian by statistical moments, and binary QLs are obtained by the measured moments. To evaluate the proposed methods, we performed speech recognition experiments on a simple speech recognition task. Experimental results show that the proposed methods work well in various SNR conditions when compared to conventional methods. Future research issues include finding new contrast functions for better approximation of noise presence.

Acknowledgments This work was supported by the Basic Science Research Program through the National Research Foundation of Korea (NRF) funded by the Ministry of Education, Science and Technology (No. 2012-0008090).

References

1. Boll S (1979) Suppression of acoustic noise in speech using spectral subtraction. *IEEE Trans Acoust Speech Signal Process* 2:113–120
2. Martin R (1994) Spectral subtraction based on minimum statistics. In: *Proceeding of 7th European signal processing conference, EUSIPCO-94, Edinburgh, Scotland*, pp 1182–1185
3. Stahl V, Fischer A, Bippus R (2000) Quantile based noise estimation for spectral subtraction and wiener filtering. In: *Proceeding of ICASSP*, vol 3, pp 1875–1878
4. Lee T-W, Girolami M, Sejnowski TJ (1999) Independent component analysis using an extended infomax algorithm for mixed subgaussian and supergaussian sources. *Neural Comput* 11(2):417–441
5. Cooke M, Hershey J, Rennie S (2010) Monaural speech separation and recognition challenge. *Comput Speech Lang* 24(1):1–15

6. Jang G-J, Cho H-Y (2011) Efficient spectrum estimation of noise using line spectral pairs for robust speech recognition. *Electron Lett* 47(25):1399–1401
7. Pearce D, Hirsch H (2000) The AURORA experimental framework for the performance evaluations of speech recognition systems under noisy condition. In: *Proceeding of INTERSPEECH*, pp 29–32

An Efficient Resource Management Scheme Based on Locality for P2P Overlay Network

Chung-Pyo Hong, Jin-Chun Piao, Cheong-Ghil Kim, Sang-Yeob Na
and Tae-Woo Han

Abstract In a mobile environment, there are limitations: limited power supply, smaller user interface, limited computing power, limited bandwidth and limited storage space; and above limitations must be considered for deploying a p2p overlay network. Locality and mobility are important factors as well as the limitations in a mobile environment. Based on the above assumption, we propose a mobile locality-based hierarchical p2p overlay network (MLH-Net) to address locality problems without any other services. In this paper, we introduce a novel profile called PCSN-List and node management scheme. MLH-Net is constructed as two layers, an upper layer formed with super-nodes and a lower layer formed with normal-nodes. Because super-nodes can share advertisements, we can guarantee physical locality utilization between a requestor and a target during any discovery process. To overcome a node failure, we propose a simple recovery mechanism. The simulation results demonstrate that the hop value of MLH-Net is 21 % decreased compared with JXTA when discovering nodes. And also, the average distance is decreased by 45 % as the number of max-hop is increased.

C.-P. Hong (✉) · J.-C. Piao
Yonsei University, 5-4, Sinchon-dong, Seodaemun-gu, Seoul, South Korea
e-mail: hulkboy@yonsei.ac.kr

J.-C. Piao
e-mail: kumcun@yonsei.ac.kr

C.-G. Kim · S.-Y. Na
Namseoul University, 21, Mae Ju-ri, Seonghwan-eup, Seobuk-gu,
Cheonan-si, Chungnam, South Korea
e-mail: cgkim@nsu.ac.kr

S.-Y. Na
e-mail: nsy@nsu.ac.kr

T.-W. Han
Woosong University, 171, Dongdaeyeon-ro, Dong-gu, Daejeon, South Korea
e-mail: bluebird@wsu.ac.kr

1 Introduction

DHT-based p2p systems distribute nodes and resources uniformly over a p2p overlay network. These p2p systems provide good load-balancing, but they have a locality problem. In a mobile environment, there are many mobile devices such as PDAs and cell phones, and query results from resources that are physically close to the requestor should be more efficient and useful. Therefore, we should support both locality and mobility when deploying a p2p overlay network in a mobile environment.

In this paper, we propose a mobile locality-based hierarchical p2p overlay network, called MLH-Net. It is based on the p2p overlay network of JXTA. MLH-Net is motivated to address locality problems without other external services, to provide load-balancing of DHT simultaneously, and to support mobility. In a mobile environment, there are major limitations such as limited power, computing capability, bandwidth, storage space, and an insufficient user interface. To deploy a p2p overlay network in a mobile environment, these limitations should be considered. In particular, we have considered mobility and locality as important features. MLH-Net addresses the locality problem by using mobility without any other external services such as GPS. Second, we provide a recovery mechanism within a given p2p overlay network to support mobility because the p2p overlay network should be dynamically reconfigured. Because the MLH-Net guarantees one hop during the locality-based discovery process, simulation results show that the hop value of MLH-Net is 21 % decreased compared with JXTA when discovering nodes. And also, the average distance is decreased by 45 % as the number of max-hop is increased.

The rest of this paper is organized as follows. Other p2p systems for improving locality are described in [Sect. 2](#). The system overview is introduced in [Sect. 3](#). In [Sect. 4](#), the evaluation result is presented. And finally, the conclusion is shown in [Sect. 5](#).

2 Related Work

To address the locality problem, p2p systems such as Grapes [1], SkipNet [2], Brocade [3], and Jelly [4] have designed their own approaches. Grapes uses a hierarchical virtual network to support lookup services. The hierarchical virtual network consists of sub-networks which consist of physically close nodes and a super-network which consists of the leaders of sub-networks. Resources and nodes increase in a sub-network and then the leader of that sub-network sacrifices load-balancing in a super-network. Our goal is to deploy a p2p overlay network for improving locality in a mobile environment. These systems cannot support both locality and mobility.

SkipNet [2] uses a scalable overlay network to provide two kinds of locality: content locality and path locality. Content locality distributes data to a specific node in a given organization, and path locality prevents messages between two nodes in the same organization from being routed outside that organization. To provide efficient message routing, they use two separate, but related address spaces: a string name ID space and a numeric ID space. The string name ID space is mapped by node names and content identifier strings, and the numeric ID space is mapped by hash values of the node names and content identifiers. SkipNet cannot provide load-balancing for the overall system but instead provides constrained load-balancing for a subset of nodes in a system.

3 Proposed Scheme

In this section, we overview the proposed p2p system, a mobile locality-based hierarchical p2p overlay network. Specifically, its structure and management mechanism are explained. MLH-Net is constructed as two layers, i.e., the upper layer and the lower layer. The upper layer is configured with super-nodes and the lower layer is configured with normal-nodes, where each normal-node is connected to its associated super-node.

3.1 *The Proposed P2P Architecture*

An example of the proposed p2p system, as shown in Fig. 1, shows the basic structure of MLH-Net. As in Fig. 1, a super-node is connected to a group of normal-nodes, which are connected to each other. When a normal-node needs to identify some specific resources, a discovery query is propagated through the upper layer. If this request can be serviced by any specific target, which is physically close to itself, propagating this query may waste network bandwidth and cause unnecessary traffic. The main goal of MLH-Net is to prevent a discovery query from being propagated through the overall p2p overlay network and thus to guarantee a physically short distance between requestor and target.

3.2 *The Recovery Mechanism*

To recover our hierarchical p2p overlay network, two kinds of nodes, i.e., a normal-node and a super-node have to be able to change their roles dynamically. Because all normal-nodes need one connected super-node to publish advertisements and to discover resources, we need a recovery mechanism for super-node failure. A failed

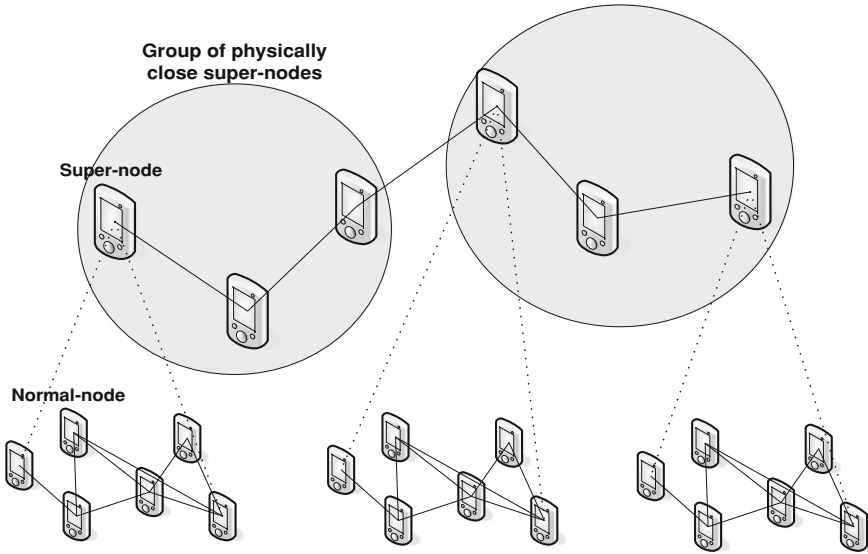


Fig. 1 The conceptual model of the proposed architecture

super-node will exit the p2p overlay network. In this section, we discuss this recovery mechanism.

The recovery mechanism is very important because the method is directly related to the safety of the p2p overlay network and each sub-network requires one super-node to participate in a p2p overlay network. Super-nodes communicate with each other through an upper layer network.

One example of the recovery method, in Fig. 2, shows the case where one normal-node becomes a super-node. In Fig. 2, S1 is a super-node and N1–N3 are normal-nodes. If S1 exits the network, the sub-network of S1 is destroyed and N1–N3 (which were connected to S1) cannot participate in a p2p overlay network. The data which are propagated and which are related to N1 become inconsistent. Because S1 exits the p2p overlay network, a normal-node must become a super-node. The recovery process is described in Fig. 2.

4 Evaluation

In this section, we describe the evaluation result of the proposed architecture compared with the conventional P2P model called JXTA. In this experiment, some parameters are chosen as limited values. The map size is 200.200, the percentage of super-nodes is 20 % over the total number of nodes: 1000, the number of movements is 1000, and the number of discoveries is 1000.

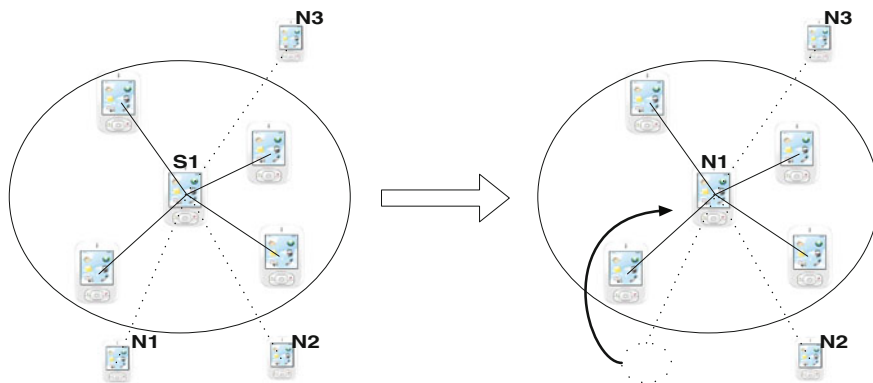


Fig. 2 An example of the node recovery

In Fig. 3, the hop value of JXTA is 3.42 in all graphs. The hop values of MLH-Net are 3.11, 2.98, 2.79, and 2.7, respectively. The gap between MLH-Net and JXTA increases while the max-hop value increases. For the first bar case, the hop value of MLH-Net is 3.11 and this is 9 % decreased compared with that of JXTA. For the last bar case, the hop value of MLH-Net is 2.7. This is a 21 % decrease compared with JXTA.

In Fig. 4, the y-axis shows the average total distance to target for any discovery query being propagated. While the max-hop value increases, the y-axis value of MLH-Net decreases and the gap between MLH-Net and JXTA increases.

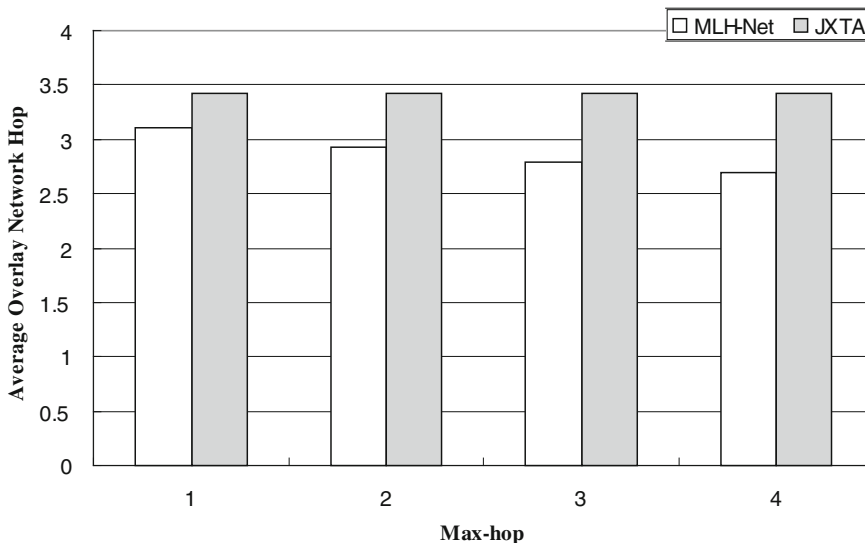


Fig. 3 Hop for the increasing number of max-hop

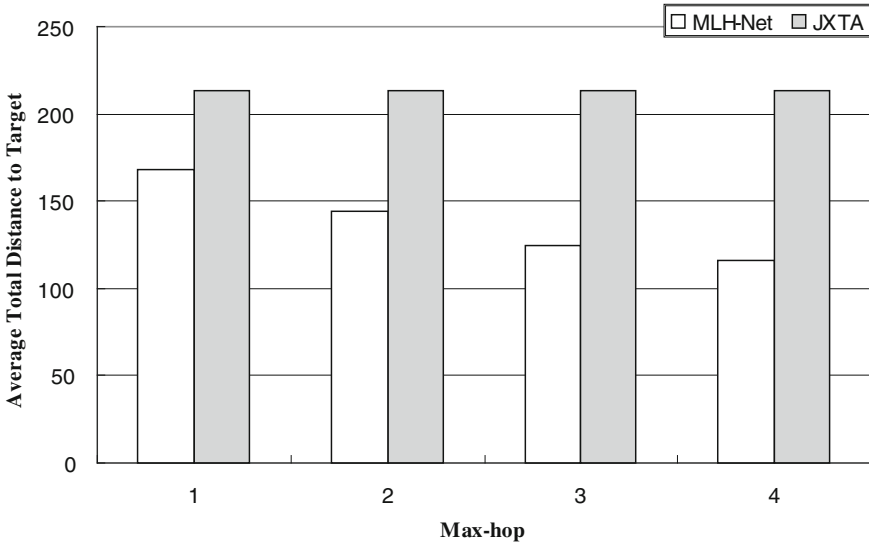


Fig. 4 Average distance for the increasing number of max-hop

The y-axis value of JXTA is 213 for all cases and the y-axis values of MLH-Net are 168, 144, 125, and 116, respectively. For the first bar case, the y-axis value of MLH-Net is 168. This is a 21 % decrease compared with JXTA. For the last bar case, the y-axis value of MLH-Net is 116. This is a 45 % decrease compared with that of JXTA.

5 Conclusion

DHT-based p2p systems distribute nodes and resources uniformly over a p2p overlay network. These p2p systems provide good load-balancing, but they have a locality problem. In a mobile environment, there are many mobile devices such as PDAs and cell phones, and query results from resources that are physically close to the requestor should be more efficient and useful. Therefore, we should support both locality and mobility when deploying a p2p overlay network in a mobile environment. In this paper, we introduce a novel profile called PCSN-List and node management scheme. MLH-Net is constructed as two layers, an upper layer formed with super-nodes and a lower layer formed with normal-nodes. And also, we propose a simple recovery mechanism. The simulation results demonstrate that the hop value of MLH-Net is 21 % decreased compared with JXTA when discovering nodes. And also, the average distance is decreased by 45 % as the number of max-hop is increased.

References

1. Shin K, Lee S, Lim G, Yoon H, Ma J (2002) Grapes: topology-based hierarchical virtual network for peer-to-peer lookup services. In: Proceedings of international conference on parallel processing workshops, pp 159–166
2. Harvey NJA, Jones MB, Saroiu S, Theimer M, Wolman A (2003) SkipNet: a scalable overlay network with practical locality properties. In: Proceedings of 4th USITS, pp 113–126
3. Zhao BY, Duan Y, Huang L (2002) Brocade: landmark routing on overlay networks. In: Proceedings of the 1st international workshop on peer-to-peer systems, pp 34–44
4. Hsiao R, Wang S (2004) Jelly: a dynamic hierarchical P2P overlay network with load balance and locality. In: Proceedings of the international conference on distributed computing systems workshops, pp 534–540

Parallel SAD for Fast Dense Disparity Map Using a Shared Memory Programming

Cheong Ghil Kim

Abstract The depth map extraction from stereo video is a key technology of stereoscopic 3D video as well as view synthesis and 2D-3D video conversions. Sum of Absolute Differences (SAD) is a representative method to reconstruct disparity map. However, dense disparity map implementation requires heavy computations and extensive memory accesses. In this situation, the rapid advance of computer hardware and popularity of multimedia applications enable multi-core processors to become a dominant market trend in desk-top PCs as well as high end mobile devices; this movement allows many parallel programming technologies to be realized in users computing devices. Therefore, this paper proposes a parallel algorithm for SAD operation using a shared memory programming, OpenMP, which can provide the advantage to simplify managing and synchronization of program threads. The parallel implementation results show the 2.5 times of performance improvements on the processing speed compared with the serial implementation.

1 Introduction

In order to keep increasing PC performance, the architecture of modern micro-processors had put emphasis on increasing CPU clock speed and putting more transistors in single core processors. As a result, the complexity of a chip continued to grow at roughly the same rate as stated in Moore's law in transistor count and the speed of CPU, with no doubt, was expected to increase continuously over 10 GHz at an accelerating pace. However, this trend is facing the theoretical and practical limit of power dissipation which is proportional to both clock speed and

C. G. Kim (✉)

Department of Computer Science, Namseoul University, #91 Daehak-ro,
Senghwn-eub, Seobuk-gu, Cheonan, Chungnam 331-707, Korea
e-mail: cgkim@nsu.ac.kr

transistor count. In consequence, multi-core processor architecture [1] has emerged as a dominant market trend in desk-top PCs while preserving the CPU clock speed between 3 and 4 GHz. This movement enables a single chip to increase the performance capability without requiring a complex system and increasing the power requirements. Therefore, single-core CPUs are actually hard to find and two-, three-, and four-core CPUs become normal in the market [2].

In this situation, another solution to increase PC performance could be improving efficiency by taking advantage of parallelism in software rather than depending on hardware technologies. Therefore, parallel programming becomes an important issue of a multi-core system, since it enables full use of the market dominant hardware system. Especially, Open Multi-processing (OpenMP) [3], an open specification Application Programming Interface (API), provides an easy low-burdensome method for threading applications based on shared memory architecture. In the OpenMP programming model, the parallelization has been implemented on a high abstraction level, which allows efficient parallelized C/C++ -programs for parallel processors featuring a shared memory by adding specific OpenMP directives into the C-program code. These directives support the distribution of autonomous subtasks (threads) over the available processor cores [4].

This paper presents the effectiveness of parallel programs in multi-core hardware architecture. For this purpose, we parallelize SAD algorithm, a representative method to reconstruct disparity map requiring heavy computations and extensive memory accesses, using OpenMP. And the performance evaluation was made by comparing its processing time with the serial implementation.

The organization of this paper is as follows. Section 2 introduces the background of SAD algorithm and OpenMP. Section 3 discusses the design of parallel SAD using OpenMP. Section 4 covers the results of simulation about the the implementation of parallel SAD with comparison with its serial implementation. In Sect. 5, we conclude our result and discuss further perspectives.

2 Background

2.1 Disparity Map and SAD

Stereoscopic 3D has been studied extensively due to its usefulness in many applications like 3D scene reconstruction, robot navigation, civil engineering, manufacturing, and so on. Especially, stereo matching is one of the most active research areas and many different algorithms have been introduced [5]. In stereoscopic 3D, two images of a scene from different viewpoints, called as left and right images, are utilized and the difference in the positions of the two corresponding points in the image pairs is called disparity. From the disparity, we can calculate depth.

Sum of absolute differences (SAD) is an algorithm for measuring the similarity between image blocks. It works by taking the absolute difference between each

pixel in the original block and the corresponding pixel in the block being used for comparison. These differences are summed to create a simple metric of block similarity. It computes the intensity differences for each center pixel (i, j) in a window $W(x, y)$ as follows:

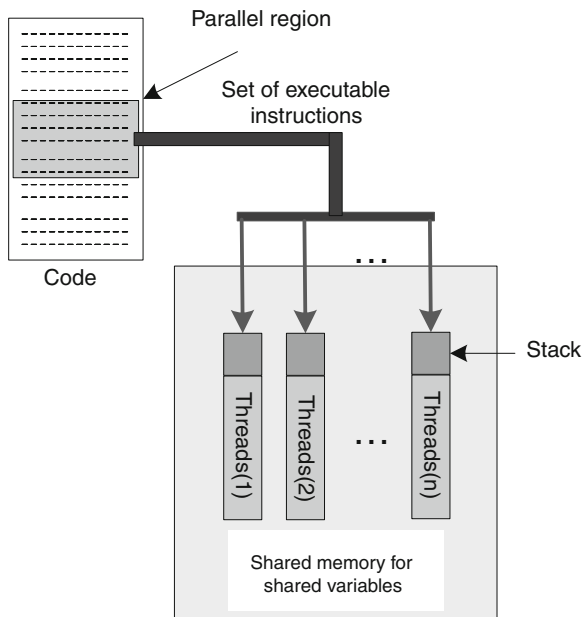
$$SAD(x, y, d) = \sum_{(i,j) \in W(x,y)}^N |I_L(i, j) - I_R(i - d, j)|, \tag{1}$$

where I_L and I_R are pixel intensity functions of the left and right image, respectively. $W(x, y)$ is square window that surrounds the position (x, y) of the pixel. The disparity $SAD(x, y, d)$ calculation is repeated within the x -coordinate frame in the image row, defined by zero and maximum possible disparity d_{max} of the searched 3D scene. The minimum difference value over the frame indicates the best matching pixel, and position of the minimum defines the disparity of the actual pixel [6, 7].

2.2 OpenMP

In OpenMP, all threads can access global and shared memories. Programmers can control the number of threads. Optimal performance occurs when the number of threads represents the number of processors. Figure 1 depicts the operational block diagram of OpenMP in which how a process can be divided into several threads.

Fig. 1 Operational block diagram of OpenMP



Here, a master thread exists to assign tasks to threads, i.e., fork-join. Fork-join time increases when there are more threads than processors. Moreover, data can be labeled with private or shared. In particular, private data are visible to one thread while all threads can spot shared data. In practical programs, local variables which are about to be parallelized should be private. Additionally, global variables must be assigned as shared data. OpenMP requires a compiler. Most IDEs today accommodate OpenMP. Numerous benefits exist to using OpenMP, e.g., preservation of serial code, simplicity, flexibility and portability. Nevertheless, explicit synchronization remains as an issue that to be addressed [8].

3 Parallel SAD

Disparity map calculation is a estimation is a pixel-by-pixel basis to find corresponding pixels for the left and right image pair. Generally, this computing procedure can be characterized as having no dependency between processes. This means that these kinds of application are inherently suitable for making use of parallel processing. The basic processing concept of SAD is accumulating absolute differences of left image and right image pixels within a given window. Using the Eq. (1), the least SAD is determined to be the disparity.

By using OpenMP, initially SAD program is executed by one process; and then it activates light-weight processes (threads) at the entry of a parallel region. After that each thread executes a task comprised of a group of instructions. An OpenMP program is an alternation of sequential regions and parallel regions. A sequential region is always executed by the MASTER thread, the one whose rank equals 0. A parallel region can be executed by many threads at once. Threads can share the work contained in the parallel region.

Figure 2 shows the possible parallelizable code blocks in SAD program. The work-sharing consists mainly of executing a loop by dividing up iterations between the threads; executing many code sections but only one per thread; executing many occurrences of the same procedure by different threads. During the execution of a task by a thread, a variable can be read and/or updated in memory. When it is defined either in the stack (local memory space) of a thread, it becomes a private variable; when in a shared-memory space accessible by all the threads, it is a shared variable.

4 Simulation Result

In order to evaluate the performance improvement of OpenMP SAD implementation over its serial one, the processing time was measured. Table 1 describes the experimental environment using Intel Core I7 CPU Q 740 @ 1.73 GHz. In this

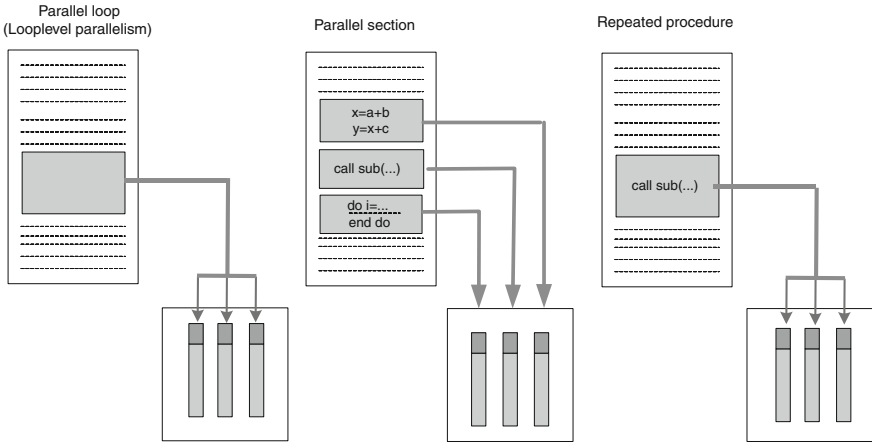
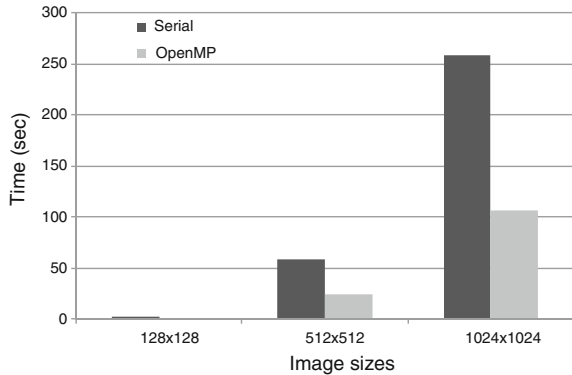


Fig. 2 Parallel SAD implementation

Table 1 Simulation environment

	Description
CPU	Intel(r) Core(TM) I7 CPU Q 740 @ 1.73 GHz
RAM	8.00 GB
System	Windows 7 (64 bit)
IDE	Microsoft visual studio 2010

Fig. 3 Performance improvement of OpenMP over the serial implementation



work, we just estimate the processing time of SAD algorithm so that for the simplicity we used the pixel data only rather than reading from real image pairs.

As for the number of thread, we used 4 threads. The increase of number of threads over 4 resulted in the degradation of the overall performance. This was because the increased threads caused the overhead of thread distribution of master thread.

Figure 3 shows the performance improvements of OpenMP implementations on various image sizes. In all image sizes, over two times improvements was achieved and the ratios become larger as the increase of image sizes.

5 Conclusion

In this paper, we presented basic concepts of parallel implementation of SAD using OpenMP. SAD is a representative method to reconstruct disparity map from stereo video and a key technology of stereoscopic 3D. Because it requires heavy computation, SAD computation is suitable for parallel processing. The parallel implementation results show the 2.5 times of performance improvements on the processing speed compared with the serial implementation. Our future work will include the disparity map computations with real image pairs and this will increase the performance improvement of OpenMP over the serial implementation more.

Acknowledgments This research is supported by Ministry of Culture, Sports and Tourism (MCST) and Korea Creative Content Agency (KOCCA) in the Culture Technology (CT) Research and Development Program 2013.

References

1. Kayi A, Yao Y, El-Ghazawi T, Newby G (2007) Experimental evaluation of emerging multi-core architectures. In: Proceeding of IPDPS 2007, pp 1–6
2. Kim CG, Kim JG, Lee DH Optimizing image processing on multi-core CPUs with Intel parallel programming technologies. Multimedia tools applications, Springer. doi:[10.1007/s11042-011-0906-y](https://doi.org/10.1007/s11042-011-0906-y)
3. OpenMP official web site: www.openmp.org
4. Blume H, von Livonius J, Rotenberg L, Noll TG, Bothe H, Brakensiek J (2008) OpenMP-based parallelization on an MPCore multiprocessor platform—a performance and power analysis. J Syst Architect 54:1019–1029
5. Scharstein D, Szeliski R (2002) A taxonomy and evaluation of dense two-frame stereo correspondence algorithms. Int J Comput Vis 47:7–42
6. Kamencay P, Breznán M, Jarina R, Lukac P, Zachariasova M (2012) Improved depth map estimation from stereo images based on hybrid method. Radioengineering 21(1):70–78
7. Kuhl A (2005) Comparison of stereo matching algorithms for mobile robots. Centre for Intelligent Information Processing System, University of Western Australia, pp 4–24
8. Song Y, Ho YS (2011) Fast disparity map estimation using multi-thread parallel processing. In: International Conference on Embedded Systems and Intelligent Technology (ICESIT), pp 1–4

A Study on Object Contour Tracking with Large Motion Using Optical Flow and Active Contour Model

Jin-Woo Choi, Taek-Keun Whangbo and Nak-Bin Kim

Abstract In this study, an object contour tracking method is proposed for an object with large motion and irregular shapes in video sequences. To track object contour accurately, an active contour model was used, and the initial snake point of the next frame is set by calculating an optical flow of feature points with changing curvature in the object contour tracked from the previous frame. Here, any misled optical flow due to irregular changes in shapes or fast motion was filtered by producing an edge map different from the previous frame, and as a solution to the energy shortage of objects with complex contour, snake points were added according to partial curvature for better performance. Findings from experiments with real video sequences showed that the contour of an object with large motion and irregular shapes was extracted precisely.

Keywords Object contour tracking · Optical flow · Active contour model

1 Introduction

With the growing interest in the 3D videos, displays such as 3D TV and broadcasting technologies that make it possible to watch 3D videos have been developed and gaining popularity in a quick pace recently. However, despite ever-growing

J.-W. Choi (✉)
CT Research Institute, Seongnam-si,
Republic of Korea
e-mail: cjw49@paran.com

T.-K. Whangbo · N.-B. Kim
Department of Interactive Media, Gachon University, Seongnam-si,
Gyeonggi-do, Republic of Korea
e-mail: tkwhangbo@gachon.ac.kr

N.-B. Kim
e-mail: nabkim@gachon.ac.kr

demands for the 3D contents, available 3D contents are very rare due to limited production time and money [1, 2]. The 2D-to-3D technology that converts existing 2D images to 3D videos has been drawing attention lately as a solution to this. Although there are a number of ways of realizing such a technology, generally, 2D-to-3D conversion works in the following manner [1].

- Object Extraction or Segmentation
- Depth Map Assignment or Generation
- Rendering or Occlusion
- Re-touch

In this technology, conversion is conducted by means of (1) manual conversion, (2) non real-time software automatic conversion, and (3) real-time hardware automatic conversion, depending on the use of contents, costs, and the quality of videos [1]. It usually takes six months and 300 staffers to carry out manual conversion to attain the level of movie-like quality, and a hybrid conversion technology that combines software conversion based on an image-processing function and manual work has been emerging to reduce manual work necessary for video conversion and meet quality requirements [1]. To produce quality scene-based video sequences that are properly classified, the operator intervenes to deliberately extract individual objects and subtract the background for the first frame before producing depth map through geometric analysis. The next frames are converted automatically within a reasonable time on the basis of data used for the first frame. Here, it is highly important for the operator to correctly track the contour of an object subtracted from the first frame in subsequent frames, and the more irregular the shape of the object is and the larger its movement becomes, the harder tracking gets.

In this study, we propose a method of tracking contour of an object with larger motion and irregular shapes in video sequences for the 2D-to-3D conversion in a stable manner. Regarding this issue, we explain existing object contour tracking technologies in [Chap. 2](#) and how to track the contour of objects with larger motion using the proposed optical flow and active contour model in [Chap. 3](#). In [Chap. 4](#), we assess the performance of the proposed method through experiments, and [Chap. 5](#) discusses the conclusion.

2 Existing Object Contour Tracking Technologies

Object tracking methods of video sequences are classified largely into the method of using modified object extracting algorithm of the past and the one of using object tracking algorithm [3]. Technologies to apply the object extraction algorithm to video sequences include the method of forming an energy function considering the relationship between time-dimensional nodes together with background subtraction and graph-cut algorithm [4, 5]. These methods often cause errors in the adjacent areas with complex background. In object tracking algorithm, features such as point, kernel, and silhouette are extracted from the previous

frames, with the object extracted from the following frame by matching them [6]. Designed mainly to situate an object, this method needs additional algorithms to ensure accurate extraction of the shape of an object and has disadvantages such as occlusion of the object or vulnerability for objects with large motion [3].

In recent years, extensive studies have been made on an active contour model-based method that effectively captures the modification of an object and divides in flexible lines surrounding the object [7–11], a method to find the shape of an object based on its contour energy data. In this study, the outermost closed curve of an irregular object extracted from the first frame of video sequences by the operator are being tracked continuously in the following frames using the active contour model.

2.1 Snake Algorithm

The snake algorithm, as the most common active contour model, was first proposed in 1987 by Kass [7]. In this algorithm, initial snake points are set around the object to extract from the input video, and the contour of the object is extracted in the course of minimizing the energy function by moving snake points iteratively according to the defined energy function.

Snake energy function is the sum of internal energy determining the shape of snake contour and external energy that serves to pulling snake points toward the object contour.

$$E_{\text{snake}}(v) = \sum_{i=0}^{N-1} (E_{\text{internal}}(v_i) + E_{\text{external}}(v_i)) \quad (1)$$

where snake point is set as v_i , v_i is $v_i = (x_i, y_i)$, which means the i th snake point, and N refers to the number of snake points.

Internal energy consists of continuity energy that determines the distance between snake points and curvature energy that determines the movement of snake points.

$$E_{\text{internal}}(v_i) = E_{\text{continuity}}(v_i) + E_{\text{curvature}}(v_i) \quad (2)$$

External energy functions to attract snake contour to features or contour of an object. Features of frequently used videos include gradient meaning the boundary of the object where brightness changes sharply. External energy at individual points of 9-neighbor including the current control point is calculated to move to the location with a larger gradient.

$$E_{\text{external}}(v_i) = \frac{-|\nabla f(v_i)|}{e_{\text{max}}} \quad (3)$$

2.2 Problems with Snake Algorithm

Since it can extract the object contour in a simple and effective manner, snake algorithm is being used broadly and has following problems although there have been many minimization algorithms proposed [12]. The algorithm

- (1) is highly dependent on the location and shape of initial snake points.
- (2) cannot extract the contour of an object with complex shape by means of functions of internal energy function.
- (3) takes enormous time due to the limited range where fixed points move at a time.

As this study aims at applying to the non real-time 2D-to-3D conversion, the problem as in (3) is not taken into account seriously. By calculating optical flow with the previous frame and setting the location of initial snake points for object tracking of the current frame, the problem of dependence on the location and shape of initial snake points as mentioned in (1) is solved. As far as the problem described in (2) is concerned, object contour, no matter how complex, is effectively extracted by inserting new snake points after calculating partial curvature between snake points.

3 The Proposed Method

This study proposes a new tracking method that follows in order to solve the problem of object tracking using existing snake algorithm. The proposed method is designed to track exactly object contour in the $n + 1$ th frame from object extraction result data in the n th frame. In the $n + 1$ th frame, optical flow of object contour feature points in the n th frame is calculated to set the initial snake points. In this case, any optical flow as a result of wrong algorithm due to irregular object or large motion is filtered, compared to the result of morphology algorithm of difference edge map between two frames. Afterwards, activation contour is converged to the target object in the $n + 1$ th frame in the course of finding activation contour solution in the snake algorithm. To solve the problem of energy shortage caused by complex contour of the object to track, we took into consideration of the method of adding snake points using partial curvature of Lee [13] (Fig. 1).

3.1 Calculation of Optical Flow

In the case of non real-time 2D-to-3D conversion, objects are classified generally by the operator for the first frame ($n = 0$) in video sequences of the scene to convert. From the object contour classified in this way, end points of horizontal, vertical, and diagonal components are set as feature points of object contour.

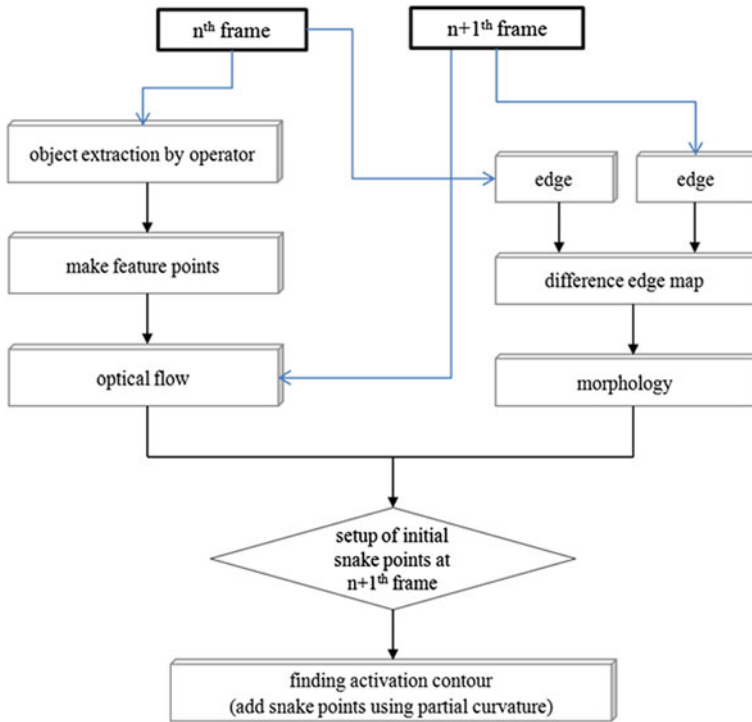


Fig. 1 Flow of the proposed object contour tracking

Afterwards, referring to the $n + 1$ th frame, optical flow off feature points is calculated. Optical flow means the motions of individual pixels created by 3D movement of the object in the video or the camera represented by vector field [14]. Among many methods of tracking the motion of pixels, the Lucas-Kanade [15] algorithm, most widely known, was used in this study. The Lucas-Kanade algorithm is based on three hypotheses: brightness constancy, temporal persistence, and spatial coherence. Brightness constancy means that brightness values among video frames never change, while temporal persistence means that compared to motion of an object in a video, time change faster, causing less motions of the object between frames. Under these two hypotheses, the optical flow between time t and $t + \Delta t$ is expressed as follows:

$$\begin{bmatrix} V_x \\ V_y \end{bmatrix} = \begin{bmatrix} \sum I_{x_i}^2 & \sum I_{x_i} I_{y_i} \\ \sum I_{x_i} I_{y_i} & \sum I_{y_i}^2 \end{bmatrix} \begin{bmatrix} \sum I_{x_i} I_t \\ \sum I_{y_i} I_t \end{bmatrix} \quad (4)$$

V_x and V_y in Eq. (4) refer to speed component of each axle, and I to brightness degree of each pixel. Figure 2 shows the results of motion of feature points following the calculation of optical flow with the $n + 1$ th frame, once feature points are created along the object contour extracted by the operator from the n th frame.



Fig. 2 Creation of feature points and calculation of optical flow from object contour. **a** Object extracted from the n th frame by the operator, **b** Feature points created from the object contour in **(a)**, **c** Results of tracking feature points of **(b)** along optical flow in the $n + 1$ th frame

3.2 Setup of Initial Snake Points

The 15frame/s videos were used for this study and have tracking points where as a result of creating optical flow, quickly moving irregular objects are unable to move precisely to the object contour as shown in Fig. 2. Therefore, these tracking points cannot be used for snake algorithm as they are due to higher dependence on the location and shape of initial snake points set in 2.2, so it is impossible to track object contour properly. To solve this problem, a difference edge map between frames is created for filtering purposes. To make a difference edge map, edge maps of the n th frame and the $n + 1$ th frame are made first of all. To reduce the impacts of surrounding noises and obtain thick gradient data, the Sobel operator is used for an edge map. The difference edge map $D_{\text{edge}}(x, y)$ for the two frames is defined as follows:

$$D_{\text{edge}}(x, y) = \begin{cases} S_{n+1}(x, y) - S_n(x, y) & \text{if } S_{n+1}(x, y) - S_n(x, y) > I_{th} \\ 0 & \text{otherwise} \end{cases} \quad (5)$$

where $S_n(x, y)$ and $S_{n+1}(x, y)$ refer to edge extraction result of using the Sobel operator of the n th frame and the $n + 1$ th frame, respectively, and 10 is used for I_{th} as a threshold to prevent the mixture of noises. Figure 3 is the result of creating difference edge map. Figure 3a, b show the results of the Sobel edge extraction for the n th frame and the $n + 1$ th frame, respectively, and Fig. 3c is the result of creating difference edge map. Fixed background and still object in a scene where the camera does not move are set to values close to 0. Then, considering the scope of filtering, dilation algorithms as a morphological algorithm are performed many times to obtain a map for final snake point filtering as in Fig. 3d.

Using the difference edge map obtain in this way, the feature points produced through optical flow in 3.1 are filtered. Specifically, any optical flow surpassing a set value (here 5 set from many experiments) becomes subject to filtering, while the one found not included in the value as a result of comparison with the difference edge map is removed. Figure 4 shows that almost all of the feature points not included in the object contour have been removed.

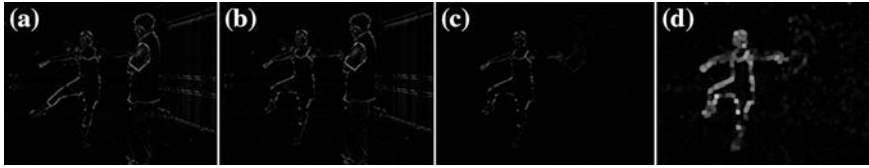


Fig. 3 Creation of difference edge map to set reference snake points. **a** Result of edge extraction in the n th frame, **b** Result of edge extraction of the $n + 1$ th frame, **c** Difference edge map, **d** Dilation for (c)

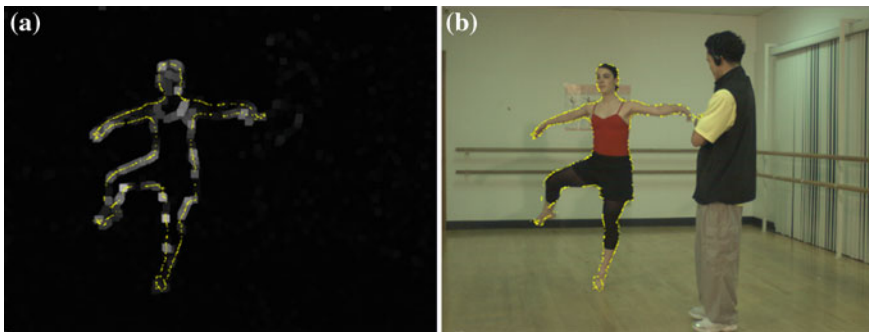


Fig. 4 Filtering of feature points according to difference edge map. **a** Filtering method of feature points, **b** Filtering results

3.3 Finding Activation Contour Solution

Feature points filtered by difference edge map are set as reference snake points in the $n + 1$ th frame and converged to object contour with gradient of grey image as external energy. For an object with irregular shape, we considered a method of adding snake points using partial curvature of Lee [13] in the stage of renewing individual snake points in order to detect the contour in the areas where the curvature among and between snake points changes severely. Discrete curvature k_d is calculated using three snake points v_{i-1}, v_i, v_{i+1} as follows:

$$\overrightarrow{T_{d1}} = v_{i-1} - v_i, \quad \overrightarrow{T_{d2}} = v_{i+1} - v_i \tag{6}$$

$$\cos \theta = \frac{\overrightarrow{T_{d1}} \bullet \overrightarrow{T_{d2}}}{\|\overrightarrow{T_{d1}}\| \cdot \|\overrightarrow{T_{d2}}\|} \tag{7}$$

$$k_d = \frac{2 \sin \theta}{d}, \text{ where } d = v_{i+1} - v_{i-1} \tag{8}$$

In the above equation, \bullet means inner area of two vectors, and $\| \cdot \|$ means the norm of vector. Since the curvature value more than the critical value means complex object contour, two new snake points are inserted into $v_{i-1} + v_i/2$ and $v_i + v_{i+1}/2$.

4 Results and Discussion

To test the proposed method, a ballet video (1024*768, 15frame/s) [16] and a foreman video (352*288, 50frame/s) containing irregularly changing object were used. To assess the performance, mean error of actual contour point coordinates and estimated contour point coordinates was calculated. Actual contour point coordinates were obtained from the object contour extracted manually.

Figure 5 shows the experiment of the foreman video with a sufficient number of frames and smaller motion of the object. Tracking was conducted in the 159th frame for the object manually extracted from the 158th frame. Weights for continuity energy, curvature energy, and external energy of the snake algorithm were set to 0.2, 0.3, and 0.5, respectively, through many experiments, and convergence condition was that the rate of change of the snake points was below 10 %. The mean error was 2.23 pixels, almost similar to the actual object contour.

Figure 6 indicates the experiment of the ballet video with less frames and larger motion. Tracking was performed in the 84th frame for the object manually extracted from the 83th frame. Weights of continuity energy, curvature energy,



Fig. 5 Results of experiments with the foreman video. **a** The 158th frame, **b** Reference snake points estimated from the 159th frame, **c** Result of activation contour tracking of the 159th frame



Fig. 6 Results of experiments with the ballet video. **a** The 83th frame, **b** Reference snake points estimated from the 84th frame, **c** Results of activation contour tracking of the 84th frame

and external energy of the snake algorithm are 0.2, 0.15, and 0.65, respectively. The mean error was 5.61 pixels, almost similar to the actual object contour. Figure 6c reveals that some contour points near the left hand and foot are not converged properly to the object. Motion blur is considered to cause the object contour blurred near the left hand, while external energy shortage due to highly similar brightness of the object and the background seemed to cause the problem near the left foot. Nevertheless, most are found to have been tracked as the boundary of the object.

5 Conclusion

In this study, we proposed a method of tracking object contour with large motion and irregular shape in video sequences in a stable manner using the optical flow and active contour model. Setting optical flow of feature points along the object contour extracted by the operator from video sequences as snake reference for the next frame, activation contour tracking was conducted with addition of snake points by partial curvature. Findings from experiments with actual videos indicate that irregular objects with large motion are easier to track. To apply this method to a non real-time 2D-to-3D conversion where precise tracking of object is important, however, research is necessary to solve the problem of motion blur or energy shortage due to smaller brightness difference from the background.

Acknowledgments This research is supported by Ministry of Culture, Sports and Tourism (MCST) and Korea Creative Content Agency (KOCCA) in the Culture Technology (CT) Research and Development Program [R2012030006].

References

1. Lee YS (2011) The trends and prospects of 2D-3D conversion technology. *J. Korean Inst Electron Eng* 38(2):37–43
2. Okino T, Murata G, Taima K, Inuma T, Oketani K (1996) New television with 2D/3D image conversion technologies. *Proc SPIE* 2653:96–103
3. Kim J, Lee J, Kim C (2011) Video object extraction using contour information. *J Korean Inst Electron Eng* 48(1):33–45
4. Li Y, Sun J, Shum HY (2005) Video object cut and paste. *J ACM Trans Graph* 24(3):595–600
5. Li B, Yuan B, Sun Y (2006) Moving object segmentation using dynamic 3D graph cuts and GMM. *IEEE Int Conf Signal Process* 2:16–20
6. Javed O, Rasheed Z, Shafique K, Shah M (2003) Tracking across multiple cameras with disjoint views. *IEEE Int Conf Comp Vis* 2:952–957
7. Kass M, Witkin A, Terzopoulos D (1988) Snakes - active contour models. *Int J Comp Vis* 1(4):321–331
8. Bing X, Wei Y, Charoensak C (2004) Face contour tracking in video using active contour model. *Int Conf Image Process* 2:1024–1024

9. Chenyang X, Prince JL (1997) Gradient vector flow: a new external force for snakes. In: IEEE computer society conference on computer vision and pattern recognition, pp 66–71
10. Leymarie F, Levince MD (1993) Tracking deformable object in the plane using an active contour model. *IEEE Trans Pattern Anal Mach Intell* 15(6):617–634
11. Ling P, Fan J, Shen C (2007) Color image segmentation for objects of interest with modified geodesic active contour method. *J Math Imaging Vis* 27(1):51–57
12. Kim D, Lee D, Paik J (2007) Combined active contour model and motion estimation for real-time object tracking. *J Inst Electron Eng Korea* 44(5):64–72
13. Lee JH (2009) A study on an improved object detection and contour tracking algorithm based on local curvature. Master's Thesis, Paichai University, Daejeon, Korea
14. Lee JW, You S, Neumann U (2000) Large motion estimation for omnidirectional vision. In: *Proceedings of IEEE Workshop on Omnidirectional Vision*, pp 161–168
15. Lucas BD, Kanade T (1981) An iterative image registration technique with an application to stereo vision. In: *Proceedings of 1981 DARPA Imaging Understanding Workshop*, pp 121–130
16. Zitnick CL, Kang SB, Uyttendaele M, Winder S, Szeliski R (2004) High-quality video view interpolation using a layered representation. In: *Proceedings of ACM SIGGRAPH and ACM transaction on graphics*, Los Angeles, CA, pp 600–608

Correction to: 3D Trajectory Planning for a 6R Manipulator Robot Using BA and ADAMS

Correction to:

**Chapter 84 in: J. J. (Jong Hyuk) Park et al. (eds.),
Information Technology Convergence,
Lecture Notes in Electrical Engineering 253,
https://doi.org/10.1007/978-94-007-6996-0_84**

In the original version of the Chapter 84, an author name “A Gün” was added in the reference 7. The book and the chapter have been updated with the changes.

The updated version of this chapter can be found at
https://doi.org/10.1007/978-94-007-6996-0_84

J. J. (Jong Hyuk) Park et al. (eds.), *Information Technology Convergence*,
Lecture Notes in Electrical Engineering 253,
https://doi.org/10.1007/978-94-007-6996-0_114,
© Springer Science + Business Media Dordrecht 2024

C1

Author Index

A

Abe, T., 847
Aikebaier, A., 417
Akieda, S., 855
Akita, H., 1019
Ariff, R. M., 255, 273, 295

B

Barolli, A., 47, 131, 223
Barolli, L., 37, 47, 77, 89, 161, 169, 193,
223, 243, 281, 451, 863
Bohari, A. A., 255, 273, 295
Byambasuren, B.-E., 835

C

Cao, K.-X., 341
Chae, S.-H., 203, 213
Chae, Y. N., 933
Chang, A. Y., 783
Chang, B.-J., 341
Chang, C.-s., 617
Chang, C.-W., 111
Chang, R.-C., 773
Chang, S.-F., 557
Chang, T.-J., 57
Chang, W.-C., 617
Chang, X., 161
Chao, C.-Y., 683
Chen, C.-L., 575
Chen, H., 333
Chen, H.-M., 723
Chen, J.-S., 445
Chen, K.-Y., 793
Chen, S.-Y., 723
Chen, S.-W., 111
Chen, T.-S., 723

Chen, W.-Y., 743
Chen, Y.-J., 355
Chen, Y.-S., 717
Chen, Y.-H., 669, 683
Chiang, D.-J., 587
Chiang, H.-S., 761
Chien, H.-F., 111
Ching, K. B., 273
Chiou, S.-F., 461
Chiou, Y.-S., 151
Cho, N., 977
Choi, J.-W., 1061
Choi, W.-H., 509
Choi, Y.-H., 185
Chou, S.-C., 751
Chung, T.-M., 185
Chung, Y.-H., 111

D

Debnath, N. C., 519
Deng, L. Y., 659, 669, 683
Doo, S., 435

E

Enokido, T., 417
Eom, J.-H., 185
Fujioka, H., 941

G

Ghanbarzadeh, A., 807
Ghosh, D., 519
Go, S. j., 485
Guo, J.-Z., 717
Guo, Y.-M., 575

H

Hammood, M. M., 13, 407
 Han, ByungOk, 933
 Han, T.-W., 1047
 Hanafi, D., 273
 Haron, Z. A., 255, 295
 Hasegawa, J., 847
 Herrero, X., 131
 Hidaka, N., 855
 Hiyama, M., 77, 89
 Ho, C. C., 311
 Honda, J., 101
 Honda, S., 1011
 Honda, T., 29
 Hong, C.-P., 1047
 Hsiao, K.-F., 121
 Hsieh, C.-H., 67
 Hsu, C.-L., 693, 793
 Hu, W.-P., 743
 Huang, C.-L., 677
 Huang, C.-P., 67
 Huang, J.-Y., 659, 683
 Huang, P. S., 57
 Huang, S.-C., 3
 Huang, S.-Y., 121
 Huang, T.-C., 707
 Huang, Y.-M., 717
 Hung, C.-J., 677
 Hung, J. M., 67
 Hwang, G.-H., 461

I

Ihm, S.-Y., 531
 Ikeda, M., 29, 37, 77, 89, 161, 169, 281
 Ishikawa, S., 985
 Iwamoto, Y., 855
 Iwashige, J., 281, 451

J

Jang, G.-J., 817, 949, 1037
 Jen, C.-Y., 567
 Jeon, H.-B., 957
 Jeong, H. Y., 501
 Jhan, F.-J., 733
 Jheng, M.-R., 617
 Jheng, Y.-S., 659, 683
 Jian, M.-S., 707, 733
 Jiang, X., 397
 Jo, A., 817
 Jui-Yu, Chiu, 627
 Jullakarn, I., 1011

Jung, D.-Y., 957

Jung, S.-Y., 967

K

Kato, T., 1011
 Kawabata, K., 873
 Ke, C.-K., 567
 Khil, A., 995
 Kikuchi, S., 827
 Kim, C. G., 1047, 1055
 Kim, D.-H., 835
 Kim, D.-K., 509
 Kim, J.-H., 949
 Kim, J.-H., 957, 977, 1037
 Kim, J.-H., 387
 Kim, J. Y., 469
 Kim, K.-H., 977
 Kim, N.-B., 1061
 Kim, Y. J., 913
 Kimura, H., 847
 Kino, H., 827
 Koo, K.-M., 913
 Koo, M.-W., 957, 977
 Ku, D. T., 635
 Kulla, E., 77, 89, 169, 243, 281
 Kumar, J. V., 743
 Kuo, K.-P., 121

L

Lai, C.-Y., 761
 Lee, C.-C., 547
 Lee, D. G., 213
 Lee, D., 977
 Lee, D.-L., 669, 683, 693, 793
 Lee, E.-S., 387
 Lee, H.-J., 957
 Lee, I.-Y., 477, 485
 Lee, J. D., 495
 Lee, J., 881
 Lee, J., 21
 Lee, K.-H., 995, 1003
 Lee, K., 1037
 Lee, K.-W., 733
 Lee, S.-H., 477, 485
 Lee, S., 923
 Lee, Y.-K., 957
 Li, J.-H., 723
 Li, W.-C., 557
 Liang, Y.-H., 341
 Lim, J., 435
 Lim, S.-H., 469

Lin, C.-J., 635
 Lin, K.-C., 723
 Lin, K.-H., 659, 683
 Lin, S.-L., 607
 Lin, S.-H., 355
 Lin, Y.-H., 121
 Lin, Z.-Y., 311
 Lin, Z.-W., 597
 Liu, L.-C., 761
 Liu, Y.-J., 669
 Lu, C.-T., 707
 Lu, Y.-F., 751

M

Ma, J., 397
 Maeda, E., 1019
 Maeda, H., 333
 Maki, T., 263, 323
 Manaskasemsak, B., 365, 375
 Masajedi, P., 807
 Masuda, H., 1011
 Matsuda, S., 855
 Matsuo, K., 193, 451, 863
 Matsutani, Y., 827
 Miho, R., 193
 Min, J.-W., 185
 Mino, G., 243, 281
 Miura, H., 855
 Moon, D., 213
 Morizono, T., 1027
 Mukhopadhyay, S., 519

N

Na, S.-Y., 1047
 Nagoya, T., 941
 Nakayama, K., 855
 Nasridinov, A., 531

O

Oda, T., 47, 161, 169, 223
 Ogiela, L., 177, 427
 Ogiela, M. R., 177, 427
 Okamoto, T., 1019
 Okamura, K., 1019
 Oyun-Erdene, Mandakh, 835

P

Pan, I.-H., 57
 Pan, S. B., 203, 213
 Papajorgji, P., 223

Park, G.-L., 21
 Park, J.-S., 817, 881, 949, 957, 977, 1037
 Park, J. S., 495
 Park, J. H., 495, 501
 Park, M.-W., 185
 Park, S.-J., 897, 905, 967
 Park, S.-Y., 957
 Park, Y.-H., 531
 Piao, J.-C., 1047
 Rahim, A. S. B. A., 985
 RamTeja, N., 519
 Rungsawang, A., 365, 375

S

Sagara, S., 873
 Sagheer, A. M., 13, 407
 Sakagami, N., 985
 Sakamoto, S., 169
 Samretwit, D., 323
 Sasaki, H., 855
 Seo, Y., 817
 Seo, Y.-H., 881, 897, 923, 931, 933, 967
 Shen, J.-H., 707, 733
 Shen, Y., 397
 Shi, W., 397
 Shibata, M., 889
 Shieh, S.-L., 461
 Shigetomi, K., 101
 Shih, H.-Y., 717
 Shih, Y.-H., 445
 Shimoto, T., 855
 Shin, D., 977
 Shin, Y., 435
 Shirazi, K. H., 807
 Siangkhio, S., 365
 Sim, S. Y., 255, 273, 295
 Spaho, E., 37, 47, 161, 193, 451, 863
 Sula, A., 193
 Surarerk, A., 365, 375
 Suzuki, M., 1027

T

Tahara, K., 827
 Tajima, T., 847
 Takematsu, M., 101
 Takemura, F., 873
 Takizawa, M., 47, 77, 89, 131, 223, 243, 417
 Tang, S.-W., 567
 Teerasetmanakul, P., 375
 Tokuyasu, T., 1019
 Tomiura, K., 333

Tongtip, K., 375
Toshimitsu, K., 1019
Tsai, J. J. P., 743
Tsai, T.-S., 773
Tseng, C.-H., 649
Tzeng, Y.-S., 3

U

Uchida, K., 101
Uechi, N., 873
Umezaki, K., 451
Utomo, W. M., 255, 273, 295

W

Wakahara, T., 233, 263, 305, 323
Wan, L.-T., 121
Wan, T.-L. J., 677
Wang, C.-S., 607
Wang, C.-S., 717
Wang, Ching-Sheng, 575, 587
Wang, Chu-Fu, 141
Wang, Jen-Ya, 445
Wang, Lung-Cheng, 677
Wang, Qi, 281
Wang, Rong-Sheng, 751
Wang, Yu-Hui, 541
Wattanavarangkul, N., 233
Wei, J.-S., 311
Wei, Y.-C., 587
Wen-C., C., 627
Whangbo, T.-K., 1061
Wong, W.-T., 597
Wu, M.-Y., 557

Wu, S.-H., 151
Wu, W.-C., 597

X

Khafa, F., 37, 47, 89, 131, 161, 169, 193,
223, 451, 863
Xia, Y., 547

Y

Yamamoto, N., 305, 323
Yang, H.-L., 607
Yang, H.-C., 617
Yang, H. S., 923, 933
Yang, S.-Y., 793
Yang, T.-K., 897, 905, 967
Yang, T., 243
Yang, Y.-C., 141
Yao, L., 773
Yasumoto, K., 333
Yeh, S.-C., 151
Yeh, Y.-J., 567
Yeh, Y.-C., 461
Yoon, H., 435
Yoshigoe, K., 13, 407
Yoshiura, K., 1019
You, K.-B., 1003

Z

Zeng, W.-S., 355
Zin, N. M., 255, 273, 295

Subject Index

B

Biomechanics, modeling and computing

C

Cloud computing, [502](#), [503](#), [506](#), [551](#), [718](#),
[734](#), [794](#)

Cryptographic, [13](#), [14](#), [19](#), [398](#), [408](#), [431](#)

Data integrity, [961](#)

Dependability, [961](#)

E

e-Health and e-Hospital

e-Learning Pedagogical Strategies

Electronic Commerce, Business and Management, [568](#), [608](#), [670](#)

I

Intelligent Manufacturing Technology, [v](#)

Intelligent Robotics, [195](#), [870](#)

Intelligent Vehicular Systems and Communications

M

Medical Knowledge Mining

Medicine and Education with IT

N

New Computational Science and Applications

New Electrical and Electronics Engineering and Technology

R

Robot sensing and data fusion

S

Security and Privacy issues with e-learning, [204](#)

Security and Trust computing

Sensor network and data, [101](#), [196](#), [243](#),
[281](#), [547](#), [548](#), [552](#), [790](#)